

1996

***XVII BRAZILIAN
NATIONAL
MEETING ON
PARTICLES
AND FIELDS***

 **FAPESP**

 **SBF**
SOCIEDADE BRASILEIRA DE FÍSICA

**XVII Brazilian National
Meeting on
Particles and Fields**

September 2-6, 1996

Serra Negra - Brasil

Published with financial support of FAPESP
Fundação de Amparo à Pesquisa do Estado de São Paulo.

The Brazilian National Meeting on Particles and Fields

The Brazilian National Meeting on Particles and Fields (Encontro Nacional de Física de Partículas e Campos) is a scientific meeting held every year that assembles the Brazilian Physics community working in Field Theory, Cosmology and Gravitation, Particle Physics Phenomenology, and Experimental High Energy Physics. The aim of this meeting is the interchange of information among the whole community through invited review talks, presentation of contributed short communications and panels on current research activities of the participants.

The first of these meetings was held in 1978 and had about 80 participants. In the following years this number has grown considerably and in 1996 we have more than 250 participants, including Master and Ph.D. graduated students, and 115 submitted papers.

The meeting is organized under the auspices of Sociedade Brasileira de Física (SBF) with the support of Coordenação de Aperfeiçoamento de Pessoal de Nível Superior (CAPES), Centro Latino-Americano de Física (CLAF), Conselho Nacional de Desenvolvimento Científico e Tecnológico (CNPq), Fundação de Amparo à Pesquisa do Estado de São Paulo (FAPESP), do Rio de Janeiro (FAPERJ), do Rio Grande do Sul (FAPERGS), and Financiadora de Estudos e Projetos (FINEP).

We would like to thank the SBF staff for all their efforts, in particular Neusa M. L. Martin and Fernando L.C.da Silva Braga for organizing these Proceedings.

December, 1996

Adilson J. da Silva, IFUSP
Anderson Fauth, UNICAMP
Angela Focrster, UFRGS
Dionisio Bascia, UFPB
Nelson R. F. Braga, UFRJ
Rogério Rosenfeld, IFT-Unesp
Ronald Shellard, CBPF-Lafex
Samuel Oliveira, UNB

Desde a criação deste Encontro em 1978 o Prof. J. J. Giambiagi esteve sempre presente, trazendo sua contribuição científica, entusiasmo pela Física, companheirismo e alegria. Este ano sentimos muito sua ausência. Dedicamos esta publicação à sua memória.

ÍNDICE

PALESTRAS DE REVISÃO E SEMINÁRIOS

Electric Magnetic Duality and Quark Confinement <i>F. Gliozzi</i>	1
Some Aspects Physics Beyond the Standard Model <i>F. de Campos</i>	8
Teoria de Campos em Espaços Curvos: Nova Luz Para Velhos Problemas <i>G. E. A. Matsas</i>	30
A Profusion of Black Holes From Two to Ten Dimensions <i>J. P. S. Lemos</i>	40
Black Holes as Atoms: Classical Hair and Quantum Levels in the Light of General Relativity <i>J. D. Bekenstein</i>	59
Selected Topics on DØ Physics <i>J. M. de Miranda</i>	70
Turbulence and Quantum Field Theory <i>L. Moriconi</i>	82
Topological and Quasi-Topological Field Theories in Two Dimensions <i>P. Teotonio Sobrinho, B. G. C. da Cunha</i>	96
Physics of the Standard Model and Beyond <i>R. S. Chivukula</i>	117
Casimir Effect for the Real Boundaries <i>V. M. Mostepanenko</i>	137

CONTRIBUIÇÕES CIENTÍFICAS

A. COSMOLOGIA E GRAVITAÇÃO

Black-Body Spectrum of the CBR and its (possible) relation to the Topological Degree of Connectedness <i>A. Bernui Leo</i>	149
The Radiation-Reaction Problem in Topologically Different FRW Space-times <i>A. Bernui Leo, M. J. Rebouças</i>	151
Desenvolvimento de um Transdutor Indutivo Supercondutivo de Dois Modos com Alto Fator de Qualidade Mecânico para uma Antena Ressonante Massiva de Ondas Gravitacionais <i>C. Frajuca, Nadja S. Magalhães, O. D. Aguiar, Z. K. Geng, William O. Hamilton W. W. Johnson, N. D. Solomonson</i>	157
On The Higher Derivative Quantum Gravity <i>M. Asorey, J.L. López, I.L. Shapiro</i>	161

On the conformal transformation in (quantum) gravity <i>Ilya I. Shapiro</i>	165
On the parameters of the Levi-Civita solution <i>A. Wang, M. F. A. da Silva, N. O. Santos</i>	169
Formalismo do Tempo Extrínseco para o Buraco Negro Euclidiano em uma Caixa <i>G. Oliveira-Neto</i>	174
Comparative Study Between the Thermodynamics of the 2-Dimensional Black Hole in the 'Teitelboim-Jackiw Theory and the 4-Dimensional Schwarzschild Black Hole <i>José P. S. Lemos</i>	178
Bundles in a Supersymmetric Yang-Mills Theory <i>M. F. Borges, S. R. M. Musalskiene, W. Seizas</i>	184
The Causal Interpretation of Quantum Mechanics and The Singularity Problem in Quantum Cosmology <i>J. A. de Barros, N. Pinto Neto</i>	186
Classical Fields and the Quantum concept <i>M. M. de Souza</i>	190
Black Hole Formation in Lovelock Theory <i>A. Ilha, José P. S. Lemos</i>	196
'The Detection of Gravitational Waves as a Test for Theories of Gravitation <i>Nadja S. Magalhães, O. D. Aguiar, W. W. Johnson, C. Frajuca</i>	202
Self-Similar Planar Newtonian Collapse <i>O. S. Ventura, José P. S. Lemos</i>	205
Model Independent Analysis of Proton-Proton Elastic Scattering <i>P. A. S. Carvalho, M. J. Menon</i>	215
Radiative Processes for Accelerating Observers <i>R. De Paola, N. F. Svaiter</i>	220
Regge Law in Astrophysics <i>R. Murááian</i>	224
Anomalous Higgs Boson Contribution to $e^+e^- \rightarrow b\bar{b}\gamma$ at LEP2. <i>S. M. Lietti, S. F. Novaes, R. Rosenfeld</i>	232
Topology Change in Canonical Quantum Cosmology <i>V. A. De Lorenci, J. Martin, N. Pinto Neto, I. D. Soares</i>	236
Vacuum Quantum Effects of Nonconformal Scalar Field in the Friedmann Cosmology <i>V. D. Bezerra, V. M. Mostepanenko, C. Romero, A. Friedmann</i>	242
Computer-aided classification of the Segre types [11(1,1)] and [(11)1,1] <i>W. Seizas, M. F. Borges</i>	246
Chaos in Gravitational Core-Halo Systems <i>W. M. Vieira, P. S. Letelier</i>	251
Formação de Defeitos Topológicos no Universo Primordial <i>S. E. Jorás e C.A.A. de Carvalho</i>	252

B. FÍSICA EXPERIMENTAL DE ALTAS ENERGIAS

O Detector de Chuveiros Atmosféricos EASCAMP-II <i>A.R. Biral, J.A. Chinellato, A.C. Fauth, E. Kemp, E.G.S. Luna, H. Nogima, M.A.L. de Oliveira, L.G. dos Santos, M.C. Souza Jr., F. Tessari, A. Turtelli Jr.</i>	255
Performance of Resistive Plate Counters with Ar/Bu/CCl ₂ F ₂ and Ar/Iso/CBrF ₃ <i>A. Campos Fauth, A. Guidi</i>	259
Estimate of the Arrival Direction of Primary Particles Inducing Air Showers, From Data Obtained by the Top Cluster in the Cascade Experiment <i>C. Dobrigkeit</i>	263
Teste e Calibração de Componentes para a Torre de Destilação do detector Barrel RICH do DELPHI <i>D. Magalhães Moares</i>	268
Cascatas Hadrônicas Iniciadas Por Um Único Núcleo <i>H.M. Portella, A.S. Gomes, R.H.C. Maldonado, A.L.V. Silva, A.M.M. Lima, E.M. Fernandes, N. Amato</i>	274
Production of Sinner Layer of Si-Tracker 1996 DELPHI 96-38 MVX 12 <i>E. Polycarpo, I. Stavitski</i>	277
Projeto Microsul: Um Telescópio de Múons Cósmicos Horizontais <i>E. W. Hamburger, O. Dietzsch, N. Canzian da Silva, A. Bonini, E. M. Kubo, F. B. M. Saleme, L. M. R. Falco de França, S. A. Pereira, M. A. Schmidt, L. Galhardo</i>	284
τ Polarisation from the $\tau \rightarrow \rho\nu_\tau$ Channel in Delphi <i>J. R. P. Mahon, M. E. Pol, R. C. Shellard</i>	294
Search for Pair-Produced Neutral Higgs Bosons Using B-Tagging <i>M. Berggren</i>	298
A Medida de R_b no DELPHI/LEP <i>M. Gandelman, R. Shellard</i>	304
Synchrotron Radiation Monitoring for LEP2 using the DELPHI-TPC Silicon Detector <i>M. A. Gaspar, M. Barbi, B.M. Maréchal, L. de Paula, P. Siegrist, M. Besançon, T. Bolognese, X. Bravo, M. Gros, J. P. Passerieux, F. Picre, J. Poinsignon, D. Vilanova, E. Merle, J. Renaud</i>	306
DELPHI Event Server <i>L. M. Mundim</i>	312
Eventos Denominados Centauro <i>S.L.C. Barroso, P.C. Beggio, A.O. de Carvalho, M.D.D.O. Marques, R. de Oliveira, E.H. Shibuya, C.R.A. Augusto, C.E. Navia, F.A. Pinto</i>	315
A Medida da Polarização do τ no DELPHI/LEP <i>S. Amato e L. de Paula</i>	324
Teste do Protótipo do Novo Anel Cintilador do STIC e Testes das Fotomultiplicadoras e dos Cabos de Fibras Óticas do Contadores de 40° <i>T. da Silva</i>	328

C. FENOMENOLOGIA DE PARTÍCULAS ELEMENTARES

Critical Coupling for Dynamical Chiral-Symmetry Breaking with an Infrared Finite Gluon Propagator <i>A. A. Natale, P. S. Rodrigues da Silva</i>	335
Derivative Analyticity Relation and Parton-Parton Scattering Amplitude <i>A. F. Martini, M. J. Menon, J. T. S. Paes, M. J. Silva Neto</i>	343
Análise Bi-Dimensional de χ^2 em Interferometria de Kaons <i>C. G. Roldão, S. S. Padula</i>	347
Hadronic Size Dependence in High-Energy Scattering <i>E. Ferreira, F. Pereira</i>	351
Probing Higgs Couplings in $e^+e^- \rightarrow \gamma\gamma\gamma$ <i>F. de Campos, S. M. Lietti, S. F. Novaes, R. Rosenfeld</i>	357
The fermion families replication question <i>F. Pisano</i>	360
Espectro de Muons e Neutrinos ao Nível do Mar <i>H.M. Portella, A.S. Gomes, A.L.V. Silva, R.H.C. Maldonado N. Amato, C.E.C. Lima, L.C. Oliveira</i>	365
Difração de Solitons Bidimensionais <i>J. E. Cieza Montalvo, Y. P. Rybakov</i>	368
Spin-flip Conversion and Time Variations of Solar Neutrino Data Provoked by Solar Magnetosonic Waves <i>J.H. Colonia, M.M. Guzzo, N. Reggiani</i>	371
Busca de Ressonâncias na Conversão de Helicidade de Neutrinos em Interações com Campos Magnéticos Rotantes <i>J. Bellandi, M. M. Guzzo, Pedro C. de Holanda</i>	374
A Geração da Massa do Pion na Quantização dos Skyrmions <i>J. Ananias Neto</i>	378
Otimização de Tempo na Simulação de Cascatas Eletromagnéticas na Atmosfera <i>L. Américo de Carvalho, C. Dobrigkeit, J. A. Chinellato</i>	380
Bounds on Excited Leptons from Precise Electroweak Measurements <i>M. C. Gonzalez-Garcia, S. F. Novaes</i>	385
Aspectos de SUSY com Quebra de Paridade-R <i>M. Bernardino Magro</i>	392
Colorless States in Perturbative QCD: Charmonium Production <i>O.J.P. Éboli, E.M. Gregores, F. Halzen</i>	397
A Produção Associada de Bósons de Gauge e Jatos Através de Interações Múltiplas de Pártons <i>O. J. P. Éboli, J. K. Mizukoshi, F. Halzen</i>	400
Looking for Invisibly Decaying Higgs Bosons Through the Final State $b\bar{\nu}p_T$ <i>O.J.P. Éboli, F. de Campos, J. Rosiek, J.W.F. Valle</i>	405
Hadronic Inelastic Cross Sections from Analyses of the Elastic Channel <i>P.C. Beggio, A.F. Martini, M.J. Menon</i>	411

The Importance of Thermal Fluctuations During the Electroweak Phase Transition	
<i>Rudnei O. Ramos</i>	417
Produção de Pares do Top com um Gluon Extra no Tevatron	
<i>V. Barger, P. G. Mercadante, R. J. N. Phillips</i>	420

D. TEORIA DE CAMPOS

Fixed Points and Vacuum Energy of Dynamically Broken Gauge Theories	
<i>A. A. Natale, P. S. Rodrigues da Silva</i>	426
Von Neumann Algebra and Thermofield Dynamics	
<i>A. Matos Nctos, J.D.M. Vianna, A.E. Santana, F.C. Khanna</i>	429
Hamilton-Jacobi formulation for singular higher order systems	
<i>B. M. Pimentel, R. G. Teixeira</i>	433
Fermions and Bubble Nucleation	
<i>D. G. Barci, E. S. Fraga, C.A.A. de Carvalho</i>	438
Cordas Magnéticas Quânticas a Temperatura Finita	
<i>D. G. G. Sasaki, E. C. Marino</i>	443
Blindagem versus Confinamento na QCD em 2 Dimensões	
<i>E. Abdalla, R. Mohayaec, A. Zadra</i>	448
The q -Virasoro Algebra Obtained by an Analogue of the Hamiltonian Reduction Procedure	
<i>E. Batista, J.F. Gomes, I.J. Lautenschleguer</i>	452
Remark on Shape Invariant Potential	
<i>E. Drigo Filho, R. M. Ricotta</i>	456
Superspace Formulation for the BRST Quantization of the Chiral Schwinger Model	
<i>E. M. C. Abreu, N. R. F. Braga</i>	458
Zeta Function Method for Repulsive Casimir Forces at Finite Temperature	
<i>F. C. Santos, A. Tenório, A. C. Tort</i>	463
Spherical Collapse in Higher Order Gravity	
<i>F. Kokubun</i>	467
Atomic Levels Shifts Between Plates: the Influence of Vacuum Polarization	
<i>G.L. Klimchitskaya, I.L. Tomashevsky</i>	473
New Experiment for Obtaining Stronger Constraints on Hypothetical Particles of Modern Field Theory	
<i>G.L. Klimchitskaya, Ye.P. Krivtsov, V.M. Mostepanenko, C. Romero, A.Ye. Sinelnikov</i> ..	476
The $(\lambda\phi^4 + \sigma\phi^6)_{D=3}$ Model at Finite Temperature and the Tricritical Phenomena	
<i>G. N. J. Añaños, N.F. Svaiter</i>	482
Vacuum, Chiral Symmetry and Condensates in two-dimensional QCD	
<i>H. R. Christiansen</i>	489
Negative Dimensional Integration Method and Massive Feynman Diagrams	
<i>I. G. Halliday, R. M. Ricotta, A. T. Suzuki</i>	495
A Note on Moments of Gaussian Grassmann Multivariable Integrals	
<i>I. C. Charret, S. M. de Souza, M. T. Thomaz</i>	499
Expansão a Altas Temperaturas para Sistemas Fermiônicos Autointeragentes até ordem β^3	
<i>I. C. Charret, S.M. de Souza, M.T. Thomaz, E.V. Corrêa Silva</i>	502

Violação de Desigualdades Quânticas com Campos Clássicos <i>J. A. de Barros, P. Suppes, Gary Oas, A. S. Sant'Anna</i>	507
Hamiltonian Structures for the Generalized Dispersionless KdV Hierarchy <i>J. C. Brunelli</i>	511
The Connes-Lott program on the Sphere and the Static Magnetic Monopole <i>J. A. Mignaco, C. Sigaud, F. J. Vanhecke, A. R. da Silva</i>	516
The Virasoro algebra of a 1+1 black hole model <i>J. F. Gomes, F. E. Mendonça da Silveira, A. H. Zimmerman</i>	521
Asymptotic Dynamics in QED ₃ <i>J. L. Boldo, B. M. Pimentel, J. L. Tomazelli</i>	525
Explicit Demonstration of How the Zeta Function Method Removes the Divergences <i>J. A. Nogueira, Adolfo Maia Jr.</i>	530
Estudo das Ressonâncias em um Cilindro com Incidência Oblíqua <i>J. P. R. F. de Mendonça, L. G. Guimarães</i>	537
Acoplamento Interplanos e Propriedades Magnéticas em Supercondutor a Alta T_c <i>L. C. Malacarne, R. S. Mendes, P. R. Veroneze</i>	540
Álgebra Super $(W_{\frac{m}{2}} \oplus W_{\frac{1+\infty}{2}})$ no Modelo de Super-Autovalores <i>L. O. Buffon, D. Dalmazi, A. Zadra</i>	544
Sobre o Modelo de Chern-Simons na Frente de Onda da Luz <i>L. R. Ururahy Manssur</i>	549
Sewing string tree vertices with ghosts <i>L. Sandoval Junior</i>	554
The one loop measure in String Theory: the case of two finite fixed points <i>L. Sandoval Junior</i>	557
On Pseudospherically Symmetric Repulsive Gravitational Field <i>L. A. Anchordoqui, J. D. Edelstein, C. Núñez, G. S. Birman</i>	560
Scalar-Time Parametrization of Klein-Gordon Equation: The Harmonic Oscillator Solution <i>L. A. Anchordoqui, A. G. Grunfeld, M. C. Rocca</i>	563
More on Renormalization Ambiguities: Effective Action and Mode Summation <i>L. C. de Albuquerque</i>	569
Casimir Mass and Coupling Constant at Finite Temperature <i>L. C. de Albuquerque, C. Farina, A. Tort</i>	574
$O(p^2/m^2)$ Corrections to the Aharonov-Bohm Scattering <i>M. Gomes, J.M.C. Malbouisson, A. J. da Silva</i>	579
Soluções Tipo Vórtice em Eletrodinâmica Escalar em $D = 2 + 1$ Acoplada à Gravitação <i>M.S. Cunha, A. Penna Firme, O.S. Ventura</i>	585
Método de Gibbons para Função Zeta em Teoria de Campos <i>M.V. Cougo-Pinto, C. Farina, A. Tenório</i>	589
Factored coset approach to bosonization in the context of topological backgrounds and massive fermions <i>M.V. Manías, C.M. Naón, M.L. Trobo</i>	595
The Weakly Disordered 2D Electron Gas in a Magnetic Field <i>N. Brahić, R. M. Cavalcanti, C. A. A. de Carvalho, P. Donatis</i>	601

Chiral Decomposition For Non-Abelian Bosons <i>N.R.F. Braga, C. Wotzasek</i>	604
Função Partição Generalizada para Campos Quase-Periódicos com Potencial Químico <i>P. F. Borges, H. Boschi-Filho, C. Farina</i>	608
Action Principle for the Classical Dual Electrodynamics <i>P.C.R. Cardoso de Mello, S. Carneiro, M.C. Nemes</i>	613
Schwinger Model With Current-Current Interaction <i>R. L. P. G. Amaral, L.V. Belvedere, C. P. Natividade</i>	618
SUSY QM for the Two-Component Wave Functions <i>R. de Lima Rodrigues, A. N. Vaidya</i>	622
Uma Classe de Potenciais Isoespectrais com o q-Oscilador Relativístico 1D <i>R. de Lima Rodrigues, S. Bezerra de Oliveira</i>	625
Perturbative Analysis of the Schwinger Model (QED_2) for Gauge Non-Invariant Regularizations <i>R. C. Sifuentes, M. B. da Silva Neto, S. Alves Dias</i>	628
On Bosonization Ambiguities of Two Dimensional Quantum Electrodynamics <i>S. A. Dias, M. B. Silva Neto</i>	633
Path-integral Computation of Multipoint Spin Correlators in 2d Statistical Mechanics Models <i>V. I. Fernández, C.M. Naón</i>	636
Sobre a Expansão Perturbativa do Modelo de Gross-Neveu $(2 + 1)D$ <i>V. S. Alves, M. Gomes, L. C. Malacarne, S.V.L. Pinheiro, A. J. da Silva</i>	640
Regularização de um modelo tipo $\lambda\varphi^4$ tensorial, via “point-splitting” <i>W. A. Moura Melo, J. A. Helayël-Neto</i>	643
O Tensor Energia-Momentum do Campo de Radiação sob Vínculos Macroscópicos e o Efeito Casimir <i>F. P. A. Farias, Arthur M. Neto</i>	648
Energia de Casimir em geometrias retangulares d-dimensionais sob condições de contorno mistas <i>J. C. da Silva, H. Q. Plácido, A. E. Santana, Arthur M. Neto</i>	653
Lista de Participantes	659

ELECTRIC MAGNETIC DUALITY AND QUARK CONFINEMENT ^a

F. GLIOZZI

*Dipartimento di Fisica Teorica, Università di Torino,
via P. Giuria 1, 10125 Torino, Italy*

We give an elementary account of the Seiberg and Witten approach to $N=2$ super Yang-Mills theory which yields an exact form of the low energy effective action and suggests a simple confinement mechanism generated by monopole condensation.

1 Introduction

It is now widely believed that the phase of quark confinement observed or conjectured in many gauge theories in three or four space-time dimensions is described, as first suggested by t'Hooft, Mandelstam and Parisi ¹, by a sort of dual Higgs mechanism: a (composite) field ϕ_M carrying a magnetic charge acquires a non-vanishing vacuum expectation value $\langle \phi_M \rangle \neq 0$. This condensation gives a mass to the gauge field and a mass gap is generated like in ordinary Higgs effect. The important difference is that it is the dual or magnetic description of the gauge field which couples locally to the magnetized field ϕ_M . As a consequence, the chromoelectric field is expelled from the vacuum (dual Meissner effect) and the flux lines connecting a quark pair are squeezed in a thin flux tube (dual Abrikosov vortex), giving rise to a confining potential proportional to the interquark distance.

Unfortunately the above description for almost all known models remains at a conjectural stage. The only explicit example of this mechanism can be found in the Polyakov proof of confinement of $U(1)$ gauge model in three space-time dimensions ².

More recently, Seiberg and Witten worked out a new approach to four-dimensional $N = 2$ supersymmetric gauge theories leading to some exact results on their spectrum and on their low energy behaviour which strengthen and sheds new light on the dual picture of confinement. In this talk I would like to give an elementary account of this new approach.

2 $N = 2$ super Yang-Mills Theory

The minimal $N = 2$ super Yang-Mills theory for $SU(2)$ gauge group is described by a Lagrangian of the following form

$$L = \frac{1}{4\pi} \Im m \left\{ \left(\frac{\theta}{2\pi} + i \frac{4\pi}{e^2} \right) \left[-\frac{1}{4} \left(F_{\mu\nu}^a F_{\mu\nu}^a - \frac{1}{2} \epsilon^{\mu\nu\rho\sigma} F_{\mu\nu}^a F_{\rho\sigma}^a \right) + \overline{(D_\mu \phi)}_a (D_\mu \phi)_a - \frac{1}{2} (\epsilon^{abc} \phi_b \bar{\phi}_c)^2 + \text{fermions} \right] \right\} \quad (1)$$

where, in the usual notations, $F_a^{\mu\nu} = \partial^\mu A_a^\nu - \partial^\nu A_a^\mu - e \epsilon^{abc} A_b^\mu A_c^\nu$, the complex Higgs field ϕ is in the adjoint representation, and $(D^\mu \phi)_a = \partial^\mu \phi_a - e \epsilon^{abc} A_b^\mu \phi_c$.

We need not to write out explicitly the fermionic part of the Lagrangian which contains the contribution of the two Weyl fermions (the gaugino and the higgsino) which complete the chiral $N = 2$ supermultiplet.

The structure of the bosonic part of the Lagrangian in eq. (1) is pretty much the same as the one in the Georgi-Glashow model. There is, however, an important difference. Unlike the Georgi-Glashow case, here the potential

$$V(\phi) = \frac{1}{2e^2} (\epsilon^{abc} \phi_b \bar{\phi}_c)^2 \quad (2)$$

^aTalk given at the XVII Encontro Nacional de Física de Partículas e Campos, september 2-6, Serra Negra - S.P., Brazil

does not fix uniquely the vacuum. In fact any field configuration of the type $\phi^a = (0, 0, a)$ corresponds to a minimum of the potential with vanishing value (in order not to break the supersymmetry) for any value of the complex variable a . The set of all values of a is called the classical moduli space of the theory.

If $a \neq 0$ the $SU(2)$ gauge symmetry is broken to $U(1)$ by the Higgs phenomenon and the charged components of the gauge fields get a non vanishing mass, while the Higgs and the gauge field of the unbroken $U(1)$ remain massless. Thus the bosonic massless spectrum for a generic value of a consists of a photon A_μ , that is the gauge field of the unbroken $U(1)$, and of a complex, neutral scalar particle ϕ . If we are interested in studying the low-energy dynamics of these fields, we need to restrict ourselves to an effective Lagrangian with at most two derivatives and with no more than four-fermion couplings. The requirement of $N = 2$ supersymmetry fixes completely its form giving the following Lagrangian³

$$L = \frac{1}{4\pi} \Im m \left\{ \tau(\phi) \left[\partial_\mu \bar{\phi} \partial^\mu \phi - \frac{1}{4} (F^2 + i\bar{F}F) + \text{fermions} \right] \right\} \quad (3)$$

where

$$\tau(\phi) = \frac{\partial^2 \mathcal{F}}{\partial \phi^2} \quad (4)$$

is given in terms of a single holomorphic function $\mathcal{F}(\phi)$ of the scalar field ϕ which fulfills the important constraint

$$\Im m \left(\frac{\partial^2 \mathcal{F}}{\partial \phi^2} \right) > 0 . \quad (5)$$

As a consequence, the low-energy dynamics is completely determined by the function \mathcal{F} that in general will receive both perturbative and non-perturbative contributions.

Comparing eq. (3) with eq. (1) we see that at the tree level the function \mathcal{F} is given by

$$\mathcal{F}_{cl} = \frac{1}{2} \tau_d \phi^2 \quad \tau_d = \frac{\theta}{2\pi} + i \frac{4\pi}{e^2} \quad (6)$$

As a direct consequence of the fact that this theory is asymptotic free with a β -function $\beta(e) = -\frac{e^3}{4\pi^2}$ one gets for the sum of the tree and one-loop contributions the expression^{4,5}

$$\mathcal{F}_{cl} + \mathcal{F}_1 = \frac{i}{2\pi} \phi^2 \log \frac{\phi^2}{\Lambda^2} , \quad (7)$$

where Λ is a dynamically generated scale. Conversely, inserting this expression in Eq.(4) one obtains how the running coupling constant varies with the scale a showing that for large a the asymptotic freedom takes over and the theory becomes weakly coupled.

It can be shown that higher loops do not give any contribution to \mathcal{F} . Only non perturbative effects, as for instance instantons, can give an additional contribution to it.

We have seen that the moduli space of the $N = 2$ theory is parametrised, in the semiclassical theory, by the vacuum expectation value of the scalar field $a = \langle \phi \rangle$. We can endow this 2D manifold with a (Kähler) metric ds^2 expressed in terms of \mathcal{F} with the constraint (5) as follows

$$ds^2 = \Im m \tau(a) da d\bar{a} \quad , \quad \tau(a) = \frac{\partial^2 \mathcal{F}(a)}{\partial a^2} \quad (8)$$

However a cannot provide a global description of the moduli space. In fact any holomorphic function $f(a)$ of the complex plane a with an everywhere positive imaginary part should be a constant (because $\exp if(a)$ is bounded), while asymptotic freedom tells us that $\Im m(\tau(a))$ diverges for $|a| \rightarrow \infty$. Therefore in Ref.³ it was proposed to choose the gauge invariant quantity $u = \frac{1}{2} \langle \text{tr } \phi^2 \rangle$ as the one providing a global parametrization of the moduli space and to regard both $a(u)$

and the auxiliary variable $a_D(u) \equiv \frac{\partial \mathcal{F}}{\partial a}$ as functions of u . In terms of both a and a_D the metric in eq. (8) assumes the more symmetric form

$$ds^2 = \Im m \left(\frac{da_D}{da} da d\bar{a} \right) = \Im m (da_D d\bar{a}) = -\frac{i}{2} (da_D d\bar{a} - da d\bar{a}_D) \quad (9)$$

Introducing the vector $v = \begin{pmatrix} da_D \\ da \end{pmatrix}$ it is easily shown the invariance of ds^2 under the transformation $v \rightarrow Mv$, where M is an arbitrary matrix of $SL(2, R)$. This isometry group may be generated by the repeated action of two independent matrices T_b and S , defined by

$$T_b = \begin{pmatrix} 1 & b \\ 0 & 1 \end{pmatrix}, \quad S = \begin{pmatrix} 0 & 1 \\ -1 & 0 \end{pmatrix}. \quad (10)$$

The former leaves da invariant and transforms da_D according to

$$da_D \rightarrow da_D + b da. \quad (11)$$

This implies that $\tau(a)$ is just translated

$$\tau(a) \rightarrow \tau(a) + b \quad (12)$$

yielding, when inserted in the effective Lagrangian, a translation for the vacuum angle θ

$$\theta \rightarrow \theta + 2\pi b. \quad (13)$$

Since physical quantities are invariant when

$$\theta \rightarrow \theta + 2\pi n \quad (14)$$

for any integer n , we deduce that the transformation associated to the matrix $T_{b=1}$ is a symmetry of the theory. Thus only the $SL(2, Z)$ subgroup of the isometric group $SL(2, R)$ of the moduli space is compatible with the physical interpretation of the model.

It remains to understand the meaning of the inversion S in terms of the gauge fields. Note that S transforms $\tau(a)$ according to

$$\tau(a) \rightarrow -\frac{1}{\tau(a)} = -\frac{da}{da_D} \equiv \tau_D(a_D), \quad (15)$$

or, equivalently, it exchanges the field ϕ with the auxiliary field $\phi_D = \frac{\partial \mathcal{F}}{\partial \phi}$:

$$\begin{aligned} \phi &\rightarrow \phi_D, \\ \phi_D &\rightarrow -\phi. \end{aligned} \quad (16)$$

In order to see more clearly the meaning of such a transformation, it is convenient going into the weak-coupling region and set the vacuum angle $\theta = 0$. Then we see that, if $\Im m \tau(a) = \frac{4\pi}{g^2}$, then $\Im m \tau_D(a_D) = \frac{g^2}{4\pi}$, which is the typical effect of the electric-magnetic duality^{6,7}. Thus the auxiliary variable ϕ_D is nothing but that the dual Higgs field in a dual formulation of the theory.

Notice that the action of S does not correspond necessarily to a symmetry of the theory, but provides a transformation between two different descriptions of the same physics. In fact the bosonic part of the low energy effective Lagrangian can be represented either in terms of the variables $(A^\mu, \phi, \tau(\phi))$ or in terms of the dual ones $(A_D^\mu, \phi_D, \tau_D(\phi_D) = -1/\tau(\phi))$. One description may be more suitable for weak coupling, while the other for strong coupling.

2.1 The spectrum

We shall see now that in this $N = 2$ theory the holomorphic function $\mathcal{F}(\phi)$ fixes not only the low energy effective Lagrangian, but also its exact spectrum. Indeed, as in the Georgi-Glashow model, in the $N = 2$ super Yang-Mills theory there are also time-independent solutions⁸ of the classical equations of motion corresponding to magnetic monopoles and dyons. These states survive after quantization and their mass, in the semiclassical limit, is given by

$$M = \sqrt{2}|Z_{cl}| \quad (17)$$

with

$$Z_{cl} = a(n_e + \tau_{cl}n_m)$$

where n_e and n_m are the electric and magnetic charges and a is the vacuum expectation value of ϕ . It has been shown⁹ that Z_{cl} is the semiclassical limit of the central charge of the $N = 2$ superalgebra. This algebra yields, in the same limit, the positivity constraint $M \geq \sqrt{2}|Z_{cl}|$, with equality precisely for the so called “small” representations. States saturating the inequality are known as BPS-saturated states^{10,11}.

Noticing that the coefficient of n_m is equal to a_D in the classical limit, the mass spectrum of the possible BPS states can be rewritten as follows

$$M = \sqrt{2}|Z| \quad , \quad Z = an_e + a_D n_m \quad (18)$$

Seiberg and Witten³ proposed eq. (18) as an exact formula and made several checks for confirming its validity. It is easy to show (see for instance³) that, when a_D/a is not real, these states are stable provided that the integers n_e and n_m be relatively prime.

2.2 Singularity structure of moduli space

In this section we study the singularity structure of a and a_D as functions of the variable u , that provides a global parametrization of the moduli space.

In the semiclassical region, corresponding to a large value of u , we get

$$a = \sqrt{2u} \quad , \quad a_D = i\frac{\sqrt{2u}}{\pi} \left[2 \log \frac{\sqrt{u}}{\Lambda} + 1 \right] \quad (19)$$

Thus there is a branch point at $u = \infty$. Under a rotation around such a point given by $\log u \rightarrow \log u + 2i\pi$ a and a_D are not monodromic functions, but transform according to

$$M_\infty : \quad a \rightarrow -a \quad , \quad a_D \rightarrow -a_D + 2a \quad (20)$$

The existence of a branch point requires the existence of another, at least. No other kind of singularity is allowed, because the physical quantities a and a_D cannot diverge. But, if we had only one additional branch point, it should be at $u = 0$, because there is a global $Z(2)$ symmetry that transforms u in $-u$. The only holomorphic functions a and a_D with two branch points in 0 and ∞ and the asymptotic behaviour given in Eq. (19) coincide with (19) everywhere in the whole u -plane. As a consequence, the positivity condition (5) cannot be fulfilled near $u = 0$. Thus we must require the existence of at least two additional branch points.

Following the example of what is happening in some $N = 1$ supersymmetric theories Seiberg and Witten assume that the singularities occur at those points of the moduli space where additional massless particles appear in the spectrum. In the classical theory this occurs for $a = 0$ where the $SU(2)$ symmetry is restored and W^\pm become massless. This singularity at $u = 0$ does not survive quantization because of the positivity argument given before. On the other hand, restoration of the $SU(2)$ gauge symmetry should be accompanied by conformal invariance in the infrared region, then this restoration cannot happen at a finite $u \neq 0$, because it introduces an explicit breaking

of the scale invariance. There are instead indications that one at least of these singularities is associated at the point u_0 where the monopole with $(n_m, n_e) = (1, 0)$ becomes massless.

Using the exact formula in eq. (18) we see that this occurs when $a_D(u_0) = 0$ with $a(u_0) \neq 0$. With an obvious rescaling it is always possible to choose $u_0 = 1$.

The monodromy M_1 around the singularity at $u = 1$ can be easily computed by observing that the low energy theory at the point $u = 1$ consists of a "magnetic" $N = 2$ super QED (the matter has magnetic and non electric charge). This theory is not asymptotically free and the coefficient of the β -function, besides a sign, has a factor $1/2$ of difference with respect to the β -function previously used for studying the singularity around $u = \infty$. By taking into account this difference in the β -function one arrives at the following monodromy transformation around the point $u = 1$:

$$M_1 : \quad a_D \rightarrow a_D \quad a \rightarrow a - 2a_D \quad . \quad (21)$$

The $Z(2)$ symmetry implies that there is another singularity at $u = -1$. The monodromy M_{-1} around the point $u = -1$ must be consistent with the previous ones, i.e. $M_1 M_{-1} = M_\infty$. One obtains

$$M_{-1} : \quad a_D \rightarrow -a_D + 2a \quad a \rightarrow -2a_D + 3a \quad . \quad (22)$$

In order to see what massless state is associated to this singularity, note that these monodromies act also on the spectrum of BPS-saturated states because a transformation on the pair (a_D, a) induces a corresponding transformation on the charges n_m, n_e . A massless state associated to the singularity around which we are looping should remain invariant. Using this criterion one finds that the massless state associated with $u = -1$ is the dyon with $(n_m, n_e) = (1, -1)$.

2.3 Exact solution

Having established the singularities and the monodromy transformations of a and a_D their form is uniquely determined: any pair of functions with the same monodromies in the same points and with the positivity constraint (5) can differ only by a multiplicative constant. Such a constant is fixed by their asymptotic behaviour. Seiberg and Witten have built up an explicit solution by mapping the space of the quantum vacua into the moduli space of Riemann surfaces of genus one, where an explicit solution of such a monodromy problem is known.

Here I would like to outline an elementary approach to this problem, based on some general properties of the \wp -function of Weierstrass. This is a meromorphic, doubly periodic function. Let us denote by $\{\omega\}$ the period lattice, namely the set of points of the complex plane of the form $\{\omega = m\omega_1 + n\omega_2\}$, with m and n integral coefficients and ω_1, ω_2 two complex numbers (periods) with non real ratio ω_1/ω_2 . Then the double periodicity means

$$\wp(z + \omega) = \wp(z) \quad . \quad (23)$$

It satisfy the first order differential equation

$$\wp'^2 = 4(\wp(z) - e_1)(\wp(z) - e_2)(\wp(z) - e_3) \quad , \quad (24)$$

where e_i are all distinct and given by

$$e_1 = \wp(\omega_1/2) \quad e_2 = \wp(\omega_2/2) \quad e_3 = \wp((\omega_1 + \omega_2)/2) \quad . \quad (25)$$

In terms of the new variables

$$x = \frac{2\wp(z)}{e_1 - e_2} - \frac{e_1 + e_2}{e_1 - e_2} \quad , \quad y = \sqrt{2} \frac{\wp'(z)}{(e_1 - e_2)^{3/2}} \quad (26)$$

Eq.(24) can be rewritten as the elliptic curve

$$y^2 = (x - 1)(x + 1)(x - u) \quad \quad u = \frac{e_1 + e_2 - 2e_3}{e_1 - e_2} \quad . \quad (27)$$

This algebraic equation describes a generic torus as a double cover of the x plane branched over $\infty, 1, -1$ and u . It becomes singular when two branch points coincide, and this occurs precisely for $x = \infty, 1, -1$.

Using the uniformizing parametrization (26) one can verify at once that

$$\frac{2}{\sqrt{e_1 - e_2}} \frac{dx}{y} = \frac{dp}{2\sqrt{(\rho(z) - e_1)(\rho(z) - e_2)(\rho(z) - e_3)}} = dz, \quad (28)$$

telling us that dx/y is a holomorphic differential and that its integral along a topologically non trivial closed path is proportional to a point of the period lattice $\{\omega\}$. In particular, denoting with γ_1 a path looping around the pair $1, -1$ and with γ_2 the one looping around $1, u$, the two periods defined by

$$\omega_i = \sqrt{2(e_1 - e_2)} \oint_{\gamma_i} \frac{dx}{y}, \quad i = 1, 2 \quad (29)$$

have precisely the same monodromies of da/du and da_D/du . Moreover $\Im m(\omega_2/\omega_1) > 0$, thus

$$\frac{da_D}{du} \propto \omega_2, \quad \frac{da}{du} \propto \omega_1 \quad \Rightarrow \quad \tau(u) = \frac{\omega_2}{\omega_1}. \quad (30)$$

Integrating on u and adjusting the proportionality constant one gets the exact result

$$a(u) = \frac{\sqrt{2}}{\pi} \int_{-1}^1 dx \frac{\sqrt{x-u}}{\sqrt{x^2-1}}, \quad a_D(u) = \frac{\sqrt{2}}{\pi} \int_1^u dx \frac{\sqrt{x-u}}{\sqrt{x^2-1}}. \quad (31)$$

Generalizations of these formulas are now available for many other gauge groups¹² also with matter in the fundamental representation¹³.

3 Monopole Condensation and Confinement

One of the interesting properties of the $N = 2$ super Yang-Mills model described before is that a small perturbation produces a dramatic modification of the space of the possible vacua, leading to monopole condensation and confinement.

Suppose to break explicitly the $N = 2$ supersymmetry to $N = 1$ by adding a mass term $m\phi^2$ to the Lagrangian. Then the quantum moduli space collapses to the two points $\frac{1}{2} \langle \text{tr } \phi^2 \rangle = \pm u_0$. If u_0 is non vanishing the $Z(2)$ symmetry is spontaneously broken and there is a simple argument³ indicating that u_0 does correspond precisely to the value u_0 where the monopole or the dyon become massless and that these monopoles condense. The argument goes as follows. Let U be the chiral superfield whose first component is $\frac{1}{2}\phi^2$. In order to break the $N = 2$ supersymmetry to $N = 1$ we have to add to low energy Lagrangian an effective superpotential $W = mU$. Near the point at which there are massless monopoles, they can be represented by chiral superfields Q and \tilde{Q} . Since the monopoles couple in a non-local way to the original "electric" photon, we cannot use that photon in the effective Lagrangian. Instead we should perform a dual transformation and write an effective superpotential in terms of dual vector supermultiplet A_D , i.e. the supermultiplet formed by the dual potential A_D^μ the gaugino and the dual Higgs field ϕ_D . The total effective superpotential is

$$W = A_D Q \tilde{Q} + mU(A_D), \quad (32)$$

where the first term is required by gauge and $N = 2$ invariances of the $m = 0$ theory. The possible vacua correspond to solution of $dW = 0$, which yields for the bosonic component the following conditions:

$$Q \tilde{Q} + m \frac{du}{da_D} = 0;$$

$$a_D Q = a_D \tilde{Q} = 0 \quad (33)$$

One of the fundamental properties of the parameter u as defined in Eq. (27) is that du is always different from zero, because u is a good global coordinate on the space of moduli of the torus and hence on the space of quantum vacua. Then the first equation tells us that Q and \tilde{Q} are different from zero, *i.e.* there is a condensate of monopoles, while the second equation requires $a_D = 0$, which expresses the vanishing of the mass of the monopole at $u = v_0$. This condensation gives a mass to the photon. However, since the photon around the point u_0 is described by the dual A_D^μ of the usual electric potential, we have actually the confinement of the electric charge.

References

1. G. 'tHooft, EPS International Conference, Palermo 1975; S.Mandelstam, *Phys. Rep. C* **23** (1976) 245; G.Parisi, *Phys. Rev. D* **11** (1975) 970.
2. A.Polyakov, *Phys. Lett.* **B59** (1975) 82; and *Nucl. Phys.* **B120** (1977) 429.
3. N. Seiberg and E. Witten, *Nucl. Phys.* **B298** 36 (1994).
4. P. Di Vecchia, R. Musto, F. Nicodemi and R. Pettorino, *Nucl. Phys. B* **252** 635 (1985).
5. N. Seiberg, *Phys. Lett.* **206B** 75 (1988).
6. P.A.M. Dirac, *Proc. Roy. Soc.* **A33** 60 (1931).
7. P. Goddard and D. Olive, *Rep. on Prog. in Phys.* **41** 1357 (1978).
8. A. D'Adda, R. Horsley and P. Di Vecchia, *Phys. Lett.* **76B** 298 (1978).
9. E. Witten and D. Olive, *Phys. Lett.* **78B** 97 (1978).
10. E.B. Bogomolny, *Sov. J. Nucl. Phys.* **24** 449 (1976).
11. M.K. Prasad and C.M. Sommerfield, *Phys. Rev. Lett.* **35** 760 (1975).
12. A.Klemm, W. Lerche, S. Yankielowicz and S. Theisen, *Phys. Lett.* **B344** (1995) 169; P.C. Argyres and A. Faraggi, *Phys. Rev. Lett.* **73** (1995) 3931; P.C. Argyres, R. Plesser and A. Shapere, *Phys. Rev. Lett.* **75** (1995) 1699; U.H. Danielsson and B. Sundborg, *Phys. Lett.* **B358** (1995) 273.
13. A. Hanany and Y. Oz, *Nucl. Phys.* **B452** (1995) 73; P.C. Argyres and A. Shapere, hep-th/9609175; I.M. Krichever and D.H. Phong, hep-th/9604199.

Some Aspects of Physics Beyond the Standard Model

F. de Campos *

Instituto de Física Teórica

UNESP - São Paulo - SP

Abstract

We discuss some phenomenological aspects of extensions of the Standard Model related to the electroweak symmetry breaking sector with supersymmetry. The physics potential for Higgs boson searches at LEP200, including Majoron extensions of the Standard Model, the physics of invisibly decaying Higgs bosons, as well as some possible signatures associated to models with R parity violation are included.

1 Introduction

Although very successful wherever it has been tested, the Standard Model leaves unanswered many fundamental issues in particle physics to be an ultimate theory of nature.

A basic assumption of the Standard Model is the Higgs mechanism, which is introduced in order to generate the masses of all the fundamental particles. This mechanism implies the existence of a fundamental scalar bosons [1]. If such an elementary boson exists some stabilising principle - like supersymmetry (SUSY) - should be operative at the electroweak scale in order to explain the stability of its mass scale against quantum corrections associated with physics at very high energies. The unification of the three gauge coupling constants as they are evolved from the presently accessible energies up to a common scale of $\sim 10^{16}$ GeV provides a hint that supersymmetry seems to set in somewhere around $M_{SUSY} \sim 10^3$ GeV. Probing the details of this structure constitutes one of the main goals in the next generation of elementary particle colliders.

Another fundamental issue in the Standard Model refers to the properties of neutrinos, in the sense that there is no principle that dictates that neutrinos are massless, as postulated in the Standard Model. In fact, nonzero masses may be required in order to account for the data on solar and on atmospheric neutrinos, as well as for an explanation of the dark matter in the universe.

The above two different extensions of the Standard Model may be connected *via*, for example, supersymmetric models with spontaneously broken R parity, which necessarily imply non-vanishing neutrino masses. As a result in some of these models there are novel processes that could be observed at high energy colliders. One interesting aspect of these models is that they may affect the physics of the electroweak sector in such a remarkable way, that can be probed in various present and future experiments.

*E-mail: fernando@ifit.unesp.br

	$SU_c(3) \otimes SU_L(2) \otimes U_Y(1)$
W	$(1, 3, 0)$
B	$(1, 1, 0)$
ϕ	$(1, 2, 1)$
ℓ_a	$(1, 2, -1)$
e_a^c	$(1, 1, 2)$
Q_a	$(3, 2, 1/3)$
u_a^c	$(\bar{3}, 1, -4/3)$
d_a^c	$(\bar{3}, 1, 2/3)$

Table 1:

1.1 Standard Model Basics

The Standard Model is a Yang-Mills theory based on the $SU(3) \otimes SU(2) \otimes U(1)$ gauge group, and described by the field representations in table 1, where all fermions are left-handed. The fundamental constituents of matter - quarks and leptons - interact mainly due to the exchange of the gauge bosons. In order to comply with the fact that the weak interaction is mediated by massive vector bosons, the W and the Z , the gauge symmetry has to be broken. The way to accomplish this is through the nonzero vacuum expectation value (VEV)

$$\langle \phi^0 \rangle = v/\sqrt{2} \quad (1)$$

of the neutral component of a complex Higgs scalar doublet ϕ

$$\phi = \begin{pmatrix} \phi^+ \\ \phi^0 \end{pmatrix}. \quad (2)$$

The surviving electrically neutral Higgs scalar, the so-called Standard Model Higgs boson, has a mass given by

$$m_h \propto \sqrt{\lambda} \langle \phi \rangle \quad (3)$$

where λ is the quartic coupling in the Higgs potential. A great effort has been devoted in designing a search for the Standard Model Higgs boson. This is one of the main open questions of the Standard Model [2]. As a result, the massless vector boson A_μ is the photon, while Z_μ has a mass

$$m_Z = \frac{gv}{2 \cos \theta_W} \quad (4)$$

while the charged gauge bosons $W^\pm = \frac{1}{\sqrt{2}}(W_1 \mp iW_2)$ have a mass

$$m_W = \frac{gv}{2}. \quad (5)$$

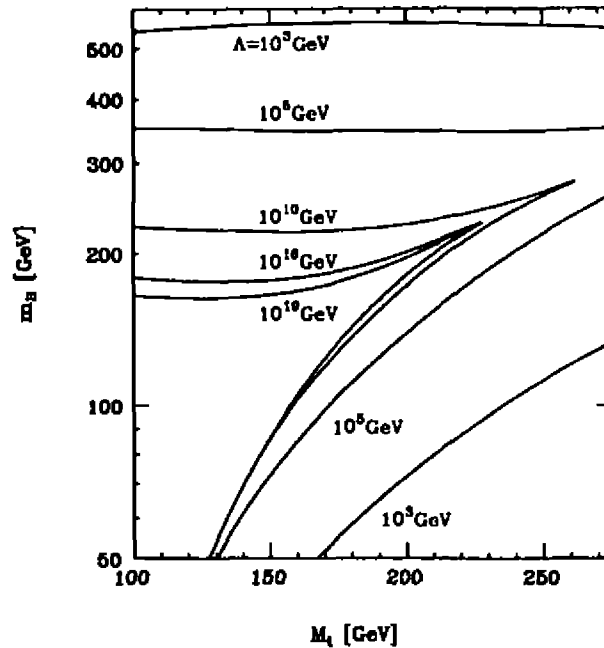


Figure 1: Theoretical Bounds on the Standard Model Higgs Boson.

The W and the Z gauge bosons have been discovered at CERN. The properties of the Z have now been precisely determined by the LEP experiments [3], while those of the W mostly come from CERN and Fermilab [4]. The measured gauge boson mass values agree well with the electroweak theory predictions, once radiative corrections are included. The success of the LEP experiments in the precise determination of the electroweak parameters has been so remarkable that just the internal consistency of the various measurements is sufficient to provide a very good determination of the mass of the top quark $m_t = 180 \pm 14$ GeV, with the error largely due to the lack of knowledge of the Higgs boson mass [3]. This is in excellent agreement with the direct measurement at Fermilab [4]. In the same way, the agreement among the theoretical and experimental R_b and R_c values are improved [5].

The total Z decay width, as well as its partial widths have been precisely measured by the LEP collaborations, leaving little room for new physics. Of special interest to us is the measurement of the invisible Z width [6]

$$\Gamma_{inv}^Z = 499.9 \pm 2.5 \text{ MeV} \quad (6)$$

which can be translated into a measurement of the effective number of Standard Model neutrino generations. This places a very stringent constraint on models of neutrino mass where lepton number is a global symmetry spontaneously broken at low energies.

1.2 Standard Model Higgs

Unfortunately both the mass and self-coupling strengths of the Higgs boson are undetermined by the theory. However, an upper bound on the Higgs boson mass depending on the top quark mass through the renormalization group equation, is illustrated in Fig. (1).

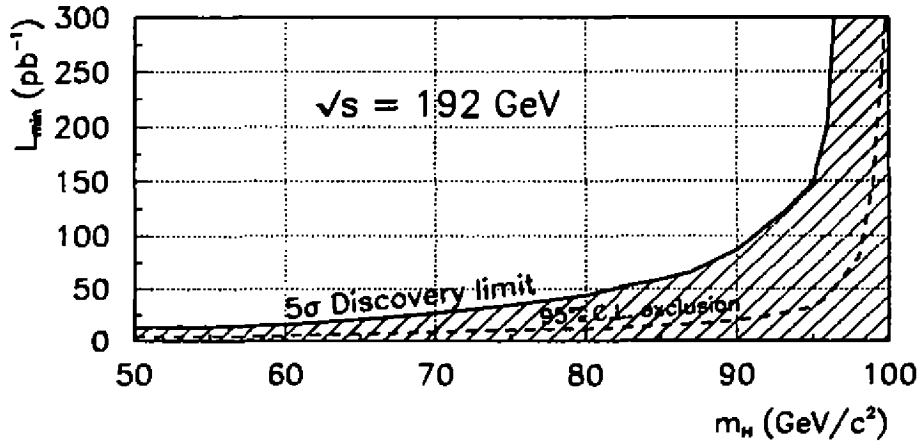


Figure 2: Standard Model Higgs boson search potential at LEP200.

The limit varies from $m_H \lesssim 600 \text{ GeV}$ down to $m_H \lesssim 200 \text{ GeV}$ if one also assumes that there is no new physics below M_{Planck} [7].

From the analysis of the data collected at LEP one can place the following lower limit on the Standard Model Higgs boson mass [8]

$$m_H \gtrsim 65 \text{ GeV} \quad (7)$$

As illustrated in Fig. (2), if lighter than $\sim 100 \text{ GeV}$, the Standard Model Higgs boson should be found at LEP 200 [9]. The minimum required luminosity per experiment, in pb^{-1} , for a 5σ Higgs boson discovery is displayed in the solid line of Fig. (2), while the corresponding 95% C.L. exclusion limit is shown as dashed. Heavier Higgs boson can be probed at higher centre-of-mass energies, such as at NLC, or at the LHC. Unfortunately the prospects for finding the Higgs boson in the intermediate mass range between m_Z and $2m_Z$ at the LHC are not too optimistic [11]. Above this mass the detection would be very easy, through the 4-lepton signal [11]. In addition to testing the Standard Model, one has the possibility of constraining the value of the Higgs mass, which enters through the radiative corrections to the Z and W boson self-energies. Combining the most recent LEP and SLC electroweak results [12] with the recent top-quark mass measurement at the Tevatron [4], a weak preference is found for a light Higgs boson mass of order m_Z [12]. Fig. (3) illustrate a typical χ^2 Standard Model fit constraining the Standard Model Higgs mass. The solid line includes all LEP, SLD, $p\bar{p}$ and deep inelastic neutrino data. The dashed one excludes the measurements of the Z width into $b\bar{b}$ and $c\bar{c}$. The dotted line corresponds to the LEP data including R_b and R_c . In all cases one includes the direct top mass determination from the Tevatron.

2 Supersymmetry

The physics associated to the electroweak breaking sector plays a central role in particle physics. One of the most important physics motivations in favour of supersymmetry is the fact that it is the only symmetry one knows which can stabilize the elementary Higgs boson mass with respect to divergent radiative corrections. These would be expected in any fundamental unified theory including gravity, or simply encompassing the electroweak and strong interactions. Either way one has a very large mass

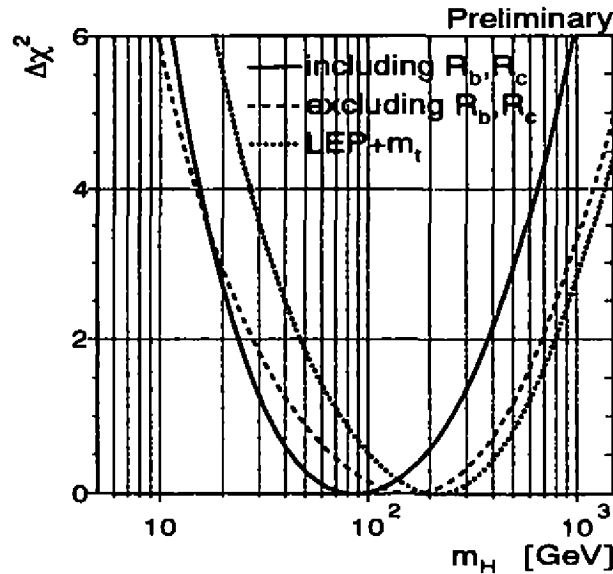


Figure 3: Standard Model Higgs mass determination from precision data.

scale - the Planck scale or the grand unification scale - which can mix through loops and destabilize the electroweak scale in eq. (1). This is the so-called *hierarchy problem*, which can be solved through supersymmetry [13], to the extent that it holds at TeV energies and helps to cancel the loops.

Supersymmetry is also theoretically attractive as it is the most general symmetry consistent with the basic principles of field theory [14]. Unlike most symmetries discussed in particle physics, that relate particles of the same spin, SUSY relates bosons to fermions, and vice-versa (see table).

Finally, the experimental determination of gauge couplings at low energies plays in favour of the existence of SUSY particles[†] at the TeV scale. This hint is provided by the joining of these gauge couplings at high energies of order of the unification scale 10^{16} GeV [15] as illustrated in Fig. (4) [16]. For these reasons the study of supersymmetric extensions of the Standard Model has attracted a lot of effort, including the theoretical understanding of supersymmetric models as well as the simulation of the expected signals at present and future particle colliders.

2.1 The MSSM

The simplest supersymmetric model is the so-called Minimal Supersymmetric Standard Model (MSSM) [17], defined by the particle content given in table. and supplemented by the hypothesis that the basic interactions conserve a discrete R parity (R_p) symmetry, under which all Standard Model particles are even while their partners are odd. As a result the interactions of the MSSM are such that all SUSY particles must be only produced in pairs, with the lightest of them (LSP) being absolutely stable.

The presence of two doublets of Higgs superfields is required by supersymmetry, anomaly cancellation,

[†]For definiteness, one assumes here those present in the so-called MSSM.

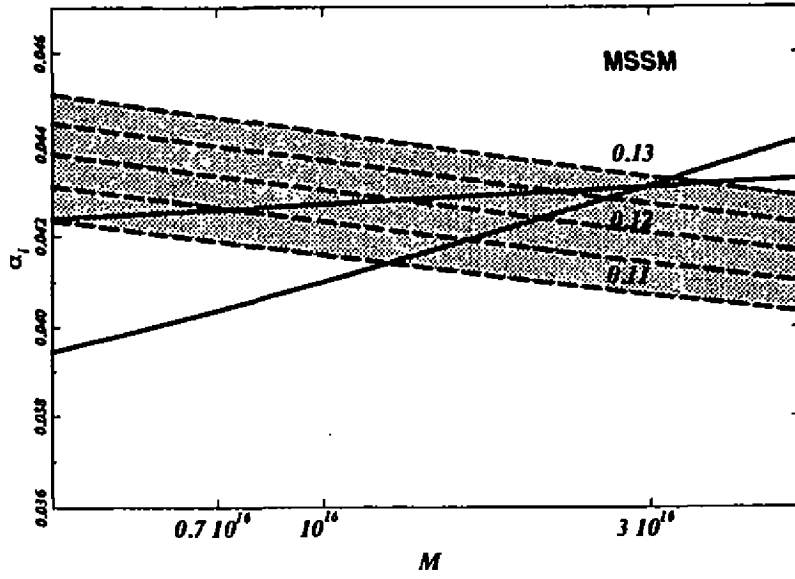


Figure 4: Gauge coupling unification in the MSSM.

Vector	Supermultiplet	Chiral	Supermultiplet
$J = 1$	$J = 1/2$	$J = 1/2$	$J = 0$
g	\tilde{g}	Q_L, U_L^c, D_L^c	$\tilde{Q}_L, \tilde{U}_L^c, \tilde{D}_L^c$
W^\pm, W^0	$\tilde{W}^\pm, \tilde{W}^0$	L_L, E_L^c	$\tilde{L}_L, \tilde{E}_L^c$
B	\tilde{B}	\tilde{H}_d, \tilde{H}_u	H_d, H_u

Table 2:

and in order to give different masses to both up and down-type charged fermions.

With this assumption the MSSM is characterised by the following superpotential,

$$W_0 = \epsilon_{ab} \left[h_{ij} \hat{L}_i^a \hat{H}_1^b \hat{E}_j^c + h'_{ij} \hat{Q}_i^a \hat{H}_1^b \hat{D}_j^c + h''_{ij} \hat{Q}_i^a \hat{H}_2^b \hat{U}_j^c + \mu \hat{H}_1^a \hat{H}_2^b \right] \quad (8)$$

For our subsequent discussion we need the chargino and neutralino mass matrices. The form of the chargino mass matrix is given by

$$\begin{array}{c|cc} & \tilde{H}_u^+ & -i\tilde{W}^+ \\ \hline \tilde{H}_d^- & \mu & \sqrt{2}g_2v_d \\ -i\tilde{W}^- & \sqrt{2}g_2v_u & M_2 \end{array} \quad (9)$$

Two matrices U and V are needed to diagonalize the 2×2 (non-symmetric) chargino mass matrix

$$\chi_i^+ = V_{ij}\psi_j^+ \quad (10)$$

$$\chi_i^- = U_{ij}\psi_j^- \quad (11)$$

where $\psi_j^+ = (\tilde{H}_u^+, -i\tilde{W}^+)$ and $\psi_j^- = (\tilde{H}_d^-, -i\tilde{W}^-)$.

On the other hand the neutralino mass matrix is 4×4 and has the following form

$$\begin{array}{c|cccc} & \tilde{H}_u & \tilde{H}_d & -i\tilde{W}_3 & -i\tilde{B} \\ \hline \tilde{H}_u & 0 & -\mu & -g_2v_u & g_1v_u \\ \tilde{H}_d & -\mu & 0 & g_2v_d & -g_1v_d \\ -i\tilde{W}_3 & -g_2v_u & g_2v_d & M_2 & 0 \\ -i\tilde{B} & g_1v_u & -g_1v_d & 0 & M_1 \end{array} \quad (12)$$

This matrix is diagonalized by a 4×4 unitary matrix N,

$$\chi_i^0 = N_{ij}\psi_j^0 \quad (13)$$

where $\psi_j^0 = (\tilde{H}_u, \tilde{H}_d, -i\tilde{W}_3, -i\tilde{B})$, (the indices i and j run from 1 to 4).

In the above two equations $M_{1,2}$ denote the supersymmetry breaking gaugino mass parameters and $g_{1,2}$ are the $SU(2) \otimes U(1)$ gauge couplings divided by $\sqrt{2}$. We assume the canonical relation $M_1/M_2 = \frac{5}{3}\tan^2\theta_W$. Typical values for the SUSY parameters μ , M_2 and $\tan\beta$ lie in the range given by

$$-1000\text{GeV} \leq \mu \leq 1000\text{GeV} ; 20\text{GeV} \leq M \leq 1000\text{GeV} ; 1 \lesssim \tan\beta \lesssim 40 \quad (14)$$

Adding the soft supersymmetry breaking scalar mass terms to the supersymmetric gauge interactions(D terms) and the supersymmetric Yukawa interactions following from eq. (8) one can write the scalar potential characterising the MSSM. Its general form may be written schematically as

$$V_{MSSM} = \sum_i \left| \frac{\partial W}{\partial z_i} \right|^2 + \tilde{m}_0 [AW_3 + BW_2 + h.c.] + \sum_i \tilde{m}_i^2 |z_i|^2 + \alpha (|H_u|^2 - |H_d|^2)^2 \quad (15)$$

where W_3 and W_2 denote the cubic and quadratic parts of the superpotential, $\alpha \equiv \frac{g^2 + g'^2}{8}$ and z_i denotes any neutral scalar field in the theory. The parameter A is the cubic soft breaking parameter and B=A-1 is the corresponding quadratic one [17].

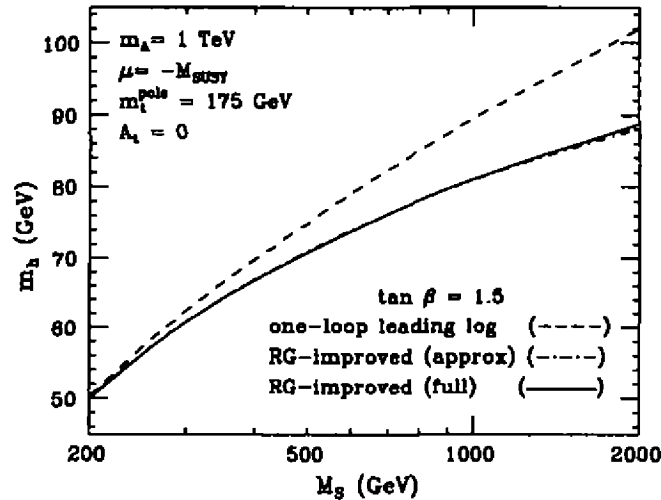


Figure 5: Radiatively corrected MSSM lightest Higgs mass versus SUSY scale.

2.2 The MSSM Higgs Sector

Due to the presence of two Higgs boson doublets in the MSSM there are two physical CP-even neutral Higgs scalars (h , H), a CP-odd neutral scalar particle, A , and a physical electrically charged scalar boson H^\pm . At the tree level the mass of the lightest CP-even neutral Higgs boson h can be calculated in terms of two parameters, which may be chosen as m_A and the ratio of Higgs VEVs $\tan\beta$ [18].

There is an upper bound on the lightest CP even Higgs boson mass due to the special structure of the MSSM Higgs potential. At the tree level, this bound is exactly the Z mass. However, it is sensitive to radiative corrections, which depend on the soft supersymmetry breaking parameters [19].

The full one-loop radiatively corrected h mass is given in [20] and [21]. A simple procedure for accurately approximating m_h was described by Haber [22]. We assume that the ratio of Higgs VEVs lies in the range $1 \lesssim \tan\beta \lesssim \frac{m_t}{m_b}$ and that the scale characterizing supersymmetry breaking M_S is less than 2 TeV. This scale can be roughly regarded as a common supersymmetric scalar mass. A large M_S value takes into account the possibility of large radiative corrections to the lightest CP even Higgs boson mass. We used a top quark mass in the range $m_t = 175 \pm 35$ GeV which covers the region indicated by the recent experimental data from the Tevatron. In Fig. (5) we illustrate the dependence of the radiatively corrected lightest CP-even Higgs mass with respect to M_S for $\tan\beta = 1.5$. The one-loop leading logarithmic computation is compared with the RG-improved result which was obtained by numerical analysis and by using the simple analytic result [22].

The dependence of the upper bound on the lightest CP-even Higgs boson mass in the MSSM with respect to the top quark mass is given by the solid line in Fig. (6). The dashed line shows the corresponding result for the special case of b - τ unification under several assumptions, explained in [21]. The complete spectrum of MSSM scalar boson masses, including the h , H , A and H^\pm masses is shown in Fig. (7) from ref. [21]. The dashed, solid and dot-dashed lines refer to h , H and H^\pm masses respectively. The region of interest is above 40 GeV, which is roughly the lower limit on the A mass accessible at LEP1. On the other hand, one sees that for m_A above 200 GeV or so there is a very slow variation in m_h .

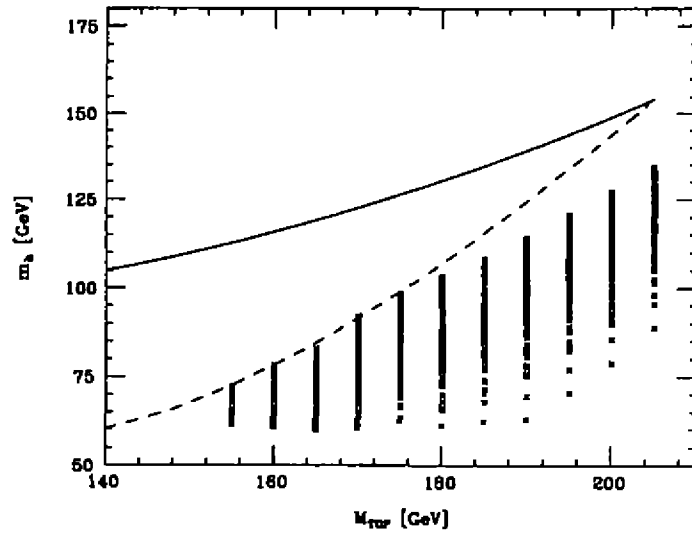


Figure 6: Radiatively corrected MSSM lightest Higgs mass versus m_t .

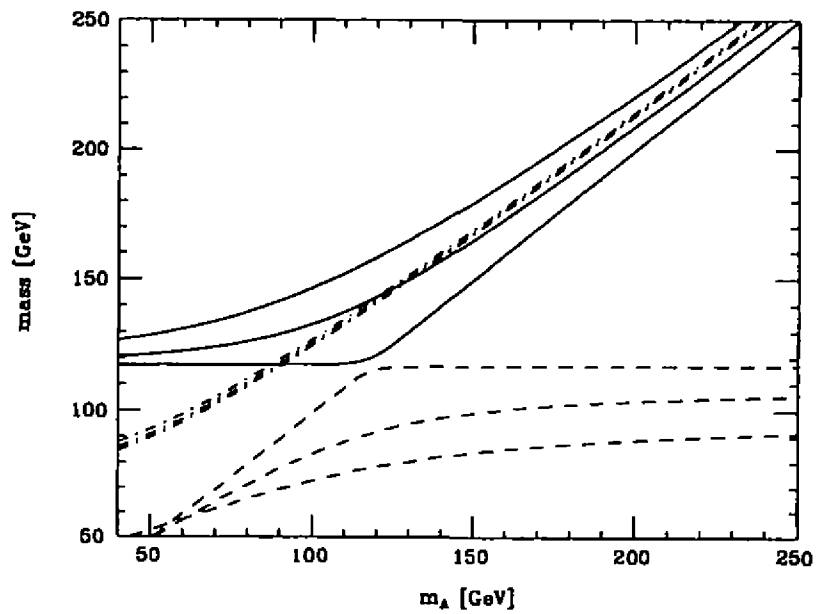


Figure 7: Radiatively corrected MSSM Higgs boson masses.

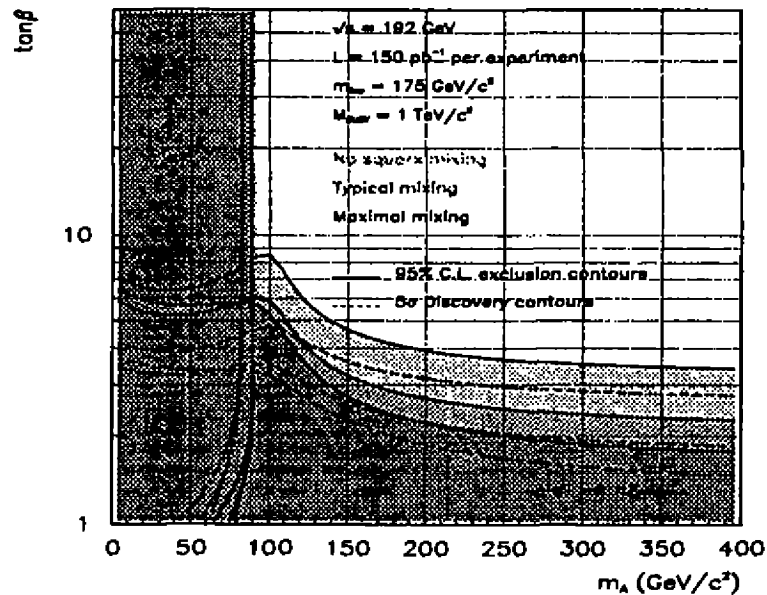


Figure 8: MSSM Higgs boson discovery contours at LEP200.

The MSSM Higgs boson discovery contours at LEP200 are illustrated in Fig. (8) [10]. This plot corresponds to centre-of-mass energies 192 GeV, substantially better for Higgs bosons searches at LEP than 175 GeV, and for three stop quark mixing assumptions $A_t = 0$ and $|\mu| \ll M_S$ (no mixing), $A_t = M_S$ and $\mu = -M_S$ (typical mixing), and $A_t = \sqrt{6}M_S$ and $|\mu| \ll M_S$ (maximal mixing), with $M_S = 1$ TeV.

2.3 Limits on SUSY Particles

So far all searches for supersymmetric particles have been negative. The best existing search site for the weakly interacting SUSY particles is the LEP accelerator. The most recent results follow from searches performed at 130 and 136 GeV centre-of-mass energies and supersede some of the previous LEP1 results.

From the non-observation of acoplanar lepton pairs, hadronic events with isolated leptons, hadronic events with missing energy, and acoplanar jet topologies, the Aleph collaboration has recently placed the following limits [8]:

- 1 $m_{\chi_{\pm}} \gtrsim 65$ GeV If the chargino is mostly gaugino this assumes that the sneutrino mass exceeds 200 GeV and, when it is mostly Higgsino, it assumes that the chargino-neutralino mass difference exceeds 10 GeV.
- 2 The searches for neutralinos at Aleph lead to the excluded region in Fig. (9), for the case $\mu = 1$ TeV and $\tan\beta = 2$. Note that it depends on the assumption of universal soft-breaking gaugino masses and on the value of the selectron mass. The limits also substantially depend on the assumed decay modes of the heavier neutralino.
- 3 Searches for dilepton + missing momentum events have been performed by the LEP collaborations.

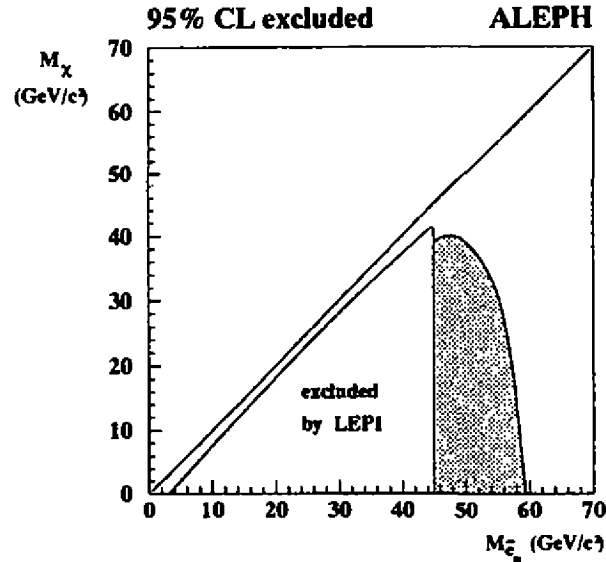


Figure 9: Limits on neutralino and selectron masses in the MSSM.

The Aleph data give the following limit [8]

$$m_{\tilde{\tau}_{\pm}} \gtrsim 60 \text{ GeV} \quad (16)$$

For the smuons and staus there is no improvement over the 45 GeV LEP1 limit. For sneutrinos, the limit is worse than for charged sleptons.

The limits on squark and gluino masses come mostly from hadron collisions [23]. These limits are correlated. For a very heavy gluino, one has $m_{\tilde{q}} \gtrsim 100$ GeV for the lower limit on the squarks, with a weaker limit on the top squark. On the other hand, in the limit of very heavy squarks one gets $m_{\tilde{g}} \gtrsim 140$ GeV as the corresponding limit on the gluino mass. The limits given depend on simplifying assumptions, and some of them may become stronger if one adopts specific parameter choices in the MSSM. On the other hand, they may get weaker in extended models.

The limits for SUSY fermion searches may be combined in order to determine the shape of the corresponding allowed region of region of SUSY parameters μ and M_2 , for given choices of the ratio of Higgs doublet VEVs $\tan\beta$, as shown in Fig. (10).

The region excluded by the chargino search is the shaded region, while the dashed line indicates the previous LEP1 region. The slepton masses are assumed to be 500 GeV. The dark area corresponds to the case that the chargino is lighter than all neutralinos. The searches for neutralinos at Aleph lead to the hatched excluded region displayed in Fig. (9), for the case $\mu = 1$ TeV and $\tan\beta = 2$.

In short, there is still a very large domain of parameters where SUSY would be a meaningful symmetry. From this point of view it is of great interest to look for its possible effects at higher energies, such as will be accessible at the LHC and other future elementary particle accelerators such as the NLC.

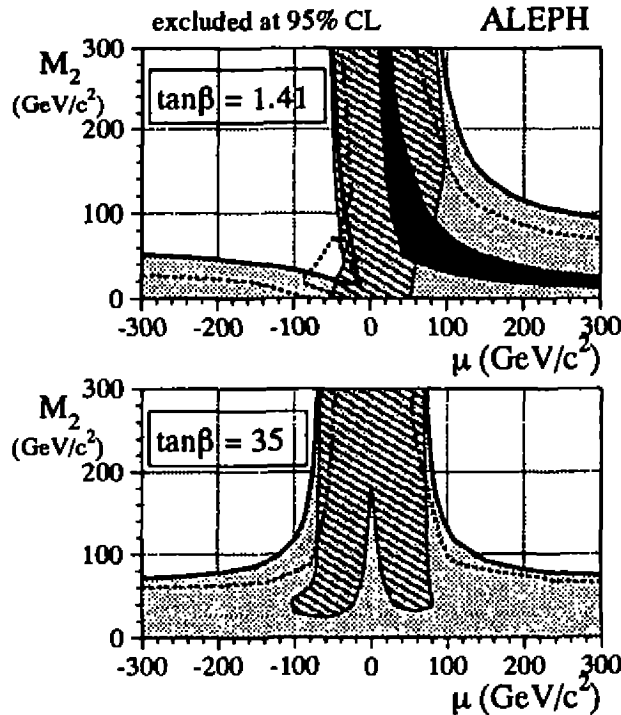


Figure 10: Presently allowed region of MSSM parameters.

An important assumption underlying all SUSY searches conducted so far, is that of R parity conservation. This assumption dictates that all SUSY particles must be produced in pairs, the lightest of these (LSP), typically a neutralino, being absolutely stable. Thus the signal associated to the LSP is missing momentum. These properties have been taken as the basis of all searches of SUSY particles.

Unfortunately there is no clue as to how SUSY is realized. Whether or not R parity is conserved is an important dynamical issue. However, for all we know so far, R parity conservation may very well break down at some level.

Present SUSY particle search strategies are not adequate for the analysis of extended models where SUSY is realized with broken R parity. For example, if R parity is broken, it would be possible to probe SUSY even at the LEP1 energies through new signatures, such as single SUSY particle production [24]. Therefore one needs to re-analyse the existing data in order to place limits on these models.

2.4 Explicit and Spontaneous R Parity Violation

The minimal supersymmetric extension of the $SU(2) \otimes U(1)$ theory *in general violates lepton and baryon number conservation*. Indeed, $SU(2) \otimes U(1)$ gauge invariance and SUSY are consistent with adding to the basic superpotential, eq. (8), many Yukawa terms that violate lepton number conservation, such as

$$W_R = \epsilon_{ab} \left[\lambda_{ijk} \hat{L}_i^a \hat{L}_j^b \hat{E}_k^C + \lambda'_{ijk} \hat{L}_i^a \hat{Q}_j^b \hat{D}_k^C + \epsilon_i \hat{L}_i^a \hat{H}_u^b \right] \quad (17)$$

Here i,j,k denote flavour indices and λ is anti-symmetric in ij . Similarly, one could add terms such as $\hat{U}^c \hat{D}^c \hat{D}^c$, as they are consistent with all symmetries of the Standard Model, plus supersymmetry. The presence of such terms, along with those in eq. (17), will lead to baryon number violating processes such as proton decay. In their presence R parity symmetry is broken explicitly, as can easily be checked. There are several constraints on these couplings, some of which are quite stringent [25]. Recent results by the Aleph collaboration has placed limits on explicitly broken R-parity models [26]. One normally forbids these terms by hand, invoking R parity conservation. It is possible, however, that R parity is explicitly broken only by a subset of these terms, at a sizeable level, yet fully consistent with observation. The missing terms could arise by imposing some global and/or discrete symmetry. Moreover, explicit R_p violating interactions could be tolerated in the presence of a mechanism that could generate a nonzero baryon asymmetry at low energy, as suggested in [27].

In Spontaneous R Parity Violation scenarios the breaking of R-parity is driven by right-handed *isosinglet* sneutrino vacuum expectation values (VEVS) [28, 29], so that the associated Goldstone boson (Majoron) is mostly singlet. As a result the Z does not decay by Majoron emission, in agreement with LEP observations [3].

Here we focus on what is the conceptually simplest model for Spontaneous R Parity Violation, in which two $SU(2) \otimes U(1)$ singlet leptons, instead of one, are added in each family [28] The simplicity of the model follows from the fact that the magnitude of all R Parity violating effects is strictly correlated to the mass of the tau neutrino. We will focus on the simplest model and start by recalling its main ingredients. Indeed, many of the phenomenological features relevant for the accelerator studies already emerge in an effective model where the spontaneous violation of R parity is reproduced through a the addition of the explicit bilinear superpotential term in eq. (17) [30].

The superpotential is given by

$$h_u Q H_u U^c + h_d H_d Q D^c + h_e \ell H_d E^c + (h_0 H_u H_d - \epsilon^2) \Phi + h_\nu \ell H_u \nu^c + h \Phi S \nu^c + h.c. \quad (18)$$

where we have omitted the hats in the superfields, as well as generation space indices in the coupling matrices h_u, h_d, h_e, h_ν, h . This superpotential conserves *total* lepton number and R parity. The superfields (Φ, ν^c_i, S_i) are singlets under $SU(2) \otimes U(1)$ and carry a conserved lepton number assigned as $(0, -1, 1)$, respectively. These additional singlets ν^c, S [31] and Φ [32] may drive the spontaneous violation of R parity in the model [28]. This leads to the existence of a Majoron given by the imaginary part of

$$\frac{v_L^2}{V v^2} (v_u H_u - v_d H_d) + \frac{v_L}{V} \tilde{\nu}_\tau - \frac{v_R}{V} \tilde{\nu}^c_\tau + \frac{v_S}{V} \tilde{S}_\tau \quad (19)$$

where the isosinglet VEVS

$$v_R = \langle \tilde{\nu}_{R\tau} \rangle, \quad v_S = \langle \tilde{S}_\tau \rangle \quad (20)$$

with $V = \sqrt{v_R^2 + v_S^2}$ characterize R-parity or lepton number breaking and the isodoublet VEVS

$$v_u = \langle H_u \rangle, \quad v_d = \langle H_d \rangle \quad (21)$$

drive electroweak breaking and the fermion masses. The combination $v^2 = v_u^2 + v_d^2 + v_L^2$ is fixed by the W, Z masses. Finally, there is a small seed of R parity breaking in the doublet sector, i.e.

$$v_L = \langle \tilde{\nu}_{L\tau} \rangle \quad (22)$$

whose magnitude is now related to the Yukawa coupling h_ν . Since this vanishes as $h_\nu \rightarrow 0$, we can naturally obey the limits from stellar energy loss [33].

The form of the chargino mass matrix is common to a wide class of $SU(2) \otimes U(1)$ SUSY models with spontaneously broken R parity. It is given by

$$\begin{array}{c|ccc}
 & e_j^+ & \tilde{H}_u^+ & -i\tilde{W}^+ \\
 \hline
 e_i & h_{eij}v_d & -h_{\nu ij}v_{Rj} & \sqrt{2}g_2v_{Li} \\
 \tilde{H}_d^- & -h_{eij}v_{Li} & \mu & \sqrt{2}g_2v_d \\
 -i\tilde{W}^- & 0 & \sqrt{2}g_2v_u & M_2
 \end{array} \quad (23)$$

Two matrices U and V are needed to diagonalize the 5×5 (non-symmetric) chargino mass matrix

$$\chi_i^+ = V_{ij}\psi_j^+ \quad (24)$$

$$\chi_i^- = U_{ij}\psi_j^- \quad (25)$$

where the indices i and j run from 1 to 5 and $\psi_j^+ = (e_1^+, e_2^+, e_3^+, \tilde{H}_u^+, -i\tilde{W}^+)$ and $\psi_j^- = (e_1^-, e_2^-, e_3^-, \tilde{H}_d^-, -i\tilde{W}^-)$.

Under reasonable approximations, we can truncate the neutralino mass matrix so as to obtain an effective 7×7 matrix of the following form [28]

$$\begin{array}{c|ccccc}
 & \nu_i & \tilde{H}_u & \tilde{H}_d & -i\tilde{W}_3 & -i\tilde{B} \\
 \hline
 \nu_i & 0 & h_{\nu ij}v_{Rj} & 0 & g_2v_{Li} & -g_1v_{Li} \\
 \tilde{H}_u & h_{\nu ij}v_{Rj} & 0 & -\mu & -g_2v_u & g_1v_u \\
 \tilde{H}_d & 0 & -\mu & 0 & g_2v_d & -g_1v_d \\
 -i\tilde{W}_3 & g_2v_{Li} & -g_2v_u & g_2v_d & M_2 & 0 \\
 -i\tilde{B} & -g_1v_{Li} & g_1v_u & -g_1v_d & 0 & M_1
 \end{array} \quad (26)$$

This matrix is diagonalized by a 7×7 unitary matrix N ,

$$\chi_i^0 = N_{ij}\psi_j^0 \quad (27)$$

where $\psi_j^0 = (\nu_i, \tilde{H}_u, \tilde{H}_d, -i\tilde{W}_3, -i\tilde{B})$, with ν_i denoting weak-eigenstate neutrinos (the indices i and j run from 1 to 7).

Here we make the same parameter assumptions and conventions as used in the MSSM. Typical values for the SUSY parameters μ and M_2 are as before. The parameters $h_{\nu i,3}$ lie in the range given by

$$10^{-10} \leq h_{\nu 13}, h_{\nu 23} \leq 10^{-1} \quad 10^{-5} \leq h_{\nu 33} \leq 10^{-1} \quad (28)$$

while the expectation values are chosen as

$$\begin{aligned}
 v_L = v_{L3} &= 100 \text{ MeV} & v_{L1} = v_{L2} &= 0 \\
 v_R = v_{R3} &= 1000 \text{ GeV} & v_{R1} = v_{R2} &= 0 \\
 v_S &= 1000 \text{ GeV} & 1 \lesssim \tan \beta = \frac{v_u}{v_d} &\lesssim \frac{m_t}{m_b}
 \end{aligned} \tag{29}$$

The diagonalization of eq. (26) gives rise to the mixing of the neutralinos with the neutrinos, leading to R-parity violating gauge couplings and to neutrino masses, mainly the ν_τ mass. Although the ν_τ can be quite massive, it is perfectly consistent with cosmology [34], including primordial nucleosynthesis, as it can both decay through Majoron emission $\nu_\tau \rightarrow \nu_\mu + J$ [35, 36] due to flavour non-diagonal couplings such as $h_{\nu 23}$, as well as annihilate to a Majoron pair due to the diagonal coupling $h_{\nu 33}$ [37].

In what concerns the R-parity breaking couplings, the largest ones correspond to the case when the standard lepton belongs to the third family. These couplings can reach a few per cent or so for mass values accessible in accelerator studies [38].

2.5 Implications of Spontaneous R Parity Breaking

2.5.1 Invisibly Decaying Higgs boson searches in the $e^+e^- \rightarrow HZ$ and $e^+e^- \rightarrow HA$ channels

The mass spectrum for both CP-even and CP-odd scalar bosons was studied numerically in this model, both at the tree level and after including radiative corrections [39]. For centre-of-mass energies attainable either at LEP200, LHC or NLC, not all of the scalar bosons are kinematically accessible. Typically one or two of the CP-even ones (h, H) will be accessible and one of the massive CP-odd (A) scalar bosons. Although the Majoron has very tiny couplings to matter and gauge bosons, it can have significant couplings to the Higgs bosons, leading to the possibility that the Higgs boson may decay with a substantial branching ratio into the channel [40]

$$h \rightarrow J + J \tag{30}$$

Since the Majoron J is weakly coupled to the rest of the particles, once produced in the accelerator, it will escape detection, leading to a missing momentum signal. Since the strategies to search for the Higgs boson depend heavily on its expected decay pattern, the presence of such an invisible decay signal affects them in a very remarkable way.

The production and subsequent decay of a Higgs boson which may decay visibly or invisibly via the process $e^+e^- \rightarrow HZ$ production involves three independent parameters: its mass M_H , its coupling strength to the Z boson, normalized by that of the Standard Model, ϵ^2 , and its invisible decay branching ratio. The LEP searches for various exotic channels can be used in order to determine the regions in parameter space that are already ruled out, as described in ref. [41]. The exclusion contour in the plane ϵ^2 vs. M_H , can be found in ref. [41].

The invisible decay of the Higgs boson may also affect the strategies for searches at higher energies. For example, the ranges of parameters that can be covered by LEP200 searches for various integrated luminosities and centre-of-mass energies have been investigated [42], and the results are illustrated in Fig. (11). Similar analysis can be made for the case of a high energy linear e^+e^- collider (NLC) [43], as well as

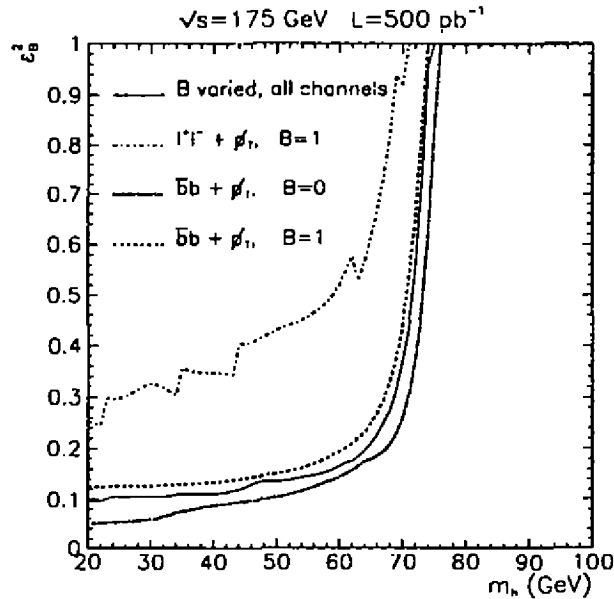


Figure 11: Higgs mass and coupling that can be explored at LEP200 in $e^+e^- \rightarrow H Z$ production.

the LHC [44]. In the latter case the invisible decay has an advantage for searches in the intermediate mass region, namely, that the invisible decay branching ratio can be of order 1, while the standard $H \rightarrow \gamma\gamma$ decay branching ratio in either the SM or the MSSM is rather small, $\mathcal{O}(10^{-3})$. Although it can lead to sizeable signals, the invisible decay has the disadvantage that the Higgs mass can not be reconstructed at a hadron collider. In any case, Higgs boson masses in this range can be probed in less than a year LHC running. However, the NLC would be a cleaner machine for invisibly decaying Higgs boson searches beyond the LEP200 reach.

Due to the existence of two $SU(2) \otimes U(1)$ doublets of scalar bosons, there is another mode of production of invisibly decaying Higgs bosons, in which a CP-even Higgs boson is produced in association with a massive CP-odd scalar.

Present LEP1 limits on the corresponding coupling strength parameter were given in [45]. The region of parameters that can be explored at LEP200 is shown in Fig. (12), as a function of the A and H masses, for the case of a visibly decaying A boson and an invisibly decaying H boson.

2.6 The Fermionic Sector

In the MSSM all supersymmetric particles are always produced in pairs. If R parity is broken, they may be singly-produced. As we have seen, in models with spontaneous R parity breaking the mixing of the standard leptons with the supersymmetric charginos and neutralinos leads to the existence of R-parity violating couplings in the Lagrangian when written in terms of the mass eigenstates. It is in the couplings of the W and the Z where the main R-parity violating effects reside [38]. As a result one is no longer forced to produce the SUSY particles in pairs (standard MSSM production) as well as singly, in association with

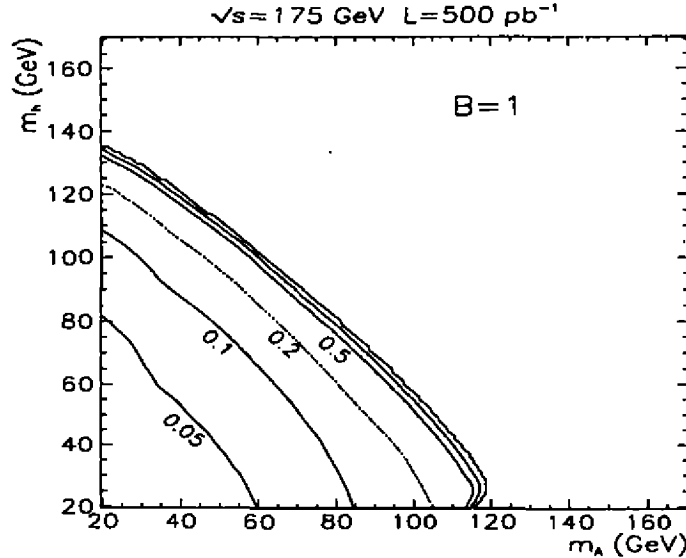


Figure 12: Higgs masses and coupling that can be probed at LEP200 in $e^+e^- \rightarrow H A$ production.

a τ or ν_τ (R-parity breaking single production).

On the other hand the RPSUSY model rates for pair production of SUSY particles are similar to those in the MSSM. However, in contrast to the MSSM, where all supersymmetric particles have cascade decays finishing in the LSP which is normally a neutralino, in the RPSUSY case there are new decay channels and the supersymmetric particles can decay directly to the standard states breaking R-parity. Alternatively, they may decay through R-parity conserving cascade decays that will finish in the lightest neutralino, which then decays. This way one can generate novel supersymmetric signatures in R parity violating models even when the single production SUSY particle cross sections are small.

The lightest neutralino can decay to standard states breaking R-parity. If its mass is lower than the mass of the gauge bosons there are three-body decays such as

$$\chi^0 \rightarrow \nu_j f \bar{f} \quad \chi^0 \rightarrow l_j f_u \bar{f}_d \quad (31)$$

where the first decays are mediated by the neutral current, while the second are charged-current mediated. Here f denotes any fermion, while f_u and f_d denote up or down-type fermions, respectively.

If the neutralino is heavier than the W it may have the two body decays

$$\chi^0 \rightarrow l_j W \quad \chi^0 \rightarrow \nu_j Z \quad (32)$$

The explicit expressions for the widths are given in [38]. Neutralinos of mass accessible at LEP have mostly three-body decay modes mediated by charged and neutral currents. The only exception will be the two-body Majoron decay, characteristic of the simplest spontaneous R parity breaking models eq. (33).

In $SU(2) \otimes U(1)$ models of spontaneous breaking of R-parity the LSP is not the neutralino, but rather the Majoron, which is massless and therefore stable. The existence of the Majoron implies that in $SU(2) \otimes U(1)$

spontaneously broken R-parity, the neutralino can always decay invisibly to

$$\chi^0 \rightarrow \nu_j J \quad (33)$$

For definiteness let us consider the case of the lightest neutralino and chargino, which one expects could be the earliest-produced supersymmetric particles. Here are some examples of signals related to their production in the spontaneously broken R parity (RPSUSY) models:

- Single chargino production in Z decays

$$Z \rightarrow \chi^\pm \tau^\mp \quad (34)$$

where the lightest chargino mass is assumed to be smaller than the Z mass. This decay is characteristic of spontaneous R parity violation. In the simplest models, the magnitude of R parity violation is correlated with the nonzero value of the ν_τ mass and is restricted by a variety of experiments. Nevertheless the R parity violating Z decay branching ratios can easily exceed 10^{-6} and thus lie within the sensitivities of the LEP experiments performed at the Z pole. The maximum branching ratio allowed by other experiments and by theory is directly correlated with m_{ν_τ} , which is a characteristic feature of the model of [28].

- Single neutralino production in Z decays

$$Z \rightarrow \chi^0 \nu_\tau \quad (35)$$

To the extent that χ decays into charged particles are dominant the neutralino is not necessarily an origin of events with missing energy, as in the MSSM. Thus the decay $Z \rightarrow \chi^0 \nu_\tau$ would give rise to zen events, similar to those of the MSSM, but where the missing energy is carried by the ν_τ and the visible tracks come from the decays of the χ . The searches for single particle SUSY production at LEP1 should place restrictions on the parameter space available for studies at LEP200 energies [46].

- Pair production of the lightest neutralino in Z decays, followed by neutralino decays.
Even if its single production cross section is small, the $\chi \chi$ pair production process at LEP will generate zen events where one χ decays visibly and the other invisibly. The corresponding zen-event rates can therefore be larger than in the MSSM and may occur even if there is no energy to produce the next-to-lightest neutralino χ' .

The allowed rates for single Majoron emitting μ and τ decays have been determined in [47] and are compatible with present experimental sensitivities [6]. An illustration of the ν_τ mass dependence of the allowed decay branching ratios can be found in [47]. This example also illustrates how the search for rare decays can be a more sensitive probe of neutrino properties than the more direct searches for neutrino masses, and therefore complementary. Moreover, they are ideally studied at a tau-charm factory [48, 49].

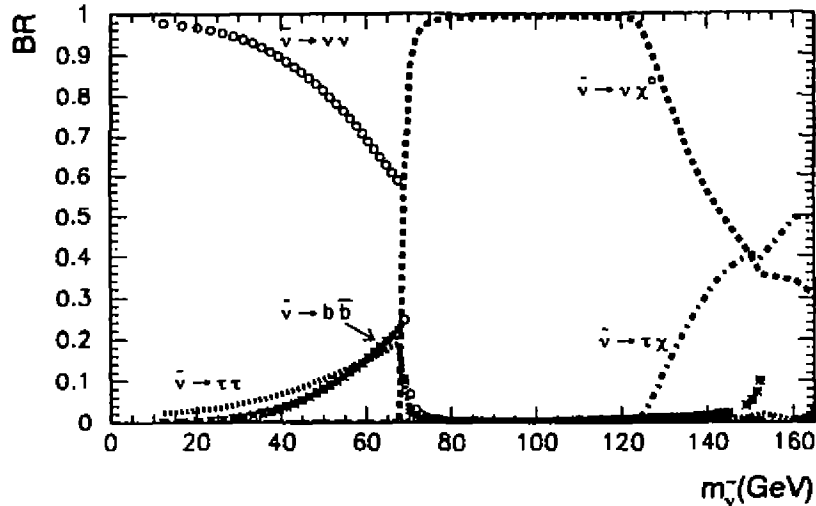


Figure 13: Sneutrino decay branching ratios in the RPSUSY model.

2.7 R Parity Breaking Scalar Boson Decays

Explicit violation of R parity in the minimal supersymmetric model through bilinear terms $\hat{L}\hat{H}_u$ plays an important role in the scalar sector [30]. The presence of such bilinear superpotential term will induce the mixing of sleptons with Higgs bosons, thus affecting the decays of both.

The most illustrative example of this is the possibility that, below the threshold for SUSY particle production, the sneutrino mostly decays to Standard Model particles, as shown in Fig. (13) However, even when the sneutrino is not the lightest SUSY particle, there may be a sizeable branching ratio for the R parity violating sneutrino decays, even for a moderately small value of the Higgsino-lepton superpotential mixing parameters c_i .

As shown in [30] this may lead also to sizeable branching ratio for the supersymmetric Higgs boson decay mode $H \rightarrow \chi\ell$, where χ denotes the lightest supersymmetric particle - LSP - or a chargino, and ℓ is either a neutrino or a tau lepton. This R parity violating Higgs boson decay mode may compete favourably with the conventional decay $H \rightarrow b\bar{b}$, at least for some ranges of parameters of the model. In these estimates one has taken into account the relevant constraints on R parity violation, as well as those coming from SUSY particle searches.

3 Acknowledgements

I thank R. Rosenfeld for carefully reading the manuscript.

References

- [1] See, for example, P. W. Higgs, *Phys. Lett.* **12** (1964) 132; *Phys. Rev. Lett.* **13** (1964) 508.
- [2] G. Altarelli et al, *Interim Report on the Physics Motivations for an Energy Upgrade of LEP2*, CERN-TH/95-151 (1995); M. Carena and P. Zerwas, in ref. [10]; T. L. Barklow, S. Dawson, H. Haber and J. L. Siegrist, SLAC-PUB-95-6893 [hep-ph/9505296], in *Particle Physics - Perspectives and Opportunity*, edited by R. Pecci et al (World Scientific, 1995); J. F. Gunion, A. Stange, and S. Willenbrock, UCD-95-28 (1995), in *Electroweak Symmetry Breaking and New Physics at the TeV Scale*, ed. by T. Barklow et al (World Scientific, to be published).
- [3] M. Martinez, in proceedings of Int. Workshop on Elementary Particle Physics: Present and Future, ed. A. Ferrer and J. W. F. Valle, World Scientific, in press.
- [4] CDF collaboration, *Phys. Rev. D* **52** (1995) 2609; *Phys. Rev. Lett.* **74** (1995) 2626; D0 collaboration, *Phys. Rev. D* **52** (1995) 4877; *Phys. Rev. Lett.* **74** (1995) 2632; see also J. M. Benlloch, in *Elementary Particle Physics: Present and Future*, ed. A. Ferrer and J. W. F. Valle, (World Scientific, 1996) in press.
- [5] M. Gandelman, talk given at this conference.
- [6] L. Montanet et al *Phys. Rev. D* **50** (1994) 1173 and 1995 off-year update for the 1996 edition (URL: <http://pdg.lbl.gov/>).
- [7] See M. Sher, *Phys. Rep.* **179** (1989) 273 and references therein.
- [8] ALEPH collaboration, CERN-PPE/96-10, submitted to *Phys. Lett. B* (1996) .
- [9] D. Treille, in proceedings of Int. Workshop on Elementary Particle Physics: Present and Future, ed. A. Ferrer and J. W. F. Valle, World Scientific, in press.
- [10] M. Carena, P. Zerwas, et al, in *Higgs Physics at LEP II*, CERN-96-01, hep-ph/9602250
- [11] D. Denegri, in proceedings of Int. Workshop on Elementary Particle Physics: Present and Future, ed. A. Ferrer and J. W. F. Valle, World Scientific, in press.
- [12] P. Antilogus et al. [LEP Electroweak Working Group], LEPEWWG/95-02 (1995), contributions of the LEP Experiments to the 1995 International Europhysics Conference on High Energy Physics, 27 July–2 August, 1995, Brussels, Belgium; P. H. Chankowski and S. Pokorski, *Phys. Lett.* **B356** (1995) 307; MPI-PH-95-39 [hep-ph/9509207]; J. Ellis, G. L. Fogli, and E. Lisi, CERN-TH/95-202 [hep-ph/9507424].
- [13] G. G. Ross, *Grand Unified Theories* (Benjamin, 1984), and references therein.
- [14] J. Wess, B. Zumino, *Nucl. Phys.* **B89** (1975) 535; S. Coleman, J. Mandula, *Phys. Rev.* **159** (1967) 1251; R. Haag et al *Nucl. Phys.* **B88** (1975) 257
- [15] U. Amaldi, W. de Boer, H. Furstencau, *Phys. Lett.* **B260** (1991) 447; F. Anselmo et al, *Nuovo Cim.* **104A** (1992) 1335; J. Ellis et al, *Nucl. Phys.* **B373** (1992) 55, *Phys. Lett.* **B287** (1992) 95

- [16] P. Langacker, N. Polonski, *Phys. Rev. D* **52** (1995) 3081
- [17] H. Haber and G. Kane, *Phys. Rep.* **117** (1985) 75; H. P. Nilles, *Phys. Rep.* **110** (1984) 1
- [18] J. F. Gunion, H. E. Haber, G. L. Kane and S. Dawson, *The Higgs Hunter's Guide* (Addison-Wesley, Redwood City, CA, 1990).
- [19] H. E. Haber and R. Hempfling, *Phys. Rev. Lett.* **66** (1991) 1815; Y. Okada, M. Yamaguchi and T. Yanagida, *Prog. Theor. Phys.* **85** (1991) 1; J. Ellis, G. Ridolfi and F. Zwirner, *Phys. Lett.* **B257** (1991) 83.
- [20] P. Chankowski, S. Pokorski, and J. Rosiek, *Phys. Lett.* **B274** (1992) 191; *Nucl. Phys.* **B423** (1994) 437; A. Dabelstein, *Z. Phys.* **C67** (1995) 495.
- [21] M. Carena, J. R. Espinosa, M. Quiros, and C. E. M. Wagner, *Phys. Lett.* **B355** (1995) 209; J. A. Casas, J. R. Espinosa, M. Quiros, A. Riotto, *Nucl. Phys.* **B436** (1995) 3, [E: *Nucl. Phys.* **B439** (1995) 466]; M. Carena, M. Quiros, and C.E.M. Wagner, CERN-TH-95-157 (1995).
- [22] H. Haber, talk at EPS HEP Conference, Brussels [hep-ph/9601330]
- [23] D0 collaboration, *Phys. Rev. Lett.* **75** (1995) 618; and references therein, CDF collaboration, *Phys. Rev. Lett.* **69** (1992) 3439; UA2 collaboration, *Phys. Lett.* **B235** (1990) 363.
- [24] P. Nogueira, J. C. Romão, J. W. F. Valle, *Phys. Lett.* **B251** (1990) 142; R. Barbieri, L. Hall, *Phys. Lett.* **B238** (1990) 86. M. C. Gonzalez-Garcia, J. W. F. Valle, *Nucl. Phys.* **B355** (1991) 330
- [25] V. Barger, G. F. Giudice, T. Han, *Phys. Rev. D* **40** (1989) 2987.
- [26] D. Buskulic et al *Phys. Lett.* **B349** (1995) 238
- [27] R. Mohapatra, J. W. F. Valle, *Phys. Lett.* **B186** (1987) 303; S. Dimopoulos, L.J. Hall, *Phys. Lett.* **196B** (1987) 135; J. Cline, S. Raby, *Phys. Rev. D* **43** (1991) 1781-1787
- [28] A Masiero, J. W. F. Valle, *Phys. Lett.* **B251** (1990) 273; J. C. Romão, C. A. Santos, and J. W. F. Valle, *Phys. Lett.* **B288** (1992) 311
- [29] G. Giudice, A. Masiero, M. Pietroni, A. Riotto, *Nucl. Phys.* **B396** (1993) 243; M. Shiraishi, I. Umemura, K. Yamamoto, *Phys. Lett.* **B313** (1993) 89; see also I. Umemura, K. Yamamoto, *Nucl. Phys.* **B423** (1994) 405
- [30] F. de Campos, M. A. Garcia-Jarño, A. Joshipura, J. Rosiek, J. W. F. Valle, *Nucl. Phys.* **B451** (1995) 3-15
- [31] R. Mohapatra, J. W. F. Valle, *Phys. Rev. D* **34** (1986) 1642; J. W. F. Valle, *Nucl. Phys. B (Proc. Suppl.)* **B11** (1989) 118-177
- [32] R. Barbieri, S. Ferrara, and C. Savoy, *Phys. Lett.* **B119**, 343 (1982).
- [33] J. E. Kim, *Phys. Rep.* **150** (1987) 1 D. Dearborn, et al., , *Phys. Rev. Lett.* **56** (1986) 26; M. Fukugita et al., , *Phys. Rev. Lett.* **48** (1982) 1522; *Phys. Rev. D* **26** (1982) 1841; J. Ellis, K. Olive, *Nucl. Phys.* **B223** (1983) 252

- [34] E. Kolb, M. Turner, *The Early Universe*, Addison-Wesley, 1990, and references therein.
- [35] J. W. F. Valle, *Phys. Lett.* **B131** (1983) 87; G. Gelmini, J. W. F. Valle, *Phys. Lett.* **B142** (1984) 181; J. W. F. Valle, *Phys. Lett.* **B159** (1985) 49; M. C. Gonzalez-Garcia, J. W. F. Valle, *Phys. Lett.* **B216** (1989) 360 A. Joshipura, S. Rindani, *Phys. Rev.* **D46** (1992) 3000; for an early discussion see J. Schechter and J. W. F. Valle, *Phys. Rev.* **D25** (1982) 774
- [36] J. C. Romão and J. W. F. Valle. *Phys. Lett.* **B272** (1991) 436; *Nucl. Phys.* **B381** (1992) 87.
- [37] A.D. Dolgov, S. Pastor, J.C. Romão and J.W.F. Valle, hep-ph/9610507.
- [38] M. C. Gonzalez-Garcia, J. C. Romão, J. W. F. Valle, *Nucl. Phys.* **B391** (1993) 100
- [39] J. C. Romão, F. de Campos, and J. W. F. Valle, *Phys. Lett.* **B292** (1992) 329.
- [40] A. Joshipura and J. W. F. Valle, *Nucl. Phys.* **B397** (1993) 105; J. C. Romão, F. de Campos, and J. W. F. Valle, *Phys. Lett.* **B292** (1992) 329. A. S. Joshipura, S. Rindani, *Phys. Rev. Lett.* **69** (1992) 3269; R. Barbieri, and L. Hall, *Nucl. Phys.* **B364** (1991) 27; G. Jungman and M. Luty, *Nucl. Phys.* **B361** (1991) 24; E. D. Carlson and L. B. Hall, *Phys. Rev.* **D40** (1989) 3187; S. Bertolini, A. Santamaria, *Phys. Lett.* **B213** (1988) 487
- [41] A. Lopez-Fernandez, J. Romão, F. de Campos and J. W. F. Valle, *Phys. Lett.* **B312** (1993) 240; B. Brahmachari, A. Joshipura, S. Rindani, D. P. Roy, K. Sridhar, *Phys. Rev.* **D48** (1993) 4224; F. de Campos et al., proceedings of Moriond94, hep-ph/9405382
- [42] F. de Campos, O. J. P. Eboli, J. Rosiek, J. W. F. Valle, hep-ph/9601269.
- [43] O. Eboli, M. C. Gonzalez-Garcia, A. Lopez-Fernandez, S. Novaes, and J. W. F. Valle, *Nucl. Phys.* **B421** (1994) 65
- [44] J. W. F. Valle, *Nucl. Phys. B (Proc. Suppl.)* **31** (1993) 221-232; J. C. Romão, F. de Campos, L. Diaz-Cruz, and J. W. F. Valle, *Mod. Phys. Lett.* **A9** (1994) 817; J. Gunion, *Phys. Rev. Lett.* **72** (1994) 199; D. Choudhury, D. P. Roy, *Phys. Lett.* **B322** (1994) 368.
- [45] F. de Campos, M. A. Garcia-Jareño, A. Joshipura, J. Rosiek, D. P. Roy, J. W. F. Valle, *Phys. Lett.* **B336** (1994) 446-456
- [46] F. de Campos, M. A. Garcia-Jareño, M. B. Magro, J. Romão, J. W. F. Valle, in preparation; M. Pimenta et al, in preparation
- [47] J. C. Romão, N. Rius, J. W. F. Valle, *Nucl. Phys.* **B363** (1991) 369.
- [48] J. W. F. Valle, in Proceedings of *Second Workshop on Tau-Lepton Physics*, Ohio, ed. K. K. Gan (World Scientific, 1993); see also *Third Workshop on the Charm Tau Factory*, Marbella, Spain, June 1993, (World Scientific, 1994), Ed. J. Kirkby and R. Kirkby.
- [49] R. Alemany et. al. hep-ph/9307252, published in ECFA study group report for a B Meson factory, ed. R. Aleksan, A. Ali, p. 191-211

Teoria de campos em espaços curvos: Nova luz para velhos problemas.

George E.A. Matsas
Instituto de Física Teórica
Universidade Estadual Paulista
Rua Pamplona 145
01405-900 - São Paulo, SP, Brasil

Revisitamos alguns efeitos preditos pela gravitação semi-clássica e em particular discutimos neste contexto o conceito de partícula elementar. Uma breve introdução histórica é incluída para situar a Teoria de Campos em Espaços Curvos no cenário da gravitação clássica. Encerramos com alguns resultados recentes que dizem respeito à solução do problema se cargas estáticas em campos gravitacionais também estáticos irradiam.

Prefácio

O presente artigo foi parcialmente inspirado em minha palestra intitulada "*Bremsstrahlung, efeito Davies-Unruh, radiação Hawking. Gravitação semi-clássica: Nova luz para velhos problemas*" proferida no XIII Encontro Nacional de Partículas e Campos em Caxambu-1992 e parcialmente em minha palestra intitulada "*Solution to the paradox whether or not static charges in gravitational fields radiate*" proferida no XVII Encontro Nacional de Partículas e Campos em Serra Negra-1996. Isso me pareceu propício já que a palestra de Serra Negra é uma continuação natural daquela proferida em Caxambu, cujos proceedings nunca foram publicados. De fato, a presente contribuição foi construída sobre uma versão preparada em 92 e acrescida da seção 7 que trata do paradoxo se cargas estáticas em campos gravitacionais também estáticos irradiam ou não.

1 Introdução

A gravitação semi-clássica, também conhecida como Teoria de Campos em Espaços Curvos, pretende ser mais um passo na construção de uma teoria quântica da gravitação. Sua gênese remonta aos fins dos anos 60 quando L. Parker e Ya.B. Zel'dovich decidiram analisar a criação de partículas em Cosmologia (veja por exemplo [1] e suas referências para uma abrangente revisão.) Em síntese, a idéia resume-se em fixar um espaço-tempo¹ de fundo onde se efetua a quantização dos campos. As propriedades geométricas da variedade podem ser artificialmente dadas ou definidas pelas equações de Einstein, $G_{\mu\nu} = 8\pi T_{\mu\nu}$, onde $G_{\mu\nu}$ é o tensor de Einstein, e $T_{\mu\nu}$ é o tensor de energia momento. Restringindo-nos, por simplicidade, à solução de vácuo, reescrevemos as equações de Einstein como

$$G_{\mu\nu} = 0. \quad (1)$$

Contudo, apesar de no vácuo o tensor de energia momento clássico ser nulo, a curvatura e/ou topologia do espaço podem perturbar a flutuação do vácuo quântico, fazendo com que em geral $\langle 0|T_{\mu\nu}|0\rangle$ seja diferente de zero. Esse tipo de fenômeno constitui uma espécie de efeito Casimir gravitacional. É natural então se perguntar qual a auto-reação do valor esperado no vácuo do tensor de energia momento sobre a geometria. A maneira mais natural de se introduzir correções semi-clássicas na métrica é conseguida modificando-se (1) para

$$G_{\mu\nu} = \langle 0|T_{\mu\nu}|0\rangle. \quad (2)$$

Para campos livres, por exemplo, o lado direito de (2) é de ordem \hbar , o que evidentemente induz correções quânticas na métrica. Note que sendo $\langle T_{\mu\nu} \rangle \equiv \langle 0|T_{\mu\nu}|0\rangle$ de origem quântica, o valor esperado no vácuo do tensor de energia momento não precisa satisfazer as condições clássicas de positividade de energia, usadas na maior parte dos teoremas de singularidade deduzidos por Hawking e Penrose via técnicas globais. Isso permite a evasão de importantes resultados por eles demonstrados no contexto clássico, assim como veremos depois.

Apesar de não podermos esperar que a validade da teoria possa ser extrapolada para além da escala de Planck, a gravitação semi-clássica já tem antecipado efeitos de origem puramente quântica em gravitação, tal como a radiação Hawking sobre a qual voltaremos a falar brevemente mais adiante². A existência de um mecanismo no qual buracos negros evaporam levando possivelmente ao seu desaparecimento³ foi uma predição notável [3], e mudou completamente o conceito de indestrutibilidade que a teoria clássica conferia aos buracos negros. Isso levou muitos pesquisadores a analisarem mais cuidadosamente a construção de teorias de campos em diversas variedades não triviais. Com isso, o estudo da Teoria de Campos em Espaços Curvos acabou enriquecendo em conteúdo velhos conceitos. Em especial, notou-se que o conceito de partícula elementar é fortemente dependente do referencial no qual o campo é quantizado. Tal fato pode ser ilustrado pelo assim chamado efeito Davies-Unruh [4]. Suponha um detetor acelerado no vácuo de Minkowski.⁴ Ao contrário do que esperado inicialmente, tal detetor acusa a presença de partículas. Mais especificamente, um detetor com aceleração própria constante no vácuo de Minkowski deteta um banho térmico de partículas caracterizado por uma temperatura proporcional à sua aceleração própria. Voltaremos a isso nas seções seguintes.

O objetivo principal desta palestra é o de enfatizar as principais conquistas na área, discutindo rapidamente ao final alguns novos resultados. Na seção 2 faremos um breve (e incompleto) histórico de alguns resultados da Relatividade Geral como motivação à Teoria de Campos em Espaços Curvos. Para tanto, enfatizaremos a física de buracos negros como paradigma guia. Na seção 3 será evidenciado no contexto clássico como a estrutura da variedade influencia na construção de teorias de campos. Na seção 4 veremos que a existência de simetrias temporais são cruciais para o conceito de partícula elementar. Dedicaremos a seção 5 para discutir mais detalhadamente o efeito Davies-Unruh. Na seção 6 responderemos à questão se cargas uniformemente aceleradas irradiam com respeito

¹ Formalmente definimos o espaço-tempo como uma variedade \mathcal{M} munida de uma métrica Lorentziana g_{ab} [2]. Intuitivamente uma variedade é uma superfície de dimensão n que localmente possui as propriedades do R^n . No espaço de Minkowski, \mathcal{M} está associado a R^4 e g_{ab} à métrica de Lorentz η_{ab} .

² Atualmente tem sido uma prática comum se usar o efeito Hawking como um teste a baixas energias para possíveis teorias quânticas de gravitação

³ Os estágios finais da evaporação de buracos negros tem sido fonte de especulação. Não é claro se buracos evaporam completamente ou se permanece alguma estrutura estável ao final. Apenas uma teoria quântica completa da gravitação poderia trazer uma resposta.

⁴ O vácuo de Minkowski é o estado no qual observadores inerciais não medem a presença de partículas.

a observadores em co-movimento. Finalmente na seção 7 abordaremos o problema se cargas estáticas em campos gravitacionais também estáticos irradiam. Comentários finais serão reservados para a seção 8.

2 Notas Históricas

Pouco tempo depois de Einstein ter publicado suas equações para descrever o campo gravitacional no vácuo (1), K. Schwarzschild as resolveu para o caso estático e com simetria esférica.⁵ O elemento de linha encontrado por Schwarzschild

$$ds^2 = \left(1 - \frac{2M}{r}\right) dt^2 - \left(1 - \frac{2M}{r}\right)^{-1} dr^2 - r^2 (d\theta^2 + \sin^2\theta d\phi^2) \quad (1)$$

não é apenas importante para o estado do campo gravitacional ao redor da enorme maioria dos corpos celestes que são aproximadamente esféricos, como também descreve a solução para buracos negros estáticos de massa M que passaram a ser chamados buracos de Schwarzschild. Contudo, foi apenas em 1933 que Lemaître reconheceu que o raio de Schwarzschild $r_s = 2M$ não era uma singularidade física [6]. A única singularidade física presente se encontra em $r = 0$ onde se "concentra" a massa do buraco negro. O raio de Schwarzschild define a região denominada horizonte de eventos dentro da qual os cones de luz encontram-se tão distorcidos que nada pode escapar.⁶ Qualquer fonte de energia adentrando o horizonte, inevitavelmente colapsa para o centro.

Depois de um período de relativa latência, a gravitação voltou a ganhar impulso na década de 60. Uma solução de vácuo descrevendo buracos negros estacionários axialmente simétricos, caracterizados por sua massa e momento angular, foi descoberto por Kerr em 1963. Com efeito, uma série de teoremas demonstrados entre 1967 e 1975 particularmente por Israel, Carter, Hawking e Robinson mostraram que buracos negros estacionários, derivados das soluções de vácuo das equações de Einstein, devem ser tipo Kerr, ou seja, são caracterizados apenas por sua massa e momento angular (veja [7] e suas referências.) A generalização destes teoremas, conhecidos como teoremas *no-hair*, nos faz crer que buracos negros são completamente descritos por sua massa M , momento angular J e carga elétrica Q . Para evitarmos a presença de singularidades nuas, (i.e. não vestidas de um horizonte de eventos,) tais parâmetros devem satisfazer $M^2 \geq Q^2 + J^2/M^2$.

Neste mesmo período Hawking e Penrose mostraram que buracos negros, uma vez formados, não podem ser destruídos ou se bifurcarem.⁷ Finalmente em 1971 Hawking provou que num espaço fortemente predizível assintoticamente, e satisfazendo $R_{ab}k^ak^b \geq 0$ para todo k^a tipo luz,⁸ a soma total da área dos horizontes de evento nunca decresce.

A área do horizonte de eventos associado a um buraco negro de Kerr-Newmann (i.e. caracterizado por sua massa M , momento angular J e carga elétrica Q) é dada por [8]

$$A = 4\pi \left[2M^2 - Q^2 + 2M \left(M^2 - Q^2 - \frac{J^2}{M^2} \right)^{1/2} \right] \quad (2)$$

É interessante inverter (2) para isolar a massa

$$M^2 = \frac{A}{16\pi} + \left(\frac{4\pi}{A} \right) \left(J^2 + \frac{Q^4}{4} \right) + \frac{Q^2}{2} \quad (3)$$

Diferenciando (3) obtemos

$$dM = \frac{\kappa}{8\pi} dA + \Omega dJ + \Phi dQ, \quad (4)$$

⁵Um espaço-tempo é dito esféricamente simétrico se o grupo de isometrias contiver um subgrupo $SO(3)$.

⁶De maneira mais geral, buracos negros podem ser definidos em espaços assintoticamente planos, como $B = \mathcal{M} - J^-(I^+)$, onde \mathcal{M} denota a variedade associada ao espaço-tempo, e $J^-(I^+)$ é o passado causal do infinito futuro nulo. O horizonte de eventos \mathcal{H} é definido por $\mathcal{H} = J^-(I^+) \cap \mathcal{M}$. O conceito de horizonte de eventos está intimamente relacionado com o conceito de horizonte de Killing, i.e. uma hipersuperfície nula com um campo de Killing ξ^a normal à hipersuperfície.

⁷De passagem comentamos que tanto este como o teorema seguinte assumem que o espaço-tempo é fortemente predizível assintoticamente, i.e. todos os observadores externos a buracos negros ou sobre o horizonte de eventos não podem ser influenciados por singularidades nuas.

⁸Note que esta condição em conjunto com as equações de Einstein implicam em $T_{ab}k^ak^b \geq 0$.

que relaciona a diferença de massa entre dois buracos negros com pequenas diferenças de área, momento angular e carga elétrica. A gravidade superficial é definida por

$$\mathcal{K} = 4\pi \frac{[M^2 - Q^2 - J^2/M^2]^{1/2}}{\mathcal{A}}, \quad (5)$$

a frequência angular como

$$\Omega = \frac{4\pi J}{M\mathcal{A}} \quad (6)$$

e o potencial elétrico sobre o horizonte de eventos como

$$\Phi = \frac{4\pi Q}{\mathcal{A}} \left[M + \sqrt{M^2 - Q^2 - J^2/M^2} \right]. \quad (7)$$

A semelhança entre (4) e a forma diferencial da primeira lei da termodinâmica nos faz associar a $\mathcal{K}/8\pi$ uma grandeza tipo temperatura, e à área \mathcal{A} uma grandeza tipo entropia⁹ [10]. O próprio Hawking, um ano depois, ao estudar a quantização de campos no espaço externo ao de estrelas colapsando mostrou que buracos negros irradiam com uma temperatura¹⁰

$$T^* = \frac{\mathcal{K}}{2\pi}, \quad (8)$$

assim como observado no infinito¹¹, e fica associada uma entropia ao buraco negro de

$$S_{bn} = \frac{\mathcal{A}}{4}. \quad (9)$$

Especificamente no caso de Schwarzschild $T = 1/8\pi M$ e $S_{bn} = 4\pi M^2$. Foi com enorme surpresa que este resultado foi recebido, pois ao contrário do que previsto classicamente, buracos negros poderiam eventualmente evaporar até seu possível desaparecimento. Outras consequências marcantes são a violação de algumas leis de conservação,¹² e a generalização da segunda lei da termodinâmica que passa a ter o seguinte enunciado: Em qualquer processo físico, $\delta S' \geq 0$, onde $S' = \sum S_{matéria} + \sum S_{bn}$. $S_{matéria}$ é a entropia termodinâmica usual externa ao horizonte de eventos e S_{bn} é a entropia associada aos buracos negros.

3 Espaço-tempo e teorias de campos clássicos

Nesta seção pretendemos evidenciar através de exemplos, como a estrutura da variedade determina e limita a construção da teoria de campos ainda a nível clássico. Para tanto supomos um campo escalar real não massivo descrito pela equação de Klein-Gordon

$$\square\phi = 0. \quad (1)$$

Suponha que a variedade \mathcal{M} associada ao espaço-tempo (\mathcal{M}, g_{ab}) é um 4-toro de lado espacial L e temporal T . Então se T^2/L^2 for irracional, (1) não admite solução.

Em contrapartida, se (\mathcal{M}, g_{ab}) for globalmente hiperbólico,¹³ com Σ sendo uma superfície de Cauchy suave, então a solução de (1) é um problema a valores iniciais bem posto, no seguinte sentido: Dadas funções suaves (ϕ_0, π_0) de

⁹Note-se que, segundo o teorema de Hawking, a área total dos horizontes de evento nunca decresce, em perfeita analogia com a entropia total de um sistema termodinâmico fechado. Contudo, antes de 1974, isso parecia apenas uma coincidência [9]:

"It should however be emphasized that $\mathcal{K}/8\pi$ and \mathcal{A} are distinct from the temperature and entropy of the black hole. In fact the effective temperature of a black hole is absolute zero."

¹⁰A gravidade superficial \mathcal{K} é definida como segue: Seja ξ^a um campo de Killing normal ao horizonte de Killing H . Então $\nabla^b(\xi^a\xi_a) \equiv -2\mathcal{K}\xi^b$ sobre H . Também podemos escrever igualmente $\mathcal{K} = \lim_{\rightarrow H}(V\alpha)$, onde $V = \sqrt{-\xi_a\xi^a}$, $\alpha = \sqrt{a^b a_b}$, e $a^b = \frac{\xi^a}{V} \nabla_a \frac{\xi^b}{V}$.

¹¹Em geral, a temperatura para um outro observador será $T_{loc} = \frac{T}{\sqrt{-\xi^a\xi_a}}$.

¹²Suponha que uma estrela com número leptônico (bariônico) não nulo colapse em um buraco negro. Pelos teoremas de no-hair, não somente a informação sobre estes números quânticos será perdida, como também haverá explícita violação destes números devido à radiação térmica na qual o buraco evapora.

¹³O conceito de espaço-tempo globalmente hiperbólico está intimamente relacionado com o de domínio de dependência. Seja Σ uma superfície acronal, i.e. $I^+(\Sigma) \cap \Sigma = \emptyset$. Definimos o domínio de dependência de Σ por $D(\Sigma) = \{p \in \mathcal{M} \mid \text{ toda curva causal que passe por } p, \text{ intercepte } \Sigma\}$. Se $D(\Sigma) = \mathcal{M}$, então Σ é dita uma superfície de Cauchy e \mathcal{M} globalmente hiperbólica.

ordem C^∞ sobre Σ , então existe uma única solução suave de (1) sobre \mathcal{M} tal que $\phi|_\Sigma = \phi_0$, $n^\alpha \nabla_\alpha \phi|_\Sigma = \pi_0$, onde n^α é o campo vetorial normal a Σ .

Fica claro assim que as propriedades da variedade de fundo influenciam na construção das possíveis teorias de campo mesmo a nível clássico. Evidentemente isso deve se refletir na quantização como veremos a seguir.

4 Partículas e teorias de campos

Antes de prosseguir devemos averiguar qual a dependência do conteúdo de partícula de uma dada teoria de campos com as simetrias temporais do espaço de fundo em questão. Para tanto, voltemos a analisar o campo escalar real não massivo no bem conhecido espaço de Minkowski.¹⁴ Os modos normais de vibração são dados pela solução de $\square\phi = 0$. Ondas planas $u_\pm = e^{\mp i(\omega t - \vec{k} \cdot \vec{x})}$ ($\omega > 0$) são solução e formam um conjunto completo. Na representação do espaço das configurações, $E \rightarrow i\frac{\partial}{\partial t}$. Assim, como

$$i\frac{\partial}{\partial t}u_\mp(x) = \mp\omega u_\mp(x), \quad (1)$$

definimos $u_-(x)$ como modos de frequência negativa e $u_+(x)$ como modos de frequência positiva. Fazemos então a expansão em Fourier do campo em ondas planas

$$\phi(x^\nu) = \int \frac{d^3k}{\sqrt{2\omega(2\pi)^3}} \left\{ \hat{a}(\vec{k})e^{-i(\omega t - \vec{k} \cdot \vec{x})} + \text{H.c.} \right\}. \quad (2)$$

A questão que se coloca é como discernir modos de frequência positiva de modos de frequência negativa numa teoria invariante por transformações gerais de coordenadas. Para responder a isso é necessário generalizar a relação (1). Dizemos que $u_+(x^\mu)$ é um modo de frequência positiva ω com relação a um campo de Killing ξ tipo tempo se

$$i\mathcal{L}_\xi u_+ = \omega u_+, \quad (3)$$

onde $\omega > 0$ e \mathcal{L} indica derivação de Lie.¹⁵ Lembramos que se ξ é um campo de Killing então $\mathcal{L}_\xi g = 0$. O grupo a um parâmetro de difeomorfismos λ_t associado ao campo vetorial ξ define uma isometria.

Analogamente, se uma função de onda u_- satisfizer

$$i\mathcal{L}_\xi u_- = -\omega u_-, \quad (4)$$

então dizemos que $u_-(x)$ é um modo de frequência negativa ω , com relação ao campo de Killing ξ tipo tempo.

Assim, uma vez dado o campo de Killing tipo tempo ξ e descoberto um conjunto completo de modos de frequência positiva e negativa, procedemos de maneira usual a expansão do campo

$$\hat{\phi}(x^\nu) = \sum_j \left\{ \hat{a}_j u_-^j(x^\nu) + \text{H.c.} \right\}, \quad (5)$$

onde somamos sobre os números quânticos que rotulam o campo.

Pela definição acima, não é claro como definir o conceito de partícula em espaços sem alguma simetria temporal. Podemos contornar parcialmente esse problema quando o espaço-tempo tende a Minkowski assintoticamente no passado e futuro. Neste caso pode-se comparar o número de partículas nos espaços assintoticamente planos, e atribuir uma possível criação de quanta à variação do campo gravitacional. Uma situação análoga pode ser encontrada no eletromagnetismo [11]. Uma situação mais interessante é o caso de espaços que admitem mais de um campo de Killing tipo tempo. Neste caso pode-se extrair diferentes conteúdos de partícula, associados a cada campo de Killing, de uma mesma teoria de campos.

¹⁴O espaço de Minkowski é obviamente globalmente hiperbólico.

¹⁵Definimos a derivada de Lie de um campo tensorial T com relação a um campo vetorial ξ no ponto p de uma variedade \mathcal{M} como $\mathcal{L}_\xi T = \lim_{t \rightarrow 0} \frac{\lambda_t^* T - T}{t}$, onde ξ gera o grupo a um parâmetro de difeomorfismos λ_t e denotamos por λ_t^* o isomorfismo induzido por λ_t ($\lambda_t^* : T_p \rightarrow T_{\lambda_t(p)}$).

5 Efeito Fulling-Davies-Unruh

Afim de analisar o efeito Hawking num contexto mais simples, Davies e Unruh (vide [4]) analisaram o caso de um observador com aceleração própria constante no vácuo de Minkowski. De fato, descobriu-se que um observador acelerado no espaço de Minkowski deteta um banho térmico de partículas cuja temperatura é dada por [veja (8)],

$$T = \frac{a}{2\pi}, \quad (1)$$

onde a corresponde à aceleração própria do observador. Para discutirmos o efeito Davies-Unruh [4] investigaremos brevemente a resposta de um detetor acelerado no vácuo de Minkowski.

A amplitude de transição em primeira ordem de perturbação para um detetor no estado fundamental $|E_0\rangle$ e acelerado no vácuo de Minkowski $|0\rangle$ de se excitar para um estado $|E_1\rangle$ ($E_1 > E_0$) e ainda emitir um quantum $|1_{\mathbf{k}}\rangle$ pode ser escrita como

$$A_{|0, E_0\rangle \rightarrow |1_{\mathbf{k}}, E_1\rangle} = i\alpha \langle E_1, 1_{\mathbf{k}} | S_I | 0, E_0 \rangle, \quad (2)$$

onde α é uma constante de acoplamento pequena e

$$S_I = \int_{-\infty}^{+\infty} d\tau \hat{m}(\tau) \hat{\phi}(x^\mu(\tau)) \quad (3)$$

denota a ação de interação entre o campo escalar $\hat{\phi}(x^\mu)$ e o detetor¹⁶ descrito por um monopolo $m(\tau)$. A linha de Universo do detetor é descrito por $x^\mu = x^\mu(\tau)$ com τ sendo seu tempo próprio.

Usando a Hamiltoniana H onde $H|E\rangle = E|E\rangle$, podemos evoluir o monopolo $m(\tau)$ associado ao detetor como

$$\hat{m}(\tau) = e^{iH\tau} \hat{m}(0) e^{-iH\tau}, \quad (4)$$

e com isso reduzimos (2) a

$$A_{|0, E_0\rangle \rightarrow |1_{\mathbf{k}}, E_1\rangle} = i\alpha \langle E_1 | m(0) | E_0 \rangle \int_{-\infty}^{+\infty} e^{i(E_1 - E_0)\tau} \langle 1_{\mathbf{k}} | \hat{\phi}(x^\mu) | 0 \rangle d\tau, \quad (5)$$

Expandindo o campo em termos de ondas planas (2), obtemos

$$\langle 1_{\mathbf{k}} | \hat{\phi}(x^\mu) | 0 \rangle = (16\pi^3\omega)^{-1/2} e^{i(\omega t - \vec{k} \cdot \vec{x})},$$

com o que podemos reescrever (5)

$$A_{|0, E_0\rangle \rightarrow |1_{\mathbf{k}}, E_1\rangle} = i\alpha \langle E_1 | m(0) | E_0 \rangle (16\pi^3\omega)^{-1/2} \int_{-\infty}^{+\infty} e^{i(E_1 - E_0)\tau} e^{i(\omega t - \vec{k} \cdot \vec{x})} d\tau. \quad (6)$$

A probabilidade de transição será simplesmente

$$P_{|0, E_0\rangle \rightarrow |1_{\mathbf{k}}, E_1\rangle} = |A_{|0, E_0\rangle \rightarrow |1_{\mathbf{k}}, E_1\rangle}|^2. \quad (7)$$

Note agora que (6) depende da trajetória do detetor $\vec{x} = \vec{x}(\tau)$.

É fácil ver [1] que se o detetor está numa trajetória inercial ($\vec{x} = \vec{x}_0 + \vec{v}t = \vec{x}_0 + \frac{\vec{v}}{\sqrt{1-v^2}}\tau$), então (7) se anula como esperado. No entanto, se o detetor possui uma aceleração própria constante a , a probabilidade de transição (7) (por unidade de tempo próprio) não se anula, podendo ser escrita como

$$\frac{P_{|0, E_0\rangle \rightarrow |1_{\mathbf{k}}, E_1\rangle}}{\tau} = \frac{\alpha^2 (E_1 - E_0) |\langle E_1 | m(0) | E_0 \rangle|^2}{2\pi (e^{2\pi(E_1 - E_0)/a} - 1)}. \quad (8)$$

O fator tipo Planck $[e^{2\pi(E_1 - E_0)/a} - 1]^{-1}$ indica que o detetor no seu referencial de repouso sente um banho térmico caracterizado pela temperatura¹⁷ $T = a/2\pi$. Com efeito, a função de Green para um detetor com aceleração

¹⁶Basicamente o detetor pode ser encarado como um sistema de dois níveis.

¹⁷Um fenômeno também algo contra-intuitivo pode ser encontrado em eletrodinâmica clássica: Suponha uma carga com aceleração própria constante. Um observador inercial deteta radiação provinda da carga, enquanto que um observador co-accelerado com a carga não. Interpretando radiação como sendo fótons, vemos mesmo neste contexto que a observação de fótons dependerá do referencial. (Veja discussão na seção 6.)

própria constante a corresponde à função de Green térmica para um detetor inercial num banho com temperatura $T = a/2\pi$.

O fato do detetor emitir simultaneamente um quantum e se excitar a um nível de energia mais elevado somente é possível porque o agente que acelera o detetor fornece essa energia. É interessante notar também [12] que cada partícula de Minkowski emitida pelo detetor assim como observada no referencial inercial, é descrita pelo observador acelerado como a *absorção* de uma partícula de Rindler presente no banho térmico. As denominações *partícula de Minkowski* e *partícula de Rindler* estão associadas à quantização do campo com respeito aos vetores de Killing ∂_t e ∂_τ respectivamente.

A busca pela confirmação observacional da radiação Hawking continua intensa [13], mas até o momento os resultados negativos têm sido apenas úteis para fixar limites superiores sobre a densidade de mini-buracos negros. Em contra-partida, a observação da depolarização do feixes de partículas em aceleradores pode ser interpretado no referencial co-acelerado como devido à presença do banho térmico que induziria um flipping no spin [14]. Em seguida veremos como o banho térmico de Davies-Unruh é importante na re-interpretação da emissão de radiação por cargas aceleradas.

6 Cargas aceleradas irradiam segundo observadores co-acelerados?

Nesta seção vamos re-interpretar o efeito de irradiação por cargas clássicas uniformemente aceleradas no contexto da QED em primeira ordem de perturbação no referencial em co-movimento com a carga [15]. É bem sabido que cargas aceleradas irradiam tal como observado em referenciais inerciais. Classicamente, contudo, havia alguma controvérsia sobre se observadores co-acelerados com a carga mediria alguma radiação. Atualmente existe um consenso no contexto clássico de que observadores co-acelerados com a carga não medem qualquer radiação, porque *toda ela se dirige a uma região inacessível para estes observadores* [16]. No contexto da mecânica quântica, a investigação destas questões se torna ainda mais interessante, devido ao papel desempenhado pelo banho térmico no qual a carga está imersa em seu referencial de repouso.

Existem dois ingredientes básicos que devem ser levados em conta neste estudo:

- A corrente que descreve a carga no seu referencial de repouso não pode excitar modos de Rindler de energia finita pois é estática.
- Existem infinitos “fotons de Rindler de energia nula”, i.e. modos de energia nula com respeito ao tempo próprio da carga acelerada, no banho térmico de Davies-Unruh.

O primeiro ingrediente antecipa porque apenas “modos de Rindler de energia nula” serão excitados. O segundo ingrediente permite que a taxa de emissão e absorção destes modos não se anulem, apesar de sua energia nula. A maneira de contornar estas duas tendências concorrentes é introduzir um regulador na corrente, suprimindo-o ao final dos cálculos.

Suponha uma carga q com aceleração própria constante a na direção z . O regulador é introduzido substituindo a corrente estática

$$j^\tau = q\delta(\xi)\delta(x)\delta(y), \quad (1)$$

$$j^\xi = j^x = j^y = 0 \quad (2)$$

que descreve a carga no seu referencial de repouso, pelo dipolo

$$j^\tau = \sqrt{2}q \cos(E\tau) [\delta(\xi) - e^{-2aL}\delta(\xi - L)] \delta(x)\delta(y), \quad (3)$$

$$j^\xi = \sqrt{2}qE \sin(E\tau)e^{-2a\xi}\theta(\xi)\theta(L - \xi)\delta(x)\delta(y), \quad (4)$$

$$j^x = j^y = 0. \quad (5)$$

Ao final dos cálculos o regulador é removido, i.e. $E \rightarrow 0$, $L \rightarrow +\infty$.¹⁸

¹⁸São usadas coordenadas de Rindler para cobrir o Rindler wedge. O Rindler wedge é a região do espaço de Minkowski vinculada por $x > |t|$. Estas coordenadas estão relacionadas com as coordenadas de Minkowski por $t = \frac{e^{a\xi}}{a} \sinh a\tau$, $z = \frac{e^{a\xi}}{a} \cosh a\tau$.

A corrente (3)-(5) se acopla ao campo de Maxwell \hat{A}_μ via a Lagrangiana de interação

$$\mathcal{L}_{int} = \sqrt{-g} j^\mu \hat{A}_\mu, \quad (6)$$

através do que os modos de Rindler podem se excitar.

Depois de quantizar adequadamente o campo eletromagnético no Rindler wedge, podemos obter a taxa total de emissão de fons de Rindler com momento transversal $k_\perp = \sqrt{k_x^2 + k_y^2}$ (por unidade de tempo próprio total τ) tal como calculado no referencial acelerado

$${}^{ac}P_{k_\perp}^{em} = \int_0^{+\infty} \frac{d\omega}{\tau} |A_{(\omega, k_\perp)}^{em}|^2 \left(1 + \frac{1}{e^{2\pi\omega/a} - 1} \right). \quad (7)$$

Os termos dentro do parênteses em (7) estão relacionados com emissão espontânea e estimulada respectivamente. Analogamente, a taxa de absorção de fons de Rindler do banho é dada por

$${}^{ac}P_{k_\perp}^{abs} = \int_0^{+\infty} \frac{d\omega}{\tau} |A_{(\omega, k_\perp)}^{abs}|^2 \frac{1}{e^{2\pi\omega/a} - 1}. \quad (8)$$

Efetuando os cálculos e então retirando o regulador ($E \rightarrow 0, L \rightarrow +\infty$), obtém-se a resposta total da carga com respeito a fons de Rindler de energia nula

$${}^{ac}P_{(k_x, k_y)}^{tot} = \frac{q^2}{4\pi^3 a} |K_1(k_\perp/a)|^2, \quad (9)$$

onde ${}^{ac}P_{(k_x, k_y)}^{tot} = {}^{ac}P_{(k_x, k_y)}^{em} + {}^{ac}P_{(k_x, k_y)}^{abs}$.

Afirmamos em seguida que a taxa total de emissão de fons de Minkowski com momento transversal k_\perp , assim como calculado no referencial inercial coincide inteiramente com esse resultado

$${}^{in}P_{(k_x, k_y)}^{tot} = \frac{q^2}{4\pi^3 a} |K_1(k_\perp/a)|^2. \quad (10)$$

Note que k_\perp é invariante por boosts na direção z , e portanto tem o mesmo valor em ambos os referenciais. Esta igualdade (i.e. ${}^{ac}P_{(k_x, k_y)}^{tot} = {}^{in}P_{(k_x, k_y)}^{tot}$) ilustra nossa principal conclusão:

A emissão de fons com momento transversal k_\perp assim como visto no referencial inercial, pode ser interpretada como a emissão/absorção de fons de Rindler de energia nula com o mesmo momento transversal k_\perp para o banho térmico de Davies-Unruh no qual a carga está imersa em seu referencial de repouso.

Com respeito à mensurabilidade dos fons de Rindler de energia nula, notamos que apesar de carregarem momento transversal finito, fons de Rindler emitidos pela carga não são detetáveis. Isso se deve não apenas ao fato de que existem infinitos fons de energia nula no banho térmico, mas também porque a taxa de emissão e absorção destas partículas é a mesma e o banho não sofre disrupção (i.e., $|n\rangle \rightarrow |n+1\rangle$ tem a mesma taxa de transição de $|n+1\rangle \rightarrow |n\rangle$.) Esta conclusão está de acordo com a análise feita no contexto clássico de que observadores co-acelerados com a carga não observam radiação (veja por exemplo [16]).

7 Cargas estáticas em campos gravitacionais também estáticos irradiam?

Nessa seção tratamos da clássica controvérsia se deveríamos esperar pelo Princípio de Equivalência que cargas estáticas em campos gravitacionais também estáticos irradiassem. O "paradoxo" pode ser enunciado como segue: *É sabido que cargas aceleradas irradiam com respeito a observadores inerciais. Como radiação pode ser interpretada quantum-mecanicamente em termos de fons, seria natural esperar que observadores co-acelerados com a carga também observassem radiação. Por fim, usando ingenuamente o Princípio de Equivalência, poderíamos ser levados a concluir que cargas estáticas em campos gravitacionais também estáticos emitem radiação, o que seria inconsistente do ponto de vista de conservação de energia.* Como já vimos acima, o fato do conceito de partícula elementar ser dependente do observador permite que observadores em co-movimento com uma carga uniformemente acelerada não

observem fons de energia finita sendo irradiados pela carga, ao contrário de observadores inerciais. Entretanto, como já visto, esses observadores co-acelerados atribuem à carga emissão e absorção de fons de energia nula. É natural então se perguntar se observadores estáticos com uma carga num campo gravitacional também estático podem igualmente atribuir a ela a emissão e absorção de algum tipo de partícula de energia nula. Tratamos aqui especificamente do caso no qual uma carga se encontra em repouso fora de um buraco negro de Schwarzschild emitindo radiação Hawking. Por simplicidade, consideramos [17] uma fonte escalar clássica interagindo com um campo escalar não massivo, ao invés de tratar de uma carga elétrica interagindo com o campo de Maxwell. Os cálculos e demais considerações são bastante análogas às feitas na seção anterior, contanto que as devidas adaptações sejam feitas.

A fonte escalar q em repouso fora do buraco negro nas coordenadas de Schwarzschild (r_0, θ_0, ϕ_0) será descrita pela corrente escalar

$$j = \frac{q}{\sqrt{h}} \delta(r - r_0) \delta(\theta - \theta_0) \delta(\phi - \phi_0), \quad (1)$$

onde $h = \det[h_{ij}]$ é o determinante da métrica espacial. Para evitar resultados indeterminados introduzimos novamente um regulador oscilatório, ω_0 , na corrente acima

$$j = \frac{q}{\sqrt{h}} \sqrt{2} \cos(\omega_0 t) \delta(r - r_0) \delta(\theta - \theta_0) \delta(\phi - \phi_0), \quad (2)$$

que é naturalmente suprimido ao final. A corrente (2) se acopla ao campo escalar ϕ via a Lagrangiana de interação

$$\mathcal{L}_{int} = \sqrt{-g} j \hat{\phi}. \quad (3)$$

Em seguida, depois de quantizar o campo escalar no espaço de Schwarzschild (1) e repetir o procedimento acima descrito para o caso de uma carga no espaço de Rindler, podemos calcular a taxa total de emissão e absorção de fons de energia nula [17], tal como calculado no referencial de repouso da fonte:

$${}^{ac} P^{tot} = \frac{q^2}{4\pi^2} a(r_0). \quad (4)$$

onde ${}^{ac} P^{tot} \equiv {}^{ac} P^{em} + {}^{ac} P^{abs}$ e $a(r_0)$ é a aceleração própria experimentada pela fonte quando em repouso em $r = r_0$. Assim, um observador parado com a fonte estática fora do buraco não observa nenhum fóton de energia não-nula sendo emitido pela fonte e por conseguinte nenhuma inconsistência com o princípio de conservação de energia é verificado!

8 Comentários finais

A gravitação semi-clássica, assim como preconizado no início não pretende ser uma teoria completa de gravitação quântica. No entanto, esperamos ter conseguido convencer o leitor da riqueza de informações que ela acrescenta aos nossos conhecimentos de gravitação como um todo. A fórmula para a temperatura com que buracos irradiam consegue agrupar as constantes fundamentais G , c , \hbar , k e talvez acabe sendo o primeiro resultado intrinsecamente quântico observado na gravitação. Mas mesmo que isso não se confirme, não devemos esquecer os benefícios que a Teoria de Campos em Espaços Curvos já trouxe para uma melhor compreensão de alguns de nossos velhos conceitos tais como o de partícula elementar. Guardadas as devidas proporções, a relevância das partículas de energia nula introduzidas acima, por exemplo, deve ser comparada com a relevância do conceito de partículas virtuais: Apesar de, por definição, serem não-observáveis, são muito importantes para a intelecção da física subjacente a vários fenômenos tais como do efeito Lamb shift, efeito Casimir, etc. Apenas o futuro poderá aquilatar com propriedade o quão relevante esta teoria será para o desenvolvimento da Física Teórica.

Agradecimentos

Inicialmente gostaria de agradecer a Atsushi Higuchi e Daniel Sudarsky por inúmeras discussões que tem levado a uma profícua colaboração. Agradeço também a R. Aldrovandi, G. Francisco e V. Pleitez por comentários e sugestões

que me permitiram melhorar a versão anterior do manuscrito e ao Instituto de Física da USP onde permaneci como pós-doutorando durante a elaboração dessa mesma versão. O suporte financeiro nesse período ficou completamente a cargo da Fundação de Amparo à Pesquisa do Estado de São Paulo, enquanto que a presente versão foi parcialmente financiada pelo Conselho Nacional de Desenvolvimento Científico e Tecnológico.

References

- [1] N.D. Birrell and P.C.W. Davies, *Quantum Field Theory in Curved Space*, (Cambridge University Press, Cambridge, 1982). S.A. Fulling, *Aspects of Quantum Field Theory in Curved Space-Time*, (Cambridge University Press, Cambridge, 1989.)
- [2] R.M. Wald, *General Relativity*, (The University of Chicago Press, 1984.)
- [3] S.W. Hawking, *Nature* **248**, 30 (1974); S.W. Hawking, *Commun. Math. Phys.* **43**, 199 (1975).
- [4] S.A. Fulling, *Phys. Rev. D* **7**, 2850 (1973); P.C.W. Davies, *J. Phys. A: Gen. Phys.* **8**, 609 (1975); W.G. Unruh, *Phys. Rev. D* **14**, 870 (1976).
- [5] R. Penrose, *Riv. Nuov Cim.* **1** (número speciale), 252 (1969).
- [6] G. Lemaitre, *Ann. Soc. Sci. Bruxelles I* **A53**, 51 (1933).
- [7] S.W. Hawking, G.F.R. Ellis *The Large Scale Structure of Spacetime*, Camb. Univ. Press, Cambridge, England.
- [8] L. Smarr, *Phys. Rev. Lett.* **30**, 71 (1973).
- [9] J.M. Bardeen, B. Carter, e S.W. Hawking, *Commun. Math. Phys.* **31**, 161 (1973).
- [10] J.D. Bekenstein, *Phys. Rev. D* **7**, 2333 (1973).
- [11] D.M. Gitman, *J. Phys. A Gen. Phys.* **10**, 2007 (1977).
- [12] W.G. Unruh e R.M. Wald, *Phys. Rev. D* **29**, 1047 (1984).
- [13] F. Halzen, E. Zas, J.H. MacGibbon e T.C. Weeks, *Nature* **353**, 807 (1991).
- [14] J.S. Bell e J.M. Leinaas, *Nucl. Phys.* **B212**, 131 (1985).
- [15] A. Higuchi, G.E.A. Matsas e D. Sudarsky, *Phys. Rev. D* **45**, R3308 (1992); *Phys. Rev. D* **46**, 3450 (1992).
- [16] D.G. Boulware, *Ann. Phys. (N.Y.)* **124**, 169 (1980).
- [17] G.E.A. Matsas, D. Sudarsky e A. Higuchi, *Bremsstrahlung by static charges outside black holes?*, gr-qc/9605030; A. Higuchi, G.E.A. Matsas e D. Sudarsky, *Interaction of static classical source with Hawking radiation in Schwarzschild spacetime*, gr-qc/9609025.

A Profusion of Black Holes From Two to Ten Dimensions

José P. S. Lemos

Departamento de Astrofísica, Observatório Nacional-CNPq,

Rua General José Cristino 77, 20921 Rio de Janeiro, Brasil,

Departamento de Física, Instituto Superior Técnico,

Av. Rovisco Pais 1, 1096 Lisboa, Portugal

Black holes in several dimensions and in several theories are studied and discussed. The theories are, general relativity, Kaluza-Klein, Brans-Dicke, Lovelock gravity and string theory.

1. Introduction

Black hole physics and black holes (BHs) have by now a long and interesting history since they were first predicted in 1939 by the prescient work of Oppenheimer and Snyder [1] following some hints left by Zwicky in 1934 [2] that neutron stars, stars of very high densities and very small radii, could form as the end product of a supernova explosion.

It is not here the place to comment on the development of these ideas, but maybe, some would like to know that in the same year, Einstein published a paper [3] arguing forcefully that the gravitational radius, what we now call the event horizon of a BH, could never be surpassed. Einstein was, in a sense, isolated in Princeton, while Oppenheimer was on the west coast, the other side of the country, commuting with his students between Berkeley and Caltech each six months. In Caltech he could share ideas with Tolman the great relativist, and Zwicky a master of prophesying correctly (although there is no direct sign of communication between Zwicky and Oppenheimer). With hindsight, it seems that Caltech was the right place to study gravitational collapse and predict BH formation.

It is also relevant to note that 150 years before, dark stars, the Newtonian BHs, were predicted by Michell [4] in Cambridge, an idea that Laplace followed 12 years later [5]. In modern terms Michell's idea can be put in the form: give a mass M of an astronomical object; find its radius so that the escape velocity is the velocity of light c . The answer is $R = \frac{2GM}{c^2}$, where G is the gravitational constant. Objects with radii below this value are dark stars. However, the argument is not strictly valid because c does not have a fundamental meaning in Newton's gravity. One could detect tachyonic particles emitted from the surface of the star, or an observer not placed at infinity, in the neighborhood of the star, say, could still see the light coming from the star. However entertaining was the dark star idea, it was dropped down for one or other reason until 1939, where it appeared in the right context, the theory of general relativity. Curiously enough, a good condition for the formation of a BH is that the radius of the star obeys Michell condition $R = \frac{2GM}{c^2}$, although now M and R have the corresponding relativistic meanings and G and c are both fundamental constants.

So, what is the picture of a star collapsing into a BH? One can best see it through a spacetime diagram. As the star collapses there is a last ray emerging from the center that can reach spatial infinity. This is the event horizon, signaling the existence of a BH, see figures 1 and 2.

When the BH forms there are two distinct but connected regions, the inside and the outside of the event horizon, explicitly showing that time in relativity is observer dependent. As the matter of the star continues to collapse inside the event horizon it will form a singularity where curvatures and densities of infinite strength are formed and the usual concept of spacetime is lost. Inside the event horizon light is trapped. Light not only does not escape to infinity, it cannot escape to the outside of the BH. However, to an outside observer the story is different. As the BH is being formed, the luminosity of the original star decays exponentially, $L = L_0 e^{-\frac{t}{\tau}}$ where the characteristic time is very short, $\tau = 3\sqrt{3}\frac{GM}{c^3} = 2.6 \times 10^{-6} \frac{M}{M_\odot} \text{s}$, i.e., in a few millionths of a second the star turns totally black ($M_\odot = \text{solar mass}$). In addition, to an outside observer the collapse of the star results in a BH whose properties are characterized by three parameters only: mass, charge and angular momentum. One then says that BHs have no hair (in fact, they have three hairs). All the other properties, or 'hairs', of the matter of the star that formed

the BH disappear. No observation can reveal the nature of the original star, whether it possessed anti-matter, or was made of fermions, or bosons, or whether it had any other hairs.

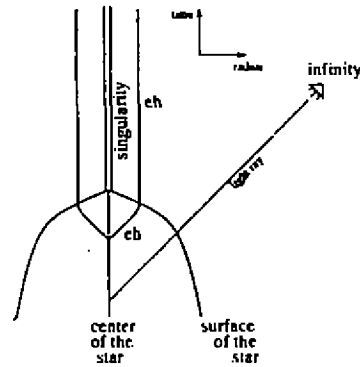


Figure 1. Eddington-Finkelstein diagram for the collapse of a star, (eh = event horizon). A double line in all figures represents a polynomial singularity.

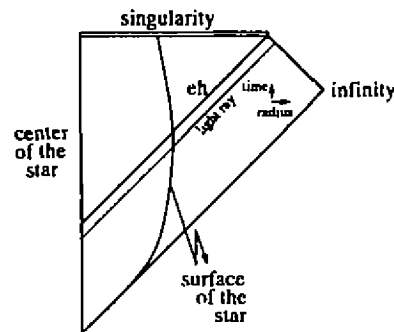


Figure 2. Penrose diagram for the collapse of the same star of figure 1. Light rays move at $\pm 45^\circ$ and each point in the diagram represents a 2-sphere.

This picture is drastically altered if the collapse produces a singularity first, not dressed by an event horizon. BHs are well studied and their existence is highly plausible. Naked singularities do not enjoy the same status. They are a threat to the predicability power of general relativity, and for this reason a cosmic censorship conjecture forbidding the existence of such nasty objects was formulated [6]. There are many theoretical counter-examples to the cosmic censorship conjecture [7, 8], although it is still arguable that these examples cannot occur in nature, either because they may be physically unrealistic or possibly highly unstable. One drawback to the conjecture, often invoked, is that its validity implies the impossibility of observing quantum gravity phenomena, coming out right from the singularity.

BHs formed from the collapse of stars can have masses between $3 - 100M_\odot$. There is also the possibility that supermassive stars or the core of star clusters collapse to form BHs with masses of the order of $1000M_\odot$. BHs with much higher masses $10^6 - 10^9M_\odot$ may form in the center of a galaxy via gravitational collapse of a mixture of clusters of stars and gas. Primordial BHs with masses ranging up to $10^{-19}M_\odot \simeq 10^{14}g$, and the radius of a proton $10^{-13}cm$, could have been formed in the fluctuations of the early and very early universe.

For stellar size objects, the mass is a good indicator to separate BHs from neutron stars. If the compact object has a mass $M \gtrsim 3.5M_\odot$ then there is no equation of state, however stiff, able to support the neutron star (a cold star with a radius of $\sim 10Km$) against complete collapse. There are strong candidates in the sky to stellar BHs, the most famous of all is Cygnus X1, a binary system emitting X-rays and harboring a dark compact object with $\sim 16M_\odot$ (see e.g. [9] for a review). There are no candidates for BHs with $\sim 1000M_\odot$ (even the existence of supermassive stars is pure theoretical speculation). Galactic BHs should inhabit the center of active galactic nuclei, compact sources which can shine more than an entire galaxy. In some cases like quasars, the nuclei of the galaxy

has a brightness equivalent to the brightness of several thousands of galaxies, in a region not bigger than the solar system. In two galaxies with active galactic nuclei the value of the central mass points to the existence of a BH: (i) in the elliptical galaxy M87 the Hubble Space Telescope measured a rotation velocity of $v \sim 550 \text{ km/s}$ for the gas at an orbital radius of 60 light years, which, through Kepler's law gives $M = \frac{v^2 R}{2G} \sim 2 - 3 \times 10^9 M_\odot$; (ii) for the spiral galaxy NGC 4258 Keplerian velocities of $\sim 1000 \text{ km/s}$ in an inner orbit of very small radius, $R \sim 0.4 \text{ ly}$, have been measured through water masers which imply a central mass of $M \sim 2 \times 10^7 M_\odot$. This work is considered to provide the strongest case for a supermassive BH in the center confirming the predictions of Lynden-Bell [10], (see [9] for a review). All these methods are indirect, and to probe directly the existence of a BH one should measure relativistic speeds of the matter circulating in the disk very near the event horizon. In addition, when the gravitational antennas are operating we should directly detect the formation of BHs either through collapse of a single star, or through the merging of binary systems. There is no observational evidence of the existence of primordial BHs.

A quantity that gives some insight to the physical processes occurring during the collapse is the average density of the collapsing matter ρ when the BH is forming, i.e., when $R = \frac{2GM}{c^2}$, yielding $\rho = \frac{3c^6}{32\pi G^3} \left(\frac{1}{M}\right)^2 \simeq 1.3 \times 10^{16} \left(\frac{M_\odot}{M}\right)^2 \frac{\text{g}}{\text{cm}^3}$. For a $1M_\odot$ BH this gives a density ten times larger than the nuclear density, whereas for a $10^8 M_\odot$ BH it gives the density of water. This means the larger the mass the less uncertain is the physics at the BH formation. Even if BHs have not been produced in our cosmos, one could envisage an astronomical experiment, by assembling a very large mass in the form of dust and let it alone to collapse to form a BH. After the matter has passed its own gravitational radius, the singularity theorems [11] plus theoretical models indicate that the density raises to infinity, $\rho \rightarrow \infty$. Is it really infinity? In principle there are strong suggestions that there is a minimum scale, the Planck scale (constructed from G , c and Planck's constant \hbar), below which the usual physical concepts break down. At the Planck scales, $R_{\text{pl}} = \sqrt{\frac{\hbar G}{c^3}} \simeq 10^{-33} \text{ cm}$ and $M_{\text{pl}} = \sqrt{\frac{\hbar c}{G}} \simeq 10^{-5} \text{ gm}$, the density of the matter is $\rho \simeq \frac{M}{R^3} \simeq 10^{92} \left(\frac{M}{M_{\text{pl}}}\right) \text{ gm/cm}^3$. At these scales it is expected that the topology of the spacetime breaks down in order to accommodate these large masses in such a small volume. It is interesting to note that the Planck density $\rho_{\text{pl}} = \frac{c^5}{G^2 \hbar} \simeq 10^{92} \text{ gm/cm}^3$ is the density at which a Planck mass turns into a BH, as well as merging into the singular structure of the spacetime. General relativity provides an adequate description of BHs that are much bigger than the Planck mass. On the other hand for Planckian BHs a description in terms of general relativity breaks down and it has to be replaced by a quantum theory of gravity.

Even much before the quantum gravity regime starts to be important, the BH already presents a quantum mechanical behavior. Indeed following hints that a BH has an associated entropy and therefore, through the relation $S = Q/T$, an associated temperature, Hawking [12] using quantum field theory on a BH background found that BHs are not black but radiate with a blackbody spectrum at a temperature $T = \frac{\hbar c^3}{8\pi G k_B} \frac{1}{M} \simeq 6 \times 10^{-8} \left(\frac{M_\odot}{M}\right) \text{ K}$, and have an associated entropy S_{BH} given by $S_{\text{BH}} = \frac{k_B c^3}{4G} \frac{A}{4}$, where A is the area of the BH and k_B is the Boltzmann constant. Since so many fundamental constants enter these formulas one can say that quantum mechanics, general relativity and thermodynamics must merge together in a unified theory. For $M \sim 1M_\odot$ one has $T \sim 10^{-7} \text{ K}$, whereas for a Planckian BH, $M \sim 10^{-5} \text{ gm}$, $T \sim 10^{32} \text{ K}$. An important unsolved problem raised by this thermal evaporation is the information paradox, which is the problem of knowing to where all the information contained inside the original star has gone after the BH has evaporated completely [13, 14].

Classically, BHs are stable objects, however quantum mechanically they are unstable. As the BH radiates energy its mass decreases, the temperature increases in a runaway process which probably ends in a final explosion. Suppose now that instead of neutral BHs one considers a charged non-rotating BH. Then $T = \frac{1}{2\pi} \frac{\sqrt{M^2 - Q^2}}{(M + \sqrt{M^2 - Q^2})}$. If the charge is large enough, $|Q| = M$, then $T = 0$ and one could expect these objects to be stable. However, vacuum polarization effects will discharge the BH itself rapidly. There are two ways to stabilize the situation:

1. Take a topological charge so that there are no particles to radiate [15].
2. A charged BH will preferentially radiate away its charge, depending on the charge to mass ratio of the particles in the theory. If $\frac{q}{m}$ is small most of the radiation will be in the form of neutral particles and Q will remain constant. Take then that the lightest charged particles are heavy enough so that they cannot be created by the BH. This could be done in two instances.

(a) For example, suppose that the BH carries magnetic charge instead of electric charge. The only way for

the BH to lose this charge would be via the creation of monopoles. However, if the monopoles are heavy enough the probability of decay is heavily suppressed [16].

- (b) A variant of this scenario is to suppose that the charge arises as a central charge in a supersymmetric algebra. It is known that in $N = 2$ supergravity the bosonic sector is Einstein-Maxwell theory with a Bogomolnyi bound given by $Q \leq M$. One can then show that extreme Reissner-Nordstrom solutions $|Q| = M$ (which saturate the bound) are supersymmetric, in the sense that under a supersymmetric operation the metric remains invariant and the fermionic sector remains null [17]. These BHs have zero T and are stable.

Stable BHs can be considered as solitons of the theory and as such belong to the non-perturbative sector and should be put on the same foot as the elementary particles of the theory. To see more directly that the distinction between BHs and elementary particles can be blurred, suppose there is an elementary particle with a mass greater or equal to the Planck mass. Then its Compton wavelength is smaller or equal to its Schwarzschild radius. At these scales it is therefore hard to distinguish between what is an elementary particle from what is a BH. It is then natural to think of such particles as BHs and conversely BHs may be viewed as elementary particles [18]. It is expected that gravity must become the dominant field at the quantum Planck scale 10^{-33}cm , which as we have said represents the minimum scale at which spacetime can be considered smooth. BHs, viewed as elementary particles, are the objects to test this scale, through Hawking radiation. Imagine the following futuristic experiment: two incoming particles in a huge accelerator are set to collide face-on, such that, a center of mass energy of $\sim 10^{19}\text{Gev}$ is produced. Then, one might form a Planckian BH which will evaporate quickly in a burst, allowing us to study the physics at the Planck scale. One might think that by increasing the energy the study of sub-Planckian scales would follow. However, this is not the case, since one would produce a BH with larger mass, which would decay slowly.

From all this one can see that quantum gravity plays an essential role in every theory of extremely strong gravitational fields such as BHs and singularities. One could think of reconciling general relativity with quantum mechanics, but it is known that general relativity is perturbatively unrenormalizable which is taken at face value by many people as an indication that the quantum theory does not exist. At present, the best candidate to a consistent theory of quantum gravity is string theory, a theory remarkable in some respects. The idea of string theory is to use strings as fundamental entities and treat its vibrations as manifestations of the physical world, as fields, particles, etc. The string action plus some rules (like preservation of conformal invariance at the quantum level) place strong restrictions on the possible theories and on the spacetime itself. For instance, string theories treat the dimension of spacetime as a parameter to be settled by the theory. For the pure bosonic string theory (inconsistent at the quantum level), the dimension is $D = 26$, while $D = 10$ for the four consistent supersymmetric string theories which seem to belong to a $D = 11$ M-theory [19, 20] or even a $D = 12$ F-theory [21]. Although apparently incorrect, these dimensions can, in principle, be dynamically compactified into the $D = 4$ dimensions actually observed in our universe. Superstring theories can also be formulated in any dimension $D \leq 10$, with the left $10 - D$ dimensions treated as being compactified somehow [22]. A remarkable feature of the theory is the presence of a bewildering variety of BH solutions in any dimension from 2 to 10. The study of BH solutions in $D \geq 4$ dimensions is not new [23], although string theory has made an important impact in their appearance and development in the lower 2 and 3 dimensions. Besides string theory, BHs in different dimensions also appear in theories like general relativity, Kaluza-Klein theory, Brans-Dicke theory, Lovelock gravity and in their corresponding supersymmetric versions. In the subsequent sections we will discuss some of these solutions and some of their properties.

2. BHs in 4D

Let us start with general relativity in 4D, i.e., Einstein-Maxwell theory, characterized by the action

$$S = \frac{1}{16\pi G} \int d^4x \sqrt{-g} (R - F^2), \quad (1)$$

where g and R are the determinant of the metric and the curvature scalar, respectively, and $F^2 = F_{\mu\nu} F^{\mu\nu}$, where

$F_{\mu\nu}$ is the Maxwell tensor ($c = 1$). Uncharged BHs are described by the Schwarzschild solution

$$ds^2 = -\left(1 - \frac{2M}{r}\right)dt^2 + \frac{dr^2}{1 - \frac{2M}{r}} + r^2 d\Omega_2^2, \quad (2)$$

where $d\Omega_2^2$ is the line element of the 2-sphere, M is the mass of the BH, and we have put $G = 1$. The causal structure is conveniently described by the Penrose diagram of figure 3, where light rays move at $\pm 45^\circ$ and each point in the diagram represents a 2-sphere. The event horizon is located at $r = 2M$ (where $g^{rr} = 0$).

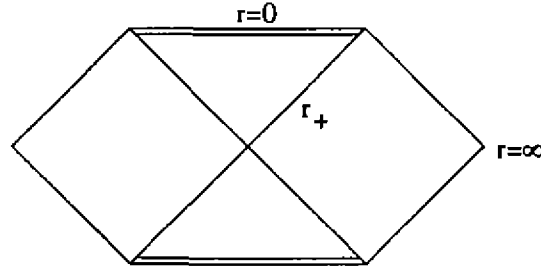


Figure 3. Penrose diagram for the Schwarzschild solution.

A charged BH in general relativity is described by the Reissner-Nordstrom solution,

$$ds^2 = -\left(1 - \frac{2M}{r} + \frac{Q^2}{r^2}\right)dt^2 + \frac{dr^2}{1 - \frac{2M}{r} + \frac{Q^2}{r^2}} + r^2 d\Omega_2^2, \quad (3)$$

where Q is the charge, $F_{rt} = \frac{Q}{r^2}$ for electric Q , and $F_{\theta\phi} = Q \sin\theta$ for magnetic Q . The causal structure is richer now. There are three distinct cases depending on the charge to mass ratio. For $0 < |Q| < M$ there are two horizons (the event and the Cauchy horizon) given by the roots of $g^{rr} = 0$, r_{\pm} . The Penrose diagram is sketched in figure 4. For an extreme BH, $|Q| = M$, the two horizons merge in one, and for $Q > M$ the singularity is timelike and naked.

The Hawking temperature of static BHs can be calculated in several ways. The original calculation involves the analysis of quantum matter fields in the BH background [24]. A cleaner calculation is achieved by analytically continuing the metric in time t and requiring that the resulting Riemannian space be non-singular. This implies a periodic identification in imaginary time with the temperature being equal to the inverse of the period [25]. One can then show that this BH instanton is related to a real BH in thermal equilibrium with radiation. As mentioned, for the Reissner-Nordstrom BH $T = \frac{1}{2\pi} \frac{\sqrt{M^2 - Q^2}}{(M + \sqrt{M^2 - Q^2})}$, which for $Q = 0$ yields the familiar $T = \frac{1}{8\pi M}$.

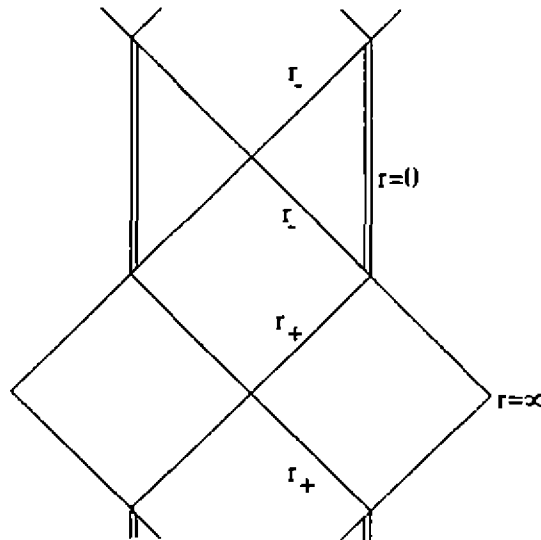


Figure 4. Penrose diagram for the Reissner-Nordstrom solution.

Near singularities general relativity should be replaced by a quantum theory. String theory is a consistent theory that may give some clues at the Planckian scales. This raises the question of whether BHs in string theory are different from BHs in general relativity. We will see that these two theories give distinct BHs. Due to the existence of dilaton, axion and other fields in string theory there are even BHs without singularities. There are also solutions describing one-, two-, and p -dimensional objects surrounded by event horizons, i.e., black strings, black membranes and black p -branes. We will also show in the next section that general relativity also possesses these type of objects, a feature not known until recently [26, 27].

Without further details for the time being, let us consider the low energy action to heterotic string theory [22, 28]

$$S = \frac{1}{4\pi} \int d^D x \sqrt{-g} e^{-2\phi} \left[R - 2\Lambda + 4(\nabla\phi)^2 - F^2 - \frac{1}{12}H^2 \right], \quad (4)$$

where the new fields are the dilaton scalar field ϕ , and the 3-form field $H_{\mu\nu\rho}$, such that $H^2 = H_{\mu\nu\rho}H^{\mu\nu\rho}$ and defined by $H = dB - A \times F$ where $B_{\mu\nu}$ is the axion 2-form potential and A_μ is the vector potential that defines the $U(1)$ Maxwell field, $F = dA$. These fields arise naturally in string theory. The cosmological constant Λ is set by the internal consistency of the theory and related to the dimension D of the spacetime and the central charge of a possible internal conformal field theory. The constant factor $\frac{1}{4\pi}$ in front of the integral in the action (4) is somewhat arbitrary. This arbitrariness will remain throughout this article, although without loss of precision, since we are dealing mostly with classical results.

To have a full theory and not only the low energy action (4) one would have to add higher order correction terms R^2 , R^3 , F^4 , etc. All the higher order terms are important for studying BHs of Planckian size and the spacetime singularities. However, using (4) one can study the properties of larger BHs away from the singularities. For $D = 4$ and in a background where $\Lambda = 0 = H$ the action simplifies to

$$S = \frac{1}{4\pi} \int d^4 x \sqrt{-g} e^{-2\phi} [R + 4(\nabla\phi)^2 - F^2]. \quad (5)$$

Note that ϕ plays the role of a coupling constant, since comparing (1) and (5) roughly one has $G \sim e^{2\phi} \equiv g_s$, where g_s is the string coupling constant. In order to directly compare with the Einstein-Maxwell action one rescales the string metric $g_{\mu\nu}$ (which is the metric seen by the strings) to the Einstein metric $g_{\mu\nu}^E \equiv e^{-2\phi} g_{\mu\nu}$ (the metric that puts the string action in an Einstein form) to have the action,

$$S_E = \frac{1}{4\pi} \int d^4 x \sqrt{-g_E} [R_E + 4(\nabla\phi)^2 - e^{-2\phi} F^2]. \quad (6)$$

For $F = 0$, i.e., uncharged solutions, one deduces from (6) and the no-hair theorems [29] that uncharged BHs in the low energy string action are the same as the Schwarzschild BH of general relativity. On the other hand, for $F \neq 0$ and $\phi \neq 0$ the charged BHs in string theory are different from the Reissner-Nordstrom BHs. This could give a low energy test of string theory: if string theory is the correct one then charged BHs are not described by the Reissner-Nordstrom metric but instead by the solution [30, 31, 32]

$$ds^2 = -\left(1 - \frac{2m}{\bar{r}}\right) \left(1 + \frac{2m \sinh^2 \alpha}{\bar{r}}\right) dt^2 + \frac{d\bar{r}^2}{1 - \frac{2m}{\bar{r}}} + \bar{r}^2 d\Omega_2^2$$

$$e^{-2\phi} = 1 + \frac{2m \sinh^2 \alpha}{\bar{r}} \quad A_t = -\frac{m \sinh 2\alpha}{\sqrt{2[\bar{r} + 2m \sinh \alpha]}} \quad (7)$$

where the mass and charge are given by $M = m \cosh^2 \alpha$, $Q = \sqrt{2} m \sinh 2\alpha$. For $\bar{r} = 2m$ there is an event horizon whereas for $\bar{r} = 0$ there is a singularity. At the singularity $g_s = e^{2\phi} \rightarrow 0$ which might mean that in the full string theory, the string coupling remains negligible and quantum effects are suppressed. To compare with general relativity we then do the conformal rescaling mentioned above ($ds_E^2 = e^{-2\phi} ds^2$) and obtain

$$ds_E^2 = -\left(1 - \frac{2M}{r}\right) dt^2 + \frac{dr^2}{1 - \frac{2M}{r}} + r \left(r - \frac{Q^2}{r}\right) d\Omega_2^2,$$

$$e^{2\phi} = 1 - \frac{Q^2}{Mr}, \quad r_{,t} = \frac{Q}{r^2}, \quad (8)$$

where for convenience we have defined $r = \bar{r} + \frac{Q^2}{M}$. The charged string metric is identical to Schwarzschild in the $r - t$ plane (same Penrose diagram as in figure 1), however the spheres have smaller radii. There is the extremal

limit $|Q| = M$ given by the diagram of figure 5. For $|Q| > M$ the singularity is naked. The string metric (7) has the same corresponding Penrose diagrams since these diagrams are unaltered by conformal transformations.

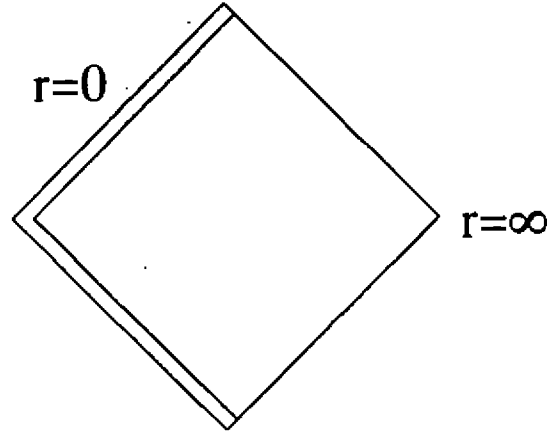


Figure 5. Penrose diagram for the charged extreme BH in string theory. The singularity is null, or in other words, the event horizon is singular.

What about magnetic BHs? We have seen that in general relativity, electric and magnetic BHs have the same metric, i.e., neutral particles do not distinguish the two types of BHs. In string theory one can find magnetic BHs by performing an S-duality (or strong-weak) transformation, which transforms weak coupling into strong coupling and vice-versa. The transformation is [28]

$$F \rightarrow \tilde{F}, \phi \rightarrow -\phi, g_E \rightarrow g_E \quad (9)$$

where \tilde{F} is the dual of F , $\tilde{F}_{\mu\nu} = \frac{1}{2}e^{-2\phi}\epsilon_{\mu\nu}{}^{\alpha\beta}F_{\alpha\beta}$, transforming electric into magnetic charge. Since the Einstein metric is unchanged the Penrose diagrams for magnetic BHs are identical to the Penrose diagrams for electric BHs. In terms of the string metric we have

$$ds^2 = -\frac{1-\frac{2M}{r}}{1-\frac{Q^2}{Mr}}dt^2 + \frac{dr^2}{(1-\frac{2M}{r})(1-\frac{Q^2}{Mr})} + r^2d\Omega_2^2$$

$$e^{-2\phi} = 1 - \frac{Q^2}{Mr}, \quad F_{\theta\phi} = Q \sin\theta \quad (10)$$

The singularity happens at a finite area, when $r = \frac{Q^2}{M}$. The extremal limit is given by $Q^2 = 2M^2$, for which the temperature is zero. On the other hand for the non-extreme BH given in equation (10), the temperature is $T = \frac{1}{8\pi M}$, independent of the charge. This means that the BH radiates past beyond the extremal limit, indicating in turn that the semi-classical approximation for the calculation of the temperature breaks down.

We have only mentioned non-rotating BHs. In string theory, uncharged rotating BHs have the same metric as Kerr BHs. However the charged rotating BHs are different [33].

3. BHs in 3D

It is now known that 3D general relativity is important to study as it provides a bedtest for 4D and higher D theories [34, 35, 36]. Two features in 3D general relativity are relevant: (i) the theory has no Newtonian limit (it is still an open question which 3D theory has a Newtonian limit), (ii) there are no propagating degrees of freedom, which means that in vacuum, outside matter, spacetime is locally flat, anti-de Sitter or de Sitter depending on the value of the cosmological constant, $\Lambda = 0$, $\Lambda < 0$, and $\Lambda > 0$, respectively. Due to this simplicity and lack of structure it can be thought that there is no interesting object emerging from the theory. Surprisingly, from the action

$$S = \frac{1}{2\pi} \int d^3x \sqrt{-g}(R - 2\Lambda). \quad (11)$$

and its equations of motion, Bañados, Teitelboim and Zanelli [37] found a 3D rotating BH metric known as the

BTZ BH, given by

$$ds^2 = -\left(\frac{r^2}{l^2} - M + \frac{J^2}{4r^2}\right)dt^2 + \frac{dr^2}{\frac{r^2}{l^2} - M + \frac{J^2}{4r^2}} + r^2\left(d\varphi - \frac{J}{2r^2}dt\right)^2, \quad (12)$$

where $l^2 \equiv -\frac{1}{\Lambda}$ and J is the angular momentum. For $|J| < Ml$ there are two horizons r_{\pm} given by the zeros of g^{rr} . There are also ergoregions for $r_+ < r < r_{\text{erg}}$ where particles and observers are dragged along certain trajectories. In the extremal case, $|J| = Ml$, the two horizons merge. For $J = 0$ the BH is static. The rotating case resembles in many aspects the Kerr metric and the non-rotating case the Schwarzschild solution, although there are no polynomial singularities, only (milder) causal singularities. The maximal analytical extension of the static and rotating BHs are given in the Penrose diagrams of figures 6 and 7.

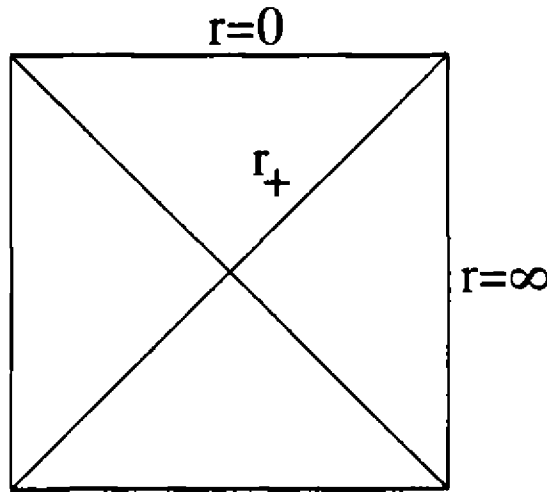


Figure 6. Penrose diagram for the 3D static BH. The line $r = 0$ in this figure and in figure 7 is a milder causal (not polynomial) singularity. Spacetime is asymptotically anti-de Sitter.

Besides the BH solution, 3D general relativity with $\Lambda < 0$ also has the anti-de Sitter (ADS) spacetime as a vacuum solution with metric given by

$$ds^2 = -\left(\frac{r^2}{l^2} + 1\right)dt^2 + \frac{dr^2}{\frac{r^2}{l^2} + 1} + r^2d\varphi^2. \quad (13)$$

We note that for $r \rightarrow \infty$ the BH solution (12) is asymptotically ADS. Asymptotically ADS solutions and ADS spacetime itself are interesting to study for various reasons: (i) theories of extended supergravity in which some group, like $O(N)$, is gauged have ADS as a vacuum state, and (ii) there exists a positive energy theorem, i.e., it is possible to give Witten's proof of the positive mass theorem of Schoen and Yau to asymptotically ADS spacetimes, implying in turn that asymptotically ADS solutions are stable.

Now, in 3D there is the relation $R^{ab}{}_{cd} = \epsilon^{abe}\epsilon_{cdf}G^e{}_f$. Therefore, a solution of $G_{ab} = 0$ is flat, and a solution of $G_{ab} = -\Lambda g_{ab}$ has constant curvature. Since the BII metric and the ADS solution have both constant curvature, one concludes that patches in the BH spacetime have an isometric neighborhood to the ADS spacetime and the BH spacetime can be defined by a collection of such neighborhoods. Indeed, it was shown in [38] that the BH can be represented as a quotient space of the universal covering of ADS, $\tilde{\text{ADS}}$, by some group of isometries, which provides a powerful mathematical tool in examining the BH spacetime.

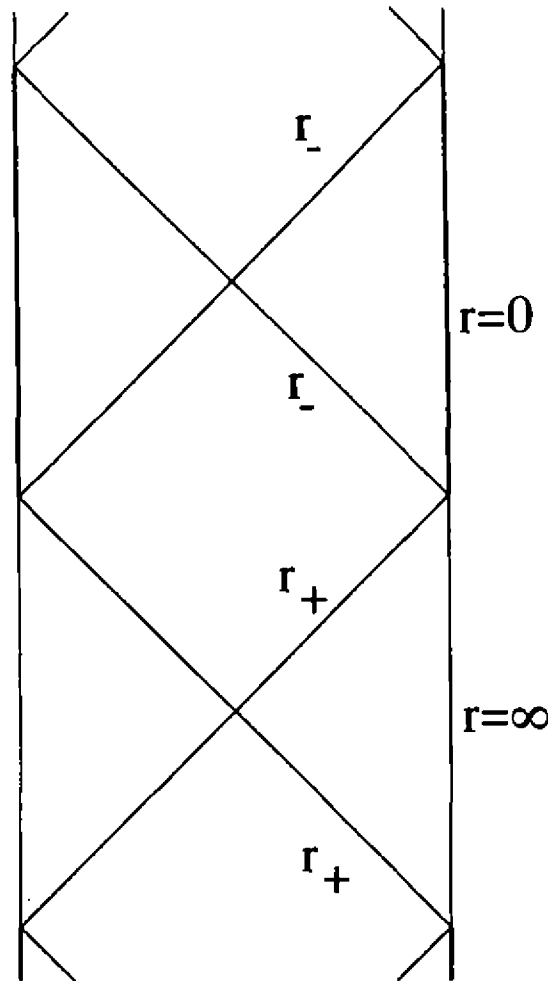


Figure 7. Penrose diagram for the 3D rotating BII.

3D ADS spacetime can be obtained from the plane R^4 with two time and two space coordinates (X_1, X_2, T_1, T_2) (we follow [39] here). The ADS metric is then the induced metric taken from the 4D flat metric,

$$ds^2 = -dT_1^2 - dT_2^2 + dX_1^2 + dX_2^2, \quad (14)$$

restricted to the hyperboloid

$$X_1^2 - T_1^2 + X_2^2 - T_2^2 = -l^2. \quad (15)$$

From (14) and (15) the isometry group is $SO(2, 2)$, of course. One can go further and combine (X_1, X_2, T_1, T_2) in a 2×2 matrix,

$$\underline{X} = \begin{pmatrix} T_1 + X_1 & T_2 + X_2 \\ -T_2 + X_2 & T_1 - X_1 \end{pmatrix} \quad (16)$$

with $\det|\underline{X}| = 1$ and $\underline{X} \in SL(2, R)$. Here, the isometries can be represented as elements of the group $SL(2, R) \times SL(2, R)$, $SO(2, 2)$, with each $SL(2, R)$ acting by left and right multiplication, such that $\underline{X}' = \rho_L \underline{X} \rho_R$, with $(\rho_L, \rho_R) \sim (-\rho_L, \rho_R)$.

Now, given ADS spacetime one may cover it using three different regions parametrized by (r, t, φ) with $0 \leq r < \infty$, $-\infty < t < \infty$, and $-\infty < \varphi < \infty$. For instance, in the region $r \geq r_+$ we have $X_1 = l\sqrt{\alpha(r)} \sinh(\frac{r_+}{l} \varphi - \frac{r_-}{l} t)$, $T_1 = l\sqrt{\alpha(r)} \cosh(\frac{r_+}{l} \varphi - \frac{r_-}{l} t)$, $X_2 = l\sqrt{\alpha(r) - 1} \cosh(\frac{r_+}{l} t - \frac{r_-}{l} \varphi)$, and $T_2 = l\sqrt{\alpha(r) - 1} \sinh(\frac{r_+}{l} t - \frac{r_-}{l} \varphi)$, where, $\alpha(r) = \frac{r_+^2 - r^2}{r_+^2 - r_-^2}$. This corresponds to give region I of the Penrose diagram in figure 7. Analogous transformations can be given to the regions $r_- < r < r_+$ and $0 < r < r_-$, i.e., to regions II and III of the figure 7. By repeating these regions ad infinitum one covers the entire ADS spacetime. One can pick up X_1, T_1, X_2, T_2 from these transformations,

put back in the induced metric (14)–(15), and recover the form of the BH metric (12). However, note that this is not the BH spacetime since φ ranges from $-\infty$ to $+\infty$. To make φ an angular variable one has to identify φ with $\varphi + 2\pi$. In this construction it is easy to see that such an identification is an isometry of ADS, in fact it is a boost in the $X_1 - T_1$ and $X_2 - T_2$ planes. Indeed, it leads to, $X_1 \rightarrow X_1' = (\cosh \frac{2\pi r \pm}{l})X_1 + (\sinh \frac{2\pi r \pm}{l})T_1$, $T_1 \rightarrow T_1' = (\sinh \frac{2\pi r \pm}{l})X_1 + (\cosh \frac{2\pi r \pm}{l})T_1$, and analogously for X_2 and T_2 . This corresponds in the $SL(2, R)$ formulation to an element (ρ_L, ρ_R) given by $\rho_L = \text{diag} \left(e^{\pi(\frac{r+\tilde{r}}{l})}, e^{-\pi(\frac{r+\tilde{r}}{l})} \right)$, $\rho_R = \text{diag} \left(e^{\pi(\frac{r+\tilde{r}}{l})}, e^{-\pi(\frac{r+\tilde{r}}{l})} \right)$. The BTZ BH may then be viewed as a group manifold given by the quotient space ADS/P , where P denotes the group generated by (ρ_L, ρ_R) .

This formulation has great advantages: the ADS spacetime is an extremely simple manifold and if one makes appropriate global identifications one finds a 3D BH which has inherit its own complex structure. The implications are many: (i) one can compute the Green functions in the ADS spacetime and then make a direct connection to the BH; (ii) one can find Killing spinors fairly easily, which provides an identification of the existence of supersymmetry; if the BH is embedded in a supergravity theory with vanishing gravitino field, then the existence of Killing spinors leave the metric and gravitinos invariant. It was found that Killing spinors exist for extreme BHs only [40]; (iii) the temperature of the BH is $T = \frac{r_+^2 - r_-^2}{2\pi r_+^2}$, which for zero rotation yields, $T = \frac{\sqrt{M}}{2\pi l}$ and an entropy $S = \frac{2\pi r_+}{4hG}$. Unfortunately, this does not help in solving the long standing problem in 4D, to know whether or not the BH evaporates completely, since in 3D $T \rightarrow 0$ as $M \rightarrow 0$; (iv) on the other hand, one can show that the 3D BH forms from gravitational collapse of 3D matter, as in the 4D case [41]; (v) 4D gravity can be written in a first order formalism as a Chern-Simons theory. Viewing the BH as an ADS space with proper identifications helps in the study of the holonomies (see [39] for a complete list of references).

Another important result, is that the 3D BH we have been discussing is also a solution of 3D string theory [42, 43]. Using the action (4) with $D = 3$, $\phi = 0$ and $H_{\mu\nu\rho} = \frac{2}{l}\epsilon_{\mu\nu\rho}$ one obtains the same 3D BH. This displays the versatility of string theory. One can also find a black string solution by applying a duality transformation. We have already seen the S-duality at work. There is another well known symmetry of string theory that maps any solution with a translational symmetry of the low-energy action into another solution. This symmetry is usually called T-duality or target-duality. Given a target-space solution $(g_{\mu\nu}, B_{\mu\nu}, \phi)$ which is independent of one coordinate, like φ in the BH solution, then there is another solution $(\tilde{g}_{\mu\nu}, \tilde{B}_{\mu\nu}, \tilde{\phi})$ related to the previous one by a T-duality [28]. The T-dual solution for the 3D BH is a black string.

What else can we do with the 3D BH? It can be embedded in 4D general relativity [44, 45]. One takes the product of the BTZ BH with the real line R , with metric $ds^2 = ds_{\text{BTZ}}^2 + dz^2$, and imposes that it satisfies the 4D Einstein equations derived from the action $S = \frac{1}{16\pi} \int d^4x \sqrt{-g} [(R - 2\Lambda) + \mathcal{L}_{\text{matter}}]$. By suitably choosing the energy-momentum tensor $T_{\mu\nu} \equiv -\frac{2}{\sqrt{-g}} \frac{\delta \mathcal{L}_{\text{matter}}}{\delta g_{\mu\nu}}$ one finds that the 3D BH can be converted into a black string in 4D general relativity. The idea is analogous to the well-known result that point particles in 3D are related to straight infinite strings in 4D.

There is yet a different solution which relates vacuum black strings in 4D general relativity with 3D BHs of a dilaton-gravity theory. Starting with the Einstein-Maxwell action $S = \frac{1}{16\pi} \int d^4x \sqrt{-g} (R - 2\Lambda - F^2)$ one imposes the existence of a Killing vector such that the metric can be written in the form $ds^2 = g_{ab}^{(3)} dx^a dx^b + e^{-4\phi} dz^2$, where $a, b = 1, 2, 3$ and g_{ab} , and ϕ are functions of x^a . Then by dimensional reduction one obtains a dilaton-gravity action, $S = \frac{1}{16\pi} \int d^3x \sqrt{-g} e^{-2\phi} (R - 2\Lambda - F^2)$. It is then easy to relate 4D and 3D solutions. In 4D general relativity there is a black string solution, with charge and rotation, given by [46]

$$\begin{aligned}
 ds^2 = & - \left(\alpha^2 r^2 - \frac{4M(1 - \frac{a^2 \alpha^2}{2})}{\alpha r} + \frac{4Q^2}{\alpha^2 r^2} \right) dt^2 + \\
 & - \frac{4\alpha M \sqrt{1 - \frac{a^2 \alpha^2}{2}}}{\alpha r} \left(1 - \frac{Q^2}{M(1 - \frac{a^2 \alpha^2}{2}) \alpha r} \right) 2dt d\varphi + \\
 & + \left(\alpha^2 r^2 - \frac{4M(1 - \frac{3}{2} a^2 \alpha^2)}{\alpha r} + \frac{4Q^2}{\alpha^2 r^2} \frac{(1 - \frac{1}{2} a^2 \alpha^2)}{(1 - \frac{a^2 \alpha^2}{2})} \right)^{-1} dr^2 + \\
 & + \left[r^2 + \frac{4M a^2}{\alpha r} \left(1 - \frac{Q^2}{(1 - \frac{a^2 \alpha^2}{2}) M \alpha r} \right) \right] d\varphi^2 + \alpha^2 r^2 dz^2, \tag{17}
 \end{aligned}$$

where here $\alpha \equiv -\frac{1}{3}\Lambda$, M and Q are the mass and charge, respectively, and a is related to the angular momentum

J via $J = \frac{3}{2}aM\sqrt{1 - \frac{a^2\alpha^2}{2}}$, with $0 \leq \alpha a \leq 1$. This solution has many similarities with the Kerr-Newman BH. For instance, the causal structure for the non-extreme BH, i.e., $0 < a^2\alpha^2 < \frac{2}{3} - \frac{128}{81} \frac{Q^6}{M^4(1 - \frac{1}{4}a^2\alpha^2)^3}$, is given by the Penrose diagram of figure 7, with $r = 0$ being now a polynomial singularity. However, unlike the Kerr-Newman BH, the topology of the horizon is cylindrical or toroidal, rather than spherical, violating Hawking's theorem [47] due to the presence of a negative Λ . It also has implications on the hoop conjecture [48]: gravitational collapse in such a background can generate a black string even if one is not able to pass a hoop of given circumference through the matter. If there is no charge then the causal structure changes drastically, resembling the Schwarzschild-ADS BH rather than the Kerr BH [26].

The 3D BH generated through dimensional reduction of 4D general relativity, has a dilaton in addition to the metric and Maxwell fields. A study to put these black solutions in a supersymmetric context is being carried [49]. Generalizations of the 3D action to a Brans-Dicke type of action, given by $S = \frac{1}{2\pi} \int d^3x \sqrt{-g} e^{-2\phi} (R + 4\omega(\nabla\phi)^2 - 2\Lambda)$ also yield static and stationary BH solutions [50, 51]. Using a metric with two Killing vectors, one can find black membranes in general relativity, related through dimensional reduction to 2D dilatonic BHs. This is a matter for the end of the next section.

4. BHs in 2D

To analyse BHs in 2D we first return to string theory. In 2D there is less freedom for dynamics, for obvious reasons. For instance, for a compact orientable 2D manifold of genus g (e.g., sphere $g = 0$, torus $g = 1$, etc), the Einstein-Hilbert action, $\frac{1}{2\pi} \int d^2x \sqrt{-g} R = 2(1 - g)$, is the Euler characteristic of space, a topological invariant with no dynamics. Therefore, if one wants to go further in 2D one has to find a different action. An interesting action is provided by string theory. For understanding the appearance of BHs in 2D string theory is now important to introduce some basic concepts of the theory itself. In string theory one has to distinguish the world-sheet action for the string from the target-space or spacetime action for the usual spacetime fields. The latter follows from the former upon imposing certain restrictions related to renormalization procedures. (In particle theory there is also such a distinction but the respective actions are not inter-related a priori.) The propagation of strings in a generic curved spacetime is described by the Polyakov action

$$S = \frac{1}{4\pi\alpha'} \int d^2\sigma \sqrt{h} h^{\alpha\beta} \nabla_\alpha x^\mu \nabla_\beta x^\nu g_{\mu\nu} \quad (18)$$

where $h^{\alpha\beta}$ is the world-sheet metric of the string, x^μ are the spacetime (or target-space) coordinates, $g_{\mu\nu}$ is the metric of the background, and α' is the string coupling constant (see figure 8). Such an action is also called a non-linear sigma model. It is invariant under reparametrizations of the string world-sheet $\sigma \rightarrow \sigma'$ and moreover, is conformal invariant (i.e, local scale invariant), $h_{\alpha\beta} \rightarrow \Omega^2 h_{\alpha\beta}$. In principle, one should also include in the action, besides the graviton, the other massless states or fields of the (closed) bosonic string, namely, the antisymmetric tensor $B_{\mu\nu}$ and the dilaton ϕ (see [22] also for the inclusion of fermionic fields and supersymmetry). The bosonic world-sheet action or σ -model is then,

$$S = \frac{1}{4\pi\alpha'} \int d^2\sigma \sqrt{h} h^{\alpha\beta} \nabla_\alpha x^\mu \nabla_\beta x^\nu g_{\mu\nu}(x) - \frac{1}{4\pi\alpha'} \int d^2\sigma \epsilon^{\alpha\beta} \nabla_\alpha x^\mu \nabla_\beta x^\nu B_{\mu\nu}(x) + \frac{1}{4\pi} \int d^2\sigma \sqrt{h} R_\alpha \phi(x), \quad (19)$$

where R_α is the curvature of $h^{\alpha\beta}$. Imposing Weyl invariance at the 1-loop level to get rid of the ultraviolet divergences translates into the requirement that the so called beta-functions associated with the background fields vanish. The beta-function associated to the metric $g_{\mu\nu}$ is $\beta_{\mu\nu}^g = R_{\mu\nu} - \frac{1}{4} H_\mu^{\lambda\sigma} H_{\nu\lambda\sigma} + 2\nabla_\mu \nabla_\nu$ which should be set to zero. The 3-form H is related to B through $H_{\mu\nu\lambda} = \nabla_\mu B_{\nu\lambda} + \nabla_\nu B_{\lambda\mu} + \nabla_\lambda B_{\mu\nu}$. The other β -functions are $\beta_{\mu\nu}^B = \nabla_\lambda H_{\mu\nu}^\lambda - 2(\nabla_\lambda \phi H^\lambda_{\mu\nu}) = 0$, $\beta^\phi = R + 2\Lambda + 4\nabla^2 \phi - 4(\nabla\phi)^2 - \frac{1}{12} H^2 = 0$. The constant Λ is connected to the dimension of spacetime. For the bosonic string $\Lambda = \frac{D-26}{6\alpha'}$, whereas for the supersymmetric string with fermions $\Lambda \propto (D - 10)$. The dimensions $D = 26, 10$ are the critical dimensions for the bosonic and supersymmetric strings, respectively, because in these dimensions the theory is free from divergences and anomalies. However, one can go away from these dimensions to the more familiar 2, 3 or 4, by considering additional internal conformal field theories with central charges to complete, so to speak, the other extra dimensions.

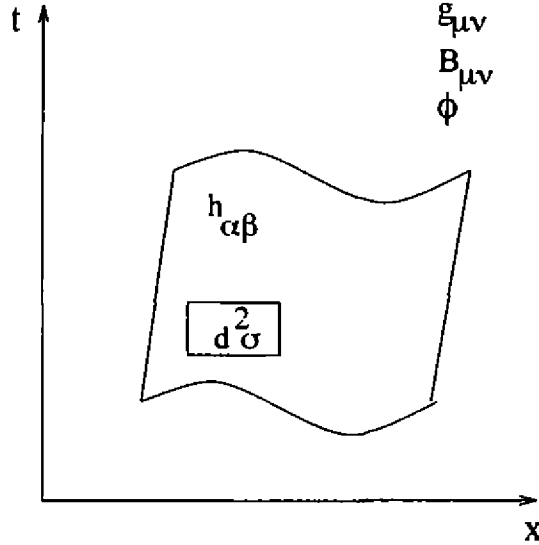


Figure 8. Spacetime diagram showing the nomenclature for the propagation of strings.

The equations for the three β -functions are the field equations of first order string theory, which can be derived from a spacetime effective action given by

$$S_{\text{eff}} = \frac{1}{4\pi} \int d^D x \sqrt{-g} e^{-2\phi} \left(R - 2\Lambda + 4(\nabla\phi)^2 + \frac{1}{12} H^2 \right). \quad (20)$$

The Maxwell field $F_{\mu\nu}$ has been left out in this discussion (compare (20) and (4)), as well as other fields like the tachyon T of the bosonic string, but they can be included consistently. Putting $D = 2$ and $H = 0$ in the equations of motion derived from (20) one finds a 2D BH solution in [52] given by

$$ds^2 = -(1 - e^{-2\lambda r}) dt^2 + \frac{dr^2}{1 - e^{-2\lambda r}}, \quad e^{-2\phi} = e^{-\lambda r}, \quad (21)$$

where $\lambda^2 \equiv -\frac{\Lambda}{2}$. This solution has horizons at $r_+ = 0$ and a singularity at $r = -\infty$. The Penrose diagram is identical to the Schwarzschild diagram in figure 1. Since this is a solution of the low-energy action it is only valid as long as the curvature is small compared to the Planck curvature. Is there a way to find an exact solution of the full action, i.e., of the world-sheet action, without resorting to perturbation theory? Yes, and the idea was initiated in [53]. One starts with the Wess-Zumino-Novikov-Witten (WZNW) model described by the action

$$S_{\text{WZNW}}[g] = \frac{k}{8\pi} \int d^2\sigma \sqrt{h} h^{\alpha\beta} \text{tr} (\nabla_\alpha g^{-1} \nabla_\beta g) + ik\Gamma(g), \quad (22)$$

where g is an element of some group, function of a field x^μ , k is a real and positive number (called the level of the Kac-Moody algebra) and the last term is the Wess-Zumino term which guarantees conformal invariance of the action and for the purposes used here is of no importance. The motivation for this model comes from the need to simplify the background in order to find solutions. One good simplification is to assume string propagation in a group manifold of a Lie group G with elements g . Note the analogy of (22) with the world-sheet action (18), where the trace has the role of a metric. Now, if one supposes that $g \in SL(2, R)/U(1)$ one can parametrize it by

$$\begin{pmatrix} a & u \\ -v & b \end{pmatrix} \quad (23)$$

with $ab + uv = 1$. Since $SL(2, R)$ has dimension 3, and $U(1)$ has dimension 1, the quotient space group manifold $SL(2, R)/U(1)$ has dimension 2, which, in turn, can be parametrized by the coordinates u, v . After imposing that the action (22) is gauge invariant and solving the equations of motion one finds [53]

$$S_{\text{WZNW}}[g] = -\frac{k}{4\pi} \int d^2\sigma \sqrt{h} h^{\alpha\beta} \frac{\nabla_\alpha u \nabla_\beta v}{1 - uv}. \quad (24)$$

Comparing with the world-sheet action (18) one immediately finds that the target space metric is

$$ds^2 = \frac{dudv}{1-uv}, \quad (25)$$

which upon further coordinate transformation can be put in the form (21). The dilaton can also be made to enter in this picture, see [53]. Since one has to solve the classical equations of motion this treatment is semiclassical. The full treatment was attempted in [54] where it was found without approximations that the metric and dilaton are given by

$$ds^2 = 2(k-1) \left[- \left(\frac{x+1}{x-1} - \frac{2}{k} \right)^2 dt^2 + \frac{dx^2}{4(x^2-1)} \right] \\ e^{-2\phi} = \frac{x^2-1}{\left(\frac{x+1}{x-1} - \frac{2}{k} \right)^2}, \quad (26)$$

where x is a new radial coordinate. In the semiclassical approximation, when $k \rightarrow \infty$ one recovers Witten's result. The causal structure is given in figure 9 [55], the novel feature being that in the exact solution of the full theory the BH has no singularities! This indicates that string theory has indeed new things to show at the singularities.

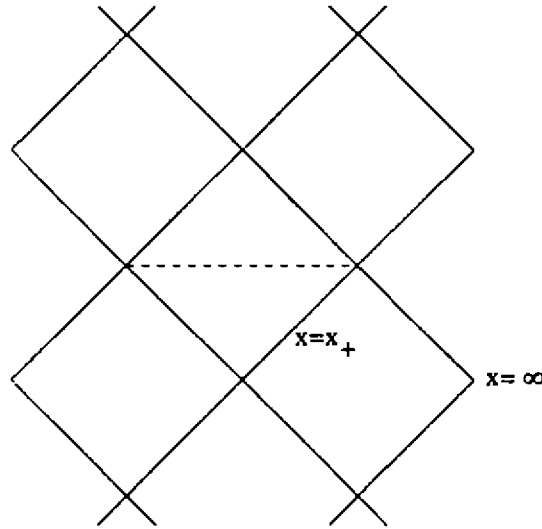


Figure 9. Penrose diagram for the non-singular 2D BH in string theory.

Having this exact solution and using the tools of string theory, namely, conformal field theory, one can in principle know how strings propagate in the BH background, calculate the latest stages of the BH evaporation and solve the information paradox. However, in practice the problem is still out of reach [56]. Extensions to 4D of the idea of using a WZNW model to find exact solutions with associated conformal field theories have been tried with some interesting but limited progress [57].

We have just seen that the dilaton gives non-trivial dynamics to 2D. This has been known since the works of Teitelboim [58] and Jackiw [59] where the power of 2D theories was first understood. They proposed the theory

$$S = \frac{1}{2\pi} \int d^2x \sqrt{-g} e^{-2\phi} (R - 2\Lambda), \quad (27)$$

with $\Lambda < 0$. Although spacetime has constant and negative curvature it is possible to find a BH solution which is asymptotically ADS [60, 61, 62]. The thermodynamics of this BH has been studied (see this volume [63] and [64]).

In trying to find meaningful 2D actions one can look for connections with 4D general relativity, as it was done for 3D theories (see last section). Starting with the Einstein-Hilbert action $S = \frac{1}{16\pi} \int d^4x \sqrt{-g} (R - 2\Lambda)$ and imposing planar symmetry (two-killing vectors), with a metric given by $ds^2 = g_{ab} dx^a dx^b + e^{-2\phi} (dx^2 + dy^2)$, one finds upon dimensional reduction the following 2D action [27]

$$S = \frac{1}{2\pi} \int d^2x \sqrt{-g} e^{-2\phi} (R + 2(\nabla\phi)^2 - 2\Lambda). \quad (28)$$

This theory also possesses a BH which, when reinterpreted in 4D yields a black membrane in general relativity [27]. An obvious generalization of these three 2D theories is given by the Brans-Dicke action [65]

$$S = \frac{1}{2\pi} \int d^2x \sqrt{-g} e^{-2\phi} (R + 4\omega(\nabla\phi)^2 - 2\Lambda), \quad (29)$$

where ω is a free parameter, and $\omega = -1, -\frac{1}{2}, 0$ corresponding to string theory, planar general relativity and the Teitelboim-Jackiw theory, respectively. When $\omega \rightarrow \infty$ one obtains the 2D analogue of general relativity [66], also called the $R = T$ theory [67]. The BH in this case is a massless BH as has been shown in [65]. The BHs of action (28) for all rational ω s have been analysed in detail in [65] and the quantum version in [68]. What about the temperature of these BHs? Usually the temperature goes with some power of the mass M , $T \propto M^\gamma$, where for instance for $\omega = 0$, $\gamma = \frac{1}{2}$ [63, 64]. Thus, these 2D theories cannot tell much about the latest stages of the BH evaporation. A notable exception is string theory ($\omega = -1$) for which $\gamma = 0$ and $T \propto \text{constant}$, independent of the mass. Thus, following this result, the BH radiates indefinitely, which cannot be correct. In order to remedy the situation one has to make a full quantum treatment of the backreaction (see e.g. [69, 70]).

5. BHs in higher D

We have been considering BHs in general relativity, Brans-Dicke and string theories in 4 and lower dimensions. However, higher dimensional BHs are also important to study since they may shed some light on the understanding of non-perturbative effects in quantum gravity (such as the compactification scheme), as well as expose which of the features of the usual four-dimensional BH solutions remain in higher dimensions. Let us then go on to higher dimensions and consider, for a change, the original Kaluza-Klein theory in 5D. This is simply 5D general relativity in which the fifth dimension is a Killing direction, i.e., the fields are independent of the 5th dimension, x^5 , say. The theory has two descriptions, the first given by the action

$$S = \frac{1}{16\pi} \int d^5x \sqrt{-g} R, \quad (30)$$

and metric components $g_{\mu\nu}^{(5)}$, $g_{\mu 5}^{(5)}$ and $g_{55}^{(5)}$, $\mu, \nu = 0, 1, 2, 3$. In the other description the action takes the form

$$S = \frac{1}{16\pi} \int d^4x \sqrt{-g} \left(R - 2(\nabla\phi)^2 - e^{2\sqrt{3}\phi} F^2 \right), \quad (31)$$

with the 5D metric related to the 4D fields by the usual Kaluza-Klein ansatz, $g_{\mu\nu}^{(5)} = e^{\frac{2\phi}{\sqrt{3}}} \left(g_{\mu\nu}^{(4)} + e^{-2\sqrt{3}\phi} A_\mu A_\nu \right)$, $g_{\mu 5}^{(5)} = e^{-\frac{4\phi}{\sqrt{3}}} A_\mu$, and $g_{55}^{(5)} = e^{-\frac{8\phi}{\sqrt{3}}}$. Due to this connection, one can generate with little effort static non-vacuum solutions from static vacuum solutions. Given a static vacuum 4D metric one can take its product with the real line R , 4D solution $\times R$, to obtain a 5D solution with two symmetry directions (t, x^5). If one boosts this 5D solution in the 5th direction it still satisfies the 5D equations. However, when reinterpreted in 4D one obtains a solution with non-zero Maxwell and dilaton fields. In other words, given a 4D metric $g_{\mu\nu}$ one obtains a new solution $(\tilde{g}_{\mu\nu}, \tilde{A}_\mu, \tilde{\phi})$ given by the transformations,

$$\begin{aligned} \tilde{g}_{tt} &= \frac{g_{tt}}{(\cosh^2 \alpha + g_{tt} \sinh^2 \alpha)^{\frac{1}{2}}}, \\ \tilde{g}_{ij} &= g_{ij} (\cosh^2 \alpha + g_{tt} \sinh^2 \alpha)^{\frac{1}{2}}, \\ \tilde{A}_t &= \frac{1 + g_{tt} \sinh 2\alpha}{2(\cosh^2 \alpha + g_{tt} \sinh^2 \alpha)}, \\ e^{-\frac{4\tilde{\phi}}{\sqrt{3}}} &= \cosh^2 \alpha + g_{tt} \sinh^2 \alpha \end{aligned} \quad (32)$$

where α is the boost parameter and $i, j = 1, 2, 3$. Example: given the Schwarzschild solution (2) one obtains after performing the above transformations, the following [71, 72, 73]

$$\begin{aligned} ds^2 &= -\frac{1 - \frac{r_-}{r}}{\sqrt{1 - \frac{r_-}{r}}} dt^2 + \frac{dr^2}{(1 - \frac{r_+}{r})(1 - \frac{r_-}{r})} + r^2 \left(1 - \frac{r_-}{r} \right) d\Omega_2^2, \\ A_t &= \frac{\sqrt{r_+ r_-}}{r}, \quad e^{-\frac{4\tilde{\phi}}{\sqrt{3}}} = 1 - \frac{r_-}{r}, \end{aligned} \quad (33)$$

where we have redefined the Schwarzschild radial coordinate (r_S , say) in (2) to $r_S = r(1 - \frac{r_-}{r})$, and put $r_- = 2m \sinh^2 \alpha$, $r_+ = 2m \cosh^2 \alpha$, m being the Schwarzschild mass. The ADM mass and electric charge are $M = m \sinh 2\alpha$, $Q = m \cosh 2\alpha$, respectively. There are horizons at $r = r_{\pm}$ and the singularity is at $r = 0$. Another type of transformation, called Harrison transformation [74], transforms metrics within general relativity, taking for instance, the Schwarzschild metric into the Reissner-Nordstrom metric. Now, in string theory there is the analogue of these boost transformed solutions. In a simple case, one starts with a static solution $(g_{\mu\nu}, \phi)$, with $B_{\mu\nu} = 0$ and $A_{\mu} = 0$. Then one gets a new solution $(\tilde{g}_{\mu\nu}, \tilde{A}_{\mu}, \tilde{\phi})$ by making the following transformations [75]

$$\begin{aligned}\tilde{g}_{tt} &= \frac{g_{tt}}{(\cosh^2 \alpha + g_{tt} \sinh^2 \alpha)^2}, \\ \tilde{A}_t &= \frac{1 + g_{tt} \sinh 2\alpha}{2\sqrt{2}(\cosh^2 \alpha + g_{tt} \sinh^2 \alpha)}, \\ e^{-2\tilde{\phi}} &= e^{-2\phi} \cosh^2 \alpha + g_{tt} \sinh^2 \alpha.\end{aligned}\quad (34)$$

Recalling that the Schwarzschild solution (2) is a solution of string theory, one can apply (34) to obtain the electric charged BHs given in equation (7). But we are still discussing 4D BHs.

To obtain charged BHs in higher D , one starts with a D -dimensional uncharged BH [23],

$$ds^2 = -\left(1 - \frac{cm}{r^n}\right)dt^2 + \frac{dr^2}{1 - \frac{cm}{r^n}} + r^2 d\Omega_{n+1}^2, \quad (35)$$

where $n = D - 3$ and c is a constant. This is a solution of both D -dimensional general relativity and string theory. By using the transforming equations (34) one can obtain the D -dimensional electrically charged BHs in string theory [31],

$$\begin{aligned}ds^2 &= -\left(1 - \frac{cm}{r^n}\right) \left(1 + \frac{cm \sinh^2 \alpha}{r^n}\right) dt^2 + \frac{dr^2}{1 - \frac{cm}{r^n}} + r^2 d\Omega_{n+1}^2, \\ A_t &= -\frac{cm \sinh 2\alpha}{2\sqrt{2}(r^n + cm \sinh^2 \alpha)}, \\ e^{-2\phi} &= 1 + \frac{cm}{r^n} \sinh^2 \alpha.\end{aligned}\quad (36)$$

The ADM mass and charge are given by $M = m(1 + \frac{2n}{n+1} \sinh^2 \alpha)$ and $Q = \frac{cmn \sinh 2\alpha}{\sqrt{2}}$. The event horizons are at $r = (cm)^{\frac{1}{n}}$, and the singularities at $r = 0$. In contrast with 4D we have that in the extremal limit the singularity is timelike rather than null, and the temperature of the extreme BH is zero. There are no higher D magnetically charged BHs because there are no Maxwell magnetic charges (one cannot integrate a 2-form F over a $D - 2$ sphere). However, using a magnetic charge associated with the 3-form field H , one can find magnetically charged BH solutions in string theory [76].

From BHs in D -dimensions one can find straightforwardly black strings in $(D + 1)$ -dimensions. It is only necessary to take the product of the BH with R [76],

$$ds^2 = -\left(1 - \frac{cm}{r^n}\right)dt^2 + \frac{dr^2}{1 - \frac{cm}{r^n}} + r^2 d\Omega_{n+1}^2 + dx^2. \quad (37)$$

If one takes the product of the BH with R^2 , R^3 , R^p , one obtains a black membrane, a black 3-brane, and a black p -brane. These branes are simple products. For instance, to get a black string that is not a simple product one performs, after Lorentz boosting to get charge, a T-duality transformation on the simple product black string to obtain

$$\begin{aligned}ds^2 &= -\frac{\left(1 - \frac{cm}{r^n}\right)}{\left(1 + \frac{cm \sinh^2 \alpha}{r^n}\right)} dt^2 + \frac{dr^2}{1 - \frac{cm}{r^n}} + r^2 d\Omega_{n+1}^2 + \frac{dx^2}{1 + \frac{cm \sinh^2 \alpha}{r^n}}, \\ B_{xt} &= -\frac{cm \sinh 2\alpha}{2(r^n + cm \sinh^2 \alpha)}, \\ e^{-2\phi} &= 1 + \frac{cm}{r^n} \sinh^2 \alpha.\end{aligned}\quad (38)$$

The causal structure is identical to Schwarzschild. In the extremal limit the metric field is given by

$$ds^2 = \frac{-dt^2 + dx^2}{1 + \frac{cm}{r^n}} + dr^2 + r^2 d\Omega_{n+1}^2. \quad (39)$$

where \bar{c} is a redefinition of c . There are two novel features in this solution (39): (i) an extra symmetry has appeared, the metric is now boost-invariant in the (x, t) plane, and (ii) the solution is the same solution found in [77] for a straight fundamental macroscopic string. These objects appear as stable extended sates of closed-string theories and are distinct from the cosmic strings of string theory. This means that fundamental strings are extreme black strings. There is no such analogue in general relativity. The electron, a fundamental particle is not an extreme BH.

Ultimately, one would like to get a BII solution of $10D$ string theory, suitably dimensionally reduced to $4D$. One starts with the $10D$ action

$$S = \frac{1}{16\pi} \int d^{10}x \sqrt{-G} \left[R_G + \nabla_M \Phi \nabla^M \Phi - \frac{1}{12} H^2 - \frac{1}{4} F^I{}^2 \right] \quad (40)$$

where $H^2 = H_{MNP} H^{MNP}$, $F^I{}^2 = F_{MN}^I F^{IMN}$, capital letters denote $10D$ fields and indices, and I is an internal index. Through a Kaluza-Klein reduction to $4D$, one can find an effective $4D$ action, with the other dimensions compactified on a six torus. One writes the ansatz,

$$G_{MN} = \begin{pmatrix} e^{2\phi} g_{\mu\nu} + G_{mn} A_\mu^m A_n^n & A_\mu^m G_{mn} \\ A_\nu^n G_{mn} & G_{mn} \end{pmatrix} \quad (41)$$

with the $4D$ spacetime indices $\mu\nu = 0, 1, 2, 3$, $m, n = 1, \dots, 6$, and ϕ and A are the $4D$ dilaton and Kaluza-Klein $U(1)$ fields, respectively. The action (39) then turns into

$$S = \frac{1}{16\pi} \int d^4x \sqrt{-g} \left(R - \frac{1}{2} \nabla_\mu \phi \nabla^\mu \phi - \frac{1}{2} e^{2\phi} \nabla_\mu \psi \nabla^\mu \psi - \frac{1}{4} e^{-\phi} F_{\mu\nu} F^{\mu\nu} + \frac{1}{8} \text{tr}(\nabla_\mu M \nabla^\mu M) \right), \quad (42)$$

where M is a $O(6, 22)$ matrix of the scalar (moduli) fields appearing in the reduction process and ψ is the axion related to $H_{\mu\nu\lambda}$ by $H_{\mu\nu\lambda} = \frac{e^{2\phi}}{\sqrt{-g}} \epsilon^{\mu\nu\lambda\rho} \nabla_\rho \psi$, see [78] for all details. This is quite complicated to solve, but applying a generalized boosting procedure and using all the symmetries it is possible to find the most general BH solution with all charges [78]. An important consequence brought from this $4D$ analysis is that the extreme BH solutions correspond to massive excitations of $4D$ superstrings, suggesting that BHs are simple string states [79] and confirming the idea that elementary particles (represented here by those string states) might behave like BHs. These BHs saturate the Bogomolnyi-Prasad-Somerfield bound of the underlying supersymmetric theory and are called extreme BPS BHs.

There are also studies on black p -branes in string theory (e.g. [80]) motivated by their importance in the non-perturbative dynamics of the $11D$ M-theory [19], a theory not explicitly formulated, but known to agglutinate the four consistent (heterotic, type I, type IIA and B) superstring theories.

We have been presenting higher dimensional BH solutions in Kaluza-Klein theory, string theory and general relativity. Yet, although pure general relativity can be formulated in other dimensions, when one goes to dimensions higher than four it is not anymore unique. The natural generalization is given by the Lovelock action [81] so that the field equations for the metric remain of second order. The theory can also be considered as a dimensional continuation of the Euler densities of lower dimensions [82, 83, 84]. In four dimensions one has to take in consideration two Euler densities. The Euler density of the 0 -dimensional space which is proportional to $\sqrt{-g}$, and the Euler density of the 2 -dimensional space, proportional to $\sqrt{-g}R$, where g is the determinant of the metric and R the Ricci curvature scalar. Thus Lovelock gravity in four dimensions reduces to Einstein gravity, with action $\frac{1}{16\pi G} \int d^4x \sqrt{-g} (-2\Lambda + R)$. A similar construction and action is obtained for three dimensions. In six dimensions one has still to add the Euler characteristic of four dimensional space, i.e. the Gauss-Bonnet term, to have the Lanczos action, given by, $\frac{1}{16\pi G} \int d^6x \sqrt{-g} (-2\Lambda + R + \alpha_2 (R_{\alpha\beta\gamma\sigma} R^{\alpha\beta\gamma\sigma} - 4R_{\alpha\beta} R^{\alpha\beta} + R^2))$, where α_2 is a new constant. A similar construction and action can be obtained for five dimensions. For each two new dimensions there exists a new constant α_p . These constants do not seem to have a direct physical meaning. In order to find a meaningful set of constants in any dimension D , it was proposed in [85, 86] a method which restricts drastically the number of independent constants to two, G and Λ , thus yielding a restricted Lovelock gravity. This method separates, in a natural manner, theories in even dimensions ($D = 2n$, with $n = 1, 2, \dots$) from theories in odd dimensions ($D = 2n + 1$). The BII solutions are given by [86]

$$ds^2 = - \left[1 - \left(\frac{2sM}{r^p} + q \right)^{\frac{1}{n-1}} + \left(\frac{r}{l} \right)^2 \right] dt^2 + \frac{dr^2}{1 - \left(\frac{2sM}{r^p} + q \right)^{\frac{1}{n-1}} + \left(\frac{r}{l} \right)^2} + r^2 d\Omega_{D-2}^2, \quad (43)$$

where for odd D one puts ($s = \frac{1}{2}, p = 0, q = 1$), and for even D one has ($s = 1, p = 1, q = 0$). There are horizons at $r = r_+$ given by the zeros of g^{rr} and the singularity is at $r = 0$. Note that there is no restriction in the dimension of spacetime, it can be any natural number from 3 to ∞ . Since in general relativity BHs appear as the final state of gravitational collapse it is important to know if the BH solutions found in Lovelock gravity can, in an analogous manner, form from gravitational collapse. It was shown that, indeed, Lovelock BHs form from regular initial data [87]. The collapsing matter is modelled by a Friedmann type metric, and the solution can be viewed as a dimensional continued Oppenheimer-Snyder gravitational collapse. A possible scenario for the occurrence of this collapse in D dimensions, would be in the very early universe, before the $(D - 4)$ extra dimensions have been compactified. In turn, these newly formed higher dimensional BHs could play a role in the compactification process. It is interesting to note that these BH and collapsing solutions show that some important features of classical general relativity are preserved and carried into Lovelock gravity in any dimension.

5. Conclusions

We have investigated BH, black string and black membrane solutions in several dimensions and in several theories (general relativity, Kaluza-Klein, Brans-Dicke, Lovelock gravity and string theory). We have seen that new properties come into play. For instance, in string theory there are BHs without singularities. It was also shown that the existence of a negative cosmological term can be important in producing black solutions, as was the case of black strings in 4D general relativity. We have also seen that some features appearing in general relativity remain in other theories, like in Lovelock gravity, where the BHs also form from gravitational collapse of matter. Other important developments not discussed here are solutions of BHs with both electric and magnetic charges, rotating BHs, and multi-BH solutions in the various theories, to name a few.

With such a profusion of BHs in all these gravity theories, one could hope to understand in some detail the BH evaporation process, at least, in one of those solutions. However, the problem of calculating Hawking radiation of BHs, black strings and black membranes, through the latest stages of the evaporation process, remains.

A remarkable property of BHs is that they appear in all scales, from the Planck length to astronomical dimensions. This seems to be unique. Electrons, molecules, stars and galaxies have well defined scales, BHs do not.

Acknowledgements – I thank Paulo Sá and Vilson Zanichin for collaborations and conversations. I also thank Antares Kleber for reading the manuscript carefully.

References

- [1] J. R. Oppenheimer, H. Snyder, *Phys. Rev.* **56**, 455 (1939).
- [2] W. Baade, F. Zwicky, *Phys. Rev.* **45**, 138 (1934).
- [3] A. Einstein, *Ann. Math. (Princeton)* **40**, 922, (1939).
- [4] J. Michell, *Phil. Trans. R. Soc. (London)* **74**, 35 (1784).
- [5] P. S. Laplace, *Exposition du Système du Monde* (J. B. M. Duprat, Paris, 1796).
- [6] R. Penrose, *Riv. Nuovo Cimento* **1**, 252 (1969).
- [7] J. P. S. Lemos, *Phys. Rev. Lett.*, **68**, 1447 (1992).
- [8] P. S. Joshi, *Global Aspects in Gravitation and Cosmology*, (Clarendon Press, Oxford, 1993).
- [9] J. P. S. Lemos, in *Proceedings of the XXIVth Annual Meeting of the Sociedade Astronômica Brasileira (August 1995)*, eds. F. Jablonski, F. Elizalde, L. Sodré Jr., V. Jatenco-Pereira, (IAG 1996), p. 57.
- [10] D. Lynden-bell, *Nature* **223**, 690 (1969).
- [11] R. Penrose, *Phys. Rev. Lett.* **14** (1965) 57.
- [12] S. W. Hawking, *Nature* **248**, 30 (1974).
- [13] S. W. Hawking, *Phys. Rev. D* **13**, 191 (1976).
- [14] A. Strominger, *Phys. Rev. Lett.* **77** (1996) 3498.
- [15] S. Coleman, J. Preskill, F. Wilczek, *Nucl. Phys.* **B378**, 175 (1992).
- [16] B. Carter, *Phys. Rev. Lett.* **33**, 558 (1974).
- [17] G. Gibbons, C. M. Hull, *Phys. Lett.* **B109**, 190 (1982).

- [18] S. W. Hawking, *Mon. Not. R. astr. Soc.* **152**, 75 (1971).
- [19] P. K. Townsend, *M-Theory for mortals*, Lectures delivered at the XVIIth UK Institute for Theoretical High Energy Physicists (1996).
- [20] E. Witten, *Nucl. Phys.* **B443**, 85 (1995).
- [21] C. Vafa, hep-th/9602022.
- [22] M. B. Green, J. H. Schwarz, E. Witten, *Superstring theory*. (Cambridge University Press, Cambridge 1987).
- [23] F. R. Tangherlini, *Il Nuovo Cim.* **XXVII**, 636 (1963).
- [24] S. W. Hawking, *Comm. Math. Phys.* **43**, 149 (1975).
- [25] S. W. Hawking, in *General Relativity*, eds. S. W. Hawking, W. Israel (Cambridge University Press, Cambridge 1979).
- [26] J. P. S. Lemos, *Phys. Lett. B* **352**, 46 (1995).
- [27] J. P. S. Lemos, *Class. Quantum Gravity* **12**, 1081 (1995).
- [28] G. Horowitz, *Proceedings of The 1992 Trieste Spring School on String Theory and Quantum Gravity*, (World Scientific, Singapore 1993), hep-th/921019.
- [29] P. T. Chrusciel, *Contemporary Mathematics - AMS* **170**, 23 (1994).
- [30] G. Gibbons, *Nucl. Phys.* **B207**, 337 (1982).
- [31] G. Gibbons, K. Maeda, *Nucl. Phys.* **B208**, 741 (1988).
- [32] D. Garfinkle, G. Horowitz, A. Strominger, *Phys. Rev. D* **43**, 3140 (1991); **45**, 3888(E) (1992).
- [33] A. Sen, *Phys. Rev. Lett.* **69**, (1992).
- [34] S. Deser, R. Jackiw, G. 't Hooft, *Ann. Phys.* **152**, 220 (1984).
- [35] A. Achúcarro, P. K. Townsend, *Phys. Lett.* **B180**, 89 (1988).
- [36] E. Witten, *Nucl. Phys.* **B311**, 46 (1988).
- [37] M. Bañados, C. Teitelboim and J. Zanelli, *Phys. Rev. Lett.* **69**, 1849 (1992).
- [38] M. Bañados, M. Henneaux, C. Teitelboim and J. Zanelli, *Phys. Rev. D* **48**, 1506 (1993).
- [39] S. Carlip, *Class. Quantum Grav.* **12**, 2853 (1995).
- [40] O. Coussaert, M. Henneaux, *Phys. Rev. Lett.* **72**, 183 (1994).
- [41] R. B. Mann, S. F. Ross, *Phys. Rev. D* **47**, 3319 (1993).
- [42] G. T. Horowitz, D. L. Welch, *Phys. Rev. Lett.* **71**, 328 (1993).
- [43] N. Kaloper, *Phys. Rev. D* **48** (1993) 2598.
- [44] N. Kaloper, *Phys. Rev. D* **48** (1993) 4658.
- [45] J. P. S. Lemos, V. T. Zanchin, *Phys. Rev. D* **53**, 4684 (1996).
- [46] J. P. S. Lemos, V. T. Zanchin, *Phys. Rev. D* **54**, 3840 (1996).
- [47] S. W. Hawking, G. F. R. Ellis, *The Large Scale Structure of Space-Time*, (Cambridge University Press, Cambridge, 1973).
- [48] K. S. Thorne, in *Magic without Magic*, ed. J. R. Klauder, (Freeman and Company, San Francisco 1972), p. 231.
- [49] J. P. S. Lemos, P. V. Moniz, "Supersymmetry of the black strings", in preparation.
- [50] P. M. Sá, A. Kleber, J. P. S. Lemos, *Class. Quantum Grav.* **13**, 125 (1996).
- [51] P. M. Sá, J. P. S. Lemos, hep-th/9503089.
- [52] G. Mandal, A. M. Sengupta, S. R. Wadia, *Mod. Phys. Lett. A* **6**, 1685 (1991).
- [53] E. Witten, *Phys. Rev. D* **44**, 314 (1991).
- [54] R. Dijkgraaf, H. Verlinde, E. Verlinde, *Nucl. Phys.* **B371**, 269 (1992).
- [55] M. J. Perry, E. Teo, *Phys. Rev. Lett.* **70**, 2669 (1993).
- [56] K. Becker, *Strings, Black Holes and Conformal Field Theory*, (PhD thesis, University of Bonn 1994), hep-th/9404157.
- [57] C. V. Johnson, R. C. Myers, *Phys. Rev. D* **52**, 2294 (1995).
- [58] C. Teitelboim, in *Quantum Theory of Gravity*, ed. S. M. Christensen (Hilger, Bristol, 1984).
- [59] R. Jackiw, in *Quantum Theory of Gravity*, ed. S. M. Christensen (Hilger, Bristol, 1984).
- [60] J. P. S. Lemos, P. M. Sá, *Mod. Phys. Lett. A* **9**, 771 (1994).
- [61] M. Cadoni, S. Mignemi, *Phys. Rev. D* **51**, 4139 (1995).

- [62] A. Achúcarro, M. E. Ortiz, *Phys. Rev. D* **48**, 3600 (1993).
- [63] J. P. S. Lemos, "Comparative study between the thermodynamics of the 2-dimensional black hole in the Teitelboim-Jackiw theory and the 4-dimensional Schwarzschild black hole", this volume.
- [64] J. P. S. Lemos, *Phys. Rev. D* **54**, 6206 (1996).
- [65] J. P. S. Lemos, P. M. Sá, *Phys. Rev. D* **49**, 2897 (1994).
- [66] J. P. S. Lemos, Paulo Sá, *Class. Quantum Gravity* **11**, L11 (1994).
- [67] R. B. Mann, S. F. Ross, *Phys. Rev. D* **47**, 3312 (1993).
- [68] J. D. Hayward, hep-th/9508090.
- [69] C. G. Callan, S. B. Giddings, J. A. Harvey, A. Strominger, *Phys. Rev. D* **45**, R1005 (1992).
- [70] S. W. Hawking, *Phys. Rev. Lett.* **69**, 406 (1992).
- [71] P. Dobiasch, D. Maison, *Gen. Rel. Grav.* **14**, 231 (1982).
- [72] A. Chodos, S. Detweiler, *Gen. Rel. Grav.* **14**, 870 (1982)
- [73] G. Gibbons, D. Wiltshire, *Ann. Phys.* **167**, 201 (1986); **176**, 393(E) (1987).
- [74] B. Harrison, *J. Math. Phys.* **9**, 1744 (1968).
- [75] S. Hassan, A. Sen, *Nucl. Phys.* **B375**, 103 (1992).
- [76] G. Horowitz, A. Strominger, *Nucl. Phys.* **B360**, 197 (1991).
- [77] A. Dabholkar, G. Gibbons, J. A. Harvey, F. Ruiz Ruiz, *Nucl. Phys.* **B340**, 33 (1990).
- [78] M. Cvetic, D. Youm, *Nucl. Phys.* **B472**, 249 (1996).
- [79] M. J. Duff, R. R. Khuri, R. Minasian, J. Rahmfeld, *Nucl. Phys.* **B418**, 195 (1994).
- [80] J. M. Maldacena, *Black Holes in String Theory*, (PhD thesis, University of Princeton 1996), hep-th/9607235.
- [81] D. Lovelock, *J. Math. Phys.* **12**, 498 (1971).
- [82] T. Regge, *Phys. Rep.* **137**, 31 (1986).
- [83] B. Zumino, *Phys. Rep.* **137**, 109 (1986).
- [84] C. Teitelboim, J. Zanelli, in *Constraint Theory and Relativistic Dynamics*, eds. G. Longhi, L. Lussana, (World Scientific, Singapore 1987).
- [85] M. Bañados, C. Teitelboim, J. Zanelli, in *J. J. Giambiagi Festschrift*, edited by H. Falomir, R. Gamboa, P. Leal, F. Schasposnik (World Scientific, Singapore 1991).
- [86] M. Bañados, C. Teitelboim, J. Zanelli, *Phys. Rev. D* **49**, 975 (1994).
- [87] A. Ilha, J. P. S. Lemos, "Dimensionally continued Oppenheimer-Snyder gravitational collapse solutions in even dimensions", *Phys. Rev. D*, to appear (1997), hep-th/9608004.

Black Holes as Atoms: Classical Hair and Quantum Levels in the Light of General Relativity

Jacob D. Bekenstein

*Racah Institute of Physics, Hebrew University of Jerusalem,
Givat Ram, Jerusalem 91904, Israel*

I marshal the heuristic arguments, based squarely on general relativity and elementary quantum notions, that suggest the quantum numbers relevant for a black hole in a stationary state. The evidence for believing that horizon area is an adiabatic invariant is reviewed. This fact when combined with an argument going back to P. Ehrenfest points to a discrete spectrum of black hole horizon area with uniform spacing between eigenvalues, as also found on other grounds by V. Mukhanov as well as others. This immediately leads to quantization of black hole mass with the spacing between neighboring “energy levels” roughly inversely proportional to mass, in harmony with N. Bohr’s correspondance principle. The degeneracy of the “energy levels” can be gotten by identifying degeneracy with the exponent of black hole entropy. I delineate an algebra for the relevant black hole operators which reproduces the uniformly spaced area spectrum. It also, independently of other arguments in physics, leads to charge quantization for black holes and free particles in multiples of a universal charge unit. I remark on the differences between the conclusions listed here and those from the loop quantization of gravity.

1 INTRODUCTION

In classical general relativity the mass spectrum of black holes is a continuum. However, venerable arguments [1, 2] suggest that in quantum theory this spectrum must be discrete and highly degenerate. The simplest way to summarize these conclusions is by stating that black hole horizon area is quantized with equispaced levels whose degeneracy corresponds, by the usual Boltzmann–Einstein formula, to the black hole entropy associated with each area eigenvalue. The first of these conclusions has been recovered by a number of workers using diverse ideas [3]. On the other hand, the loop quantization scheme for general relativity [4] seems to give a different spectrum [5]. Here I shall marshal the arguments favoring the equispaced area spectrum, and point out the clarification they afford of the nature of the quantum black hole.

In what follows I use units for which $G = c = 1$. Then $\hbar^{1/2}$ is the Planck–Wheeler length ℓ_P .

2 NO HAIR – NO NEW CLASSICAL PARAMETERS

A primary question here is what is the complete set of quantum numbers that describe a black hole in a stationary quantum state. In the absence of a lucid quantum theory of gravity, I here opt to infer the answer from the generic parameters of a black hole in classical general relativity. The issue is the same as that in Wheeler’s “no hair” conjecture [6] which has illuminated so much of black hole physics. Inspired by Israel’s and Carter’s early black hole uniqueness theorems [7], Wheeler anticipated that “collapse leads to a black hole endowed with mass and charge and angular momentum, but, so far as we can now judge, no other free parameters”. He stressed that quantum numbers such as baryon number or strangeness can have no place in the external description of a black hole. Support for this last expectation was soon forthcoming from the “no hair” theorems of Chase, Teitelboim, Hartle and myself [8].

Wheeler's characterized a 'free parameter' as one subject to a Gauss type law, which circumstance permits its determination from measurements made far away from the black hole. It is entirely in harmony with this philosophy to add magnetic charge to Wheeler's list: magnetic monopole is subject to a Gauss law, and duality invariance of the Maxwell-Einstein equations implies that there should be analogues of the Kerr-Newman solution with magnetic charge alongside electric charge (these are in fact known). The question of whether charges of nonabelian gauge theories - color in modern parlance - should be added to the list arose early. I [9] found no obstruction to such "hair", while Yasskin [10] provided explicit, if trivial, solutions of black holes with nonabelian gauge hair. Nevertheless, the discovery of the black hole solution with $SU(2)$ gauge hair by Volkov and Gal'tsov [11] took everybody by surprise. The ensuing plethora of black hole solutions with "hair" (for reviews see ref. [12]) was interpreted by some as debunking the "no hair" principle.

But, at least for spherical static black holes, this reaction has proved premature. The Volkov-Gal'tsov black hole as well as the Green-Mathur-O'Neill Proca-hair and sphaleron-hair black hole solutions [13] have turned out to be unstable [14]. In like manner the hoary Bronnikov-Bocharova-Melnikov conformal scalar hair black hole [15] was found unstable [16]. The Skyrme hair black hole [17] and the black hole with a nonabelian monopole [18] are the only known general relativistic *spherical* black hole solutions which have hitherto evaded instability symptoms. In addition powerful new theorems rule out the *existence* of static solutions with scalar hair, whether charged and interacting with an Abelian gauge field [19, 20], or neutral [21, 20] (in the latter case the proof still does not cover the range $0 < \xi < \frac{1}{2}$ of the nonminimal coupling parameter).

What about nonspherical black holes? The Kerr-Newman family contains all known general relativistic solutions representing stationary rotating black holes. For static black holes, three nonspherical examples are known. The first is the the Zel'dovich and Novikov [22] quadrupolar black hole; this is not asymptotically flat and, therefore, represents a nonisolated black hole. The second is the Achucarro-Gregory-Kuijken [23] black hole transfixed by a cosmic string. Again this is not asymptotically flat, and is not ostensibly equipped with a parameter not already present in the spherical black hole or straight cosmic string. Thus these examples fail to supply us with new black hole parameters beyond the usual ones; they are not hairy black holes. The third nonspherical example is Ridgway and E. Weinberg's black hole [24]; it is a solution of a rather contrived gauge theory, and as such not directly of interest to our search for parameters that may translate into quantum numbers.

Reviewing all this evidence we see that today only the Skyrmeion black hole and the black-hole-in-a-monopole deserve the status of *viable (that is stable) hairy black holes*. Things have not changed much since Wheeler made his clever guess. We do have to add to his list of black hole parameters magnetic monopole, both the Maxwell kind and the kind in some specific nonabelian gauge theories, as well as Skyrme topological number.

3 BLACK HOLE QUANTUM NUMBERS

How do we convert information about classical parameters to a selection of quantum numbers? Again, the lack of a lucid quantum gravity motivates us to seek illumination from analogy. Consider then the case of the Higgs field with Mexican hat potential in flat spacetime. A configuration with the Higgs field taking on values on a slope of the potential is not a stationary classical solution. No stationary quantum state corresponds to it. A configuration with the field at a minimum of the potential is a classical stationary stable solution. It is well known that small perturbations away from it, which classically oscillate around it, are interpreted in quantum theory as excitations of the field arising from the minimum state. By contrast, a configuration with the field at a maximum of the potential is a classical stationary but unstable solution. A small perturbations away from it runs away. In the quantum theory such perturbations are reinterpreted as tachyonic excitations which, at the level of this discussion, certify the underlying stationary configuration as pathological.

By analogy we may conclude that to each *stable stationary* classical black hole solution corresponds a stationary quantum state which is capable of excitation. Again by analogy, the excited state can be interpreted as the base black

hole state plus quanta of various fields propagating on its background. By contrast, an unstable stationary classical black hole solution cannot be associated with a stationary quantum state because excitations of the later would be tachyonic in nature. Thus, the unstable nonabelian hair black holes and the Bocharova–Bronnikov–Melnikov black hole *do not* furnish classical analogues of quantum stationary states.

The classical *nonstationary* solutions of the Higgs theory include some which have the field shuttle in time from one potential well to the other and back. These are big perturbations which are not confined around a single minimum. In the quantum theory the appropriate base state is a linear superposition of two quantum stationary states, one for each well. It would seem that in the black hole case the appropriate analog is a linear superpositions of two distinct black hole stationary states. In other words, the shuttling solutions do not imply new quantum stationary black hole states.

Although the above arguments cannot rule out quantum stationary black hole states without classical analogs, they are suggestive that, as far as present evidence requires, the only quantum numbers of a stationary black hole state are mass, electric and magnetic charge (this last including nonabelian varieties) and Skyrmionic topological number. I am not too clear about what to do with this last number, so I will ignore it at this preliminary stage. I thus focus on black hole eigenstates of mass \hat{M} , electric charge \hat{Q} , magnetic monopole \hat{K} , angular momentum $\hat{\mathbf{J}}^2$ and \hat{J}_z and, of course, linear momentum $\hat{\mathbf{P}}$. This last can be set to zero if we agree to work in the black hole's center of mass. The eigenvalues of \hat{Q} , \hat{K} , $\hat{\mathbf{J}}^2$, \hat{J}_z are well known. By making the standard assumption that this last set of operators are mutually commuting, we may immediately establish the spectrum of the mass for the extremal black holes.

The classical *extremal* Kerr–Newman black hole is defined by the constraint

$$M^2 = Q^2 + K^2 + J^2/M^2 \quad (1)$$

so that

$$M = 2^{-1/2} \left[Q^2 + K^2 + \sqrt{(Q^2 + K^2)^2 + 4J^2} \right]^{1/2} \quad (2)$$

where the negative root solution has been discarded because it gives imaginary M . By replacing in this expression $Q \rightarrow q(\alpha\hbar)^{1/2}$, $K \rightarrow g(\hbar/4\alpha)^{1/2}$ and $J^2 \rightarrow j(j+1)\hbar^2$ with q, g integers, j a positive integer or half-integer and α the fine-structure constant, we enforce the quantization of charge, magnetic monopole and angular momentum, and obtain the mass eigenvalues (also discussed by P. Mazur [25])

$$M_{qgj} = (\hbar/2)^{1/2} \left[\alpha q^2 + g^2/4\alpha + \sqrt{(\alpha q^2 + g^2/4\alpha)^2 + 4j(j+1)} \right]^{1/2} \quad (3)$$

Substituting these in the classical expression for horizon area of an extremal black hole

$$A = 4\pi [Q^2 + K^2 + 2J^2/M^2] \quad (4)$$

we obtain the area eigenvalues. It should be noted that these last, which can hardly be quibbled with, are at variance with the area eigenvalues claimed to follow from the loop quantization program [4, 5]. Therefore, since the eigenvalues of charges which force this conclusion cannot be tampered with, one must conclude that either the algorithm from loop quantization is manifestly inapplicable to extremal black holes, or else that extremal black holes are forbidden by loop gravity theory. Most would view the last alternative as highly unpalatable.

For generic black holes I shall use other arguments. As I shall make clear, for them horizon area is more immediately quantized than is mass. I shall avail myself of the relation between mass and area of the generic Kerr–Newman black hole to write, as first done for the classical quantities by Christodoulou and Ruffini, [26]

$$\hat{M}^2 = \frac{\hat{A}}{16\pi} \left(1 + \frac{4\pi(\hat{Q}^2 + \hat{K}^2)}{\hat{A}} \right)^2 + \frac{4\pi\hat{\mathbf{J}}^2}{\hat{A}} \quad (5)$$

This relation allows one to read off eigenvalues of \hat{M} from those of \hat{A} , the charges and the angular momentum; it was first used in this sense long ago [1].

4 BLACK HOLE AREA: AN ADIABATIC INVARIANT

In the absence of a complete theory of quantum gravity, I seek to quantize the black hole area of a generic Kerr-Newman black hole in the style of the old quantum theory, by exploiting its similarity to an adiabatic invariant in mechanics. What is an adiabatic invariant?

A physical system governed by a hamiltonian which depends on an exterior parameter λ is said to undergo an adiabatic change if λ varies on a timescale long compared to the longest timescale of the internal motions T . Thus if $H(q, p, \lambda(t))$, the change in the system is regarded as adiabatic when $\lambda^{-1}d\lambda/dt \ll T^{-1}$. An adiabatic invariant is any dynamical quantity $A(q, p)$ which changes little during the period when H accumulates a large total change. Ehrenfest [27] showed that for a quasiperiodic system, all action integrals of the form $A = \oint p dq$ are adiabatic invariants. For instance, for an harmonic oscillator of frequency ω , the action integral equals $2\pi E/\omega$. Thus when the spring constant varies on a timescale $\gg \omega^{-1}$, E/ω remains constant even when E has changed sizeably.

One can understand this adiabatic invariance of E/ω in quantum terms. For an harmonic oscillator in a stationary state labelled by quantum number n , $E/\omega = (n + \frac{1}{2})\hbar$. One expects n to remain constant during an adiabatic change because the perturbations imposed on the system have frequencies $\ll \omega$, so that transitions between states of different n are strongly suppressed. Therefore, the ratio E/ω is preserved. Now in the Bohr-Sommerfeld theory (old quantum mechanics), action integrals are quantized in integers: $\oint p dq = 2\pi n\hbar$. The above logic then explains why the classical action integrals are adiabatic invariants.

Actually Ehrenfest stated a broader hypothesis [27]: any classical adiabatic invariant (action integral or not) corresponds to a quantum entity with discrete spectrum. The rationale is that an adiabatic change, by virtue of its slowness, is expected to lead only to continuous changes in the system, not to jumps that change a discrete quantum number. The preservation of the value of the quantum entity would explain the classical invariant property. I shall apply Ehrenfest's hypothesis to black hole area of generic Kerr-Newman black holes, which, as I show now, shows all the signs of being the analog of the mechanical adiabatic invariant.

Consider a Reissner-Nordström black hole of mass M and charge Q . We shoot in a classical point particle of charge ϵ with (conserved) energy $E = \epsilon Q/r_{\mathcal{H}}$, where $r_{\mathcal{H}}$ is the radius of the black hole in Boyer-Lindquist coordinates. In Newtonian terms the particle should marginally reach the horizon where its potential energy just exhausts the total energy. Study of the exact equation of motion supports this conclusion: the particle's motion has a turning point at the horizon. Because of this the assimilation of particle by the black hole takes place especially slowly; it is an adiabatic process.

Now the area of the horizon is originally

$$A = 4\pi r_{\mathcal{H}}^2 = 4\pi \left(M + \sqrt{M^2 - Q^2} \right)^2 \quad (6)$$

and the (small) change inflicted on it by the absorption of the particle is

$$\Delta A = \theta_{RN}^{-1} \cdot (\Delta M - Q \Delta Q/r_{\mathcal{H}}) \quad (7)$$

where

$$\theta_{RN} \equiv \frac{1}{2} A^{-1} \sqrt{M^2 - Q^2} \quad (8)$$

Thus if the black hole is not extremal, $\Delta A = 0$ because $\Delta M = E$ while $\Delta Q = \epsilon$ and $E = \epsilon Q/r_{\mathcal{H}}$. Therefore, the horizon area is invariant in the course of an adiabatic change of the black hole. For an extremal black hole this conclusion fails: when $Q = M$, $\sqrt{M^2 - Q^2}$ in Eq.(6) is unchanged to $O(\epsilon^2)$ during the absorption, so that $\Delta A = 8\pi M E \neq 0$.

As a second example consider a Kerr black hole of mass M and angular momentum J . Send onto it a scalar wave of the form $Y_{\ell m}(\theta, \phi)c^{-i\omega t}$. It is known [28] that the absorption coefficient has the form

$$\Gamma = K_{\omega \ell m}(M, J) \cdot (\omega - \Omega m) \quad (9)$$

where

$$\Omega \equiv \frac{J/M}{r_H^2 + (J/M)^2} \quad (10)$$

is the rotational angular frequency of the hole, while $K_{\omega \ell m}(M, J)$ is a positive coefficient. If we choose $\omega = m \Omega$, the wave is perfectly reflected. By choosing $\omega - \Omega m$ slightly positive, we arrange for a small fraction of the wave to get absorbed. If the reflected wave is repeatedly reflected back towards the black hole by a large spherical mirror surrounding it, one can arrange for a sizeable fraction of the wave's energy and angular momentum to eventually get absorbed. But since this takes place over many cycles of reflection, the change in the hole is an adiabatic one.

The horizon area of the Kerr black hole is

$$A = 4\pi \left[\left(M + \sqrt{M^2 - (J/M)^2} \right)^2 + (J/M)^2 \right] \quad (11)$$

and small changes of it are given by

$$\Delta A = \theta_K \cdot (\Delta M - \Omega \Delta J) \quad (12)$$

where

$$\theta_K \equiv \frac{1}{2} A^{-1} \sqrt{M^2 - (J/M)^2} \quad (13)$$

In our case the overall changes ΔM and ΔJ must stand in the ratio ω/m (as a mental aid just think of the wave as made of quanta, each with energy $\hbar\omega$ and angular momentum $\hbar m$). But since we chose $\omega \approx \Omega m$, we see from Eq.(12) that if the black hole is not extremal, $\Delta A \approx 0$, to the accuracy of the former equality. Evidently, here too horizon area is invariant during adiabatic changes. This conclusion fails for the extremal black hole for reasons similar to those in our first example.

The two examples and the one in the next section support the thesis that for a generic black hole, horizon area A is, classically, an adiabatic invariant. By taking Ehrenfest's hypothesis seriously, I conclude that horizon area of a generic quantum black hole, \hat{A} , must have a discrete eigenvalue spectrum:

$$a_n = f(n); \quad n = 1, 2, 3, \dots \quad (14)$$

The function f is supposed to be positive and monotonically increasing (this last just reflects the ordering of eigenvalues by magnitude); however, nothing else can be deduced about f from this argument. At any rate, in light of Eq.(5), and the quantization of charge, magnetic monopole, and angular momentum, this result tells us that black hole mass has a discrete spectrum. The form of it will be elucidated in Sec.V

5 AREA QUANTIZATION

For generic Kerr–Newman black holes, Eq.(14) raises the pressing question, what is the spacing of the area levels, and how does this spacing vary along the spectrum? Here I shall answer this question by recalling a modification [29] of Christodoulou and Ruffini's reversible process [26]. Christodoulou asked, can assimilation of a point particle by a Kerr black hole be made reversible in the sense that all changes of the black hole can be undone by absorption of a suitable second particle? His answer, as later generalized to the Kerr–Newman black hole [26], is that the process is reversible if the particle, which may be electrically charged and carry angular momentum, is injected at the horizon from a turning point in its orbit. In this case the horizon area (or the irreducible mass in the original terminology) is left unchanged. Since horizon area cannot decrease [31], it is plain that the effects on the black hole can be undone by another reversible process which adds charges and angular momentum opposite in sign to those added by the first. For generic Kerr–Newman black holes Christodoulou's reversible process is an adiabatic process (in the sense that assimilation from a turning point proceeds slowly) which leaves the horizon area unchanged. It supplies us with a further example of the adiabatic invariance of horizon area.

Note that the particle in the reversible process has to be a point particle in order for its absorption to leave the area unchanged. In fact, recalculation of the process for a particle of mass μ and radius b shows [29] that there is a minimum increase in area,

$$\Delta A = 8\pi\mu b, \quad (15)$$

which is attainable if the particle is captured when its center of mass is at a turning point of its motion a proper distance b away from the horizon. Classically one can here take the limit $b \rightarrow 0$ and recover Christodoulou's reversible process. However, a quantum point particle is subject to quantum uncertainty. If it is known to be at the horizon with high accuracy, its radial momentum is highly uncertain; this prevents the turning point condition from being fulfilled. And, of course, a relativistic quantum point particle cannot even be localized to better than a Compton length \hbar/μ . Thus in quantum theory the limit $b \rightarrow 0$ is not a legal one. One can get an idea of the smallest possible (quantum) increase in horizon area by replacing $b \rightarrow \gamma\hbar/8\pi\mu$ in Eq.(15), where γ is a number of order unity and the 8π is for later convenience. That minimal increase is

$$(\Delta A)_{\min} = \gamma\ell_P^2 \quad (16)$$

The surprising thing here is that $(\Delta A)_{\min}$ is independent of M, Q and J of the black hole. This strongly suggests that it corresponds to the spacing between eigenvalues of \dot{A} in the quantum theory, a uniform spacing. For it would be strange indeed if that spacing were to vary, say with mass of the black hole, and yet the increment in area resulting from the best approximation to a reversible process would contrive to come out universal, as in Eq.(16), by involving a number of quantum steps inversely proportional to the eigenvalue spacing.

A check of our identification is furnished by a calculation of the mass spacing between area eigenvalues. For a black hole with zero charges and angular momentum, it is easy to derive from Eq.(5) that

$$\omega = \frac{\Delta M}{\hbar} = \frac{1}{32\pi M} \cdot \frac{\Delta A}{\ell_P^2} = \frac{\gamma}{32\pi M} \quad (17)$$

This result is in pleasant agreement with Bohr's correspondence principle: "transition frequencies at large quantum numbers should equal classical oscillation frequencies" because a classical Schwarzschild black hole displays 'ringing frequencies' of order M^{-1} , just as Eq.(17) predicts. The agreement would be destroyed if the area eigenvalues were unevenly spaced. Thus there are two good grounds for replacing Eq.(14) for a generic Kerr–Newman black hole by

$$a_n = \gamma\ell_P^2 (n + \eta); \quad \eta > -1; \quad n = 1, 2, \dots \quad (18)$$

where η allows for the possibility, entirely consistent with all that has been said, that the *smallest* area eigenvalue is either very small or very large on the scale of the spacing $\gamma\ell_P^2$.

Our conclusion that the minimal area increase is given by Eq.(15) fails for extremal black holes because the analog of the quantity θ_K in Eq.(13) diverges. Just as we found in Sec.IV that for an extremal Kerr black hole the area does increase during the adiabatic process, so we find here that the minimal increase in area is not Eq.(15), but a quantity dependent on M, Q and J . We cannot thus deduce that the area eigenvalues of an extremal black hole are evenly spaced. This is entirely consistent with Eqs.(3-4) which show the area spectrum of the extremal black hole to be very complex.

To get an idea about the magnitude of γ in Eq.(18), I now consider the degeneracy g_n of the eigenvalue a_n , first discussed in these terms by Mukhanov [2]. We know that black hole entropy $S_{HH} = A/4\ell_P^2 + \text{const.}$ (recall that black hole entropy is determined by thermodynamic arguments only up to an additive constant) quantifies how many internal microstates of the black hole correspond to the particular externally describable black hole macrostate. Accordingly, in the spirit of the Boltzmann–Einstein formula, I make the identification $\exp(S_{HH}) \leftrightarrow g_n$, or

$$g_n = \exp\left(\frac{a_n}{4\ell_P^2} + \text{const.}\right) = g_1 \exp(\gamma(n-1)/4) \quad (19)$$

As stressed by Mukhanov, g_n has to be a whole number for every n ; this is only possible if [32]

$$g_1 = 1, 2, \dots \quad \text{and} \quad \gamma = 4 \times \{\ln 2, \ln 3, \dots\} \quad (20)$$

I now consider some special cases.

In case $g_1 = 1$ (nondegenerate black hole groundstate), the additive constant in Eq.(19) must be retained, for were it to vanish, a_1 would also vanish; however, in any state a black hole should have nonvanishing horizon area. Just this case was studied in Ref. [32]; it is a bit ugly in that the eigenvalue law Eq.(18) and the black hole entropy include related but undetermined additive constants. For $g_1 = 1$ the simplest choice for γ is $\gamma = 4 \ln 2$.

The next case, $g_1 = 2$ (doubly degenerate black hole groundstate), no longer requires an additive constant in the black hole entropy. I view this as a virtue. With zero additive constant and $\gamma = 4 \ln 2$, Eq.(18) specifies that $\eta = 0$. Thus this is an economical option in that both the additive constant in the entropy and the offset η vanish. The area spectrum is

$$a_n = 4\ell_P^2 \ln 2 \cdot n; \quad n = 1, 2, \dots \quad (21)$$

If instead we take $\gamma = 4 \ln x$ with $x = 3, 4, \dots$, then $\eta = -1 + 1/\ln_2 x$. The resulting spectrum is $a_n = 4\ell_P^2 \ln x \cdot (n - 1 + 1/\ln_2 x)$. For instance, if $x = 4$, the horizon area is quantized in half integers.

For $g_1 = 3, 4, \dots$, the choices $\gamma = 4 \ln 3, 4 \ln 4, \dots$, respectively correspond to $\eta = 0$ and vanishing additive constant in the entropy. They are as elegant as the case $g_1 = 2$ with $\gamma = 4 \ln 2$ discussed above, but in the present state of ignorance I prefer this last one for its lowest ground state degeneracy.

For an extremal black hole the area eigenvalues that follow from Eqs.(4) and (3), if substituted in Eq.(19), would in general give nonintegral values of g_n . However, we recall that the black hole entropy of an extremal black hole is thought to vanish [33]. This decoupling of area from entropy means we must ignore Eq.(19) and set $g_1 = 0$.

For the nonextremal black holes we still have to decide among the various choices of γ for $g_1 = 2$. I now propose a new kind of argument.

6 ALGEBRAIC APPROACH

In quantum theory one usually obtains spectra of operators from the algebra they obey. With Mukhanov I have been studying various algebras that might enlighten us on the quantum basis of the results just discussed. Let me here describe one algebra of this kind; it has the advantage of simplicity, and offers as a surprising bonus the quantization of electric (or magnetic charge), which in this paper has so far been assumed to be a given.

In ordinary quantum theory the algebra of operators usually reflects symmetries in the system. I cannot claim that I know how to derive the relevant algebra of observables from the underlying symmetries of black holes. My approach here shall be axiomatic. Our earlier heuristic arguments have already pointed us to the operators that should be involved, and have even suggested that one should focus on horizon area quantization as the key step. I shall thus try to guess, by appealing to analogies with well known physics and simplicity, the form of the algebra that is required. In the final analysis what is being done here is trying an algebra for consistency with our previous conclusions.

I now state and discuss three axioms:

- Horizon area is represented by a *positive semi-definite* operator \hat{A} with a *discrete* spectrum $\{a_n; n = 0, 1, 2, \dots\}$.
Discreteness of the area spectrum, as suggested by the adiabatic invariant character of horizon area, is formalized in this axiom. One imagines the eigenvalues to be arranged so that $a_0 = 0$ corresponds to the vacuum $|0\rangle$ (no black hole case) while the rest of the a_n are arranged in order of increasing value. These eigenvalues have various degeneracies g_n ; I take $g_0 = 1$.
- The operators \hat{A} , \hat{Q} , \hat{K} , \hat{J}^2 and \hat{J}_z mutually commute, and for each set of their joint eigenvalues there exists *at least* one black hole creation operator \hat{R}_{nqjms} such that $\hat{R}_{nqjms}|0\rangle$ is a one-black hole state with area a_n , with

electric and magnetic charges $q(\alpha\hbar)^{1/2}$ and $g(\hbar/4\alpha)^{1/2}$, and with total spin $j(j+1)\hbar$ and z-component of spin $m\hbar$. The index s represents internal quantum numbers invisible to an external observer.

That \hat{Q} , \hat{K} , \hat{J}^2 and \hat{J}_z mutually commute requires no explanation. That \hat{A} commutes with all of them is in agreement with the feeling that horizon area is invariant under gauge transformations and bodily rotations of the black hole. Creation operators are common in field theory. In view of the similarities between black hole and elementary particle, it seems not farfetched to treat black holes as particles of some field. Internal quantum numbers are necessary because we know from the black hole entropy that each state seen by an external observer corresponds to many internal states; these need to be distinguished by additional quantum numbers.

• The subalgebra spanned by \hat{A} , \hat{Q} , \hat{K} , \hat{J}_z and all the \hat{R}_{nqgjm_s} and $\hat{R}_{nqgjm_s}^\dagger$ for $n \geq 1$ is linear and closed.

In general it is always possible to choose operators such that their algebra is linear, but there is no guarantee that these will be the physically interesting operators. Thus the third axiom is a physical one and nontrivial. Note that I have left out \hat{J}^2 ; this is because being a square it cannot have a linear algebra: it is easily verified that even \hat{J}_z^2 cannot have commutators with the \hat{R}_{nqgjm_s} which are linear in \hat{R}_{nqgjm_s} if \hat{J}_z has such.

In applying these axioms, it will be convenient to use the index κ as an alias for $nqgjm$. One example of a commutator consistent with the axioms is

$$[\hat{A}, \hat{R}_{\kappa s}] = h_{\kappa s}^{\kappa' s'} \hat{R}_{\kappa' s'} + k_{\kappa s}^{(A)} \hat{A} + k_{\kappa s}^{(Q)} \hat{Q} + k_{\kappa s}^{(K)} \hat{K} + k_{\kappa s}^{(J_z)} \hat{J}_z \quad (22)$$

where $h_{\kappa s}^{\kappa' s'}$ and the $k_{\kappa s}^{(x)}$ are suitable structure constants. Clearly all of \hat{A} , \hat{Q} , \hat{K} and \hat{J}_z annihilate the vacuum; therefore,

$$[\hat{A}, \hat{R}_{\kappa s}]|0\rangle = \hat{A}\hat{R}_{\kappa s}|0\rangle = h_{\kappa s}^{\kappa' s'} \hat{R}_{\kappa' s'}|0\rangle \quad (23)$$

However, $\hat{R}_{\kappa s}$ is to create an eigenstate of \hat{A} from the vacuum; therefore we must set

$$h_{\kappa s}^{\kappa' s'} = a_n \delta_{\kappa}^{\kappa'} \delta_s^{s'} \quad (24)$$

with n identical to the n in the group κ for consistency. Now suppose we redefine

$$\hat{R}_{\kappa s} \rightarrow \hat{R}_{\kappa s}^{\text{new}} = \hat{R}_{\kappa s} + a_n^{-1} \left[k_{\kappa s}^{(A)} \hat{A} + k_{\kappa s}^{(Q)} \hat{Q} + k_{\kappa s}^{(K)} \hat{K} + k_{\kappa s}^{(J_z)} \hat{J}_z \right] \quad (25)$$

$\hat{R}_{\kappa s}^{\text{new}}$ obviously still creates a state with quantum numbers κs out of the vacuum. But in terms of it the commutation relation (22) becomes

$$[\hat{A}, \hat{R}_{\kappa s}^{\text{new}}] = a_n \hat{R}_{\kappa s}^{\text{new}} \quad (26)$$

From now on I drop the superscript "new".

Now we operate with $\hat{R}_{\kappa' s'}$, $\hat{R}_{\kappa s}$ on the vacuum and employ the said commutation relation to get

$$\hat{A}\hat{R}_{\kappa s}\hat{R}_{\kappa' s'}|0\rangle = \hat{R}_{\kappa s}(\hat{A} + a_n)\hat{R}_{\kappa' s'}|0\rangle = (a_n + a_{n'})\hat{R}_{\kappa s}\hat{R}_{\kappa' s'}|0\rangle \quad (27)$$

so that $\hat{R}_{\kappa s}\hat{R}_{\kappa' s'}|0\rangle$ has area which is the sum of the areas of $\hat{R}_{\kappa s}|0\rangle$ and $\hat{R}_{\kappa' s'}|0\rangle$. Analogy with field theory might lead us to believe that the state $\hat{R}_{\kappa s}\hat{R}_{\kappa' s'}|0\rangle$ is just a two-black hole state. In this case the result just obtained would seem to be trivial. But in fact, the axiomatic approach allows other possibilities.

To clarify the matter, let us write down one more generic commutation relation allowed by the axioms:

$$[\hat{R}_{\kappa s}, \hat{R}_{\kappa' s'}] = \epsilon_{\kappa s \kappa' s'}^{\kappa'' s''} \hat{R}_{\kappa'' s''} + f_{\kappa s \kappa' s'}^{(A)} \hat{A} + f_{\kappa s \kappa' s'}^{(Q)} \hat{Q} + f_{\kappa s \kappa' s'}^{(K)} \hat{K} + f_{\kappa s \kappa' s'}^{(J_z)} \hat{J}_z \quad (28)$$

Here the $\epsilon_{\kappa s \kappa' s'}^{\kappa'' s''}$ and $f_{\kappa s \kappa' s'}^{(x)}$ are additional structure constants antisymmetric under the exchange $\kappa s \kappa' s' \leftrightarrow \kappa' s' \kappa s$. Operating with this relation on the vacuum gives

$$\hat{R}_{\kappa s}\hat{R}_{\kappa' s'}|0\rangle - \hat{R}_{\kappa' s'}\hat{R}_{\kappa s}|0\rangle = \epsilon_{\kappa s \kappa' s'}^{\kappa'' s''} \hat{R}_{\kappa'' s''}|0\rangle \quad (29)$$

Since on the R.H.S. of this relation stands a one-black hole state, any state like $\hat{R}_{\kappa s} \hat{R}_{\kappa' s'} |0\rangle$ is a linear combination containing one-black hole states. The statement that $a_n + a_{n'}$ is also an eigenvalue of \hat{A} must thus also accrue to one-black hole states.

The last result means that $2a_1$ must be an eigenvalue of \hat{A} at least as big as the second eigenvalue, a_2 . Likewise $2a_1 + a_1 = 3a_1$ must be eigenvalue at least as large as the third, a_3 . Continuing this scheme we see that $\{na_1; n = 1, 2, \dots\}$ is a series of eigenvalues of \hat{A} . The only question is, are there other eigenvalues sprinkled in between these? I shall show, by contradiction, that there cannot be.

Suppose that the k -th eigenvalue is given by $a_k = (k' + \zeta)a_1$ where k' is an integer below k while $0 < \zeta < 1$. Let us take recourse to the adjoint of Eq.(26)

$$[\hat{A}, \hat{R}_{\kappa s}^\dagger] = -a_n \hat{R}_{\kappa s}^\dagger \quad (30)$$

In entire analogy with Eq.(27) we have

$$\hat{A} \hat{R}_{\kappa s}^\dagger \hat{R}_{\kappa' s'} |0\rangle = \left(\hat{R}_{\kappa s}^\dagger \hat{A} - a_n \hat{R}_{\kappa s}^\dagger \right) \hat{R}_{\kappa' s'} |0\rangle = (a_{n'} - a_n) \hat{R}_{\kappa s}^\dagger \hat{R}_{\kappa' s'} |0\rangle \quad (31)$$

We may now conclude that the *difference* of two area eigenvalues of one black hole is also an eigenvalue. In addition, it follows from the postulated positive definiteness of \hat{A} that $\hat{R}_{\kappa s}^\dagger \hat{R}_{\kappa' s'}$ annihilate the vacuum whenever $n > n'$ (from the fact that eigenvalues are ordered by magnitude). Anyway, the difference $(k' + \zeta)a_1 - k'a_1 = \zeta a_1$ of two eigenvalues singled out by our previous discussion must also be an eigenvalue. But this contradicts the assumption that a_1 is the lowest area eigenvalue. Thus the assumption that ζ can be nonvanishing must be wrong. We thus come out with the spectrum

$$a_n = na_1; \quad n = 0, 1, 2, \dots \quad (32)$$

Comparing with Eq.(18) we see that the axiomatic approach requires $\eta = 0$. Further, referring to the discussion accompanying Eq.(21), we find that necessarily $\gamma = 4 \ln 2$. Thus if we accept the argument from simplicity that $g_1 = 2$, all free parameters in the formula for area eigenvalues are fixed by the algebraic approach.

7 QUANTIZING CHARGE AND SPIN

A bonus of the algebra just described is that it gives quantization of black hole charge, as well as of the z component of black hole spin. To see this consider the Jacobi identity

$$[[\hat{Q}, \hat{A}], \hat{R}_{\kappa s}] + [[\hat{R}_{\kappa s}, \hat{Q}], \hat{A}] + [[\hat{A}, \hat{R}_{\kappa s}], \hat{Q}] \equiv 0 \quad (33)$$

As argued already, $[\hat{Q}, \hat{A}] = 0$; taking Eq.(26) into account this can be written as

$$[\hat{A}, [\hat{Q}, \hat{R}_{\kappa s}]] = a_n [\hat{Q}, \hat{R}_{\kappa s}] \quad (34)$$

Now the third axiom allows us to write in analogy with Eq.(22)

$$[\hat{Q}, \hat{R}_{\kappa s}] = H_{\kappa s}^{\kappa' s'} \hat{R}_{\kappa' s'} + l_{\kappa s}^{(Q)} \hat{Q} + l_{\kappa s}^{(A)} \hat{A} + l_{\kappa s}^{(K)} \hat{K} + l_{\kappa s}^{(J_s)} \hat{J}_s \quad (35)$$

By operating with this equation on the vacuum we get, in analogy with Eq.(24), that

$$H_{\kappa s}^{\kappa' s'} = q \delta_{\kappa}^{\kappa'} \delta_s^{s'} \quad (36)$$

with q identical to the q in the group κ . If we now substitute these two results in Eq.(35) we get

$$a_n \left(l_{\kappa s}^{(Q)} \hat{Q} + l_{\kappa s}^{(A)} \hat{A} + l_{\kappa s}^{(K)} \hat{K} + l_{\kappa s}^{(J_s)} \hat{J}_s \right) = 0 \quad (37)$$

Thus so long as κ is not null (so that $a_n \neq 0$), the $l_{\kappa s}$ coefficients must vanish because the four operators in Eq.(37) are independent. Hence

$$[\hat{Q}, \hat{R}_{\kappa s}] = q \hat{R}_{\kappa s} \quad (38)$$

Eq.(37) is entirely analogous to Eq.(26). By analogy with the discussion of Eqs.(27) and (31), we conclude that if q and q' are two eigenvalues of \hat{Q} , then so are $q + q'$ and $q - q'$. Here there is no reason to forbid negative eigenvalues. Thus all positive and all negative integer multiples of some smallest charge ϵ are eigenvalues of \hat{Q} . So is zero (because $q - q = 0$). The proof that there are no eigenvalues in between these proceeds just as in the case of area eigenvalues. Hence,

$$q = k\epsilon \quad k = 0, \pm 1, \pm 2, \dots \quad (39)$$

And because two black holes may merge, and charge is conserved in the merger and subsequent relaxation to stationarity, the charge ϵ must be the same for all black holes.

Not only that, but if there is just one black hole in the universe, all particles in the universe must have their charges quantized according to the same rule (39) since particles can always fall into the black hole, and charge is conserved in that event. We thus get for free an explanation of why electric (or magnetic) charge is quantized in integers. In physics there are only a couple of ways to understand charge quantization: existence of magnetic monopoles (which maybe do not exist) and grand unification (which may not happen), so it is gratifying to find another one here.

From the point of view of our algebra, there is very little difference between \hat{Q} and \hat{J}_z . By arguments similar to the above we can show that the eigenvalues of \hat{J}_z are restricted to zero and all the positive and negative integer multiples of some fundamental unit. But this is precisely the spectrum that follows in the well known manner from the $SU(2)$ algebra of \hat{J}^2 and \hat{J}_z when both integer and half integer values of j are allowed, and when the fundamental unit is identified with $\hbar/2$. Thus the algebra expounded here is consistent with angular momentum quantization. We note that as far as the formalism goes, black holes may be bosonic or fermionic.

8 ACKNOWLEDGMENTS

Many issues discussed here first surfaced in inspiring conversations with Slava Mukhanov. I also thank Avraham Mayo for a comment on extremal black holes. This research is supported by a grant from the Israel Science Foundation.

References

- [1] J. D. Bekenstein, *Lett. Nuovo Cimento* **11**, 467 (1974).
- [2] V. Mukhanov, *Pis. Eksp. Teor. Fiz.* **44**, 50 (1986) [*JETP Letters* **44**, 63 (1986)], and in *Complexity, Entropy and the Physics of Information*. SFI Studies in the Sciences of Complexity, vol. III, ed. W. H. Zurek (Addison-Wesley, New York 1990).
- [3] Ya. I. Kogan, *Pis. Eksp. Teor. Fiz.* **44**, 209 (1986) [*JETP Letters* **44**, 267 (1986)]; M. Schiffer, "Black hole spectroscopy", São Paulo preprint IFT/P-38/89 (1989); J. Bellido, "Quantum black holes", hep-th/9302127 (unpublished); U. H. Danielsson and M. Schiffer, *Phys. Rev. D* **48**, 4779 (1993); Y. Peleg, hep-th/9307057 (unpublished); M. Maggiore, *Nucl. Phys. B* **429**, 205 (1994); I. I. Kogan, hep-th/9412232 (unpublished); C. O. Lousto, *Phys. Rev. D* **51**, 1733 (1995); H. A. Kastrup, gr-qc/9605038; A. Barvinsky and G. Kunstatter, gr-qc/9606134.
- [4] A. Ashtekar, C. Rovelli and L. Smolin, *Phys. Rev. Letters* **69**, 237 (1992).
- [5] C. Rovelli, preprint gr-qc/9608032; A. Ashtekar and J. Lewandowski, preprint gr-qc/9602046.
- [6] R. Ruffini and J. A. Wheeler, *Physics Today* **24**, 30 (1971).
- [7] W. Israel, *Phys. Rev.* **164**, 1776 (1967) and *Commun. Math. Phys.* **8**, 245 (1968); B. Carter, *Phys. Rev. Letters* **26**, 331 (1971).
- [8] J. E. Chase, *Commun. Math. Phys.* **19**, 276 (1970); J. D. Bekenstein, *Phys. Rev. Letters* **28**, 452 (1972); *Phys. Rev. D* **5**, 1239 and 2403 (1972); C. Teitelboim, *Lett. Nuov. Cim.* **3**, 326 and 397 (1972); J. Hartle, *Phys. Rev. D* **3**, 2938 (1971).

- [9] J. D. Bekenstein, Dissertation, Princeton University. (1972).
- [10] P. Yasskin (1972), unpublished.
- [11] M.S. Volkov and D.V. Gal'tsov, JETP Lett. **50**, 312 (1989).
- [12] G. W. Gibbons, in *The Physical World*, Lecture Notes in Physics **383** (Springer, Berlin 1991); M. Heusler, *Black Hole Uniqueness Theorems* (Cambridge University Press, Cambridge, 1996).
- [13] B. R. Greene, S. D. Mathur and C. M. O'Neill, Phys. Rev. D**47**, 2242 (1993).
- [14] N. Straumann and Z.H. Zhou, Phys. Lett. **B237** 353 (1990) and **B243**, 53 (1991); Nucl. Phys. **B369** 180 (1991); E. Mavromatos and E. Winstanley, Phys. Rev. D**53** 3190 (1996).
- [15] N. Bocharova, K. Bronnikov and V. Melnikov, Vestn. Mosk. Univ. Fiz. Astron. **6**, 706 (1970); J. D. Bekenstein, Ann. Phys. (NY) **82**, 535 (1974) and **91**, 72 (1975).
- [16] K. A. Bronnikov and Yu. N. Kireyev, Phys. Lett. **67A**, 95 (1978).
- [17] S. Droz, M. Heusler and N. Straumann, Phys. Lett. **B268**, 371 (1991).
- [18] K-Y. Lee, V.P. Nair and E. Weinberg, Phys. Rev. Lett. **68**, 1100 (1992).
- [19] S. A. Adler and R. P. Pearson, Phys. Rev. D **18**, 2798 (1978); A. Lahiri, Mod. Phys. Lett. **A8**, 1549 (1993).
- [20] A. E. Mayo and J. D. Bekenstein, Phys. Rev. D**54**, 5059 (1996).
- [21] M. Heusler, J. Math. Phys. **33**, 3497 (1992); Class. Quant. Grav. **12**, 779 (1995); B. C. Xanthopoulos and T. Zannias, J. Math. Phys. **32**, 1875 (1991); T. Zannias, J. Math. Phys. **36**, 6970 (1995); D. Sudarsky, Class. Quant. Grav. **12**, 579 (1995); J. D. Bekenstein, Phys. Rev. D **51**, R6608 (1995); A. Saa, J. Math. Phys. **37**, 2346 (1996).
- [22] Ya. B. Zel'dovich and I. D. Novikov, *Relativistic Astrophysics: Stars and Relativity* (Univ. of Chicago Press, Chicago 1971).
- [23] A. Achúcarro, R. Gregory and K. Kuijken, Phys. Rev. D **52**, 5729 (1995).
- [24] S. A. Ridgway and E. J. Weinberg, Phys. Rev. D**52**, 3440 (1995).
- [25] P. Mazur, Gen. Rel. Grav. **19**, 1173 (1987).
- [26] D. Christodoulou, Phys. Rev. Letters **25**, 1596 (1970); D. Christodoulou and R. Ruffini, Phys. Rev. D**4**, 3552 (1971).
- [27] M. Born, *Atomic Physics* (Blackie, London 1969), eight edition.
- [28] A. A. Starobinskii, Sov. Phys. JETP **37**, 28 (1973).
- [29] J. D. Bekenstein, Phys. Rev. D**7**, 2333 (1973).
- [30] D. Christodoulou, Phys. Rev. Letters **25**, 1596 (1970).
- [31] S. W. Hawking, Phys. Rev. Letters **26**, 1344 (1971).
- [32] J. D. Bekenstein and V. F. Mukhanov, Phys. Lett. **B360**, 7 (1995).
- [33] S. W. Hawking, G. Horowitz and S. Ross, Phys. Rev. D**51**, 4302 (1995).

Selected Topics on DØ Physics

Jussara M. de Miranda
Lafex/CBPF - Rio de Janeiro

I Introduction

In this paper we cover a few selected topics on DØ physics. Top physics, the W mass measurement and the inclusive jet cross section were taken as examples of fundamental tests of the Standard Model. Several interesting results were presented in the summer conferences[1]. We do not mean to exhaust the three chosen topics nor to compare our results with the ones from the other Tevatron Collider experiment, CDF [2].

Our intention is to show some of the newest results from DØ as well as presenting to a non specialist audience a flavour of how we extract physics from the data. For that reason we've decided to emphasize the top analysis description. We did not have time to detail all the topics.

The DØ detector was designed to study high transverse momentum (p_T) physics topics [3] in $\bar{p}p$ collisions. It does not have a central magnetic field, making possible a compact, hermetic detector with almost full solid angle coverage. A vertex, central and forward drift chambers provide charged particle detection in the region $|\eta| < 3.2$, where $\eta = -\ln \tan \frac{\theta}{2}$ and θ is the polar angle. The tracking system is surrounded by finely segmented uranium liquid-argon calorimeters (one central and two end-caps). The overall resolution of the DØ calorimeter is $\frac{\sigma_E}{E} = \frac{0.15}{\sqrt{E}} \oplus 0.004$ for electromagnetic showers and $\frac{\sigma_E}{E} = \frac{0.60}{\sqrt{E}}$ for hadrons. Electrons and photons are identified by the shape of their energy deposition in the calorimeter and a matching track (for electrons). A muon system consisting of proportional drift tubes and magnetized iron toroids (1.9 Tesla) located outside the calorimeter provides good muon identification in the region $|\eta| < 3.3$. The deflection of the muon candidates in the magnetic field provides the momentum measurement with a resolution of $\sigma\left(\frac{1}{p}\right) = \frac{0.18(p-2)}{p^3} \oplus 0.008$ where p is the muon momentum measured in GeV/c. Neutrinos are not identified in the detector but their transverse momentum is inferred from the missing transverse energy in the event(\cancel{E}_T)¹

II Top Physics

After the announcement of the top quark discovery by the DØ [4] and CDF [5] collaborations at the Fermilab Tevatron Collider, the DØ analysis was redone with more than twice the statistics ($\sim 100 \text{ pb}^{-1}$), now focussing on the best possible measurement of the top production cross section and mass.

Presently only Fermilab's Tevatron has sufficient energy to produce top quarks. Fortunately the top mass is such that the quark is produced with low enough momentum to keep its decay products well isolated and large enough to pass the detector thresholds, thus enabling it's observation over a huge background.

At the Tevatron, top quarks are predominantly pair produced, via $q\bar{q}$ annihilation ($\sim 85\%$) or gg fusion($\sim 15\%$) [6]. Due to its large mass, top quark decays before hadronization [7]. According to Standard Model expectations the branching ratio of process $t \rightarrow W + b$ is 99.8%. The various DØ analysis are classified by the subsequent W decay, as follows:

- *Dilepton*: both W 's decay leptonically to $e\nu$ or $\mu\nu$ (the $\tau\nu$ channel is in progress). The rather small branching ratio of these channels (5%) is compensated by the extremely small backgrounds.

¹ $\cancel{E}_T^{cal} = -\sum_i E_i \sin\theta$ where the sum i extends over all cells in the calorimeter. \cancel{E}_T includes muon in its calculation.

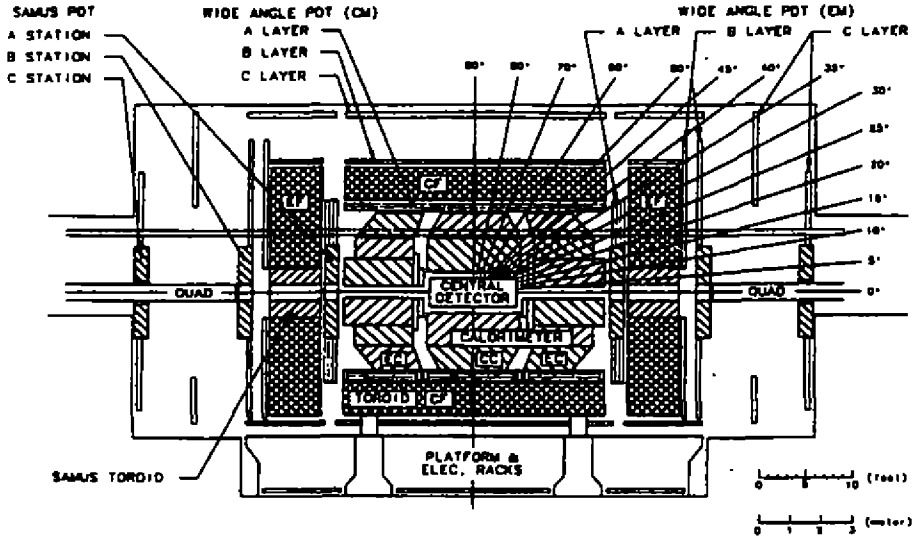


Figure 1. The DØ detector

- *Lepton+jets*: one W decays leptonically to $e\nu$ or $\mu\nu$ and the other hadronically. This is the compromising mode with a sizable branching ratio (30%) and a reasonable background. The dominant background comes from $W + jets$ direct production. These channels are subdivided into b -tagged or untagged according to whether or not a soft muon consistent with the b quark decaying semileptonically is observed. Selection criteria based on the topology of the top-like event are applied to the μ -untagged to further clean the sample. The best top mass measurement comes from these channels and will be described below.

Two other analyses are being pursued by DØ. The *all jets* channel, where both W 's decay hadronically [8] and an inclusive $e\nu + jets$ where some of the kinematic cuts are relaxed to try and recover some of the efficiency lost. We will not present these analysis. Particle identification and detector techniques are described elsewhere [3], [9].

In the various analysis that we'll present here the topology of the top-like events is explored. As result of a grid search process using Monte Carlo (to represent top signal) and data (for the background) two variables prove to be effective on reducing the background: aplanarity (\mathcal{A}) and H_T .

Aplanarity \mathcal{A} is defined after the normalized three-momentum tensor constructed from the selected jets in the event:

$$M^{ab} \equiv \frac{\sum_i p_i^a p_i^b}{\sum_i p_i^2},$$

in such a way that

$$\mathcal{A} \equiv \frac{3}{2} \times (\text{smallest eigenvalue of } M).$$

The maximum value for the aplanarity is 0.5 for a spherical event. For a planar or linear event, it is zero. Top events tend to be more spherical than events due to radiative QCD background processes. Large aplanarity means that there is little difference between the jet with the highest E_T and the one with the lowest E_T and that the jets are spherically distributed ².

H_T is defined as the scalar sum of the transverse energies of all jets which pass the selection cuts:

$$H_T \equiv \sum_i |E_T(\text{jet}_i)|$$

²Aplanarity would not be a good variable if the top quarks themselves carried very high E_T , or in the case of a much larger top mass where the b jets would take more momentum than the W decays.

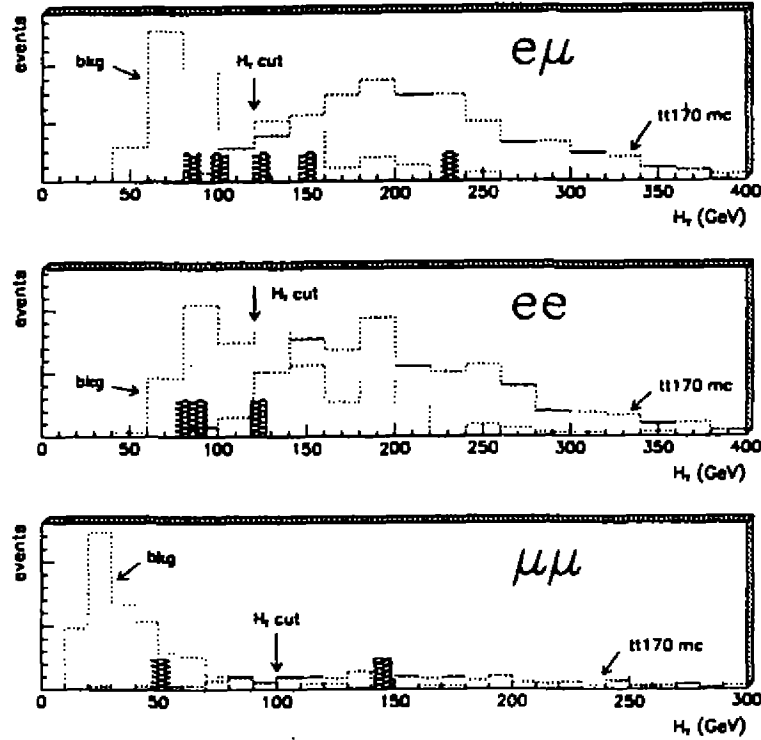


Figure 2. H_T distribution of dilepton events. The open histograms show the expected distributions for $t\bar{t}$ events for $m_t = 170$ GeV/c^2 and background. The hatched rectangles show the events from our data before the H_T cut.

A large H_T is a signature of the decay of a massive particle. It is a good variable because the top is very heavy, and it would be a poor variable for a light top.

II.1 Cross section

The Top quark production cross section is given by

$$\sigma_{t\bar{t}} = \frac{N - B}{A\mathcal{L}}$$

where N is the total number of events that survive the analysis cuts, \mathcal{L} is the integrated luminosity, B is the estimated background and A is the acceptance for top events to correct for detector, trigger and selection cuts effects, weighted by the branching ratios for the specific modes. In principle we would like to have a model independent measurement but we cannot avoid using Monte Carlo to estimate acceptances and some aspects of the background. Various generators are used and discrepancies among them are accounted for on systematic error estimation. In the following we summarize the various analysis used in the cross section measurement [14]³.

The dilepton channels are characterized by two high p_T isolated leptons (ee , $e\mu$, $\mu\mu$), two or more jets and missing E_T . Table 1 summarizes the kinematic cuts as well as topological and specific selection criteria for these modes. For the ee channel the electron's E_T are included in calculating H_T . In figure 2 we compare H_T distributions for MC top signal ($m_t = 170$ GeV/c^2), expected major backgrounds and final cuts data events. Physics backgrounds are Drell-Yan Z , $\gamma^* \rightarrow ll$, vector boson pair and heavy flavour production. To remove the specific background $Z \rightarrow ee$ we require $|m_{ee} - m_Z| > 12$ GeV/c^2 . The $\mu\mu$ events are required not to be consistent with the $Z \rightarrow \mu\mu$ hypothesis by a global kinematic fit ($\text{prob}\chi^2_{2\sigma}$). Unphysical backgrounds due to jets misidentified as electrons are estimated using data controlled samples. Typical value for the misidentification probability is 2×10^{-4} . The unphysical muon backgrounds were found to be negligible.

³We use ISAJET [10] or HERWIG [11] for top event generation, VECBOS [12] for backgrounds, and GEANT [13] to model the detector.

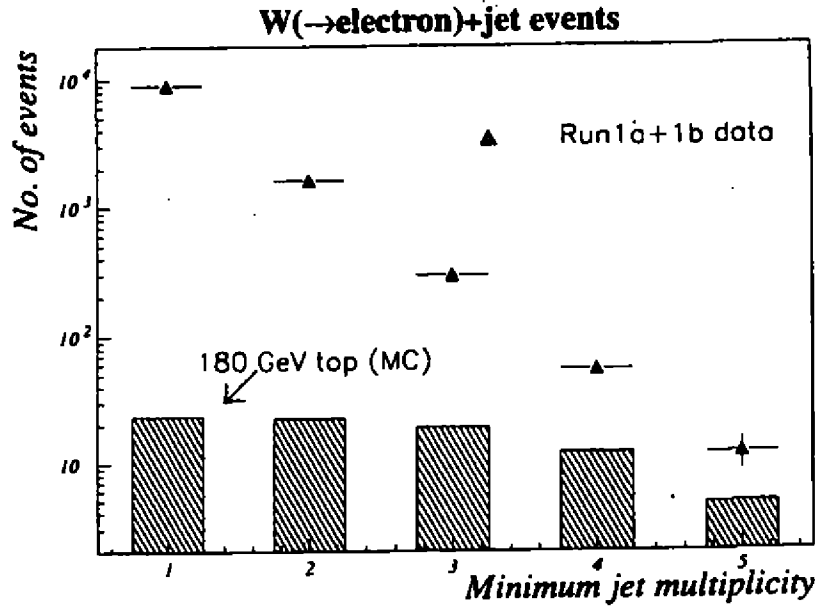


Figure 3. Multiplicity distribution of $e + jets$ after lepton identification and kinematic cuts applied.

For the three dilepton channels four events altogether survive the cuts. The background is estimated to account for 1.6 ± 0.3 events.

The signature for the $lepton + jets$ channels is one high p_T isolated lepton (e or μ), missing E_T and a number of high E_T jets (in principle top events should produce at least 4 jets, but we study the background content as a function of the jet multiplicity). Figure 3 shows the jet multiplicity spectrum for $W \rightarrow e + jets$ data, as compared to absolutely normalized $m_t = 180 \text{ GeV}/c^2$ Monte Carlo where we required p_T isolated electron and missing E_T . It becomes clear that we need more stringent selection cuts to see top events under the huge $W + jets$ background, even at large jet multiplicity. Two independent and non overlapping analyses were pursued by DØ. The first, “ μ -tag”, requires a muon to tag a semileptonic decay for one of the b quarks. These are usually soft muons running close by the jet. This is imposed by $p_{t\mu} > 4 \text{ GeV}/c^2$ and $\Delta R(\mu, jet) < 0.5$ ⁴. Since “all” top events should have two b and taking into account the inclusive branching ratio for $b \rightarrow \mu + X$, $\sim 44\%$ of the top events should have at least one μ tag. DØ reconstructs 45% of those muons leaving $\sim 20\%$ of the events with a μ -tag.

Events not selected by the μ -tag are submitted to the topological analysis. Here the emphasis is the overall shape of the top-like events. To select the events the already mentioned H_T and \mathcal{A} variables are used in such a way that minimizes the relative error in the cross section measurement, not necessarily the best signal to background ratio. In figure 4 we show a scatter plot of H_T vs. \mathcal{A} for top Monte Carlo, backgrounds and final data.

Two major backgrounds are considered. The physical background is dominant and comes from direct W production with jets. The second comes from QCD multijet production where one jet is misidentified as an e . In either case one of the jets can be a real b or c that undergoes a semileptonic decay contributing to the background on the μ -tag analysis. To estimate the background the basic ingredients are real data and the fact that $W + jets$ production follows the Berends scaling [15]:

$$\frac{NW_i}{NW_{i-1}} = \alpha,$$

where NW_i is the number of $W - l + i jets$. The estimative of the various sources of background is specific for each analysis, we take the $W + jets$ background on the $l + jets$ mode as an example. Before applying the topological cuts, and having already subtracted the unphysical background, we can write:

⁴ $\Delta R(i, j) = \sqrt{\Delta\eta_{ij}^2 + \Delta\phi_{ij}^2}$ being the distance in the $\eta - \phi$ of the objects i and j

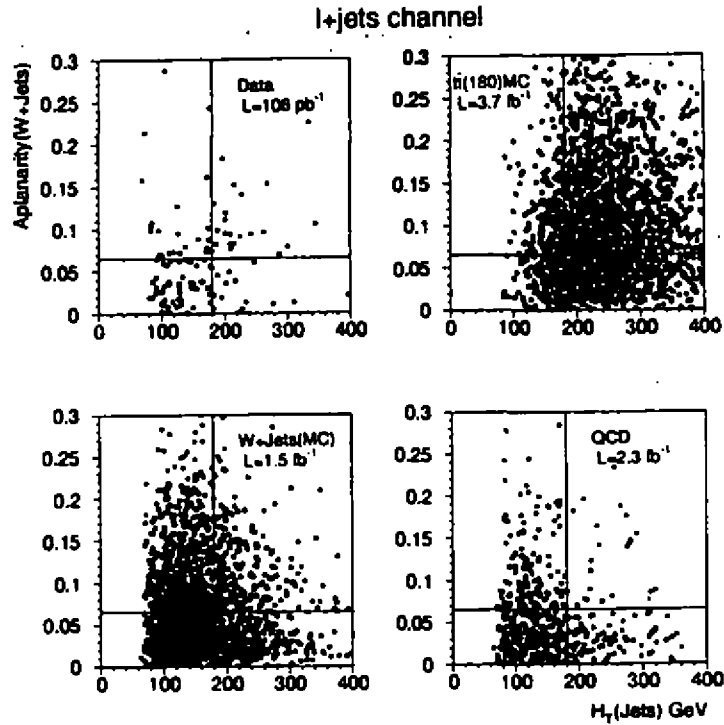


Figure 4. $A(W + jets)$ vs. H_T for data, Monte Carlo signal and $W - l\nu + jets$ and QCD multijet backgrounds.

$$N_i^{observed} = NW_1 * \alpha^{i-1} + f_i * N_t$$

Where $N_i^{observed}$ is the number of events with i or more jets, lepton identification and missing E_T . The first term on the right accounts for the direct $W + jets$ contribution. f_i is the fraction of $t\bar{t}$ expected for multiplicity i and N_t is the total number of top events surviving the kinematic cuts. NW_1 , α and N_t are extracted from an $N_i^{observed}$ vs. inclusive multiplicity plot and f_i comes from Monte Carlo. Next the topological cuts are applied and their efficiency for both top and background are extracted from Monte Carlo. As a result of this process we estimate a $W + jets$ background of 7.68 ± 2.83 and a QCD multijet contribution of 1.55 ± 0.49 events for $e/\mu + jets$ channel.

Tables 1 and 2 summarize the results for these seven channels. We observe 37 events with an expected background of 13.4 ± 3.0 events. The cross section measurement as a function of the top mass hypothesis is shown in figure 5.

Table 1: Summary of dilepton channels

channel	$e\mu + jets$	$ee + jets$	$\mu\mu + jets$
lepton p_T	> 15	> 20	> 15
electron $ \eta $	< 2.5	< 2.5	--
muon $ \eta $	< 1.7	--	< 1.0
\cancel{E}_T^{cal}	$> 20^\dagger$	> 25	--
# of jets	≥ 2	≥ 2	≥ 2
jet p_T	> 20	> 20	> 20
jet $ \eta $	< 2.5	< 2.5	< 2.5
H_T	> 120	> 120	> 100
specific cuts	--	$ M_{ee} - M_{Z^0} > 12$	$\text{prob}(\chi^2_{Z^0 fit}) < 1\%$
signal [†] ($m_t = 180$)	1.69 ± 0.27	0.92 ± 0.11	0.53 ± 0.11
$\int \mathcal{L}(\text{pb}^{-1})$	90 ± 5	106 ± 6	87 ± 5
events observed	3	1	1
Backgrounds			
$Z - \tau\tau$	0.31 ± 0.07	0.17 ± 0.04	0.03 ± 0.01
WW	0.03 ± 0.01	0.04 ± 0.02	0.009 ± 0.003
Drell-Yan $\rightarrow \tau\tau$	0.02 ± 0.03	--	--
Fake e	0.02 ± 0.01	0.32 ± 0.14	--
$Z - ll$	--	0.13 ± 0.03	0.46 ± 0.26
QCD	--	0.00 ± 0.05	0.05 ± 0.01
total	0.36 ± 0.09	0.66 ± 0.17	0.55 ± 0.28

Energy in GeV, mass in GeV/c^2 [†] Additional cut of $\cancel{E}_T \geq 10$ (includes μ)[‡] Expected number of top events based on ref [16]

Table 2: Summary of lepton+jets channels

channel	$e + jets$	$\mu + jets$	$e + jets/\mu$	$\mu + jets/\mu$
lepton p_T	> 20	> 20	> 20	> 20
lepton $ \eta $	< 2.0	< 1.7	< 2.0	< 1.7
\cancel{E}_T^{cal}	> 25	$> 20^\S$	> 20	$> 20^\S$
# of jets	≥ 4	≥ 4	≥ 3	≥ 3
jet E_T	> 15	> 15	> 20	> 20
jet $ \eta $	< 2	< 2	< 2	< 2
tagging μ^\dagger	--	--	1	1
E_T^W	> 60	> 60	--	--
A	> 0.065	> 0.065	> 0.04	> 0.04
H_T	> 180	> 180	> 110	> 110
signal [†] ($m_t = 180$)	6.5 ± 1.5	6.4 ± 1.4	2.4 ± 0.4	2.8 ± 0.9
events observed	10	11	5	6
$\int \mathcal{L}(\text{pb}^{-1})$	106 ± 6	96 ± 5	91 ± 5	96 ± 5
background	3.8 ± 1.4	5.4 ± 2.0	1.4 ± 0.4	1.1 ± 0.2

Energy in GeV, mass in GeV/c^2 [§] Additional cut of $\cancel{E}_T > 20$ (includes μ)[‡] Expected number of top events based on ref [16][†] $p_T^\mu > 4 \text{ GeV}$, $\Delta\mathcal{R}(\mu, jet) < 0.5$ ^{*} $E_T^W = |\cancel{E}_T| + |E_T^{\text{lepton}}|$

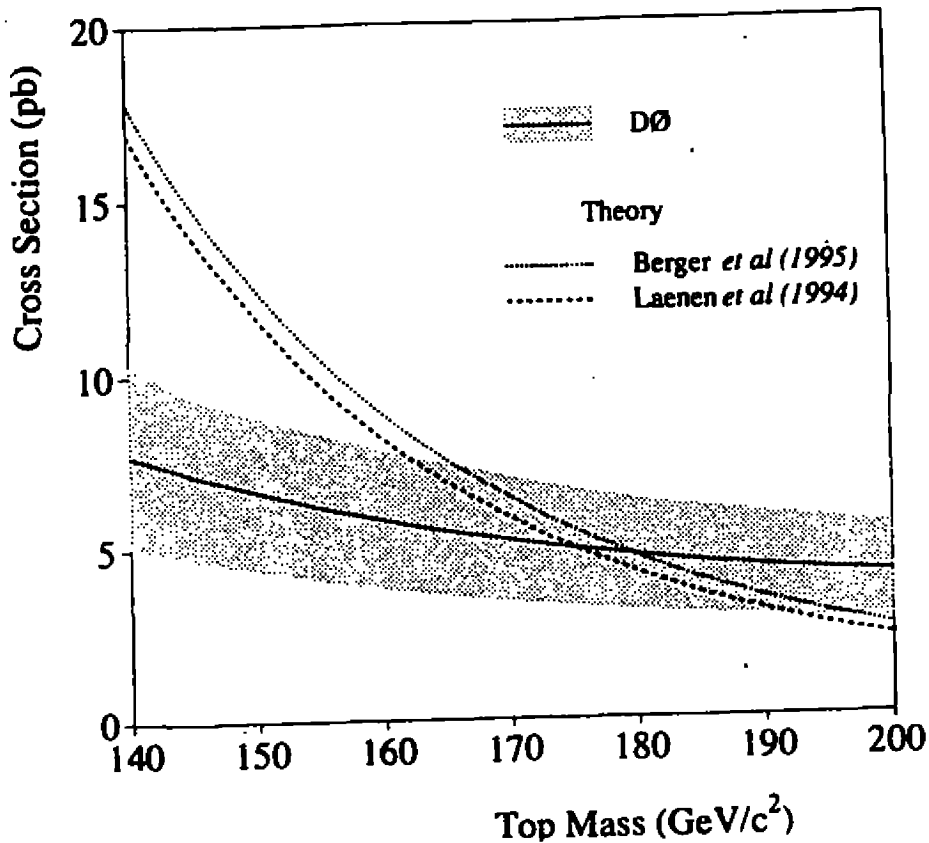


Figure 5. Top production cross section.

II.2 Mass Measurement [17]

In the direct measurement of the top mass there are two major problems. First, we don't fully measure the neutrino momentum, the transverse component is obtained from the total energy balance and its z component is undetermined. Second, except for μ -tagged jets there is no way to uniquely identify them. Here we will present the DØ measurement using only the $l + jets$ modes, that has evolved considerably since the observation. We apply the kinematic cuts listed in table 2 for the topological $l + jets$ analysis. For the subsample without a μ -tag we require $E_T^W > 60$ GeV and $|\eta_W| < 2.0$. In this selections process, 93 events survive, 8 of which have a μ -tag. Notice that the focus of the analysis changed from cross section to mass measurement and consequently, the variables chosen to select the events are very weakly correlated with the mass.

The 6 final state particles are fully determined by 18 parameters, of which we measure 17. We then perform a constrained fit to the hypothesis $m(l\nu) = m(q\bar{q}) = m_W = 80.9$ GeV/ c^2 and $m_t = m(W^+b) = m_{\bar{t}} = m(W^-\bar{b})$ to obtain what we call fitted mass (m_{fit}). As we have no *a priori* way to assign the jets (except the tagged ones) we do all combinations retaining only the best χ^2 one provided that $\chi^2 < 7$. The jet permutation runs over the 4 most energetic jets in the event. The Monte Carlo m_{fit} distribution peaks at the correct value (m_t) and the width is dominated by jet combinatorics.

After all the mentioned cuts (referred as precut), we are left with 73 events, most of which are background (signal/background $\sim 1/2$). To discriminate between signal and background we use two multivariate techniques based on the following variables:

$$v_1 \equiv E_T$$

$$v_2 \equiv \mathcal{A}$$

$$v_3 \equiv \frac{H_{T2} \equiv H_T - E_T^{j1}}{H_{||}}$$

$$v_4 \equiv \frac{K_{Tmin} \equiv (\min \text{ of } 6 \Delta \mathcal{R}_{jj}) \cdot E_T^{\text{lesser } j}}{E_T^W}$$

$$v_5 \equiv H_{T2}$$

$$v_6 \equiv K_{Tmin}$$

where $\Delta \mathcal{R}_{jj}$ is the distance between any two jets, $H_{||}$ is the scalar sum of $|p_z|$ of the jets, charged leptons, and neutrino. In the first method we construct a top likelihood discriminant (\mathcal{D}) based on the the variables $v1$ through $v4$. These variables are weakly correlated with the m_t . We fit simultaneously the mass and a likelihood discriminant distributions. The second method consist on using neural network techniques to construct a top probability discriminant (t_{prob}) based on all variables listed above. Figure 6 illustrates the discrimination power of the method.

Using the variables above mentioned we obtain a top enriched sub-sample of 32 events refered as low bias (LB), where signal/background $\sim 2/1$. The top mass results for the two samples obtained with the two methods are listed in table 3 below.

Table 3: Top mass for the precut and low bias samples obtained with the two methods

	\mathcal{D}		t_{prob}	
	PR	LB	PR	LB
m_t (Gev/ c^2)	168 ± 10	168 ± 8	169 ± 10	168 ± 7
n_s	27.5 ± 7.0	$24.5^{+9.7}_{-5.0}$	26.4 ± 7.6	26.6 ± 5.5
n_b	45.5 ± 10.0	$4.9^{+7.7}_{-2.2}$	39.5 ± 7.6	2.4 ± 2.0

III W Mass

The Standard Model requires interrelations among its parameters, and, given other measurements, the theory may predict the parameters of the W . At lowest order, an important relation holds between the weak boson masses and the weak mixing angle: $\rho = M_W/M_Z \cos\theta = 1$. Deep inelastic scattering, forward-backward and left-right asymmetries at the Z^0 resonance establish a value for the weak mixing angle, $\sin\theta_W$, that, together with the LEP precision measurement of the Z^0 mass, give a prediction for M_W . So, a precision measurement of M_W can be compared with the theory prediction.

More than that, a precise measurement of M_W , combined with other electroweak precision measurements and the measurement of the top quark mass, tests the consistency of the standard electroweak model, and within the framework of the model, can give an indication of the Higgs mass (M_H). In figure 7, the curves show the dependence of M_W on m_t in the minimal Standard Model using several Higgs masses. The data point represents the DØ current result.

DØ plans to measure the W -boson mass within ~ 50 MeV/ c^2 for the next run [18]. This measurement, coupled with a 10 GeV/ c^2 for the top mass, would severely constrain the theory and give information about the Higgs. As we will see below, the challenge here for a hadron collider is to control the momentum scale to such precision. LEP 200 also plans to measure M_W with an equivalent precision, and there the problem is to achieve the necessary statistics.

The DØ measurement is based on $W \rightarrow e\nu$ decays⁵ where the electron is detected in the central calorimeter. The calorimeter is not calibrated independently to the precision needed and therefore the ratio of the W to Z

⁵The muon mode is not used in this analysis since the electron momentum is better measured.

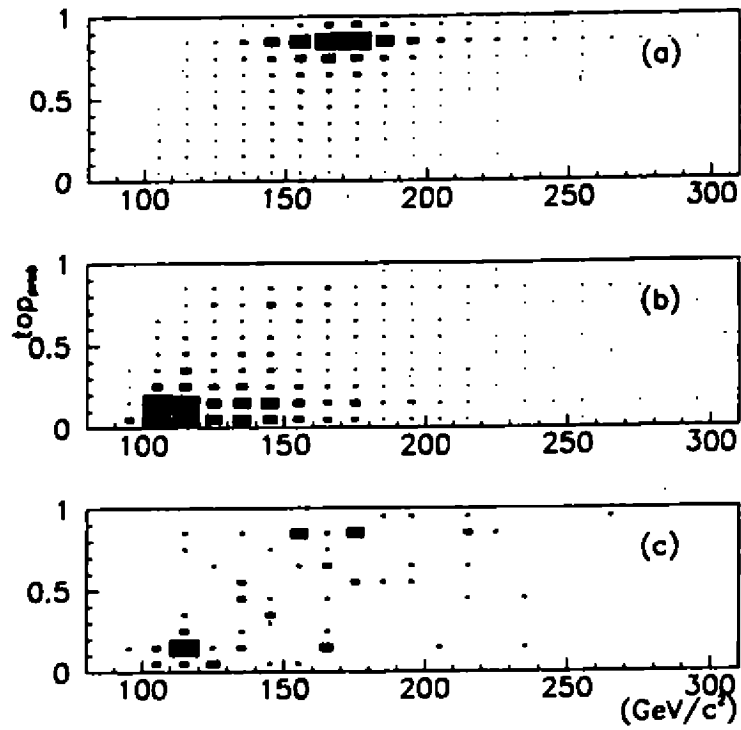


Figure 6. top_{prob} vs. m_{top} . a) $t\bar{t}$ Monte Carlo for $m_t = 170 \text{ GeV}/c^2$, b) background c) data .

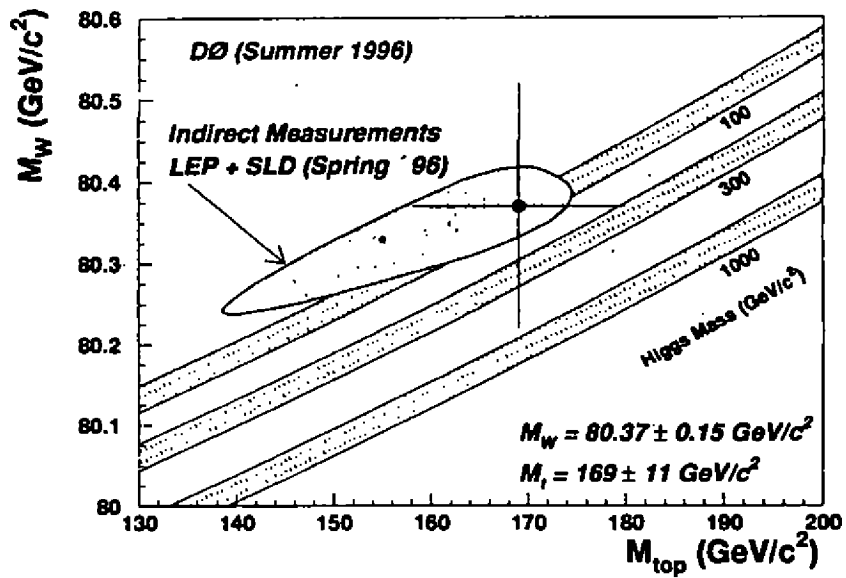


Figure 7. M_W vs. m_t .

masses was measured and scaled to the precisely known LEP/SLC Z mass. This ratio cancels various systematic uncertainties.

The longitudinal momentum of the neutrino cannot be determined because the detector cannot measure with enough precision the longitudinal component of the total energy flow of the hard scatter. The invariant mass cannot be reconstructed, which imposes the use of the “transverse mass”, the invariant mass using only the transverse components of the momentum vectors. It is defined as

$$M_T^W = \sqrt{2p_T^\nu p_T^e - 2\vec{p}_T^\nu \cdot \vec{p}_T^e}$$

where \vec{p}_T^ν and \vec{p}_T^e are the transverse momentum of the neutrino and of the electron, respectively.

The mass of the W was determined by a maximum likelihood fit of the measured M_T^W distribution to Monte Carlo distributions which were generated for several values of M_W . The fast Monte Carlo simulation used a theoretical prediction of W production and decay and a parameterized model of the detector response. The same applies to Z events. The underlying event was modelled by superimposing the W event onto a minimum bias event obtained from data. QCD multi-jet production and $Z \rightarrow ee$ events where one electron is not identified were the considered backgrounds to the W event sample.

The result is $M_W = 80.340 \pm 0.140(stat.) \pm 0.160(scale) \pm 0.165(syst.)$ GeV/ c^2 . The systematic uncertainties are dominated by the electromagnetic energy resolution, hadronic energy resolution, input $p_T(W)$ distribution and parton distribution functions, number of minimum bias events, hadronic energy scale and electron angle determination.

IV Inclusive Jet Cross Section [19] [20]

The experimental determination of the inclusive jet cross section ($\sigma(p\bar{p}) \rightarrow jet + X$) is probably one of the simplest tests of QCD, yet a very fundamental one. The complete next-to-leading order $\mathcal{O}(\alpha_s^2)$ calculations [21][22][23] have small theoretical uncertainties (10-20)%. In addition, this measurement can be used to test the validity of different sets of parton distribution functions. It is also a good place to look for “new physics”, for example quark compositeness. The Tevatron enables probing a wide portion of the phase space producing jets with large statistics up to nearly 500 GeV. DØ is particularly well suited for the task due to its highly segmented liquid argon calorimeter with $|\eta| < 4.0$ coverage.

The basic entity for this analysis is the hadronic jet. In principle we would like that the experimental definition of a jet represent theoretical quarks and gluons. More over we would like that the various experiments use the same definition in a way to simplify comparisons. In DØ jets are reconstructed offline using an interactive jet cone algorithm, with a cone radius of $\mathcal{R} = 0.7$ in the $\eta - \phi$ space [24]. Starting with preclusters formed from ≥ 1 GeV calorimeter tower seeds, the algorithm builds up a jet by including neighbouring cells. The jet E_T is defined as the sum of each cell E_T . After all jets are formed, they are split or merged according to whether they share more or less than 50% of the smaller energy jet. Effects like out of cone energy deposition, non linearity of the calorimeter for soft particles (≤ 2 GeV) and extra energy from the underlying event may deteriorate the measurement of the jet energy [19]. Calorimeter energy scale calibration is of course fundamental. We use the expected energy balance of $\gamma + 1$ jet to estimate the jet energy scale correction.

In figure 8 we show the inclusive jet cross section measurement with very good agreement with the NLO parton event generator JETRAD [22] over seven orders of magnitude. The NLO calculations require specification of the renormalization scale ($\mu = E_T/2$, where E_T is the maximum jet E_T in the generated event), parton distribution function and the parton clustering algorithm. Figure 8b shows the ratio $(D - T)/T$ for data (D) and theoretical (T) prediction based on different choices of parton distribution functions. We see that the shapes of all predictions are in very good agreement with data.

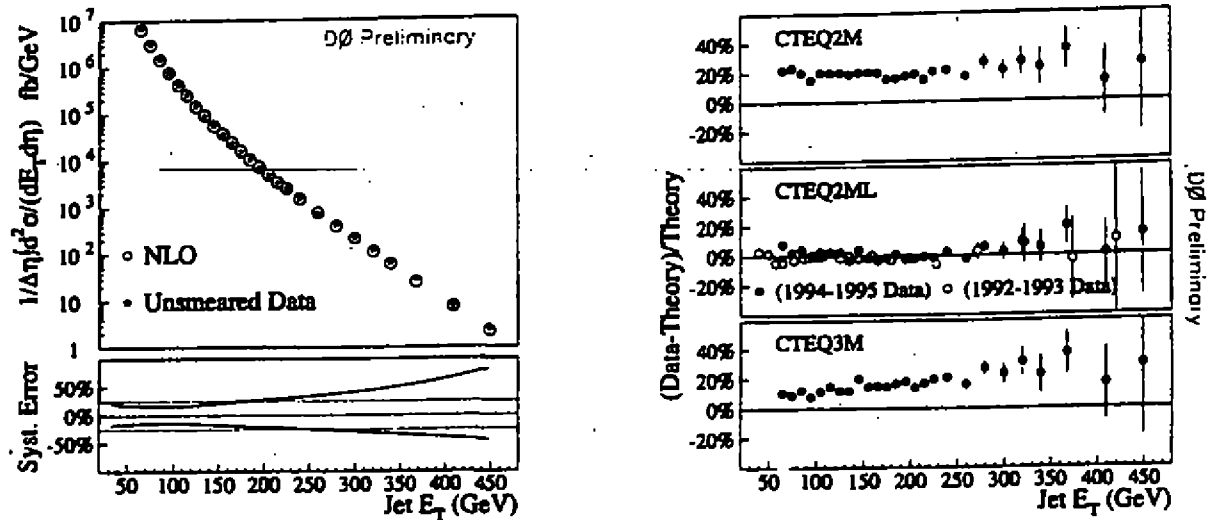


Figura 8. left) Central inclusive jet cross section, data points include statistical error. right) Difference of data and three QCD predictions normalized to theoretical prediction. The solid (open) symbols are for 1994-1995 (1992-1993) data.

V Conclusion

We presented the latest D0 results on top physics and briefly discussed the W mass measurement and the inclusive jet cross section. The D0 collaboration is working actively on the upgrade of the detector for the next run when there will be a factor of twenty increase in integrated luminosity.

References

- [1] http://d0wop.fnal.gov/d0pubs/conf_byname.html
- [2] <http://www-cdf.fnal.gov/physics/physics.html>
- [3] S. Abachi *et al.* (D0 Collaboration), Nucl. Instrum. and Methods Phys. Res., Sect. A **338**, 185 (1994).
- [4] D0 Collaboration, S. Abachi *et al.*, Phys. Rev. Lett. **74**, 2632 (1995)
- [5] CDF Collaboration, F. Abe *et al.*, Phys. Rev. Lett. **74**, 2626 (1995)
- [6] C.-P. Yuan, "Top Quark Physics", Lecture given at the VI Mexican School for Particle Physics, Villahermosa, Mexico, (1994)- HEP-PH-9503216
- [7] J.L. Lopez, D.V. Nanopoulos, G.T. Park, Xu Wang and A. Zichichi, Phys. Rev. **D50**, 2164 (1994)
- [8] E. Won, *Top Quark Study in All-Jets channel at D0*, submitted to the 1996 APS Meeting, Minneapolis, (1996)
- [9] D0 Collaboration, S. Abachi *et al.*, Phys. Rev. **D52**, 4877 (1995)
- [10] F. Paige and S. Protopopescu, BNL Report no. BNL38034, 1986 (unpublished), release 6.49
- [11] G. Marchesini *et al.*, Comput. Phys. Commun., **67**, 465, (1992)
- [12] W. T. Giele, E. Glover and D. Kosower, Nucl. Phys. **B403**, 633, (1993)
- [13] F. Carminati *et al.*, "GEANT Users Guide", CERN Program Library, December 1991 (unpublished).
- [14] M. Narain, *Top Production at D0*, presented at 1996 Rencontre de Physique de la Vallée d'Aoste on Results and Perspectives in Particle Physics La Thuile, Italy (1996); J. Bantly, *D0 Top Quark Cross Section for the 1992-1995 Tevatron Run* Proceedings of the 28th International Conference on High Energy Physics, Warsaw, Poland, (1996)
- [15] F.A. Herends, H. Kuijf, B. Takusk, and W.T. Giele, Nucl. Phys. **B357**, 32, (1991).
- [16] E. Laenen, J. Smith, and W. van Neerven, Phys. Rev. Lett. **63**, 115 (1995), Phys. Rev. D **54**, 3085 (1996)
- [17] S. Protopopescu, *Measurement of the Top Quark Mass at D0*. Proceedings of the 28th International Conference on High Energy Physics, Warsaw, Poland, (1996)
- [18] Editors D. Amidei, and R. Brock, "future ElectroWeak Physics at the Fermilab Tevatron: Report of the te2000 Study Group", FERMILAB-Pub-96/082

- [19] S. Abachi *et al.* (D0 Collaboration), "The Dijet Mass Spectrum and Angular Distributions with the DØ Detector" Proceedings of the 28th International Conference on High Energy Physics, Warsaw, Poland, (1996)
- [20] G. C. Balsey, "Preliminary Measurement of the Inclusive Jet and Dijet Cross Sections in $p\bar{p}$ Collisions at $\sqrt{s} = 1.8$ TeV", Presented at the XXXIst Rencontres de Moriond QCD and High Energy Hadronic Interactions, Les Arcs, France (1996). FERMILAB conf-96/132-E.
- [21] S. Ellis, Z. Kunszt, and D. Soper, Phys. Rev. Lett., **62**, 2188, (1989); Phys. Rev. Lett, **64**, 2121, (1990).
- [22] W. T. Giele, E. W. N. Glover and D. A. Kosower, Phys. Rev. Lett. **73** 2019 (1994) and Private communications. We use the program JETRAD written by these authors.
- [23] F. Aversa *et al.*, Phys. Rev. Lett. **65** (1990)
- [24] DØ Collaboration, S. Abachi *et al.*, Phys. Rev. Lett. **B257**, 232 (1995)

Turbulence and Quantum Field Theory

L. Moriconi

Instituto de Física, Universidade Federal do Rio de Janeiro

C.P. 68528, Rio de Janeiro, RJ — 21945-970, Brasil

We briefly review some attempts towards a field-theoretical comprehension of turbulence. After a discussion of basic phenomenological ideas, like the laminar-turbulent transition and the Kolmogorov's cascade picture of the inertial range, we introduce the fundamental set of Hopf's equations, describing the stationary statistical state of a turbulent fluid. The application of conformal field theory methods in two-dimensional turbulence is studied, as well as the computation of corrections due to realistic three-dimensional effects.

1 Introduction

Turbulence is one of the most common experiences of our everyday life. Nevertheless, its understanding has been a real challenge along the centuries. It is amazing to know that the phenomenon of turbulence was formerly studied around 500 years ago by Leonardo da Vinci, who clearly noticed the generation of eddies across a certain range of length scales in turbulent water flows, an observation that could be regarded as an anticipation of some relatively recent ideas [1, 2]. A large historical gap followed Leonardo's studies until the very first systematic investigations of turbulence by O. Reynolds [3] and Lord Rayleigh [4] in the last decades of the 19th century. Since then, many approaches and new insights have been devised, originated from completely different branches of science and technology. Even though a unified theoretical description grasping most of experimental turbulence is still lacking, we believe that field theory methods are promising, not only by their fundamental character, from which phenomenological results should be derived, but also by a number of suggestive ideas by now accumulated in the study of a plethora of models, like short-distance expansions and anomalies.

Besides the interest we may have in turbulence by itself, it is important to note that there are physical phenomena like localization in condensed matter systems [5], hadronic jets in high energy physics [6], or the dynamics of chaotic systems [7], which seem to be deeply connected with the cascade processes happening in a turbulent fluid. Essentially, all of these phenomena exhibit some kind of intermittency, or, in other words, strong deviations from simple gaussian statistics, leading to an infinite set of anomalous exponents, typical of multifractal distributions [8].

Our aim in this short review is to describe first basic phenomenological ideas and then some of the modern field theory attempts in the study of turbulence. The interested reader is also encouraged to take a look at other "classic" and recent accounts on turbulence [2, 9, 10, 11].

This paper is organized as follows. In section II, we explain in an elementary way how the laminar-turbulent transition comes into place in fluid dynamics. Furthermore, we describe the celebrated Kolmogorov's picture of the energy cascade process in fully developed turbulence [12], as well as deviations from it due to intermittency [13]. In section III, we establish the fundamental statistical equations (Hopf's equations) of turbulence and a field theory formulation for the computation of velocity correlation functions [14]. We, then, comment on some advances obtained in this way by means of renormalization group [15, 16] and saddle point techniques [17, 18]. In the next section, we examine the problem of two-dimensional turbulence. After a discussion of the orthodox view [19], the recent conformal field theory approach [20] is introduced. It should be clear, however, that purely two-dimensional turbulence is just an idealization, possibly corresponding, in the real world, to rotating fluids. An analysis of perturbations associated to the three-dimensional nature of space is carried out in section V, in the framework of the conformal approach [21]. Finally, in section VI, we comment on some problems not touched in this review, along with general conclusions and possible directions of research.

2 Phenomenological Aspects

Our basic assumption is that an incompressible fluid may be described, either in laminar or turbulent regimes, by the Navier-Stokes equations,

$$\partial_t v_\alpha + v_\beta \partial_\beta v_\alpha = -\partial_\alpha P + f_\alpha + \nu \partial^2 v_\alpha, \quad (1)$$

$$\partial_\alpha v_\alpha = 0. \quad (2)$$

Above, v_α is the velocity field, P is the pressure, f_α is an external force and ν is the viscosity. Boundary and initial conditions have also to be defined. The role of pressure is just to assure the incompressibility constraint, given by (2). Taking the divergence of (1) and using (2) we get an expression for P that may be replaced back in (1), yielding

$$\partial_t v_\alpha + \Pi_{\alpha\gamma} v_\beta \partial_\beta v_\gamma = \Pi_{\alpha\gamma} f_\gamma + \nu \partial^2 v_\alpha, \quad (3)$$

where $\Pi_{\alpha\gamma} = \delta_{\alpha\gamma} - \partial_\alpha \partial_\gamma / \partial^2$ is the projector on transverse modes. The nonlinear term of (3) is associated to convection, representing eddy interaction at different length scales, while the viscosity term is the one responsible for energy dissipation, through diffusion.

In order to discuss the laminar-turbulent transition, it is simpler to assume that there are no external forces acting on the system, that is, $f_\alpha = 0$. The transition is related, roughly, to a competition between convective and diffusive processes. To understand it, let us imagine that the fluid, initially at rest, was perturbed in a small region, Ω , such that the rms velocity in this region is now V . As the fluid evolves, Ω will grow and we may ask how long it will take to reach a size of order L . There are, in fact, two time scales here, corresponding to different physical regimes. One follows from convection and is given by $T_c \simeq L/V$. The other characteristic time is due to diffusion. If the convection term in (3) could be discarded, meaning that diffusion is the dominating process, the dynamics would be completely described by the heat equation. Therefore, the time spent in the propagation of the initial velocity configuration would be $T_d \simeq \nu/L^2$. We may define, thus, a dimensionless quantity, the "Reynolds number", given by

$$R \equiv \frac{T_d}{T_c} = \frac{LV}{\nu}. \quad (4)$$

According to the above definition, $R \rightarrow 0$ means that diffusion is much more important than convection, implying that the fluid is laminarly flowing. On the other hand, as R grows, convection starts mixing more and more portions of the fluid, diffusion is not relevant anymore and turbulence appears. We regard, more concretely, L and V as typical values for these quantities in an experiment, like the size of an object immersed in the fluid and the rms velocity close to its boundary layer, respectively. In the case of turbulence sustained by random external forces, L may be considered to be their correlation length, a natural macroscopic scale characterizing the effective system size. Perhaps the most well-known example of the laminar-turbulent transition is given by a flow past a circular cylinder. From experimental observations, it turns out that there are flow patterns below a critical Reynolds number R_c , like Kármán vortex streets. Above R_c , the flow loses its regular aspect and becomes turbulent [22]. For many diverse water flows, $R_c \simeq 10^3$, explaining why turbulence is so easily generated: for $L \simeq 1\text{cm}$, the critical velocity is $V_c \simeq 10\text{cm/s}$. The laminar-turbulent transition at a finite critical Reynolds number is still a very open problem, waiting for more experimental and theoretical investigations. In most of the fundamental studies, the interest has been concentrated in "fully developed turbulence," related to the limit $R \rightarrow \infty$.

In 1941, Kolmogorov [12] proposed a cascade theory of turbulence, establishing, through simple dimensional arguments, the universal decay of the energy spectrum in Fourier space, for the region of higher wave numbers. The cascade mechanism, qualitatively foreseen by L. Richardson [23] several years before Kolmogorov's work, is something that may be understood directly from equations (3). As mentioned before, in a slightly diverse way, the convection term in the Navier-Stokes equations represents a coupling between different Fourier modes of the velocity field. On the other hand, the viscosity term implies that energy dissipation is more intense at higher wave numbers. Kolmogorov's idea, combining these two effects, is that in fully developed turbulence, eddies will "break" into smaller ones until they reach a minimum size, where dissipation acts. It is assumed that there is an

energy cascade from large to small scales, characterized by an energy transfer rate which is constant and viscosity independent.

We may express the averaged energy density in the fluid as

$$\frac{1}{2} \langle v^2(x) \rangle = \int_0^\infty E(k) dk, \quad (5)$$

where $E(k)$ is the energy spectrum at wave number k . In order to define the energy transfer rate, $\epsilon(\bar{k})$, at wave number \bar{k} , we imagine that at some time, t_0 , when the fluid was already in a stationary statistical regime, all the external forces were turned off, so that

$$\epsilon(\bar{k}) = -\partial_t \left[\int_0^{\bar{k}} E(k, t) dk \right]_{t=t_0^+} \equiv \epsilon. \quad (6)$$

Thus, according to Kolmogorov's reasoning, it follows that in general, $E(k) = F(\epsilon, k)$. The only possible choice, considering the dimensions of ϵ and k , is to take $F(\epsilon, k) = C_{\text{ko}} \epsilon^{2/3} k^{-5/3}$, where C_{ko} is a dimensionless and universal constant. In a similar way, the "Kolmogorov length scale," η , where dissipation starts being relevant and viscosity cannot be discarded anymore, may be proposed to depend only on ϵ and ν . Using again dimensional analysis, we get $\eta \sim (\nu^3/\epsilon^2)^{1/4}$. It is important to observe that as viscosity vanishes so does η . Also, if one wants to study turbulence in a discrete version of space, at Reynolds number R , the number of lattice sites should be, roughly, $N \simeq (L/\eta)^3 \simeq R^{9/4}$, showing why it is so hard to perform straightforward computer simulations of turbulence at higher Reynolds numbers, without the use of additional assumptions.

The Kolmogorov's picture of turbulence may be summarized by noticing that it distinguishes essentially three different physical processes happening in Fourier space, each one associated to well-defined length scales:

- Energy pumping occurs at scales given by $0 \leq k < 1/L$, where L is the length scale of external random forces. This is not a universal region, since velocity correlation functions will depend on the specific forcing mechanisms or on the system geometry;
- The energy generated at larger scales is transferred to smaller wave numbers across the region $1/L < k < 1/\eta$. In particular, we hope that velocity fluctuations will have a universal character for $1/L \ll k \ll 1/\eta$, the so-called "inertial range," where energy pumping and dissipation are not relevant and the energy spectrum decays as $E(k) \sim k^{-5/3}$. It is also believed that translation symmetry and isotropy, broken at larger scales, are restored in the inertial range;
- Finally, at scales given by $k > 1/\eta$, energy is completely dissipated, through annihilation of the small eddies created at the end of the inertial range.

In the field theory approach to turbulence, one is mainly interested to find results in the inertial range, working in the presence of natural infrared and ultraviolet cutoffs, given by $1/L$ and $1/\eta$, respectively. In principle, the limits $L \rightarrow \infty$ and $\eta \rightarrow 0$ should be taken, leading to physically acceptable answers, like velocity correlation functions or probability distribution functions.

A large amount of experimental and numerical data has been collected supporting Kolmogorov's theory in its general aspects [24]. However, there are deviations concerning predictions for the scaling exponents of the structure functions, $S_p(|\vec{x} - \vec{y}|) \equiv \langle |\vec{v}(\vec{x}) - \vec{v}(\vec{y})|^p \rangle$. From Kolmogorov's analysis, it follows that in the inertial range, defined by $\eta \ll |\vec{x} - \vec{y}| \equiv r \ll L$, we must have $S_p(r) \sim r^{\zeta(p)}$, with $\zeta(p) = p/3$. In this respect, general arguments tell us that $\zeta(3) = 1$, one of the few quantitative exact results in turbulence [25], and also that $\zeta(p)$ is a convex curve, that is $\zeta''(p) \leq 0$, as it follows from probability theory [26]. Anselmetti et al. [13] obtained experimentally that $\zeta''(p) < 0$, in contradiction with the expected linear behavior of $\zeta(p)$. The physics behind this disagreement has to do with an old comment by Landau [10], regarding Kolmogorov's theory. The point is that in the eddy fragmentation process, it was assumed that the energy transfer rate is a non-fluctuating quantity. However, it is likely that, while the mean energy transfer rate is really scale independent, fluctuations might introduce a length scale in the problem, modifying the scaling exponents. Later on, and even before experimental studies, Kolmogorov [27] and Obukhov [28] tried to include the effects of possible energy transfer fluctuations in the original cascade theory. Anyway, experiments still show deviations when these improvements are taken into account.

A better phenomenological understanding of the scaling exponents is due to the multifractal theory of eddy fragmentation [7], where it is supposed that the eddies generated in the cascade towards smaller scales do not fill all space, but in fact give rise to a multifractal structure. The multifractal model is physically related to the phenomenon of intermittency [9], viz., the existence of strong fluctuations of the velocity field, far beyond the ones predicted by any simple gaussian statistics. It is, however, a very phenomenological model, containing a certain number of arbitrary parameters whose values are defined so that the best agreement with experiments may be achieved. Recently, a conceptually simpler phenomenological model with no arbitrary parameters was proposed [29], based on a hierarchy of singular structures like vortex filaments, leading to an accurate prediction of the scaling exponents.

Another recent progress concerns the behavior of $S_p(r)$ for the dissipative region, $r < \eta$, where no simple scaling relation exists. Surprisingly, the crossover from the inertial range to the dissipative region was found to be well described by $S_p(r) \sim [f(r)r]^{\zeta(p)}$, where $f(r)$ gives corrections to the scaling behavior in the dissipative region [30]. This result, named "Extended Self Similarity" (ESS), has been useful for the analysis of experimental data, yielding more precise values for $\zeta(p)$, resorting to the fact that $\zeta(3) = 1$. We believe that ESS is indeed a property shared by a larger class of multifractal systems, like strange attractors and localized electrons in random potentials, as indicated in some numerical computations [31].

3 Statistical Field Theory Formulation

In the statistical field theory approach to sustained turbulence, we are interested to compute N-point correlation functions, like

$$G_{\{\alpha_i\}}^{(N)}(\{\vec{x}_i, t_i\}) \equiv \langle \prod_{i=1}^N v_{\alpha_i}(\vec{x}_i, t_i) \rangle . \quad (7)$$

There are many ways to define the averaged product of fields considered in (7). We may choose a set of different initial conditions and, then, after a long time, when the fluid has reached a stationary statistical state, take the average over the ensemble generated in this way. Another procedure, this time independent of initial conditions, is based on an ergodic hypothesis, yielding

$$\langle \prod_{i=1}^N v_{\alpha_i}(\vec{x}_i, t_i) \rangle = \lim_{T \rightarrow \infty} \frac{1}{T} \int_0^T dt \prod_{i=1}^N v_{\alpha_i}(\vec{x}_i, t_i + t) . \quad (8)$$

A third method of computing averages, which will be the one we will consider in practice, is to imagine that the fluid is evolving under the influence of external random forces. Averages are now taken over the ensemble corresponding to all realizations of the stochastic forces. Of course, in order to obtain meaningful results, we have to suppose that the random forces f_α act at large length scales, without spoiling general features of the inertial range, which is the region we want to describe. The simplest choice for the statistics of random forces is the gaussian case, where

$$\langle f_\alpha(\vec{x}, t) f_{\alpha'}(\vec{x}', t') \rangle = g \delta_{\alpha, \alpha'} \delta(t - t') F(|\vec{x} - \vec{x}'|) . \quad (9)$$

Above, $F(r)$ is a function which decays quickly for $r > L$. We may take $F(r) \sim L^3 \exp(-r^2/L^2)$. Physical results correspond to the large scale limit, $L \rightarrow \infty$, such that the Fourier transform of $F(r)$ approaches $\tilde{F}(\vec{k}) \sim \delta^3(\vec{k})$.

Defining the correlation function (7) at equal times, $t_i = t$, an equation describing the asymptotic stationary statistical limit may be promptly obtained: $\partial_i G_{\{\alpha_i\}}^{(N)}(\{\vec{x}_i, t\}) = 0$, that is,

$$0 = \sum_{j=1}^N \langle v_{\alpha_1}(\vec{x}_1, t) \dots \partial_i v_{\alpha_j}(\vec{x}_j, t) \dots v_{\alpha_N}(\vec{x}_N, t) \rangle . \quad (10)$$

Using now equations (3), we may replace the above time derivatives by expressions containing random forces and space derivatives of the velocity field. We get

$$0 = \sum_{j=1}^N \left[- \langle \Pi_{\alpha_j \gamma} v_\beta(\vec{x}_j, t) \partial_\beta v_\gamma(\vec{x}_j, t) \prod_{i=1, i \neq j}^N v_{\alpha_i}(\vec{x}_i, t) \rangle \right]$$

$$+ g \sum_{i=1, i \neq j}^N \delta_{\alpha_j, \alpha_i} F(|\vec{x}_j - \vec{x}_i|) < \prod_{l=1, l \neq i, j}^N v_{\alpha_l}(\vec{x}_l, t) > + \nu \frac{\partial^2}{\partial x_j^2} < \prod_{i=1}^N v_{\alpha_i}(\vec{x}_i, t) > \Big], \quad (11)$$

where we used the result that for gaussian random forces, described by (9), holds [32]

$$< f_{\alpha}(\vec{x}, t) \prod_{i=1}^N v_{\alpha_i}(\vec{x}_i, t) > = g \sum_{i=1}^N \delta_{\alpha, \alpha_i} F(|\vec{x} - \vec{x}_i|) < \prod_{j=1, j \neq i}^N v_{\alpha_j}(\vec{x}_j, t) > . \quad (12)$$

The so-called Hopf's equations, given by (11), mix correlation functions with different number of points. We have, therefore, an infinite chain of coupled equations, similar to the Schwinger-Dyson equations of quantum field theory. In the past, many (modestly successful) attempts based on closure techniques were devised, consisting of truncations which would render (11) a finite and closed set of equations [33].

A further simplification is obtained if these correlation functions are studied in the inertial range, that is, taking $\eta \ll |\vec{x}_i - \vec{x}_j| \ll L$. In this situation, we may neglect in (11) terms proportional to g and ν , since external forces and viscosity play their roles out of the inertial range. Hopf's equations become now

$$0 = \sum_{j=1}^N < \Pi_{\alpha_j, \gamma} v_{\beta}(\vec{x}_j, t) \partial_{\beta} v_{\gamma}(\vec{x}_j, t) \prod_{i=1, i \neq j}^N v_{\alpha_i}(\vec{x}_i, t) > . \quad (13)$$

The consequence of neglecting the mechanisms of energy injection and dissipation is that we need to do more than merely solve (13). We could find, in principle, many solutions of the simplified Hopf's equations, with none of them satisfying the physical imposition of a constant energy flux through the inertial range. In order to establish a relation for the energy flux in Fourier space, let us consider the fluid as initially at rest and contained in a volume $V \rightarrow \infty$, where periodic boundary conditions were imposed. Its evolution, as governed by the stochastic N-S. equations, will be described, therefore, by translation invariant and isotropic correlation functions. The time dependence of the energy spectrum is obtained from

$$\frac{\partial}{\partial t} E(k, t) + \frac{\partial}{\partial k} J(k, t) = \frac{1}{2V} [< \tilde{f}_{\alpha}(\vec{k}, t) \tilde{v}_{\alpha}(-\vec{k}, t) > + c.c. >] - \nu k^2 E(k, t) , \quad (14)$$

where

$$J(k, t) = \frac{1}{V} \int_{|\vec{k}'| \leq k} d^3 \vec{k}' < [\Pi_{\alpha\gamma} v_{\beta} \partial_{\beta} v_{\gamma}]_{\vec{k}} \tilde{v}_{\alpha}(-\vec{k}', t) > \quad (15)$$

and $[\Pi_{\alpha\gamma} v_{\beta} \partial_{\beta} v_{\gamma}]_{\vec{k}}$, is a notation for the Fourier components of the convection term. Equation (14) gives the energy balance in the fluid. In the asymptotic statistical limit, $\partial_t E(k, t) \rightarrow 0$. In this case, taking a wave number k in the inertial range, $1/L \ll k \ll 1/\eta$, the RHS of (14) may be discarded, implying that $\partial_k J(k) = 0$. This means that in real space, for $\eta \ll |\vec{x} - \vec{y}| \ll L$, we must have

$$< (\Pi_{\alpha\gamma} v_{\beta} \partial_{\beta} v_{\gamma}) \Big|_{\vec{x}} v_{\alpha}(\vec{y}) > \sim |\vec{x} - \vec{y}|^0 = const. \quad (16)$$

In this way, Hopf's equations (13) are supplemented by the constraint of a constant energy flux in the inertial range, written as (16). If (13) and (16) admit more than one solution, further work will be necessary to single out the answer compatible with the large scale statistics of the random forces. In three dimensions, the solution of the above equations is still a major problem of turbulence theory. In two dimensions, as we will see in the next sections, some advances were obtained recently, through the application of conformal field theory methods.

A field theory formalism, developed by Martin, Siggia and Rose [14], from which Wyld's perturbative expansion [34] may be obtained, addresses in a fundamental way the problem of computing velocity correlation functions. It amounts in defining the generating functional

$$Z[j] = \mathcal{N} \int D\hat{v} Dv \exp \left(-S[v, \hat{v}] + i \int d^d \vec{x} dt j_{\alpha}(\vec{x}, t) v_{\alpha}(\vec{x}, t) \right) , \quad (17)$$

where

$$\begin{aligned} S[v, \hat{v}] &= i \int d^d \vec{x} dt \hat{v}_{\alpha} (\partial_t v_{\alpha} + \Pi_{\alpha\gamma} v_{\beta} \partial_{\beta} v_{\gamma} - \nu \partial^2 v_{\alpha}) \\ &+ g \int d^d \vec{x}_1 d^d \vec{x}_2 dt \hat{v}_{\alpha}(\vec{x}_1, t) \hat{v}_{\gamma}(\vec{x}_2, t) \Pi_{\alpha\gamma} F(|\vec{x}_1 - \vec{x}_2|) , \end{aligned} \quad (18)$$

in such a way that N-point correlation functions may be written as

$$G_{\{\alpha_i\}}^{(N)}(\{\vec{x}_i, t_i\}) = \frac{1}{i^N} \prod_{i=1}^N \frac{\delta}{\delta j_{\alpha_i}(\vec{x}_i, t_i)} Z[j] \Bigg|_{j=0} \quad (19)$$

For the sake of simplicity, we omitted, in (17), a jacobian which just cancels tadpole diagrams in a perturbative expansion, where the only vertex is given by the nonlinear convection term.

Straightforward perturbation theory is faded to fail here. As the limit $L \rightarrow \infty$ is carried out, individual terms in the perturbative expansion will show infrared divergencies, suggesting, due to unsuccessful efforts to regularize them, that the problem has to be attacked essentially by nonperturbative methods. Anyway, a renormalization group procedure, based on a perturbative approach has been studied [15], where the force-force correlation function (9) is replaced by a different expression, which would, hopefully, correspond somehow to an effective theory of the inertial range. The replacement is given, in Fourier space, by

$$\tilde{F}(k) = D_0 k^{4-d} (m_0^2 + k^2)^{-\epsilon/2} \quad (20)$$

Above, d is the dimension of space, $\epsilon \geq 0$ is an arbitrary parameter, playing a role similar to the one in the ϵ -expansion in critical phenomena, and $m_0 \rightarrow 0$ is an infrared regulator. It turns out that the field theory given by (17) has an infrared stable fixed point, with $E(k) \sim k^{1-\frac{2}{3}\epsilon}$ and renormalized Reynolds number $R \sim \epsilon^{1/2}$. As $\epsilon \rightarrow 4$, we recover Kolmogorov's law of energy spectrum decay. Even though there are conceptual problems (turbulence should not be associated to a stable infrared fixed point) and also technical difficulties (there are infrared divergencies as $\epsilon > 3$) in this ad hoc formulation, a number of quantitative results [16] show a remarkable agreement with experiments, like the prediction of the Kolmogorov's constant, $C_{ko} \sim 1.6$.

An important problem of turbulence is the evaluation of probability distribution functions of velocity dependent observables, like $\mathcal{O}(v_\alpha) = (\vec{v}(\vec{x}) - \vec{v}(\vec{y})) \cdot \hat{n}$, where \hat{n} is an arbitrary unit vector. They are defined as

$$P(\mathcal{O}(v_\alpha)) = \frac{1}{2\pi} \int_{-\infty}^{\infty} d\lambda \langle \exp(i\lambda \mathcal{O}(v_\alpha)) \rangle \quad (21)$$

Recently, it has been proposed that the saddle-point solutions obtained from the modified action

$$S_\lambda[v, \hat{v}] = S[v, \hat{v}] + i\lambda \mathcal{O}(v_\alpha) \quad (22)$$

may give the non-gaussian tails of probability distribution functions related to intermittency [17]. The first investigations so far have been motivating, specially regarding applications in one-dimensional turbulence, where many diverse techniques may be compared [18, 35, 36, 37].

4 Two-dimensional Turbulence

Investigation of turbulence in other than three dimensions has shown, in general, interesting concrete applications. In the real world, approximately two-dimensional motion may be observed in many systems, like soap films, stratified flows, or rotating fluids [38]. The later, in particular, have been receiving much attention due to their relevance to oceanic and atmospheric sciences. One of the advantages of lower-dimensional turbulence is that higher Reynolds numbers may be achieved in numerical simulations. Also, as a general rule, intermittency effects are more pronounced here than in the three-dimensional case, making it easier, in principle, to study their generation mechanisms.

Defining the stream function ψ by the relation $v_\alpha = \epsilon_{\beta\alpha} \partial_\beta \psi$ and the vorticity $\omega = \partial^2 \psi$, the two-dimensional N-S. equations for ω may be written as

$$\partial_t \omega + \epsilon_{\alpha\beta} \partial_\alpha \psi \partial^2 \partial_\beta \psi = \epsilon_{\alpha\beta} \partial_\alpha f_\beta + \nu \partial^2 \omega \quad (23)$$

In the inviscid case ($\nu = 0$) and in the absence of external forces, the above equation implies that there is, besides energy, an infinite number of conserved quantities, given by

$$I_n = \int d^2 \vec{x} \omega^n, \quad (24)$$

where n is a positive integer. I_2 is known as “enstrophy,” having an important role in the cascade picture of two-dimensional turbulence. Kraichnan [19] advanced the hypothesis that not only energy, but also these additional conserved quantities would flow across the inertial range. A careful analysis of the energy and enstrophy fluxes leads to a surprising result. Energy is transported now to larger length scales, while enstrophy flows towards smaller ones, in such a way that both fluxes cannot coexist in the same range of wave numbers. Regarding the energy spectrum, if the system is forced at wave number k_0 , the energy transport to wave numbers $k < k_0$ is characterized by $E(k) \sim k^{-5/3}$, as in the Kolmogorov’s theory, and the constant enstrophy flux towards $k > k_0$ is associated with $E(k) \sim k^{-3}$. It is believed that Kraichnan’s idea of the enstrophy cascade is physically correct, but numerical simulations [39] show that the energy spectrum decay is given by exponents close to -3.5 , varying according to the nature of the large scale external forcing.

Polyakov has suggested, recently, a conformal field theory approach to two-dimensional turbulence [20], from which the exponents describing the energy spectrum decay may be found exactly. Conformal methods have been very important in the understanding of critical phenomena in two dimensions, where specific models were seen to correspond to different realizations of the Virasoro algebra. Among the conformal theories, the “minimal models” play a special role, since they have a finite number of scaling operators. These models [40] are generically defined by a pair of relatively prime numbers, (p, q) , with $p < q$. They contain a subset of $(p-1)(q-1)/2$ scalar primary operators, $\psi_{(m,n)}$, labelled by $1 \leq m < p$ and $1 \leq n \leq (q-1)/2$, if p is even, or $1 \leq m \leq (p-1)/2$ and $1 \leq n < q$, otherwise, having dimensions $\Delta_{(m,n)} = ((pn - qm)^2 - (p - q)^2) / 4pq$. The reason for the choice of scalar operators is that we deal with isotropic correlation functions in the turbulence problem. The operator product expansion (OPE) of two primary operators $\psi_{(r_1,s_1)}(z)$ and $\psi_{(r_2,s_2)}(z')$, with $|z - z'| \rightarrow 0$ is written as

$$\begin{aligned} \psi_{(r_1,s_1)}(z)\psi_{(r_2,s_2)}(z') &= \sum_{(r_3,s_3)} (a\bar{a})^{(\Delta_{(r_3,s_3)} - \Delta_{(r_1,s_1)} - \Delta_{(r_2,s_2)})} \sum_{(n,m)} C_{\{(n_1,\dots,n_k);(m_1,\dots,m_l)\}}^{(r_3,s_3)} \\ &\times L_{-n_1} \dots L_{-n_k} \bar{L}_{-m_1} \dots \bar{L}_{-m_l} a \sum^n \bar{a} \sum^m \psi_{(r_3,s_3)}(z), \end{aligned} \quad (25)$$

where $|r_1 - r_2| + 1 \leq r_3 \leq \min(r_1 + r_2 - 1, 2p - r_1 - r_2 - 1)$, $|s_1 - s_2| + 1 \leq s_3 \leq \min(s_1 + s_2 - 1, 2q - s_1 - s_2 - 1)$ and we have introduced, in (25), the Virasoro generators of conformal transformations, L_{-n} and \bar{L}_{-n} . The interest in these models is related not only to their finite number of primary operators, but also to the fact that their dimensions and the form of short distance products are completely known.

Let us now apply the above operator structures in the problem of two-dimensional turbulence. We may write Hopf’s equations for the vorticity correlation functions,

$$\partial_t [\langle \omega(x_1, t) \omega(x_2, t) \dots \omega(x_n, t) \rangle] = 0, \quad (26)$$

where time derivatives are expressed through equations (23). In the inertial range, as discussed in the previous section, both forcing and viscosity terms may be neglected in order to formulate a simplified set of Hopf equations. Considering, furthermore, the convection term in (23) as a vanishing point-split product of fields, that is, $\oint_{|z-z'|=|a|} (dz'/a) \epsilon_{\alpha\beta} \partial_\alpha \psi(z) \partial^2 \partial_\beta \psi(z') \rightarrow 0$, when $|z - z'| \rightarrow 0$, we would have, then, an exact solution of (26). A concrete realization of this possibility may be achieved if we regard the stream function ψ as a primary operator of some conformal minimal model. In this case, we may use all the available information on operator dimensions and OPE’s to obtain physical results. According to this assumption, let ϕ be the primary operator which has the lowest dimension, $\Delta\phi$, appearing in the OPE $\psi\psi$, between fields with the same dimension $\Delta\psi$. Taking $a \equiv |a| \exp(i\theta)$, we will have, thus,

$$\begin{aligned} &\lim_{|a| \rightarrow 0} \oint_{|z-z'|=|a|} \frac{dz'}{a} \epsilon_{\alpha\beta} \partial_\alpha \psi(z) \partial^2 \partial_\beta \psi(z') \\ &\sim \int d\theta [\partial_\alpha^2 \partial_a \partial_z - \partial_a^2 \partial_a \partial_z] (a\bar{a})^{(\Delta\phi - 2\Delta\psi)} \sum C_{(n,m)} L_{-n_1} \dots L_{-n_k} \bar{L}_{-m_1} \dots \bar{L}_{-m_l} a \sum^n \bar{a} \sum^m \phi(z, \bar{z}) \\ &\sim (a\bar{a})^{(\Delta\phi - 2\Delta\psi)} [L_{-2} \bar{L}_{-1}^2 - \bar{L}_{-2} L_{-1}^2] \phi, \end{aligned} \quad (27)$$

as the dominant contribution in this short distance product. It is important to note that in order to get (27) it was necessary to set $C_{\{1,2\}} = C_{\{2,1\}}$ and $C_{\{1,(1,1)\}} = C_{\{(1,1),1\}}$, as it follows from the pseudoscalar nature of the ϵ factor

above. We see, then, that (27) vanishes with $|a| \rightarrow 0$ if

$$\Delta\phi > 2\Delta\psi, \quad (28)$$

which is one of the constraints that the chosen minimal model has to satisfy. An additional constraint comes from the condition of a constant enstrophy or energy flux through the inertial range. In the energy cascade case this means, according to (16), that $\langle \dot{v}_\alpha(x)v_\alpha(0) \rangle \sim x^0$. Analogously, it may be proved that the condition for a constant enstrophy flux is $\langle \dot{\omega}(x)\omega(0) \rangle \sim x^0$, which gives

$$\langle \dot{\omega}(x)\omega(0) \rangle \sim (u\bar{a})^{(\Delta\phi-2\Delta\psi)} \langle [(L_{-2}\bar{L}_{-1}^2 - \bar{L}_{-2}L_{-1}^2)\phi(x)]\partial^2\psi(0) \rangle. \quad (29)$$

The correlation function at the RHS of (29) is now evaluated by means of a purely dimensional argument, as $L^{-2(\Delta\phi+\Delta\psi+3)}$, which makes sense if one thinks that there is an effective infrared cutoff in the theory at the length scales given by L , where random forces act. Imposing (29) to be independent of L , we get

$$\Delta\phi + \Delta\psi + 3 = 0. \quad (30)$$

In the case of an energy cascade, the argument is the same and the constraint turns out to be

$$\Delta\phi + \Delta\psi + 2 = 0. \quad (31)$$

It is known that there is an infinite number of minimal models compatible with (28) and (30) or (31) [41, 42]. The general belief, and still an open problem, is that there may be universality classes, associated to the statistical properties of the forcing terms, which would single out one or another of the possible solutions. Let us note that the minimal models found in this way are non-unitary, since the short-distance product $\psi(z)\psi(z')$ goes to zero when $z \rightarrow z'$.

An alternative analysis of conformal turbulence regards the existence of boundary effects on the vacuum expectation values (VEV's) of single operators in non-unitary theories [43]. In this case, one has to consider the OPE between $\phi(x)$ and $\psi(0)$ in (29), picking up the most relevant operator, let us say, χ . Now, (30) is modified to $\Delta\phi + \Delta\psi - \Delta\chi + 3 = 0$, with an analogous change for the constant energy flux condition. Some of these further solutions (in the enstrophy cascade picture) were obtained in ref. [44].

The connection of the conformal approach with real experiments or numerical simulations is made through the computation of inertial range exponents, which describe the decrease of energy in the region of higher Fourier modes. In the situation where VEV's of single operators vanish, the inertial range exponents are given by $4\Delta\psi + 1$ and, in the opposite case, by $4\Delta\psi - 2\Delta\phi + 1$. A good agreement has been reached between the former possibility, for the direct enstrophy cascade case, and numerical simulations [39, 45, 46] of the two-dimensional Navier-Stokes equations. There are, however, deviations with the results obtained in real laboratory investigations [47]. In fact, as we will show next, the inclusion of three-dimensional effects in the conformal field theory approach may give corrections to the inertial range exponents, in reasonable agreement with experimental data [21].

5 3-D Perturbations in Conformal Turbulence

In a series of interesting experiments, Hopfinger et al. [48, 49, 50] studied the turbulence phenomenon as it happens in a rotating tank, where at its bottom there was an oscillating grid responsible for perturbations of the fluid motion. According to the Taylor-Proudman theorem [51, 52, 53] a rotating fluid tends to behave as if it were two-dimensional and in fact this was observed in the form of coherent structures (vortices) organized in the direction parallel to the rotation axis of the tank. However, "defects" in the vortices were seen to propagate from the very turbulent region at the bottom of the tank up to the effectively two-dimensional system. The essential picture extracted from these observations is that the fluid should be best described in terms of two-dimensional equations containing not only large scale forcing terms but also small scale random perturbations, originated from either vortex-breakdown or soliton pulses propagating along vorticity filaments. The experimental data suggested then the existence of an inertial range, likely to be related to a direct enstrophy cascade and well approximated by $E(k) \sim k^{-2.5}$, which

represents a less steep energy spectrum than the one obtained by Kraichnan, $E(k) \sim k^{-3}$, or even other proposals [54, 55], not excluding conformal turbulence [41]. This puzzling result is presently understood to be due only to the measurement techniques used in the experiments, based on the analysis of the dispersion of suspended particles in the fluid [50]. More recently, similar experiments were conducted by Narimousa et al. [47] and direct measurements of the turbulent velocity field were recorded. The results pointed out the existence of a possible energy spectra $E(k) \sim k^{-5/3}$ at lower wave numbers, in agreement with the conjecture of an inverse energy cascade [19], and a range at higher wave numbers, where $E(k) \sim k^{-5.5 \pm 0.5}$. In this region, the spectral slope was seen to depend on the controlling external conditions, with results varying from $E(k) \sim k^{-5.0}$ up to $E(k) \sim k^{-6.0}$. It is worth to note that a spectral law $E(k) \sim k^{-5}$ follows from Rhines theory of β -plane turbulence [56] and, alternatively, is closely approximated by some solutions of the constant enstrophy flux condition in the conformal approach, like the minimal models (9, 71) or (11, 87).

The variation of exponents obtained in the experiments may have a theoretical counterpart in the existence of a set of operator anomalous dimensions, making it interesting to analyze the problem from the conformal field theory point of view. It is clear, however, that the inertial range exponents, found in ref. [41], cannot reproduce the experimental situation. We believe that the important ingredient, missing in the previous conformal approach, is precisely the existence of three-dimensional perturbations, which must be taken into account in any realistic model of a quasi two-dimensional fluid.

In view of the above considerations, let us write the two-dimensional Navier-Stokes equations as

$$\partial_t v_\alpha + v_\beta \partial_\beta v_\alpha = \nu \partial^2 v_\alpha + f_\alpha^{(1)} + g f_\alpha^{(2)} - \partial_\alpha P, \quad (32)$$

where $f_\alpha^{(1)}$ and $f_\alpha^{(2)}$ are stirring forces defined at large (L) and small ($\mu \ll L$) scales, respectively. The dimensionless constant g represents, roughly, a coupling with the three-dimensional modes of the fluid. We assume that the dissipation scale, η , is related, in principle, to the other scales of the problem as $\eta \ll \mu \ll L$. This means that even though the perturbations act at very small scales, when compared to the macroscopic size of the system, they are still much larger than the scale where dissipation occurs.

An important point here is that the condition of incompressibility, when formulated in three dimensions, reads $\partial_1 v_1 + \partial_2 v_2 + \partial_3 v_3 = 0$, suggesting that the "projection" of this constraint to the two-dimensional world has to be given by $\partial_\alpha v_\alpha = \mathcal{O}(g)$, in the framework of equations (32). The velocity field may be described, then, by means of a stream function, ψ , and a velocity potential, ϕ , as

$$v_\alpha = \epsilon_{\beta\alpha} \partial_\beta \psi + g \partial_\alpha \phi. \quad (33)$$

It is of further interest to study, besides the vorticity ω , the divergence of v_α , given by $\rho = g \partial^2 \phi$. An exact, although infinite, chain of equations may be generated if we expand ψ and ϕ in powers of g , substituting them into (32) and collecting the coefficients of the obtained series. Defining, in this way,

$$\begin{aligned} \psi &= \sum_{n=0}^{\infty} g^n \psi^{(n)}, & \omega &= \sum_{n=0}^{\infty} g^n \omega^{(n)}, \\ \phi &= \sum_{n=0}^{\infty} g^n \phi^{(n)}, & \rho &= \sum_{n=0}^{\infty} g^{n+1} \rho^{(n)}, \end{aligned} \quad (34)$$

we get the following set of coupled equations,

$$\begin{aligned} \text{i) } \partial_t \omega^{(n)} &+ \sum_{p=0}^n \epsilon_{\alpha\beta} \partial_\alpha \psi^{(p)} \partial_\beta \partial^2 \psi^{(n-p)} + \sum_{p=0}^{n-1} \left[\partial_\beta \phi^{(p)} \partial_\beta \partial^2 \psi^{(n-p-1)} + \partial^2 \phi^{(p)} \partial^2 \psi^{(n-p-1)} \right] \\ &= \nu \partial^2 \omega^{(n)} + \epsilon_{\alpha\beta} \partial_\alpha f_\beta^{(2)} \delta_{n,1}, \\ \text{ii) } \partial_t \omega^{(0)} &+ \epsilon_{\alpha\beta} \partial_\alpha \psi^{(0)} \partial_\beta \partial^2 \psi^{(0)} = \nu \partial^2 \omega^{(0)} + \epsilon_{\alpha\beta} \partial_\alpha f_\beta^{(1)}, \\ \text{iii) } \partial_t \rho^{(n)} &+ \sum_{p=0}^{n-1} \left[\partial_\alpha \partial_\beta \phi^{(p)} \partial_\alpha \partial_\beta \phi^{(n-p-1)} + \partial_\alpha \phi^{(p)} \partial_\alpha \partial^2 \phi^{(n-p-1)} \right] \end{aligned}$$

$$\begin{aligned}
& + \sum_{p=0}^n \left[2c_{\alpha\beta} \partial_\beta \partial_\sigma \phi^{(p)} \partial_\alpha \partial_\sigma \psi^{(n-p)} + c_{\alpha\beta} \partial_\alpha \psi^{(n-p)} \partial_\beta \partial^2 \phi^{(p)} \right] \\
& + \sum_{p=0}^{n+1} \left[\partial_\alpha \partial_\beta \psi^{(p)} \partial_\alpha \partial_\beta \psi^{(n-p+1)} - \partial^2 \psi^{(p)} \partial^2 \psi^{(n-p+1)} \right] = \nu \partial^2 \rho^{(n)} , \\
\text{iv) } \partial_t \rho^{(0)} & + 2\partial_\alpha \partial_\beta \psi^{(0)} \partial_\alpha \partial_\beta \psi^{(1)} + 2c_{\alpha\beta} \partial_\beta \partial_\sigma \phi^{(0)} \partial_\alpha \partial_\sigma \psi^{(0)} + c_{\alpha\beta} \partial_\alpha \psi^{(0)} \partial_\beta \partial^2 \phi^{(0)} \\
& - 2\partial^2 \psi^{(0)} \partial^2 \psi^{(1)} = \nu \partial^2 \rho^{(0)} + \partial_\alpha f_\alpha^{(2)} , \tag{35}
\end{aligned}$$

and, finally, the constraint of incompressibility for the g -independent part of the velocity field, which defines the pressure term,

$$\left(\partial_\alpha \partial_\beta \psi^{(0)} \right) \left(\partial_\alpha \partial_\beta \psi^{(0)} \right) - \partial^2 \psi^{(0)} \partial^2 \psi^{(0)} = \partial_\alpha f_\alpha^{(1)} - \partial^2 P . \tag{36}$$

In the above expressions, $n \geq 1$. We have obtained, therefore, a set of stochastic partial differential equations. In a statistical description, reflecting a stable asymptotic limit for the correlation functions of ω and ρ , Hopf equations may be straightforwardly written as

$$\partial_t \left\langle \prod_{i=1}^N \omega^{(n_i)}(x_i, t) \prod_{j=N+1}^M \rho^{(n_j)}(x_j, t) \right\rangle = 0 . \tag{37}$$

We observe now that in (35), equation ii) is identical to the one which corresponds to an unperturbed ($g = 0$) two-dimensional fluid. This means that the field $\psi^{(0)}$ will be related to an enstrophy or energy cascade, even in the presence of three-dimensional effects. This field plays the role of an external random variable in the other equations, since its dynamics is independent of the other components $\psi^{(n)}$ or to the field ϕ (in general, the subset $\{\psi^{(0)}, \psi^{(1)}, \dots, \psi^{(n)}, \phi^{(0)}, \phi^{(1)}, \dots, \phi^{(n-1)}\}$ contains fields which act like external random perturbations in the equations for $\psi^{(p)}$ and $\phi^{(p-1)}$, with $p \geq n+1$). Considering that (35) gives relatively complex equations, the analysis of the problem might seem hopeless, being perhaps addressed only to a numerical treatment. However, we can extend the conformal approach, applied previously to the unperturbed case, to find here solutions of the Hopf equations. Our basic assumption is that not only $\psi^{(0)}$ but also the other components in the power expansions of ψ and ϕ are primary operators which belong to some minimal model in a conformal field theory. It is necessary, then, to define a scale ℓ , possibly associated to intermittency effects, which allows us to write the following dimensionally correct expansion,

$$\begin{aligned}
\psi & = \sum_{n=0}^{\infty} f_n \ell^{2(\Delta\psi^{(n)} - \Delta\psi^{(0)})} g^n \psi^{(n)} , \\
\phi & = \sum_{n=0}^{\infty} f'_n \ell^{2(\Delta\phi^{(n)} - \Delta\psi^{(0)})} g^n \phi^{(n)} , \tag{38}
\end{aligned}$$

where $\psi^{(n)}$ and $\phi^{(n)}$ have dimensions $\Delta\psi^{(n)}$ and $\Delta\phi^{(n)}$, respectively.

The introduction of a scale ℓ in (38) means that the perturbed system exhibits a breaking of scale invariance in the inertial range. It may be seen that this phenomenon is signaled by the existence of constant enstrophy or energy fluxes which depend on the small scales of three-dimensional perturbations. It is conceptually important to understand the physical origin of ℓ . A clue for this comes from the structure of couplings between $\psi^{(0)}$ and the other fields, as expressed in (35). As we have already observed, $\psi^{(0)}$ is effectively an external field in the equations for $\psi^{(n)}$ (with $n \geq 1$) and $\phi^{(n)}$ (for any n). In this way, it is plausible to have a relation between ℓ and the scales involved in the dynamics of $\psi^{(0)}$. Now, if we consider the turbulent limit of the equations for $\psi^{(0)}$, corresponding to $\nu \rightarrow 0$ (or, alternatively, $\eta \rightarrow 0$), we are left essentially with the correlation length L of large scale random forces. A simple choice, thus, is to consider $\ell = L$. In this respect, one may observe that the small scale μ could also be used in the definition of ℓ . We have, however, physical reasons to believe that this does not happen: μ is related to the forcing terms in the equations for $\psi^{(1)}$ and $\phi^{(1)}$, which we expect to be irrelevant when compared to the nonlinear convection terms in the range of wave numbers given by $|\vec{k}| \ll 1/\mu$.

It is interesting to note that there is an analogy between our problem and the statistical mechanics of second order phase transitions for a system close to its critical point. In this case, one can study deviations of the critical temperature T_c by means of an expansion in $(T - T_c)$ and through the use of the operator structure of the critical theory [57]. Here, in the turbulence context, the "critical theory" is just what we get when $g \rightarrow 0$.

We are interested to get possible combinations of primary operators in equations (38) that would not affect, in the limit $\mu \rightarrow 0$, the constant enstrophy or energy fluxes, derived from the dynamics of the field $\psi^{(0)}$. We may write a set of operator product expansions from equations (35), generalizing (27). In this way, all the conditions necessary to find minimal models related to an enstrophy or energy cascade in a quasi two-dimensional fluid may be obtained. We will not write these conditions here, which would render our discussion very technical. The important observation is that the models we have to find must belong to the infinite set of solutions found in the former study of unperturbed conformal turbulence. This follows directly from the conditions which depend only on $\psi^{(0)}$. A strategy of computation could be, thus, just a numerical analysis of all possible combinations of fields for these previously known minimal models. As straight it may sound, this approach is hardly useful when the number of primary operators becomes large, a fact that happens already for the first few minimal models.

A more interesting computational scheme is provided if we look for solutions of the form

$$\begin{aligned}\psi &= \psi_0 + f_a(g)\psi_1, \\ \phi &= \frac{f_b(g)}{g}\phi_0,\end{aligned}\quad (39)$$

where $f_a(0) = f_b(0) = 0$, that is, we are considering solutions with $\psi^{(p)} = \psi_1$, for $p \geq 1$, and $\phi^{(p)} = \phi_0$, for any p . This approach is valuable since it turns out that if it is impossible to satisfy the constant flux conditions through any pair of fields ψ_1 and ϕ_0 , then there are no further solutions for the model under consideration. All our task is, therefore, to consider the set of minimal models representing conformal turbulence without perturbations, from which the fields ψ_0 may be immediately obtained, and add, according to the new constraints associated to three-dimensional effects, the fields ψ_1 and ϕ_0 .

In the study of the inertial range exponents, we may think of, at least, three limits for $f_{a,b}(g)$: a) $g \rightarrow 0$, that is, $f_{a,b}(g) \rightarrow 0$, b) $f_{a,b}(g) \simeq 1$, and c) $g \gg 1$, which may be defined as a "strong coupling" regime. In the first case, the perturbations play a negligible role and everything is described by unperturbed conformal turbulence. A competition between exponents appears in the second case, where the less steep spectral slope will be the most relevant in the limit of higher wave numbers. We see, in this way, that cases a) and b) cannot give any of the steeper spectral slopes observed in real experiments. The third case is, in fact, where we have some hope to find a relation with experimental results. It would be unphysical to have $f_{a,b}(g) \rightarrow 0$, for large values of g , since in this limit we would recover the unperturbed system. Let us assume that $f_{a,b}(g)$ diverges as $g \rightarrow \infty$. This means that the inertial range exponent derived from ψ_0 may be discarded and we have to analyze only the competition between the exponents obtained from ψ_1 and ϕ_0 .

An investigation of the first six minimal models for both the enstrophy and energy cascade cases was carried out. In the enstrophy case, there are solutions for all the models studied. The results show a good agreement with experimental verifications, with the only considerable deviation occurring for the very small set of two solutions for the model (2,21). The solutions, excluding the model (2,21), are organized in the table below, where values of mean exponents and standard deviations are described. It is clearly seen that the perturbed exponents are in general lesser than the exponents of the unperturbed fluid.

minimal model	exponent ($g=0$)	mean exponent ($g \neq 0$)	standard deviation
(3,25)	-4.6	-4.90	0.28
(3,26)	-4.23	-5.25	0.27
(6,55)	-3.73	-5.89	0.21
(7,62)	-4.03	-5.46	0.28
(8,67)	-4.51	-4.90	0.34

Table I: Statistical data related to the solutions for the constant enstrophy flux condition, in the strong-coupling regime, where a comparison is made with the unperturbed values of the inertial range exponents.

In the energy case, an interesting fact happens: most of the models studied do not yield any solution for the fields ψ_1 and ϕ_0 . Only the model (10,59) gives solutions, all of them with inertial range exponents close to -3.0 , which do not support the conjecture of a Kolmogorov exponent $-5/3$ for the range of lower wave numbers. It is worth to note that $E(k) \sim k^{-3.0}$ has been observed in atmospheric studies, which have been puzzlingly for a long time, since they refer to large length scales. Thus, the apparent agreement with Kraichnan's prediction seems to be fortuitous. However, more theoretical and experimental work is necessary in order to arrive at a conclusive answer on this point.

6 Conclusions

We discussed briefly the field theory approach to turbulence, keeping in mind its most important phenomenological aspects. We focused, then, in a more detailed way, on the application of conformal methods to the problem of two-dimensional turbulence, considering also the effects of three-dimensional perturbations.

We believe that the large experience accumulated in the last decades, through the study of field theory models, will be extremely useful towards a better understanding of turbulence. Of course, the connection of turbulence and field theory is not expected to be only one way. Perhaps one of the important advances to follow from this relationship regards multifractality, which is a peculiar scaling behavior observed in many different systems. The problem here is to find a general description, similar to a renormalization group treatment. In this respect, Gawedzki [58] evokes the idea of an "inverse renormalization group" analysis of turbulence, where the scaling behavior of correlation functions arises in the ultraviolet region, opposite to what happens in critical phenomena. It would be desirable to have also some perturbative expansion in turbulence, free of infrared divergencies. A recent proposal by L'vov and Procaccia [59] seems to generate a well-behaved perturbative series, from the replacement of velocity by a galilean invariant field, which would cancel the infrared divergencies.

Another interesting recent idea worth of mentioning, is the "loop" formulation of turbulence [60], similar to the well-known loop approach of gauge theories. The interest here is concentrated on the galilean invariant order parameter

$$F[C] \equiv \left\langle \exp \left[i \oint_C \vec{v} \cdot d\vec{x} \right] \right\rangle, \quad (40)$$

where C is an arbitrary loop. Migdal conjectured that $F[C]$ should depend only on the minimal area enclosed by C . Related numerical investigations [61] show that further theoretical work is in order, mainly regarding an account of intermittency effects.

Turbulence is, at the present moment, a fundamental open problem of theoretical physics. S. Orszag once observed that we know more about the small scale structure of the proton than about turbulence in some atmospheric layers. There is some truth in this comment, even if we know that "quantification" of scientific knowledge is always a vague concept.

7 acknowledgments

I would like to thank the organizers of the ENFPC-1996, in particular N. Braga, for kindly inviting me to give this talk. This work was supported by CNPq.

References

- [1] B. Mandelbrot, *The Fractal Geometry of Nature*, W. H. Freeman and Company, New York (1983).
- [2] U. Frisch, *Turbulence - The Legacy of A. N. Kolmogorov*, Cambridge University Press, Cambridge (1995).
- [3] O. Reynolds, *Phil. Trans. R. Soc. London A* **174**, 935 (1883).

- [4] Lord Rayleigh, Proc. London Math. Soc. **11**, 57 (1880).
- [5] M. Jansen, O. Viehweger, U. Fastenrath and J. Hadju, *Introduction to the Theory of the Integer Quantum Hall Effect*, VCH, Weinheim (1994).
- [6] P. Brax, J.-L. Meunier and R. Peschanski, Z. Phys. C **62**, 649 (1994).
- [7] R. Benzi, G. Paladin, G. Parisi and A. Vulpiani, J. Phys. A **17**, 3521 (1984).
- [8] G. Paladin and A. Vulpiani, Phys. Rep. **156**, 147 (1987).
- [9] G.K. Batchelor, *The Theory of Homogeneous Turbulence*, Cambridge University Press, Cambridge (1953).
- [10] L.D. Landau and E.M. Lifshitz, *Fluid Mechanics*, 2nd edition. Pergamon Press, Oxford (1987).
- [11] A.J. Chorin, *Vorticity and Turbulence*, Springer, Berlin (1994).
- [12] A.N. Kolmogorov, Dokl. Akad. Nauk SSSR **30**, 9 (1941). Reprinted in Proc. R. Soc. London A **434**, 9 (1991).
- [13] F. Anselmet, Y. Gagne, E.J. Hopfinger and R.A. Antonia, J. Fluid Mech. **140**, 63 (1984).
- [14] P.C. Martin, E.D. Siggia and H.A. Rose, Phys. Rev. A **8**, 423 (1973).
- [15] C. DeDominicis and P.C. Martin, Phys. Rev. A **19**, 419 (1979).
- [16] V. Yakhot and S.A. Orszag, J. Sci. Comp. **1**, 3 (1986).
- [17] G. Falkovich, I. Kolokov, V. Lebedev and A. Migdal, "Instantons and Intermittency," chaos-dyn/9512006.
- [18] V. Gurarie and A. Migdal, "Instantons in Burgers Equation," hep-th/9512128.
- [19] R.H. Kraichnan, Phys. Fluids **10**, 14177 (1967).
- [20] A.M. Polyakov, Nucl. Phys. **B396**, 367 (1993).
- [21] L. Moriconi, Phys. Rev. E **54**, 1550 (1996).
- [22] M. Van Dyke, *An Album of Fluid Motion*, The Parabolic Press, Stanford, CA (1982).
- [23] L.F. Richardson, *Weather Prediction by Numerical Process*, Cambridge University Press, Cambridge (1922).
- [24] M. Nelkin, Adv. Phys. **43**, 143 (1994).
- [25] A.N. Kolmogorov, Dokl. Akad. Nauk SSSR **32**, 16 (1941). Reprinted in Proc. R. Soc. London A **434**, 15 (1991).
- [26] W. Feller, *An Introduction to Probability Theory*, vol. 2. Wiley, New York (1971).
- [27] A.N. Kolmogorov, J. Fluid Mech. **13**, 82 (1962).
- [28] A.M. Obukhov, J. Fluid Mech. **13**, 77 (1962).
- [29] Z.S. She and E. Lévêque, Phys. Rev. Lett. **72**, 336 (1994).
- [30] R. Benzi, S. Ciliberto, R. Tripiccone, C. Baudet, F. Massaioli and S. Succi, Phys. Rev. E **48**, R29 (1993).
- [31] L. Moriconi, to be published.
- [32] E.A. Novikov, Zh. Exper. Teor. Fiz. **47**, 1919 (1964).
- [33] H.A. Rose and P.-L. Sulcm, J. Phys. France, **441** (1978).
- [34] H.W. Wyld, Ann. Phys. **14**, 143 (1961).
- [35] A.M. Polyakov, Phys. rev E **52**, 6183 (1995).
- [36] J. Bouchad, M. Mézard and G. Parisi, Phys. Rev. E **52**, 3656 (1995).
- [37] A. Cheklov and V. Yakhot, Phys. Rev. E **52**, 5681 (1995).
- [38] R.H. Kraichnan and D. Montgomery, Rep. Prog. Phys. **43**, 547 (1980).
- [39] B. Legras, P. Santangelo and R. Benzi, Europhys. Lett. **5**, 37 (1988).
- [40] A.A. Belavin, A.M. Polyakov, and A.B. Zamolodchikov, Nucl. Phys. **B241**, 33 (1984).
- [41] D. Lowe, Mod. Phys. Lett. A **8**, 923 (1993).
- [42] G. Falkovich and A. Hanany, "Spectra of Conformal Turbulence," WIS-92-88-PH, hep-th/9212015.
- [43] A.B. Zamolodchikov, Nucl. Phys. **B358**, 497 (1991).
- [44] B.K. Chung, S. Nam, Q-Han Park, and H.J. Shin, Phys. Lett. B **317**, 92 (1993).
- [45] A. Babiano, B. Dubrulle, and P. Frick, Phys. Rev. E **52**, 3719 (1995).
- [46] R. Benzi, B. Legras, G. Parisi and R. Scardovelli, Europhys. Phys. Lett. **29**, 203 (1995).
- [47] S. Narimousa, T. Maxworthy, and G.R. Spedding, J. Fluid Mech. **223**, 113 (1991).
- [48] E.J. Hopfinger, M. Mory, and Y. Gagne, in *Turbulence and Chaotic Phenomena in Fluids*, edited by T. Tatsumi, Elsevier Science Publishers B.V. (1984).

- [49] M. Mory and E.J. Hopfinger, in *Macroscopic Modelling of Turbulent Flows*, Lect. Notes in Phys., **230**, edited by U. Frisch et al., Springer-Verlag, Berlin-New York (1985).
- [50] M. Mory and E.J. Hopfinger, *Phys. Fluids* **29**, 2140 (1986).
- [51] J. Proudman, *Proc. R. Soc. A* **92**, 408 (1916).
- [52] G.I. Taylor, *Proc. R. Soc. A* **104**, 213 (1923).
- [53] D.R. Inglis, *Rev. Mod. Phys.* **47**, 841 (1975).
- [54] P.G. Saffmann, *Stud. Appl. Math.* **50**, 277 (1971).
- [55] H.K. Moffat, in *Advances in Turbulence*, edited by G.Comte-Bellot and J. Mathieu, Springer-Verlag, Berlin (1986).
- [56] P.B. Rhines, *J. Fluid Mech.*, **69**, 417 (1975).
- [57] D.J. Amit, *Field Theory, the Renormalization Group, and Critical Phenomena*, World Scientific (1984).
- [58] K. Gawedzki, "Turbulence Under a Magnifying Glass," hep-th/9610003.
- [59] V. L'vov and I. Procaccia, *Phys. Rev. E* **52**, 3840 (1995).
- [60] A. Migdal, *Int. J. Mod. Phys.* **9**, 1197 (1994).
- [61] N. Cao, S. Chen and K. Sreenivasan, *Phys. Rev. Lett.* **76**, 616 (1996).

Topological and Quasi-Topological Field Theories in Two Dimensions

Bruno G. Carneiro da Cunha
and
Paulo Teotonio-Sobrinho

*Universidade de Sao Paulo, Instituto de Fisica-DFMA
Caixa Postal 66318, 05315-970, Sao Paulo, SP, Brazil*

Abstract

We study a class of lattice field theories in two dimensions that include quantum Yang-Mills theory as a particular example. Given a two dimensional orientable surface of genus g , the partition function Z is defined for a triangulation with n triangles of size ϵ . These models are called quasi-topological in the sense that Z is a function of g , n and ϵ only. We compute the partition function and show that the continuum limit is well defined if when $\epsilon \rightarrow 0$ the model approaches a topological theory. We show that the universality classes of such models can be easily classified.

1 Introduction

Exactly soluble models in statistical mechanics [1] and field theory are extremely valuable examples where one hopes to learn about the physics of more realistic models where exact calculations are not available. The Ising model, for instance, has proven to be an incredible source of important ideas, such as duality and finite size scaling [2], that can be applied to much more general situations.

The simplest examples of soluble models are probably the so called lattice topological field theories [3, 4, 5, 6]. Let M be an oriented 2-dimensional compact manifold and T_M

a triangulation of M . Starting from a quite general ansatz, the authors of [4] determined what are the conditions that the local Boltzmann weights must satisfy in order that the partition $Z(T_M)$ do not depend on the specific triangulation T_M of M . In other words, $Z(T_M)$ is a topological invariant of M . A large class of models, corresponding to semi-simple associative algebras, were found. The reason we say that these lattice topological theories are soluble is because to compute $Z(T_M)$ for a triangulation T_M with an arbitrary number n of triangles, it is enough to take another triangulation T_M^0 with the minimal number of triangles, and compute $Z(T_M^0)$ explicitly.

Lattice topological field theories (LTFT for short) are in a sense too simple. They are almost trivial from the dynamical point of view. Consider for example a cylinder with boundaries $S^1 \cup S^1$, and the corresponding evolution operator U (or transfer matrix in the language of statistical systems). It is trivial to show that for a LTFT U is equal to the identity when restricted to physical observables. (However, if instead of a cylinder one has some other manifold interpolating the two circles $S^1 \cup S^1$, U is no longer the identity.) Despite their simplicity, topological models represent an attractive class of models since they can be generalized to higher dimensions and still be exactly soluble. The same type of models considered in [4] have being carried out in 3 dimensions [5]. A different approach have been used by the authors of [6] to produce subdivision invariant theories in several dimension, including four.

There is a large variety of fully dynamical soluble theories in $d = 2$ [1], but in dimensions bigger than 2 this is far from being true. Unfortunately the general situation is that physical models in higher dimensions are either soluble but too simple as LTFT's, or dynamically nontrivial but too hard be exactly solved, as for example lattice gauge theories in 3 dimensions. It would be desirable to find a class of models interpolating these two extreme situations. We want to look for models that are a little more dynamical than LTFT and still can have its partition function computed. The answer is not known in general, but in two dimension Yang-Mills theories (YM_2) are legitimate examples of such models. It is well known that the partition function of a gauge theory on a 2-manifold M is not a topological invariant. Nevertheless its partition function can be explicitly computed both in the continuum and in the lattice [7]. It turns out that the partition function depends not only on the topology of M but also on its area α . This is an example of what can be called a $2d$ quasi-topological field theory [7]. Another feature of YM_2 is that the theory is a perturbation in α of a topological theory. When the area α goes to zero, the model becomes topological.

In this report we shall discuss how to construct quasi-topological theories on the lattice. They will include gauge theories as a particular example. Let M_g be an orientable 2d surface with genus g , and $T(g, n)$ a triangulation of M_g consisting of n triangles. For simplicity, we will assume that all triangles have the same area ϵ . To each link in $T(g, n)$ we associate a dynamical variable taking values in a discrete (or even continuous) set I . Then we follow [4] and look for models such that the partition function $Z(T(g, n), \epsilon)$ depends on the topology through g , on the total number n of triangles, and on ϵ but not on the details of the triangulation T . In other words, Z is a function $Z(g, n, \epsilon)$ of the

global topology, the number of triangles and their size. That will be our definition of a lattice quasi-topological field theory (LQTFT). We will show that the continuum limit of a LQTFT is well defined whenever the model is a deformation of a lattice topological theory. The partition function $Z(g, n, \epsilon)$ can always be computed and the continuum limit is recovered by taking $n \rightarrow \infty$ and $\epsilon \rightarrow 0$, while keeping the total area $\alpha = n\epsilon$ fixed.

We start by defining what we mean by a lattice quasi-topological field theories in Section 2. In Section 3 we compute the partition function in full generality. The dynamics of LQTFT is discussed in Section 4. There we compute the evolution operator U for the case of a cylinder and comment on how to extend the answer to the generic situation. We also determine what are the physical observables and compare with the topological case. In Section 5 we study the continuum limit. Section 6 is dedicated to a simple example. Finally on Section 7, we conclude with some remarks. Some results used through this report are given in the Appendix.

2 Quasi-Topological Lattice Theories

The definition of the model follows the basic steps of [4]. Let $T(g, n)$ be a triangulation with n triangles of a two dimensional surface M_g with genus g . A configuration is determined by assigning to each edge of the triangulation a "color" i belonging to a index set I . If the set I is finite, we may think of i as a sort of spin variable sitting on the links of the lattice. For gauge theories, I is nothing but the gauge group G . To each triangle Δ , with edges colored by i, j, k and area ϵ , we associate a Boltzmann weight $C_{ijk}(\epsilon)$. We assume that all triangles have the same area ϵ and that $C_{ijk}(\epsilon)$ is invariant by cyclic permutation of the color indexes, i.e.,

$$C_{ijk}(\epsilon) = C_{jki}(\epsilon) = C_{kij}(\epsilon). \quad (2.1)$$

The weight associated with two triangles, as indicated in Fig. 1, is determined by a gluing operator g^{kl} and is given by

$$C_{ija}(\epsilon) g^{ab} C_{bkl}(\epsilon) \quad (2.2)$$

where the summation on the repeated indexes a and b is understood. One may use g^{ab} to lift indexes and write (2.2) as $C_{ij}{}^b(\epsilon)C_{bkl}(\epsilon)$ or $C_{ija}(\epsilon)C^a{}_{kl}(\epsilon)$.

It will be convenient to restrict the gluing operator g^{ij} in such way that there exists a inverse g_{ij} ,

$$g_{ia}g^{aj} = \delta_i^j. \quad (2.3)$$

The partition function for the triangulation $T(g, n)$ is obtained by performing the gluing operation on all pair $\langle ab \rangle$ of edges that should be identified in order to build the triangulation. In other words

$$Z(T(g, n), \epsilon) = \prod_{\Delta \in T} \prod_{\langle ab \rangle} C_{ijk}(\epsilon) g^{ab}. \quad (2.4)$$

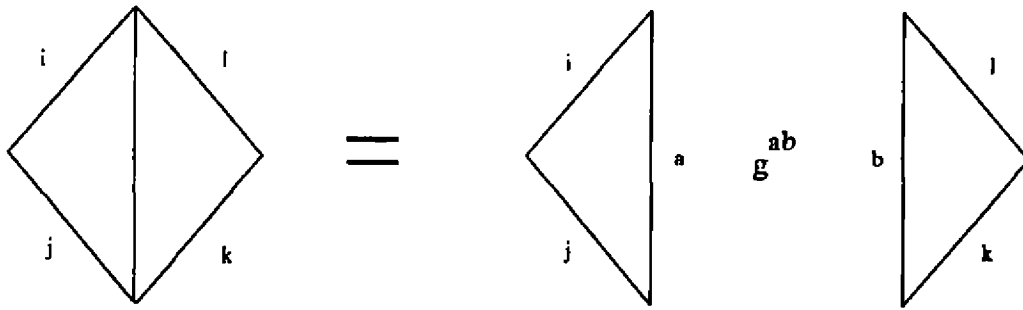


Fig.1. The figure shows how the gluing operator g^{ab} is used to give the weight corresponding to a pair of glued triangles

If the weights $C_{ijk}(\epsilon)$ are not restricted, the partition function (2.4) depends on the triangulation and it represents a complicated and fully dynamical theory.

It is convenient to represent a given triangulation $T(g, n)$ by its dual graph $\Gamma(g, n)$. Figure 2 (a) shows the gluing of triangles in terms of the dual graphs and Fig. 2 (b), an example of the graph corresponding to some triangulation. The graphs must have double lines in order to encode the same information as the triangulation.

Given two triangulations $T(g, n)$ and $T'(g, m)$, or the corresponding graphs $\Gamma(g, n)$ and $\Gamma'(g, m)$, of a surface with genus g , it is possible to transform one into another by a set of local moves that do not change the topology, namely g . It is well known that two basic moves are needed in order to go from one triangulation to another. We are going to use the so called flip move and the bubble move. In terms of the dual graphs, these moves are given in Fig. 3. Note that the flip move preserves the number n of triangles; whereas the bubble move, change it n by 1.

The theory is called topological [4] if $C_{ijk}(\epsilon)$ do not depend on ϵ

$$\frac{dC_{ijk}(\epsilon)}{d\epsilon} = 0 \tag{2.5}$$

and it is invariant under any topological move. Invariance under the flip move implies that

$$C_{ij}{}^k C_{kl}{}^m = C_{ik}{}^m C_{jl}{}^k, \tag{2.6}$$

whereas the bubble move is equivalent to

$$C_{iab} C^{ba}{}_j = g_{ij}. \tag{2.7}$$

A partition function that is invariant under both moves, can not depend on the triangulation, and therefore is a topological invariant. In other words, Z is a function $Z(g)$ depending only on the genus g of the surface M_g .

A topological theory defined by C_{ijk} has a enormous symmetry. Thanks to this fact, the partition function can be computed. Since Z do not depend on the triangulation, one

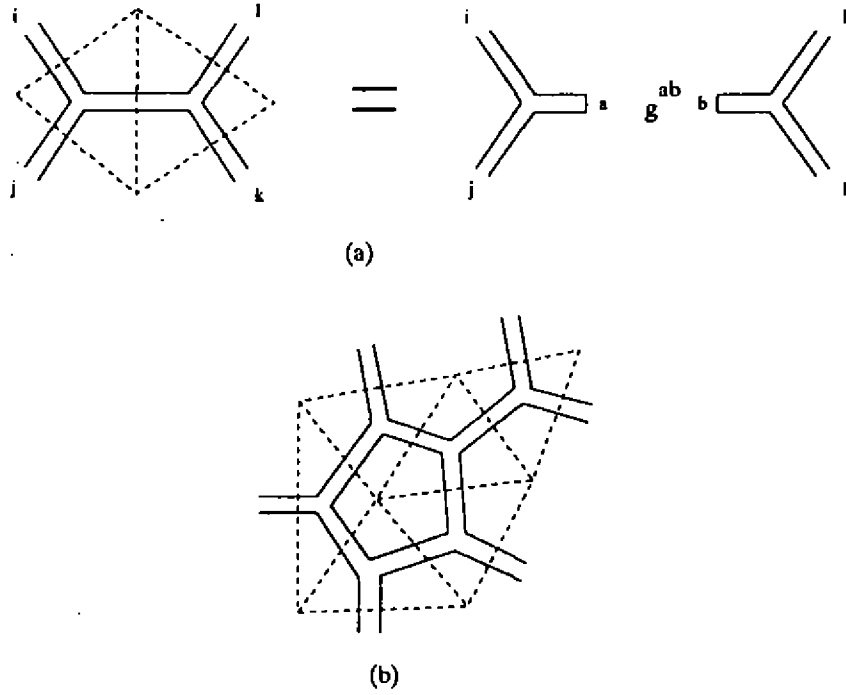


Fig.2. Figure (a) shows the gluing of triangles in terms of the dual graph. Figure (b) is a simple example of a triangulation and its dual graph.

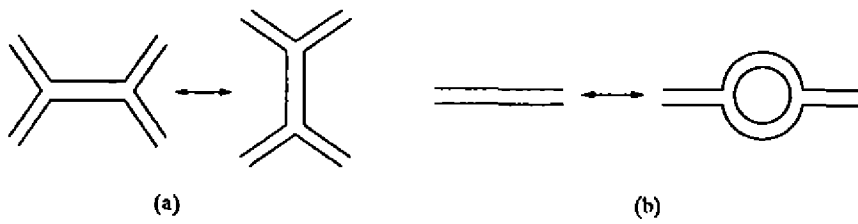


Fig.3. The two basic topological moves in terms of the dual graphs. Figure (a) is the flip move and figure (b) is the bubble move

chooses the minimal triangulation and writes down $Z(g)$ explicitly. Topological models are very special when compared to a generic theory given by (2.4) that has little or no symmetry at all. What we are going to do, is to consider an intermediate situation where part of the full topological symmetry is not present. That is the reason for the name quasi-topological models.

The simplest thing to do is to give up the invariance under one of the two topological moves described before. It will be interesting to have a partition function that depends on the size of the lattice, so we choose to break the invariance under the bubble move and keep the invariance under the flip move. We also want to allow for variation on the size ϵ of the triangles. Therefore, the model is defined by a set of local weights $C_{ijk}(\epsilon)$ invariant under the flip move, and partition function given by (2.4). In our class of models, we will assume the flip move, or in other words

$$C_{ij}^k(\epsilon)C_{kl}^m(\epsilon) = C_{ik}^m(\epsilon)C_{jl}^k(\epsilon) \tag{2.8}$$

for any value of the parameter ϵ .

It may happen that for some value ϵ_0 of the parameter ϵ , the weights $C_{ijk}(\epsilon)$ also satisfy equation (2.7). At this critical point, the full topological symmetry is restored. As we shall see, if $\epsilon = 0$ is a critical point, the model has a well defined continuum limit.

Let us assume for simplicity that the index set I is a finite set with r elements. Consider a vector space V with bases $\{\phi_1, \dots, \phi_r\}$. Then, for each value of the parameter ϵ the numbers $C_{ij}^k(\epsilon)$ define a product structure in V , namely

$$\phi_i\phi_j := C_{ij}^k(\epsilon)\phi_k. \tag{2.9}$$

Because of the flip symmetry (2.8) the product $\phi_i\phi_j$ is associative. We may think of $C_{ij}^k(\epsilon)$ as given a family A_ϵ of algebras on the space of associative algebras defined on V .

Since we are assuming that g^{ij} has an inverse g_{ij} we can define a dual base $\{\phi^i\}$ given by

$$\phi^i = g^{ij}\phi_j. \tag{2.10}$$

For the dual basis, the product is

$$\phi^i\phi^j := C^{ij}_k(\epsilon)\phi^k. \tag{2.11}$$

3 Partition Function

For a triangulation $T(0, n)$ of the sphere, the corresponding graphs $\Gamma(0, n)$ are planar. Let $\Gamma(0, n)$ and $\Gamma'(0, n)$ two planar graphs representing two different triangulations of S^2 but with the same number n of triangles. It is a well known fact that $\Gamma(0, n)$ and $\Gamma'(0, n)$ can

always be connected via a sequence of flip moves [8]. Therefore if $C_{ijk}(\epsilon)$ fulfills equation (2.8) the partition function (2.4) computed for $\Gamma(0, n)$ and $\Gamma'(0, n)$ have to be identical.

Using a variation on the proof presented in [8] we were able to show that any pair of dual graphs $\Gamma(g, n)$ and $\Gamma'(g, n)$, for arbitrary genus g can also be connected by a sequence of flip moves. For completeness we give a demonstration of this fact on the Appendix. As a result, our partition function (2.4) depends only on g, n and ϵ , provide that (2.8) is fulfilled. We will write $Z = Z(g, n, \epsilon)$ for this matter.

The particular graph $\Gamma(g, n)$ we use to compute Z is immaterial. The result of the Appendix shows us that $\Gamma(g, n)$ can be reduced to the canonical graph $\Gamma^0(g, n)$ given on Fig. 4(a) via a sequence of flip moves. The canonical graph is obtained by gluing the

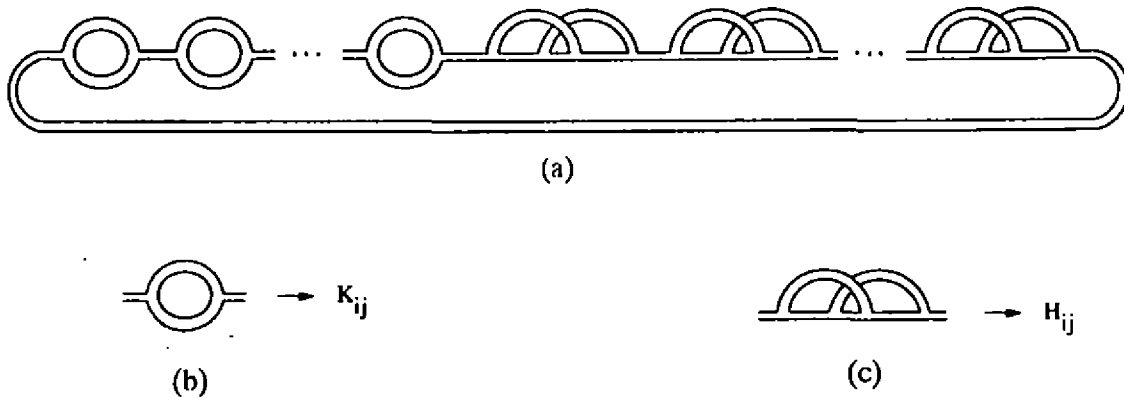


Fig.4. The dual graph corresponding to the standard triangulation of a surface of genus g is given in Figure (a). It can be constructed by repeating the basic blocs shown in Figures (b) and (c) respectively $\frac{n-4g}{2}$ and g times.

elementary blocks on Fig. 4(b) and Fig. 4(c). They correspond to operators

$$K_{ij}(\epsilon) := C_{iab}(\epsilon) C^{ba}_j(\epsilon) \tag{3.1}$$

and

$$H_{ij}(\epsilon) := C_{ikl}(\epsilon) C^{kmn}(\epsilon) C_m^{pl}(\epsilon) C_{npj}(\epsilon) \tag{3.2}$$

respectively. If we define matrices K_ϵ and H_ϵ with matrix elements $(K_\epsilon)_i^j = K_{ik}(\epsilon)g^{kj}$ and $(H_\epsilon)_i^j = H_{ik}(\epsilon)g^{kj}$, then the graph on Fig. 4(a) shows that $Z(g, n)$ can be written as

$$Z(g, n, \epsilon) = Tr \left(K_\epsilon^{\frac{n-4g}{2}} H_\epsilon^g \right) \tag{3.3}$$

Due to the flip symmetry, the computation of the partition function for a two dimensional lattice has been reduced to a one dimensional problem. If the set of states I is a

finite set with r elements, K_ϵ and H_ϵ are $r \times r$ matrices. In this case, (3.3) can be calculated for an arbitrary g and n . For this note that the algebra of observables $\{\phi_1, \dots, \phi_r\}$ has a natural inner product given by the g_{ij} :

$$\langle \phi_i, \phi_j \rangle = g_{ij},$$

and that K_ϵ and H_ϵ are both self-adjoint with respect to this inner product. Moreover, we will see below that they also commute

$$K_\epsilon H_\epsilon = H_\epsilon K_\epsilon, \tag{3.4}$$

therefore they can be simultaneously diagonalized. As the trace is unchanged by a coordinate transformation, the partition function can be computed as

$$Z(g, n, \epsilon) = \sum_l k_l^{\frac{n-4g}{2}} h_l^g, \tag{3.5}$$

where k_l and h_l are the eigenvalues of K_ϵ and H_ϵ .

We now show that equation (3.5) is fulfilled. This is a direct consequence of the flip symmetry. Consider the graphic representation of $K_i^a(\epsilon)H_{aj}(\epsilon)$ on Fig. 5(a). By

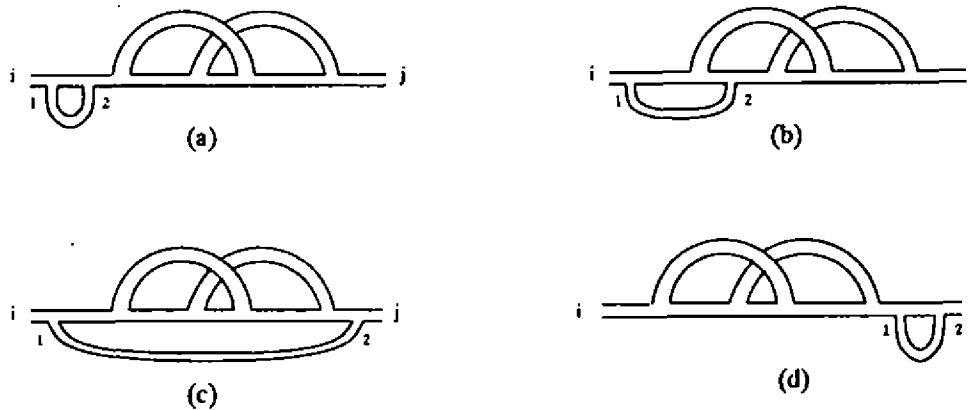


Fig.5. The figure shows equation (3.6).

performing a flip transformation, the leg of the graph marked with 2 can be moved to the position presented on Fig. 5(b). Repeating the same step one can move it further, arriving at Fig. 5(c). Finally, Fig. 5(d) is obtained by repeating the process with leg 1. This sequence of flips shows that

$$K_i^a(\epsilon)H_{aj}(\epsilon) = H_i^a(\epsilon)K_{aj}(\epsilon) \tag{3.6}$$

and therefore K_ϵ and H_ϵ commute

4 Dynamics and Observables

The dynamics of a model is controlled by its evolution operator U . For a topological theory, U is equal to the identity when restricted to the physical observables (see [4]). Since our models have less symmetry than a LTFT we expect that it must have some dynamics.

Let $T(p_1, p_2, n)$ be a triangulation of a cylinder where n is the number of triangles and p_1, p_2 are the number of edges on the boundaries σ_1 and σ_2 . We enumerate the edges on the boundary in a clockwise fashion, as in Fig. 6. We define the operator $U_{i_1, \dots, i_{p_1}; j_1, \dots, j_{p_2}}$

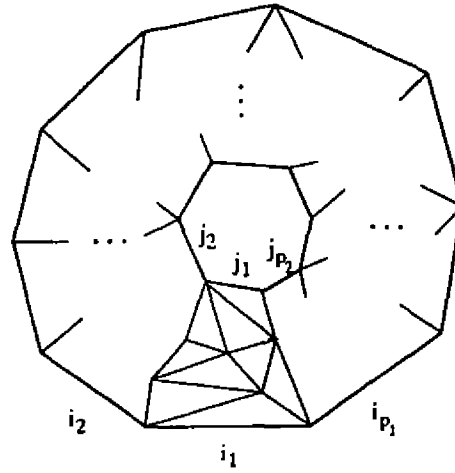


Fig.6. A cylinder with boundary given by two polygons with p_1 and p_2 links. The boundary elements are enumerated in a clockwise fashion.

as the one given by coloring the boundary links at σ_1 and σ_2 respectively with (i_1, \dots, i_{p_1}) and (j_1, \dots, j_{p_2}) , and then gluing (summing over) the internal links by the rules explained in Section 2. In other words,

$$U_{i_1, \dots, i_{p_1}; j_1, \dots, j_{p_2}} = \prod_{\Delta \in T} \prod_{\langle ab \rangle} C_{ijk}(\epsilon) g^{ab} \quad (4.1)$$

where $\langle ab \rangle$ runs over the pairs of glued internal links. What we will call the evolution operator is the matrix

$$U_{i_1, \dots, i_{p_1}}^{j_1, \dots, j_{p_2}} := U_{i_1, \dots, i_{p_1}; k_1, \dots, k_{p_2}} g^{k_1 j_1} \dots g^{k_{p_2} j_{p_2}} \quad (4.2)$$

It is clear from the definition that $U_{i_1, \dots, i_{p_1}}^{j_1, \dots, j_{p_2}}$ fulfills the factorization properties of an evolution operator. If the triangulation $T(p_1, p_2, n)$ splits in two cylinders $T_a(p_1, p, n_a)$ and $T_b(p, p_2, n_b)$, $n_a + n_b = n$, then

$$U_{i_1, \dots, i_{p_1}}^{j_1, \dots, j_{p_2}}(T) = U_{i_1, \dots, i_{p_1}}^{k_1, \dots, k_p}(T_a) U_{k_1, \dots, k_p}^{j_1, \dots, j_{p_2}}(T_b). \quad (4.3)$$

We are going to assume for the moment that the set of I of colors is equal to $1, 2, \dots, r$. Then, the vector space $V \sim A_\epsilon$ of states associated with a single link is generated by a basis $\{\phi_1, \phi_2, \dots, \phi_r\}$. In other words, a generic state ψ is given by $\psi = \psi^i \phi_i$. The space of states $V^{(p_1)}$ corresponding to a boundary with p_1 links is just the tensor product $V^{(p_1)} = V \otimes V \otimes \dots \otimes V$ with p_1 factors. At the boundary σ_2 the space of states $V^{(p_2)}$ is defined in the same way. We recall the usual interpretation for U as an linear operator from $V^{(p_1)}$ to $V^{(p_2)}$ given by

$$U(\phi_{i_1} \otimes \dots \otimes \phi_{i_{p_1}}) = U_{i_1, \dots, i_{p_1}}^{j_1, \dots, j_{p_2}} \phi_{j_1} \otimes \dots \otimes \phi_{j_{p_2}}. \tag{4.4}$$

The computation of U follows the same idea as in the calculation of the partition function on Section 3. Given two triangulations $T(p_1, p_2, n)$ and $T'(p_1, p_2, n)$ with the same number of triangles, and the same number of links on the boundary, we were able to show that they can be connected by a sequence of flip moves. Therefore the U only depend on the triangulation through the numbers p_1, p_2 and n . In fact any triangulation can be brought to the canonical form given on Fig. 7. Note that once more, the computation

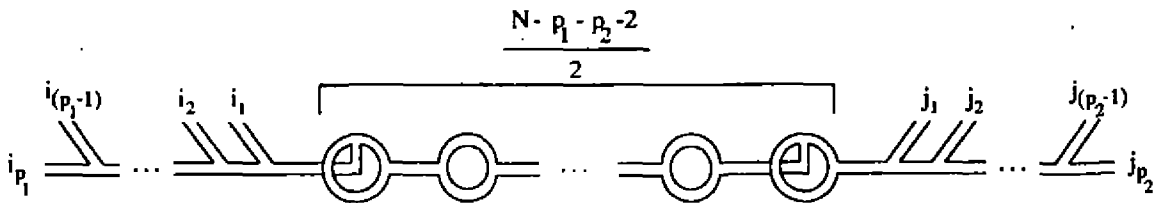


Fig.7. The canonical graph for a cylinder.

has been reduced to a one dimensional problem. It involves the product of the operator $K_i^j(\epsilon)$ defined in (3.1), and a new operator

$$S_i^j(\epsilon) := C_{iab}(\epsilon) C^{abj}(\epsilon) \tag{4.5}$$

We are going to use the following property of $S_i^j(\epsilon)$:

$$S_i^m(\epsilon) C_{mjk}(\epsilon) = S_i^m(\epsilon) C_{mkj}(\epsilon). \tag{4.6}$$

A graphic proof of (4.6) is given in Fig. 8.

Now let us consider the linear map $S_\epsilon : A_\epsilon \rightarrow A_\epsilon$ given by $S_i^j(\epsilon)$. On a generic element $a = a^i \phi_i \in A_\epsilon$ it act as

$$S_\epsilon(a) = a^i S_i^j(\epsilon) \phi_j. \tag{4.7}$$

As a consequence of (4.6) and (2.1), it is very simple to verify that for any $a_1, a_2 \in A_\epsilon$

$$a_1 S_\epsilon(a_2) = S_\epsilon(a_2) a_1 \quad \text{and} \quad S_\epsilon(a_1 a_2) = S_\epsilon(a_2 a_1). \tag{4.8}$$

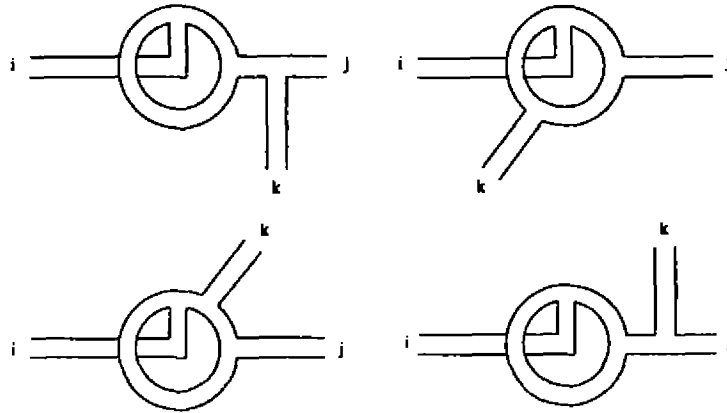


Fig.8. The figure shows a sequence of moves that proofs equation (4.6).

The first part of (4.8) shows that $S_\epsilon(a)$ belongs to the center $Z(A_\epsilon)$ of the algebra A_ϵ . Contrary to the topological case, S_ϵ is not a projector from A_ϵ to $Z(A_\epsilon)$. Actually, one can show that

$$S_i^l(\epsilon)S_i^j(\epsilon) = K_i^l(\epsilon)S_i^j(\epsilon) = S_i^l(\epsilon)K_i^j(\epsilon) \tag{4.9}$$

One can see from Fig. 7 that the form of $U_{i_1, \dots, i_{p_1}}^{j_1, \dots, j_{p_2}}(p_1, p_2, n, \epsilon)$ is

$$U_{i_1, \dots, i_{p_1}}^{j_1, \dots, j_{p_2}}(p_1, p_2, n, \epsilon) = [S_\epsilon(\phi_{k_1} \phi_{k_2} \dots \phi_{k_p})]^a \left(K_\epsilon^{\frac{n-p_1-p_2-2}{2}} \right)_a^m [S_\epsilon(\phi^{j_{p_2}} \phi^{j_{p_2-1}} \dots \phi^{j_1})]_m \tag{4.10}$$

Therefore the evolution given by $U(p_1, p_2, n, \epsilon)$, is actually an evolution for the data $S_\epsilon(\phi_{i_1} \dots \phi_{i_{p_1}})$ and $S_\epsilon(\phi^{j_{p_2}} \phi^{j_{p_2-1}} \dots \phi^{j_1})$ in $Z(A_\epsilon)$. Note that S_ϵ is invariance under cyclic permutations of the factors ϕ 's. This is clear from the second part of (4.8). Therefore the functions $S_\epsilon(\phi_{i_1} \dots \phi_{i_{p_1}})$ and $S_\epsilon(\phi^{j_{p_2}} \phi^{j_{p_2-1}} \dots \phi^{j_1})$ depend only on the oriented loops σ_1 and σ_2 and associate to each one of them a well defined elements of $Z(A_\epsilon)$. It is useful to introduce variable $W(\sigma) \in Z(A_\epsilon)$ analogue of the trace of the Wilson loop in gauge theories, where σ is any loop given by an oriented sequence of p links. We define

$$W(\sigma) = S_\epsilon(\phi_{i_1} \dots \phi_{i_{p_1}}). \tag{4.11}$$

Analogous, we define its conjugate $\tilde{W}(\sigma) = W(-\sigma)$, where $-\sigma$ is the same loop with reverse orientation, by

$$\tilde{W}(\sigma) = S_\epsilon(\phi^{j_{p_2}} \phi^{j_{p_2-1}} \dots \phi^{j_1}) \in Z(A) \tag{4.12}$$

The observables, or loop variables $W(\sigma)$, are elements of the center of the form $S_\epsilon(a)$ for some $a \in A_\epsilon$. The question is whether $S_\epsilon(a)$ span the entire $Z(A_\epsilon)$ or just a subspace. That will depend on the particular set of weights $C_{ijk}(\epsilon)$. Consider an element $b \in Z(A_\epsilon)$. One can show that $S_i^j(\epsilon)b^i = K_i^j(\epsilon)b^i$. Therefore if K_ϵ restricted to the center is invertible, then the image of S_ϵ is the whole $Z(A_\epsilon)$.

Note that, when restricted to the observables, the evolution U is given by

$$U|_{\text{phy}} = K_\epsilon^{\frac{n-p_1-p_2-2}{2}}. \quad (4.13)$$

A Cylinder is topologically equivalent to a sphere with two holes. For this reason U is also called the two point correlation function for genus zero. To complete our discussion we would need to consider the corresponding operator for a surface with g handles and N holes, i.e., the N points correlation function for genus g . It is a well known result that it is sufficient to compute the three point correlation function Y for genus zero. Any other correlator can be written in terms of Y and U . Consider a sphere with 3 holes representing a cobordism from $S^1 \times S^1$ to S^1 . Let $T(p_1, p_2, p_3, n)$ be a triangulation with n triangles and p_i links on the oriented boundary σ_i . It is not difficult to show that analogously to (4.10) we have

$$Y_{i_1, \dots, i_{p_1}; j_1, \dots, j_{p_2}}^{k_1, \dots, k_{p_3}}(p_1, p_2, p_3, n) = [W(\sigma_1)]^a [W(\sigma_2)]^b C_{ab}{}^l(\epsilon) [K_\epsilon^{\frac{q}{2}}]_l^m \tilde{W}(\sigma_3)_m, \quad (4.14)$$

where $q = n - p_1 - p_2 - p_3 - 4$.

5 Continuum Limit

The continuum limit is obtained by making the number n of triangles going to infinity. We will be interested in the scaling situation, when the area ϵ of each triangle becomes smaller but the total area α of the surface remains constant. Therefore

$$\epsilon = \frac{\alpha}{n}. \quad (5.1)$$

At the limit, the partition function will be a function $Z(g, \alpha)$ of genus g and area α .

In the continuum limit, the weights associated with the two triangles of Fig. 9 (a) should be the same, since both would be triangles of zero area. The corresponding diagrams are shown in Fig. 9 (b). It is clear from the figure that $C_{ijk}(0)$ should satisfy

$$C_{iab}(0)C_j{}^{ba}(0) = g_{ij} \quad (5.2)$$

or, in other words $K_i{}^j(0) = \delta_i^j$. But (5.2) is exactly the condition (2.7) to have a lattice topological field theory. In other words, to have a well defined continuum limit, the weights $C_{ijk}(\epsilon)$ have to be a perturbation of a LTFT, or

$$C_{ijk}(\epsilon) = C_{ijk}^{\text{top}} + \epsilon \frac{\partial}{\partial \epsilon} C_{ijk}(0) + \mathcal{O}(\epsilon^2). \quad (5.3)$$

Similarly

$$K_i{}^j(\epsilon) = \delta_i^j + 2\epsilon B_i{}^j + \mathcal{O}(\epsilon^2) \quad (5.4)$$

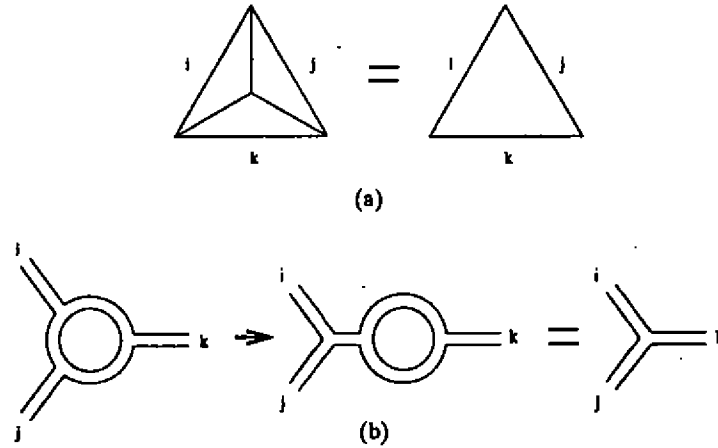


Fig.9. In the limit of $\epsilon \rightarrow 0$ both triangles in (a) have zero area. The restriction on the weights can be derived from (b).

where B_i^j is defined by

$$B_i^j := \frac{1}{2} \frac{\partial}{\partial \epsilon} (C_{ikl}(\epsilon) C^{lkj}(\epsilon)) \Big|_{\epsilon=0} \tag{5.5}$$

Therefore

$$\lim_{n \rightarrow \infty} K_{\alpha/n}^{\frac{n-4g}{2}} = \lim_{n \rightarrow \infty} (I + \frac{2\alpha}{n} B)^{\frac{n-4g}{2}} = e^{\alpha B} \tag{5.6}$$

From (3.3) one sees that in the limit the partition function is

$$Z(g, \alpha) = Tr (e^{\alpha B} (H_0)^g) \tag{5.7}$$

The continuum theory is clearly a perturbation of a topological theory.

The operator U also has a well defined continuum limit when restricted to the physical observable. In the limit $n \rightarrow \infty$ the algebra A_ϵ becomes A_0 . Let σ_1 and σ_2 be the boundary of a cylinder. The observable are given by two loop variables $W(\sigma_1)$ and $W(\sigma_2)$ belonging to the center of $Z(A_0)$. From (4.13) we have to compute

$$U|_{\text{phy}} = \lim_{n \rightarrow \infty} K_{\alpha/n}^{\frac{n-p_1-p_2-2}{2}} \tag{5.8}$$

As p_1 and p_2 are of the order \sqrt{n} , we get

$$U|_{\text{phy}} = e^{\alpha B} \tag{5.9}$$

where α is the area of the cylinder interpolating between σ_1 and σ_2 .

It is clear from the above discussion that the continuum theories are determined by a topological theory and an operator B_i^j . The pair $C_{ijk}(0), g^{ij}$ defines a topological lattice field theory and B_i^j contributes with a non trivial dynamics. Note that B_i^j in (5.5) is fixed by the derivative of $C_{ijk}(\epsilon)$ at zero. The global behavior of $C_{ijk}(\epsilon)$ is irrelevant. To classify the possible continuum theories, or universality classes, one has to determine

what are the possible dynamics B_i^j that can come from a generic $C_{ijk}(\epsilon)$ via (5.5). As we shall see, for a given $C_{ijk}(0), g^{ij}$, the allowed B_i^j are not arbitrary.

Consider the matrices C_m^ϵ , defined by

$$[C_m^\epsilon]_i^j := C_{mi}^j(\epsilon) \tag{5.10}$$

As it is illustrated by Fig. 10, the matrices C_m^ϵ fulfill

$$C_m^\epsilon K_\epsilon = K_\epsilon C_m^\epsilon. \tag{5.11}$$

This equation has to be valid in all orders of $\epsilon = \alpha/n$. It is easy to see that at first order in ϵ , equation (5.11) is equivalent to

$$C_m^0 B = B C_m^0 \text{ or } [B, C_m^0] = 0 \tag{5.12}$$

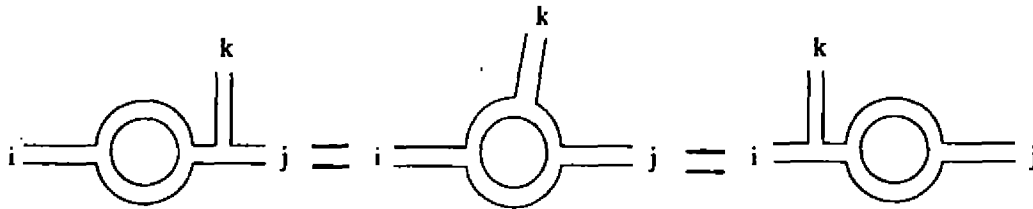


Fig.10. A proof that $C_m^\epsilon K_\epsilon = K_\epsilon C_m^\epsilon$.

Any pair $C_{ijk}(0), g^{ij}$ and B_i^j coming from (5.3) and (5.5) has to satisfy equation (5.12). Actually this is the only restriction on B_i^j . Given a topological theory C_{ijk}, g^{ij} and an operator B_i^j fulfilling (5.12) we can always find at least one $C_{ijk}(\epsilon)$ where they came from. A simple calculation shows that it is enough to take

$$C_{ijk}(\epsilon) = [e^{\epsilon B}]_i^l C_{ljk} \tag{5.13}$$

Therefore, given a topological lattice theory $C_{ijk}(0), g^{ij}$, the the set of allowed quasi-topological theories, are given by all matrices

$$B_i^j = B_{ia} g^{aj}, \quad B_{ij} = B_{ji}$$

commuting with C_m . It is easy to verify that any element $z = z^i \phi_i$ in the center $Z(A_0)$ defines a possible operators $B(z)$

$$B(z) = z^m C_m^0. \tag{5.14}$$

Actually, as we will see next, all operators B are of the form (5.14).

We will show that there is a bijection between the space of all B and the center of the algebra. For a given symmetrical M^{ij} commuting with the C_m^0 we can associate an element of the center of the algebra by the mapping

$$\beta(M) = C_{ia}^a M^{ij} \phi_j. \tag{5.15}$$

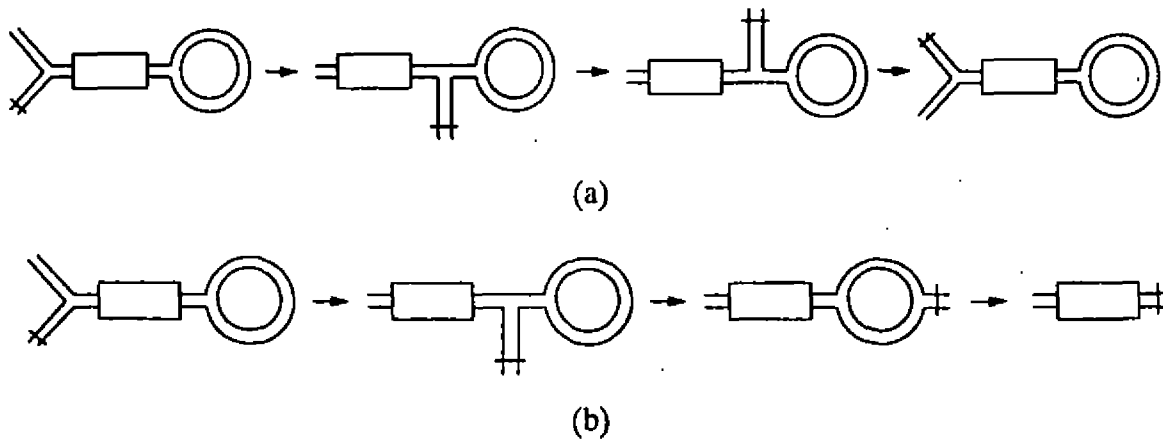


Fig.11. Figure (a) shows that the image of β is in the center. Figure (b) shows that $B \circ \beta$ is the identity map.

Fig. 11 (a) proves that $C_{ij}^k B^{ib} C_{ba}^a = C_{ji}^k B^{ib} C_{ba}^a$ and therefore $\beta \phi_j = \phi_j \beta$ and β is indeed an element of the center of the algebra. We can see that (5.15) is the inverse of (5.14) in Fig. 11 (b). The symmetrical matrix commuting with the C_m^0 is displayed as a box. It follows from the commutation that we can attach the box on any side of the C_{ij}^k . Fig 11 (b) shows that $[(B \circ \beta)(M)]_j^i = M_j^i$ for any M commuting with C_m^0 . Hence $B \circ \beta$ is the identity map. On the other hand, $\beta \circ B$ is also the identity map on the algebra. Given an element of the algebra $z^m \phi_m$ we will have

$$[(\beta \circ B)(z^m \phi_m)] = \beta(z^m C_m) = C_{ia}^a z^m C_m^{il} \phi_l = z^m \phi_m. \tag{5.16}$$

Hence β is a bijection and therefore any operator B is of the form (5.14).

6 Example

We will now consider an example of quasi-topological theory. We will study the case where the topological constants C_{ij}^k are derived from a group algebra.

Given a group G , we can construct a group algebra over the complex numbers in the usual way:

$$C[G] = \bigoplus_{g \in G} C \phi_g,$$

with the algebra product inherited from the group, i.e., $\phi_x \phi_y \equiv \phi_{xy}$.

We can then calculate the topological part of C_{ij}^k :

$$C_{ij}^k(0) = \delta(ij, k), \quad g_{ij} = \delta(i, j^{-1}), \quad C_{ijk}(0) = \delta(ijk, 1),$$

where 1 is the group identity.

We saw in the last section that the two constraints on B are i) $B_{ij} = B_{ji}$ and ii) the matrix B with entries B_i^j must commute with the C_m^0 defined above. In other words,

$$\sum_{l \in G} \delta(ij, l) B(l, k) = \sum_{l \in G} \delta(il, k) B(j, l),$$

where we use $B(i, j)$ for B_i^j . Working out the details, we will have

$$B(ij, k) = B(j, ki^{-1}).$$

We then realize that $B(i, j) = B(j^{-1}i, 1) \equiv B(j^{-1}i) = B_{j^{-1}i}$. As B_{ij} is symmetrical, it follows that $B(ij^{-1})$ is a function which depends only on the conjugacy class of the product ij^{-1} . In other words, B is given by a class function. It can be therefore expanded on the characters χ_R of the group as

$$B(ij^{-1}) = \sum_R B_R d_R \chi_R(ij^{-1}). \tag{6.1}$$

The sum runs over representations and the complex constants B_R spans all possible B . This is consistent with the discussion of Section 5, since there is a one to one correspondence between the set of all class functions and the center of the group algebra.

The relation with the elements of the center of the group algebra is easily seen as follows. Let F be the set of all functions $f : G \rightarrow \mathbb{C}$ such that

$$f(hgh^{-1}) = f(g).$$

For each class function $\phi \in F$ we can assign an element of the center of the group algebra by the map

$$\begin{aligned} b : F &\rightarrow \mathbb{C}[G] \\ f &\mapsto b[f] = \sum_{g \in G} f(g)g \end{aligned}$$

Note that the image of b is the whole group algebra, for arbitrary functions f . Therefore, for $b[f]$ be an element of the center of the group algebra, it suffices to prove that we have $b[f]b[h] = b[h]b[f]$ for any class function f and any function from the group to the complex numbers h .

$$b[f]b[h] = \sum_{x \in G} f(x)x \sum_{y \in G} h(y)y$$

making the transformation on x , $x \rightarrow yxy^{-1}$, we will have

$$\sum_{x,y} f(yxy^{-1})h(y)yxy^{-1}y = \sum_y h(y)y \sum_x f(x)x$$

which equals $b[h]b[f]$. The reverse is also true: if $b[f]b[h] = b[h]b[f]$ for all h , then f is a class function. Note also that each element of the group algebra defines a unique

function $f : G \rightarrow \mathbb{C}$, the coefficient of each group element giving explicitly the value of the function on that element. Therefore b is invertible and the space of all B have a bijective correspondence with the center of the group algebra.

It is interesting to go a little further and calculate the partition function for a triangle on the continuum limit. For this consider a single triangle with a triangulation such that an external edge of the triangle belongs to only one triangle of the triangulation. After reorganization by flip moves, this will correspond to a single triangle, whose weight tends to the topological one, attached to a chain of operators $K_i^j(\epsilon)$, whose weights tend, on the continuum limit, to the exponential of B (5.9). Note that we can easily compute the exponential of B , using (6.1) and the orthogonality of the characters:

$$(e^{BA})_i^j = \sum_R e^{BRA} d_R \chi_R(ij^{-1}).$$

So the partition function for the triangle at this limit is:

$$Z(i, j, k, A) = C_{ijl}^0 (e^{BA})_k^l = \sum_R e^{BRA} d_R \chi_R(ijk). \quad (6.2)$$

The reader will recognize the Yang-Mills partition function [7] if we take the quadratic Casimir operator $C_2(R)$ as B_R for continuum groups, such as $SU(N)$.

7 Concluding Remarks

Two dimensional lattice quasi-topological field theories are less trivial than the corresponding topological models. They have less symmetry but it is enough to reduce the two dimensional model to an equivalent one dimensional problem. If the link variables assume values in a finite dimensional set, the partition function can be exactly computed.

The set of Boltzmann weight $C_{ij}^k(\epsilon)$ and the gluing operator g^{ij} give a one parameter family of associative algebras A_ϵ together with a bilinear form. The scaling limit $\epsilon \rightarrow 0$ is well defined whenever $C_{ij}^k(0)$ and g^{ij} define a lattice topological field theory. At $\epsilon = 0$ the topological symmetry is restored and the theory becomes invariant by subdivision. The continuum theory is not topological in the sense that the partition function depends also on the total area of the surface. However, in the limit of zero area, the theories become topological. This is usually what is meant by a quasi-topological field theory, the prototype being YM_2 [7]. It is clear that a single topological theory can be the zero area limit of more than one continuum quasi-topological theory. That will depend on how $C_{ij}^k(\epsilon)$ approaches the critical point. We have seen that the set of all quasi-topological theories associated with $C_{ij}^k(0)$ is in one to one correspondence to the center $Z(A_0)$ of the semi-simple algebra A_0 .

It is not clear whether our continuum theories can be described by means of a Lagrangian field theories. The continuum approach is certainly possible in the case of YM_2 . It would be very interesting to find other examples of such Lagrangian theories. The simplest approach is to look for the analog of a Schwarz type topological field theory, i.e., one considers Lagrangians that are invariant under area preserving diffeomorphisms. If there is no anomalies, the zero area limit should be a Schwarz type topological field theory. Volume preserving theories have been considered in [9]. However this may not be generic enough and one may need to find the quasi-topological analog of the Witten's type topological field theories. This possibility is presently under investigation and results will be reported elsewhere.

A Appendix

We will now present a proof that any triangulation representing a surface with genus g and consisting of n triangles is equivalent. This will be done by an argument somewhat similar to the one of [8]. Our idea is to reduce any triangulation to a special one which we will refer as standard. This one is constructed by attaching several bubble-like structures composed of two triangles, as well as some double-handled structures composed of four triangles, the latter giving information about the genus. These two are shown in their dual representation on Fig. 4 (b) and Fig. 4 (c) respectively.

It is well known that any surface of genus g can be represented as the inner part of a $4g$ -sided polygon with its sides identified suitably. Hence any triangulation of the surface can be viewed as a triangulation of the polygon itself. We will make a distinction between the triangles by now. We will call "external" triangles those which share an edge with the outer boundary of the polygon. As the polygon has $4g$ sides, that will be the minimum number of "external" triangles. We will now prove that no matter how complicated the triangulation is, we can always reduce the number of "external" triangles per one side of the polygon by one and therefore reduce it to the minimal number. In other words, we can consider only one triangle per side of the polygon. Suppose that there is some side with two such triangles. As the graph is connected, we can always do some flip bonds in order to make these two triangles share an edge. Now we flip this common edge and the result will look like Fig. 12. To proceed, remember that this polygon is in fact a genus g surface, and therefore this side we are considering is identified with another side of the polygon. Note also that this identification is somewhat arbitrary. The edge defined as the side of the polygon could be in fact any edge nearby. In particular, let us pick that common edge we flipped as the side of the polygon. Now our number of "external" triangles has decreased by one.

The action on the dual graph will now be the cutting the lines which connect each side with its "opposite". We are then left with a triangulation of a $4g$ sided polygon with just one triangle at each side. Our problem reduces now to getting the standard triangulation

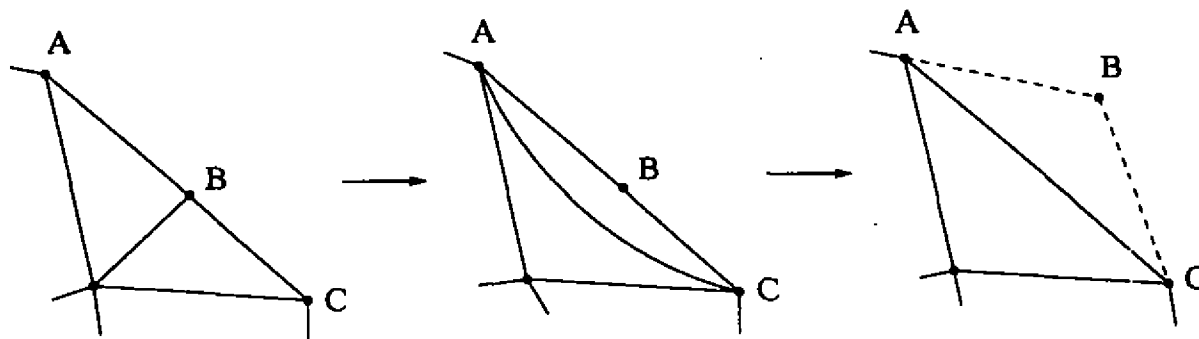


Fig.12. How we can decrease the number of "external" triangles. From left to right: in the first figure we have two triangles, and the external edges are \overline{ABC} , in the second we made a flip move, in the third we redefined our external edge as \overline{AC} . The dashed line means that B has been sent "to the other side".

of a sphere with $4g$ boundary elements. As this graph are planar, we can draw them with single lines and still encode the same information as the triangulation. The action of the flip bond move will be then the simple sliding of one edge over another as shown on Fig. 13.

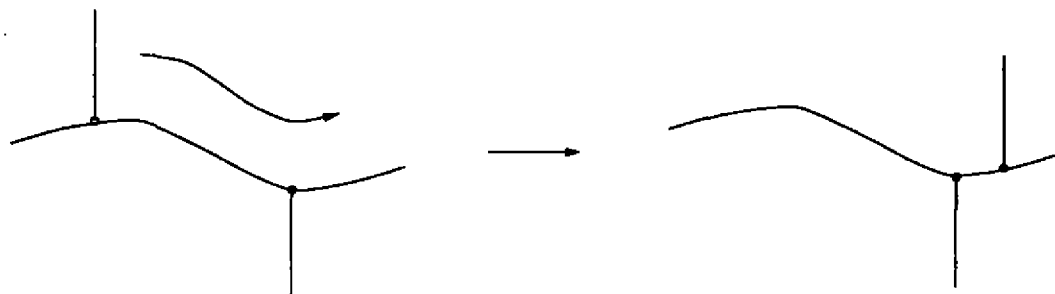


Fig.13. The action of the flip move on dual graphs. As the graph is planar, we can represent it by single lines. The figure shows the flip move as the sliding of lines one over another.

This triangulation is, in terms of the dual graphs, represented by internal loops, connected by several links among them, and some links connecting this complex to a greater loop, formed by the external triangles. This greater loop has several links pointing outwards, which will be suitably identified among them later on in order to re-build the g -torus. Consider now the internal loops. As we can slide one edge over another, we can then arrange all the edges of a given loop to link it to at most two different loops, these three loops interconnected. Fig. 14 shows how to disentangle this compound, forming "pins" in the process.

We are left then with structures like two loops linked by some edges. Fig. 15 shows

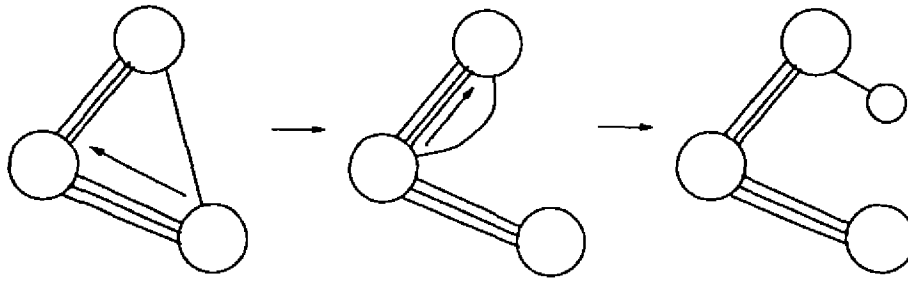


Fig.14. The action of disentanglement of three internal loops with edges linking them. This results in a number of “pins” attached to any of them.

how to transform it into two loops linked by just one edge, again forming pins. We have

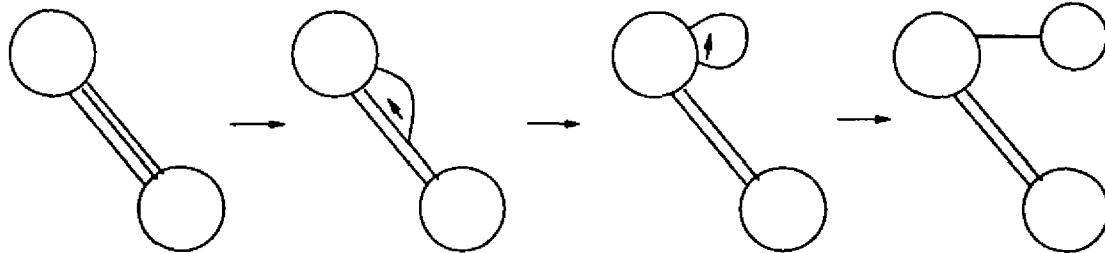


Fig.15. The action of disentanglement of two internal loops creating “pins”.

by now some internal loops, with some pins attached, connected by just one edge to at most two different loops, and this compound connected by just one edge to a greater loop which encompasses all internal loops. The pins can be carried one by one to the last internal loop – the only loop that is connected to just one different loop – and thus becoming the last one. Repeating this process, we will eventually reach a triangulation with a chain of loops linked by only one edge with one end of the chain linked by inside with the big “external” loop. This end will have an edge finishing at a vertice with two other edges, these two belonging to the outer loop. Then carry one edge of these two to the other end of the chain. We will have then a chain of bubbles attached in each end to a chain of “external” edges. Now we identify the external edges by the usual way $a_1 b_1 a_1^{-1} b_1^{-1} \dots a_g b_g a_g^{-1} b_g^{-1}$, we will have our standard triangulation as depicted is Fig. 4 (a).

One may notice that, although all we did was for a surface with genus greater than zero, we could also extend the argument for genus zero. With a given triangulation of the sphere get a vertice with coordination number 3. If it does not exist, create one by some flips. cut these three out and we will have a structure just like we had before in

the non vanishing genus case. One goes through all the procedures listed above and will end with a chain of loops on the dual graph, with one end attached to the other plus a single vertex with three edges attached to the chain. We will then merge it into the chain making two more loops, as shown in Fig. 16.

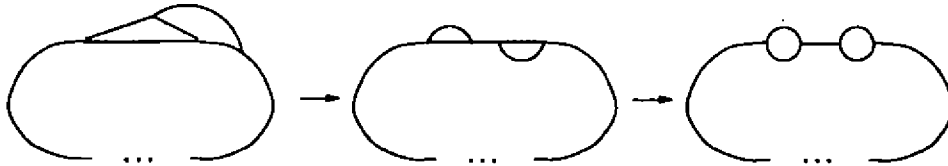


Fig.16. (a) How a vertex with coordination number 3 can be transformed into Fig. 4 (a). The vertex is represented by a triangle in the dual graph.

Acknowledgments

This work was supported by CNPq.

References

- [1] R.J. Baxter, *Exactly Solved Models in Statistical Mechanics* (Academic Press, New York, 1982)
- [2] S. M. Bhattacharjee and A. Khare, *Fifty Years of the Exact Solution of the Two-dimensional Ising Model by Onsager*, preprint IOP-BBSR/95, cond-mat/9511003.
- [3] J.F. Wheeler, *Phys. Lett.* **B223** (1989), 551; T. Jonsson, *Phys. Lett.* **B265** (1991), 141; C. Bachas and P.M.M. Petropoulos, *Commun. Math. Phys.* **152** (1993), 191.
- [4] M. Fukuma, S. Hosono, H. Kawai, *Commun. Math. Phys.* **161** (1994), 157.
- [5] S-W Chung, M. Fukuma, A. Shapere, *Int. J. Mod. Phys.* **A9** (1994) 1305.
- [6] D. Birmingham and M. Rakowski, *Commun.Math.Phys.* **173** (1995)135, hep-th/9405108; *Int.J.Mod.Phys.* **A10** (1995), hep-th/9303110.
- [7] E. Witten, *Commun. Math. Phys.* **141** (1991), 153; M. Blau, G. Thompson, *Int. J. Mod. Phys.* **A7** (1992) 3781.
- [8] D. V. Boulatov, V.A. Kazakov, I.K. Kostov and A.A. Migdal, *Nucl. Phys.* **B275**, (1986), 641.
- [9] R. Brooks, *Nucl. Phys.* **B423** (1994) 197.

Physics of the Standard Model and Beyond*

R. S. Chivukula
Boston University - USA

1. The Standard Model
 - Precision Electroweak Tests
 - R_b & R_c
2. What's Wrong with the Standard Model?
 - Unanswered Questions
 - Naturalness and Hierarchy Problems
 - Triviality
3. Dynamical Electroweak Symmetry Breaking
 - Technicolor
 - Phenomenological Signatures
 - The Top Quark & Top-Color
4. Compositeness
 - Composite Vector Bosons: W^\pm & Z
 - Composite Fermions
5. Conclusions

*Invited Plenary talk at the XVII Brazilian Annual Meeting in Particles and Fields -
October 2-6 1996, Serra Negra - Brazil

The Standard $SU(3)_C \times SU(2)_W \times U(1)_Y$ Model

Gauge Bosons: γ, W^\pm, Z^0, g

Leptons:

$$\begin{pmatrix} \nu_e \\ e \end{pmatrix}_L, \begin{pmatrix} \nu_\mu \\ \mu \end{pmatrix}_L, \begin{pmatrix} \nu_\tau \\ \tau \end{pmatrix}_L$$

$$e_R, \mu_R, \tau_R$$

Quarks:

$$\begin{pmatrix} u \\ d \end{pmatrix}_L, \begin{pmatrix} c \\ s \end{pmatrix}_L, \begin{pmatrix} t \\ b \end{pmatrix}_L$$

$$u_R, c_R, t_R$$

$$d_R, s_R, b_R$$

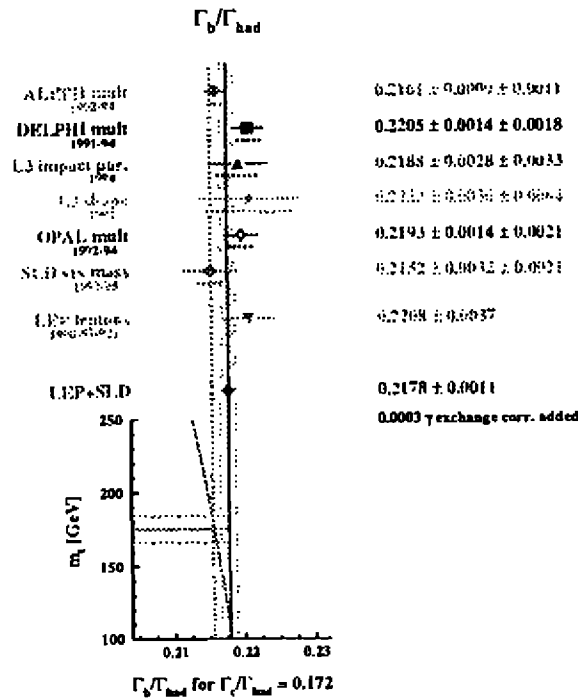
Fundamental Higgs Doublet:

$$\begin{pmatrix} \phi^+ \\ \phi^0 \end{pmatrix} \quad V(\phi) = \lambda \left(\phi^\dagger \phi - \frac{v^2}{2} \right)^2$$

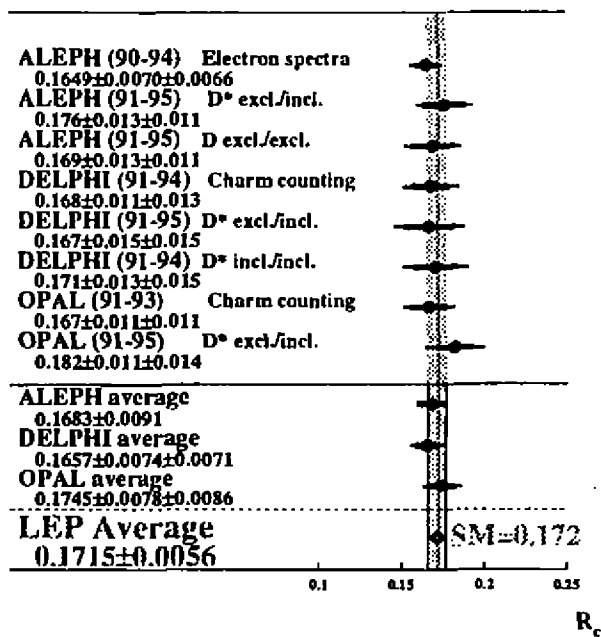
Precision Tests of the Standard Model*

	Measurement with Total Error	Standard Model	Pull
a) LEP			
line shape and lepton asymmetries:			
m_Z [GeV]	91.1863 ± 0.0020	91.1881	0.1
Γ_Z [GeV]	2.4966 ± 0.0027	2.4980	-0.5
σ_e^0 [nb]	41.508 ± 0.054	41.465	0.8
R_e	20.778 ± 0.029	20.757	0.7
$A_{FB}^{e,\tau}$	0.0174 ± 0.0010	0.0159	1.4
+ correlation matrix Table 6			
ν polarization:			
A_e	0.1401 ± 0.0067	0.1458	-0.9
A_μ	0.1382 ± 0.0076	0.1458	-1.0
b and c quark results:			
$R_b^{(e)}$	0.2170 ± 0.0012	0.2168	1.6
$R_c^{(e)}$	0.1715 ± 0.0056	0.1723	-0.1
$A_{FB}^{b(c)}$	0.0979 ± 0.0023	0.1022	-1.6
$A_{FB}^{c(b)}$	0.0733 ± 0.0049	0.0730	0.1
+ correlation matrix Table 13			
qq charge asymmetry:			
$\sin^2 \theta_{eff}^{qq} ((Q_{FB}))$	0.2320 ± 0.0010	0.23187	0.3
b) SLD			
$\sin^2 \theta_{eff}^{lepton} (A_{LR} [82,83])$	0.23061 ± 0.00047	0.23187	-2.2
$R_b [8]^{(e)}$	0.2149 ± 0.0038	0.2168	-0.2
$A_b [7]$	0.063 ± 0.048	0.035	-1.4
$A_c [7]$	0.025 ± 0.084	0.047	-0.5
c) $p\bar{p}$ and eN			
m_W [GeV] ($p\bar{p}$ [73])	80.356 ± 0.125	80.353	0.3
$1 - m_{H_u}^2/m_h^2$ (eN [8-10])	0.2244 ± 0.0042	0.2235	0.2
m_t [GeV] ($p\bar{p}$ [16-17])	175 ± 6	172	0.6

*A. Blondel, ICHEP Warsaw '96

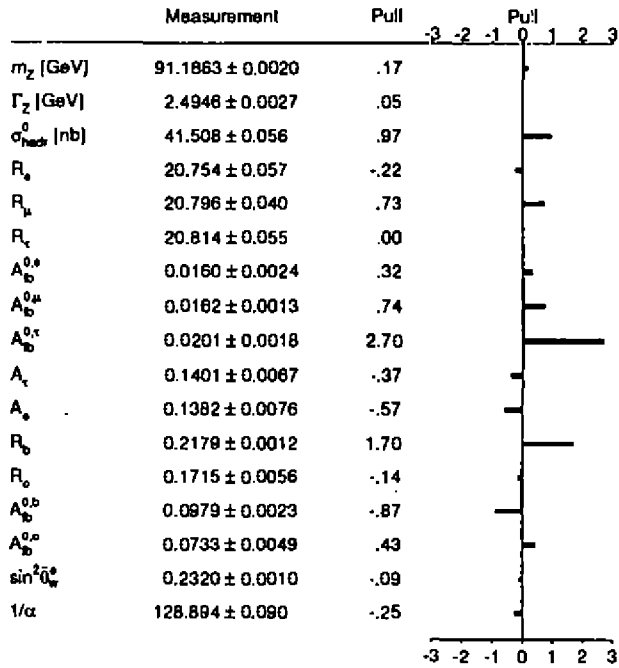


http://www.cern.ch/LEPEWWG/plots/rb_bar.eps



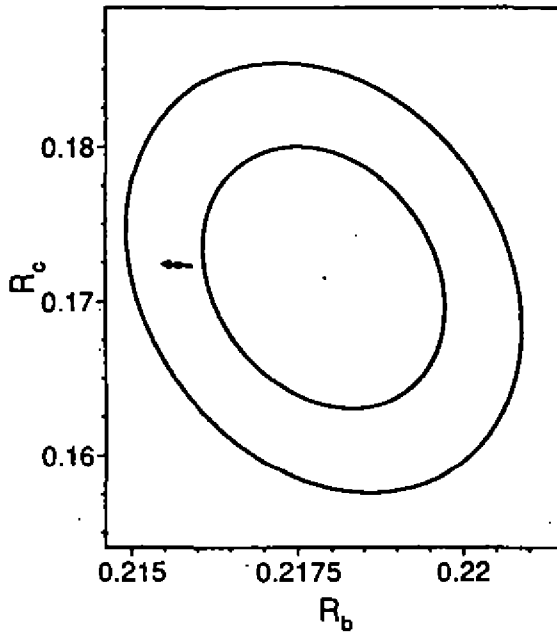
http://www.cern.ch/LEPEWWG/plots/rc_bar.eps

Warsaw 1996



<http://www.cern.ch/LEPEWWG/plots/summer96 lep-pulls.ps>

Preliminary



http://www.cern.ch/LEPEWWG/plots/rb_rc.eps

Unanswered Questions...

- What is responsible for Electroweak Symmetry Breaking?
 - Technicolor, Composite Higgs, Dynamical SUSY Breaking,...
- What is responsible for Flavor?
 - Extended Technicolor, Family-Symmetries,...
- What is the origin of CP-violation?
 - ??
- What explains the gauge structure of the standard model?
 - Grand-Unified Theories, Compositeness
- Why is the cosmological constant small?
 - ??
- What is the quantum theory of gravity?
 - String Theory

What's Wrong with the Standard Model?

Fundamental Scalar Doublet:

$$\phi = \begin{pmatrix} \phi^+ \\ \phi^0 \end{pmatrix} ,$$

with potential:

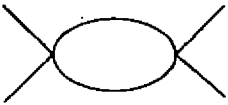
$$V(\phi) = \lambda \left(\phi^\dagger \phi - \frac{v^2}{2} \right)^2$$

- No *explanation* of Electroweak Symmetry Breaking
- Hierarchy and Naturalness Problem



$$\Rightarrow m_H^2 \propto \Lambda^2 .$$

- Triviality Problem



$$\Rightarrow \beta = \frac{3\lambda^2}{2\pi^2} > 0 .$$

Wilson Renormalization Group

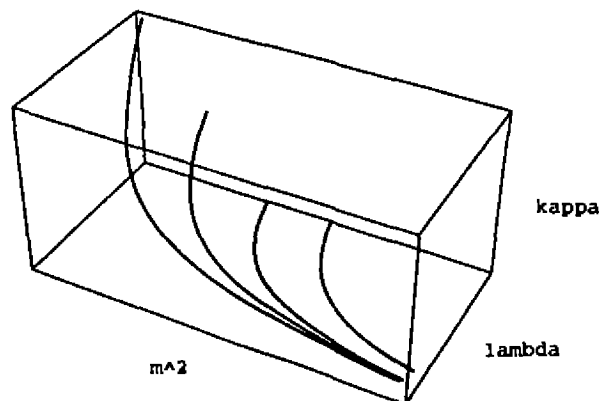
Define theory with a fixed UV-cutoff:

$$\mathcal{L}_\Lambda = D^\mu \phi^\dagger D_\mu \phi + m^2(\Lambda) \phi^\dagger \phi + \frac{\lambda(\Lambda)}{4} (\phi^\dagger \phi)^2 + \frac{\kappa(\Lambda)}{36\Lambda^2} (\phi^\dagger \phi)^3 + \dots$$

Integrate out states with $\Lambda' < k < \Lambda$:

$$\begin{aligned} \mathcal{L}_\Lambda &\Rightarrow \mathcal{L}_{\Lambda'} \\ m^2(\Lambda) &\rightarrow m^2(\Lambda') \\ \lambda(\Lambda) &\rightarrow \lambda(\Lambda') \\ \kappa(\Lambda) &\rightarrow \kappa(\Lambda') \end{aligned}$$

Consider evolution of couplings in the IR-limit....



Implications:

- $\kappa \rightarrow 0$ — Renormalizability.
- $m^2 \rightarrow \infty$ — Naturalness/Hierarchy Problem:

$$\frac{\Delta m^2(\Lambda)}{m^2(\Lambda)} \propto \frac{v^2}{\Lambda^2}$$

- $\lambda \rightarrow 0$ — Triviality.

Perturbative analysis, but Wilson approach in principle non-perturbative:

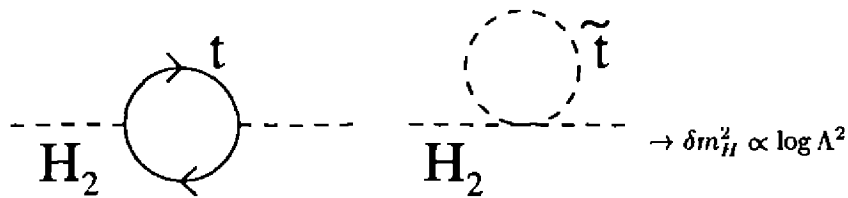
- Nontrivial Fixed Points
- Large Anomalous Dimension

Solving the Naturalness/Hierarchy Problems

Stabilize the Hierarchy

While scalar masses are *susceptible* to $\mathcal{O}(\Lambda^2)$ mass renormalization, they can be protected by a symmetry.

1. Supersymmetry



2. Composite Higgs

- Higgs as Goldstone Boson
- EWSB due to “vacuum (mis)-alignment”

Eliminate the Hierarchy...

- EWSB due to χ -symmetry breaking in a gauge theory with massless fermions

Dynamical Electroweak Symmetry Breaking

Technicolor: $SU(N_{TC})$ gauge theory,

$$\Psi_L = \begin{pmatrix} U \\ D \end{pmatrix}_L \quad U_R, D_R$$

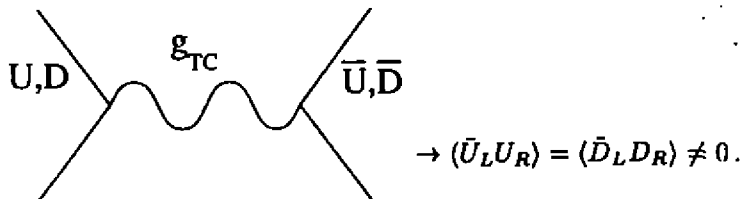
with massless fermions

$$\mathcal{L} = \bar{U}_L i \not{\partial} U_L + \bar{U}_R i \not{\partial} U_R + \quad (1)$$

$$\bar{D}_L i \not{\partial} D_L + \bar{D}_R i \not{\partial} D_R \quad (2)$$

Like QCD in $m_u, m_d \rightarrow 0$ limit:

- Chiral $SU(2)_L \times SU(2)_R$ symmetry
- Dynamically broken $SU(2)_L \times SU(2)_R \rightarrow SU(2)_V$



Broken Chiral Symmetries \Rightarrow Goldstone Bosons

Gauge $SU(2)_W \times U(1)_Y \Rightarrow$ Higgs Mechanism

$$\pi^\pm, \pi^0 \rightarrow W_L^\pm, Z_L$$

$$M_W = \frac{g F_{TC}}{2} \rightarrow F_{TC} \approx 250 \text{ GeV}$$

Scale up QCD by

$$\frac{F_{TC}}{f_\pi} \approx 2500.$$

Generalizations:

- Any strongly interacting gauge theory with

$$SU(2)_W \times U(1)_Y \subseteq G \rightarrow H \supseteq SU(2)_C \supset U(1)_{em}$$

- where "custodial" $SU(2)_C$ symmetry insures that

$$\rho = \frac{M_W}{M_Z \sin \theta_W} = 1$$

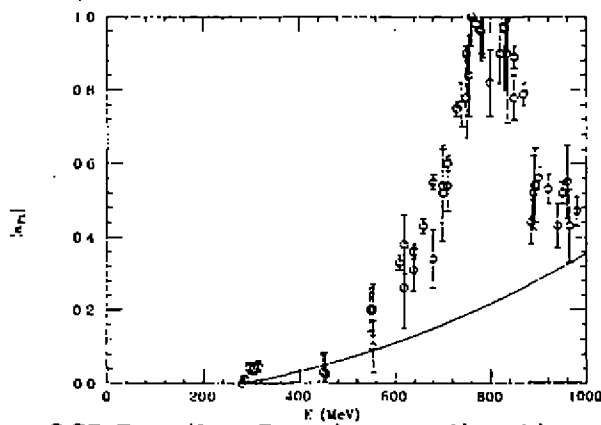
at tree-level.

This results in Universal Low-Energy Theorems:

$$\begin{aligned}
 \mathcal{M}[W_L^+ W_L^- \rightarrow W_L^+ W_L^-] &= \frac{4u}{v^2 \rho} \\
 \mathcal{M}[W_L^+ W_L^- \rightarrow Z_L Z_L] &= \frac{4s}{v^2} \left(4 - \frac{3}{\rho}\right) \\
 \mathcal{M}[Z_L Z_L \rightarrow Z_L Z_L] &= 0
 \end{aligned}
 \tag{3}$$

What dynamics cuts off growth in amplitude?

- New particles.
- Born approximation fails \rightarrow strong interactions.
- Both.

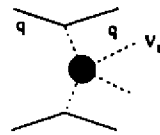


QCD Data (from Donoghue, *et. al.*) and low-energy theorem prediction for the spin-1/isospin-1 pion scattering amplitude.

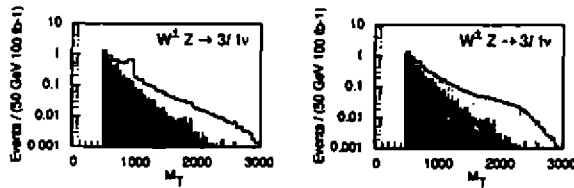
To get predictions for QCD-like technicolor, scale by $v/f_\pi \approx 2600$. That is,

$$M_{\rho_{TC}} \approx 2 \text{ TeV} \sqrt{\frac{3}{N_{TC}}}$$

Gauge-Boson Scattering at the LHC*



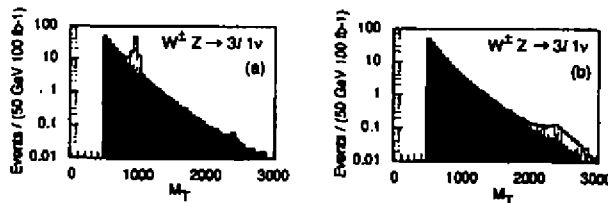
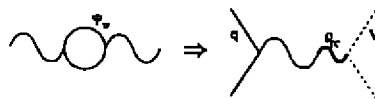
For $M_{\rho TC} = 1.0 \text{ TeV}, 2.5 \text{ TeV}$:



leptonic cuts	jet cuts
$ \eta(\ell) < 2.5$	$E(j_{tag}) > 0.8 \text{ TeV}$
$p_T(\ell) > 40 \text{ GeV}$	$3.0 < \eta(j_{tag}) < 5.0$
$p_T^{min} > 50 \text{ GeV}$	$p_T(j_{tag}) > 40 \text{ GeV}$
$p_T(Z) > \frac{1}{2} M_T$	$p_T(j_{miss}) > 60 \text{ GeV}$
$M_T > 500 \text{ GeV}$	$ \eta(j_{miss}) < 3.0$

*J. Bagger *et. al.*, hep-ph/9306256, 9504426.

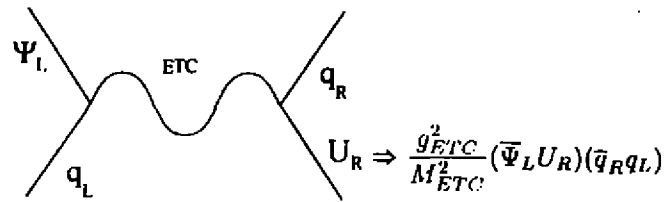
Gauge Boson — Vector Meson Mixing at LHC*



*M. Golden, *et. al.*, hep-ph/9511206.

Fermion Masses & ETC Interactions

Extended Technicolor Interactions — Connect chiral-symmetries of TFs to quarks & leptons.



$$m_q \approx \frac{g_{ETC}^2}{M_{ETC}^2} \langle \bar{U}U \rangle_{ETC}$$

$$\langle \bar{U}U \rangle_{ETC} = \langle \bar{U}U \rangle_{TC} \exp \left(\int_{\Lambda_{TC}}^{M_{ETC}} \frac{d\mu}{\mu} \gamma_m(\mu) \right)$$

For QCD-like TC (“precociously” asymptotically free), γ_m is small over this range:

$$\langle \bar{U}U \rangle_{ETC} \approx \langle \bar{U}U \rangle_{TC} \approx 4\pi F_{TC}^3$$

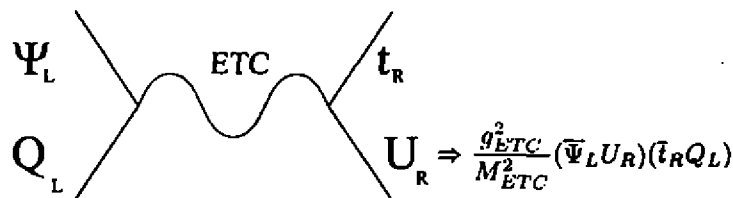
$$\frac{M_{ETC}}{g_{ETC}} \approx 40 \text{ TeV} \left(\frac{F_{TC}}{250 \text{ GeV}} \right)^{\frac{1}{2}} \left(\frac{100 \text{ MeV}}{m_q} \right)^{\frac{1}{2}}$$

The Status of Models of DEWSB...

- Dynamical electroweak symmetry breaking can provide a natural explanation for M_W & $M_Z \neq 0$.
- Fermion masses require additional, ETC interactions.
- ETC is a dynamical theory of flavor, no complete theory exists.
- The following obstructions to an ETC theory may be alleviated in a theory of "walking technicolor":
 1. Flavor-Changing Neutral-Currents
 2. Light Pseudo-Goldstone Bosons
 3. S(?)

Top (and Bottom) pose a particular challenge...

Top Mass in Models of DEWSB



$$m_t \approx \frac{g_{ETC}^2}{M_{ETC}^2} \langle \bar{U}U \rangle_{ETC}$$

Using

$$\langle \bar{U}U \rangle_{ETC} \approx \langle \bar{U}U \rangle_{TC} \approx 4\pi F_{TC}^3$$

we find

$$\frac{M_{ETC}}{g_{ETC}} \approx 1 \text{ TeV} \left(\frac{F_{TC}}{250 \text{ GeV}} \right)^{\frac{3}{2}} \left(\frac{175 \text{ GeV}}{m_t} \right)^{\frac{1}{2}}$$

Scale of top-quark ETC-dynamics is *very* low.

Since $M_{ETC} \simeq \Lambda_{TC}$,

$$\langle \bar{U}U \rangle_{ETC} = \langle \bar{U}U \rangle_{TC} \exp \left(\int_{\Lambda_{TC}}^{M_{ETC}} \frac{d\mu}{\mu} \gamma_m(\mu) \right)$$

walking doesn't alter this conclusion.

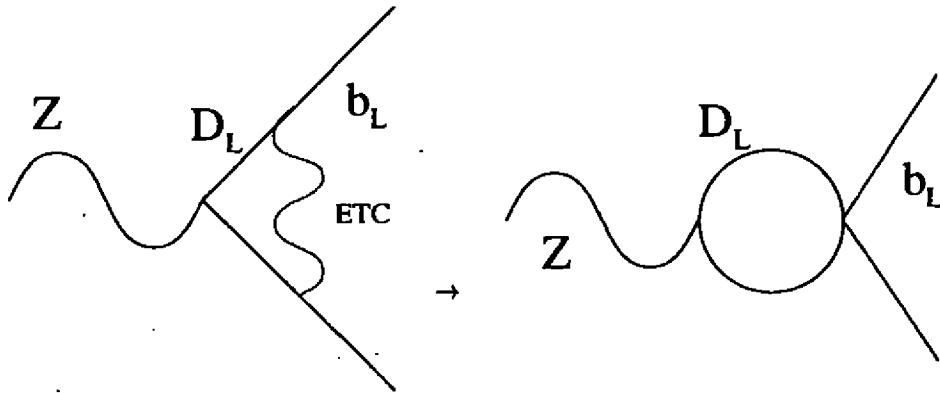
ETC Effects on $Z \rightarrow b\bar{b}$

Top-quark ETC-boson couples to the current

$$\xi(\bar{\Psi}_L^{i\alpha} \gamma^\mu Q_L^i) + \xi^{-1}(\bar{U}_R^\alpha \gamma^\mu t_R)$$

(or *h.c.*) where α is a TC index, and the contracted i are weak-indices.

N.B.: We assume here that $[SU(2), ETC] = 0$.



Defining $R_b = \Gamma_b/\Gamma_h$,

$$\frac{\delta R_b}{R_b} \approx \frac{\delta \Gamma_b}{\Gamma_b} (1 - R_b) \approx -5.1\% \cdot \xi^2 \cdot \left(\frac{m_t}{175 \text{ GeV}}\right)$$

Isospin Violation: $\Delta\rho$

ETC-interactions *must* violate weak-isospin in order to give rise to $m_t \gg m_b$.
 \Rightarrow This could induce dangerous $\Delta I = 2$ technifermion operators (Appelquist, *et. al.*).

$$\begin{array}{c} Z \\ \text{---} \\ \Psi \\ \text{---} \\ \text{ETC} \\ \text{---} \\ \Psi \\ \text{---} \\ Z \end{array} \Rightarrow \frac{g_{ETC}^2}{M_{ETC}^2} (\bar{\Psi}_R \gamma_\mu \tau_3 \Psi_R)^2$$

In the vacuum-insertion approximation

$$\Delta\rho \simeq \frac{2g_{ETC}^2}{M_{ETC}^2} \frac{N_D^2 F_{TC}^4}{v^2} \Rightarrow$$

$$\Delta\rho \approx 12\% \cdot \left(\frac{\sqrt{N_D} F_{TC}}{250 \text{ GeV}} \right)^2 \cdot \left(\frac{1 \text{ TeV}}{M_{ETC}/g_{ETC}} \right)^2$$

If we require that $\Delta\rho \leq 0.4\%$, then

$$\frac{M_{ETC}}{g_{ETC}} > 5.5 \text{ TeV} \cdot \left(\frac{\sqrt{N_D} F_{TC}}{250 \text{ GeV}} \right)^2,$$

to large to produce $m_t \simeq 175 \text{ GeV}$.

Another possibility: It is possible that $N_D F_{TC}^2 \ll (250 \text{ GeV})^2$, if the sector responsible for the top-quark mass does not give rise to the bulk of EWSB.

In this scenario, the constraint is

$$F_{TC} < \frac{105 \text{ GeV}}{N_D^{1/2}} \cdot \left(\frac{M_{ETC}/g_{ETC}}{1 \text{ TeV}} \right)^{1/2}$$

Topcolor-Assisted Technicolor (TC2)

C. T. Hill, *Physics Letters B* 345, 488 (1995)

- Strong Technicolor dynamics at 1 TeV dynamically generates most of EWSB.
- Extended Technicolor dynamics at scales much higher than 1 TeV generate the light quark and lepton masses, and ETC contributions to the third generation masses ($m_{t,b,\tau}^{ETC}$) of order 1 GeV. (No large ΔF_b).
- Strong Topcolor dynamics also at a scale of order 1 TeV generates $\langle \bar{t}t \rangle \neq 0$, $m_t \sim 170 \text{ GeV}$.
- Topcolor does not form $\langle \bar{b}b \rangle$.
- Topcolor contributes a small amount to EWSB ($f_t \sim 60 \text{ GeV}$).
- Low-Energy Phenomena: Extra pseudo-Goldstone bosons ("Top-pions"), "Top-gluons", etc.

Compositeness

Composite Vector Bosons: W^\pm, Z

- Weinberg: As $M_V \rightarrow 0$, consistency requires that the coupling to a conserved current, hence...
- Gauge couplings (& universality) inevitable in the limit $M_V/\Lambda \rightarrow 0$

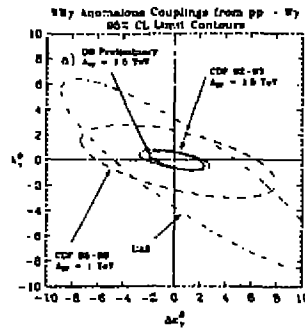
Following Hagiwara, *et. al.*:

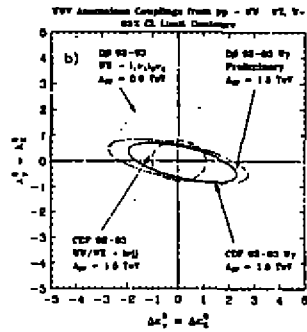
$$\frac{i}{e \cot \theta} \mathcal{L}_{WWZ} = g_1(W_{\mu\nu}^\dagger W^\mu Z^\nu - W_\mu^\dagger Z_\nu W^{\mu\nu}) + \kappa_Z W_\mu^\dagger W_\nu Z^{\mu\nu} + \frac{\kappa_\gamma}{\cot \theta} W_\mu^\dagger W_\nu F^{\mu\nu}$$

Where:

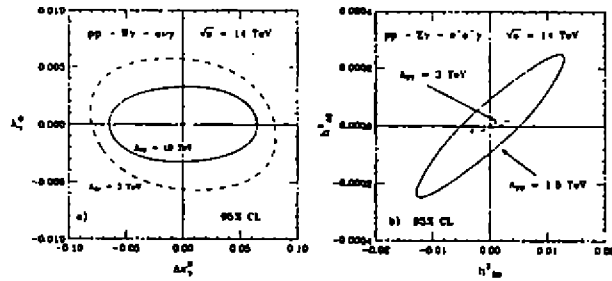
$$\left. \begin{matrix} g_1 - 1 \\ \kappa_Z - 1 \\ \kappa_\gamma - 1 \end{matrix} \right\} = \mathcal{O}\left(\frac{M_V^2}{\Lambda^2}\right)$$

Current Limits[†]:



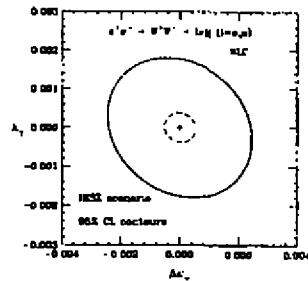


† Aihara *et. al.*, hep-ph/9503425.
 Experimental Prospects at the LHC†:



$$\sqrt{s} = 14 \text{ TeV}, 100 \text{ fb}^{-1}$$

and NLC†:



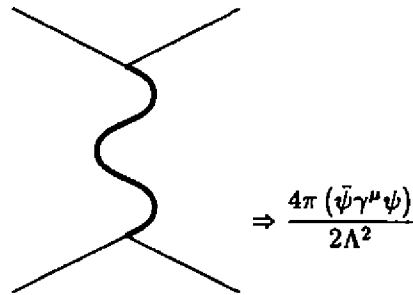
$$\sqrt{s} = 500, 1500 \text{ GeV}, 80 \text{ \& } 190 \text{ fb}^{-1}$$

† Aihara *et. al.*, hep-ph/9503425.

Composite Fermions

- 't Hooft: confinement & unbroken chiral symmetry \Rightarrow massless composite fermions.
- In limit $m_f \rightarrow 0$, SM has $(SU(3) \times U(1))^5$ global chiral symmetry: can fundamental theory have fewer fermions?

Following Eichten, *et. al.*, low-energy effects:



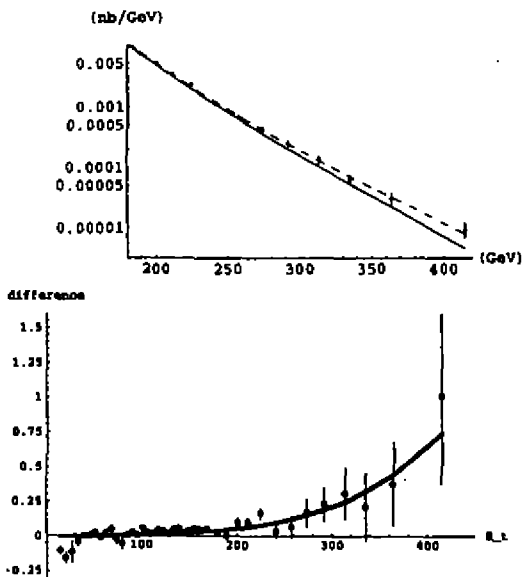
$$\Rightarrow \frac{4\pi (\bar{\psi}\gamma^\mu\psi)}{2\Lambda^2}$$

Leads to rise in cross-section:

$$\sigma(s) \sim \frac{\alpha^2}{s} \left(1 + \frac{4\pi s}{\alpha\Lambda^2} + \dots \right)$$

Current limits: $\Lambda(\ell\ell\ell) > 2.9$ TeV

High- E_T Jet Data at the Tevatron:

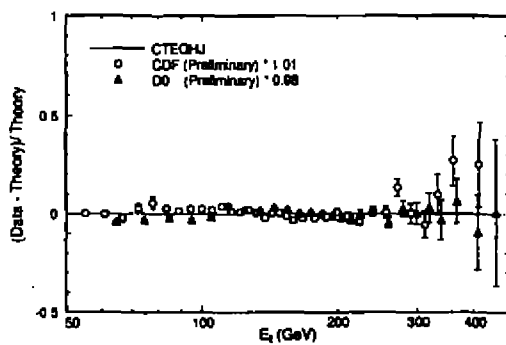


$$\frac{4\pi}{2!\Lambda^2} J^{\alpha\mu} J_{\mu}$$

Dashed lines for a model* with $\Lambda(qqqq) \approx 2$ TeV.

* hep-ph/9603311

However, this effect could be due* to lack of understanding of structure functions:



* CTEQ Collaboration hep-ph/9606399

Conclusions

- There is still **NO DIRECT EVIDENCE** for physics beyond the standard model.
- There are strong theoretical reasons to believe that there is, probably at energies of $O(1 \text{ TeV})$ or below.
- Models of Dynamical Electroweak Symmetry Breaking provide a natural and dynamical explanation of EWSB.
 - Accommodating the t mass \Rightarrow TC2 or related model(s).
- Gauge-Boson or Fermion Compositeness would result in interesting phenomenological signatures and remain a possibility.

However, no complete, consistent, & compelling models exist ...



“Oh, yeah! Well I’d rather be a living corpse made from dismembered body parts than a hunchbacked little grave robber like you!”

We Need Experimental Direction!

(Apologies to Larson, and thanks to K. Lane.)

Additional References

- **DYNAMICAL ELECTROWEAK SYMMETRY BREAKING AND THE TOP QUARK.** By R.Sekhar Chivukula (Boston U.). BUHEP-95-23A, Sep 1995. 18pp. Talk given at SLAC Summer Inst., Jul 10-24, 1995. e-Print Archive: hep-ph/9509384
- **STRONG W(L) W(L) SCATTERING.** By R.Sekhar Chivukula (Boston U.). BUHEP-95-17, Feb 1995. 11pp. Contributed to International Symposium on Vector Boson Self-interactions (WGZ95) (To be followed by Topics in Particle Physics with CMS, Los Angeles, CA, 6-8 Feb 1995), Los Angeles, CA, 1-3 Feb 1995. e-Print Archive: hep-ph/9505202
- **THEORY OF A STRONGLY INTERACTING ELECTROWEAK SYMMETRY BREAKING SECTOR.** By R.Sekhar Chivukula, Michael J. Dugan (Boston U.), Mitchell Golden (Harvard U.), Elizabeth H. Simmons (Boston U.). BUHEP-95-09, Feb 1995. 44pp. Published in *Ann.Rev.Nucl.Part.Sci.*45:255-294,1995.
- **STRONGLY COUPLED ELECTROWEAK SYMMETRY BREAKING: IMPLICATION OF MODELS.** By R.Sekhar Chivukula, Rogerio Rosenfeld, Elizabeth H. Simmons, John Terning (Boston U.). BUHEP-95-07, Feb 1995. 31pp. To be published in 'Electroweak Symmetry Breaking and Beyond the standard Model, ed. by T. Barklow, et al. (World Scientific).
- **PHYSICS BEYOND THE STANDARD MODEL: PROSPECTS AND PERSPECTIVES.** By R.Sekhar Chivukula (Boston U.). BU-HEP-94-22, Aug 1994. 21pp. Talk given at 1994 Meeting of the American Physical Society, Division of Particles and Fields (DPF 94), Albuquerque, NM, 2-6 Aug 1994. Published in *DPF Conf.1994:273-296 (QCD161:A6:1994)*

Casimir Effect for the Real Boundaries

V.M. Mostepanenko

Departamento de Física - Universidade Federal da Paraíba - João Pessoa
(On leave from St.Petersburg State Technological Institute (Technical University)
and A. Friedmann Laboratory for Theoretical Physics (Russia))

1 Introduction

The physical phenomena generally known as the Casimir effect are interesting because of their exclusively quantum nature associated with the presence of zero-point oscillations in the vacuum states of quantized fields. Due to the change of zero-point oscillation spectrum in restricted quantization domain some force arises acting upon the boundaries. For two perfect plane parallel uncharged metallic plates placed in a vacuum at a distance a the Casimir attractive force per unit area is [1]

$$F_0 = -\frac{\pi^2}{240} \frac{\hbar c}{a^4}, \quad (1)$$

where \hbar is Plank's constant, c is the velocity of light. A unique peculiarity of this force is that it does not depend on mass, charge or any other coupling constant. The attraction (1) was observed experimentally [2]. For plates of area 1 cm^2 and $a = 0.5 \mu\text{m}$ the value of the force was $\approx 0.2 \cdot 10^{-5} \text{ N}$ in agreement with (1).

We will discuss here the corrections to the Casimir force (1) due to non-ideality of the electrical properties and of the geometry of the boundaries restricting the quantization domain. Such corrections must be taken into account in experiments on measuring the Casimir force and in applications of the Casimir effect for obtaining more strong constraints for the constants of hypothetical long-range interactions [3,4].

In Sec. 2 the corrections to the Casimir force (1) will be studied due to the electrical imperfections of the plate metal. In Sec. 3 the new formalism will be presented which helps to calculate corrections to (1) due to the small geometrical imperfections of the plates material. In Sec. 4 the configurations which are important for experiment will be considered.

Below the units in which $\hbar = c = 1$ are used.

2 Corrections due to the electrical imperfections

We begin with the corrections due to the non-ideality of plates metal. The result (1) was obtained for the ideal metal, i.e. when on the surface of the plates the boundary condition is fulfilled:

$$E_t|_S = 0, \quad (2)$$

where E_t is the tangential component of the electromagnetic zero oscillations electric field.

It is known [5] that the penetration of an electromagnetic field into a real metal can be modelled by imposing a so called "impedance" condition at the boundary:

$$E_t = Z(\omega) [H_t \times n], \quad (3)$$

where $Z(\omega)$ is the impedance, n is the internal ("into" the medium) normal, and the tangential components of the electric and magnetic fields are given by

$$E_t = E - n(E \cdot n), \quad H_t = H - n(H \cdot n). \quad (4)$$

When the medium is characterized by definite electric permittivity $\epsilon(\omega)$ and magnetic permeability $\mu(\omega)$ the impedance can be expressed as

$$Z(\omega) = \sqrt{\frac{\mu(\omega)}{\epsilon(\omega)}}. \quad (5)$$

Below we shall assume that $|Z| \ll 1$; for an ideal metal $Z(\omega) \equiv 0$.

We impose condition (3) on surfaces of plates bounding the quantization domain and pose the problem of calculating the resulting electromagnetic field vacuum energy densities and Casimir forces [6].

Condition (3) similarly to the simpler boundary condition (2) changes the vacuum fluctuation spectrum. We determine it for the case of two plane parallel plates modelling half-spaces separated by an empty gap $-a/2 < z < a/2$.

We will look for eigenfunctions to the Maxwell equations obtained after separating the time variable in the form

$$E = e(z) \exp(iQ \cdot \rho); \quad (6)$$

$$G \equiv i\omega H = g(z) \exp(iQ \cdot \rho) = \nabla \times E, \quad (7)$$

where Q, ρ are two-dimensional vectors in the plane of the plates (x, y) ; the vectors e and g satisfy the equations

$$e'' + \kappa^2 e = 0; \quad g'' + \kappa^2 g = 0; \quad \kappa^2 \equiv \omega^2 - Q^2. \quad (8)$$

Here the prime denotes the derivative with respect to z .

Substituting (6), (7) into (3) and taking account to the direction of the normal, we find that at the boundaries $z = \pm a/2$

$$\begin{aligned} e_x &= \pm \frac{iZ}{\omega} [iQ_x e_z - e'_x]; \\ e_y &= \pm \frac{iZ}{\omega} [iQ_y e_z - e'_y]. \end{aligned} \quad (9)$$

In addition from $\nabla \cdot E = 0$ it follows that

$$i(Q \cdot e) + e'_z = 0 \quad (10)$$

everywhere.

Without loss of generality we will assume that $Q_y = 0$. If $e_y \equiv 0$ then by symmetry considerations the solutions of (7) has the form

$$e_z \sim \cos \kappa z; \quad e_x \sim \sin \kappa z \quad (11)$$

or vice-versa. Substituting (11) into (9) we obtain the dispersion equation for the determination of the spectrum:

$$\sin \frac{\kappa a}{2} + \frac{iZ(Q^2 + \kappa^2)}{\kappa \omega} \cos \frac{\kappa a}{2} = 0 \quad (12)$$

or

$$\cos \frac{\kappa a}{2} - \frac{iZ(Q^2 + \kappa^2)}{\kappa \omega} \sin \frac{\kappa a}{2} = 0. \quad (13)$$

Equations (8) also have the solutions

$$e_z = e_x = 0; \quad e_y \neq 0, \quad (14)$$

leading to the equation

$$\cos \frac{\kappa a}{2} - \frac{iZ}{\omega} \kappa \sin \frac{\kappa a}{2} = 0 \quad (15)$$

or

$$\sin \frac{\kappa a}{2} + \frac{iZ}{\omega} \kappa \cos \frac{\kappa a}{2} = 0 \quad (16)$$

It is obvious that in (12)–(16) $Q = (Q_x, Q_y)$ may be considered as arbitrary.

When the penetration depth $\delta = iZ/\omega$ and the eigenfrequencies are real, the vacuum energy averaged over z is given by the half-sum of frequencies

$$E_0 = \frac{1}{2} \sum_n \omega_n \quad (17)$$

and the argument principle may be used to calculate it. We obtain

$$E_0 = E_0(a, Z) = \frac{1}{2\pi} \int_0^\infty d\zeta \int_0^\infty \frac{Q dQ}{2\pi} \ln D[Q, i\zeta], \quad (18)$$

where $Q = |Q|$ and the replacements are used $\omega \rightarrow i\zeta$, $\kappa \rightarrow i\sqrt{\zeta^2 + Q^2} \equiv iR$, and D is a function that vanishes for every solution of (10), (13), (15), (16).

For arbitrary complex Z the eigenfrequencies $\omega = \sqrt{\kappa^2 + Q^2}$ governed by (12)–(16) will have an imaginary part. It is known that in this case the vacuum energy should be determined from the solution of an auxiliary electromagnetic problem [7] and does not coincide with the half-sum of the eigenfrequencies (which is already clear from the complexity of the ω_n). However, formula (18) is in fact still valid: we recall that after the contour rotation $\omega \rightarrow i\zeta$ the integral in (18) evidently real.

Multiplying (12) and (13), and using the previous replacements, we obtain

$$D^I = \sinh Ra + \frac{2\sigma}{1 + \sigma^2} \cosh Ra, \quad (19)$$

where $\sigma \equiv Z\zeta/R$.

To ascribe a finite value to E_0 it is suitable to use a subtraction procedure which reduces to the subtraction from E_0 of its asymptotic behaviour as $a \rightarrow \infty$. This subtraction eliminates fictitious divergences of lower orders as well as the vacuum divergence $\sim R^4$.

The subtraction is equivalent to replacing of D^I by the regularized value

$$D_{\text{reg}}^I = D^0 \left[1 + \frac{4\sigma}{(1 + \sigma^2)^2} \frac{1}{\exp(2Ra) - 1} \right], \quad (20)$$

$$D^0 \equiv 1 - \exp(-2Ra).$$

Here D^0 describes the spectrum for perfect metallic plates and the second factor gives the corrections caused by imperfection.

From (15) and (16) we similarly obtain

$$D_{\text{reg}}^{II} = D^0 \left[1 + \frac{4ZR\zeta}{(\zeta + RZ)^2} \frac{1}{\exp(2Ra) - 1} \right]. \quad (21)$$

The renormalized energy U_R is thus given by formula (18) in which $D[Q, i\zeta]$ is replaced by the product $D_{\text{reg}}^I D_{\text{reg}}^{II}$ from (20), (21). For the force acting per unit area, $F = -\partial U_R / \partial a$ we obtain

$$F = -\frac{1}{2\pi^2} \int_0^\infty d\zeta \int_0^\infty dQ QR \frac{\partial}{\partial(2Ra)} \ln(D_{\text{reg}}^I D_{\text{reg}}^{II}). \quad (22)$$

For perfect plates with $Z = 0$ we have $D_{\text{reg}}^I = D_{\text{reg}}^{II} = D^0$, and from (22) we obtain once more the result (1). The main contribution to F is given by the frequencies $\zeta = |\omega| \leq a^{-1}$. Direct computation shows that any approximation to $Z(\omega)$ that is exact for wavelengths $1.4a < \lambda < 30a$ and satisfies $d[Z(i\zeta)]/d\zeta > 1$ gives F with an error no greater than 0.01%.

When $Z \neq 0$ the value of the force is $F = F_0 + \Delta F$. In linear approximation with $Z(i\zeta)/\zeta a$ as a small parameter we obtain from (22) the following correction to the force:

$$\Delta^{(1)} F = -\frac{2}{\pi^2} \int_0^\infty d\zeta \int_0^\infty dQ QR \left(\sigma + \frac{Z}{\zeta} R \right) \frac{\partial}{\partial(2Ra)} \frac{1}{\exp(2Ra) - 1}. \quad (23)$$

To obtain the second-order correction to the force $\Delta^{(2)}F \sim F_0 Z^2 / \zeta^2 a^2$ it is necessary to identify those terms in the expansion of $\ln D_{\text{reg}}^{I,II}$ in (22) that are quadratic in δ and ZR/ζ . Because the neighbouring terms in the expansion of $\ln(1+z)$ in powers of z have opposite signs, it is obvious that the corrections $\Delta^{(1)}F$ and $\Delta^{(2)}F$ have opposite signs. We finally get

$$\Delta^{(2)}F = \frac{4}{\pi^2} \int_0^\infty d\zeta \int_0^\infty dQ QR \left(\sigma^2 + \frac{Z^2}{\zeta^2} R^2 \right) \times \frac{\partial}{\partial(2Ra)} \left[\frac{1}{\exp(2Ra) - 1} \left(1 + \frac{1}{\exp(2Ra) - 1} \right) \right]. \quad (24)$$

We underline that in the integrals (23), (24) Z is taken with the replacement $Z(\omega \rightarrow i\zeta)$. Here, by its analytic properties, $Z(i\zeta)$ has real values independently of the behaviour of $Z(\omega)$ on the real axis [5].

The results (22)–(24) obtained above enable us to determine the influence of dispersive properties of real metals on the magnitude of the Casimir force. To obtain the specific dependence of ΔF on a one should use an expression for the impedance Z in terms of the frequency ω and other parameters such as the conductivity σ , electron Fermi momentum p_F etc. The main contribution to the Casimir effect comes from vacuum fluctuations with wavelengths of the order of the distance between the plates. Because for fields with different wavelengths the impedance Z behaves differently, to calculate the dispersive corrections to the Casimir force one must consider several cases.

We first consider the domain with plate separation from a few tenths of a micrometer to around a hundred micrometers (infra-red optics). In this domain impedance is purely imaginary: $Z(\omega) = -i\omega/\Omega$, where Ω is the effective plasma frequency of the electrons. For such impedance the penetration depth of the field into metal is frequency-independent [8]

$$\delta(\omega) = \delta_0 = iZ(\omega)/\omega = 1/\Omega. \quad (25)$$

The domain of applicability of the condition $\delta(\omega) = \text{const}$ depends on the specific metal from which the plates are made, and also on the temperature (which should be sufficiently low) when the distances between the plates are large. Here the small parameter of the perturbation theory may be interpreted as the relative penetration depth: $Z/\zeta a = \delta_0/a$.

Changing the variable of integration in (23) according to $Q = \zeta\sqrt{t-1}$ we obtain the first-order correction to the force

$$\Delta^{(1)}F = \frac{\delta_0}{4\pi} \int_1^\infty dt (1+t) \int_0^\infty \frac{d\zeta \zeta^4}{\sinh^2(a\zeta\sqrt{t})}. \quad (26)$$

Performing this integration and using the result (1), we find

$$F \approx F_0 + \Delta^{(1)}F = -\frac{\pi^2}{240a^4} \left(1 - \frac{16}{3} \frac{\delta_0}{a} \right) \quad (27)$$

or, in the same approximation,

$$F(a) = F_0(a_{\text{eff}}), \quad a_{\text{eff}} = a_0 + \frac{4\delta_0}{3}. \quad (28)$$

We note that the first-order correction in δ_0/a was found in [9] with a coefficient differing by a factor of 5 from the correct value which was firstly found in [10].

We consider now corrections of second order in δ_0/a for the same values of a . With the change of variable $Q = \zeta t$ and integrating with respect to ζ , the integrals in (24) may be found from tables. We finally get

$$\Delta^{(2)}F = -\frac{\pi^2 \delta_0^2}{10a^6}. \quad (29)$$

The total force in two orders of perturbation theory is [6]

$$F = F_0 + \Delta^{(1)}F + \Delta^{(2)}F = -\frac{\pi^2}{240a^4} \left(1 - \frac{16}{3} \frac{\delta_0}{a} + 24 \frac{\delta_0^2}{a^2} \right). \quad (30)$$

From (22), using (20), (21), it follows that the force F has the constant sign for all δ and tends to zero in the formal limit $\delta \rightarrow \infty$. This allows us to obtain a simple interpolating formula giving the same result for small δ_0/a as (30), but applicable over the broader range $0 < \delta_0/a \leq 0.2$:

$$F = -\frac{\pi^2}{240a^4} \left(1 + \frac{11}{3} \frac{\delta_0}{a}\right)^{-\frac{18}{11}}. \quad (31)$$

For good metals $\delta_0 \sim 0.1a$ when $a \sim 1 \mu\text{m}$, and so it is clear that corrections to the Casimir force due to the imperfection of the plate metal are rather significant.

We now consider the normal skin-effect domain, which corresponds to the distances between plates of $a \geq 0.1 \text{ cm}$. In this domain the impedance Z is complex

$$Z(\omega) = (1 - i) \sqrt{\frac{\omega}{8\pi\sigma}}. \quad (32)$$

where σ is the conductivity of the plate metal. The field penetration depth δ is connected with the impedance by the relation

$$\delta = (1 + i) \frac{Z(\omega)}{\omega} = \frac{1}{\sqrt{2\pi\sigma\omega}}. \quad (33)$$

Substituting (32) into (23) and performing the change of variable $Q = \zeta\sqrt{l-1}$ we obtain expression for the first-order correction to the force:

$$\Delta^{(1)}F = \frac{1}{8\pi^2\sqrt{\pi\sigma}} \int_1^\infty dt (1+t) \int_0^\infty \frac{d\zeta \zeta^{7/2}}{\sinh^2(a\zeta\sqrt{t})}. \quad (34)$$

Calculating these integrals and using the result (1), the Casimir force in the first order of perturbation theory is

$$F = -\frac{\pi^2}{240a^4} \left(1 - \frac{1.93}{\sqrt{a\sigma}}\right). \quad (35)$$

We note that this expressions holds only at absolute zero.

The anomalous skin-effect domain lies between the domain of infra-red optics and the normal skin-effect domain. The quantity $\varepsilon(\omega)$ has then only a formal meaning because of the strong non-locality, and the impedance acquires a vectorial nature and depends on the shape and sizes of the Fermi surface. In the isotropic approximation

$$Z(\omega) \sim \left(\frac{\omega}{ep_F}\right)^{\frac{2}{3}}, \quad \delta(\omega) \sim \left(\frac{1}{\omega e^2 p_F^2}\right)^{\frac{1}{3}}, \quad (36)$$

where p_F is the Fermi momentum of the electrons. Substituting (36) into (23) and performing the integration, we get the first-order correction

$$\Delta^{(1)}F \sim \frac{1}{a^4} (ep_F a)^{-\frac{2}{3}}. \quad (37)$$

3 Perturbation approach for taking into account small geometrical imperfections

The configuration, for which the Casimir force has been investigated for the first time, consists of two plane parallel metal plates. At once this is the simplest geometry. In this Section we investigate the Casimir force for configurations with small deviations from that geometry. Our aim now is to give a complete description for all possible deviations. Hereby we consider plates made up of arbitrary materials.

The exact result for the Casimir force per unit area between two plane parallel plates made of arbitrary materials may be expressed in the form [11]

$$F_0 = -\Psi(\varepsilon_1, \varepsilon_2) \frac{\pi}{10a^4}, \quad (38)$$

where a is the distance between the plates, $\varepsilon_{1,2}$ are the dielectric permittivities of the plates, and we note that

$$\Psi(\varepsilon_1, \varepsilon_2) = \frac{5}{16\pi^3} \int_0^\infty dx \int_1^\infty dp \frac{x^3}{p^2} \left\{ \left[\frac{(s_1 + p)(s_2 + p)}{(s_1 - p)(s_2 - p)} e^x - 1 \right]^{-1} + \left[\frac{(s_1 + p\varepsilon_1)(s_2 + p\varepsilon_2)}{(s_1 - p\varepsilon_1)(s_2 - p\varepsilon_2)} e^x - 1 \right]^{-1} \right\}. \quad (39)$$

Here, $s_{1,2} \equiv (\varepsilon_{1,2} - 1 + p^2)^{1/2}$. For example, for perfect conductors we have $\varepsilon_1 = \varepsilon_2 \rightarrow \infty$ and $\Psi(\varepsilon_1, \varepsilon_2) \rightarrow \pi/24$. More information — a graphical representation, for instance — concerning this function can be found in Ref. [11].

Under small deviations from the plane parallel geometry we understand all kinds of deviations whose amplitude is small in comparison with the distance between the plates. All these deviations can be described by some function depending on the point on the plate, i.e. on two variables. The deviations from the plane parallel geometry give rise to corrections to the Casimir force (38).

First let us outline the main features of an approximative method which may be applied for the calculation of the Casimir force for configurations of arbitrary form [12]. According to this method the potential of the Casimir force acting between two test bodies can be obtained by summation of the interatomic potentials over all atoms of the test bodies with a subsequent multiplicative renormalization:

$$U_R(u) = -\frac{CN_1N_2}{K} \int_{V_1} dr_1 \int_{V_2} dr_2 |r_1 - r_2|^{-7}. \quad (40)$$

Here the integrations run over the volumes V_1 resp. V_2 of the test bodies, N_1 resp. N_2 are the numbers of atoms per unit volume, C is the constant of the retarded van der Waals interaction potential, K is a special renormalization constant and a is the distance between the test bodies. Note that even the simple summation of the interatomic potentials (i.e. (40) without the correction factor K^{-1}) gives the proper dependence of U_R on a for three-dimensional configurations. But the values of the coefficients in such dependencies come out to be larger than their true values due to the screening effects.

The renormalization procedure allows us to take into account approximately the effects of screening of the farther layers of the test bodies matter by the nearer ones. The value of constant K is determined in [12] as the ratio of the Casimir force potential between two infinite plane parallel plates obtained by the summation method (using integrations (40) without the correction factor K^{-1}) and by the exact solution (38). The result is

$$K = \frac{CN_1N_2}{\Psi(\varepsilon_1, \varepsilon_2)} > 1, \quad (41)$$

where the function $\Psi(\varepsilon_1, \varepsilon_2)$ is as defined in (39).

Equations (40) and (41) may be rewritten in the form

$$U_R(u) = -\Psi(\varepsilon_1, \varepsilon_2) \int_{V_1} dr_1 \int_{V_2} dr_2 |r_1 - r_2|^{-7}. \quad (42)$$

As was shown in [12], the relative error of the potential (42) is less than 3.8% for configurations of an arbitrary body over a plane plate. For the configuration of two plates with small deviations from planes it is even much smaller.

For zero approximation in our perturbation theory we consider the Casimir force between a square plane plate V_1 with thickness D and sides of length $2l$, and another plane plate V_2 which is parallel to V_1 and has the same sides and thickness. Our aim is to calculate the Casimir force between plates with surfaces that deviate slightly from plane geometry. We describe the surface of the first plate by the equation $z_1^{(s)} = A_1 f_1(x_1, y_1)$ and the surface of the second plate by the equation $z_2^{(s)} = a + A_2 f_2(x_2, y_2)$, where a is the mean value of the distance between the plates. The values of the amplitudes are chosen so that $\max |f_i(x_i, y_i)| = 1$. We can choose the zero point on the

z -axis so that

$$\begin{aligned} \langle z_1^{(s)} \rangle &\equiv A_1 \langle f_1(x_1, y_1) \rangle \equiv \frac{A_1}{(2L)^2} \int_{-L}^L dx_1 \int_{-L}^L dy_1 f_1(x_1, y_1) = 0, \\ \langle z_2^{(s)} \rangle &\equiv a + A_2 \langle f_2(x_2, y_2) \rangle = a. \end{aligned} \quad (43)$$

The perturbation expansion assumes that $A_i \ll a$, $a \ll D$ and $a \ll L$. At the same time, in all real situations we have $a/D, a/L \ll A_i/a$, so that we are looking for a perturbation expansion in powers of A_i/a and of zeroth order in a/D and a/L .

The Casimir force per unit area between the plates is given by

$$F = -\frac{1}{(2L)^2} \frac{\partial U_R}{\partial a}, \quad (44)$$

where U_R is defined in (42).

We represent the force (44) as a sum of terms of up to fourth order in the small parameters $A_1/a, A_2/a$:

$$F = F_0 \sum_{i=0}^4 \sum_{k=0}^{4-i} c_{ik} \left(\frac{A_1}{a}\right)^i \left(\frac{A_2}{a}\right)^k. \quad (45)$$

Here F_0 is the Casimir force (38) for perfectly plane parallel plates.

The coefficients in (45) are found in [13]. We first note that

$$c_{00} = 1, \quad c_{01} = c_{10} = 0, \quad (46)$$

where the last two equalities follow from our choice (43).

Coefficients with a single zero index are

$$\begin{aligned} c_{02} &= 10 \langle f_2^2 \rangle, & c_{03} &= -20 \langle f_2^3 \rangle, & c_{04} &= 35 \langle f_2^4 \rangle, \\ c_{20} &= 10 \langle f_1^2 \rangle, & c_{30} &= 20 \langle f_1^3 \rangle, & c_{40} &= 35 \langle f_1^4 \rangle, \end{aligned} \quad (47)$$

where notations for averaged values are the same as in (43).

Expressions for the "mixed" coefficients (which depend on the deviation functions of both plates) are quite complicated. The results are [13]

$$\begin{aligned} c_{11} &= -\frac{4}{3} \sqrt{\frac{2}{\pi}} \sum_{m=0}^{\infty} \sum_{n=0}^{\infty} G_{mn}^{(1,1)}(z_{mn})^{\frac{1}{2}} K_{\frac{1}{2}}(z_{mn}), \\ c_{12} &= \frac{2}{3} \sqrt{\frac{2}{\pi}} \sum_{m=0}^{\infty} \sum_{n=0}^{\infty} G_{mn}^{(1,2)}(z_{mn})^{\frac{1}{2}} \left[z_{mn} K_{\frac{3}{2}}(z_{mn}) - K_{\frac{1}{2}}(z_{mn}) \right], \\ c_{13} &= -\frac{2}{9} \sqrt{\frac{2}{\pi}} \sum_{m=0}^{\infty} \sum_{n=0}^{\infty} G_{mn}^{(1,3)}(z_{mn})^{\frac{3}{2}} \left[z_{mn} K_{\frac{5}{2}}(z_{mn}) - K_{\frac{3}{2}}(z_{mn}) \right], \\ c_{22} &= 210 g_{00}^{(2)} h_{00}^{(2)} \\ &+ \frac{1}{3} \sqrt{\frac{2}{\pi}} \sum_{m=0}^{\infty} \sum_{n=0}^{\infty} G_{mn}^{(2,2)}(z_{mn})^{\frac{3}{2}} \left[z_{mn} K_{\frac{5}{2}}(z_{mn}) - K_{\frac{3}{2}}(z_{mn}) \right]. \end{aligned} \quad (48)$$

The $K_\nu(z)$ are Bessel functions of imaginary argument and

$$z_{mn} \equiv \frac{2\pi a}{L} \sqrt{n^2 + m^2}.$$

The quantities $G_{m,n}^{(i,k)}$ from (48) are given by

$$G_{m,n}^{(i,k)} = \frac{1}{4} (1 + \delta_{m0} + \delta_{n0}) \sum_{p=1}^4 g_{p,mn}^{(i)} h_{p,mn}^{(k)},$$

where $g_{p,mn}^{(i)}$, $h_{p,mn}^{(k)}$ are Fourier coefficients of the functions f_1^i and f_2^k , considered as periodic functions with the period $2L$. The quantities $g_{00}^{(2)}$ and $h_{00}^{(2)}$ are zeroth terms in the Fourier expansions of the functions f_1^2 and f_2^2 respectively. The coefficient c_{21} differs from c_{12} by its sign and by the sequence of upper indices of G . To obtain c_{11} it is sufficient just to change the sequence of upper indices of G in c_{13} .

We now give some particular results which follow from (45)–(48) for various deviations from plane parallel geometry [13]. But first it is interesting to consider the configuration of the plane plates with an angle α_0 between them. The angle α_0 is assumed to be small, so that $\alpha_0 L \ll a$ holds. This configuration is an example of a plate perturbation with a length scale much larger than a . For all such perturbations the coefficients (48) may be calculated in general form. So the result for the Casimir force (45) is [13]

$$\begin{aligned}
 F = F_0 \left\{ 1 + 10 \left[\langle f_1^2 \rangle \left(\frac{A_1}{a} \right)^2 - 2 \langle f_1 f_2 \rangle \frac{A_1 A_2}{a^2} + \langle f_2^2 \rangle \left(\frac{A_2}{a} \right)^2 \right] \right. \\
 + 20 \left[\langle f_1^3 \rangle \left(\frac{A_1}{a} \right)^3 - 3 \langle f_1^2 f_2 \rangle \frac{A_1^2 A_2}{a^3} + 3 \langle f_1 f_2^2 \rangle \frac{A_1 A_2^2}{a^3} \right. \\
 \left. \left. - \langle f_2^3 \rangle \left(\frac{A_2}{a} \right)^3 \right] \right. \\
 + 35 \left[\langle f_1^4 \rangle \left(\frac{A_1}{a} \right)^4 - 4 \langle f_1^3 f_2 \rangle \frac{A_1^3 A_2}{a^4} + 6 \langle f_1^2 f_2^2 \rangle \frac{A_1^2 A_2^2}{a^4} \right. \\
 \left. \left. - 4 \langle f_1 f_2^3 \rangle \frac{A_1 A_2^3}{a^4} + \langle f_2^4 \rangle \left(\frac{A_2}{a} \right)^4 \right] \right\}. \quad (49)
 \end{aligned}$$

As is seen from (49), the mixed terms produce interference. For example, when $f_2 = \mp f_1$ we have

$$\begin{aligned}
 F = F_0 \left[1 + 10 \langle f_1^2 \rangle \left(\frac{A_1 \pm A_2}{a} \right)^2 \right. \\
 \left. + 20 \langle f_1^3 \rangle \left(\frac{A_1 \pm A_2}{a} \right)^3 + 35 \langle f_1^4 \rangle \left(\frac{A_1 \pm A_2}{a} \right)^4 \right]. \quad (50)
 \end{aligned}$$

We apply these results to the case of two plane plates with an angle α_0 between them. This configuration can be realized in two different ways. In the first way the upper plate is not perturbed and deviations of the lower plate from the parallel position is described by the function $f_1(x_1, y_1) = x_1/L$ with amplitude $A_1 = \alpha_0 L$. Substituting this information into (49) and putting $A_2 = 0$ we obtain:

$$F = F_0 \left[1 + \frac{10}{3} \left(\frac{\alpha_0 L}{a} \right)^2 + 5 \left(\frac{\alpha_0 L}{a} \right)^4 \right]. \quad (51)$$

In the second way one may imagine the same configuration where both plates are perturbed with the amplitudes $A_1 = \alpha_1 L$ and $A_2 = \alpha_2 L$. Here the angle between the plates is $\alpha_0 = \alpha_1 + \alpha_2$ or $\alpha_0 = |\alpha_1 - \alpha_2|$. The function f_1 is $f_1 = x/L$ in both cases and the function f_2 is $f_2 = \mp f_1$ respectively.

It is easy to see that calculation of the Casimir force according to (50) repeats result (51). This example is interesting because it allows the possibility of observing the presence of the interference terms in (49). These contributions must be included in order to obtain correct results.

It can be seen that (51) coincides with the result obtained for the same configuration by using the exact expression for the Casimir energy density inside a wedge [14]. So, at least up to fourth order inclusive in the parameter $\alpha_0 L/a$, (42), (44) yields the same result as the exact calculation. This allows us to estimate the real relative error of (42), (44) for configurations which deviate slightly from plane parallel geometry. Taking a realistic value $\alpha_0 L \approx 10^{-1}$ we conclude that the relative error of results (42) and (44) is much smaller than $10^{-2}\%$. Applying the described above approximate method to the configuration under consideration can therefore be expected to give reliable results up to the fourth order inclusive in the parameters A_i/a .

We now consider the case of large-scale plate inhomogeneities described by periodic functions with periods T_x and T_y in the coordinates x and y respectively. Here $a/T_x, a/T_y \ll 1$ and the result (49) is again valid. As an example we take longitudinal deviations with amplitudes $A_{1,2}$ described by functions:

$$f_1(x_1, y_1) = \sin \omega x_1, \quad f_2(x_2, y_2) = \sin(\omega x_2 + \delta). \quad (52)$$

Calculating all the coefficients of (49) using the functions (52) we obtain

$$\begin{aligned} F = F_0 \left\{ 1 + 5 \left[\left(\frac{A_1}{a} \right)^2 - 2 \cos \delta \frac{A_1 A_2}{a^2} + \left(\frac{A_2}{a} \right)^2 \right] \right. \\ \left. + \frac{105}{8} \left[\left(\frac{A_1}{a} \right)^4 - 4 \cos \delta \frac{A_1^3 A_2}{a^4} + 2(2 + \cos 2\delta) \frac{A_1^2 A_2^2}{a^4} \right. \right. \\ \left. \left. - 4 \cos \delta \frac{A_1 A_2^3}{a^4} + \left(\frac{A_1}{a} \right)^4 \right] \right\}. \quad (53) \end{aligned}$$

We see that the results depend significantly on the value δ .

For short-scale distortions whose size is smaller than a the general result for the Casimir force (see (45) with coefficients (46)–(49)) acquires a simpler form than that presented in (49). If the functions $f_{1,2}$ are nonperiodic or periodic with the different periods (at last in one coordinate) then (49) takes the form [13]

$$\begin{aligned} F = F_0 \left\{ 1 + 10 \left[\langle f_1^2 \rangle \left(\frac{A_1}{a} \right)^2 + \langle f_2^2 \rangle \left(\frac{A_2}{a} \right)^2 \right] \right. \\ \left. + 35 \left[\langle f_1^4 \rangle \left(\frac{A_1}{a} \right)^4 + 6 \langle f_1^2 f_2^2 \rangle \frac{A_1^2 A_2^2}{a^4} + \langle f_2^4 \rangle \left(\frac{A_2}{a} \right)^4 \right] \right\}. \quad (54) \end{aligned}$$

If the periods T_x and T_y of f_1 and f_2 are equal in both coordinates respectively and $T_{x,y} \ll a$ then (54) can be simplified because

$$\langle f_1^2 f_2^2 \rangle = \langle f_1^2 \rangle \langle f_2^2 \rangle. \quad (55)$$

For particular example (52) we have from (54), (55):

$$\begin{aligned} F = F_0 \left\{ 1 + 5 \left[\left(\frac{A_1}{a} \right)^2 + \left(\frac{A_2}{a} \right)^2 \right] \right. \\ \left. + \frac{105}{8} \left[\left(\frac{A_1}{a} \right)^4 + 4 \frac{A_1^2 A_2^2}{a^4} + \left(\frac{A_2}{a} \right)^4 \right] \right\}. \quad (56) \end{aligned}$$

We see that the result does not depend on the phase-shift δ , which is to be expected in this case.

For the case $T_{x,y} \sim a$ we have to calculate the coefficients of (48) according to non-simplified formulas. An example of such a calculation can be found in [13].

The approximate method which has just been used to calculate corrections to the Casimir force may also be applied to the case of stochastic deviations from plane parallel geometry. This is very interesting from the experimental point of view. In this case small deviations are deviations whose dispersions are small in comparison with the distance between the plates. The deviations of the surfaces of both plates from the plane geometry are described by two stochastic functions $\{\delta_i f_i(x_i, y_i)\}$, $i = 1, 2$ with dispersions δ_i and mean values

$$\langle \delta_i f_i(x_i, y_i) \rangle_i = 0. \quad (57)$$

Here, $\langle \dots \rangle_i$ denotes averaging over ensembles of all particular realizations $\delta_i f_i(x_i, y_i)$ of the corresponding stochastic functions. The factor δ_i is placed in front of f_i to make the dispersion of the functions $\{f_i(x_i, y_i)\}$ equal to unity. For the bodies with surfaces $z_1^{(s)} = \delta_1 f_1(x_1, y_1)$, $z_2^{(s)} = a + \delta_2 f_2(x_2, y_2)$ the energy U_R in (42) has to be replaced by $\langle \langle U_R \rangle \rangle_2$. The Casimir force is then given by [15]

$$F = -\frac{1}{4L^2} \frac{\partial}{\partial a} \langle \langle U_R \rangle \rangle_2 \quad (58)$$

instead of (44).

For stationary stochastic functions ($\delta_i = \text{const}$) it is possible to perform calculations according to (42), (58) in general form. Using the normal distribution at every point of the surfaces together with expansions with respect to the small parameters δ_i/a we obtain the result [15]

$$F = F_0 \left\{ 1 + 10 \left[\left(\frac{\delta_1}{a} \right)^2 + \left(\frac{\delta_2}{a} \right)^2 \right] + 105 \left[\left(\frac{\delta_1}{a} \right)^2 + \left(\frac{\delta_2}{a} \right)^2 \right]^2 \right\}. \quad (59)$$

It is seen that the correction to the Casimir force only depends on the sum $\delta_1^2 + \delta_2^2$ and does not depend on the correlation radii of the stochastic functions describing the distortions. For a typical value of $\delta_{1,2}/a \approx 0.1$ the correction given by (59) is 24% to F_0 where 4% results from the fourth order. So one has to take it into account in experiments on Casimir force measurements.

4 Configurations used in experiments

Here we discuss the contribution of small distortions of different types to the Casimir force for the configurations of the spherical lense situated at height a above the plate and of two crossed cylinders [16]. These configurations are of direct interest for experiments on Casimir force measurements. Let us consider the first of them. As the zero approximation for our perturbation theory we will use the Casimir force between the square plane plate B_1 with the sidelength $2L$ and the thickness D and the ideal spherical lens B_2 with radius r , height h and curvature radius R . We suggest in our perturbation expansion that $a \ll h, r, D, L$ and $r \ll R$. Our aim is to calculate the Casimir force between a plate and a lens which surfaces possess some small deviations from the perfect geometry with amplitudes A_1, A_2 . In all real situations one has $a/h, a/r, a/D, a/L \ll A_i/a$, so that we are looking for the perturbation expansion in the powers of A_i/a and in the zeroth orders in other parameters.

Note that it is convenient to use the cylindric coordinate system for integration over the volume V_2 of the lens. So for configuration under consideration the zero approximation is

$$U_R^{(0)} = -\psi(\varepsilon_1, \varepsilon_2) \int_0^{2\pi} d\varphi \int_0^r \rho d\rho \int_a^{a+h} dz_2 \int_{-L}^L dx_1 \int_{-L}^L dy_1 \int_{-D}^0 dz_1 \times [(x_1 - \rho \cdot \cos \varphi)^2 + (y_1 - \rho \cdot \sin \varphi)^2 + (z_1 - z_2)^2]^{-7/2}. \quad (60)$$

Upon integrating (60) one has in zeroth order in the above-mentioned parameters

$$U_R^{(0)} = -\psi(\varepsilon_1, \varepsilon_2) \frac{\pi^2 R}{30a^2}. \quad (61)$$

The corresponding Casimir force is [17]

$$F_0 = -\psi(\varepsilon_1, \varepsilon_2) \frac{\pi^2 R}{15a^3}. \quad (62)$$

Let us consider now two crossed cylinders with radiuses R_1, R_2 and lengths $2L_1, 2L_2$. Let a be a distance between their nearest points. In all real situations one has $a \ll R_1, R_2, L_1, L_2$. In this case the zero approximation may be written as

$$U_R^{(0)} = -\psi(\varepsilon_1, \varepsilon_2) \int_{-\infty}^{\infty} dz_2 \int_0^{R_2} \rho_2 d\rho_2 \int_0^{2\pi} d\varphi_2 \Phi(\rho). \quad (63)$$

Here we use the notation

$$\Phi(\rho) = \int_0^{R_1} \rho_1 d\rho_1 \int_0^{2\pi} d\varphi_1 \int_{-\infty}^{\infty} dz_1 [z_1^2 + (\rho_1 \cos \varphi_1)^2 + (\rho - \rho_1 \sin \varphi_1)^2]^{-7/2}, \quad (64)$$

where $\rho = [z_2^2 + (R_1 + R_2 + a - \rho \sin \varphi_2)^2]^{1/2}$ is the distance from the points of the second cylinder to the axis of the first one.

So in zeroth orders one has

$$U_R^{(0)} = -\psi(\varepsilon_1, \varepsilon_2) \frac{\pi^2 \sqrt{R_1 R_2}}{30a^2}. \quad (65)$$

The corresponding Casimir force is

$$F_0 = -\psi(\varepsilon_1, \varepsilon_2) \frac{\pi^2 \sqrt{R_1 R_2}}{15a^3}. \quad (66)$$

For the equal cylinders ($R_1 = R_2$) equations (65), (66) give the results (61), (62).

Our aim is to obtain the corrections to the Casimir forces (62), (66) due to the small deviations the surfaces from the ideal configurations.

The surface of the plate with some small deviations from the plane may be described by the same equation as in Sec. 3: $z_1^{(s)} = A_1 f_1(x_1, y_1)$ with the condition (43). Let us consider the surface of the lens with small deviations from the ideal spherical form. There may be two types of distortions, which are described separately. For the first type of distortions the surface of the lens may be described by equation [16]

$$z_2^{(s)} = a + R - \sqrt{R^2 - \rho^2} + A_2 f_2(\rho, \varphi). \quad (67)$$

For the other type of distortions equation of the surface is [16]

$$\rho^{(s)} = \sqrt{R^2 - (z_2 - R - a)^2} + A_2' f_2'(z_2, \varphi). \quad (68)$$

The values of amplitudes are chosen as specified above. It is suitable also to choose the curvature radius of the lens R in (67), (68) so that the corresponding mean values $\langle f_2 \rangle$, $\langle f_2' \rangle$ be equal to zero. Then this value of radius R is used for calculation of F_0 in accordance with (62).

As to configuration of two crossed cylinders, their surfaces are most conveniently described in their own cylindrical coordinate systems. The corresponding equations are:

$$\rho_i^{(s)} = R_i + A_i f_i(\varphi_i, z_i). \quad (69)$$

The quantities R_i and A_i in (69) are chosen from the same considerations as R in (67), (68).

In the paper [16] numerous results for the described configurations are obtained. By way of example let us consider the longitudinal periodic distortions of the plate

$$f_1(x) = \cos(2\pi x/l_x + \delta_1) \quad (70)$$

and the concentric distortions of the lens of (67) type

$$f_2(\rho) = \cos(2\pi\rho/l_\rho + \delta_2), \quad (71)$$

where the quantities l_x , l_ρ are the periods of distortions. For long-scale inhomogeneities there are $l_x \sim L$, $l_\rho \sim r$. The parameter δ_2 in (71) defines the type of deviation in the lens center: convex or concave, smooth ($\delta_2 = 0$ or $\delta_2 = \pi$) or sharp. The parameter δ_1 in (70) fixes the position of the lens above the plate.

Calculating the coefficients of (45) by the formulae obtained in [16] one may write the Casimir force (45) in the form [16]

$$F = F_0 \left[1 + 3 \cos \delta_1 \left(\frac{A_1}{a} \right) - 3 \cos \delta_2 \left(\frac{A_2}{a} \right) + 3 \left(\frac{A_1}{a} \right)^2 + 3 \left(\frac{A_2}{a} \right)^2 - 12 \cos \delta_1 \left(\frac{A_1}{a} \right) \left(\frac{A_2}{a} \right) \right]. \quad (72)$$

Here the dependence of the Casimir force on parameters δ_1, δ_2 is given in an explicit form. At the same time the Casimir force for the extremely short-scale distortions (70), (71) with $l_x, l_\rho \ll a$ naturally does not depend on parameters δ_1, δ_2 at all.

For the crossed cylinders, as an example, let us consider distortions (69) of the form

$$f_i = \cos \left(\pi \frac{z_i}{l_{z,i}} + \delta_i \right). \quad (73)$$

If $l_{z,i} \sim L_i$ the first non-zero coefficients of (45) are [16]

$$c_{10} = 12 \cos \delta_1, \quad c_{01} = 12 \cos \delta_2, \quad (74)$$

so that the Casimir force takes the form

$$F' = F'_0 \left[1 + 12 \cos \delta_1 \left(\frac{A_1}{a} \right) + 12 \cos \delta_2 \left(\frac{A_2}{a} \right) \right]. \quad (75)$$

Let us estimate the relative corrections $\delta F = (F - F_0)/F_0$ to the Casimir force F_0 for different configurations. These estimations are made using the realistic value $(A_i/a) \sim 10^{-1}$. In case of short-scale distortions we have for both configurations under consideration $\delta F = 6\%$ [16]. It is less than the corresponding correction for the configuration of two parallel plates.

However the corrections may be very large in the case of long-scale deviations. In such a manner the lens surface distortion (71) with $l_\rho = r/2$ and $\delta_2 = 0$ gives us $\delta F = 30\%$. It is significant that the correction caused by the long-scale deviations may be both positive and negative. Such corrections must be taken into account in the precise experiments on Casimir force measurements.

The detailed discussion of different applications of the Casimir effect in condensed matter physics, elementary particle theory and cosmology may be found in the monograph [17] on which this report is also partly based.

The author is grateful to Prof., Dr. G.L. Klimchitskaya for helpful discussions. It is a pleasure also to thank the Department of Physics of the Federal University of Paraiba for kind hospitality.

References

- [1] H.B.G. Casimir. *Proc. Kon. Nederl. Akad. Wet.*, **51**, 793, 1948.
- [2] M.J. Sparnaay. *Physica*, **24**, 751, 1958.
- [3] V.M. Mostepanenko and I.Yu. Sokolov. *Phys Rev.*, **D47**, 2872, 1993.
- [4] M. Bordag, V.M. Mostepanenko and I.Yu. Sokolov. *Phys. Lett.*, **A187**, 35, 1994.
- [5] L.D. Landau and L.D. Lifshitz. *Electrodynamics of Continuous Media*. Pergamon Press, Oxford, 1982.
- [6] V.M. Mostepanenko and N.N. Trunov. *Sov. J. Nucl. Phys. (USA)*, **42**, 812, 1985.
- [7] Yu.S. Barash and V.L. Ginzburg. *Sov. Phys. Usp. (USA)*, **27**, 467, 1984.
- [8] E.M. Lifshitz and L.P. Pitaevsky. *Physical Kinetics*. Pergamon Press, Oxford, 1981.
- [9] N.E. Dzyaloshinskii, E.M. Lifshitz and L.P. Pitaevsky. *Sov. Phys. Usp. (USA)*, **4**, 153, 1979.
- [10] C.M. Hargreaves. *Proc. Kon. Nederl. Akad. Wet.*, **68B**, 231, 1965.
- [11] E.M. Lifshitz and L.P. Pitaevsky. *Statistical Physics*. Pergamon Press, Oxford, 1980.
- [12] V.M. Mostepanenko and I.Yu. Sokolov. *Sov. Phys. Dokl. (USA)* **33**, 140, 1988.
- [13] M. Bordag, G.L. Klimchitskaya and V.M. Mostepanenko. *Int. J. Mod. Phys.*, **A10**, 2661, 1995.
- [14] Yu.B. Zayaev and V.M. Mostepanenko. *Theor. Math. Phys. (USA)*, **79**, 487, 1989.
- [15] M. Bordag, G.L. Klimchitskaya and V.M. Mostepanenko. *Phys. Lett.*, **A200**, 95, 1995.
- [16] G.L. Klimchitskaya and Yu.V. Pavlov. *Int. J. Mod. Phys.*, **A11**, 3723, 1996.
- [17] V.M. Mostepanenko and N.N. Trunov. *The Casimir Effect and its Applications*, Clarendon Press, Oxford, 1997.

Black-Body Spectrum of the CBR and its (possible) relation to the Topological Degree of Connectedness

A. Bernui Leo^{*†}

** Centro Brasileiro de Pesquisas Físicas
Departamento de Relatividade e Partículas
Rio de Janeiro, Brazil*

*[†] Facultad de Ciencias
Universidad Nacional de Ingeniería
Lima, Peru*

1 Introduction

Recently we investigated the role that some topological features of space-times [1, 2] play in the time evolution of physical phenomena [3]. More specifically we have studied how the compactness and the topological degree of connectedness of Friedmann-Robertson-Walker (FRW) space-times could have influenced cosmological events. Here we apply these ideas to analyze the spectrum of the Cosmic Microwave Background Radiation (CBR).

It has been observed –and carefully measured [4, 5]–that the CBR, remnant of the period when matter and radiation of our universe were in thermal equilibrium, has a Planckian nature. That is the proper energy-density of the leftover photons has a spectrum corresponding to radiation of a black-body at the present temperature $T = 2.7258 K$.

The proper energy-density of this photons, with frequency at the present time t_{now} , between ν and $\nu + d\nu$, is given by ($k = h = 1$) [6]

$$\rho(t_{now}, \nu) = 8\pi\nu^3 \int_0^{t_{now}} \left[\exp\left(\frac{\nu A(t_{now})}{T(t')A(t')}\right) - 1 \right]^{-1} \times \frac{dP(t_{now}, t'; \nu)}{dt'} dt'$$

where $P(t_{now}, t'; \nu)$ is the probability, taking account of stimulated emission, that a photon of frequency $\nu (A(t_{now})/A(t'))$ present at time t' will survive until t_{now} , T is the temperature and A is the scale factor of the FRW spacetime.

The (theoretical) criteria usually adopted to integrate the above equation in order to obtain a Planckian spectrum are [6]:

- (i) $T \sim A^{-1}$, or
- (ii) the opacity (of the system) drops sharply.

Regarding hypothesis (i) we observe that it relates a thermodynamical property of the system (T) with a dynamical property of the space-time containing it (A). Recently it has been proved that if the CBR is Planckian to first order (i.e. considering a perturbation of relation (i)) then the space-time is *almost*-FRW (see [7]).

Hypothesis (ii) instead could be related to global properties of the space-time. In principle it deals with a physical property that however, as we shall see in the next section, **could be interpreted** as a consequence of a topological effect. In fact, the passage from a opaque to a transparent universe could have been generated by the developing of a Future Event Horizon (FEH). In such a case the Topological Degree of Connectedness (TDC) of the space-time goes rapidly from 1 (representing a connected or opaque universe) to 0 (representing a disconnected or transparent universe) in a finite time.

^{*}internet: bernui@novell.cnt.cbpf.br

[†]This work was supported by a CLAF/CNPq fellowship

2 Physical & Topological Analogies

As we know [3], the TDC of a space-time manifold is a measure of the geodesic-null flux available for emission or absorption of photons at each instant. It constraints the mean free-path of the photons. Thus, one can establish the following analogies between physical and topological variables.

P1. $P(t_{now}, t; \nu)$ is the probability that a photon of frequency ν , present at time t , survives until t_{now} , where $P \in [0, 1]$.

T1. \mathcal{G} is the spacetime's degree of connectedness, with $\mathcal{G} \in [0, 1]$.

P2. In an opaque universe, when matter & radiation were in thermodynamical equilibrium ($P \sim 0$) the photon's mean free path (i.e. the optical depth) is finite.

T2. In a spacetime with compact space slices null geodesics (i.e. light rays) have finite lengths.

P3. If the opacity drops sharply ($P : 0 \rightarrow 1$): $dP/dt = \delta(t - t_d)$, i.e. the Universe becomes transparent at $t = t_d$.

T3. If $\lim_{t \rightarrow \infty} f(t) < \infty$, where $f(t) \equiv \int ds / A(s)$, the spacetime develops a FEH, then $\mathcal{G} : 1 \rightarrow 0$.

3 Results

Considering that the absorption rate for photons (Λ , from which the probability P depends) of a matter-radiation equilibrium system is driven by the TDC of an expanding FRW spacetime, we performed numerical integrations of the radiation-density relation. For this we have considered relation (i) and perturbations of it, and also relation (ii). The corresponding plots of the radiation-density ρ vs. the frequency of the photons ν give, in all the situations considered, a Planckian black-body radiation spectrum with decreasing temperature and the corresponding cosmological redshift.

Acknowledgements

I am grateful to M.J. Rebouças and J. Santos for valuable discussions. I also thank a CLAF-CNPq fellowship.

References

- [1] J.R. Weeks. *The Shape of Space*, "Pure & App. Math." 26, M. Dekker, N.Y. (1985).
- [2] M. Lachièze-Rey & J.-P. Luminet, *Phys. Rep.* 254, 135 (1995).
- [3] A. Bernui & M.J. Rebouças, submitted (1996).
- [4] R. A. Muller, *Scientific American* 238, 64, May (1978).
- [5] R. Schwarzschild, *Physics Today* 17, March (1990).
- [6] S. Weinberg, "Gravitation and Cosmology", John Wiley & Sons, N.Y. (1972).
- [7] R. Maartens, G.F.R. Ellis & W.R. Stoeger, *Phys. Rev. D* 51, 1525 (1995).

The Radiation-Reaction Problem in Topologically Different FRW Space-times

A. Bernui Leo* and M.J. Rebouças†

* † *Centro Brasileiro de Pesquisas Físicas*
Departamento de Relatividade e Partículas
Rua Dr. Xavier Sigaud 150
22290-180 Rio de Janeiro - RJ, Brazil

* *Facultad de Ciencias*
Universidad Nacional de Ingeniería
Apartado 31 - 131, Lima 31 - Peru

1 Introduction

General relativity is a purely metrical (local) theory and leaves unsettled the global structure (topology) of the space-time. Consider, for example, the Friedmann-Robertson-Walker (FRW) space-times, whose line element can be given by

$$ds^2 = dt^2 - A^2(t) \left[\frac{dr^2}{1 - \kappa r^2} + r^2 (d\theta^2 + \sin^2 \theta d\varphi^2) \right], \quad (1)$$

where $A(t)$ is the scale factor, t is the cosmic time, and the constant spatial curvature $\kappa = 0, \pm 1$ specifies the type of geometry (flat, elliptic or hyperbolic) of the $t = \text{const}$ spacelike section \mathcal{M}_3 . Clearly FRW space-time manifolds \mathcal{M}_4 can be splitted into $\mathcal{R} \times \mathcal{M}_3$. The number of three-dimensional spacelike orientable and compact manifolds \mathcal{M}_3 which can be endowed with these three possible geometries is quite large: for $\kappa = 0$ there are 6 topologically distinct 3-spaces, while for both $\kappa = \pm 1$ an infinite number of 3-spaces exist [1, 2].

Since physical laws are usually expressed in terms of local differential equations, in order to be confident about the physical results one derives it is often necessary to have some degree of control over the topological structure of the space-time manifold so as to include constraints imposed by the topology of the space-time [3, 4]. One is then confronted with the question of what topologies are (or are not) physically acceptable for a given space-time geometry. In the present work we study the role played by the compactness and the topological degree of connectedness of \mathcal{M}_3 in the time evolution of the energy of a radiating system in the flat FRW space-times, whose spacelike $t = \text{const}$ sections are endowed with seven different topologies, namely the simply connected 3-space \mathcal{R}^3 , and the six multi-connected orientable compact 3-spaces shown in table 1 [5]. For a detailed account of our results see ref. [6].

2 Physical System and Evolution Equations

The radiating system we shall be concerned with is represented by a harmonic oscillator (energy source) coupled with a relativistic massless scalar field (the energy radiated by the source are scalar waves propagating at speed of light) [7, 8]. In our model the gravitational field is treated as external.

*internet: bernui@novell.cat.cbpf.br

†internet: reboucas@cat.cbpf.br

Topology Type	Basic Cell	Identifications of Faces
\mathcal{T}_1	cube	3 pairs non rotated
\mathcal{T}_2	cube	2 pairs non rotated, 1 pair rotated 90°
\mathcal{T}_3	cube	2 pairs non rotated, 1 pair rotated 180°
\mathcal{T}_4	cube	3 pairs rotated 180°
\mathcal{H}_1	hexagonal prism	top and bottom rotated 60°
\mathcal{H}_2	hexagonal prism	top and bottom rotated 120°

Table 1: The six compact orientable topologies for flat 3-spaces, according to ref. [5].

The dynamics of our system is described by the action integral ($c = 1$),

$$S = \frac{1}{2} \int d^4x \sqrt{-g} [g^{\mu\nu} \partial_\mu \phi \partial_\nu \phi] + \frac{1}{2} \int dt [\dot{Q}^2 - \omega_c^2 Q^2] + \lambda \int d^4x \sqrt{-g} \rho(t, x) Q(t) \phi(t, x), \quad (1)$$

where $t \in [t_0, \infty)$, $x \in \mathcal{M}_3$, $g_{\mu\nu}$ is the metric tensor on \mathcal{M}_4 , $g \equiv \det(g_{\mu\nu})$, overdot means derivative with respect to t , and λ is the coupling constant. The (normalized) density-function ρ , which accounts for the coupling between the harmonic oscillator and the scalar field, is choosed $\rho(t, x) = \delta^{(3)}(x)/\sqrt{-g(t, x)}$. This type of point-like coupling requires a renormalization of the frequencies [8].

Varying the action (1) with respect to Q and ϕ one obtains the coupled evolution equations of the system, namely

$$\square \phi(t, x) = \lambda \rho(t, x) Q(t), \quad (2)$$

$$\ddot{Q}(t) + \omega_c^2 Q(t) = \lambda \int d^3x \sqrt{-g} \rho(t, x) \phi(t, x), \quad (3)$$

where $\square \phi \equiv (\sqrt{-g})^{-1} \partial_\mu (\sqrt{-g} g^{\mu\nu} \partial_\nu \phi)$ is the d'Alembertian operator, hereafter simply called wave-operator. Solving first equation (2) as an initial value problem, we write the solution in the form [9]

$$\phi(t, x) = \int dt' d^3x' \sqrt{-g} G(t', x'; t, x) \lambda \rho(t', x') Q(t'), \quad (4)$$

with $t' \in [t_0, t]$, $x' \in \mathcal{M}_3$ and where the homogeneous part $\phi_H(t, x) = 0$ if we assume the initial condition $(\phi(t_0, x), \partial_t \phi(t_0, x)) = (0, 0)$. In (4) $G(t', x'; t, x)$ is the retarded Green function, often referred to as fundamental solution of the wave-operator.

3 The Green Functions

Now we shall obtain the Green functions for the wave-operator through the study of null geodesics of the space-time manifolds for each distinct 3-spaces shown in table 1 [5]. We consider here static space-times, however the Green functions can be easily calculated for dynamic space-times if one uses the conformal time τ , defined by $\tau \equiv f(t) \equiv \int dt'/A(t')$, for $t' \in [t_0, t]$. Thus, the metric tensor we shall be concerned is $g_{\mu\nu}(t, \vec{r}) = \text{diag}(1, -1, -1, -1)$, where $\vec{r} \equiv (x, y, z) \in \mathcal{R}^3$, and where the topological identifications for each 3-space will be suitably considered.

The manifold \mathcal{T}_1 , best known as the three-torus T^3 [1], is a compact multi-connected manifold obtained by identifying the opposite faces of cube of side a (see table 1). A useful way of thinking about \mathcal{T}_1 in terms of a simply connected 3-manifold is to imagine the cube repeated endlessly in a three-dimensional grid (basic cell and its images) where each repetition consists of the same physical region of space. To construct the Green function of the wave-operator we shall examine the light rays emitted (null geodesic flow) by the point-like energy source located at the origin of coordinates $\vec{r}' = (0, 0, 0)$ (the center of the cubic cell). Note that the images of the point-like source are located at $\pm a(i, j, k)$, for any integers i, j, k . Observe that not all light rays emitted return to the origin: a light

ray directed to the point (p_1, p_2, p_3) , where at least one of the ratios p_i/p_j is an irrational number, never comes back. Baking in mind these points one can find that the Green function for the wave-operator in \mathcal{T}_1 is

$$G(t-t', r) = \frac{1}{4\pi r} \left\{ \delta(t-t'-r) + \frac{1}{M} \sum_{n=1}^{\infty} c_n \left[\Theta(t-r-a_n) \delta(t-t'-r-a_n) - \Theta(t+r-a_n) \delta(t-t'+r-a_n) \right] \right\}, \quad (1)$$

where $t' \in [t_0, t]$, $a_n \equiv a \sqrt{i^2 + j^2 + k^2}$ for all i, j, k integers. M is the total number of images under consideration, it depends upon the time interval under investigation. The above coefficients c_n give the number of the n -th neighbours source-images: $c_1 = 6, c_2 = 12, c_3 = 8, c_4 = 6, c_5 = 24$, and so forth; whereas the a_n give the discrete set of elapsed times (since t') to reach the corresponding n -th neighbours: $a_1 = a, a_2 = a\sqrt{2}, a_3 = a\sqrt{3}, a_4 = 2a, a_5 = a\sqrt{5}$, etc. Note that using the first term of G in eq. (2.4) gives rise to the term $2(\lambda^2/4\pi) \int d\chi \delta(\chi)/\chi$, that formally diverges. After a suitable renormalization procedure, for arbitrary initial data $(Q(t_0), \dot{Q}(t_0))$, we find

$$\ddot{Q}(t) + 2\Gamma \dot{Q}(t) + \Omega^2 Q(t) = -\frac{4\Gamma}{M} \sum_{n=1}^{\infty} \Theta(t-t_0-a_n) c_n \dot{Q}(t-a_n), \quad (2)$$

for $t \in [t_0, \infty)$, where $\Omega^2 \equiv \omega_s^2 - 2\Gamma \int d\chi \rho_\epsilon(\chi)/\chi$, $\Omega^2 \in (0, \infty)$ and $2\Gamma \equiv \lambda^2/(4\pi)$.

The Green functions for the wave-operator in $\mathcal{T}_2, \mathcal{T}_3, \mathcal{T}_4, \mathcal{H}_1, \mathcal{H}_2$ can be similarly worked out, they has the same form except for the values of the constants a_n, c_n .

For the simply connected manifold \mathcal{R}^3 ($t = \text{const}$ section of the Minkowski space-time) the Green function is $G = \delta(t-t'-r)/4\pi r$. Thus the radiation-reaction equation in this manifold reduces to (2) with right hand side equal to zero, for all $t \in [t_0, \infty)$.

4 Numerical Analysis and Conclusions

Now we investigate the time behaviour of the energy-function of the source: $E(t) = \frac{1}{2} [\dot{Q}^2(t) + \Omega^2 Q^2(t)]$, where the functions $Q = Q(t)$ are the corresponding solutions of the radiation-reaction equations for each manifold in study. For the present numerical analysis we have chosen as initial data $(Q(t_0), \dot{Q}(t_0)) = (\sqrt{2}/\Omega, 0)$, (i.e., $E(t_0) = 1$) and $\Gamma = \Omega = 1; a = 1$.

In figure 1 we observe the exponential decay of the energy in Minkowski space-time (that is the 3-space is the non-compact \mathcal{R}^3). Figures 2 and 3 show the damping of the energy in FRW space-times with compact \mathcal{T}_1 and \mathcal{H}_1 space slices respectively, for different ratios h/a (h is the height of the basic cells, a is the side of the square basis of the \mathcal{T}_1 -cell or the shortest distance between two opposite sides of the \mathcal{H}_1 -cell). The fact that the relative maxima occur at different times and are of different amplitudes for distinct tessellations (different ratios h/a) of the covering manifold [2], basically reveals the differences in their degree of connectedness (returning light rays take different times to return to the source).

According to the concept of degree of connectedness one learns from figures 2 and 3 that the greater is the topological degree of connectedness the earlier is the occurrence of the first relative maximum in the energy function. Note also that these maxima are due to the retarded terms, present in the right hand sides of the radiation-reaction equations, demanded by the compactness and the connectedness, and incorporated in the corresponding Green functions. It should be noticed that the extension of the above concept of topological degree of connectedness to non-compact 3-manifolds implies that \mathcal{R}^3 has a null topological degree of connectedness. This, of course, is indicated in figure 1, which shows an exponential decay of the energy with the time, no relative maxima come about, which means that no light rays (null geodesics) return to the origin.

For completeness we show in figure 4 the time evolution of the energy in a FRW space-time with $\mathcal{M}_3 = \mathcal{P}^3$ (the multi-connected real projective 3-space), where we notice the absence of the radiation damping phenomenon (a suitable time-average for the energy is constant). This pattern for the energy is typical of the space-times with spherical ($\kappa = 1$) spacelike sections. In fact, in these space-time manifolds all emitted light rays return to the source within a finite time (for finite radii of the 3-worlds, of course), then we associate to them the maximum topological degree of connectedness, i.e. one.

Acknowledgements

We are grateful to A.F.F. Teixeira and G. Gomero for valuable discussions. We also thank CNPq for financial support.

References

- [1] J.R. Weeks, *The Shape of Space*, "Pure & App. Math." 26, M. Dekker, N.Y. (1985).
- [2] M. Lachièze-Rey & J.-P. Luminet, *Phys. Rep.* 254, 135 (1995).
- [3] W. Oliveira, M.J. Rebouças & A.F.F. Teixeira, *Phys. Lett. A* 188, 125 (1994).
- [4] A. de Oliveira-Costa & G. Smoot, *Astrophys. J.* 448, 447 (1995).
- [5] G.F.R. Ellis & G. Schreiber, *Phys. Lett. A* 115, 97 (1986).
- [6] A. Bernui & M.J. Rebouças, submitted (1996).
- [7] F. Schwalb & W. Thirring, *Ergeb. exakten Naturwiss.* 36, 219 (1964).
- [8] A. Bernui, *Ann. Physik* 3, 408 (1994).
- [9] P. Morse & H. Feshbach, *Methods of Theoretical Physics*, Mc Graw-Hill, N.Y. (1953).

Fig. 1

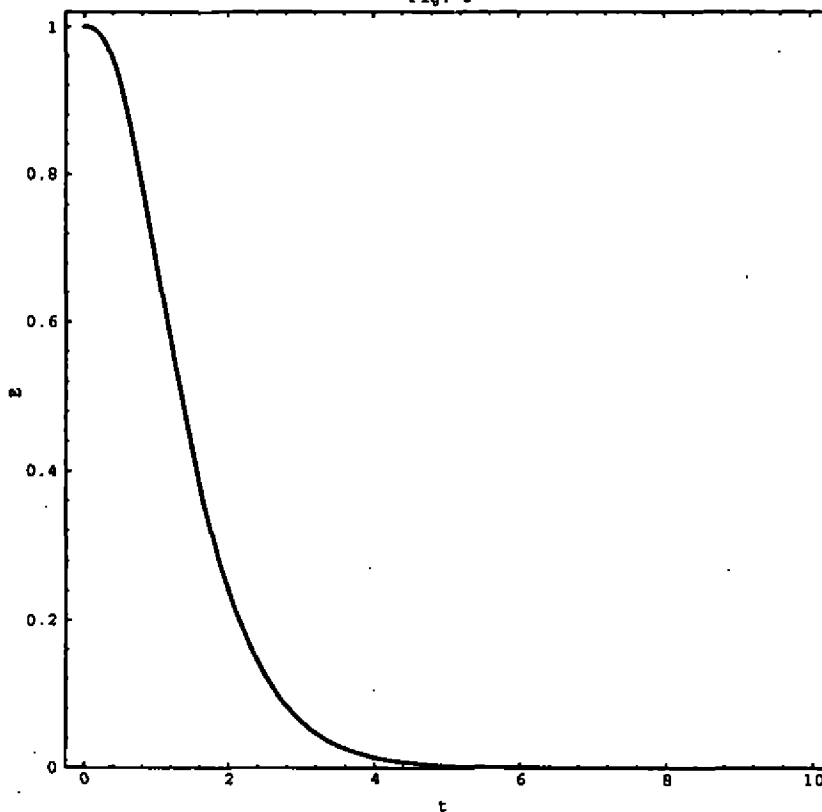


Fig. 2

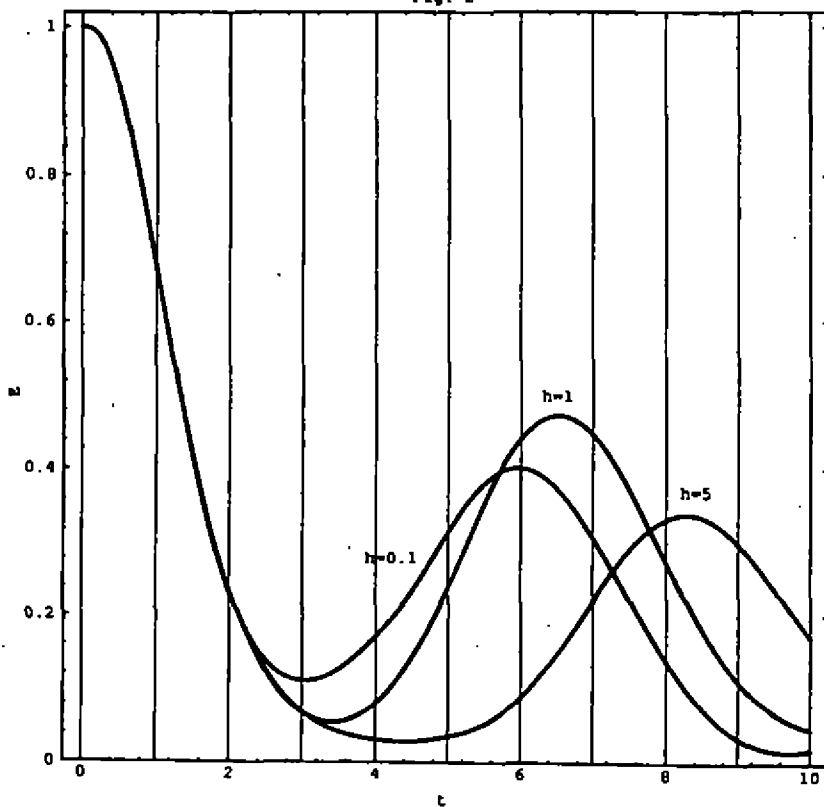


Fig. 3

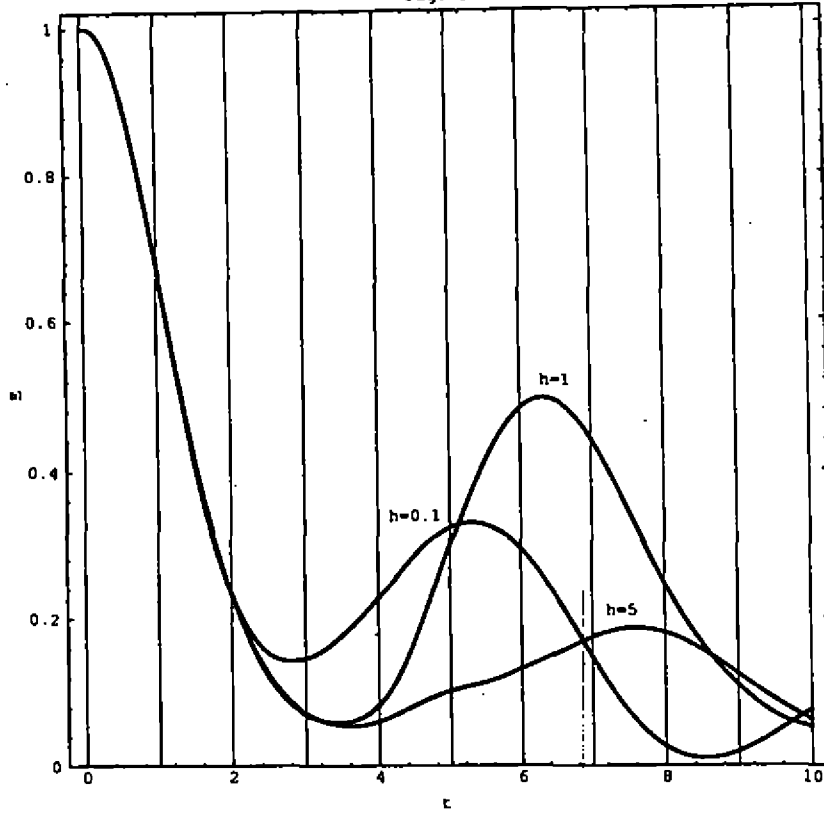
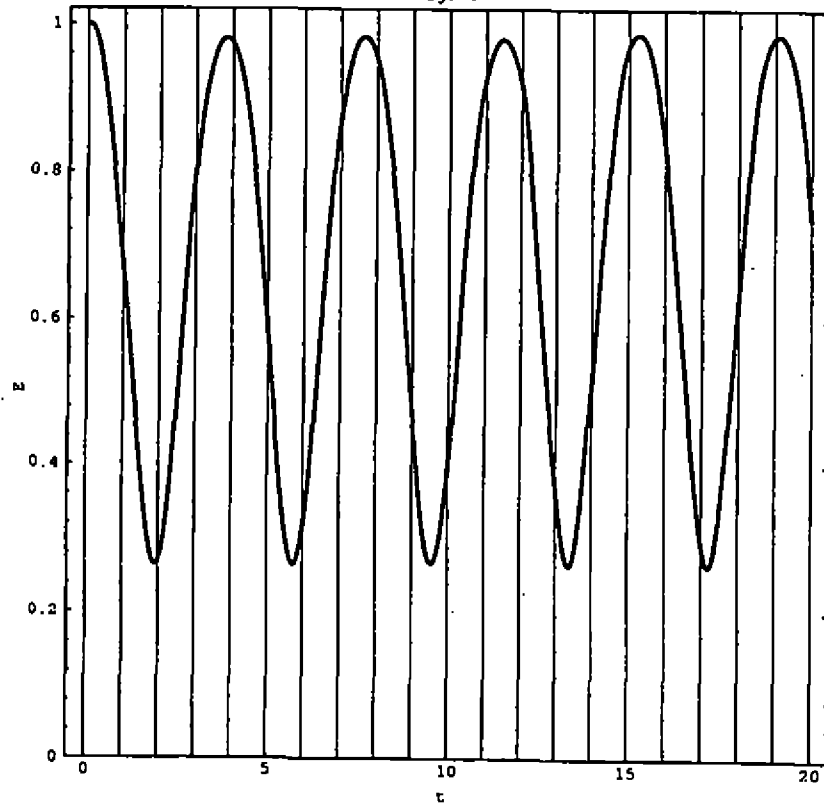


Fig. 4



Desenvolvimento de um Transdutor Indutivo Supercondutivo de Dois Modos com Alto Fator de Qualidade Mecânico para uma Antena Ressonante Massiva de Ondas Gravitacionais

Carlos Frajuca

*Escola Técnica Federal de São Paulo, Rua Pedro Vicente 625,
Canindé, São Paulo, SP 01109, Brazil*

Nadja S. Magalhães, Odylio D. Aguiar

*Divisão de Astrofísica, Instituto Nacional de Pesquisas Espaciais,
C.P. 515, São José dos Campos, SP 12201-970, Brazil*

Z. K. Geng, William O. Hamilton, Warren W. Johnson and Norbert D. Solomonson

*Department of Physics and Astronomy, Louisiana State University,
Baton Rouge, LA 70803-4001, USA*

Um dos métodos propostos para a detecção de ondas gravitacionais (e o único em operação no momento) é o de massas ressonantes, onde o fator de qualidade tem um ponto decisivo na sensibilidade da antena, assim como a largura de banda de detecção. Para incrementar esses dois fatores, foi desenvolvido um transdutor de dois modos para ser usado em uma antena de 3 modos. Nesse transdutor indutivo supercondutor, o último modo do transdutor é um ressonador de nióbio que sozinho apresenta um fator de qualidade de 16 milhões (a 4 Kelvin). O segundo modo do transdutor é um ressonador de alumínio que sozinho apresenta um fator de qualidade de 13 milhões (a 4 Kelvin). Esses dois modos são acoplados através de contração térmica, pois o alumínio contrai mais do que o nióbio ao ser resfriado. A frequência dos dois ressonadores não foram perfeitamente sintonizadas para que o fator de qualidade dos dois modos pudessem ser medidos separadamente. Os resultados obtidos foram de 10 milhões para o ressonador de alumínio e 15 milhões para o ressonador de nióbio. Esses resultados permitem construir antenas ressonantes massivas com sensibilidade em h da ordem de 10^{-21} .

1 Introdução

A detecção de ondas gravitacionais é um dos maiores desafios a que se propõe a ciência em nossos dias e com a conquista desse desafio teremos a abertura de uma nova janela na astronomia: a astronomia gravitacional. A própria causa das ondas gravitacionais serem tão difíceis de detectar (a sua interação muito fraca com a matéria) nos permitirá sondar o interior de estrelas colapsantes ou eventos que estejam escondidos de nós por nuvens de poeira ou gases. Além disso poderemos ter acesso a alguns dos fenômenos mais espetaculares da natureza como a formação de buracos negros, coalescência de binárias compostas por buracos negros e/ou estrelas de nêutrons e outros tantos fenômenos que permanecem até hora fora de nossa observação.

A detecção de ondas gravitacionais tem mais de 30 anos [1]. Ela começou com Joseph Weber que inventou o detector de massa ressonante (uma onda gravitacional ao passar por um cilindro transfere parte da sua energia para este, se a frequência deste for ressonante com a da antena, fazendo este cilindro vibrar, esta vibração pode agora ser amplificada por amplificadores mecânicos e/ou eletrônicos e finalmente medida). Desde a época de Weber, esses

detectores já tiveram sua sensibilidade muito melhorada, passaram a ter melhor isolamento vibracional (para diminuir ruído sísmico), passaram a ser esfriados até temperaturas criogênicas (existem três em operação resfriados a 4 K, e dois que estão em fase final de montagem e que devem atingir temperaturas da ordem de 50 mK), a eletrônica de amplificação passou a ser mais sofisticada (algumas das antenas usam como amplificadores os chamados SQUIDs: "Superconducting Quantum Interference Devices") e começou-se a usar uma amplificação mecânica (um segundo ressonador mecânico sintonizado na frequência da antena, acoplado a ela aumenta a amplitude do movimento pela relação das massa entre os dois ressonadores) a partir da qual a vibração é transformada em sinal elétrico para ser amplificado.

Esse segundo ressonador constitui-se o segundo modo ressonante da antena e tem como função , além de amplificar a vibração , também aumentar a banda de frequência de detecção (banda esta dada pela frequência ressonante multiplicada pela raiz quadrada da razão entre as massas dos dois modos). Para aumentar ainda mais essa banda de interação , um outro ressonador pode ser introduzido em série com os outros dois, o que permite aumentar mais ainda a razão das massas e por conseguinte a banda de detecção .

A transformação do sinal mecânico em sinal elétrico é feita através de um transdutor eletromecânico, neste caso um transdutor indutivo, onde uma bobina supercondutora plana é colocada paralelamente e muito próxima de uma superfície plana do último ressonador feito de material também supercondutor (no nosso caso nióbio). Os movimentos do último ressonador alteram a indutância da bobina gerando o sinal elétrico que, passando por um transformador casador de impedâncias, é amplificado no SQUID e aí amplificado pela eletrônica convencional.

O objetivo deste trabalho é o de se obter altos fatores de qualidade mecânico nos ressonadores de nióbio, e ao mesmo tempo conseguir fazer um acoplamento entre ressonadores feitos de diferentes materiais (no nosso caso: nióbio e alumínio 5056) sem que haja uma degradação no fator de qualidade mecânico. O motivo disso é que as antenas geralmente são feitas de materiais diferentes dos materiais do último ressonador (nióbio). O método escolhido aqui foi o da contração térmica diferencial. O ressonador de nióbio ao ser resfriado contrai menos do que um anel da mesma medida usinado no centro do segundo ressonador de alumínio, a pressão desse contato numa área de contato suficientemente grande, garante um acoplamento forte suficiente que não degrade o fator de qualidade mecânico. 20

2 O ressonador de nióbio

Primeiramente se mediu o fator de qualidade mecânico (Q) do ressonador de nióbio sozinho e como o Q se comportava com a temperatura nas proximidades da temperatura de 4 K, e o resultado é apresentado na figura 1. Podemos ver que o maior Q se encontra perto de 7,5 K, na região abaixo de 4K há um pico de dissipação (em outros experimentos este pico foi localizado ao redor de 2K), e à temperatura de 9,2K aparece um degrau devido à transição supercondutora do nióbio.

3 O ressonador de nióbio e o de alumínio

Para testar como o fator de qualidade se comportava com a pressão da contração térmica diferencial, primeiro testes com apenas um anel de alumínio em torno do ressonador foram realizados e os resultados podem ser vistos na tabela 1. Note-se que quanto maior a pressão, maior o fator de qualidade, ou que este fator de qualidade poderia ser melhorado se fosse colocada graxa de vácuo de silicone na interface entre os ressonadores.

Ao se decidir pelo melhor acoplamento, optou-se pelo de maior pressão sem a presença de graxa.

Finalmente a montagem final dos dois ressonadores foi feita como aparece na figura 2, e os resultados finais dos fatores de qualidade mecânicos aparecem indicados na tabela 2.

4 Conclusões

O transdutor desenvolvido aqui pode ser usado tanto para antenas cilíndricas quanto para antenas esféricas.

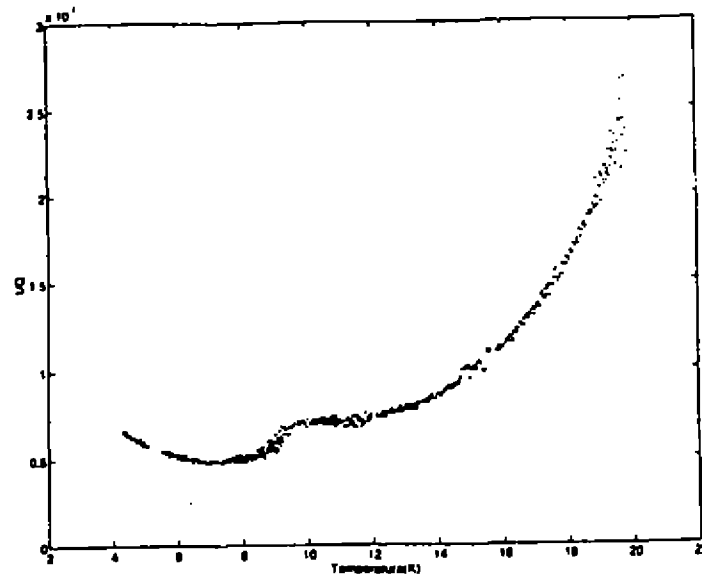


Figure 1.: Gráfico do Q Inverso versus a Temperatura do ressonador de nióbio

Anel 20 (índice)	diâmetro (cm)	Pressão na interface(kgf/cm ²)	Q (10 ⁶) sem graxa	Q (10 ⁶) com graxa
só ressonador	6,985	0	20,7	
1	7,005	80	19,0	20,7
2	7,003	170	19,1	20,5
3	6,995	330	20,7	19,3 *

Table 1: Tabela dos fatores de qualidade(*Neste teste foi encontrado um parafuso solto, podendo ser este o motivo do baixo Q)

O processo de contração térmica diferencial pode ser usado também para acoplar um ressonador de alumínio com a massa principal da antena, faz-se um furo do mesmo diâmetro (com a menor ovalização possível) e coloca-se um cilindro de nióbio nesse furo.

Pelos resultados aqui mostrados, o motivo da dissipação mecânica na interface de contato é a existência de regiões com contato fraco, ou seja as superfícies não estão rigidamente fixas uma na outra.

Agradecimentos

CF agradece CNPq (Brasil) pelo suporte de sua pesquisa. NSM agradece a FAPESP (Brasil) pelo apoio financeiro. A pesquisa desenvolvida por ZKG, WOH, WWJ e NDS é (ou foi) apoiada pela NSF(National Science Foundation) (USA).

	ressonador sozinho	ressonador acoplado
ressonador Al	13×10^6	10×10^6
ressonador Nb	16×10^6	15×10^6

Table 2: Tabela dos fatores de qualidade dos dois ressonadores acoplados

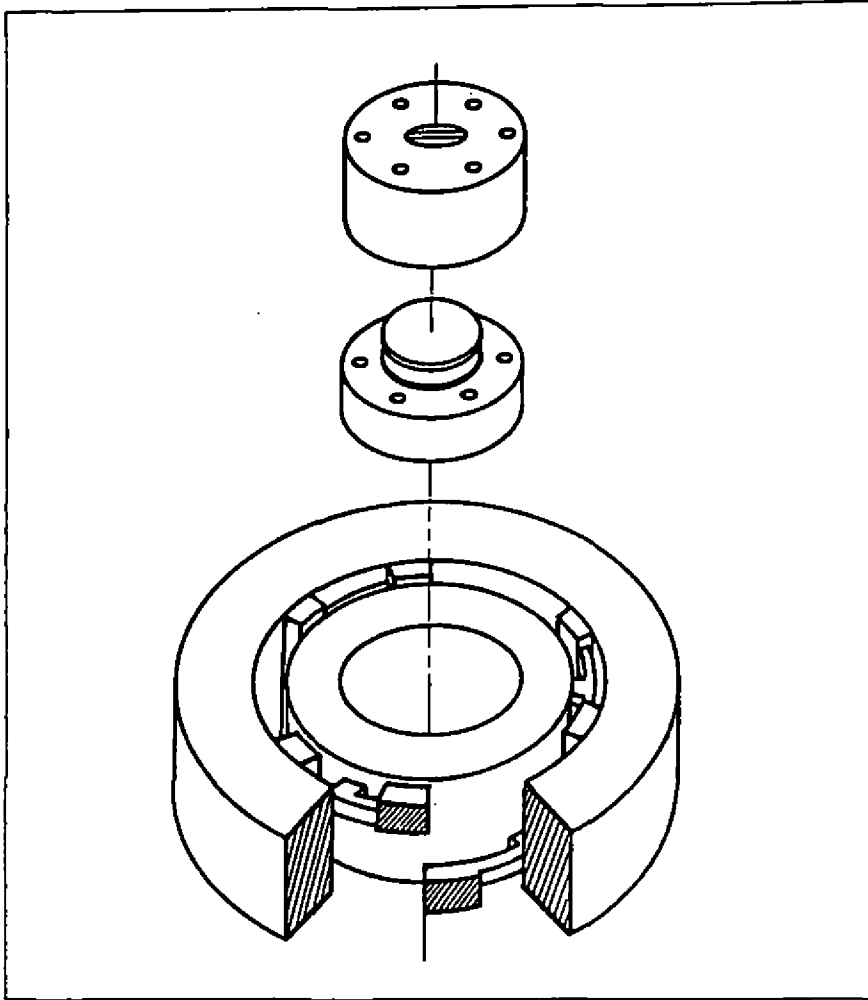


Figure 2.: Desenho da montagem final do ressonador de dois modos

References

- [1] Para uma bibliografia recente em detectores de ondas gravitacionais recomenda-se: Proceedings of the First Edoardo Amaldi Conference on Gravitational Wave Experiments (Singapore: World Scientific, 20 1995.)

On The Higher Derivative Quantum Gravity

M. Asorey^a, J.L. López^a, I.L. Shapiro^{a,b}

a) Departamento de Física Teórica Universidad de Zaragoza 50009, Zaragoza, Spain

b) Departamento de Física -ICE,

Universidade Federal de Juiz de Fora, 33036-330 MG - Brazil

We analyze the perturbative implications of the most general high derivative approach to quantum gravity based on a diffeomorphism invariant local action. In particular, we consider the super-renormalizable case with a large number of metric derivatives in the action. The structure of ultraviolet divergences is analyzed and it is shown that the cosmological counterterm vanishes under certain parameter conditions. The divergences are gauge fixing and parametrization independent. We elaborate on the unitarity problem of high derivative approaches and the distribution of masses of the unphysical ghosts. We also discuss the properties of the low energy regime and explore the possibility of having a multi-scale gravity with different scaling regimes compatible with Einstein gravity at low energies.

The formulation of a consistent theory of Quantum Gravity is still one of the major challenges in theoretical physics. One of the main fundamental problems is that there is no experimental evidence of any Quantum Gravity effect whereas the classical theory covers from cosmology to current precision tests with great success. Due to the lack of any experimental evidence, the models of Quantum Gravity are necessarily based on purely theoretical principles without phenomenological constraints. On spite of this freedom the construction of consistent models for Quantum Gravity meets very serious difficulties. In particular, the quantum theory based on the Einstein-Hilbert action is non-renormalizable, and thus one has to imply an infinite number of renormalization conditions in order to extract finite part of the diagrams.

Recently, it was pointed out [1] that some large distances effects remain, however, independent of the renormalization conditions involving higher order terms of the effective action. In particular this occurs for the quantum corrections to the gravitational Newtonian potential. However, the analysis of other effects like the scaling dependence of the cosmological and gravitational constants, requires a concrete formulation of the quantum theory. One can always imagine that the extremely high energy UV regime is described by qualitatively different theory like string theory, free of renormalizability problems which will provide a natural reduction parameter scheme at intermediate scales. In this scheme the field theoretical approaches to quantum gravity should be considered as an effective field theories. At the same time, the string effective action is well defined only on shell because of the reparameterization invariance. For such a reason, we consider the most general effective action which can be generated by string theory [2] in an arbitrary parametrization

$$\Gamma_{eff}[g_{\mu\nu}] = \sum_{n=0}^{2N+4} \alpha_n m^{4-n} \int d^4x \sqrt{-g} O_n[(\partial_\lambda g_{\mu\nu})^n] \quad (1)$$

where $N \rightarrow \infty$. m^2 is the dimensional parameter of the fundamental theory (in string theory it is the inverse of the string tension α'), $O_n(\partial_\lambda g_{\mu\nu})$ denotes the general covariant scalar terms containing n derivatives of the metric $g_{\mu\nu}$ and α_n are dimensionless couplings. Although theories with higher derivatives like (1) are in general non-unitary at the quantum level, string theory is both unitary and renormalizable. While studying the effective theory (1) one meets massive ghosts. On the other hand the first few ghosts have the masses of the Planck order, and therefore the truncated theory has the same status as the well known fourth derivative gravity [3,4] (see [5] for introduction and references), it can be used as an effective low energy theory for quantum gravity in the same fashion as the the fourth derivative gravity.

One can always choose a special parameterization without unphysical ghosts [6,7], although from a pure string point of view there are no means to distinguish this special parameterization of the metric except for the absence of unphysical massive ghosts [8].

Here we consider a finite value of N without taking the infinite limit $N \rightarrow \infty$. If $N \geq 0$ the corresponding theory contains more than four derivatives of the metric and it becomes super-renormalizable. This provides a natural framework to study the possibility of different scaling regimes compatible with Einstein gravity at low energies and different scenarios for the ultraviolet behaviour of the cosmological constant.

The $n = 0$ term of the action (1) is cosmological term, $n = 1$ - Einstein term. For $n = 2$ one meets the fourth derivative gravity. In higher orders, when $n > 2$, the action contains terms which are composed by curvature tensor, Ricci tensor, scalar curvature and their covariant derivatives. We suppose that the perturbation theory is constructed for the quantum metric $h_{\mu\nu}$ on flat background where $g_{\mu\nu} = \eta_{\mu\nu} + h_{\mu\nu}$. Then the contributions of the $n > 2$ terms to the propagator are only through the terms of second order in curvature, while others can contribute to the vertexes only, because they necessary contain more than two $h_{\mu\nu}$ fields. Therefore, the terms relevant for the propagator have the form

$$S = \int d^4x \sqrt{-g} \left[\sum_{i=0}^N (a_i R_{\mu\nu} \square^i R^{\mu\nu} + b_i R \square^i R) - \frac{1}{G} R + \Lambda \right] \quad (2)$$

If $a_N \neq 0$ and $a_N + 3b_N \neq 0$, the highest order terms are nondegenerate (after introducing the gauge fixing) and then, at high momentum k , the propagator behaves like $k^{-(2N+4)}$. The gauge fixing can be introduced within the standard Faddeev-Popov prescription, but with an additional weight functional [4,5] (see also [11,12] for the recent general discussion of higher derivative theories), and thus provide the ghost propagator to have the same UV asymptotics.

The spin-2 sector of the propagator are gauge-fixing independent, just as in the fourth derivative gravity, and if $a_N \neq 0$, then $G^{(2)} = O(k^{-(2N+4)})$. Some comment on the form of the propagator is in order. In the general theories like (1), one always meets the following structure of propagator.

$$G(k) = (l_{2N+4} k^{2N+4} + l_{2N+2} k^{2N+2} + l_{2N} k^{2N} + \dots + l_2 k^2)^{-1} \quad (3)$$

where l_i are real numbers related with the values of a_i , b_i coefficients in (2). The expression (3) can be rewritten in the form

$$G(k) = \frac{A_0}{k^2} + \frac{A_1}{k^2 + m_1^2} + \frac{A_2}{k^2 + m_2^2} + \dots + \frac{A_{N+1}}{k^2 + m_{N+1}^2} \quad (4)$$

where m_j^2 , depending on the values of l_i (3) can be real or complex. In the last case there are always complex conjugate couples of the m^2 's. As one can prove [9], that for real $0 < m_1^2 < m_2^2 < m_3^2 < \dots < m_{N+1}^2$, one has $sign[A_j] = -1 sign[A_{j+1}]$. This shows the structure of massive poles in the higher derivative theory (1). The contributions of the massive unphysical particles make the theory superrenormalizable while all the masses are of the Planck orders. Consequently the violation of unitarity is not visible while we consider an effective theory valid for the energies below the Planck scale. Above this scale all quantum effects should be derived from the string loops directly.

The standard estimate for the superficial degree of divergency for arbitrary p -loop diagram gives

$$d_{ext} \leq 4 + 2N - 2Np \quad (5)$$

where d_{ext} is the total number of derivatives acting on an external lines. Therefore the theory (1) is superrenormalizable. In all the $N > 0$ cases the possible divergences have the powers of curvature less than in the starting action, and moreover, this power is decreasing with the loop order.

Since the local covariant counterterms have smaller amount of derivatives than the classical action, the coefficients of terms with more derivatives don't need the infinite renormalization. In the framework of the theory (1) these

coefficients are arbitrary. In principle their values should be derived from the fundamental theory, or taken from experiment. The sector of any theory (1) (with $N > 0$), which is subject of infinite renormalization, has the form

$$\int d^4x \sqrt{-g} \left\{ a_0 R_{\alpha\beta} R^{\alpha\beta} + b_0 R^2 - \frac{1}{G} R + \Lambda \right\} + (\text{surface terms}) \quad (6)$$

Now we consider the renormalization group equations in the theory (1). In fact, since only the parameters of the lower derivative part (6) of the action need to be renormalized, the effective theory (1) depends on scale only via the beta-functions for these parameters: β_{a_0} , β_{b_0} , β_G , β_Λ . Thus it is reasonable to evaluate these beta-functions. Here we develop the method [9] which enables one to calculate the above beta-functions in the one-loop approximation for general theory (1), and moreover perform an explicit calculation of β_Λ .

Before the discussion of the calculation of the beta-functions, let us show that they do not contain the gauge fixing and parametrization arbitrariness. The local counterterms, in principle, can be gauge and parametrization dependent, but these dependence has to vanish on the mass-shell. For the one-loop counterterms one can go on shell by just substituting the classical equations of motion into the expression for counterterms. For $N > 0$ these equations contain derivatives of the metric of degree higher than four. However, we already know that in the theory (1) the counterterms are local expressions with maximum four derivatives of the metric. Therefore the one-loop divergences of the theory are invariant and unambiguous. At higher loops one has to take into account quantum corrections to the equations of motion, but the above result holds.

Now we can proceed with the one-loop calculation. Technically it is reduced to the evaluation of the divergent part of the *Det* of the operator ¹ (see [9] for details).

$$\left[\frac{a_N}{4} \delta_{\mu\nu}^{\rho\sigma} - \frac{a_N (a_N + 4b_N)}{16b_N} g_{\mu\nu} g^{\rho\sigma} \right] \left\{ \delta_{\rho\sigma\alpha\beta} \square^{N+2} + V_{\rho\sigma\alpha\beta}^{\lambda_1\lambda_2\dots\lambda_{2N+2}} \nabla_{\lambda_1} \nabla_{\lambda_2} \dots \nabla_{\lambda_{2N+2}} + \right. \\ \left. + Z_{\rho\sigma\alpha\beta}^{\tau_1\tau_2\dots\tau_{2N+1}} \nabla_{\tau_1} \nabla_{\tau_2} \dots \nabla_{\tau_{2N+1}} + U_{\rho\sigma\alpha\beta}^{v_1v_2\dots v_{2N}} \nabla_{v_1} \nabla_{v_2} \dots \nabla_{v_{2N}} + O(\nabla^{2N+1}) \right\}$$

Unfortunately it is difficult to apply the general algorithm [9] for the real calculations for general N . The only one thing which can be traced up to the end in a general form is the calculation of the cosmological counterterm. The reason is that this counterterm can be derived for the flat background metric, when only the (2) terms are relevant.

Let us first consider the case $N > 1$. One can apply the general formula [9] and find the cosmological counterterm in the form

$$W_{N>1}^{div} = \frac{1}{\epsilon} \int d^4x \sqrt{-g} \left[-\frac{2}{a_N(a_N + 3b_N)} u(N, N > 1) + \frac{1}{a_N^2(a_N + 3b_N)^2} v(N) \right] \quad (7)$$

where

$$u = 6a_N a_{N-2} + 15b_N a_{N-2} + 3b_{N-2} a_N, \quad v = a_N^2 (a_{N-1} + 3b_{N-1})^2 + 5a_{N-1}^2 (a_N + 3b_N)^2$$

In the case $N = 1$ one meets a different expression for u [9]. It is important that the obtained result is gauge and parametrization independent. In this respect it differs from the counterterms which appears in GR and fourth derivative quantum gravities. Thus, taking into account the higher orders in the effective theory (1) we get some advantage. With the use of dimensional consideration one can write down the counterterm of the Einstein type with accuracy to the numerical coefficients. The same concerns the renormalization of the parameters a_0, b_0 .

Let us now discuss the possible physical applications of the above result. One can fine tune the coefficients $a_N, b_N, a_{N-1}, b_{N-1}, a_{N-2}, b_{N-2}$ in such a way that the cosmological constant does not need an infinite renormalization. This can give an additional constraint for these coefficients, in fact such a constraints are rather restrictive if we require the finiteness for arbitrary N . In this case the zero (or very small) value of Λ is not in a conflict with the renormalization.

On the other hand we can consider the nonzero beta-function for Λ . In this case after the renormalization the one-loop expression gives the leading logarithmic term in the dependence of the contribution of quantum gravity to the cosmological constant. One can start at the Planck scale with the nonzero cosmological constant. This should

¹ Here V, Z, U depend on the dimensionful ratios like $\frac{a_{N-1}}{a_N}$, and also on curvature and on it's covariant derivatives.

lead to the cosmological model with the cosmological constant term, which depends on the scale factor $a(t)$ as follows

$$\Lambda[a(t)] = - \left[-\frac{2}{a_N(a_N + 3b_N)} u(N, N > 1) + \frac{1}{a_N^2(a_N + 3b_N)^2} v(N) \right] \ln[a(t) M_{Pl}] \quad (8)$$

where we have used the relation $\mu \sim a^{-1}$. Such a consideration can be interesting for the analysis of the quantum gravitational effects in the evolution of the bubbles in the Universe, or for the solution of the problem of the age of the Universe.

It is worth to mention that the coupling of the superrenormalizable gravity (1) to the matter fields doesn't affect the β -functions of (gauge, Yukawa and scalar) couplings in the matter fields sector. This follows directly from the power counting. In this respect our model differs from both GR where adding matter fields spoils the renormalizability, and from the four derivative gravity where the Yukawa and scalar couplings are affected by gravitational corrections [10]. In fact two diagrams with external scalar legs can be divergent for $N = 1$ case, but they give contribution only to the beta-function of the scalar mass. One can find this correction to mass' beta-function in [9].

As it was mentioned above, the masses of ghosts (4) have the same order as the Planck mass. At low energies (corresponding to the macroscopic length) they all are not propagating, and the only one relevant excitation is that related with the massless particle - graviton. To evaluate the quantum corrections to the gravitational potential, one has to proceed in the same way as in the recent paper [1]. In the far IR the quantum effects of the higher derivative theory (1) are the same as in Einstein gravity. By the algebraic reasons they are linked with the UV counterterms of the Einstein gravity rather than with the ones of the theory we are discussing here. Thus the low energy (long distance) effects in the theory (1) are essentially the same as in the Einstein gravity. At the intermediate scales, however, quantum gravity effects will be related with the more general theory (1) and one can regard (8) as an example of such an effects.

Authors are grateful to S.Ketov for discussion on string reparametrizations. I.Sh. is grateful to Departamento de Física Teórica, Universidad de Zaragoza and to Departamento de Física - ICE, Universidade Federal de Juiz de Fora, MG - Brazil, for kind hospitality.

1. J.F. Donoghue, *Phys.Rev.D***50** (1994) 3874.
2. M.B.Green, J.H.Schwarz, E. Witten, *Superstring Theory*(Cambridge Univ.,1987).
3. K.S.Stelle *Phys.Rev.***16D** (1977) 953.
4. E.S.Fradkin, A.A.Tseytlin, *Nucl.Phys.***201B** (1982) 469.
5. I.Buchbinder,S.Odintsov, I.Shapiro,*Effective Action in Quantum Gravity*(IOP,Bristol,1992).
6. B.Zwiebach, *Phys.Lett.* **156B** (1985) 315.
7. S.Deser, A.N.Redlich, *Phys.Lett.***176B** (1986) 350.
8. A.A.Tseytlin, *Phys.Lett.***176B** (1986) 92.
9. M.Asorey, J.L. López , I.L.Shapiro, *DFTUZ* 96-15 (1996).
10. I.L.Buchbinder, O.K.Kalashnikov, I.L.Shapiro, V.B.Vologodsky, Yu.Yu. Wolfengaut, *Phys.Lett.***216B**(1989)127; I.L.Shapiro, *Clas.Quant.Grav.***6**(1989)1197.
11. M. Asorey and F. Falceto, DFTUZ795-3 preprint, hep-th/9502025 (Phys. Rev. D in press).
12. T.D.Bakeyev and A.A.Slavnov, SMI-02-96 preprint, hep-th/9601092 (Int. J. Mod. Phys.in press)

On the conformal transformation in (quantum) gravity

Ilya L. Shapiro*

*Departamento de Física - ICE,
Universidade Federal de Juiz de Fora - MG, Brazil*

We consider several aspects of conformal transformation in second and fourth derivative metric-dilaton gravity theories. The local conformal symmetry and conformal duality are formulated in $n \neq 2$ dimensions. In order to use the conformal duality for the study of strong gravitational field regime in quantum gravity the first term in the Schwinger-DeWitt expansion for the effective action and its gauge fixing dependence are derived. In $n = 4$ we consider the possible form of the one-loop divergences and obtain an infinite family of higher derivative conformal invariant metric-dilaton actions. Another (inequivalent) family of metric-dilaton generalizations of the Weyl gravity comes from the study of the anomaly-induced effective action of vacuum.

1. It is well known that the study in the field of quantum gravity meets serious difficulties. On classical level General Relativity is in a good accordance with the known tests, but quantum theory based on GR is nonrenormalizable. Indeed there were a number of approaches to develop quantum gravity, however the principal problem with the lack of quantum gravitational experiments doesn't enable one to choose among the numerous theories and therefore the models for quantum gravity are subjects of wide arbitrariness. This concerns, for instance, the choice of the model for the description of low-energy quantum gravitational phenomena, while the string-inspired action contains, along with the metric, massless dilaton field. In such a situation a lot of attention has been attracted by the models which have more symmetries than GR, and in particular, by the theories with local conformal invariance [1].

On the other hand, the standard perturbative techniques give the effective action in a form of a power series in the curvature tensor and its derivatives. At the same time one of the most important applications of quantum gravity should be the regions of extremely strong gravitational field in the vicinity of cosmological and black hole singularities, where this approximation doesn't look efficient. One way to study this strong field limit is to develop essentially nonperturbative methods in quantum gravity. Another one is to explore a specific models for quantum gravity which have a symmetry linking the regimes of strong and weak gravitational field. Below we consider an example of such a symmetry - conformal duality, which has been originally discovered by Bekenstein [2] as a property of dynamical equations for the conformal scalar field coupled to gravity.

2. Consider the action of metric-dilaton theory in n -dimensional space-time.

$$S[g_{\mu\nu}, \phi] = \int d^n x \sqrt{-g} \{ A(\phi) g^{\mu\nu} \partial_\mu \phi \partial_\nu \phi + B(\phi) R + C(\phi) \} \quad (1)$$

This theory possesses general covariance and, for some special choice of the functions A, B, C (otherwise arbitrary), an extra conformal symmetry. If one performs an arbitrary reparametrization of the scalar field $\phi = \phi(\psi)$, and the conformal transformation of the metric $\tilde{g}_{\mu\nu} = g_{\mu\nu} e^{2\sigma(x)}$ then the condition of symmetry for the action (1) is $S[\tilde{g}_{\mu\nu}, \psi] = S[g_{\mu\nu}, \phi]$. The solution for the last equation has the form

$$e^{(n-2)\sigma(\phi)} = \frac{B(\phi)}{B(\psi(\phi))}, \quad A(\phi) = \frac{n-1}{n-2} \frac{B_1^2(\phi)}{B(\phi)}, \quad C(\phi) = \lambda B^{\frac{n}{n-2}}(\phi) \quad (2)$$

*On leave from Tomsk Pedagogical University, 634041, Tomsk, Russia. E-mail: shapiro@fisica.ufjf.br

where $\lambda = \text{const}$ and $X_i = d^i X / d\phi^i$. The equations (2) show the relation between arbitrary reparametrization of scalar field and the corresponding conformal transformation for the metric and also give the constraints on $A(\phi)$, $C(\phi)$ which are caused by the conformal symmetry.

Following [3] we denote the action (1) which satisfies the conformal constraints (2) as $S_{B(\phi),\lambda}$. The particular case of $S_{B(\phi),\lambda}$ is GR with $B = \gamma\kappa^{-2}$. Here the Newton constant is divided into dimensional $[\kappa^2]$ and dimensionless γ factors for convenience. Another particular case of $S_{B,\lambda}$ is the conventional conformal scalar field, for which $B(\phi) = \frac{n-2}{2(n-1)}\psi^2$ where ψ is some other scalar.

GR is classically equivalent to conformal scalar field [1]. To see this one has to perform the conformal transform of symmetric model. It turns out that the result also satisfies (2) so that

$$S_{B(\phi),\lambda}[\bar{g}_{\mu\nu}, \phi] = S_{K(\phi),\lambda}[g_{\mu\nu}, \phi] \quad (3)$$

for any given function $K(\phi)$ (with only sign restrictions), if only $\bar{g}_{\mu\nu} = \left[\frac{K(\phi)}{B(\phi)}\right]^{\frac{2}{n-2}} g_{\mu\nu}$. In particular one can choose $K = \text{const}$ and demonstrate the conformal equivalence between the models $S_{B(\phi),\lambda}$ with nonconstant different B including GR.

2. The equality (3) can be used as a basis for another interesting symmetry, which holds for some of the nonconformal versions of (1) [2, 3, 4]. Let us consider the sum

$$S_{B(\phi),\lambda}[\bar{g}_{\mu\nu}, \phi] + S_{L(\phi),\tau}[\bar{g}_{\mu\nu}, \phi] \quad (4)$$

where $L(\phi)$ is some function and $\tau = \text{constant}$. One can show that after the conformal transformation (4) becomes

$$S_{K(\phi),\lambda}[g_{\mu\nu}, \phi] + S_{M(\phi),\tau}[g_{\mu\nu}, \phi], \quad M(\phi) = \frac{L(\phi)K(\phi)}{B(\phi)} \quad (5)$$

Especially interesting particular case of the above symmetry takes place when one of the components in (4) is GR

$$S = \frac{1}{\kappa^2} \int d^n x \sqrt{-g} \left\{ \frac{n-1}{n-2} \frac{1}{\phi} g^{\mu\nu} \partial_\mu \phi \partial_\nu \phi + (\phi + \gamma)R + \lambda \phi^{\frac{n}{n-2}} + \tau \gamma^{\frac{n}{n-2}} \right\} \quad (6)$$

For this specific case we face a conformal duality which exchanges

$$\phi \leftrightarrow \phi^{-1}, \quad \gamma \leftrightarrow \gamma^{-1}, \quad \tau \leftrightarrow \lambda, \quad g_{\mu\nu} \leftrightarrow \bar{g}_{\mu\nu} = g_{\mu\nu} (\phi\gamma)^{-\frac{2}{n-2}}$$

The dual symmetry links different metrics, different values of scalar field and different values of coupling constants. Let us, for instance, choose weakly changing $\phi \ll 1$ and also $\gamma \ll 1$. Then we arrive at the transformation which links the regimes of strong and weak gravitational field. Thus, contrary to the dual symmetries in string theory the conformal duality does not link the regimes of weak and strong coupling. However the conformal duality can be important in the study of quantum gravity effects in the regime of strong gravitational field in a given order of the loop expansion. Consider the one-loop effective action in the theory of quantum gravity with classical action (6). The effective action Γ can be derived on the basis of the background field method and Schwinger-DeWitt expansion. The last gives the local representation of Γ as an infinite power series in the proper time parameter s . Since this parameter is dimensional, the local $\text{Tr} a_k(x, x)$ coefficients have dimensions of $(\text{curvature})^k$, and then the conformal duality may help one to extract an information about the opposite strong gravity regime.

3. Since all the theories with conformal duality (5) differ from the most simple one (6) by the reparametrization of the scalar field only, we shall perform the calculations for this simple case, with an accuracy to the first order in curvature and to the corresponding second order in the derivatives of the scalar field. This approximation corresponds to the first a_1 coefficient of the Schwinger-DeWitt expansion. After some calculations we obtain [4]

$$\text{Tr} a_1(x, x) = \int d^n x \sqrt{-g} \{ A(\phi) g^{\mu\nu} \partial_\mu \phi \partial_\nu \phi + B(\phi)R + C(\phi) \} \quad (7)$$

where $B(\phi) = \frac{3n-5n^2-1}{12} + \frac{n\phi}{2\gamma(n-1)}$

$$\begin{aligned}
\mathcal{A}(\phi) &= \frac{1}{8(n-2)(n-1)(\gamma+\phi)^2} \left\{ \frac{\gamma^2}{\phi^2} (6n-4-2n^2) + \frac{\gamma}{\phi} (16-28n+4n^2+12n^3-4n^4) - \right. \\
&\quad \left. -26n+49n^2-30n^3+7n^4 + \frac{\phi}{\gamma} (16-28n+16n^2-2n^3) \right\} \\
\mathcal{C}(\phi) &= \frac{\lambda n \phi^{\frac{n-2}{2}}}{\gamma(n^2-3n+2)} (n\phi+\phi+\gamma) + \frac{n(-\gamma+\gamma n^2+\phi)(\lambda \phi^{\frac{n-2}{2}} + \gamma^{\frac{n-2}{2}} \tau)}{2\gamma(1-n)(\gamma+\phi)} \quad (8)
\end{aligned}$$

Unfortunately the physical analysis of the expression (8) is difficult because it contains a gauge fixing arbitrariness which can be fixed only on shell. In particular, the dependence of $\Gamma_1^{(1-loop)}$ on the gauge fixing parameters is proportional to the classical equations of motion. In our case only one combination of the functions $\mathcal{A}(\phi)$, $\mathcal{B}(\phi)$, $\mathcal{C}(\phi)$ is gauge independent.

To go on (classical) mass shell one needs the equations of motion for (6), from which follows

$$R = R(\phi) = \frac{n\tau}{2-n} \gamma^{\frac{n-2}{2}}, \quad \frac{1}{\phi^2} (\nabla\phi)^2 - \frac{2}{\phi^2} (\square\phi) = \frac{n}{n-1} \left(\tau \gamma^{\frac{n-2}{2}} - \lambda \phi^{\frac{n-2}{2}} \right) = S(\phi)$$

After some consideration (which we miss for the sake of brevity) one arrives at the following on-shell expression

$$a_1(x, x)_{ms} = \int d^4x \sqrt{-g} \left\{ \phi^{-1/2} \int_{\phi_0}^{\phi} d\phi \phi^{1/2} \mathcal{A}(\phi) S(\phi) + \mathcal{B}(\phi) R(\phi) + \mathcal{C}(\phi) \right\} \quad (9)$$

where the value of ϕ_0 is not relevant if ϕ and metric satisfy the equations of motion. An explicit form of the last expression can be found in [4].

The first approximation which we have explored here, shows the general structure of quantum corrections, but unfortunately it provides too little information because of the strong gauge-fixing arbitrariness. In particular, the on-shell result (9) doesn't allow one to restore the effective potential and thus to investigate in which way the quantum corrections change the expansion rate of the early Universe, or how they affect the black hole solutions in the vicinity of singularity. Indeed it should be interesting to use a more complicated methods of calculations, in order to evaluate the nonlocal part of the effective action, which can be free of the above arbitrariness.

4. Let us turn to the $n = 4$ and consider the possible form of the one-loop divergences in a conformal invariant theory (1), (2). The symmetric action $S_{B(\phi),\lambda}$ differs from the action of GR $S_{\gamma/\kappa^2,\lambda}$ in one respect. The first one has one more field variable that is compensated by an extra conformal-like symmetry. On classical level both theories are equivalent. However on quantum level the equivalence may be broken by anomaly which can violate the symmetry. We suppose that the one-loop divergences of $S_{B(\phi),\lambda}$ are not affected by anomaly and hence they can be derived in a field variables corresponding to the General Relativity with the cosmological constant. Since we suppose that the Jacobian of the corresponding conformal transformation is finite, the one-loop divergences in the theory $S_{B(\phi),\lambda}$ are given by the conformally transformed ones of the GR. The one-loop divergences in the last case have the form

$$\Gamma_{div}^{GR} = \frac{1}{n-4} \int d^4x \sqrt{-g} \{ a_1 C^2 + a_2 \hat{R}^2 + a_3 \hat{R} + a_4 \} \quad (10)$$

where C^2 is the square of the Weyl tensor. The values of $a_{1,2,3,4}$ depend on the gauge fixing parameters. One can easily find the form of the conformal transformation which links $S_{\gamma,\lambda}$ and $S_{B(\phi),\lambda}$, and so obtain the expression for the divergences of the last

$$\begin{aligned}
\Gamma_{div} &= \frac{1}{n-4} \int d^4x \sqrt{-g} \left\{ a_1 C^2 + a_2 \left[R - \frac{3(\square B)}{B} + \frac{3(\nabla B)^2}{2B^2} \right]^2 + \right. \\
&\quad \left. + \frac{a_3 B}{\gamma} \left[R - \frac{3(\square B)}{B} + \frac{3(\nabla B)^2}{2B^2} \right] + \frac{a_4 B^2}{\gamma^2} \right\} + \dots \quad (11)
\end{aligned}$$

Here the dots stand for the terms, proportional to the classical equations of motion, they indicate to the gauge fixing dependence of the counterterms. On shell the expressions (11), (10) coincide, and the mentioned dependence disappears.

(11) gives, as a by-product, the action of higher derivative conformal invariant (in $n = 4$) metric-dilaton action [5, 3]. Another generalization of the Weyl gravity has been formulated in [6] in the form, inspired by the anomaly induced effective action of gravity [7] (see also [8], [9] and [10]).

$$S_c = \int d^4x \sqrt{-g} \left\{ q(\varphi) C^2 + \frac{1}{2} p(\varphi) \varphi \Delta \varphi + f(\varphi) (\nabla \varphi)^4 \right\} \quad (12)$$

where $\Delta = \square^2 + 2R^{\mu\nu} \nabla_\mu \nabla_\nu - \frac{2}{3} R \square + \frac{1}{3} (\nabla^\mu R) \nabla_\mu$ and $(\nabla \varphi)^2 = \nabla^\mu \varphi \nabla_\mu \varphi$.

Three higher derivative theories (10), (11), (12) have equal number of degrees of freedom, but two last have an extra conformal symmetry. At the moment it is unclear whether (11) and (12) can be transformed into each other. One can only mention that while the conformal continuation of (11) to $n \neq 4$ is straightforward, the same procedure for (12) is very difficult and maybe impossible.

Author is grateful to I.G. Avramidi and M.S. Plyushchay for useful discussions and thanks for the warm hospitality the Departamento de Fisica Teorica en Universidad de Zaragoza and the Departamento de Fisica en Universidade Federal de Juiz de Fora, where this work has been started and completed.

References

- [1] S. Deser, Ann. Phys. **59**, 248, (1970).
- [2] J.D. Bekenstein, Ann.Phys. **82**,535,(1974).
- [3] I.L. Shapiro and H. Takata, Phys. Lett. **B361**,31 (1995); Rhys.Rev. **52D**, 2162 (1995).
- [4] I.L. Shapiro, Preprint *NF-DE - 03/96*, (08/08/96 - UFJF).
- [5] I. Antoniadis, J. Iliopoulos and T.N. Tomaras, Nucl.Phys. **B261** 157 (1985);
- [6] I.L. Shapiro and A.G. Jacksenaev, Phys.Lett. **324B**, 284 (1994).
- [7] R.Y. Reigert, Phys.Lett. **134B**, 56, (1984); E.S. Fradkin and A.A. Tseytlin, Phys.Lett. **134B**, 187 (1984).
- [8] I.L. Buchbinder, S.D. Odintsov and I.L. Shapiro, *Effective Action in Quantum Gravity* (IOP, Bristol, 1992).
- [9] I. Antoniadis and E. Mottola, Phys. Rev. **45D**, 2013 (1992).
- [10] I.L. Shapiro and G. Cognola, Phys.Rev. **51D** 2775 (1995); I.L. Shapiro, Mod. Phys. Lett. **9A**, 1985 (1994).

On the parameters of the Levi-Civita solution

A. Wang*, M. F. A. da Silva* and N. O. Santos**

*Departamento de Física Teórica - UERJ,

**Departamento de Astrofísica, CNPq-Observatório Nacional,

Author's internet address respectively:

a.wang@symbcomp.uerj.br, mfas@symbcomp.uerj.br and nos@on.br

The Levi-Civita solution is matched to a cylindrical shell of an anisotropic fluid. The fluid satisfies the energy conditions when the mass parameter σ is in the range $0 \leq \sigma \leq 1$. The mass per unity length of the shell is given implicitly in terms of σ , which has a finite maximum. The relevance of the results to the non-existence of horizons in the LC solution and to gauge cosmic strings is pointed out.

1 Introduction

The Levi-Civita metric for the static vacuum, cylindrically symmetric[1] is characterized by two parameters which we will call " σ " and " a ". One of them, σ , is generally associated with the energy density per unit length of the cylindrical source[2, 3, 5]. The other one, a , is associated with the topological defect of the cylindrical spacetimes[5, 6].

To interpret the parameters of the Levi-Civita metric, and then to comprehend the meaning of the cylindrical static vacuum spacetimes, it is useful to know the possible sources of these spacetimes. Some of them may be found in the literature[4, 7, 8, 9, 10, 11, 12, 13, 14]. Most of them refer to perfect fluids except one [7] which consider a particular case of an anisotropic fluid. To study the junction conditions which are necessary to match the matter's solutions to the Levi-Civita solution would give us a good way to interpret the physical meaning of these parameters. Some authors [3, 4, 5, 7] interpreted the parameter σ as the linear energy density of the source and found that $0 \leq \sigma \leq \frac{1}{4}$ [4] and $0 \leq \sigma < \frac{1}{2}$ [3]. Besides this results, Bonnor and Martins (1991) had concluded that $0 \leq \sigma \leq \frac{1}{4}$ based on geodesic arguments. The same conclusion had been found by another author [15].

So, until now, there is no any known source which admits the matching with the Levi-Civita spacetime to $\sigma \geq \frac{1}{2}$.

In the present paper we consider a cylindrical shell constituted by a completely anisotropic fluid dividing the vacuum spacetime in two regions: the interior, described by the Minkowski metric and the exterior, described by the Levi-Civita metric. The junction conditions on the shell allow us to find its energy density and its pressure in the principal directions. Imposing that the energy conditions must be satisfied by this solution we find $0 \leq \sigma \leq 1$. Thus we obtain the first matter solution which represents a source to Levi-Civita spacetime with $\sigma \geq \frac{1}{2}$. However this result must not to be considered in contradiction with the previous results since these considered particular fluids, i. e. perfect fluids. Instead of this, in our present work, we have the most general fluid constituting a shell of matter. Besides, we get the energy density per unit length of the shell and show that it only coincides with the parameter σ when $\sigma < \frac{1}{2}$.

The paper is organized as follows. In the next section we present the static cylindrical spacetime, including the three regions: the interior (Minkowski), the shell and the exterior spacetime (Levi-Civita). In section three the junction conditions are presented and applied on the shell. In section four we find the limits to the parameter σ in order that our solution satisfied the energy conditions. The energy density per unit length is given in section five. In the conclusion we sum up our main results.

2 The spacetime

The spacetime is divided into two regions: the interior V^- , with $0 \leq r \leq R$, to a cylindrical Σ shell of radius R centered along z ; and the exterior V^+ , with $R \leq r < \infty$. The shell is constituted by a static completely anisotropic

fluid.

The interior spacetime is described by the Minkowski metric [16], that is

$$ds_-^2 = \alpha^2 dt^2 - dr^2 - \beta^2 dz^2 - d\varphi^2, \quad (1)$$

where α and β are constants and the ranges of the coordinates t , z and φ are

$$-\infty < t < \infty, \quad -\infty < z < \infty, \quad 0 \leq \varphi \leq 2\pi, \quad (2)$$

with the hypersurfaces $\varphi = 0$ and $\varphi = 2\pi$ being identified. The coordinates are numbered

$$x^0 = t, \quad x^1 = r, \quad x^2 = z, \quad x^3 = \varphi. \quad (3)$$

The indexes $-$ and $+$ stand for the interior and exterior spacetimes, respectively, from now on.

The exterior spacetime is also formed by vacuum but the presence of the static shell suggests us that it should be described by the Levi-Civita metric, which is given by

$$ds_+^2 = f_0(r)dt^2 - dr^2 - f_2(r)dz^2 - f_3(r)d\varphi^2, \quad (4)$$

being

$$f_0 = [A(r-a)]^{4\sigma/A}, \quad (5)$$

$$f_2 = [A(r-a)]^{4\sigma(2\sigma-1)/A}, \quad (6)$$

$$f_3 = \frac{1}{C}[A(r-a)]^{2(1-2\sigma)/A}, \quad (7)$$

where

$$A = 4\sigma^2 - 2\sigma + 1.$$

The energy momentum tensor $T_{\mu\nu}^\pm$ to the interior and exterior regions are

$$T_{\mu\nu}^\pm = 0$$

We are supposing that the cylindrical shell is filled with a static anisotropic fluid. Hence the energy momentum tensor is given by

$$T_{\mu\nu} = \rho U_\mu U_\nu + p_z Z_\mu Z_\nu + p_\varphi \Phi_\mu \Phi_\nu, \quad (8)$$

where ρ is the energy density, p_z and p_φ are the principal stresses, and U_μ , Z_μ and Φ_μ are four vectors satisfying

$$U_\mu U^\mu = 1; \quad Z_\mu Z^\mu = -1; \quad \Phi_\mu \Phi^\mu = -1;$$

$$U_\mu Z^\mu = U_\mu \Phi^\mu = Z_\mu \Phi^\mu = 0.$$

The previous conditions and the general metric (4) provide

$$U^\mu = \left(\frac{1}{\sqrt{f_0}}, 0, 0, 0 \right)$$

$$Z^\mu = \left(0, 0, \frac{1}{\sqrt{f_2}}, 0 \right)$$

$$\Phi_\mu = \left(0, 0, 0, \frac{1}{\sqrt{f_3}} \right)$$

3 Junction conditions

The discontinuities surfaces can be characterized by boundary surfaces or by surface layers. In the first case we have a jump discontinuity in the energy density. In the second one the energy density becomes infinite, and this is the case of a shell. Surface layers are well represented by Dirac delta function.

The Lichnerowicz's formalism was modified [17], considering the distribution's theory, to obtain a new formalism which preserves the Bianchi identities.

The junction conditions obtained by Taub, to static metrics, can be summarized as follows.

$$(g_{\mu\nu}^+)_{\Sigma} - (g_{\mu\nu}^-)_{\Sigma} = 0, \quad (1)$$

$$(g_{\mu\nu,\lambda}^+)_{\Sigma} - (g_{\mu\nu,\lambda}^-)_{\Sigma} = K_{\lambda}\gamma^{\mu\nu}, \quad (2)$$

with K_{λ} being the normal vector to Σ surface, and given by

$$K_{\lambda} = \frac{\partial F(r)}{\partial x^{\lambda}} \quad (3)$$

where $F(r)$ is the function describing the surface Σ .

The energy momentum tensor of the shell is given by

$$\begin{aligned} T_{\mu\nu} = & \frac{1}{2} [\gamma^{\delta}_{\delta} (K^{\lambda} K_{\lambda} g_{\mu\nu} - K_{\mu} K_{\nu}) + (K_{\mu} \gamma^{\lambda}_{\nu} + K_{\nu} \gamma^{\lambda}_{\mu}) K_{\lambda}] \\ & - \frac{1}{2} [K^{\lambda} K_{\lambda} \gamma_{\mu\nu} + g_{\mu\nu} K_{\delta} K_{\lambda} \gamma^{\delta\lambda}]. \end{aligned} \quad (4)$$

From (1) and (2), with the metrics (1) and (4), we can get the tensor $\gamma_{\mu\nu}$. Substituting $\gamma_{\mu\nu}$ into (3.5) we are able to know the energy momentum tensor and the pressures which must have the shell in order to permit the matching with the Minkowski interior spacetime and the Levi-Civita exterior spacetime. This procedure provides

$$\rho = \frac{2\sigma(1-2\sigma)(r_0+a) + 4\sigma^2 r_0 - a}{8\pi A r_0 (r_0 - a)}, \quad (5)$$

$$p_z = \frac{2\sigma(1-2\sigma)(r_0-a) + a}{8\pi A r_0 (r_0 - a)}, \quad (6)$$

$$p_{\varphi} = \frac{4\sigma^2}{8\pi A (r_0 - a)}, \quad (7)$$

where

$$r_0 = \frac{1}{C} [A(r_0 - a)]^{\frac{1-\sigma}{\sigma}}, \quad (8)$$

and $r_0 - a > 0$ and $r_0 > 0$.

Here we can see that if $\sigma = 0$, which should reduce the Levi-Civita metric in the string metric, we have the string momentum energy tensor as expected, i. e.

$$\rho = -p_z = \frac{-a}{r_0(r_0 - a)} = \frac{1}{r_0} \left(1 - \frac{1}{C}\right); \quad p_{\varphi} = 0.$$

Equation (8) shows us still that if we put $a = 0$, the parameter C have to be equal the unit, meaning that we cannot have a string in $a = 0$.

4 The energy conditions

The energy momentum tensor should satisfy certain inequalities which are physically reasonable. They constituted the energy conditions [18].

The first of them is the *weak energy condition*. For fields with non-zero rest mass it holds if

$$\rho \geq 0, \quad (1)$$

$$\rho + p_i \geq 0. \quad (2)$$

with $i = 1, 2, 3$.

The second one is the *dominant energy condition*. For that same fields it imposes that

$$\rho \geq 0, \quad (3)$$

$$-\rho \leq p_i \leq \rho. \quad (4)$$

This condition is the weak energy condition with the additional imposing that the pressure, in any direction, should not exceed the energy density. In fact, to limit the sound velocity v_s to be less than or equal to 1 (because no signal can propagate faster than light) implies $p_i \leq \rho$.

Finally we have the *strong energy condition*. It is satisfied if

$$\rho + p_i \geq 0, \quad (5)$$

$$\rho + \sum_{i=1}^3 p_i \geq 0. \quad (6)$$

This condition is more restrictive than the weak energy condition.

Using these energy conditions we find that our solution (5)–(7) is physically reasonable only if $0 \leq \sigma \leq 1$.

5 The energy density per unit length

Here we consider two different definitions of the energy density: the first one by Marder and the second one by Israel. The energy density per unit length μ as defined by Marder (1958), is given, in the case of a cylindrical shell, by

$$\mu = \int_S \rho \delta(r - r_0) \sqrt{g_{(2)}} dr d\varphi, \quad (1)$$

because we have $r = \text{const.} = r_0$. The $\delta(x)$ is the delta Dirac function.

Using the metric (1) on the surface Σ , we get $\sqrt{g_{(2)}} = R$. Substituting this and ρ given by (6) in the equation (1) we have

$$\mu = \frac{2\sigma(1 - 2\sigma)(r_0 + a) + 4\sigma^2 r_0 - a}{4A(r_0 - a)}. \quad (2)$$

If we consider $\sigma = 0$, which transforms the Levi-Civita metric (2) in the string metric, and considering yet equation (3.10) we have that the linear energy density is

$$\mu = \frac{1}{4} \left(1 - \frac{1}{C} \right), \quad (3)$$

which represents the linear energy density of the string [6]. In the particular case where $a = 0$, we have

$$\mu = \frac{\sigma}{2(4\sigma^2 - 2\sigma + 1)}. \quad (4)$$

The energy density defined by Israel (1977) furnishes

$$\mu = \int (\rho + p_z + p_\varphi) \delta(r - r_0) \sqrt{g} dr d\varphi = \sigma. \quad (5)$$

Clearly, in the present case Marder's definition does not give the correct Newtonian limit, while Israel's does.

6 Conclusion

In this paper, we have shown that the Levi-Civita solution with $0 \leq \sigma \leq 1$ can be produced by physically realistic sources, and the mass per unity length of the cylinder, μ , depends on the parameter σ , and is given explicitly by equations (4) and (5). Equation (4) shows that as σ increases, μ is monotonically increasing until $\sigma = 1/2$, where it reaches its maximum $\mu = 1/4$. This could explain the fact why in the Levi-Civita solution no horizons exist. However, it shows that $\mu \approx \sigma/2$ if $0 \leq \sigma \ll 1$, which is inconsistent with its Newtonian limit. The other definition of energy density, equation (5), reproduces the Newtonian limit but, on the other hand, it does not include the string solution as a particular case.

References

- [1] Levi-Civita, T. (1917) *Rend. Acc. Lincei* **26**, 307.
- [2] Bonnor, W. B. and Martins, M. A. P. (1991) *Class. Quantum Grav.* **8**, 727.
- [3] Bonnor, W. B. and Davidson, W. (1992) *Class. Quantum Grav.* **9**, 2065.
- [4] da Silva, M. F. A., Herrera, L., Paiva, F. M. and Santos, N. O. (1995a) *J. Math Phys.* **36**, 3625.
- [5] da Silva, M. F. A., Herrera, L., Paiva, F. M. and Santos, N. O. (1995b) *Gen. Rel. Grav.* **27**, 859.
- [6] Linet, B. (1985) *Gen. Rel. Grav.* **17**, 1109.
- [7] Marder, L. (1958) *Proc. Roy. Soc. Lond., Ser. A*, **244**, 524.
- [8] Raychaudhuri, A. K. and Som, M. M. (1962) *Proc. Camb. Phil. Soc.* **58**, 338.
- [9] Teixeira, A. F. F., and Som, M. M. (1974) *Il Nuovo Cimento* **B21**, 64.
- [10] Evans, A. B. (1977) *J. Phys. A:Math. Gen.* , 1303.
- [11] Teixeira, A. F. F., Wolk, I. and Som, M. M. (1977) *Il Nuovo Cimento* **B41**, 387.
- [12] Wainwright, J., Ince, W. C. W. and Marshman, B. J. (1979) *Gen. Rel. Grav.* **10**, 259.
- [13] Bronnikov, K. A. (1979) *J. Phys. A:Math. Gen.* **12**, 201.
- [14] Davidson, W. (1990) *Gen. Rel. Grav.* **22**, 553.
- [15] Lathrop, J. D. and Orsenc, M. S. (1980) *J. Math. Phys.* **21**, 152.
- [16] Apostolatos, T. A. and Thorne, K. S. (1992) *Phys. Rev. D* **46**, 2435.
- [17] Taub, A. H. (1980) *J. Math. Phys.* **21**, 1423.
- [18] Hawking, S. W. and Ellis, G. F. R. (1973) *"The large scale structure of spacetime"* (Cambridge University Press - Cambridge - UK).
- [19] Israel, W. (1977) *Phys. Rev. D* **15**, 935.

Formalismo do Tempo Extrínscico para o Buraco Negro Euclidiano em uma Caixa

G. Oliveira-Neto *

*DCP, CBPF, R. Dr. Xavier Sigaud 150, Urca,
CEP 22290-180, Rio de Janeiro, Brasil.*

Neste trabalho nós retornamos ao problema de buracos negros de Schwarzschild Euclidianos em equilíbrio com a radiação, sobre as condições do *ensemble* canônico de estatística. Desta vez nós usamos o formalismo do tempo extrínscico, desenvolvido por K. Kuchař, para selecionarmos o correto conjunto de variáveis dinâmicas. Com esse conjunto de variáveis canônicas, $\{\tilde{R}, P_{\tilde{R}}, M, P_M\}$, e a proposta de J. York, Jr., para os termos de fronteira e 'horizonte', nós calculamos uma ação total, consistente classicamente, para o buraco negro Euclidiano. Nós mostramos explicitamente que a função de partição a *zero - loop* derivada dessa ação total é idêntica a uma que já havia sido calculada na literatura desta área.

1 Motivações.

Neste trabalho vamos estudar, a nível quântico, a termodinâmica do sistema composto por um Buraco Negro de Schwarzschild Euclidiano (BNSE) e radiação, sobre as condições do *ensemble* canônico de mecânica estatística [1].

A relevância do *ensemble* canônico, para esse sistema, foi demonstrada por J. York, Jr. [2]. Ele mostrou que juntamente com a configuração instável, existe uma outra meta ou localmente estável.

Estudaremos a termodinâmica desse sistema com a ajuda do Formalismo do Tempo Extrínscico (FTE), para sistemas compostos por buracos negros, introduzido por K. Kuchař [3].

Essa proposta de Kuchař, tem por objetivo identificar, dentro do conjunto de variáveis canônicas da teoria, uma variável temporal apropriada e seu momento canonicamente conjugado.

2 Sistema a ser estudado e objetivos.

Escreveremos uma ação consistente para a configuração de equilíbrio meta-estável do sistema composto de um BNSE e radiação.

O sistema se encontra imerso em uma caixa ou cavidade com somente uma fronteira, a qual tem uma topologia $S^2 \times S$. De acordo com as propriedades do *ensemble* canônico, adaptadas para a presente situação, o volume da fronteira é fixo e a caixa está em contato com um reservatório de calor que mantém a temperatura da fronteira fixa.

Essa ação será escrita em termos de novas variáveis canônicas $\{\tilde{R}, P_{\tilde{R}}, M, P_M\}$, introduzidas com a ajuda do FTE.

A consistência dessa ação será demonstrada, após calcularmos a função de partição à *zero - loop*, e notarmos que esta é idêntica a expressão já conhecida na literatura.

3 Formalismo canonico em termos das variaveis R, P_R, Γ, P_Γ .

Cometemos escrevendo, em termos do formalismo ADM, o ansatz mais geral para o espaço - tempo Euclidiano, esfericamente simétrico, sendo folheado por hipersuperfícies tri - dimensionais Σ , caracterizadas por valores constantes de r :

*Email: n04c7@cat.cbpf.br

$$ds^2 = [N^2(r, t) + \Gamma^2(r, t)(N'(r, t))^2] dr^2 + 2\Gamma^2(r, t) N'(r, t) dr dt + \Gamma^2(r, t) dt^2 + R^2(r, t) d\Omega^2 \quad (1)$$

onde

$$0 \leq r \leq r_b \quad ; \quad 0 \leq t \leq p; \quad (2)$$

nós estamos usando um sistema de unidades em que todas as constantes físicas são feitas iguais a identidade ; e $d\Omega^2$ é o elemento de linha da superfície esférica, bi-dimensional, de raio unitário.

O valor do parâmetro r , $r = r_b$, localiza a fronteira da caixa e o valor, $r = 0$, é uma superfície esférica bi-dimensional e uma singularidade do sistema de coordenadas.

A dependência nos parâmetros (r, t) , dá uma liberdade maior na descrição do sistema e é uma exigência do FTE [3].

A partir do ansatz (1), podemos escrever, seguindo as instruções do formalismo ADM [1], a ação das hipersuperfícies I_Σ , em sua forma Hamiltoniana:

$$I_\Sigma[\Gamma, R, P_\Gamma, P_R, N, N'] = \int_0^{2\pi} dt \int_0^{r_b} dr (P_\Gamma \Gamma' + P_R R' - NH - N' H_t) \quad (3)$$

onde: ' é a derivada em relação a r , e o ponto é a derivada em relação a t ;

$$P_\Gamma = -\frac{R}{N} (R' - N' \dot{R}); \quad (4)$$

$$P_R = -\frac{1}{N} \{ \Gamma (R' - N' \dot{R}) + R [\Gamma' - (\Gamma N')'] \}; \quad (5)$$

$$H = \frac{\Gamma P_\Gamma^2}{2R^2} - \frac{P_R P_\Gamma}{R} - \frac{R \ddot{R}}{\Gamma} + \frac{R \dot{R} \dot{\Gamma}}{\Gamma^2} - \frac{\dot{R}^2}{2\Gamma} + \frac{\Gamma}{2}; \quad (6)$$

$$H_t = P_R \dot{R} - \Gamma \dot{P}_\Gamma. \quad (7)$$

O funcional H é a superhamiltoniana e H_t é o supermomentum.

Uma vez que temos uma fronteira, devemos incluir um termo, que não havia sido considerado no formalismo ADM [4], do tipo [5]:

$$-\frac{1}{8\pi} \int_{\Sigma_{r_b}} K_0 \sqrt{h} d^3x, \quad (8)$$

onde K_0 é a curvatura extrínseca para o espaço Euclidiano plano, calculada na fronteira.

Uma vez que $r = 0$ não é uma fronteira, devemos retirar um termo, que já havia sido considerado no formalismo ADM [4], do tipo:

$$-\frac{1}{8\pi} \int_{\Sigma_{r_0}} K \sqrt{h} d^3x. \quad (9)$$

Desta forma, a ação total I , em sua forma Hamiltoniana, fica dada por:

$$I = \int_0^{2\pi} dt \left\{ \int_0^{r_b} dr (P_\Gamma \Gamma' + P_R R' - NH - N' H_t) - \frac{1}{2} R_0^2 + \Gamma_b R_b \right\}. \quad (10)$$

Pode-se mostrar que essa ação (10) é consistente, no sentido que variações de I em relação as variáveis canônicas $\{R, P_R, \Gamma, P_\Gamma\}$ e (N, N') , levam as equações de movimento e vínculos, nada mais.

4 Formalismo canonico em termos das variáveis $\tilde{R}, P_{\tilde{R}}, M, P_M$.

Baseados no trabalho de Kuchař, nós aplicamos as seguintes transformações nas variáveis canônicas:

$$\tilde{R} = R \quad (11)$$

$$M = -\frac{1}{2}R^{-1}P_{\tilde{R}}^2 - \frac{1}{2}R\dot{R}^2\Gamma^{-2} + \frac{1}{2}R \quad (12)$$

$$P_M = R^{-1}F^{-1}\Gamma P_{\tilde{R}} \quad (13)$$

$$P_{\tilde{R}} = P_R - \frac{1}{2}R^{-1}\Gamma P_{\tilde{R}} - \frac{1}{2}R^{-1}F^{-1}\Gamma P_{\tilde{R}} \\ - R^{-1}F^{-1}\Gamma^{-2}[(\Gamma P_{\tilde{R}})R\dot{R} - \Gamma P_{\tilde{R}}(R\dot{R})] \quad (14)$$

onde

$$F = \left(\frac{P_{\tilde{R}}}{R}\right)^2 + \left(\frac{\dot{R}}{\Gamma}\right)^2 \quad (15)$$

Usando as transformações (11) - (15), podemos reescrever a ação total (10), da seguinte forma:

$$I = \int_0^{2\pi} dt \left\{ \int_0^{r_b} dr (P_M M' + P_{\tilde{R}} \tilde{R}' - NH - N' H_t) \right. \\ \left. - \frac{1}{2} \tilde{R}_0^2 - P_{M_b} \tilde{F}_b^{1/2} \tilde{R}_b + P_{M_b} \tilde{F}_b \tilde{R}_b \right\}, \quad (16)$$

onde

$$\tilde{F}(\tilde{R}) = 1 - \frac{2M}{\tilde{R}}, \quad (17)$$

$$H_t = \dot{\tilde{R}} P_{\tilde{R}} + \dot{M} P_M, \quad (18)$$

$$H = \frac{\tilde{F}^{-1} \dot{\tilde{R}} M - \tilde{F} P_M P_{\tilde{R}}}{\sqrt{\tilde{F}^{-1} \dot{\tilde{R}}^2 + P_M^2 \tilde{F}}}. \quad (19)$$

Pode-se mostrar a consistência de (16), no mesmo sentido do caso anterior (10), desta vez em termos de $\{\tilde{R}, P_{\tilde{R}}, M; P_M\}$ e (N, N') .

5 Função de partição a 'zero-loop'.

Vamos escrever abaixo quais são as condições necessárias para obtermos a função de partição a zero-loop e os resultados dessas condições, para o nosso modelo, até o nosso resultado final.

- (i) Restrição ao caso em que não há dependência em t .
- (ii) Imposição dos vínculos (18) e (19), levando aos resultados:

$$\Gamma(r) = \tilde{F}^{1/2}(r); \quad P_M = -1; \quad M = \text{constante}. \quad (20)$$

- (iii) Substituição dos resultados obtidos até agora na ação (16) e obtenção da ação reduzida I^* :

$$I^* = \beta \tilde{R}_b (1 - \sqrt{1 - \tilde{R}_0/\tilde{R}_b}) - \pi \tilde{R}_0^2 \quad (21)$$

onde β , é o inverso da temperature (T) na fronteira r_b , e é dado por:

$$\beta = \frac{1}{T} = 2\pi\Gamma_b \quad (22)$$

- (iv) Determinação do valor do raio do 'horizonte' \tilde{R}_0^E , que extremiza a ação reduzida I^* (21). Substituição desse valor \tilde{R}_0^E em I^* , levando a nova ação que chamamos de \tilde{I} .

(v) Com \bar{I} , escrevemos a função de partição à zero - loop Z_0 :

$$Z_0 = \exp\{-\beta\bar{R}_b(1 - \sqrt{1 - \bar{R}_0^E(\beta, \bar{R}_b)/\bar{R}_b}) + \pi\bar{R}_0^E(\beta, \bar{R}_b)\} \quad (23)$$

Essa quantidade (23), é idêntica a função de partição à zero-loop dada em [6].

6 Conclusões e Perspectivas.

O nosso resultado principal é a ação total (16).

Demonstramos a consistência dessa ação ao calcularmos a função de partição à zero - loop Z_0 (23), e verificarmos que o valor encontrado, está de acordo com o valor já obtido por outros métodos.

Podemos usar essa ação para calcular Z em ordens superiores. Em particular, pode-se verificar se a previsão qualitativa de S. W. Hawking para Z à um - loop (Z_1), é correta:

$$\log Z_1 = \frac{4\pi^5 \bar{R}_b^3}{135\beta^3}. \quad (24)$$

Uma outra aplicação deste formalismo, se daria ao estudarmos o sistema composto por buracos negros Euclidianos de Reissner - Nordström e radiação sobre as condições do ensemble canônico de mecânica estatística.

AGRADECIMENTOS.

Gostaria de agradecer Ian Moss, Jorma Louko e J. A. Helajel - Neto por proveitosas discussões e a CAPES e a FAPERJ pela indispensável ajuda financeira.

References

- [1] G. Oliveira-Neto, *Phys. Rev. D* **53**, 1977 (1996)
- [2] J. W. York, Jr., *Phys. Rev. D* **33**, 2092 (1986)
- [3] K. V. Kuchař, *Phys. Rev. D* **50**, 3961 (1994)
- [4] C. W. Misner, K. S. Thorne & J. A. Wheeler, *Gravitation*, (San Francisco: Freeman) (1973)
- [5] S. W. Hawking, in *General Relativity - An Einstein Centenary Survey*, edited by S. W. Hawking & W. Israel (Cambridge: Cambridge University Press), 746 (1979)
G. W. Gibbons & S. W. Hawking, *Phys. Rev. D* **15**, 2752 (1977)
- [6] J. D. Brown, G. L. Comer, E. A. Martinez, J. Melmed, B. F. Whiting and J. W. York, Jr., *Class. Quantum Grav.* **7**, 1433 (1990)

Comparative Study Between the Thermodynamics of the 2-Dimensional Black Hole in the Teitelboim-Jackiw Theory and the 4-Dimensional Schwarzschild Black Hole

José P. S. Lemos

*Departamento de Astrofísica, Observatório Nacional-CNPq,
Rua General José Cristino 77, 20921 Rio de Janeiro, Brasil*

Hawking's and York's prescriptions for finding the temperature and other thermodynamic quantities of a static black hole are briefly reviewed and applied to the Schwarzschild black hole. Then, we exploit York's formalism to study the thermodynamics of the black hole in the two-dimensional Teitelboim-Jackiw theory.

1. Thermodynamics of the Schwarzschild black hole

Analysis of the behavior of quantum fields in a black hole (BH) background has shown that BHs steadily emit thermal radiation at a given temperature T [1]. Although physically sounding, the original calculation was untidy, and other cleaner ways to obtain and interpret this temperature were devised by Hawking himself [2]. Hawking's prescription for the computation of the temperature T of a static BH, consists essentially of four steps, (i) write the BH metric in static (Schwarzschild) coordinates, (ii) Euclideanize the time $t \rightarrow it$ and periodically identify t , (iii) adjust the period of t , $2\pi\alpha$ say, to remove conical singularities, and (iv) find the temperature by putting the inverse temperature β precisely equal to this period at infinity, $\beta = 2\pi\alpha$ and then $T = \frac{1}{\beta}$.

This prescription comes from a formal calculation of the partition function $Z(\beta)$ as a functional integral over all Euclidean geometries g with period β and Euclidean action $I[g]$. In more detail: the probability that a thermodynamic system is in a state of energy E_n is proportional to $e^{-\beta E_n}$. The partition function is then defined as $Z(\beta) = \sum_n e^{-\beta E_n}$, and for a quantum mechanical system this can be written as $Z(\beta) = \sum_n \langle g_n | e^{-\beta H} | g_n \rangle$ where H is the Hamiltonian and $\langle g_n | e^{-\beta H} | g_n \rangle$ gives the expectation value of $e^{-\beta H}$ on a state g_n of the field g . Now, from the work of Feynmann [3] one can also write Z as $Z = \int D[g] e^{-I[g]}$, a functional integral over all fields g . In the Lorentzian formulation the integral is a propagator, but Feynmann understood that by Euclideanizing the time, $t \rightarrow \beta = it$, one could have a well defined statistical mechanics formalism. Hawking extended this idea to include the gravitational field itself. By starting with a BH geometry g , such as the Euclidean-Schwarzschild metric, one obtains through the partition function, an appropriate thermodynamics for the BH.

How does this prescription work for the Schwarzschild BH with mass M ? First one writes the metric in the Euclideanized form $ds^2 = N^2(r)dt^2 + \frac{dr^2}{1-\frac{2M}{r}} + r^2 d\Omega^2$ with $0 \leq t < 2\pi$ and $2M \leq r < \infty$. Then, one insures that the metric has no conical singularities in the (r, t) plane, i.e., near $r \sim 2M$ one imposes $2\pi N(r) \sim 8\pi \sqrt{1 - \frac{2M}{r}}$. Then, by fixing the period at infinity to the inverse temperature, i.e., equating $2\pi N(\infty) = \beta$, one finds $T = \frac{1}{8\pi M}$.

Now, the Euclidean action is $I_E = -\frac{1}{16\pi} \int_V d^4x \sqrt{g} R - \frac{1}{8\pi} \int_{\partial V} d^3x \sqrt{h} (K - K^0)$, where g is the determinant of the metric, R is the Ricci scalar, h is the induced metric on the boundary, K is the extrinsic curvature and K^0 is a term necessary to choose the background (the zero point energy). Putting in the appropriate quantities from the Schwarzschild metric into this action (recalling that $R = 0$ and thus the integral over the volume does not contribute) one obtains $I(M) = M\beta - 4\pi M^2$, yielding in turn $Z = \int dM e^{-I(M)}$. The extremum of the

action satisfies $\partial I/\partial M = 0$, which gives $\frac{\beta}{8\pi} = M$, i.e., $T = 1/8\pi M$ as required. Then the partition function is classically approximated by $Z(\beta) = e^{-I(M_{extremum})} = e^{-I(\frac{\beta}{8\pi})}$. Since Z and the Helmholtz free energy F are related, $-\ln Z = I = \beta F$, one can obtain other physical quantities. The expectation value of the energy of the system is $\langle E \rangle \equiv \frac{\partial I}{\partial \beta} = \frac{\beta}{8\pi} = M$, and the entropy is $S \equiv \beta \frac{\partial I}{\partial \beta} - I = 4\pi M^2 = \frac{A}{4}$ (where A is the area of the BH), closing the scheme. However, there is a problem. Indeed, $\frac{\partial^2 I}{\partial M^2} < 0$ at the extremum $M = \frac{\beta}{8\pi}$, and therefore the Euclidean BH does not dominate the integral. The calculations, although giving the write results are physically incorrect. This BH, in fact, makes an imaginary contribution to the partition function and should be interpreted as an instanton that may govern black hole nucleation [4], i.e., it gives the probability of a spontaneous transition through a quantum fluctuation from hot flat space (space filled with gravitons and other massless fields) to a BH.

In order to circumvent these problems York [5] defined a canonical ensemble for the BH and hot gravity in equilibrium. The ensemble is defined by a heat reservoir with radius R where a temperature $T(R)$ is kept fixed. York's prescription for the computation of the temperature says that steps (iii) and (iv) above should be replaced by (iii') adjust the mass M to remove conical singularities, and (iv') fix the proper period at R , to β . Then, one finds two values for the mass M . The larger M is the mass of the stable BH. The smaller M gives the mass of the instanton, i.e., of the unstable BH that can be created through quantum tunneling and subsequently decay thermodynamically to the stable BH. Let us see, how it works. Since the boundary is at R the range of the radial coordinate is $2M \leq r \leq R$. Then by (iv') the inverse temperature is fixed to $2\pi N(r) = \beta$ yielding (after removing the conical singularities) $T = \frac{1}{8\pi M \sqrt{1 - \frac{2M}{R}}}$. Now, putting the appropriate quantities into the Euclidean action, one gets the following reduced action $I(M) = R\beta \left(1 - \sqrt{1 - \frac{2M}{R}}\right) - 4\pi M^2$. The extrema of this action, $\frac{\partial I}{\partial M} = 0$, are given by $\beta = 8\pi M \sqrt{1 - \frac{2M}{R}}$. There are two solutions M_1 and M_2 , with $M_1 < M_2$. But now, $\frac{\partial^2 I}{\partial M^2} < 0$ at the extremum M_1 ($M_1 \rightarrow \frac{\beta}{8\pi}$ as $R \rightarrow \infty$), and $\frac{\partial^2 I}{\partial M^2} > 0$ at M_2 ($M_2 \rightarrow \frac{R}{2} - \infty$ as $R \rightarrow \infty$). Thus, M_2 can be used to approximate the partition function, $Z(\beta) = e^{-I(M_2)}$. Then one obtains, $\langle E \rangle = R \left(1 - \sqrt{1 - \frac{2M_2}{R}}\right)$ and $S = 4\pi M^2 = \frac{A}{4}$. In this approach, one sees that the temperature of the BH is Hawking's temperature $T = \frac{1}{8\pi M}$ multiplied by Tolman's redshift factor $\frac{1}{\sqrt{1 - \frac{2M}{R}}}$. One can ask in what sense is the temperature of the BH equal to $\frac{1}{8\pi M}$ as yielded by the original approach which made use of quantum field theory in a BH geometry. The idea [6] is that Hawking's temperature corresponds to drilling a small hole in the reservoir at R and letting some radiation escape to infinity. In this case, the Tolman redshift factor goes to unity yielding the Hawking temperature. If the hole is large enough, so that its thermodynamic equilibrium changes very slowly, one can imagine the complete withdrawal of the reservoir, and identify the BH temperature at infinity as $T = \frac{1}{8\pi M}$.

2. Thermodynamics of the two-dimensional black hole in the Teitelboim-Jackiw theory

The analysis of thermodynamic processes involving BHs has first appeared in four dimensional (4D) general relativity. It was then extended to lower dimensions and other theories, following indications that these are important and useful to study. Two dimensions (2D) has been of particular interest after a black hole in string theory has appeared [7, 8]. Hawking radiation and thermodynamics of this black hole has been analysed by several authors (e.g., [9]). Another 2D theory which has been studied in some detail is the Teitelboim-Jackiw theory [10, 11]. Although in this theory the curvature is constant and negative, it has a black hole solution [12, 13, 15, 16, 17]. The existence of a black hole implies a non-trivial causal structure which in turn generates interesting non-trivial thermodynamics. Hawking radiation of this black hole has been analysed in [15], and thermodynamics of a black hole in versions of the theory with electromagnetic and scalar fields have been studied [18, 19]. Here we study the black hole of the original Teitelboim-Jackiw theory using York's formalism [5, 20]. For an extended detailed study see [21].

In the Teitelboim-Jackiw 2D theory the action is $I = \frac{1}{2\pi} \int d^2x \sqrt{-g} e^\Phi (R - 2\Lambda) + I_B$, where g is the determinant of the metric, R is the curvature scalar, Λ is the cosmological constant (sometimes written as $\Lambda = -2\lambda^2$, although here we put $\alpha^2 \equiv -\Lambda$), and I_B is a boundary term to specify later. This action has got a black hole solution given

by $ds^2 = -(\alpha^2 r^2 - b)dt^2 + \frac{dr^2}{\alpha^2 r^2 - b}$, $e^\Phi = c\alpha r$ where b and c are positive constants. The maximal analytical extension of this solution is given in figure 1..

The curvature scalar of the solution is $R = -\alpha^2$ which is a constant. Therefore, spacetime has constant negative curvature and, in principle, is isomorphic to the anti-de Sitter (ADS) spacetime. However, one can indeed interpret this solution as a BH solution by truncating spacetime at $r = 0$. The reason for this cut off comes from the interpretation of this 2D theory either as a theory derived from dimensional reduction of (a) a low energy 4D action of heterotic string theory, with e^Φ representing the string coupling [14], or (b) 3D general relativity with e^Φ representing the circumference radius [13]. In either case $e^\Phi = c\alpha r$ has to be positive, and the Penrose diagram is simply the $r \geq 0$ square of figure 1.. Thus, the dilaton sets new boundary conditions, making two locally indistinguishable solutions, namely the BH and ADS spacetimes, topologically and globally different. Yet another interpretation can be given. One can notice that the BH metric represents a portion of the 2D anti-de Sitter spacetime in accelerated coordinates. Indeed, a stationary observer with $r = \text{constant}$ has four acceleration a^μ with magnitude $a = \sqrt{a^\mu a_\mu} = \frac{\alpha^2 r}{\sqrt{\alpha^2 r^2 - b}}$ with $b > 0$. The radius $r = \frac{\sqrt{b}}{\alpha}$, where the acceleration is infinite, corresponds to the trajectory of a light ray. Thus, observers held at $r = \text{constant}$ see this light ray as a horizon, they will never see events beyond this ray. They are accelerated observers and can see only a portion of anti-de Sitter spacetime. In this sense, region II in figure 1, can be considered a black hole for region I accelerated observers. The mass of the black hole can be calculated by the standard procedures [17] and is given by, $M = \frac{\alpha c}{2} b$. $M = 0$ gives the extremal black hole.

The Euclidean action of the theory is $I_E = -\frac{1}{2} \int_V d^2x \sqrt{g} e^\Phi (R + \alpha^2) - \int_{\partial V} d\rho \sqrt{h} e^\Phi (K - K^0)$, where the surface term is required to make the variational procedure self-consistent, which is important in analysing the thermodynamics, and the other quantities have been defined previously. The equations of motion are, $e^\Phi T_{ab} \equiv \frac{1}{2} D_a \Phi D_b \Phi + \frac{1}{2} D_a D_b \Phi - \frac{1}{2} g_{ab} D_c D^c \Phi + \frac{1}{2} g_{ab} D_c \Phi D^c \Phi - \frac{1}{2} g_{ab} \alpha^2 = 0$. Then the T_{00} constraint, $T_{00} = 0$, gives upon integration, $P\Phi'^2 - \alpha^2 = -\alpha^2 b e^{-2\Phi}$, where we have chosen the constant of integration as $-\alpha^2 b$ appropriately.

Then, integrating the action and using the constraints and boundary conditions we find,

$$I(h^{-1}) = -(G^{-1})\beta e^{\Phi_B} \alpha \sqrt{1 - e^{2(\Phi_H - \Phi_B)}} - (h^{-1})2\pi e^{\Phi_H} + (G^{-1})\beta e^{\Phi_B} \alpha,$$

where Φ_H is the value of Φ at the horizon and $I_0 \equiv \beta e^{\Phi_B} \alpha$ was chosen appropriately. We have put back Newton's constant G and Planck's constant h (still putting Boltzmann's constant and the velocity of the light equal to one). Note that in 2D we use the following units for the constants: $[G] = LM^{-1}T^{-1}$ and $[h] = MT^{-1}$. As in 4D [20], one sees that a quantum term has appeared in the action, namely the term $2\pi e^\Phi$, which is associated with the entropy of the system. The above equation is thus the reduced action $I = I(\beta, \Phi_B, \Phi_H)$ which yields the important thermodynamic quantities.

To find the temperature we have to obtain the stationary point of the reduced action with respect to Φ_H . This gives, $\frac{2M}{\alpha c} = \alpha^2 r_H^2 = \frac{\alpha^2 r_B^2}{1 + \frac{\alpha^2 r_B^2}{4\pi T}}$, where $\beta = \frac{1}{T}$. Thus as $T \rightarrow 0$ we have $M \rightarrow 0$. As $T \rightarrow \infty$ we have a maximum mass $M_{\max} = \frac{1}{2} \alpha^3 c r_B^2$ for the BH in the thermal bath. That is, for a given r_B the mass of the hole cannot be larger than the one which gives a horizon radius equal to r_B . There is nothing like the instanton solution of the Schwarzschild bath in 4D.

The entropy is given by $S_H = \beta \left(\frac{\partial I}{\partial \beta} \right)_{\Phi_B} - I = 2\pi e^{\Phi_H} = 2\pi \sqrt{\frac{2M}{\alpha c}}$. It is interesting to note that this functional dependence on the dilaton is the same for all black holes having a simple 2D Brans-Dicke action [22]. This is analogous to the 4D case, where the entropy is equal to $\frac{A}{4}$. Note also that the extreme case ($M = 0$) has zero entropy.

The thermodynamic energy E is defined by $E \equiv \left(\frac{\partial I}{\partial \beta} \right)_{\Phi_B} = c\alpha^2 r_B (1 - \sqrt{1 - \frac{r_H^2}{r_B^2}})$. We see here that the zero point was chosen so that when there is no mass ($r_H = 0$) the thermal energy is zero. Since $r_H^2 = \frac{2M}{\alpha^2 c}$ we can invert expression for the energy to yield $\frac{1}{\alpha^2 c} M = E - \frac{1}{\alpha^2 c} \frac{E^2}{2r_B}$, which relates the ADM mass and the thermal energy. The ADM mass (the mass at infinity) is equal to the thermal energy times the length (in intrinsic units) of the reservoir minus a self-energy thermal term. This expression is the closest one can get to the Schwarzschild expression found in [5] for the Schwarzschild mass, i.e., $M = E - \frac{1}{2} \frac{E^2}{r_B}$.

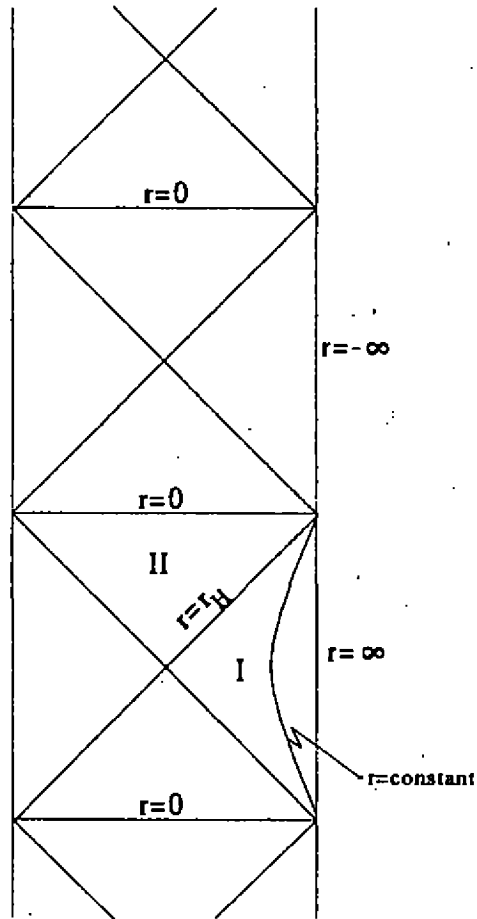


Figure 1.: The Penrose diagram for the non-singular black hole.

Now, the Euler relation for this thermodynamic system can be found to be $E = TS - pr_B$, where p is the linear pressure defined by $p = -\frac{\partial E}{\partial r_B}$. Upon scaling, $r_B \rightarrow lr_B$ and $r_H \rightarrow lr_H$ or $(S \rightarrow lS)$ one has $E \rightarrow lE$, showing that E is homogeneous of degree 1 in S and r_B . This is in contrast with the Schwarzschild solution where E is homogeneous of degree one-half in S and the A .

To analyse thermodynamic stability we find the heat capacity, $C_{r_B} \equiv T \left(\frac{\partial S}{\partial T} \right)_{r_B} = 2\pi c \alpha \frac{r_H}{r_B} (r_B^2 - r_H^2)$. Thus the heat capacity is positive always, implying thermal stability always. For the Schwarzschild BH thermal stability exist only within a limited range of the reservoir radius.

One can now compare the free energies of the 2D BH and hot ADS (HADS) space, in order to know the ground state of the system. One state cannot jump to another classically, but of course, quantum mechanically the topologies can change. The free energy of the BH can be taken from the relation $I_{BH} = \beta F_{BH} = -\beta e^{\Phi_D} \alpha + 2\pi e^{\Phi_D} \sqrt{1 + \frac{\alpha^2 g^2}{4\pi^2}}$. The free energy for HADS in 2D can be found to be $-I_{HADS} = \frac{\pi}{6\alpha} g T \arctan(\alpha r_B)$ [21], where g is the number of massless spin states. The ground state is the state of least free energy. Thus, we find that HADS dominates whenever $I_{HADS} \leq I_{BH}$, i.e.,

$$T \geq \alpha \frac{12c}{g} \frac{\alpha r_B}{\arctan(\alpha r_B)} \sqrt{1 - \frac{g}{12\pi c} \frac{\arctan(\alpha r_B)}{\alpha r_B}}.$$

Whenever the number of particle species is relatively large then HADS is favored for sufficiently small r_B . Indeed, if $g > 12\pi c$, then the quantity inside square brackets is negative up to some boundary radius given implicitly by $\frac{\alpha r_B}{\arctan(\alpha r_B)} = \frac{12\pi c}{g}$. This means that up to this radius HADS dominates and for larger r_B HADS dominates if T obeys the above inequality. A detailed analysis is found in [21]. Note that when the boundary $r_B \rightarrow \infty$ one obtains that, for finite temperature, the black hole is the ground state. A similar analysis, albeit more complex, can be done for the Schwarzschild BH [5].

In conclusion we can say that the Teitelboim-Jackiw theory has, in absence of matter, constant curvature spacetime solutions. Therefore the black hole solution of the theory has no singularities. In the first studies exploring this theory it was thought that such a black hole did not exist. However, solutions containing point particles and horizons were found [23] which also had some interesting thermodynamic properties. To establish the existence of the black hole in this theory one has to invoke topological arguments, which appear through the addition of boundary conditions. We have then showed that this black hole yields non-trivial thermodynamics in York's scheme, with some of its properties being analogous to the Schwarzschild BH. Through an analysis of the free energies of both the black hole solution and hot anti-de Sitter spacetime it was possible to infer that for small enough ambient temperature the black hole is the ground state.

References

- [1] S. W. Hawking, *Nature* **248**, 30 (1974).
- [2] S. W. Hawking, in *General Relativity*, eds. S. W. Hawking, W. Israel (Cambridge University Press, Cambridge 1979).
- [3] R. P. Feynmann, A. R. Hibbs, *Quantum Mechanics and Path Integrals*, (McGraw-Hill, New York 1965).
- [4] D. J. Gross, M. J. Perry, L. G. Yaffe, *Phys. Rev. D* **25**, 330 (1982).
- [5] J. W. York, *Phys. Rev. D* **33**, 2092 (1986).
- [6] D. J. Brown, gr-qc/9404006 (1994).
- [7] G. Mandal, A. M. Sengupta, S. R. Wadia, *Mod. Phys. Lett. A* **6**, 1685 (1991).
- [8] E. Witten, *Phys. Rev. D* **44**, 314 (1991).
- [9] V. P. Frolov, *Phys. Rev. D* **46**, 5383 (1992).
- [10] C. Teitelboim, in *Quantum Theory of Gravity*, ed. S. M. Christensen (Hilger, Bristol, 1984).
- [11] R. Jackiw, in *Quantum Theory of Gravity*, ed. S. M. Christensen (Hilger, Bristol, 1984).
- [12] D. Christensen, R. B. Mann, *Class. Quantum Grav.* **6**, 9 (1992).
- [13] A. Achúcarro, M. E. Ortiz, *Phys. Rev. D* **48**, 3600 (1993).
- [14] M. Cadoni, S. Mignemi, *Nucl. Phys. B* **427**, 669 (1994).

- [15] M. Cadoni, S. Mignemi, *Phys. Rev. D* **51**, 4139 (1995).
- [16] J. P. S. Lemos, P. M. Sá, *Mod. Phys. Lett. A* **9**, 771 (1994).
- [17] J. P. S. Lemos, P. M. Sá, *Phys. Rev. D* **49**, 2897 (1994).
- [18] A. Kumar, K. Ray, *Phys. Lett. B* **351**, 431 (1995).
- [19] E. Elizalde, P. Fosalba-Vela, S. Naftulin, S. D. Odintsov, *Phys. Lett. B* **352**, 235 (1995).
- [20] H. W. Braden, J. D. Brown, B. F. Whiting, J. W. York, *Phys. Rev. D* **42**, 3376 (1990).
- [21] J. P. S. Lemos, *Phys. Rev. D*, to appear, 15 October (1996).
- [22] J. P. S. Lemos, unpublished.
- [23] D. J. Brown, M. Henneaux, C. Teitelboim, *Phys. Rev. D* **33**, 319 (1986).

Bundles in a Supersymmetric Yang-Mills Theory

M. F. Borges, S. R. M. Masalskiene and W. Seixas

DCCE - Ibilce - Unesp

Campus de São José do Rio Preto -SP.

The notion of a fibre bundle is appropriate for solving local problems of differential geometry, field theory, gauge transformations and general relativity. In this letter motivated by Trautman [2] and in recent results given in [1], a fibre bundle structure is suggested as a consequence of the integrability conditions, as the Bianchi identities, of a supersymmetric Yang-Mills theory.

In general relativity there is no natural isomorphism of $(F(M), M, \pi)$ onto a product $M \times F$ but it is possible to show that the bundle $(F(F(M)), F(M), \pi)$ is a product bundle. In this way, as Ivanenko suggest [2], generalizations of general relativity are admitted. He call it as the "second relativization". From this motivation a fibre bundles approach to an extended Einstein-Cartan theory recently obtained [1] is briefly proposed as it follows. In supergravity $N=2, d=5$ theory [3] the curvature does not have componentes along ω^{ab} and B (ω^{ab} = Cartan connection and B =eletromagnetic field). It is then said that theory is factorized respect to the group $H' = SO(1,4) \otimes U(1)$. The supergravity theory being gauge invariant under H' , the group $SU(2,2/1)$ acquires a bundle structure with fibre H' , represented by $SO(1,4) \otimes U(1)$ and bais space the quocient $\frac{G}{H'}$, identifiable with the superspace. In the other words, the first condition implies ω^{ab} is a connection on a principal bundle with basis given by $SU(2,2/1)/SO(1,4)$, with gauge group $H = SO(1,4)$ as the fibre. The second condition implies that also B is a connection on a principal bundle. The basis in this case is $SU(2,2/1)/U(1)$ with gauge group $U(1)$ as the fibre. The extended Eisntein-Cartan gravity theory proposed in [1] has the same structure of the coupled supergravity, enriched with the general gauge group G . That is asserted by its gauge invariance with respect to $G \otimes SO(1,4) \otimes U(1)$, whic is a consequence of the integrability conditions of the Yang-Mills exterior covariant derivatives fields presents in the group G . For the mentioned proposed theory those conditions are satisfied throughout the solution of the Bianchi identities for the fields λ_A (spinorial field, rrelated to the Dirac Equation, $\Gamma^m \Delta_{mA} = 0$), A (gauge fields, related to Yang-Mills Potential) and σ (scalar field), that means:

$$DDA = DD\lambda_A = DD\sigma = 0 \quad (1)$$

The system I provides a compatible set of equation for the free parameters appearing in the exterior covariant derivatives, and is usually called the Bianchi identities.

By solving the system of equations for the free parameters after solving the Bianchi identities, we will find that:

$$n = 1; k = \frac{1}{2}; p = d = 1; l = \frac{1}{2}; t = z = -\frac{1}{2}; g = h = -\frac{1}{2} \quad (2)$$

That will mean that $H'' = G \otimes SO(1,4) \otimes U(1)$ is the fibre of the proposed theory [1], and $\frac{G}{H''}$ is its basis spaces.

Conclusion

Fibre bundles play a fundamental role in theoretical physics, to clarify both what symmetry groups are present in a theory and the way they may bring new developments towards unifying process of physical forces.

References

- [1] Borges, M.F., "*Bianchi identities for an $N = 2$, $d = 5$ supersymmetric Yang-Mills theory on the group manifold*" in *Journal of Geometry and Physics*, Elsevier, Amsterdam, Holland.,(2)20: 142 (1996).
- [2] Trautman, A., "*Fibre Bundles associated with space-time*", *Reports on Mathematical Physics*,(1)1: 29 (1970).
- [3] D'Àuria, R; Fré, P; Maina, E; Regge, T. "*Geometrical first order supergravity in 5 space-time dimensions*, *Ann.Phys.*,135: 237 (1981).

The Causal Interpretation of Quantum Mechanics and The Singularity Problem in Quantum Cosmology

José Acácio de Barros and Nelson Pinto Neto

UFJF, Juiz de Fora - MG - Brazil and LAFEX/CPBF/CNPq - Rio de Janeiro, RJ - Brazil

In this paper we will close our attention to the interpretation and time issues of quantum cosmology in order to study the problem of appearance of singularities in the early Universe. The difficult technical problems coming from the quantization of the full gravitational field will be circumvented by taking advantage of minisuperspace models. In these models, all but a finite number of degrees of freedom are frozen out alleviating considerably the technical problems. In the framework of these minisuperspace models, a number of papers have been written showing how the issue of time is important for the singularity problem: different choices of time imply different quantum gravity theories, some of them still presenting singularities, others not [1]. The interpretation adopted is the conventional probabilistic one. Here, we will adopt a non-probabilistic interpretation to quantum cosmology which circumvents the measurement problem because it is an ontological interpretation of quantum mechanics: it is not necessary to have a measuring apparatus or a classical domain in order to bring home physical reality; it is there "ab initio". It is the causal interpretation of quantum mechanics [2, 3]. We will apply this interpretation to a minisuperspace model and show that the question about the persistency of the singularities at the quantum level does not depend on the choice of time but only on the quantum state of the system.

Let us review the ontological interpretation of quantum mechanics, and then apply it to quantum cosmology.

Take the Schrödinger equation, in the coordinate representation, for a non-relativistic particle with the hamiltonian $H = \frac{P^2}{2m} + V(x)$:

$$i\hbar \frac{d\Psi(x, t)}{dt} = \left[-\frac{\hbar^2}{2m} \nabla^2 + V(x) \right] \Psi(x, t) \quad (1)$$

Writing $\Psi = R \exp(iS/\hbar)$, and substituting it into (1), we obtain the following equations:

$$\frac{\partial S}{\partial t} + \frac{(\nabla S)^2}{2m} + V - \frac{\hbar^2}{2m} \frac{\nabla^2 R}{R} = 0 \quad (2)$$

$$\frac{\partial R^2}{\partial t} + \nabla \cdot \left(R^2 \frac{\nabla S}{m} \right) = 0 \quad (3)$$

The usual probabilistic interpretation takes Eq. (3) and understands it as a continuity equation for the probability density R^2 for finding the particle at position x and time t . All physical information about the system is contained in R^2 , and the total phase S of the wave function is completely irrelevant. In this interpretation, nothing is said about S and its evolution equation (2). However, examining Eq. (3), we can see that $\nabla S/m$ may be interpreted as a velocity field, suggesting the identification $p = \nabla S$. Hence, we can look to Eq (2) as a Hamilton-Jacobi equation for the particle with the extra potencial term $-\frac{\hbar^2}{2m} \frac{\nabla^2 R}{R}$.

After this preliminary, let us then introduce the ontological interpretation of quantum mechanics, which is based on the two equations (2) and (3), and not only in the last one as it is the Copenhagen interpretation:

i) The quantum particles follow trajectories $x(t)$, independent of observations. Hence, in this interpretation, we can talk about trajectories of quantum particles, contrary to the Copenhagen interpretation where only positions at one instant of time have a physical meaning.

ii) The particles are never separated from a quantum field Ψ which acts on them, and satisfies the Schrödinger equation (1).

iii) The momentum of the particle is $p = \nabla S$.

iv) Equation (2) is a Hamilton-Jacobi type equation for a particle submitted to an external potential which is the classical potential plus a new quantum potential

$$Q \equiv -\frac{\hbar^2}{2m} \frac{\nabla^2 R}{R} \tag{4}$$

Hence, the particle trajectory $x(t)$ satisfies the equation of motion

$$m \frac{d^2 x}{dt^2} = -\nabla V - \nabla Q \tag{5}$$

v) For a statistical ensemble of particles in the same quantum field Ψ , the probability density is $P = R^2$. Equation (3) guarantees its conservation in time.

Let us make some comments:

a) The quantum potential is non-local and responsible for the quantum effects.

b) This interpretation can be applied to a single particle. In this case, R is not interpreted as a probability density and hence needs not be normalized.

c) The classical limit is very simple: we only have to find the conditions for having $Q = 0$.

d) There is no need to have a classical domain because this interpretation is ontological.

As the causal interpretation does not require a classical domain, and can be applied to a single system, we think that it should be relevant to examine what it can say about quantum cosmology. In fact, we will see that quantum cosmology becomes very simple to interpret in the light of this interpretation.

The fundamental equation in canonical quantum gravity is:

$$(G^{ijkl} \frac{\delta}{\delta h^{ij}} \frac{\delta}{\delta h^{kl}} + \hbar^{1/2} R^{(3)})\Psi(h^{ij}) = 0. \tag{6}$$

(we have set $\hbar = 1$), which is called the Wheeler-DeWitt equation. The tensor h^{ij} represents the metric of the spacelike hypersurfaces which foliate the spacetime. The Wheeler-DeWitt equation should determine the evolution of the wave function. However, time has disappeared from it. This fact makes people advocates another quantization scheme, the ADM approach, where time is chosen before quantization by a gauge fixing procedure. However, different choices of time lead to inequivalent quantum theories and there is no criterium to choose one of them.

Others say that the fact which makes not easy to find what should play the role of time in the Wheeler-DeWitt equation simply means that there is no time at all in quantum gravity [4, 5]. We should consider the Wheeler-DeWitt equation as a time-independent Schrödinger equation with zero energy. This is consistent with the fact that a closed Universe has, by definition, a null total energy.

Using a non-ontological interpretation, we can understand this fact in another way. Space geometry is like position in ordinary particle mechanics while spacetime geometry is like a trajectory. As trajectories have no sense in the quantum mechanics of particles following a non-epistemological interpretation, we can conclude that spacetime has no meaning in quantum gravity.

However, if we apply the ontological interpretation to quantum cosmology, we should expect that the notion of a spacetime would have a meaning exactly like the notion of trajectories have in the quantum mechanics of non-relativistic particles. Indeed, if we substitute $\Psi = R \exp(iS/\hbar)$ into the Wheeler-DeWitt equation (6), we obtain the two equations:

$$\frac{1}{2} G_{ijkl} \frac{\delta S}{\delta h_{ij}} \frac{\delta S}{\delta h_{kl}} + \hbar^{1/2} R^{(3)}(h_{ij}) + \hbar^{1/2} Q(h_{ij}) = 0 \tag{7}$$

$$G_{ijkl} \frac{\delta}{\delta h_{ij}} (R^2 \frac{\delta S}{\delta h_{kl}}) = 0 \tag{8}$$

where the quantum potential is given by:

$$Q = -\frac{1}{R} G_{ijkl} \frac{\delta^2 R}{\delta h_{ij} \delta h_{kl}} \tag{9}$$

As before, we postulate that $h^{ij}(x, t)$ is meaningful even at the Planck length and set:

$$\Pi_{ij} = -h^{1/2}(K_{ij} - h_{ij}K) = \frac{\delta S}{\delta h^{ij}} \quad (10)$$

recalling that

$$K_{ij} = -\frac{1}{2N}(\partial_t h_{ij} - \nabla_i N_j - \nabla_j N_i) \quad (11)$$

Hence, as K_{ij} is essentially the time derivative of h_{ij} , equation (10) gives the time evolution of h_{ij} , which will be different from the time evolution of classical general relativity due to the presence of the quantum potential in equation (7). As we see, there is no issue of time. The notion of spacetime is meaningful in this interpretation, exactly like the notion of trajectory is meaningful in particle quantum mechanics following this interpretation. However, the dynamics will be modified by the presence of the quantum potential which can, among other things, prevents the formation of the singularities predicted by the classical theory.

The question about the persistency of classical cosmological singularities at the quantum level has been studied extensively in the literature. In a first approach, the dynamical evolution of the quantum states is obtained by fixing the time gauge before quantization [1]. As we mentioned above, different choices of time gauge imply different quantum theories with different answers to the question we are addressing.

Let us show with a simple mini-superspace example that the existence of cosmological singularities at the quantum level does not depend on the choice of the time-gauge, if we assume the causal interpretation of quantum mechanics. This minisuperspace is the Bianchi I model.

The mini-superspace metric is given by:

$$ds^2 = -N^2(t)dt^2 + e^{(2\beta_0(t)+2\beta_+(t)+2\sqrt{3}\beta_-(t))}dx^2 + e^{(2\beta_0(t)+2\beta_+(t)-2\sqrt{3}\beta_-(t))}dy^2 + e^{(2\beta_0(t)-4\beta_+(t))}dz^2 \quad (12)$$

The gravitational hamiltonian for this minisuperspace model is:

$$\mathcal{H} = \frac{N}{24 \exp 3\beta_0} (p_0^2 - p_+^2 - p_-^2). \quad (13)$$

where the p 's are the canonical momenta of the β 's.

The classical equations of motion are:

$$p_0^2 - p_+^2 - p_-^2 = 0, \quad (14)$$

$$\dot{\beta}_0 = \frac{\partial \mathcal{H}}{\partial p_0} = \frac{N}{12 \exp 3\beta_0} p_0, \quad (15)$$

$$\dot{\beta}_+ = \frac{\partial \mathcal{H}}{\partial p_+} = -\frac{N}{12 \exp 3\beta_0} p_+, \quad (16)$$

$$\dot{\beta}_- = \frac{\partial \mathcal{H}}{\partial p_-} = -\frac{N}{12 \exp 3\beta_0} p_-, \quad (17)$$

and all momenta are constants of motion.

To discuss the appearance of singularities, we need the Weyl square tensor. In the gauge $N = 12 \exp 3\beta_0$ and using the fact that the p 's are constants, the Weyl square tensor is proportional to $\exp(-3\beta_0)$. Solving Eq. (15), we can see that $\beta_0 = p_0 t$, and the singularity is at $t = -\infty$. It is a fast time gauge in the terminology of Ref. [1]. If we choose $N = 1$, then $\beta_0 = \frac{1}{3} \ln(\frac{p_0}{4} t)$ and the singularity appears at $t = 0$. It is a slow time gauge.

The classical singularity can be avoided only if we set $p_0 = 0$. But then, due to Eq. (14), we would also have $p_{\pm} = 0$, implying that the Weyl square tensor be identically zero, corresponding to the trivial case of Minkowski spacetime.

The Dirac quantization scheme yields the following Wheeler-DeWitt equation:

$$\left(\frac{\partial^2}{\partial \beta_0^2} - \frac{\partial^2}{\partial \beta_+^2} - \frac{\partial^2}{\partial \beta_-^2} \right) \Psi = 0. \quad (18)$$

In Ref. [6], a consistent inner product is constructed, and gauge invariant observables which depend on a parameter, which is nothing but β_0 , are constructed. In this way, the Weyl square observable is built, exhibiting a singularity at $\beta_0 = -\infty$, as in the classical case. As β_0 plays the role of time, this is equivalent to a quantization in the fast-time gauge.

Let us now make use of the causal interpretation. Take the following solution to the Wheeler-DeWitt equation (18):

$$\Psi = \exp i(\sqrt{k_+^2 + k_-^2} \beta_0 + k_+ \beta_+ + k_- \beta_-) + \exp -i(-\sqrt{l_+^2 + l_-^2} \beta_0 + l_+ \beta_+ + l_- \beta_-) \quad (19)$$

where the k 's and l 's are constants.

Note that this function is not normalizable, but this is not important for the ontological interpretation.

Calculating $\frac{\partial S}{\partial \beta_0}$, $\frac{\partial S}{\partial \beta_+}$, and $\frac{\partial S}{\partial \beta_-}$, where S is the phase of the wave function (19), we obtain:

$$p_0 \equiv \frac{\partial S}{\partial \beta_0} = \frac{1}{2} \sqrt{k_+^2 + k_-^2} - \frac{1}{2} \sqrt{l_+^2 + l_-^2}, \quad (20)$$

$$p_+ \equiv \frac{\partial S}{\partial \beta_+} = \frac{1}{2} k_+ - \frac{1}{2} l_+ \quad (21)$$

$$p_- \equiv \frac{\partial S}{\partial \beta_-} = \frac{1}{2} k_- - \frac{1}{2} l_- \quad (22)$$

It is easy to see in the above equations that it is possible to have $p_0 = 0$ and $p_{\pm} \neq 0$. We can also understand it by the fact that Eq. (14) is no longer valid at the quantum level; the quantum potential must be added to it and thus $p_0 = 0$ does not imply $p_{\pm} = 0$. Hence, it is possible to find a curved spacetime without singularities, i.e., a spacetime with a Weyl square tensor which is neither null nor infinite, for the quantized Bianchi I model. Note that this result is independent of the value chosen for N . In particular, we could have chosen the fast time gauge mentioned previously and still have a non-singular quantum spacetime. Hence, using the ontological interpretation, we have presented a simple example where the appearance of singularities in the quantum regime depends only on the state of the system, and not on the time-gauge choice we make.

References

- [1] M. J. Gotay and J. Demaret; Report gr-qc/9605025 and references therein.
- [2] D. Bohm and B. J. Hiley; *The undivided universe: an ontological interpretation of quantum theory* (Routledge, London, 1993).
- [3] P. R. Holland; *The Quantum Theory of Motion: An Account of the de Broglie-Bohm Interpretation of Quantum Mechanics* (Cambridge University Press, Cambridge, 1993).
- [4] J. Barbour; *Class. Quantum Grav.* 11, 2853 (1994).
- [5] J. Barbour; *Class. Quantum Grav.* 11, 2875 (1994).
- [6] A. Ashtekar, R. Tate and C. Uggla; Report gr-qc/9302027.

Classical Fields and the Quantum concept

Manoelito M de Souza

Universidade Federal do Espírito Santo - Departamento de Física

29065.900 - Vitória-ES-Brasil

We do a critical review of the Faraday-Maxwell concept of classical field and of its quantization process. With the hindsight knowledge of the essentially quantum character of the interactions, we use a naive classical model of field, based on exchange of classical massless particles, for a comparative and qualitative analysis of the physical content of the Coulomb's and Gauss's laws. It enlightens the physical meaning of a field singularity and of a static field. One can understand the problems on quantizing a classical field but not the hope of quantizing the gravitational field right from General Relativity.

1 Introduction

The concept of interacting field introduced by Faraday-Maxwell is on the basis of Field Theory and of Quantum Mechanics. It is necessary for a relativistic description of the wave-particle duality of the quantum theories. The idea of a classical interaction as a wave, continuous and distributed over the whole space, is put against the modern idea of a quantum interaction, discrete and localized in "corpuscles" or interaction quanta. The passage from the first to the second idea requires a so called quantization process, and this passage, it is well known, in the best of the cases (QED) has deep problems, and in the worst case (QG) it has proved to be not viable. In the search of solutions to this problem of quantizing the gravitational field the observed tendency is the one of replacing complex models and formalisms for others of increasing complexity. On the other hand, the Classical Electrodynamics, the best known and "well succeeded" paradigm of all subsequent field theory, has old and well known problems of inconsistency with the description of fields in the neighborhood of their sources. In a recent work (hep-th/9610028) we show that taking the correct zero distance limit to the charge solves these problems and shows unequivocal clues of quantum features in Classical Electrodynamics: the flux of field from a charge is discontinuous in time. The problems of CED in its zero distance limit, which are erroneously attributed to the working hypothesis of a pointlike electron, are rather unequivocal signs that our concepts of fields are unappropriate for describing interactions. The idea of a continuous classical field is misleading; it is valid only for large distances and large number of photons. Out of this limit this discontinuity is masqueraded by the field spacetime-average character.

We want to make a critical review of the Faraday-Maxwell concept of classical field under the perspective of modern physics that understands it as being of a fundamentally quantum nature. It is well known that the pioneers of classical field theory worked with a model for the electromagnetic phenomena based on an analogy with the fluid mechanics. The electromagnetic effects would be propagated through an all-pervading fluid, the ether. This, at the time, new vision of field-mediated interactions between distant charges was an advance with respect to the Newtonian concept of action at a distance. The fluid analogy implies on a field distributed all over the space around its source, like it happens with the sound waves, for example. This image was certainly reinforced by what at that time seemed to be an apparently definitive victory of the concept of light as a wave phenomena against the Newtonian model of light as a stream of corpuscles. The phenomena of interference, diffraction and polarization of light had been decisive for this conviction. Only much later the first clues of a discreteness, like the photoelectric and the Compton effects, would be discovered. But even Quantum Mechanics that was created from the necessity of explaining these new effects received also the influence of this fluid-mechanics concept of field: the wave function is a space-distributed field representing a fluid of amplitude of probabilities. In this qualitative analysis we want to oppose this historical vision of classical fields as some waves, continuous and distributed all over the space, against the vision of interactions mediated by localized point-like objects, their quanta, discretely emitted, propagated

and absorbed. In the modern perspective all the four fundamental interactions of nature are mediated by their respective quanta. We will try to obtain a qualitative view on how a classical field theory could be formulated if the interaction were seen as mediated by massless point-like objects propagating on straight-line trajectories between their emitters and their absorbers.

2 The Gauss's law and the singularity problem

The Coulomb's law (or in the case of gravitation, the Newton's law) describes the **effectively** observed interaction between two static electric charges in terms of forces acting on the charges along the straight-line defined by the charges positions and with a magnitude that is directly proportional to the product of the two charges and to the inverse of the square of the distance between them. The observed spherical symmetry around a point charge is the assurance that nothing changes in the above description if the second point charge is moved to any other point of a spherical surface centered at the first charge. The forces acting on the charges are what is actually observed and they require the presence of the two charges and they are observed only at the charges sites. The concept of a field existing everywhere around a single charge, regardless the presence of any other charge is an extrapolation of what is effectively observed. There is, therefore, a very deep distinction between the physical content of the Coulomb's and of the Gauss's laws. This last one describes the *inferred* electric field as existing around a single charge, independent of the presence of the other charge. The electric field, as it is well known, is extracted from the Gauss's law through the integration of its flux across a surface, having the appropriate symmetry, *enclosing* the charge,

$$\vec{E}(x) = \hat{e} \frac{\int_V \rho dv}{\int_{\partial V} dS}, \quad (1)$$

where \hat{e} is the unit vector normal to the closed surface ∂V . (1) puts in evidence the effective or average character of the Faraday-Maxwell's concept of field; it gives also a hint on the meaning and origin of the field singularity. If the electric field can be visualized in terms of exchanged photons, then according to (1), the frequency or the number of these exchanged photons must be proportional to the enclosed net charge. And if we take \vec{E} , as suggested by the Gauss's law, as a measure of the flux of photons emitted/absorbed by a point charge, we can schematically write, $E \sim \frac{n}{4\pi r^2}$, where n is the number of photon per unit of time crossing an spherical surface of radius r and centered on the charge. Then, the divergence of E in the limit when $r \rightarrow 0$ does not represent a physical fact like an increasing number of photons, but just an increasing average number of photons per unit area, as the number of photons remains constant but the area tends to zero. So, a field singularity would have no physical meaning, because it would just be a consequence of this average nature of the Faraday-Maxwell's field, and contrary to what is usually thought, it would not be a consequence of the electron point-like nature.

Taken the exchange of "quanta" (here in the sense of discrete and localized chunks of energy and momenta, like in a classical particle) as a model for a classical interaction one must conclude that the Faraday-Maxwell concept of field, which lies behind the justification of the use of the Gauss's law, must be seen as the smearing of the effect of the "quantum" exchanging on the whole space around a charge, and during a time interval larger than the time (period) between two consecutive exchange of a "quantum". Under this perspective, the Faraday-Maxwell concept of a classical field corresponds in fact to an average in space and in time of the actual quantum interaction. It replaces something discrete in space and in time and localized on the straight-line between the two interacting charges by something isotropically spread in space around each charge and in time. The quantization process is a tentative of reversing this operation. Does it make sense, in this new perspective? Is it the more appropriate approach? The answer to both questions, in this context, seems to be no. It seems to be more appropriate to reformulate the description of classical physics in terms of discrete interactions before trying to quantizing it. The two concepts (classical and quantum) of interaction are associated to domains with distinct topologies: the light-cone and the straight-line, respectively. The quantization process does not account for this difference. The classical field, as a massless wave, propagates on the light-cone, which is not a manifold because of the singularity on its vertex. The quantum interaction, on the contrary, is defined on a light-cone generator, a straight-line, and therefore, has no singularity.

3 Quantum Gravity and General Relativity

The problems with the description of fields in a close vicinity of their sources seem to be that we are taking the fields by their averages. This seems to be true for the electromagnetic field and it may also be true for the other known classical interaction, the gravitation. For the gravitational field there is a further complication given by the General Theory of Relativity which replaces the description of a gravitational force by the picture of a curved (Riemannian) spacetime. In the context of discrete interactions, this geometrization is an added averaging process as it changes a polygonal trajectory of an interacting test mass smoothing it into a geodesic. With discrete interactions, the events of emission and absorption of a gravitational quantum by a mass form the vertices of a polygonal trajectory; they are connected by straight-line segments that correspond to the, in between, mass's free motion. This geometrization not only hides the interaction discreteness as it also makes more difficult any tentative of retrieving it by quantization, since it mixes the geometry of the background Minkowski spacetime (its metric) with the actual physical effect (the exchange of quanta) incorporating them into the metric tensor of a Riemannian manifold. To quantize this metric tensor would be, therefore, tantamount to a discretization not only of the gravitational interaction but also of the spacetime. The physicists who see this picture of a curved spacetime not as an approximation but as a fundamental aspect of nature does not, of course, agree with this; but in this context of discrete interactions any whole-metric quantization does not make sense.

The Einstein field equations, like the Maxwell's equations, deal with spacetime-average fields. The General Theory of Relativity has a solid basis of experimental confirmation, but like Classical Electrodynamics, only for situations where the classical approximation of the field as an spacetime average is a good description: far from their sources and involving a large number of quanta. In this perspective of discrete classical interactions, one can understand the nature of the problems that show up in the quantization of the classical fields but it seems then that there is no justification for a hope that the gravitation field may be quantized starting from the General Theory of Relativity.

This is more than just an academic discussion. If such observations are correct and if the above considerations about the physical meaning of the classical field singularities are valid also for the gravitational field of Einstein, described by a metric tensor, one must worry about the enormous intellectual efforts that are being devoted to a detailed comprehension of black-hole physics. It is opportune to remember that all known indirect evidences of black-holes are just indications of possibly very intense gravitational fields produced by very compact objects but not necessarily black-holes.

4 The Coulomb's law and the meaning of static field

The Gauss's law, in a picture of continuous interaction, has a natural explanation for the dependence of the interaction with the inverse of the squared distance as a consequence of the 3-dimensionality of the space. The origin of this $\frac{1}{r^2}$ -dependence must be entirely distinct if the interactions are seen as the result of exchange of particles.

This is a nagging problem in this picture of a classical field in terms of discrete interactions, which is also related, in the context of an actual quantum field theory, to the conceptual meaning of a static field. The $\frac{1}{r^2}$ -dependence of the static force between two point charges (or masses) is an experimental fact as stated in the Coulomb's law (or Newton's law). In the context of the present analysis the question now is how to understand this $\frac{1}{r^2}$ -dependence as well as the meaning of a static field in terms of a discrete exchange of particles. In QFT theory one deals with quantum fluctuation and virtual-particle exchange. Here, in a classical context, there is no virtual particle and no quantum fluctuation. All particles are real with positive and definite energy and mass (which may be null). Strict conservation laws for energy and (angular and linear) momentum must be always observed.

But before proceeding further on this, we must remind some well-known experimental facts:

1. Only an accelerated charge can radiate. A non-accelerated charge never radiates.

On the other hand, as a consequence of the energy-momentum conservation, the act of emitting or absorbing

radiation by a charge necessarily results on its acceleration. So, for a charge, we can put it this way:

RADIATION \Leftrightarrow ACCELERATION

2. A charge under an external periodic stimulation (force) emits radiation with the same frequency of the external stimulus. Or:

FREQUENCY OF THE EMITTED RADIATION = FREQUENCY OF THE EXTERNAL FORCE

Accepting the above empirical fact 1 as being also valid in a fundamental level has some immediate logical implications:

- An isolated charge will never radiate, will never emit a single photon, will never be accelerated or will never accelerate itself (by emitting/absorbing a photon, as it is isolated).
- So, it does not make sense talking of the electric field of a single isolated charge (taken as in the elementary pedagogical hypothesis of the only existing charge in the world and not under any external force).
- This is contrary to the ideas of quantum fluctuations (in QFT) and of self-interactions.
- The fundamental (in the sense of irreducible) electromagnetic interaction does not correspond to a 3-legs Feynmann diagram (which does not obey the conservation laws, anyway) but to a connected set of two of them, accounting for the fact that an electron must be stimulated (accelerated by the absorption of a photon) to irradiate (emit a photon). See the figure 1.

For both pictures of interaction, mediated by a continuous and distributed field or discretely produced by the exchange of particles, some external forces must be provided to assure that the charges remain in a static equilibrium. The first immediate distinction is that in the continuous case the force must act continuously at both charges while in the particle-exchange picture the forces act only in the brief instant of emission and absorption of a quantum, as a kind of elastic reaction force. See figure 2, where we are neglecting a possible time delay, δt , between the absorption and the consequent re-emission of a photon.

Each charge then emits a photon after being stimulated (accelerated) by the absorption of a photon emitted by the other charge. There is a much diffused false premise that the wave concept of field, in classical field theories, or of the emission followed by the reabsorption of virtual quanta, in quantum field theory, are necessary for explaining the interaction between two separated charges, otherwise, it is argued, how could the charges know the presence of each other? But this is indeed a not well posed question. What we really know from experiment (and confirmed by our best theories) is that interactions and the emission and absorption process are closely interdependent concepts: an electric charge does not radiate unless it is under the action of an external force (interaction) and, according to our modern understanding, any change in the state of motion of the charges is a consequence of the exchange (emission or absorption) of quanta. It is not a question of what comes first, the emission or the interaction: they are just two aspects of a same thing. A complete understanding of this may be a subject of scientific investigation in the future; today this question still belongs to the domain of plain philosophy. All we can say now, as physicists, is that a charge is accelerated with the emission and absorption of radiation and that it radiates only when accelerated. In quantum mechanics the condition that a charge be accelerated without emitting electromagnetic radiation leads to stationary states or the quantization of its energy.

Let us consider an imaginary Coulomb's experiment for measuring the repulsive force between two electrons. Let r be the separation between the two point electric charges, fixed in their positions, each one, by a dynamometer on which one can read the value of the applied force on each electron. There is a force acting on a charge just in the instants when it receives a photon (emitted by the other electron) and emits also (as a reaction) a photon in the direction of the other electron. So, each dynamometer indicates a discrete, instantaneous force, discontinuous but periodical, with a period T ,

$$T = \frac{2r}{c},$$

where c is the speed of light. According to our listed experimental fact number 2, each electron, stimulated by this periodical force, emits photons with this same frequency, $f = \frac{c}{2r}$. This seems to introduce a non-locality in the electrostatic interaction because the emitted photon depends on the distance between the interacting charges. But this is just apparent because this dependence on r comes from the photon's (two-ways) travelling time between the charges. Using the quantum information (the de Broglie's relation: $E = hf = h/T$), we have for the change in the momentum of an electron, Δp , during a time interval Δt ,

$$\Delta p = \left(\frac{2hf}{c}\right)(f\Delta t) = \frac{2hf^2\Delta t}{c}, \quad (2)$$

or

$$F = \frac{\Delta p}{\Delta t} = \frac{hc}{2r^2}. \quad (3)$$

Then, with $\alpha = \frac{e^2}{4\pi\hbar c}$, in rationalized Gaussian units, we have

$$F = \frac{1}{4\alpha} \frac{e^2}{r^2}, \quad (4)$$

or

$$F = \frac{1}{4\alpha_g} \frac{Gm^2}{r^2} \quad (5)$$

with $\alpha_g = \frac{Gm^2}{4\pi\hbar c}$. (4) and (5) are, respectively, the Coulomb's law and the Newton's gravitation law, up to a multiplicative constant. It is amazing that all of their qualitative aspects can be so easily obtained from such a simple and naive model of interaction. The two laws describe interactions between two static sources, but while the Coulomb's law gives an exact description, the Newton's law is just a weak field approximation. This difference may be explained by the mixing of the Minkowski metric with the graviton-exchange effects in the Einstein's field and by its space average nature. The attractive or repulsive character of the electrostatic force requires the use of angular momentum conservation in which an essential role (like in QFT) belongs to the photon's spin. For simplicity, as this is not the point on the present focus, we will neglect the particles' spins. They will be treated as scalar objects. Only linear momentum conservation is involved and this only leads to repulsive force. The point here is to understand the $\frac{1}{r^2}$ -dependence of the force.

The spin of the exchanged quantum makes the differences among distinct kind of interactions (scalar, vectorial and tensorial). For the validity of (4), $\Delta t \gg T \gg \delta t$, must be satisfied. As the distance between the two interacting charges in any Coulomb's experiment is of the order of centimeters, the lapse of time (T) between two consecutive emissions is about 10^{-10} s. So, $\Delta t \gg 10^{-10}$ s. This is in the reach of an experimental detection, and so, it would be possible, at least in principle, to observe discrete interactions with a carefully done Coulomb's experiment.

In summary, according to this view of interactions as exchanges of quanta both statements, the Gauss's law and the Coulomb's law, correspond to smoothing approximative averages hiding the process natural discreteness: the Gauss's law is an average in space and time while the Coulomb's law is an average in time. But they are not equivalent as they produce distinct consequences. The space average causes a topological change as it replaces the action of a single quantum, which propagates along a light-cone generator by a continuous field or wave propagating on the light-cone. It replaces, therefore, the simple topology of a straight-line (the light-cone generator, domain of the quantum) by the topology of the light-cone (domain of the wave). The light-cone is not a manifold because of its singularity on its vertex which is a reflection of the wave singularity.

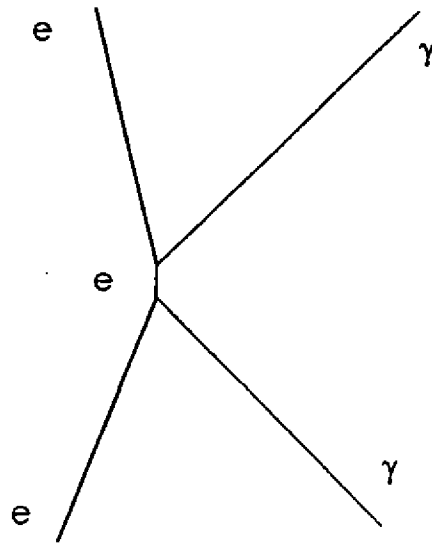


Figure 1.: Classical picture of the fundamental quantum process: an electron must be stimulated (accelerated) by the absorption of a photon in order to emit a photon.

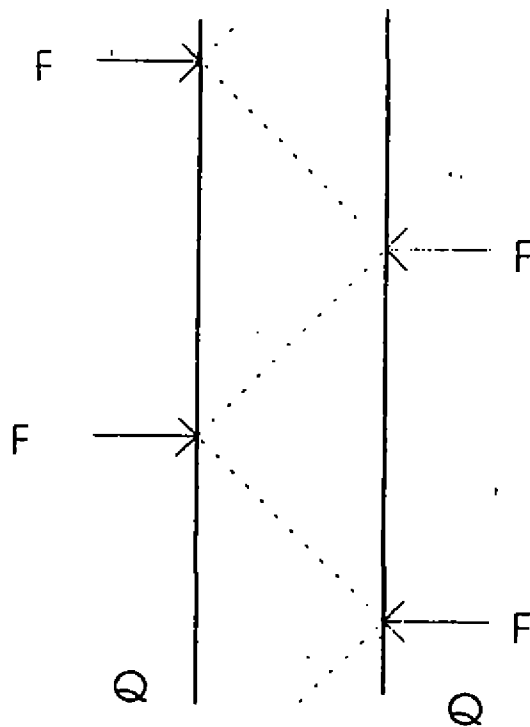


Figure 2.: The Coulomb's experiment or the static field seen as the exchange of real photons between two fixed charges.

Black Hole Formation in Lovelock Theory

Anderson Ilha and José P. S. Lemos

*Departamento de Astrofísica, Observatório Nacional/CNPq
Rua General José Cristino 77, 20921-400 Rio de Janeiro, Brazil*

1 Introduction

The concept of a multidimensional spacetime picture has been around in theoretical physics long since 1926, when Kaluza and Klein (KK) published their version of a theory of everything that lived in five dimensions. Since then this idea has been brought a mixture of reactions from the scientific community. It was only in seventies that a really new and improved framework for this idea emerged in the physical scenario, when the Grand Unified Theories (GUT's) and supergravity begun to take shape and force via the always dreamed final theory of nature. However, these tentatives always broke in one or another point. The common point in these two rather distinct theories is that, like the KK theory, both live in $\mathcal{D} > 4$ dimensions. The last attempt to create a final theory has been the superstring theory (in its heterotic form). In this theory, the nature's basic building blocks live in 10 dimensions, in the realms of the Planck scale.

So we might wonder what is the natural extension of the General Theory of Relativity (GR) to spacetimes whose dimension is greater than four. Although GR can be formulated in these spacetimes, in its usual formulation the theory is no more unique, and we must seek for a mathematical formulation that maintains the same degrees of freedom from the original theory. It turns out that the natural extension is given by the so called Lovelock theory [1], which albeit nonlinear in the curvature, gives second-order field equations for any spacetime dimension. This theory has many constant arbitrary coefficients. However, it is possible in a natural way to parametrize these set in terms of only two constants, the Newton's and the cosmological constants. In this process one separates theories in even and odd dimensions. It was found that these theories have static black hole solutions. In general relativity, black holes appear as a final state of a gravitational collapse process. In this work, we are seeking for the formation of black holes in this more general context for even dimensions [2]. For odd dimensions, see [3]. In particular, we are using the Oppenheimer-Snyder model, in which a dust hyperball collapses towards a final black hole state.

2 Lovelock theory

The most general action in $\mathcal{D} \geq 3$ spacetime dimensions that yields the same degrees of freedom of Einstein theory is the so called Lovelock action, which is given by [1]

$$S = \kappa \sum_{p=0}^{[(\mathcal{D}-1)/2]} \alpha_p \int_M \epsilon_{a_1 \dots a_{\mathcal{D}}} R^{a_1 a_2} \wedge \dots \wedge R^{a_{2p-1} a_{2p}} \wedge e^{a_{2p+1}} \wedge \dots \wedge e^{a_{\mathcal{D}}} + S_m, \quad (1)$$

where $R^{ab} = d\omega^{ab} + \omega_c^a \wedge \omega^{cb}$ is the curvature two-form, e^a is the local frame one-form, and ω^{ab} is the spin connection, with $a_i = 0, 1, \dots, \mathcal{D} - 1$. The symbol $[\]$ over the summation symbol means one should take the integer part of $(\mathcal{D} - 1)/2$. S_m is a phenomenological action which describes the macroscopic matter sources.

In general, the constant coefficients α_p are arbitrary. However, it is shown in [4, 5] that taking certain special choices one is able to get simple meaningful solutions. Following [5] one first considers embedding the Lorentz group $SO(\mathcal{D} - 1, 1)$ into the anti-de Sitter group $SO(\mathcal{D} - 1, 2)$, and then separates into two distinct classes of Lagrangians: Lagrangians for even dimensions and Lagrangians for odd dimensions.

For even dimensions, $\mathcal{D} = 2n$, ($n = 2, 3, \dots$), the set of coefficients are given by

$$\alpha_p = \binom{n}{p} l^{-\mathcal{D}+2p}, \quad (2)$$

where, for convenience one can choose κ as

$$\kappa = \frac{l^{\mathcal{D}-2}}{32 \pi G n}, \quad (3)$$

Given the action (1), the field equations are obtained by the variation with respect to the one-forms e^a . Under the assumption of zero torsion, the variation with respect to the spin connection ω^{ab} vanishes identically. Although the equations have powers in the curvatures, they remain by construction second order in the metric. The field equations are given by

$$-\kappa \sum_{p=0}^{[(\mathcal{D}-1)/2]} \alpha_p (\mathcal{D} - 2p) \epsilon_{a_1 \dots a_{\mathcal{D}}} R^{a_1 a_2} \wedge \dots \wedge R^{a_{2p-1} a_{2p}} \wedge e^{a_{2p+1}} \wedge \dots \wedge e^{a_{\mathcal{D}-1}} = Q_{a_{\mathcal{D}}}, \quad (4)$$

where $Q_{a_{\mathcal{D}}}$ is a $(\mathcal{D} - 1)$ -form associated with the energy momentum tensor T_b^a through the following expression

$$Q_i = \frac{1}{(\mathcal{D} - 1)!} T_i^{a_1} \epsilon_{a_1 \dots a_{\mathcal{D}}} e^{a_2} \wedge \dots \wedge e^{a_{\mathcal{D}}}. \quad (5)$$

3 Exterior Vacuum Solutions

In the vacuum all components of the energy-momentum tensor vanish, so that we will have $Q_a = 0$ in the field equations (4). In order to solve these equations, we consider a static spherically symmetric spacetime, given by

$$ds_+^2 = -g^2(r_+) dt_+^2 + g^{-2}(r_+) dr_+^2 + r_+^2 d\Omega_{\mathcal{D}-2}^2, \quad (6)$$

where t and r are the time and radial coordinates and $d\Omega_{\mathcal{D}-2}^2$ is the arc-element of a unit $(\mathcal{D} - 2)$ -sphere. The subscript $+$ reminds that (6) is to be viewed as an exterior spacetime. With metric (6) and the equation (4), Bañados, Teitelboim and Zanelli were able to find the following exact solution for $\mathcal{D} = 2n$ [5],

$$ds_+^2 = - \left[1 - (2M/r_+)^{\frac{1}{n-1}} + (r_+/l)^2 \right] dt_+^2 + \frac{dr_+^2}{1 - (2M/r_+)^{\frac{1}{n-1}} + (r_+/l)^2} + r_+^2 d\Omega_{\mathcal{D}-2}^2. \quad (7)$$

These solutions describe black holes. We will show that they also represent the exterior vacuum solution to a collapsing (or expanding) dust cloud in Lovelock's theory.

4 Interior Matter Solutions

The interior spacetime is modeled by a homogeneous collapsing (or expanding) dust cloud, whose metric is described by the Friedmann-Robertson-Walker in \mathcal{D} dimensions

$$ds^2 = -dt^2 + a^2(t) \left[\frac{dr^2}{1 - k r^2} + r^2 d\Omega_{\mathcal{D}-2}^2 \right]. \quad (8)$$

The coordinates t and r are comoving coordinates (we omit throughout the subscript $-$ to indicate an interior solution). The constant k can take the values $k = 0, \pm 1$. From (8), Lovelock equations (4) and the energy-momentum tensor for a perfect fluid we obtain the following first integral for the scale factor $a(t)$,

$$\dot{a}^2 = -k - \left(\frac{\dot{a}}{l}\right)^2 + \left(\frac{\dot{a}}{l}\right)^2 \left[\frac{16 \pi G l^2 \rho_0}{(\mathcal{D} - 1)!} \left(\frac{a_0}{a}\right)^{\mathcal{D}-1} \right]^{2/(\mathcal{D}-2)}, \quad (9)$$

where ρ_0 and a_0 are constants. There is a conservation law relating the cloud density $\rho(t)$ and $a(t)$, which is given by

$$\dot{\rho} + (\mathcal{D} - 1)(\rho + p) \frac{\dot{a}}{a} = 0, \quad (10)$$

where p is the pressure of the cloud. We now assume a dust fluid, $p = 0$. For such an equation of state we can integrate (10) to give

$$\rho = \rho_0 \left(\frac{a_0}{a}\right)^{\mathcal{D}-1}, \quad (11)$$

where ρ_0 and a_0 are the constants defined above.

In general it is not possible to obtain an exact analytical solution of (9) for $k = \pm 1$. However, restricting to $\mathcal{D} = 4$, one of course obtains the Lemaître models, of which the closed and open Friedmann universes are the particular cases found for $l \rightarrow \infty$. The marginally bound case, $k = 0$, allows a second integral of (9) given by

$$a = a_0 \left\{ \frac{16\pi}{(\mathcal{D}-1)!} G \rho_0 l^2 \sin^{\mathcal{D}-2}(\bar{l}) \right\}^{\frac{1}{\mathcal{D}-1}}, \quad (12)$$

where

$$\bar{l} \equiv -\frac{\mathcal{D}-1}{\mathcal{D}-2} \left(\frac{t-t_0}{l} \right). \quad (13)$$

Here t_0 gives the time for which $a = 0$, and without loss of generality, one can put $t_0 = 0$. We take $-\pi < \bar{l} < 0$. For $-\pi < \bar{l} < -\pi/2$ the cloud is expanding. For $-\pi/2 < \bar{l} < 0$ the cloud is collapsing. And $\bar{l} = \pi/2$ is a moment of time-symmetry. Inserting (12) in (11) we obtain the evolution of the density in the $k = 0$ dust model,

$$\rho(t) = \frac{(\mathcal{D}-1)!}{16\pi G} \left(\frac{1}{\bar{l}} \right)^2 \sin^{-(\mathcal{D}-2)}(\bar{l}), \quad (14)$$

which blow up at $\bar{l} = -\pi$ (representing the appearance of a singularity), and $\bar{l} = 0$ (representing the formation of a singularity). This can also be viewed by the curvature scalars, the Ricci scalar

$$R^{ab} R_{ab} = -(\mathcal{D}-1)^2 \left(\frac{\ddot{a}}{a} \right)^2 + (\mathcal{D}-1) \left[\frac{\ddot{a}}{a} + (\mathcal{D}-2) \frac{\dot{a}^2 + k}{a^2} \right]^2, \quad (15)$$

and the Kretschmann scalar

$$R^{abcd} R_{abcd} = (\mathcal{D}-1) \left[\left(\frac{\ddot{a}}{a} \right)^2 + \left(\frac{\dot{a}^2 + k}{a^2} \right)^2 \right], \quad (16)$$

both of which diverge when $a = 0$ at $\bar{l} = 0$.

5 Junction Conditions

Now we match the exterior and interior spacetimes found in sections 3 and 4, respectively, across an interface of separation Σ . The junction conditions are [6]

$$ds_+^2 \Big|_{\Sigma} = ds_-^2 \Big|_{\Sigma} \quad (17)$$

$$K_{\alpha\beta}^+ \Big|_{\Sigma} = K_{\alpha\beta}^- \Big|_{\Sigma} \quad (18)$$

where $K_{\alpha\beta}$ is the extrinsic curvature. The subscripts \pm represent the quantities taken in the exterior and interior spacetimes. Both the metrics and the extrinsic curvatures in (17)-(18) are evaluated at Σ . The metric intrinsic to Σ is written as

$$ds_{\Sigma}^2 = -d\tau^2 + R^2(\tau) d\Omega_{\mathcal{D}-2}^2. \quad (19)$$

Where τ is the proper time on Σ and $d\Omega_{\mathcal{D}-2}^2$ denotes the line element on a $(\mathcal{D}-2)$ -dimensional sphere. The equations (17) and (18) establish constraints on the interior and exterior spacetimes geometries, so that we could make a smooth transition between these two spacetimes. For example, using the junction condition (17), metric (19) and the exterior metric (7) we obtain

$$r_+ = R(\tau), \quad (20)$$

and

$$\frac{dt_+}{d\tau} = \frac{\sqrt{\left[1 - (2M/R)^{\frac{1}{\mathcal{D}-1}} + (R/l)^2 \right] + \dot{R}^2}}{\left[1 - (2M/R)^{\frac{1}{\mathcal{D}-1}} + (R/l)^2 \right]}. \quad (21)$$

where $\dot{} \equiv \frac{d}{d\tau}$, and both equations are evaluated at Σ . Although we started back with two different spacetimes (the interior and exterior geometries), equations like (20) and (21) will guarantee to us a unique physical picture from the

problem. From now on, we will usually omit the subscript Σ to denote evaluation at the interface. Using now the junction conditions (18), metric (20) and the interior metric (8), we get

$$\dot{R}^2 + \left(\frac{R}{l}\right)^2 + k (r_\Sigma)^2 = \left(\frac{2M}{R}\right)^{2/(\mathcal{D}-2)} \quad (22)$$

The only component K_{ab} needed for use in with work is $K_{\theta\theta}$. Multiplying equation (9) by $(r_\Sigma)^2$, and then comparing it with equation (22), we have

$$M = \left(\frac{1}{l}\right)^{\mathcal{D}-4} \frac{8\pi}{(\mathcal{D}-1)!} \rho_0 G R_0^{\mathcal{D}-1}, \quad (23)$$

which is the mass of the cloud expressed in terms of the constants given in the problem. This expression is valid for any value of k , $k = 0, \pm 1$.

6 Black Hole Formation

In order to study black hole formation in this theory we work with the $k = 0$ model solution found in (12). The interior metric is then the equation (8) with k set to zero. The exterior metric is given in (7) and as we have shown in section 5, it is possible to make a smooth junction between both spacetimes.

To know whether a black hole as formed or not, one has to search for the appearance of an apparent horizon and an event horizon. The apparent horizon is defined in to be the boundary of the region of trapped two-spheres in spacetime. To find this boundary on the interior spacetime one looks for two spheres $Y \equiv a(t)r = \text{constant}$ whose outward normals are null [7]. Using the metric (24) we obtain

$$\left(\frac{da(t)}{dt}\right)^2 = \frac{1}{r^2}. \quad (24)$$

Using (12) in (24) gives the evolution of the apparent horizon in comoving coordinates,

$$r = r_\Sigma \left(\frac{1}{2m}\right)^{1/\mathcal{D}-1} \frac{\sin^{1/\mathcal{D}-1}(\bar{t})}{\cos(\bar{t})}. \quad (25)$$

where $m \equiv \frac{M}{l}$. For $\mathcal{D} = 4$ and $l \rightarrow \infty$ this expression reduces to the usual expression for the apparent horizon in the Friedmann metric [7].

Now, the apparent horizon first forms at the surface r_Σ . Then, for $r = r_\Sigma$, equation (25) gives the time t at which the apparent horizon first forms. On the other hand, one should also be able to find the formation time of the apparent horizon on the surface Σ through an equation on Σ , equation (22). Indeed, at the junction one has $R = a(t)r_\Sigma$. Then from junction condition (22) and equation (24) we have that the apparent horizon first forms when

$$x [1 + x^2]^{(\mathcal{D}-2)/2} = 2m \quad (26)$$

where $x \equiv R/l$. For Friedmann ($l \rightarrow \infty$ and $\mathcal{D} = 4$) the above expression reduces to $R = 2M$, as expected. Now, the time of formation of the apparent horizon can be found through equation

$$\begin{aligned} x_{AH} &= a(t_{AH}) x_\Sigma \\ &= \left\{ 2m \sin^{\mathcal{D}-2} \left[-\frac{\mathcal{D}-1}{\mathcal{D}-2} \left(\frac{t_{AH}}{l} \right) \right] \right\}^{1/(\mathcal{D}-1)} \end{aligned} \quad (27)$$

Given a dimension \mathcal{D} and an m one can obtain x through equation (26). Then equation (27) gives implicitly t_{AH} , the time of the formation of the apparent horizon on the surface Σ . For instance, for $\mathcal{D} = 6$ and $m = 1$ we find $t_{AH} = -0.53l$. Putting this value back in equation (25) we verify that everything checks.

The event horizon, being a null spherical surface, is determined through the null outgoing lines of metric (8), i.e., $dt/dr = a(t)$. This equation can be put in the following integral form,

$$\frac{r}{r_\Sigma} = -\frac{\mathcal{D}-2}{\mathcal{D}-1} \left(\frac{1}{2m}\right)^{1/(\mathcal{D}-1)} \int_{u_0}^{u_1} \frac{du}{\sin^{(\mathcal{D}-2)/(\mathcal{D}-1)}(u)}, \quad (28)$$

$u \equiv -\frac{\mathcal{D}-1}{\mathcal{D}-2} \frac{t}{l}$ and m has been defined above. Now, the time u_1 is precisely equal to the formation time of the apparent horizon, since in vacuum both horizons coincide [8]. One has then to integrate (28) to find the time

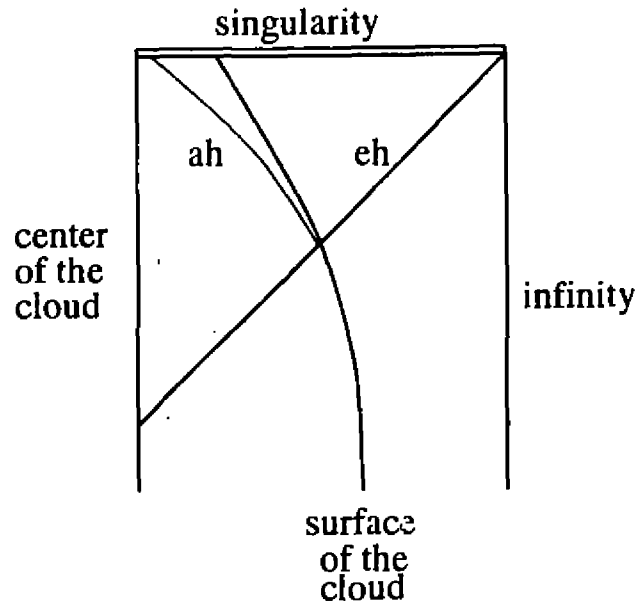


Figure 1.: Penrose diagram for the collapse of a dust cloud in anti-de Sitter spacetime. Each point in the diagram represents a $\mathcal{D} - 2$ sphere. (eh = event horizon), ah = apparent horizon).

u_0 at which the event horizon first forms, at $r = 0$. This can be done numerically. For $\mathcal{D} = 6$ and $m = 1$ we obtain $t_0 = -\frac{4}{5}u_0 l = -1.57 l$. A plot in comoving coordinates (t, r) shows the evolution of the apparent and event horizons. See [2] for plots for $\mathcal{D} = 4, 6, 10, 26$. Making a matching to the vacuum exterior spacetime one finds the usual Penrose diagram for gravitational collapse and formation of a black hole in an anti-de Sitter background, see figure below.

7 Conclusions

We have analysed gravitational collapse in Lovelock gravity which is a natural extension of Einstein's general relativity to higher dimensions. It was shown that within a restricted set of Lovelock coefficients, gravitational collapse of a regular initial non-rotating dust cloud proceeds, to form event and apparent horizons, and terminates at a spacelike curvature singularity, in much the same way as the Oppenheimer-Snyder collapse. As in the case of the wormhole solutions found in [9] and the black hole solutions found in [5] the collapsing solutions studied here show that some important features of classical general relativity are preserved and carried into Lovelock gravity.

References

- [1] D. Lovelock, *J. Math. Phys.* **12**, 498 (1971).
- [2] A. Ilha e J. P. S. Lemos, *Phys. Rev. D*, to appear.
- [3] A. Ilha e J. P. S. Lemos, in preparation.

- [4] M. Bañados, C. Teitelboim, J. Zanelli, in *J. J. Giambiagi Festschrift*, edited by H. Falomir, R. Gamboa, P. Leal, F. Schasposnik (World Scientific, Singapore, 1991).
- [5] M. Bañados, C. Teitelboim, J. Zanelli, *Phys. Rev. D* **49**, 975 (1994).
- [6] W. Israel, *Nuovo Cimento* **44B**, 463 (1967).
- [7] D. M. Eardley and L. Smarr, *Phys. Rev. D* **19**, 2239 (1979).
- [8] S. W. Hawking, G. F. R. Ellis, *The Large Scale Structure of Space and Time*, (Cambridge University Press, Cambridge 1973).
- [9] X. Li, *Phys. Rev. D* **50**, 3787 (1994).

The Detection of Gravitational Waves as a Test for Theories of Gravitation

Nadja S. Magalhães, Odylio D. Aguiar

*Divisão de Astrofísica, Instituto Nacional de Pesquisas Espaciais,
C.P. 515, São José dos Campos, SP 12201-970, Brazil*

Warren W. Johnson

*Department of Physics and Astronomy, Louisiana State University,
Baton Rouge, LA 70803-4001, USA*

Carlos Frajuca

*Escola Técnica Federal de São Paulo, Rua Pedro Vicente 625,
Canindé, São Paulo, SP 01109, Brazil*

We present a geometric and pictorial method that relates the data from fourth generation resonant-mass gravitational wave detectors to the different metric theories of gravitation. Such detectors use spherical antennas and allow for the determination of five out of the six independent "electrical" components of the Riemann tensor. These components can be written in terms of the Newmann-Penrose parameters, which allow for the discrimination among the different metric theories of gravitation. We present how the experimental results may be used to discriminate among these theories.

1 Introduction

Gravitational waves are a phenomenon predicted by several theories of gravitation. In this paper we will focus our attention on metric theories of gravitation, which have more experimental support than the non-metric ones. Also, metric theories can be conveniently classified according to its spin content that is responsible for the generation of the gravitational wave. Therefore, by detecting a gravitational wave and determining its spin it is possible to obtain information about the metric theories that may describe it.

The detection of gravitational waves is a field more than thirty years old[1]. It began with the research by Joseph Weber in the 60's using a massive aluminum cylinder at room temperature. In the 70's and 80's such detectors were improved: the cylinders (also known as antennas for gravitational waves) got bigger, better isolated from mechanical noises and were cooled down to 4K. Also, in those decades other kinds of detectors were introduced, like the interferometric ones.

Nowadays, the best cylindrical antennas are cooled down to temperatures less than 1K and they are protected against cosmic rays. Also, full-scale interferometric detectors are being built to operate in cooperation with the massive ones, and experiments are being designed to be performed in space. And the last, fourth generation of massive antennas is about to be built, using large, spherical masses. Such spherical antennas have several improvements over the cylindrical ones: they are expected to be omnidirectional and to detect five out of the six components of h (the dimensionless amplitude of the wave.) Because of this feature, for instance, a single spherical antenna could inform the direction of astrophysical sources of gravitational waves described by general relativity[2].

The resonant-mass detectors that use spherical antennas are those we will be interested on in this work. We will show how their data can be used to discriminate among the different metric theories of gravitation.

2 The Newmann-Penrose parameters

The Newmann-Penrose parameters (NPP) allow the identification of the spin content of a metric theory responsible for the generation of a gravitational wave[3]. For instance, general relativity (g.r.) (spin 2) has the following values for the NPP: $\Psi_4 \neq 0$ and $\Psi_2 = \Psi_3 = \Phi_{22} = 0$; on the other hand, Kaluza-Klein theories (spin 2, 1 and 0) have $\Psi_4 \neq 0$, $\Psi_3 \neq 0$, $\Phi_{22} \neq 0$ and $\Psi_2 = 0$. Such differences appear in the corresponding six independent “electric” components of the Riemann tensor, $E_{ij} \equiv R_{0i0j}$, which, to lowest non-trivial order in the perturbative expansion, may be expressed in terms of the NPP as

$$(E_{ij}) = \begin{pmatrix} -Re\Psi_4 - \Phi_{22} & Im\Psi_4 & -2\sqrt{2} Re\Psi_3 \\ Im\Psi_4 & Re\Psi_4 - \Phi_{22} & 2\sqrt{2} Im\Psi_3 \\ -2\sqrt{2} Re\Psi_3 & 2\sqrt{2} Im\Psi_3 & -6\Psi_2 \end{pmatrix}. \tag{1}$$

The six NPP can also be associated to 3×3 linearly independent matrices[4], forming a complete basis that describes any 3×3 matrix. These six matrices are also known as “basis polarization matrices” and each of them can be associated to one of the six polarization modes of a weak, plane, null gravitational wave permitted in the generic metric theory of gravity (these modes are illustrated in Ref.[4].) For instance, comparing the NPP of Kaluza Klein theories to those of g.r. we see that those theories allow three more polarization modes for a gravitational wave than g.r. does because $\Psi_3 \neq 0$ and $\Phi_{22} \neq 0$ for them. Differences in polarizations are the ones we expect to detect with a spherical antenna, which responds differently to different polarizations, as we present below. . .

3 The antenna’s response

A gravitational wave is commonly described in terms of its dimensionless amplitude h , which is basically a perturbation on the Minkowskian metric[5]. This amplitude can be written in terms of a 3×3 , symmetric matrix, and in general it has six independent terms. The observable h is the one that gravitational wave detectors are intended to detect.

The first quadrupole modes of a spherical antenna sensitive to gravitational waves are five-fold degenerate[6]. Such degeneracy allows the determination of five out of the six independent components of h . As we mentioned before, because of the use of the TT gauge in g.r. the number of independent components of h is reduced to five in this theory, and in principle only one spherical detector should suffice to inform the direction of the wave’s source. But in practice at least two detectors should work in coincidence so that the detected signal is reliable.

The response of a spherical antenna to a g.r. gravitational wave was presented in another paper[7]: the antenna’s shape is distorted to that of an ellipsoid. This geometric figure is described by an equation of the form

$$\frac{x^2}{a^2} + \frac{y^2}{b^2} + \frac{z^2}{c^2} = 1, \tag{2}$$

which can also be put in a convenient matrix form so that a 3×3 , real, symmetric matrix can characterize the figure:

$$\begin{pmatrix} x \\ y \\ z \end{pmatrix} \begin{pmatrix} a & 0 & 0 \\ 0 & b & 0 \\ 0 & 0 & c \end{pmatrix} \begin{pmatrix} x \\ y \\ z \end{pmatrix} = 1. \tag{3}$$

Because in general h is also described by this kind of matrix, not only g.r. but any metric theory of gravitation is expected to distort the spherical antenna into an ellipsoid. But since each theory allows different polarizations for a wave the antenna’s distortion should follow distinct patterns for each theory, basically the ones presented in Figure 1 of Ref.[4].

A prototype of a spherical antenna is already being tested[8] and its data can be organized so that h can be given in matrix form. From this the ellipsoidal picture follows naturally. With enough sensitivity, therefore, a spherical detector should to give important information on the polarization of the wave, among other things. This should be of major importance in confirming metric theories of gravitation.

4 Concluding Remarks

The first five quadrupole modes of a spherical antenna are five-fold degenerate and thus are adequate to inform about h described by traceless matrices. However, monopole modes are predicted by several metric theories and are not described by this kind of matrices. In order to detect the monopole and the quadrupole modes of a gravitational wave two spherical detectors should work in coincidence, one bigger than the other and adequately tuned, so that the smaller one is sensitive to the quadrupole modes and the bigger one is sensitive to the monopole mode.

The construction of an array of spherical detectors is now under study by an international collaboration named OMEGA[9], which includes a Brazilian group[10]. It is expected that spherical detectors of gravitational waves will be in operation in the beginning of the next century.

A more complete and detailed version of this work will be presented in a forthcoming paper.

Acknowledgements

NSM acknowledges FAPESP (Brazil) for the financial support. The research by WWJ is supported by the National Science Foundation (USA) under grant No. PHY-9311731. CF acknowledges CNPq (Brazil) for supporting his research.

References

- [1] For a recent bibliography on detectors of gravitational waves we recommend the *Proceedings of the First Edoardo Amaldi Conference on Gravitational Wave Experiments* (Singapore: World Scientific, 1995.) See also *Proceedings of the First International Workshop for an Omnidirectional Gravitational Radiation Observatory* (São José dos Campos, Brazil, May 26-31, 1996: To appear.)
- [2] N. S. Magalhães, W. W. Johnson, C. Frajuca and O. D. Aguiar, *Mon. Not. R. Astr. Soc.* **274**, 670 (1995.)
- [3] C. M. Will, *Theory and Experiment in Gravitational Physics* (Cambridge: Cambridge Univ. Press, 1993.)
- [4] D. M. Eardley, D. L. Lee and A. P. Lightman, *Phys. Rev.* **D8**,3308(1973.)
- [5] For a simple explanation of this concept we refer the reader to the book by B. Schutz, *A first course in general relativity* (Cambridge: Cambridge Univ. Press, 1990.)
- [6] R. V. Wagoner and H. J. Paik, *Proceedings of International Symposium on Experimental Gravitation* (Roma: Roma Accademia Nazionale dei Lincei), 257 (1977.)
- [7] N. S. Magalhães, W. W. Johnson, C. Frajuca and O. D. Aguiar, *The Astrophysical Journal*, Oct 10, 1996 issue.
- [8] S. M. Merkowitz and W. W. Johnson, *Phys. Rev.* **D51**,2546(1976.)
- [9] More information on this collaboration can be found by contacting the email address omegaimail@phgrav.phys.lsu.edu or from the WWW pages at <http://phwave.phys.lsu.edu/omega/>.
- [10] The Brazilian project is called GRAVITON and its WWW homepage can be found at <http://cruz.das.inpe.br/graviton/home.html>.

Self-Similar Planar Newtonian Collapse

Ozemar S. Ventura¹ and José P. S. Lemos²

¹*Centro Brasileiro de Pesquisas Físicas,*

Departamento de Partículas e Campos,

Rua Xavier Sigaud 150, 22290-180, Urca, RJ, Brazil

e-mail: ozc1.cbpf@cbpf.br

²*Observatório Nacional,*

Departamento de Astrofísica, Rua General José Cristino 77, 20921-400, São Cristóvão, RJ, Brazil

e-mail: lemos@on.br

In this work, two different classes of planar solutions for cold dust are analysed within the Newtonian framework. The first class contains planar collapsing solutions for a general set of self-similar initial conditions extending, in this way, Penston's original results. The second class consists of solutions without prescribing any initial conditions. In both classes, the solutions exhibit shell-crossing outside the plane of symmetry. The range of validity for both classes of solutions is then presented.

1 Introduction

Planar symmetry occurs as the limiting case in a number of geometrical configurations. For instance, (i) the central region of a disc whose edge is at a very large distance from the center, can be considered a region with planar symmetry, (ii) a spherical surface with radius incomparably larger than typical distances of interest within the surface, can also be locally approximated by planes. In these examples the planar approximation in the geometry can also be extended to symmetry in the dynamical laws. Indeed, it is well known that the gravitational potential generated by discs and spheres approach in the above well-defined limits the gravitational potential of a plane.

On the other hand, self-similar solutions are expected whenever the system under analysis does not have a characteristic scale, e. g., the basic constants and boundary conditions of the problem are insufficient to build up a scale. This may happen if the system loses at an intermediate stage of its evolution the memory of the initial or boundary conditions (see e. g. Zeldovich and Raizer 1991 or Lynden-Bell 1986).

Self-similar collapsing solutions have been widely studied. Self-similar spherically symmetric solutions for cold dust have been analysed by Penston (1969), Dyer (1979), Lynden-Bell and Lemos (1989), Lemos and Lynden-Bell (1989), as well as for other types of fluid, Fillmore and Goldreich (1984) and, in general relativity, by Cahill and Taub (1971) among others. Self-similar collapse of flat cold axisymmetric Newtonian discs has been studied by Boily and Lynden-Bell (1993).

Self-similar gravitational collapse with planar symmetry, within the context of Newton's gravitational theory, has been mainly studied to understand the formation of structures, like stars, galaxies and clusters of galaxies (Penston 1969, Fillmore and Goldreich 1984). In particular, Penston (1969) has presented a study of the self-similar Newtonian collapse for cold dust. This work considered a quadratic profile in the density and included the spherical, cylindrical and planar symmetries. It was shown that the spherical collapse of nearby shells is well described by a planar equation for those shells. It was also shown that thermal forces start to be important earlier for planar collapse than for spherical collapse. Therefore, the plane flatten instability, which drives spheres into flatten systems (Lynden-Bell 1964, Lin, Mestel and Shu 1965), is opposite to the thermal pressure gradient appearing in these nearly planar regions. That phenomenon obstructs the formation of a plane with infinite density.

In the case of large scale structure formation, Fillmore and Goldreich (1984) investigated self-similar planar solutions. It was given time a prescription to continue the solutions past the shell-crossing singularities, confirming earlier numerical simulation results (Mellot 1980).

Planar collapse has also been studied in General Relativity within the context of singularities and black holes. Thorne (1972) has argued that the relativistic collapse of oblate spheroids of mass m with size bigger than $\frac{Gm}{c^2}$ (where G is the gravitational constant and c is the light velocity) is well approximated by Newtonian gravitation until the final stage when a singular disk forms. The collapse of the inner regions of these oblate spheroids can be approximated by collapse of planes. In the Newtonian framework the collapse to a disk was earlier analysed by Lin, Mestel and Shu (1965), whereas a full relativistic numerical analysis was done by Shapiro and Teukolsky (1991).

In this work we investigate two distinct cases. In section 2, we study self-similar planar systems that collapse from rest. In this case, we obtain a general class of self-similar initial conditions for the collapsing system. In section 3, we analyse self-similar planar systems that do not remember the initial conditions.

2 Dust self-similar solutions with self-similar initial conditions

In this section, we consider self-similar cold dust solutions in collapse with planar symmetry. This configuration was also treated in the Appendix I of Penston's paper. Here, we generalize Penston's solutions finding a general class of initial conditions for a self-similar collapse.

2.1 The solutions

Self-similar solutions, in this case, are such that the form of the density's profile distribution remains unchanged with time. Consider a cold plane of gas with mean volumetric density $\bar{\rho}(z)$ at a distance z from the plane of symmetry. Then its interior effective mass $\sigma(z)$ (i. e., the mass per unit area within distance z) is given by $\sigma(z) = 2z\bar{\rho}(z)$. The equation of motion for such a plane is

$$\frac{\partial^2 z}{\partial t^2} = -2\pi G\sigma(z), \quad (1)$$

We may analyse only the case $z \geq 0$. The $z \leq 0$ case has an analogous treatment.

Self-similarity requires $z = z_0(t)z_*(\sigma_*)$, where $\sigma_* = \sigma/\sigma_0(t)$ is a time independent variable (see e. g. Lynden-Bell and Lemos 1989 for the spherical symmetric analogue). Let us go on now analysing one class of solutions for the plane distribution of cold dust.

A solution of (1) is

$$z = z_i(\sigma) - \pi G\sigma t^2, \quad (2)$$

$$v = -2\pi G\sigma t, \quad (3)$$

where $z_i(\sigma)$ is an integration function. We have set the initial velocity of the planes equal to zero (we prove in the Appendix that the condition $v_i \neq 0$ is irrelevant). In order to obtain the functional dependence of z_i , we introduce the self-similar condition in equation (2). Then,

$$F(\sigma_*) = f(t) \left[t^2 - \frac{z_i(\sigma_0\sigma_*)}{\pi G\sigma_0\sigma_*} \right], \quad (4)$$

where

$$f(t) = -\frac{\pi G\sigma_0}{z_0}, \quad (5)$$

$$F(\sigma_*) = \frac{z_*}{\sigma_*}. \quad (6)$$

Differentiating (4) with respect to σ_* , we obtain

$$F'(\sigma_*) = \sigma_0 f \left[\frac{z_i}{(\sigma_0\sigma_*)^2} - \frac{z_i'}{\sigma_0\sigma_*} \right], \quad (7)$$

where the dash denotes a derivative with respect to its own argument. Next, we take logarithms in (7), differentiate the resulting equation with respect to σ_0 , and multiply by σ_0 to obtain

$$\sigma_0^2 f \frac{d}{d\sigma_0} \left(\frac{1}{\sigma_0 f} \right) = \sigma \frac{d}{d\sigma} \log \left[\frac{z_i}{\sigma^2} - \frac{z_i'}{\sigma} \right]. \quad (8)$$

Since the functional dependence in both sides of (8) is different, we have that each side of this equation is a constant b , say. Therefore, integrating the right hand side of (8) we have

$$\frac{dz_i}{d\sigma} - \frac{z_i}{\sigma} = \pi G B_1 \sigma^b, \quad (9)$$

where B_1 is also a constant. The general solution of (9), for $b \neq 0$, is

$$z_i = \pi G \sigma (B \sigma^b + t_{c0}^2) \quad (10)$$

with $B = bB_1$ and t_{c0}^2 a new integration constant. When $b \rightarrow 0$ we have $z_i \rightarrow \pi G \sigma (B_1 \log \sigma + c_1)$, where c_1 is a new constant. These results give the general class of self-similar initial conditions for planar collapse.

If we now put

$$z = \pi G \sigma [t_c^2(\sigma) - t^2], \quad (11)$$

we may identify $t_c^2(\sigma) = z_i(\sigma) / \pi G \sigma$. So,

$$t_c^2(\sigma) = B \sigma^b + t_{c0}^2. \quad (12)$$

We see that $t_c(0) = t_{c0}$ which is the time the central plane collapses to the origin. With (12) and (11), we obtain:

$$z = \pi G \sigma (B \sigma^b + t_{c0}^2 - t^2). \quad (13)$$

We impose $b \geq 0$ to avoid initial shell-crossing in order that planes with larger interior masses start the collapse at greater distances.

Shell-crossing happens when two nearby planes with densities σ and $\sigma + d\sigma$ pile up into the same distance z , i. e., $dz = 0$ for these two planes. In this case the volumetric density diverges, $\rho = \frac{d\sigma}{dz} \rightarrow \infty$. The solution is no more valid when plane-crossing starts. To find a full solution one has to give a precise prescription for the continuation of the solution after the shell-crossing. Indeed, when $t = t_{c0}$, we have from equation (14) $\frac{d\sigma}{dz} \Big|_{\sigma \rightarrow 0} \rightarrow \infty$. For later times there will be shell-crossings in the region $z > 0$.

The density profile $\frac{d\sigma}{dz}$ is given by

$$\pi G \rho = [B(b+1)\sigma^b + t_{c0}^2 - t^2]^{-1}. \quad (14)$$

From (14) we see that there is shell-crossing for distances $z > z_l$ where,

$$z_l = \frac{\pi G b}{B^{1/b}} \left[\frac{t^2 - t_{c0}^2}{b+1} \right]^{\frac{b+1}{b}}. \quad (15)$$

Thus, the region with plane-crossing increases with time.

From equation (13), we can see that it is possible to choose the scale $\sigma_0(t)$ as

$$\sigma_0 = \left| \frac{t_{c0}^2 - t^2}{B} \right|^{1/b}, \quad (16)$$

yielding then the other sides,

$$z_* = \sigma_* (\sigma_*^b \pm 1), \quad (17)$$

$$z_0 = \frac{\pi G}{B^{1/b}} |t_{c0}^2 - t^2|^{\frac{b+1}{b}}, \quad (18)$$

where \pm , in (17) is the signal of $t_{c0}^2 - t^2$. Immediately, we have the profile of $\rho_*(\sigma_*)$, $\rho_0(t)$, $v_*(\sigma_*)$ and $v_0(t)$, given by:

$$\rho_* = [(b+1)\sigma_*^b \pm 1]^{-1}, \quad (19)$$

$$\pi G \rho_0 = |t_{c0}^2 - t^2|^{-1}, \quad (20)$$

$$v_* = -\frac{1}{2}\sigma_*, \quad (21)$$

$$v_0 = 4\pi Gt \left| \frac{t_{c0}^2 - t^2}{B} \right|^{1/b} \quad (22)$$

Therefore, we have two distinct forms for ρ_* . When the signal is positive, σ_* takes any value greater or equal to zero (being zero only in the centre of symmetry). When the signal is negative, i. e., $t^2 > t_{c0}^2$, then we have the condition $\sigma_* \geq 1$. However, the no-shell crossing condition imposes a stronger requirement:

$$z_* \geq \frac{b}{(b+1)^{(b+1)/b}} \quad (23)$$

Note that the self-similar profiles are always valid in the $z_* > 1$ regions.

2.2 Illustration of the solutions

From equations (17), (19) and (21), one can check that before the central shell collapses, the $z_* \ll 1$ region can be described by the approximation

$$\rho_* \cong 1 - (b+1)z_*^b, \quad (24)$$

$$v_* \cong -\frac{1}{2}z_*. \quad (25)$$

On the other hand, the region with $z_* \gg 1$ can be approximated by

$$\rho_* \cong \frac{1}{(b+1)}z_*^{-b/(b+1)}, \quad (26)$$

$$v_* \cong -\frac{1}{2}z_*^{1/(b+1)}. \quad (27)$$

Using the time-scales $\sigma_0(t)$ and $z_0(t)$ given in equations (16) and (18) respectively, one can verify that the regions at large z have identical density and velocity profiles for all times, taking the following asymptotic forms: $\rho \propto z^{-\alpha}$, and $v \propto z^\beta$, where $\alpha = b/(b+1)$ and $\beta = 1/(b+1)$. Using (24) and (25), we have that, for $t < t_{c0}$, the regions with relatively small values of z have density and velocity profiles given by

$$\rho \cong \frac{1}{\pi G(t_{c0}^2 - t^2)} \left[1 - \frac{B(b+1)}{(\pi G)^b (t_{c0}^2 - t^2)^{b+1}} z^b \right] \quad (28)$$

and

$$v \cong -\frac{2t}{(t_{c0}^2 - t^2)} z. \quad (29)$$

The value of the constant b is constrained by the chosen density initial profile. Firstly, we analyse Penston's particular solution which is characterized by $b = 2$. His results are linked to the initial condition

$$\rho(0, z) = \rho_i \left(1 - \frac{z^2}{A^2} \right), \quad (30)$$

where ρ_i and A are constants. In this case we see that, when $z \rightarrow \infty$, $\rho \rightarrow z^{-2/3}$ and $v \rightarrow z^{1/3}$. In the other limit ($z \rightarrow 0$), ρ presents a quadratic top. For $t^2 > t_{c0}^2$, there is plane-crossing but, the asymptotic dependence of ρ and v is invariant.

Penston's ($b = 2$) case separates two types of solutions. For $b > 2$, the solutions present a smooth flat top in the $z \rightarrow 0$ regions while for $b < 2$ the solutions have a cusp in the same small z region.

Another case of analytical interest is given by $b = 1$. This solution has the property of being invertible. Then, the density and velocity profiles can be described as explicit functions of z and t . This solution has the form:

$$\sigma = \frac{t^2 - t_{c0}^2}{2B} + \frac{1}{2B} \sqrt{(t_{c0}^2 - t^2)^2 + \frac{4B}{\pi G} z}, \quad (31)$$

$$\rho = \frac{(\pi G)^{3/2}}{\sqrt{\pi G(t_{c0}^2 - t^2)^2 + 4Bz}}$$

and

$$v = -\frac{\pi G t}{B} \left[t^2 - t_{c0}^2 + \sqrt{(t_{c0}^2 - t^2)^2 + \frac{4B}{\pi G} z} \right]. \quad (32)$$

It is straightforward to note that when $z_* \rightarrow 0$, the profile does present a cusp at $z = 0$.

A case of physical importance is $b = 0.2$. This exponent has been studied by Fillmore and Goldreich (1984) and illustrates qualitatively Mellot's numerical results (Mellot 1980). This numerical calculations simulates the large scale planar collapse of massive neutrinos, which can be considered candidates to generate condensations for the formation of the large scale structures. The asymptotic forms of the ρ and v given by $\rho \rightarrow z^{-1/6}$ and $v \rightarrow z^{5/6}$.

3 Solutions for self-similar dust without initial conditions

In the previous section, we obtained and illustrated one class of self-similar solutions with initial conditions. Now, we shall find another self-similar class of solutions for cold dust planar distribution of matter. Here, we do not impose any initial conditions.

3.1 The solutions

First, we note that the equation of motion (1) has a first integral given by

$$E(\sigma) = \frac{1}{2} \dot{z}^2 + 2\pi G \sigma z. \quad (33)$$

Now, to obtain self-similar solutions without memory of initial conditions we first use the self-similar requirement and put Eq. (1) in the form:

$$\frac{\partial^2}{\partial t^2} [z_0(t) z_*(\sigma_*)] \Big|_{\sigma} = -2\pi G \sigma_0(t) \sigma_*. \quad (34)$$

writing

$$\frac{\partial}{\partial t} \Big|_{\sigma} = \frac{\partial}{\partial t} \Big|_{\sigma_*} - \frac{\sigma_* \dot{\sigma}_0}{\sigma_0} \frac{\partial}{\partial \sigma_*} \Big|_t,$$

eq. (34) may be rewritten as

$$\begin{aligned} \left[\frac{\ddot{L}}{L^2} l' + l'^2 + l'' \right] - \left[2l' + \frac{\dot{L}}{L^2} \right] \frac{dl_*}{dL_*} + \left(\frac{dl_*}{dL_*} \right)^2 + \frac{d^2 l_*}{dL_*^2} &= \\ &= -\frac{2\pi G \sigma_0}{z_* L^2} \frac{\sigma_*}{z_*}, \end{aligned} \quad (35)$$

where $L = \ln \sigma_0$, $l = \ln z_0$, $L_* = \ln \sigma_*$ and $l_* = \ln z_*$. The dash denotes derivation with respect to L and the dot with respect to time. Without gravitation (i. e., $G = 0$), the right hand side of (35) is zero. In this zero gravity case, the left hand side of (35) can be used without distinction for the three most used symmetries, planar, cylindrical and spherical.

One can find which constraints self-similarity imposes on the energy per unit mass $E(\sigma)$ and on the time function $t_c(\sigma)$. Noting that the difference to the spherically symmetric case is in the RHS of (35), one can follow closely the work of Lemos and Lynden-Bell 1989b, and without repeating here the whole calculation, we find (Ventura, 1992).

$$E = A \sigma^a \quad (36)$$

$$t_c(\sigma) = B \sigma^b + t_0 \quad (37)$$

where A , B , b are constants of integration and $a = 2(b + 1)$. There is a special case, when $b \rightarrow 0$, given by

$$t_c(\sigma) = B_1 \log \left(\frac{\sigma}{\sigma_1} \right) + t_1 \quad (38)$$

where B_1 , σ_1 and t_1 are constants. The equations (36), (37) and (38) give then a set of self-similar solutions without initial conditions.

One can write the distance z of the planes in the form

$$z = -\pi G \sigma (t + B \sigma^b) \left[t - \left(\frac{\sqrt{2A}}{\pi G B} - 1 \right) B \sigma^b \right]. \quad (39)$$

3.2 Illustration of the solutions

We will present now a study of the solutions obtained in the previous sub-section. Unlike the spherical case, such solutions always have positive total energy, which follows a power-law in the interior effective mass, $E = A \sigma^a$. The other integration function is $t_c(\sigma) = B \sigma^a$, where, without loss of generality, we have set $t_0 = 0$. This, leads us to write the self-similar solutions as $\sigma = \sigma_0 \sigma_*$ and $z = z_0 z_*$, where now

$$\sigma_0 = \left| \frac{t}{B} \right|^{1/b}, \quad (40)$$

$$z_0 = \pi G B^2 \sigma_0^{2b+1} \quad (41)$$

and

$$z_* = \sigma_* (\sigma_*^b \pm 1) \left[\left(\frac{\sqrt{2A}}{\pi G B} - 1 \right) \sigma_*^b \mp 1 \right]. \quad (42)$$

Here the sign \pm is the same as the one of t . We analyse the expansion and recollapse of the shells. To avoid initial plane-crossing, we impose $b \geq 0$. We also see that equation (42) represents a physical solution if $\frac{\sqrt{2A}}{\pi G B} > 1$.

Let us verify if these self-similar solutions have subsequent plane-crossing. From the equations (39), we have $\rho = \frac{d\sigma}{dt}$ given by

$$\begin{aligned} \pi G \rho = & \left[\left(\frac{\sqrt{2A}}{\pi G B} - 1 \right) (2b + 1) B^2 \sigma^{2b} + \right. \\ & \left. + \left(\frac{\sqrt{2A}}{\pi G B} - 2 \right) (b + 1) B \sigma^b t - t^2 \right]^{-1}. \end{aligned} \quad (43)$$

Then, there is shell-crossing for distances $z \leq z_1$, where

$$z_1 = \pi G B (1 + \beta_{\pm}) \left[1 + \beta_{\pm} - \frac{\sqrt{2A}}{\pi G B} \right] \left[\left| \frac{t}{B \beta_{\pm}} \right| \right]^{\frac{2b+1}{b}}, \quad (44)$$

and

$$\begin{aligned} \beta_{\pm} = & \frac{1}{2} \left[(b + 1) \left(\frac{\sqrt{2A}}{\pi G B} - 2 \right) \pm \left[\frac{2A (b + 1)^2}{\pi^2 G^2 B^2} + \right. \right. \\ & \left. \left. - 4B^2 \left(\frac{\sqrt{2A}}{\pi G B} - 1 \right) \right]^{1/2} \right] \end{aligned} \quad (45)$$

The validity of this solution is restricted to the regions with $|z| > |z_1|$. We analyse only the regions where there is no shell-crossing.

For large negative times the planes are expanding and the plane-crossing region decreases with time. For large positive times the planes are collapsing and the plane-crossing regime increases with time. At $t = 0$ there is a plane expanding and recollapsing instantaneously. Since the planes reach their maximum distances when $t = \frac{B \sigma^b}{2} \left(\frac{\sqrt{2A}}{\pi G B} - 2 \right)$, solutions with $\frac{\sqrt{2A}}{\pi G B} > 2$ have their maximum for $t > 0$, while solutions with $\frac{\sqrt{2A}}{\pi G B} < 2$ reach their maximum for $t < 0$. The marginal case $\left(\frac{\sqrt{2A}}{\pi G B} = 2 \right)$ gives us that all the planes have their maximal expansion point at $t = 0$.

The self-similar form of the profile's density is given by:

$$\rho = \frac{1}{\pi G B^2 \sigma_0^{2b}} \left[(2b+1) \left(\frac{\sqrt{2A}}{\pi G B} - 1 \right) \sigma_*^{2b} + \right. \\ \left. \pm \left(\frac{\sqrt{2A}}{\pi G B} - 2 \right) (b+1) \sigma_*^b - 1 \right]^{-1} \quad (46)$$

and the velocity's profile by

$$v = \pi G B \sigma_0^{b+1} \sigma_* \left[\left(\frac{\sqrt{2A}}{\pi G B} - 2 \right) \sigma_* \mp 2 \right]. \quad (47)$$

In the limit $z \rightarrow \infty$, the density has the form $\rho \rightarrow z^{-2b/(2b+1)}$, while the velocity goes as $v \rightarrow z^{(b+1)/(2b+1)}$. For large or intermediate z , such that $B \sigma^b \left(\frac{\sqrt{2A}}{\pi G B} - 2 \right) \ll 2$ (see equation (47)), the velocity's profile is $v \rightarrow z^{1/(2b+1)}$. When $\frac{\sqrt{2A}}{\pi G B} = 2$, we have that this intermediate region is pushed to infinity.

For $t = 0$, the time-scale of the density, $\rho_0(t)$, diverges. The profiles of the density and velocity take the same form of the limiting $z \rightarrow \infty$ case, given by:

$$\rho = \frac{1}{(2b+1) \left[\pi G B^2 \left(\frac{\sqrt{2A}}{\pi G B} - 1 \right) \right]^{1/(2b+1)}} z^{-2b/(2b+1)}, \quad (48)$$

$$v = \begin{cases} \frac{(\pi G B^2)^{\frac{b+1}{2b+1}} \left(\frac{\sqrt{2A}}{\pi G B} - 2 \right)}{B \left(\frac{\sqrt{2A}}{\pi G B} - 1 \right)^{\frac{b+1}{2b+1}}} z^{\frac{b+1}{2b+1}}, & \text{if } \frac{\sqrt{2A}}{\pi G B} \neq 2 \\ -\frac{2(\pi G B^2)^{\frac{b+1}{2b+1}}}{B^2 \left(\frac{\sqrt{2A}}{\pi G B} - 1 \right)^{\frac{b+1}{2b+1}}} z^{1/(2b+1)}, & \text{if } \frac{\sqrt{2A}}{\pi G B} = 2. \end{cases} \quad (49)$$

The solution with $b = 0$ and $B = 0$ is described by $z = \pi G \sigma \left[\frac{\sqrt{2A}}{\pi G} t - t^2 \right]$, $v = \pi G \sigma \left[\frac{\sqrt{2A}}{\pi G} - 2t \right]$ and $\pi G \rho = \left[\frac{\sqrt{2A}}{\pi G} t - t^2 \right]^{-1}$ where $0 < t < \frac{\sqrt{2A}}{\pi G}$. We verify that, in spite of the motion of planes, the volumetric density does not exhibit functional dependence on σ . This solution seem to have no direct physical interpretation.

4 Appendix

In Section 2 we analysed collapsing solutions for systems initially at rest. Now, we will show that the dynamical description of the self-similar system is invariant when the initial velocity of the shells is non-vanishing. The general solution for such cases is:

$$z = z_i(\sigma) + v_i(\sigma)t - \pi G \sigma t^2 \quad (A1)$$

and

$$v = v_i(\sigma) - 2\pi G \sigma t. \quad (A2)$$

We impose the self-similarity condition, $v = v_0(t) v_*(\sigma_*)$ and $z = z_0(t) z_*(\sigma_*)$. From (A2), we have

$$F_1(\sigma_*) = f_1(t) [k_i(\sigma_0 \sigma_*) - t], \quad (A3)$$

where

$$F_1 = \frac{v_*(\sigma_*)}{\sigma_*}, \quad (A4)$$

$$f_1 = \frac{2\pi G \sigma_0(t)}{v_0(t)}, \quad (A5)$$

$$k_i = \frac{v_i(\sigma_0 \sigma_*)}{2\pi G \sigma_0 \sigma_*}. \quad (A6)$$

Differentiating (A3) with respect to σ_* , and taking the logarithm of the resulting equation, we are lead to

$$\log F' = \log(\sigma_0 f) + \log k'_i, \quad (\text{A7})$$

where the dash denotes derivation with respect to its own argument. Differentiating (A7) with respect to σ_* , and multiplying afterwards by σ_* , we have

$$-\sigma_0 \frac{d}{d\sigma_0} \log(\sigma_0 f) = \sigma_* \frac{d}{d\sigma_*} \log k'_i = b - 1 = \text{constant}. \quad (\text{A8})$$

For $b \neq 0$, the equation (A8) has the solution

$$k_i = \frac{1}{2} (B_1 \sigma_*^b + B_2), \quad (\text{A9})$$

where B_1 and B_2 are constants. With (A6) and (A9), we have

$$v_i = \pi G \sigma (B_1 \sigma_*^b + B_2). \quad (\text{A10})$$

Then (A10) and (A1) yield

$$F_2(\sigma_*) = f_2(t) [H(\sigma_* \sigma_*) + (B_1 \sigma_*^b \sigma_*^b + B_2) t - t^2], \quad (\text{A11})$$

where,

$$H = \frac{z_i}{\pi G \sigma}, \quad (\text{A12})$$

$$F_2 = \frac{z_*}{\sigma_*}, \quad (\text{A13})$$

and

$$f_2 = \frac{\pi G \sigma_0}{z_0}. \quad (\text{A14})$$

Differentiating (A11) with respect to σ_* , dividing by σ_*^{b-1} and differentiating again with respect to σ_* , we obtain:

$$\frac{d}{d\sigma_*} \left[\frac{F'_2}{\sigma_*^{b-1}} \right] = \sigma_0^b f_2 \frac{d}{d\sigma_*} \left[\frac{H'}{\sigma_*^{b-1}} \right]. \quad (\text{A15})$$

Taking the logarithm of the equation (A15), differentiating with respect to σ_* and multiplying by σ_* , gives

$$\sigma_0 \frac{d}{d\sigma_0} \{ \sigma_0^{b+1} f_2 \} + \sigma_* \frac{d}{d\sigma_*} \left[\frac{H'}{\sigma_*^{b-1}} \right] = 0. \quad (\text{A16})$$

Since the two terms of the equation (A16) are functions of different variables, each side must be a constant. In this case, the general solution for $H(\sigma)$ is

$$H(\sigma) = B_3 \sigma^b + B_4 + \alpha I(\sigma), \quad (\text{A17})$$

where B_3 , B_4 and α are constants and $I(\sigma)$ is given by

$$I(\sigma) = \begin{cases} \sigma^b [\log \sigma - 1], & \text{for } b \neq 1; \\ (\log \sigma)^2, & \text{for } b = 1. \end{cases} \quad (\text{A18})$$

Introducing (A10), (A12) and (A17) in (A1), we have

$$z = \pi G \sigma \left[(B_3 + B_1 t) \sigma^b + \alpha I + B_4 + \frac{B_2^2}{4} - \left(t - \frac{B_2}{2} \right)^2 \right] \quad (\text{A20})$$

When we take $v_i = 0$, i. e., $B_1 = B_2 = 0$, the solutions obtained in Section 3 should be reproduced. But this occurs only if $\alpha = 0$. Therefore, (A19) is written as

$$z = \pi G \sigma \left(1 + \frac{B_1}{B_3} t \right) \left[B_3 \sigma^b + - \frac{\left(t - \frac{B_2}{2} \right)^2 - \left(B_4 + \frac{B_2^2}{4} \right)}{1 + \frac{B_1}{B_3} t} \right]. \quad (\text{A20})$$

From (A20), we see that the general form of the time scale for the surface density is

$$\sigma_0 = \gamma \left| \frac{\left(t - \frac{B_2}{2}\right)^2 - \left(B_4 + \frac{B_2^2}{4}\right)}{1 + \frac{B_1}{B_3}t} \right|^{1/b}, \quad (A21)$$

where γ is a constant which we set to one, without loss of generality, $\gamma = 1$. Then from (A20) and (A21) we have

$$z_0 = \pi G \left(1 + \frac{B_1}{B_3}t\right) \sigma_0^b. \quad (A22)$$

We know that $v_0(t) = \frac{dz_0}{dt}$. From (A21), (A22), (A2) and (A10) we have:

$$v_*(\sigma_*) = b\sigma_* J(t, \sigma_*) \quad (A23)$$

with

$$\begin{aligned} J = & \left[(B_2 - 2t) \left(1 + \frac{B_1}{B_3}t\right) + B_1 \left(t - \frac{B_2}{2}\right)^2 \sigma_*^b \right] \times \\ & \times \left[(b+1)(B_2 - 2t) \left(1 + \frac{B_1}{B_3}t\right) - \frac{B_1}{B_3} \left\{ \left(t - \frac{B_2}{2}\right)^2 + \right. \right. \\ & \left. \left. - \left(B_4 + \frac{B_2^2}{4}\right) \right\} \right]^{-1} \end{aligned} \quad (A24)$$

From (A23) one finds that $J(t, \sigma_*)$ cannot depend on t . Then, we impose that the equation (A24) has dependence only on σ_* . In such case, we have only one possibility: $B_1 = 0$ and $J = \frac{1}{b+1}$. This condition, along with a time translation $(t \rightarrow t - \frac{B_2}{2})$, allows us to write (A20) as

$$z = \pi G \sigma \left[B_3 \sigma^b + t_{c0}^2 - t^2 \right]. \quad (A25)$$

Similarly

$$v = -2\pi G \sigma t. \quad (A26)$$

The demonstration for the logarithmic ($b = 0$) case goes along the same steps.

5 Acknowledgments

Ozemar Souto Ventura acknowledges Observatório Nacional do Rio de Janeiro, where this work has been done.

References

- [jf] Boily, C., and Lynden-Bell, D., *Mon. Not. R. Astr. Soc.*, **204**, 1003 (1993).
- [kl] Cahil, M. E. and Taub, A. H., *Comm. Math. Phys.*, **21**, 1 (1971).
- [1] Dyer, C. C., *Mon. Not. R. Astr. Soc.*, **189**, 189 (1979).
- [2] Fillmore, J. A. and Goldreich, P., *Ap. J.*, **281**, 1 (1984) and Fillmore, J. A. and Goldreich, P., *Ap. J.*, **281**, 9 (1984).
- [h] Lemos, J. P. S. and Lynden-Bell, D., *Mon. Not. R. Astr. Soc.*, **240**, 303 (1989a).
- [yt] Lemos, J. P. S. and Lynden-Bell, D., *Mon. Not. R. Astr. Soc.*, **240**, 317 (1989b).
- [sa] Lin, C., Mestel, L. and Shu, F. H., *Ap. J.*, **142**, 1431 (1965).
- [lk] Lynden-Bell, D., in " *Gravitation in Astrophysics* ", Cargèse 86, eds: Carter, B., Hartle, J., Plenum, New York (Ch 1).
- [3] Lynden-Bell, D., *Ap. J.*, **139**, 1195 (1964).
- [po] Lynden-Bell, D. and Lemos, J. P. S., *Mon. Not. R. Astr. Soc.*, **233**, 197 (1989).
- [4] Mellot, A. L., *Ap. J.*, **84**, 1138 (1980).
- [l] Mestel, L., *Q. Jl. R. astr. Soc.* **6**, 161 (1965).
- [g] Penston, M. V., *Mon. Not. R. astr. Soc.*, **144**, 425 (1969).
- [l] Shapiro, S. L. and Teukolsky, S. A., *American Scientist*, **79**, 330 (1991).
- [12] Thorne, K. S., *Magic Without Magic*, editor: Klauder, J., Freeman, San Francisco (1972).
- [13] Ventura, O. S., M.S. Thesis, Observatório Nacional - Rio de Janeiro - Brasil, (1992).
- [jg] Zel'dovich, Ya. B. and Raizer, Y. P., *Phys. of Shock Waves and High Temperature Hydrodynamic Phenomena*, Academic Press, New York (1991).

Model Independent Analysis of Proton-Proton Elastic Scattering*

P. A. S. Carvalho and M. J. Menon

Instituto de Física 'Gleb Wataghin'

Universidade Estadual de Campinas - Unicamp

13083-970 Campinas, São Paulo, Brasil.

We present an impact parameter analysis of pp elastic scattering between $\sqrt{s}=13.8$ GeV and $\sqrt{s}=62.5$ GeV. Parametrizing the scattering amplitude by a sum of exponentials with complex parameters, we fit the differential cross section data through the CERN program MINUIT. From the analysis of 7 sets of experimental data we compute the Profile and Inelastic Overlap Functions. We have improved a previous analysis taking into account the error propagation and achieving better confidence intervals in the statistical analysis ($\chi^2/\text{d.o.f.}$). We conclude that the central opacity is nearly constant at 20 ~ 60 GeV (92% ~ 93%) and that the peripheral opacity ($b=1$ fm) increases with the energy at 20 ~ 60 GeV (34% \rightarrow 38%). We calculate the eikonal in the transferred momentum space and the results suggest the existence of a zero at $q^2 \simeq 10 \sim 11$ GeV².

1 Introduction

In the absence of a pure QCD description for elastic hadron scattering, model-independent analyses play an important role in the search for connections between experimental data and gauge field theories. To this end the impact parameter formalism and eikonal approach have been presently used.

In the impact parameter representation the elastic scattering amplitude, F , is given by the Fourier-Bessel transform of the Profile Function [1],

$$F(q, s) = i \int b db J_0(qb) \Gamma(b, s) \equiv i \langle \Gamma(b, s) \rangle, \quad (1)$$

where b is the impact parameter, q^2 the transferred momentum, \sqrt{s} the center-of-mass energy, J_0 the Bessel Function and $\Gamma(b, s)$ the Profile Function. The s -channel unitarity in the impact parameter space connects $\Gamma(b, s)$ with the Inelastic Overlap Function, $G_{in}(b, s)$, by [1],

$$2\text{Re}\Gamma(b, s) = |\Gamma(b, s)|^2 + G_{in}(b, s). \quad (2)$$

In the optical analogy (Fraunhofer diffraction), $\text{Re} \Gamma(b, s)$ represents the degree of absorption of an incident wave caused by the obstacle and so, may be seen as describing the hadronic opacity as a function of b and s . The $G_{in}(b, s)$ represents the absorption into open inelastic channels and its integration over the impact parameter plane leads to the total inelastic cross section:

$$\sigma_{in}(s) = 2\pi \int b db G_{in}(b, s). \quad (3)$$

The $\Gamma(b, s)$ is connected to the eikonal, $\Omega(b, s)$, by

$$\Gamma(b, s) = 1 - e^{-\Omega(b, s)}, \quad \Omega(b, s) = \langle \Omega(q, s) \rangle. \quad (4)$$

*Financial Support: FAPESP, CNPq

Extraction of $\Gamma(b, s)$ and $G_{in}(b, s)$ from experimental data is usually performed by suitable parametrizations for the scattering amplitude $F(q, s)$ and fits to experimental differential cross section and ρ -parameter data:

$$\frac{d\sigma}{dq^2} = \pi |F(q, s)|^2, \quad \rho(s) = \frac{\text{Re}F(0, s)}{\text{Im}F(0, s)} \quad (5)$$

2 Fits to the Experimental Data

We introduce the following model-independent parametrization for the scattering amplitude

$$F(q, s) = i \sum_{j=1}^2 \alpha_j (1 + i\lambda) e^{-\beta_j q^2} + i \sum_{j=3}^n \alpha_j e^{-\beta_j q^2}, \quad (6)$$

with the constraint

$$\lambda(s) = -\rho(s) \frac{\sum_{j=1}^n \alpha_j}{\alpha_1 + \alpha_2}, \quad (7)$$

where $\alpha_i, \beta_i, i=1,2,\dots,n$ are real free parameters and $\rho(s)$ is the experimental ρ -value at each energy.

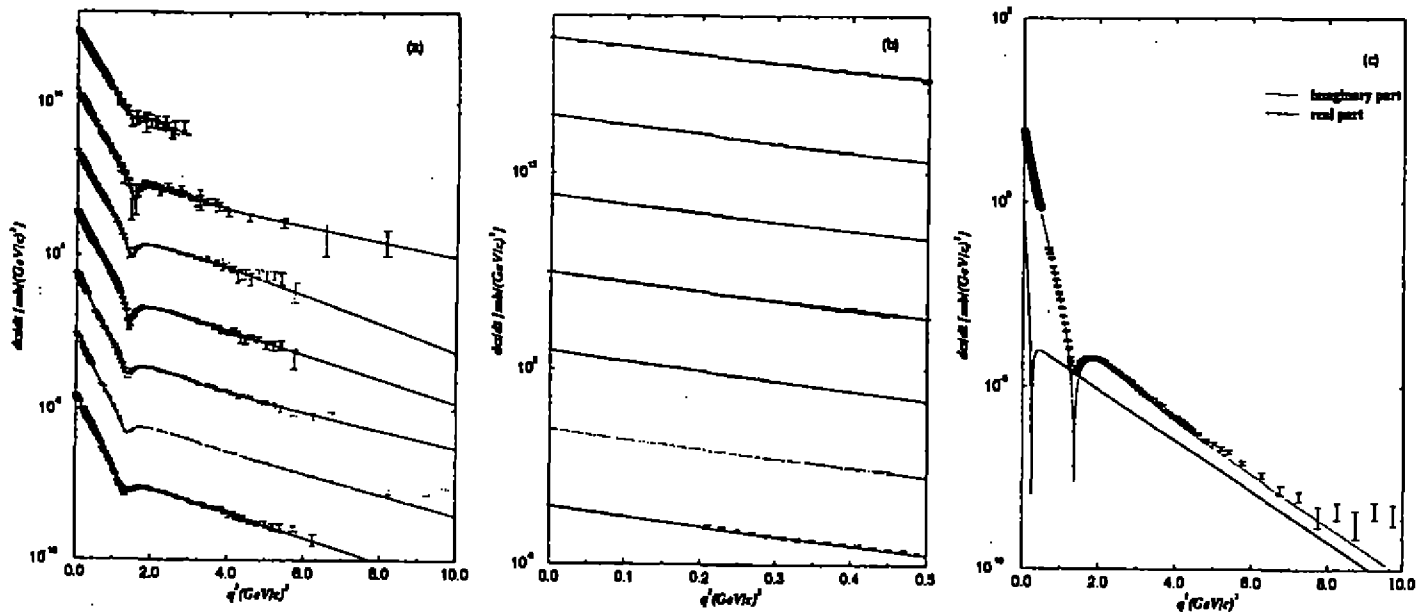


Figure 1. Fit to pp differential cross section data: (a) complete region in transferred momentum with available data; (b) diffraction peak; (c) contribution of the real and imaginary part of the scattering amplitude at the energy of 52.8 GeV. Experimental data are from references [3,4].

Making use of the CFRN-minuit routine [2] we fit seven sets of pp differential cross section data above $\sqrt{s} = 10$ GeV. These sets may be classified into two groups: G1: $\sqrt{s}=13.8$ and 19.4 GeV [3], G2: $\sqrt{s}=23.5, 30.7, 44.7, 52.8$ and 62.5 GeV [4]. The group G2 was critically analysed by Amaldi and Schubert [4] and corresponds to a coherently normalized data set. This is not true for the group G1. The fits were performed with $n=4$ at 23.5 and 62.5 GeV, $n=3$ at 30.7 and $n=5$ at the other energies¹. The results are shown in figure 1 and table 1 (numerical values of the free parameters are available from the authors).

¹The determination of n was based on the analysis of $\chi^2/\text{d.o.f.}$ and confidence levels [6]

$\sqrt{s}(\text{GeV})$	$\cdot N$	$\chi^2/\text{d.o.f.}$
13.8	100	2.08
19.4	124	2.88
23.5	134	1.14
30.7	173	1.01
44.7	207	2.14
52.8	206	1.65
62.5	124	1.17

Table 1 Number of experimental data points and chi square per degree of freedom at each energy.

From table 1, our fits present $\chi^2/\text{d.o.f.}=1\sim 2$ for group G2 and $\chi^2/\text{d.o.f.}=2\sim 3$ for group G1, which is statistically satisfactory (figure 1a, 1b). In figure 1c we observe that the real part of the scattering amplitude changes sign at high energies, as predicted from dispersion relations analysis [5]. Also, we see that the contribution of the real part is important only in the dip region. From this result, in what follows, we will only take into account the imaginary part of the scattering amplitude.

3 Profile and Inelastic Overlap Functions

Substitution of parametrization (6)-(7) into equation (1) reads,

$$\text{Re}\Gamma(b, s) = \frac{1}{2} \sum_{j=1}^n \frac{\alpha_j}{\beta_j} e^{-b^2/4\beta_j} \quad (8)$$

Then, through equation (2) we obtain $G_{in}(b, s)$. Error propagation from the fits parameters has been taken into account analitically [6]. The results for $\text{Re}\Gamma$ and G_{in} at $\sqrt{s} = 23.5$ and 62.5 GeV are displayed in figure 2, as function of the impact parameter. Conversely, for G_{in} , figure 3 shows the energy dependence of G_{in} for two different values of the impact parameter.

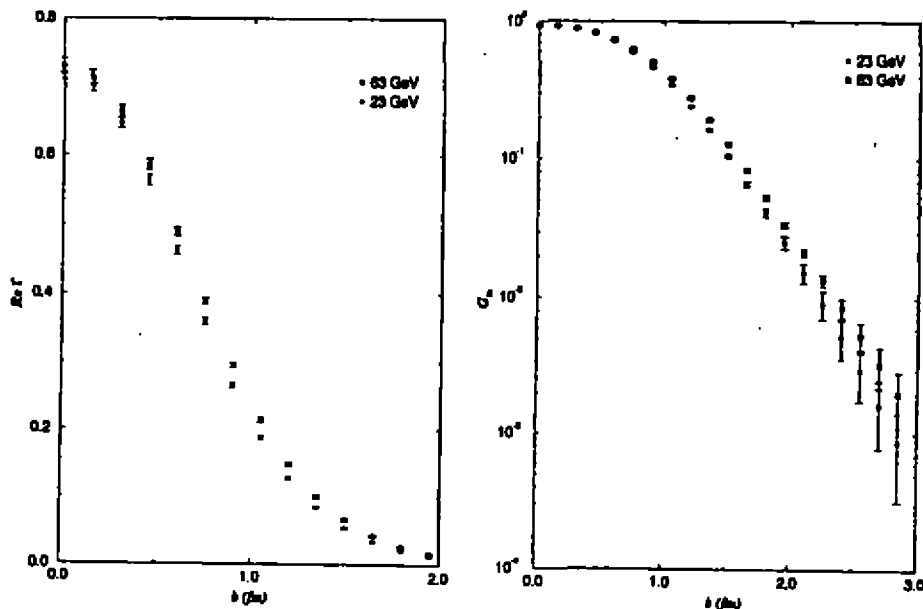


Figure 2. Real part of Γ and G_{in} as function of the impact parameter in the ISR energy region.

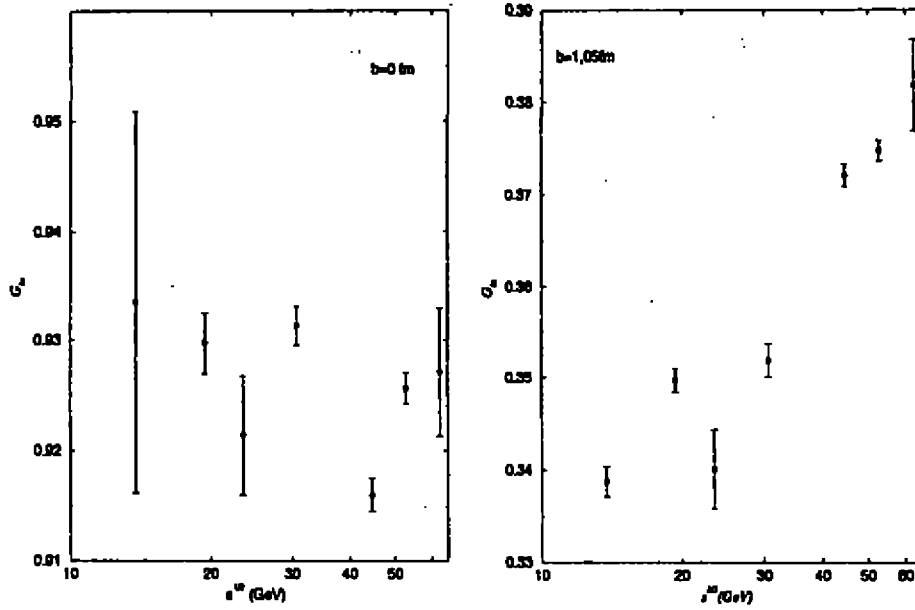


Figure 3. Extracted values of G_{in} as function of the energy at two fixed parameters.

From figure 2 we conclude that hadrons become blacker and larger as the energy increases in the ISR region (group G2) and that at fixed energies, $G_{in}(b)$ is nearly exponential above $b \sim 1.0$ fm. From figure 3 the central opacity, $G_{in}(0, s)$, is nearly constant at 23-62 GeV. However in the peripheral region ($b \sim 1.0$ fm) it increases at 23-62 GeV. Similar results were obtained by Amaldi and Schubert [4].

4 The Eikonal in the Transferred Momentum Space

From equation (4), the eikonal in the transferred momentum space is given by

$$\Omega(q, s) = -\langle \ln[1 - \text{Re}\Gamma(b, s)] \rangle. \quad (9)$$

Following [7] we evaluate this quantity by making use of the expansion,

$$\Omega(q, s) = \langle \text{Re}\Gamma(b, s) \rangle + \langle O[(\text{Re}\Gamma)^2] \rangle \quad (10)$$

where $\langle \text{Re}\Gamma(b, s) \rangle = \text{Im}F(q, s)$, and fitting $\langle O[(\text{Re}\Gamma)^2] \rangle$ by a sum of gaussians using CERN-minuit. The results for $\sqrt{s} = 23.5$ and 62.5 are shown in Figure 4, in a suitable form. We observe a change of signs, indicating the existence of zeros at finite values of the transferred momentum.

Similar results were obtained by Buenerd, Furget and Valin [8] through a parametrization for $F(q, s)$ introduced by Amaldi and Schubert [4]. However, as in our case, the error propagation to the eikonal in the transferred momentum space was not taken into account. We are presently investigating this subject.

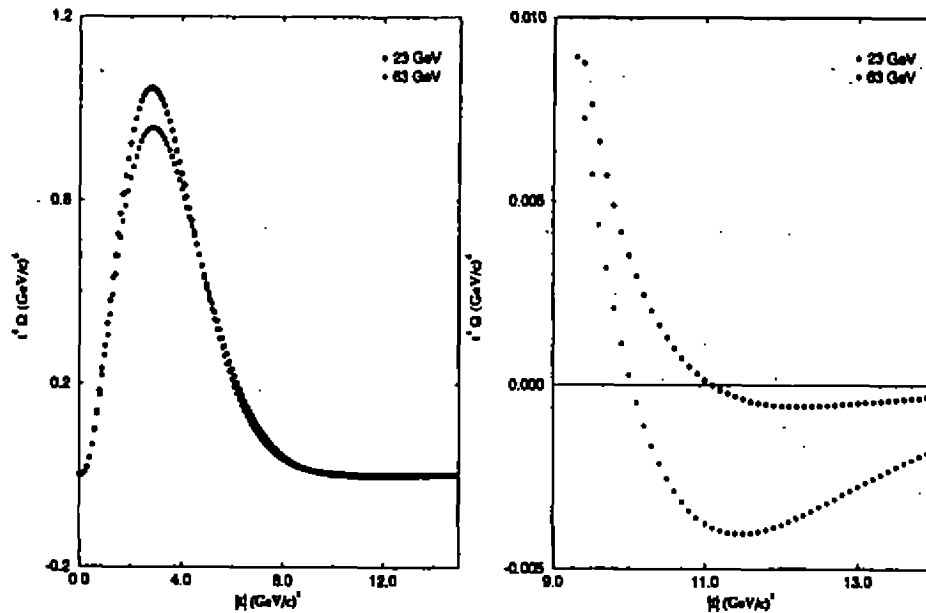


Figure 4. Eikonal in transferred momentum space multiplied by t^4 , $q^2 = -t$.

Acknowledgements

We are grateful to Professor Erasmo Ferreira for useful discussions during this meeting and to C. D. Chinellato for reading the manuscript. We are thankful to the CNPq and Fapesp for financial support.

References

1. - U. Amaldi, M. Jacob, G. Matthiae, *Ann. Rev. Nucl. Sci* **26** (1976) 385.
2. - F. James and M. Roos, "Minuit, Function Minimization and Error Analysis", CERN **D506** (1994).
3. - Group G1: D. S. Ayres et al., *Phys. Rev. D* **15** (1977) 3105; C. W. Akerlof et al., *Phys. Rev. D* **14** (1976) 2864; R. Rubinstein, *Phys. Rev. D* **30** (1984) 1413; G. Fidicaro, *Phys.Lett.* **105B** (1981) 309 (differential cross section); L. A. Fajardo et al., *Phys. Rev. D* **24** (1981) 46 (ρ -parameter).
4. - Group G2: K. R. Schubert, 'Tables on Nucleon-Nucleon scattering, in Landolf-Bornstein, Numerical Data and Functional Relationships in Science and Tecnology, New Series, vol. 1/9a (1979) (diferential cross section); U. Amaldi and K.R. Schubert, *Nucl. Phys.* **B166** (1980) 301 (ρ -parameter).
5. - J. B. Bronzau, G. L. Kane, U. P. Sukhatme, *Phys. Lett.* **B49** (1974) 272.
6. - P. R. Bevington and D. K. Robinson, "Data Reduction and Error Analysis for the Physical Sciences" (Mc Graw-Hill, NY, 1992).
7. - C. Furget, Ph. D. thesis, Université Joseph Fourier, Grenoble, 1989.
8. - C. Furget, M. Buenerd, P. Valin, *Z. Phys.* **C47** (1990) 377.

Radiative Processes for Accelerating Observers

R. De Paola

*Pontifícia Universidade Católica do Rio de Janeiro
Rua Marques de São Vicente 110, Rio de Janeiro 22460, RJ, Brazil*

N.F. Svaiter

*Centro Brasileiro de Pesquisas Físicas - CBPF
Rua Dr. Xavier Sigaud 150, Rio de Janeiro 22290 RJ, Brazil*

We consider a monopole detector interacting with a massive scalar field. We analyse radiative processes for the monopole detector travelling in a world line that is inertial in the infinite past and has a constant proper acceleration in the infinite future.

1 Introduction

It has been known that an uniformly accelerated detector interacting with a massless scalar field in the Minkowski vacuum behaves like an inertial detector in equilibrium with a thermal bath at temperature $\beta^{-1} = \frac{1}{2\pi\alpha}$, where α^{-1} is the proper acceleration of the detector[1].

In a recent paper, Svaiter and Svaiter [2], studied the spontaneous and induced emission problem, using a very simple model of an atom consisting of a pointlike object with an internal structure defining two energy levels introduced by DeWitt [3]. Assuming that the atom (detector) interacts with a real massless scalar field, and it is travelling in inertial or non inertial world lines, the authors obtained the probability of transition per unit proper time as $\frac{dP(E, \Delta\tau)}{d\Delta\tau}$, (normalized by the selectivity of the detector) between different eigenstates of the detector and also presented the rate of spontaneous excitation after a finite observation or switching time ΔT . The extension of these calculations for the detector in the presence of parallel plates at zero and finite temperature was given by Ford, Svaiter and Lyra [4]. A more mathematically involved case of the monopole detector in the presence of cosmic strings was discussed more recently by Svaiter and Svaiter[5].

The purpose of this paper is to discuss the radiative processes for the asymptotic accelerated detector.

The main difference among our approach and all the previous papers is that we use the rotating wave approximation. In a real quantum detector prepared in the ground state, the detector goes to an excited state by an absorption process. Of course we are assuming asymptotically measurements, i.e., the observation time is large when compared with times on the order E^{-1} , where E is the energy gap between the excited and the ground state of the detector. Consequently it is possible to assume the normally ordered field correlation function in the probability of transition, i.e., the rotating wave approximation.

The paper is prepared as follows. In section II, the asymptotic accelerated detector is discussed. Conclusions are given in section III. In this paper we use $\hbar = c = 1$.

2 The asymptotic accelerated detector

The aim of this section is to discuss the following physical situation. How the monopole detector behaves if is traveling along a world line in such a way that the detector is inertial in the infinite past and has a constant proper acceleration in the infinite future.

Let us consider the following transformation of coordinates between the inertial (t, x) and non-inertial coordinates (η, ξ) ,

$$t + x = \frac{2}{a} \sinh a(\eta + \xi) \tag{1}$$

$$t - x = -\frac{1}{a} e^{a(\eta + \xi)} \tag{2}$$

This coordinate system was investigated by Kalnins and Miller[6], and for this reason we will call it the Kalnins-Miller coordinate system.

The line element in this coordinate system can be written as:

$$ds^2 = (e^{2a\xi} + e^{-2a\eta})(d\eta^2 - d\xi^2) \tag{3}$$

In this coordinate system the curves $\xi = cte$ are the world lines for asymptotic accelerated observers (see [7] for a more complete discussion regarding this coordinate system). Note that the hypersurface $\eta = \eta_0$ is a Cauchy surface for the region $t - x < 0$.

The massive Klein-Gordon equation in the Kalnins-Miller manifold reads

$$\left[\frac{\partial^2}{\partial \eta^2} - \frac{\partial^2}{\partial \xi^2} + m^2(e^{-2a\eta} + e^{2a\xi}) \right] \varphi(\eta, \xi) = 0. \tag{4}$$

Since the coordinate system (η, ξ) allows the separation of variables, writing $\varphi(\eta, \xi) = F(\eta)G(\xi)$, the Klein-Gordon equation separates in the following equations:

$$\left(\frac{d^2}{d\eta^2} + m^2 e^{-2a\eta} + a\nu \right) F(\eta) = 0 \tag{5}$$

and

$$\left(\frac{d^2}{d\xi^2} - m^2 e^{2a\xi} + a\nu \right) G(\xi) = 0. \tag{6}$$

Equations(7) and (8) are Bessel equations with imaginary order. A straightforward calculation reveals that there are two well behaved complete sets $(\phi_\nu(x), \phi_\nu^*(x))$ and $(\varphi_\nu(x), \varphi_\nu^*(x))$, basis in the space of the solutions of the massive Klein-Gordon equation in the Kalnins-Miller manifold. These two complete sets are given by

$$\phi_\nu(\eta, \xi) = \frac{1}{2} \left(\frac{\nu(1 - e^{-2\pi\nu})}{\pi a} \right)^{\frac{1}{2}} H_{i\nu}^{(1)} \left(\frac{m}{a} e^{-a\eta} \right) K_{i\nu} \left(\frac{m}{a} e^{a\xi} \right) \tag{7}$$

$$\phi_\nu^*(\eta, \xi) = \frac{1}{2} \left(\frac{\nu(1 - e^{-2\pi\nu})}{\pi a} \right)^{\frac{1}{2}} H_{i\nu}^{(2)} \left(\frac{m}{a} e^{-a\eta} \right) K_{i\nu} \left(\frac{m}{a} e^{a\xi} \right) \tag{8}$$

and

$$\varphi_\nu(\eta, \xi) = \left(\frac{\nu}{\pi a} \right)^{\frac{1}{2}} J_{i\nu} \left(\frac{m}{a} e^{-a\eta} \right) K_{i\nu} \left(\frac{m}{a} e^{a\xi} \right) \tag{9}$$

$$\varphi_\nu^*(\eta, \xi) = \left(\frac{\nu}{\pi a} \right)^{\frac{1}{2}} J_{-i\nu} \left(\frac{m}{a} e^{-a\eta} \right) K_{i\nu} \left(\frac{m}{a} e^{a\xi} \right). \tag{10}$$

Since the line element is time dependent, there is no simple way to define positive and negative frequency modes. Different solutions for the problem were presented by di Sessa [8] and Sommerfield [9]. Combining both criteria (which we do not discuss here), we have that the modes given by eqs.(9) and (10) are the positive and negative frequency modes in the infinite past, and the modes given by eqs.(11) and (12) are those for the infinite future. By this reason we will call them "inertial" and "accelerated" modes respectively.

The Bogoliubov coefficients between the Minkowski modes and the inertial and accelerated modes are given respectively by :

$$|\beta_{\nu\mu}|_{in}^2 = \frac{1}{2\pi^2\nu\epsilon\delta\sinh\pi\nu} (Re)^2 (-i\nu)! [2a(\epsilon - \mu)]^{i\nu} \quad (11)$$

and

$$|\beta_{\nu\mu}|_{ac}^2 = \frac{1}{2\pi\epsilon a} \frac{1}{e^{2\pi\nu} - 1} \quad (12)$$

where ϵ is the energy of the Minkowski modes. Using eq.(13) and (14) it is possible to obtain the transition rate of the detector. The problem is that it is not possible to make asymptotic measurements, but only for finite time $\Delta T = \eta_f - \eta_i$. For small ΔT it is possible to assume that the metric is static and we have two different outcomes if the measurement is made in the infinite past or in the infinite future. The calculation of the response function in the infinite past is very difficult to evaluate exactly. Nevertheless the response function in the infinite future can be evaluated. To obtain this result we have to substitute eqs.(11) and (12) in the response function and use the expression of the Bogoliubov coefficient between the Minkowski modes and the accelerated modes. Thus if we prepare the detector in the ground state and the field in the di Sessa vacuum the rate of spontaneous excitation is

$$R(E, \eta, \eta', \xi, \xi') = \int_{-\Delta T}^{\Delta T} d\tau e^{iE\tau} \int d\eta \frac{1}{e^{2\pi\mu}} \frac{\mu}{(\pi a)^2} (J_{-i\mu}(\frac{m}{a}e^{-a\eta}) J_{i\mu}(\frac{m}{a}e^{-a\eta'}) + J_{-i\mu}(\frac{m}{a}e^{-a\eta'}) J_{i\mu}(\frac{m}{a}e^{-a\eta})) K_{i\mu}(\frac{m}{a}e^{a\xi}) K_{i\mu}(\frac{m}{a}e^{a\xi'}). \quad (13)$$

Substituting the asymptotic expression for the Bessel function of first kind given by

$$\lim_{x \rightarrow 0} J_\nu(x) = \frac{x^\nu}{2^\nu \Gamma(1 + \nu)}$$

we have

$$R(E, \Delta T, \xi, \xi') = \frac{\Delta T}{\pi^2} \int_0^\infty d\mu f(\mu, E, \Delta T) K_{i\mu}(m\xi) K_{i\mu}(m\xi'), \quad (14)$$

We obtain that if a measurement is made in the asymptotic future we have a similar result as Rindler's (the case in which the detector has constant proper acceleration during all time). Nevertheless if the measurement is made in the infinite past we obtain a non-expected result, i.e, the rate is not zero although the detector is inertial in this region. This result can be understood since although the detector is travelling in an inertial world line the coordinate system is non-cartesian.

3 Conclusions

In this paper we discussed radiative processes of a monopole detector interacting with a massive scalar field. The probability of transition per unit proper time of the asymptotic accelerated detector is obtained.

We used the RWA in order to simplify the calculations of a detector with nonconstant proper acceleration. We want to remark that the standard "photodetection" scheme is based on absorption of quantum of the field by the detector. Using first order perturbation theory the rate of excitation is proportional to the Fourier transform of a normal ordered product of the negative and positive parts of the field operator. Nevertheless, normal ordering with respect to the asymptotic accelerated time is not normal ordered with respect to the Minkowski time. This explains the non-zero probability of excitation of the detector.

4 Acknowledgement

We would like to thank Prof.L.Ford, for valuable comments. This paper was supported by Conselho Nacional de Desenvolvimento Científico e Tecnológico (CNPq) of Brazil.

References

- [1] P.C.W.Davies, *J.Phys.A* **8**, 609 (1975), W.G.Unruh, *Phys.Rev.D* **14**, 870 (1976).
- [2] B.F.Svaiter and N.F.Svaiter, *Phys.Rev.D* **46**, 5267 (1992), *ibid*, *Phys. Rev.D* **47**,4802 (1993)E.
- [3] B.DeWitt, in *General Relativity - An Einstein Centenary Survey*, edited by S.W.Hawking and W.Israel (Cambridge University Press, Cambridge, Englad, 1980).
- [4] L.H.Ford, N.F.Svaiter and M.L.Lyra , *Phys.Rev.A* **49**, 178 (1994).
- [5] B.F.Svaiter and N.F.Svaiter, *Class.Quant.Grav.* **11**, 347 (1994).
- [6] E.G.Kalnins and W.Miller, *J.Math.Phys.* **15**, 1025 (1974), *ibid* *J.Math.Phys.* **19**, 1233 (1978).
- [7] I.Costa, *J.Math.Phys.* **30**, 888 (1989).
- [8] A.di Sessa, *J.Math.Phys.* **15**, 1892 (1974).
- [9] C.M.Sommerfield, *Ann.Phys.* **84**, 285 (1974).

Regge Law in Astrophysics

Rudolf Muráđian*

*Instituto de Física, Universidade Federal da Bahia
Salvador, BA, Brasil*

It is shown that the generalized Regge law allows to explain the origin and magnitude of angular momenta of cosmic bodies – planets, stars, galaxies, clusters of galaxies and the Universe itself.

1 Introduction

The Regge-Chew-Frautschi spin-mass relation $J \sim m^2$ for usual string-like hadrons is generalized for hadronic objects having geometrical shape of disc and ball. The galaxies, their clusters, superclusters and Universe itself are described by Regge trajectory for disc-like two-dimensional objects with spin-mass dependence $J^2 \sim m^3$, and planets and stars corresponds to trajectory with dependence $J^3 \sim m^4$, characteristic for three-dimensional spherical hadrons.

The Chew-Frautschi plot for cosmic objects is constructed, and two important cosmological points are revealed on it. These points are named as Eddington and Chandrasekhar points and their coordinates are expressed via definite combinations of the classical and quantum-mechanical fundamental constants:

$$\text{Eddington point} \Rightarrow \left\{ m_{\text{Universe}} = m_p \left(\frac{m_{Pl}}{m_p} \right)^4, J_{\text{Universe}} = \hbar \left(\frac{m_{Pl}}{m_p} \right)^6 \right\}$$

$$\text{Chandrasekhar point} \Rightarrow \left\{ m_{\text{star}} = m_p \left(\frac{m_{Pl}}{m_p} \right)^3, J_{\text{star}} = \hbar \left(\frac{m_{Pl}}{m_p} \right)^4 \right\}$$

where m_{Pl} is the Planck mass: $m_{Pl} = (\frac{\hbar c}{G})^{1/2}$.

It is shown that the spin of the Universe has interesting property: the density of spin in the proton and in the Universe are equal

$$\frac{\hbar}{r_p^3} = \frac{J_{\text{Universe}}}{r_{\text{Universe}}^3}$$

where $r_p = \frac{\hbar}{m_p c}$ — proton radius, and $r_{\text{Universe}} = r_p \left(\frac{m_{Pl}}{m_p} \right)^2$ — radius of the Universe.

For the first time in the history of astronomy and physics the angular momentum J of astronomical objects are described using only fundamental constants. The successful application of Regge-Chew-Frautschi concept in astrophysics witnessed on unity and simplicity of Nature in the range from elementary particles up to Universe and opens the new way towards complete solution of the great mystery of the origin and magnitude of the angular momentum of cosmic bodies.

*Electronic address: muradian@ufba.br

2 Regge Law for n-Dimensional Objects

The *Regge-Chew-Frautschi* spin-mass relation for one-dimensional string-like hadrons [1], [2] can be generalized for *n*- dimensional hadrons and represented at large *m* in the form, containing only fundamental constants $m_p = 1.673 \cdot 10^{-27} \text{ kg}$ — proton mass and $\hbar = 1.055 \cdot 10^{-34} \text{ J} \cdot \text{s}$ — Planck's constant (see [3] – [10] and [11],[12]):

$$J^{(n)} = \hbar \left(\frac{m}{m_p} \right)^{1+1/n} \tag{1}$$

The number $n = 1, 2, 3$ characterizes the geometrical shape of the hadron:

$$n = 1, \text{ string} : J^{(1)} = \hbar \left(\frac{m}{m_p} \right)^2 \tag{2}$$

$$n = 2, \text{ disc} : J^{(2)} = \hbar \left(\frac{m}{m_p} \right)^{3/2} \tag{3}$$

$$n = 3, \text{ ball} : J^{(3)} = \hbar \left(\frac{m}{m_p} \right)^{4/3} \tag{4}$$

The Regge trajectories are linear for *string* in the plane (J, m^2) , for *disc* in the plane (J^2, m^3) , and for *ball* in the the plane (J^3, m^4) .

2.1 Leading (Yrast) Regge Trajectory

In fact, the general formula (1) can be understood from simple dimensional considerations and requirement of similarity. Since $m \sim r^n$, for *n*-dimensional object and consequently $r \sim m^{1/n}$, it follows from classical angular momentum relation $J = m v r$ that $J \sim m m^{1/n} \sim m^{1+1/n}$ at constant velocity.

In the following we shall show that formula (1) corresponds to the leading (yrast) Regge trajectory, i. e. trajectory with maximal angular momentum for fixed mass (see, also, [12]).

The total mass *m* of the spinning *n*-dimensional object with radius *r*, angular velocity $\omega = \frac{c}{r}$ and density ρ is:

$$\begin{aligned} m &= \rho r^n + m_{rot} \\ &= \rho r^n + \frac{J \omega}{2 c^2} \\ &= \rho r^n + \frac{J}{2 c r} \end{aligned} \tag{5}$$

The leading trajectory corresponds to maximal *J* at minimal *m*. Minimalizing *m* with respect to *r*

$$\frac{\partial m}{\partial r} = 0 = -\frac{J}{2 c r^2} + n \rho r^{n-1} \tag{6}$$

we find

$$r = \left(\frac{J}{2 n \rho c} \right)^{\frac{1}{n+1}} \tag{7}$$

This gives from (5):

$$J = m^{1+1/n} \frac{2 n \rho^{-1/n} c}{(n+1)^{1+1/n}} \tag{8}$$

This is well-known formula (1), if we take the following value for *n*-dimensional density ρ :

$$\rho = \frac{m_p}{\left(\frac{\hbar}{m_p c} \right)^n} \frac{(2n)^n}{(n+1)^{n+1}} \sim \frac{m_p}{\left(\frac{\hbar}{m_p c} \right)^n} \tag{9}$$

As noticed by V.A.Matveev the same result follows from minimalizig the semirelativistic expression ¹:

$$m = \sqrt{(\rho r^n)^2 + \left(\frac{J}{2 c r} \right)^2} \tag{10}$$

¹I am indebted to Prof. V.A.Matveev for this remark

2.2 The Kerr gravitational angular momentum

The horizon for rotating black hole meets requirement

$$r = r_g + \sqrt{r_g^2 - \left(\frac{J}{mc}\right)^2} \quad (11)$$

where $r_g = \frac{Gm}{c^2}$ is a half of the Shwarzshild radius and the gravitational spin-mass relation for maximally rotating black hole follows

$$J^{(Kerr)} = m c r_g \quad \text{or} \quad J^{(Kerr)} = \frac{G m^2}{c} \quad (12)$$

where $G = 6.673 \times 10^{-11} \text{ m}^3 \cdot \text{kg}^{-1} \cdot \text{s}^{-2}$ - Newton gravitational constant and $c = 2.998 \times 10^8 \text{ m} \cdot \text{s}^{-1}$ - speed of light. The Kerr relation can also be expressed in Regge-string form, by means of Planck's mass

$$J^{(Kerr)} = \hbar \left(\frac{m}{m_{Pl}}\right)^2 \quad (13)$$

We see that (2) and (13) are interconnected by substitution $m_p \leftrightarrow m_{Pl}$. Let us notice the identity

$$J^{(Kerr)} \equiv \frac{G m_p^2}{\hbar c} J^{(1)} \quad (14)$$

The gravitational angular momentum for n -dimensional object follows from (1) by substitution $m_p \rightarrow m_{Pl}$:

$$J_{grau}^{(n)} = \hbar \left(\frac{m}{m_{Pl}}\right)^{1+1/n} = \hbar \left(\frac{G m^2}{\hbar c}\right)^{\frac{1}{2}(1+1/n)} \quad (15)$$

By definition $J^{(Kerr)} \equiv J_{grau}^{(1)}$.

It is interesting to note that since the sixties it has been known that hadrons exhibit features resembling gravity. The relation (14) can be viewed as a new example. Recently Y. Ne'eman and Dj. Šijački suggested that this feature can be explained by component of QCD due to exchange of zero-color two-gluon effective graviton-like spin 2 combination $G_{\mu\nu}(x) = \delta_{ab} B_\mu^a B_\nu^b$, where $B_\mu^a(x)$ is the gluon field [13].

2.3 Disc: $J \sim m^{3/2}$

For practical applications different expressions for $J^{(2)}$ can be used:

$$\begin{aligned} J^{(2)} &= \hbar \left(\frac{m}{m_p}\right)^{3/2} \\ &= \hbar N^{3/2} \\ &= 1.542 \times 10^6 m^{3/2} \quad (\text{in SI units}) \\ &= 4.324 \times 10^{51} \left(\frac{m}{m_\odot}\right)^{3/2} J \cdot s \end{aligned}$$

where N is the number of nucleons $N = \frac{m}{m_p}$ and $m_\odot = 1.98892(25) \times 10^{30} \text{ kg}$ is the solar mass.

The $J^{(2)}$ trajectory describes sufficiently well the angular momentum of galaxies.

2.4 Ball: $J \sim m^{4/3}$

The relation (4) describes the spin-mass connection for planets and stars. We display for practical purposes different forms of $J^{(3)}$:

$$\begin{aligned} J^{(3)} &= \hbar \left(\frac{m}{m_p}\right)^{4/3} \\ &= \hbar N^{4/3} \\ &= 53.114 \times m^{4/3} \quad (\text{in SI units}) \\ &= 1.329 \times 10^{42} \left(\frac{m}{m_\odot}\right)^{4/3} J \cdot s \end{aligned}$$

3 Cosmic Chew–Frautschi Plot

The main objective of our approach is the construction of generalized Chew–Frautschi plot [2] for cosmic objects in double logarithmic $\log_{10}(m) - \log_{10}(J)$ plane.

3.1 Observational data

Below in Tables 1 & 2 the observational data on masses and spins of celestial bodies are presented and graphically reproduced on Fig.1. (see also [8] & [10]).

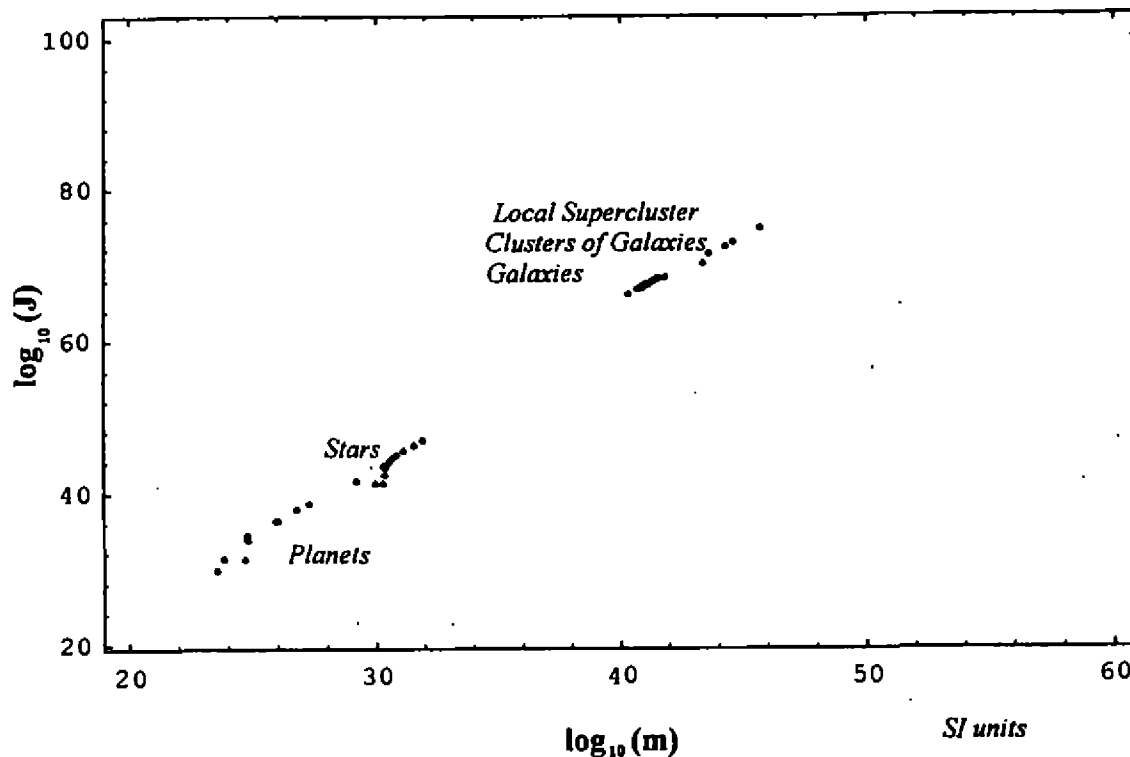


Figure 1. Observational data from Tables 1 and 2.

Table 1

Clusters of galaxies, spiral galaxies and globular clusters ³

Object	Mass	Spin(<i>observ.</i>)	Spin(<i>theor.</i>)
<i>Clusters of galaxies</i>			
Local Supercluster	5×10^{45}	6×10^{74}	5.45×10^{74}
A 1656 (Coma)	4×10^{44}	0.9×10^{73}	1.23×10^{73}
A 2199	2×10^{44}	2.2×10^{72}	4.36×10^{72}
Virgo	4×10^{43}	2.6×10^{71}	3.90×10^{71}
Shakhbazian I	2.4×10^{43}	1.8×10^{71}	1.81×10^{71}
<i>Spiral galaxies</i>			
Andromeda (M31)	6.78×10^{41}	2.36×10^{68}	8.61×10^{68}
Our Galaxy	3.38×10^{41}	1.92×10^{68}	3.03×10^{68}
NGC 3031 (M81)	2.78×10^{41}	1.30×10^{68}	2.26×10^{68}
5005	1.98×10^{41}	6.82×10^{67}	1.36×10^{68}
7331	1.86×10^{41}	6.82×10^{67}	1.24×10^{68}
5055 (M63)	1.31×10^{41}	2.91×10^{67}	7.31×10^{67}
1832	1.11×10^{41}	2.85×10^{67}	5.70×10^{67}
1808	9.55×10^{40}	2.11×10^{67}	4.55×10^{67}
5194 (M51)	9.54×10^{40}	2.48×10^{67}	4.54×10^{67}
0681	7.76×10^{40}	1.67×10^{67}	3.33×10^{67}
6574	8.15×10^{40}	1.18×10^{67}	3.59×10^{67}
1084	4.97×10^{40}	7.44×10^{66}	1.71×10^{67}
3504	2.19×10^{40}	1.61×10^{68}	5.00×10^{66}
<i>Globular clusters</i>			
NGC 104 (47 Tuc)	2.1×10^{36}	1.3×10^{58}	4.69×10^{60}
362	3.6×10^{35}	2.4×10^{57}	3.33×10^{59}

Table 2

Stars and planets ⁴

Object	Mass	Spin(<i>observ.</i>)	Spin(<i>theor.</i>)
<i>Main sequence stars</i>			
O5	7.92×10^{31}	7.07×10^{46}	1.81×10^{44}
B0	3.54×10^{31}	1.46×10^{46}	6.17×10^{43}
B5	1.28×10^{31}	3.12×10^{45}	1.59×10^{43}
A0	6.44×10^{30}	8.56×10^{44}	6.36×10^{42}
A5	4.16×10^{30}	3.01×10^{44}	3.55×10^{42}
F0	3.38×10^{30}	1.27×10^{44}	2.69×10^{42}
F5	2.56×10^{30}	2.57×10^{43}	1.86×10^{42}
G0	2.18×10^{30}	2.54×10^{42}	1.50×10^{42}
<i>Solar System</i>			
The Sun (G2)	1.99×10^{30}	3.15×10^{43}	1.33×10^{42}
K0	1.54×10^{29}	$< 3.65 \times 10^{41}$	4.38×10^{40}
M0'	9.31×10^{28}	$< 1.63 \times 10^{41}$	2.24×10^{40}
<i>Planets</i>			
Jupiter	1.90×10^{27}	4.32×10^{38}	1.25×10^{38}
Saturn	5.68×10^{26}	7.68×10^{37}	2.50×10^{37}
Uranus	8.72×10^{25}	2.09×10^{36}	2.05×10^{36}
Neptune	1.02×10^{26}	2.10×10^{36}	2.53×10^{36}
Earth/Moon	5.97×10^{24}	2.81×10^{34}	5.75×10^{34}
Earth	5.97×10^{24}	5.91×10^{33}	5.75×10^{34}
Pluto	6.6×10^{23}	2.3×10^{31}	3.05×10^{33}
Venus	4.87×10^{24}	1.8×10^{31}	4.38×10^{34}
Mercury	3.33×10^{23}	6.5×10^{29}	1.23×10^{33}

²For clusters of galaxies and globular clusters observed spins are estimated from data on velocity dispersion and linear sizes. For clusters of galaxies the results of [14] are used. The masses and spins of spiral galaxies are taken from [15]. The SI units are used, where kg is the unit of mass, and spins are measured in $\frac{kg \cdot m^2}{s} \equiv J \cdot s$.

³Observational data are taken from [16] [17]. The total angular momentum of satellites in the systems of of Jupiter, Saturn and Uranus is much smaller than the spin momentum of the central planet. In the Jupiter system the total orbital moment of satellites is 4.24×10^{36} , of Saturn - 9.6×10^{35} , and of Uranus - $0.7 \times 10^{34} J \cdot s$.

3.2 Eddington and Chandrasekhar points

Fig.2 presents three straight lines, corresponding to the two Regge relations - $J^{(2)}$ for disc and $J^{(3)}$ for ball, intersected by Kerr trajectory $J^{(Kerr)}$. The two important points appear in this plot:

- *Eddington point* at the crossover of Regge trajectory for *disc* $J^{(2)}$ with Kerr angular momentum $J^{(Kerr)}$. The coordinates of crossing points can be readily found by solving equation $J^{(2)} = J^{(Kerr)}$, or $\hbar \left(\frac{m}{m_p}\right)^{3/2} = \frac{G m^2}{c}$.
- *Chandrasekhar point* corresponds to the crossover of Regge trajectory for *ball* $J^{(3)}$ with Kerr trajectory $J^{(Kerr)}$, $J^{(3)} = J^{(Kerr)}$ or $\hbar \left(\frac{m}{m_p}\right)^{4/3} = \frac{G m^2}{c}$.

The Chew-Frautschi plot for cosmic objects reveals two important cosmological points on it. These points are named as Eddington and Chandrasekhar points and their coordinates are expressed via definite combinations of the classical and quantum fundamental constants G , c , \hbar , m_p . Using the Plank mass

$$m_{Pl} = \left(\frac{\hbar c}{G}\right)^{1/2} \equiv m_p \left(\frac{\hbar c}{G m_p^2}\right)^{1/2}$$

our main result reads

$$\text{Eddington point} \Rightarrow \left\{ m_{Universe} = m_p \left(\frac{m_{Pl}}{m_p}\right)^4, J_{Universe} = \hbar \left(\frac{m_{Pl}}{m_p}\right)^6 \right\} \tag{16}$$

$$\text{Chandrasekhar point} \Rightarrow \left\{ m_{star} = m_p \left(\frac{m_{Pl}}{m_p}\right)^3, J_{star} = \hbar \left(\frac{m_{Pl}}{m_p}\right)^4 \right\} \tag{17}$$

4 Conclusion:

Origin of the Universe from Primeval Hadron

The arguments presented here and in [3]-[10] make probable the possibility of the cosmic objects origin due to the decay of macroscopic superhadrons with Regge-like spin. Sometime in the past the Universe have had an extremely anisotropic planar disc-like configuration, and the observed astronomical objects are products of the hierarchical fragmentation and evolution of this Primeval Hadron. Our scenario according to the Peebles [18] classification corresponds *top* → *down*, in contrast to the more accepted *bottom* → *up* scenario. (CH&3y → BBepx).

Using the numerical value for angular momentum of the Primeval Hadron it is possible to estimate the angular velocity of the Universe as $\omega_U \approx 10^{-13} \frac{\text{radian}}{\text{year}}$. The period of rotation 10^{13} year is larger than the age of the Universe 1000 times, in agreement with Birch [19], [20] result. The angular velocity

$$\omega_U = 10^{-3 \pm 1} \frac{\text{radian}}{\text{age of Universe}} \tag{18}$$

The spin of the Universe

$$J_{Universe} = \hbar \left(\frac{\hbar c}{G m_p^2}\right)^3$$

has interesting interpretation, that the the density of spin in proton and in the Universe are equal

$$\frac{\hbar}{r_p^3} = \frac{J_{Universe}}{r_{Universe}^3}$$

where $r_p = \frac{\hbar}{m_p c}$ — proton radius, and $r_{Universe} = r_p \frac{\hbar c}{G m_p^2}$.

References

- [1] Regge T., *Nuovo Cimento*, 1959, **14**, 951.
- [2] Chew G.F. and Frautschi S.C., *Phys. Rev. Lett.*, 1961, **7**, 394.
- [3] Muradian R., *Astrofizika*, 1975, **11**, 237.
- [4] Muradian R., *Astrofizika*, 1977, **13**, 63.
- [5] Muradian., *Astrofizika*, 1978, **14**, 439.
- [6] uradian R., *Astrophys. Space Sci.*, 1980, **69**, 339.
- [7] Muradian R., *Proceedings IAU Symposium* **121**.
- [8] Muradian R. *The primeval hadron: origin of rotation and magnetic fields in the Universe*, preprint Yerevan Physics Institute - 701(16)-84, 1984.
- [9] Muradian R., *On the rotation of astronomical Universe*, preprint Yerevan Physics Institute - 636(26)-83, 1983.
- [10] Muradian R., *Regge in the sky: origin of the cosmic rotation*, preprint ICTP, IC/94/143, Trieste, 1994.
- [11] Sistero R.F., *Astrophys. Lett.*, 1983, **23**, 235.
- [12] Vasconcellos C.A.Z., Dottori H.A., Schmidt A.A., *Astrophys. Space. Sci.*, 1985 **113**, 383.
- [13] Ne'eman Y. and Šijački Dj., *Phys.Lett.* 1990, **B247**, 571; *Phys.Lett.* 1992, **B276**, 173.
- [14] Rood H.J., *Astropys. J.*, 1974, **188**, 451.
- [15] Nordsieck K.H., *Astrophys. J.*, 1973, **184**, 735.
- [16] Allen K., *Astrophysical quantities*, M. Millp, 1977.
- [17] Alfvén H. & Arrenius G., *Structure and evolutionary history of the Solar System*, Kiev, Naukova Dumka, 1981.
- [18] Peebles P.J.E., *Principles of Physical Cosmology*, Princeton University Press, Princeton, N. J., 1993.
- [19] Birch P., *Nature*, 1982, **298**, 452.
- [20] Birch P., *Nature*, 1982, **298**, 452.

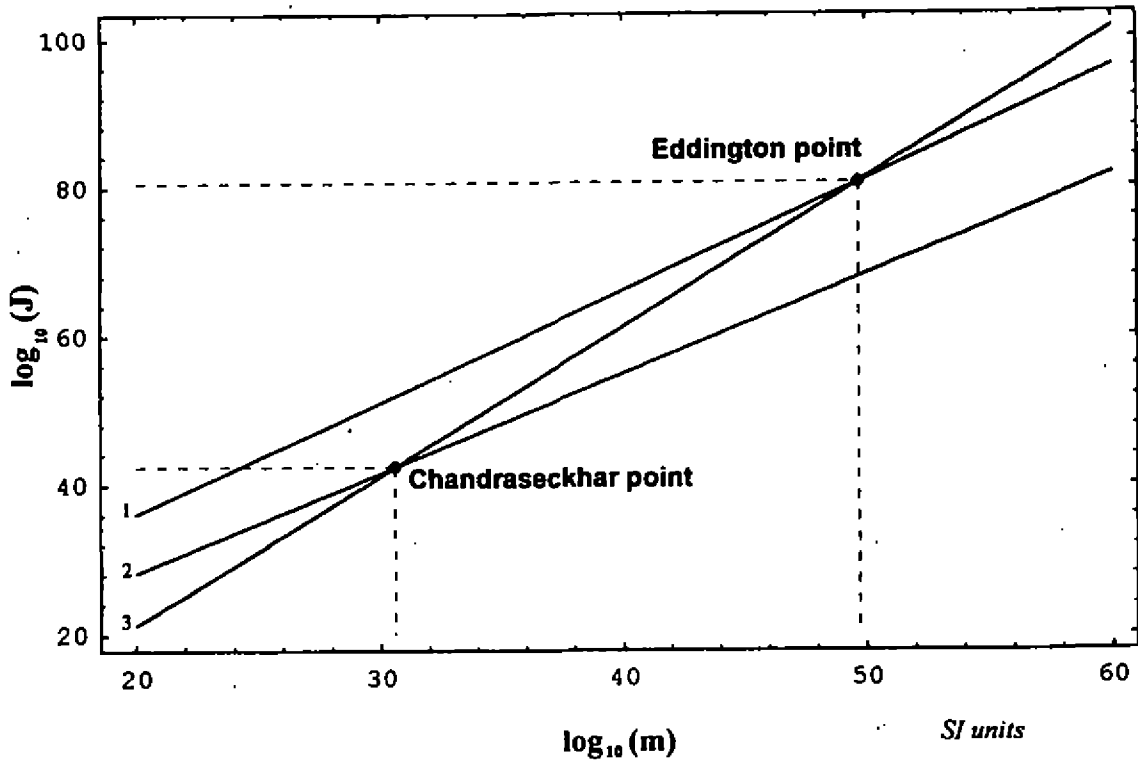


Figure 2. Theoretical spin-mass relations in $\log_{10} - \log_{10}$ plane for disc-like and ball-like hadrons and for Kerr solution:

1. *disc*: $J^{(2)} = \hbar \left(\frac{m}{m_p}\right)^{3/2}$
2. *ball*: $J^{(3)} = \hbar \left(\frac{m}{m_p}\right)^{4/3}$
3. *Kerr*: $J^{(Kerr)} = \frac{G m^2}{c}$

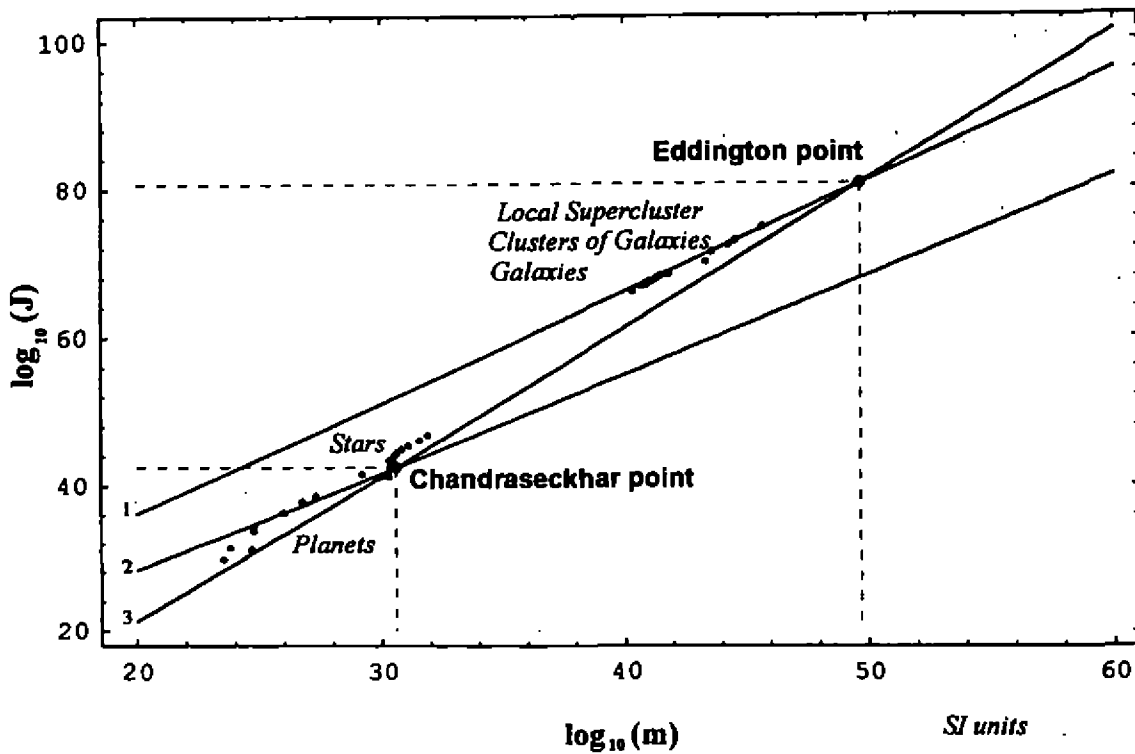


Figure 3. Generalized Chew-Frautschi plot as a result of addition of the Fig.1 and Fig.2.

Anomalous Higgs Boson Contribution to $e^+e^- \rightarrow b\bar{b}\gamma$ at LEP2.

S. M. Licetti, S. F. Novaes and R. Rosenfeld

Instituto de Física Teórica, Universidade Estadual Paulista,

Rua Pamplona 145, CEP 01405-900 São Paulo, Brazil

We study the effect of anomalous $H\gamma\gamma$ and $HZ\gamma$ couplings, described by a general effective Lagrangian, on the process $e^+e^- \rightarrow b\bar{b}\gamma$ at LEP2 energies. We include the relevant irreducible standard model background to this process, and from the photon energy spectrum, we determine the reach of LEP2 to unravel the anomalous couplings by analyzing the significance of the signal for Higgs boson with mass up to 150 GeV.

The Standard Model (SM) has been tested to an unprecedented degree of accuracy of 0.1% in some of the physical observables at LEP1, with many implications to physics beyond the SM [1]. However, the Z -pole experiments are able to probe with great precision just the fermionic couplings to the vector bosons while furnishing very little information about the interaction between the gauge bosons and the Higgs sector of the SM. In principle, it is conceivable that the interactions of the Higgs boson, which is responsible for the spontaneous breaking of the electroweak symmetry and for generating fermion masses, are different from those prescribed by the SM. In this case, an effective Lagrangian formalism can be used to describe possible anomalous interactions between the Higgs boson and the vector bosons.

The effective Lagrangian approach is a convenient model-independent parametrization of the low-energy effects of new physics beyond the SM that may show up at higher energies [2]. Effective Lagrangians, employed to study processes at a typical energy scale E , can be written as a power series in $1/\Lambda$, where the scale Λ is associated with the new particle masses belonging to the underlying theory. The coefficients of the different terms in the effective Lagrangian arise from integrating out the heavy degrees of freedom that are characteristic of a particular model for new physics. Invariant amplitudes, generated by such Lagrangians, will be an expansion in E/Λ , and in practice one can only consider the first few terms of the effective Lagrangian, *e.g.* dimension six operators, which are dominant for $E \ll \Lambda$.

In order to define an effective Lagrangian, it is necessary to specify the symmetry and the particle content of the low-energy theory. In our case, we require the effective Lagrangian to be CP-conserving, invariant under the SM symmetry $SU(2)_L \times U(1)_Y$ and to have as fundamental fields the same ones appearing in the SM spectrum. In particular, the Higgs field will be manifest and the symmetry is realized linearly. There are eleven independent dimension-six operators [3] of which only five are relevant for our discussions. Following the notation of reference [4], we can write,

$$\mathcal{L}_{eff} = \frac{1}{\Lambda^2} \left[f_{BW} \Phi^\dagger \hat{B}_{\mu\nu} \hat{W}^{\mu\nu} \Phi + f_W (D_\mu \Phi)^\dagger \hat{W}^{\mu\nu} (D_\nu \Phi) + f_B (D_\mu \Phi)^\dagger \hat{B}^{\mu\nu} (D_\nu \Phi) + f_{WW} \Phi^\dagger \hat{W}_{\mu\nu} \hat{W}^{\mu\nu} \Phi + f_{BB} \Phi^\dagger \hat{B}_{\mu\nu} \hat{B}^{\mu\nu} \Phi \right], \quad (1)$$

where Φ is the Higgs field doublet, and $\hat{B}_{\mu\nu} = i\frac{q}{2} B_{\mu\nu}$, $\hat{W}_{\mu\nu} = i\frac{g}{2} \sigma^a W_{\mu\nu}^a$, with $B_{\mu\nu}$ and $W_{\mu\nu}^a$ being the field strength tensors of the respective $U(1)$ and $SU(2)$ gauge fields.

This Lagrangian gives rise to the following anomalous $H\gamma\gamma$ and $HZ\gamma$ couplings, in the unitary gauge [5],

$$\mathcal{L}_{eff}^{H\gamma\gamma, HZ\gamma} = g_{H\gamma\gamma} H A_{\mu\nu} A^{\mu\nu} + g_{HZ\gamma}^{(1)} A_{\mu\nu} Z^\mu \partial^\nu H + g_{HZ\gamma}^{(2)} H A_{\mu\nu} Z^{\mu\nu}, \quad (2)$$

where $A(Z)_{\mu\nu} = \partial_\mu A(Z)_\nu - \partial_\nu A(Z)_\mu$, and the coupling constants $g_{H\gamma\gamma}$, and $g_{HZ\gamma}^{(1,2)}$ are related to the coefficients of the operators appearing in (1) through,

$$g_{H\gamma\gamma} = - \left(\frac{gM_W}{\Lambda^2} \right) \frac{s^2(f_{BB} + f_{WW} - f_{BW})}{2},$$

$$\begin{aligned}
g_{HZ\gamma}^{(1)} &= \left(\frac{gM_W}{\Lambda^2} \right) \frac{s(f_W - f_B)}{2c}, \\
g_{HZ\gamma}^{(2)} &= \left(\frac{gM_W}{\Lambda^2} \right) \frac{s(2s^2 f_{BB} - 2c^2 f_{WW} + (c^2 - s^2)f_{BW})}{2c},
\end{aligned} \tag{3}$$

with g being the electroweak coupling constant, and $s(c) \equiv \sin(\cos)\theta_W$.

The coefficients f_B and f_W can be related to triple vector boson anomalous couplings and are bounded, for instance, by the direct measurement of $WW\gamma$ vertex at hadron colliders. However, more stringent bounds on the coefficients of the effective Lagrangian (1) come from the precision measurements of the electroweak parameters obtained at LEP1 [4]. Typically one has that $|f_{W,B,WW,BB}/\Lambda^2|$ can be as large as 100 TeV^{-2} , whereas $|f_{BW}/\Lambda^2|$ should be at most $\sim 1 \text{ TeV}^{-2}$. The anomalous $H\gamma\gamma$ and $HZ\gamma$ couplings have already been considered in Z and Higgs decays [5], in e^+e^- collisions [5, 6] and at $\gamma\gamma$ colliders [7].

An interesting option to test the couplings described by (2) at LEP2 is via the reaction $e^+e^- \rightarrow H\gamma$, with the subsequent decay of the Higgs boson into a $b\bar{b}$ pair. A SM Higgs boson contribution to this process appears only at one-loop level, and is extremely small, and the observation of any $H\gamma$ event at LEP2 will be a clear signal of new physics. In this way, we neglect this loop contribution in our calculation.

In the SM, at tree-level, there are eight Feynman diagrams that contribute to the process $e^+e^- \rightarrow b\bar{b}\gamma$ (see Fig.1(a) - (d)). The bulk of the SM cross section comes from the Z boson contribution to the diagrams (a) - (b) when the Z boson is on-mass-shell, and the process is effectively a 2-body one. This implies that the majority of the photons emitted are monochromatic, with energy given by $E_\gamma^Z = (s - M_Z^2)/(2\sqrt{s})$.

When we take into account the anomalous Higgs boson couplings described above, two additional diagrams should be considered (see Fig.1(e)). Their contributions are dominated by the on-mass-shell $H\gamma$ production, with $H \rightarrow b\bar{b}$. Therefore, we can anticipate the existence of a secondary peak in the photon energy spectrum, generated at an energy

$$E_\gamma^H = \frac{s - M_H^2}{2\sqrt{s}} \tag{4}$$

which would be a very clear signal for the Higgs boson.

In order to evaluate the total cross section and kinematical distributions for the process $e^+e^- \rightarrow b\bar{b}\gamma$, we have used the package MadGraph [8] coupled to DPELAS, the double precision version of HELAS [9], for generating the tree-level SM amplitudes. We have written the relevant subroutines for the Higgs anomalous couplings, and included in the MadGraph generated file the two additional anomalous amplitudes. In this way, all interference effects between the SM and the anomalous amplitudes were taken into account. We checked for electromagnetic gauge invariance of the whole invariant amplitude, and incorporated a three-body phase space code, based on [10]. Since the Higgs boson resonance is very narrow, $\Gamma(H \rightarrow b\bar{b}) \sim 5 \text{ MeV}$, for $M_H \sim 100 \text{ GeV}$, we make sure to use appropriate variables to take care of the Higgs events close to the resonance peak. Finally, we used VEGAS [11] to perform the phase space integration.

In our analyses we have assumed a center-of-mass energy of $\sqrt{s} = 175 \text{ GeV}$ for the LEP2 collider, with a luminosity of 0.5 fb^{-1} . Our results were obtained using the energy cut $E_\gamma \geq 20 \text{ GeV}$, and the following angular cuts, $|\cos\theta_{e^-(e^+)\gamma}| \leq 0.87$ and $|\cos\theta_{b(\bar{b})\gamma}| \leq 0.94$. The photon energy is intended to reject the background from unresolved pair of photons from π^0 decays and assures, in principle, a sensitivity to M_H up to 150 GeV . The cuts in $\cos\theta_{e^-(e^+)\gamma}$ and $\cos\theta_{b(\bar{b})\gamma}$ were introduced to reduce initial and final state radiation, respectively.

Our purpose is to determine the range of anomalous $H\gamma\gamma$ and $HZ\gamma$ couplings that could be probed at LEP2 by searching for a signal of the Higgs boson in the process $e^+e^- \rightarrow b\bar{b}\gamma$. We assume that the Higgs couplings to fermions are the standard ones, which makes the $BR(H \rightarrow b\bar{b})$ dominant in the range $70 < M_H < 150 \text{ GeV}$, for $|f_i/\Lambda^2| \sim \text{TeV}^{-2}$ [5].

Figure 2 shows our typical results for the photon energy distribution presented as a 1 GeV bin histogram. We have taken $g_{H\gamma\gamma} = 10^{-3} \text{ GeV}^{-1}$, $g_{HZ\gamma}^{(1,2)} = 0$ and varied the Higgs mass between 70 and 120 GeV. We should point out that the general behavior of the energy distribution remains the same when we consider the other couplings, $g_{HZ\gamma}^{(1,2)}$, different from zero. We can identify the Z -boson peak around $E_\gamma \simeq 64 \text{ GeV}$ and also the various secondary peaks due to the Higgs boson at the energies given by (4). We can notice that the smaller the Higgs mass, the larger is its effect in the E_γ distribution. Its detectability should rely on a careful analyses of the tail (in the case where $M_H \neq M_Z$) of the SM contribution to the photon energy spectrum in the process $e^+e^- \rightarrow b\bar{b}\gamma$. It is important to

note that, for the sake of comparison between the signal (H) and background (Z) behavior, one can analyse the normalized angular distributions for SM and anomalous contributions [12].

In order to estimate the reach of LEP2 to disentangle the anomalous Higgs boson couplings, we have evaluated the significance ($S = \text{Signal}/\sqrt{\text{Background}}$) of the signal based on the Higgs boson peaks in the E_γ distribution, assuming a Poisson distribution for both signal and background. We have scanned the parameter space for the three anomalous couplings keeping only one non-zero coupling in each run, for different values of the Higgs boson mass. We took the coupling constants $g_{H\gamma\gamma}$, $g_{HZ\gamma}^{(1,2)}$ in the range $10^{-4} - 10^{-2} \text{ GeV}^{-1}$, and we assumed a b -tagging efficiency of 68% [13]. In Table 1, we show the values of the coupling constants $g_{H\gamma\gamma}$, $g_{HZ\gamma}^{(1,2)}$ that corresponds to a 5σ effect in the 1 GeV bin of the E_γ distribution around the Higgs peaks, for different Higgs boson masses. We also present the total number of signal and background events in these bins. For $M_H = 90 \text{ GeV}$, a large numbers of events is needed due to the Z boson peak. Since the signal increases with the square of the anomalous couplings, for some values of the coupling constants, we could expect to have a reliable signal for the anomalous Higgs boson in less than one year of LEP2 run.

In this study, we have not taken into account initial state radiation, which would result in an energy degradation of the original e^+e^- beams, and we have not included a realistic simulation of the electromagnetic energy resolution. It is important to notice that an increase in the b -tagging efficiency, and a good resolution of the electromagnetic calorimeter can help to select the $b\bar{b}$ events, increasing the signal over background ratio and improving the resolution of the Higgs boson peak in the photon energy distribution.

In conclusion, searching for the anomalous Higgs at LEP2 provides a complementary way to the indirect precision measurements at LEP1 in probing effective Lagrangians that are the low-energy limit of physics beyond the SM. We have shown that the study of the process $e^+e^- \rightarrow b\bar{b}\gamma$ can be a very important tool in the search of these particles at LEP2. We found that anomalous couplings $g_{H\gamma\gamma}$, $g_{HZ\gamma}^{(1,2)} \sim 10^{-2} \text{ GeV}^{-1}$ are necessary for identifying an anomalous Higgs of 150 GeV. However, for a lighter Higgs boson, couplings as small as $4 \times 10^{-4} \text{ GeV}^{-1}$ should suffice.

References

- [1] See, e.g., K. Hagiwara, talk presented at the *XVII International Symposium on Lepton and Photon Interactions at High Energies, 10-15 August 1995, Beijing, China*, KEK preprint 95-184, hep-ph/9512425.
- [2] S. Weinberg, *Physica* **96A**, 327 (1979); J. F. Donoghue, E. Golowich and B. R. Holstein, *Dynamics of the Standard Model* (Cambridge University Press, 1992).
- [3] W. Buchmuller and D. Wyler, *Nucl. Phys.* **B268**, 621 (1986).
- [4] K. Hagiwara, S. Ishihara, R. Szalapski and D. Zeppenfeld, *Phys. Rev. D* **48**, 2182 (1993).
- [5] K. Hagiwara, R. Szalapski, and D. Zeppenfeld, *Phys. Lett.* **B318**, 155 (1993).
- [6] K. Hagiwara, and M. L. Stong, *Z. Phys.* **C62**, 99 (1994); B. Grzadkowski, and J. Wudka, *Phys. Lett.* **B364**, 49 (1995); G. J. Gounaris, J. Layssac and F. M. Renard, *Z. Phys.* **C65**, 245 (1995); G. J. Gounaris, F. M. Renard and N. D. Vlachos, preprint PM-95-30, and hep-ph/9509316.
- [7] G. J. Gounaris and F. M. Renard, preprint PM-95-20, and hep-ph/9505429.
- [8] T. Stelzer and W. F. Long, *Comput. Phys. Commun.* **81**, 357 (1994).
- [9] H. Murayama, I. Watanabe and K. Hagiwara, KEK Report 91-11.
- [10] V. D. Barger and R. J. N. Phillips, *Collider Physics* (Addison-Wesley, 1987).
- [11] G. P. Lepage, *J. Comp. Phys.* **27**, 192 (1978), and "Vegas: An Adaptive Multidimensional Integration Program", CLNS-80/447, 1980 (unpublished).
- [12] S. M. Lietti, S. F. Novaes and R. Rosenfeld, *Phys. Rev. D*, (1996)
- [13] P. Bambade *et al.*, *Delphi Collaboration*, preprint DELPHI 95-57 PHYS 493 (1995) (unpublished).

M_H (GeV)	$ g_{H\gamma\gamma} $ (GeV ⁻¹)	$ g_{HZ\gamma}^{(1)} $ (GeV ⁻¹)	$ g_{HZ\gamma}^{(2)} $ (GeV ⁻¹)	Signal / Background
70	3.89×10^{-4}	1.93×10^{-3}	9.62×10^{-4}	4.69/0.88
80	5.63×10^{-4}	2.66×10^{-3}	1.37×10^{-3}	7.32/2.14
90	1.52×10^{-3}	7.47×10^{-3}	3.74×10^{-3}	43.09/74.20
100	1.04×10^{-3}	4.98×10^{-3}	2.49×10^{-3}	13.61/7.41
110	8.00×10^{-4}	4.30×10^{-3}	2.14×10^{-3}	7.16/2.05
120	1.02×10^{-3}	4.91×10^{-3}	2.43×10^{-3}	5.81/1.35
130	1.36×10^{-3}	6.44×10^{-3}	3.24×10^{-3}	4.77/0.91
140	2.70×10^{-3}	1.09×10^{-2}	5.45×10^{-3}	4.72/0.89
150	5.16×10^{-3}	2.65×10^{-2}	1.24×10^{-2}	4.92/0.97

Table 1: Values of the anomalous couplings $g_{H\gamma\gamma}$, $g_{HZ\gamma}^{(1)}$, and $g_{HZ\gamma}^{(2)}$ corresponding to a significance of 5σ , and the ratio of the total number of signal and background events.

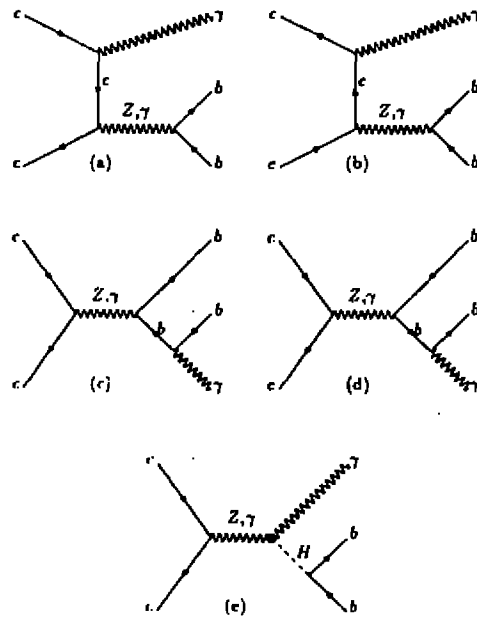


Figure 1: Feynman diagrams for $e^+e^- \rightarrow b\bar{b}\gamma$ in the standard model at tree-level (a, b, c, d) and the anomalous Higgs boson contribution (e).

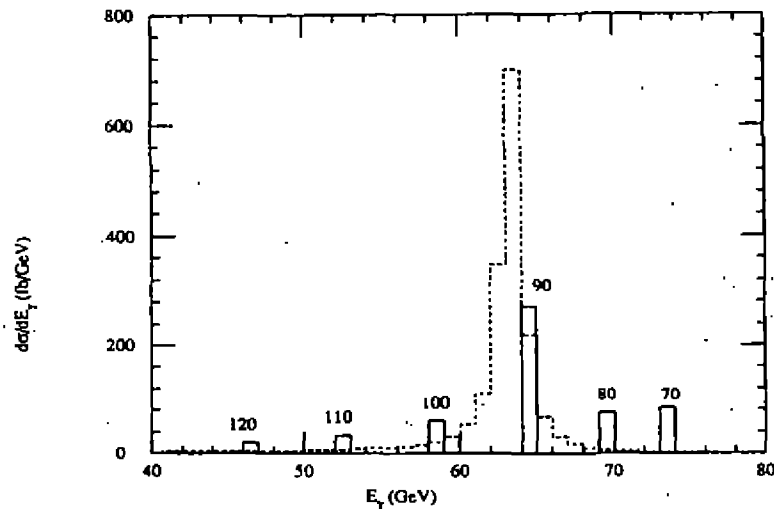


Fig. 2

Figure 2: Photon energy distribution ($d\sigma/dE_\gamma$) of the process $e^+e^- \rightarrow b\bar{b}\gamma$, for the standard model contribution (dashed histogram). We also show the Higgs boson peaks (solid histogram) for different values of its mass, and $g_{H\gamma\gamma} = 10^{-3}$ GeV⁻¹.

Topology Change in Canonical Quantum Cosmology

Vitorio A. De Lorenci ^(a), Jérôme Martin ^{(a),(b)}, Nelson Pinto Neto ^(a)
and Ivano Damião Soares ^(a)

^(a) Laboratório de Cosmologia e Física Experimental de Altas Energias,
Centro Brasileiro de Pesquisas Físicas,
Rua Dr. Xavier Sigaud, 150, Urca
Rio de Janeiro CEP 22290-180-RJ. Brazil.

^(b) Laboratoire de Gravitation et Cosmologies Relativistes,
Université Pierre et Marie Curie, CNRS/URA 769,
Tour 22/12, Boite courrier 142, 4 place Jussieu,
75252 Paris, France.

1 Introduction

The aim of this paper is to exhibit *some scenarios* where classically forbidden changes of topology in the Universe are indeed possible in the quantum domain.

Our model is based on the following minisuperspace metric:

$$ds^2 = -N^2(t)dt^2 + a^2(t) \left\{ d\chi^2 + \left[\frac{\sin(\sqrt{k(t)}\chi)}{\sqrt{k(t)}} \right]^2 d\Omega^2(\theta, \phi) \right\}. \quad (1)$$

where $d\Omega^2(\theta, \phi)$ is the usual line element of a two-sphere. For $k(t) > 0$, the domain of variation of χ is $0 \leq \chi < 2\pi/\sqrt{k(t)}$, in order to avoid conical singularities. We are assuming a S^3 topology for these values of $k(t)$. For $k(t) \leq 0$, the domain of variation of χ is $0 \leq \chi \leq \chi_0(\theta, \varphi)$, where the function $\chi_0(\theta, \varphi)$ will depend on the topology of the particular closed space that we choose. We use the terminology *closed spaces* for a compact space without boundary. We consider only closed spaces in order to avoid surface terms in the Hamiltonian formalism.

The metric (1) is a Friedman-Lemaître-Robertson-Walker (FLRW) like metric with a time dependent $k(t)$. It is clear from Eq. (1) that, when $k(t)$ passes through zero, there is a change of topology. For instance, when $k(t)$ changes from a positive number to zero, the topology of the three-dimensional space V^3 changes because the S^3 topology cannot be realized in spaces with $k = 0$.

However, things are not so simple. It is not possible to construct a minisuperspace hamiltonian from the metric (1) because, as far as k depends on time, this metric does not represent a spatially homogeneous spacetime, in the sense that the components of the 4-dimensional curvature tensor in a local frame are functions of t and χ . The existence of the non-null component of the Einstein tensor $R_{t\chi} = \chi \dot{k}(t)/a(t)N(t) \neq 0$ is a consequence of this fact. Hence we are forced to introduce a midisuperspace model having a shift function $N_\chi(\chi, t)$. The midisuperspace metric, which was already proposed in Ref. [1] to study different problems, and also in Refs. [2, 3] to study the quantum black hole, will then be:

$$ds^2 = \left[-N^2(\chi, t) + \frac{N_\chi^2(\chi, t)}{a^2(\chi, t)} \right] dt^2 + 2N_\chi(\chi, t)d\chi dt + a^2(\chi, t)[d\chi^2 + \sigma^2(\chi, t)d\Omega^2(\theta, \phi)]. \quad (2)$$

Our new idea is then to quantize this midisuperspace model, and after impose to the quantum solutions the restrictions on the configuration variables from which we can obtain the metric (1). We will have to treat the midisuperspace problem to come back to the minisuperspace one, in order to be consistent, and in order to have a single Wheeler-DeWitt equation which can be applied to the different topologies mentioned above. Adopting a suitable interpretation, we want to know if any of the wave functions found exhibits a change of topology.

2 The Hamiltonian Formalism for the Classical Model

The total Hamiltonian density is given by:

$$\mathcal{H} = N\mathcal{H}^0 + N_X\mathcal{H}^X, \quad (3)$$

where \mathcal{H}^0 and \mathcal{H}^X are the super-Hamiltonian and super-momentum constraints,

$$\mathcal{H}^0 = \left[\frac{\pi_a^2}{8a\sigma^2} + \frac{3\pi_\sigma^2}{8a^3} - \frac{\pi_a\pi_\sigma}{2a^2\sigma} + \frac{\pi_\phi^2}{2a^3\sigma^2} \right] + \sigma^2 a^3 \mathcal{V} + \left(\frac{\xi'^2}{2a^2} + 1 \right)^{\frac{1}{2}} \pi_\xi, \quad (4)$$

$$\mathcal{H}^X = \frac{1}{a^2} \left(-a\pi'_a + \sigma\pi'_\sigma + 2\sigma'\pi_\sigma + \phi'\pi_\phi + \xi'\pi_\xi \right), \quad (5)$$

where \mathcal{V} is defined by

$$\mathcal{V} = -{}^3\mathcal{R} + \frac{\phi'^2}{2a^2} + U(\phi) + V(\xi). \quad (6)$$

Before proceeding in the quantization of the above system, it will be useful to perform a change to new variables $\alpha(\chi, t)$ and $\beta(\chi, t)$ defined by

$$\alpha = \ln a, \quad \beta = -2 \ln(\sigma a). \quad (7)$$

The momenta π_α and π_β are related to the old momenta π_a and π_σ by

$$\pi_a = e^{-\alpha} (\pi_\alpha - 2\pi_\beta), \quad (8)$$

$$\pi_\sigma = -2e^{\alpha+\frac{\beta}{2}} \pi_\beta.$$

In the new variables α and β , the super-Hamiltonian and super-momentum constraints can be expressed as

$$\mathcal{H}^0 = e^{-\alpha+\beta} \left[\frac{\pi_\alpha^2}{8} + \frac{\pi_\alpha\pi_\beta}{2} + \frac{\pi_\phi^2}{2} \right] + e^{\alpha-\beta} \mathcal{V} + \left(e^{-2\alpha}\xi'^2 + 1 \right)^{\frac{1}{2}} \pi_\xi \approx 0, \quad (9)$$

$$\mathcal{H}^X = e^{-2\alpha} \left[\alpha'\pi_\alpha + \beta'\pi_\beta + \phi'\pi_\phi + \xi'\pi_\xi - \pi'_\alpha \right] \approx 0, \quad (10)$$

where the functions \mathcal{V} and ${}^3\mathcal{R}$ in the α, β variables have the form:

$$\mathcal{V} = -{}^3\mathcal{R} + e^{-2\alpha} \frac{\phi'^2}{2} + U(\phi) + V(\xi), \quad (11)$$

$${}^3\mathcal{R} = e^{-2\alpha} \left[-\frac{3}{2}\beta'^2 - 2\alpha'\beta' + 2\beta'' + 2e^{2\alpha+\beta} \right]. \quad (12)$$

For further reference we introduce the two variables $u(\chi, t)$ and $v(\chi, t)$ given by

$$u = \ln \sigma = -\alpha - \frac{\beta}{2}, \quad v = \ln(a^3\sigma^2) = \alpha - \beta. \quad (13)$$

3 Quantization

The space of wave functionals must be endowed with the structure of a Hilbert space in order to associate operators with observables. Also, the super-Hamiltonian and super-momentum constraints, turn into a restriction on the Hilbert space of wave functionals, namely

$$\hat{\mathcal{H}}^0 \Psi[a, \sigma, \phi, \xi] = 0, \quad (14)$$

$$\hat{\mathcal{H}}^\chi \Psi[a, \sigma, \phi, \xi] = 0. \quad (15)$$

Eq. (14) is the well-known Wheeler-DeWitt equation, and Eq. (15) is the so-called momentum constraint equation, the solutions of which will be the main interest in the remainder of this paper. Note that equations (14) and (15) are valid for all possible domains of variation of χ , and thus applicable to all possible topologies we are considering.

We obtain the following expression for \mathcal{H}^0 :

$$\begin{aligned} \hat{\mathcal{H}}^0 = & \left[\frac{\hat{\pi}_\alpha e^{-\alpha+\beta} \hat{\pi}_\alpha}{8} + \frac{1}{4} (\hat{\pi}_\alpha e^{-\alpha+\beta} \hat{\pi}_\beta + \hat{\pi}_\beta e^{-\alpha+\beta} \hat{\pi}_\alpha) + \frac{\hat{\pi}_\phi^2}{2} \right] \\ & + e^{\alpha-\beta} \nu + \left(e^{-2\alpha} \xi'^2 + 1 \right)^{\frac{1}{2}} \hat{\pi}_\xi. \end{aligned} \quad (16)$$

The equation $\hat{\mathcal{H}}^0 \Psi = 0$ is a Schrödinger like functional equation with ξ playing the role of time, because $\hat{\mathcal{H}}^0$ is linear in the momentum operator π_ξ .

The general wave functionals can always be put under the following form

$$\Psi[\alpha, \beta, \phi, \xi] = e^{i/\hbar S[\alpha, \beta, \phi, \xi]}, \quad (17)$$

where the complex functional S must satisfy the equations

$$\begin{aligned} -i\hbar e^{-\alpha+\beta} \left[\frac{1}{8} \frac{\delta^2 S}{\delta \alpha^2} + \frac{1}{2} \frac{\delta^2 S}{\delta \alpha \delta \beta} + \frac{1}{2} \frac{\delta^2 S}{\delta \phi^2} + \left(\frac{1}{8} \frac{\delta S}{\delta \alpha} - \frac{1}{4} \frac{\delta S}{\delta \beta} \right) \delta(0) \right] \\ + e^{-\alpha+\beta} \left[\frac{1}{8} \left(\frac{\delta S}{\delta \alpha} \right)^2 + \frac{1}{2} \left(\frac{\delta S}{\delta \alpha} \right) \left(\frac{\delta S}{\delta \beta} \right) + \frac{1}{2} \left(\frac{\delta S}{\delta \phi} \right)^2 \right] + e^{\alpha-\beta} \nu \\ + \left(e^{-2\alpha} \xi'^2 + 1 \right)^{\frac{1}{2}} \frac{\delta S}{\delta \xi} = 0, \end{aligned} \quad (18)$$

$$e^{-2\alpha} \left[\alpha' \frac{\delta S}{\delta \alpha} + \beta' \frac{\delta S}{\delta \beta} + \phi' \frac{\delta S}{\delta \phi} + \xi' \frac{\delta S}{\delta \xi} - \partial_\chi \left(\frac{\delta S}{\delta \alpha} \right) \right] = 0. \quad (19)$$

At order \hbar^0 , Eq. (18) reduces to the Hamilton-Jacobi (H-J) functional equation, whose solution is the phase of the WKB wave functional. The momentum constraint equation (19) remains unchanged.

It's clear that Eqs. (18) and (19) are very complicated and we were not able to find solutions valid in the full midisuperspace. The solutions we obtained are only valid in the minisuperspace, i.e., they are solutions in the subdomain \mathcal{M} of the midisuperspace defined by

$$a' = 0, \quad \phi' = 0, \quad \xi' = 0, \quad (20)$$

$$\sigma = \frac{\sin(\sqrt{k(t)}\chi)}{\sqrt{k(t)}}. \quad (21)$$

For $U(\phi) = 0 = V(\xi)$, we display the following solutions to the H-J and momentum constraint functional equations

$$\begin{aligned} \Psi_1 = e^{iS/\hbar} = \exp \left\{ \frac{i}{4\pi\hbar} \int d\theta d\varphi \sin \theta \left[\frac{Ca \sin(2\lambda_0)\xi}{\sqrt{k}} - \sqrt{3-C} \frac{\phi a^2 \sin^2 \lambda_0}{k} + \right. \right. \\ \left. \left. - \sqrt{6-2C} \frac{a^2}{k} \left(\sin^2 \lambda_0 \ln \left(\frac{a \sin \lambda_0}{2\sqrt{k}} \right) + \cos^2 \lambda_0 \ln(\cos \lambda_0) \right) \right] \right\}, \end{aligned} \quad (22)$$

$$\Psi_2 = e^{iS_2/\hbar} = \exp \left\{ \frac{i}{4\pi\hbar} \int d\theta d\phi \sin \theta \left[\frac{Ca \sin(2\lambda_0)\xi}{\sqrt{k}} - i\sqrt{2C+3} \frac{\phi a^2 \sin^2 \lambda_0}{k} + 8i\sqrt{C+3} \frac{a^2}{k} \sin^2 \left(\frac{\lambda_0}{2} \right) \right] \right\} \quad (23)$$

where $\lambda_0 = \sqrt{k}\chi_0(\theta, \phi)$.

The above wave functions Ψ_1 and Ψ_2 are the main result of this section.

4 The Conditional Probability Interpretation

The conditional probability, for fixed a and ϕ , of having k equal to $-1, 0$ or $+1$ knowing that $k \in \{-1, 0, +1\}$ is defined by:

$$P_c(k) \equiv \frac{|\Psi(k)|^2}{\sum_{k=0,\pm 1} |\Psi(k)|^2}. \quad (24)$$

The constraint $\sum_{k=0,\pm 1} P_c(k) = 1$ can be immediately checked. Let us compute and discuss $P_c(k)$ for the wave function Ψ_2 . At this stage, boundary conditions on Ψ_2 should be chosen. In the present context, this amounts to fix the value of the constant C . Many proposals have been made to answer this question [16, 17]. In this article, we will just consider two different possible values for C in order to illustrate that different choices actually lead to different predictions.

As a first example, let us assume that $C = -i$. The term multiplying ξ in the exponential of Eq. (23) becomes:

$$F_1 \equiv \frac{a}{4\pi\hbar} \int_0^{2\pi} \int_0^\pi d\theta d\phi \sin \theta \sin \left[2\chi_0^{(1)}(\theta, \phi) \right] \quad (25)$$

for $k = 1$, where $\chi_0^{(1)} = 2\pi$ for S^3 and $\chi_{max}^{(1)} = \text{Max}\chi_0^{(1)}(\theta, \phi) \approx 0.163$ for Poincaré's dodecahedral space (D^3);

$$F_0 \equiv \frac{a}{4\pi\hbar} \int_0^{2\pi} \int_0^\pi d\theta d\phi \sin \theta 2\chi_0^{(0)}(\theta, \phi) \quad (26)$$

for $k = 0$, where $\chi_{max}^{(0)} = \text{Max}\chi_0^{(0)}(\theta, \phi)$ is arbitrary for T^3 (and for any other closed topology in $k=0$); and,

$$F_{-1} \equiv \frac{a}{4\pi\hbar} \int d\theta d\phi \sin \theta \sinh \left[2\chi_0^{(-1)}(\theta, \phi) \right] \quad (27)$$

for $k = -1$, where $\chi_{max}^{(-1)} = \text{Max}\chi_0^{(-1)}(\theta, \phi) \approx 1.3824$ and $\chi_{min}^{(-1)} = \text{Min}\chi_0^{(-1)}(\theta, \phi) \approx 0.8683$.

As the integrands in F_{-1}, F_0, F_1 are equal or greater than zero in all cases, we have: $F_1 = 0$ for S^3 space, $F_1 < a \sin(0.326)/\hbar$ for D^3 space, and $a \sinh(2\chi_{insc})/\hbar < F_{-1} < a \sinh(2\chi_{circ})/\hbar$ for I^3 space. The integral F_0 will be as big as the volume of T^3 , which is arbitrary because χ_{max}^0 is not fixed. Note that $F_{-1} > F_1$ for all cases in considerations.

Using the definition (24) and Eq. (23), we obtain, for the conditional probabilities:

$$P_c(k = -1) = \frac{A(a, \phi)e^{F_{-1}\xi}}{C(a, \phi)e^{aF_1\xi} + B(a, \phi)e^{aF_0\xi} + A(a, \phi)e^{aF_{-1}\xi}}, \quad (28)$$

$$P_c(k = 0) = \frac{B(a, \phi)e^{F_0\xi}}{C(a, \phi)e^{aF_1\xi} + B(a, \phi)e^{aF_0\xi} + A(a, \phi)e^{aF_{-1}\xi}}, \quad (29)$$

$$P_c(k = +1) = \frac{C(a, \phi)e^{F_1\xi}}{C(a, \phi)e^{aF_1\xi} + B(a, \phi)e^{aF_0\xi} + A(a, \phi)e^{aF_{-1}\xi}}, \quad (30)$$

where the positive functions $A(a, \phi)$, $B(a, \phi)$ and $C(a, \phi)$ can be obtained by substituting $k = -1, 0, +1$ in Eq. (23), respectively. These functions are not relevant for what follows because they do not depend on ξ .

Let us study $P_c(k)$ at the boundaries of the minisuperspace in ξ , for fixed values of the scale factor and the scalar field. For clarity we will distinguish the two set of closed spaces: (i) $\{S^3, T^3, I^3\}$, and (ii) $\{D^3, T^3, I^3\}$.

i) In this case $F_1 = 0$ and we have two possibilities: $F_0 > F_1$ or $F_0 < F_{-1}$. From the previous expressions, we get:

$$\lim_{\xi \rightarrow -\infty} P_c(k = -1) = \lim_{\xi \rightarrow -\infty} P_c(k = 0) = 0, \quad (31)$$

and,

$$\lim_{\xi \rightarrow -\infty} P_c(k = +1) = 1. \quad (32)$$

On the other hand, if we compute the same probabilities but this time when the dust field goes to $+\infty$, we obtain:

$$\lim_{\xi \rightarrow +\infty} P_c(k = +1) = 0, \quad (33)$$

$$\lim_{\xi \rightarrow +\infty} P_c(k = -1) = \begin{cases} 0, & F_0 > F_{-1} \\ 1, & F_0 < F_{-1}, \end{cases} \quad (34)$$

and,

$$\lim_{\xi \rightarrow +\infty} P_c(k = 0) = \begin{cases} 0, & F_{-1} > F_0 \\ 1, & F_{-1} < F_0, \end{cases} \quad (35)$$

Therefore, in this case, definite predictions can be made since conditional probabilities are either equal to 0 or 1. There is a change of topology from $k = 1$ to $k = 0$ when in the minisuperspace we go from $\xi = -\infty$ to $\xi = +\infty$ and $F_0 > F_{-1}$; an the other hand, if $F_0 < F_{-1}$ there is a change of topology from $k = 1$ to $k = -1$ when in the minisuperspace we go from $\xi = -\infty$ to $\xi = +\infty$.

It is clear that this is a quantum mechanical effect since it is not possible that a classical path could connect the two regions. A similar result would have been obtained if we had used Ψ_1 instead of Ψ_2 .

If we choose $C = i$ we will obtain the results of $C = -i$ with $\xi \rightarrow -\xi$. This shows the importance of the choice of boundary conditions.

ii) For the set $\{D^3, T^3, I^3\}$, we have $0 < F_1 < F_{-1}$ and three possibilities:

- a) $F_0 < F_1$. The conditional probabilities (28 - 30) gives for $\xi \rightarrow \infty$ $P_c(k = +1) = 1$ and for $\xi \rightarrow -\infty$ $P_c(k = -1) = 1$;
- b) $F_1 < F_0 < F_{-1}$. For $\xi \rightarrow -\infty$ we have $P_c(k = +1) = 1$ and for $\xi \rightarrow \infty$, $P_c(k = -1) = 1$;
- c) $F_1 < F_{-1} < F_0$. For $\xi \rightarrow -\infty$ we have $P_c(k = +1) = 1$ and for $\xi \rightarrow \infty$, $P_c(k = 0) = 1$.

A most important remark must be made here. Although the dimension and volume of the fundamental cube ($k = 0$) is arbitrary, its relation to the dimensions of the fundamental dodecahedron ($k = 1$) and the fundamental icosahedron ($k = -1$) is crucial to fix what will be the allowable transitions of topology, according to the conditional probability interpretation. For example, for the WKB wave function (23) with $C = -i$, the transition of a dodecahedral closed space ($k = 1$) to an icosahedral closed space ($k = -1$) is permitted if and only if the dimension of the cube is such that $F_1 < F_0 < F_{-1}$. It seems that the change of topology depends crucially on the volume of the $k = 0$ space. For $c = -i$, for instance, topology tends to change in the direction of the space of bigger volume between T^3 and I^3 .

Let us conclude this section by emphasizing that different interpretations actually lead to very different results. For instance, the "selection rule" established previously is violated in the conditional probability interpretation. This shows how crucial the problem of the interpretation of Quantum Gravity is.

It should be also clear that the two wave functions Ψ_1 and Ψ_2 do not represent automatically states of cosmological interest. Our aim was just to exhibit at least one state for which the change of topology considered in this article is indeed possible.

5 Conclusion

In this paper we tried to settle down in a proper way an interesting and simple physical question: in a Friedman-Lemaître-Robertson-Walker Universe with a scalar field, is it possible to have a quantum change of topology of the spacelike hypersurfaces of homogeneity by changing the sign of their intrinsic curvatures? As we have shown in section 2, a consistent hamiltonian treatment to this problem involves an enlargement of the minisuperspace to a midisuperspace model. This enlarged configuration space is, *per se*, very interesting to analyze because it has an

infinity number of degrees of freedom: it is a quantum field theory and it is closer to the full quantum gravity than the usual minisuperspaces models. New problems arise, like anomalies and regularization, and the Wheeler-DeWitt equation becomes a functional differential equation.

We have seen how the physical predictions we can obtain from the quantum solutions depends crucially on the interpretation we adopt. For our class of solutions and choice of topology, in the probabilistic interpretation, the requirement of normalizability implies that only wave functions which vanishes for $k = 1$ and S^3 topology are possible. Hence, topology change from $k = 1$ with S^3 topology to some other value of k is impossible. However, if we adopt the conditional probability interpretation, where there is no requirement of normalizability, we have shown a wave function exhibiting a quantum change of topology from $k = 1$ with S^3 topology to $k = 0$ or $k = -1$, with a preference to the space of bigger volume.

It is also evident the importance of imposing boundary conditions in order to obtain definite predictions. We have shown that, adopting the conditional probability interpretation, different quantum solutions exhibit different types of topology change or even no change of topology at all if we choose, e.g., C real in Eq. (23).

References

- [1] W. Fischler, D. Morgan and J. Polchinski; *Phys. Rev.* **D42**, 4042 (1990).
- [2] D. Louis-Martinez et al, *Phys. Lett.* **B 321**, 193 (1994); J. G. Demers and C. Kiefer, *Phys. Rev.* **D 53**, 7050 (1996).
- [3] T. Brotz and C. Kiefer, Report gr-qc/9608031.
- [4] K. V. Kuchař and C. G. Torre, *Phys. Rev.* **D43**, 419 (1991).
- [5] D. S. Salopek, *Phys. Rev.* **D46**, 4373 (1992).
- [6] M. Lachièze-Rey and J. P. Luminet, *Phys. Report* **254**, 135 (1995)
- [7] H. Seifert and W. Threlfall, *Math. Ann.* **104**, 1 (1930); *A textbook of Topology*, ed. J. S. Birman and J. Eisner (New York: Academic) 1980.
- [8] H. S. M. Coxeter, *Twelve Geometric Essays*, Southern Illinois University Press (1968)
- [9] W. G. Unruh and R. M. Wald, *Phys. Rev.* **D40**, 2598 (1984).
- [10] C. Teitelboim, *Phys. Lett.* **B 50**, 376 (1975).
- [11] K. Kuchař, in *Quantum Gravity II* edited by C. J. Isham, R. Penrose and D. W. Sciama, (Clarendon Press, Oxford, 1982).
- [12] J. H. Van Vleck, *Proc. Natl. Acad. Sci.* **14** (1928) 178.
- [13] M. C. Gutzwiller, *Chaos in Classical and Quantum Mechanics* (Springer-Verlag, Berlin, 1990).
- [14] B. Hatfield, "Quantum Field Theory of Point Particles and Strings". (Addison-Wesley, Redwood City, 1992).
- [15] J.J. Halliwell, in *Quantum Cosmology and Baby Universes* edited by S. Coleman, J. B. Hartle, T. Piran and S. Weinberg, (World Scientific, Singapore, 1991).
- [16] J. B. Hartle and S. W. Hawking, *Phys. Rev.* **D28**, 2960 (1983).
- [17] A. Vilenkin, *Phys. Rev.* **D37**, 888 (1988).

Vacuum Quantum Effects of Nonconformal Scalar Field in the Friedmann Cosmology

V. B. Bezerra, V. M. Mostepanenko*, C. Romero

Departamento de Física - Universidade Federal da Paraíba - João Pessoa

A. Friedmann

Laboratory for Theoretical Physics (Russia)

Particle creation and vacuum polarization are considered for the quantized scalar field of mass m with arbitrary coupling ξ in isotropic cosmology. The conformal case was investigated in the latter half of the seventies [1]. As to the nonconformal one the mention may be made only of the paper [2] where the anomalous trace was derived and of the paper [3] where the total vacuum stress-energy tensor (SET) was obtained for the de Sitter space-time.

The case of the scalar field with nonconformal coupling is important as such a field drives the inflation process. It may contribute also to solve the cosmological constant problem. Here we calculate the total vacuum SET of the quantized scalar field with arbitrary coupling in the radiation dominated Friedmann Universe. The wave equation for the field $\varphi(x)$ is [1,4]

$$(\nabla_i \nabla^i + \xi R + m^2)\varphi(x) = 0, \quad (1)$$

where R is the scalar curvature of space-time, m is the field mass (units in which $\hbar = c = 1$ are used throughout). For $\xi = 1/6$ (in four-dimensional space-time), and $m = 0$ the Eq.(1) is conformally invariant [1,4].

We will consider the quasi-Euclidean space-time with the metric

$$\begin{aligned} ds^2 &= dt^2 - a^2(t)\gamma_{\alpha\beta}dx^\alpha dx^\beta \\ &\equiv dt^2 - a^2(t) [(dx^1)^2 + (dx^2)^2 + (dx^3)^2], \end{aligned} \quad (2)$$

where $dt = a(\eta)d\eta$ and η is the so called "conformal" time.

The variables separation procedure in Eq. (1) leads to the oscillatory equation

$$g_\lambda''(\eta) + [\omega^2(\eta) + q(\eta)]g_\lambda(\eta) = 0 \quad (3)$$

with

$$\begin{aligned} \omega^2(\eta) &\equiv \lambda^2 + m^2 a^2(\eta), & q(\eta) &\equiv -6\left(\frac{1}{6} - \xi\right) \frac{a''(\eta)}{a(\eta)}, \\ g_\lambda(\eta_0) &= \omega^{-1/2}(\eta_0), & g_\lambda'(\eta_0) &= i\omega(\eta_0)g_\lambda(\eta_0), \end{aligned} \quad (4)$$

where η_0 is some initial moment and derivative with respect to η is denoted by a prime.

Field quantization is carried out in the usual way after which we get the total renormalized expectation values of the metrical SET operator in initial vacuum state (for details see [1])

$$\langle T_{00} \rangle_{ren} = \frac{1}{\pi^2 a^2} \int_0^\infty d\lambda \lambda^2 \{\omega(s - s_2 - s_4)\}$$

*On leave from St.Petersburg State Technological Institute (Technical University)

$$\begin{aligned}
 &+ 3\left(\frac{1}{6} - \xi\right) \frac{c^2}{\omega} \left[s - s_2 + \frac{1}{2}(u - u_2)\right] \\
 &+ 3\left(\frac{1}{6} - \xi\right) c(v - v_1 - v_3), \\
 \langle T_{\alpha\beta} \rangle_{ren} = &\frac{1}{\pi^2 a^2} \int_0^\infty d\lambda \lambda^2 \left\{ \frac{\lambda^2}{3\omega} (s - s_2 - s_4) \right. \\
 &- \frac{m^2 a^2}{6\omega} (u - u_2 - u_4) + \\
 &+ 3\left(\frac{1}{6} - \xi\right) [c^2 - 4\xi(c' + c^2)] \frac{1}{\omega} \left[s - s_2 + \frac{1}{2}(u - u_2)\right] - \\
 &\left. - 2\left(\frac{1}{6} - \xi\right) \omega (u - u_2 - u_4) + 3\left(\frac{1}{6} - \xi\right) c(v - v_1 - v_3) \right\} \gamma_{\alpha\beta}.
 \end{aligned} \tag{5}$$

Here $c \equiv a'/a$ and the bilinear quantities s, u, v are defined as follows

$$\begin{aligned}
 s &= \frac{1}{4\omega} (|g'_\lambda|^2 + \omega^2 |g_\lambda|^2) - \frac{1}{2}, \\
 u &= -\frac{1}{2\omega} (|g'_\lambda|^2 - \omega^2 |g_\lambda|^2), \quad v = -\frac{1}{2} \frac{d}{d\eta} |g_\lambda|^2.
 \end{aligned} \tag{6}$$

The subtractions of the quantities $v_1, v_3, s_2, s_4, u_2, u_4$ in (5), where

$$\begin{aligned}
 s_2 &= \frac{1}{16} W^2, \quad s_4 = -\frac{1}{32} W D^2 W + \frac{1}{64} [DW]^2 + \\
 &+ \frac{3}{256} W^4 + \frac{q^2}{16\omega^4} + \frac{1}{16} W \omega D\left(\frac{q}{\omega^3}\right) - \frac{q}{16\omega^2} DW \dots, \\
 u_2 &= \frac{1}{4} DW - \frac{q}{2\omega^2}, \quad u_4 = -\frac{1}{16} D^3 W + \frac{3}{32} W^2 DW + \\
 &+ \frac{1}{8} D\omega D\left(\frac{q}{\omega^3}\right) - \frac{q}{16\omega^2} W^2 - \frac{q}{8\omega^2} DW + \frac{q^2}{4\omega^4} \dots, \\
 v_1 &= \frac{1}{2} W, \quad v_3 = -\frac{1}{8} D^2 W + \frac{1}{16} W^3 + \frac{\omega}{4} D\left(\frac{q}{\omega^3}\right) \dots,
 \end{aligned} \tag{7}$$

($D \equiv \omega^{-1}(d/d\eta)$, $W \equiv \omega'/\omega^2$) remove the divergencies in the cut-off momentum proportional to Λ^4, Λ^2 and $\ln \Lambda$. They are equivalent to renormalization of the cosmological constant, gravitational constant and constants near quadratic in curvature terms in the bare gravitational Lagrangian [1].

The scale factor of the radiation dominated Friedmann Universe vanishes by the linear law

$$a(\eta) = a_1 \eta, \tag{8}$$

where really the condition $ma_1 \gg 1$ is fulfilled with great supply.

The oscillatory equation (3) takes here the simplified form with $q(\eta) = 0$:

$$g''_\lambda(\eta) + (\lambda^2 + m^2 a_1^2 \eta^2) g_\lambda(\eta) = 0, \tag{9}$$

i.e., the same as for the conformal scalar field. Nevertheless the contributions proportional to $(\frac{1}{6} - \xi)$ are contained in the Eq.(5) for the total renormalized SET, thus distinguishing the cases of conformal field and of field with arbitrary coupling.

Using (9) we get the following system of equations for the quantities defined in (6):

$$\begin{aligned}
 s' &= \frac{1}{2} \frac{\omega'}{\omega} u, \quad v' = 2\omega u, \\
 u' &= \frac{\omega'}{\omega} (1 + 2s) - 2\omega v
 \end{aligned} \tag{10}$$

with the initial conditions

$$s(\eta_0) = u(\eta_0) = v(\eta_0) = 0, \quad (11)$$

which are equivalent to (4). Below we will put $\eta_0 = 0$. Both the Eq.(9) or the equivalent to it system of equations (10) with the scale factor (8), cannot be solved exactly. But it is possible to do the analytic calculations for the epoch $t \ll m^{-1}$ near the cosmological singularity which just corresponds to the radiation dominated equation of state of the background matter. With this in mind let us find the asymptotics of s , u and v for the regions $\lambda \ll \eta^{-1}$ and $\lambda \gg ma$ which overlap each other due to the relation

$$ma(\eta)\eta \sim m \int_0^\eta a(\eta') d\eta' = mt \ll 1. \quad (12)$$

In the region $\lambda \gg ma$ it is convenient to use the Volterra equations [1] which are equivalent to the system (10) with the initial conditions (11). The first iteration of these equations gives

$$u + iv \approx \int_0^\eta \frac{\omega'(\eta')}{\omega(\eta')} \exp[2i\lambda(\eta - \eta')] d\eta',$$

$$s \approx \frac{1}{4} \left| \int_0^\eta \frac{\omega'(\eta')}{\omega(\eta')} \exp(2i\lambda\eta') d\eta' \right|^2. \quad (13)$$

Substituting the scale factor (8) into (13), we arrive to the result

$$s = \frac{m^4 a_1^4}{16\lambda^6} \left[\eta^2 - \frac{\eta}{\lambda} \sin 2\lambda\eta + \frac{1}{\lambda^2} \sin^2 \lambda\eta \right],$$

$$u = \frac{m^2 a_1^2}{2\lambda^4} \sin^2 \lambda\eta, \quad v = \frac{m^2 a_1^2}{2\lambda^3} \left[\eta - \frac{1}{2\lambda} \sin 2\lambda\eta \right]. \quad (14)$$

In the region $\lambda \ll \eta^{-1}$ the results may be easily obtained using the method of sudden perturbations. They are given by

$$s = \frac{(\omega - \lambda)^2}{4\omega\lambda}, \quad u = \frac{m^2 a^2}{2\omega\lambda}, \quad v = 0. \quad (15)$$

It is a matter of direct verification to prove the joining of the asymptotics (14), (15) for the value of λ_0 satisfying the inequalities $ma \ll \lambda_0 \ll \eta^{-1}$.

Now it is possible to find the total renormalized SET of nonconformal field in the radiation dominated Friedmann Universe. Let us calculate the integrals from (5) using Eqs.(7) for the counter-terms, asymptotics (14) in the interval (λ_0, ∞) and asymptotics (15) in the interval $(0, \lambda_0)$. Upon integration λ_0 is absent from the results and all the divergencies are cancelled.

The end effect of long but elementary calculations of the total vacuum energy density and pressure of nonconformal field

$$\epsilon = \langle T_0^0 \rangle_{ren}, \quad P = - \langle T_\alpha^\alpha \rangle_{ren} \quad (16)$$

(the summation in α is absent) expressed in terms of the proper synchronous time t is:

$$\epsilon = \frac{m^4}{16\pi^2} \left(\ln \frac{1}{mt} - \ln 2 - C + \frac{3}{2} \right) - \frac{m^2}{192\pi^2 t^2} -$$

$$- \frac{3}{16\pi^2} \frac{m^2}{t^2} \left(\frac{1}{6} - \xi \right) \left(\ln \frac{1}{mt} - \ln 2 - C - 1 \right) + \frac{1}{7680\pi^2 t^4},$$

$$P = - \frac{m^4}{16\pi^2} \left(\ln \frac{1}{mt} - \ln 2 - C + \frac{5}{6} \right) - \frac{m^2}{576\pi^2 t^2} -$$

$$-\frac{1}{16\pi^2} \frac{m^2}{t^2} \left(\frac{1}{6} - \xi\right) \left(\ln \frac{1}{mt} - \ln 2 - C + 1\right) + \frac{1}{4608\pi^2 t^4}. \quad (17)$$

The first two terms of both ε and P coincide with the known results for the energy density and pressure of conformal quasiparticles created from vacuum by the gravitational field. The fourth terms of ε and P which do not depend on mass describe the vacuum polarization and also are the same as for the scalar field with conformal coupling. This contribution to SET may be expressed in a generally covariant form

$$\langle T_{ik} \rangle_{ren}^{(m=0)} = \frac{1}{1440\pi^2} ({}^{(3)}H_{ik} - \frac{1}{6} {}^{(1)}H_{ik}), \quad (18)$$

where ${}^{(1)}H_{ik}$, ${}^{(3)}H_{ik}$ are the quadratic in curvature tensors [1, 4].

The third terms of (17) represent the nonlocal contributions due to nonconformal coupling of the scalar field under consideration. These contributions disappear in conformal limit $\xi \rightarrow 1/6$.

It is evident from the foregoing that the vacuum polarization for the scalar field in a radiation dominated Friedmann model does not depend on the value of the coupling constant ξ . At the same time the depending on mass contribution to the SET of nonconformal field is different for different values of ξ . Due to $mt \ll 1$, it is seen from (17) that the term proportional to $(\xi - \frac{1}{6})$ dominates the other mass dependent terms (if the value of ξ is not too near $1/6$). It is interesting also to investigate the role of vacuum quantum effects of nonconformal fields in the formation of self-consistent cosmological models [5], in multi-dimensional gravity (see, e.g., [6]) and in the applications of topological defects [7].

Two of the authors (V.B.B. and C.R.) were partially supported by CNPq.

References

- [1] A.A. Grib, S.G. Mamayev and V.M. Mostepanenko, "Vacuum Quantum Effects in Strong Fields", Friedmann Laboratory Publishing, St. Petersburg 1994.
- [2] S.M. Christensen and M.J. Duff, *Nucl. Phys.* **B154** (1979), 301.
- [3] J.S. Dowker and R. Critchley, *Phys. Rev.* **D13** (1976), 3224.
- [4] N.D. Birrell and P.C.W. Davies, "Quantum Fields in Curved Space", Cambridge Univ. Press, Cambridge 1982.
- [5] S.G. Mamayev and V.M. Mostepanenko, *Sov. Phys. — JETP (USA)* **51** (1980), 9.
- [6] S. Rippl, C. Romero and R. Tavakol, *Class. Quantum Gravity* **12** (1995), 2411.
- [7] V.B. Bezerra, *Phys. Rev.* **D35** (1989), 2031.

Computer-aided classification of the Segre types $[11(1,1)]$ and $[(11)1,1]$

Wladimir Seixas and Manoel F. Borges,

DCCE - Ibilce - Unesp

Campus de São José do Rio Preto - SP

The computer implementation of the Segre classification given by Joly and MacCallum [1] and its extended version given by Seixas [3] lacks test(s) to decide between the Segre types $[11(1,1)]$ and $[(11)1,1]$. In their paper, Joly and MacCallum suggested an improvement in order to decide between these two cases. This consists of using the fact that being Plebanski-Petrov type D, it is possible to find a transformation for the four null basis vectors such that the Plebanski tensor will be in a canonical form. The new spinor components $\Phi_{AB'}$ must be in a form where the 2-planes are aligned with the principal 2-planes of the Plebanski-Petrov tensor since they must be invariant under the same isotropy group. If not, to decide between the two cases it is necessary to find the eigenvalues and eigenvectors. In this work we intend to present some ideas for a possible approach in the direction of solving this specific problem in the classification algorithm. First we verify that if a standard form was found for the Plebanski spinor, it implies that $\Phi_{AB'}$ is in canonical form. In this way, the additional information about the transformations to bring a general form of the PP type D metric into a canonical form should be useful. We give some idea by considering two possibilities of the Plebanski-Petrov type D to show how this information can be used in terms of simplifying the tests (e.g. a fourth degree test involving $\Phi_{AB'}$ is the highest order quantity).

The Plebanski-Petrov type D possibilities are [2]:

1. **00100** χ_A is in canonical form;
2. **00111** \sim **11100** with $B_9 = 2\chi_3^2 - 3\chi_2\chi_4 = 0$;
3. **10101** with $B_5 = 9\chi_2^2 - \chi_0\chi_4 = 0$;
4. **11011** with $B_{12} = \chi_0\chi_4 + 2\chi_1\chi_3 = 0$ and $G = 2\chi_3^3 - \chi_1\chi_4^2 = 0$;
5. **11111** with $G = 2\chi_3^3 - 3\chi_2\chi_3\chi_4 + \chi_1\chi_4^2 = 0$ and $C_3 = \chi_0\chi_4^2 - 9\chi_2^2\chi_4 + 2\chi_1\chi_3\chi_4 + 6\chi_2\chi_3^2 = 0$.

We are now going to consider in detail the two first possibilities.

00100: χ_A is in canonical form, i.e. χ_2 is the only non-zero component. Then, by looking at the definitions of χ_A , $\Phi_{AB'}$ satisfies the following conditions:

$$\begin{aligned}
 \Phi_{00'}\Phi_{02'} - \Phi_{01'}^2 &= 0 \\
 \Phi_{00'}\Phi_{12'} + \Phi_{10'}\Phi_{02'} - 2\Phi_{01'}\Phi_{11'} &= 0 \\
 \Phi_{22'}\Phi_{10'} + \Phi_{12'}\Phi_{20'} - 2\Phi_{21'}\Phi_{11'} &= 0 \\
 \Phi_{22'}\Phi_{20'} - \Phi_{21'}^2 &= 0
 \end{aligned} \tag{1}$$

Let us start by assuming that $\Phi_{00'} \neq 0$. From the condition (1a) we have,

$$\Phi_{02'} = \frac{\Phi_{01'}^2}{\Phi_{00'}} \tag{2}$$

Claim: $\Phi_{01'} = 0$. In fact, if $\Phi_{01'} \neq 0$, then there exists a null rotation of class I such that,

$$\begin{aligned}\Phi'_{00'} &= \Phi_{00'} \\ \Phi'_{01'} &= \Phi_{01'} + a\Phi_{00'} = 0\end{aligned}$$

and $\chi'_0 = \chi'_1 = 0$ with χ'_2, χ'_3 and χ'_4 different from zero (i.e. we have lost the canonical form). Since,

$$\Phi'_{02'} = \frac{\Phi'^2_{01'}}{\Phi'_{00'}}$$

it will imply that $\Phi'_{01'} = \Phi'_{02'} = 0$. By the condition $\chi'_1 = 0$ (1b), it follows that $\Phi'_{00'}\Phi'_{12'} = 0$ and then $\Phi'_{12'} = 0$. In this way, $\chi'_3 = \chi'_4 = 0$ which is a contradiction. Therefore, $\Phi_{01'} = 0$ must be zero.

We have only to take into account the cases where $\Phi_{11'}$ and $\Phi_{22'}$ are zero or non-zero. The case where both are zero does not make sense since this will give all the Plebanski tensor components null.

1. $\Phi_{11'} \neq 0$ and $\Phi_{22'} = 0$. Following the tests in PP type D metrics, we have for this case that $I_6 \neq 0$ and $Q = S_i = 0, i = 1, 2, 3$ with $S_4 \neq 0$. Therefore, the Segre type is $[(11)2]$.
2. $\Phi_{11'} = 0$ and $\Phi_{22'} \neq 0$. I_6 and Q are different from zero. The sign of

$$S_7 = \frac{1}{576}\Phi_{00'}^3\Phi_{22'}^3$$

will be given by the product of $\Phi_{00'}$ and $\Phi_{22'}$. If $\Phi_{00'}\Phi_{22'} < 0$ then the Segre type is $[(11)Z\bar{Z}]$. On the other hand if $\Phi_{00'}\Phi_{22'} > 0$ although this is true for two possible Segre types, only the Segre type $[(11)1,1]$ will occur since we are in its canonical form.

3. $\Phi_{11'} \neq 0$ and $\Phi_{22'} \neq 0$. We have that,

$$\chi_2 = \frac{1}{12}(\Phi_{00'}\Phi_{22'} - 4\Phi_{11'}^2)$$

with $\Phi_{00'}\Phi_{22'} \neq 4\Phi_{11'}^2$. If $\Phi_{00'} \neq \pm\Phi_{22'}$ then there exists a transformation in class III where,

$$\begin{aligned}\Phi'_{00'} &= M^2M^{*-2}\Phi_{00'} \\ \Phi'_{01'} &= 0 \\ \Phi'_{02'} &= 0 \\ \Phi'_{11'} &= \Phi_{11'} \\ \Phi'_{12'} &= 0 \\ \Phi'_{22'} &= M^{-2}M^{*-2}\Phi_{22'}\end{aligned}$$

where M is such that $\Phi'_{00'} = \Phi'_{22'}$, and the standard form of χ_A is preserved. The canonical form for Φ'_{AB} will depend on the sign of the product $\Phi_{00'}\Phi_{22'}$. In this way, if $\Phi_{00'}\Phi_{22'} < 0$ the Segre type is $[(11)Z\bar{Z}]$ otherwise, $[(11)1,1]$.

Now assume that $\Phi_{00'} = 0$. From (1a), $\Phi_{01'} = 0$. If $\Phi_{22'} \neq 0$ we are in the case of $\Phi_{00'} \neq 0$ by swapping the index $0 \leftrightarrow 2$. So, we can assume with no loss of generality that $\Phi_{22'} = 0$. Then, by (1d) we obtain that $\Phi_{12'} = 0$. Again, the subcases to be considered are:

1. $\Phi_{02'} \neq 0$ and $\Phi_{11'} = 0$. The tests will imply, since $I_6 \neq 0$ and $Q = I_7 = 0$ with $S_2 \neq 0$ that the Segre type is $[(11)2]$.
2. $\Phi_{02'} = 0$ and $\Phi_{11'} \neq 0$. We have, $I_6 \neq 0$ and $Q = S_i = 0$ for all $i = 1, \dots, 6$. In this case, the Segre type is $[(11)(1,1)]$.
3. $\Phi_{02'} \neq 0$ and $\Phi_{11'} \neq 0$. We have that,

$$\chi_2 = \frac{1}{12}(\Phi_{02'}\Phi_{20'} - 4\Phi_{11'}^2)$$

with $\Phi_{02'}\Phi_{20'} \neq 4\Phi_{11'}^2$. The non-zero quantities are,

$$\begin{aligned} I_6 &= \frac{1}{6}(\Phi_{02'}\Phi_{20'} + 2\Phi_{11'}^2) \\ S_2 &= -\Phi_{02'}\Phi_{20'} \\ I_7 &= 48\Phi_{11'}\Phi_{02'}\Phi_{20'} \\ Q &= -\frac{1}{16}\Phi_{02'}\Phi_{20'}(\Phi_{02'}\Phi_{20'} + 8\Phi_{11'}^2) \\ S_7 &= \frac{1}{576}(\Phi_{02'}\Phi_{20'} + 8\Phi_{11'}^2)(\Phi_{02'}\Phi_{20'} - 2\Phi_{11'}^2)^2 \end{aligned}$$

The Segre type will be $[11(1,1)]$.

$00111 \sim (11100)$. This case is characterized by $\chi_0 = \chi_1 = 0$ (conditions (1a) and (1b)) and $B_9 = 2\chi_3^2 - 3\chi_2\chi_4 = 0$. If $\Phi_{00'} = 0$ from (1a) we have $\Phi_{01'} = 0$. Then,

$$\begin{aligned} \chi_2 &= \frac{1}{12}(\Phi_{02'}\Phi_{20'} - 4\Phi_{11'}^2) \\ \chi_3 &= \frac{1}{4}(\Phi_{12'}\Phi_{20'} - 2\Phi_{21'}\Phi_{11'}) \\ \chi_4 &= \frac{1}{2}(\Phi_{22'}\Phi_{20'} - \Phi_{21'}^2) \\ B_9 &= \frac{1}{8}\Phi_{20}(12\chi_2\Phi_{22'} + 4\chi_3\Phi_{12'} + 4\chi_3^*\Phi_{21'}) \end{aligned}$$

Since B_9 is equal to zero we can assume two different subcases. Firstly, if $\Phi_{02'} = 0$ we obtain,

$$\begin{aligned} \chi_2 &= -\frac{1}{3}\Phi_{11'}^2 \\ \chi_3 &= -\frac{1}{2}\Phi_{21'}\Phi_{11'} \\ \chi_4 &= -\frac{1}{2}\Phi_{21'}^2 \end{aligned}$$

and consequently, to write χ_A in a canonical form, we have to apply a null rotation of class I with

$$a = -\frac{\Phi_{21'j}}{2\Phi_{11'}}$$

$\Phi_{AB'}$ will transform as follows

$$\begin{aligned} \Phi'_{00'} &= 0 \\ \Phi'_{01'} &= 0 \end{aligned}$$

$$\begin{aligned}\Phi'_{02'} &= 0 \\ \Phi'_{11'} &= \Phi_{11'} \\ \Phi'_{12'} &= 0 \\ \Phi'_{22'} &= \frac{1}{\Phi_{11'}}(\Phi_{22'}\Phi_{11'} - \Phi_{12'}\Phi_{21'})\end{aligned}$$

If $\Phi_{22'}\Phi_{11'} - \Phi_{12'}\Phi_{21'} = 0$ ($\Phi'_{22'} = 0$) then the Segre type is $[(11)(1,1)]$. Otherwise, the Segre type is $[(11)2]$. Now, by assuming that $\Phi_{02'} \neq 0$ then

$$12\chi_2\Phi_{22'} + 4\chi_3\Phi_{12'} + 4\chi_3'\Phi_{21'} = 0$$

Since $\chi_2 \neq 0$,

$$\Phi_{22'} = -\frac{\Phi_{20'}\Phi_{12'}^2 + \Phi_{02'}\Phi_{21'}^2 - 4\Phi_{12'}\Phi_{21'}\Phi_{11'}}{\Phi_{02'}\Phi_{20'} - 4\Phi_{11'}^2}$$

The null rotation in class I will bring the χ_A in canonical form with,

$$a = -\frac{\Phi_{12'}\Phi_{20'} - 2\Phi_{21'}\Phi_{11'}}{\Phi_{20'}\Phi_{02'} - 4\Phi_{11'}^2}$$

After a straightforward calculation the Segre type will be $[(11)2]$ if $\Phi_{11'} = 0$. If $\Phi_{11'} \neq 0$ then the Segre type is $[11(1,1)]$.

Let us assume now that $\Phi_{00'} \neq 0$. From the conditions (1a) and (1b) we have,

$$\begin{aligned}\Phi_{02'} &= \frac{\Phi_{01'}^2}{\Phi_{00'}} \\ \Phi_{12'} &= \frac{\Phi_{01'}(2\Phi_{11'}\Phi_{00'} - \Phi_{10'}\Phi_{01'})}{\Phi_{00'}^2}\end{aligned}$$

and,

$$B_9 = \frac{\Phi_{10'}^2\Phi_{01'}(2\Phi_{11'}\Phi_{00'} - \Phi_{10'}\Phi_{01'})\chi_3}{\Phi_{00'}^3}$$

Looking for the cases where $B_9 = 0$ one would obtain that $\Phi_{01'} = 0$. However, it does not happen since it would imply that χ_3 and χ_4 are equal to zero. In this way, B_9 is equal to zero if and only if

$$2\Phi_{11'}\Phi_{00'} - \Phi_{10'}\Phi_{01'} = 0$$

Then,

$$\Phi_{11'} = \frac{\Phi_{10'}\Phi_{01'}}{2\Phi_{00'}}$$

The Plebanski spinor will be given by,

$$\begin{aligned}\chi_0 &= 0 \\ \chi_1 &= 0 \\ \chi_2 &= \frac{1}{12}\Phi_{00'}\Phi_{22'} \\ \chi_3 &= \frac{1}{4}\Phi_{22'}\Phi_{10'} \\ \chi_4 &= \frac{\Phi_{22'}\Phi_{10'}^2}{2\Phi_{00'}}\end{aligned}$$

The null rotation in class I to write χ_A in canonical form is given by

$$a = -\frac{\Phi_{10'}}{\Phi_{00'}}$$

$\Phi_{AB'}$ will transform as,

$$\begin{aligned}\Phi'_{00'} &= \Phi_{00'} \\ \Phi'_{01'} &= 0 \\ \Phi'_{02'} &= 0 \\ \Phi'_{11'} &= -\frac{\Phi_{01'}\Phi_{10'}}{2\Phi_{01'}} \\ \Phi'_{12'} &= 0 \\ \Phi'_{22'} &= \frac{\Phi_{10'}^2\Phi_{01'}^2 + \Phi_{00'}^3\Phi_{22'}}{\Phi_{00'}^3}\end{aligned}$$

Therefore, if $\Phi_{10'}^2\Phi_{01'}^2 + \Phi_{00'}^3\Phi_{22'} = 0$ then the Segre type is [(11)2]. If $\Phi_{10'}^2\Phi_{01'}^2 + \Phi_{00'}^3\Phi_{22'} > 0$ then [(11)1,1]. Otherwise, the Segre type is [(11)Z \bar{Z}].

As we could verify from the two examples above, a significant improvement was obtained. In addition, the conjecture raised in the beginning of this section has proved to be true. The standard form for the Plebanski spinor defined a form for the Ricci spinor where its Segre type can be decided directly. The case 00111 gave some idea about how the information on the PP type and the rotations to be performed are very useful in terms of simplifying the tests (e.g. a fourth degree test involving $\Phi_{AB'}$ is the highest order quantity). The other cases are not straightforward to solve because of the complexity of the expressions obtained after the transformation which brings χ_A into a canonical form is applied. However, it is very worth while pursuing a solution for the remaining cases and this should be done elsewhere. The results in this section were obtained by utilizing the computer algebra system MAPLE.

References

- [1] G.C. Joly and M.A.H. MacCallum. Computer-aided classification of the Ricci tensor in general relativity. *Class. Quant. Grav.*, 7:541-556, 1990.
- [2] M.A.H. MacCallum and J.E.F. Skea. SHEEP: a computer algebra system for general relativity. In M.J. Rebouças and W. L. Roque, editors, *Proceedings of the first Brazilian school on computer algebra*. Oxford University Press, 1993. To appear.
- [3] W. Seixas. Extensions to the computer-aided classification of the Ricci tensor. *Class. Quant. Grav.*, 8:1577-1585, 1991.

Chaos in Gravitational Core-Halo Systems

Werner M. Vieira and Patricio S. Letelier

Departamento de Matemática Aplicada – IMECC

Universidade Estadual de Campinas

13081-970 Campinas, SP, Brazil

e-mail: vicira@ime.unicamp.br

We analyse the motion of test particles in the intermediate vacuum of a system consisting of a massive monopolar core and a far distant halo of dust in both General Relativity and Newtonian Gravity. To this end, we extend an exact relativistic core-halo model recently proposed to take account of halo dipole, quadrupole and octopole components. We compare the orbit dynamics in the relativistic and Newtonian theories and find chaotic behavior in both when either quadrupoles or octopoles are considered, with the chaotic layers extending over larger regions of phase space in the relativistic case. If only halo dipoles are taken into account, we find that the Newtonian model is integrable while the relativistic one presents chaoticity.

The authors thank CNPq and FAPESP for financial support.

Formação de Defeitos Topológicos no Universo Primordial

Sergio E. Jorás e C.A.A. de Carvalho
Depto. Física Teórica - Instituto de Física - UFRJ[†]

1 Introdução

As transições de fase pelas quais o universo passou, e que foram usadas nos modelos inflacionários, podem dar origem a outras estruturas com importantes efeitos cosmológicos: os defeitos topológicos. Os defeitos são, basicamente, configurações de campo estáveis que apresentam energia potencial confinada; desta forma, contribuem para a formação de estruturas de larga escala [1]. Além disto, podem ter grande importância na assimetria bariônica do universo. A abordagem para o estudo dos defeitos (basicamente a mesma da inflação) concentra-se no estudo da estrutura de domínios que regiões de vácuos verdadeiros formam na transição de fase. Esta estrutura definirá a distribuição espacial dos defeitos, que determinará seus efeitos.

Se lembrarmos a definição do potencial efetivo para o campo ϕ inflacionário, verificaremos que seu argumento é, na verdade, uma média espacial do valor esperado do campo Φ em equilíbrio térmico. Ou seja, em altas temperaturas, $\phi = 0$ corresponde a um estado altamente desordenado, com o campo Φ em cada ponto raramente se aproximando do zero¹. Por isso, enquanto a temperatura decresce, o campo terá acesso aos mínimos do potencial efetivo antes que eles surjam, definindo seus domínios antes da temperatura crítica [3]. Por outro lado, mesmo que o campo Φ seja levado ao equilíbrio através da interação com um outro campo, por exemplo, é necessário mostrar que este equilíbrio será em $\Phi = 0$ e não em $\Phi \neq 0$, para que o quadro inflacionário seja gerado. Uma outra falha da abordagem padrão envolvendo a inflação é não dizer quanto tempo o campo ϕ permanece na origem, antes de começar a descer o potencial. Note que isto define a duração do período inflacionário e determina se um dado modelo gera inflação suficiente ou não.

Em outras palavras, é importante estudar a dinâmica do resfriamento do campo, tanto para verificar se um cenário inflacionário é efetivamente gerado, quanto para verificar os defeitos topológicos remanescentes. Tal estudo da transição pode impor novos limites ao tamanho mínimo necessário para se obter uma região de homogeneidade do campo Φ , ou eventualmente mostrar que esta não precisa ser imposta como condição inicial para a inflação. Pode ainda mostrar se cordas cósmicas — ou outros defeitos — são responsáveis pela atual distribuição de matéria no universo.

2 Método Perturbativo

A lagrangiana de evolução do campo ϕ é

$$\mathcal{L} = \frac{1}{2} \partial_\mu \phi \partial^\mu \phi - V(\phi, t) \quad (1)$$

onde

$$V(\phi, t) = \frac{1}{2} m^2(t) \phi^2 + \frac{\lambda}{4} \phi^4$$

*joras@if.ufrj.br, aragao@if.ufrj.br

[†]Este trabalho foi em parte financiado pela FUBA/UFRJ.

¹Para que o campo λ se encontre em equilíbrio, seria necessário que $\lambda > 0.01$ [2]

e $m^2(t) \equiv m_0^2 \left(\frac{T^2(t)}{T_c^2} - 1 \right)$.

Quer-se calcular a probabilidade de uma dada configuração $\phi_0(x, t')$ — a princípio não-uniforme — evoluir para a configuração $\phi_k(x, t'')$, que descreve um defeito (kink). Tratando o último termo do potencial acima como uma perturbação, escrevemos

$$\begin{aligned} \langle \phi_k(x, t'') | U_{tot}(\phi_k, \phi_0) | \phi_0(x, t') \rangle &= \\ &= \left\{ \exp \left[-i \int_{t'}^{t''} \frac{1}{2} m_0^2 \frac{T^2(t)}{T_c^2} \left(\frac{\delta}{\delta j} \right)^2 dx \right] \langle \phi_k | U_4^j(\phi_k, \phi_0) | \phi_0 \rangle \right\}_{j=0} \end{aligned} \quad (2)$$

onde

$$\begin{aligned} \langle \phi_k | U_4^j(\phi_k, \phi_0) | \phi_0 \rangle &= \\ &= \int_{\phi_0}^{\phi_k} [D\phi] \exp \left\{ i \int dx \left[\frac{1}{2} \partial_\mu \phi \partial^\mu \phi + \frac{1}{2} m_0^2 \phi^2 - \frac{\lambda}{4!} \phi^4 + j(x)\phi \right] \right\}. \end{aligned} \quad (3)$$

Aqui concentramo-nos no cálculo de $\langle \phi_k | U_4^j(\phi_k, \phi_0) | \phi_0 \rangle$ como uma perturbação ao oscilador harmônico invertido em presença de uma força externa. Mantendo apenas termos de primeira ordem em λ , obtemos

$$\begin{aligned} \langle \phi_k | U_4^j(\phi_k, \phi_0) | \phi_0 \rangle &= \\ &= \text{Det}^{\frac{1}{2}(\partial_\mu \partial^\mu - m_0^2)} \left\{ 1 + \frac{i\lambda}{8} \int dx \Delta^3(0, 0) + \right. \\ &+ \frac{i\lambda}{48} \frac{m_0^2}{T_c^2} \int dx \int dy T^2(y_0) [\Delta^2(x, x)\Delta(x, y) + 2\Delta^2(x, x)\Delta(y, y) + \\ &\left. + 3\Delta(x, x)\Delta^2(x, y)] \right\} \end{aligned}$$

onde $\Delta(x, y)$ é dado pela equação

$$\left(\frac{\partial^2}{\partial x^\mu \partial y_\mu} - m_0^2 \right) \Delta(x, y) = \delta(x - y) \quad (4)$$

O tratamento perturbativo para o termo dependente do tempo, porém, não é indicado, uma vez que só poderíamos nos restringir aos primeiros termos se $m_0^2 T^2(t)/T_c^2 \ll 1$. Esta condição é satisfeita quando a temperatura é bem menor que

3 Métodos Não-perturbativos

Começamos com a mesma lagrangiana, ou seja, de um oscilador harmônico de massa variável e termo ϕ^4 :

$$\mathcal{L}\{\phi\} = \frac{1}{2} \partial_\mu \phi \partial^\mu \phi - V(\phi, t) \quad (5)$$

$$V(\phi, t) = \frac{1}{2} m_0^2 \left(\frac{T(t)}{T_c} - 1 \right) \phi^2 + \frac{\lambda}{4} \phi^4 \quad (6)$$

Definimos então um novo campo

$$\sigma \equiv \sqrt{\lambda} \phi^2 \quad (7)$$

e uma nova lagrangiana

$$\mathcal{L}'\{\phi, \sigma\} \equiv \frac{1}{2} \partial_\mu \phi \partial^\mu \phi - \frac{1}{2} \sqrt{\lambda} \sigma \phi^2 + \frac{1}{4} \sigma^2 - \frac{1}{2} m_0^2 \left(\frac{T^2(t)}{T_c^2} - 1 \right) \phi^2 \quad (8)$$

de tal forma que $\mathcal{L}' = \mathcal{L}$ se substituirmos σ .

A nova lagrangiana, porém, pode ser escrita sob a forma

$$\mathcal{L}' = \frac{1}{2} \partial_\mu \phi \partial^\mu \phi + \frac{1}{4} \sigma^2 - \frac{1}{2} (m^2(t) + \sqrt{\lambda} \sigma) \phi^2 \quad (9)$$

Da mesma forma que antes, queremos calcular a probabilidade de formação de um kink ϕ_k , partindo de uma configuração ϕ_0 . Então, devemos calcular

$$\begin{aligned} \langle \phi_k | U | \phi_0 \rangle &= \\ &= \int \mathcal{D}\sigma \int \mathcal{D}\phi \exp \left[i \int \left(\frac{1}{2} \partial_\mu \phi \partial^\mu \phi + \frac{1}{4} \sigma^2 - \frac{1}{2} (m^2(t) + \sqrt{\lambda} \sigma) \phi^2 \right) dx \right] \end{aligned}$$

A integral funcional em $\mathcal{D}\phi$, acima, é exatamente a integral de um oscilador harmônico forçado com massa dependente do tempo, cuja solução é $\text{Det}^{-1/2} [\partial_\mu \partial^\mu + m^2(t) + \sqrt{\lambda} \sigma]$.

Deste modo,

$$\langle \phi_k | U | \phi_0 \rangle = \int \mathcal{D}\sigma \left\{ \exp \left[i \int \frac{1}{4} \sigma^2 dx \right] \text{Det}^{-1/2} [\partial_\mu \partial^\mu + m^2(t) + \sqrt{\lambda} \sigma] \right\} \quad (10)$$

Os próximos passos incluem completar o cálculo não-perturbativo acima usando a abordagem de Hartree-Fock.

Uma abordagem totalmente não-perturbativa pode ser feita através de instantons, soluções dependentes do tempo que tunelam de um vácuo a outro. No entanto, a dependência temporal do termo de massa torna bastante difícil a resolução analítica das equações em questão. Esta linha de trabalho está em andamento. Acreditamos que a resposta possa ser encontrada pela abordagem de catástrofes no ponto onde a solução $\phi = \phi_0$ bifurca entre uma solução onde todo o sistema está em um vácuo e outra onde a configuração do campo é de um kink.

O objetivo final do trabalho é aplicar os formalismos aqui apresentados em cordas cósmicas e outros defeitos. Neste caso, algumas quantidades de interesse seriam a proporção numérica entre cordas fechadas e cordas infinitas², a taxa de probabilidade de formação de cada tipo de corda, a distância média entre duas cordas e a distribuição espacial de cordas.

References

- [1] Robert H. Brandenberger, Invited Lectures at the 7th Swieca Summer School in Particles and Fields, Brazil, January 10-23, 1993;
- [2] Daniel Boyanovsky, Da-Shin Lee, Phys. Rev D48, 2 (1993) 800
- [3] Gene F. Mazenko, William G. Unruh, Robert M. Wald, Phys. Rev. D31, 2 (1985) 273.

²já que cada uma contribui de maneira diferente para a formação de estruturas de larga escala

O Detector de Chuveiros Atmosféricos EASCAMP-II

A.R. Biral, J.A. Chinellato, A.C. Fauth, E. Kemp, E.G.S. Luna, H. Nogima
M.A.L. de Oliveira, L.G. dos Santos, M.C. Souza Jr., F. Tessari, A. Turtelli Jr.

*Departamento de Raios Cósmicos e Cronologia
Instituto de Física 'Gleb Wataghin'
Universidade Estadual de Campinas - Unicamp
Campinas, São Paulo, Brasil.*

São apresentados o novo lay-out e a nova eletrônica do detector de chuveiros atmosféricos EASCAMP-II, instalado no campus da UNICAMP (22°54'S-47°05'W) em Campinas-SP. A ampliação em número de módulos à cintilação (de 4 para 12) e de tracejamento (2 m² para 16 m²), e a nova arquitetura da eletrônica de aquisição, resulta em sensível melhoria na resolução angular de todo o aparato, além de possibilitar estudos sobre a energia das partículas primárias. A integração no experimento de módulos de tracejamento viabiliza a reconstrução de eventos multi- μ , ampliando o intervalo de energia dos primários que pode ser investigado.

1 Introdução

No início de 1996, foi concluída a expansão física do detector de chuveiros atmosféricos (mantido pelo grupo de Léptons do DRCC-IFGW) localizado na UNICAMP^[1], que por hora será denominado EASCAMP-II. A expansão é resultado da incorporação ao detector de 8 novos módulos baseados em cintiladores plásticos (NE-102/NE-110) e fotomultiplicadoras (Philips/XP-2040), e um módulo de tracejamento de 16 m² composto por tubos *streamer*. A expansão ampliou a área nominal coberta pelo experimento de ~ 160 m² para ~ 710 m², que resultará diretamente no aumento da frequência de eventos.

Uma característica peculiar do experimento é a combinação de duas técnicas para detecção de chuveiros com vantagens complementares. A técnica de tempo de voo, com o sistema de cintiladores, tem seu melhor desempenho para eventos cujo eixo do chuveiro atinja a região próxima aos módulos detectores, onde a espessura da frente de partículas é menor e o erro causado na determinação da direção de incidência (σ_θ) devido aos efeitos da sua curvatura são minimizados. Por outro lado, nessa condição, os módulos de tracejamento não conseguem reconstruir as direções das partículas, porque quando um grande número destas atingem o detector, são introduzidas ambiguidades irremovíveis na técnica de reconstrução dos traços. O outro caso, onde o centro do chuveiro atinge regiões distantes dos módulos detectores, o erro na determinação da direção de chegada fornecida pela técnica de tempo de voo cresce (grande σ_θ). Nessa condição os módulos de tracejamento recontroem melhor a direção de chegada do evento.

Outra importante modificação, é a nova arquitetura da eletrônica de aquisição de dados. Tal modificação também é decorrência direta do aumento do número de módulos detectores do experimento, pois outras condições de disparo devem ser estabelecidas. Essa nova arquitetura minimiza efeitos provocados por *jitter* na análise do sinal vindo das fotomultiplicadoras, também contribuindo para a melhoria de σ_θ .

Nas seções seguintes discutiremos detalhes destes aspectos apresentados sobre a nova configuração do experimento.

2 O novo sistema de cintiladores plásticos

A disposição dos módulos detectores à cintilação que após a expansão compõe o experimento, é mostrada na Figura 1. Na mesma figura, para efeito de comparação, podem ser vistos os módulos operantes da antiga configuração

(denominados P1, P2, P3 e P4).

Além do aumento na área nominal coberta pelo experimento, deve-se salientar que a área efetiva (região onde caem chuviros observáveis) também foi aumentada em 2,3 vezes, atingindo $\sim 2,8 \times 10^5 \text{ m}^2$. Essa área efetiva foi obtida por simulação^[2] onde foram levados em conta a nova condição de disparo (coincidência quádrupla de sinal em quaisquer dos 12 cintiladores), a geometria com que os módulos estão dispostos e o limiar em número de partículas (~ 1 partícula/m²) no experimento. Uma consequência direta do aumento da área efetiva será a melhor estatística que deve ser alcançada na análise de dados.

O aumento no número de cintiladores também faz com que σ_θ obtido com o tempo de voo diminua em 50%, ou seja, ganha-se em um fator 2 na resolução angular, para eventos incidentes na faixa de até 45° em relação ao zênite. Esse dado também é resultante de simulações numéricas^[3] e espera-se alcançar $\sigma_\theta \sim 2^\circ$ com a nova configuração, usando a seleção de eventos ocorridos nas proximidades do aparato. A Figura 2 mostra um gráfico com o resultado da simulação, comparando o comportamento de σ_θ para os casos de 4 e 12 cintiladores.

O estudo do espectro de energia dos primários (E_0) da radiação cósmica também passa a fazer parte do escopo do experimento após a expansão. Funcionando com 12 cintiladores, pode-se tomar uma amostragem da densidade de partículas na frente do chuveiro que possibilite a obtenção (de forma indireta) de E_0 . Na configuração anterior, com apenas 4 pontos de amostragem, esse estudo não era possível por critérios meramente estatísticos.

3 O detector central e o trigger de multi- μ

Na região interna aos cintiladores foi posicionado o Detector Central^[4], composto por 4 planos de tubos *streamer* com 16 m², superpostos com 1,1 m de separação. A secção de cada célula sensível é de 3,0x3,0 cm². Essa geometria resulta em $\sigma_\theta \sim 0,5^\circ$ na reconstrução do traço da partícula. Essa boa resolução angular deve ser explorada na reconstrução da direção de chegada dos chuviros, via o tracejamento da componente carregada (em sua maioria e^\pm e μ^\pm). Esse estudo já era feito com os módulos MA e MB da Figura 1, que têm $\sim 1 \text{ m}^2$ de área sensível cada, ou seja, aumentou-se a área sensível de tracejamento em ~ 9 vezes.

Além do funcionamento integrado ao sistema de cintiladores (ver item 1), está em fase de projeto o *trigger* de multi- μ para esse detector. Esse *trigger* permitirá a detecção de grupos de μ^\pm que fazem parte de chuviros cuja componente eletromagnética já foi absorvida na atmosfera acima do detector, e conseqüentemente não disparam o sistema de cintiladores. Em geral, os μ^\pm têm distribuição angular estreita em relação ao eixo do chuveiro^[5] e preservam essa direção, assim a detecção desses eventos multi- μ possibilita o estudo de anisotropias e fontes pontuais em um intervalo de E_0 abaixo daquele em que são gerados chuviros observáveis pelos cintiladores, sendo estimado $10^{12} \leq E_0 \leq 10^{14} \text{ eV}$ para este tipo de evento.

4 A nova arquitetura da eletrônica

A Figura 3 mostra o diagrama da eletrônica de aquisição de dados. As linhas para o processamento de sinal nessa arquitetura são duas. Uma para o grupo de 4 cintiladores da antiga configuração e a outra para os 8 novos. Esse critério é por razões puramente técnicas. A diferença básica entre essas linhas, está no primeiro módulo que recebe o sinal analógico dos cintiladores. Na primeira linha, usa-se um gerador de *gate* da LeCroy mod. 4222, e na segunda o mod. 2323A. Após esses módulos todo o processamento do sinal nas duas linhas é idêntico. Estes dois módulos (4222 e 2323A), além de cumprirem sua função básica na geração de *gates*, cumprem as funções de discriminador e FanIn/FanOut, que eram anteriormente realizadas por módulos específicos para tais tarefas. Com a substituição do discriminador, reduz-se a a flutuação temporal para a digitalização do sinal (*jitter*) em até 10 vezes, que corresponde a uma redução em σ_θ de até 1,5°. O módulo FanIn/FanOut, era utilizado para derivação do sinal analógico dos cintiladores enviado aos ADC's para medidas de densidade de partículas. Esse módulo apresentava problema de saturação, que limitava o número máximo de partículas medido em cada cintilador. Valendo-nos da entrada de alta impedância desses dois geradores de *gate*, é possível utilizar o mesmo sinal, tanto no ingresso da parte lógica da eletrônica, quanto no ingresso dos ADC's.

Uma importante modificação na arquitetura de aquisição, foi a introdução da técnica de duplo-limiar. Quando o sinal analógico ingressa nos módulos 4222 e 2323A, o limiar de discriminação está ajustado para um valor mínimo (-20 mV) que elimine apenas o ruído da linha de sinal. Superado esse limiar, um pulso NIM é enviado aos ingressos dos TDC's, para medidas de tempo de voo, minimizando a flutuação temporal relativa. Uma outra saída NIM dos geradores de *gate* é conectada a um discriminador com limiar ajustado em -50 mV, que uniformiza a largura dos pulsos (em 70 ns) utilizados no ingresso da unidade lógica (LeCroy 380A) que estabelece a condição de disparo (ver item 2). Mesmo que o primeiro limiar esteja ajustado em um valor pequeno, propiciando a passagem de pulsos espúrios, estima-se que a probabilidade de disparo por coincidência casual seja da ordem de 10^{-15} .

A leitura de tempo absoluto (UT) deve ser feita por um GPS, com precisão da ordem de 10^{-3} s, conectado diretamente ao barramento ISA do micro-computador (PC) que controla a aquisição.

5 Conclusão

O detector de chuvaros atmosféricos EASCAMP-II, decorrente da expansão do antigo array localizado no campus da UNICAMP, apresenta grande melhoria em termos de resolução angular e área efetiva de detecção. Espera-se atingir $\sigma_\theta \sim 2,0^\circ$. O aumento na área efetiva com a inclusão de 8 novos cintiladores reduzirá o tempo de coleta de dados para obtenção de uma boa estatística na sua análise, e ainda, passa a ser possível a amostragem de densidade de partículas na frente dos chuvaros, necessária para estudos do espectro de primários. A utilização do módulo central de traçamento para a detecção de eventos multi- μ possibilitará estudos de anisotropias e busca de fontes, com a inclusão de duas décadas de magnitude na energia dos primários observados (agora $E_0 \geq 10^{12}$ eV) e uma melhor estabilidade na aquisição de dados.

6 Referências

1. - A.R. Biral et al., Proceedings from 24th. International Cosmic Rays Conference (Roma-Itália), HE Session, Vol. 1, 450 (1995).
2. - A.I. da Silva, A.C. Fauth, Relatório de Instrumentação para o Ensino, IFGW-UNICAMP, (1996).
3. - A.R. Biral et al., Nota Interna / Grupo de Léptons-DRCC-IFGW-UNICAMP, (1995).
4. - A.R. Biral et al., Proceedings from 24th. International Cosmic Rays Conference (Roma-Itália), HE Session, Vol. 1, 994 (1995).
5. - S. Hayakawa, Cosmic Rays Physics, J. Wiley & Sons, U.S.A., (1969)

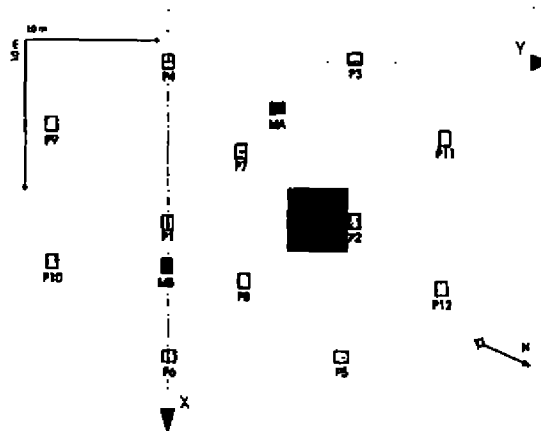


Figura 1: Disposição dos módulos detectores do EASCAMP-II. P1 (i=1,2,...,12) designa os módulos cintiladores; MA e MB e DC são os módulos de traçamento de 1 m² e 16 m² respectivamente.

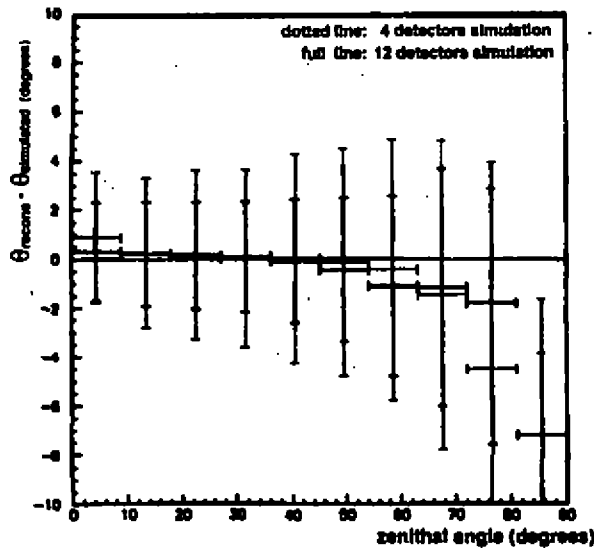


Figura 2: Diferença ente o ângulo zenital reconstruído (após flutuações nos tempos de disparo dos cintiladores) e o ângulo zenital original gerado pela simulação, para diversas faixas de ângulo zenital.

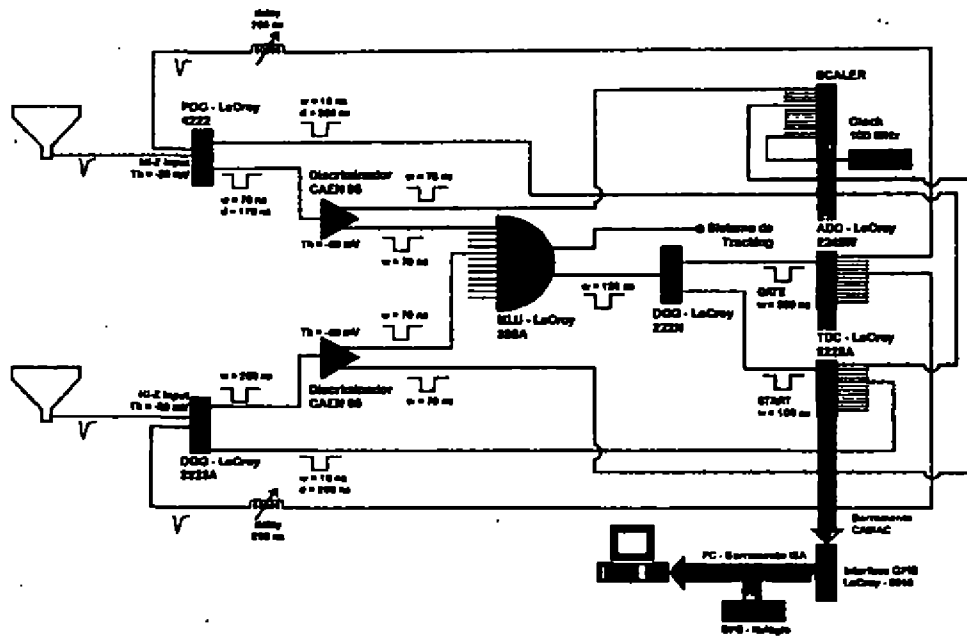


Figura 3: Diagrama da eletrônica de aquisição de dados do EASCAMP-II.

Performance of Resistive Plate Counters with Ar/Bu/CCl₂F₂ and Ar/Iso/CBrF₃

A. Campos Fauth, A. Guidi*

Departamento de Raios Cósmicos e Cronologia

Instituto de Física 'Gleb Wataghin'

Universidade Estadual de Campinas - Unicamp

Campinas, São Paulo, Brasil

**) Scholarship FAPESP*

The performance of a glass electrode resistive plate counter (RPC) has been studied as a function of high voltage and two gas mixtures. We present the time and charge results obtained with: Ar/Bu/CCl₂F₂ and Ar/Iso/CBrF₃. The detector demonstrated adequate to be used in extensive air shower experiments to measure the arrival time and particle tracking.

1 Introduction

Particle detectors with a time resolution smaller than 1 ns and that allow tracking measurements are often required in high energy physics.

The RPC (Resistive Plate Counter) is a gaseous detector which enables tracking measurements and can achieve a time resolution of 25 ps under some special conditions[1]. To obtain this performance the gas is maintained at high pressure and the gap between the electrodes is very small (≤ 1 mm).

We study the performance of a simple version of these detectors, made of commercially available materials and maintained at atmospheric pressure. We expect to achieve a time resolution of 1 ns.

The uncritical working conditions and low cost of this detector are interesting in apparatus for extensive air showers, where large detection areas are involved.

2 The Resistive Plate Counter

Figure 1 shows a scheme of a resistive plate counter studied. It is constituted of two parallel plane electrodes made of glass with volume resistivity $\rho = 10^{12} \Omega.cm$. These electrodes are 2 mm thick and the 2 mm gap between them is ensured by PVC spacers. A water based graphite painting is applied in the external surface of each electrode, in order to provide electrical connection. In usual working conditions a high voltage between 5 and 8 kV is applied. The electrodes are enclosed in a PVC box, which interior is filled with a gaseous mixture. We studied the detector performance using two different mixtures, Ar/Bu/CCl₂F₂ - 68,7/29,3/2 and Ar/Iso/CBrF₃ - 60,8/34,1/5,1 [2].

When a charged particle crosses the active region of the detector, the ionization of a gas molecule will occur. An electron resulting of this process may cause the ionization of another molecule and so on, in such a way that an avalanche of ions and electrons is formed between the electrodes[3]. Because of their high resistivity, this discharge does not propagate throughout the whole detector, being limited to an area smaller than 10 mm².

The transparency of the electrodes to transient signals[4] allows the avalanche to induce a pulse on an external pick up pad. These pads are made of copper and are 100 cm long, 8 cm wide. They are placed on each side of the PVC box so that both the positive and negative signals can be read. If orthogonal strips are used instead of pads, a good spatial resolution is achieved.

3 Experimental Setup

Two resistive plate counters were assembled and placed one 3,5 cm above the other. Their electrodes were connected to two HV sources (0-6kV) with inverted polarities. In this way it is possible to obtain up to 12 kV of potential difference in the gap.

The readout electronics scheme is shown in Figure 2. The analog induced signal from each detector goes first to a Dual Gate Generator Le Croy 2323A. The input threshold is set at 20 mV. The logic unit CAEN N18A was programmed to produce three output signals: two for each single detector signal and one for the temporal coincidence (100ns) between them. This last signal goes to the start of the TDC 2228A Le Croy, used to measure the time difference between the two detectors. The resulting curve is a distribution centered at the time spent from a relativistic particle to cross the separation distance of the two RPCs. An ADC Le Croy 2249A is used to study the charge spectrum of each RPC. A Scaler 2551 Le Croy is used to make the singles counting rate curve of the detectors and also the counting rate curve of the coincidence.

4 Results

The data acquisition trigger selects principally cosmic ray muons with angles from 0 to 88 degrees. This muons are minimum ionization particles crossing different points on the two RPCs, so the time distribution of the signal from RPCs is a sum of the detector time resolution, pad fluctuations due the interaction position, and electronic (discriminator, TDC) jitters. Figure 3 shows this total time resolution as function of the high voltage. The singles counting rate curve for the mixture Ar/Bu/CCl₂F₂ has a plateau 700 V wide (see Figure 4). The counting rate starts increasing due to the transition from the avalanche to the spark mode. The plateau is reached when this transition is completed. At this region the detector is working at the spark mode and every signal is related to the passage of an ionizing particle. After this, the rate starts increasing again because of the presence of spurious signals. It is important to notice that the rate of 40 Hz where the singles counting rate plateau lies is the one estimated for a detector of this size at an ordinary cosmic ray flux, so that its efficiency must be near 100%. A total time resolution smaller than 6 ns was obtained, for an applied voltage of 6500 V.

The singles counting rate curve presented no plateau for the Ar/Iso/CBrF₃ gas mixture. The reason may be the high percentage of Freon13B1 of this mixture, since this gas is very electronegative. The total time resolution is lying around 9 ns.

The charge spectrum is similar for both mixtures showing some after pulses due to secondary avalanches induced by the primary discharge.

5 Conclusions

Two resistive plate counters were assembled with transparent electrodes. The data acquisition system was mounted and tested. We studied the performance of the RPCs for two gas mixtures Ar/Bu/CCl₂F₂ and Ar/Iso/CBrF₃ as a function of high voltage. The first one is good for time of flight measurements on extensive air shower experiments. The other one is too unstable. Both mixtures are improper for calorimetric measurements because of the afterpulses their charge spectrums present.

A time resolution smaller than 6 ns was obtained for the first mixture. We used 100 x 8 cm² pads as readout electrodes. If the pads are replaced by strips and with selection of vertical muons we expect the time resolution drops down to 1 ns. We are now taking the first data with 2,5 cm wide strips instead of the pads. The detector is well suited for large area underground experiments, where a time-of-flight system can be used to discriminate upward, or downward going muons. The presence of afterpulses in both mixtures requires a careful analysis if an analog measurement is desired. Its design and the materials used permit a large production at low cost.

Acknowledgments - We are grateful to G. Bencivenni, F. Tessari, H. Nogima and J. Botasso for their collaboration on prototype realization. The authors are also grateful to FAPESP, CNPq and FAEP for support this research laboratory.

References

1. - Yu. N. Pestov, Nucl. Instr. and Meth. 265 (1988) 150-156.
2. - Produced by White-Martins Brazil, calibration standard.
3. - F. Sauli, Principles of Operation of Multiwire Proportional and Drift Chambers, CERN 77-09, May 1977.
4. - G. Battistoni et al., Nucl. Instr. and Meth. 202 (1982) 459-464.

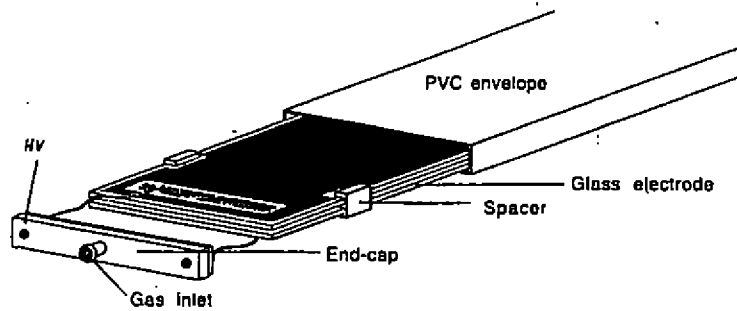


Figure 1: Sketch of a RPC module.

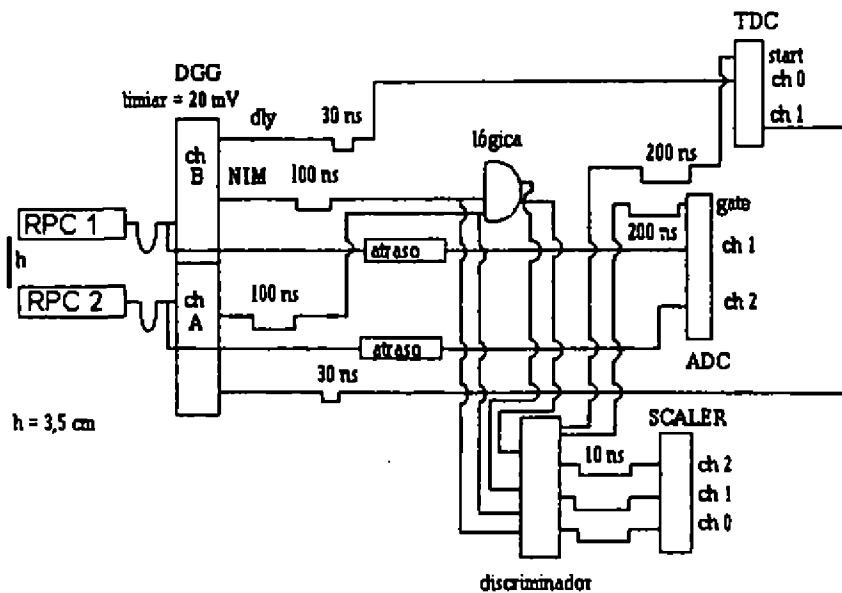


Figure 2: Block diagram of experimental arrangement.

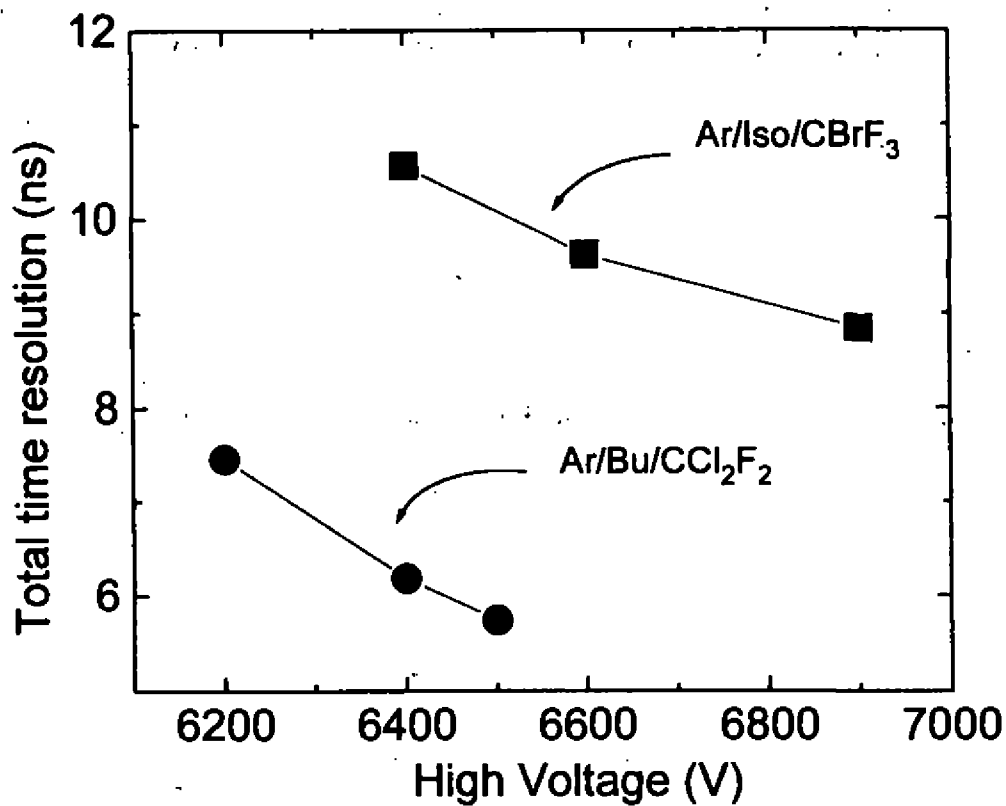


Figure 3. Total time resolution vs. operating voltage.

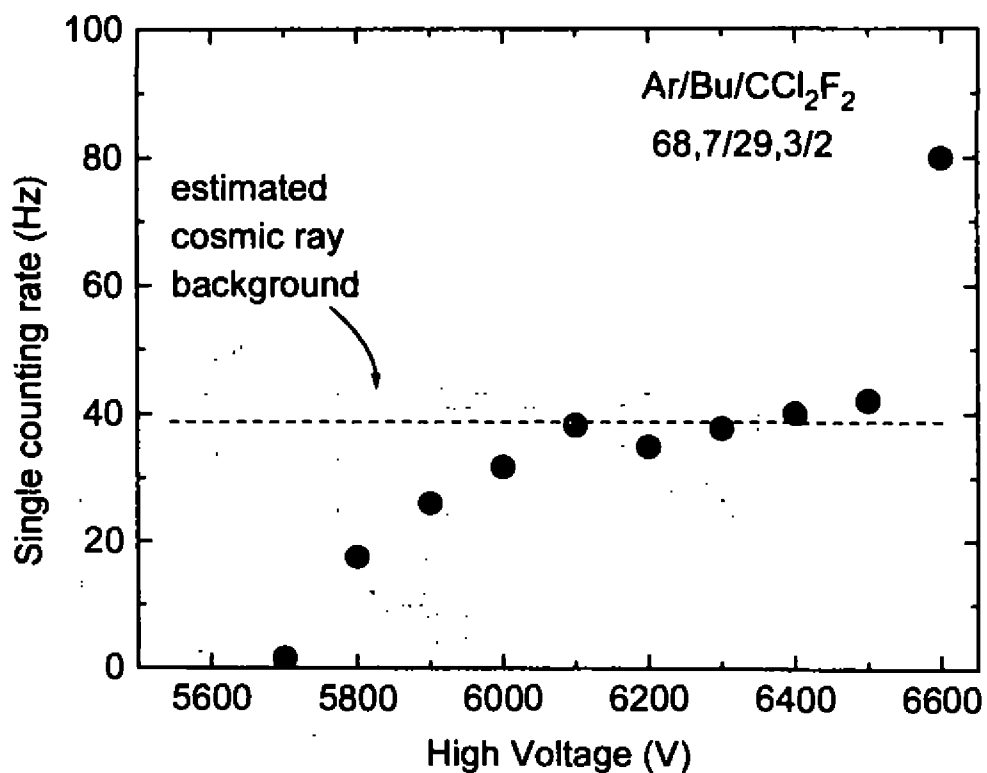


Figure 4. Single counting rate for Ar/Bu/CCl₂F₂ and cosmic ray expected counting rate.

Estimate of the Arrival Direction of Primary Particles Inducing Air Showers, From Data Obtained by the Top Cluster in the KASCADE Experiment

Carola Dobrigkeit*

*Departamento de Raios Cósmicos e Cronologia
Instituto de Física Gleb Wataghin-UNICAMP
13083-970 Campinas SP*

The intention of this work is to obtain an estimate of the incidence directions of primary particles inducing air showers, from the relative differences in arrival times of their secondaries registered by a detector array. In particular, the algebraic procedure developed here is destined to reconstruct the direction of showers detected by the top cluster in the KASCADE experiment [Ref.1].

In order to verify the goodness of the reconstruction, the method is applied to simulated events incident on the top cluster and the directions so obtained are compared with the known directions of incidence of the primary particle inducing each shower. The analysis of the relative angles between primary incidence directions and reconstructed directions shows that the procedure is perfectly adequate for a good reconstruction of events detected by the top cluster.

The method of reconstruction has also been applied to events measured by the same detector array, and the results compared to those obtained by a least-square fit of a plane to the shower front. With only a few exceptions, the directions obtained by algebraic reconstruction and by least-square fit agree within approximately 1° , on the average.

Proposition

The cosmic ray experiment KASCADE (KARlsruhe Shower Core and Array DETector) consists of an extensive air shower detector built in the Forschungszentrum Karlsruhe, Germany, 110 m above sea level [Ref.1]. Its main proposition is to measure various observable quantities for high-energy showers in the atmosphere, induced by cosmic-ray particles, in order to determine the chemical composition of primary cosmic radiation at energies above 10^{14} eV. On the top of the KASCADE central detector a small array consisting of 32 scintillation counters (0.45 m² each) has been installed [Ref.2]. This top cluster is able to measure the energy deposit of the electromagnetic component in the detectors and also the arrival times of secondary shower particles at the detectors, improving the reconstruction of high-energy showers, particularly in those cases when the shower center hits the central detector area. For lower energy showers, the reconstruction must be based only on measurements from the top cluster, due to the low density of particles in the KASCADE array.

From the arrival times of the particles impinging on the detectors, an estimate of the shower front can be obtained, and the incidence direction of the shower (assumed coincident with that from the primary particle) can be evaluated (Figure 1). Admitting that the shower front can be considered approximately plane, which is certainly a fairly good hypothesis for those showers detected by the top cluster because of its reduced dimensions, an algebraic algorithm can be used to obtain from the arrival times the estimated primary direction.

*E-mail : carola@ififi.unicamp.br

Method

Starting from the assumption of having an air shower incident on a detector array consisting of N detector stations, with known coordinates $\mathbf{r}_i = (x_i, y_i, z_i)$ and known arrival times of the first particle at each station, t_i , we look for the director cosines $\mathbf{n} = (n_x, n_y, n_z)$ of the vector normal to the plane passing through the N_{coin} responding detectors at corresponding times:

$$\mathbf{n} \cdot \mathbf{r}_i + k = ct_i \quad \text{with} \quad \mathbf{n} \cdot \mathbf{n} = 1 \quad \text{and} \quad n_z \geq 0 \quad (1)$$

where c is the assumed incidence velocity of the shower front, equal to the velocity of light (~ 30 cm/ns). This procedure is analogous to that applied in [Ref.3] for a small array of four detectors.

In principle, all station coordinates and corresponding registered times should satisfy Eq.(1). This situation corresponds to a system of N_{coin} linear equations involving four unknown variables, n_x , n_y , n_z and k , but not all independent, since $\mathbf{n} \cdot \mathbf{n} = 1$. The minimum N_{coin} for which a unique solution of this system is possible is, therefore, three, and for greater values the system is overdetermined. In the latter cases a solution is still possible, imposing Gauss's condition of minimum total distance from all points to the plane:

$$\sum_{i=1}^{N_{coin}} (\mathbf{n} \cdot \mathbf{r}_i + k - ct_i)^2 = Q = \text{minimum} \quad (2)$$

Differentiating partially Eq. (2) relative to the unknowns n_x , n_y , n_z and k , and using the additional normalization condition for \mathbf{n} , a system of four linear equations is obtained, which can be solved in the usual way. In the particular case of the top cluster array in the experiment KASCADE, all detector stations have the same z_i , which may be arbitrarily set as zero. In this way the system can be reduced to the trivial case of three unknown quantities and the fourth one, n_z , may be then obtained from the normalization condition of \mathbf{n} .

Since we are also interested in obtaining information about the goodness-of-fit, it is possible to evaluate Q from Eq.(2), obtaining an estimate for the χ^2 for each event and the corresponding confidence level. In the present case this means:

$$\chi^2 = \sum_{i=1}^{N_{coin}} (\mathbf{n} \cdot \mathbf{r}_i + k - ct_i)^2 / c^2 \sigma_i^2$$

where each σ_i describes the dispersion in the value of the arrival time t_i . As dispersion we must include the experimental error in time measurements and that derived from the natural thickness of the shower front (approximately 1m measured on the shower axis), also responsible for spreading arrival times.

The associated number of degrees of freedom is naturally $N_{coin} - 3$, since we have only three *independent* unknown quantities between n_x , n_y , n_z and k .

From the considerations above and the usual assumptions [Ref.5], the confidence level can be obtained for each event, knowing χ^2 and the number of degrees of freedom. In all cases with $N_{coin} > 3$ the confidence level can be used as an indicator in the case of having no possible solution for the direction. Since its value varies between 0 and 1, having no solution can be made to correspond to a confidence level outside this interval, say -2. Also in the case $N_{coin} = 3$, for which the number of degrees of freedom is zero and the confidence level is not even defined, this trick can be applied, attributing another value outside the interval mentioned for the case with a solution, let us say, -1.

Results

The algebraic procedure exposed above was applied to reconstruct the direction of the axis of 31900 simulated showers and also to 12219 real showers detected by the top cluster.

1) Simulated showers

The showers were supposed to be initiated by a proton, whose energy was sampled from a power spectrum, in the range between $5 \cdot 10^{12}$ and 10^{14} , and whose angles were sampled from an isotropic distribution. The CORSIKA

code [Ref.6] was used, including VENUS as the model for high-energy proton-air interactions, GEISHA for those interactions at energies below, and EGS for the simulation of the resulting electromagnetic cascades. The shower axis is located inside a square 30 m on the side around the top cluster. In order to imitate the effect of experimental errors in time measurements, simulated times were folded with a Gaussian distribution ($\sigma_{exp} \approx 1ns$) and the resulting arrival times were used for reconstruction.

An important aspect for the correct interpretation of the measured arrival times must be kept in mind. For calculations of χ^2 's, the actual dispersion in arrival times σ_t has to be known. This σ_t , here assumed the same for each station, includes, on the one hand, the natural dispersion $\sigma_{thick} \approx 2.6ns$ in the shower front (its thickness) and, on the other, the experimental error mentioned above. In this way the total dispersion can be estimated to be $\sigma_t \approx 2.8ns$. This assumed value is crucial, not only for the χ^2 values here obtained, but also for the resulting confidence levels.

The simulated air showers were analyzed and all events with the minimum of three detectors responding were reconstructed applying the algebraic procedure exposed above. In this "first" attempt of reconstruction all times of the responding stations were considered. As already mentioned, there are cases for which no reconstruction is possible, simply because no direction can be found that reproduces the arrival times of those events. For each event the procedure is repeated excluding one or two stations whenever possible and the combination with best confidence level is chosen as the "best" estimated direction. All possible combinations of minus-one-station and minus-two-stations are compared. In this way, it is practically always possible to obtain an estimate of the direction, since there is only one five-station event impossible to be reconstructed after excluding one station.

In the analysis of the reconstructed directions it is necessary to distinguish between showers in which only a small number of stations was hit and those with a large number of stations responding, typically more than ten.

When only three or four stations were hit, no station can be excluded. The mean angles between reconstructed and primary direction for the events effectively reconstructed is rather large, 15° and 11° , respectively.

In the cases of five to seven stations hit, it is possible to exclude one (five stations) and one or two stations (six/seven stations), but doing so does not improve for sure the resolution. In these cases an advantage of excluding one or two stations is the possibility to obtain an estimate for the direction in those cases for which no first solution was initially possible.

When comparing the angular resolution obtained in those cases where eight to eleven stations were hit, it is interesting to observe that, as expected, excluding stations results in greatest improvement for those showers which initially presented a lower confidence level, say with their first confidence level between 0 and 0.7. Generally speaking, those events with first confidence level greater than 0.7 obviously are the cases for which an already good resolution is attained *ab initio*, and to exclude a station only makes things worse. Table 1 below resumes the mean angular resolutions obtained for those cases, separated by intervals of first confidence levels. From Tab.1 it is possible to deduce that resolution can be improved by approximately 2° when excluding one or two stations, for those showers with $9 \leq N_{stat} \leq 11$ and first confidence level below 0.7. In the same interval of confidence level, exclusion makes angular resolution better by ca. 1.4° , even when only eight stations were hit. As in the previous case, to exclude one/two stations also opens the possibility to estimate directions of those showers that previously did not admit any solution.

For those showers in which 12 or more stations were hit, it is practically always an advantage to try a better resolution through the exclusion of one or two stations. It is easy to observe that, for those events that already had a high first confidence level, the exclusion brings an improvement of $0.1^\circ \sim 0.3^\circ$. Again for those showers with first confidence level below 0.7 or without any first solution, the exclusion of one or two stations improves the resolution in circa 2.3° to 3° . As an example, Figures 2a and 2b show the angular resolutions for showers with 16 stations hit and with the first confidence level below 0.7, before and after excluding one or more stations, respectively. The improvement in the angular resolution by 2, on the average, is easily seen, as in Figures 3a and 3b, which include the 7640 showers where more than 8 stations were hit and considering the same interval for the first confidence level.

Number of stations	Number of events	Mean angles (degrees) (conf.lev.>2)		Number of events	Mean angles (degrees) (-2<conf.lev<0.7)		Number of events	Mean angles (degrees) (conf.lev.>0.7)	
		α_{first}	α_{best}		α_{first}	α_{best}		α_{first}	α_{best}
N_{stat}	#	α_{first}	α_{best}	#	α_{first}	α_{best}	#	α_{first}	α_{best}
8	3518	5.3	4.9	1767	7.1	5.7	1751	3.4	4.1
9	3554	4.9	4.2	1753	6.7	4.7	1801	3.2	3.9
10	3355	4.4	3.5	1624	6.0	3.9	1731	3.0	3.1
11	2929	4.1	3.2	1352	5.6	3.5	1577	2.8	2.9
12	2451	3.9	2.8	1062	5.5	3.1	1389	2.7	2.6
13	1978	3.7	2.6	827	5.2	2.9	1151	2.7	2.4
14	1471	3.3	2.4	519	4.8	2.6	952	2.5	2.3
15	1080	3.1	2.2	334	4.9	2.4	746	2.3	2.1
16	874	2.6	1.9	169	5.2	2.2	705	2.0	1.8

2) Measured showers

The algebraic procedure developed above was also applied to 12219 showers measured at the top cluster, where at least one particle was detected by one edge station.

These showers were measured and analyzed in [Ref.2]. Therein the reconstructed shower directions were obtained by another procedure [Ref.7], involving a numerical least-square fit, making possible a comparison between the results of both methods. For this reason all criteria used here are coincident with those in [Ref.2]. As in the case of simulated events, it is necessary to estimate the actual dispersion in the arrival times σ_t , in order to estimate the confidence levels. Following the same procedure as before, a rough estimate for σ_t , results to be ~ 3 ns. For those events with more than six stations responding, the comparison between the directions here obtained (without excluding any station) and those in [Ref.2] revealed a mean relative angle of 1.4° . Since our procedure gives the possibility to distinguish those cases without solution, these showers can be excluded from the previous comparison, decreasing the relative angle to 1.1° , as shown in Fig. 4.

Conclusions

As a rule of thumb, if up to seven stations respond, no exclusion is recommended, except in those cases where no direction can be estimated *ab initio*. If more than seven stations were hit, there is an advantage to exclude detectors if the first confidence level is lower than 0.7 or in the cases where no algebraic estimate was possible. But it must be kept in mind that this interval of confidence level is strongly dependent of the value of $\sigma_t \approx 2.8$ ns taken for calculating the χ^2 , and therefore, the confidence level. The complete analysis and results can be seen in [Ref.8].

Acknowledgments

This analysis resulted from a three-month stay at the Forschungszentrum Karlsruhe during 1996. I thank to FAPESP for the financial support for this stay, CNPq for a research scholarship during the last years and FAEP/UNICAMP for a technical support. I want to thank Prof. Dr. Gerd Schatz for his kind invitation and support during the stay in Karlsruhe and Prof. Dr. Heinigerd Rebel for proposing the theme of this work and stimulating discussions. Finally I want to express my gratitude to the whole group of experiment KASCADE, for their friendship and warm reception during the cold winter in Karlsruhe.

References

1. P. Doll et al., KfK-Report 4686, Kernforschungszentrum Karlsruhe, 1990.
2. R.Haesler, Diplomarbeit, Universität Karlsruhe und Forschungszentrum Karlsruhe, March 1996.

3. O. Schöps, KfK-Report 5263B, Kernforschungszentrum Karlsruhe, 1993
4. Bronstein, Semendjajew, Musiol and Mühlig, Taschenbuch der Mathematik, Verlag Harry Deutsch, 1995, pg. 182
5. Review of Particle Properties, Phys. Rev. D50, (1994)1173, pg 1276.
6. J.N. Capdevielle et al., KfK-Report 4998, Kernforschungszentrum Karlsruhe, 1992 and references therein.
7. H. J. Mayer, Nucl. Instr. and Meth. A311 (1992) 327
8. C. Dobrigkeit, FZK-Interner Bericht 51.02.03-Z13C, Forschungszentrum Karlsruhe, 1996

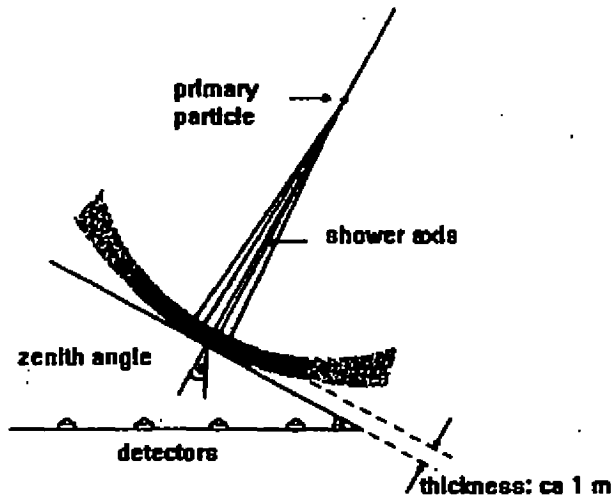


Figure 1. Schematic representation of a shower front [Ref.2]

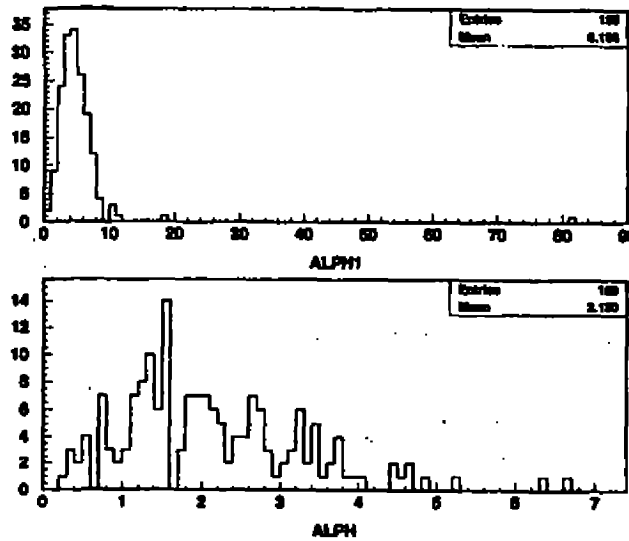


Figure 2a (top) and 2b(bottom)

Angular resolution between reconstructed and primary directions, for showers with sixteen stations hit, without and with exclusion of one/two stations, respectively

Teste e Calibração de Componentes para a Torre de Destilação do detetor *Barrel RICH* do DELPHI

Danielle Magalhães Moares

Instituto de Física, Universidade Federal do Rio de Janeiro

O DELPHI (*DEtector with Lepton, Photon and Hadron Identification*) é um dos quatro detetores presentes no colisor de e^-e^+ LEP, do CERN. Ele é composto por diversos subdetetores, classificados como: detetores de traço, contadores de luz Čerenkov, calorímetros, câmaras de muons e cintiladores.

1 O Detetor de Luz Čerenkov

O RICH (*Ring Imaging Čerenkov*) é um detetor de luz Čerenkov otimizado para a identificação de $\pi/K/p$ numa faixa de momentos abaixo de $40\text{GeV}/c$, que cobre quase todo o ângulo sólido.

Este sistema é proporcionado por dois detetores, um localizado na região da tampa, referido como Forward RICH (FRICH), e outro de geometria cilíndrica situado na região do barril. Este último é designado *Barrel RICH* (BRICH). O BRICH abrange um ângulo polar de $40^\circ < \Theta < 140^\circ$ e o FRICH de $15^\circ < \Theta < 35^\circ$ e $145^\circ < \Theta < 165^\circ$.

1.1 Descrição Técnica do *Barrel RICH*

O *Barrel RICH* (BRICH) consiste de um cilindro oco de $3,50\text{ m}$ de comprimento com um $\phi_{\text{interno}} = 246\text{ cm}$ e $\phi_{\text{externo}} = 394\text{ cm}$, dividido em duas metades por uma parede central ($Z > 0$, $Z < 0$).

Cada metade (Figura 1) é composta por 24 setores contendo um radiador líquido (LRAD) e uma câmara de deriva seguida de um radiador gasoso (GRAD) e um conjunto de espelhos. Num total de 48 radiadores líquidos de volume igual à 240 l , um radiador gasoso de 24 m^3 , 288 espelhos e 48 detetores de fótons de UV de 1200 l , com 12288 canais de aquisição eletrônica. As MWPC são formadas por 128 fios anódico de 20μ , separados de 2.62 mm e 16 tiras catódicas de 5 mm . Estas câmaras operam num ganho de 2×10^5 para cada elétron e contêm paredes de blindagem (com campos acelerativos) entre os fios, afim de reduzir o ponto de detecção da carga (Figura 2). Este detetor opera à temperatura de 40°C e a pressão constante de 1030 hPa .

1.2 Princípios Gerais de Operação

- o A identificação de partículas é baseada na detecção de cones de luz Čerenkov produzidos nos dois meios.
- o O gás Čerenkov preenche todo o espaço disponível no detetor. Espelhos focalizadores, localizados na parte mais externa do detetor, refletem os fótons na direção da câmara de projeção temporal (Figura 1).
- o Os radiadores líquidos consistem em uma camada de 1 cm de perfluorhexano (C_6F_{14}) de baixo índice de refração ($1,273$) e o lado oposto à região de interação, é composto por uma janela de quartzo com uma transparência no UV. Estes radiadores são utilizados para separação de $\pi/K/p$ acima de $\approx 4,5\text{ GeV}$ e para separação de K/p acima de 6 GeV .
- o As partículas mais rápidas são identificadas pela emissão de luz nos radiadores gasosos, que são preenchidos por perfluorpentano (C_5F_{12}).
- o Perfluorcarbonetos foram escolhidos como meio radiador, pois combinam um índice de refração apropriado com uma boa transparência para comprimentos de onda abaixo de 165 nm . E ainda são não inflamáveis e não tóxicos. Algumas das propriedades destes fluidos estão descritas na Tabela 1.

	Ponto de Ebulição (°C)	M_{mol} (g)	ρ à 25°C (g/cm ³)	n à 7 eV	Θ_{max} (mrad)
C_4F_{10}	-2	238	1.594	1.00153	55.6
C_5F_{12}	28	288	1.604	1.00178	59.1
C_6F_{14}	57	338	1.682	1.283	677.1

Table 1: Propriedades Físicas dos fluorcarbonos. O valor da densidade do C_4F_{10} corresponde ao ponto de ebulição

2 Torre de Destilação

Durante o período de *run* de 1994, a presença de vazamentos dentro do BRICH levou à mistura entre os fluorcarbonos usados como meio radiador. Juntamente com isto, aumentou o risco de condensação ou aquecimento, bem como, a variação do índice de refração. Por isto, os sistemas de radiadores do BRICH requerem uma separação *online* dos dois líquidos C_5F_{12} e C_6F_{14} utilizados como meio radiador.

A Torre de Destilação foi conectada nos dois sistemas de radiadores de maneira tal que o líquido contaminado que retorna dos radiadores seja coletado num tanque misturador e injetado na coluna. A capacidade da Torre é de 150 - 200 Kg/h e espera-se uma pureza na separação dos produtos melhor que 95%.

2.1 Descrição Geral

A Torre tem um comprimento total de 7,7m e está localizada entre o nível 2 e nível 4 do aparato DELPHI. Os componentes principais são: uma coluna de 5,5m de comprimento e 100mm de diâmetro, um boiler com potência de aquecimento de 12KW e um condensador com potência de resfriamento estimada em 6.8KW à 28°C (ponto de ebulição do C_5F_{12}).

2.2 Operação

- ▷ A coluna tem apenas uma entrada e opera a pressão absoluta constante.
- ▷ O C_5F_{12} é extraído do condensador a uma temperatura de aproximadamente 25°C e bombeado para o tanque principal do GRAD (Figura 3).
- ▷ O C_6F_{14} é removido do boiler à temperatura de aproximadamente 55°C, resfriado até 20°C e então inserido no tanque principal do LRAD (Figura 3).
- ▷ A Torre é alimentada por uma mistura numa taxa e composição estáveis. Para que a pureza exigida seja atingida, são necessários 14 estágios teóricos de separação (método McCabe-Thiele¹).
- ▷ Os gases não condensáveis (principalmente N_2), que são diluídos nos fluorcarbonos, estão saturados de C_5F_{12} e C_6F_{14} à temperatura do condensador. Para recuperar estes fluorcarbonos o vapor de pressão é transferido para a bomba do GRAD fazendo com que o gás passe pelo separador criogênico do sistema do GRAD.

2.3 Monitoração

Todas as quantidades importantes da Torre são monitoradas por um sistema de processamento de controle *Siemens Simatic*. As seguintes quantidades tem que ser monitoradas:

- fluxo e temperatura da água fria;
- temperatura da torre de destilação, incluindo o boiler e o condensador (aproximadamente 10 sensores);
- pressão absoluta do boiler, do topo da coluna e ao longo da coluna (alta precisão);
- nível de líquido no boiler e no tanque misturador;

¹McCabe and Thiele, Ind. Eng. Chem., 17, 605 (1925).

- fluxo e temperatura de entrada e saída da coluna.

O trabalho resultante da preparação e calibração de todas as peças utilizadas neste monitoramento segue adiante.

2.3.1 Medidores de Fluxo

Para monitorar o balanço de massa ao longo da torre, 3 medidores de fluxo foram instalados. Estes medidores precisam ser calibrados já que uma medida muito precisa do fluxo é requerida. Eles são conhecidos como *rotameter* e consistem em um tubo graduado com diâmetro interno crescente e uma bóia no interior. Inicialmente os medidores existentes mediam um fluxo de até 90 l/h, o que era insuficiente. As especificações do projeto exigiam dois medidores de 120 l/h e um de 25 l/h. Para que isto fosse atingido foi necessário estudar as forças atuantes na bóia tais como, o empuxo (1), a força de fricção (2) e a gravidade (3), para que novas bóias fossem construídas.

$$E = v_L \times \eta \times A_{livre}^{-1} \quad (1)$$

$$F = m_b \times g - v_b \times \rho_l \cdot g \quad (2)$$

$$G = m_b \times g \quad (3)$$

onde v_b \equiv velocidade da bóia, v_L \equiv velocidade do líquido, ρ \equiv densidade específica, η \equiv viscosidade e A_{livre} \equiv área livre.

Utilizando um esquema experimental que representa as ramificações da torre de destilação, e conhecendo a dependência da velocidade do líquido com a área livre (4), foi possível redimensionar as bóias e obter a calibração requerida para os medidores de fluxo.

$$v_L = \frac{\phi}{\pi(r_t^2 - r_b^2)} \quad (4)$$

2.3.2 Sondas de Temperatura

Outros parâmetros importantes a serem monitorados são a temperatura ao longo da coluna, incluindo o boiler e o condensador. Este objetivo será alcançado através de sondas conhecidas como PT100.

O PT100 consiste em uma resistência de platina de 100 Ω à 0°C e com $\frac{\Delta R}{\Delta T} \approx 0.4\Omega/K$.

Apesar de estarem conectados de maneira a compensar a resistência dos cabos, eles precisam ser calibrados pois possuem uma incerteza de $\pm 0.5^\circ C$. Para esta calibração, foram comparados com um termômetro de mercúrio num banho à temperatura entre 25°C e 41°C.

2.3.3 Sistema de Regulagem de Pressão

A Torre de Destilação tem que ser equipada com um sistema de regulagem de pressão passivo que opera independente do sistema de controle, assim como, independente de força elétrica. Este aparato é constituído de duas válvulas de regulagem de pressão mecânicas², uma que injeta nitrogênio na coluna se a pressão for menor que um limiar (tipo FRS) e a outra que abre (tipo FRU), permitindo a retirada de líquido da coluna, se a pressão exceder o limite.

Estas válvulas podem ser reguladas de maneira a estabelecer a pressão exata de abertura ou vedação. Isto foi obtido estudando-se todo o mecanismo destas válvulas e das suas conexões. As válvulas foram reguladas para uma pressão relativa mínima de 130 mbar e máxima de 180 mbar (Figura 4).

²DUNGS technic - Druckregelgerät typ FRS, typ FRU Korrespondenzanschrift - Karl Dungs GmbH & Co. Postfach 12 29 D-73602 Schorndorf

2.4 Performance

Os testes dos componentes para a **Torre de Destilação** foram realizados durante os meses de janeiro e fevereiro de 1996 no CERN. A torre foi conectada no sistema do *Barrel RICH* em maio de 1996 e está em pleno funcionamento, como a seguinte performance:

- A taxa de extração do boiler (C_6F_{14}) é igual a 40 ± 10 l/h.
- A taxa de extração do condensador (C_5F_{12}) é igual a 10 ± 5 l/h.
- A mistura enviada para a torre é composta por 24,4% de C_5F_{12} e 75,25% de C_6F_{14} .
- O fluorcarbono extraído do boiler e enviado para o LRAD contém 96,68% de C_6F_{14} e 3,23% de C_5F_{12} .
- A pressão ao longo da torre é mantida constante utilizando-se as válvulas de regulagem de pressão, como demonstra a Figura 5.
- O fluorcarbono extraído do condensador e enviado para o GRAD é formado por 0,05% de C_6F_{14} e 98,39% de C_5F_{12} .

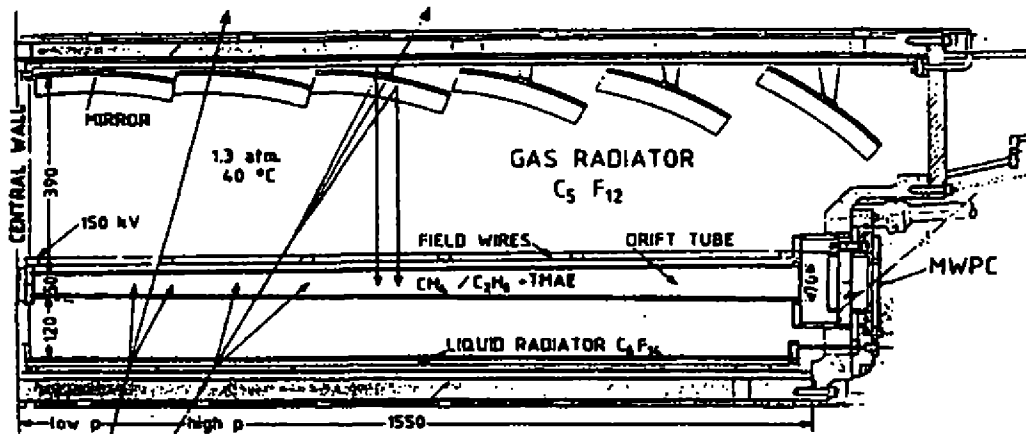


Figure 1: Seção longitudinal do detector *Barrel RICH*.

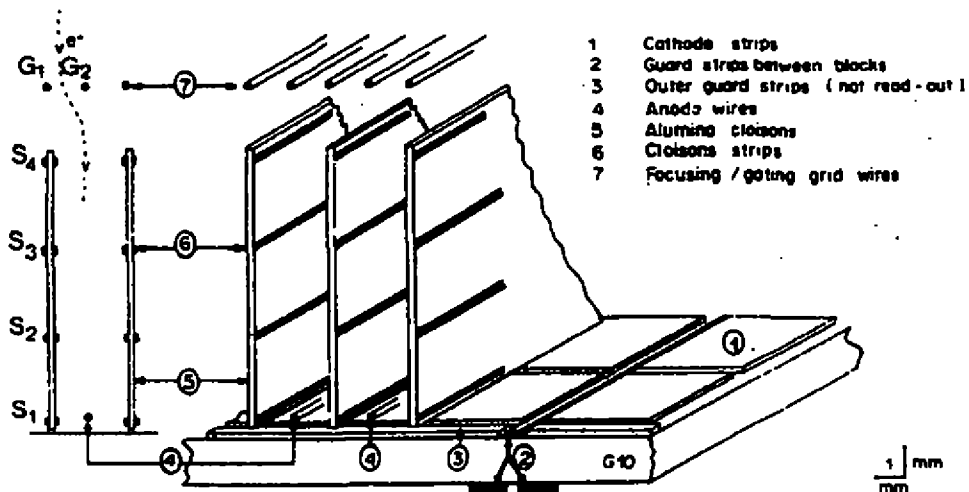
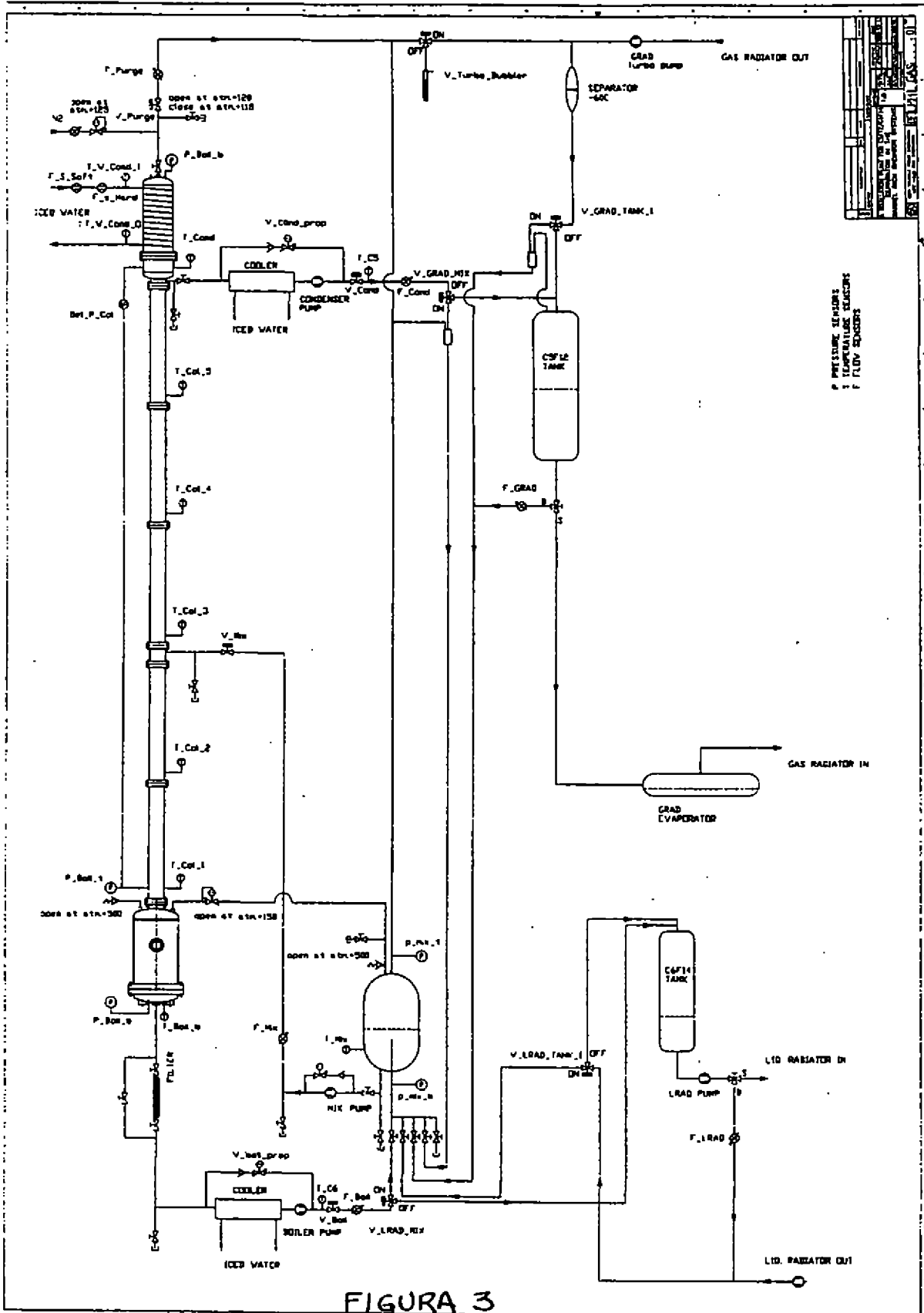


Figure 2: Detalhamento da MWPC do detector *Barrel RICH*.



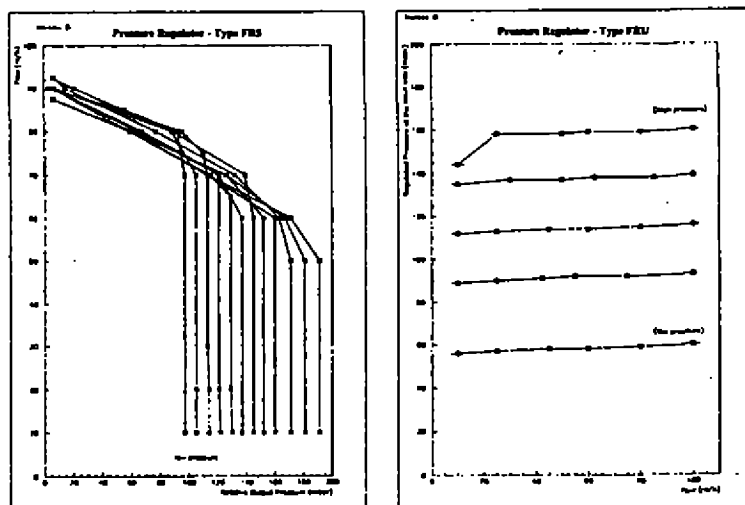


Figure 4: Calibração das válvulas de regulação de pressão mecânicas.

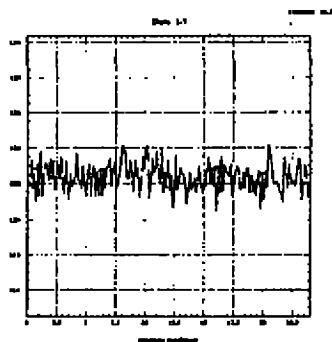


Figure 5: Pressão da coluna medida no condensador em relação à pressão atmosférica (escala em mbar).

Cascatas Hadrônicas Iniciadas Por Um Único Núcleo

H.M.Portella, A.S.Gomes, R.H.C.Maldonado, A.L.V.Silva, A.M.M.Lima, E.M.Fernades
Instituto de Física/UFF - Niterói - RJ

Neusa Amato

Centro Brasileiro de Pesquisas Físicas-CBPF/CNPq - Rio de Janeiro - RJ

As equações de difusão dos hadrons são resolvidas analiticamente considerando que esses chuviros atmosféricos são originados por um único núcleo (p, α , CNO, Ca, Mn e Fe). As distribuições de elasticidade dos hadrons na atmosfera foram consideradas uniformes.

1 Cascata iniciada por um nucleon

1.1 Equação de difusão dos nucleons na atmosfera

A difusão dos nucleons na atmosfera é descrita pela seguinte equação:

$$\frac{\partial F_N(x, x_0, E, E_0)}{\partial x} = -\frac{F_N(x, x_0, E, E_0)}{\lambda_N} + \int_0^1 F_N(x, x_0, E/\eta, E_0) f_{NN}(\eta) \frac{d\eta}{\eta}$$

Que está sujeita a seguinte condição de contorno:

$$F_N(x = x_0, E, E_0) = \delta(E - E_0)$$

onde:

$f_{NN}(\eta)$ = distribuição de elasticidade dos nucleons na atmosfera,

λ_N = livre percurso médio dos nucleons na atmosfera,

x_0 = ponto de origem da cascata,

E_0 = energia do nucleon incidente.

Usando uma distribuição uniforme para $f_{NN}(\eta)$ e $\lambda_N = \text{cte.}$ solução da equação acima é [1]:

$$F_N(x, x_0, E, E_0) = e^{-(x-x_0)/\lambda_N} \left[\delta(E - E_0) + \frac{2(x-x_0)}{Z\lambda_N} I_1(Z) \right]$$

com:

$$Z = 2\sqrt{\frac{(x-x_0)}{\lambda_N} \ln(E_0/E)}$$

e $I_1(Z)$ = função de Bessel modificada de primeira espécie

1.2 Equação de difusão dos pions na atmosfera

A difusão dos pions na atmosfera é descrita pela equação diferencial:

$$\frac{\partial F_\pi(x, x_0, E, E_0)}{\partial x} = -\frac{F_\pi(x, x_0, E, E_0)}{\lambda_\pi} + \int_0^1 \frac{F_\pi(x, x_0, E/\eta, E_0)}{\lambda_\pi} f_{\pi\pi}(\eta) \frac{d\eta}{\eta} +$$

$$+ \int_E^{E_0} \frac{f_{N\pi}(E', E_0)}{\lambda_\pi} F_N(x, x_0, E', E_0) dE'$$

com:

$$F_\pi(x = x_0, E, E_0) = 0$$

onde:

λ_π = livre percurso médio dos pions na atmosfera,

$f_{N\pi}(E', E_0)$ = distribuição de energia dos pions secundários originados na interação nucleon-núcleo do ar.

Usando uma distribuição de elasticidade uniforme para os pions nós obtivemos a solução [2]:

$$F_\pi(x, x_0, E, E_0) = \frac{1}{1 - \frac{\lambda_N}{\lambda_\pi}} f_{\pi N}(E, E_0) (e^{-(x-x_0)/\lambda_\pi} - e^{-(x-x_0)/\lambda_N}) + \int_{x_0}^x \frac{T(t)}{E_0} \frac{e^{-T(t)}}{\lambda_N} dt \int_E^{E_0} f_{N\pi}(E', E_0) \frac{2}{u_\pi} I_1(u_\pi) dE'$$

onde:

$$u_\pi = 2\sqrt{T(t)\ln(E_0/E')}$$

$$T(t) = \frac{x-t}{\lambda_\pi} + \frac{t-x_0}{\lambda_N}$$

1.3 Fluxo integral de hadrons

Com o objetivo de compararmos nossos resultados com o espectro integral de hadrons de algumas superfamílias ($\Sigma E_h^\gamma > 1000$ TeV) detetadas em Chacaltaya devemos somar os fluxos dos nucleons obtidos na seção 1.1 com os dos pions da seção 1.2 e integrarmos desde $E_{min}(E_h^\gamma)$ até E_0 .

$$F_h(\geq E, E_0, x, x_0) = \int_{E_{min}}^{E_0} (F_N(x, x_0, E', E_0) + F_\pi(x, x_0, E', E_0))$$

2 Cascata iniciada por um único núcleo

2.1 Equação de difusão dos nucleons na atmosfera

A difusão dos nucleons na atmosfera provenientes de uma cascata iniciada por um núcleo é descrita pela seguinte equação:

$$\frac{\partial F_N(x, x_0, E, E_0)}{\partial x} = \frac{-F_N(x, x_0, E, E_0)}{\lambda_N} + \int_0^1 \frac{F_N(x, x_0, E, E_0)}{\lambda_N} f_{NN}(\eta) \frac{d\eta}{\eta} + \sum_{j>1} \int_E^{E_0} \frac{F_j(E', E_0, x, x_0)}{\lambda_j} f_{j1}(E', E) dE'$$

onde:

$f_{j1}(E', E)$ = probabilidade de um núcleo j se fragmentar no nucleon,

λ_j = livre percurso médio do núcleo j na atmosfera.

j	1	2	3	4	5
núcleo	proton	α	CNO	Ca, Mn	Fe

Considerando uma distribuição de elasticidade dos núcleons na atmosfera uniforme e um livre percurso médio dos diferentes núcleos, constantes, nós obtivemos a seguinte solução:

$$F_N(x, x_0, E, E_0) = \sum_{j>1} \frac{1}{1 - \frac{\lambda_j}{\lambda_N}} f_{j1}(E, E_N) (e^{-(x-x_0)/\lambda_N} - e^{-(x-x_0)/\lambda_j}) +$$

$$+ \int_{x_0}^x \sum_j \frac{T(w)e^{-T(w)}}{\lambda_j} dw \int_E^{E_0} f_{j1}(E', E) \frac{2}{E_0 Z_j} I_1(Z_j)$$

onde:

$$Z_j = 2\sqrt{T(w)\ln(E_0/E')}$$

$$T(w) = \frac{x-w}{\lambda_N} + \frac{w-x_0}{\lambda_j}$$

Os núcleos da radiação cósmica primária são agrupados de acordo com a tabela acima:

2.2 Equação de difusão dos pions na atmosfera

A difusão dos pions na atmosfera segue a seguinte equação diferencial:

$$\frac{\partial F_\pi(x, x_0, E, E_0)}{\partial x} = -\frac{F_\pi(x, x_0, E, E_0)}{\lambda_\pi} + \int_0^1 \frac{F_\pi(x, x_0, E/\eta, E_0)}{\lambda_\pi} f_{\pi\pi}(\eta) \frac{d\eta}{\eta} +$$

$$+ \sum_{j=1}^3 \int_E^{E_0} \frac{F_j(x, x_0, E', E_0)}{\lambda_j} f_{j\pi}(E, E') dE'$$

Cuja solução é a seguinte:

$$F_\pi(x, x_0, E, E_0) = \sum_{j=1}^3 \frac{1}{1 - \frac{\lambda_j}{\lambda_\pi}} f_{j\pi}(E, E_0) (e^{-(x-x_0)/\lambda_\pi} - e^{-(x-x_0)/\lambda_j}) +$$

$$\sum_{j=1}^3 \int_{x_0}^x \frac{T'(t)e^{-T'(t)}}{\lambda_j} dt \int_E^{E_0} f_{j\pi}(E', E) \frac{2}{E_0 Z_\pi} I_1(Z_\pi)$$

onde:

$$Z_\pi = 2\sqrt{T'(t)\ln(E'/E)} \quad e \quad T'(t) = \frac{x-t}{\lambda_\pi} + \frac{t-x_0}{\lambda_j}$$

Referências

- [1] - N. Arata e F. M. Oliveira Castro, Revista Brasileira de Física, 18 (1988) 261
- [2] - J. Bellandi et al., Phys. Rev. D 50 (1994) 6836

Production of Sinner Layer of Si-Tracker 1996 DELPHI 96-38 MVX 12

E. Polycarpo*

UFRJ, Instituto de Física, Rio de Janeiro, Brasil

I. Stavitski

Dipartimento di Fisica, Università di Padova and INFN, Padova, Italy

1 Introduction

The DELPHI silicon microvertex detector is being upgraded for 1996. To improve the forward coverage there will be two layers of pixel detectors and two planes of ministrips detectors [1] on each side of it. In the barrel region the Outer and Inner layers will have their lengths increased and the Closer, which was already a longer layer, will remain unchanged. To avoid confusion with the old detector, the layers of the new Si-tracker are called Scloser, Souter and Sinner. The aim of this note is to fully describe the process of production of Sinner modules. In the second section the layer itself is described, the third gives an overview of the assembly and the fourth explains the test procedures. Finally, the fifth section makes a summary of the results obtained.

2 The Sinner Layer

The intermediate layer of 1996 Delphi Si-tracker lies at a radius of between 89.5 and 93.5 mm and covers the θ angle from approximately 21 to 159 degrees. It is composed of twenty overlapping modules, each one 55.47 cm long and made of four single sided and four double sided plaquettes of microstrip detectors, making a total of 160 silicon detectors for the whole layer. The double sided plaquettes, which are taken in pairs from the previous VD'94-95, have on the p-side 1280 diodes with 25 μm pitch and a readout pitch of 50 μm , providing R- ϕ coordinate in DELPHI. On the n-side the strips are read out with a second metal layer, providing R-z coordinate in DELPHI. The plaquette closest to the hybrid has a readout pitch of 84 μm with no multiplexing, while the furthest is multiplexed into two compartments with a readout pitch of 42 μm . A full description of them can be found in [2]. The single sided plaquettes are the same as those used in the new Souter layer [4] and have only p-side R- ϕ readout strips, similar to the one described above.

3 Assembly

The first step of module construction consists of separating an Outer'95 module, taking it apart into two Sinner quarter modules, each with one hybrid and two flipped double sided plaquettes of silicon. The hybrid provides all the necessary voltages and supports 10 MX6 readout chips with 1280 channels in total. The flipped module design is well detailed in [2], while the features of the MX6 can be found in [3]. A preliminary test is done and if it is necessary the module is repaired. For the second step a pair of single sided detectors, previously glued and bonded together, is glued to the quarter module and has the readout lines bonded. Two half modules are tested once more and glued together by means of a composed kevlar-carbon-fiber rail, which provides mechanical firmness. So the assembling of the full Sinner module is done. Then it is surveyed on a special optico-mechanical setup¹ to prepare a 3-dimensional data base for each plaquettes with precision of 2 μm in the strips plane and 15 μm in the direction orthogonal to this plane. An automatic search for dead strips is done and they are ready to be mounted. Figure ??

*This work was partially supported by the European community, contract number C11-CT94-0118.

¹POLI S.p.a., Varallo Sesia, Italy and Mondo Machine Development Ltd., Leicester, UK

gives a global idea of the whole process. The steps described are carried out at CERN, apart from the gluing and bonding of the single sided pair, which is carried out at Padova and Cracow. The final product consists of two electrically isolated half modules. The different sides of the module are named top (corresponding to the first 640 channels) and bottom (corresponding to the last 640 channels) (fig.1). Top channels are connected to two plaquettes with p+n strips in chain and bottom channels to four plaquettes with n+p+p+p strips in chain.

4 Test Procedure

The test setup consists of a black box where the detector, which is sensitive to light, will be housed and connected by means of a motherboard to the supply voltages, timing signals and to the data acquisition system based on CAMAC standard (see diagram 2). The readout is done using a flash ADC SIROCCO connected to an oscilloscope and a Macintosh. At each stage two kinds of analysis are done. A preliminary inspection with the oscilloscope can quickly reveal noisy regions associated to defects (locally in the working group nicknamed pinholes and Fujis) which need to be treated. After this a more quantitative evaluation is performed on the Macintosh.

4.1 Pinholes and Fujis

Figure 3 shows a schematic illustration of a readout line connected to four plaquettes. In the first plaquette there is a n-strip connected to 60 V and on the other side a p-strip is around 3 V. The second plaquette is flipped and the biasing voltages are opposite to the first. The two last detectors are single sided. All the metal readout lines lie at approximately 3 V. A pinhole is a breakdown in the coupling capacitance between the diode and the metal line. If it is created on the p-side it is possible to regulate the p-bias voltage in order to minimize the potential difference between the readout line and the strip. On the other hand, if it is created on the n-side the potential difference of about 60 V will produce a current flow to the electronics and usually this current will be spread over the neighbouring strips. To prevent current inside electronics this strip must have its bond wire removed. A similar problem that can be solved by removing the bond wire of the affected channel is called Fuji. In this case, a short is created through the bulk of the silicon between the n-side and a p-side diode, connecting the p-strip to 60 V and producing a potential difference that cannot be regulated. The coupling capacitor on the p-diode quickly breaks down, causing a current flow into the readout chips. This can occur in both single or double sided detectors. It creates in the pedestal distributions a region with volcanic shape, the origin of its name, affecting up to 40 neighbouring channels. Fujis and n-side pinholes are some of the major sources of noise. The presence of these defects also corresponds to unbalanced currents on the sides of the plaquettes. Figure 4 shows the shape of Fuji on the fourth chip of a half module.

Removing the bond wire from the affected channel normally reduces the current unbalance and avoids both noise or pedestals saturation. Actually this strip becomes dead, but not really invisible because the charge from a m.i.p. will not be lost but distributed over neighbours due to the interstrip capacitance.

4.2 Qualitative Test - Oscilloscope

This test is done looking at the pedestal distributions on the scope for all 1280 channels. At this time the state of the module is qualitatively evaluated. It's possible to check if there is any short on it, if the chips are working well and to look for pinholes and Fujis. Very noisy regions are at this point repaired (if it is possible), often removing n-pinholes and p-side Fujis.

4.3 Quantitative Test - Macintosh/HP

After being qualitatively evaluated and accepted the module has the signal over noise ratio (S/N) calculated and an analysis of bad strips made. The test consists of measuring pedestals and noise with a FORTRAN program that reads the data file from the computer. The program makes the pedestals and noise plots for each side of the module. To be accepted as a good strip the channel must satisfy the following criteria :

- Pedestals: The channel must lie within the dynamic range of the ADC. Those with too high or too low pedestals are rejected.
- Noise: The noise of the channel must be such that the S/N for a m.i.p. does not fall below 3. This value provides a cut in the specification of levels used in the data acquisition and cluster reconstruction algorithm (reference [2]). Channels with too high noise after common mode subtraction are rejected. Also channels

with too low noise, either before or after common mode subtraction, are rejected because this indicates a dead channel. This test serves as an estimation of the quality of the module.

The total number of bad strips is the sum of the strips that are rejected at least in one of the categories above. Figure 5 shows the plots mentioned for the module which had the Fuji repaired. It is possible to see a difference between the mean values of the noise on different sides of the detector, coming from the extra capacitive load of the readout lines of the extra plaquettes connected on the bottom side. Also the percentage of channels failing each cut is shown.

4.4 Dead Strips Search

To have more reliable information about the percentage of dead channels a special test was performed on this final step. This is done by placing the module in a setup with red LEDs illuminating separately each plaquette. Every normal strip saturates, but the dead strips do not. Thus dead channels can easily be found. In the first plaquette strips saturate up on the top side and down on the bottom side. In the next plaquette they saturate down on the top side and up on the other. The two last only saturate up on the bottom side. The visual check of interrupted channels was in precise agreement with this test. The existence of a dead strip in the center of a cluster of strips responding to the passage of a m.i.p. can result in the reconstruction of two separate clusters at the wrong positions. Using a database of dead strips it is possible to repair these clusters and recuperate the correct cluster position.

For the 95 detector the dead strips were found by directly searching in the data, but for runs after 1996 we don't expect enough tracks to extract this information more clear.

5 Results of the tests

The results obtained for Sinner layer modules are summarized in figures 6 to 8. The first plot (figure 6) gives the percentage of channels outside the limits imposed by the pedestals and noise cuts for each module. Figure 7 gives the percentage of dead channels in each plaquette, according to the test with the LEDs. Each point in the vertical line is related to a different module and each vertical line corresponds to a different plaquette. The first line corresponds to the plaquette closest to the hybrid. To measure the signal over noise ratio for the final modules, an Am241 source, which deposits 60 keV in the silicon, was used. The signal and the noise for each side of the detector are illustrated on figure 8. The source was placed on the first plaquette, hence the signals are positive on the top side and negative on the bottom side. This represents a S/N for a minimum ionizing particle, that deposits 84 keV in the silicon, of 14. and 13.3 for the top and bottom sides, respectively.

6 Conclusions

Twenty sinner modules have been fully tested up to now. The addition of the pair of single sided detectors on the bottom side has not brought a significant increase of noise. This could be expected because the noise is dominated by the n-side of the detectors and due to the second metal layer that produces a more significant capacitive load in the input amplifiers. The average percentage of bad channels is 5 % and of dead channels is 4 %. These numbers are comparable to the last year and show that the complex assembly of this layer has not had a detrimental effect.

7 Acknowledgments

The work described represents the efforts of many people in the VD group. We would like to thank all them and to express our gratitude to P. Collins, H. Dijkstra, M. Gandelman, Y. Michalowski and A. Nomerotski for their many contributions to our work at CERN.

References

- [1] M. Krammer, "The construction of the DELPHI Very Forward ministrip detector." DELPHI 96-11 MVX11, 12 February, 1996
- [2] V. Chabaud *et al.*, "The DELPHI Silicon Strip Microvertex Detector with Double Sided Readout." CERN-PPE/95-86, 14 June, 1995. NIM A 368 (1996) 314-332
- [3] I. Stanton and N. Kurtz, "An Introduction to MX chip", RAL-89-028
- [4] P. Collins, Experience with Silicon Detectors at the DELPHI Experiment, LEP. DELPHI 95-173 MVX8, 1 December, 1995

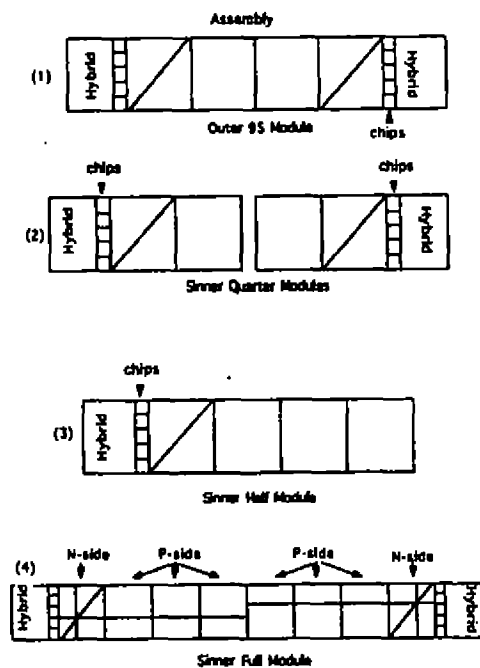


Figure 1: Assembly steps for Sinner module production. The Outer 95 module (1) is first separated to make two Sinner quarter modules (2). A half module (3) is made by gluing and bonding them to a pair of single sided plaquettes. Finally the half modules are joined to make a full Sinner module (4) consisting of two electrically isolated halves.

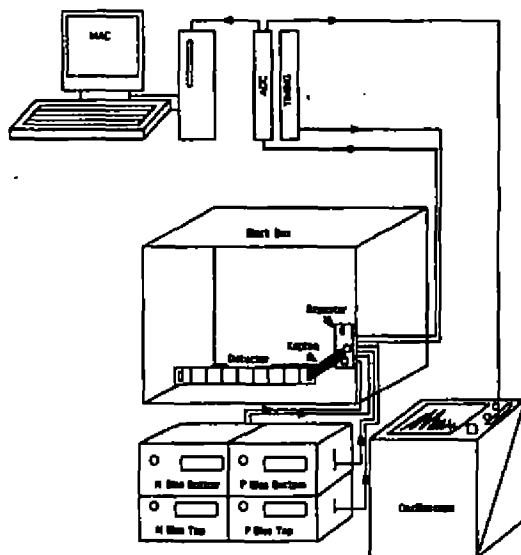


Figure 2: An schematic illustration of the test setup.

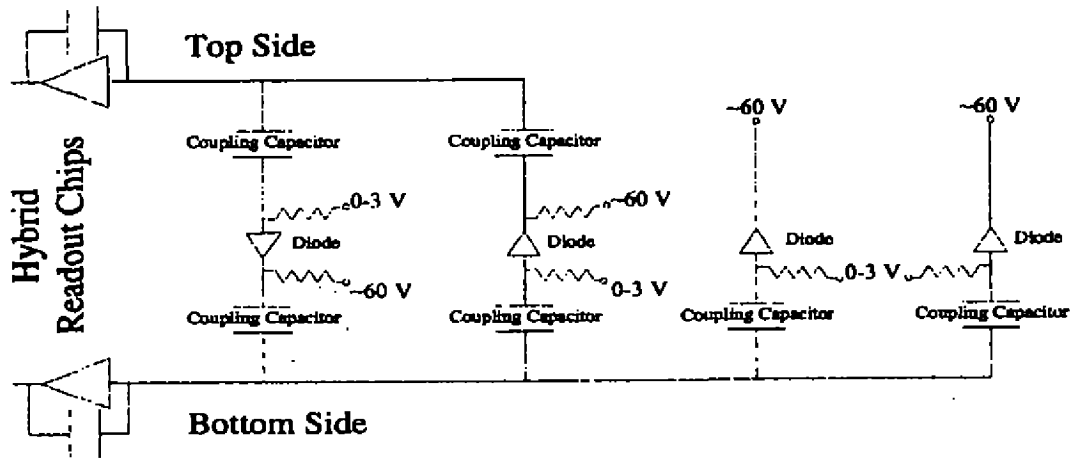


Figure 3: Schematic view of the connection read-out lines and the detector regarding only two strips on the top and bottom sides. A top read-out connects to two plaquettes while bottom one connects to all four plaquettes.

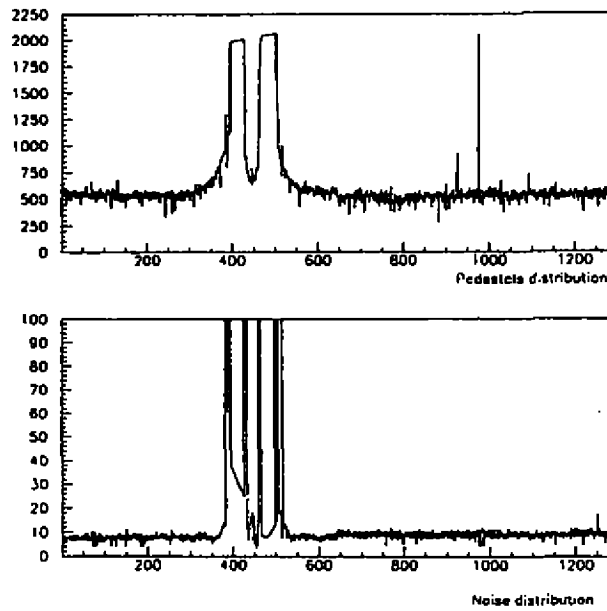


Figure 4: The volcanic shape of a Fuji. The symmetry makes it possible to find the strip that must be disconnected to the readout. A very noisy region associated to the region of saturated pedestals can be seen.

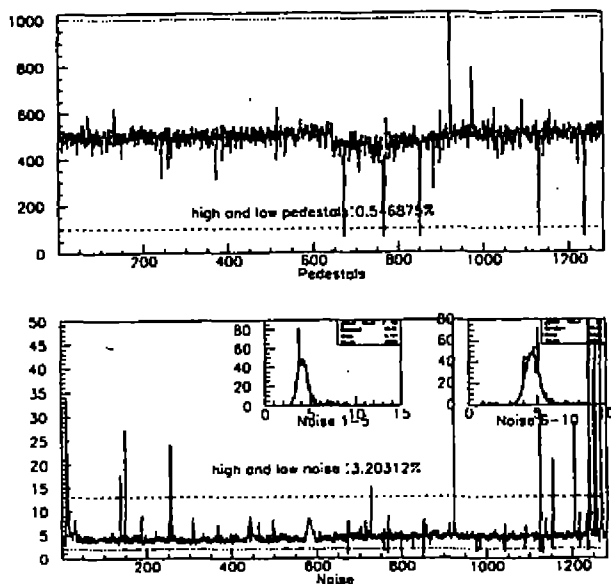


Figure 5: The pedestal (upper plot) and noise (lower plot) distributions of a completed full module after removal of the Fuji shown in figure 4. The plots show the noise for each side of the detector. There is an increase of 10 % for the noise on the bottom side. The percentage of channels falling outside the pedestals and noise cuts are shown. The total percentage of bad channels is 3.8 .

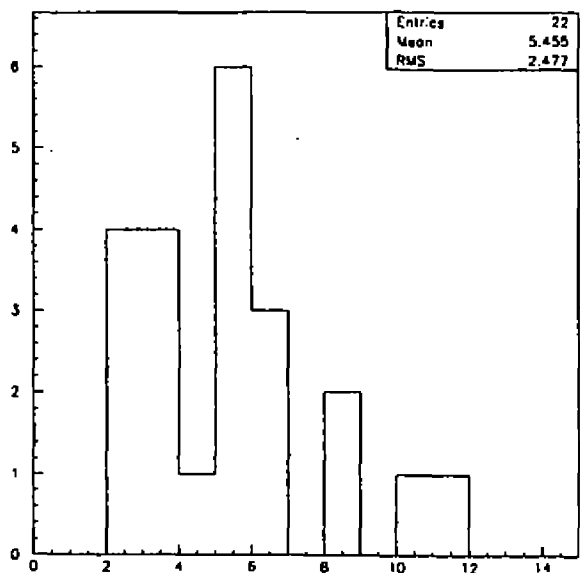


Figure 6: The percentage of bad strips for each full module, including the number of channels outside the dynamic range of the SIROCCO, the noisy and the dead channels.

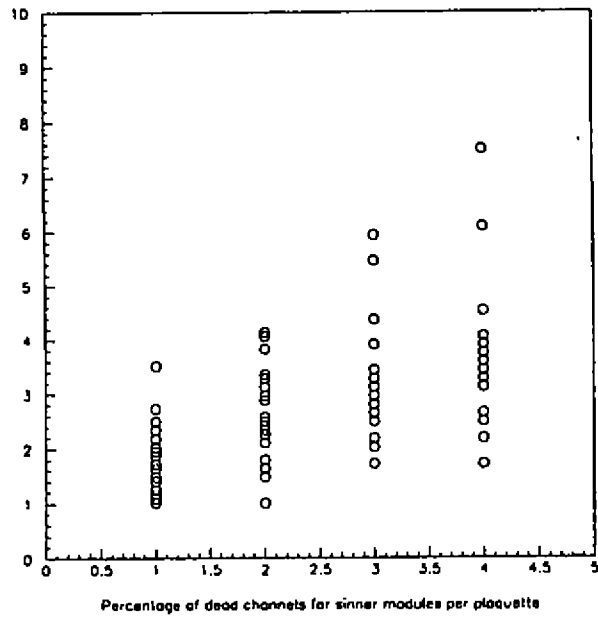


Figure 7: The percentage of dead channels of Sinner final modules. Each vertical line corresponds to a different plaquette, where plaquette 1 is the one closest to the hybrid.

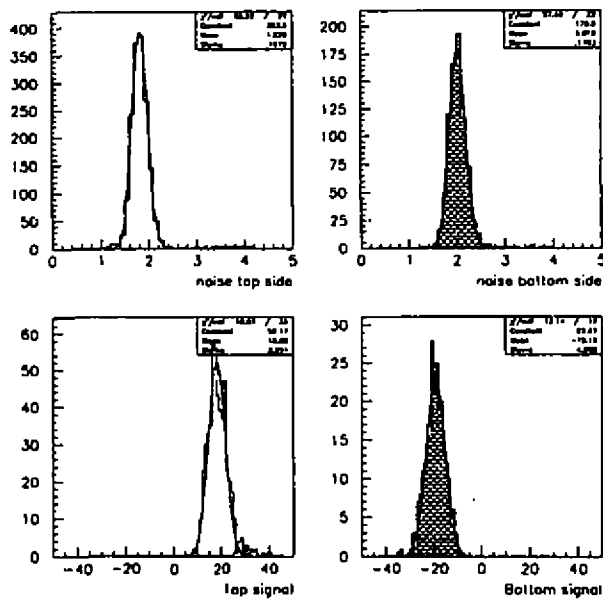


Figure 8: Am241 test - The noise corresponds to 1860 electrons RMS on the top side and to 2000 on the bottom. The mean signal should be multiplied by 1.4 in order to represent the signal of a m.i.p. .

Projeto Microsul: Um Telescópio de Múons Cósmicos Horizontais

E. W. Hamburger, O. Dietzsch, N. Canzian da Silva, A. Bonini,
E. M. Kubo, F. B. M. Salemme, L. M. R. Falco de França,
S. A. Pereira, M. A. Schimdt, L. Galhardo*

Instituto de Física da Universidade de São Paulo, Depto. de Física Experimental

** Instituto Astronômico e Geofísico da Universidade de São Paulo*

1 Experimento Microsul

Motivação: inexistência de um mapeamento, no hemisfério sul, da distribuição de fontes de raios cósmicos em médias energias. É baseado no experimento MICRO [1], realizado em 1987, em Frascati, Itália.

Objetivo: o telescópio procurará anisotropias largas e estreitas na distribuição dos múons cósmicos horizontais.

Localização: cúpula de antigo observatório óptico no Instituto Astronômico e Geofísico da USP, São Paulo.

O Experimento Microsul (Figura 2) comporta 6 planos verticais, distribuídos 3 a 3 em faces paralelas de um cubo, e separados por uma distância de 1 m. Cada plano é constituído por 12 módulos de 8 tubos de Iarocci [2,3] de $100 \times 1 \times 1 \text{ cm}^3$ (Figura 3). Os tubos funcionam com mistura de gás carbônico, argônio e isobutano em regime "streamer" limitado, com descargas localizadas [4]. Os tubos estão colocados entre dois planos de faixas metálicas, um na direção X (paralela ao eixo dos tubos), e o outro na direção Y , e são responsáveis pela obtenção dos sinais induzidos devido à ionização (Figura 4). Tais sinais fornecem as coordenadas (x_i, y_i) do múon em cada um dos 6 planos. Isso permite reconstruir a trajetória da partícula e determinar a direção de incidência.

A condição de planos verticais garante que apenas partículas praticamente horizontais, geradas com energia acima de 10 GeV na alta atmosfera, serão detetadas.

A resolução angular, de aproximadamente 1° , é determinada através das dimensões de cada tubo detetor, $1 \times 1 \text{ cm}^2$, a resolução ao longo do anodo e a distância entre os planos.

2 Telescópio Didático

Motivação: divulgação e ensino de Física Moderna, particularmente de Raios Cósmicos, para público geral e escolas de 1o. e 2o. graus.

Instalações: foram construídos dois exemplares, um com 4 planos detetores, em exposição permanente na Estação Ciência, Lapa, São Paulo, operando continuamente desde o início de 1995, e outro em exposições itinerantes (Casa das Rosas, São Paulo, SP, abril-maio de 1996 e Metrô Ana Rosa, julho de 1996).

O telescópio didático da Estação Ciência consiste de 4 planos com 1 módulo de detetores de Iarocci cada. São dispostos horizontalmente e, por isso, detetam múons verticais. Utiliza em sua eletrônica cartões LeCroy 4200 e circuitos de coincidências e aquisição de dados projetados e construídos por A. Bonini (IFUSP). No telescópio didático itinerante há 3 planos horizontais e os cartões LeCroy foram substituídos por novos SGS (Figura 9).

Os telescópios didáticos têm servido para ensaios da eletrônica e dos tubos detetores. Foram elaborados programas de aquisição e análise de dados para os telescópios didáticos [5], que posteriormente foram adaptados para o Experimento Microsul, e realizado um estudo sistemático das características do detector [6]. Estudou-se os padrões de disparos e a distribuição angular dos múons. Resultados preliminares são apresentados e discutidos nas Figuras 10 a 13. Os resultados experimentais concordam bem com os obtidos a partir de uma simulação do experimento utilizando método de Monte Carlo.

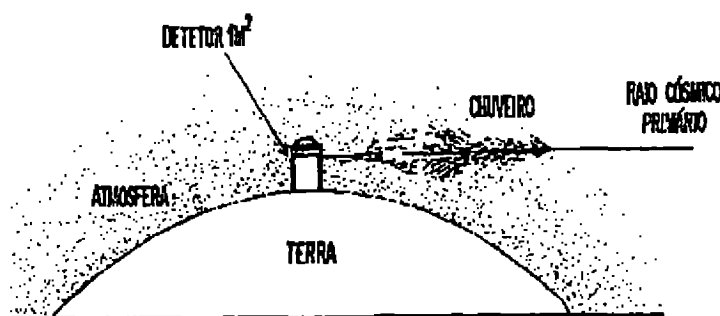


Figura 1. Representação esquemática de um chuva quase horizontal provocado por um raio cósmico primário durante penetração na alta atmosfera. Os múons produzidos serão detectados pelo Experimento Microsul [7].

Referências

1. G. Battistoni et. al.; *Il Nuovo Cimento*, vol. 11C, N2.
2. Iarocci, E.; *Plastic streamer tubes and their applications in high energy physics*, Nucl. Inst. and Methods, 217 (30-42), 1983.
3. Monica Techio, Tesi di Laurea, Università degli studi di Padova, Facoltà di Scienze MM. FF. NN., Dipartimento di Fisica "G. Galilei", *Prestazioni dei tube a streamer del Warm Iron Calorimeter di SLD*, 1988-1989.
4. SLD-WIC Collaboration, *Survey of the response of standard limited streamer tubes over the complete range of three-component gas mixtures of Isobutane, CO₂, Argon*, Nucl. Inst. and Methods, A289 (449-462), 1990.
5. N. C. da Silva, S. A. Pereira, E. W. Hamburger, A. Bonini, O. Dietzsch, *A Muon Telescope for Scientific Research and Public Demonstrations in a Science Museum*, em elaboração.
6. Sérgio A. Pereira, *Construção e caracterização de um telescópio de múons cósmicos*, dissertação de Mestrado a ser apresentada, IFUSP, setembro de 1996.
7. Eduardo J. Pacheco (IAGUSP), Elly Silva (CBPF), Ernst W. Hamburger (IFUSP), Hélio M. Portela (IFUFF), José A. F. Pacheco (IAGUSP), Jorge Horvath (IAGUSP), Luis Galhardo (IAGUSP), Margaret O. Silva (CBPF), Nelson Canzian da Silva (IFUSP), Nilton A. Alves (CBPF), Olácio Dietzsch (IFUSP), Regina H. C. Maldonado (IFUFF), Walter Velloso (IAGUSP), Alfredo Bonini (IFUSP), A. F. Assis (CBPF), C. A. M. Mesquita (CBPF), E. M. Kubo (IFUSP), F. B. M. Salemme (IFUSP), Laura M. R. Falco de França (IFUSP), M. A. Guimarães (CBPF), Marco A. Schmidt (IFUSP), Marcos Mansueto (IFUSP), S. A. Pereira (IFUSP), *Microsul: A Cosmic Ray Muon Monitor*, XV Encontro Nacional de Física de Partículas e Campos, Angra dos Reis, RJ, 1994.

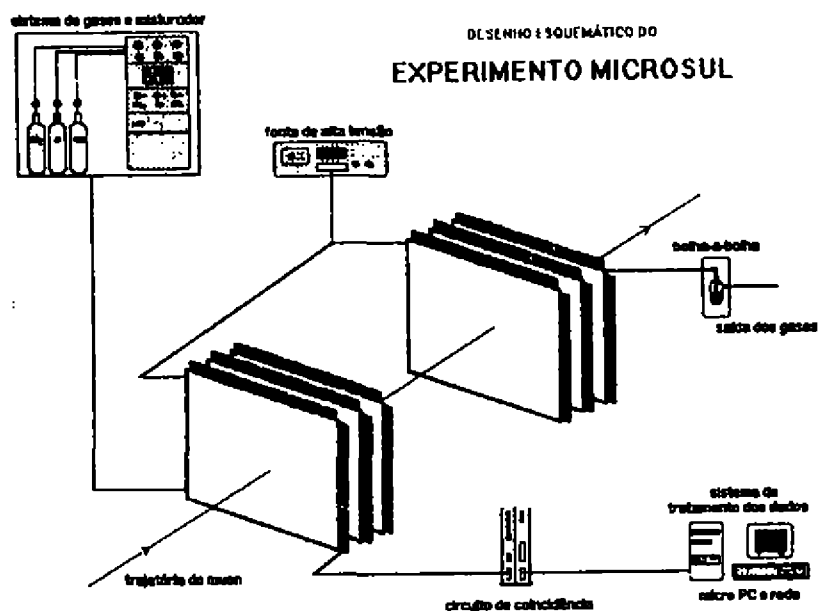


Figura 2. Principais componentes do Experimento Microsul: ocupando a região central estão os seis planos de módulos de tubos de larocci, agrupados três a três e 36 cartões de aquisição LeCroy 4200. Ao redor, a fonte de alimentação, o sistema misturador de gases, o circuito de coincidências e o microcomputador tipo IBM-PC utilizado para aquisição de dados.

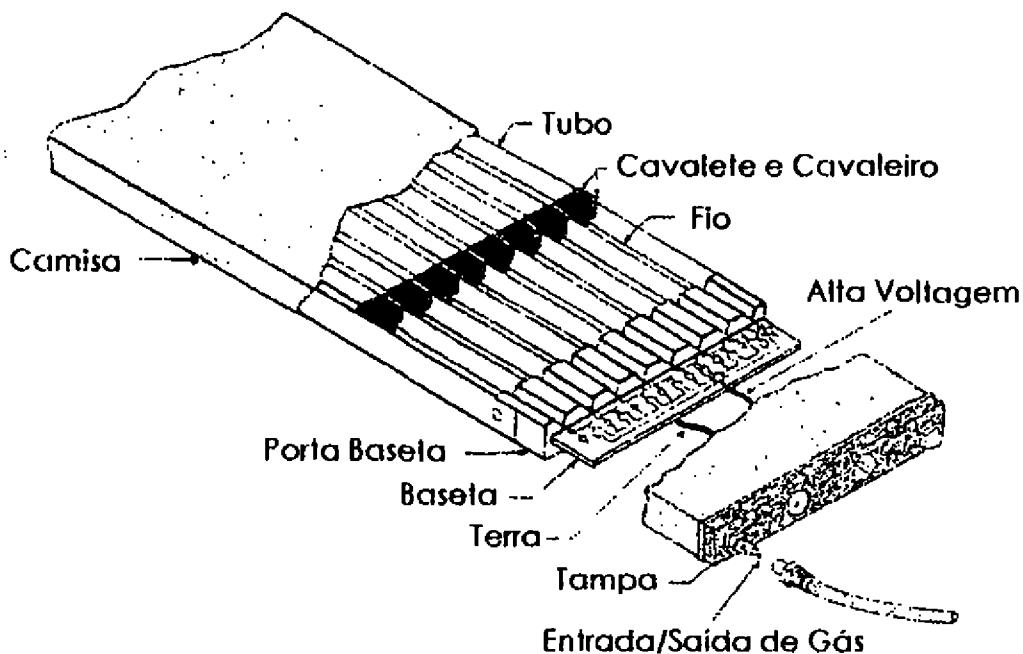


Figura 3. Módulo de 8 tubos de larocci. Cada plano do telescópio possui 12 módulos. O telescópio didático possui apenas um módulo por plano.

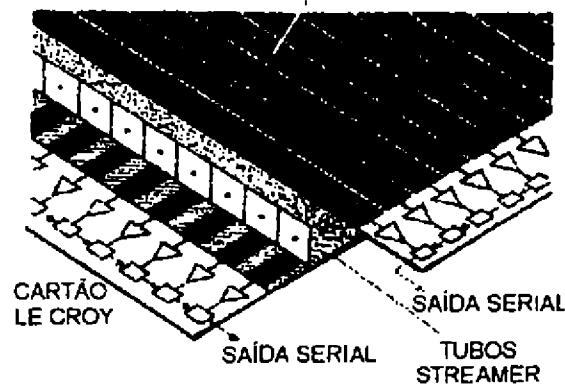


Figura 4. Estrutura dos tubos de larocci e os planos de faixas metálicas responsáveis pela obtenção das coordenadas (x, y) a partir das quais é determinada a trajetória dos múons.

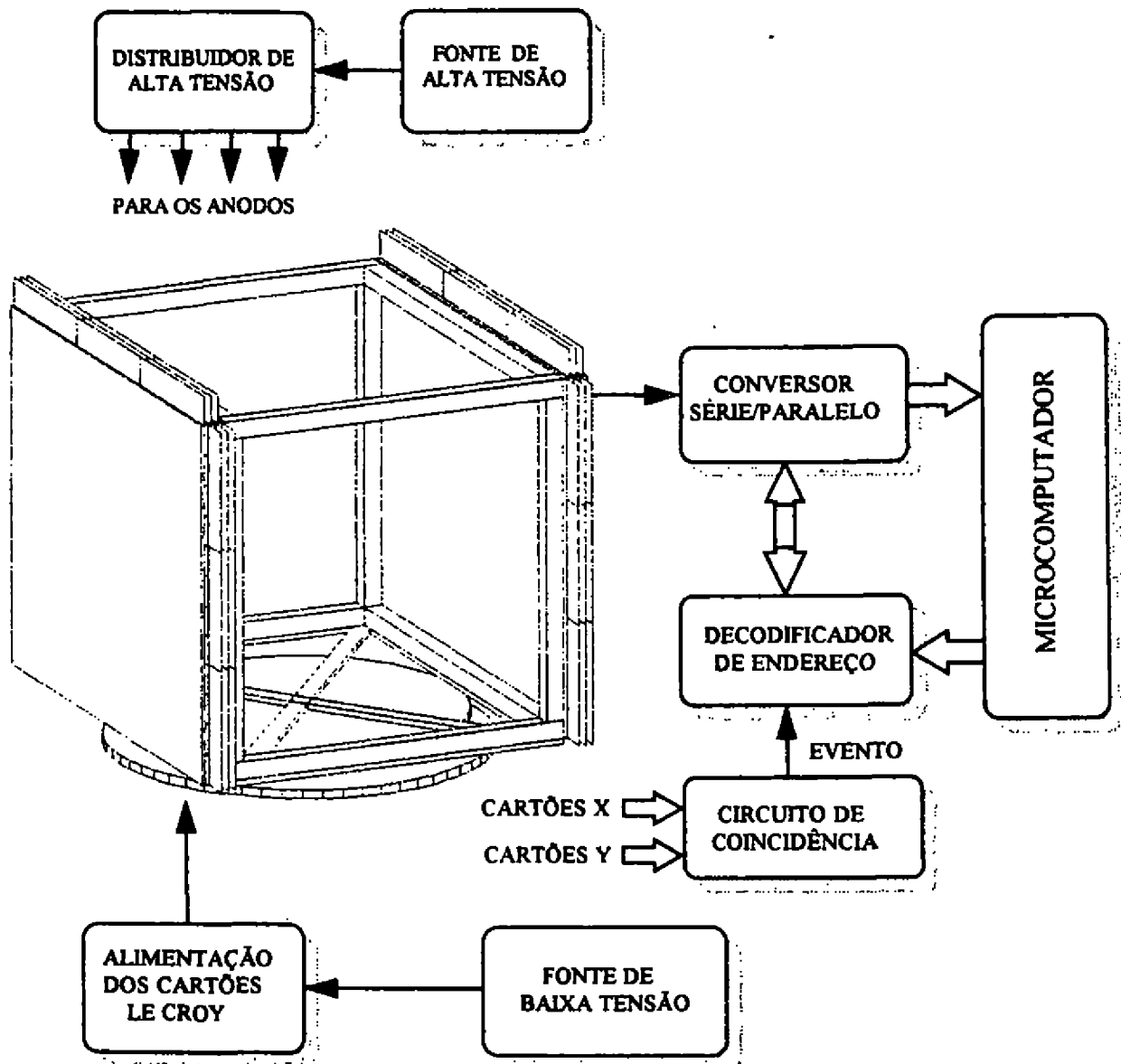


Figura 5. Estrutura em madeira que acomoda os planos verticais do telescópio do Projeto Microsul, e o diagrama de blocos da eletrônica atualmente utilizada.

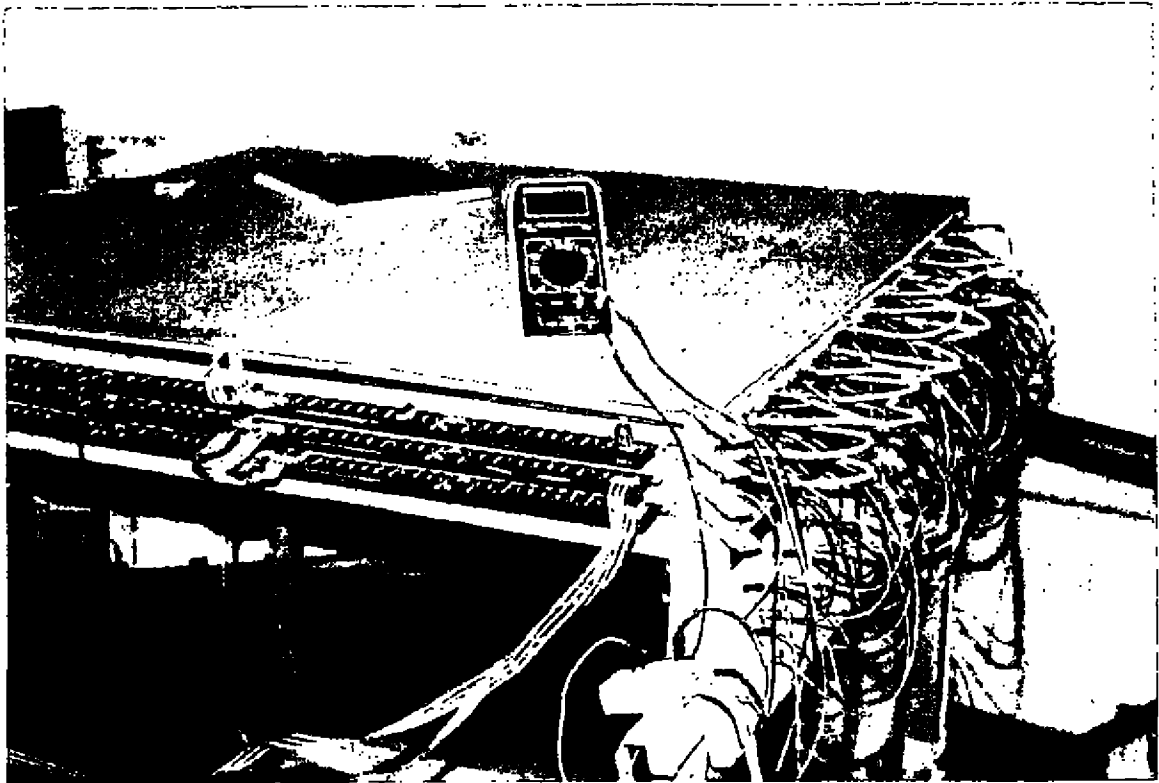


Figura 6. Foto dos três planos de detecção em posição horizontal. Vê-se os cartões de aquisição de sinais (LeCroy 4200) e os distribuidores de alta tensão para os tubos larocci. Em posição de testes, detecta os múons que incidem verticalmente.

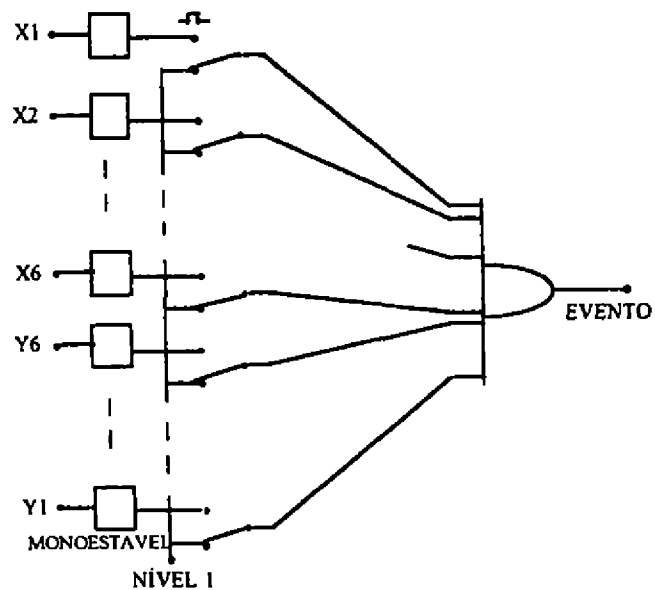


Figura 7. Circuito de coincidência atualmente utilizado, e que deverá ser substituído por um circuito de coincidências majoritário.

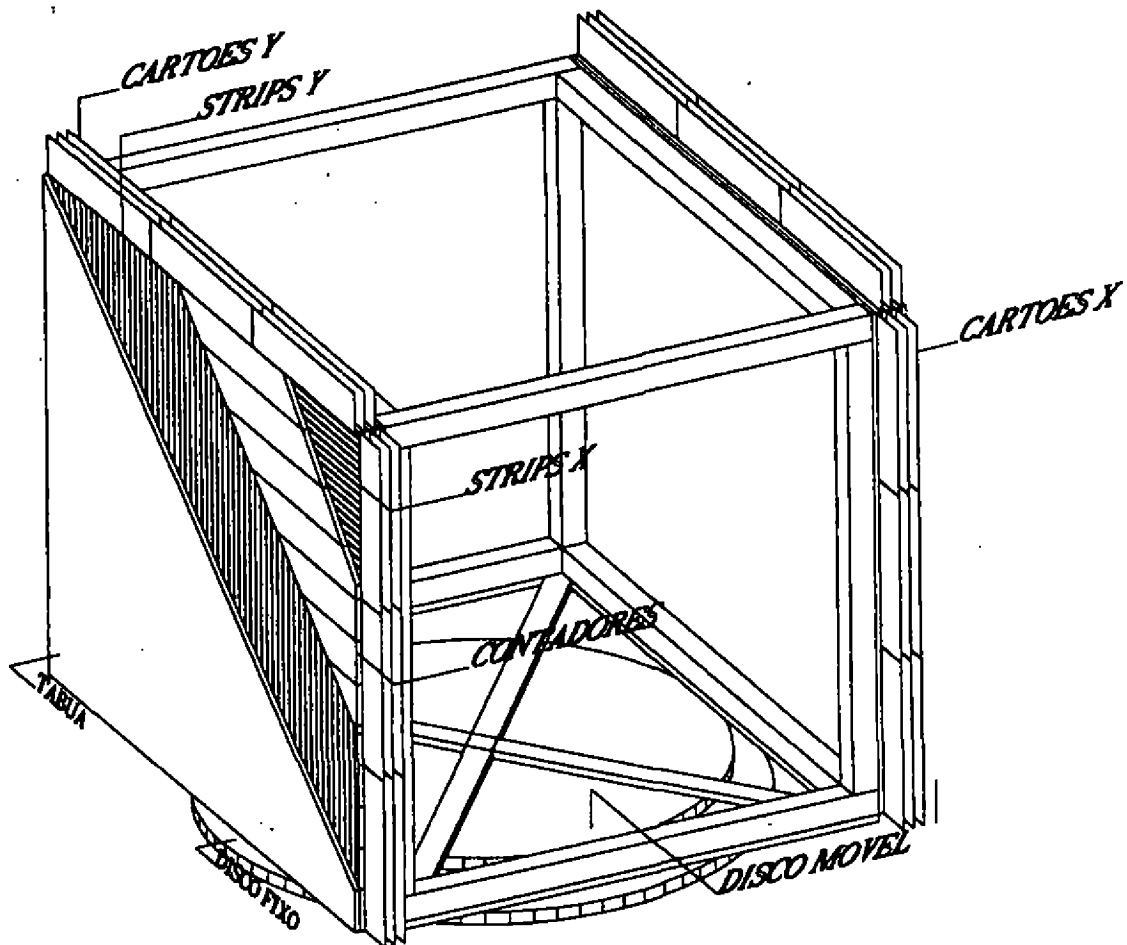


Figura 8. O telescópio de múons em sua configuração definitiva de planos verticais e sobre a mesa giratória para orientação astronômica. No primeiro plano de detetores vê-se, em corte, o conjunto de módulos de larocci e as faixas metálicas ("strips") x e y .

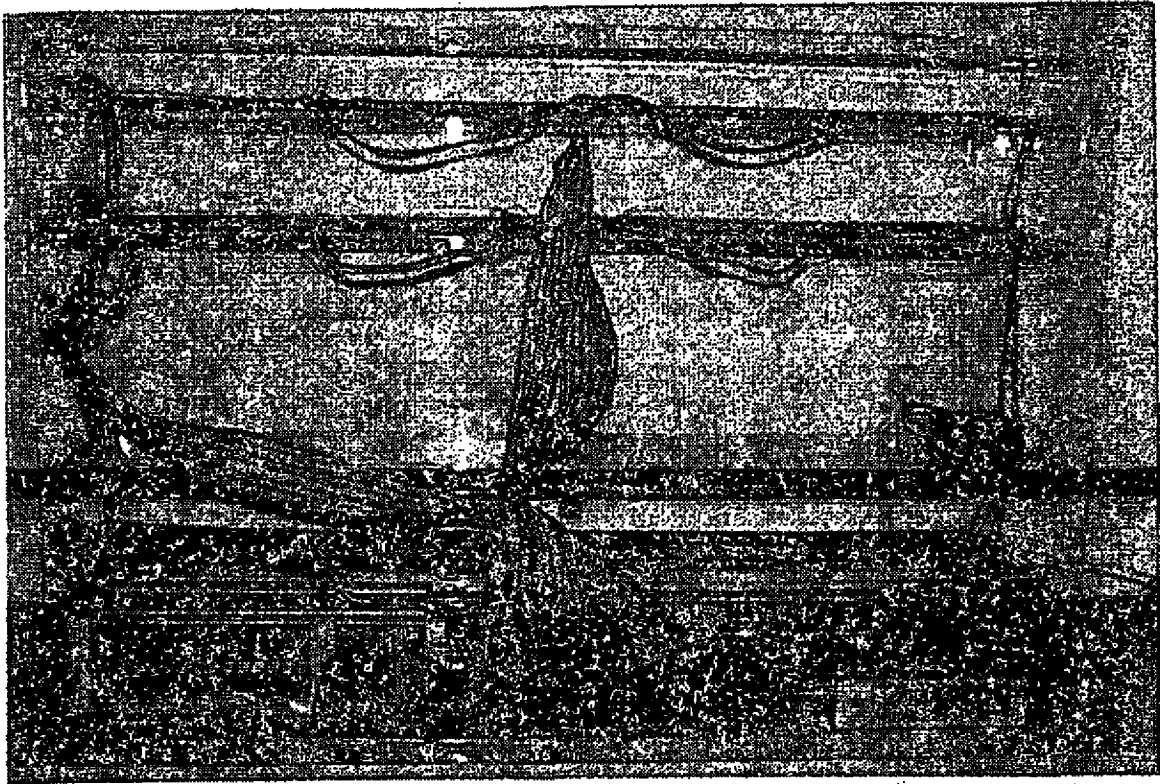


Figura 9. Foto do telescópio didático itinerante com três planos de detecção e cartões SGS.

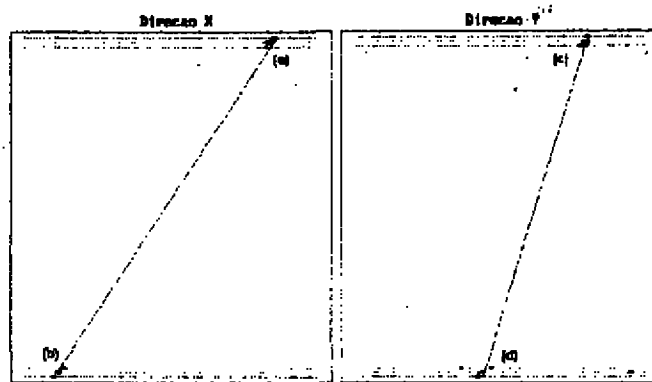


Figura 10. Evento registrado pelo telescópio de nêutrons do Projeto Microsul. Em (a) as posições x nos três planos superiores ativados pela passagem da partícula; em (b) as posições x nos três planos inferiores; em (c) e (d) o análogo para as coordenadas y . As coordenadas (x_i, y_i) e (y_i, x_i) , onde i corresponde à posição do plano, são utilizadas num algoritmo de ajuste de retas que determina a trajetória da partícula, representada pela reta que liga os pontos.

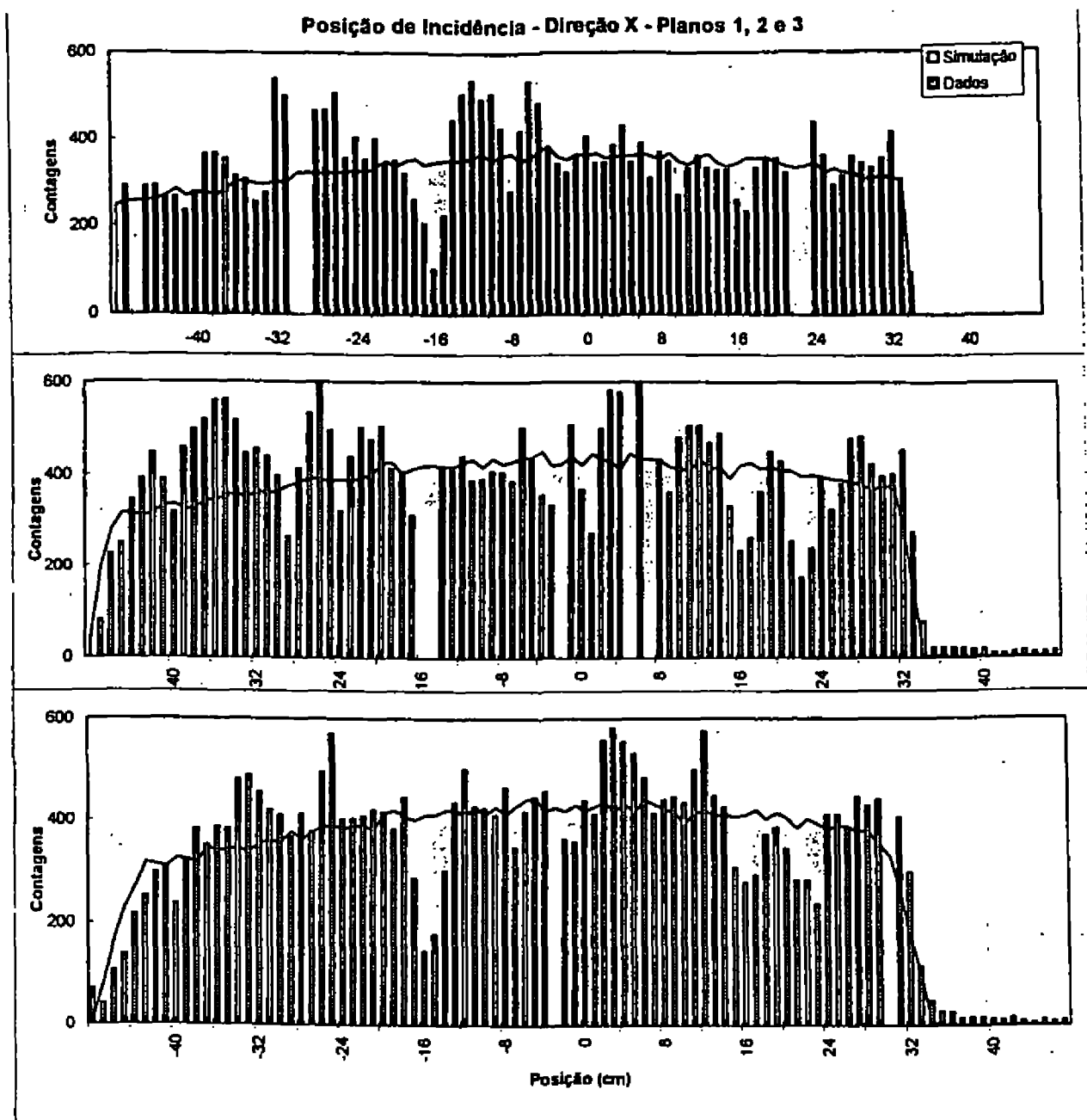


Figura 11. Distribuições medidas e simuladas das posições de incidência das partículas nos três primeiros planos do telescópio, ao longo da direção x , para um conjunto de aproximadamente 20000 eventos. Cada barra representa quantas vezes aquele canal foi ativado. A área preenchida ao fundo é a distribuição prevista por uma simulação do detector pelo método de Monte Carlo. Nos dados, muitos canais estão ausentes por defeitos eletrônicos. Em particular, há ausência total de disparos em canais correspondentes a $x > 33$ cm no primeiro plano, ocasionando uma drástica redução das contagens nos respectivos canais dos outros dois planos devido à coincidência requerida para a aquisição do evento ("trigger").

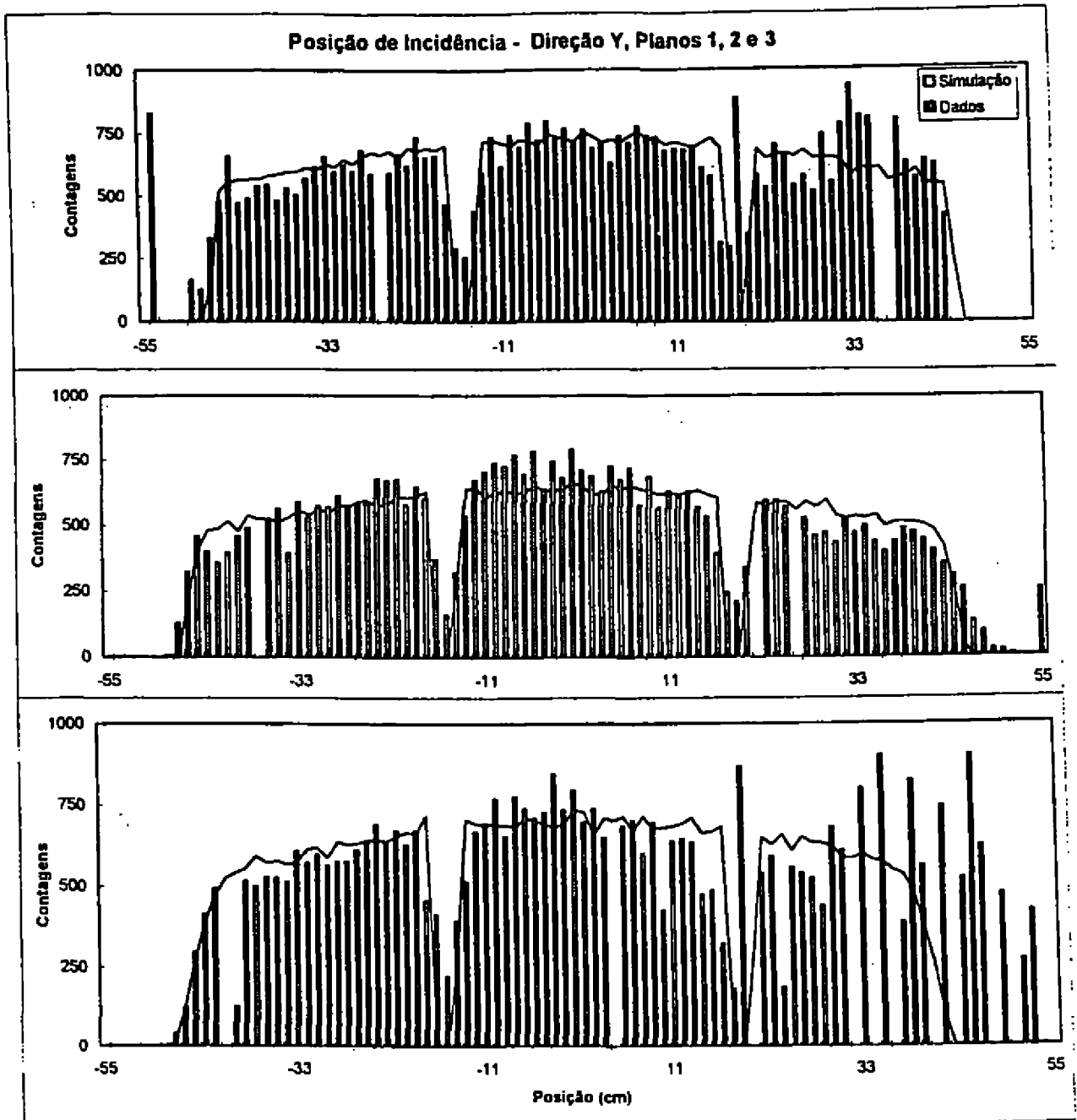


Figura 12. Distribuições medidas e simuladas das posições de incidência das partículas nos três primeiros planos do telescópio, no longo da direção y , para o mesmo conjunto de dados da Figura 2. Os canais de cada extremidade não apresentam atividade por encontrarem-se fora da região sensível dos contadores. Os "vales" próximos a ± 15 cm também correspondem a regiões insensíveis devido a cavaletes plásticos que servem de suportes aos fios de anodo. Na extremidade direita do terceiro plano observa-se um elevado número de canais inativos e ruidosos.

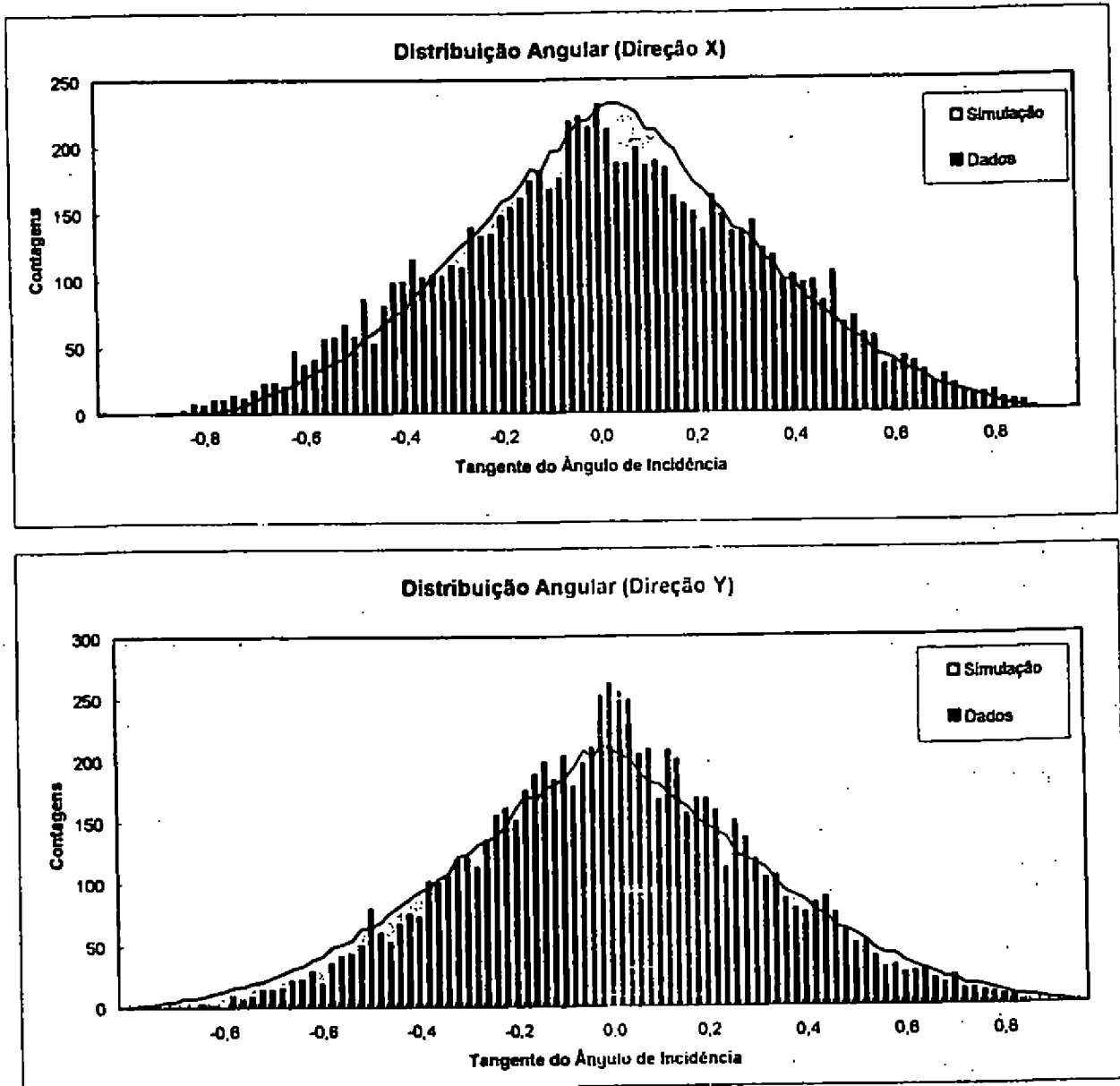


Figure 13. Distribuições dos coeficientes angulares das trajetórias das partículas, obtidas a partir do ajuste de $x = a_x \cdot z + b_x$ e $y = a_y \cdot z + b_y$, onde a_x e a_y são os coeficientes angulares e b_x e b_y coeficientes lineares, aos dados. A área preenchida ao fundo é a distribuição prevista pela simulação. Há bom acordo entre as distribuições medidas e simuladas, com pequenas discrepâncias que podem ser eliminadas com refinamentos no equipamento e na simulação. A utilização de vários planos próximos e em coincidência fornece uma redundância de medidas que minimiza o efeito dos canais inativos ou ruidosos observados nas Figuras 2 e 3. As diferenças entre as distribuições medidas e simuladas podem ser utilizadas para determinar, a partir dos dados, certos parâmetros não mensuráveis diretamente, bem como verificar o alinhamento entre diferentes partes do sistema.

τ Polarisation from the $\tau \rightarrow \rho\nu_\tau$ Channel in Delphi

J. R. P. Mahon*, M. E. Pol† and R. C. Shellard‡

1 Introduction

Studying the reaction $e^+e^- \rightarrow Z^0 \rightarrow \tau^+\tau^-$, we determine the τ polarisation from the decay $\tau \rightarrow \rho\nu_\tau$ at the DELPHI experiment at LEP, using data taken in 1993.

For the reaction $e^+e^- \rightarrow Z^0 \rightarrow \tau^+\tau^-$, both the Z^0 and the τ lepton are polarised due to parity violation in the weak neutral current. The LEP beams are unpolarised and the inequality of the Z^0 couplings to left-handed and right-handed leptons induces a polarisation of the Z^0 as well as a polarisation of the taus. The polarisation of the τ can be measured from the τ decay products, assuming the V-A structure of the weak charged current, and has, due to the Z^0 polarisation, a dependence on the production angle.

2 ρ selection

The DELPHI detector [1] and the $\tau\tau$ selection [2] have already been described.

In order to reconstruct the ρ , we selected τ decays containing one charged particle, π^\pm and a π^0 through its decays seen as two (one) photons in the electromagnetic calorimeter. We then required that the angle between the reconstructed track and the π^0 was less than 20° and that the effective mass of these two particles lies in the interval $0.48 < M_{\tau\pi^0} < 1.2 \text{ GeV}/c^2$.

2.1 Track selection

The charged π^\pm was selected as a single 'good' track in the hemisphere of the decay considered, registered by the tracking detectors within the central region $45^\circ < \theta < 135^\circ$, being θ the polar angle with the beam axis, having a momentum greater than $0.5 \text{ GeV}/c$, track length greater than 30 cm, impact parameter in $r\phi$ less than 2.5 cm and in z less than 5 cm consistent with origin at the collision point and vetoed with DELPHI particle identification programs as not being an electron or muon.

2.2 π^0 selection

The π^0 reconstruction, which is the most delicate point of the analysis, was done with the following three different criteria:

2.2.1 2 photons

Photons were selected if they were reconstructed in the fiducial region of the barrel electromagnetic calorimeter (HPC), which corresponds to $45^\circ < \theta < 135^\circ$. It was also required that their energy was greater than 0.5 GeV and that the longitudinal and transverse profiles of the showers in the calorimeter were compatible with the structure of a photon. Photons that converted in the tracking detectors were also accepted when the effective mass of the e^+e^- pair allowed to reconstruct unambiguously the original photon.

*Inst. de Física, Univ. Estadual do Rio de Janeiro, Rio de Janeiro, Brasil

†Centro Brasileiro de Pesquisas Físicas, Rio de Janeiro, Brasil

‡CBPF, Rio de Janeiro, Brasil and Pontifícia Universidade Católica, Rio de Janeiro, Brasil

Pairs of photons were combined and considered as a π^0 candidate when their effective mass was $0.04 < M_{\gamma\gamma} < 0.3$ GeV/c² and the angle between them was less than 10°. This last cut was done in order to minimise the combinatorial background, as the typical angle between two photons coming from π^0 at LEP energies is of the order of 2.5°-3.0°.

2.2.2 1 photon

We also considered the case where only one of the two photons is seen in the detector. This may be due to losses in the cracks of the calorimeter or, in the case of a very energetic π^0 , the angle between the photons is so small that the two photons are reconstructed as one.

In order to accept one photon as a ' π^0 ', we required that its energy was greater than 2.5 GeV.

2.2.3 Merged π^0

This category corresponds to the last case of the previous selection, in the special situation where the profile of the shower in the calorimeter is such that clearly there are indeed two 'merged' photons.

3 Data analysis and results

Background and efficiencies were estimated using simulated events, which were generated with KORALZ [3], fully simulated through the detector with DELSIM [4] and reconstructed with the same algorithm as the real data.

The data collected in 1993 corresponds to 15.7 pb⁻¹ at $E_{cm} = 91.2$ GeV, 9.4 pb⁻¹ at $E_{cm} = 89.2$ and 4.5 pb⁻¹ at GeV $E_{cm} = 93.2$ GeV. We selected 18371 $\tau\tau$ pairs and 4933 $\tau \rightarrow \rho\nu_\tau$ decays, with an efficiency of 23% in 4 π and a background of 15%.

The method used in this analysis takes into account the kinematic distributions of single τ decays. The τ polarisation is reflected in the angular distributions of its decay products in the τ rest frame. The angular distribution affects the momenta of the final state particle in the laboratory frame, which can thus be used to infer the τ polarisation. Due to the fact that the ρ is a spin-1 particle, the possibility of several polarisation states reduces the sensitivity of the measurement. We increased this sensitivity using also information from the decay of the ρ . Therefore, the extraction of the τ polarisation involves a multidimensional ξ distribution [5], in terms of functions of the angles of the final state particles and momenta.

The usual ξ distribution was made for the real data taken at the Z^0 peak, together with the helicity ± 1 from the simulated Monte Carlo events, all of them passing the above cuts for ρ selection. To obtain the polarisation, the data was fitted using a maximum likelihood method including Monte Carlo statistics [6], to a function:

$$NN\left[\frac{1+P}{1+P_0}N_i^+ + \frac{1-P}{1-P_0}N_i^-\right]$$

where N_i^+ and N_i^- are the distributions of the set of variables for positive and negative τ helicities respectively. We also considered the six slices in $\cos\Theta$ ($\cos\Theta = -Q\cos\theta$, where Q is the τ charge) to fit the distribution [7]. Table 1 shows the P_τ for the six slices, which gives a weighted mean average:

$$\langle P_\tau \rangle = -0.208 \pm 0.045$$

$\cos\Theta_{min}$	$\cos\Theta_{max}$	P_τ
-0.732	-0.488	0.068±0.119
-0.488	-0.244	-0.164±0.112
-0.244	0.000	-0.193±0.122
0.000	0.244	-0.202±0.117
0.244	0.488	-0.342±0.103
0.488	0.732	-0.331±0.101

Table 1

3.1 Systematic error

In order to evaluate the systematic error we calculated the polarisation varying the selection cuts one at the time. For τ selection we considered just one variation:

a) relax the requirement of total reconstructed energy and momentum.

We introduced an error from Monte Carlo Statistics

For the ρ analysis itself, we took the following variations:

- 1) energy of '1 photon' $\pi^0 > 5$. GeV.
- 2) energy of '1 photon' $\pi^0 > 0$. GeV.
- 3) energy of photons (for pairs) > 1 . GeV
- 4) π^0 mass < 0.5 GeV/c²
- 5) $0.3 < m_p < 1.35$ GeV/c²
- 6) track momentum > 1.0 GeV/c
- 7) accept standard identification for electron and muon
- 8) just one track in the hemisphere
- 9) angle between pair of photons $< 20^\circ$
- 10) angle between photons and charged track $< 60^\circ$

In order to estimate the systematic error, we took into account the fact that some of the variations are independent of the internal background, and also their correlations: The ρ selection variations 1 and 2 are not independent, we take the average of their contribution to ΔP . The variation due to ρ selection 4 (π^0 mass) is included in 5 (ρ mass). Finally contributions due to ρ selection variables 8 and 10 are negligible.

Table 2 shows the individual contributions to the systematic error.

Contributions	ΔP
τ selection a)	0.005
MONTE CARLO	0.008
ρ selection 1) and 2)	0.018
ρ selection 3)	0.022
ρ selection 4) and 5)	0.017
ρ selection 6)	0.010
ρ selection 7)	0.005
ρ selection 8)	-
ρ selection 9)	0.008
ρ selection 10)	-
Total	0.037

Table 2

Our final result is:

$$P_{\tau_{03}} = -0.208 \pm 0.045 \pm 0.037$$

The ξ distribution summed over all bins in $\cos\Theta$ is shown in the figure, with the simulated data distribution using the fitted value of $\langle P_\tau \rangle$ superimposed.

From our result for the τ polarisation, which agrees with other LEP measurements, the τ and e asymmetries can be obtained, giving $\mathcal{A}_\tau = -0.199 \pm 0.046$ and $\mathcal{A}_e = -0.192 \pm 0.071$, which show that these values are compatible with universality.

References

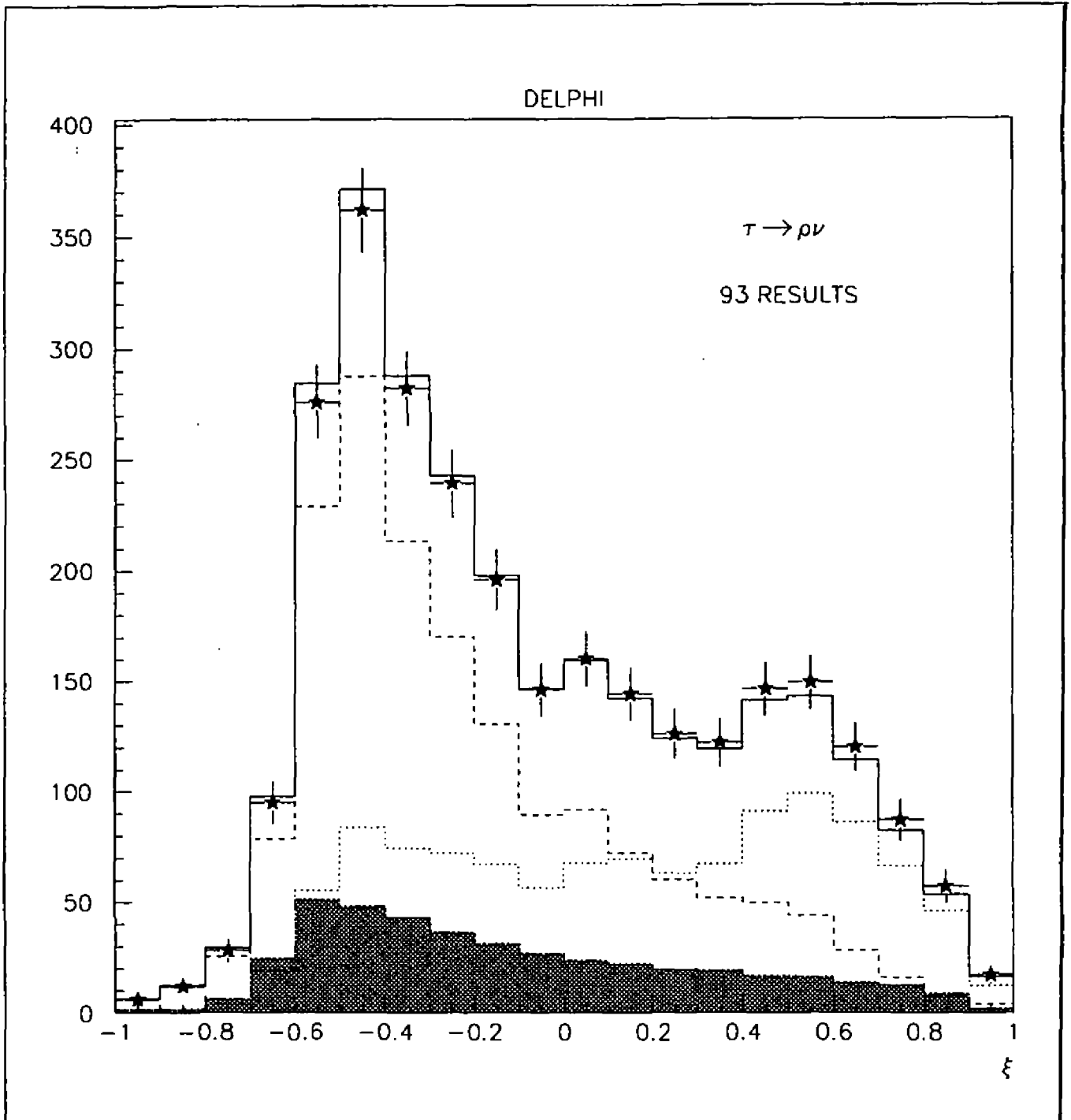
- [1] DELPHI Collaboration, Nucl. Instr. and Meth. **A303** (1991) 233.
- [2] DELPHI Collaboration, Phys. Lett. **B357** (1995) 715.
- [3] S.Jadach and Z.Was, Comp. Phys. Com. **36** (1985) 191.
S.Jadach, B.F.L. Ward and Z.Was, Comp. Phys. Com. **66** (1991) 276.

[4] DELSIM Reference Manual, DELPHI 89-68 Prog 143, CERN, September 1989.

[5] A. Rougé, Z. Phys. C48 (1990) 75.

[6] P. Eberhard, G. Lynch and D. Lambert, NIM A328 (1993) 574.

[7] F. Matorras, DELPHI 94-155 PHYS 462, 1 December 1994.



Search for Pair-Produced Neutral Higgs Bosons Using B-Tagging

Mikael Berggren*

Instituto de Física, UFRJ, Rio de Janeiro, RJ

Supported in part by European Union, grant # CII CT94-0118*

Based on DELPHI data from 1991 and 1992, and, preliminarily, from 1994 and 1995, a search for pair-produced neutral heavy Higgs bosons decaying into $b\bar{b}$ has been carried out using hadronic decays of the Z boson into four jet final states. The two production mechanisms present in the two Higgs doublet scheme, bremsstrahlung hZ^* and pair production hA , may lead to four beauty jets well recognizable using the precise microvertex detector measurements. Limits on $BR(Z \rightarrow hA \rightarrow 4b)$ from 3 to 5×10^{-4} are obtained; the preliminary analysis of the 94 and 95 data decreases this limit to 1×10^{-4} . When combined with the recent DELPHI standard Higgs search, this result allows to reach the kinematical limit for the masses of h and A in the MSSM scheme. Results are also given in the general two doublet scheme.

1 Introduction

In MSSM, the Higgs sector has a two doublet structure, and two of the predicted Higgs particles, the neutral scalar h , and the neutral pseudo-scalar A , can be light. Hence the possibility for the decay $Z \rightarrow hA$. The presently best limits are obtained using h (or A) $\rightarrow \tau^+\tau^-$, yielding a rather weak limit (10^{-3}) due to the low branching ratio and detection efficiency of this channel.

In this paper, a search for events with four jets containing beauty particles is presented. This is done by selecting events with at least four well separated jets, combined with an efficient b-tagging method.

In the two doublet Higgs scheme, the doublets mix with angles α and β . These angles enter into the branching ratios of Z^0 to hA and hZ^* , and these two processes are complementary. The mixing effects are also present in the decays: For $\tan\beta \geq 1$, A decays dominantly into b quarks[1], while h may or may not do so, depending on α ; for $\alpha=0$, h completely decouples from $b\bar{b}$. Because of the complementarity of the two channels, constraining both is necessary to exclude regions in the m_h - m_A plane. The hZ^* channel is the one studied in SM-Higgs searches, with two important differences: The expected branching-ratio is reduced by a factor $\sin^2(\alpha - \beta)$, and if $\alpha = 0$, h will not decay to $b\bar{b}$. The observed branching ratio limit at some m_h sets limits on α , if β is limited. From this one can deduce if the hA channel can produce a $b\bar{b}c\bar{c}$, or if $b\bar{b}b\bar{b}$ will dominate, and therefore which branching ratio limit to apply to find allowed m_A values for the given m_h . To constrain the hZ^* channel, the results of the SM Higgs search of reference 2 were used. For the above reasons, we supplemented this analysis with one not using b-tagging. This analysis is relevant for m_h above 45 (37) GeV/c^2 ($\tan(\beta) \geq 1$ (0.5)); at lower masses $\alpha=0$ is excluded.

In the MSSM Higgs sector, which is a special case of the two doublet scheme, the allowed parameter domain for m_h , m_A , α , and β is restricted, and in particular one does not expect α to vanish. The relations between the parameters depend on the top and squark masses through radiative corrections [3] [4].

2 Data analysis

The analysis presented is mainly based on the events collected by DELPHI in '91-'92, and was published in [5]. A preliminary analysis of data recorded in '94 and '95 is also presented here. A description of the detector can

*Representing the DELPHI Collaboration.

be found in reference [6]. The standard DELPHI selection of $Z \rightarrow$ hadrons [7] was applied to the data and MC samples. 96 % of the events in the data (in total 950 000) and the background QCD MC sample passed this cut; all simulated signal events also did. To select events with at least four well separated reconstructed jets[8], we retained only those four-jet events in which the sum of the two lowest, even Fox-Wolfram moments[9] greater than 0.6. In the 92-93 data and in the corresponding QCD-MC, 8.2 % of the events fulfilled this, while 88 (67) % in the signal-MC remained, if the lightest of the two Higgs bosons has a mass of 40 (15) GeV/c^2 . In the data from 94-95 (in total 2 100 000 events), 7.0 % passed the cuts, while 6.8 % in the corresponding QCD-MC did. In the signal-MC for the later period, 86 % passed, for a Higgs mass of 45 GeV/c^2 .

The b-tagging was done using the three-layer silicon microvertex detector (VD): A track with well-associated hits in the VD, $p \geq 0.5 \text{ GeV}/c$, and a impact parameter [10] w.r.t. the fitted main vertex $\leq 2 \text{ mm}$ and $\geq 2.5 \sigma_{ip}$ was regarded to have an *offset*. In order to define the sign of the impact-parameter, the directions of the b quarks were estimated by clustering the particles into jets using the JADE algorithm[8] with the parameter y_{cut} set to 0.01. The sign was taken to be positive if the projected track intersected the jet axis after the point of closest approach (in the direction of the momentum) and negative otherwise.

The impact parameter resolution in the simulation was increased by approximately 10% to match that observed in data. This correction was calculated on generic hadronic events and mostly affects the central part of the impact parameter distribution. Figure 1. a shows a comparison between simulation and data for the impact parameter distribution after this correction.

The main experimental difference in the later and earlier periods concerns the impact-parameters. As of 1994, the DELPHI VD also measured the track coordinate along the beam- direction (the z-direction), as well as in $r\phi$. Hence, for the later period the b-tagging procedure was modified: also offsets in the z-direction were counted. Since the measurements in the two projections are independent, the offset-counting was done independently in the two directions, i.e. a single track could have zero, one or two offsets. The same criteria as for the offsets in the $r\phi$ projection was used to select tracks with valid offsets in z; the only difference was that the cut on absolute size was at 5 mm (rather than 2 mm).

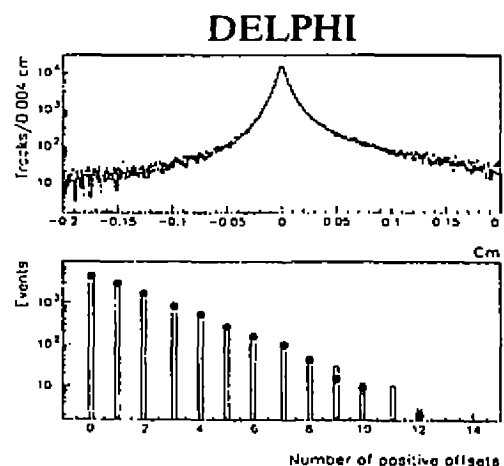


Figure 1.: The top figure shows the distribution of the impact parameter of accepted tracks in a sample of hadronic events. The solid line is the Monte Carlo prediction and the crosses represent the data. The lower figure shows the distribution of the number of positively signed impact parameters for the same sample with the same convention. While the general agreement is good a certain difference arises for big number of offsets.

Because of the long lifetime and high mass of beauty particles, their decays produce many secondaries with

offsets. This method is well known to provide a robust selection of beauty particles which is not very sensitive to various backgrounds such as wrong associations, strange particle decays, or photon conversions [10].

Good agreement was observed in the distribution of the number of offsets between data and simulation, as shown in fig 1b.

3 The data samples

The data was classified in three samples, reflecting the different relevant channels, and the difference of the experimental setup. Sample I and II both concerns data from the earlier period; while sample III takes into account the increase in sensitivity gained by the two-coordinate read-out in the VD.

Sample I, aimed at constraining the $b\bar{b}c\bar{c}$ channel, contained events with more than four offsets in total. This sample consisted of 1899 events in the data, $1956 \pm 38 \pm 140$ in the QCD-MC. The efficiency for the relevant signal-MC was $(8.0 \pm 0.5) \%$.

Sample II, aimed at the $b\bar{b}b\bar{b}$ channel, contained events having either three jets with at least two offsets each, or having two jets with at least two offsets and two other jets with one offset each. Here, the sample consisted of 105 events in the data, $97 \pm 9 \pm 10$ in the QCD-MC. For the signal-MC, the efficiency was between (8.0 ± 0.5) and $(5.0 \pm 0.5) \%$, depending on the mass of the lightest Higgs boson. Among the selected candidates, one had four jets tagged, i.e. with at least 2 offsets in each jet. This event is shown in figure 2.

Sample III, also aimed at the $b\bar{b}b\bar{b}$ channel, but takes advantage of the new VD in the later period. It contained events having either three jets with at least four offsets each, or having two jets with at least four offsets and two other jets with at least two offsets each. Here, the sample consisted of 116 events in the data, 110 ± 8 in the QCD-MC. For the signal-MC, the efficiency was between (8.0 ± 0.5) and $(5.0 \pm 0.5) \%$, depending on the mass of the lightest Higgs boson.

The most important background was $b\bar{b}$ events with two additional gluon jets. The probability to mistake a gluon jet for a b jet is small, but the cross section is quite large. A second background source is the pure QCD production of 4 b quarks (or 2 b and 2 c quarks), which occurs at a low rate: From standard QCD processes, events with 4 b quarks are expected to be produced in about 0.03 % of the hadronic Z^0 decays (this figure was extracted with the JETSET[11] event generator, using the Parton Shower model). Events with two b quarks and two c quarks are seven times more abundant . This latter source of background constitutes 28 % of the total background in sample II, while it represents 10 (15) % in sample I(III).

The uncertainties of the size of these sources was taken into account in the systematic errors stated. Other sources of systematic uncertainty arises from the slight discrepancy between the simulation of the VD and the observed data (the fraction of events (with any number of jets) with more than four offsets was 10% higher in the simulated events than in the data), and a likewise small discrepancy on the efficiency to select four jets (the number of events classified as four jets after the event preselection was 10% larger in the data than in the simulation, an effect uncorrelated with the b-tagging cuts).

The background extracted from simulation was accordingly corrected and systematic errors of half the size of the corrections was assigned to it.

Other possible systematic effects such as those due to variation of the beauty lifetime and the effects of the cuts were found to be negligible.

All systematic errors were added in quadrature, giving a total contribution of 7% for *Sample I* and 10% for the *Sample II*.

4 Results and Conclusions

The number of events in all samples are clearly compatible with the expected numbers. Sample I therefore yields that $BR(Z \rightarrow hA \rightarrow b\bar{b}c\bar{c}) < 3 \times 10^{-3}$, and sample II that $BR(Z \rightarrow hA \rightarrow b\bar{b}b\bar{b}) < 3 (5) \times 10^{-4}$ for the lightest Higgs at 40 (15) GeV/c².

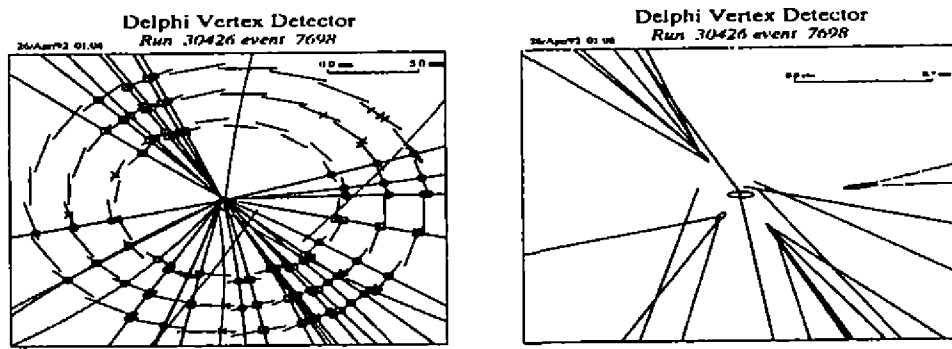


Figure 2.: Display of a 4b candidate showing the microvertex information. In the left-hand figure, dotted tracks were not within the acceptance of the micro-vertex detector. Circles (squares) represent VD hits associated to tracks in the half detector with $z > 0$ ($z < 0$) and crosses hits which were not associated to tracks. The right hand figure displays the same candidate on an expanded scale. Only tracks measured by the micro-vertex detector and with momenta above 0.5 GeV/c are displayed. The central ellipse indicates the beam position. Three displaced vertices have been reconstructed; the ellipses define the four-standard-deviation contours around them. A K_S^0 candidate is reconstructed on the right.

The preliminary analysis of sample III yields that $BR(Z \rightarrow hA \rightarrow b\bar{b}b\bar{b}) < 1 \times 10^{-4}$ for the lightest Higgs at 45 GeV/c². Note, however, that the systematic uncertainties have not yet been evaluated for this sample.

In the region below the limit in m_h where h decouples from $b\bar{b}$, sample II can be used, above it sample I must be used. Figures 3a and 3b show the exclusion regions in the m_A - m_h plane. In the region where h must couple to $b\bar{b}$, the process $Z \rightarrow hA$ is excluded; if m_h is higher, it might possibly occur.

In MSSM, samples II or III applies everywhere. Figure 3c shows that the decay of the Z^0 to hA is excluded. Note that the published results [5] left a small window open for this process. The reason we can now exclude this is purely theoretical: since the publication of [5], two-loop calculations of the radiative corrections have been performed [4], and the corrections to the one-loop calculations sufficiently modified the cross-sections to exclude this possibility. The only dependence on parameters of the MSSM is the m_A limit, which depends on the squark mass between 500 and 800 GeV/c²; it is 39 (45) GeV/c² at $m_{sq} = 1$ (0.5) TeV/c². In the unlikely case [13] that $0.5 \leq \tan\beta < 1$, ($\tan\beta < 0.5$ is theoretically excluded [14]), we constrain m_h to be above 55 GeV/c². There is, however, no lower limit on m_A when $m_h \geq 60$ GeV/c².

We conclude that, within MSSM, $m_h \geq 44$ GeV/c² for any $\tan\beta$ and $m_A \geq 39$ GeV/c² for $\tan\beta \geq 1$ (at 95% CI, with $m_t = 170$ GeV/c² and $m_{sq} = 1$ TeV/c²).

In figure 4, the exclusion region in the $\tan\beta$ - m_A plane is shown for different values of the top quark mass. Note that $\tan\beta = 1$ is excluded if $m_t = 150$ GeV/c² (one standard-deviation below the central value stated in ref [12]).

The preliminary analysis of the most recent data excludes $m_A \leq 45$ GeV/c², for $m_t = 170$ GeV/c² and $m_{sq} = 1$ TeV/c² and with little dependence on these masses.

Beyond this result, some further increase in the excluded region might be attained by more stringent limits on h/Z production. However, no further progress on the mass limits (ie. the edge of the allowed region at the lowest masses) can be expected from studies of Z^0 decays. To extend the limits further, and hence to perform a crucial test of MSSM, data from LEP200 will be needed.

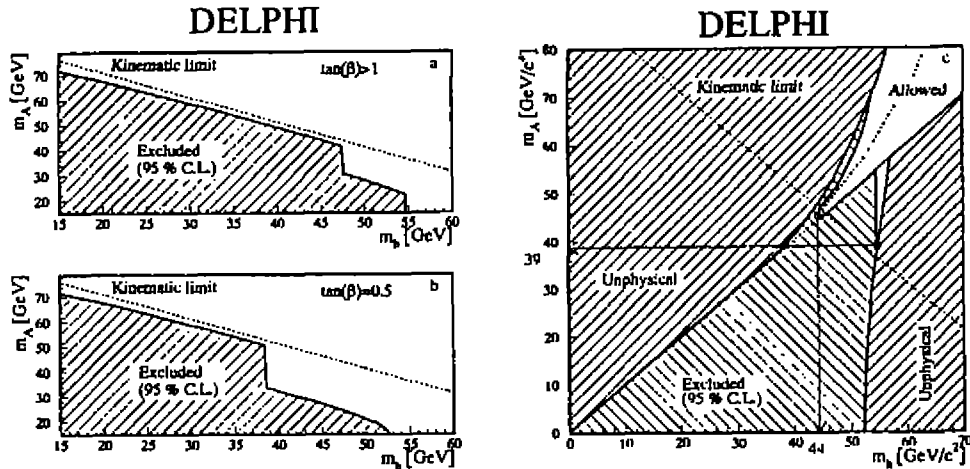


Figure 3.: m_A - m_h limit contour (at 95 % CL) obtained from searches for hA and hZ^* for : a. The two doublet case with $\tan\beta \geq 1$, b. The two doublet case with $\tan\beta \geq 0.5$, and c. The MSSM case with $\tan\beta \geq 1$, assuming $m_t = 170$ GeV/c^2 and $m_{sq} = 1$ TeV/c^2 .

In c, the dash-dotted line indicates the preliminary result using the data from 94 and 95.

References

- [1] See J.F. Gunion, H.E. Haber, G. Kane and S. Dawson, *The Higgs Hunters Guide* (Addison-Wesley, Reading, MA, 1990) and references therein.
- [2] P. Abreu et al., DELPHI Coll., *CERN-PPE 94-46-REV*.
- [3] Y. Okada, M. Yamaguchi and T. Yanagida, *Prog. Theor. Phys. Lett.* **85** (1991) 1.
J. Ellis, G. Ridolfi and F. Zwirner, *Phys. Lett.* **B257** (1991) 83.
H.E. Haber and R. Hempfling, *Phys. Rev. Lett.* **66** (1991) 1815.
- [4] J. Kodaira, Y. Yasui and K. Sasaki, *Phys. Rev.* **D50** (1994) 7035.
R. Hempfling and A. H. Hoang, *Phys. Lett.* **B331** (1994) 99;
J.A. Casas, J.R. Espinosa, M. Quirós and A. Riotto, *Nucl. Phys.* **B429** (1995) 466 and *Nucl. Phys.* **B436** (1995) 3.
- [5] P. Abreu et al., DELPHI Coll., *Z. Phys.* **C67** (1995) 69.
- [6] P. Aarnio et al., DELPHI Coll., *NIM* **A303** (1991) 233.
- [7] P. Abreu et al., DELPHI Coll., *CERN-PPE 94-08*.
- [8] S. Bethke et al., *Phys. Lett.* **B213** (1988) 235.
- [9] G.C. Fox and S. Wolfram, *Phys. Lett.* **B82** (1979) 134.
- [10] R. G. Jacobsen, *SLAC 381* (July 1991).
- [11] T. Sjöstrand, *Comp. Phys. Comm.* **30** (1986) 347.
- [12] F. Abe et al., *Phys. Rev. Lett.* **73** (1994) 225.
- [13] See e.g. A.B. Lahanas and D.V. Nanopoulos, *Phys. Rep.* **145** (1987), 1.
- [14] J. Bagger, S. Dimopoulos and E. Masso, *Phys. Lett.* **B156** (1985) 357.

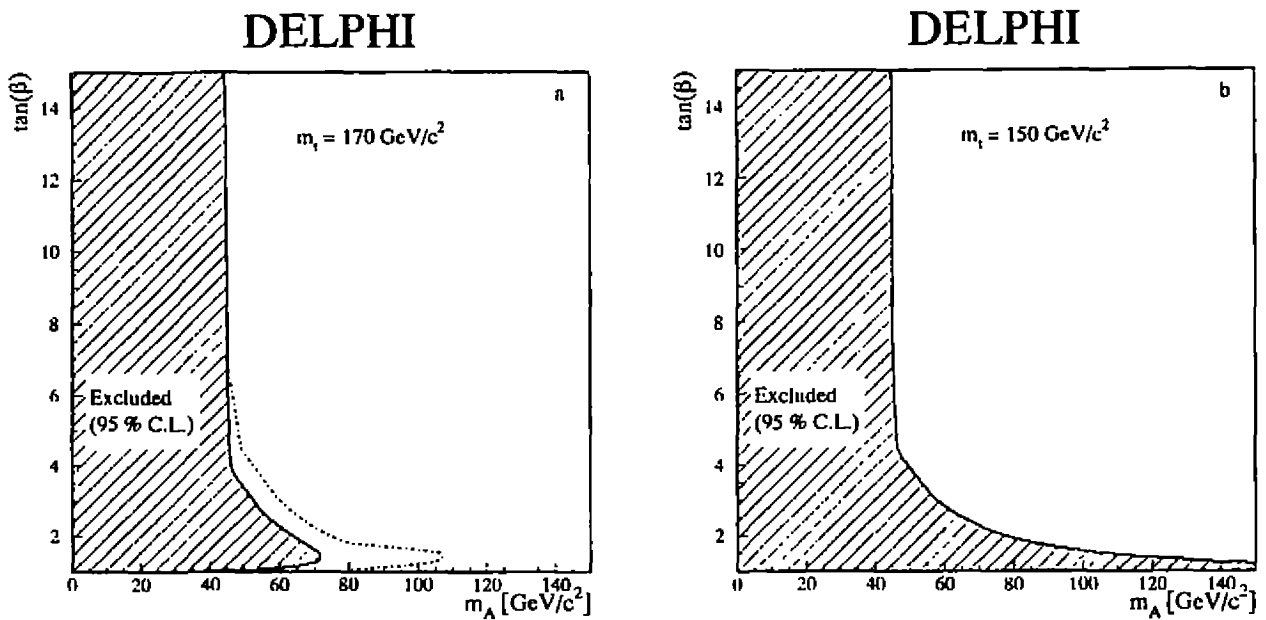


Figure 4.: $\tan\beta/m_A$ limit contour (at 95 % confidence level) obtained from searches for hA and hZ^* channels in the MSSM case with $m_{3q}=1 \text{ TeV}/c^2$. The two figures correspond to : a. $m_t=150 \text{ GeV}/c^2$ and b. $m_t=170 \text{ GeV}/c^2$. In a, the dash-dotted line indicates the preliminary result using the data from 94 and 95.

A Medida de R_b no DELPHI/LEP

Miriam Gandelman e Ronald Shellard

O Modelo Padrão tem sido testado exaustivamente pelas experiências do LEP 1 com precisão sensível às correções quânticas do modelo. Essa grande precisão permitiu prever a massa do quark top, por exemplo, e pode ainda ser sensível para o estudo dessa possível discrepância já que nesse ano foram coletados um número de eventos igual à soma dos eventos coletados em todos os outros anos e portanto podemos dobrar a estatística existente. Além disso é muito importante do DELPHI [2], o ano de 1994 é ainda mais especial pois nesse ano foi instalado um novo detetor vértices tri-dimensional fundamental para essa medida, como explicado a seguir.

Uma vez que a identificação de um evento onde há produção de quark b se dá pela evidência do decaimento de um méson B, o detetor mais importante para a identificação desses eventos é o detetor de vértices que tem resolução suficiente para separar os vértices de produção e decaimento desses mésons. Os primeiros detetores desse tipo u Com o intuito de melhorar ainda mais a identificação de quarks b, foi desenvolvida uma primeira geração de detetores tridimensionais, constituídos por duas placas de detetores com apenas um lado sensível, coladas uma de encontro à outra, o que dobra a quantidade de material a ser atravessada pelas partículas detetadas. Recentemente foi desenvolvida uma nova tecnologia que permite construir detetores tridimensionais com a mesma quantidade de material que os bidimensionais [4]. Esses novos detetores têm duas camadas de *strips* perpendiculares entre si implantadas na mesma placa de silício e também duas camadas metálicas, o que permite que a leitura seja feita na mesma extremidade do detetor. A colaboração DELPHI foi a primeira a construir e instalar um detetor que usa essa tecnologia, em 1994.

Nesse trabalho foram apresentados os resultados da análise de dados feita no DELPHI utilizando como método para a identificação de eventos onde houve a produção de um par $b\bar{b}$ o método do parâmetro de impacto [5]. Com esse método obtivemos uma pureza de seleção de 95% para uma eficiência de 17%. Para um mesmo valor de pureza esse resultado é 70% mais eficiente que o obtido com os dados de 1993 quando tínhamos um detetor bi-dimensional. A curva de eficiência versus pureza para os anos de 1993 e 1994 pode ser visto na figura [1].

Os resultados obtidos nessa análise podem ser vistos na figura[2], onde os erros na figura são a soma em quadratura dos erros estatístico e sistemático. Fazendo a medida para 95% de pureza, o que nesse gráfico significa ler o valor para $\log_{10}(prob) = 4.4$, o valor obtido é:

$$R_b = 0,2164 \pm 0,0019(stat) \pm 0,0020(sist) \pm 0,0017(R_c\ sist) \quad (1)$$

Onde o erro relativo à variação de R_c é colocado explicitamente, já que a medida depende diretamente desse valor que pode ser a média dos valores medidos ou o valor previsto pelo Modelo Padrão. O resultado obtido é compatível com as previsões do Modelo padrão e com as demais medidas feitas em 1994 no LEP.

References

- [1] J. Ellis *et al.*, CERN-TH/95-202
- [2] DELPHI Collaboration, The DELPHI detector at LEP, NIM A303 (1991) 233.
- [3] N. Bingefors *et al.*, The DELPHI Microvertex detector, NIM A328 (1993) 447.
- [4] Vertex Detector DELPHI Collaboration, The DELPHI Silicon strip Microvertex detector with double sided readout, NIM A368 (1996) 314.
- [5] D. Brown e M. Frank, ALEPH 92-135 ou PHYSICS 92-124.

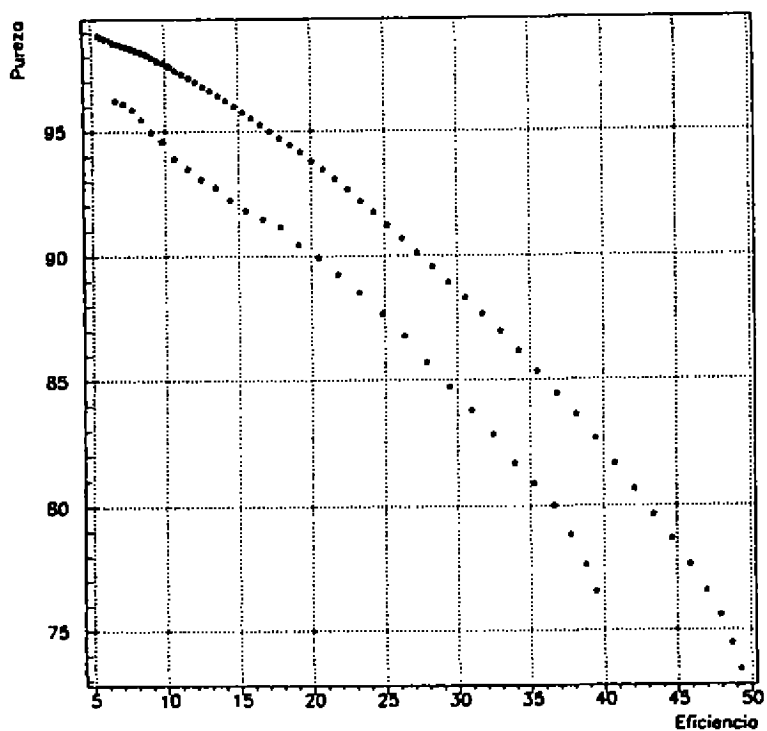


Figura 1. Eficiência versus pureza. A curva superior representa os dados de 1994 e a inferior, os de 1993.

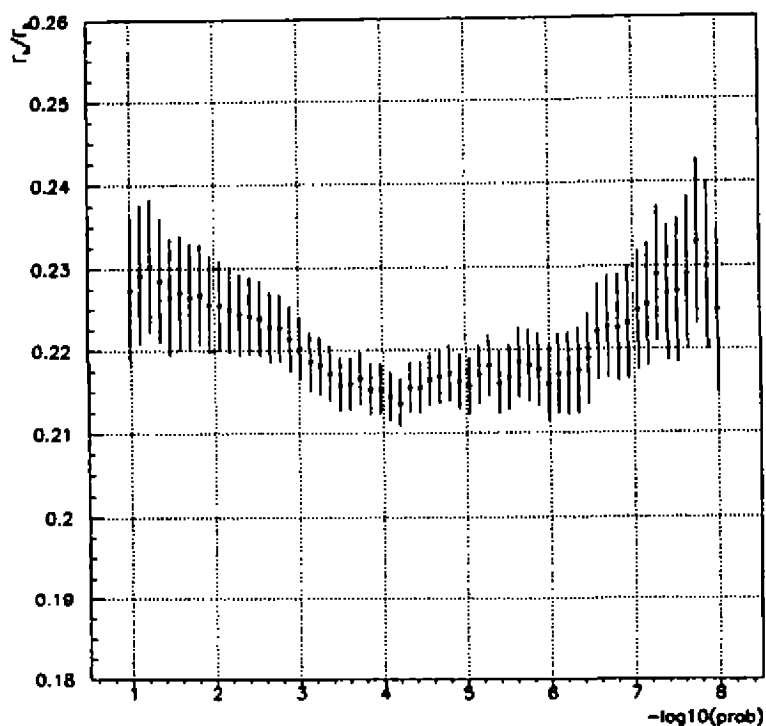


Figura 2. R_b como função do corte na probabilidade. O erro nesse caso é a soma em quadratura do erro estatístico e da estimativa do erro sistemático.

Synchrotron Radiation Monitoring for LEP2 using the DELPHI-TPC Silicon Detector

M. A. Gaspar, M. Barbi, B.M. Maréchal, L. de Paula
(*Instituto de Física - UFRJ*)

P. Siegrist, M. Besançon, T. Bolognese, X. Bravo, M. Gros,
J. P. Passerieux, F. Pierre, J. Poinsignon, D. Vilanova

(*CEN-Saclay, France*)
E. Merle, J. Renaud
(*CERN, Geneva*)

Partially supported by EC (Contract CII*-CT94-0118)

1- Motivation

The Time Projection Chamber/TPC (fig.1) of the DELPHI detector suffers contamination due to Synchrotron Radiation (small ionized cloud with slow drift velocity which causes a magnetic field perturbation), specially during the new phase of operation of the LEP2. Therefore one needs to monitor this radiation by means of an independent detector. This detector, which has been developed during the last 20 months, uses the silicon technique and allows precise measurements of both the energy and time of flight of the photons, either direct, or back-scattered by the quadrupoles, masks or collimators in front of the TPC (see fig. 2). Typical time delay and energy range are of the order of 50 ns and 100 to 400 KeV, respectively. The detector being independent of the DELPHI acquisition system, it allows a good monitoring task that can give some clue on the state of the beams and non-stop trace plot. In addition, MIP's monitoring (e^+ and e^- that escape from the beam pipe) can be done.

2- First tests (1995): Design and Results

During the year 1995 two prototypes have been installed on side C of the TPC (one between the collimators, 1.9 m from the Intersection Point, and the other outside, 6.3 m from this IP - see fig. 2). The design of the detectors was:

- * One plate/prototype
- * 24 strips/plate (either single or double-sided)
- * Plate surface and thickness: $40 \times 50 \text{ mm}^2$ and $300 \mu\text{m}$
- * Strip surface: $2 \times 40 \text{ mm}^2$

The acquisition system (fig. 3) consisted of 2 Amplifiers, 2 Constant Fraction Discriminators, ADC (12 channels) and TDC modules, CAMAC electronics and a VME computer (OS9 system). The time and energy resolutions have been found to be 3.4 ns and 6.4 KeV and the peak energies about 90 KeV for MIPs and 56 KeV for photons, the LEP being running at 130 GeV. The counting rate was about 0.5 Hz during the physics regime. Prior to any beam measurements, the detectors were energy calibrated using an Am^{241} source. Using double-sided strips, it has been proved that MIP's and photon separation was possible.

3- Set-up and results during 1996

The final set-up for normal operation was defined as shown in fig. 4, the Gamma monitor consisting now of:

- * 4 modules on each side of the TPC
- * 1.9 m from the Intersection Point (close to the TPC laser box)
- * 24 strips/module
- * 12 channels/module (double strips!) - 96 total

The acquisition system is using the DELPHI Standard Fastbus, 96-channel ADC-1885F and TDC-1877 LeCroy modules, crates CAMAC for the discriminators and the shapers and the OS9 system. Figs. 5 and 6 show the results of energy calibration with an Am^{241} source and the time and energy spectra obtained, the LEP being running at 160 GeV center of mass energy. Separation of photons coming up from e^+ and e^- synchrotron radiations is shown in fig. 7. As may be observed in fig. 8, the synchrotron radiation, important during the squeezing regime, appears also from time to time during the physics (normal data taking) regime.

4- Present status and Conclusions

The gamma monitor is now installed and ready for normal operation, sending a signal to Background-1 (Synchrotron+MIP's) trace-plot at control room, being so able to give information on beam state. Some problems concerning the discrimination between photons and MIP's above 60 KeV are still to be solved. With higher rates, and so with higher statistics, one expects to be able to identify the synchrotron sources (Qpoles, collimators, tungsten mask).

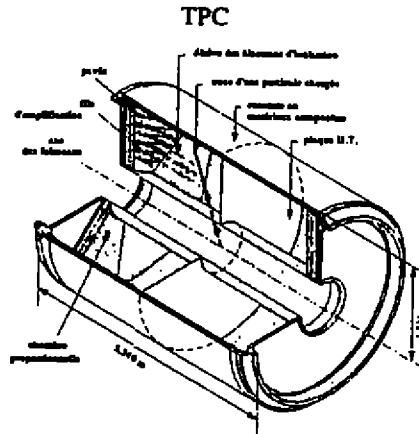


Fig. 1: Schematic view of the DELPHI Time Projection Chamber

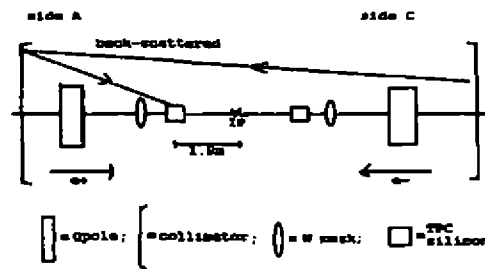


Fig. 2: Localization of the TPC silicon detectors

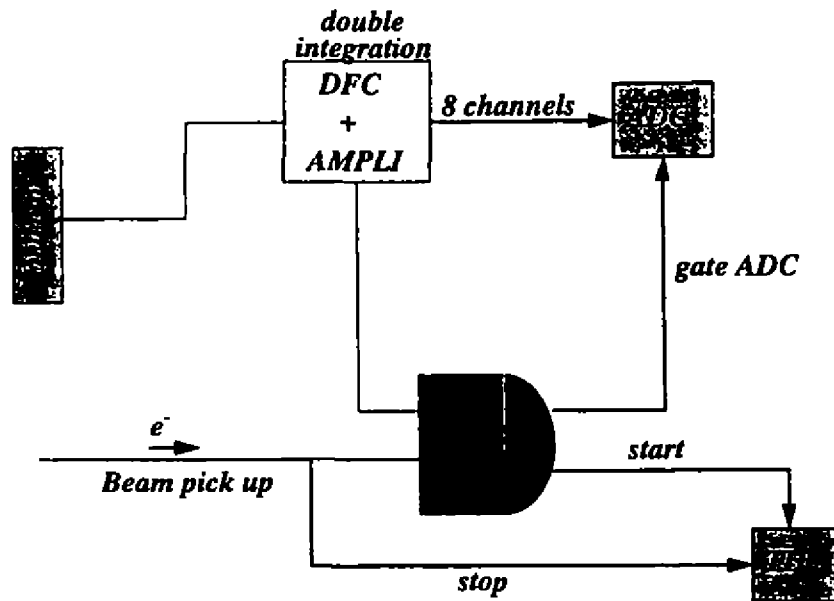


Fig. 3: Principle of the acquisition system for the Gamma monitor

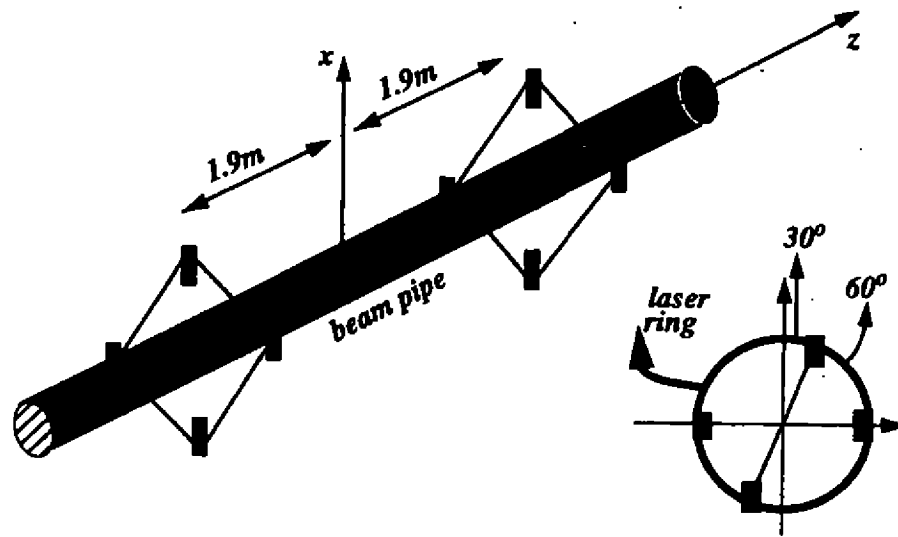


Fig. 4: Spatial distribution of the 8 modules of the Gamma monitor

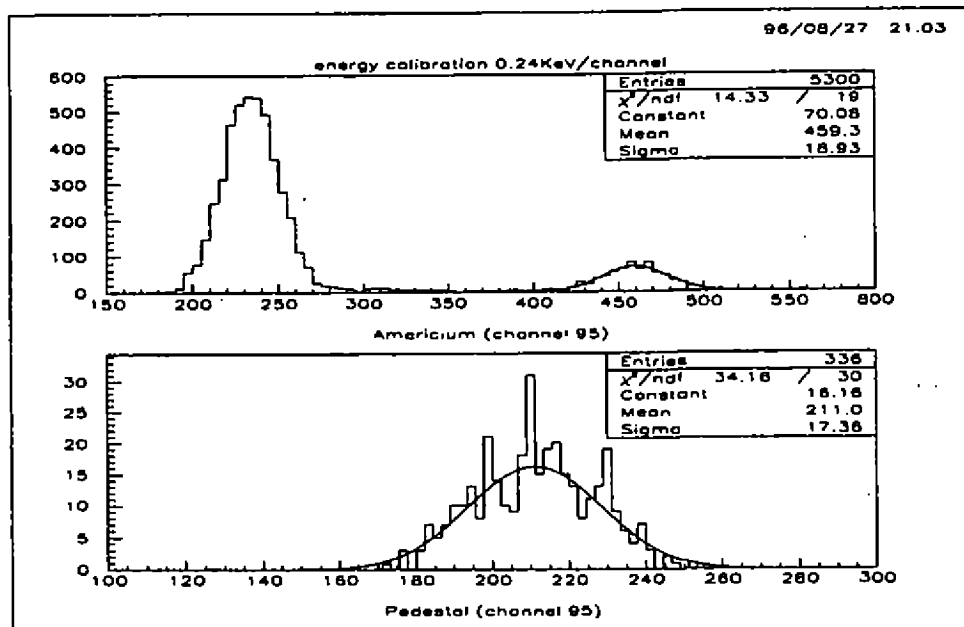


Fig. 5: Energy calibration of the silicon strips using Am²⁴¹

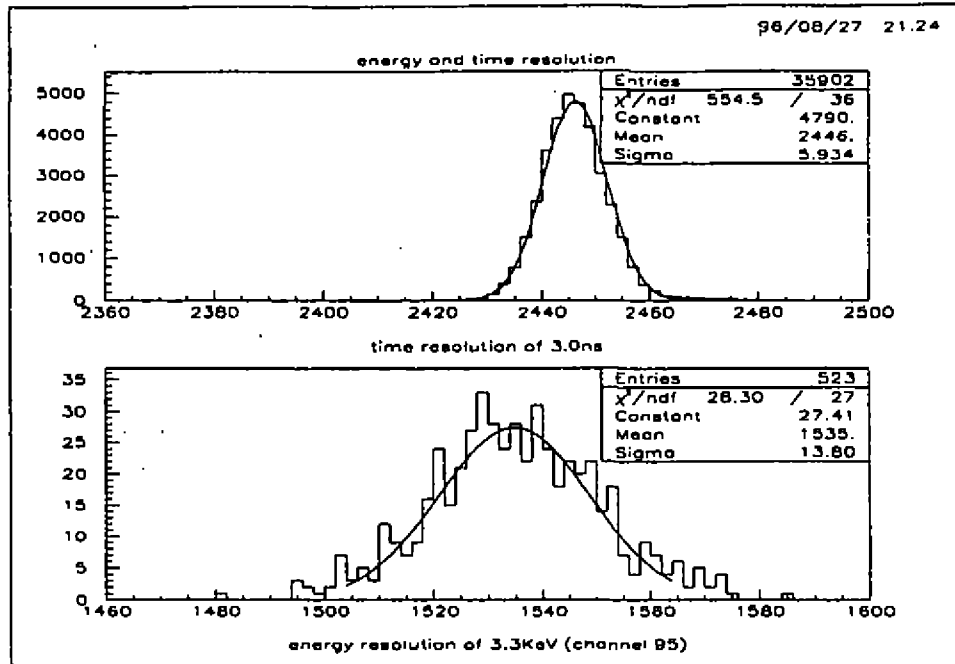


Fig. 6: Energy and time resolutions of the Gamma monitor

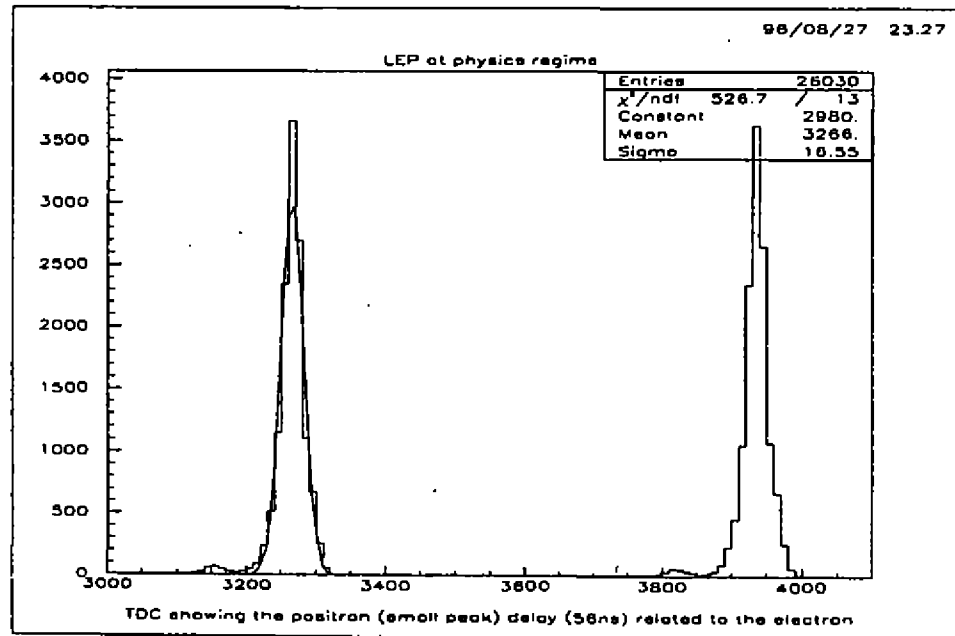


Fig. 7: Photons peaks for two successive bunch trains. While the higher peaks are due to direct photons produced by the electron beam, the small ones are back-scattered photons associated to the positron beam.

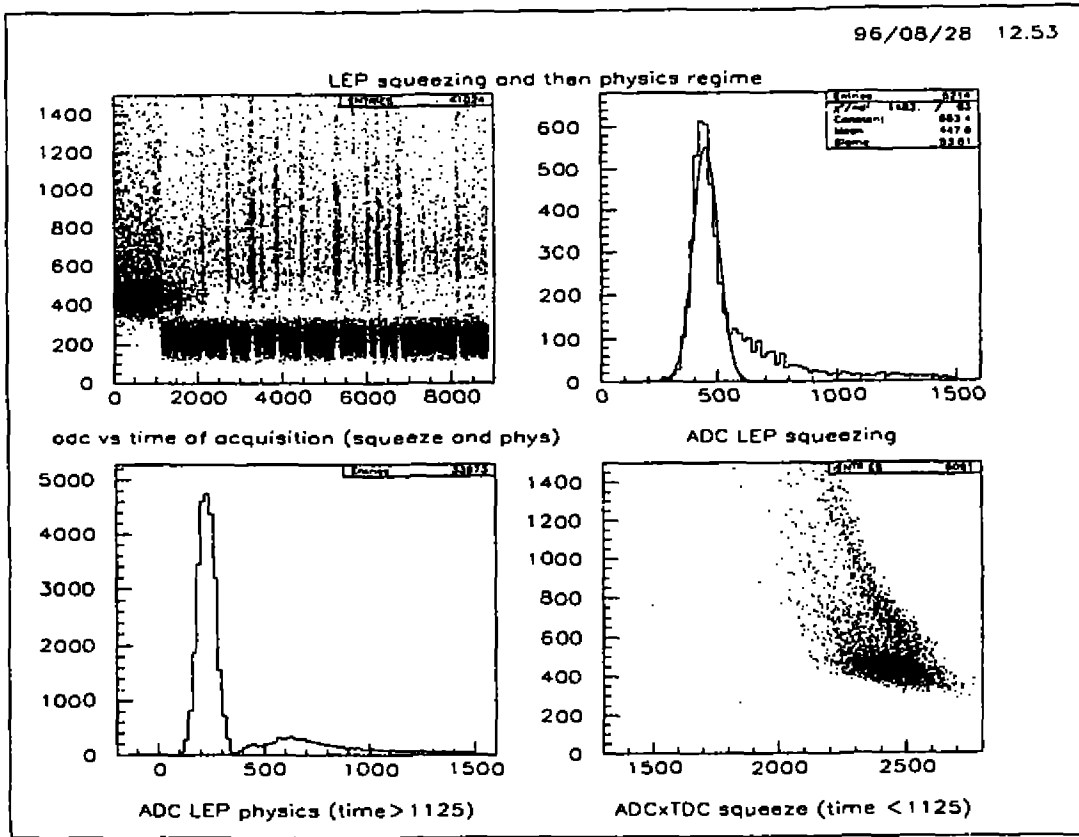


Fig. 8: Time distribution of the radiation synchrotron during a typical LEP operation. A clear difference can be noted between squeezing and physics regime.

DELPHI Event Server

L. M. Mundim

CBPF/LAFEX

R. Xavier Sigaud, 150 - 22290-180 Rio de Janeiro

A *World-Wide Web* - WWW - é o ramo das telecomunicações que sofreu um dos maiores saltos tecnológicos já visto na atualidade. Em pouco mais de 3 anos, ela saiu dos laboratórios e passou a atender as necessidades de pessoas comuns (atendendo a uma variada gama de aplicações como acesso a jornais, publicidade, jogos, etc...) até as de grandes instituições como o CERN, onde foi criada e desempenha um papel fundamental, mesmo no controle de experiências, como no sistema *Online* do DELPHI [1]

1 Introdução

Em um grande experimento como o DELPHI, apesar de se obter eventos aos milhares por dia, existem certas tarefas que são executadas na base de um único evento, como por exemplo estudo de subdetectores, *debug* e desenvolvimento de *software* de reconstrução, além da visualização gráfica de eventos de interesse especial.

A fim de suprir essa necessidade no âmbito da Colaboração DELPHI, foi desenvolvido o *DELPHI Event Server* (DES), partindo de alguns requisitos básicos, tais como rodar em sistema operacional Unix, usar uma interface padronizada e ser facilmente acessível dentro e fora do CERN. O resultado foi um pacote de programas modular que utiliza como interface entre o usuário e os programas do DELPHI os navegadores da WWW.

A escolha do WWW foi fundamental para se cumprir com os requisitos de padronização e acessibilidade, pois assim o DES pode ser acessado de qualquer computador no mundo que esteja ligado à internet (desde que seja autorizado a acessar os dados do DELPHI), utilizando um terminal gráfico ou simplesmente um terminal texto normal.

2 Estrutura do DES

O DES fornece ao físico três opções:

1. LIST - verifica em qual fita se encontra um dado evento;
2. PICK - copia um dado evento, enviando-o no formato *raw data*¹;
3. DELANA - reconstrói o evento usando o programa DELANA [2].

O DES é composto de dois módulos principais, um para receber e processar uma determinada tarefa requerida pelo usuário, chamada *SUBMIT*² e outro responsável em fornecer informações sobre o estado dos pedidos que tenham sido feitos, chamado *QUERY*.

Estes módulos consistem por sua vez de outros módulos menores que podem ser divididos em dois níveis. O primeiro nível, constituído de uma interface CGI [3], é responsável pela interpretação dos dados enviados pelo navegador da WWW (netscape, mosaic, etc.) e o segundo nível, constituído de todos os programas necessários à execução da tarefa requerida pelo usuário, de acordo com as informações processadas no primeiro nível.

¹ O evento como foi originalmente medido pelo detector, sem reconstrução.

² Alguns termos em inglês vão ser mantidos neste artigo.

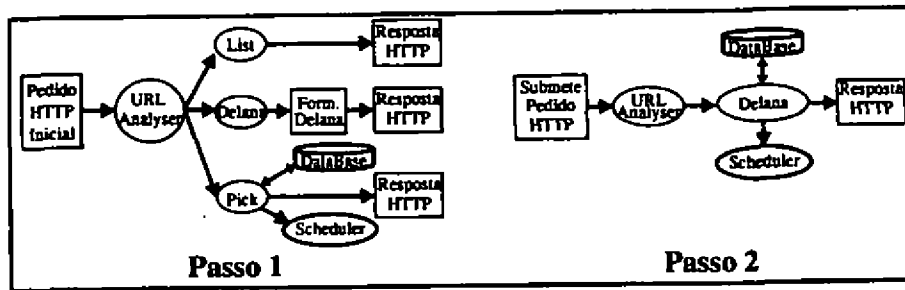


Figura 1. Fluxo de dados do módulo *SUBMIT*, responsável pelo processamento das opções Delana, List, Pick.

A CGI do módulo *SUBMIT* é composta de um analisador de URL (*Uniform Resource Locator* [4]), o *URL Analyser* e dos sub-módulos *Delana*, *List* e *Pick* (veja fig. 1), enquanto que a CGI do módulo *QUERY* é constituída dos sub-módulos *URL Analyser*, *GetStatus*, *DiscardFile* e *SendFile* (veja fig. 2).

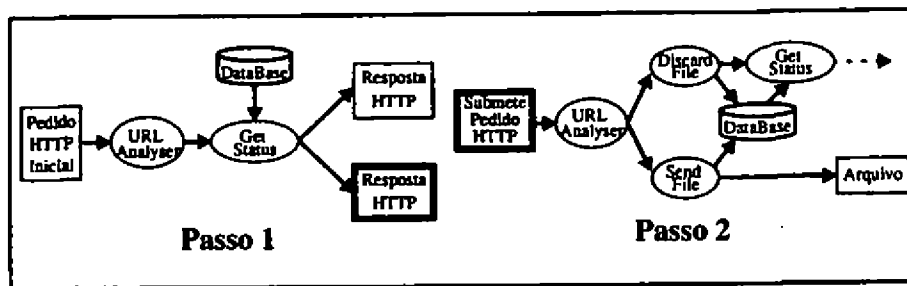


Figura 2. Fluxo de dados do módulo *QUERY*, que verificar e informar o usuário a respeito do estado em que se encontra uma tarefa submetida.

O *URL Analyser* checa a consistência do pedido HTTP (*HyperText Transfer Protocol* [4]) e o envia aos sub-módulos correspondentes à opção escolhida, que se encarregam de executar os programas oficiais do DELPHI. A função dos outros módulos é explicada a seguir.

2.1 Fluxo de dados do módulo *SUBMIT*

O sub-módulo *List* fornece a informação ao usuário imediatamente, pois não necessita de nenhum processamento complexo. Ele se comunica com o banco de dados FATMÉN [5], formata a informação obtida em linguagem HTML [4, 3] e a envia usuário.

Os sub-módulos *Delana* e *Pick*, como demandam operações mais complexas, como cópia de fita em disco (cerca de 200 Mbytes), necessita de um esquema de filas de execução. O usuário receberá ao final do processo de submissão um documento HTML informando se o DES recebeu corretamente o pedido e nesse caso, a identificação do mesmo também é fornecida. Essa identificação corresponde a um número único, que em caso de erro posterior, servirá para que o gerenciador do DES possa verificar as causas do problema.

O sub-módulo *Pick* recebe as informações do *URL Analyser*, atualiza o banco de dados e envia o pedido para uma fila de execução. A posição deste pedido na fila dependerá do número de pedidos a serem executados e de quantos pedidos do usuário em questão estão esperando para serem processados.

O sub-módulo *Delana* é um caso especial e exige dois passos para completar a submissão de um pedido, como abaixo:

1. ao receber o pedido inicial do usuário, o sub-módulo *Delana* envia de volta um formulário HTML [3] com as opções adicionais para o programa DELANA [2], que permitirá ao usuário alterar a configuração do mesmo;

2. o formulário criado no passo anterior é submetido novamente ao DES, repetindo o item anterior, porém ao checar que as informações necessárias ao DELANA estão completas, o sub-módulo Delana remete o pedido à fila para execução.

2.2 O fluxo de dados do módulo *QUERY*.

Este módulo também funciona em dois passos (veja a fig. 2), fornecendo a informação requerida imediatamente. No passo 1 o URL Analyser envia o pedido ao sub-módulo GetStatus, o qual se comunica com o banco de dados do DES, verificando se existe algum pedido submetido pelo usuário em questão e o estado dos eventuais pedidos. A informação é enviada em duas formas, dependendo deste estado:

- **nenhum pedido recebido ou pedido na fila de execução:** uma simples mensagem informando que não houve nenhum pedido deste usuário ou a posição do(s) pedido(s) na fila, respectivamente;
- **pelo menos um pedido concluído:** um formulário HTML que possibilitará o usuário copiar os arquivos com as mensagens do programa executado ou o evento em si (*raw data* ou o resultado da reconstrução) ou ainda apagar do banco de dados o presente pedido, caso o mesmo não interesse mais ao usuário. É também incluído a posição de pedidos que estejam esperando para serem processados, se existirem.

O segundo passo só é executado caso a resposta enviada ao usuário no primeiro passo seja um formulário (item 2 acima). Neste caso, o URL Analyser envia as informações para os sub-módulos DiscardFile ou SendFile dependendo da ação requerida pelo usuário. No primeiro caso, este sub-módulo se comunica com o banco de dados do DES, atualizando-o e executa o sub-módulo GetStatus, voltando ao passo 1, conforme já explicado acima. No segundo caso, o sub-módulo SendFile simplesmente envia o arquivo para o usuário e atualiza o banco de dados.

3 Conclusões

Apesar de esta ter sido uma versão de teste e desenvolvimento do DES atual, ela realizou todas as tarefas para a qual tinha sido planejada com uma performance além da esperada, pois manteve-se em operação durante 11 meses processando dezenas de pedidos por dia e com uma taxa de erros muito baixa.

Este período coincidiu com a fase LEP1.5 (o LEP operando com energia no centro de massa de 140 GeV) e início do LEP2 (200 GeV), justamente o período onde a necessidade de se estudar eventos individualmente foi maior, devido aos testes de novas versões de *softwares* e procura por eventos exóticos.

O DES veio provar mais uma vez os benefícios da WWW em um ambiente característico da Física de Altas Energias, ou seja, grandes colaborações onde é fundamental propagar informações para centenas de pessoas espalhadas em várias partes do mundo.

References

- [1] M. Dönszelman, D. Carvalho, L. M. Mundim, S. Du, K. Rodden and F. Tennebo, " *Advanced Use of World-Wide Web in the Online System of Delphi*, Computing for High Energy Physics 95 - CIIEP95, Rio de Janeiro, (1995).
- [2] Delphi Collaboration, " *Delphi Data Analysis Program (DELANA) - User's Guide*", Internal Delphi Note, 89-44 PROG 137, CERN, Geneva, Switzerland (1989).
- [3] NCSA Team, " *CGI, Common Gateway Interface (specification)*", <http://hoohoo.ncsa.uiuc.edu/cgi/overview.html>, (1994).
- [4] T. J. Berners-Lee, R. Cailliau, J. F. Groff and B. Pollermann, " *World-Wide Web: The Information Universe*", Electronic Networking: Research, Applications and Policy, 2(1), pp.52-58 (1992).
- [5] CN/AS Division, " *FATMEN*", CERN Program Library Long Write-up Q123, CERN, Geneva, Switzerland (1993).

Eventos Denominados Centauro

S.L.C.Barroso¹, P.C. Beggio¹, A.O. de Carvalho¹, M. D.D.O.Marques¹,
R. de Oliveira¹, E.H.Shibuya¹, C.R.A. Augusto², C.E. Navia², F.A. Pinto²

1. Departamento de Raios Cósmicos e Cronologia,
Instituto de Física 'Gleb Wataghin', UNICAMP

2. Instituto de Física, Universidade Federal Fluminense

December 2, 1996

A CBJ-Colaboração Brasil Japão de Raios Cósmicos observou alguns eventos (Interações Hadrônicas) com características inusitadas, denominados CENTAURO. Entre estas características podemos citar a significativamente alta multiplicidade de hádrons e a significativamente baixa multiplicidade de fótons produzidos na Interação, quando comparadas às respectivas multiplicidades dos eventos normais. Outra destas características é o alto momento transversal médio dos secundários, novamente quando comparado aos eventos normais. Serão apresentadas neste trabalho características como distribuições de energia fracionária, angular e de momento transversal de dois destes eventos (detectados pela CBJ), selecionados devido a determinação direta de seus pontos de interação (vértices). Ambos apresentam características de decimento isotrópico e momento transversal médio da ordem de 1 GeV/c. A interpretação dada é de que se trata de eventos indicadores de Produção Múltipla de Bárions e Anti-Bárions.

I Breve descrição do detector

O detector é constituído de duas câmaras. Cada câmara é composta por um arranjo de blocos. Os blocos estão arrumados como azulejos em um piso. Cada azulejo seria um bloco, e o piso seria a câmara, sendo que não há espaço entre os blocos adjacentes de uma mesma câmara. Um bloco consiste de uma pilha de envelopes contendo material fotossensível, com placas de chumbo intercaladas entre os envelopes. Cada envelope contém em geral dois filmes de Raio-X e uma placa de Emulsão Nuclear. As duas câmaras estão separadas por um alvo de material rico em carbono e por um vão livre de cerca de 1,7 m. Cada bloco mede cerca de 40 cm x 50 cm. O número de blocos por câmara e o número de envelopes por bloco varia de acordo com a câmara. O detector é capaz de registrar os fótons (mais especificamente, a parte carregada das cascatas eletromagnéticas produzidas por estes fótons¹) produzidos direta ou indiretamente pela Interação Hadrônica. Basicamente, ele fornece a energia (ver [2], [3] e [4]), os ângulos zenital e azimutal, e a posição de cada fóton detectado. Para maiores detalhes ver [1].

II Métodos de análise

O conjunto de fótons provenientes de uma mesma Interação Hadrônica é denominado família. De acordo com a região do detector onde ocorreu a Interação Hadrônica (IH), seus secundários o detector), C-Jatos (IH no alvo de carbono) ou Pb-Jatos (IH numa placa de chumbo). A altura do ponto onde ocorreu a IH, ou simplesmente a altura de interação, é também determinada. No caso destes dois eventos (ou famílias), a altura foi determinada por triangulação, que consiste basicamente em determinar-se a separação entre os vários chuveiros da família em diversas camadas.

Identificadas as famílias, verifica-se então se cada uma delas é realmente resultante de uma única IH com produção isotrópica de secundários. Isto é feito usando-se uma relação, chamada de \mathcal{R} , dada por:

$$\mathcal{R}_{\theta_n} = \frac{\sum_{i=1}^n E_{\gamma_i} \sum_{i=1}^n E_{\gamma_i} \theta_{\gamma_i}^2}{\left(\frac{4}{\pi} \sum_{i=1}^n E_{\gamma_i} \theta_{\gamma_i} \right)^2}, \quad \theta_{\gamma_i} \leq \theta_{\gamma_{i+1}} \quad (1)$$

¹ Chamada simplesmente de chuveiro.

onde:

- θ_{γ_i} é o ângulo de incidência do i -ésimo γ ,
- E_{γ_i} é a energia do i -ésimo γ .

Supondo decaimento isotrópico no referencial de repouso do Estado Intermediário, obtêm-se, para a expressão analítica de \mathcal{R} :

$$\mathcal{R}(\theta, \Gamma) = \left(\frac{\pi}{2}\right)^2 \frac{(\Gamma^2\theta^2 + 2)\Gamma^6\theta^6}{[(1 + \Gamma^2\theta^2)^2 \arctan(\Gamma\theta) - (1 - \Gamma^2\theta^2)\Gamma\theta]^2} \quad (2)$$

onde:

- Γ é o fator de Lorentz do Estado Intermediário.

A qualidade do ajuste da expressão 2 aos pontos experimentais obtidos usando-se a expressão 1, permite avaliar se a família é resultante de uma única IH isotrópica. Os dados que atendem a tal critério são então submetidos a um segundo algoritmo, chamado de mDW, em referência a sua semelhança com o algoritmo de Duller-Walker[5]. A expressão do mDW é dada por:

$$mDW_n = \frac{1}{4M\Gamma} \left[\sum_{i=1}^n E_{\gamma_i} + \frac{4}{\pi} \sum_{i=1}^n E_{\gamma_i} \Gamma \theta_{\gamma_i} + \sum_{i=1}^n E_{\gamma_i} + \frac{4}{3\pi} \sum_{i=1}^n E_{\gamma_i} (\Gamma \theta_{\gamma_i})^3 \right], \quad \theta_{\gamma_i} \leq \theta_{\gamma_{i+1}} \quad (3)$$

Nota-se então que o conjunto de dados se divide em grupos. A cada grupo associa-se um Estado Intermediário Discreto² diferente, batizados de Mirim, Açú, Guaçú e Centauro.

III Conclusões

Na figura 1 nota-se como as IH parecem se dividir em alguns tipos diferentes. Na figura 2 vemos a distribuição de energia fracionária dos dois Centauros (neste gráfico os fótons não foram diferenciados dos hádrons). Nota-se como as distribuições dos dois são semelhantes, indicação de que são eventos do mesmo tipo. Na tabela 1 são mostradas algumas grandezas características de cada um destes tipos.

Uma das características dos Centauros que mais se destaca é a baixa multiplicidade de chuveiros iniciados por fótons. Neste ponto cabe uma pequena explicação sobre os critérios usados para se identificar uma cascata iniciada por um fóton e uma iniciada por um hádron. Nas IH's comuns (Mirim e Açú) ocorre o fenômeno conhecido como Produção Múltipla de Mésons (PMM). Dentre estes, o π (carregado ou neutro) é o mais abundante. A maioria dos chuveiros detectados, neste caso, é proveniente dos fótons (produzidos aos pares) no decaimento do π^0 ($\pi^0 \rightarrow \gamma + \gamma$), cuja vida média é muito menor que a dos seus "irmãos" carregados. Os chuveiros destes fótons (que são identificados como γ 's) começam, na grande maioria das vezes, nas primeiras camadas da câmara. Os pions carregados, por sua vez, podem interagir hadronicamente com as placas de chumbo do detector (Pb-Jato), na maioria dos casos em profundidades bem maiores (nas últimas camadas do detector). Esta segunda IH irá resultar em uma segunda PMM, e consequentemente em mais π^0 's, que por sua vez vão produzir mais fótons cujos chuveiros serão detectados. Este tipo de chuveiro será identificado como hádron. Desta definição surge o primeiro critério para se identificar um chuveiro como γ ou hádron, a profundidade em que o mesmo começa. Chuveiros "rasos" são γ 's, chuveiros profundos são hádrons. O segundo critério está relacionado com a variação do tamanho da cascata (número de partículas³) em função da profundidade na câmara. Um hádron secundário pode sobreviver a primeira IH e interagir novamente produzindo um segundo Pb-Jato. Analisando então a curva número de partículas x profundidade deste chuveiro (que na realidade são dois), observar-se-ão dois picos. A chance de um chuveiro iniciado por fóton apresentar um comportamento deste tipo é muito baixa⁴. O terceiro critério está associado a diferença de resolução dos materiais fotossensíveis utilizados. Os chuveiros são observados como manchas nos filmes de Raios-X, e traços (dos e^{+-}) nas

²Em vários modelos para IH's, costuma-se supor a formação de um Estado Intermediário entre a colisão e o decaimento. Em geral este Estado Intermediário (EI) é um objeto termodinâmico que decai ao atingir equilíbrio térmico. Este tipos de EI's são conhecidos na literatura como *bolas de fogo*.

³Estas partículas são de fato elétrons e pósitrons, produzidos pelos vários fenômenos eletromagnéticos envolvidos no desenvolvimento do chuveiro.

⁴Na realidade a chance é nula, mas casos extremos (falha no material fotossensível, por exemplo) de falhas experimentais podem levar a picos falsos na curva.

Placas de Emulsão Nuclear. No caso de um chuva iniciado por hádron, a mancha do filme de Raios-X pode aparecer com varios nucleos de traços de e^{+-} na Placa de Emulsão, devido aos vários pions produzidos nas IH dos Pb-Jatos. Novamente, a chance de um chuva iniciado por fóton apresentar um comportamento como este (principalmente se o número de núcleos for maior que dois) é muito baixa.

Assim, a maioria dos componentes dos dois eventos do tipo Centauro foram identificados como hádrons e a sua multiplicidade é bem maior que a dos eventos normais. Isto poderia ser explicado supondo que, por algum motivo, π^0 's não foram produzidos na IH do primario. Entretanto corrigindo-se o momento transversal médio de hádrons em forma de fótons ($P_{t_h}^{(\gamma)}$), usando-se uma multiplicidade média de 0.3 e levando em conta que só é detectada a parte eletromagnética da IH, obtém-se $\langle P_{t_h} \rangle$ da ordem de 1 GeV/c para os Centauros⁵. Como as famílias Centauro analisadas foram produzidas isotropicamente (segundo o algoritimo usado para verificar isotropia, figuras 1 e 5, podemos descreve-las através de modelos termodinâmicos para IH. Tais modelos mostram que há uma relação entre $\langle P_t \rangle$ do Estado Intermediário e a(s) massa(s) da(s) partícula(s) produzida(s). Seguindo esta linha de raciocínio, o valor de 1 GeV/c para o $\langle P_t \rangle$ do Centauro pode ser visto como sinal da produção de partículas mais pesadas que aquelas produzidas nos eventos normais (Mirim e Açú). Assim, o valor relativamente alto de $\langle P_t \rangle$ dos Centauros, associado a esta singular multiplicidade de hádrons e fótons, sugere que os Centauros sejam resultantes não do fenômeno de *Produção Múltipla de Mésons* com supressão de π^0 's, mas sim de uma *Produção Múltipla de Bárions e Anti-Bárions*.

		fótons		π^0		hádrons	
		$\langle N_\gamma \rangle$	$\langle P_t \rangle$ (MeV/c)	$\langle N_{\pi^0} \rangle$	$\langle P_t \rangle$ (MeV/c)	$\langle N_h \rangle$	$\langle P_{t_h}^{(\gamma)} \rangle$ (MeV/c)
Mirim	A-Jatos	7 ± 0.4	168 ± 13	2.5 ± 0.3	280 ± 17	-	-
	C-Jatos	7 ± 0.5	125 ± 11	2.5 ± 0.4	192 ± 14	-	-
Açú	A-Jatos	15 ± 0.4	385 ± 20	4.6 ± 0.3	547 ± 23	-	-
	C-Jatos	17 ± 0.6	258 ± 16	6.4 ± 0.6	387 ± 20	-	-
Centauro 1	A-Jatos	-	-	-	-	42 ± 2	366 ± 56
Centauro 5	A-Jatos	-	-	-	-	39 ± 4	267 ± 43

Table 1: Resumo dos resultados obtidos. $\langle N_\gamma \rangle$, $\langle N_{\pi^0} \rangle$ e $\langle N_h \rangle$ são, respectivamente, as multiplicidades médias por IH de fótons, π^0 's e hádrons.

References

- [1] • M.Akashi & outros, Prog. Theor. Phys. Suppl. 32 (1964), 1-2
• Chacaltaya Emulsion Chamber Experiment, Prog. Theor. Phys. Suppl. 47 (1971), 1-125
- [2] • B.Rossi & K.Greisen, Rev. Mod. Phys. 13 (1941), 240-309
• K.Kamata & J.Nishimura, Prog. Theor. Phys. Suppl. 6 (1958) 93-154
• J.Nishimura, Prog. Theor. Phys. Suppl. 32 (1964), 72-81
• J.Nishimura, Handbuch der Physik (Springer Verlag), XLVI/2 (1967), 1-114
- [3] • I.Ohta Prog. Theor. Phys. Suppl. 47 (1971), 271-299
• I.Ohta & outros, Nucl. Inst. Meth. 161 (1979), 35-43
- [4] • M.Okamoto & T.Shibata, Nucl. Inst. Meth. A 257(1987), 155-176
• T.Fujinaga & outros, Nucl. Inst. Meth. A 276 (1989), 317-339
- [5] N.M.Duller & W.D.Walker, Phys. Rev. 93 (1954), 215-226

⁵ Esta correção é necessária, porque $\langle P_{t_h}^{(\gamma)} \rangle$ não é o $\langle P_t \rangle$ das primeiras partículas produzidas pela IH, enquanto que $\langle P_{t_h} \rangle$ dos eventos normais é.

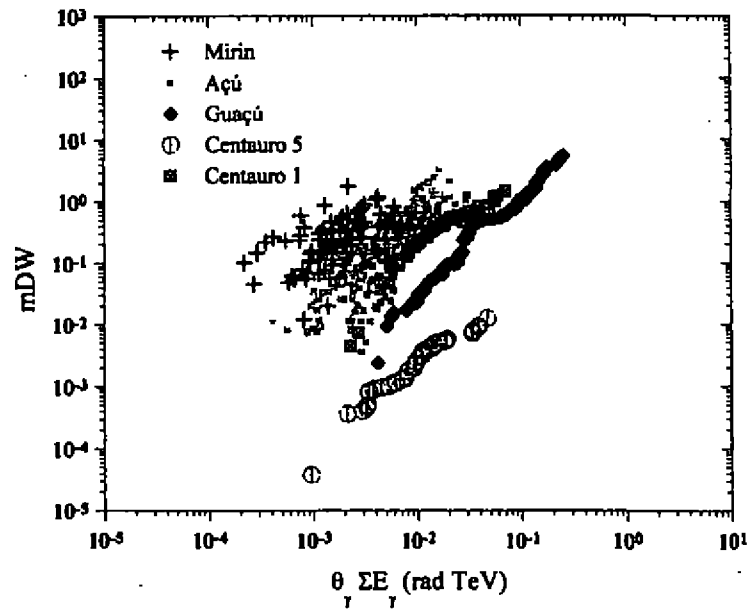


Figura 1. Gráfico do mDW para os Centauro 1 e 5, Guaçu e as famílias A-Jatos. Notar a separação entre os quatro tipos de Estado Intermediário identificados.

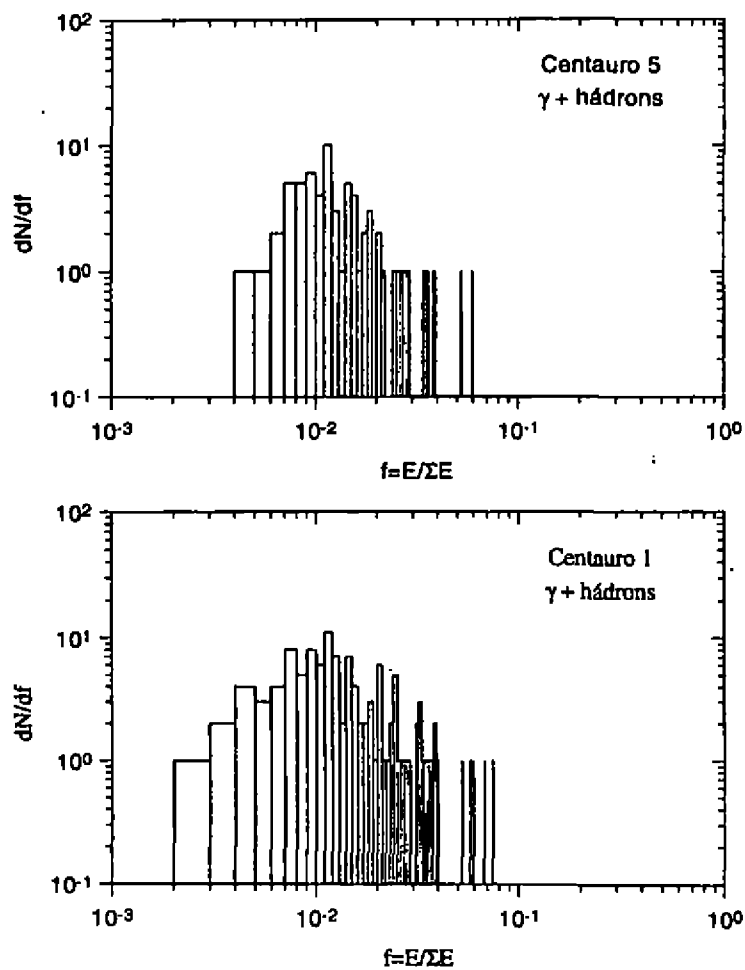


Figura 2. Abaixo: distribuição de energia fracionária para o Centauro 1. Acima: A mesma para o Centauro 5

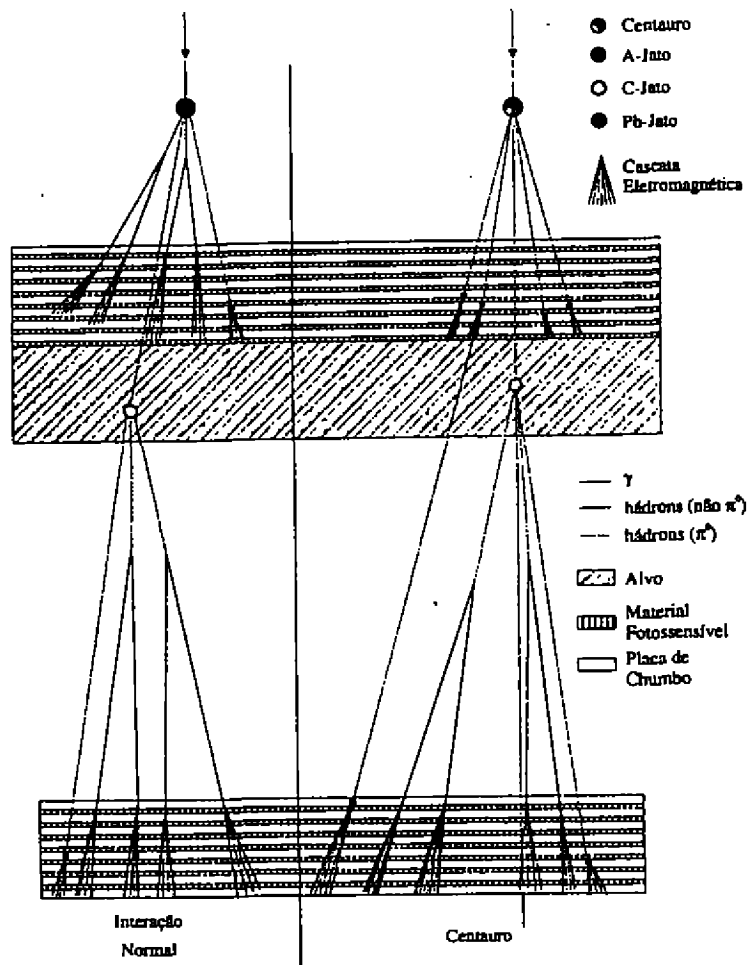


Figura 3. Figura simplificada das diferenças entre uma interação Centauro e uma comum.

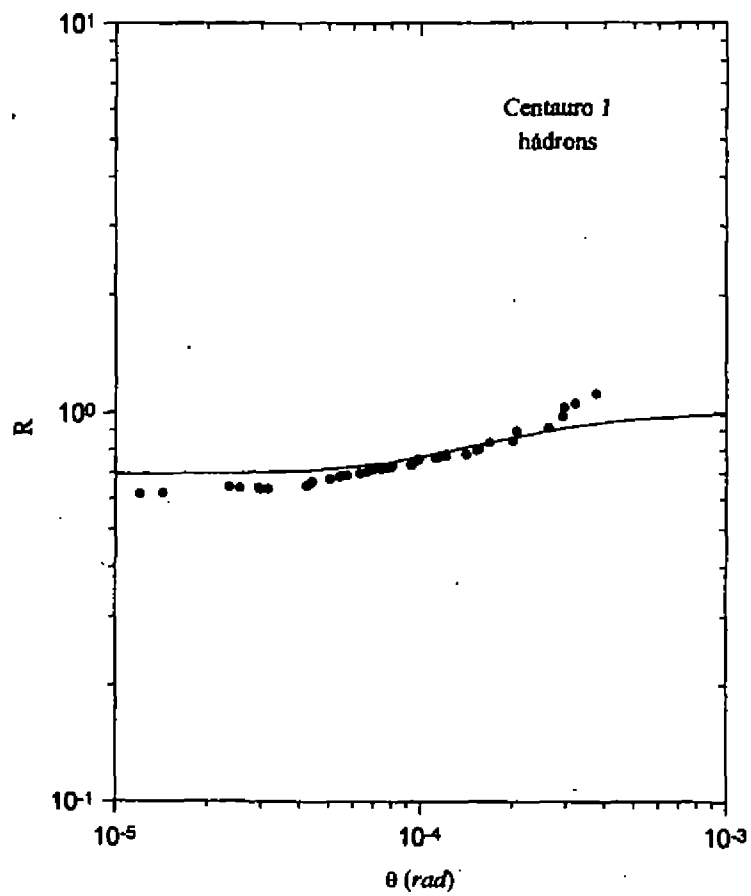


Figura 4. Gráfico do ajuste da função R usada para teste de isotropia para o Centauro 1. Notar que a qualidade do ajuste é boa, indicando que a família Centauro 1 atende o critério de isotropia.

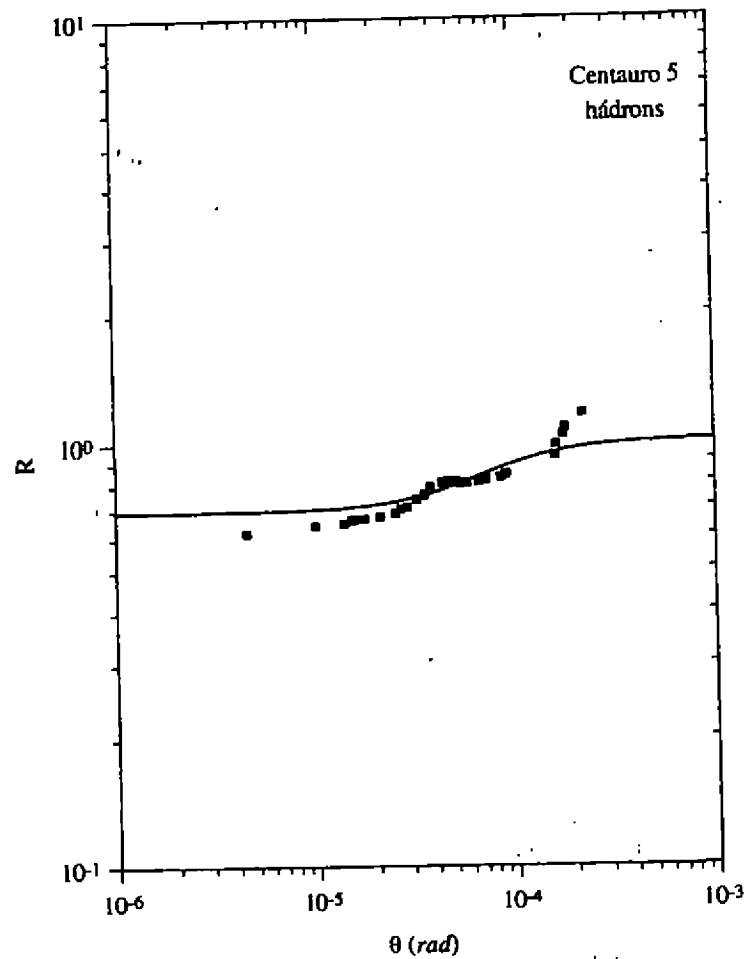


Figura 5. Gráfico do ajuste da função R usada para teste de isotropia para o Centauro V. Notar novamente a qualidade do ajuste é boa, indicando que a família Centauro V também atende o critério de isotropia.

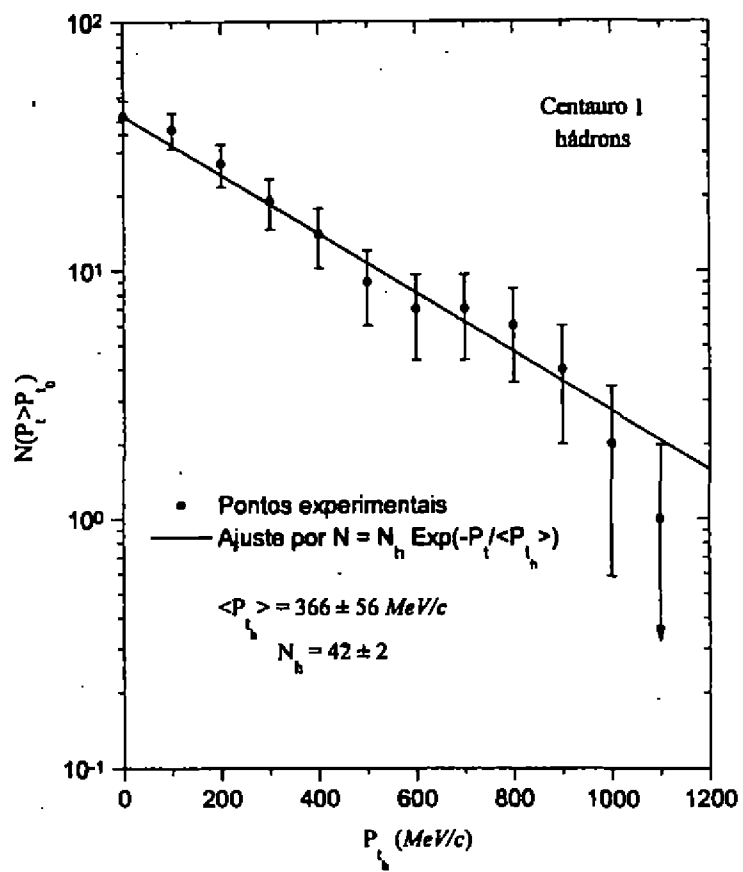


Figura 6. Distribuição integral de momento transversal dos hádrons detectados (em forma de grupos de Centauro 1).

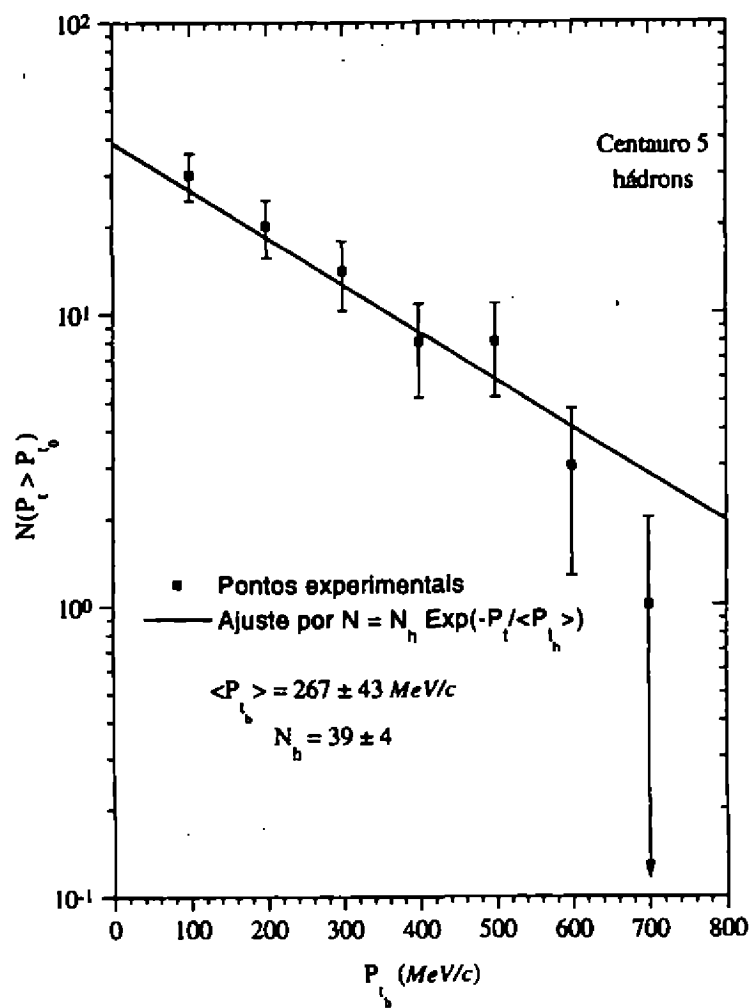


Figura 7. Distribuição integral de momento transversal dos hádrons detectados (em forma de grupos de Centauro 5).

A Medida da Polarização do τ no DELPHI/LEP

Sandra Amato e Leandro de Paula

Instituto de Física, Universidade Federal do Rio de Janeiro

A medida da polarização do τ , produzido no decaimento do Z^0 , é uma das maneiras mais precisas de se ter acesso às constantes de acoplamento axial e vetorial e, conseqüentemente, ao ângulo de Weinberg uma vez que

$$\langle P_\tau \rangle = A_\tau \approx \frac{2v_l}{a_l} = 2(1 - 4\text{sen}^2\theta_W)$$

Quando o Z^0 é produzido por colisões de feixes não polarizados de elétrons e pósitrons a polarização do lépton produzido, em função de sua distribuição angular, é dada por:

$$P_\tau(\cos\theta) = \frac{\langle P_\tau \rangle (1 + \cos^2\theta) + 2 \langle P_e \rangle \cos\theta}{(1 + \cos^2\theta) + 2 \langle P_\tau \rangle \langle P_e \rangle \cos\theta}$$

onde $\langle P_e \rangle$ é a polarização do elétron e não foi levada em conta a universalidade leptônica[1].

No DELPHI[2], de 90 a 95, foram observados da ordem de 3,6 milhões de decaimentos do Z^0 . Já foi publicado o resultado da análise da medida da polarização do τ relativo aos 3 primeiros anos[1], que correspondem a um pouco menos de 1/4 do total de dados. No presente trabalho estamos analisando aproximadamente os 2 milhões de eventos coletados em 93 e 94.

Dentre os vários modos de decaimento aquele que propicia uma medida mais direta é o canal $\tau \rightarrow \pi + \nu$ por se tratar da produção de uma partícula de spin nulo.

A seleção de eventos tem uma eficiência de 57% quando trabalhamos na região central do detetor e o *background* é de 10.2%, sendo que 9.4% são devidos a outros decaimentos do τ .

Selecionamos 4360 candidatos produzidos com uma energia do feixe igual a 92 GeV. Da observação da figura 1 observa-se que há um bom acordo entre a simulação, histograma, e os dados, pontos. A medida da polarização se faz através do ajuste das distribuições de momento dos dados com as esperadas para eventos com polarização +1 e -1, figura 2.

Identificamos as principais causas de erros sistemáticos e realizamos uma primeira avaliação visando a determinar um limite superior para este erro. Nosso resultado foi combinado com o obtido para os 2956 candidatos selecionados no trabalho anterior.

Na figura 3 é mostrada a polarização em função de θ e o valor médio é calculado através do ajuste da função apresentada anteriormente. Constata-se que a universalidade leptônica é respeitada pois os valores de $\langle P_\tau \rangle$ e $\langle P_e \rangle$ são praticamente os mesmos.

Os resultados preliminares, para a análise do canal do π , são:

$$B.R.(\tau \rightarrow \pi(K) + \nu) = (12.18 \pm 0.21 \pm 0.4)\%$$

$$\langle P_\tau \rangle = -0.169 \pm 0.028 \pm 0.050$$

Combinando-se com os resultados, também provisórios, obtidos por análises de outros canais de decaimento temos

$$\langle P_\tau \rangle = -0.139 \pm 0.007 \pm 0.005$$

Este trabalho foi parcialmente financiado pelo CNPq e pela C.E. contrato CII-CT94-0118.

References

- [1] Measurements of the τ Polarization in Z^0 Decays, Z. Phys. C67: 183-202, 1995.
- [2] Delphi Collaboration, Nucl. Instr. and Meth. A303: 103, 1991.
- [3] Particle Data Group.

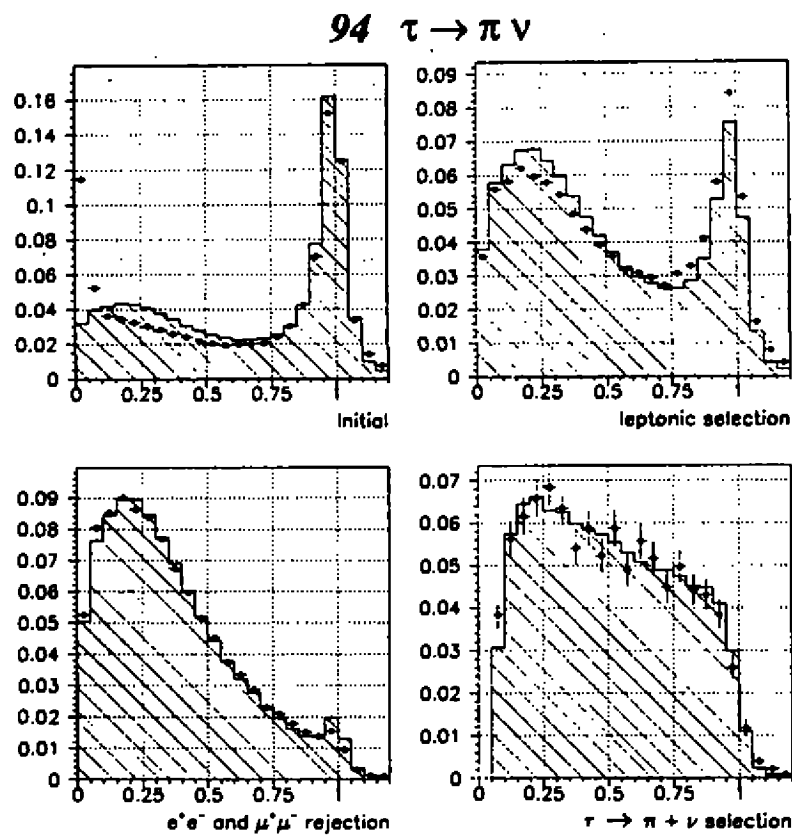


Figure 1: Comparação entre dados, pontos, e simulação, histograma. Da esquerda para a direita e de cima para baixo são apresentadas as distribuições de momento da amostra para as seguintes situações: eventos com até 6 partículas produzidas; seleção de decaimentos leptônicos do Z^0 ; seleção de eventos onde há produção de τ ; seleção final.

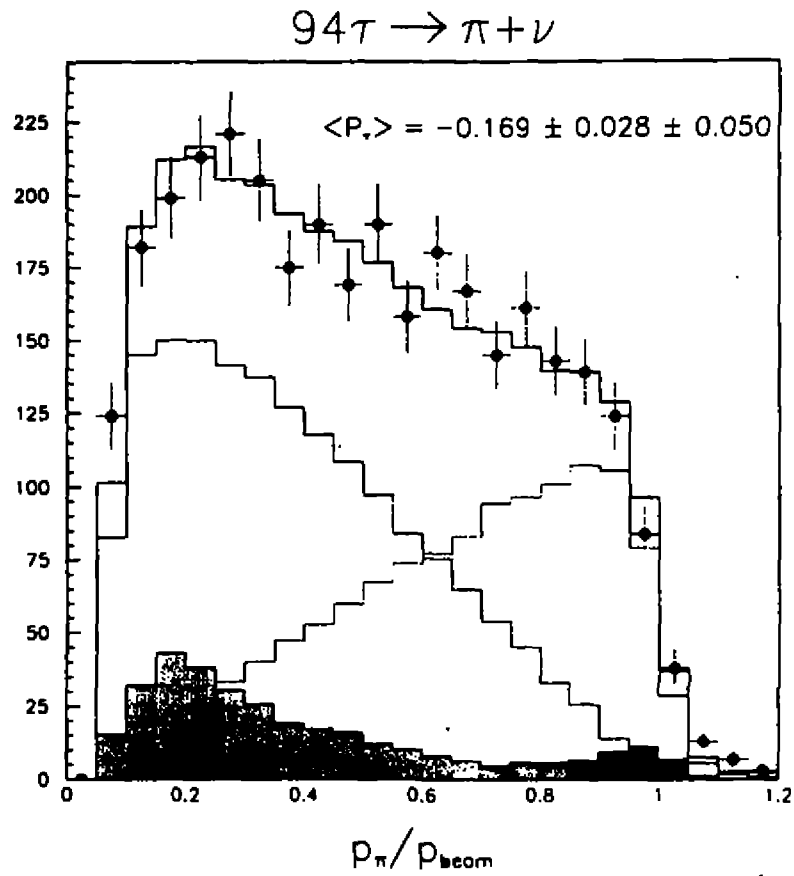


Figure 2: Distribuição de momento dos dados, pontos, e simulação: em cinza é apresentado o *background*, os dois histogramas a meia altura representam as distribuições para as polarizações -1 e $+1$ e a curva superior é a soma.

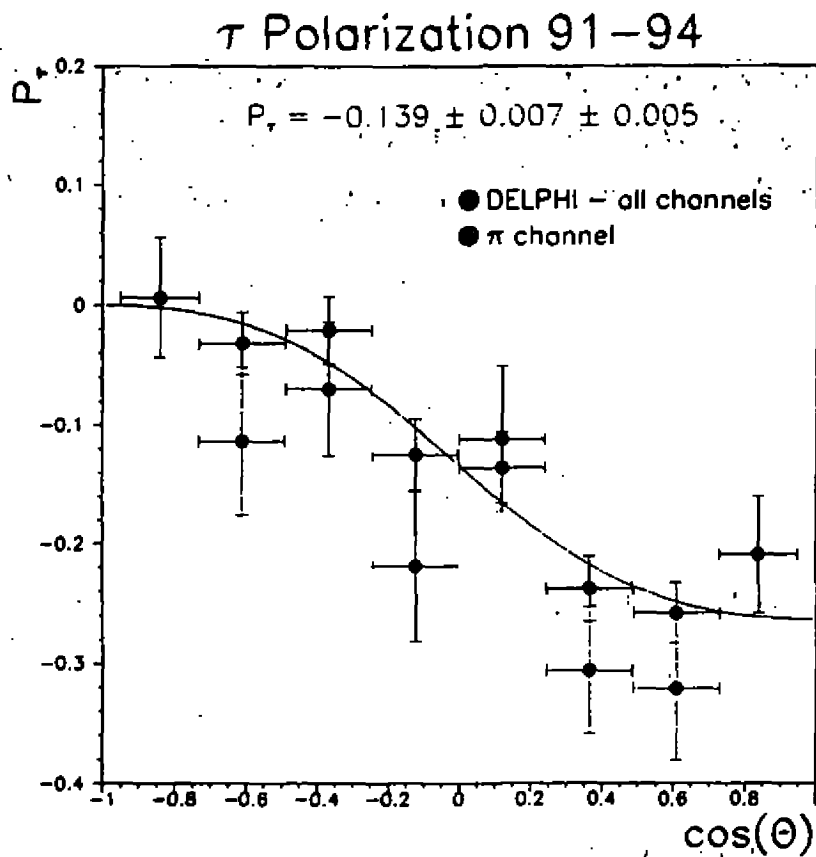


Figure 3: Polarização do τ em função de θ para dados de 91 a 94. As duas curvas ajustadas, supondo-se ou não a universalidade léptonica, se superpõem.

Teste do Protótipo do Novo Anel Cintilador do STIC e Testes das Fotomultiplicadoras e dos Cabos de Fibras Óticas do Contadores de 40^0

Tatiana da Silva-IF/UFRJ

1 Introdução

A colaboração DELPHI instalou o STIC (figura 1) no início de 1994, procurando aumentar a hermeticidade do detector na região frontal - havia um *gap* entre 8^0 e 11^0 deixado pelos calorímetros eletromagnéticos (*SAT+FEMC*) - e medir a luminosidade com uma precisão de 0.2%.

A principal tarefa do STIC é permitir uma medida precisa do ponto de impacto do elétron no limite interno de aceitação.

2 Descrição do Detetor :

2.1 Calorímetro :

O STIC consiste de dois cilindros localizados simetricamente a 2.2 m do ponto de interação, cobrindo uma região angular $29\text{mrad} \leq \theta \leq 188\text{mrad}$ e uma radial $65\text{mm} \leq r \leq 420\text{mm}$. É constituído por 47 sanduiches compostos por placas de chumbo laminadas com aço e telhas cintiladoras, correspondendo num total de $27X_0$.

A luz produzida nas telhas pelo chuveiro eletromagnético é transportada para os fotodetetores, localizados na parte de trás do detector, por fibras WLS (posicionadas ortogonalmente às placas do calorímetro) que têm um pico de absorção em 420nm e um de emissão em 520nm, ou seja, absorve no azul e emite no verde.

As telhas cintiladoras se encontram segmentadas em 16 setores azimutais de 22.5^0 e 10 radiais. As bordas dos setores se encontram deslocadas de um plano para outro em $375\mu\text{m}$ num total de 18 mm do primeiro ao último plano. Este deslocamento foi feito a fim de se obter uma completa hermeticidade e se evitar que partículas escapem do calorímetro através dos buracos destinados às fibras óticas ou através das falhas entre as duas metades cilíndricas que compõem o calorímetro.

As não uniformidades na resposta em energia típicas de detetores deste tipo são resolvidas, então, com uma estrutura de torres compostas por planos contínuos de conversão e com uma alta densidade de fibras.

2.2 Detetores de Silício :

Os planos 8 ($4.0X_0$) e 15 ($7.4X_0$) do calorímetro foram substituídos por detetores de silício, cobrindo a região interna do detetor ($29\text{mrad} \leq \theta \leq 80\text{mrad}$).

Cada um dos planos é constituído por silício altamente resistivo do tipo-n, com *strips* tipo-p implantadas na frente e uma camada n^+ atrás.

As *strips* são circulares com uma separação radial de 1.712 mm (1.754 mm) para o primeiro (segundo) plano, cobrindo 22.5^0 em ϕ .

Estes detetores permitem a reconstrução da direção do chuveiro, impedida pela geometria do calorímetro.

2.3 Sistema de Veto :

É composto por 64 contadores trapezoidais dispostos em 2 planos posicionados em frente aos cilindros do calorímetro, a uma distância entre 2010 e 2050 mm do ponto de interação, cobrindo uma região angular, $43.7\text{mrad} \leq \theta \leq 185\text{mrad}$, e uma radial, $87.8\text{mm} \leq r \leq 379\text{mm}$.

A luz é coletada por 16 fibras WLS sendo 8 em cada lado do cintilador.

Este sistema permite a separação entre partículas carregadas e neutras.

2.4 Nariz e Sistema de Máscara de Tungstênio :

Extendem-se radialmente de 61-96 mm a partir da linha do feixe e cobrem uma região angular de 30-44 mrad. Encontram-se no lado C do calorímetro, definindo o limite interno do detetor para medidas de luminosidade.

Existe um *gap* de 5mrad entre este sistema e a proteção de tungstênio que foi deixado para permitir uma maior clareza na instalação dos contadores de veto.

Este *trigger* de energia neutra foi operacional para o *run* de 95 no qual o LEP rodou à energia de 140 GeV, mas forneceu uma taxa de *trigger* alta demais para uma operação segura no DELPHI dentro de um tempo morto razoável. Por este motivo decidiu-se instalar um novo anel cintilador posicionado bem próximo ao *beam-pipe* cobrindo este *gap*.

3 Teste do protótipo semicircular do novo anel cintilador com leitura feita por fibras WLS:

O objetivo deste protótipo é checar a coleta de luz e investigar um método para se colar fibras numa superfície circular sem provocar o aparecimento de bolhas de ar que podem limitar a transmissão de luz.

O contador têm uma forma semicircular com um raio interno de 56 mm e um externo de 120 mm.

A coleta de luz é feita usando-se um dispositivo, que se encontra nas duas extremidades do contador, no qual 8 fibras WLS são coladas com cimento ótico. Estas fibras eram terminadas com conectores que permitiam a fácil ligação com fibras transparentes que transportam a luz para os fotodetetores (fotomultiplicadoras Hamamatsu H3165).

A resposta do contador foi estudada com uma fonte de raios beta (Rutênio). Os dados foram armazenados para comparação com os resultados obtidos nos testes feitos com raios cósmicos.

No teste com a fonte as fibras nas extremidades interna e externa do contador eram conectadas com cabos de fibras óticas, de 1m de comprimento, a fotomultiplicadoras separadas a fim de se medir a transmissão de luz separadamente. Um pequeno contador de 2 mm de espessura foi colocado em baixo do contador teste (8mm) e a fonte

O sinal era mandado para um *fanin fanout* linear que tinha como função copiar a entrada fornecendo duas saídas exatamente iguais à entrada. Uma saída seguia para o ADC e a outra era discriminada, somente sinais acima de -20mV eram aceitos, gerando o *trigger*. Após a geração do *trigger* a coincidência é bloqueada, a unidade de tempo atrasa o *trigger* para o computador até que o ADC termine a digitalização do sinal e também impede que *triggers* adicionais sejam gerados até que o sistema de aquisição gere um *busy*. A coincidência é vetada pelo tempo morto do sistema de aquisição.

A aquisição foi baseada no sistema MACUA1 que rodava num Macintosh ligado à um módulo Camac (ver figura 2).

A fim de se estudar a uniformidade na coleta de luz foram obtidos dados em diversos pontos do contador.

3.1 Análise dos Dados :

1. Qualidade do contador é dada pelo número de fotoelétrons (tabela 1):

$$N_{pe} = \frac{(Pico - Pedestal)^2}{\sigma^2}, \text{ sendo } \sigma = \sqrt{\sigma_{dist}^2 - \sigma_{ped}^2}$$

2. Análise de uma fotomultiplicadora impondo um corte na outra para eliminar sinais que não correspondiam ao de uma partícula carregada que tivesse atravessado o contador.

O efeito é mostrado superimpondo o espectro do ADC após o corte e o espectro sem o corte (figura 3).

4 Teste dos Cabos de Fibras Óticas e das Fotomultiplicadoras usadas nos Contadores de 40°

4.1 Os Contadores de 40°

São um conjunto de contadores constituídos por chumbo e material cintilador, instalados na região entre o barril e os calorímetros eletromagnéticos na região frontal no lado C do DELPHI. O propósito é identificar a energia eletromagnética que não é detetada por escapar nas falhas entre o barril e as tampas, aumentando a hermeticidade do detetor.

Cada contador consiste de 2 cm de chumbo e 1 cm de material cintilador. A coleta de luz é feita usando-se fibras WLS. São três os tipos de contador: A, B, C. Possuem formas diferentes mas têm a mesma espessura e se encontram dispostos em três anéis concêntricos.

O raio mais externo é constituído pelos contadores A que cobrem um ângulo polar (θ) entre 39° e 42° , e um intervalo azimutal de 15° . Os raios mediano e interno consistem dos contadores B e C, respectivamente. Eles cobrem um intervalo polar entre 36° e 40° e cobrem a mesma região azimutal estando acoplados à mesma fotomultiplicadora.

4.2 Teste dos Cabos de Fibras Óticas Usados nos Contadores de 40°

O objetivo deste teste é verificar a existência de algum cabo danificado medindo-se a transmissão de luz através dos mesmos.

A medida foi realizada iluminando-se os cabos com a mesma fonte de luz.

A aquisição é semelhante à do teste anterior, mas o *trigger* é dado por um pulsador que faz com que o LED pisque. Este led emite luz verde para reproduzir a situação, em que estes cabos de fibra transparente recebem luz no verde das fibras WLS e a transporta até os fotodetetores (figura 4).

4.3 Teste das Fotomultiplicadoras usadas nos Contadores de 40°

Procurou-se através deste teste investigar a estabilidade das fotomultiplicadoras (figura 5). O número de fotoelétrons e o ganho (tabela 2) foram calculados em relação a uma determinada fotomultiplicadora. Os resultados foram importantes para a comparação com medidas realizadas em 95.

$$N_{pe} = \frac{(ADC \cdot ATT - PED)^2}{(\sigma \cdot ATT)^2}, \quad ATT = 10^{-\frac{E_{ph}}{E_0}}$$

$$Ganho = \frac{(ADC \cdot ATT - PED)}{N_{pe} \cdot G_{ref}}$$

DELPHI STIC

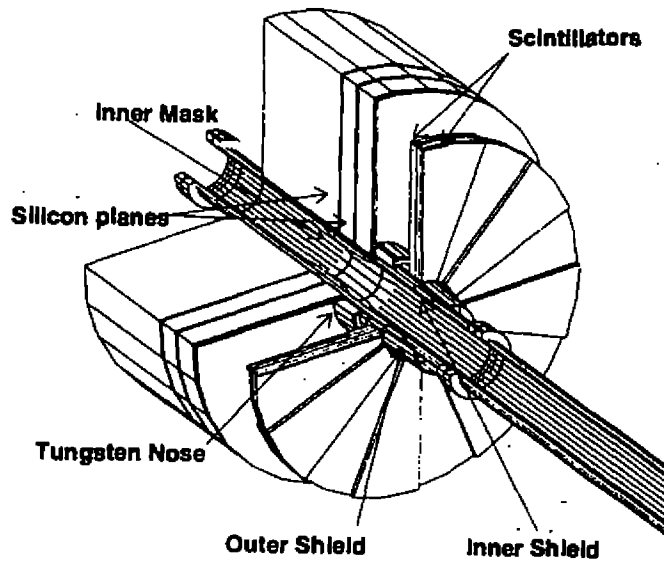


Figure 1: STIC e Cintiladores do Sistema de Veto

APARATO EXPERIMENTAL :

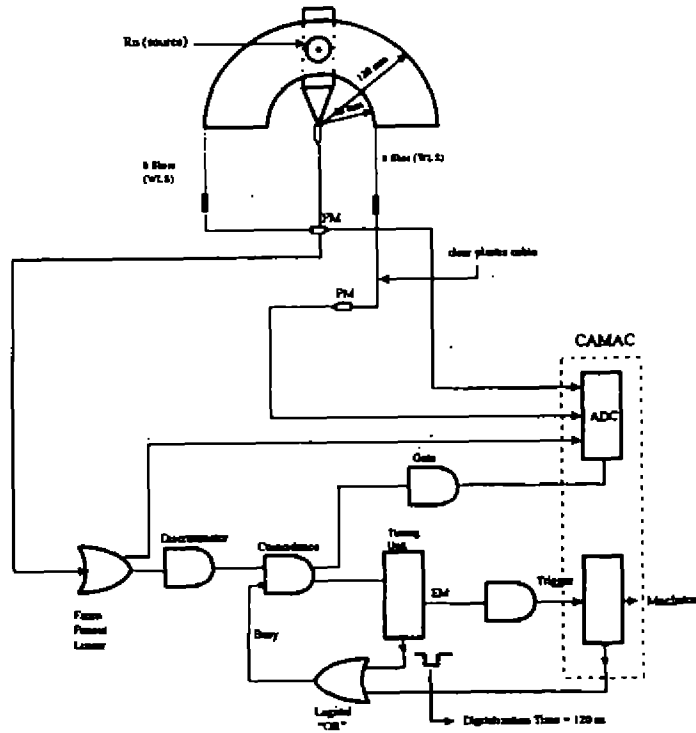
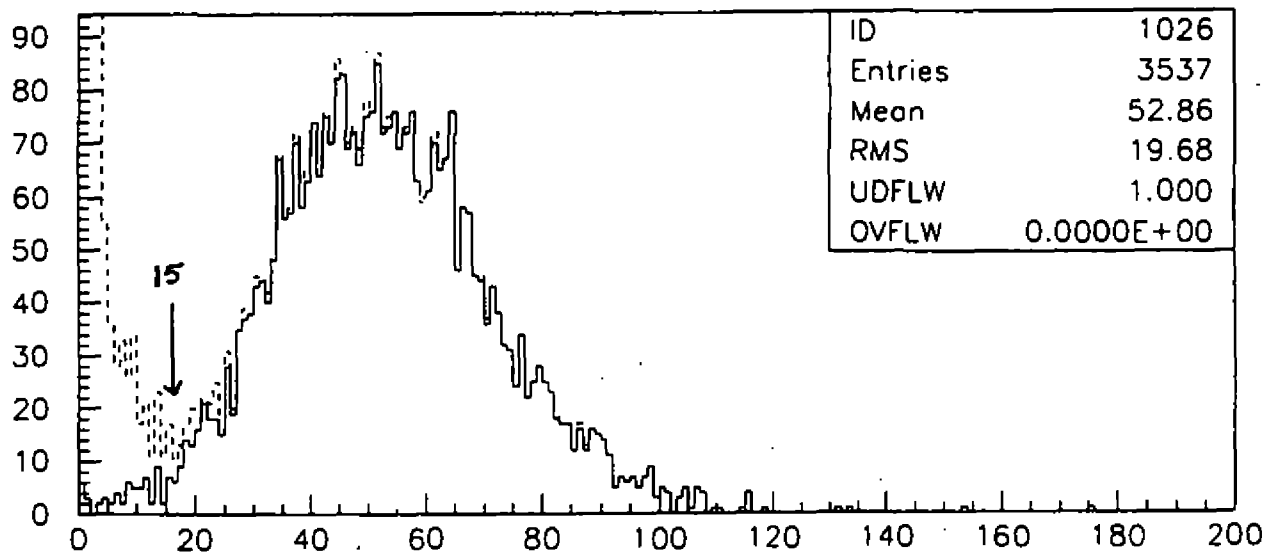
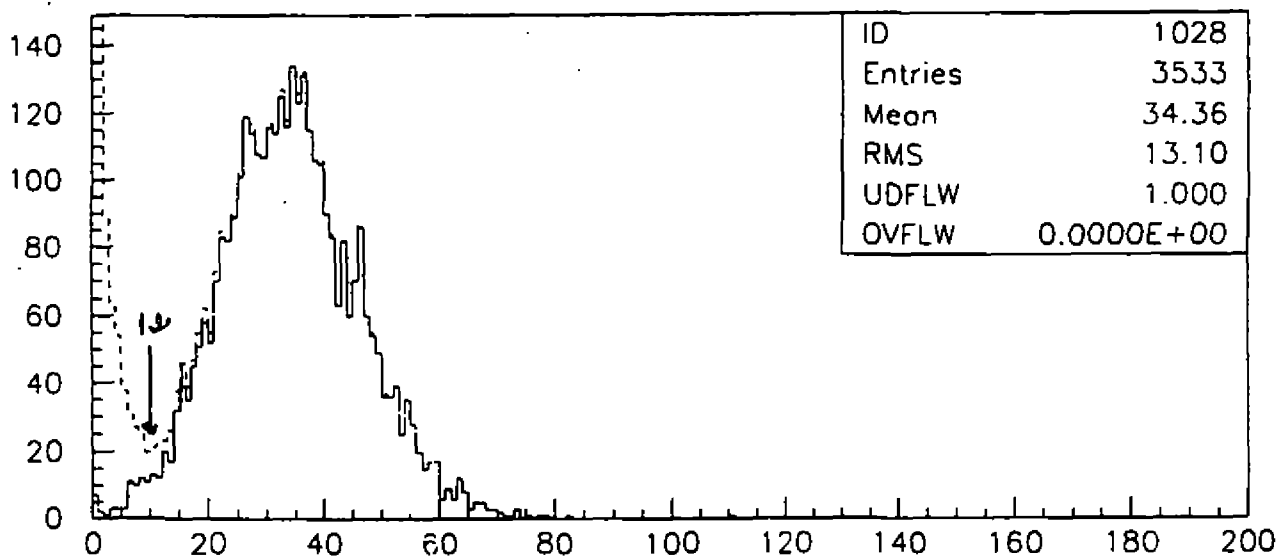


Figura 2: Esquema Experimental usado no Teste do Protótipo do Nove Anos Cintilador do STIC

Figura 3: Superposição do espectro do ADC após corte e o sem corte



MIPEDzVETOR CUT VETOL



MIPEDzVETOR CUT VETOL

Aparato Experimental

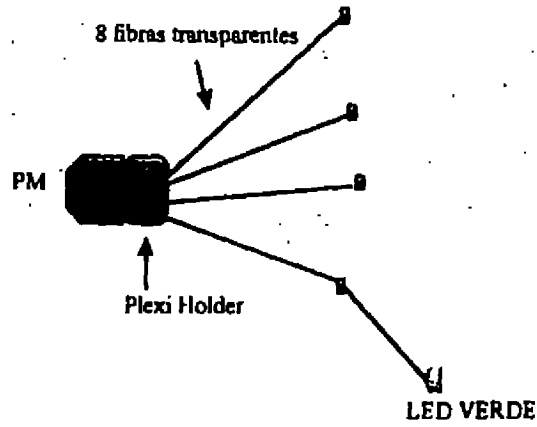


Figura 4 : Aparato experimental do Teste dos Cabos de Fibras Óticas dos Contadores de 40 °.

Aparato Experimental

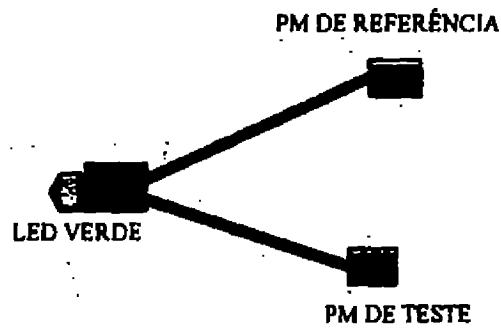


Figura 5: Aparato Experimental do Teste das Fotomultiplicadoras dos Contadores de 40 °.

Table 1: Número de Fotoelétrons

	l	lmid	mid	rmid	r
miped_veto_r cut veto l	9.5 ± 0.4	8.6 ± 0.4	9.8 ± 0.2	9.4 ± 0.3	8.1 ± 0.3
miped_veto_l cut veto r	9.8 ± 0.4	10.2 ± 0.5	9.2 ± 0.3	10.9 ± 0.4	9.6 ± 0.4
sum(l+r) cut l	18 ± 1	15 ± 2	18 ± 1	17 ± 2	15 ± 1
sum(l+r) cut r	20 ± 1	16 ± 2	20 ± 1	18 ± 2	17 ± 1
sum(l+r) cut lr	22 ± 2	21 ± 2	24 ± 1	20 ± 2	23 ± 1

Table 2: Resultados

PM	N_{pe}	Ganho	PM	N_{pe}	Ganho
082	1.52	0.26	312	2.01	0.57
083	1.42	0.87	323	1.18	1.38
087	1.91	0.60	344	1.91	0.87
091	1.80	0.44	379	1.13	0.34
092	1.61	0.41	460	1.38	2.33
093	1.45	0.67	461	0.87	2.98
097	0.95	2.77	462	1.03	2.85
102	1.78	0.63	465	0.92	3.47
109	1.24	1.01	472	1.56	0.71
103	1.42	0.36	480	1.69	1.72
139	1.59	0.83	511	1.33	1.42
172	1.88	1.18	549	1.52	0.35
177	1.09	1.34	655	1.59	1.90
193	1.57	0.75	670	1.41	0.69
203	1.95	0.98	677	1.33	1.79
209	1.00	1.00	688	2.04	0.32
212	1.00	1.56	693	0.85	2.39
222	1.50	0.71	739	2.21	0.25
232	2.26	0.21	750	0.85	0.56
240	1.65	2.22	751	0.80	1.32
242	1.27	0.85	752	0.89	1.06
301	1.45	1.02	771	1.30	0.37

Critical Coupling for Dynamical Chiral-Symmetry Breaking with an Infrared Finite Gluon Propagator

A. A. Natale* and P. S. Rodrigues da Silva†

Instituto de Física Teórica, Universidade Estadual Paulista

Rua Pamplona, 145, 01405-900, São Paulo, SP Brazil

We compute the critical coupling constant for the dynamical chiral-symmetry breaking in a model of quantum chromodynamics, solving numerically the quark self-energy using infrared finite gluon propagators found as solutions of the Schwinger-Dyson equation for the gluon, and one gluon propagator determined in numerical lattice simulations. The gluon mass scale screens the force responsible for the chiral breaking, and the transition occurs only for a larger critical coupling constant than the one obtained with the perturbative propagator. The critical coupling shows a great sensibility to the gluon mass scale variation, as well as to the functional form of the gluon propagator.

1 Introduction

The idea that quarks obtain effective masses as a result of a dynamical breakdown of chiral symmetry (DBCS) has received a great deal of attention in the last years [1, 2]. One of the most common methods used to study the quark mass generation is to look for solutions of the Schwinger-Dyson equation for the fermionic propagator. It is known that above a certain critical coupling ($\alpha_c \equiv g_c^2/4\pi$) a nontrivial self-energy solution bifurcates away from the trivial one. Numerical evaluation of this critical coupling in QCD with three and four flavors gives $\alpha_c \sim \mathcal{O}(1)$ [3, 4].

Parallel to the study of DBCS a lot of effort has also been done to obtain the nonperturbative behavior of the gluon propagator [5, 6, 7], and perhaps one of the most interesting results is the one where it is argued that the gluon may have a dynamically generated mass [5]. The study of the infrared behavior of the gluon propagator was also performed numerically on the lattice [8], and more recent numerical simulation give strong evidence for an infrared finite gluon propagator in the Landau gauge [9]. It is worth mentioning that from the phenomenological point of view, the existence of a “massive gluon” may shed light on several reactions where long distance QCD effects can interfere, and examples of the possible consequences can be found in the literature, see, for instance, Ref. [10, 11, 12].

Much work has yet to be done about the infrared behavior of the gluon propagator, but it is clear that its implications have to be tested in all possible problems. It is possible that the constraint coming from DBCS, and other phenomenological studies [10, 11, 12] will provide a map of the infrared gluon propagator. Since the bifurcation point for DBCS was studied up to now with the perturbative $1/k^2$ gluon propagator, it is natural to ask what is going to happen with the infrared finite propagators that have been found through solutions of the gluonic Schwinger-Dyson equation or using Monte Carlo methods, and, moreover, to look for the consequences of different forms of non-perturbative gluon propagators. It is intuitive that the force necessary for condensation is going to be screened if the gluon propagator is infrared finite, therefore, the actual critical coupling constant should be larger, and this is what we will investigate in this work.

We will present the Schwinger-Dyson equation of our problem, and first we will discuss the critical coupling for the linear approximated problem in the case of a bare gluon mass. This will teach us on the general behavior of the critical coupling constant as a function of the gluon mass. Secondly, we perform a numerical calculation of the full

* e-mail: natale@axp.ift.unesp.br

† e-mail: fedel@axp.ift.unesp.br

nonlinear equation, for two different gluon propagators resulting from solutions of the gluon polarization tensor, and one obtained from numerical simulation on the lattice. In the conclusions we discuss the differences in the critical coupling for each of the "massive" gluon propagators, arguing that its value definitively gives information about the infrared gluon propagator.

2 Quark propagator Schwinger-Dyson equation

The Schwinger-Dyson equation for the quark propagator in Minkowski space is

$$S^{-1}(p) = \not{p} - \frac{4}{3} \int \frac{d^4 q}{(2\pi)^4} \gamma_\mu S(q) \Gamma_\nu(p, q) g^2 D^{\mu\nu}(p - q). \quad (1)$$

where we write the gluon propagator in the form

$$g^2 D^{\mu\nu}(q) = \frac{4\pi\alpha(-q^2/\Lambda^2)}{q^2} \left(-g^{\mu\nu} + \frac{q^\mu q^\nu}{q^2} \right). \quad (2)$$

The propagator has been written in the Landau gauge, which will be used throughout our work. In the above equations $\Gamma_\nu(p, q)$ is the vertex function, and $\alpha(-q^2/\Lambda^2)$ is the QCD running coupling constant, for which we know only the ultraviolet behavior, and to solve Eq.(1) we make the same ansatz of Ref. [3, 4] about its behavior for the full momentum scale

$$\alpha(-q^2/\Lambda^2) = \frac{12\pi/(33 - 2n_f)}{\ln(\tau + \frac{-q^2}{\Lambda^2})}. \quad (3)$$

Eq.(3) goes continuously to the perturbative result, and has already been used in phenomenological applications.

To proceed further we also need to introduce an ansatz for the quark-gluon vertex $\Gamma^\mu(p, q)$, which must satisfy a Slavnov-Taylor identity that, when we neglect ghosts, reads

$$(p - q)_\mu \Gamma^\mu(p, q) = S^{-1}(p) - S^{-1}(q). \quad (4)$$

This identity constrains the longitudinal part of the vertex, and if we write $S^{-1}(p)$ in terms of scalar functions

$$S^{-1}(p) = A(p) \not{p} - B(p), \quad (5)$$

we find the solution [13]

$$\begin{aligned} \Gamma^\mu(p, q) = & A(p^2) \gamma^\mu + \frac{(p - q)^\mu}{(p - q)^2} ([A(p^2) - A(q^2)] \not{p} - [B(p^2) - B(q^2)]) \\ & + \text{transverse part}, \end{aligned} \quad (6)$$

which is a much better approximation than the use of the bare vertex. Assuming that the transverse vertex part vanishes in the Landau gauge we obtain

$$D^{\mu\nu}(p - q) \Gamma_\nu(q, p) = D^{\mu\nu}(p - q) A(q^2) \gamma_\nu. \quad (7)$$

and arrive at the approximate Schwinger-Dyson equation

$$[A(p^2) - 1] \not{p} - B(p^2) = \frac{4}{3} \int \frac{d^4 q}{(2\pi)^4} g^2 D^{\mu\nu}(p - q) \gamma_\mu \frac{A(q^2)}{A(q^2) \not{p} - B(q^2)} \gamma_\nu. \quad (8)$$

Going to Euclidean space, we will be working with the following nonlinear coupled integral equations for the quark wave-function renormalization and self-energy

$$\begin{aligned} [A(P^2) - 1] P^2 = & \frac{16\pi}{3} \int \frac{d^4 Q}{(2\pi)^4} \frac{\alpha((P - Q)^2/\Lambda^2)}{\Phi[(P - Q)^2]} \\ & \times \left(P \cdot Q + 2 \frac{P \cdot (P - Q) Q \cdot (P - Q)}{(P - Q)^2} \right) \\ & \times \frac{A^2(Q^2)}{A^2(Q^2) Q^2 + B^2(Q^2)}. \end{aligned} \quad (9)$$

$$B(P^2) = 16\pi \int \frac{d^4Q}{(2\pi)^4} \frac{\alpha((P-Q)^2/\Lambda^2)}{\Phi[(P-Q)^2]} \frac{A(Q^2)B(Q^2)}{A^2(Q^2)Q^2 + B^2(Q^2)}, \quad (10)$$

where $Q^2 = -q^2$ and $P^2 = -p^2$, and we introduced a function $\Phi[(P-Q)^2]$ which, in the case of the perturbative propagator, is simply $\Phi[(P-Q)^2] = (P-Q)^2$, for the massive bare gluon it will have the form $\Phi[(P-Q)^2] = (P-Q)^2 + m_g^2$, and will be a more complex expression in the case of a dynamically generated mass.

3 The linear problem with a massive bare gluon

Eq.(9) and Eq.(10) possess the trivial solution $A(P^2) = 1$ and $B(P^2) = 0$ for small values of the coupling constant. We can also see that $B(P^2)$ depends on $B(P^2)$ at first order, whereas $A(P^2)$ has a higher order dependence on $B(P^2)$. In order to examine the possibility that a nontrivial solution, $B(P^2)$, branches away from the trivial one at a critical coupling, α_c , we examine the so-called bifurcation equation [14]. This involves differentiating Eq.(9) and Eq.(10) functionally with respect to B and then setting $B = 0$. Since the equation for $A(P^2)$ depends at least quadratically on $B(P^2)$ it will be dropped at leading order from the bifurcation problem, and we substitute $A(P^2)$ by 1 in the bifurcation equation that will come out from Eq.(10). We define the dynamical fermion mass (m_f) by the normalization condition

$$\delta B(0) = m_f, \quad (11)$$

and finally arrive at our bifurcation equation

$$\begin{aligned} \delta B(P^2) &= \frac{16\pi}{(2\pi)^3} \int dQ^2 \int d\theta \sin^2 \theta \frac{Q^2}{Q^2 + m_f^2} \\ &\times \frac{\alpha[(P-Q)^2/\Lambda^2]}{(P-Q)^2 + m_g^2} \delta B(Q^2), \end{aligned} \quad (12)$$

where we already assumed a bare massive gluon.

Our main intention in this section is to verify the gross behavior of the critical coupling constant with the existence of an infrared finite gluon propagator, stressing that the results obtained here have a qualitative meaning only. In order to do this, we can still make some simpler approximations before estimating α_c , making the angle approximation (which consists in separating the integration over the momenta in two regions, $P \gg Q$ and $Q \gg P$) in the coupling constant as well as in the gluon propagator, and this introduces an error of about 10% in the calculation [4]. Defining the variables $x = P^2/m_f^2$, $y = Q^2/m_f^2$, $\ell = \Lambda^2/m_f^2$, $\kappa = m_g^2/m_f^2$, and $f(P^2) = \delta B(P^2)/m_f$, we obtain

$$f(x) = \frac{1}{\pi} \int dy K(x, y) f(y), \quad (13)$$

where

$$K(x, y) = \frac{\alpha(x/\ell)}{x + \kappa} \frac{y}{y + 1} \theta(x - y) + \frac{\alpha(y/\ell)}{y + \kappa} \frac{y}{y + 1} \theta(y - x). \quad (14)$$

The kernel K is square integrable, therefore Eq.(13) has a nontrivial L^2 solution for α_c on a point set. The smallest eigenvalue (α_c) for which Eq.(13) has a nontrivial square integrable solution, is the first bifurcation of the nonlinear equation, and satisfy

$$\frac{1}{\pi} \|K\| = 1, \quad (15)$$

where $\|K\|$ means the integrated kernel in x and y over the whole space. Table 1 gives the critical value α_c as a function of ℓ and κ .

The values of Table 1 were obtained with $n_f = 4$ but they do not change appreciably as we change n_f . As we can see from table 1, if we increase the gluon masses we can satisfy Eq.(15) only with larger critical coupling constants, and this is what we can expect from the numerical solution of the complete nonlinear problem.

ℓ	κ	α_c
10^4	1	0.6971
10^4	10^2	0.9440
10^4	10^3	1.4853
10^5	1	0.5568
10^5	10^2	0.6607
10^5	10^4	0.9489
10^{10}	10^4	0.6226
10^{10}	10^5	0.7822
10^{10}	10^5	1.2278

Table 1: Critical coupling constant (α_c) as a function of $\ell = \Lambda^2/m_f^2$, and $\kappa = m_g^2/m_f^2$ for $n_f = 4$

4 The critical coupling for infrared finite propagators

In this section we solve Eq.(9) and Eq.(10) numerically without further approximations. The numerical code we used is the same of Ref. [16], and the criterion to determine the critical coupling is the one of Ref. [4]. With the perturbative gluon propagator we obtain (with $n_f = 4$)

$$\alpha_c = 0.854. \quad (16)$$

which is compatible with the calculations of Ref. [3, 4]. We will solve the gap equations with three different propagators which we discuss in the sequence.

One of the infrared finite propagators found in the literature was determined by Cornwall [5]

$$\Phi(Q^2) = D_c^{-1}(Q^2) = [Q^2 + m_g^2(Q^2)]bg^2 \ln\left[\frac{Q^2 + 4m_g^2(Q^2)}{\Lambda^2}\right], \quad (17)$$

where $m_g^2(Q^2)$ is the momentum-dependent dynamical gluon mass

$$m_g^2(Q^2) = m_g^2 \left[\frac{\ln\left(\frac{Q^2 + 4m_g^2}{\Lambda^2}\right)}{\ln\frac{4m_g^2}{\Lambda^2}} \right]^{-12/11} \quad (18)$$

$g^2 \sim 1.5 - 2$ is the strong coupling constant, and $b = (33 - 2n_f)/48\pi^2$ is the leading order coefficient of the β function of the renormalization group equation. This form for the propagator was obtained as a fit to the numerical solution of a gauge invariant set of diagrams for the gluonic Schwinger-Dyson equation.

Another infrared finite gluon propagator has been found by Stingl *et al.* [6]. Its form agrees with that derived by Zwanziger based on considerations related to the Gribov horizon [17], and is given by

$$\Phi(Q^2) = D_s^{-1}(Q^2) = Q^2 + \mu^4/Q^2. \quad (19)$$

where μ is a scale not determined in Ref. [6]. It is interesting to note that the Bernard *et al.* [9] lattice result for the gluon propagator can be fitted by Eq.(17) as well as Eq.(19). These propagators, apart from some multiplying constant, approach the perturbative gluon propagator in the small mass limit.

Finally, Marenzoni *et al.* [9] also performed a lattice study of the gluon propagator in the Landau gauge, obtaining for its infrared behavior the following fit

$$\Phi(Q^2) = D_m^{-1}(Q^2) = m_g^2 + ZQ^2(Q^2/\Lambda^2)^\eta. \quad (20)$$

where m_g , Z and η are constants determined with the numerical simulation. m_g is of $\mathcal{O}(\Lambda)$, $Z \simeq 0.4$ and $\eta \simeq 0.5$, what is slightly different from the previous propagators. The results of Bernard *et al.* also show the behavior $(Q^2)^\eta$, but with a smaller value for η .

With the above propagators we computed the dynamical fermion mass as a function of the coupling constant. As in Ref. [4] the results were fitted by a function

$$h(\alpha) = \beta(\alpha - \alpha_c)^\gamma, \quad (21)$$

characteristic of a phase transition phenomena. We have not found large differences in the values of the critical coupling as we varied the number of fermions, therefore, the fitting will be presented for $n_f = 4$. In Fig.1 we plot $-1/\ln B(0)$ as a function of the coupling constant, for the Cornwall propagator, which was studied by Haeri and Haeri [18] whom performed a cancellation between the coupling constant in the vertex function and the factor g in Eq.(17), something far from clear to for $m_g = 2\Lambda$ and $m_g = 2.2\Lambda$, and as expected from the example of the previous section if we increase the gluon mass the critical coupling also increases. These gluon masses are consistent with the values determined phenomenologically in the last work of Ref. [5]. The parameters of Eq.(21) and the critical coupling are given by

$$\beta = 1.0785, \quad \gamma = 0.2535, \quad \alpha_c = 0.8692, \quad (m_g = 2.0\Lambda); \quad (22)$$

$$\beta = 0.8424, \quad \gamma = 0.2682, \quad \alpha_c = 1.4211, \quad (m_g = 2.2\Lambda). \quad (23)$$

As will become clear in the following, not only the value of the gluon mass scale is important to characterize the phase transition, but the precise form of the gluon propagator will affect considerably the value of the critical coupling. In this case, as well as in the next ones, we verified that for small gluon masses we start having dynamically generated quark masses for critical couplings quite close to the value obtained with the $1/Q^2$ propagator (see Eq.(25)). After some value of the gluon mass the critical coupling deviates very fast from the value of Eq.(19). An example of this behavior is shown in Eq.(26), where the coupling constant is almost twice the value of Eq.(25), although we obtained it increasing the previous gluon mass value only by 10%!

Using the propagator determined by Stingl *et al.* [6], we obtain the curves shown in Fig.2 for $\mu^2 = 0.25\Lambda^2$ and $\mu^2 = 0.30\Lambda^2$, and described by Eq.(21) with

$$\beta = 0.2482, \quad \gamma = 0.4784, \quad \alpha_c = 2.9038, \quad (\mu^2 = 0.25\Lambda^2); \quad (24)$$

$$\beta = 0.2946, \quad \gamma = 0.3362, \quad \alpha_c = 6.4720, \quad (\mu^2 = 0.30\Lambda^2). \quad (25)$$

Note that the values for the critical coupling constants are quite large. We rely on these numbers based on the continuous growth of the coupling constant from a value near the one of Eq.(19) for small gluon masses, to the ones of Eq.(27) and (28) as the mass is increased. It is known for several other theories with chiral breaking for coupling constants of $\mathcal{O}(1)$, that higher order corrections do not modify the critical behavior shown by the ladder approximation [19], and we expect the same to hold here. Comparing Fig.2 to Fig.1 we see that the dynamically generated mass is much smaller for this propagator, than with the Cornwall one. Performing the calculation for $\mu \approx \mathcal{O}(3.0\Lambda)$ we do not obtain a significative signal of chiral symmetry breaking, i.e. if there is a dynamical mass it is much smaller than Λ , and do not satisfy our numerical criterion to recognize mass generation [4]. This result is compatible with the one of Ref. [20], where it was verified that the quark condensate is consistent with zero above a certain critical value of μ for this same gluon propagator. Here we foresee a problem for the Stingl *et al.* [6] propagator, because as shown by Cudell and Nguyen [11] we need $\mu \approx \mathcal{O}(3.0\Lambda)$ to obtain a correct description of diffractive scattering with this propagator.

Fig.3 contains the critical curve for the lattice propagator (Eq.(20)) in the case of $m_g = 0.7\Lambda$, and with

$$\beta = 0.4588, \quad \gamma = 0.2870, \quad \alpha_c = 3.9712, \quad (m_g = 0.7\Lambda). \quad (26)$$

The Marenzoni *et al.* propagator gives a value for the critical coupling constant which is intermediate between the other two propagators that we discussed up to now. If we increase the gluon mass we will also find a point where the symmetry is not broken anymore, however, this will occur for larger masses than the one predicted in Ref. [9] ($m_g \approx \Lambda$). Comparing all the results it becomes clear that, for masses of the same order, the softer is the propagator in the infrared the larger will be the critical coupling for chiral symmetry breaking. We believe that the value of the critical coupling constant can be a good indicator of the gluon propagator infrared behavior.

5 Conclusions

We studied the chiral-symmetry breaking in a model of quantum chromodynamics, using infrared finite gluon propagators found as solutions of the Schwinger-Dyson equation for the gluon. We first solved numerically the linearized equation of the quark self-energy, and found that a bare gluon mass scale screens the force responsible for the chiral breaking, and the transition occurs at a larger critical coupling constant if we increase the ratio of the gluon to fermion mass. Secondly, we solved numerically the full quark self-energy equation for some infrared finite gluon propagators. The result confirm our linear approximation. We also verified that the functional form of the propagator is also important to characterize the chiral transition.

With the Cornwall propagator (Eq.(17)) and gluon masses of the order that are expected phenomenologically, we obtain critical coupling constants not far away from the one obtained with the $1/k^2$ propagator. With the Stingl *et al.* propagator (Eq.(19)) the chiral transition will occur only for quite large values of the coupling constant. If the gluon mass scale is of $O(\Lambda)$ the critical coupling is one order of magnitude larger than the one obtained with the perturbative propagator. Unfortunately, a phenomenological study of diffractive scattering with the Stingl propagator demand gluon masses of $O(3\Lambda)$, for which there is no symmetry breaking! This means that this propagator does not represent the actual gluon infrared behavior, or the model of diffractive scattering of Ref. [11] must be modified. The Marenzoni *et al.* propagator leads to a picture of the chiral transition that is consistent phenomenologically, but with a larger value for the critical coupling constant. In general, the softer is the propagator in the infrared the larger will be the critical coupling. The value of this coupling can be used as a tool to study the infrared behavior of the gluon propagator, and associated with other phenomenological calculations (like the ones of Ref. [10, 11, 12]) may provide a map of the gluon propagator for every momenta scale.

Acknowledgments

We have benefited from discussions with G. Krein and J. Montero. This research was supported in part by the Conselho Nacional de Desenvolvimento Científico e Tecnológico (CNPq) (AAN), and in part by Fundação de Amparo a Pesquisa do Estado de São Paulo (FAPESP) (PSRS).

References

- [1] Y. Nambu and G. Jona-Lasinio, *Phys. Rev.* **122**, 345 (1961).
- [2] E. Farhi and R. Jackiw, *Dynamical Gauge Symmetry Breaking*, World Scientific Pub. Co., Singapore, 1982; P. Fomin, V. Gusynin, V. Miranskii and Y. Sitenko, *Rev. Nuovo Cimento* **6**, 1 (1983); C. D. Roberts and A. G. Williams, *Dyson-Schwinger Equations and their Applications to Hadronic Physics*, *Progress in Particle and Nuclear Physics*, **33**, 477 (1994).
- [3] D. Atkinson and P. W. Johnson, *Phys. Rev.* **D37**, 2296 (1988).
- [4] C. D. Roberts and B. H. J. McKellar, *Phys. Rev.* **D41**, 672 (1990).
- [5] J. M. Cornwall, in *Deeper Pathways in High-Energy Physics*, edited by B. Kursunoglu, A. Perlmutter and L. Scott (Plenum, New York, 1977), p.683; *Nucl. Phys.* **B157**, 392 (1979); *Phys. Rev.* **D26**, 1453 (1982).
- [6] M. Stingl, *Phys. Rev.* **D34**, 3863 (1986); U. Habel *et al.*, *Z. Phys.* **A330**, 423, 435 (1990).
- [7] J. R. Cudell and D. A. Ross, *Nucl. Phys.* **B350**, 247 (1991).
- [8] C. Bernard, *Phys. Lett.* **B108**, 431 (1982); P. A. Amundsen and J. Greensite, *Phys. Lett.* **B173**, 179 (1986); J. E. Mandula and M. Ogilvie, *Phys. Lett.* **B185**, 127 (1987); R. Gupta *et al.* *Phys. Rev.* **D36**, 2813 (1987).
- [9] C. Bernard, C. Parrinello and A. Soni, *Phys. Rev.* **D49**, 1585 (1994); P. Marenzoni, G. Martinelli, N. Stella and M. Testa, *Phys. Lett.* **B318**, 511 (1993); *ibid.* preprint Southampton - hep-ph 9410355; P. Marenzoni, G. Martinelli and N. Stella, *Nucl. Phys.* **B455**, 339 (1995).
- [10] G. Parisi and R. Petronzio, *Phys. Lett.* **B94**, 51 (1980).
- [11] F. Halzen, G. Krein and A. A. Natale, *Phys. Rev.* **D47**, 295 (1993); M. B. Gay Ducati, F. Halzen and A. A. Natale, *Phys. Rev.* **D48**, 2324 (1993); J. R. Cudell and B. U. Nguyen, *Nucl. Phys.* **B420**, 669 (1994).
- [12] J. H. Field, *Int. J. Modern Physics* **A9**, 3283 (1994).
- [13] G. Krein, P. Tang and A. G. Williams, *Phys. Lett.* **B215**, 145 (1988).

- [14] G. H. Pimbley, *Eigenfunction branches of nonlinear operators, and their bifurcations*, Lecture Notes in Mathematics, 104 (Springer, Berlin, 1969); see also D. Atkinson, J. Math. Phys. 28, 2494 (1987).
- [15] D. Atkinson, V. P. Gusynin and P. Maris, Phys. Lett. B303, 157 (1993).
- [16] A. G. Williams, G. Krein and C. D. Roberts, Ann. Phys. (NY) 210, 464 (1991).
- [17] D. Zwanziger, Nucl. Phys. B378, 525 (1992).
- [18] B. Haeri and M. B. Haeri, Phys. Rev. D43, 3732 (1991).
- [19] U. Mahanta, Phys. Lett. B225, 181 (1989); B. Holdom, Phys. Rev. Lett. 62, 997 (1989); U. Mahanta, Phys. Rev. Lett. 62, 2349 (1989).
- [20] F. T. Hawes, C. D. Roberts and A. G. Williams, Phys. Rev. D40, 4683 (1994).

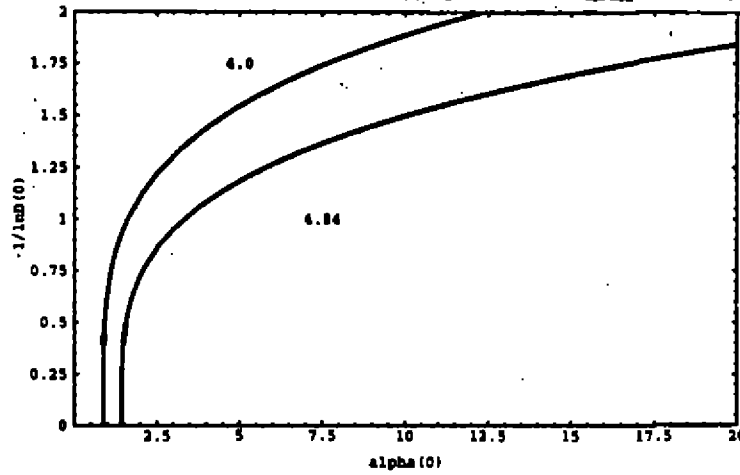


Figure 1: Results of the evaluation of Eq.(10) as a function of the coupling constant with the propagator of Eq.(17). We show some of the calculated points, and the curve is the result of the fitting by Eq.(21). The calculation was performed for $n_f = 4$, the upper curve is for $m_p^2 = 4.0\Lambda^2$ and the lower one is for $m_p^2 = 4.84\Lambda^2$.

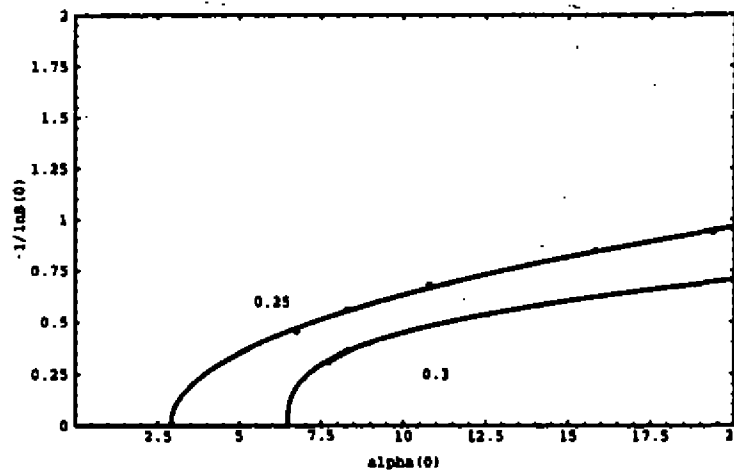


Figure 2: The same as Fig.1 for the propagator of Eq.(19), with $\mu^2 = 0.25\Lambda^2$ (upper curve) and $\mu^2 = 0.30\Lambda^2$ (lower curve).

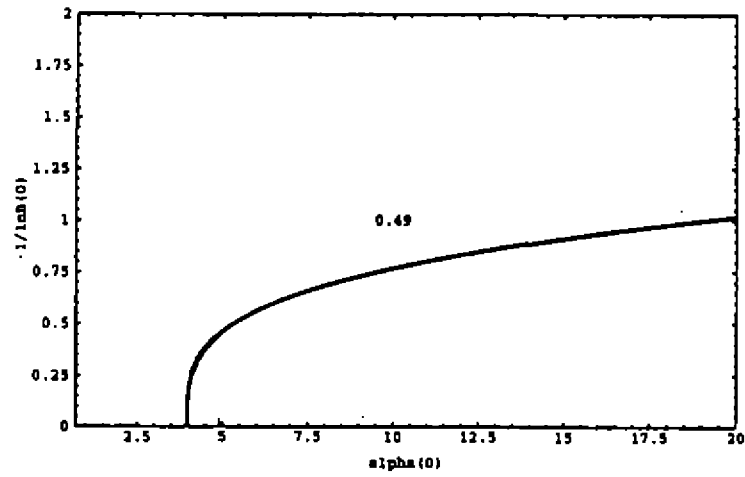


Figure 3: The same as Fig.2 for the propagator of Eq.(20), with $m_0^2 = 0.49\Lambda^2$.

Derivative Analyticity Relation and Parton-Parton Scattering Amplitude*

A. F. Martini¹, M. J. Menon¹, J. T. S. Paes² and M. J. Silva Neto²

1- Instituto de Física 'Gleb Wataghin'

Universidade Estadual de Campinas - Unicamp

13089-970 Campinas, São Paulo, Brasil

2-Centro de Ciências Exatas e Naturais

Departamento de Física - Universidade Federal do Pará

Campus Universitário - Guamá

CEP 66075-900 - Belém - Pará.

The real part of the elementary (parton-parton) amplitude is calculated, using a derivative analyticity relation and a phenomenological parametrization for the imaginary part. As a first test for future analysis, physical observables are calculated through a multiple diffraction approach early develop. With this formalism global-descriptions of the experimental data on pp elastic scattering above 10 GeV are achieved. The predicted ρ parameter reaches the maximum value 0.15 at $\sqrt{s} \approx 500$ GeV and then goes asymptotically to zero through positive values.

1 - Introduction

Phenomenological aspect of the high-energy elastic hadron scattering have been investigated through multiple diffraction models [1]. In the framework of the impact parameter formalism and eikonal approximation, this approach connects the hadronic scattering amplitude with the hadronic form factors and elementary (parton-parton) amplitude. In a previous work it was shown that the real of the hadronic amplitude may be calculated by assuming proportionality between real and imaginary parts of the elementary amplitude, the coefficient being a free parameter depending on the energy. With suitable parametrizations for the form factors and for the imaginary part of the elementary amplitude, a satisfactory description of the experimental data on pp elastic scattering above 10 GeV was obtained [2]. In this communication we make use of a derivative dispersion relation in order to compute the real part of the elementary amplitude. Assuming that the elementary part factorizes in the energy and momentum transferred, the result leads also to a proportionality relation. Beside the elimination of one free parameter, this could be viewed as a theoretical justification for the proportionality early assumed. The paper is organized as follows. In section 2 we briefly review the multiple diffraction formalism and the phenomenological model early developed. In the section 3 we introduce the derivative analyticity relation in the context of the model, showing the predictions for physical observables and comparisons with experimental data. Some critical and final remarks are the content of section 4.

2 - Multiple Diffraction Model

The eikonal approach connects the hadronic elastic scattering amplitude F with the eikonal function χ through the well known formula [3].

$$F(s, q) = i \int_0^\infty b db J_0(qb) [1 - \exp[i\chi(s, b)]] \equiv i < 1 - \exp[i\chi(s, b)] >, \quad (1)$$

*Financial Support: CAPES-PICD/CNPq

where \sqrt{s} is the c.m. energy, q the transferred momentum, b the impact parameter, J_0 the Bessel function and the angular brackets denote the symmetrical two-dimensional Fourier transform. In the first order multiple diffraction theory, the eikonal is expressed by [4]

$$\chi(s, b) = \langle G_A G_B f \rangle, \quad (2)$$

where G_A, G_B are the hadronic form factors of the hadrons A and B and f the averaged elementary (parton-parton) amplitude.

Recently Martini and Menon investigated elastic pp scattering with the following parametrizations for the form factors and elementary amplitude [2]:

$$G_A = G_B = \frac{1}{1 + q^2/\beta^2} \cdot \frac{1}{1 + q^2/\alpha^2}, \quad (3)$$

$$f = \text{Re}f + i\text{Im}f, \quad (4)$$

$$\text{Im}f = C \frac{1 - q^2/a^2}{1 + q^4/a^4}, \quad (5)$$

and assuming

$$\text{Re}f = \lambda \text{Im}f, \quad (6)$$

where $\alpha^2, \beta^2, a^2, C$ and λ are free parameter. Defining

$$\Omega(s, b) = \langle G^2 \text{Im}f \rangle \quad (7)$$

the complex eikonal reads

$$\chi(s, b) = (\lambda + i)\Omega(s, b) \quad (8)$$

and the real and imaginary parts of the hadronic amplitude, eq.(1), are expressed by

$$\text{Re}F(s, q) = \langle e^{-\Omega(s, b)} \text{sen}(\lambda\Omega) \rangle, \quad (9)$$

$$\text{Im}F(s, q) = \langle 1 - e^{-\Omega(s, b)} \text{cos}(\lambda\Omega) \rangle. \quad (10)$$

With this, physical observables may be investigated, such as the differential cross section

$$\frac{d\sigma}{dq^2} = \pi |F(s, q)|^2, \quad (11)$$

the ρ parameter (ratio of the real and imaginary parts of the forward scattering amplitude)

$$\rho = \frac{\text{Re}F(s, 0)}{\text{Im}F(s, 0)}, \quad (12)$$

and total cross sections

$$\sigma_{tot} = 4\pi \text{Im}F(s, 0). \quad (13)$$

Analysis of pp elastic scattering above 10 GeV leads to the following values and parametrizations for the five free parameters [2]:

$$a^2 = 8.2 \text{ GeV}^2, \quad \beta^2 = 1.8 \text{ GeV}^2, \quad (14)$$

$$C(s) = 14.26 - 1.65(\ln s) + 0.159(\ln s)^2, \quad (15)$$

$$\frac{1}{\alpha^2(s)} = 2.57 - 0.217(\ln s) + 0.0243(\ln s)^2, \quad (16)$$

$$\lambda(s) = \frac{0.0695 \ln(s/s_0)}{1 + 0.118[\ln(s/s_0)] + 0.015[\ln(s/s_0)]^2}. \quad (17)$$

With this, a satisfactory description of the observables in eqs. (11), (12) and (13) was obtained.

3 - Derivative Analyticity Relation and Results

In spite of the satisfactory description achieved with the above model, the hypothesis of proportionality between $Ref(q, s)$ and $Imf(q, s)$, eq.(6), was assumed by simplicity, without a theoretical justification. More yet, this introduces one free parameter, $\lambda(s)$, and its dependence with the energy, eq. (17), has also no theoretical justification.

Attempting to formalize these aspects, we applied a derivative dispersion relation directly in the elementary amplitude [5]

$$Ref(s, q) = \frac{\pi}{2} \frac{d}{d \ln s} Imf(s, q). \quad (18)$$

Making use of $Imf(s, q)$ given by eq.(5) and parametrization (15), we yet obtain

$$Ref(s, q) = \lambda(s) Imf(s, q), \quad (19)$$

but now $\lambda(s)$ is explicitly determined:

$$\lambda(s) = \left(\frac{\pi}{2}\right) \left[\frac{-1.65 + 0.318 \ln s}{14.26 - 1.65 \ln s + 0.159 (\ln s)^2} \right]. \quad (20)$$

As a first test, we introduce this theoretical result directly in the formalism described in the last section. To this end, we substitute the phenomenological parametrization (17) by the analytic result (20). With this, eqs. (3) to (10) and parametrizations (14) to (16) lead to the observables (11), (12) and (13). The predictions for pp differential cross section, total cross section and ρ parameter are shown in figs. 1, 2 and 3, respectively.

From fig.1 we see that, with the exception of the dip region, all the differential cross section data are well described. Figure 2 shows that the predictions for the total cross section are in agreement with the experimental data at ISR energies; extrapolations to cosmic ray energies show agreement with the reanalysis performed by N.N.Nikolaev [6] on the Akeno data [7]. This result was also obtained in the previous formalism [2]. From fig. 3, predictions for $\rho(s)$ overestimate the experimental data. Extrapolations to higher energies indicate a maximum value $\rho = 0.15$ at $\sqrt{s} \approx 500$ GeV. In the region $\sqrt{s} : 10-20$ TeV (LHC) the predictions are $\rho : 1.02-1.03$

4 - Final Remarks

In high-energy hadron-hadron scattering, dispersion relations are usually applied to the hadronic amplitude. Up to our knowledge this work presents the first test of use in the elementary (parton-parton) amplitude. In order to compute physical observables, use was made of the multiple diffraction formalism and previous parametrizations for the hadronic form factors and the for the imaginary part of the elementary amplitude. With this, global characteristics of the experimental data on pp elastic scattering above 10 GeV could be described.

A crucial point concerns the overestimation of the differential cross section in the dip region and of the $\rho(s)$ at ISR energies. However, all these results depend strongly on the phenomenological parametrizations and previous assumptions, e.g. the factorization of the imaginary part of the elementary amplitude and the energy dependence of the free parameters. Although we did not attempt a general "best fit", we see that the gross features of the experimental data may be reproduced. We hope this first test may bring insights on the subject.

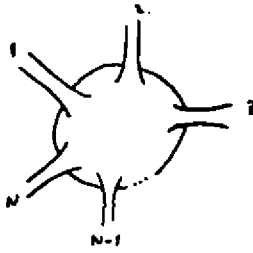
Fig.1: scattering of N closed bosonic strings.

Fig.2: scattering after conformal transformations.

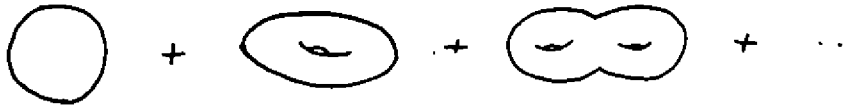


Fig.3: all orders of perturbation theory.

References

1. G. Matthiae, Rep. Prog. Phys. **57** (1994) 743.
2. A.F. Martini, M. J. Menon, "Phenomenological Approach to Elastic Proton-Proton Scattering above 10 GeV", in XVI Brazilian National Meeting on Particles and Fields - 1995 (to be published); preprint IFGW - ABSTRACTA CO19 - 96.
3. R. J. Glauber, in Lectures on Theoretical Physics; edited by W. E. Britten et al (Interscience, New York, 1959) Vol I, p.315.
4. W. Czyz and L. C. Maximon, Ann. Phys. (N-Y) **52** (1969) 59; V. Franco and K. Varma, Phys. Rev **c18** (1978) 349; M.J. Menon, Phys. Rev. **D48** (1993) 2007.
5. J. B. Bronzan, G. L. Kane and U. P. Sukhatme, Phys. Lett. **49B** (1974) 272.
6. N. N. Nikolaev, Phys. Rev **D48** (1993) R 1904.
7. M. Honda et al. , Phys. Rev. Lett. **70** (1993) 525.

Análise Bi-Dimensional de χ^2 em Interferometria de Kaons

C. G. Roldão * and S. S. Padula †

Instituto de Física Teórica, Universidade Estadual Paulista

Rua Pamplona, 145, 01405-900, São Paulo, SP - Brazil

Este trabalho apresenta resultados preliminares, uma vez que está em fase inicial, da análise de χ^2 sobre dados obtidos da Colaboração E859. O principal objetivo aqui é quantificar o poder de resolução da interferometria bidimensional em kaons.

1 Introdução

Na década de 50 Hunbury-Brown e Twiss [1] propuseram um novo método para determinar os raios, ou ao menos ângulos, subentendidos por fontes de rádio e estrelas próximas. Este método fundamenta-se na correlação do tempo de chegada dos fótons, oriundos da fonte, em dois detectores separados. Em 1959 Goldhaber *et al.* [2] observaram que pions produzidos em colisões $p\bar{p}$ possuíam um efeito semelhante. A interferometria de partículas idênticas é utilizada para determinar a dimensão espaço-temporal de reações a altas energias, sendo por este motivo sugerida como assinatura para o plasma de quarks e glúons, pois pode oferecer informações sobre a distribuição de matéria durante o último estágio do processo da reação.

A função de correlação, na sua forma mais simples, é dada por

$$C(k_1, k_2) = \frac{P(k_1, k_2)}{P(k_1)P(k_2)} = \{1 \pm \lambda |\rho(q)|^2\}, \quad (1)$$

onde $P(k_i)$, $i = 1, 2$, e $P(k_1, k_2)$ são as distribuições inclusivas para um e dois kaons, respectivamente. $q = k_1 - k_2$ é a diferença de quadri-momenta dos dois kaons, λ é o parâmetro de caoticidade e $\rho(q)$ é a transformada de Fourier da densidade espaço-temporal, $\rho(x)$, da partícula emitida.

O método utilizado para a obtenção das referidas dimensões no espaço-tempo consiste na análise do gráfico da função de correlação fornecida pela Eq.(1) versus a diferença de momenta do par, sendo a largura desta curva o inverso do raio, R , do volume da reação. Mas esta interpretação estritamente geométrica é válida apenas no limite semi-clássico e quando não existe nenhuma correlação no espaço de fase dos kaons. Frequentemente efeitos dinâmicos podem levar a existência de uma forte correlação entre o quadri-momentum, p^μ , e o espaço-tempo, x^μ , causando distorções em $C_2(k_1, k_2)$, o que invalida esta interpretação. Por estes motivos será usado, no lugar de (1), uma forma mais genérica para a função de correlação

$$C(k_1, k_2) = \left(1 + \frac{|G(k_1, k_2)|^2}{G(k_1, k_1)G(k_2, k_2)}\right),$$

onde $G(k, k)$ é a distribuição inclusiva para um único kaon e $G(k_1, k_2)$ é a amplitude complexa que contém o termo de interferência.

Para pacotes Gausseanos com mínima incerteza e ausencia de ressonancias, $G(k_1, k_2)$, será [3, 4, 5]

$$G(k_1, k_2) = \int d^4x d^4p D(x, p) e^{iqx} e^{i/2 \Delta x^2 / \Delta p^2} e^{i(p-k)^2 / 2 \Delta p^2} \propto \{e^{iqx} e^{-\mathcal{K} \cdot p / \Delta p^2}\}. \quad (2)$$

*e-mail: roldao@xpc.ift.unesp.br

†e-mail: padula@xpc.ift.unesp.br

onde Δp é a largura do momento do pacote e Δx é a largura no espaço-tempo. Os colchetes (...) indicam que foi feita a média sobre a distribuição no espaço de fase desacoplado dos kaons, $D(x, p)$, e (x_f, p_f) são as coordenadas de freeze-out no espaço de fase dos mesmos. Quando efeitos devido a ressonâncias de longa vida são considerados, a amplitude complexa será

$$G(k_1, k_2) \approx \left(\sum_r f_{K^+ / r} (1 - i q u_r / \Gamma_r)^{-1} \exp(i q x_r - \mathcal{K} p_r / \Delta p^2) \right), \quad (3)$$

sendo $f_{K^+ / r}$ a fração de K^+ decorrente de decaimentos de ressonâncias do tipo r com quadri-velocidade final u_r^μ , e para kaons é $f_{K^+ / \text{direto}} \approx 0.50$ [3, 4, 5]. Tanto na Eq.(2) quanto na Eq.(3) foi utilizada a notação padrão, onde $q = k_1 - k_2$ e $\mathcal{K} = (k_1 + k_2)/2$.

As Ref.[3] e [5] mostram que as ressonâncias distorcem a função de correlação, simulando fontes de longa vida e parcialmente coerentes, o que justifica o interesse em testar sua abundância em baixas energias através da interferometria. Neste contexto dois cenários serão analisados, um sem a produção de ressonâncias e outro com ressonâncias previstas pelo modelo de Lund [6], ambos a energias do AGS.

2 Análise Bidimensional de χ^2

Como na Ref [8], a interferometria em uma dimensão, $C_2(k_1, k_2) \times q_\perp$, onde q_\perp é a diferença de momenta transversal dos dois kaons, não é suficiente para determinar qual dos dois cenários, com ou sem ressonâncias, adequa-se melhor aos dados experimentais, uma vez que os parâmetros geométricos R_T e τ , raio transversal e tempo próprio da bola de fogo, respectivamente, podem ser escolhidos, em ambos os casos, para concordar com os dados experimentais. Desta forma surgiu a ideia de estudar a interferometria em duas dimensões.

Para comparar os dados experimentais projetados em duas das seis dimensões com a função de correlação teórica, calculamos a função de correlação projetada

$$C_{proj}(q_T, q_L) = \frac{\int d^3 k_1 d^3 k_2 P_2(\mathbf{k}_1, \mathbf{k}_2) A_2(q_\perp, q_L; \mathbf{k}_1, \mathbf{k}_2)}{\int d^3 k_1 d^3 k_2 P_1(\mathbf{k}_1) P_1(\mathbf{k}_2) A_2(q_\perp, q_L; \mathbf{k}_1, \mathbf{k}_2)}$$

onde P_1 e P_2 são as distribuições inclusivas para um e dois kaons, respectivamente, e A_2 é a função de aceitação experimental. Todos os cálculos foram realizados usando CERES [3], onde a função de aceitação experimental para os dados da Colaboração E859 foram aproximados por

$$A_2(q_T, q_L; \mathbf{k}_1, \mathbf{k}_2) = A_1(k_1) A_1(k_2) \Theta(22 - |\phi_1 - \phi_2|) \times \delta(q_L - |k_{z1} - k_{z2}|) \delta(q_\perp - |k_{\perp 1} - k_{\perp 2}|). \quad (4)$$

Os ângulos de corte experimentais, ϕ_1 e ϕ_2 , são medidos em graus e os momenta em GeV/c. Os cortes da distribuição inclusiva são especificados por

$$A_1(\mathbf{k}) = \Theta(14 < \theta_{lab} < 28) \Theta(p_{lab} < 2.9 \text{ GeV/c}) \Theta(y_{min} > 0.75).$$

As flutuações nos dados experimentais não permitem nenhuma conclusão a respeito de qual dos dois casos analisados está em melhor concordância com os dados obtidos pela Colaboração E859, que podem ser vistos na figura (1.a). A fig.(1.d) mostra seus erros experimentais. As fig.(1.b) e (1.c) ilustram as funções de correlação filtradas pela Eq.(4) correspondendo aos cálculos com e sem ressonâncias, respectivamente, no intervalo $0.005 < q_\perp, q_L < 0.125 \text{ GeV/c}$. Os parâmetros que fornecem as melhores curvas são $R_T = 2.5 \text{ fm}$ e $\tau = 2.5 \text{ fm/c}$, no caso sem ressonâncias, e $R_T = 2.5 \text{ fm}$ e $\tau = 1.5 \text{ fm/c}$ para o caso com ressonâncias. Uma alternativa a este impasse é calcular a qualidade do ajuste de χ^2 no plano (q_\perp, q_L) , para ambos os cenários. Para isso usaremos a sugestão dada por Zajc [7] para χ^2 .

$$\chi^2(i, j) = \frac{[A(i, j) - \mathcal{N}_\chi^{-1} C_{th}(i, j) B(i, j)]^2}{[(\Delta A(i, j))^2 + (\mathcal{N}_\chi^{-1} C_{th}(i, j) \Delta B(i, j))^2]}$$

onde \mathcal{N}_χ é um fator de normalização escolhido para minimizar χ^2 médio e depende do intervalo q_\perp , q_L no plano sob análise. Os índices i e j referem-se ao correspondente *bin* (q_\perp , q_L) [9, 10]. $\chi^2(i, j)$ pode ser visto em (1.e), na ausência de ressonâncias, e em (1.f), quando as mesmas estão presentes.

3 Procedimento de Minimização

A minimização de χ^2 é feita variando-se os parâmetros R_T e $\Delta\tau$ e então $\langle\chi^2\rangle$ é calculado sobre uma grade de 30×30 no plano dos momentos, onde $0,005 < q_\perp$, $q_L < 0.605$ GeV/c. Na vizinhança onde R_{T_0} e τ_0 (os mínimos de R_T e τ) deve-se determinar os parâmetros α e β da superfície quadrática

$$\langle\chi^2(R_T, \Delta\tau)\rangle = \chi_{min}^2 + \alpha(R_T - R_{T_0})^2 + \beta(\Delta\tau - \Delta\tau_0)^2.$$

Este procedimento foi proposto por [11], onde dados da Colaboração E802 foram analisados, nesta ocasião uma clara distinção entre os dois cenários foi encontrada, os cálculos sem ressonância estavam em melhor concordância com os dados experimentais.

Este trabalho visa realizar a mesma análise para kaons, e os resultados por nós obtidos, embora preliminares e ainda em fase inicial, indicam que nas duas referidas situações os conjuntos de parâmetros (R_T, τ) são similares, o que acreditamos refletir a menor sensibilidade dos kaons à influência de ressonâncias.

References

- [1] R. Hanbury-Brown and R. Q. Twiss, *Phil. Mag.* 45 (1954) 663; *Nature* 177 (1956) 27; *ibidem* 178 (1956) 1447.
- [2] G. Goldhaber, et al., *Phys. Rev.* 120 (1960) 300.
- [3] M. Gyulassy, S. S. Padula, *Phys. Lett.* 217B (1989) 181.
- [4] S.S. Padula, M. Gyulassy, and S. Gavin, *Nucl. Phys.* B329 (1990) 357.
- [5] S. S. Padula and M. Gyulassy, *Nucl. Phys.* B339 (1990) 378.
- [6] B. Anderson et al., *Nucl. Phys.* B281 (1987) 289. M. Gyulassy, *CERN-TH 4794* (1987), *Proc. Eight Balaton Conf. on Nucl. Phys.*, ed by Z. Fodor, KFKI, Budapest 1987.
- [7] W. Zajc, *Proc. of CAMP (LESIP IV)*, p. 439, ed. by M. Plümer, S. Raha and R. M. Weiner, World Scientific (1991). (1990) R21.
- [8] S.S. Padula and M. Gyulassy, *Nucl. Phys.* A544 (1992) 537c-542c.
- [9] Y. Akiba et al. (E859 collab.), *Phys. Rev. Lett.* 70 (1993) 1057; V. Cianciolo (E859), *Nucl. Phys.* A590 (1995) 459c.
- [10] V. Cianciolo (E859 Collab.), *private communication*.
- [11] S.S. Padula and M. Gyulassy, *Phys. Lett.* 348B (1995) 303.

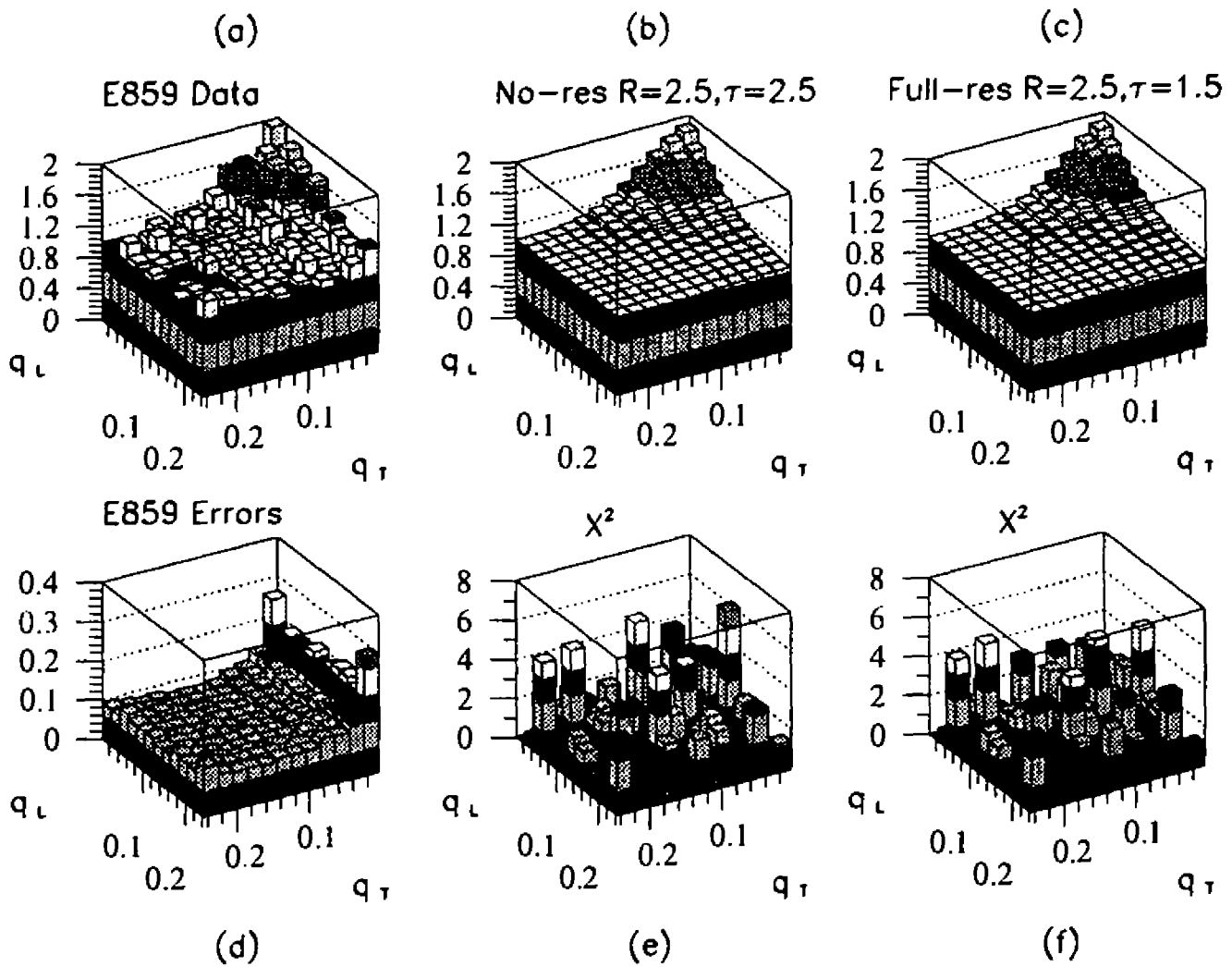


Figura 1. Função de correlação para K^+ produzidos na colisão Si+Au. Os dados da Colaboração E859 podem ser vistos em (a) e seus erros em (d). Em (c) e (b) estão as funções de correlação teóricas sem e com ressonâncias, respectivamente, e suas correspondentes distribuições de χ^2 em (e) e (f).

Hadronic Size Dependence in High-Energy Scattering

Erasmus Ferreira

*Instituto de Física, Universidade Federal do Rio de Janeiro
Rio de Janeiro 21945-970, RJ, Brazil*

Flavio Pereira

*DAGE, Observatório Nacional, CNPq
Rio de Janeiro 20921-400, RJ, Brazil*

The functional dependence of the high-energy observables of total cross-section and slope parameter on the sizes of the colliding hadrons predicted by the model of the stochastic vacuum and the corresponding relations used in the geometric model of Povh and Hüfner are confronted with the experimental data. The existence of a universal term in the expression for the slope, due purely to vacuum effects, and independent of the energy and of the particular hadronic system, is investigated.

1 The Model of the Stochastic Vacuum and the Geometric Models

Diffraction high energy scattering is largely determined by the non-perturbative regime of QCD. The extended character of the interaction, involving correlation properties of the gauge field, determines the properties of the observables, which are fixed by the sizes and global structures of the colliding systems, rather than by the number of constituents and their couplings. These features have led to models of geometric nature for high-energy scattering [1, 2].

A non-perturbative QCD description of the main features of high-energy scattering is given by the model of the stochastic vacuum [3, 4], which combines QCD quantities (gluon condensate and correlation length) and hadronic sizes in an eikonal framework, leading to a unified description of the data for different hadronic systems. In the present work we explore further the results of the model for the pp and $\bar{p}p$ and other hadronic systems and compare them with those from the geometric model of B.Povh and J.Hüfner [2].

The hadronic structures enter in the form of transverse wave-functions [3, 5], with the hadron size represented by a parameter S_H . The dimensionless scattering amplitude $T_{H_1 H_2}$ is given in terms of the dimensionless profile function $J_{H_1 H_2}$ for hadron-hadron scattering. We define the dimensionless moments of the profile function (with b in units of the correlation length a)

$$I_k = \int d^2\vec{b} b^k J(b) \quad , \quad k = 0, 1, 2, \dots \quad (1)$$

which depend only on S_1/a , S_2/a , and the Fourier-Bessel transform

$$I(t) = \int d^2\vec{b} J_0(ba\sqrt{|t|}) J(b) \quad (2)$$

Then

$$T_{H_1 H_2} = is\{(g^2 FF)a^4\}^2 a^2 I(t) \quad (3)$$

and

$$\sigma^T = I_0 \{(g^2 FF)a^4\}^2 a^2 \quad , \quad B = \left. \frac{d}{dt} \left(\ln \frac{d\sigma^T}{dt} \right) \right|_{t=0} = \frac{1}{2} \frac{I_2}{I_0} a^2 \equiv K a^2 \quad (4)$$

This conveniently factorizes the dimensionless QCD strength $(g^2 FF)a^4$ in the expressions for the observables. The correlation length a , which is an intrinsic parameter of the correlation function of the QCD field, appears as the natural length scale for the observables and for the geometric aspects of the interaction, contained in the quantities $I_0(S_1/a, S_2/a)$ and $I_2(S_1/a, S_2/a)$, which depend on the hadronic structures. σ^T measures the strength, while the slope B has the strength cancelled out and is only related to the hadron geometry.

2 pp and $\bar{p}p$ systems

We first discuss pp and $\bar{p}p$ systems, with $S_1 = S_2 = S$. The curves for $I_0 = \sigma^T / [(g^2 FF)^2 a^{10}]$ and $K = B/a^2$ can be parametrized as simple powers of S/a with good accuracy. The convenient expressions are

$$I_0 = \alpha \left(\frac{S}{a} \right)^\eta \quad K = \eta + \gamma \left(\frac{S}{a} \right)^\delta \quad (5)$$

The parameter values result from integrations over correlation functions, are intrinsic to the model of the stochastic vacuum, and do not contain dependence on experimental quantities. Their values are $\eta = 2.03$, $\beta = 8/3$, $\gamma = 3/8$, $\delta = 2$, $\delta/\beta = 3/4$, $\alpha = 0.76 \times 10^{-2}$.

The QCD parameters are the gluon condensate $\langle g^2 FF \rangle$ and the correlation length a . The proton radius can be eliminated from eqs.(4) and (5), and we obtain a relation between σ^T and B at a given energy

$$(B - \eta a^2) = \frac{a^2}{[\langle g^2 FF \rangle a^4]^{2\delta/\beta}} \frac{\gamma}{\alpha^{\delta/\beta}} \left(\frac{\sigma_{\text{pom}}^T}{a^2} \right)^{\delta/\beta} \quad (6)$$

The two QCD parameters can then be determined using the experimental data for σ^T and B at two different energies.

The available data on σ^T and B for pp and $\bar{p}p$ scattering at high energies consist mainly [6] of ISR (CERN) measurements at energies ranging from $\sqrt{s} = 23$ GeV to $\sqrt{s} = 63$ GeV, of the $\sqrt{s} = 541 - 546$ GeV measurements in CERN SPS and in Fermilab, and of the $\sqrt{s} = 1800$ GeV data from the E-710 Fermilab experiment. Since we are here concerned with non-perturbative contributions only, at the ISR energies we take for total cross-sections the values given by Donnachie-Landshoff parametrization [7] for the pomeron-exchange contribution, and for the values of the slope we take those of the pp system. Using as input the data for the highest energies (541 and 1800 GeV), where the process is essentially non-perturbative and no separation is needed, we obtain [4]

$$a = 0.32 \pm 0.01 \text{ fm} \quad \langle g^2 FF \rangle a^4 = 18.7 \quad \langle g^2 FF \rangle = 2.7 \pm 0.1 \text{ GeV}^4 \quad (7)$$

The relation between the experimental values is well represented at all energies from 23.5 to 1800 GeV with the form

$$B = B_\Delta + C_\Delta (\sigma^T)^\Delta \quad (8)$$

This form is similar to eq.(6), with an obvious correspondence of parameters. In our calculation with the model of the stochastic vacuum the exponent $\Delta = \delta/\beta$ does not depend on QCD quantities and is equal to about 0.75. Eq.(8) is also used in the geometric model, with $\Delta = 0.5$ and $B_\Delta = 0$.

In fig.1 we show the description of the data through eq.(8), with $\Delta = 1$, 0.75 and 0.5. There are no free parameters, since B_Δ and C_Δ are fixed by the input data. The values of χ^2 are also shown, and, although $\Delta = 0.75$ is favoured, we cannot say that the differences are statistically meaningful. However, the model of the stochastic vacuum gives precise meaning to the parameters B_Δ and C_Δ in terms of QCD quantities, and successfully fixes

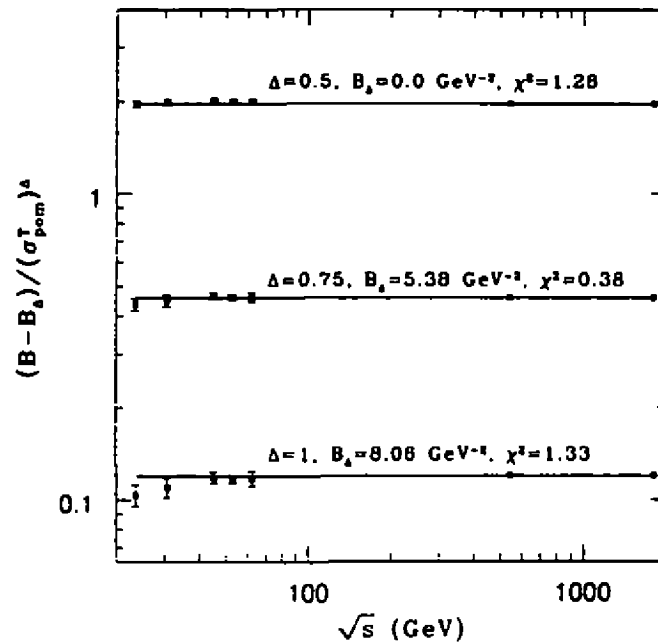


Figure 1.: Relation between experimental quantities of the pp and pp systems. At energies up to 62.3 GeV the values of σ^T shown in this figure are those given by the parametrization $\sigma_{\text{pom}}^T = (21.70 \text{ mb})s^{0.0808}$ of Donnachie-Landshoff and the values of B are those of the pp data. The point at 1800 GeV is from the Fermilab E-710 experiment. The values of B_Δ and C_Δ are obtained taking the 541 GeV and 1800 GeV data as inputs. The horizontal lines represent the constant C_Δ with values for $\Delta=1, 0.75$ and 0.5 . The values of χ^2 represent the average deviation of the five ISR points from the constant line.

$\Delta = 0.75$ a priori. It is remarkable the presence in this case of a bounding minimum B_Δ for the slope, which occurs for all hadron-proton systems.

B.Povh and J.Hüfner [2] write for Hp (hadron-proton) scattering

$$B_{Hp} = R_p^2 + R_H^2 \quad , \quad \sigma_{Hp}^T = g R_H^2 R_p^2 \quad (9)$$

The expression for B_{Hp} is to be considered as a definition of effective hadronic radii. For proton-proton scattering, with $R_H = R_p$, these relations lead to

$$B = C_{1/2} (\sigma^T)^{1/2} \quad (10)$$

which is of the form of eq.(8), and it is remarkable that using the input data and $\Delta = 1/2$, one obtains the same $B_\Delta = 0$, as shown in fig.1.

The radii are functions of the energy in both kinds of model, with values near electromagnetic radii, and a slow increase with the energy.

3 Hadron-Proton Systems

In the treatment of the pp system we are constrained by $\sqrt{s} \geq 20$ GeV, and cannot observe clearly the effect of the minimum slope B_Δ . The presence of this term can be better observed in Hp systems, where H represents hadrons of small size. Since we deal with radii which are energy dependent quantities, we must compare different hadronic systems at the same center-of-mass energy.

The parametrization of the results obtained with the model of the stochastic vacuum for general Hp systems is

$$\sigma_{pom}^T = [(g^2 FF)a^4]^2 a^2 \alpha \left(\frac{S_p}{a} \frac{S_H}{a} \right)^{\beta/2} \cdot B = \eta a^2 + \frac{1}{2} \gamma (S_p^2 + S_H^2) . \quad (11)$$

With $a = 0.32$ fm, we have $\eta a^2 = 5.38$ GeV⁻².

In order to compare the models, it is important to eliminate the influence of specific values of radii, since they have different definitions. Thanks to the convenient factorization in the final expressions, we may actually build relations involving only the observables, or involving only the ratios of radii, which we may assume to follow the ratios of electromagnetic radii. We thus have for $\sigma_{Hp}/\sigma_{H'p}$, the ratios $(r_H/r_{H'})^{4/3}$ and $(r_H/r_{H'})^2$ in the stochastic vacuum and geometric models respectively. Entering with the known values [9] for the radii of the proton (0.862 ± 0.012 fm), of the pion (0.66 ± 0.01 fm) and of the kaon (0.58 ± 0.04 fm) we obtain the results shown in table 1. The experimental ratio refers to the pomeron exchange contribution. We observe that the value 2/3 given for the ratio $\sigma_{\pi p}/\sigma_{pp}$ by the quark additivity rule is here obtained as a simple consequence of the sizes of the hadrons. Also the ratio $\sigma_{Kp}/\sigma_{\pi p}$ is consistently obtained with a value close to the data, without need for different couplings of the pomeron to strange and non-strange quarks, as must be the case with quark additivity rules. The factorization relation $\sigma_{\pi\pi} = \sigma_{\pi p}^2/\sigma_{pp}$ is identically satisfied in both cases considered here.

Table 1 - Ratios of the pomeron exchange contributions to the total cross-sections for different hadronic systems.

Cross-section ratios	stochastic vacuum	geometric model	Experimental values
$\sigma_{\pi\pi}/\sigma_{pp}$	0.69 ± 0.02	0.59 ± 0.02	0.63
$\sigma_{pK}/\sigma_{p\pi}$	0.83 ± 0.08	0.77 ± 0.08	0.87

Considering all Hp systems at a given energy, eqs.(11) lead to a nonzero minimum possible value for the slope, given by

$$B_{Hp}^{\min}(s) = \eta a^2 + \frac{\gamma}{2} S_p^2 = \frac{1}{2} \eta a^2 + \frac{1}{2} B_{pp}(s) = 2.69 \text{ GeV}^{-2} + \frac{1}{2} B_{pp}(s) . \quad (12)$$

The existence of this minimum is characteristic of the model of the stochastic vacuum. We call $G = \alpha [(g^2 FF)a^4]^2 a^2$ and for a given energy we write

$$\frac{B_{pp} - B_{Hp}}{\sigma_{pp}^{4/\beta} - \sigma_{Hp}^{4/\beta}} = \frac{(\gamma/2)(S_p^2 - S_H^2)}{G^{4/\beta}(S_p^2/a^2)^2 - G^{4/\beta}(S_p S_H/a^2)^2} = \frac{(\gamma/2) a^2}{G^{2/\beta} \sigma_{pp}^{2/\beta}} . \quad (13)$$

The last quantity is fixed, for a given energy. We obtain a straight line in a plot of B_{Hp} against $\sigma_{Hp}^{4/\beta}$, going from the point representing the observables for the pp system to the point representing the limit point B^{\min} , $\sigma = 0$ given by eq.(12). This plot is shown in fig.2, together with data for the pp, πp and Kp systems at $\sqrt{s} \approx 20$ GeV. The limit point is shown inside a square window in the figure.

A similar plot built from the equations (9) of the geometric model is shown in fig.3. In this case we have

$$B_{Hp}^{\min}(s) = R_p^2 = \frac{1}{2} B_{pp}(s) , \quad \frac{B_{pp} - B_{Hp}}{\sigma_{pp} - \sigma_{Hp}} = \frac{1}{(\sigma_{pp} g)^{1/2}} . \quad (14)$$

Comparing figs 2 and 3 we may, with some subjective influence, decide which case reproduces better the data. The existence or not of a universal term $\frac{1}{2} \eta a^2$, representing a pure non-perturbative QCD contribution to hadronic scattering, is an important question. The model of the stochastic vacuum predicts for the $\pi\pi$ system at $\sqrt{s} \approx 20$ GeV that $B_{\pi\pi} = \eta a^2 + \gamma 2 S_p^2 = 9.6$ GeV⁻², while the geometrical model predicts $B_{\pi\pi} = (2/3) S_p^2 = 7.5$ GeV⁻².

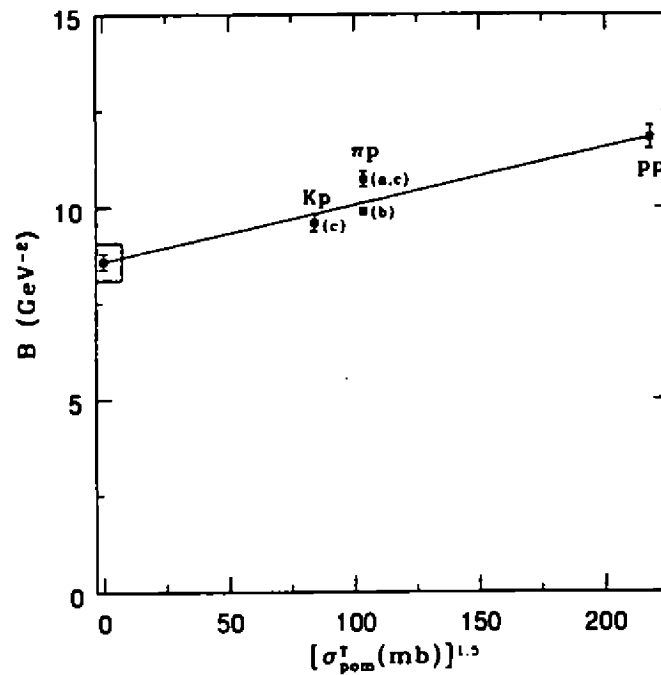


Figure 2.: Observables for different hadronic systems at 20 GeV. The straight line is the prediction of the model of the stochastic vacuum, and the square window shows the minimum value obtained in the limit of small hadrons colliding with protons at this energy.

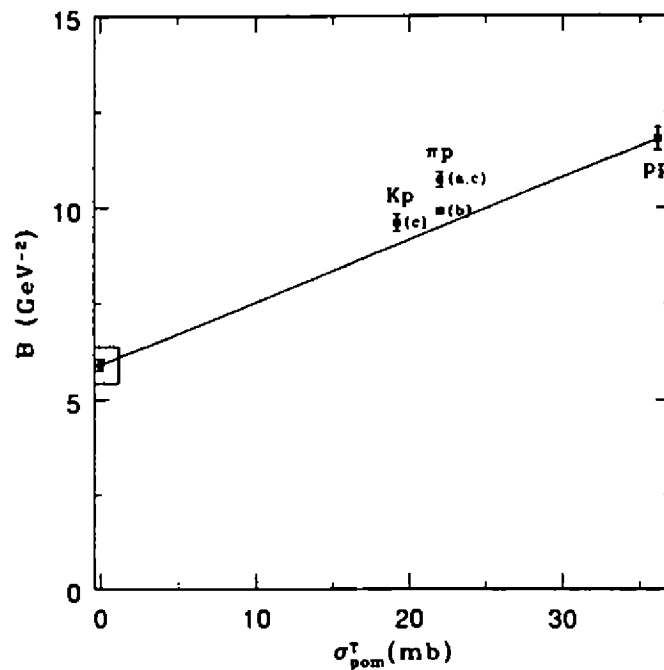


Figure 3.: Observables for different hadronic systems at 20 GeV. The straight line is the prediction of the geometric model. The square window shows the minimum value obtained when very small hadrons collide with protons at this energy.

References

- [1] C.Bourrely, J.Soffer and T.T.Wu, *Nucl. Phys.* **B247** (1984) 15, *Phys. Rev. Lett.* **54** (1985) 757, and *Phys. Lett.* **B196** (1987) 237; J.Dias de Deus and P.Kroll, *Nuovo Cimento* **A37** (1977) 67, *Acta Phys. Pol.* **B9** (1978) 157, and *J. Phys.* **G9** (1983) L81; P.Kroll, *Z. Phys.* **C15** (1982) 67; T.T.Chou and C.N.Yang, *Phys. Rev.* **170** (1968) 1591 and **D19** (1979) 3268, *Phys. Lett.* **B128** (1983) 457 and **B244** (1990) 113.
- [2] B.Povh and J.Hüfner, *Phys. Rev. Lett.* **58** (1987) 1612, *Phys. Lett.* **B215**(1988) 772 and **B245** (1990) 653, *Phys. Rev.* **D46** (1992) 990.
- [3] H.G.Dosch, E.Ferreira and A.Krämer, *Phys. Lett.* **B289** (1992) 153; *Phys. Lett.***B318** (1993) 197; *Phys. Rev.* **D50** (1994) 1992.
- [4] E.Ferreira and F.Pereira, *Phys. Lett.* submitted (1996).
- [5] H.G.Dosch and M. Ruster, *Phys. Lett.* **B205** (1996) 117.
- [6] Data on pp and $\bar{p}p$ systems. (a) N. Amos et al, *Nucl. Phys.* **B262** (1985) 689; (b) R. Castaldi and G. Sanguinetti, *Ann. Rev. Nucl. Part. Sci.* **35** (1985) 351; (c) C. Augier et al, *Phys. Lett.* **B316** (1993) 448; (d) M. Bozzo et al, *Phys. Lett.* **B147** (1984) 392; M. Bozzo et al, *Phys. Lett.***B147** (1984) 385; (e) N. Amos et al, *Phys. Lett.***B247** (1990) 127; *Phys. Rev. Lett.* **68** (1992) 2433;
- [7] A.Donnachie and P.V.Landshoff, *Phys. Lett.* **B296** (1992) 227.
- [8] Slopes of πp and Kp systems. (a) J.B.Burq et al, *Nucl. Phys.***B217** (1983) 285; (b) A.Schiz et al, *Phys. Rev.* **D24** (1981) 26; (c) L.A.Fajardo et al, *Phys. Rev.* **D24** (1981) 46; (d) N.Adamus et al, *Phys. Lett.* **B186** (1987) 223.
- [9] Electromagnetic radii. (a) Proton : G.G. Simon et al, *Z. Naturforschung* **35A** (1980) 1; (b) Pion : S.R. Amendolia et al, *Nucl. Phys.* **B277** (1986) 168; (c) Kaon : S.R. Amendolia et al, *Phys. Lett.* **B178** (1986) 435.

Probing Higgs Couplings in $e^+e^- \rightarrow \gamma\gamma\gamma$

F. de Campos, S. M. Lietti, S. F. Novaes and R. Rosenfeld*

Instituto de Física Teórica, Universidade Estadual Paulista,

Rua Pamplona 145, CEP 01405-900 São Paulo, Brazil.

We present a summary of a recent investigation [1] about the existence of anomalous Higgs boson couplings, $H\gamma\gamma$ and $HZ\gamma$, through the analysis of the process $e^+e^- \rightarrow \gamma\gamma\gamma$ at LEP2 energies. We suggest some kinematical cuts to improve the signal to background ratio and determine the capability of LEP2 to impose bounds on those couplings by looking for a Higgs boson signal in this reaction.

1 Introduction

The predictions of Standard Model (SM) for the structure of the fermion-vector boson couplings have been exhaustively tested in the last few years. In particular, the recent data of LEP1 at the Z -pole have confirmed with an unprecedented degree of precision the properties of the neutral weak boson and its vector and axial couplings with the different fermion flavors. Nevertheless, we do not have the same level of confidence on other sectors of the SM, like the self-couplings among the vector bosons and the Higgs boson couplings with fermions and bosons. The determination of these interactions can either confirm the non-abelian gauge structure of the theory and the mechanism of the spontaneous breaking of the electroweak symmetry or provide some hint about the existence of new physics beyond the SM.

A convenient way to parameterize possible deviations of the SM predictions is through the effective theory approach [2]. In this scenario, we assume that the existence of new physics, associated to a high-energy scale Λ , can manifest itself at low energy via quantum corrections, where the heavy degrees of freedom are integrated out. These effects are then described by effective operators involving the spectrum of particles belonging to the low-energy theory, *i.e.* the usual fermions and bosons.

In the linear representation, a general dimension six effective Lagrangian can be written as,

$$\mathcal{L}_{\text{eff}} = \sum_n \frac{f_n}{\Lambda^2} \mathcal{O}_n \quad (1)$$

where the operators \mathcal{O}_n involve simultaneously both vector boson and Higgs boson fields which share the same coefficients f_n . Therefore, the study of anomalous Higgs boson couplings can be an important tool to investigate the effect of new physics and concomitantly furnish information about the self-coupling of the vector bosons. In particular, anomalous $H\gamma\gamma$ and $HZ\gamma$ couplings have already been considered in Z and Higgs boson decays [3], in e^+e^- collisions [3, 4] and at $\gamma\gamma$ colliders [5].

We make an exhaustive analysis of the anomalous Higgs boson contribution to the reaction $e^+e^- \rightarrow \gamma\gamma\gamma$ at LEP2 in order to extract information about possible anomalous $H\gamma\gamma$ and $HZ\gamma$ couplings. This process is an ideal place to look for deviations from the SM since it only involves well known purely QED contributions at tree level [6]. Our Monte Carlo analysis of the contribution $e^+e^- \rightarrow \gamma, Z \rightarrow \gamma H (-\gamma\gamma)$ includes all the irreducible QED background and the respective interferences. After detailed study of the signal and background distributions, we find optimum cuts to maximize the signal to background ratio. We show how to use energy and invariant mass spectra of the final state photons in order to identify the presence of a Higgs boson and extract information about its couplings. Finally, we compare the bounds on the anomalous couplings that could be provided by this reaction with the present direct information on the triple vector boson coupling.

*Presented by R. Rosenfeld at the XVII Brazilian Meeting of Particle and Fields, Serra Negra, September 1996.

2 Anomalous Higgs Couplings and $e^+e^- \rightarrow \gamma\gamma\gamma$

The anomalous $H\gamma\gamma$ and $HZ\gamma$ can be written in a compact form as.

$$\mathcal{L}_{\text{eff}}^H = g_{H\gamma\gamma} H A_{\mu\nu} A^{\mu\nu} + g_{HZ\gamma}^{(1)} A_{\mu\nu} Z^\mu \partial^\nu H + g_{HZ\gamma}^{(2)} H A_{\mu\nu} Z^{\mu\nu} . \quad (2)$$

where $A(Z)_{\mu\nu} = \partial_\mu A(Z)_\nu - \partial_\nu A(Z)_\mu$.

In order to reduce the number of free parameters and, at the same time relate the anomalous Higgs and the triple vector boson couplings, we make the natural assumption that all the coefficients of the dimension 6 operators have a common value f [7]. In this scenario, $g_{HZ\gamma}^{(1)} = 0$, and we can relate the other Higgs boson anomalous couplings with the coefficient of the usual anomalous vector boson coupling, $\Delta\kappa_\gamma = (M_W^2/\Lambda^2)f$, through.

$$\begin{aligned} |g_{H\gamma\gamma}| &= \frac{gs^2}{2M_W} |\Delta\kappa_\gamma| \simeq 9.2 \times 10^{-4} \text{ GeV}^{-1} \times |\Delta\kappa_\gamma|, \\ |g_{HZ\gamma}^{(2)}| &= \frac{gsc(1-s^2/c^2)}{2M_W} |\Delta\kappa_\gamma| \simeq 1.2 \times 10^{-3} \text{ GeV}^{-1} \times |\Delta\kappa_\gamma|. \end{aligned} \quad (3)$$

We should point out that the anomalous vector boson couplings, like $\Delta\kappa_\gamma$, are basically unconstrained by the current high precision electroweak data. Presently, the best direct bound on $\Delta\kappa_\gamma$ was the one obtained by the CDF Collaboration [8] and constraints $-1.0 < \Delta\kappa_\gamma < 1.1$, at 95% C.L.. At LEP2, the angular distribution of final state fermions of the reaction $e^+e^- \rightarrow W^+W^- \rightarrow \ell\nu jj$ will be able to further restrict the allowed values of $\Delta\kappa_\gamma$ to $-0.19 < \Delta\kappa_\gamma < 0.21$, at 95% C.L. [7], for $\sqrt{s} = 176$ GeV.

An interesting option to test the couplings described by (2) is through the reaction $e^+e^- \rightarrow \gamma, Z \rightarrow H(\rightarrow \gamma\gamma)$. This process has already been tested at the Z pole by LEP1 which established an upper limit on the branching ratio $B(Z \rightarrow \gamma\gamma\gamma) < 1.0 \times 10^{-5}$. We found that this bound is not able to further restrict $\Delta\kappa_\gamma$ beyond the existent direct bounds [8]. For instance, for a 70 GeV Higgs, the above limit requires $\Delta\kappa_\gamma > 1.4$.

Here we make a detailed analysis for the two expected runs of LEP2 collider *i.e.* $\sqrt{s} = 176$ GeV, with $\mathcal{L} = 0.5$ fb $^{-1}$, and $\sqrt{s} = 190$ GeV, with $\mathcal{L} = 0.3$ fb $^{-1}$. We performed a Monte Carlo analysis using the package MadGraph [9] coupled to HELAS [10]. Special subroutines were constructed for the anomalous contributions which enable us to take into account all interference effects between the QED and the anomalous amplitudes. The phase space integration was performed by VEGAS [11].

In order to search for optimum cuts to maximize the signal to background ratio, we label the three final state photons as $\gamma_{1,2,3}$ according to decreasing value of their energy, *i.e.* $E_{\gamma_1} > E_{\gamma_2} > E_{\gamma_3}$. We start our analysis applying the following standard cuts on the events: $|\cos\theta_{ei}| \leq 0.97$, $\theta_{ij} > 15^\circ$, $E_{\gamma_i} \geq 5$ GeV, where θ_{ei} is the angle between the photon i and the electron/positron beam direction, and θ_{ij} is the angle between the photon pair (i, j) .

An analysis of the angular distributions suggests that, if we require the maximum angle between any pair of photons to be less than 165° ($\cos\theta_{ij} > -0.97$), we can eliminate a large portion of the background events. On the other hand, from the photon spectra we learn that cutting the maximum energy of each photon, for instance $E_{\gamma_i} < 70$ GeV, can significantly reduce the background. Finally, the angular distribution of the softest photon with the beam suggests a cut $|\cos\theta_{r3}| \leq 0.8$, which reduces the background to the same order of the signal cross section. We should notice that the above cuts are less efficient for heavier Higgs bosons, restricting our analysis to a Higgs boson with mass up to 100 GeV.

From the above considerations, we have further imposed the energy cut,

$$5 \leq E_{\gamma_i} \leq 70 \text{ (80) GeV} . \quad (4)$$

for $\sqrt{s} = 176$ (190) GeV, and the following angular cuts,

$$|\cos\theta_{r1,e2}| \leq 0.97 . \quad (5)$$

$$|\cos\theta_{r3}| \leq 0.80 . \quad (6)$$

$$15^\circ < \theta_{ij} < 165^\circ . \quad (7)$$

3 Conclusions

In order to estimate the reach of LEP2 to disentangle the anomalous Higgs boson couplings via the reaction $e^+e^- \rightarrow \gamma\gamma\gamma$, we have evaluated the significance of the signal based both on the total cross section and on the Higgs boson enhancement in the $d\sigma/dE_\gamma dM_{inv}$ distribution. We have scanned the values of $\Delta\kappa_\gamma$, for $M_H = 80, 90,$ and 100 GeV.

We studied the minimum values of $\Delta\kappa_\gamma$ that can be probed in two runs of LEP2, for a center-of-mass energy of 176 and 190 GeV, with luminosities of $\mathcal{L} = 0.5$ and 0.3 fb^{-1} , respectively. The combined result for both runs is also presented. We required a 95 % of C.L. effect in the total cross section (σ_{tot}) and also in the double differential distribution ($d\sigma/dE_\gamma dM_{inv}$). In the latter case, we have added up the events in the eight 1 GeV bins around the expected Higgs boson signal.

We found that, if the anomalous coupling $|\Delta\kappa_\gamma| \gtrsim 0.8$ it will be possible to identify an anomalous Higgs boson in the range 80–100 GeV with 95 % C.L.. However, the signature of a heavier Higgs boson will not be so clear since the reaction $e^+e^- \rightarrow \gamma, Z \rightarrow \gamma H (-\gamma\gamma)$ is particularly important when the Higgs boson is almost on-mass shell.

In conclusion, the search for anomalous Higgs boson couplings at LEP2 provides a complementary way to probe effective Lagrangians that are low-energy limit of physics beyond the SM. We have shown that the study of the process $e^+e^- \rightarrow \gamma\gamma\gamma$ is able to improve the present limits on the anomalous vector boson couplings that are concomitantly involved in operators that modify the bosonic sector of the Standard Model.

Acknowledgments

This work was supported by Conselho Nacional de Desenvolvimento Científico e Tecnológico (CNPq), and by Coordenação de Aperfeiçoamento de Pessoal de Nível Superior (CAPES).

References

- [1] F. de Campos, S. M. Lietti, S. F. Novaes and R. Rosenfeld, preprint IFT-P-021-96, hep-ph/9607241, to be published in Phys. Lett. B.
- [2] S. Weinberg, *Physica* **96A** (1979) 327; J. F. Donoghue, E. Golowich and B. R. Holstein, *Dynamics of the Standard Model* (Cambridge University Press, Cambridge, England, 1992).
- [3] K. Hagiwara, R. Szalapski, and D. Zeppenfeld, *Phys. Lett.* **B318** (1993) 155.
- [4] K. Hagiwara, and M. L. Stong, *Z. Phys.* **C62** (1994) 99; B. Grzadkowski, and J. Wudka, *Phys. Lett.* **B364** (1995) 49; G. J. Gounaris, J. Layssac and F. M. Renard, *Z. Phys.* **C65** (1995) 245; G. J. Gounaris, F. M. Renard and N. D. Vlachos, *Nucl. Phys.* **B459** (1996) 51; W. Kilian, M. Krämer and P. M. Zerwas, Report No. hep-ph/9603409; S. M. Lietti, S. F. Novaes and R. Rosenfeld, *Phys. Rev.* **D54**, 3326 (1996).
- [5] G. J. Gounaris and F. M. Renard, *Z. Phys.* **C69** (1996) 513.
- [6] See, for instance: M. Baillargeon, F. Boudjema, E. Chopin and V. Lafage, Report No. hep-ph/9506396 and references therein.
- [7] H. Aihara *et al.*, in "Electroweak Symmetry Breaking and Beyond the Standard Model", edited by T. Barklow, S. Dawson, H. Haber and J. Siegrist (World Scientific, Singapore), Report No. hep-ph/9503425.
- [8] S. M. Errede, in Proceedings of the XXVII International Conference on High Energy Physics, Glasgow, Scotland, p. 433, edited by P. J. Bussey and I. G. Knowles.
- [9] T. Stelzer and W. F. Long, *Comput. Phys. Commun.* **81** (1994) 357.
- [10] H. Murayama, I. Watanabe and K. Hagiwara, KEK Report 91-11 (unpublished).
- [11] G. P. Lepage, *J. Comp. Phys.* **27** (1978) 192; "Vegas: An Adaptive Multidimensional Integration Program", CLNS-80/447, 1980 (unpublished).

The fermion families replication question*

Felice Pisano

*Instituto de Física Teórica, Universidade Estadual Paulista
Rua Pamplona 145 - 01405-000 - São Paulo, S.P. Brazil*

We consider the simplest way for solving the flavor question by embedding the three-family Standard Model in a semisimple gauge group extending minimally the weak isospin factor. Our demonstration shows how the theory leads to determination of families structure when the Standard Model is the input at low energies.

In the Standard Model [1] the fundamental fermions come in families. In writing down the theory one may start by first introducing just one family, then one may repeat the same procedure by introducing copies of the first family. Why do quarks and leptons come in repetitive structures (families)? How many families are there? How to understand the inter-relation between families? These are the central issues of the weak interaction physics known as the flavor question or the family problem. Nowhere in physics this question is replied [2]. One of the most important experimental results in the past few years has been the determination of the number of these families within the framework of the Standard Model. In the minimal electroweak model the number of families is given by the number of the neutrino species which are all massless, by definition. We wish to suggest here that some very fundamental aspects of the Standard Model, in particular the flavor question, might be understood by embedding the three-family version in a Yang-Mills theory with the gauge semisimple group [3, 4]

$$G_{331} \equiv SU(3)_C \otimes SU(3)_L \otimes U(1)_N$$

with a corresponding enlargement of the quark representations. In particular, the number of families will be related by anomaly cancellation to the number of quark colors. In the

$$G_{321} \equiv SU(3)_C \otimes SU(2)_L \otimes U(1)_Y$$

low-energy limit all three families appear similar and cancel anomalies separately. The G_{331} model is a dilepton gauge theory which is chiral and has nontrivial anomaly cancellation. This novel method of anomaly cancellation requires that at least one family transforms differently from the others, thus breaking generation universality. Unlike the G_{321} Standard Model, where anomalies cancel family by family, anomalies in the G_{331} model only cancel when all three families are taken together. With this meaning we present here the simplest solution for the flavor question just enlarging the $SU(2)_L$ weak isospin group to $SU(3)_L$. This does not explain why $N_{\text{fam}} > 1$ for the number of families but is sufficiently impressive to suggest that $N_{\text{fam}} = 3$ may be explicable by anomaly cancellation in the simplest gauge extension of the Standard Model with a very particular representation content. The electroweak gauge group extension from $SU(2)$ to $SU(3)$ will add five gauge bosons.

The adjoint gauge octet of $SU(3)$ breaks into $8 = 3 + (2+2) + 1$ under $SU(2)$. The 1 is a Z' and the two doublets are readily identifiable from the leptonic triplet or antitriplet (ν_l, l^-, l^+) as dilepton gauge bosons (U^{--}, V^-) and (U^{++}, V^+). Such dileptons appeared first in stable-proton GUT [5] but there the fermions were non-chiral and one needed to invoke mirror fermions: this is precisely what is avoided in the G_{331} model. Contrary to the GUT case, there is no "grand desert" if G_{331} models are realized in nature and new physics could arise at not too high energies, say in the TeV range [6].

We start with the way the electric charge operator Q is embedded in the neutral generators of the $SU(3)_L$ group. The fermion contents depend on the electric charge operator

$$Q = \frac{1}{2}(\lambda_3^L + \xi \lambda_8^L) + N \quad (1)$$

*Talk presented at XVII Brazilian National Meeting on Particles and Fields, Serra Negra, September 1996

where $\lambda_{3,8}^L$ are the neutral generators of $SU(3)_L$, ξ is the embedding parameter and N is the $U(1)_N$ charge proportional to the unit matrix. The $SU(3)_L$ generators are normalized as $\text{Tr}(\lambda_a^L \lambda_b^L) = 2\delta_{ab}$; $a, b = 1, 2, \dots, 8$. In the G_{331} models with lepton charges $0, \pm 1$ there is always a set of families transforming as $(1, 3, 0)$ under the gauge group. In these families there is charge quantization in the sense of GUTs; the electric charge operator is a linear combination of the simple group generators.

In the $\xi = -\sqrt{3}$ model [3] three families of leptons belong to representation

$$\psi_{iL} \equiv \begin{pmatrix} \nu_i \\ l \\ l^c \end{pmatrix}_L \sim (1, 3, N_{\psi_{iL}} = 0); \quad l = e, \mu, \tau \quad (2)$$

where $l^c = C\bar{l}^T$ and C being the charge conjugation matrix. The right-handed neutrinos may be included in the theory if desired [7].

A result of this embedding is that there are no new leptons in the G_{331} model. While all three lepton families are treated identically, anomaly cancellation requires that one of the quark families transforms differently from the other two. In particular, canceling the pure $SU(3)_L$ anomaly requires that there are the same number of triplets and antitriplets. Taking into account the three quark color degrees of freedom we must introduce the multiplets of chiral quarks

$$Q_{iL} \equiv \begin{pmatrix} u \\ d \\ J \end{pmatrix}_L \sim (3, 3, N_{Q_{iL}}); \quad Q_{2,3L} \equiv \begin{pmatrix} j_1, j_2 \\ c, t \\ s, b \end{pmatrix}_L \sim (3, 3^*, N_{Q_{2,3L}}) \quad (3)$$

with the respective right-handed fields in $SU(3)_L$ singlets.

$$\begin{aligned} u_R &\sim (3, 1, N_{u_R}), & c_R &\sim (3, 1, N_{c_R}), & t_R &\sim (3, 1, N_{t_R}); \\ d_R &\sim (3, 1, N_{d_R}), & s_R &\sim (3, 1, N_{s_R}), & b_R &\sim (3, 1, N_{b_R}), \end{aligned} \quad (4)$$

and the exotic quarks

$$J_R \sim (3, 1, N_{J_R}), \quad j_{1R} \sim (3, 1, N_{j_{1R}}), \quad j_{2R} \sim (3, 1, N_{j_{2R}}) \quad (5)$$

where we have suppressed the color index. We are dealing with a gauge theory of chiral fermions. There are two quite distinct ways in which the G_{331} model establish the inter-relation between fermion families. Firstly, there are a set of constraints which follow from the consistency of the theory at the classical level, such as the requirement that the Lagrangian be gauge invariant, while there are other constraints which follow from the consistency of the theory at the quantum level which are the anomaly cancellation conditions. Anomalies imply the loss of a classical symmetry in the quantum theory [8]. For chiral gauge theories in four dimensions our basic tool will be freedom from the triangle perturbative chiral gauge anomaly which must be canceled to avoid the breakdown of gauge invariance and the renormalizability of the theory. Of course, it is clear that anomalies alone cannot lead to a definite theory without some way to specify the underlying chiral fermions and some knowledge of the gauge symmetry that is responsible for the dynamics.

Let us first obtain the classical constraints. In order to generate Yukawa couplings we introduce the minimal set of scalar fields $SU(3)_L$ triplets $\eta \sim (1, 3, N_\eta)$, $\rho \sim (1, 3, N_\rho)$, and $\chi \sim (1, 3, N_\chi)$. The Yukawa Lagrangian, without considering the mixed terms between quarks is

$$\begin{aligned} -\mathcal{L}_Y^q &= \bar{Q}_{1L}(G_u u_R \eta + G_d d_R \rho + G_J J_R \chi) + (G_c \bar{Q}_{2L} c_R + G_t \bar{Q}_{3L} t_R) \rho^* \\ &+ (G_s \bar{Q}_{2L} s_R + G_b \bar{Q}_{3L} b_R) \eta^* + (G_{j_1} \bar{Q}_{2L} j_{1R} + G_{j_2} \bar{Q}_{3L} j_{2R}) \chi^* + \text{H.c.} \end{aligned} \quad (6)$$

where all fields are weak eigenstates and η^*, ρ^*, χ^* denote the respective antitriplets [9]. The requirement of gauge invariance leads to the classical constraints

$$\begin{aligned} N_{Q_{1L}} - N_{u_R} &= N_\eta \\ N_{Q_{1L}} - N_{d_R} &= N_\rho \\ N_{Q_{1L}} - N_{J_R} &= N_\chi \end{aligned} \quad (7)$$

for the first family and

$$\begin{aligned} N_{Q_{3L}} - N_{j_{1R}} &= N_{\chi^*} \\ N_{Q_{2L}} - N_{c_R} &= N_{\rho^*} \\ N_{Q_{2L}} - N_{s_R} &= N_{\eta^*} \end{aligned} \quad (8)$$

for the second family. The constraints for the third family are obtained from those of the second family making the replacements $Q_{2L} \rightarrow Q_{3L}$, $j_{1R} \rightarrow j_{2R}$, $c_R \rightarrow t_R$, and $s_R \rightarrow b_R$. The above equations with $N_{\eta^*} = -N_{\eta}$, $N_{\rho^*} = -N_{\rho}$, and $N_{\chi^*} = -N_{\chi}$ imply

$$\begin{aligned} N_{Q_{1L}} + N_{Q_{2L}} &= N_{u_R} + N_{s_R} \\ N_{Q_{1L}} + N_{Q_{3L}} &= N_{d_R} + N_{c_R} \\ N_{Q_{1L}} + N_{Q_{2L}} &= N_{j_{1R}} + N_{j_{2R}} \end{aligned} \quad (9)$$

constraining the first and second families and

$$\begin{aligned} N_{Q_{2L}} - N_{Q_{3L}} &= N_{j_{1R}} - N_{j_{2R}} \\ N_{Q_{2L}} - N_{Q_{3L}} &= N_{c_R} - N_{t_R} \\ N_{Q_{2L}} - N_{Q_{3L}} &= N_{s_R} - N_{b_R} \end{aligned} \quad (10)$$

which relates the second and third families. This step illustrates how the Lagrangian is used as the primary source of constraints. In contrast to the minimal Standard Model, the classical and the quantum constraints enclose all three families of fermions. Although each family is anomalous, this type of construction is only anomaly-free when the number of families is divisible by the number of colors. Thus three families are singled out as the simplest nontrivial anomaly-free G_{331} model.

The flavor question of the Standard Model might be understood by embedding the three family version in the G_{331} group with a corresponding enlargement of the quark representations. In the G_{331} low-energy limit all three families appear similarly and cancel anomalies separately. By matching the coupling constants at the G_{331} symmetry breaking an upper limit on the symmetry-breaking scale of a few TeVs can be placed by the requirement that $\sin^2 \theta_W < 1/4$, implying that the physics associated with the $(U^{\pm\pm}, V^{\pm})$ dilepton gauge bosons, the additional Z' neutral gauge boson, and the $J, j_{1,2}$ exotic quarks will be accessible to the next generation of colliders [6, 10]. The Standard Model is the effective low energy theory of the G_{331} model and it enjoys considerable support from experiment. As such we can take it to be a safe input to G_{331} . According to Eq. (2) we have directly $N_{\psi_{lL}} = 0$ for any leptonic family $l = e, \mu, \tau$. Let us set the following notation

$$N_{u_R} = N_{c_R} = N_{t_R} \equiv N_{U_R} \quad (11)$$

$$N_{d_R} = N_{s_R} = N_{b_R} \equiv N_{D_R} \quad (12)$$

and from the constraints given in Eqs. (10) we obtain the following two conditions

$$N_{Q_{2L}} = N_{Q_{3L}} \equiv N_{Q_{aL}}, \quad a = 2, 3; \quad (13)$$

and

$$N_{j_{1R}} = N_{j_{2R}} \equiv N_{j_R}. \quad (14)$$

Thus we write the quantum constraints in the concise form

$$\begin{aligned} \text{Tr}[\text{SU}(3)_C]^2[\text{U}(1)_N] &= 0 : \\ 3(N_{Q_{1L}} + 2N_{Q_{aL}}) - 3(N_{U_R} + N_{D_R}) - N_{j_R} - 2N_{j_R} &= 0 \\ \text{Tr}[\text{SU}(3)_L]^2[\text{U}(1)_N] &= 0 : \end{aligned} \quad (15)$$

$$3(N_{Q_{1L}} + 2N_{Q_{\alpha L}}) = 0 \tag{16}$$

$$\text{Tr}[U(1)_N]^3 = 0 :$$

$$3(N_{Q_{1L}}^3 + 2N_{Q_{\alpha L}}^3) - 3(N_{U_R}^3 + N_{D_R}^3) - N_{J_R}^3 - 2N_{j_R}^3 = 0 \tag{17}$$

and the mixed gravitational-gauge constraint [11] coincides with the

$$[\text{SU}(3)_C]^2[U(1)_N]$$

anomaly. In the new notation the classical constraints given in Eqs. (9) becomes

$$\begin{aligned} N_{Q_{1L}} + N_{Q_{2L}} &= N_{U_R} + N_{D_R} \\ N_{Q_{1L}} + N_{Q_{2L}} &= N_{j_R} + N_{J_R} \end{aligned} \tag{18}$$

From these classical constraints we obtain

$$N_{U_R} + N_{D_R} = N_{j_R} + N_{J_R} \tag{19}$$

which through Eq. (16) the quantum constraint of Eq. (15) gives a relation between N -charges of the exotic quarks

$$4N_{J_R} + 5N_{j_R} = 0 \tag{20}$$

and from Eq. (19) we find

$$N_{U_R} + N_{D_R} = \frac{1}{5}N_{j_R} \tag{21}$$

If the Standard Model is the input at low energies we know that

$$N_{U_R} = \frac{2}{3} \quad \text{and} \quad N_{D_R} = -\frac{1}{3} \tag{22}$$

and then from Eqs. (20) and (21) we obtain the electric charges of the exotic quarks

$$N_{J_R} = \frac{5}{3} \quad \text{and} \quad N_{j_R} = -\frac{4}{3} \tag{23}$$

At this stage it is also possible to establish the last $U(1)_N$ charges of the new G_{331} attributions. Let us take the quantum constraint of Eq. (16)

$$N_{Q_{1L}} = -2N_{Q_{\alpha L}} \tag{24}$$

and the cubic quantum constraint of Eq. (17) which, in turn, may be related to give

$$N_{Q_{1L}} = \frac{2}{3} \tag{25}$$

and

$$N_{Q_{\alpha L}} = -\frac{1}{3}, \quad \alpha = 2, 3 \tag{26}$$

for the three families of chiral left-handed quarks.

The G_{331} model is indistinguishable from the Standard Model at low energies. In this class of models in order to cancel anomalies the number of families, N_{fam} , must be divisible by the number of colors degrees of freedom, N_C . Hence the simplest possibility is $N_{\text{fam}}/N_C = 1$. An interesting fact concerns the generalization from $\text{SU}(3)_L$ to $\text{SU}(4)_L$. Using again the lightest leptons as the particles which determine the approximate symmetry, if each family is treated separately, $\text{SU}(4)$ is the highest symmetry group to be considered in the electroweak sector [12]. In this sense this is the maximal generalization of G_{331} model. There is no room for $\text{SU}(5)_L \otimes U(1)$ if the nature restrict to the case of leptons with $0, \pm 1$ electric charges.

Much of the appeal of the G_{331} model is that the new physics is guaranteed to be below a few TeV, well within the reach of future colliders [6]. Finally, could be that 331 models are not just an embedding of the Standard Model but an alternative to describe these same interactions and new ones.

I would like to thank the Fundação de Amparo à Pesquisa do Estado de São Paulo (FAPESP) for a research fellowship.

References

- [1] S.L. Glashow, Nucl. Phys. **22**, 279 (1961); S. Weinberg, Phys. Rev. Lett. **19**, 1264 (1967); A. Salam, in *Proceedings of the VIII Nobel Symposium*, Edited by N. Svartholm (Almqvist and Wiksell, Stockholm, 1968) 367; H. Fritzsch, M. Gell-Mann and H. Leutwyler, Phys. Lett. B **47**, 365 (1973).
- [2] S.L. Glashow, in *The Unity of the Fundamental Interactions*, Edited by A. Zichichi, (Plenum Press, 1983) 14.
- [3] F. Pisano and V. Pleitez, Phys. Rev. D **46**, 410 (1992); R. Foot, O.F. Hernandez, F. Pisano and V. Pleitez, Phys. Rev. D **47**, 4158 (1993).
- [4] P.H. Frampton, Phys. Rev. Lett. **69**, 2889 (1992).
- [5] P.H. Frampton and B.H. Lee, Phys. Rev. Lett. **64**, 619 (1990); P.B. Pal, Phys. Rev. D **43**, 236 (1991).
- [6] D. Ng, Phys. Rev. D **49**, 4805 (1994).
- [7] P.H. Frampton, P.I. Krastev and J.T. Liu, Mod. Phys. Lett. A **9**, 761 (1994).
- [8] S. Adler, Phys. Rev. **177**, 2426 (1969); J.S. Bell and R. Jackiw, Nuovo Cimento **60A**, 49 (1969).
- [9] J.C. Montero, F. Pisano and V. Pleitez, Phys. Rev. D **47**, 2918 (1993).
- [10] D.G. Dumm, F. Pisano and V. Pleitez, Mod. Phys. Lett. A **9**, 1609 (1994).
- [11] R. Delbourgo and A. Salam, Phys. Lett. B **40**, 381 (1972); L. Alvarez-Gaumé and E. Witten, Nucl. Phys. B **234**, 269 (1983).
- [12] M.B. Voloshin, Sov. J. Nucl. Phys. **48**, 512 (1988); R. Foot, H.N. Long and T.A. Tran, Phys. Rev. D **50**, R34 (1994); F. Pisano and V. Pleitez, Phys. Rev. D **51**, 3865 (1995).

Espectro de Muons e Neutrinos ao Nível do Mar

H.M.Portella, A.S.Gomes, A.L.V.Silva, R.H.C.Maldonado
Instituto de Física/UFF - Niterói - RJ

N.Amato, C.E.C.Lima, L.C.Oliveira
Centro Brasileiro de Pesquisas Físicas-CBPF/CNPq - Rio de Janeiro - RJ

Os fluxos de muons e neutrinos são calculados analiticamente para energias entre 1 GeV e 100 TeV e para diferentes ângulos zenitais. As razões lepton/antilepton são também estimadas. As razões μ^+/μ^- calculadas ao nível do mar é de 1.37 quando se considera muons vindos unicamente dos pions e um valor de 0.74 para a razão neutron/proton no topo da atmosfera. As razões $\frac{\nu_e + \bar{\nu}_e}{\nu_e + \bar{\nu}_e}$ são usadas no cálculo do *rate* do detector de Kamiokande.

Hipóteses Usadas no Cálculo

Os fluxos de hadrons e leptons são obtidos analiticamente com o uso do Método das Aproximações Sucessivas considerando uma seção de choque constante, um espectro primário na forma usual de potência com $\gamma = 1.7$ e para as distribuições de energia dos mesons secundários, as parametrizadas por A. Hillas [1] de dados de aceleradores e também as usadas por Gaisser [2].

Para as densidades atmosféricas foi usada a U. S. Standard para altitudes menores que 11 km e a isotérmica para valores maiores que 11 km.

Introduziu-se nas equações de difusão dos muons os termos de ionização e do decaimento dessas partículas em elétrons e neutrinos. A perda de energia dos muons ao atravessar a atmosfera foi considerada contínua e da forma: $\frac{dE}{dx} = a + bE$, com a e b constantes.

Para ângulos zenitais maiores que 60° fez-se às correções nos fluxos devido à curvatura da Terra [3].

Na região de energia entre 300 MeV e 1 GeV introduziu-se efeitos geomagnéticos que são importantes na estimativa dos fluxos dos neutrinos muônicos e eletrônicos. Esses fluxos são comparados com os obtidos por simulação por T.K.Gaisser *et al* [4].

Como fonte de muons (μ^\pm) e dos neutrinos ($\nu_\mu, \bar{\nu}_\mu$) e ($\nu_e, \bar{\nu}_e$) considerou-se os decaimentos dos mesons π^\pm, K^\pm, K_L e também o decaimento dos μ^\pm em $e^\pm, \nu_\mu, \bar{\nu}_\mu$ e $\nu_e, \bar{\nu}_e$.

Resultados e Conclusões

Na figura 1 mostra-se que os fluxos de muons vindos dos π^\pm são sempre maiores que os vindos de K^\pm . Para 1 GeV os muons originados do decaimento dos kaons é aproximadamente 5,2% dos muons originados do decaimento dos pions atingindo um valor de $\sim 40\%$ para 100 TeV. Esse fato está intimamente ligado com a escolha do valor da razão neutron/proton do espectro primário e das razões π^+/π^- e K^+/K^- .

Na figura 2 observa-se que acima de 1 TeV os ν_μ e $\bar{\nu}_\mu$ são dominados pelo decaimento dos K^\pm , enquanto que na figura 3 verifica-se que os ν_e e $\bar{\nu}_e$ são originados unicamente dos decaimentos dos K_L e K^\pm .

As razões lepton/antilepton variam de 1 GeV até 100 TeV da seguinte forma:

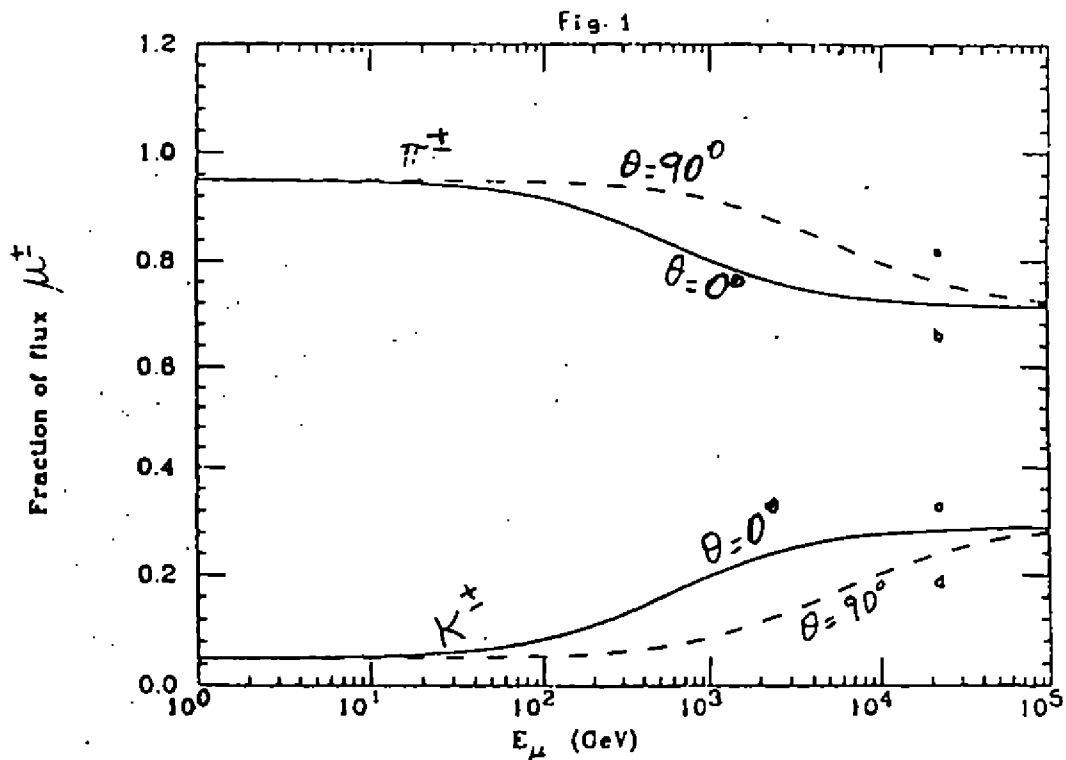
$$\theta = 8,9^\circ \quad \left\{ \begin{array}{l} 1,3 \leq \mu^+/\mu^- \leq 1,51 \\ 1,05 \leq \nu_\mu/\bar{\nu}_\mu \leq 2,4 \\ 1,28 \leq \nu_e/\bar{\nu}_e \leq 1,6 \end{array} \right.$$

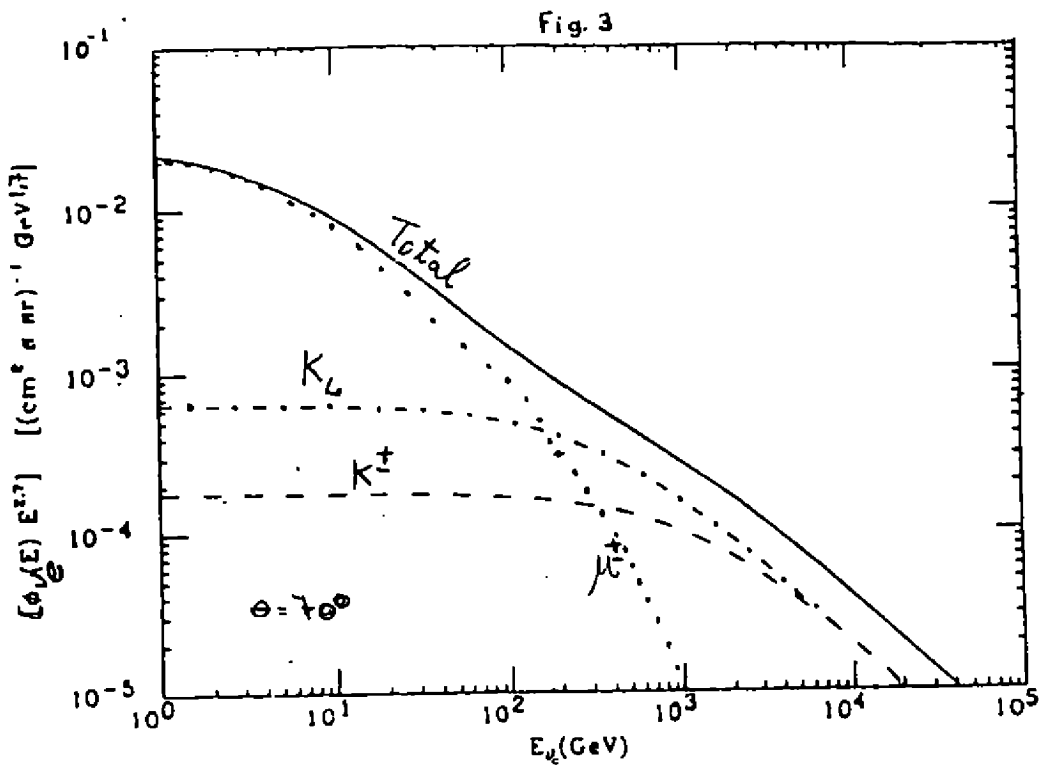
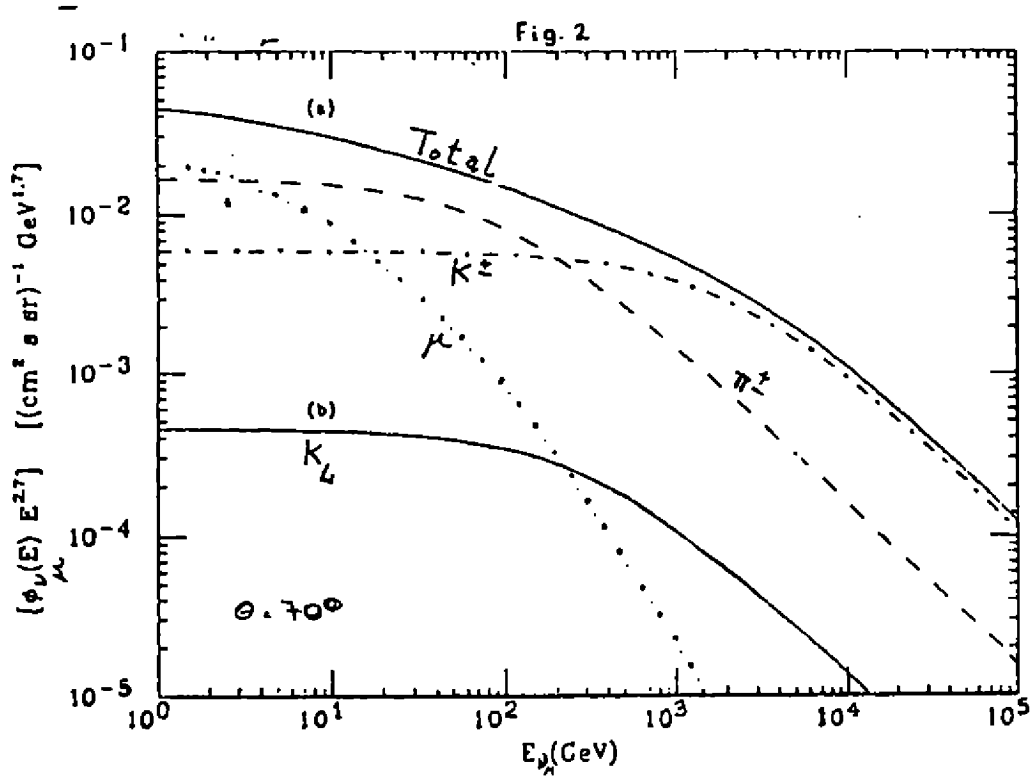
$$\theta = 0^\circ \rightarrow \begin{cases} 1,26 \leq \mu^+/\mu^- \leq 1,51 \\ 1,9 \leq \nu_\mu/\bar{\nu}_\mu \leq 2,42 \\ 1,32 \leq \nu_e/\bar{\nu}_e \leq 1,6 \end{cases}$$

A razão $\frac{(\nu_\mu/\nu_e)_{exp}}{(\nu_\mu/\nu_e)_{teo}}$ por nós calculada, na região de energia entre 300 MeV e 1 GeV, para os eventos detetados em Kamiokande, cujo vértice da interação está contido no interior do detector, é de aproximadamente 0.73. Como os neutrinos eletrônicos teóricos e experimentais são aproximadamente iguais, enquanto que os neutrinos muônicos teóricos são 1,4 dos obtidos experimentalmente e se considerarmos como uma explicação possível para esse fato a oscilação dos neutrinos, o canal viável seria então uma oscilação do tipo $\nu_\mu - \nu_\tau (\nu_s)$.

References

- [1] A.Hillas, Proc. of 19th ICRC, Kioto-Japão (1979).
- [2] T.K.Gaisser, Cosmic Rays and Particle Physics, Cambridge Univ. Press (1990).
- [3] K.Maeda, J. Geophys. Res. 69, n^o9 (1964) 1723.
- [4] T.K.Gaisser, Phys. Rev. D 36 (1993) 2650.





Difração de Solitons Bidimensionais

J. E. Cieza Montalvo*

*Instituto de Física, Universidade do Estado do Rio de Janeiro
CEP 20559 - 900 Rio de Janeiro, Brazil*

Y. P. Rybakov†

*Instituto de Física, Universidade de Patricio Lumumba
PO BOX 37, 117419 Moscow, Russia*

1 Introdução

Nos últimos anos o interesse pelas soluções dos solitons (soluções regulares e localizadas com energia finita) que recebem-se das equações não-lineares, cresceu muito. De acordo com isto o soliton pode ser considerada uma partícula elementar com extensão. Para esclarecer o quanto esta correspondência é verdadeira, estudamos a possibilidade dos solitons aparecerem com propriedades ondulatórias.

Com este objetivo nós estudaremos a difração de solitons bidimensionais sobre um cilindro impenetrável de raio c . Consideraremos que na região $x_0 \ll c$, onde x_0 é o parâmetro de impacto, o soliton interage fortemente com o cilindro e somente na região $x_0 > c$ acontece a difração.

2 Difração de Solitons sobre um Cilindro

Descreveremos o soliton como um campo escalar complexo $\varphi(t, \rho)$ no modelo de Synge [1], com a densidade de Lagrangeana

$$L = \frac{1}{2} \left(|\partial_\mu \varphi|^2 - m^2 |\varphi|^2 + \frac{2g}{3} |\varphi|^3 \right),$$

onde m e g são constantes.

A solução regular com simetria cilíndrica do soliton em repouso não excitado é $\varphi_0 = u(\rho) \exp(-i\omega t)$, mais no entanto o soliton real é sempre excitado e seu campo φ diferencia-se de φ_0 . Considerando que o campo φ tem uma simetria cilíndrica e ainda devido ao soliton ser estável, as interações irão variar φ somente na região $\rho > a$, ou seja a função $\varphi(t, a)$ e sua transformada de Fourier φ_ω serão dadas. Então na região $\rho \geq a$, onde o termo não linear é pequeno, o soliton excitado descreve-se aproximadamente pela solução da equação linear $(\square - m^2)\psi = 0$:

$$\Psi(t, \rho) = \frac{1}{2\pi} \int d\omega \psi(\omega, \rho) \exp(-i\omega t),$$

onde $\psi(\omega, \rho)$ é a solução da equação de Bessel de ordem zero, então

$$\Psi(t, \rho) = \frac{1}{2\pi} \int d\omega \varphi_\omega \frac{k_0(\mu, \rho)}{k_0(\mu, a)} \exp(-i\omega t),$$

*Na presença do cilindro o problema inicial não linear de contorno é formulada na forma integral

*E-mail address: CIEZA@USPIF.IF.USP.BR (internet) or 47602::CIEZA (dlnet).

†E-mail address: RYBAKOV@UDN.MSK.SU (internet).

$$\varphi = \varphi_{in} + \frac{g}{4\pi} \int_{-\infty}^{+\infty} dt' \int d^2\rho' G(t-t', \rho-\rho') \varphi' |\varphi'| + \frac{1}{4\pi} \int_{-\infty}^{+\infty} dt' \int_r dt'' \left[G \frac{\partial \varphi'}{\partial n'} - \varphi' \frac{\partial G}{\partial n'} \right] \quad (1)$$

onde G é a função de Green retardada para o operador $\square - m^2$ e é igual a

$$G^{ret} = \Theta(t-t') \Theta(\lambda) \left[\frac{\cos(m\sqrt{\lambda})}{2\pi\sqrt{\lambda}} \right]$$

Este problema resolveremos pelo método de iterações. $\varphi = \psi_0 + \psi_1 + \dots$ considerando $c \gg a$ onde c é o raio do cilindro.

Nós escolhemos ψ_0 como aproximação zero ou seja, o campo do soliton livre transformado por Lorentz

$$\psi_0 = \frac{1}{2\pi} \int d\omega \frac{k_0(\mu, \rho_0)}{k_0(\mu, a)} \varphi_\omega \exp[-i\omega\gamma(t - v y)],$$

onde $\rho_0 = \{(x - x_0)^2 + \gamma^2(y - vt)^2\}^{1/2}$ e $v = v_y$ é a velocidade do soliton incidente.

Considerando que $\varphi = 0$ no contorno c, encontramos pela equação 1 a primeira aproximação como sendo

$$\psi_1 = \int_{-\infty}^{+\infty} dt' \int_r dt'' \left[G \frac{\partial \psi_0}{\partial n'} - \psi_0 \frac{\partial G}{\partial n'} \right] |_{r=c} \quad (2)$$

A integral (2) calcula-se pelo método de fases estacionárias, considerando como parâmetro de decomposição $\frac{c}{a} \gg 1$

$$\psi_1 \simeq \frac{1}{32\pi^2} \int \varphi_\omega d\omega \int \frac{dy'}{\sqrt{c^2 - (y')^2}} \frac{i\omega\gamma v y'}{\sqrt{\xi_1^2 + (\rho - \rho')^2}} \left(\frac{2\pi(\xi_1^2 + (\rho - \rho')^2)}{\omega\gamma(\rho - \rho')^2} \right)^{1/2} \frac{k_0(\mu, \rho)}{k_0(\mu, a)} \exp(-i(m\xi_1 - \omega\gamma\sqrt{\xi_1^2 + (\rho - \rho')^2} - \omega\gamma v y' + \omega\gamma t - \pi/4)) \quad (3)$$

Calculando agora o impulso perpendicular, o qual adquire o soliton ao passar pelo cilindro, obtemos

$$\langle P_r \rangle = - \int_0^\infty dt \oint_{\rho=a} n_r T^{rz} dS = -a^2 R c \int_0^\infty dt \oint_{r=a} d\Omega (\partial_\rho \psi_0^* \partial_r \psi_1 + (v_0^* \psi_1 - m^2 \psi_0^* \psi_1) n_r) .$$

Devido ao soliton ser estável, então o campo $\varphi(t, a)$ corresponde a um processo casual estacionário com a seguinte correlação

$$\langle \varphi_\omega \varphi_{\omega'}^* \rangle = \sigma^2(\omega) \delta(\omega - \omega') .$$

A principal contribuição em P_r vem das frequências $\omega \simeq m$. Depois de considerar isto e integrando em t, teremos

$$\langle P_r \rangle \simeq \frac{a^3 \sigma_0^2 m^{5/2} c^2}{64\pi^{3/2} \gamma^{1/2} v} \left(\frac{2c \cos(k(x_0 - c) + \pi/4)}{m\gamma v (x_0 + c)^2 (x_0 - c)^{3/2}} - \frac{(2 + c) \sin(k(x_0 - c) + \pi/4)}{\sqrt{2c} (x_0 + c)^2 (x_0 - c)^{3/2}} \right)$$

A seção de choque diferencial para o espalhamento do soliton com o parâmetro de impacto que está entre x_0 e $x_0 + dx_0$ e o impulso entre P_x e $P_x + dP_x$, tem a forma

$$d\sigma = 2\pi x_0 W(P_x, x_0) dx_0 dP_x.$$

onde W é a densidade de distribuição de probabilidade de P_x e x_0 , de onde encontramos a expressão seguinte

$$d\sigma = \frac{\pi c^2}{2} \sin \xi d\xi + \frac{\sqrt{2\pi} P d\xi}{\Delta \cos^2 \xi} \int_c^\infty dx_0 \exp\left(\frac{-(\tan \xi + \varepsilon' f(x_0))^2}{2\Delta'^2}\right) x_0.$$

onde ξ é o ângulo de espalhamento. Aqui na primeira parte desta fórmula temos a expressão dada na mecânica quântica e a segunda parte é a correção que aparece devido ao soliton ser considerada uma partícula com extensão

$$f(x_0) = \left(\frac{2c \cos(k(x_0 - c) + \pi/4)}{m\gamma v(x_0 + c)^2(x_0 - c)^{3/2}} - \frac{(2 + c) \sin(k(x_0 - c) + \pi/4)}{\sqrt{2c(x_0 + c)^2(x_0 - c)^{3/2}}} \right).$$

$$\text{com } \varepsilon = \frac{a^3 \sigma_0^2 m^{3/2} c^2}{64 \pi^{3/2} v^{1/2} r_0},$$

$$\varepsilon' = \frac{c}{v},$$

$$\Delta'^2 = \frac{\Delta^2}{v^2}.$$

Este trabalho foi em parte financiado pelo Conselho Nacional de Desenvolvimento Científico e Tecnológico (CNPq) e pela Universidade de Patricio Lumumba

References

- [1] L. Sygne Proc. Roy. Irish Acad. Sci., **62 A**, 17, 1961

Spin-flip Conversion and Time Variations of Solar Neutrino Data Provoked by Solar Magnetosonic Waves

J.H. Colonia¹, M.M. Guzzo¹ and N. Reggiani^{1,2}

¹*Instituto de Física 'Gleb Wataghin'*

Universidade Estadual de Campinas - UNICAMP

13083-970 Campinas, São Paulo, Brasil

²*Laboratório Nacional de Luz Síncrotron*

Rua Lauro Vavucchi, 1020

13083-970 Campinas, São Paulo, Brasil

Analizamos as distorções no espectro de produção dos neutrinos solares provocadas por ondas magnetossônicas lentas no Sol e usamos nossos resultados para mostrar que tais ondas magnetossônicas podem ser responsáveis pelo comportamento temporal do fluxo de neutrinos solares observado experimentalmente nos dados de Homestake e Kamiokande.

Tem sido argumentado que o fluxo de neutrinos solares detectados no experimento de Homestake mostra alguma dependência temporal [1], no entanto, os dados dos experimentos de Kamiokande [2], Gallex [3] e Sage [4] parecem não confirmar esta variação temporal. Vários autores [5] discutiram a possibilidade de explicar a dependência temporal dos dados de Homestake considerando um momento magnético não nulo do neutrino, de tal forma que esta variação temporal do fluxo de neutrinos solares poderia estar anticorrelacionado com a variação temporal do campo magnético solar. De fato, quando os neutrino atravessam o campo magnético do Sol e um momento magnético diferente de zero é assumido, parte dos neutrinos ativos de mão esquerda mudam a neutrinos estereis de mão direita, os quais escapam à detecção. Desde que a taxa de conversão é sensível ao valor do campo magnético, flutuações deste campo poderiam afetar o fluxo total de neutrinos observados na Terra.

Num artigo recente [6] analisamos um modelo onde ondas magnetossônicas lentas são produzidas a partir de deslocamentos de plasma no Sol, perturbando o campo magnético solar. Como consequência disto, quando se considera o momento magnético do neutrino não nulo, observa-se flutuações no fluxo de neutrinos solares em períodos em torno de 100 dias. Neste trabalho, analisamos as distorções do espectro de produção dos neutrinos solares provocados por tais ondas magnetossônicas. Usamos este resultado para comparar os dados experimentais de Homestake e Kamiokande.

Considerando um momento magnético diferente de zero para o neutrino, a interação com o campo magnético será dada pelas equações de evolução [7]:

$$i \frac{d}{dr} \begin{pmatrix} \nu_L(r) \\ \nu_R(r) \end{pmatrix} = \begin{pmatrix} \frac{\sqrt{2}}{2} G_F N_{ef}(r) + \frac{\Delta m}{4E} & \mu_\nu B_\perp(r) \\ \mu_\nu B_\perp(r) & -\frac{\sqrt{2}}{2} G_F N_{ef}(r) - \frac{\Delta m}{4E} \end{pmatrix} \begin{pmatrix} \nu_L(r) \\ \nu_R(r) \end{pmatrix} \quad (1)$$

onde ν_L e ν_R são as componentes de mão esquerda e mão direita do neutrino, a diferença das potências quadradas das massas é denotada por $\Delta m \equiv m_{\nu_L}^2 - m_{\nu_R}^2$, E é a energia do neutrino, G_F é a constante de acoplamento de Fermi, $N_{ef}(r)$ é a densidade de número de elétrons no Sol e $B_\perp(r)$ é a componente transversal do campo magnético solar [6].

Resolvemos a equação (1) para calcular a probabilidade de sobrevivência dos neutrinos de mão esquerda produzidos na parte central do Sol, quando estes atingem a Terra depois de interagir com o campo magnético solar, o qual é periodicamente perturbado pelas ondas magnetossônicas [6]. A probabilidade $P(E,t)$ depende do tempo e do

espectro de energia dos neutrinos solares. O espectro de energia varia entre 0–15 MeV, onde neutrinos produzidos a partir das reações de ${}^8\text{Be}$ e ${}^7\text{Be}$ são os que mais contribuem para o espectro detectado nos experimentos. Kamiokande observa somente neutrinos de ${}^8\text{B}$ e tem um limiar aproximado de 8 MeV (veja Tabela 1), entretanto Homestake observa majoritariamente neutrinos de ${}^7\text{Be}$ e ${}^8\text{B}$ e tem um limiar de 0.814 MeV.

Período	E_{Kam}
Jan 1987 - Mai 1988	9.3 MeV
Jun 1988 - Nov 1991	7.5 MeV
Nov 1991 - Jul 1993	7.0 MeV

Table 1: Limiar de Energia em Kamiokande.

Nossos resultados são integrados levando em conta os limiares de energias dos experimentos de Homestake e Kamiokande:

$$R_{Hom}(t) = \frac{\int_{0.814}^{15} [\Phi_{SSM}^{Be}(E) P^{Be}(E, t) + \Phi_{SSM}^B(E) P^B(E, t)] dE}{\int_{0.814}^{15} [\Phi_{SSM}^{Be}(E) + \Phi_{SSM}^B(E)] dE} \quad (2)$$

$$R_{Kam}(t) = \frac{\int_{E_{Kam}}^{15} \Phi_{SSM}^B(E) P^B(E, t) \sigma(E) dE}{\int_{E_{Kam}}^{15} \Phi_{SSM}^B(E) \sigma(E) dE} \quad (3)$$

onde $\Phi_{SSM} = \Phi_{Tot} f(E)$ é o espectro total de produção. Os valores do espectro $f(E)$ estão dados na referência [8] e o fluxo de neutrinos Φ_{Tot} é dado por [8]: $\Phi_{Tot}^B = 5.8 \times 10^6 \text{ cm}^{-2} \text{ s}^{-2}$, $\Phi_{Tot}^{Be} = 4.7 \times 10^6 \text{ cm}^{-2} \text{ s}^{-2}$.

A seção de choque $\sigma(E)$ incrementa-se linearmente com a energia segundo o Modelo Solar Padrão [8]: $\sigma(E) = 9.2 \times E \times 10^{-45} \text{ cm}^2$.

As relações (2-3) são novamente integradas, esta vez no tempo, considerando o período de coleta de dados dos experimentos mencionados. Observamos que nossos resultados simulam o comportamento temporal do fluxo de neutrinos solares detectados na Terra e concluímos que as ondas magnetosônicas podem ser responsáveis do comportamento temporal observado experimentalmente em Homestake e Kamiokande (veja figura 1).

Os autores agradecem à Fundação de Amparo à Pesquisa do Estado de São Paulo (FAPESP) e ao Conselho Nacional de Desenvolvimento Científico e Tecnológico (CNPq) pelo suporte financeiro.

References

- [1] R. Davis et al., Proc. of the XXI Int. Cosmic Ray Conference, Adelaide, Australia, Vol. 7 (1990) p. 155.
- [2] K.S. Hirata et al., Phys. Rev. D 44 (1991) 2241.
- [3] P. Anselmann et al., Phys. Lett. B 327 (1994) 377.
- [4] J.N. Abdurashitov et al., Phys. Lett. B 328 (1994) 234.
- [5] A. Cisneros, Astro. & Space Sci. 10 (1971) 87; M.B. Voloshin, M.I. Vysotskii and L.B. Okun, Yad. Fiz. 44 (1986) 677 [Sov. J. Nucl. Phys. 44, (1986) 440]; J. Pulido, Phys. Rep. 211 (1992) 167.
- [6] J.H. Colonia, M.M. Guzzo e N. Reggiani, *Effects of Solar Magnetosonic Waves in Future Solar Neutrino Observations*, submetida para publicação a Phys. Lett. B (1996).
- [7] A. Yu. Smirnov, Phys. Lett. B 260 (1991) 161.
- [8] J.N. Bahcall and R.K. Ulrich, Rev. Mod. Phys. 60 (1988) 297.

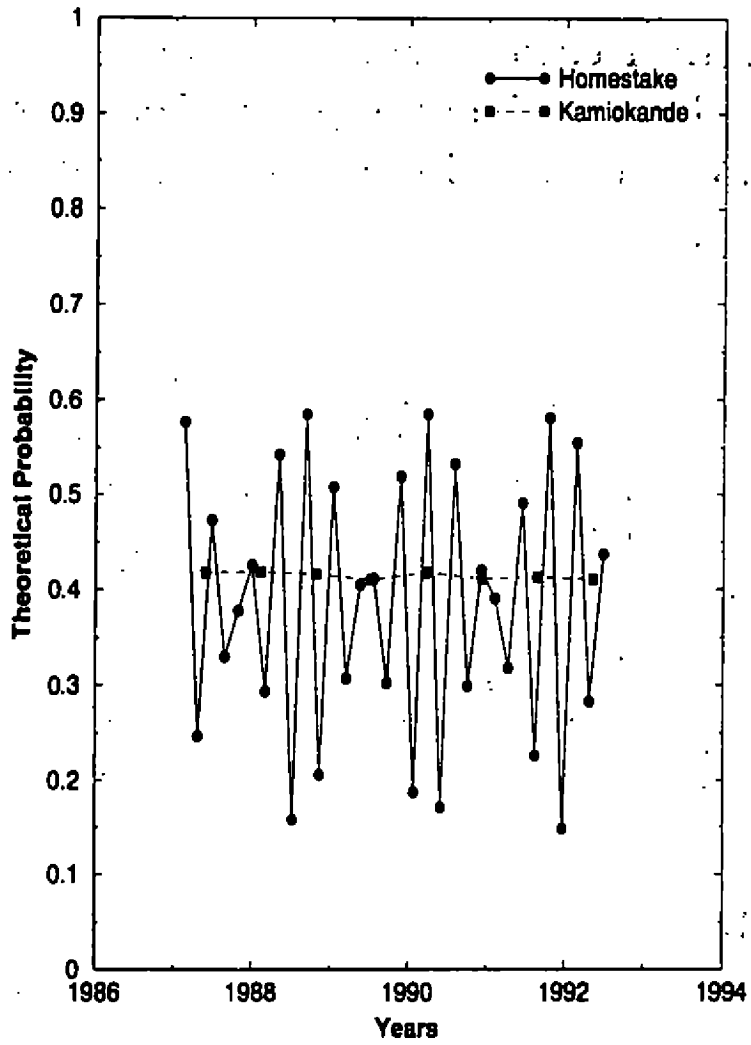


Figure 1: Neutrino flux at the Earth, normalized by the Standard Solar Model predictions.

Busca de Ressonâncias na Conversão de Helicidade de Neutrinos em Interações com Campos Magnéticos Rotantes

José Bellandi, Marcelo M. Guzzo, Pedro C. de Holanda
Instituto de Física - UNICAMP

Partindo da suposição que o momento magnético do neutrino é diferente de zero, estudamos a evolução de neutrinos sujeitos a campos magnéticos rotantes, e o modo pelo qual essa evolução poderia resultar em conversão de neutrinos de helicidade "left" (ativos) em neutrinos "right" (estéreis). Queremos utilizar o fato de que os neutrinos "right" não interagem com os detectores para conseguirmos informações sobre a magnitude do momento magnético dos neutrinos. Para resolver a equação de evolução dos neutrinos, combinou-se o método dos expansionais com o da aproximação por fase estacionária, usada para resolver as integrais dos expansionais. Feito isso, calculamos a probabilidade de conversão de neutrinos "left" em neutrinos "right" em função dos parâmetros da matriz de evolução (como o momento magnético do neutrino, a densidade de elétrons do meio, a magnitude e a fase do campo magnético). A partir daí procuramos achar condições de ajuste desses parâmetros tal que a probabilidade de transição de helicidade desses neutrinos sofra ressonâncias, de modo que a transição controlada de helicidade nestes feixes poderia nos dar novas informações sobre limites para o momento magnético dos neutrinos.

1 A Matriz de Evolução:

Consideramos neste trabalho um sistema de neutrinos composto de um auto-estado interagente (ν_L) e um auto-estado estéril (ν_R), cuja evolução se dá da seguinte forma:

$$i \frac{d}{dt} \begin{pmatrix} \nu_R \\ \nu_L \end{pmatrix} = \begin{pmatrix} \frac{\sqrt{2}}{2} G_F N_e - \frac{\Delta m^2}{4E} & \mu_\nu B(t) e^{-i\phi(t)} \\ \mu_\nu B(t) e^{+i\phi(t)} & -\frac{\sqrt{2}}{2} G_F N_e + \frac{\Delta m^2}{4E} \end{pmatrix} \cdot \begin{pmatrix} \nu_R \\ \nu_L \end{pmatrix}$$

onde:

- B : módulo da componente do campo magnético perpendicular ao eixo de propagação.
- μ_ν : momento magnético do neutrino
- ϕ : angulo relativo ao campo magnético
- G_F : constante de Fermi
- N_e : densidade de elétrons do meio
- Δm^2 : diferença dos quadrados das massas dos auto-estados físicos [$\Delta m^2 = m^2(\nu_L) - m^2(\nu_R)$]
- E : energia dos neutrinos

Consideraremos nossos neutrinos como ultra-relativísticos, que consiste em assumir que $m \ll p$, o que nos permite tratar a derivada temporal como derivada espacial, e aproximar E por p . Além disso, tomaremos neste modelo neutrinos de Dirac, o que implica que, sem a introdução de transição de sabor, o termo de diferença de massa entre os estados left e right, é nulo.

2 O Cálculo de $P(\nu_L \rightarrow \nu_R)$:

Dado um neutrino no estado ν_L no instante $t = 0$ (e esse vai ser sempre o caso, uma vez que os neutrinos são criados sempre no estado "left"), queremos calcular a probabilidade de, decorrido um certo tempo t , encontrá-lo no estado ν_L .

$$P(\nu_L \rightarrow \nu_R) = \{(\nu_R(t) | \nu_L(t = 0))\}^2$$

O processo de transição de helicidade fica mais claro se trabalharmos em outra base, que se relaciona com a base original através da relação:

$$\nu_S = \begin{pmatrix} \exp[-i \int_0^t \frac{\sqrt{2}}{2} G_F N_e(t') dt'] & 0 \\ 0 & \exp[+i \int_0^t \frac{\sqrt{2}}{2} G_F N_e(t') dt'] \end{pmatrix} \cdot \nu_S$$

Nessa nova base, a amplitude de probabilidade de transição difere da mesma amplitude na base original simplesmente por uma fase. Portanto, para o efeito de cálculo de probabilidades, as duas bases são equivalentes. Além disso, temos que $\nu_S = \nu_S$ se $t = 0$, o que nos dá as mesmas condições iniciais em ambas as bases.

Nessa nova base, temos:

$$i \frac{d \nu_S}{dt} = \begin{pmatrix} 0 & u(t) \\ u^*(t) & 0 \end{pmatrix} \cdot \nu_S$$

onde:

$$u(t) = \mu_\nu B(t) \exp[-i (\phi(t) - \sqrt{2} G_F \int_0^t N_e(t') dt')]$$

Uma solução formal pode ser obtida através do método dos Expansionais [1], onde a solução se dá em termos de múltiplas integrais da matriz de evolução. Aplicando esse método para o cálculo da amplitude de transição, encontramos a seguinte expressão:

$$\begin{aligned} (\nu_R(t) | \nu_L(t = 0)) &= -i \int_0^t u(t') dt' + \\ &+ i \int_0^t u(t') \int_0^{t'} u^*(t'') \int_0^{t''} u(t''') dt''' dt'' dt' - \dots \end{aligned}$$

Como $u(t)$ contém um termo oscilante, podemos aplicar o método da fase estacionária[3] para chegar em um resultado aproximado de sua integral em t . Esse método consiste em, caso o termo oscilante seja preponderante, considerar que a integral se anulará, a não ser que, no intervalo de integração, haja um ponto onde a fase é estacionária. Nesse caso temos:

$$\begin{aligned} f(x) &= \int_a^b g(t) e^{ixh(t)} dt \\ &\sim \left[\frac{2}{|xh''(\tau)|} \right]^{1/2} g(\tau) \exp[ixh(\tau) + \frac{i\pi}{4}] \quad \text{quando } x \rightarrow \infty \end{aligned}$$

onde τ representa o ponto de fase estacionária [$h'(\tau) = 0$].

Aplicando esse teorema ao nosso caso, chegamos no seguinte resultado:

$$\int_0^t u(t') dt' = \left(\frac{2\pi}{h''(\tau)} \right)^{1/2} \mu B(\tau) \exp[ih''(\tau) + i\frac{\pi}{4}]$$

onde $h(t) = \int_0^t \sqrt{2} G_F N_e(t') dt' - \phi(t)$ e τ é definido tal que $h'(\tau) = 0$.

Como a integral acima não depende de t , as múltiplas integrais do expansional reduzem-se a seguinte série de potências:

$$(\nu_R(t) | \nu_L(t = 0)) = -i2\xi(1 - \xi^2 + \xi^4 - \dots) \exp[ih''(\tau) + i\frac{\pi}{4}]$$

onde

$$\xi = \left[\frac{\pi}{2|h''(\tau)|} \right]^{1/2} \mu B(\tau) \exp[ih''(\tau) + i\frac{\pi}{4}]$$

Se $\xi < 1$ então a série converge e o resultado é simplesmente dado por:

$$\langle \nu_R(t) | \nu_L(t=0) \rangle = -i \frac{2\xi}{1+\xi^2} \exp[ih''(\tau) + i\frac{\pi}{4}]$$

$$P(\nu_L \rightarrow \nu_R) = |\langle \nu_R(t) | \nu_L(t=0) \rangle|^2 = 4 \left(\frac{\xi}{1+\xi^2} \right)^2$$

3 O Parâmetro de Adiabaticidade:

Antes de avançarmos em nossos cálculos, há um aspecto interessante neste problema que merece ser ressaltado. Se calcularmos o parâmetro de adiabaticidade, que se dá pela comparação dos termos não diagonais da matriz de evolução, escrita para os auto-estados de massa, com os termos diagonais, chegamos ao seguinte valor na ressonância ou fase estacionária[2]:

$$\gamma = 2 \frac{[2\mu B(\tau)]^2}{h''(\tau)}$$

Porém essa expressão se relaciona diretamente com o parâmetro ξ encontrado acima, de forma que podemos escrever a probabilidade total de transição de helicidade em termos do parâmetro de adiabaticidade, encontrando:

$$P = \frac{\pi\gamma}{(16 + \pi\gamma)^2}$$

Dessa expressão vemos que a máxima transição de helicidade se dá em um meio termo de adiabaticidade (no nosso caso, com $\gamma \approx 5$), se anulando para transições totalmente adiabáticas ($\gamma \gg 1$) ou extremamente não adiabáticas ($\gamma \ll 1$). Esse resultado já tinha sido destacado qualitativamente por Smirnov[2], mas aqui se chega a uma expressão quantitativa para essa relação. É claro que não chegamos em uma expressão geral para qualquer tipo de evolução, mas é interessante destacar a relação entre adiabaticidade e oscilação entre auto-estados em nosso caso particular.

4 Maximizando $P(\nu_L \rightarrow \nu_R)$:

Como queremos que o maior número possível de neutrinos "left" sejam convertidos em neutrinos "right", de modo que a experiência que queremos propor seja a mais sensível possível, vamos procurar valores de nossos parâmetros que maximizam $P(\nu_L \rightarrow \nu_R)$. Nota-se que o valor máximo dessa probabilidade se dá quando $|\xi| = 1$, o que nos dá uma transição completa de helicidade [$P(\nu_L \rightarrow \nu_R) = 1$]. Temos então, como condição para que o efeito da transição de helicidade seja observável:

$$\left[\frac{\pi}{2|h''(\tau)|} \right]^{1/2} \mu B(\tau) \sim 1$$

Tomando o limite do momento magnético do neutrino [$\mu \leq 10^{-12} \mu_B$] e admitindo que campos magnéticos da ordem de $10T$ são factíveis em laboratório, substituímos esses valores na condição acima, obtendo:

$$|h''(\tau)| = \left| \sqrt{2} G_F N_e(\tau) - \phi''(\tau) \right| \sim 4 \cdot 10^{-31} eV^2 \quad (1)$$

Porém há outras condições que precisam ser simultaneamente satisfeitas. Precisamos garantir que a aproximação de fase estacionária se aplique ao nosso caso. Em primeiro lugar é necessário que haja um ponto na evolução dos neutrinos onde a fase seja estacionária, um ponto onde:

$$h'(\tau) = \sqrt{2} G_F N_e(\tau) - \phi'(\tau) = 0 \quad (2)$$

Em segundo lugar, o termo $u(t)$ deve oscilar pelo menos uma vez entre o ponto de criação e o ponto de fase estacionária, e entre este ponto e a detecção, de modo que podemos desprezar a integral nessas regiões, ficando somente com o valor dado pela fase estacionária.

$$|h(\tau) - h(0)| = \left| \int_0^\tau \sqrt{2} G_F N_e(t') dt' - [\phi(\tau) - \phi(0)] \right| \geq 2\pi \quad (3)$$

$$|h(t) - h(\tau)| = \left| \int_{\tau}^t \sqrt{2} G_F N_e(t') dt' - [\phi(t) - \phi(\tau)] \right| \geq 2\pi \quad (4)$$

5 Conclusão:

Temos três condições que precisam ser satisfeitas simultaneamente para que um feixe de neutrinos ativos seja, ao menos parcialmente, convertido em neutrinos estéreis. Satisfazer essas condições é a princípio possível, uma vez que não são necessários valores de campo magnético ou de densidade de elétrons inatingíveis, ou aceleradores de extensão irrealizável. Porém existe um problema de precisão para se compatibilizar as condições 1 e 2. Se arranjamos nosso aparato para que tenhamos controle da condição 1, perdemos controle da condição 2, e vice-versa. Talvez o ajuste fino dessas duas condições seja possível experimentalmente, o que nos daria uma receita para se montar um aparato experimental para a criação, interação e detecção de neutrinos, que possa nos trazer informações adicionais para melhorar os limites de seu momento magnético. O trabalho que se seguirá portanto será o de estudar a factibilidade experimental do ajuste entre as condições citadas, procurando para isso valores que possam ser usados experimentalmente para os parâmetros do nosso problema, como a densidade eletrônica, ou o campo magnético.

References

- [1] J. Bellandi and M. M. Guzzo, Phys. Lett. B 317 (1993) 130
- [2] A. Yu. Smirnov, Phys. Lett. B 260 (1991) 161
- [3] A. Erdélyi, Asymptotic Expansions (Dover Pub. Inc., NY, 1956)

A Geração da Massa do Pion na Quantização dos Skyrmions

Jorge Ananias Neto

Departamento de Física, ICE

Universidade Federal de Juiz de Fora, 36036-330 Juiz de Fora, MG, Brasil

Através das soluções tipo sólton que minimiza todo o Hamiltoniano quântico do modelo de Skyrme, é possível gerar a massa do Pion, sem introduzir o termo de massa explicitamente na Lagrangiana da teoria.

Nas últimas décadas, o modelo de Skyrme alcançou notável sucesso devido a sua simples capacidade em descrever os fenômenos da física hadrônica. A idéia é representar os bárions e suas interações através de soluções tipo sólton num modelo que tem como base o Sigma não linear. Neste trabalho vamos mostrar que é possível obter a massa do Pion¹ através do comportamento assintótico da solução solitônica que minimiza todo o Hamiltoniano quântico. Para isso, vamos proceder, de uma maneira mais cuidadosa, a quantização operatorial do modelo, tentando prestar mais atenção no problema de ordenamento que existe nas relações de comutação entre as variáveis canônicas. Vamos iniciar pela Lagrangiana estática do modelo de Skyrme, que é dada por

$$L = \int d^3r \left[-\frac{F_\pi^2}{16} \text{Tr} (\partial_i U \partial_i U^\dagger) + \frac{1}{32e^2} \text{Tr} [U^\dagger \partial_i U \cdot U^\dagger \partial_j U]^2 \right], \quad (1)$$

onde F_π é a constante de decaimento dos Pions, e é um parâmetro adimensional e U é uma matriz $SU(2)$. Expandindo U através das coordenadas rotacionais coletivas, ou seja, $U(r)$ por $U(r, t) = A(t)U(r)A(t)^\dagger$ em (1), onde A também é uma matriz $SU(2)$, que é expandida como $A = a_0 + i\tau \cdot a$, obtemos

$$L = -M + \lambda \text{Tr} [\partial_0 A \partial_0 A^{-1}] = -M + 2\lambda \sum_{i=0}^3 (\dot{a}_i)^2, \quad (2)$$

onde M e λ são a massa e o momento de inércia do sólton, respectivamente. Como A é uma matriz $SU(2)$ temos o vínculo

$$\sum_{i=0}^3 a_i^2 = 1. \quad (3)$$

Introduzindo o momento conjugado $\pi_i = \frac{\partial L}{\partial \dot{a}_i} = 4\lambda \dot{a}_i$, podemos escrever o Hamiltoniano na forma

$$H = \pi_i \dot{a}_i - L = 4\lambda \dot{a}_i \dot{a}_i - L = M + 2\lambda \dot{a}_i \dot{a}_i = M + \frac{1}{8\lambda} \sum_{i=0}^3 \pi_i \pi_i. \quad (4)$$

O vínculo (3) é do tipo triésfera. Logo, a relação de comutação entre a coordenada a_i e o momento π_j é

$$[a_i, \pi_j] = i[\delta_{ij} - a_i a_j]. \quad (5)$$

Esta relação de comutação é não trivial. Uma possível solução da equação (5) é

¹ Sem introduzir explicitamente o termo de massa na Lagrangiana do modelo.

$$\begin{aligned} \pi_j &= \frac{1}{(1+\alpha)i} [(\delta_{i,j} - a_j a_i) \partial_i + \alpha \partial_i (\delta_{i,j} - a_i a_j)] \\ &= \frac{1}{i} (\delta_{i,j} - a_j a_i) \partial_i - \frac{5\alpha a_j}{(1+\alpha)i} \end{aligned} \tag{6}$$

onde α , a princípio, é um parâmetro livre. Substituindo a representação do momento (6) no Hamiltoniano quântico (4) obtemos a expressão para os autovalores da energia²

$$E = M + \frac{1}{8\lambda} \left[l(l+2) - \frac{5\alpha(2\alpha-3)}{(1+\alpha)^2} \right], \quad l = 1, 2, 3, \dots \tag{7}$$

Agora é possível escolher um valor do parâmetro α tal que tenhamos uma solução variacional que minimize todo o Hamiltoniano quântico³. A forma assintótica (x muito grande) da equação de Euler Lagrange na representação hedgehog, $U = \exp i\tau \cdot \hat{x} F(x)$, é dada por

$$-\frac{d^2 F}{dx^2} - \frac{2}{x} \frac{dF}{dx} + \frac{2}{x^2} F + k^2 F = 0, \tag{8}$$

onde k^2 é escrito como

$$k^2 = \frac{3l(l+2)c^4}{8\pi^2 \left(\int_0^\infty x^2 \sin^2 F \left[1 + 4 \left(F'^2 + \frac{\sin^2 F}{x^2} \right) \right] dx \right)^2} \tag{9}$$

Da equação (8) obtemos o comportamento assintótico de $F(x)$

$$F = \frac{\exp(-kx)}{x} \tag{10}$$

Do comportamento assintótico de $F(x)$, tipo *Yukawa*, podemos identificar k como sendo a massa do Pion. Para calcular este valor, temos que resolver uma equação integrodiferencial que, a princípio, não é uma tarefa fácil. Como primeira aproximação, vamos usar valores de $F(x)$, F_x e e obtidos num cálculo semiclássico. Obtemos $m_\pi \approx 140 M_e c$. O valor experimental é $m_\pi = 138 M_e c$.

Mais referências podem ser encontradas em:

1. Jorge Ananias Neto: Journal of Physics G21 (1995) 695.

²Uma típica representação dos autovetores do Hamiltoniano quântico é dado por $\frac{1}{\sqrt{N(l)}}(a_1 + i a_2)^l$.

³A escolha que elimina a divergência infravermelha é $\alpha > (21 + 5\sqrt{21})/14$ ou $\alpha < (21 - 5\sqrt{21})/14$.

Otimização de Tempo na Simulação de Cascatas Eletromagnéticas na Atmosfera

Luiz Américo de Carvalho, Carola Dobrigkeit, José Augusto Chinellato

Departamento de Raios Cósmicos e Cronologia

Instituto de Física Gleb Wataghin

Universidade Estadual de Campinas

13.083-970, Campinas, SP, Brazil

We have studied and applied two procedures with the aim of reducing the time for simulation of high energy electromagnetic cascades for high depths. The first procedure is based on the longitudinal transport of particles, i.e., without considering the deflections due to the multiple Coulomb scattering and the influence of the magnetic field of the Earth; in this way we remove subcascades that do not contribute with particles above threshold energy at the detection level. Those that contribute are then transported, now considering scattering and the influence of the magnetic field. The second procedure is based on the cut of subcascades avoiding even the longitudinal transport. For this we have studied a cut function that depends only on the depth the particle has to move till the detection level. With the use of both procedures we get a considerable profit in the time of simulation without jeopardizing the results.

Introdução

A simulação de cascatas eletromagnéticas envolve o desenvolvimento de um modelo computacional ([1]) que realize operações que representem a propagação e as interações das partículas envolvidas.

A base do modelo é que as seções de choque físicas são diretamente representadas por distribuições de probabilidade, e assim podemos amostrar a transferência de energia para a partícula-filho utilizando o método de Monte Carlo nas expressões da seção de choque diferencial dos processos de produção de pares e Bremsstrahlung ([2] e [3]).

A propagação de cada partícula carregada produzida no fenômeno envolve o processo de espalhamento múltiplo coulombiano ([2] e [4]), a influência do campo magnético terrestre e, conseqüentemente, a atualização dos cossenos diretores e das coordenadas da partículas com a parametrização da densidade atmosférica ([5] e [6]), além da perda de energia por ionização a uma razão constante (6.678×10^{-2} GeV/ X_0). Onde X_0 é o comprimento de radiação no meio, a unidade usual de distâncias no estudo do fenômeno de cascatas eletromagnéticas. Já a propagação dos fótons envolve apenas a atualização das coordenadas com a parametrização da densidade atmosférica.

A simulação inicia-se com a entrada na atmosfera de uma partícula primária que pode ser um γ , ou elétron, ou pósitron com energia entre 4 MeV e 1.000 TeV. Esse é o intervalo de energia na atmosfera no qual apenas esses processos físicos acima são relevantes e as expressões de seção de choque utilizadas são válidas.

Como a simulação de cascatas eletromagnéticas consome um considerável tempo, principalmente para primários de altas energias (acima de 1 TeV), foram utilizados dois procedimentos com a intenção de melhorar o desempenho da simulação sem o comprometimento dos resultados.

1 Otimização de tempo na simulação

O transporte de partículas pela atmosfera envolve:

Fótons

- atualização das coordenadas espaciais com a parametrização da atmosfera de Shibata/Gaisser/Chinellato ([5] e [6]), que permite transformar profundidades (dadas em g/cm^2) em alturas (dadas em mm) e vice-versa:

- registro das partículas.

Elétrons

- amostragem do ângulo Θ de espalhamento múltiplo coulombiano;
- amostragem do ângulo azimutal Φ de uma distribuição uniforme $(0, 2\pi)$;
- deflexão devida ao campo magnético terrestre (calculado para o Equador);
- atualização da direção de voo (cossenos diretores);
- atualização das coordenadas espaciais com a parametrização da atmosfera;
- registro das partículas.

Esta etapa é a que mais consome tempo na simulação do fenômeno. Para exemplificar: na simulação de uma cascata iniciada por um fóton primário de 10 TeV, com uma energia de limiar (ou registro) de 4 MeV e com a profundidade de registro de $25 X_0$ (cerca de 400m acima do nível do mar) gasta-se 75% do tempo de simulação no transporte de elétrons e 3% para o transporte de fótons. Sem a menor dúvida, a maneira mais eficiente de economizar tempo é buscar opções para realizar esta etapa sem desperdiçar tempo com partículas que não contribuirão para os resultados da simulação do fenômeno, ou seja, não contribuirão com partículas com energia acima do limiar na profundidade de detecção.

Pensando nisto, foram estudados dois procedimentos¹, os quais denominamos:

- A) Algoritmo catalisador
- B) Função corte

Assim as partículas com energia menor que determinado valor de energia, aqui denominada energia de entrada ([7]), serão propagadas por este procedimentos.

1.1 Procedimento A: Algoritmo catalisador

O algoritmo catalisador foi construído para efetuar virtualmente o transporte longitudinal das partículas. O transporte é virtual pois os dados das partículas que interagem não são eliminados da simulação. O transporte longitudinal consiste em mover a partícula de uma distância dada pelo livre caminho amostrado nas subrotinas dos processos de produção de pares e Bremsstrahlung, sem considerar as deflexões de espalhamento e no campo magnético terrestre e sem converter esses valores segundo a parametrização atmosférica. Caso a partícula pai desse subchuveiro que entrou no algoritmo catalisador, ou pelo menos um de seus descendentes, chegue à profundidade de registro com energia acima do limiar, todo o subchuveiro será transportado, agora efetivamente, considerando as deflexões e utilizando a parametrização da densidade atmosférica. Senão, todo o subchuveiro será descartado.

1.2 Procedimento B: Função corte

Neste procedimento descartam-se partículas, sem nem mesmo transportá-las virtualmente, desde que suas energias sejam menores que valores calculados a partir de uma função dependente da profundidade que a partícula ainda tem que percorrer até o nível de registro.

Esta função foi calculada a partir de um estudo na propagação longitudinal de partículas e possível registro destas, ou de pelo menos um de seus descendentes. Para isto construíram-se gráficos com as energias dos pais (fótons ou elétrons) dos subchuveiros com sobreviventes e as respectivas profundidades até o registro. Os gráficos com os subchuveiros sobreviventes e respectivas profundidades até o registro são dados, respectivamente, nas figuras (1 e 2) para elétrons e fótons.

Do estudo destes gráficos foi construída uma função corte. Esta função nos dá o valor de energia para o qual, abaixo deste, os subchuveiros muito provavelmente não terão pelo menos um sobrevivente na profundidade de registro, exceto flutuações, que, como já dito, são inerentes ao processo. A função corte é dada pela expressão:

$$f_{corte}(\Delta t) = \frac{E_{corte}(\Delta t)}{GeV} = 10^{-3,0+0,12243\Delta t+ajuste} \quad (1)$$

sendo Δt a profundidade que a partícula tem que percorrer até o registro, expressa em unidades de X_0 .

¹A idéia da utilização destes procedimentos veio de um trabalho de 1989 não publicado de Josef Spitzer quando no Instituto Max Planck, Heidelberg/Alemanha.

Pode-se notar pelos gráficos apresentados nas figuras (1 e 2) que tanto para elétrons, quanto para fótons, utilizamos a mesma função corte. Isto é feito para simplificar o corte, minimizando a necessidade de comandos condicionais na simulação. Um parâmetro de ajuste pode ser colocado para, de acordo com as necessidades do usuário, cortar maior ou menor número de subchuveiros dentro de uma margem de segurança relacionada com a probabilidade do subchuveiro não contribuir com pelo menos um sobrevivente na profundidade de registro.

É importante notar (ver figuras 1 e 2) que existem profundidades mínimas para corte, que são: $10,0X_0$ para fótons e $5,0X_0$ para elétrons. Estas são colocadas para permitir possíveis flutuações no livre caminho amostrado.

2 Resultados

O programa que executa a simulação neste trabalho foi desenvolvido ([1]) em linguagem Fortran ([8]). As simulações foram realizadas em estação de trabalho modelo Alpha.

Foram realizadas simulações para quantificar o ganho de tempo, sempre utilizando conjuntamente os dois procedimentos. Resultados que mostram estes ganhos são apresentados na tabela 1 para algumas profundidades para cascatas iniciadas por

Profundidades	ajuste +0,7	ajuste +0,3	sem ajuste	ajuste -0,3	ajuste -0,7
10,0 X_0	2,2	1,9	1,9	1,7	1,6
14,6 X_0	2,5	2,3	2,2	2,2	2,2
25,0 X_0	15,9	8,5	7,0	4,8	4,0

Table 1: Ganho de tempo com os dois procedimentos: valores para γ primário de 10 TeV, $E_{catalisador} = 6$ GeV, $E_{limiar} = 4$ MeV

Na tabela (1) podemos ver que o ganho máximo foi conseguido com a utilização dos procedimentos para o caso simulado com a profundidade de registro em $25 X_0$ (cerca de 400m acima do nível do mar) e com o parametro de ajuste da função de corte igual a +0.7. Este valor de parametro de ajuste aumenta em cerca de 5 vezes as energias de corte calculadas. Apresentamos resultados para os seguintes valores de ajuste: +0.7, +0.3, -0.3 e -0.7, e é claro,

Para justificar a utilização dos procedimentos temos que, além de quantificar o ganho de tempo, mostrar que os resultados da simulação são mantidos com a utilização dos procedimentos. Podemos comparar bem os resultados analisando os com

3 Conclusão

Com a utilização dos procedimentos estudados conseguimos um considerável ganho de tempo. A simulação foi executada até 16 vezes mais rápida (para a profundidade de $25,0 X_0$). Podemos alcançar maior economia para energias maiores que

Desta maneira, conseguimos minimizar o grande inconveniente da simulação, que é o tempo dispendido.

Os resultados da simulação com a utilização dos procedimentos são os mesmos, comparando-os ([7]) aos da simulação sem os procedimentos e considerando a influencia da flutuação, que é inerente ao fenomeno.

Uma eficiência ainda maior pode ser obtida com a utilização de funções corte diferentes para elétrons e fótons, pois para os elétrons (maiores consumidores de tempo de simulação) podemos utilizar um valor de parametro de ajuste ma

Agradecimentos

Agradecemos aos apoios da CAPES (L.A.C), do CNPq (L.A.C e C.D), da FAEP/UNICAMP (C.D) e da FAPESP (J.A.C e C.D).

References

- [1] T. Stanev e C.P. Vankov, *Comp. Phys. Comm.* 16(1979) p.363
- [2] W.R. Nelson, H. Hirayama e D.W.O. Rogers, *The EGS4 Code System* (1985)
- [3] Applications Software Group Computing and Networks Division of CERN, *GEANT : Detector description and simulation tool* (1993).
- [4] H.A. Bethe, *Phys. Rev.* 89 (1953) 1256
- [5] J.A. Chinellato, *Comunicação particular*.
- [6] T.K. Gaisser, *Cosmic rays and particle physics*, (Cambridge University, Cambridge, 1990)
- [7] L.A. Carvalho, *Otimização no tempo de simulação de cascatas eletromagnéticas na atmosfera*. Tese de Mestrado/IFGW-UNICAMP (1.996)
- [8] M.E. Hehl, *Linguagem de Programação Estruturada Fortran 77*, 2ª.. (McGraw-Hill, 1987).
- [9] W.H. Press, S.A. Teukolsky, W.T. Vetterling e B.P. Flannery, *Numerical Recipes in Fortran : The Art of Scientific Computing*, 2ª Ed. (Cambridge University, Cambridge, 1992).

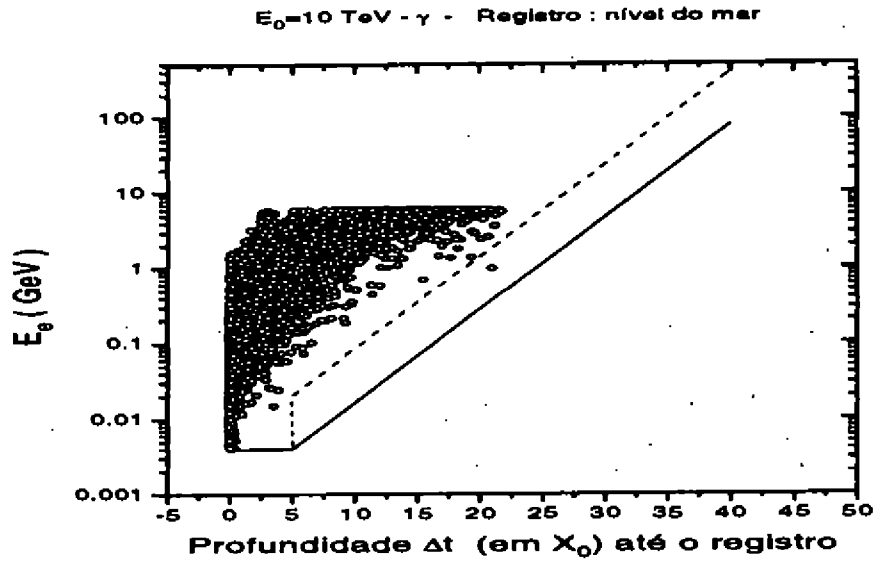


Figura 1: Gráfico da energia versus a profundidade até o registro de elétrons (pais de subchuveiros com sobreviventes) de um γ primário de 10 TeV, com transporte longitudinal desses subchuveiros abaixo de 6 GeV e energia de limiar de 4 MeV. Gráfico da função corte construída e função corte com ajuste +0,7 (reta tracejada). Foram simulados 10 eventos.

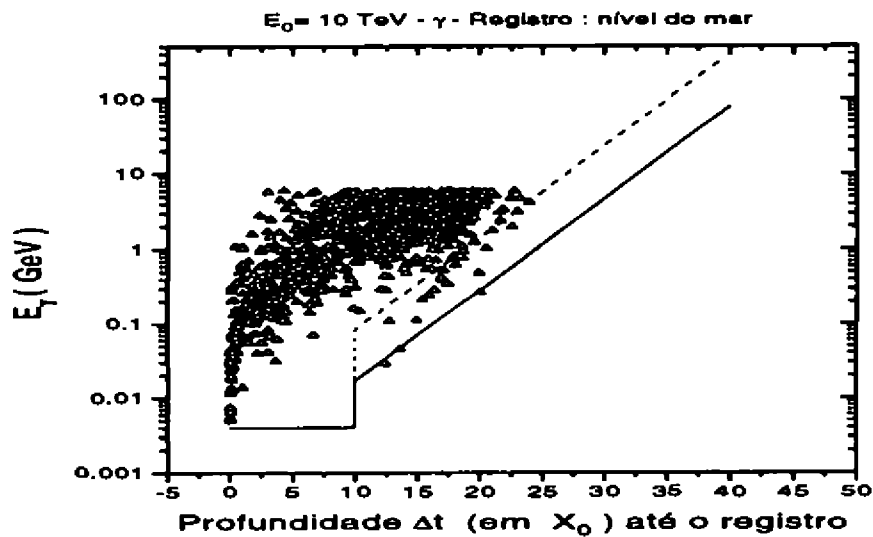


Figura 2: Gráfico da energia versus a profundidade até o registro de γ 's (pais de subchuveiros com sobreviventes) de um γ primário de 10 TeV, com transporte longitudinal desses subchuveiros abaixo de 6 GeV e energia de limiar de 4 MeV. Gráfico da função corte construída e função corte com ajuste +0,7 (reta tracejada). Foram simulados 10 eventos.

Bounds on Excited Leptons from Precise Electroweak Measurements

M. C. Gonzalez-Garcia

Theory Division, CERN, CH-1211 Geneva 23, Switzerland.

S. F. Novaes

*Instituto de Física Teórica, Universidade Estadual Paulista,
Rua Pamplona 145, CEP 01405-900 São Paulo, Brazil.*

We study the effects induced by excited leptons at the one-loop level in the observables measured on the Z peak at LEP. We compute their contributions to oblique parameters, Z partial widths, and weak-magnetic moment of the τ lepton. Our results show that the new effects are comparable to the present experimental sensitivity, but they do not lead to a significant improvement on the available constraints on the couplings and masses of these states.

The standard model of electroweak interactions (SM) obtained a remarkable agreement with the present experimental data at the Z pole performed at LEP [1]. However the SM is not able to provide a satisfactory answer to some fundamental problems like the family repetition and the fermionic mass pattern. A very appealing idea that might shed some light on these issues is to consider the possibility of these particles being composite states. Composite models assume the existence of an underlying structure, characterized by a mass scale Λ , with the fermions sharing some of the constituents [2]. In this case, excited states of each known lepton should manifest itself at some energy scale, and the SM should be seen as the low-energy limit of a more fundamental theory. We still do not have a satisfactory model, able to reproduce the whole particle spectrum. Due to the lack of a predictive theory, we should rely on a general approach to explore the possible effects of compositeness, employing effective Lagrangian techniques to describe the couplings of these excited states.

Several experimental collaborations have been searching for excited lepton states [3, 4]. Their analyses are based on an effective $SU(2) \otimes U(1)$ invariant Lagrangian, proposed some years ago [5]. Also a series of phenomenological studies of excited fermions have been carried out in electron-positron [5, 6, 7, 8, 9, 10], hadronic [8, 9], and electron-proton [5, 10] collisions.

Another important source of indirect information about new particles and interactions is the precise measurement of the electroweak parameters. Virtual effects of new heavy states can alter the SM predictions for some of these parameters, and the comparison with the experimental data can impose bounds on their masses and couplings. We report here our analysis of the effects induced by excited leptons at the one-loop level in the oblique parameters, Z partial widths measured at LEP [11] and in the anomalous weak-magnetic form factors of the leptons [12], at an arbitrary energy scale.

We consider excited fermionic states with spin and isospin $\frac{1}{2}$, and we assume that the excited fermions acquire their masses before the $SU(2) \otimes U(1)$ breaking, so that both left-handed and right-handed states belong to weak isodoublets. The coupling of the excited-usual fermions can be described by an effective Lagrangian [5, 10] which is $SU(2) \otimes U(1)$ invariant and CP-conserving.

$$\mathcal{L}_{Ff} = -\frac{1}{2\Lambda} \bar{\Psi}^* \sigma^{\mu\nu} \left(g f_2 \frac{\tau^i}{2} W_{\mu\nu}^i + g' f_1 \frac{Y}{2} B_{\mu\nu} \right) \psi_L + h.c. \quad (1)$$

where ψ_L is the standard leptonic doublet and $\Psi^* = (N \ E)^T$ is excited fermion doublet with hypercharge $Y = -1$. The constants f_2 and f_1 are weight factors associated to the $SU(2)$ and $U(1)$ coupling constants, with Λ being the compositeness scale, and $\sigma_{\mu\nu} = (i/2)[\gamma_\mu, \gamma_\nu]$.

The coupling of gauge bosons to excited leptons can also be described by a $SU(2) \otimes U(1)$ invariant and CP conserving effective Lagrangian,

$$\mathcal{L}_{FF} = -\bar{\Psi}^* \left[\left(g \frac{\tau^i}{2} \gamma^\mu W_\mu^i + g' \frac{Y}{2} \gamma^\mu B_\mu \right) + \left(\frac{g\kappa_2}{2\Lambda} \frac{\tau^i}{2} \sigma^{\mu\nu} \partial_\mu W_\nu^i + \frac{g'\kappa_1}{2\Lambda} \frac{Y}{2} \sigma^{\mu\nu} \partial_\mu B_\nu \right) \right] \Psi^* \quad (2)$$

We should notice that the particular model presented above has been used by several experimental collaborations as a guideline to the search of composite states, and our results can be directly compared with the bounds on the excited fermion mass and compositeness scale obtained by these collaborations.

Excited leptons contribute to the vector-boson-two-point functions through the diagrams shown in Fig. 1. The loop contributions of the excited leptons were evaluated in $D = 4 - 2\epsilon$ dimensions using the dimension regularization method [13], which is a gauge-invariant regularization procedure, and we adopted the unitary gauge to perform the calculations. The results in D dimensions were obtained with the aid of the Mathematica package FeynCalc [14], and the poles at $D = 4$ ($\epsilon = 0$) and $D = 2$ ($\epsilon = 1$) were identified with the logarithmic and quadratic dependence on the scale Λ [15].

FIGURES

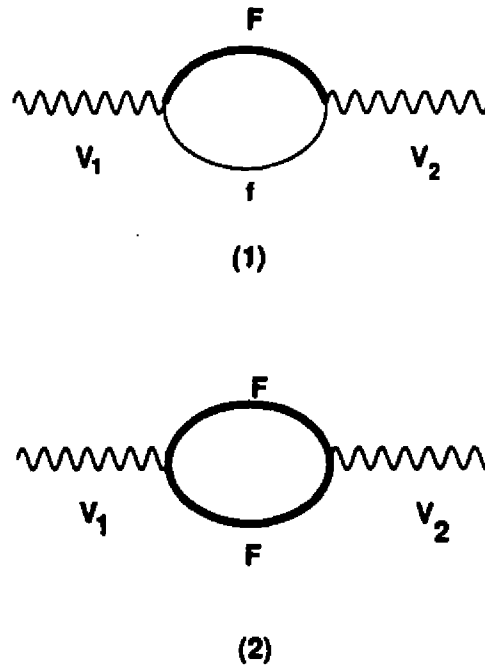


Figure 1. The contribution of the excited leptons (F) to the two-point functions.

We have studied the oblique corrections due to these particles, parametrized in terms of the variables c_1 , c_2 , and c_3 of Ref. [16]. Comparing our analytical results with recent global analyses of the LEP, SLD, and low-energy data, we verify that the constraints coming from oblique corrections are less restrictive than the available direct experimental limits.

Excited leptons affect also the $V_1 \bar{f} f$ couplings, with $V_1 = \gamma$ or Z , whose result we parametrize as,

$$J^\mu = e \bar{u}_f(p_1) \left\{ \frac{1}{2 \sin \theta_W \cos \theta_W} \gamma^\mu \left[F_V^{V_1 f}(q^2) - F_A^{V_1 f}(q^2) \gamma^5 \right] + \frac{i}{2m_f} a_f^{V_1}(q^2) \sigma^{\mu\nu} q_\nu \right\} u_f(p_2) \quad (3)$$

where $q = p_1 + p_2$. The terms $F_V^{V_1 f}$ and $F_A^{V_1 f}$ are present at tree level in the SM, e.g. for the Z boson, $F_V^{Z f} = -T_3^f + 2Q_f \sin^2 \theta_W$, and $F_A^{Z f} = -T_3^f$. The anomalous weak-magnetic form factor, $a_f^{V_1}$, is generated only at one-loop in the SM as well as in the models with excited fermions.

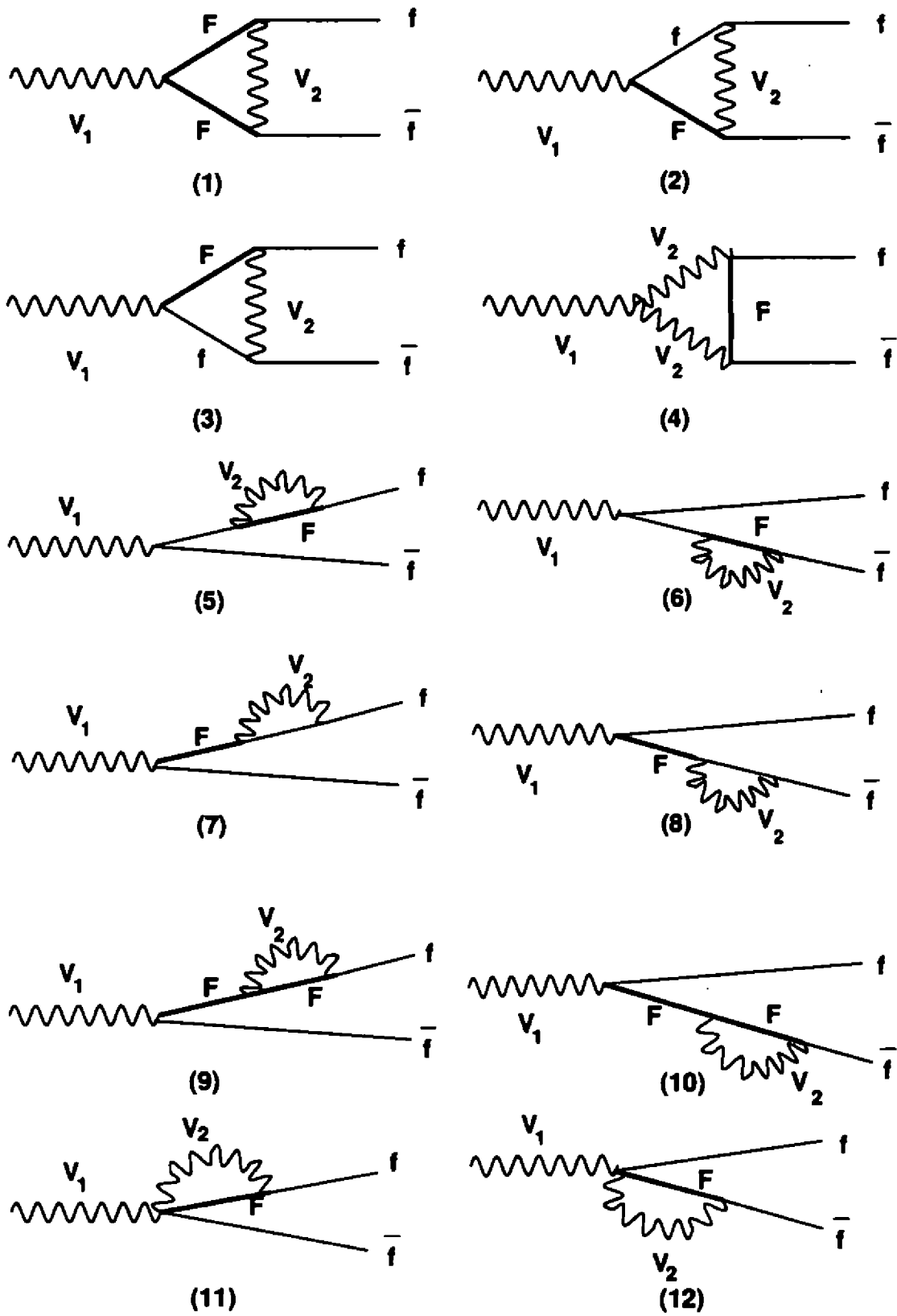


FIG. 2. The contribution of the excited leptons to the three-point functions

There are twelve one-loop Feynman diagrams involving excited fermions that contribute to the above form factors, which are shown in Fig. 2. The complete results for the excited leptons contributions are rather lengthy and can be found elsewhere [11, 12]. We should point out that we made a consistency check of the whole calculation, verifying that our exact result for the vertex $\gamma\bar{e}e$ cancels at $q^2 = 0$. This result should be expected since we are using a gauge invariant effective Lagrangian, and the QED Ward identities require that the excited fermion contribution to this vertex, at zero momentum, vanishes. In the same way, we have also checked that the contribution to the coupling $\gamma\bar{\nu}\nu$ cancels.

The form factors $F_V^{Zf} = F_A^{Zf}$ changes the Z widths, $\Gamma_e \equiv \Gamma(Z \rightarrow e^+e^-)$ and $\Gamma_{inv} \equiv 3\Gamma(Z \rightarrow \bar{\nu}\nu)$, by

$$\begin{aligned}\Delta\Gamma_e &= \alpha M_Z \frac{(s_W^2 - 1/2)}{3s_W^2 c_W^2} \times F_V^{Ze}(z), \\ \Delta\Gamma_{inv} &= \alpha M_Z \frac{1}{2s_W^2 c_W^2} \times F_V^{Z\nu}(z).\end{aligned}$$

The theoretical values for the Z partial width generated by ZFITTER [17], for $m_{top} = 175$ GeV and $M_H = 300$ GeV, are $\Gamma_e = 83.9412$ MeV and $\Gamma_{inv} = 501.482$ MeV. The most recent LEP results [18], assuming lepton universality, are $\Gamma_{\ell\ell}^{LEP}(Z \rightarrow \ell^+\ell^-) = 83.91 \pm 0.11$ MeV and for the invisible width $\Gamma_{inv}^{LEP} = 499.5 \pm 2$ MeV. Therefore, at 95% C.L., we should have $-0.25 < \Delta\Gamma_e < 0.18$ MeV, and $-5.9 < \Delta\Gamma_{inv} < 1.94$ MeV.

Our numerical results show that the most restrictive bound on the excited fermion mass and compositeness scale comes from the comparison of $\Delta\Gamma_e$ with the LEP data for this observable (see Fig. 3). In Fig. 4, we present the excluded region, at 95% C.L., in the Λ versus M plane imposed by $\Delta\Gamma_e$, for $f_1 = f_2 = \kappa_1 = \kappa_2 = 1$. We have further assumed that $M \leq \Lambda$, leading to the excluded region represented by the shadowed triangle. For comparison, we also present the regions excluded by the ZEUS [19] and H1 data [20], for $f_1 = f_2 = 1$. Since we have assumed that $BR(e^* \rightarrow e\gamma) = 1$, these curves represent the upper limit for ZEUS and H1 bounds. As we can see, we were able to exclude a small region beyond the available limit. We also show our results when we relax the condition of $M \leq \Lambda$. In the latter case, our analysis excludes all excited lepton masses with scales $\Lambda \leq 210$ GeV.

For the anomalous magnetic (a_j^γ) and weak-magnetic (a_j^Z) moments, we just present an approximate expression, assuming $M^2 = \Lambda^2 \gg M_{W,Z}^2$, and $f_1 = f_2 = f$ and $k_1 = k_2 = k$:

$$\begin{aligned}a_j^\gamma &= \frac{\alpha}{48\pi} \frac{f^2 m_j^2}{M^2} \left[\frac{37 + 74 \cos^2 \theta_W + (24 + 39 \cos^2 \theta_W)k}{\sin^2 \theta_W \cos^2 \theta_W} \right] \\ a_j^Z &= -\frac{\alpha}{96\pi} \frac{f^2 m_j^2}{M^2} \left[\frac{37 + 2 \cos^2 \theta_W (27 - 74 \cos^2 \theta_W) + 6(4 - 13 \cos^4 \theta_W)k}{\sin^3 \theta_W \cos^3 \theta_W} \right].\end{aligned}$$

Our results for the anomalous magnetic moment a_j^γ are in agreement with those of Ref. [21], for $k = 0$.

Nowadays, the most precise determination of the anomalous magnetic moment of the muon $a_\mu^\gamma \equiv (g_\mu - 2)/2$ comes from a CERN experiment [22], $a_\mu^\gamma = 11\,659\,230(84) \times 10^{-10}$. This result should be compared with the existing theoretical calculations of the QED, electroweak, and hadronic contributions, which are known with high precision. The main theoretical uncertainty comes from the hadronic contributions which is of the order of 20×10^{-10} . Therefore the present limit on the non-standard contributions to the anomalous magnetic moment of the muon is $|\delta a_\mu^\gamma| \lesssim 8 \times 10^{-9}$. The proposed AGS experiment at the Brookhaven National Laboratory [23] will be able to measure the anomalous magnetic moment of the muon with an accuracy of about $\pm 4 \times 10^{-10}$.

Taking these results into account, we plot in Fig. 5 the attainable values for the τ anomalous weak-magnetic moment, assuming universal couplings, after imposing the constraints from $g_\mu - 2$ measurements. We can see that only for a narrow band of k values around k_0 can $|a_\tau^Z(M_Z^2)|$ be large enough to be observed at LEP.

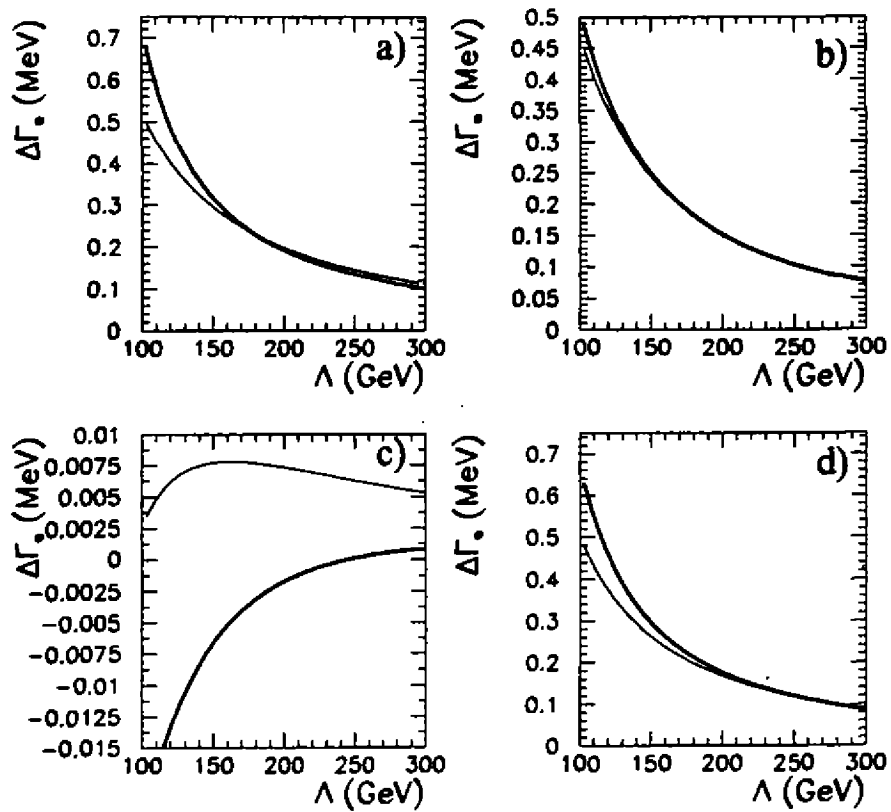


Figure 3. Attainable values for the new contributions to the width $\Gamma(Z \rightarrow \ell^+ \ell^-)$ in the model as a function of the scale Λ . The thin (thick) line correspond to excited lepton mass value of $M = 100$ (200) GeV. We have assumed different configurations of the weight factors $(f_1, f_2, \kappa_1, \kappa_2)$: (a) = (1, 1, 1, 1); (b) = (1, -1, 1, -1); (c) = (1, 0, 1, 0); (d) = (0, 1, 0, 1).

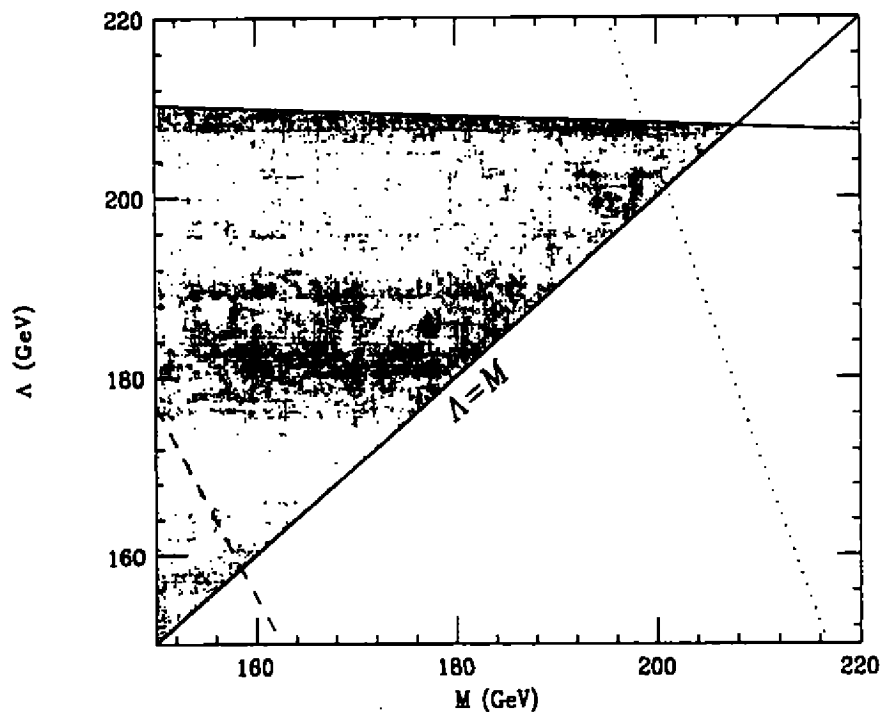


Figure 4. Excluded regions in the Λ versus M plane from the bounds on $\Delta\Gamma_{ee}$ (shaded area), from ZEUS data (below and left of the dashed curve) and H1 data (below and left of the dotted curve), at 95% C.L.

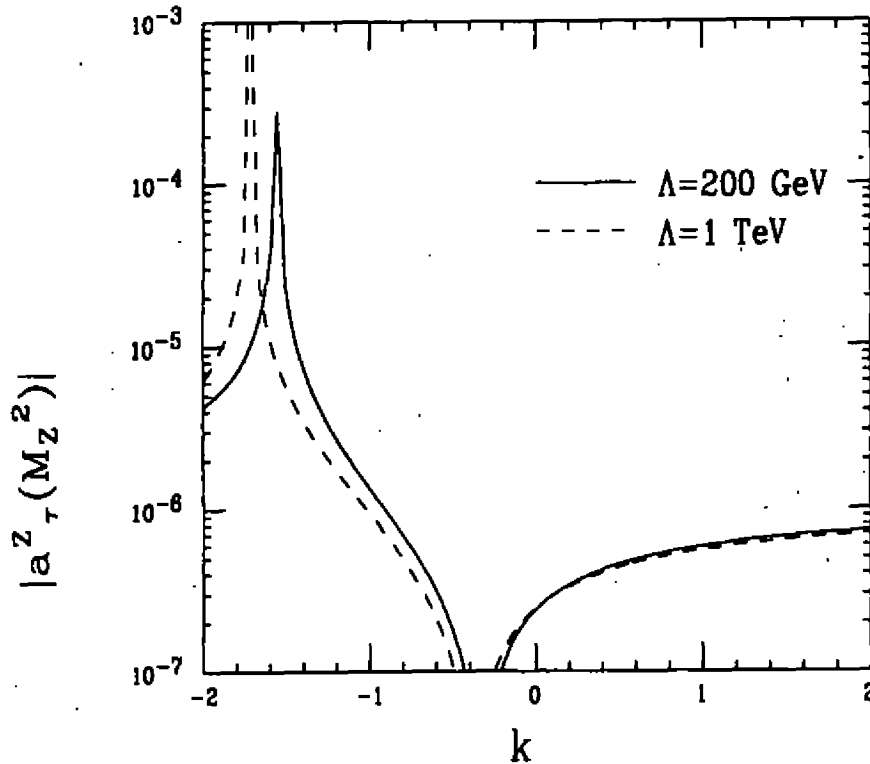


Figure 5. Attainable values of $|a_\tau^Z(M_Z^2)|$ for universal excited lepton couplings after imposing the constraints from $g_\mu - 2$.

In conclusion, we have evaluated the contribution of excited lepton states, up to the one-loop level, to the oblique variables, to the Z width to leptons, and to the anomalous magnetic and weak-magnetic form factors of the leptons. We compared our results with the recent bounds obtained through the direct search for these particles. Our results show that the present precision in the electroweak parameters attained by LEP is marginally able to constrain the parameters Λ and M beyond the present limits from direct searches. For the anomalous weak-magnetic moment of the τ , our results show that the existing limits from $g_\mu - 2$ strongly constrain the possibility of observing the anomalous weak-magnetic moment of the τ lepton at LEP.

References

- [1] The LEP Collaborations ALEPH, DELPHI, L3, OPAL, and the LEP Electroweak Working Group, contributions to the 1995 Europhysics Conference on High Energy Physics (EPS-HEP), Brussels, Belgium, and to the 17th International Symposium on Lepton-Photon Interactions, Beijing, China. Report No. CERN-PPE/95-172 (1995).
- [2] For a review, see for instance: H. Harari, Phys. Reports **104** (1984) 159; H. Terazawa, Proceedings of the XXII International Conference on High Energy Physics, Leipzig, 1984, edited by A. Meyer and E. Wieczorek, p. 63; W. Buchmüller, Acta Phys. Austriaca, Suppl. XXVII (1985) 517; M. E. Peskin, Proceedings of the 1985 International Symposium on Lepton and Photon Interactions at High Energies, Kyoto, 1985, p. 714, eds. M. Konuma and K. Takahashi.
- [3] ALEPH Collaboration, D. Decamp *et al.*, Phys. Lett. **B236** (1990) 501; *id.* **B250** (1990) 172; L3 Collaboration, B. Adeva *et al.*, Phys. Lett. **B247** (1990) 177; *id.* **B250** (1990) 199 and 205; *id.* **B252** (1990) 525; L3 Collaboration, O. Adriani *et al.*, Phys. Lett. **B288** (1992) 404; L3 Collaboration, M. Acciarri *et al.*, Phys. Lett. **B353** (1995) 136, *id.* **B370** (1996) 211; OPAL Collaboration, M. Z. Akrawy *et al.*, Phys. Lett. **B240** (1990) 497; *id.* **B241** (1990) 133; *id.* **B244** (1990) 135; *id.* **B257** (1991) 531; DELPHI Collaboration, P. Abreu *et al.*, Phys. Lett. **B268** (1991) 296; *id.* **B327** (1994) 386; Z. Phys. **C53** (1992) 41.
- [4] H1 Collaboration, I. Abt *et al.*, Nucl. Phys. **B396** (1993) 3; ZEUS Collaboration, M. Derrick *et al.*, Phys. Lett. **B316** (1993) 207, *id.* Z. Phys. **C65** (1994) 627.
- [5] K. Hagiwara, S. Komamiya and D. Zeppenfeld, Z. Phys. **C20** (1985) 115.

- [6] N. Cabibbo, L. Maiani and Y. Srivastava, Phys. Lett. **B139** (1984) 459; F. A. Berends and P. H. Daverveldt, Nucl. Phys. **B272** (1986) 131; A. Feldmaier, H. Salecker and F. C. Simm, Phys. Lett. **B223** (1989) 234; M. Martinez, R. Miquel and C. Mana, Z. Phys. **C46** (1990) 637; F. Boudjema and A. Djouadi, Phys. Lett. **B240** (1990) 485; M. Bardadin-Otwinowska, Z. Phys. **C55** (1992) 163; J. C. Montero and V. Pleitez, Phys. Lett. **B321** (1994) 267.
- [7] I. F. Ginzburg and D. Yu. Ivanov, Phys. Lett. **B276** (1992) 214; T. Kon, I. Ito and Y. Chikashige, Phys. Lett. **B287** (1992) 277; E. Boos, A. Pukhov and A. Beliaev, Phys. Lett. **B206** (1992) 452; O. J. P. Éboli, E. M. Gregores, J. C. Montero, S. F. Novaes and D. Spehler, Phys. Rev. **D53** (1996) 1253.
- [8] J. Kühn and P. Zerwas, Phys. Lett. **B147** (1984) 189.
- [9] K. Enqvist and J. Maalampi, Phys. Lett. **B135** (1984) 329.
- [10] F. Boudjema, A. Djouadi and J. L. Kneur, Z. Phys. **C57** (1993) 425.
- [11] M. C. Gonzalez-Garcia and S. F. Novaes, CERN-TH/96-123, IFT-P.013/96, hep-ph/9608309, Nucl. Phys. to appear.
- [12] M. C. Gonzalez-Garcia and S. F. Novaes, CERN-TH/96-185, IFT-P.023/96, hep-ph/9609393, Phys. Lett. to appear.
- [13] G. 't Hooft and M. Veltman, Nucl. Phys. **B44** (1972) 189; C. G. Bollini and J. J. Giambiagi, Nuovo Cim. **12B** (1972) 20.
- [14] R. Mertig, M. Böhm and A. Denner, Comput. Phys. Commun. **64** (1991) 345.
- [15] K. Hagiwara, S. Ishihara, R. Szalapski and D. Zeppenfeld, Phys. Rev. **D48** (1993) 2182.
- [16] G. Altarelli, R. Barbieri and S. Jadach, Nucl. Phys. **B369** (1992) 3; **B376** (1992) 444 (E); G. Altarelli, R. Barbieri and F. Caravaglios, Nucl. Phys. **B405** (1993) 3; Phys. Lett. **B349** (1995) 145.
- [17] D. Bardin *et al.*, Z. Phys. **C44** (1989) 493; Comput. Phys. Commun. **59** (1990) 303; Nucl. Phys. **B351** (1991) 1; Phys. Lett. **B255** (1991) 290; CERN-TH 6443/92 (May 1992).
- [18] The LEP Collaborations ALEPH, DELPHI, L3, OPAL, and the LEP Electroweak Working Group report LEPEWWG/96-02, July 1996.
- [19] ZEUS Collaboration, M. Derrick *et al.*, Z. Phys. **C65** (1994) 627.
- [20] H1 Collaboration, S. Aid *et al.*, DESY 96-163, hep-ex/9609008.
- [21] S. J. Brodsky and S. D. Drell, Phys. Rev. **D22** (1980) 2236; F. M. Renard, Phys. Lett. **B116** (1982) 264; P. Merry, S. E. Moubarik, M. Perrottet and F. M. Renard, Z. Phys. **C 40** (1990) 229; R. Escribano and E. Masso, hep-ph/9607218.
- [22] J. Bailey *et al.*, Nucl. Phys. **B150** (1979) 1; E. R. Cohen and B. N. Taylor, Rev. Mod. Phys. **59** (1987) 1121.
- [23] B. L. Roberts, Z. Phys. **C56** (1992) S101.

Aspectos de SUSY com Quebra de Paridade-R

Maurício Bernardino Magro

Instituto de Física, Universidade de São Paulo

Nos modelos supersimétricos é definido um novo número quântico multiplicativo chamado Paridade-R:

$$R_P = (-1)^{2J+3B+L} \quad (1)$$

onde J é o spin, B o número bariônico e L o número leptônico. Este novo número quântico assume o valor $+1$ para as partículas do modelo padrão e -1 para as de SUSY. Se R_P se conserva, como assume o MSSM, podemos concluir que as partículas supersimétricas são produzidas a pares e que existe uma partícula SUSY estável (LSP).

No aspecto experimental, os últimos dados dos aceleradores restringem cada vez mais os espaço cinemático para a observação de novas partículas SUSY. Este fato faz com que os físicos teóricos busquem novas alternativas que substituam o MSSM na busca de sinais de SUSY na atual escala de energia dos aceleradores em funcionamento. Uma dessas alternativas se baseia no fato de que não existe nenhuma forte razão para que R_P se conserve. É nesse contexto que se situa o modelo supersimétrico com quebra de Paridade-R [1] em que nos baseamos para desenvolver nosso trabalho.

Como no mecanismo de Higgs, o modelo com quebra espontânea de paridade-R introduz novos campos ao superpotencial do MSSM. O novo potencial é dado por¹

$$\begin{aligned} & h_u Q H_u u^c + h_d H_d Q d^c + H_e l H_d e^c + (h_0 H_u H_d - \epsilon^2) \Phi \\ & + h_\nu l H_\nu \nu^c + h \Phi S \nu^c + h.c. \end{aligned} \quad (2)$$

onde se introduz supercampos (Φ, ν_i^c, S_i) que são singletos sob $SU(2) \otimes U(1)$ e carregam número leptônico $(0, -1, 1)$ respectivamente. A esses supercampos se atribuem VEVs que levam a quebra do número leptônico e, portanto, de paridade-R.

Como consequência desse modelo surge um novo bóson de Goldstone, chamado de majoron J , singlete de $SU(2) \otimes U(1)$. É importante notar que, devido a que a paridade-R não se conserva, o LSP, que neste modelo sempre é o neutralino mais leve, não é estável e, portanto, possui canais de desintegração. Da diagonalização das matrizes de massa, observamos que sua massa está na região $25 \text{ GeV} \lesssim M_{\chi_0} \lesssim 500 \text{ GeV}$.

Para muitas aplicações práticas, este modelo pode ser substituído por um modelo efetivo [3] onde se adiciona ao superpotencial do MSSM o termo

$$\epsilon_i L_i H_u \quad (3)$$

e a conexão com o modelo espontâneo é dado por

$$\epsilon_i = \sum_j h_{ij}^j \nu_R^j \quad (4)$$

Com a finalidade de estudar os possíveis sinais que o LSP pode gerar no modelo com quebra espontânea de paridade-R, desenvolvemos um simulador de Monte Carlo que gera eventos que ocorrem em aceleradores e^+e^- . Este simulador nos permite calcular as eficiências de detecção dos processos que violam paridade-R, depois de aplicados os cortes que eliminam o *back-ground*. Este simulador nos permite, então, estudar os seguintes processos

$$e^+e^- \rightarrow Z \rightarrow \chi \nu \quad (5)$$

¹Uma descrição detalhada do modelo, bem como a apresentação dos acoplamentos e das matrizes de massa para os charginos e neutralinos pode ser encontrada na ref. [2].

$$e^+e^- \rightarrow Z \rightarrow \chi\chi; \quad (6)$$

onde o processo 5 claramente viola paridade-R e, portanto, trata-se de um novo processo predito pelo modelo. O processo 6, ao contrário, já está predito pelo MSSM.

A seção de choque diferencial para estes processos incluindo somente a troca do Z em $\sqrt{s} = M_Z$ é dada por [4]

$$\frac{d\sigma}{d\Omega} (e^+e^- \rightarrow \chi_i\chi_j) = \frac{\alpha^2}{4s} \frac{1}{2} (2 - \delta_{ij}) |Q(s)|^2 \lambda^{1/2} \left(1, \frac{m_i^2}{s}, \frac{m_j^2}{s}\right) \left(\frac{1}{\sin\theta_w \cos\theta_w}\right)^4 [G_{1ij}(s) + G_{2ij}(s) \cos\theta + G_{3ij}(s) \cos^2\theta] \quad (7)$$

onde λ é a função de Källen usual e

$$G_{1ij}(s) = (g_V^2 + g_A^2) \left[2 \frac{E_i}{\sqrt{s}} \frac{E_j}{\sqrt{s}} (O_{Lij}'' + O_{Rij}'') + 4 \frac{m_i m_j}{s} O_{Lij}'' O_{Rij}'' \right] \quad (8)$$

$$G_{2ij}(s) = 2g_V g_A (O_{Lij}'' - O_{Rij}'') \lambda^{1/2} \left(1, \frac{m_i^2}{s}, \frac{m_j^2}{s}\right) \quad (9)$$

$$G_{3ij}(s) = \frac{1}{2} (g_V^2 + g_A^2) (O_{Lij}'' + O_{Rij}'') \lambda \left(1, \frac{m_i^2}{s}, \frac{m_j^2}{s}\right) \quad (10)$$

e

$$E_i = \frac{s + m_i^2 - m_j^2}{2\sqrt{s}}; \quad E_j = \frac{s + m_j^2 - m_i^2}{2\sqrt{s}} \quad (11)$$

$$Q(s) = \frac{s}{s - M_Z^2 + iM_Z\Gamma_Z} \quad (12)$$

aqui g_V e g_A são os acoplamentos vetorial e axial usuais para o vértice Ze^+e^- do modelo padrão

$$g_V = -\frac{1}{4} + \sin^2\theta_w; \quad g_A = -\frac{1}{4} \quad (13)$$

e os acoplamentos $\chi_i \chi_j$ relevantes são determinados em [4].

O simulador também permite estudar os canais de decaimento do neutralino (LSP)

$$\chi \rightarrow \nu_\tau Z^* \rightarrow \nu_\tau l^+ l^-, \nu_\tau \nu_i \bar{\nu}_i, \nu_\tau q_i \bar{q}_i, \quad (14)$$

$$\chi \rightarrow \tau W^* \rightarrow \tau \nu_i l_i, \tau q_u \bar{q}_d. \quad (15)$$

Há também um terceiro tipo de decaimento

$$\chi \rightarrow \nu_\tau J. \quad (16)$$

que não é levado em consideração no simulador, pois apresenta um sinal de *missing P_T*, já que as partículas finais escapam do detector.

Para a produção simples $e^+e^- \rightarrow \chi\nu$ com o decaimento $\chi \rightarrow \nu_\tau \mu^+ \mu^-$ o número de eventos é dado por

$$N_{\text{expt}}(\chi\nu) = \sigma(e^+e^- \rightarrow \chi\nu) BR(\chi \rightarrow \nu_\tau \mu^+ \mu^-) \epsilon_{\chi\nu} L_{\text{int}} \quad (17)$$

onde $\epsilon_{\chi\nu}$ é a eficiência de detecção, obtida do gerador descrito anteriormente.

Usando a expressão para a seção de choque em 7 podemos escrever

$$N_{\text{expt}}(\chi\nu) = \frac{2}{3} O_{L43}''^2 \frac{\alpha^2 \pi (g_V^2 + g_A^2)}{\Gamma_Z^2 (\sin\theta_w \cos\theta_w)^4} (2 - 3x_Z^2 + x_Z^4) BR(\chi \rightarrow \nu_\tau \mu^+ \mu^-) \epsilon_{\chi\nu} L_{\text{int}} \quad (18)$$

onde $x_Z = m_\chi/m_Z$.

Ademais, a relação entre o acoplamento $O_{L43}''^2$ e o $BR(Z \rightarrow \chi\nu)$ é dada por

$$BR(Z \rightarrow \chi\nu) = \frac{2}{3} O_{L43}''^2 \frac{M_Z^2 G_F}{\Gamma_Z \pi \sqrt{2}} \left(1 - \frac{3}{2} x_Z^2 + \frac{1}{2} x_Z^4 \right) \quad (19)$$

De 18 e 19 pode-se obter um limite de 95%CL sobre o observável $BR(Z \rightarrow \chi\nu)BR(\chi \rightarrow \nu_\tau \mu^+ \mu^-)$ como função da massa do neutralino, χ . Isto é mostrado na figura 1 [4].

O número de eventos $\cancel{p}_T + \mu^+ \mu^-$ esperados para a produção a par é dada por

$$N_{\text{expt}}(\chi\chi) = \sigma(e^+e^- \rightarrow \chi\chi) 2BR(\chi \rightarrow \text{invisível})BR(\chi \rightarrow \nu_\tau \mu^+ \mu^-) \epsilon_{\chi\chi} L_{\text{int}} \quad (20)$$

e de 7 obtemos

$$N_{\text{expt}}(\chi\chi) = \frac{2}{3} O_{L44}''^2 \frac{\alpha^2}{\Gamma_Z^2} \frac{\pi(g_V^2 + g_A^2)}{(\sin\theta_w \cos\theta_w)^4} (1 - 4x_Z^2)^{3/2} \cdot 2BR(\chi \rightarrow \nu_\tau \mu^+ \mu^-)BR(\chi \rightarrow \text{invisível}) \epsilon_{\chi\chi} L_{\text{int}} \quad (21)$$

e a expressão correspondente para o *branching ratio* $Z \rightarrow \chi\chi$ é

$$BR(Z \rightarrow \chi\chi) = \frac{1}{3} O_{L44}''^2 \frac{M_Z^2 G_F}{\Gamma_Z \pi \sqrt{2}} (1 - 4x_Z^2)^{3/2} \quad (22)$$

Destas últimas expressões é possível obter um limite ilustrativo com 95%CL para $BR(Z \rightarrow \chi\chi)BR(\chi \rightarrow \nu_\tau \mu^+ \mu^-)BR(\chi \rightarrow \text{invisível})$ como função da massa do neutralino, como mostra a figura 2 [4].

Dentro do contexto deste modelo com quebra espontânea de paridade-R [1], o stop mais leve pode ter um novo modo de decaimento na terceira família de férmions, $\tilde{l}_1 \rightarrow b + \tau$, devido à mistura entre os léptons carregados e os charginos. Mostraremos aqui que este decaimento pode ser dominante ou ao menos comparável com o modo de decaimento que conserva paridade-R, $\tilde{l}_1 \rightarrow c + \tilde{\chi}_1^0$, para $m_{\tilde{l}_1} < m_b + m_{\tilde{\chi}_1^0}$, onde $\tilde{\chi}_1^0$ denota o LSP.

O decaimento $\tilde{l}_1 \rightarrow c + \tilde{\chi}_1^0$ somente é possível em ordens mais altas. Como é mostrado em [5], a contribuição dominante é devido a $\tilde{l}_1 \rightarrow \tilde{c}_L + c\tilde{\chi}_1^0$. Este processo pode ser parametrizado através de uma matriz de massa na base $(\tilde{l}_L, \tilde{l}_R, \tilde{c}_L)$ [6]. O autoestado de massa do stop leve pode ser escrito como:

$$\tilde{l}_1 = c_1 \tilde{l}_L + c_2 \tilde{l}_R + \delta \tilde{c}_L \quad (23)$$

Estimativas para δ são dadas em [5]. Para nossa discussão fenomenológica, tomamos uma mistura $\tilde{l} - \tilde{c}$ muito forte, $\delta \sim O(0.1)$. Note que esta é uma postura muito conservadora, isto é, se δ for menor, a importância relativa do nosso novo modo de decaimento é aumentada.

Os modos de decaimento em questão são dados por [6]

$$\Gamma(\tilde{l}_1 \rightarrow b + \tau) = \frac{g^2}{16\pi m_{\tilde{l}_1}^3} \sqrt{(m_{\tilde{l}_1}^2 - m_b^2 - m_\tau^2)^2 - 4m_b^2 m_\tau^2} (l^2 + k^2) \times (m_{\tilde{l}_1}^2 - m_b^2 - m_\tau^2) - 4lk m_b m_\tau \quad (24)$$

$$\Gamma(\tilde{l}_1 \rightarrow c\tilde{\chi}_1^0) = \frac{g^2}{16\pi m_{\tilde{l}_1}^3} |\delta|^2 f_1^2 (m_{\tilde{l}_1}^2 - m_{\tilde{\chi}_1^0}^2) \quad (25)$$

onde

$$l = \frac{m_t}{\sqrt{2} m_W \sin \beta} V_{34} c_2 K_{1b} - V_{35} (c_1 K_{1b} + \delta K_{cb}) \quad (26)$$

$$k = \frac{m_b K_{1b}}{\sqrt{2} m_W \cos \beta} U_{34} c_1 \quad (27)$$

$$f_1 = -\frac{\sqrt{2}}{6} (\tan \theta_W N_{47} + 3N_{46}) \quad (28)$$

$$f_2 = -\frac{\sqrt{2}}{6} (\tan \theta_W N_{57} + 3N_{56}) \quad (29)$$

Aqui V_{34} , $U_{34}(V_{35})$ denotam a mistura entre tau-higgsino e $K_{tb} = 0.999$, $K_{cb} = 0.04$ são os elementos da matriz CKM correspondentes.

Em nossa análise fixamos $m_{\tilde{t}_1} = 80$ GeV, $c_1 = 0.5$, $v_H = 100$ GeV, $v_L = 0.1$ GeV e $h_{\nu 33} = 0.03$. Variamos todos os outros parâmetros supersimétricos nos intervalos que estão permitidos experimentalmente para o MSSM. Na figura 3, mostramos o valor máximo para o *branching ratio* para $\tilde{t}_1 \rightarrow b + \tau$ em função da massa do neutralino no intervalo $1 < \tan \beta < 40$. Podemos observar que o $BR(\tilde{t}_1 \rightarrow b + \tau)$ pode facilmente alcançar 80% para massa do neutralino de 50 GeV [6].

References

- [1] A. Masiero and J. W. F. Valle, *Phys. Lett.* **B251** (1990) 273.
- [2] M. C. Gonzalez-Garcia, J. C. Romão and J. W. F. Valle, *Nucl. Phys.* **B301** (1993) 100.
- [3] F. de Campos, M. A. Garcia-Jareño, A. S. Joshipura, J. Rosiek and J. W. F. Valle, *Nucl. Phys.* **B451** (1995) 3.
- [4] J. C. Romão, F. de Campos, M. A. Garcia-Jareño, M. B. Magro and J. W. F. Valle, *pre-print hep-ph 9604244*, a ser publicado em *Nucl. Phys. B*.
- [5] K. I. Hikasa and M. Kobayashi, *Phys. Rev.* **D30** (1987) 724.
- [6] A. Bartl, W. Porod, M. A. Garcia-Jareño, M. B. Magro, J. W. F. Valle and W. Majerotto, *pre-print hep-ph 9606256*, a ser publicado em *Phys. Lett. B*.

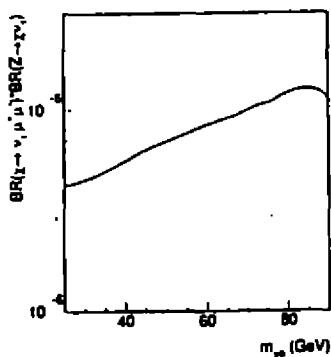


Figura 1: Região de sensibilidade com 95% C.L. para $BR(Z \rightarrow \chi\nu)BR(\chi \rightarrow \mu^+\mu^-\nu)$, em função da massa do neutralino mais leve m_{χ_0} . Isto é derivado das buscas de $b\tau + \mu^+\mu^-$ que poderiam aparecer da produção simples de neutralinos em LEP, seguida pelo decaimento $\chi \rightarrow \mu^+\mu^-\nu$

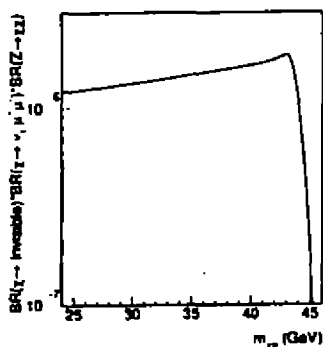


Figura 2: Região de sensibilidade com 95% C.L. para $BR(Z \rightarrow \chi\chi)(\chi \rightarrow \mu^+\mu^-\nu)BR(\chi \rightarrow \text{invisible})$ em função da massa do neutralino mais leve. Isto é derivado das buscas de $b\tau + \mu^+\mu^-$ que apareceriam a partir da produção a par de neutralinos em LEP, com um neutralino decaindo invisivelmente e o outro decaindo em $\chi \rightarrow \mu^+\mu^-\nu$.

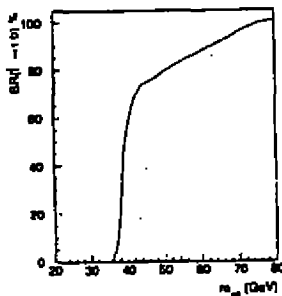


Figura 3: Máximos valores para o branching ratio de $i_1 \rightarrow b + \tau$ em porcentagem como função da massa do neutralino mais leve, m_{χ_0} . Tomamos $m_{\tilde{t}_1} = 80$ GeV, $c_1 = 0.5$, $v_R = 100$ GeV, $v_L = 0.1$ GeV e $h_{\nu 33} = 0.03$. Os outros parâmetros foram variados como explicado no texto.

Colorless States in Perturbative QCD: Charmonium Production

O.J.P. Éboli^{*†}, E.M. Gregores^{*†} and F. Halzen^{*}

^{*}Physics Department, University of Wisconsin

[†]Instituto de Física, USP

[‡]Instituto de Física Teórica, UNESP

We point out that the experimental data on the production of charmonium states support the predictions of the duality model, also known as color evaporation model, which state that the bulk of charmonium production is due to the formation of colored $c\bar{c}$. We demonstrate that the duality model gives a complete picture of charmonium production, including low energy data, the recent Tevatron results, and the HERA data on photoproduction.

There has been a renewed interest in studying the mechanism by which charmonium is produced, triggered mostly by some puzzling data from the Fermilab Tevatron. The standard perturbative QCD calculations using the color-singlet model failed to explain the data, occasionally by orders of magnitude [1]. The data incited a complete review of the treatment of color in QCD and can, in fact, be explained by allowing perturbative color octet $c\bar{c}$ states to evolve into the asymptotic colorless charmonium states. This prescription is present in both the color-evaporation[2] and in the color-octet models[3].

The color-evaporation model (CEM) quantitatively describes all charmonium photo- and hadroproduction data [4]. The model simply states that charmonium production is described by the same dynamics as $D\bar{D}$ production, i.e., by the formation of a colored $c\bar{c}$ pair. Rather than imposing that the $c\bar{c}$ pair is in a color-singlet state in the short-distance perturbative diagrams, it is argued that the appearance of color-singlet asymptotic states solely depends on the outcome of large-distance fluctuations of quarks and gluons. These large-distance fluctuations are probably complex enough for the occupation of different color states to approximately respect statistical counting. In the CEM the sum of the cross sections of all onium and open charm states is described by

$$\sigma_{\text{onium}} = \frac{1}{9} \int_{2m_c}^{2m_D} dm \frac{d\sigma_{c\bar{c}}}{dm} \quad (1)$$

and

$$\sigma_{\text{open}} = \frac{8}{9} \int_{2m_c}^{2m_D} dm \frac{d\sigma_{c\bar{c}}}{dm} + \int_{2m_D} dm \frac{d\sigma_{c\bar{c}}}{dm} \quad (2)$$

where the cross section for producing heavy quarks, $\sigma_{c\bar{c}}$, is computed perturbatively, irrespective of the color of the $c\bar{c}$ pair, and m is the invariant mass of the $c\bar{c}$ pair. The coefficients $\frac{1}{9}$ and $\frac{8}{9}$ represent the statistical probabilities that the 3×3 charm pair is asymptotically in a singlet or octet state [4].

The CEM assumes a factorization of the production of the $c\bar{c}$ pair, which is perturbative and process dependent, and the materialization of this pair into a charmonium state by a mechanism that is nonperturbative and process independent. Comparison with the ψ data requires knowledge of the fraction ρ_ψ of produced onium states that materialize as ψ 's, i.e.,

$$\sigma_\psi = \rho_\psi \sigma_{\text{onium}} \quad (3)$$

where ρ_ψ is assumed to be a constant. This assumption is in agreement with the low-energy data [5].

Quantitative tests of color evaporation are made possible by the fact that the factor ρ_ψ is the same in hadro- and photoproduction. Once ρ_ψ has been empirically determined for one initial state, the cross section is predicted without free parameters for the other. In Fig.1 we compare the photoproduction data with theory, using the NLO

perturbative QCD calculation of charm pair production. This reaction determines the only free parameter, $\rho_\psi \approx 0.5$. From this figure we can conclude that the photoproduction of J/ψ and $D\bar{D}$ is well described by the color evaporation model.

At this point the predictions of the color evaporation model for hadroproduction of ψ are completely determined, up to higher order QCD corrections. These can be estimated by fitting the hadroproduction cross section of $D\bar{D}$ pairs with a global K factor. This factor is subsequently used to correct the ψ prediction. In Fig.2 we show that the CEM is able to accommodate all data on the hadroproduction of charmonium. This is a remarkable result given that the subprocess responsible for the charmonium hadroproduction changes from $q\bar{q}$ fusion to gg fusion as the center-of-mass energy is increased. Analogously we can show that the high p_T production of charmonium at CDF can also be explained by the CEM [4].

To conclude, we would like to stress that the CEM describes extremely well all the available charmonium-production data in photon-hadron and hadron-hadron collisions, as well as in Z decays [7].

References

- [1] See, e.g., E. Braaten, S. Fleming, and T.C. Yuan, to appear in *Ann. Rev. Nucl. Part. Sci.* (hep-ph/9602374), and references therein.
- [2] H. Fritzsch, *Phys. Lett.* **B67**, 217 (1977); F. Halzen, *Phys. Lett.* **B69**, 105 (1977); F. Halzen and S. Matsuda, *Phys. Rev.* **D17**, 1344 (1978); M. Glück, J. Owens, and E. Reya, *Phys. Rev.* **D17**, 2324 (1978).
- [3] G.T. Bodwin, E. Braaten, and G. Lepage, *Phys. Rev.* **D51**, 1125 (1995).
- [4] J.F. Amundson, O.J.P. Éboli, E.M. Gregores, and F. Halzen, *Phys. Lett.* **B372**, 127 (1996), and preprint MADPH-96-942 (hep-ph/9605295).
- [5] R. Gavai, *et al.*, *Int. J. Mod. Phys.* **A10**, 3043 (1995); G.A. Schuler, preprint CERN-TH.7170/94 (hep-ph/9403387).
- [6] The data used in our plots is described in Ref. [4].
- [7] O.J.P. Éboli, E.M. Gregores, and F. Halzen, preprint MADPH-96-950 (hep-ph/0607324).

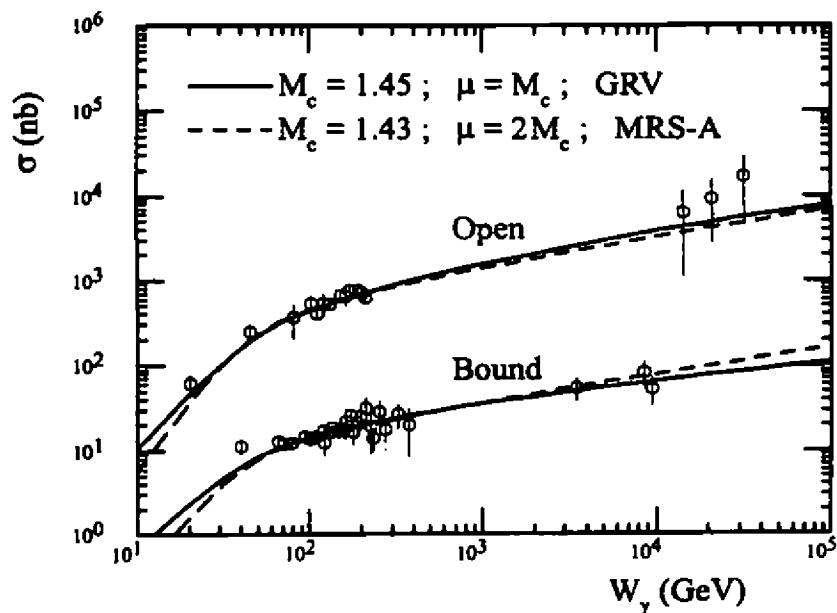


Figure 1: Photoproduction data [6] and the predictions of the CEM at next-to-leading order as a function of the photon energy in the hadron rest frame, W_γ .

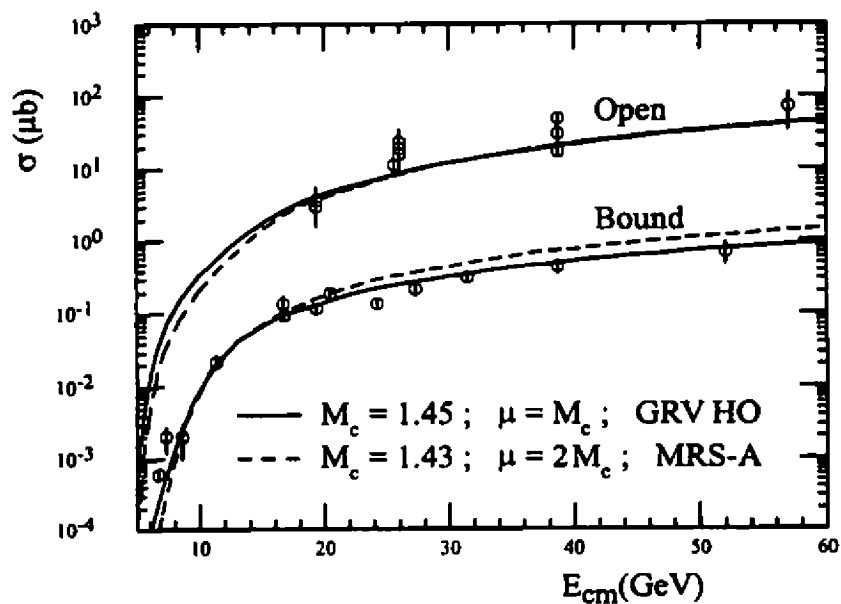


Figure 2: Hadroproduction data [6] and the predictions of the CEM at next-to-leading order as a function of the center-of-mass energy, E_{cm} .

A Produção Associada de Bósons de Gauge e Jatos Através de Interações Múltiplas de Pártons

O. J. P. Éboli, J. K. Mizukoshi

Instituto de Física, Universidade de São Paulo.

Caixa Postal 20516, 01452-990 São Paulo, Brazil

F. Halzen

Physics Department, University of Wisconsin, Madison, WI 53706

Em colisões hadrônicas, $W + n$ jatos são processos de ordens mais altas em QCD, mas também podem ser processos devido às interações múltiplas de pártons. Um subprocesso produzindo $W + k$ jatos no estado final, seguido de um outro produzindo l jatos numa mesma interação nucleon-nucleon, resultará num evento de $W + n$ jatos, caso $k + l = n$. Nós analisamos essas interações múltiplas em termos do tipo de cortes experimentais usados no Tevatron (Fermilab), considerando os casos $V = Z, W$ e γ .

1 Interações Múltiplas para $V + n$ jatos

A medida precisa dos eventos contendo $V + n$ jatos em interações próton-antipróton no Tevatron pode nos levar a um melhor entendimento da QCD. Especificamente, esses eventos têm sido usados para determinar α_s , a constante de acoplamento forte. No entanto, além de serem processos de ordem mais alta em QCD, eles podem ser originados a partir das interações múltiplas dos pártons [1].

Como exemplo, tomemos o processo $W + 2$ jatos. Neste caso, além da contribuição usual vinda da QCD, temos de levar em conta a produção do W simples devido à aniquilação quark-antiquark e a produção simultânea de 2 jatos devido a um outro par de pártons (vide fig. 1). Neste caso, a produção associada de $W + 2$ jatos pode ter como origem a interação dupla dos pártons de um mesmo "beam" (fig. 1.a) ou de "beams" diferentes (fig. 1.b), além do termo de interferência.

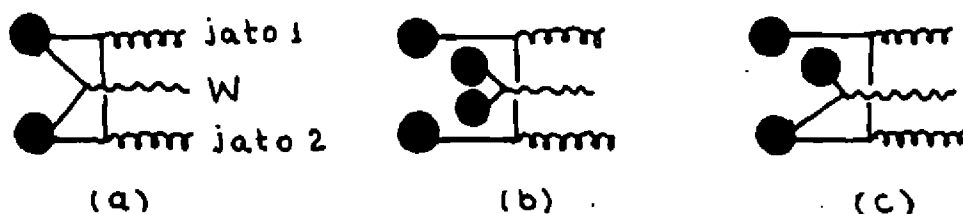


Figure 1.: Interações múltiplas para $W + 2$ jatos. Em (a) temos a interação dupla de pártons, em (b) interação múltipla $p\bar{p}$ entre os "beams" e em (c) o termo de interferência.

A seção de choque total para a produção de W associada com a de 2 jatos é dada por [2]

$$\sigma_{W+2\text{jatos}}^{\text{inter. mult.}} = \sigma_W \sigma_{2\text{jatos}} \left[\frac{1}{\pi R^2} + 2 \sqrt{\frac{1}{\pi R^2} \frac{N-1}{\sigma_{\text{inel}}} + \frac{N-1}{\sigma_{\text{inel}}}} \right], \quad (1)$$

com

$$N = \mathcal{L} \Delta t \sigma_{inel} \quad (2)$$

sendo o número médio de colisões por "bunch", onde \mathcal{L} é a luminosidade, Δt o tempo entre duas colisões e σ_{inel} a seção de choque total inelástica. O primeiro termo entre colchetes é a interação múltipla em um mesmo "beam", enquanto que o último, entre "beams" diferentes. O segundo termo é a interferência. No nosso trabalho vamos nos preocupar somente com o primeiro termo, já que o efeito das múltiplas interações dos "beams" pode ser identificado pelo detector e eliminado do conjunto de dados. Desta forma, a produção associada de $W + 2$ jatos dependerá somente da área efetiva do próton, não dependendo dos parâmetros do acelerador. Neste trabalho escolhemos $R = 0.7$ Fermi, o que corresponde à uma área efetiva de aproximadamente 15 mb.

A eq. (1) pode ser estendida para o caso $W + 3$ jatos. Neste caso, nós teremos dois tipos de contribuições: a produção de um simples W associada com a de 3 jatos e a produção de $W + 1$ jato associada com a de 2 jatos. A seção de choque total será dada por

$$\sigma_{W+3\text{jatos}}^{\text{mult. inter.}} = (\sigma_W \sigma_{3\text{jatos}} + \sigma_{W+1\text{jato}} \sigma_{2\text{jatos}}) \left[\frac{1}{\pi R^2} + 2 \sqrt{\frac{1}{\pi R^2} \frac{N-1}{\sigma_{inel}}} + \frac{N-1}{\sigma_{inel}} \right] \quad (3)$$

A expressão para o Z é análogo à do W , mas para o fóton devemos lembrar que não existe a produção simples deste na aniquilação párton-pártion. Assim, só faz sentido falarmos em interações múltiplas para $\gamma + n$ jatos quando $n \geq 3$.

2 Resultados

As seções de choque dos processos $V + k$ jatos foram calculados usando-se o método de integração por Monte Carlo, onde os elementos de matriz quadrados foram gerados por MADGRAPH [3]. Este pacote calcula a amplitude quadrada dos processos para feixes não polarizados no estado inicial e somados sobre as polarizações finais.

Nós estudamos vários cortes nos momentos transversais dos jatos. A figura (2.) mostra as distribuições dos momentos transversais para os cortes em $p_T > 5, 10, 15$ e 20 GeV do processo $W + 2$ jatos. Os cortes adicionais usados aqui correspondem aos usados recentemente pela colaboração do CDF [4] na definição de jato. Para os casos de W e Z usamos

$$\Delta R = \sqrt{\Delta\phi^2 + \Delta\eta^2} > 0.9$$

$$|\eta| \leq 3.0$$

enquanto que para o fóton usamos

$$|\eta_\gamma| \leq 1.0, \quad |\eta_{\text{jatos}}| \leq 4.0$$

Na expressão acima $\Delta\phi$ é a separação entre os ângulos azimutais dos jatos e $\Delta\eta$ a diferença de pseudorapidez entre os mesmos. As tabelas 1, 2, 3, 4 e 5 contém os resultados para $W + 2$ jatos, $W + 3$ jatos, $Z + 2$ jatos, $Z + 3$ jatos e $\gamma + 3$ jatos, respectivamente. Consideramos aqui $R \approx 0.7$ Fermi para uma simples estimativa, mas a princípio podemos considerar a área efetiva ocupada por quarks diferente daquela ocupada pelos glúons. A energia do centro de massa no Tevatron é de 1.8 TeV.

A função de distribuição dos pártons dentro do próton e anti-próton usada foi a parametrização CTEQ 3M [5], onde $\Lambda^{QCD} = 239$ MeV, listada no pacote PDFLIB [6]. Com esses dados obtemos $\sigma_W = 8.73$ nb para a produção simples do W e $\sigma_Z = 5.13$ nb para o Z .

3 Conclusões

Pelos resultados das tabelas 1 e 2 nós vemos que para o corte experimental mais realístico, $p_T > 20$ GeV e acima, as interações múltiplas de pártons tem contribuição em torno de 6 % para o processo $W + 2$ jatos e 7 % para $W + 3$ jatos. Para o caso $\gamma + 3$ jatos, os cortes usados levam a um grande valor, mas vale lembrar que estamos fazendo cortes nos processos duros e não aqueles usados pelos experimentais. De qualquer forma, é importante olharmos para processos que envolvem produção de bósons de gauge associada com a de jatos, principalmente na região de pequenos p_T 's.

p_T cut (GeV)	$\sigma_{2jets} \times 10^2$ (mb)	σ_{W2jets} (pb)	$\sigma_{W2jets}^{mult. part.}$ (pb)
5	106	1301	601
10	13.6	461	77
15	3.52	221	20
20	1.25	122	7.1
25	0.54	73.5	3.1

Table 1: Seção de choque para $W + 2$ jatos no Tevatron.

p_T cut (GeV)	σ_{3jets} (μ b)	σ_{Wjet} (nb)	σ_{W3jets} (pb)	$\sigma_{W3jets}^{mult. part.}$ (pb)
5	89	4.21	336	340
10	7.0	2.20	80	23
15	1.3	1.36	29	3.8
20	0.36	0.90	13	0.9
25	0.12	0.63	6.4	0.3

Table 2: Seção de choque para $W + 3$ jatos no Tevatron.

p_T cut (GeV)	$\sigma_{Z+2-jet}$ (pb)	$\sigma_{Z+2-jet}^{mult. part.}$ (pb)
20	78	4.2

Table 3: Seção de choque para $Z + 2$ jatos no Tevatron.

p_t cut (GeV)	σ_{Z+jet} (nb)	$\sigma_{Z+3-jet}$ (pb)	$\sigma_{Z+3-jet}^{mult.part.}$ (pb)
20	0.58	8.6	0.6

Table 4: Seção de choque para $Z + 3$ jatos no Tevatron.

p_t cut (GeV)	σ_{2jet} (nb)	$\sigma_{\gamma+jet}$ (nb)	$\sigma_{\gamma+3-jet}$ (pb)	$\sigma_{\gamma+3-jet}^{mult.part.}$ (pb)
16 for γ and leading jet 6 for secondary jet	0.86	5.0	483	279

Table 5: Seção de choque para $\gamma + 3$ jatos no Tevatron.

References

- [1] L. J. Keeble, in *The Fermilab Meeting. Proceedings of the Meeting of the Division of Particles and Fields of the APS*, Batavia, Illinois, 1992, edited by C. Albright et al. (World Scientific, Singapore, 1993), p. 1002;
R. S. Fletcher, F. Halzen e C. S. Kim, *Phys. Lett.* **B209** (1988) 351;
C. Goebel, F. Halzen e D. M. Scott, *Phys. Rev.* **D22** (1980) 2789;
F. Halzen, P. Hoyer e W. Y. Stirling, *Phys. Lett.* **B188** (1987) 375;
- [2] F. Halzen, M. C. Gonzales-Garcia, T. Stelzer e R. A. Vásquez, *Phys. Rev.* **D51** (1995) 4861;
- [3] T. Stelzer e W. F. Long, *Comput. Phys. Commun.* **81** (1994) 357;
- [4] F. Abe et al. (CDF Collaboration), *Phys. Lett.* **75** (1995) 608;
- [5] CTEQ Collaboration, MSU - HEP/41024;
- [6] H. Plathow-Besch, '*PDFLIB: Nucleon, Pion and Photon Parton Density Functions and α_s Calculations*', User's Manual - Version 6.06, W5051 PDFLIB, 1995.03.15, CERN-PPE;

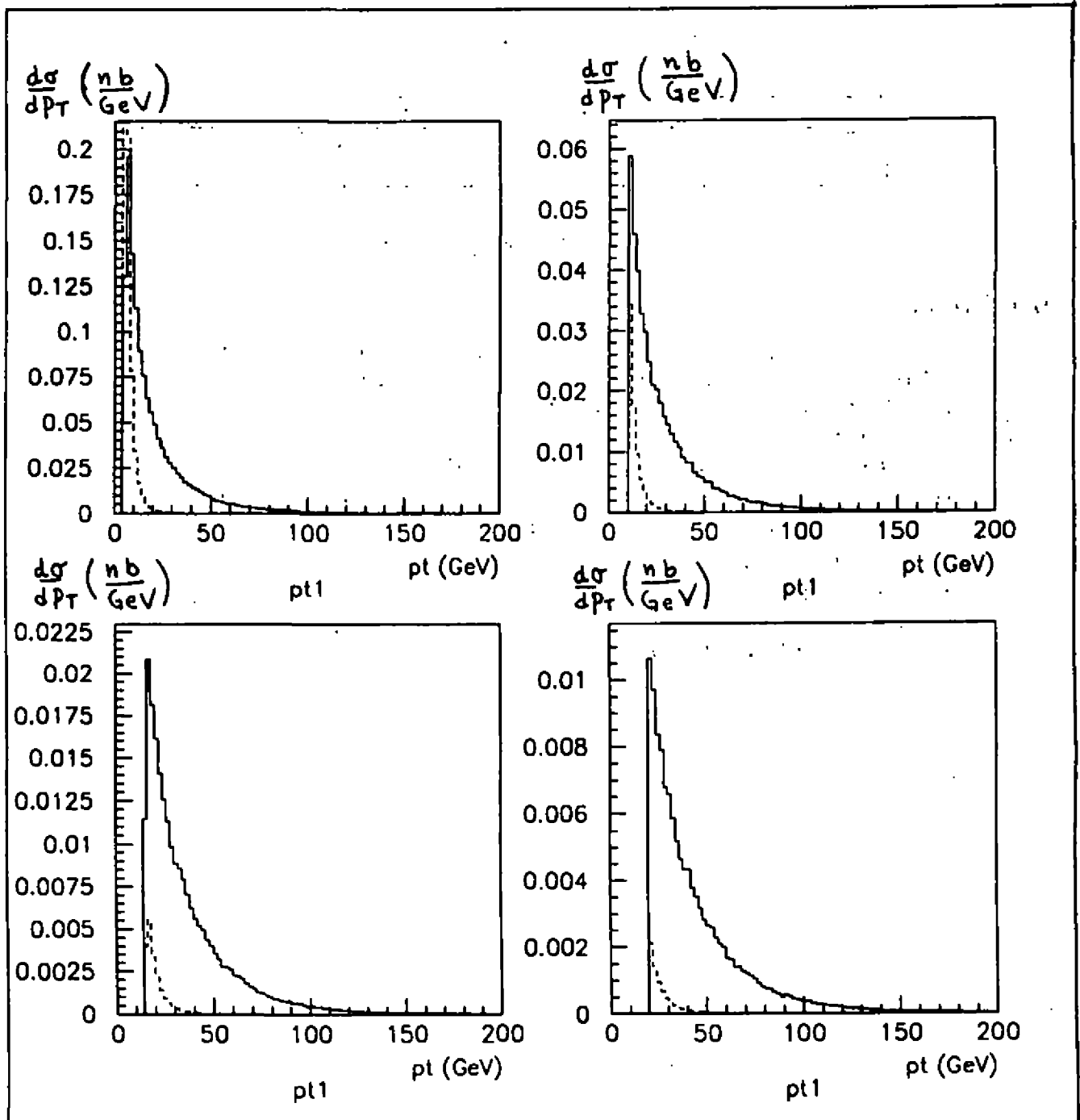


Figure 2.: As distribuições em p_T para o processo $W + 2$ jatos. A linha cheia indica a contribuição usual da QCD e a tracejada as interações múltiplas.

LOOKING FOR INVISIBLY DECAYING HIGGS BOSONS THROUGH THE FINAL STATE $b\bar{b} + \cancel{p}_T$

O. J. P. Éboli^{a,1}, F. de Campos^b, J. Rosiek^c and J. W. F. Valle^b

^aPhysics Department, University of Wisconsin, Madison, WI 53706, USA

^bInstituto de Física Corpuscular - C.S.I.C., Dept. de Física Teòrica, Universitat de València 46100 Burjassot, València, Spain

^cInstitut für Theoretische Physik, Universität Karlsruhe Postfach 6980, 76128 Karlsruhe, Germany

We study the potential of LEP II to unravel the existence of invisibly decaying Higgs bosons through the reaction $e^+e^- \rightarrow b\bar{b} + \cancel{p}_T$. We perform our analyses in a model independent way and our results show that LEP II is capable of discovering such a Higgs for a wide range of masses and couplings.

There are a variety of well motivated extensions of the standard model (SM) with an spontaneously broken global symmetry. This symmetry could be either be lepton number or a combination of family lepton numbers [1, 2]. These models are characterised by a more complex symmetry breaking sector which contain additional Higgs bosons. It is specially interesting for our purposes to consider models where such symmetry is broken at the electroweak scale [3, 4]. In general, these models contain a massless Goldstone boson, called majoron (J), which interacts very weakly with normal matter. In such models, the normal doublet Higgs is expected to have sizeable invisible decay modes to the majoron, due to the strong Higgs majoron coupling. This can have a significant effect on the Higgs phenomenology at LEP II. In particular, the invisible decay could contribute to the signal of two acoplanar jets and missing momentum. This feature of majoron models allows one to strongly constrain the Higgs mass in spite of the occurrence of extra parameters compared to the SM. In particular, the LEP I limit on the predominantly doublet Higgs mass is close to the SM limit irrespective of the decay mode of the Higgs boson [5, 6].

In this work we consider a model containing two Higgs doublets ($\phi_{1,2}$) and a singlet (σ) under the $SU(2)_L \times U(1)_Y$ group. The singlet Higgs field carries a non-vanishing $U(1)_L$ charge,

which could be lepton number. Here we only need to specify the scalar potential of the model:

$$\begin{aligned}
 V = & \mu_i^2 \phi_i^\dagger \phi_i + \mu_\sigma^2 \sigma^\dagger \sigma + \lambda_i (\phi_i^\dagger \phi_i)^2 + \lambda_3 (\sigma^\dagger \sigma)^2 + \\
 & \lambda_{12} (\phi_1^\dagger \phi_1) (\phi_2^\dagger \phi_2) + \lambda_{13} (\phi_1^\dagger \phi_1) (\sigma^\dagger \sigma) + \lambda_{23} (\phi_2^\dagger \phi_2) (\sigma^\dagger \sigma) \\
 & + \delta (\phi_1^\dagger \phi_2) (\phi_2^\dagger \phi_1) + \frac{1}{2} \kappa [(\phi_1^\dagger \phi_2)^2 + h. c.] \quad (1)
 \end{aligned}$$

where the sum over repeated indices $i=1,2$ is assumed.

Minimisation of the above potential leads to the spontaneous $SU(2)_L \times U(1)_Y \times U(1)_L$ symmetry breaking and allows us to identify a total of three massive CP even scalars H_i ($i=1,2,3$), plus a massive pseudoscalar A and the massless majoron J . We assume that at the LEP II energies only three Higgs particles can be produced: the lightest CP-even scalar h , the CP-odd massive scalar A , and the massless majoron J . Notwithstanding, our analyses is also valid for the situation where the Higgs boson A is absent [7], which can be obtained by setting the couplings of this field to zero.

At LEP II, the main production mechanisms of invisible Higgs bosons are the Bjorken process ($e^+e^- \rightarrow hZ$) and the associated production of Higgs bosons pairs ($e^+e^- \rightarrow Ah$), which rely upon the couplings hZZ and hAZ respectively. The important feature of the above model is that, because of its singlet nature, the majoron is not size-ably coupled to the gauge bosons and cannot be produced directly, therefore, thereby evading strong LEP I constraints. The hZZ and hAZ couplings depend on the model parameters via the appropriate mixing angles, but they can be effectively expressed in terms of the two parameters ϵ_A, ϵ_B :

$$\mathcal{L}_{hZZ} = \epsilon_B (\sqrt{2}G_F)^{1/2} M_Z^2 Z_\mu Z^\mu h \quad (2)$$

$$\mathcal{L}_{hAZ} = -\epsilon_A \frac{g}{\cos \theta_W} Z^\mu h \bar{\partial}_\mu A \quad (3)$$

The couplings $\epsilon_{A(B)}$ are model dependent. For instance, the SM Higgs sector has $\epsilon_A = 0$ and $\epsilon_B = 1$, while a majoron model with one doublet and one singlet leads to $\epsilon_A = 0$ and $\epsilon_B^2 \leq 1$.

The signatures of the Bjorken process and the associated production depend upon the allowed decay modes of the Higgs bosons h and A . For Higgs boson masses m_h accessible at LEP II energies the main decay modes for the CP-even state h are $b\bar{b}$ and JJ . We treat the branching fraction B for $h \rightarrow JJ$ as a free parameter. In most models B is basically unconstrained and can vary from 0 to 1. Moreover, we also assume that, as it happens in the simplest models, the branching fraction for $A \rightarrow b\bar{b}$ is nearly one, and the invisible A decay modes $A \rightarrow hJ, A \rightarrow JJJ$ do not exist (although CP-allowed). Therefore our analysis depends finally upon five parameters: $M_h, M_A, \epsilon_A, \epsilon_B$, and B . This parameterisation is quite general and very useful from the experimental point of view: limits on $M_h, M_A, \epsilon_A, \epsilon_B$, and B can be later translated into bounds on the parameter space of many specific models.

The parameters defining our general parametrisation can be constrained by the LEP I data. In fact, Refs. [5, 8] analyse some signals for invisible decaying Higgs bosons, and conclude that LEP I excludes M_h up to 60 GeV provided that $\epsilon_B > 0.4$.

The $\bar{b}b + \cancel{p}_T$ topology is our main subject of investigation and we evaluate carefully signals and backgrounds, choosing the cuts that enhance the signal over the backgrounds. Our goal is

to evaluate the limits on M_h , M_A , ϵ_A , ϵ_B , and B that can be obtained at LEP II from this final state. There are three sources of signal events with the topology $\cancel{p}_T + 2$ b -jets: one due to the associated production and two due to the Bjorken mechanism.

$$e^+e^- \rightarrow (Z \rightarrow b\bar{b}) + (h \rightarrow JJ) \quad (4)$$

$$e^+e^- \rightarrow (Z \rightarrow \nu\bar{\nu}) + (h \rightarrow b\bar{b}) \quad (5)$$

$$e^+e^- \rightarrow (A \rightarrow b\bar{b}) + (h \rightarrow JJ) \quad (6)$$

The signature of this final state is the presence of two jets containing b quarks and missing momentum (\cancel{p}_T). It is interesting to notice that for light M_h and M_A , the associated production dominates over the Bjorken mechanism [8].

There are several sources of background for this topology:

$$e^+e^- \rightarrow Z/\gamma Z/\gamma \rightarrow q\bar{q} \nu\bar{\nu} \quad (7)$$

$$e^+e^- \rightarrow (e^+e^-)\gamma\gamma \rightarrow [e^+e^-]q\bar{q} \quad (8)$$

$$e^+e^- \rightarrow Z^*/\gamma^* \rightarrow q\bar{q}[\nu\gamma] \quad (9)$$

$$e^+e^- \rightarrow W^+W^- \rightarrow q\bar{q}'[\ell]\nu \quad (10)$$

$$e^+e^- \rightarrow W[e]\nu \rightarrow q\bar{q}'[e]\nu \quad (11)$$

$$e^+e^- \rightarrow Z\nu\bar{\nu} \rightarrow q\bar{q} \nu\bar{\nu} \quad (12)$$

where the particles in square brackets escape undetected and the jet originating from the quark q is identified (misidentified) as being a b -jet.

At this point the simplest and most efficient way to improve the signal-over-background ratio is to use that the Higgs bosons A and h decays lead to jets containing b -quarks. So we require that the events contain two b -tagged jets. Moreover, the background can be further reduced requiring a large \cancel{p}_T . Having these facts in mind we impose the following set of cuts, based on the ones used by the DELPHI collaboration for the SM Higgs boson search [9]:

1. Charged multiplicity cut. We require that the event should contain more than 8 charged particles. With this cut we eliminate potential backgrounds from the production of $\tau^+\tau^-$ pairs.
2. Missing momentum cuts. We require:
 - The z component of the missing momentum to be smaller than $0.15 \times \sqrt{s}$.
 - The absolute value of cosine of the polar angle of the missing momentum to be less than 0.9.
 - The transversal component of missing momentum \cancel{p}_T should be bigger than 25 GeV for $\sqrt{s} = 175$ and 190 GeV and 30 GeV for $\sqrt{s} = 205$ GeV.
3. Acolinearity cut. The cosine of the angle between the axes of the two most energetic jets is required to be above -0.8. This is equivalent to the requirement that the angle between the axes is smaller than 145° .

4. Scaled acoplanarity cut. The scaled acoplanarity is computed as the complement of the angle in the perpendicular plane to the beam pipe between the total momenta in the two thrust hemispheres, multiplied by $\min \{ \sin \theta_{jet\ 1}, \sin \theta_{jet\ 2} \}$ in order to remove instability at low polar jet angles [9]. Scaled acoplanarity is required to be greater than 7° .
5. Thrust/number of jets cut. We require the event thrust to be bigger than 0.8. For the intermediate visibly decaying Higgs boson masses in the range 45 – 80 GeV this cut gives relatively small signal efficiency. For this mass range instead of the thrust cut we demand that the two most energetic jets should carry more than 85% of the visible energy.
6. Invariant mass cut. We assume that the visible mass should be in the range $M \pm 10$ GeV, where M is the mass of the visibly decaying particle (Z , h , or A).
7. b -tagging cut. We adopt the efficiencies for the b -tagging directly from the DELPHI note [9]: 68% efficiency for the signal and the appropriate values for the backgrounds extracted from Table 5 of ref. [9].

Depending on the h and A mass ranges, including or excluding the invariant mass cut gives better or weaker limits on the ZhA and ZZh couplings. Therefore, for each mass combination four limits are calculated (with or without invariant mass cut, with thrust cut or the cut on the minimal two-jet energy) and the best limit is kept.

We denote the number of signal events for the three production processes (4 – 6), after imposing all cuts, N_{JJ} , N_{SM} , and N_A respectively, assuming that $\epsilon_A = \epsilon_B = 1$. Then the expected number of signal events when we take into account couplings and branching ratios is

$$N_{exp} = \epsilon_B^2 [BN_{JJ} + (1 - B)N_{SM}] + \epsilon_A^2 BN_A. \quad (13)$$

In general, this topology is dominated by the associated production, provided it is not suppressed by small couplings ϵ_A or phase space. The most important background after the cuts is (7). The total numbers of background events summed over all relevant channels are 2.3, 2.8 and 5.9 for $\sqrt{s} = 175$, 190 and 205 GeV respectively.

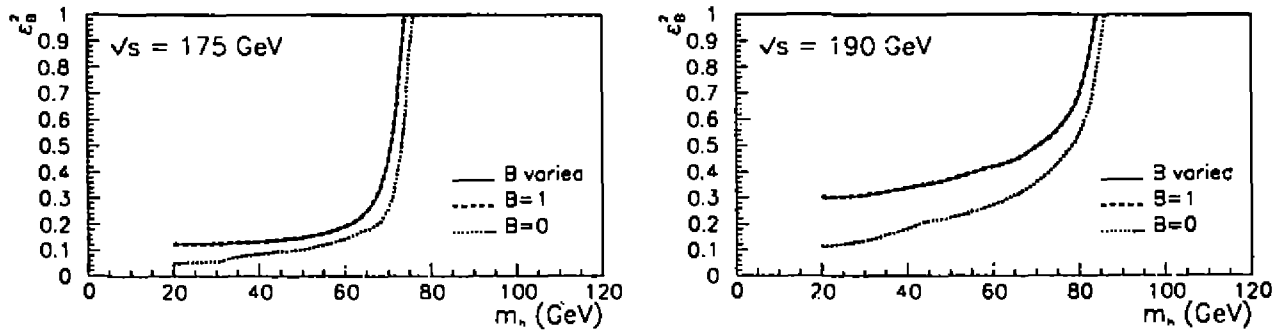


Figure 1: Limits on ϵ_B^2 as a function of M_h for $\sqrt{s} = 175, 190$ GeV and for different values of $B = Br(h \rightarrow JJ)$

In order to obtain the limits shown in Figs. 1-2, we assumed that only the background events are observed, and we evaluated the 95 % CL region of the parameter space that can

be excluded with this result. By taking the weakest bound, as we vary B , we obtained the absolute bounds on ϵ_A and ϵ_B independent of the h decay mode. The limits on ϵ_A obtained by searches for the $b\bar{b} + p_T$ final states are stronger than those given by the $b\bar{b}b\bar{b}$ topology. The bounds on ϵ_B apply directly also for the simplest model of invisibly decaying Higgs bosons, where just one singlet is added to the SM. A more complete presentation of these results will be given in ref. [10].

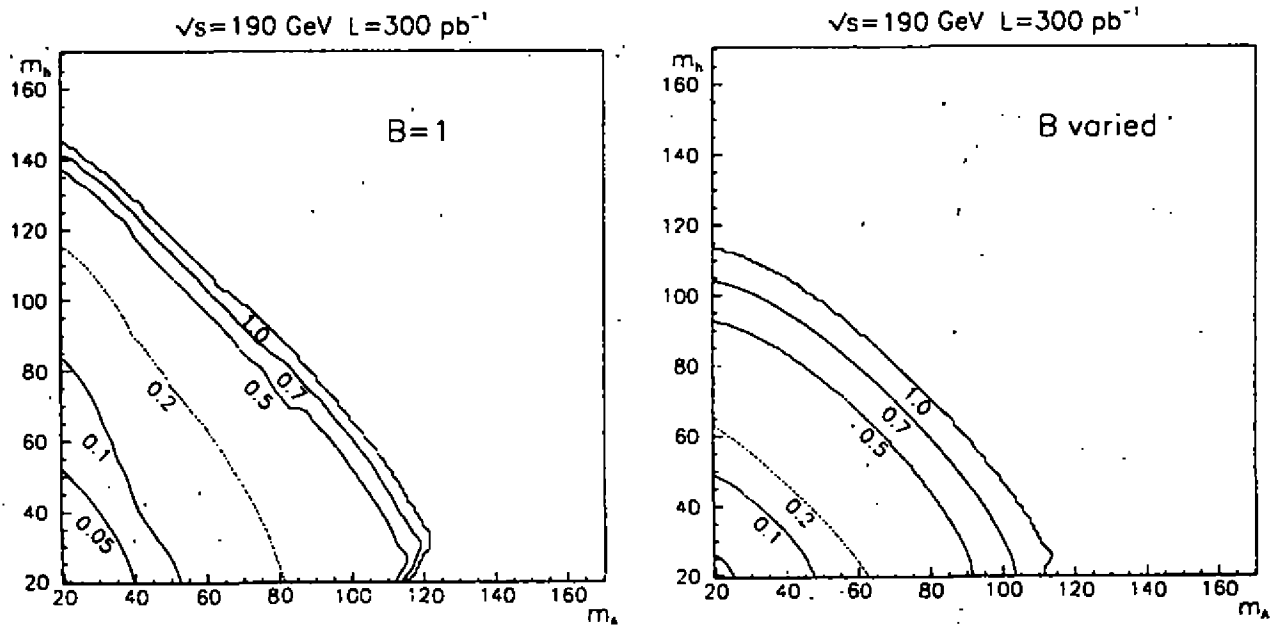


Figure 2: Limits on ϵ_A^2 as a function of M_h, M_A for $\sqrt{s} = 190 \text{ GeV}$. The left plot shows the limits obtained for $B = Br(h \rightarrow JJ) = 1$, in the right plot B is varied from 0 to 1.

ACKNOWLEDGEMENTS

This work was supported by the University of Wisconsin Research Committee with funds granted by the Wisconsin Alumni Research Foundation, by the U.S. Department of Energy under Grant No. DE-FG02-95ER40896, by DGICYT under Grant No. PB92-0084, by Conselho Nacional de Desenvolvimento Científico e Tecnológico (CNPq/Brazil), by Fundação de Amparo à Pesquisa do Estado de São Paulo (FAPESP/Brazil), and by a DGICYT postdoctoral fellowship and the Alexander von Humboldt Stiftung. We thank S. Katsanevas for useful discussions and for bringing the paper of ref. [9] to our attention.

¹ Permanent address: Instituto de Física, Universidade de São Paulo, C.P. 66318, CEP 05389-970 São Paulo, Brazil

References

- [1] Y. Chikashige, R. Mohapatra, R. Peccei, *Phys. Lett.* **98B**, 265 (1980)
- [2] For a review see J. W. F. Valle, *Prog. Part. Nucl. Phys.* **26** (1991) 91 and references therein.
- [3] A. Joshipura and J. W. F. Valle, *Nucl. Phys.* **B397** (1993) 105; A. S. Joshipura, S. Rindani, *Phys. Rev. Lett.* **69**(1992) 3269.
- [4] A. Masiero and J. W. F. Valle, *Phys. Lett.* **B251**, 273 (1990). J. C. Romao, C. A. Santos, and J. W. F. Valle, *Phys. Lett.* **B288**, 311 (1992).
- [5] A. Lopez-Fernandez et al., *Phys. Lett.* **B312** (1993) 240.
- [6] B Brahmachari et al., *Phys. Rev.* **D48** (1993) 4224; ALEPH Collab., *Phys. Lett.* **B313**, 312 (1993); **B313**, 299 (1993).
- [7] O. J. P. Éboli, et al., *Nucl. Phys.* **B421** (1994) 65, F. de Campos et al. Working Group on e^+e^- Collision at 500 GeV: The Physics Potential, edited by P. Zerwas (1993) 55.
- [8] F. de Campos et al., *Phys. Lett.* **B336** (1994) 446.
- [9] DELPHI Collaboration, DELPHI 95-57 PHYS 493.
- [10] O. J. P. Éboli, F. de Campos, J. Rosick, J. W. F. Valle, in preparation.

Hadronic Inelastic Cross Sections from Analyses of the Elastic Channel*

P.C. Beggio, A.F. Martini and M.J. Menon

Instituto de Física 'Gleb Wataghin'

Universidade Estadual de Campinas - Unicamp

13083-970 Campinas, São Paulo, Brasil

We present a comparative analysis of the Inelastic Overlap Functions predicted by three models for elastic scattering: Chou and Yang, Henzi and Valin and Martini and Menon. The results are also compared with two model independent extractions (Amaldi-Schubert and Carvalho-Menon). We then calculate the predictions for the corresponding integrated inelastic cross-sections from the three models and compare the results with the experimental data on pp and $p\bar{p}$ scattering available above 10 GeV. Similarities and differences between all models predictions are presented and discussed.

1 - Introduction

The main physical observable in elastic hadron scattering is the differential cross-section

$$\frac{d\sigma}{dq^2} = \pi |F(s, q)|^2. \quad (1)$$

The elastic scattering amplitude, $F(s, q)$, in the impact parameter representation defines the Profile Function $\Gamma(b, s)$:

$$F(s, q) = i \int_0^\infty b db J_0(qb) \Gamma(s, b) \quad (2)$$

and in the eikonal formalism the profile function $\Gamma(b, s)$ is expressed in terms of the eikonal function $\chi(s, b)$ by [1]

$$\Gamma(s, b) = 1 - \exp[i\chi(s, b)]. \quad (3)$$

Elastic scattering is usually investigated through different models for the eikonal.

On the other hand, unitarity of the S-matrix in the impact parameter space connects $\Gamma(b, s)$ with the Inelastic Overlap Function $G_{in}(b, s)$ [2]

$$2\text{Re}\Gamma(s, b) = |\Gamma(s, b)|^2 + G_{in}(s, b) \quad (4)$$

Integration of $G_{in}(s, b)$ over the impact parameter determines the inelastic cross section as function of the energy

$$\sigma_{in}(s) = \int b db G_{in}(b, s). \quad (5)$$

With this framework, starting from analysis of the elastic data, the inelastic channel may be investigated through $G_{in}(b, s)$ and $\sigma_{in}(s)$.

In this communication, as first step for further analysis, we calculate $G_{in}(b, s)$ from three phenomenological models for elastic hadron scattering: a geometrical model by Chou and Yang (CY) [3], a dispersive diffraction model by Henzi and Valin (HV) [4] and a multiple diffraction model by Martini and Menon (MM) [5]. The results are compared with two model independent analyses of the elastic scattering (fits to differential cross section data): parametrization by Amaldi and Schubert [6] and by Carvalho and Menon [7]. From $G_{in}(b, s)$ we calculate $\sigma_{in}(s)$

*Financial Support: Capes and CNPq

for the three models and compare the results with the experimental data on pp and $\bar{p}ppp$ scattering available above 10 GeV. In section 2 we review the essential formulae in the three models and in section 3 the model independent parametrizations for the scattering amplitude. The results for $G_{in}(b, s)$ and $\sigma_{in}(s)$ are presented and discussed in section 4.

2 - Phenomenological models

We are interested in three models for the elastic channel, developed from the analysis of the differential cross section data, eq.(1). Two of them are eikonal models and one introduces a direct parametrization for $G_{in}(b, s)$ (dispersive diffraction model).

2.1 - Eikonal Models

In first order Multiple Diffraction Formalism (Glauber) the eikonal is expressed by [1,8]

$$\chi(s, b) = \int_0^\infty q dq J_0(qb) G_A G_B f, \quad (6)$$

where $G_{A,B}$ are the hadronic form factors and f the averaged elementary (parton-parton) amplitude. Models are distinguished by different parametrizations for these quantities and we are interested in the following cases.

2.1.1 - Chou-Yang Model

This model is characterized by the choices [3]

$$G_A = G_B = \frac{1}{[1 + (\frac{q^2}{m^2})]^2}, \quad f(s) = iC(s), \quad (7)$$

with m^2 and C are free parameters. The real part of the scattering amplitude is introduced by the Martin prescription. In reference [3], analysis of pp scattering at 23.5 GeV and $\bar{p}ppp$ at 546 GeV leads to the determinations of m^2 and C . Following the authors we parametrized these quantities by

$$C(s) = 2.193 + 1.238[\ln(s)] \quad (GeV^{-2}), \quad \frac{1}{m^2} = 0.837 + 0.072[\ln(s)] \quad (GeV^{-2}). \quad (8)$$

2.1.2 - Martini-Menon Model

In this case the choices are [5]

$$G_A = G_B = \frac{1}{(1 + \frac{q^2}{\alpha^2})(1 + \frac{q^2}{\beta^2})}, \quad f(s, q) = \text{Re}f(s, q) + i \text{Im}f(s, q), \quad (9)$$

$$\text{Im}f(s, q) = C(s) \frac{[1 - (q^2/a^2)]}{[1 + (q^2/a^2)^2]}, \quad \text{Re}f(s, q) = \lambda(s) \text{Im}f(s, q), \quad (10)$$

with α^2 , β^2 , a^2 , C , λ free parameters. Through fits to pp elastic scattering data the following values and dependences with the energy was obtained [5]

$$a^2 = 8.20 \text{ GeV}^2, \quad \beta^2 = 1.80 \text{ GeV}^2$$

$$C(s) = 14.26 - 1.65[\ln(s)] + 0.159[\ln(s)]^2 \quad (GeV^{-2}), \quad (11)$$

$$\frac{1}{\alpha^2} = 2.57 - 0.217[\ln(s)] + 0.0243[\ln(s)]^2 \quad (GeV^{-2}). \quad (12)$$

$$\lambda(s) = \frac{0.0695[\ln(s/s_0)]}{1 + 0.118[\ln(s/s_0)] + 0.015[\ln(s/s_0)]^2}, \quad (13)$$

where $s_0 = 400 \text{ GeV}$.

In these two models the eikonal $\chi(s, b)$ is calculated from eq.(6) and then $\Gamma(s, b)$, $G_{in}(s, b)$ and $\sigma_{in}(s)$ through eqs. (3), (4) and (5), respectively. Due to its small contribution, the real part of the scattering amplitude was not taken into account in the calculations.

2.2 - Dispersive Diffraction Model

In this approach by Ilenzi and Valin, elastic differential cross section is fitted through a suitable parametrization for the inelastic overlap function. Analyses of pp data at ISR and $\bar{p}ppp$ at Collider energies lead to the following result [4]

$$G_{in}(s, b) = \frac{0.908 + 0.027 \ln^2(s/s_0)}{1 + 0.027 \ln^2(s/s_0)} \exp(-b^2/4B) (1 + \delta_2 \zeta + \frac{1}{4} \delta_2 \zeta^2) \quad (14)$$

$$\delta_2 = 0.115 + 0.000094 [\ln^2(s/s_0)], \quad \zeta = (4.24b^2/4B) \exp(-1.56b^2/4B) \quad (15)$$

$$B = 6.64 + 0.044 [\ln(s/s_0)]^2, \quad GeV^{-2} \quad (16)$$

and $s_0 = 100 GeV^2$. Integration over the impact parameter determines $\sigma_{in}(s)$, eq.(5).

III - Model independent analyses

Starting from parametrizations for $F_1(s, q)$ and fits to the differential cross section data, eq. (1), the inelastic overlap function may be extracted in a model independent way through eqs. (3) and (4). In order to discuss the model predictions for $G_{in}(s, b)$ we make use of two different parametrizations:

3.1 - Amaldi and Schubert (AS)

Elastic pp scattering data between 23.5 GeV and 62.5 GeV are well described by [6]

$$F(s, q) = i\alpha [A_1 \exp(-\frac{1}{2} b_1 \alpha q^2) + A_2 \exp(-\frac{1}{2} b_2 \alpha q^2)] - iA_3 \exp(-\frac{1}{2} b_3 q^2) \quad (17)$$

$$\alpha = \alpha(s) = \frac{\sigma_{tot}(s)}{\sigma_{tot}(23GeV)} [1 - i\rho(s)] \quad (18)$$

where $A_i, b_i, i=1,2,3$ are fixed free parameters and $\rho(s)$ is the ratio the forward real and imaginary parts of the scattering amplitude.

3.2 - Carvalho and Menon (CM)

Similar description of pp elastic scattering between 13.8 and 62.5 GeV has been also achieved with the parametrization [7]

$$F(s, q) = i \sum_{j=1}^2 \alpha_j (1 + i\mu) \exp(-\beta_j q^2) + i \sum_{j=3}^n \alpha_j \exp(-\beta_j q^2), \quad \mu(s) = -\frac{\rho(s) \sum_j \alpha_j}{\alpha_1 + \alpha_2} \quad (19)$$

where $\alpha_i, \beta_i, i=1..n$ are free parameters depending on the energy.

The results for $G_{in}(s, b)$ are presented and discussed in the next section. Error propagation from the free parameters was taken into account in the CM analysis, but not in the AS case.

4 - Results and Conclusions

As explained, we calculated the predictions for $G_{in}(s, b)$ from the two eikonal models (CY and MM) and from two model independent analyses (AS and CM). All these results are here compared with the predictions of the HV model. We limited the calculation to pp scattering in the ISR interval, 23.5 GeV and 62.5 GeV. The results are displayed in Figs. 1 and 2 up to 0.5 fm and 3.0 fm, respectively. We then integrate $G_{in}(s, b)$ over the impact

parameter space obtaining $\sigma_{in}(s)$, eq.(5), for the three phenomenological models. The results are shown in Fig.3 with the experimental data on pp and $\bar{p}ppp$ scattering at ISR, Collider and Tevatron energies.

From Figs.1 and 2 we observe a general agreement of all results for $G_{in}(s, b)$ with the exception of the CY predictions at 62.5 GeV and small values of the impact parameter (≤ 1.0 fm). Figure 3 shows that the CY model does not reproduce any experimental data, but are in agreement with some overall average behaviour of all pp and $\bar{p}ppp$ experimental data. Obviously this approach does not take account of the differences between pp and $\bar{p}ppp$ scattering observed in the ISR region. The HV model reproduces the pp data at ISR and $\bar{p}ppp$ data at Collider and Tevatron energies. This was in fact the strategy in the original analysis [4]. The MM model treat only pp data and the description of the experimental data is satisfactory. We observe that the predictions for this reaction at Collider and Tevatron energies are above the values of the experimental data on $\bar{p}ppp$ scattering.

References

1. R.J. Glauber, Lectures in Theoretical Physics: Vol.I, Ed. W.E. Britten et al. (Interscience, New York, 1959) p.315; W. Czyz and L. C. Maximon, Ann. Phys. **52** (1969) 59.
2. U. Amaldi, M. Jacob, G. Matthiae, Ann. Rev. Nucl. Sci **26** (1976) 385.
3. T.T. Chou, C.N. Yang, Phys. Rev. Lett. **B224** (1990) 113.
4. R. Henzi and P. Valin, Phys. Lett, **B160** (1985) 167.
5. A. F. Martini and M. M. Menon, "Phenomenological Approach to Elastic Proton-Proton Scattering above 10 GeV", XVI Brazilian National Meeting on Particle and Fields (to be published); preprint IFGW Abstracta CO19-96.
6. U. Amaldi and K.R. Schubert, Nucl. Phys. **B166** (1980) 301.
7. P.A.S. Carvalho and M.J. Menon, "Model Independent Analysis of Proton-Proton Elastic Scattering" these proceedings.
8. V. Franco and K. K. Varma, Phys. Rev. **C18** (1978) 349; M.J. Menon, Phys. Rev. **D48** (1993) 2007.

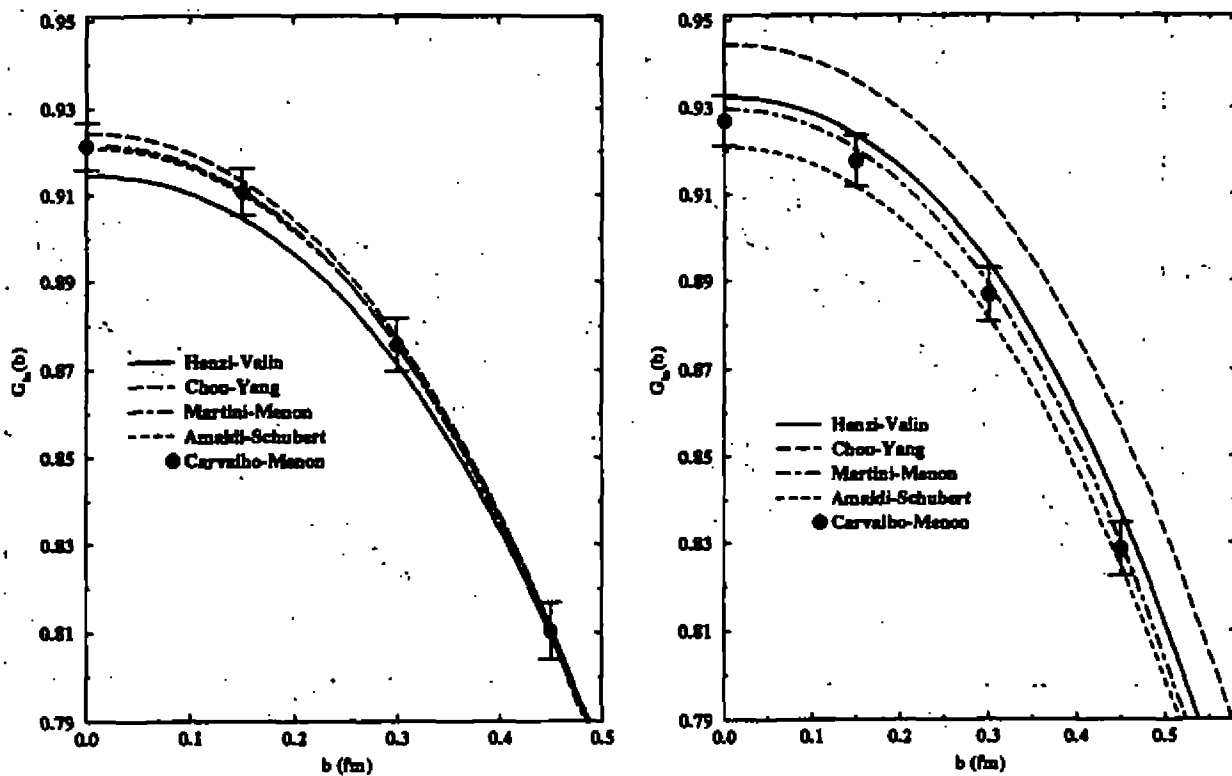


Figure 1 - Results for $G_{in}(s, b)$ (in the central collision region) for pp scattering at 23.5 GeV (left) and 62.5 GeV (right).

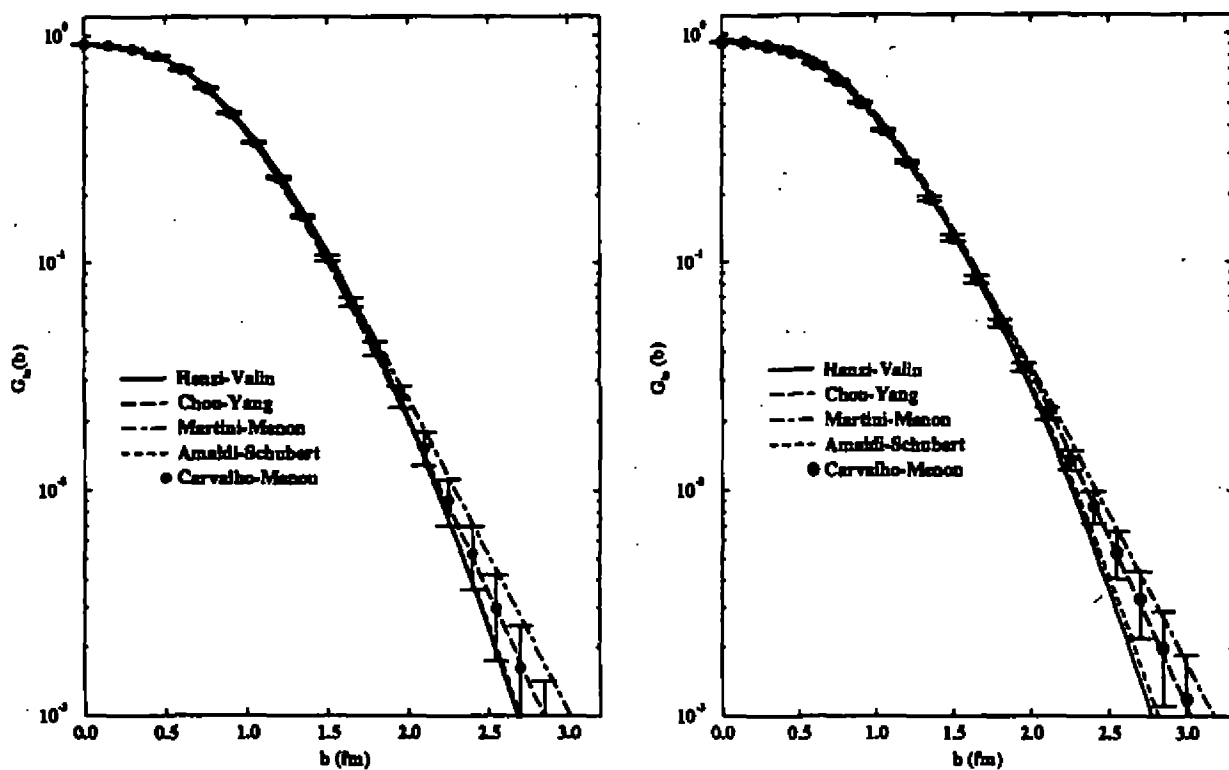


Figure 2 - Results for $G_{in}(s, b)$ for pp scattering at 23.5 GeV (left) and 62.5 GeV (right).

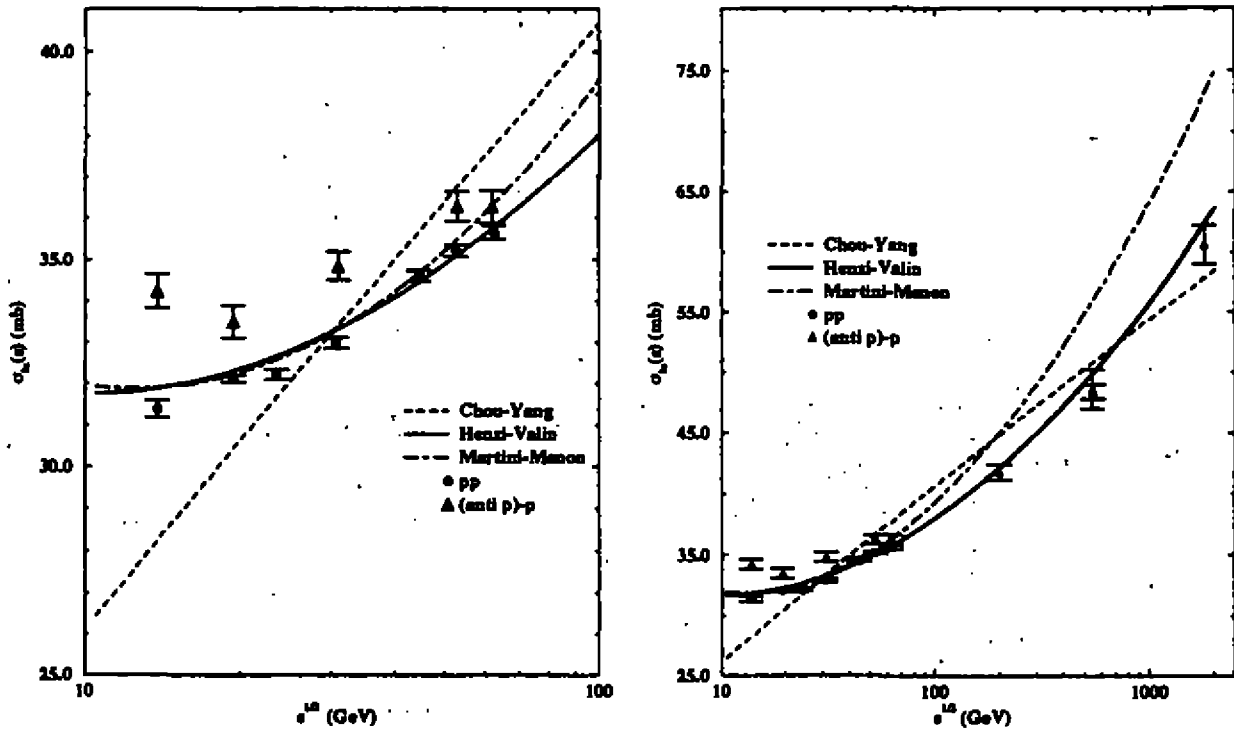


Figure 3 - Inelastic cross section predicted by CY, HV and MM models and experimental data.

The Importance of Thermal Fluctuations During the Electroweak Phase Transition*

Rudnei O. Ramos†

*Universidade do Estado do Rio de Janeiro,
Instituto de Física - Departamento de Física Teórica,
20550-013 Rio de Janeiro, RJ, Brazil*

The electroweak phase transition has been intensively studied in recent years. The possibility of generating the baryon asymmetry of the Universe during the electroweak phase transition has been the main motivation for the interest of understanding the dynamics of the phase transition. Among other things, today we learned that the phase transition is possibly too weak first order for acceptable values of the Higgs masses, within the minimal standard electroweak model. We study [1] the implications of this weak first order phase transition, in particular the rôle of thermal fluctuations to the dynamics of the phase transition. Our results show that, in the minimal standard electroweak model, for realistic higgs masses, $m_H \gtrsim 60 \text{ GeV}$, the phase transition can be completed by the percolation of the true vacuum, induced by the presence of subcritical fluctuations, ruling out the possibility of baryogenesis in the model.

Here, we further investigate [2, 3] the possible consequences of having a weak first order phase transition at the electroweak scale. Although we will restrict our analysis to the standard electroweak model, our results can be adapted to any of its extensions. In fact, we will show that the strength of the transition can be used as a new constraint on the parameters of the model, always a welcome addition to the often large parameter space of extensions to the minimal standard model.

We will model large amplitude thermal fluctuations by Gaussian-shaped bubbles of approximately correlation volume. Previous results based on a kinetic approach, have indicated that such fluctuations can destroy the first-order character of the transition for Higgs masses of order $m_H \gtrsim 55 \text{ GeV}$ [4, 2]. Here we complement this calculation by computing in detail the nucleation rate for such configurations. As these configurations are not solutions to the Euclidean equations of motion, we must treat with care the evaluation of the nucleation rate. Within reasonable approximations, we will be able to obtain the equilibrium number density of these configurations as a function of the tree-level Higgs mass, to show how the weakness of the transition is closely related to the breakdown of the dilute gas approximation.

Following the work of Ref. [3], large amplitude fluctuations describing thermal fluctuations are parameterized as:

$$\varphi_{sc}(r) = \varphi_A(T) \exp\left(-\frac{r^2}{R^2(T)}\right). \quad (1)$$

where $\varphi_{sc}(r)$ describes (spherically symmetric) fluctuations in the scalar field, with amplitude φ_A and radius given by $R(T)$. Here we adopt for R the correlation length, given by the inverse of the temperature dependent mass for the higgs effective mass, appearing in the effective action for the higgs boson field. For φ_A we take the temperature dependent true vacuum value, obtained from the effective potential for the higgs boson field. Has discussed in [1], these are the most natural choices for R and φ_A .

Let us define in the Electroweak model the partition function

*Work partially supported by CNPq
†E-mail address: rudnei@vmesa.uerj.br

$$Z = \int D\phi D\chi_i e^{-\int_0^\beta d\tau \int d^3x \mathcal{L}_{\text{Euc.}}(\phi, \chi_i)}, \quad (2)$$

where χ_i denotes gauge and fermions fields (and ghost fields) and ϕ is the SU(2) doublet

$$\phi = \frac{1}{\sqrt{2}} \begin{pmatrix} \phi_1 + i\phi_2 \\ \phi_3 + i\phi_4 \end{pmatrix}, \quad (3)$$

where ϕ_i ($i = 1, \dots, 4$) are real scalar fields. The tree level potential for the complex scalar field ϕ , given by

$$V_0(|\phi|) = -\mu^2 \phi^\dagger \phi + \lambda (\phi^\dagger \phi)^2, \quad (4)$$

for $\mu^2 > 0$, ϕ acquires a nonvanishing vacuum expectation value $\langle |\phi| \rangle = \sigma$, which one assumes real and along, for example, the real component ϕ_3 of ϕ . Thus, in the broken phase, we define $\phi'_3 = \phi_3 + \sigma$ and ϕ_1, ϕ_2 and ϕ_4 are the three Goldstone bosons.

Let us denote by g_i the coupling of the field ϕ with the χ_i fields. If $\lambda \ll g_i^2$, i.e., the interactions among the ϕ field are weak compared with the $\phi - \chi_i$ interactions, then we may formally integrate out the χ fields in (2) to obtain

$$Z = \int D\phi e^{-W(\phi)}, \quad (5)$$

where

$$W(\phi) = -\ln \int D\chi_i e^{-\int_0^\beta d\tau \int d^3x \mathcal{L}_{\text{Euc.}}(\phi, \chi_i)}. \quad (6)$$

For vector fields, the integration measure above includes the gauge fixing and ghost terms. We choose to work in the Landau gauge, which is the one usually used in the studies of the electroweak phase transition. Expanding $W(\phi)$ in a derivative expansion,

$$W(\phi) = \int_0^\beta d\tau \int d^3x \left[V_0(|\phi|) + V_\beta(|\phi|) + \hat{Z}(|\phi|) (\partial_\mu \phi)^\dagger (\partial^\mu \phi) + \dots \right], \quad (7)$$

where $V_0(|\phi|)$ is the tree level potential (4) and $V_\beta(|\phi|)$ is the contribution of the χ_i loops, coming from the integration over the χ_i fields in (2), with the scalar field ϕ in the external legs. $\hat{Z}(|\phi|)$ is the wave-function renormalization factor.

One important approximation that can be take to the above expression, as it has been shown in [1], is that, for the range of temperatures we will be interested in, we can neglect the wave function term and take $V_\beta(|\phi|)$ as the usual expression for 1-loop finite temperature effective potential, as for example given by [5]. We can now substitute in (7) the expression for φ_{sc} , Eq. (1), obtaining the usual expression for the free energy of subcritical fluctuations. However, in order to obtain the nucleation rate for these fluctuations, we need to take into account the fluctuations around the higgs field, not considered yet in (7).

In [1], we show that the equilibrium number of thermal fluctuations in the system can be obtained in terms of the nucleation rate by:

$$N_{\text{sc}} \sim \Gamma \frac{2\pi}{\omega_-} \sim \ln \frac{Z(\varphi_{\text{sc}})}{Z(\varphi_v)}, \quad (8)$$

where Γ is the transition rate given by $\Gamma \simeq \frac{\omega_-}{\pi} \text{Im} \frac{Z(\varphi_c)}{Z(\varphi_v)}$ and ω_- is the negative eigenvalue. $\frac{Z(\varphi_{\text{sc}})}{Z(\varphi_v)}$ is the partition function ratio of the system computed by expanding the scalar field ϕ around the field (vacuum) configuration φ_{sc} (φ_v).

In [1], we obtain the full expression for the equilibrium number density $n_{\text{sc}} (\equiv N_{\text{sc}}/V$, where V is the system volume) for subcritical fluctuations modeled by (1). The volume fraction V_{sc}/V , given by $\frac{4\pi R^3}{3} n_{\text{sc}} V$, evaluated at the critical temperature (when the minimum of the effective potential are degenerate) plotted in terms of the higgs boson mass m_H , shows that for higgs masses $m_H \gtrsim 60 \text{ GeV}$ the volume fraction occupied by the true vacuum

fluctuations is high enough ($V_{\text{sc}}/V \gtrsim 0.3$) to complete the phase transition by just percolation of the true vacuum phase [1]. The main consequences of this is the impossibility of baryogenesis in the minimal standard model, since we do not have nucleation of critical bubbles and not enough departure from thermal equilibrium.

References

- [1] R. O. Ramos, *Phys. Rev. D* (in press, 15 October 1996)
- [2] M. Gleiser and E. W. Kolb, *Phys. Rev. Lett.* **69**, 1304 (1992);
- [3] M. Gleiser, E. W. Kolb and R. Watkins, *Nucl. Phys.* **B364**, 411 (1991);
- [4] G. Gelmini and M. Gleiser, *Nucl. Phys.* **B419**, 129 (1994);
- [5] G. W. Anderson and L. J. Hall, *Phys. Rev.* **D45**, 2685 (1992);

Produção de Pares do Top com um Gluon Extra no Tevatron

V. Barger

Physics Department, University of Wisconsin, Madison, WI 53706, USA.

P. G. Mercadante

Instituto de Física, Universidade de São Paulo.

Caixa Postal 66318, CEP 05389-970 São Paulo, Brazil

R. J. N. Phillips

Rutherford Appleton Laboratory, Chilton, Didcot, Oxon OX11 0QX, UK

Calculamos a produção e decaimento de pares do quark top no Tevatron, com a emissão de um gluon extra. Estudamos o sinal correspondente, de $W + 5$ jatos, incluindo as correlações de spin nos decaimentos leptônico $W \rightarrow l\nu$ e hadrônico $W \rightarrow jj$. Este sinal apresenta aspectos interessantes, devido a possibilidade do gluon ser irradiado em qualquer etapa do processo, apresentando características diferentes de acordo com a fase em que ele foi emitido (antes ou depois da produção do quark top). Estudamos a possibilidade da reconstrução dos eventos considerando que um dos quarks b será identificado como tal (b-tag) e incluindo uma resolução de energia realística para os detectores. Nosso procedimento básico, baseado apenas na cinemática, apresentou 74% de eficiência sendo que, destes, 74% foram corretamente classificados (pureza). Considerando uma dupla identificação dos quarks b, estes percentuais sobem para 82% e 77%. Também apresentamos uma sugestão de refinamento baseada num critério de virtualidade em que tiramos proveito do fato do gluon ter maior possibilidade de ser irradiado próximo à partícula que o emitiu. Este novo procedimento de reconstrução apresentou uma maior pureza às custas de um menor grau de reconstrução de eventos.

1 Introdução

Recentemente o Quark Top foi detectado no Fermilab pela colaboração CDF [1]. A colaboração D0 [2] também detectou eventos confirmando a existência do Top. A principal característica do Quark Top é a sua grande massa, $176 \pm 8 \text{ GeV}$ (CDF), $199 \pm 19 \text{ GeV}$ (D0), levando a uma pequena vida média; como consequência o top decai antes do processo de hadronização ocorrer. O Top decai, portanto, através da interação eletro-fraca em um W e um Bottom.

Podemos estudar o Top como um Lepton pesado após a sua produção, uma vez que seu decaimento é puramente eletro-fraco. No entanto as correções de QCD para a produção do top são bastante grande. Para um top de 174 GeV temos, na ordem mais baixa em QCD (α_s^2)

$$\sigma_{TOT}(p\bar{p} \rightarrow bW^+\bar{b}W^- + X) = 3.8 \text{ Pb} \quad (1)$$

Na próxima ordem em QCD (α_s^3) a seção de choque de produção é

$$\sigma_{NLO}(p\bar{p} \rightarrow t\bar{t} + X) = 4.9 \text{ Pb} \quad (2)$$

onde vemos um acréscimo de mais de 25% (note que o cálculo para a correção radiativa é apenas para a produção do Top. Em primeira ordem tanto faz, pois o Top decai 100% das vezes em Wb , mas no cálculo da correção radiativa não estamos considerando emissões de gluons após o decaimento).

Nossa proposta é estudar o processo de ordem α_s^3 em nível de árvore quando teremos a emissão de um gluon real.

$$q\bar{q} \rightarrow (bW^+)(\bar{b}W^-)g \quad (3)$$

em que o gluon pode ser emitido dos quarks incidentes, dos Top produzidos, ou dos quarks b após o decaimento do Top. Este processo leva a um sinal com um jato extra.

2 Produção do Top com um Gluon Extra

O processo (3) foi estudado anteriormente [3] utilizando MADGRAPH [4] para a geração das amplitudes de helicidade. Para fazermos uma simulação mais realística iremos decair os Ws. Aproveitaremos o fato de MADGRAPH nos gerar as amplitudes de helicidade para fazermos o decaimento dos Ws conservando as relações de spin [5]. Utilizaremos a aproximação de largura zero para o decaimento dos Ws e não levaremos em consideração a radiação de gluons proveniente do decaimento hadrônico do W, uma vez que o W será identificado como um par de jatos com massa invariante M_W .

Fizemos a simulação de eventos para o caso em que um dos Ws decai leptonicamente e o outro hadronicamente, utilizando os seguintes cortes.

$$\begin{aligned} p_T(\ell) &> 20 \text{ GeV} & |\eta(\ell)| &< 2.5 \\ p_T(j) &> 10 \text{ GeV} & |\eta(j)| &< 2.5 \\ \Delta R(\ell, j) &> 0.4 & \Delta R(jj) &> 0.4 \\ \cancel{p}_T &> 25 \text{ GeV} \end{aligned} \quad (4)$$

onde ℓ se refere ao lepton (μ ou e) e j a qualquer dos cinco jatos. Temos a pseudorapidez dada por $\eta = \ln \tan(\theta/2)$. $(\Delta R)^2 = (\Delta\eta)^2 + (\Delta\phi)^2$ mede a separação angular, e θ, ϕ são os ângulos polar e azimutal em relação ao eixo dos feixes iniciais.

Incluimos também o efeito da resolução de energia dos detectores. O calorímetro mede a energia do feixe com uma certa resolução, a partir desta energia é que todo o quadri-momento do feixe é inferido. Fizemos uma simulação gerando uma distribuição gaussiana com largura dada pela resolução do detector.

$$\Delta E/E = 0.15/\sqrt{E/\text{GeV}} \quad (\text{para leptons}), \quad (5)$$

$$\Delta E/E = 0.8/\sqrt{E/\text{GeV}} \quad (\text{para quarks}), \quad (6)$$

A energia de cada partícula será gerada de forma a obedecer uma distribuição gaussiana com média no valor dado pelo espaço de fase e largura dada por ΔE . A partir desta energia reconstruímos o quadri-momento de forma que consideramos que a imprecisão no quadri-momento é devida apenas à resolução de energia (não estamos considerando possíveis desvios devido a incerteza na posição do calorímetro).

3 Reconstrução dos Eventos

Para fazermos a análise do sinal $(W \rightarrow l\nu) + 5$ jatos precisamos estabelecer alguns critérios para a identificação dos jatos. Nós consideramos que um dos jatos b será identificado (b tagg) [1] [2]. Os jatos decorrentes do decaimento dos Ws serão identificados por sua massa invariante. Temos assim três jatos identificados. Identificamos agora o gluon como sendo o jato de menor p_T , uma vez que os gluons tendem a sair com baixo p_T devido a divergências no infravermelho. Já o b tende a sair com um alto p_T , devido a um pico jacobiano em $p_T \simeq (m_t^2 - M_W^2)/(2m_t) \simeq 70 \text{ GeV}$ no referencial de repouso do top. O quadri-momento do neutrino pode ser reconstruído identificando $\cancel{p}_T = p_T(\nu)$ e impondo que a massa invariante do par $e\nu = M_W$, levando a duas soluções para o momento longitudinal do neutrino. Temos doze configurações diferentes de sinal $(W \rightarrow l\nu) + 5$ jatos que podem ser interpretadas como a produção de pares do Top (com seu subsequente decaimento) mais um gluon irradiado. Temos três possíveis classes

em que o evento pode ser caracterizado dependendo de onde que o gluon foi irradiado:

$$\text{Classe A: } g(t - W_{jj}b)(t - W_{\nu b}), \quad (7)$$

$$\text{Classe B: } (t - W_{jj}b)(t - W_{\nu bg}), \quad (8)$$

$$\text{Classe C: } (t - W_{jjbg})(t - W_{\nu b}). \quad (9)$$

Em cada classe temos quatro reconstruções diferentes para a massa do top, correspondendo a duas soluções para o neutrino e a duas formas de combinar os quarks b com os Ws. Avaliamos as massas invariantes dos candidatos ao quark top, m_1, m_2 e atribuímos um valor F que seria uma medida de quão perto esta massa estaria do quark top. $F = (m_1 - m_t)^2 + (m_2 - m_t)^2$ (assumimos que a massa do top será bem conhecida a partir do sinal $W + 4$ jatos). A configuração que der o menor valor para F é considerada a melhor configuração. A escolha do menor valor de F nos determina a classe a que ele pertence, assim como a identificação do b e do \bar{b} . Consideramos apenas eventos que tenham $F_{\min} < 500 \text{ GeV}^2$ para eliminar reconstruções erradas.

Este procedimento se mostra bastante satisfatório quando não estamos simulando a resolução de energia dos detectores. Neste caso os quarks oriundos do decaimento do W são sempre corretamente identificados enquanto que o gluon, em 85% dos casos, tem menor p_T do que o b. O teste de aceitação, $F_{\min} < 500 \text{ GeV}^2$, se encarrega de eliminar grande parte dos eventos onde o gluon não é corretamente identificado. Nossa estratégia reconstrói os eventos nas classes corretas em mais de 95% dos casos que passam pela aceitação. Quando simulamos a resolução de energia, no entanto, muitas vezes um par de jatos que não foi oriundo do decaimento do W reconstrói melhor a massa do W sendo que em um grande número de casos um destes jatos é justamente o gluon. Temos, assim, mais uma fonte de identificação errônea para os jatos. Os resultados de nossa estratégia podem ser visto na tabela 1.

Observa-se que 55% dos eventos que passaram nos cortes são reconstruídos corretamente nas classes A, B e C, enquanto que 19% são reconstruídos incorretamente e 26% não passam no teste da aceitação. Vemos ainda que dos eventos que reconstruímos como classe A, 83% estão corretamente reconstruídos, enquanto que na classe B (C), apenas 61% (65%).

Apresentamos alguns gráficos mostrando o comportamento dos gluons reconstruídos nas diferentes classes. Para efeito de comparação, apresentamos o comportamento do gluon corretamente identificado sem a simulação da resolução do calorímetro. Na Figura 1 mostramos a distribuição em P_T nas classes A e B (a classe C apresenta um comportamento similar à classe B). Notamos que na classe A temos um excesso de gluons reconstruídos com baixo P_T enquanto que a classe B apresenta o comportamento oposto. Isto ocorre porque, para um gluon com o quadri-momento pequeno, podemos reconstruí-lo facilmente na classe errada, uma vez que inclui-lo ou não na reconstrução do quadri-momento do Top não fará muita diferença. Como temos mais eventos na classe A temos mais gluons de pequeno momento sendo reconstruídos erroneamente nas classes B e C do que na direção oposta.

Table 1: Eventos reconstruídos após aplicação do teste de aceitação .

Classe Verdadeira	Porcentagem nas Classes reconstruídas					
	A	B	C	Fail		
A	59.7	⇒	32.5	4.8	4.5	17.9
B	20.2	⇒	4.1	9.9	2.0	4.2
C	20.1	⇒	2.5	1.6	12.1	3.9

Na Figura 2 temos a separação (ΔR) do gluon com o b correspondente para classes B e C. Esta curva mostra grande discordância entre os eventos reconstruídos por nós e a situação ideal, onde todos os eventos são corretamente reconstruídos. Poderíamos esperar este comportamento, lembrando que temos apenas apenas 59% (67%) dos eventos reconstruídos corretamente nas classes B (C). A curva de ΔR se mostra extremamente sensível a uma reconstrução na classe errada, uma vez que um gluon irradiado do beam-pipe (por exemplo) não está necessariamente próximo ao b.

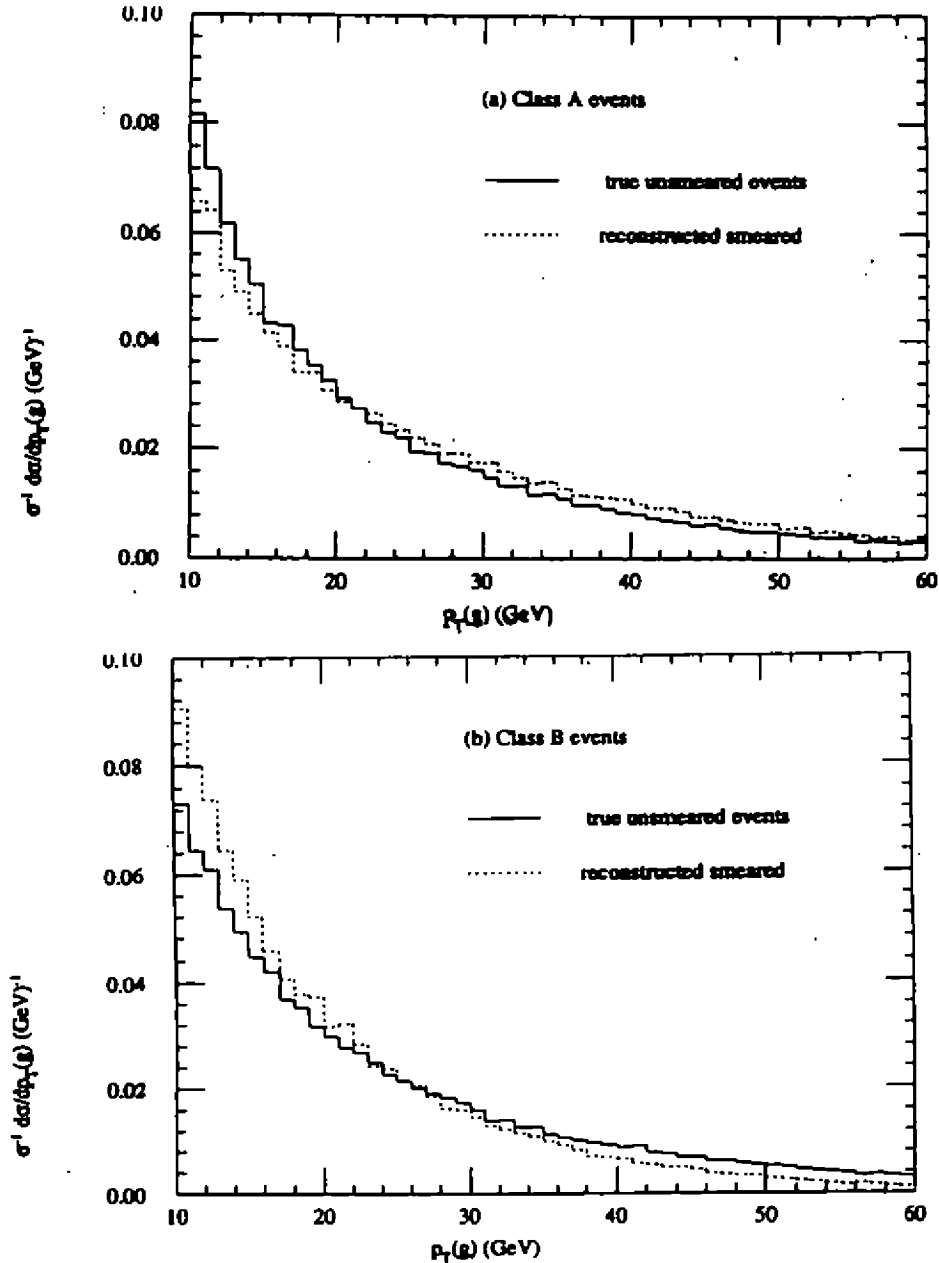


Figura 1. Distribuição de p_T do Gluon para Classes A, B e C. O histograma é para o gluon correto sem a resolução de energia enquanto que o histograma pontilhado é o resultado de nossa simulação.

4 Estratégia Refinada de reconstrução

Esta sensibilidade em ΔR pode ser utilizada como um critério extra de classificação dos eventos nas diferentes classes. Implementamos esta idéia através de um critério de virtualidade. Para a classe A consideramos a virtualidade do propagador do quark inicial após emitir um gluon, $[p(q^*)]^2 = -2p(g) \cdot p(q)$. Atribuímos o menor valor entre os dois possíveis (correspondentes ao quark ou anti-quark) para a classe A. Para as classes B e C, consideramos a virtualidade do propagador do quark b após a irradiação do gluon, $[p(b^*)]^2 - m_b^2 = -2p(g) \cdot p(b)$. Está claro que uma pequena virtualidade implica em um maior elemento de matriz portanto se o gluon foi realmente emitido na configuração considerada esperamos uma pequena virtualidade.

Estabelecemos, então, um novo critério. Para um evento ser classificado numa certa classe deve ter o mínimo F e a mínima virtualidade nesta classe. Eventos com F maior que 500 e que não obedecem ao critério anterior são

desconsiderados. Observamos os resultados desta nova estratégia na tabela 2.

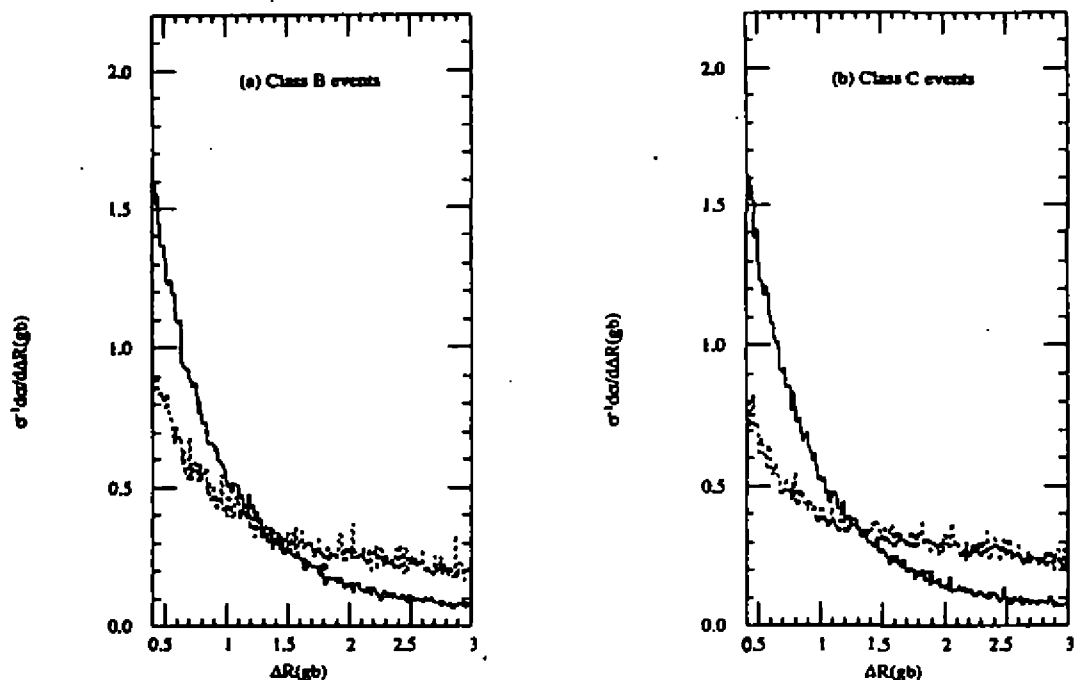


Figura 2. Distribuição de ΔR do Gluon com o b para Classes B e C. Mesma convenção de (2).

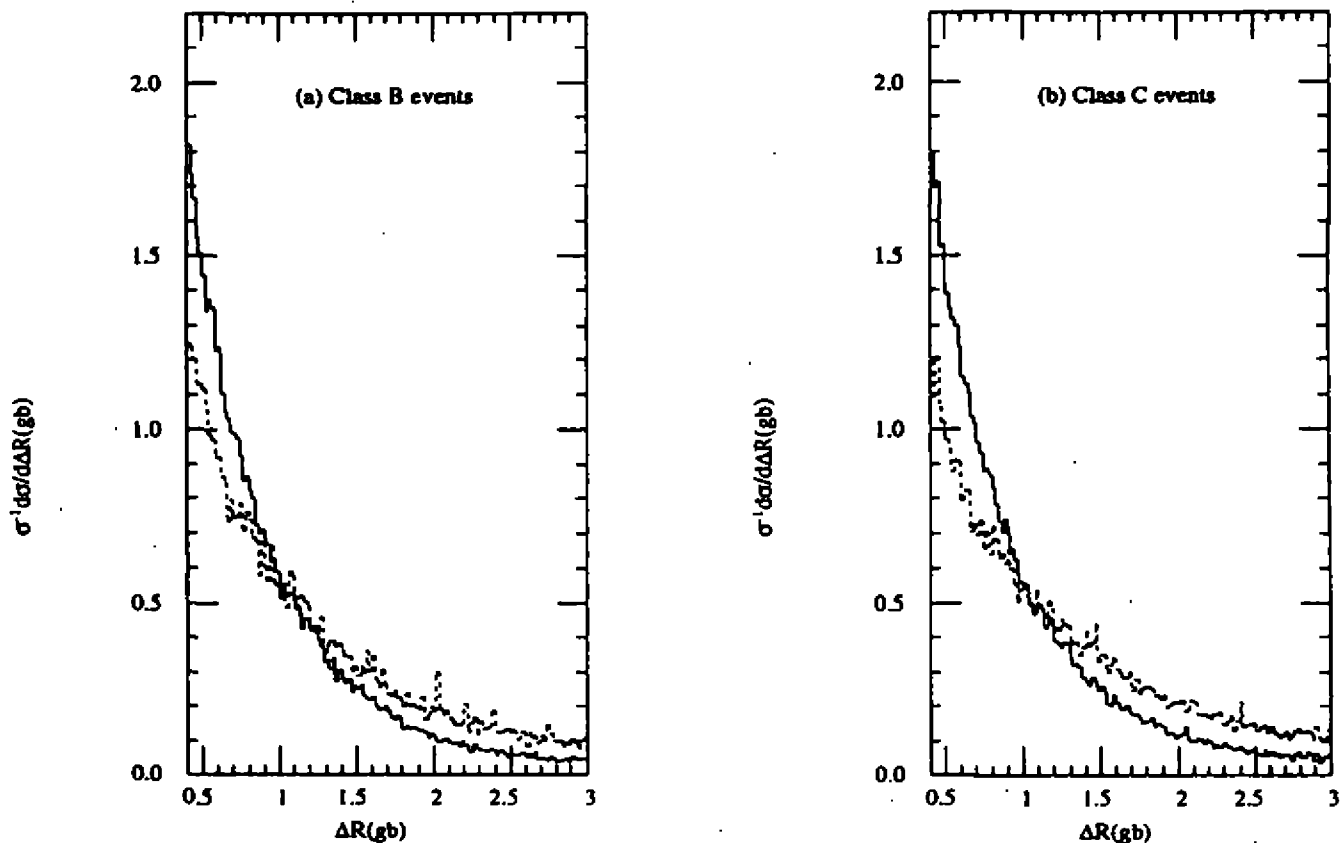


Figura 3. Distribuição de ΔR do Gluon com o b para Classes B e C após o corte em ΔR . Mesma convenção de (2).

Vemos que conseguimos melhorar a porcentagem de eventos reconstruídos corretamente, principalmente nas classes B (71%) e C (73%), embora muitos eventos foram perdidos neste processo. Na Figura 3 vemos a distribuição

de (ΔR) do gluon com o b para classes B e C após os cortes em (ΔR). Notamos que esta estratégia aproxima a curva dos eventos reconstruídos à curva ideal, em que os jatos são corretamente identificados.

Para o caso em que seja possível a identificação dos dois quarks b , continuamos com certa ambiguidade para identificar o gluon e o par de jatos que reconstrói o W , além de não sabermos qual é o b e qual o \bar{b} . O resultado de nosso procedimento de reconstrução básico é mostrado na tabela 3, a ser comparado com a tabela 1.

5 CONCLUSÕES

O ponto principal deste trabalho é apresentar uma estratégia para o estudo dos eventos com um jato extra na produção do Top. Fizemos a simulação à nível de partons, utilizando QCD perturbativa para calcular o elemento de matriz completo, o que significa que o gluon pode ser emitido em qualquer parte do processo. A distinção de regiões A B e C é feita apenas na reconstrução dos eventos e não na geração dos eventos. Este trabalho foi publicado no PLB[7].

References

- [1] CDF collaboration, F. Abe et al., Phys. Rev. Lett. **73**, 225 (1994); **74**, 2626 (1995); Phys. Rev. **D50**, 2966 (1994); **D51**, 4623 (1995); FERMILAB-PUB-95/083-E; FERMILAB-PUB-95/149-E.
- [2] D0 collaboration, S. Abachi et al., Phys. Rev. Lett. **74**, 2632 (1995).
- [3] L.H. Orr, T. Stelzer and W.J. Stirling, Phys. Rev. **D52**, 124 (1995).
- [4] T. Stelzer and W.F. Long, Comput. Phys. Commun. **81**, 357 (1991).
- [5] V. Barger, J. Ohnemus and R. Phillips, Phys. Rev. **D35**, 166 (1987)
- [6] V. Barger et al., Phys. Lett. **B 344** (1995) 329.
- [7] V. Barger, P. G. Mercadante and R. Phillips, Phys. Lett. **B 371** (1995) 117.

Table 2: Eventos reconstruídos após aplicarmos teste em ΔR .

Classe Verdadeira			Porcentagem nas Classes Reconstruídas			
			A	B	C	Fail
A	59.7	⇒	15.7	2.5	2.3	39.2
B	20.2	⇒	.5	8.3	1.1	10.4
C	20.1	⇒	.3	1.0	9.1	9.7

Table 3: Eventos reconstruídos para dupla identificação de b .

Classe Verdadeira			Porcentagem nas Classes Reconstruídas			
			A	B	C	Fail
A	59.7	⇒	38.7	4.6	4.5	11.9
B	20.2	⇒	4.0	11.1	1.8	3.3
C	20.1	⇒	2.4	1.4	13.6	2.7

Fixed Points and Vacuum Energy of Dynamically Broken Gauge Theories

A. A. Natale* and P. S. Rodrigues da Silva†

Instituto de Física Teórica, Universidade Estadual Paulista

Rua Pamplona, 145, 01405-900, São Paulo, SP, Brazil

We show that if a gauge theory with dynamical symmetry breaking has non-trivial fixed points, for values of the coupling constant within the range delimitating the dynamically broken phase, they will correspond to extrema of the vacuum energy. This relationship provides a different method to find fixed points, and we suggest that it can be tested in lattice simulations.

Gauge theories without scalar bosons may undergo the process of dynamical symmetry breaking, where dynamical masses are generated, and we have the phenomenon of dimensional transmutation [1], i.e. we basically do not have arbitrary parameters once the gauge coupling constant (g) is specified at some renormalization point (μ). In these theories all the physical parameters will depend on this particular coupling. Therefore, it would not be surprising if the dynamical masses follow a critical behavior totally related to the one of the coupling constant.

QED is one example of a theory that may show dynamical chiral symmetry breaking in the strong coupling regime. It has been suggested that QED in four dimensions at the same time that generates fermion masses, develops a non-trivial ultra-violet fixed point whose characteristics have recently been reviewed in Ref. [2]. This fixed point behavior could imply that four-dimensional QED is a non-trivial theory. In three dimensions QED also suffers from dynamical symmetry breaking, and recently it has been pointed out that it also may have a non-trivial infrared fixed point [3]. Such fixed points are determined as zeros of the renormalization group β function, and generally speaking they can be attractive or repulsive. According to the idea of dimensional transmutation we can think about how this critical behavior of the coupling constant is transmitted to other calculable physical quantities.

One of the quantities for which we have precise methods to compute in field theory is the vacuum energy, and we could naively think that the fixed points would appear as extrema of the vacuum energy. Such intuitive idea is not new. When Wilson developed the concepts of renormalization group and critical phenomena [4], he gave an example of the renormalization group equation making use of an analogy in classical physics of a ball rolling on a hill. In this example the equation of motion of the ball in the hill potential was related to the renormalization group equation, and the fixed point was related to a stationary point. Therefore, it seems natural to expect a deeper relation between fixed points and extrema of energy also in field theory. However, we have been unable to find a proof of this in the literature, and here we will present a simple demonstration of such connection. This relationship provides a completely different method to determine non-perturbative fixed points, and can be tested in lattice simulations of gauge theories.

Many years ago Cornwall and Norton [5] emphasized that the vacuum energy (Ω) in dynamically broken gauge theories could be defined as a function of the dynamical mass

$$m_{dyn} \equiv \Sigma(p) \equiv m, \quad (1)$$

where $\Sigma(p)$ is the fermion self-energy, and $\Omega = \Omega(\mu, g^2, m)$ is a finite function of its arguments, because the perturbative contribution has been subtracted out. Ω must satisfy a homogeneous renormalization group equation [6]

$$\left(\mu \frac{\partial}{\partial \mu} + \beta(g) \frac{\partial}{\partial g} \right) \Omega = 0. \quad (2)$$

*e-mail : natale@axp.ift.unesp.br

†e-mail : fedel@axp.ift.unesp.br

On the other hand, the dynamically generated masses can be written as $m = \mu f(g)$ [6], from what follows that $\mu(\partial m/\partial \mu) = m$, and consequently

$$m \frac{\partial \Omega}{\partial m} = -\beta(g) \frac{\partial \Omega}{\partial g}. \quad (3)$$

This last and simple equation will be central to our argument, because it relates the stationary condition for the vacuum energy ($\partial \Omega/\partial m = 0$) [5], to the condition of zeros of the β function, as long as $\partial \Omega/\partial g \neq 0$. Therefore, in the following we will show that in a gauge theory with dynamically generated masses (or condensation), the condition for an extrema of the vacuum energy:

$$\beta(g) \left. \frac{\partial \Omega}{\partial g} \right|_{\partial \Omega/\partial m=0 \text{ or } J=0} = 0. \quad (4)$$

always imply $\beta(g) = 0$, because in the broken phase $\partial \Omega/\partial g$ computed at the extrema condition is always different from zero.

The vacuum energy in dynamically broken gauge theories can be computed with the help of the effective action $\Gamma(G)$ for composite operators, since we are interested in theories which admit condensation of composite operators as, for instance, $\langle \bar{\psi}\psi \rangle$ [7]. If J is the source of the composite operator \mathcal{O} , we have [8]

$$\left. \frac{\delta \Gamma}{\delta J} \right|_{J=0} = \langle 0|\mathcal{O}|0 \rangle. \quad (5)$$

From the effective action we determine the effective potential $V(G)$, which depends on the complete propagator G , and finally we can define the vacuum energy as [7]

$$\Omega = V(G) - V_{\text{pert}}(G), \quad (6)$$

where we are subtracting from $V(G)$ its perturbative counterpart, and Ω is computed as a function of the nonperturbative propagators G , i.e. its self-energies, Σ or Π , whether we are working with fermions or gauge bosons, and is zero in the absence of mass generation. Ultimately, Ω is a function of the dynamical masses of the theory.

There is a long discussion in the literature if the vacuum energy Ω can be identified with the effective potential as described above [9], if the effective potential is single-valued, gauge-invariant, etc... However, we stress that all these problems are absent at the stationary points of the vacuum energy [7, 9], and it is exactly for these points that we must compute Eq.(4), which we can now write in the following form:

$$-\beta(g) \left[\frac{\partial \Omega}{\partial J} \frac{\partial J}{\partial g} \right]_{J=0} = 0. \quad (7)$$

However, $\partial \Omega/\partial J = -\partial \Gamma/\partial J$, and as a consequence of Eq.(5) we have

$$\beta(g) \langle 0|\mathcal{O}|0 \rangle \left. \frac{\partial J}{\partial g} \right|_{J=0} = 0. \quad (8)$$

The vacuum condensate $\langle 0|\mathcal{O}|0 \rangle$ is always non-zero above a certain critical coupling (g_c), which is the same for the onset of mass generation resulting a non-trivial Ω . Actually, we separate the dynamically broken phase from the symmetric one exactly by the coupling g_c for which $\langle 0|\mathcal{O}|0 \rangle \neq 0$ It remains to show that $\left. \frac{\partial J}{\partial g} \right|_{J=0}$ is also different from zero in the same conditions, what can be accomplished through the so called "inversion method" [10].

Fukuda has devised a very ingenious method to determine nonperturbative quantities [10]. He noticed that to compute a nonperturbative quantity like $\langle 0|\mathcal{O}|0 \rangle \equiv \vartheta$, the usual procedure is to introduce a source J and to calculate the series:

$$\vartheta = \sum_{n=0}^{\infty} g^n h_n(J). \quad (9)$$

In practice we have to truncate Eq.(9) at some finite order, and it gives us only the perturbative solution $\vartheta = 0$ when we set $J = 0$. The right-hand side of Eq.(9) should be double valued at $J = 0$ for another solution to exist,

which is not the present case. The alternative method proposed by Fukuda is to invert Eq.(9), solving it in favor of J and regarding ϑ as a quantity of the order of unity. We obtain the following series:

$$J = \sum_{n=0}^{\infty} g^n k_n(\vartheta), \quad (10)$$

where the k_n 's satisfying $n \leq m$ (m being some finite integer) are calculable from h_n also satisfying $n \leq m$. We can find a nonperturbative solution of ϑ by setting $J = 0$ through a truncated version of Eq.(10). The details of the method can be found in Ref. [10]. The important point for us is that by construction of Eq.(10) we verify that when $J = 0$ and $\vartheta \neq 0$ (i.e. the theory admits condensation), the same value of ϑ that satisfy Eq.(10) gives $\partial J/\partial g|_{J=0} \neq 0$ trivially. According to this and looking at Eq.(8), the only possibility to obtain $\partial\Omega/\partial m = 0$ is when we have a fixed point ($\beta(g) = 0$). From where comes our main assertion that fixed points are extrema of the vacuum energy. The other two terms of Eq.(8) never can be equal to zero in the broken phase! We have made a detailed calculation of Eq.(8) in the case of QED_4 [11].

A few years ago one of us [12] computed $\langle\Omega\rangle$, which denotes the values of Ω at the stationary points, in the case of quenched QED_4 . $\langle\Omega\rangle$ was computed using approximate solutions of the Schwinger-Dyson equations for the fermion propagator, and the minimum of energy was obtained for each value of the coupling constant (α). It was observed that the deepest minimum occurs exactly for the critical value of the coupling constant expected to be a fixed point. This fact now has been proven not to be accidental, but consistent with the relationship that we discussed here. The connection between fixed points and vacuum energy provides a totally different way to find fixed points. As $\langle\Omega\rangle$ is a gauge invariant physical quantity it can be computed in numerical lattice simulations of QED_4 for a fixed value of the coupling constant. Therefore, it is possible to obtain the curve of minima of energy in the regions of small and strong coupling, approaching the region of the phase transition, and according to our previous discussion the point of minimum energy connecting these different regions will indicate the fixed point.

In conclusion, we have shown that the extrema of the vacuum energy are associated to the fixed points of dynamically broken gauge theories, if these points occur within the range of coupling constants delimitating the dynamically broken phase. Using the "inversion method" it is possible to verify explicitly that Eq.(7) could have a zero, in the case of chirally broken QED, only if the β function has a zero. It would be interesting if such relationship could be investigated by other methods, such as direct lattice calculations.

References

- [1] S. Coleman and E. Weinberg, *Phys. Rev.* **D7**, 1888 (1973).
- [2] V. Azcoiti, *Invited Plenary Talk given at the Lattice 96 Symposium, St. Louis, Missouri, June 1996*, preprint CERN-TH/96-195 (hep-lat/9607070).
- [3] I. J. R. Aitchison, G. Amelino-Camelia, M. Klain-Kreisler, N. E. Mavromatos and D. McNeill, preprint OUTP-96-47P (hep-th/9607192).
- [4] K. G. Wilson, *Phys. Rev.* **B4**, 3174 (1971); K. G. Wilson and J. Kogut, *Phys. Rep.* **12**, 75 (1974).
- [5] J. M. Cornwall and R. E. Norton, *Phys. Rev.* **D8**, 3338 (1973).
- [6] D. J. Gross, in *Methods in Field Theory*, eds. R. Balian and J. Zinn-Justin, Les Houches, Session XXVIII, 1975, (North-Holland Pub. Company), p.141.
- [7] J. M. Cornwall, R. Jackiw and E. Tomboulis, *Phys. Rev.* **D10**, 2428 (1974).
- [8] V. P. Guz'nin, V. A. Kushnir and V. S. Miransky, *Phys. Rev.* **D39**, 2355 (1989).
- [9] T. Banks and S. Raby, *Phys. Rev.* **D14**, 2182 (1976); M. E. Peskin, in *Recent Advances in Field Theory and Statistical Mechanics*, edited by J. -B. Zuber and R. Stora, Elsevier Science Publishers/B.V., 1984, p. 217, (Les Houches, Session XXXIX, 1982).
- [10] R. Fukuda, *Phys. Rev. Lett.* **61**, 1549 (1988).
- [11] P. S. Rodrigues da Silva and A. A. Natale, preprint IFT-Unesp (in preparation).
- [12] A. A. Natale, *Phys. Lett.* **B250**, 139 (1990).

Von Neumann Algebra and Thermofield Dynamics*

A. Matos Neto, J. D. M. Vianna[†], A. E. Santana

*Instituto de Física, Universidade Federal da Bahia,
Campus de Ondina, 40210-340, Salvador, Bahia, Brazil*

F. C. Khanna

*Department of Physics, University of Alberta
Edmonton, AB, Canada, T6G 2J1; and TRIUMF, 4004 Westbrook Mall
Vancouver, BC, Canada, V6T 2A3*

Starting with the von Neumann algebra in its Tomita-Takesaki realization, structural elements of Thermofield Dynamics (TFD) are derived on an axiomatic-algebraic standing point. This approach results in a consistent (physical and mathematical) interpretation of the set of dual variables arising in thermal theories. In this context, the Ojima's work about equilibrium TFD is generalized to arbitrary states. The representation space in the Tomita-Takesaki theory is also used to define a vector manifold for representations of Lie algebras. As an example, the Galilei group is studied.

I Introduction

The von-Neumann or w^* -algebras were proposed as an attempt to build an axiomatic quantum mechanics, widening then the original formalism to embed quantum, classical and statistical theories into a broader structural approach. In a general sense, the theory of linear representations of w^* -algebras was developed by Gelfand, Naimark and Segal (known as the GNS construction), and it stresses the importance of the dynamical states as a basic element for building the representation space of the algebra[1, 2, 3]. This aspect is particularly relevant to systems with infinite degrees of freedom, for in such cases, the von Neumann's irreducibility postulate has no validity at all, resulting, for example, in the breakdown of symmetry and infrared divergences[1, 4, 5].

In this paper we present an application of the von Neumann algebra to thermofield dynamics (TFD)[4, 5, 6], in order to obtain a consistent (physical and mathematical) development to the set of dual variables arising in thermal theories[7]. In this context, we generalize the Ojima's work[8] about equilibrium TFD to arbitrary states.

In Section 2 the notation and some formal definitions related with the Tomita-Takesaki representation of the w^* -algebra, as well as some basic elements of TFD, are introduced. In Section 3 the Tomita-Takesaki representation is used to introduce a representation space for Lie algebras. In Section 4, as an example, the representations of the Galilei group are studied and the Wigner and Kirkwood functions are introduced in connection with a concept of quantum-phase-space wave function.

II Outline of von Neumann algebra and Standard Representation

A c^* -algebra \mathcal{A} is an algebra over the field of complex numbers \mathbb{C} with an involutive mapping $*$: $\mathcal{A} \rightarrow \mathcal{A}$ and another mapping $\|\cdot\|$: $\mathcal{A} \rightarrow \mathbb{R}_+$, which is the *norm*[1, 2, 3]. The set of normal forms ω on \mathcal{A} is called the *pre-dual* of \mathcal{A} and denoted by \mathcal{A}_* . When \mathcal{A} , a c^* -algebra with identity, can be identified as the dual of the pre-dual, \mathcal{A} is called a w^* -algebra or a von-Neumann algebra. (From now on, we will refer to \mathcal{A} as w^* -algebra.)

*Financial support: CAPES (a Brazilian Agency for Research) and Natural Sciences and Engineering Research Council of Canada.

[†]Senior Associated Researcher - Dep. de Física, Universidade de Brasília, 70910-900, Brasília-DF.

Let $(\mathcal{H}, \pi(\mathcal{A}))$ be a faithful realization of \mathcal{A} , where \mathcal{H} is a Hilbert space. $\pi(\mathcal{A}) : \mathcal{H} \rightarrow \mathcal{H}$ is, then, a *-isomorphism of \mathcal{A} by linear operators on \mathcal{H} . Taking $|\xi\rangle \in \mathcal{H}$ normalized, it follows that $\langle \xi | \pi(A) | \xi \rangle$, for every $A \in \mathcal{A}$, defines a state over \mathcal{A} denoted by $\omega_\xi(A) = \langle \xi | \pi(A) | \xi \rangle$. Such states are called *vector states*.

Gelfand, Naimark and Segal (GNS) demonstrated that the inverse of the proposition 2.1 is true. That is, every state ω of a w^* -algebra \mathcal{A} admits a vector representation $|\xi_\omega\rangle \in \mathcal{H}$, such that $\omega(A) = \langle \xi_\omega | \pi_\omega(A) | \xi_\omega \rangle$. This realization is called the *GNS construction*[1, 2, 3]. (In order to emphasise the dependency of the representation space and of the operators on the state $\omega \in \mathcal{A}$, it is usual to denote such a realization by $(\mathcal{H}_\omega, \pi_\omega(\mathcal{A}))$.)

A Tomita-Takesaki representation is a class of representations defined as it follows.

Let $\sigma : \mathcal{H}_\omega \rightarrow \mathcal{H}_\omega$ be a conjugation on \mathcal{H}_ω ; that is, σ is an anti linear isometry such that $\sigma^2 = 1$. $(\mathcal{H}_\omega, \pi_\omega(\mathcal{A}))$ is a Tomita-Takesaki representation of the w^* -algebra \mathcal{A} , iff $\sigma \pi_\omega(\mathcal{A}) \sigma = \tilde{\pi}_\omega(\mathcal{A})$ defines a *-anti isomorphism on the linear operators. It follows that $(\mathcal{H}_\omega, \tilde{\pi}_\omega(\mathcal{A}))$ is a faithful anti realization of \mathcal{A} . Notice that $\tilde{\pi}_\omega(\mathcal{A})$ is the commutating of $\pi_\omega(\mathcal{A})$; that is $[\pi_\omega(\mathcal{A}), \tilde{\pi}_\omega(\mathcal{A})] = 0$.

Some properties of this representation deserve to be stressed. In particular, the representative vectors of the states are invariant by σ ; that is, $\sigma | \xi_\omega \rangle = | \xi_\omega \rangle$. These vectors $| \xi_\omega \rangle$ are defined in a sub set $\mathcal{P}_\omega \subseteq \mathcal{H}_\omega$. In addition, faithful states are represented by cyclic vectors $| \xi_\omega \rangle \in \mathcal{P}_\omega$ in the representations (anti representation) $\pi_\omega(\mathcal{A})$ ($\tilde{\pi}_\omega(\mathcal{A})$). That is, $\pi_\omega(\mathcal{A}) | \xi_\omega \rangle$ and $\tilde{\pi}_\omega(\mathcal{A}) | \xi_\omega \rangle$ are dense sets in \mathcal{H}_ω .

-automorphisms on the w^ -algebra \mathcal{A} are defined through unitary operators, $U(\tau)$, such that $\{U(\tau), \sigma\} = 0$. The unitary operators $U(\tau)$ can be written as $U(\tau) = \exp(i\tau \hat{A})$, where \hat{A} is the symmetry generator. Because of property $\{U(\tau), \sigma\} = 0$, $\sigma \hat{A} \sigma = -\hat{A}$. Therefore, \hat{A} should be a combination of elements of $\pi_\omega(\mathcal{A})$ (say A) and $\tilde{\pi}_\omega(\mathcal{A})$ (say \tilde{A}) given by $\hat{A} = A - \tilde{A}$. That is, \hat{A} is an element of the set $\tilde{\pi}_\omega(\mathcal{A}) = \pi_\omega(\mathcal{A}) - \tilde{\pi}_\omega(\mathcal{A})$. The tilde and non-tilde operators, defined above by the σ conjugation, satisfy just the so-called *tilde conjugation rules*, which are derived in thermo field dynamics (TFD) in association with physical properties of free systems.

The usual (equilibrium) TFD is derived assuming that ω is given by the canonical or the grand-canonical ensemble. In such a situation, as ω is a faithful state, the vector $|\xi_\omega\rangle$ is cyclic; and so, it can be taken as the vacuum (the standard ket) for convenient realizations of the space \mathcal{H}_ω . In those cases, it is possible to use the *-isomorphism (even for ∞ degrees of freedom) and to consider $\mathcal{H}_\omega \equiv \mathcal{H} \otimes \mathcal{H}^*$. Then the representation space is a h^* -algebra (a Hilbert algebra), and we can write: $|\xi_\omega\rangle = |0(\beta)\rangle = Z(\beta, \mu)^{1/2} \sum_n \exp[\frac{1}{2}(\beta E_n - \mu N)] |n, n\rangle$, $\pi(A) = A \otimes 1$, and $\tilde{\pi}(A) = 1 \otimes A$; where $|n, n\rangle = |n\rangle \otimes \langle n|$ and $|n\rangle$ is an eigenstate of the energy with eigenvalue E_n . Notice that the basic elements of TFD are derived here without reference to any particular (equilibrium or non-equilibrium mixed) state ω of \mathcal{A} .

III w^* -Algebra and Lie Groups.

Let us consider a Lie algebra $\ell = \{a_i, i = 1, 2, 3, \dots\}$, over the field \mathbb{R} , characterized by the algebraic relations $a_i \Delta a_j = C_{ijk} a_k$, where $C_{ijk} \in \mathbb{R}$ are the structure constants and Δ is the Lie product. The space \mathcal{H}_ω can be used as a space of representation of ℓ , and according to the Tomita-Takesaki representation, there exists a reducible representation of ℓ specified by linear operators, such that $\pi_\omega(\ell) \subset \pi_\omega(\mathcal{A})$. However, as this realization is reducible, \mathcal{H}_ω is also a space of an anti realization specified by $\tilde{\pi}_\omega(\ell) \subset \tilde{\pi}_\omega(\mathcal{A})$. Using the generators of transformations, the hat operators \hat{A}_i introduced in last section, we derive the following set of commutation relations as a representation of ℓ in the standard representation:

$$[A_i, A_j] = iC_{ijk} A_k. \quad (1)$$

$$[\hat{A}_i, A_j] = iC_{ijk} A_k, \quad (2)$$

$$[\hat{A}_i, \hat{A}_j] = iC_{ijk} \hat{A}_k. \quad (3)$$

Because the properties of the standard representation, the A operators are interpreted as dynamical observables, while the hat variables are the generators of symmetries. The algebra given by Eqs.(1)-(3), which will be denoted

by \mathcal{L}_T , was derived in the context of TFD and called thermoalgebra[9].

In order to write the thermoalgebra of the Galilei group[10], we use the fact that the hat algebra is a faithful representation of the Lie algebra of the Galilei symmetries. Moreover, we consider the general situation of projective representations. Therefore, we obtain

$$[J_i, J_j] = \epsilon_{ijk} J_k, [J_i, P_j] = \epsilon_{ijk} P_k, [J_i, K_j] = \epsilon_{ijk} K_k, \quad (4)$$

$$[H, K_j] = iP_j, [K_j, P_k] = im\delta_{jk}, \quad (5)$$

$$[\hat{J}_i, \hat{J}_j] = \epsilon_{ijk} \hat{J}_k, [J_i, \hat{J}_j] = [\hat{J}_i, J_j] = \epsilon_{ijk} J_k, \quad (6)$$

$$[\hat{J}_i, \hat{P}_j] = \epsilon_{ijk} \hat{P}_k, [J_i, \hat{P}_j] = [\hat{J}_i, P_j] = \epsilon_{ijk} P_k, \quad (7)$$

$$[\hat{J}_i, \hat{K}_j] = \epsilon_{ijk} \hat{K}_k, [J_i, \hat{K}_j] = [\hat{J}_i, K_j] = \epsilon_{ijk} K_k, \quad (8)$$

$$[\hat{H}, \hat{K}_j] = i\hat{P}_j, [H, \hat{K}_j] = [\hat{H}, K_j] = iP_j, \quad (9)$$

$$[\hat{K}_i, \hat{P}_j] = im\delta_{ij}, [K_i, \hat{P}_j] = [\hat{K}_i, P_j] = im\delta_{ij}, \quad (10)$$

where ϵ_{ijk} is the Levi-Civita tensor and $i, j, k = 1, 2, 3$: the other commutation relations are null.

Considering $m \neq 0$ the invariants of \mathcal{L}_T are given by $I_1 = \frac{P^2}{2m} - H$, $I_2 = (J - \frac{1}{m} K \times P)^2$, $I_3 = \hat{I}_1 = \left(\frac{P^2}{2m}\right)^\wedge - \hat{H}$ and $I_4 = \hat{I}_2 = \left(J - \frac{1}{m} K \times P\right)^\wedge$.

From the commutation relations for the thermoalgebra of the Galilei group, \hat{H} is the generator of the time translation, and so the time evolution of an arbitrary dynamical variable is specified by $\bar{A}(t) = e^{it\hat{H}} \bar{A} e^{-it\hat{H}}$ (\bar{A} means \hat{A} or A operator). Using the Schrödinger picture we have

$$i\partial_t | \psi \rangle = \hat{H} | \psi \rangle. \quad (11)$$

Considering Eq.(4)-(10), we have several possibilities to define a frame in the Hilbert space \mathcal{H}_ω . An interesting frame can be built with the operators \underline{P} and \underline{Q} defined by $\underline{P} = P - \frac{1}{2}\hat{P}$ and $\underline{Q} = Q - \frac{1}{2}\hat{Q}$. Observe that $[\underline{P}, \underline{Q}] = 0$, and more, \underline{P} and \underline{Q} satisfy the Galilei-boost conditions: therefore, they can be taken as momentum and position operators, respectively. But despite this fact, \underline{P} and \underline{Q} can not be considered as observables, for, in this Tomita-Takesaki representation, the hat-operators are generators of symmetries, not observables.

Since \underline{P} and \underline{Q} commute with each other, a representation in which both operators are diagonal can be used to define a quantum phase space. This phase-space frame is defined by $\underline{P} | q, p \rangle = p | q, p \rangle$ and $\underline{Q} | q, p \rangle = q | q, p \rangle$, where the kets $| q, p \rangle$ are an orthonormal basis in \mathcal{H}_ω , that is, $\langle q, p | q', p' \rangle = \delta(q-q')\delta(p-p')$, $\int | q, p \rangle \langle q, p | dq dp = 1$. In this basis, we can write the observables Q and P , and the generator \hat{P} and \hat{Q} as $Q_j = q_j + \frac{1}{2}\hbar \frac{\partial}{\partial p_j}$, $P_j = p_j - \frac{1}{2}\hbar \frac{\partial}{\partial q_j}$, $\hat{Q}_j = i\hbar \frac{\partial}{\partial p_j}$, $\hat{P}_j = -i\hbar \frac{\partial}{\partial q_j}$. These results show that \mathcal{H}_ω is a reducible representation space for the observables Q_i and P_i , [11](but this is not the case for the full set of dynamical variables). From the evolution equation for the states, Eq.(11), can be written as[10]

$$\partial_t f_W(q, p; t) = \{H(q, p), f_W(q, p; t)\}_M,$$

where where $\{\cdot, \cdot\}_M$, the Moyal bracket, is given by

$$\{g, f\}_M(q, p) = g(q, p) \frac{2}{\hbar} \sin\left\{\frac{\hbar}{2}\left[\frac{\partial}{\partial q} \frac{\partial}{\partial p} - \frac{\partial}{\partial p} \frac{\partial}{\partial q}\right]\right\} f(q, p),$$

f_W is defined by $f_W(q, p) = (\psi^\dagger \circ \psi)(q, p)$, being $\psi(q, p; t) = \langle q, p | \psi(t) \rangle$, and

$$(\psi \circ \psi')(q, p) = \psi(q, p) \exp\left\{\frac{\hbar}{2}\left[\frac{\partial}{\partial q} \frac{\partial}{\partial p'} - \frac{\partial}{\partial p} \frac{\partial}{\partial q'}\right]\right\} \psi'(q, p) \quad (12)$$

We can show that the function $f_W(q, p)$ satisfies just all the properties of the Wigner function[10, 12, 13]. Then the functions $\psi(q, p)$ can be interpreted as a wave function attached to the Wigner-function approach to the quantum mechanics.

The non local product Eq.(12) equips the space $\mathcal{H}_\omega \equiv \mathcal{H} \otimes \mathcal{H}^*$ with a structure of Hilbert algebras. Therefore, we can consider other representations for such a product, giving different (but equivalent) descriptions of the quantum phase space. Indeed, let us consider two examples. The first one is defined by commutant operators $[\tilde{Q}, P] = 0$, such that $P | q, p \rangle = p | q, p \rangle$, $\tilde{Q} | q, p \rangle = q | q, p \rangle$, $Q_j = q_j + \frac{i}{2} \hbar \frac{\partial}{\partial p_j}$ and $\tilde{P}_j = p_j + \frac{i}{2} \hbar \frac{\partial}{\partial q_j}$. Then the product of the Hilbert algebra is now written as

$$(\psi \circ \psi')(q, p) = \psi(q, p) \exp\left[i \frac{\hbar}{2} \frac{\partial}{\partial q} \frac{\partial}{\partial p}\right] \psi'(q, p). \quad (13)$$

As the second example, we can consider $[Q, \tilde{P}] = 0$, such that $\tilde{P} | q, p \rangle = p | q, p \rangle$, $Q | q, p \rangle = q | q, p \rangle$, $\tilde{Q}_j = q_j - \frac{i}{2} \hbar \frac{\partial}{\partial p_j}$ and $\tilde{P}_j = p_j - \frac{i}{2} \hbar \frac{\partial}{\partial q_j}$, resulting in

$$(\psi \circ \psi')(q, p) = \psi(q, p) \exp\left[i \frac{\hbar}{2} \frac{\partial}{\partial p} \frac{\partial}{\partial q}\right] \psi'(q, p). \quad (14)$$

These products, Eq.(13) and (14), give raise to the complex distribution functions introduced by Kirkwood[12, 14]. These aspects will be studied in more detail elsewhere.

References

- [1] G. G. Emch, *Algebraic Methods in Statistical Mechanics and Quantum Field Theory* (Wiley-Interscience, New York, 1972).
- [2] O. Bratteli and D. W. Robison, *Operator Algebras and Quantum Statistical Mechanics, vols. I and II* (Springer, Berlin, 1979).
- [3] M. Takesaki, *Tomita's Theory of Modular Hilbert Algebras and its Applications*, (Springer-Verlag, Berlin, 1970)
- [4] H. Umezawa, *Advanced Field Theory : Micro, Macro and Thermal Physics* (American Institute of Physics, New York, 1993).
- [5] H. Umezawa, H. Matsumoto and M. Tachiki, *Thermofield Dynamics and Condensed States* (North-Holland, 1982).
- [6] Y. Takahashi and H. Umezawa, *Collective Phenom.* 2 (1975) 55.
- [7] H. Chu and H. Umezawa, *Int. J. Mod. Phys. A* 9 (1994) 2363.
- [8] I.Ojima, *Ann. Phys. (N.Y.)* 137 (1981) 1.
- [9] A. E. Santana and F. C. Khanna, *Phys. Lett. A* 203 (1995) 68.
- [10] A. Matos Neto, J.D.M. Vianna, A.E. Santana and F.C. Khanna, *Physics Essays*, Vol.9, N. 4(1996).
- [11] L. C. Papaloucas and J. Rembielinski, *J. Phys. A: Math. Gen.* 22 (1989) 2751; C. N. Ktorides and L. C. Papaloucas, *Prog. Theor. Phys.* 75 (1986) 465.
- [12] A. Matos Neto, *Realização de Tomita-Takesaki de w^* -álgebras Semi-Finitas e Generalização Algébrica das Teorias Clássica e Quântica*, PhD Tesis - CBPF (Centro Brasileiro de Pesquisas Físicas), Rio de Janeiro, 1992.
- [13] E. Wigner, *Phys. Rev.* 40 (1932) 749.
- [14] J. G. Kirkwood, *Phys. Rev.* 44 (1933) 31.

Hamilton-Jacobi formulation for singular higher order systems

B. M. Pimentel* and R. G. Teixeira†

*Instituto de Física Teórica - Universidade Estadual Paulista
Rua Pamplona 145 - 01405-900 - São Paulo, S.P. Brazil*

In this work we present a generalization of the Hamilton-Jacobi formulation for singular systems with arbitrarily higher order Lagrangians. We follow the procedure of obtaining the Hamilton-Jacobi equation from Carathéodory's equivalent Lagrangians method and then develop the approach for singular systems writing the equations of motion as total differential equations in many variables.

1 Introduction

Singular systems, i.e. those which have a singular Hessian matrix, have been studied widely in literature. The Lagrangian and Hamiltonian formulations for such systems have already been developed by many authors [1, 2] but, since its development, Dirac's Hamiltonian formalism [3] has been the main tool to the study of such systems [4, 5].

Recently a new approach for singular systems, based on Hamilton-Jacobi formalism, has been developed for first order singular systems [6, 7] and have also been generalized for second order systems [8] of physical systems and, as a consequence, it is still necessary to develop and analyze the applications of this formalism.

In this work we present the Hamilton-Jacobi formalism for singular systems making its generalization for singular systems with arbitrarily higher derivatives. First, we will analyze the constraints structure present in singular higher order systems and then we will apply Carathéodory's equivalent Lagrangians method to obtain the Hamilton-Jacobi partial differential equation which we will use to write the equations of motion as total differential equations.

2 Constraints structure in higher order systems

We will analyze a system described by a Lagrangian dependent up to the K -th derivative of the N generalized coordinates q_i , i.e.

$$L\left(q_i, \dot{q}_i, \dots, q_i^{(K)}\right); \quad q_i^{(s)} \equiv \frac{d^s q_i}{dt^s}, \quad (1)$$

where $s = 0, 1, \dots, K$ and $i = 1, \dots, N$. For such systems, the Euler-Lagrange equations obtained through Hamilton's principle of stationary action will be:

$$\sum_{s=0}^K (-1)^s \frac{d^s}{dt^s} \left(\frac{\partial L}{\partial q_i^{(s)}} \right) = 0 \quad (2)$$

This is a system of N differential equations of $2K$ -th order so we need $2KN$ initial conditions to solve them. These conditions are the initial values of $q_i, \dot{q}_i, \dots, q_i^{(2K-1)}$ that describe the "velocity" phase space (VPS).

*Partially supported by CNPq

†Supported by CAPES

The Hamiltonian formalism for theories with higher order derivatives, that has been developed first by Ostrogradski [9], treats the derivatives $q^{(s)}_i \equiv q_{(s)i}$ ($s = 0, \dots, K - 1$) as coordinates and introduces the momenta

$$p_{(K-1)i} \equiv \frac{\partial L}{\partial q^{(K)}_i} \tag{3}$$

$$p_{(s-1)i} \equiv \frac{\partial L}{\partial q^{(s)}_i} - \dot{p}_{(s)i}; \quad s = 1, \dots, K - 1 \tag{4}$$

conjugated respectively to $q_{(K-1)i}$ and $q_{(s-1)i}$, $s = 1, \dots, K - 1$. It is important to notice that the momenta $p_{(s)i}$ ($s = 0, 1, \dots, K - 1$) will be dependent of the derivatives up to $q^{(2K-1-s)}_i$.

The Hamiltonian is defined as

$$H = \sum_{s=0}^{K-1} p_{(s)i} q^{(s+1)}_i - L \left(q_i, \dots, q^{(K)}_i \right), \tag{5}$$

and the Hamilton's equations of motion will be written as

$$\dot{q}_{(s)i} = \frac{\partial H}{\partial p_{(s)i}} = \{ q_{(s)i}, H \} \tag{6}$$

$$p_{(s)i} = - \frac{\partial H}{\partial q_{(s)i}} = \{ p_{(s)i}, H \}. \tag{7}$$

where Einstein's summation rule is used.

The phase space (PS) is described in terms of the canonical variables $q_{(s)i}$; $p_{(s)i}$ (where $i = 1, \dots, N$ and $s = 0, \dots, K - 1$) and we have $2NK$ equations of motion (given by equations (6) and (7)) that need $2KN$ initial conditions to be solved. These initial conditions are analogue to those needed in Euler-Lagrange equations, but now they are the initial values of the canonical variables.

But the passage from VPS to PS is only possible if the momenta expressions (3) and (4) can be solved with respect to the derivatives $q^{(K)}_i, \dots, q^{(2K-1)}_i$ so that these can be expressed as functions of the canonical variables and eliminated from the theory. The necessity of express these derivatives as functions of canonical variables comes from the fact that they are present in the momenta expressions (4). So, fixing the initial conditions of the momenta in the Hamiltonian formulation is equivalent to fixing the initial conditions to the derivatives $q^{(K)}_i, \dots, q^{(2K-1)}_i$ in the Lagrangian formulation.

We can use the fact that the momenta $p_{(s)i}$ ($s = 0, 1, \dots, K - 1$) will be dependent of the derivatives up to $q^{(2K-1-s)}_i$; and that the highest derivatives appear linearly, with coefficients that are the elements of the Hessian matrix

$$H_{ij} \equiv \frac{\partial p_{(K-1)i}}{\partial q_j} = \frac{\partial^2 L}{\partial q_i \partial q_j} \tag{8}$$

to show that the derivatives $q^{(K+p)}_i$ can be solved as functions

$$q^{(K+p)}_i = f_{(K+p)i} (q_{(s)j}; p_{(K-1)j}, \dots, p_{(K-1-p)j}); \quad s, p = 0, \dots, K - 1 \tag{9}$$

if, and only if, the Jacobian matrix of the change of variables $q^{(K+p)}_j - p_{(K-1-p)j}$, with elements J_{ij} given by

$$J_{ij} = \frac{\partial p_{(K-1-p)i}}{\partial q^{(K+p)}_j} \Big|_{q^{(K+d)}_a = J_{1(K+d)}_a} = (-1)^p \frac{\partial^2 L}{\partial q_i \partial q_j} \Big|_{q^{(K+d)}_a = J_{1(K+d)}_a}$$

$$J_{ij} = (-1)^p H_{ij} \Big|_{q^{(K+d)}_a = J_{1(K+d)}_a} \tag{10}$$

($d = 0, \dots, p - 1$), be non singular. Consequently, it will be the non singularity of the Hessian matrix (8) that will determine if the passage from the VPS to PS is possible or not.

Let's suppose now that the Hessian matrix has rank $P = N - R$. In this case it will not be possible to express all derivatives $q^{(K)}_i, \dots, q^{(2K-1)}_i$; in the form described by equation (9). Anyway, without loss of generality, we can choose the order of coordinates in such a way that the $P \times P$ sub-matrix in the bottom right corner of the Hessian matrix has nonvanishing determinant:

$$\det \|H_{ab}\| = \det \left\| \frac{\partial^2 L}{\partial q^{(K)}_a \partial q^{(K)}_b} \right\| \neq 0; \quad a, b = R + 1, \dots, N \tag{11}$$

With this condition, the derivatives $q^{(K+p)}_\alpha$ ($\alpha = 1, \dots, R; p = 0, \dots, K - 1$) will remain undetermined and we will have expressions like

$$p_{(K-1-p)\alpha} = g_{(K-1-p)\alpha}(q_{(s)j}; p_{(K-1)\alpha_1}, \dots, p_{(K-1-p)\alpha}) \tag{12}$$

that will correspond to primary constraints

$$\Phi_{(K-1-p)\alpha} = p_{(K-1-p)\alpha} - g_{(K-1-p)\alpha}(q_{(s)j}; p_{(K-1)\alpha_1}, \dots, p_{(K-1-p)\alpha}) \approx 0 \tag{13}$$

in Dirac's formalism [3].

Then, we have as result that in a higher order systems the existence of constraints involving a given momentum $p_{(K-1)\alpha}$ will imply the existence of constraints involving all $p_{(s)\alpha}$ momenta conjugated to the derivatives $q_{(s)\alpha} = q^{(s)}_\alpha$ ($s = 0, \dots, K - 1$) due to the fact that the derivatives $q^{(K)}_\alpha, \dots, q^{(2K-1)}_\alpha$ can't be expressed as functions of the canonical variables. Consequently, when the Hessian matrix has rank $P = N - R$ there will be KR expressions of the kind (12) that correspond to KR primary constraints as given by (13).

The existence of such constraints structure in higher order systems have already been noticed by other authors [10, 11, 12]. But even noticing the constraints structure showed above is present in the momenta definitions, all these authors consider that only the constraints involving $p_{(K-1)\alpha}$ are primary constraints. Anyway, this makes few difference in Hamiltonian dynamics for singular systems since the others constraints will be secondary constraints obligatorily obtained as consistency conditions: $\Phi_{(K-2)\alpha}$ will be generated by the consistence condition of $\Phi_{(K-1)\alpha}$; $\Phi_{(K-3)\alpha}$ will be generated by the consistence condition of $\Phi_{(K-2)\alpha}$, and so on. Besides that, it is important to notice that the constraint structure showed above is different for a higher order Lagrangian obtained from a lower order one by adding a total time derivative. We will not discuss this case here however the reader can find a detailed analysis of the constraint structure for such Lagrangians in reference [12].

3 Hamilton-Jacobi formalism

The Hamilton-Jacobi equation for higher order systems which can be obtained through Carathéodory's equivalent Lagrangians method [13], are given by

$$\frac{\partial S}{\partial t} = -H; \quad p_{(s)i} = \frac{\partial S}{\partial q_{(s)i}}; \quad s = 0, \dots, K - 1 \tag{14}$$

where H is the Hamiltonian given by equation (5) and $S(q_i, \dots, q_{(K-1)i}, t)$ is Hamilton's principal function. An example of the application of Carathéodory's method to a second order system can be found in ref. [8].

Due to the singularity of the system we have expressions like (12) which we rewrite as:

$$p_{(d)\alpha} = -H_{(d)\alpha}(q_{(s)i}, p_{(s)\alpha}); \quad d = 0, \dots, K - 1 \tag{15}$$

Although $p_{(d)\alpha}$ is dependent only of momenta $p_{(0)\alpha}, p_{(1)\alpha}, \dots, p_{(d)\alpha}$, as it can be seen from equation (12), for simplicity we will treat them as if they were dependent of all $p_{(s)\alpha}$.

The Hamiltonian H becomes

$$H = \sum_{s=0}^{K-1} p_{(s)\alpha} q_{(s+1)\alpha} + \sum_{s=0}^{K-1} q_{(s)\alpha} p_{(s)\alpha} \Big|_{p_{(s)\alpha} = -H_{(s)\alpha}} - L \left(q_{(u)\alpha}; q_{(s)\alpha}; q_{(s)\alpha} = f_{(K)\alpha} \right) \tag{16}$$

where $d, u = 0, \dots, K-1$. The Hamiltonian H does not depend explicitly upon the derivatives $q_{(s)\alpha}, \dots, q_{(2K-1)\alpha}$ since its partial derivatives with respect to them are identically zero.

Now we adopt the following notation: t will be called $q_0 = t_0$ and $q_{(s)\alpha}$ will be called $t_{(s)\alpha}$. The "momentum" P_0 will be defined as:

$$P_0 = \frac{\partial S}{\partial t} \tag{17}$$

Then to obtain an extreme of the action integral we must find a function $S(q_i, \dots, q_{(K-1)i}, t)$ that satisfies the following set of Hamilton-Jacobi partial differential equations (HJPDE):

$$H'_0 = P_0 + H_0 \left(t_0, t_{(s)\alpha}; q_{(s)\alpha}; p_{(s)\alpha} = \frac{\partial S}{\partial q_{(s)\alpha}} \right) = 0 \tag{18}$$

$$H'_{(s)\alpha} = p_{(s)\alpha} + H_{(s)\alpha} \left(t_0, t_{(s)\alpha}; q_{(s)\alpha}; p_{(s)\alpha} = \frac{\partial S}{\partial q_{(s)\alpha}} \right) = 0 \tag{19}$$

From the definitions above we have

$$dq_0 = dt = \frac{\partial H'_0}{\partial P_0} dt_0 + \frac{\partial H'_{(s)\alpha}}{\partial P_0} dt_{(s)\alpha} \tag{20}$$

$$dq_{(s)\alpha} = \frac{\partial H'_0}{\partial p_{(s)\alpha}} dt_0 + \frac{\partial H'_{(u)\alpha}}{\partial p_{(s)\alpha}} dt_{(u)\alpha} \tag{21}$$

From the momenta definitions we get:

$$dP_0 = \frac{\partial^2 S}{\partial^2 t} dt_0 + \frac{\partial^2 S}{\partial t \partial t_{(s)\alpha}} dt_{(s)\alpha} + \frac{\partial^2 S}{\partial t \partial q_{(s)\alpha}} dq_{(s)\alpha} \tag{22}$$

$$dp_{(s)\alpha} = \frac{\partial^2 S}{\partial q_{(s)\alpha} \partial t} dt_0 + \frac{\partial^2 S}{\partial q_{(s)\alpha} \partial t_{(u)\alpha}} dt_{(u)\alpha} + \frac{\partial^2 S}{\partial q_{(s)\alpha} \partial q_{(u)\alpha}} dq_{(u)\alpha} \tag{23}$$

If we consider that we have a solution $S(q_i, \dots, q_{(K-1)i}, t)$ of the set of HJPDE given by equations (18) and (19), in a procedure analogous to that used with second order systems in ref. [8], we can reduce the equations above to:

$$dP_0 = -\frac{\partial H'_0}{\partial t_0} dt_0 - \frac{\partial H'_{(s)\alpha}}{\partial t_0} dt_{(s)\alpha} \tag{24}$$

$$dp_{(s)\alpha} = -\frac{\partial H'_0}{\partial q_{(s)\alpha}} dt_0 - \frac{\partial H'_{(u)\alpha}}{\partial q_{(s)\alpha}} dt_{(u)\alpha} \tag{25}$$

Besides that, making $Z = S(q_i, \dots, q_{(K-1)i}, t)$ and using the momenta definitions together with equation (21) we have:

$$dZ = \left(-H_0 + p_{(s)\alpha} \frac{\partial H'_0}{\partial p_{(s)\alpha}} \right) dt_0 + \left(-H_{(u)\alpha} + p_{(s)\alpha} \frac{\partial H'_{(u)\alpha}}{\partial p_{(s)\alpha}} \right) dt_{(u)\alpha} \tag{26}$$

This equation, together with equations (20), (21), (24) and (25) are the total differential equations for the characteristics curves and, if they form a completely integrable set, their simultaneous solutions determine $S(q_i, \dots, q_{(K-1)i}, t_0)$ uniquely by the initial conditions.

4 Conclusions

We have obtained a generalization of Hamilton-Jacobi formalism for singular systems that allows the study of higher order systems. For that, the constraints structure in such systems was analyzed. This is due to the fact that if we had considered only the constraints containing the momenta $p_{(K-1)\alpha}$, given by equation (12) when $p = 0$, the other constraints would have to be obtained from integrability conditions. The integrability conditions of the total differential equations for such systems will be similar to the integrability conditions for first order singular systems that have already been studied [7]. To avoid unnecessary work we consider all the constraints structure since the beginning of the formalism.

References

- [1] K. Sundermeyer, "Lecture Notes in Physics 169: Constrained Dynamics" (Springer-Verlag, 1982).
- [2] E. C. G. Sudarshan and N. Mukunda, "Classical Dynamics: A Modern Perspective" (John Wiley & Sons Inc., New York, 1974).
- [3] P. M. A. Dirac, *Lectures on Quantum Mechanics* (Belfer Graduate School of Science, Yeshiva University, New York, N. Y., 1964).
- [4] A. Hanson, T. Regge and C. Teitelboim, "Constrained Hamiltonian Systems" (Accademia Nazionale dei Lincei, Roma, 1976).
- [5] D. M. Gitman and I. V. Tyutin, "Quantization of Fields with Constraints" (Springer-Verlag, 1990).
- [6] Y. Güler, *Il Nuovo Cimento B*, **107**, 1389 (1992).
- [7] Y. Güler, *Il Nuovo Cimento B*, **107**, 1143 (1992).
- [8] B. M. Pimentel and R. G. Teixeira, *Il Nuovo Cimento B*, **111**, 841 (1996).
- [9] M. Ostrogradski, *Mem. Ac. St. Petersburg* **1**, 385 (1850).
- [10] V. V. Nesterenko, *J. Phys. A: Math. Gen.* **22**, 1673 (1989).
- [11] C. Batlle, J. Gomis, J. M. Pons and N. Román-Roy, *J. Phys. A: Math. Gen.* **21**, 2693 (1988).
- [12] Y. Saito, R. Sugano, T. Ohta and T. Kimura, *J. Math. Phys.* **30**, 1122 (1989).
- [13] C. Carathéodory, "Calculus of Variations and Partial Differential Equations of the First Order", Part II, page 205 (Holden-Day, 1967).

Fermions and Bubble Nucleation*

D.G. Barci^{a)}

Instituto de Física, Universidade Estadual do Rio de Janeiro

E. S. Fraga^{b)} and C.A.A. de Carvalho^{c)}

Instituto de Física, Universidade Federal do Rio de Janeiro

December 3, 1996

The study of the mechanism of decay of metastable systems via bubble nucleation finds a wide range of applicability in all realms of Physics. From condensed-matter physics, in polymer transitions [2, 4, 3, 8], to baryon number violation via sphaleron transitions in high-energy physics [9].

In this work, we present a study of the role of fermions in the decay of metastable states of a scalar field via bubble nucleation. We consider a system of interacting fermions and bosons that starts in a metastable vacuum and gradually decays to the true one via nucleation of bubbles. Our main purpose is the analysis of the effect of fermions on the stability of these bubbles. We analyze both two and four-dimensional systems. In order to obtain the effects of fermions on the bosonic field, we construct an effective theory, integrating over the fermions. However, integrating over the fermions implies calculating the fermionic determinant. If we focus on the long distance (small momentum) properties of the theory, we may calculate this determinant by using a systematic functional gradient expansion for an arbitrary number of dimensions ν [10, 11]. Using this procedure, we obtain the corrected form for the bubbles (now charged ones) and their energies as functions of their radii. In this way, we obtain all the information about their stability, and we may even calculate decay rates as explicit functions of time. The results for two dimensions are compared to the exact results of previous work [2].

The model Lagrangian has the following form

$$\mathcal{L} = \frac{1}{2}(\partial_\mu \phi)(\partial^\mu \phi) - [V(\phi) - V(\phi_2)] + \bar{\psi}_a(i\gamma^\mu \partial_\mu - \mu - g\phi) \psi_a \quad (1)$$

where ϕ_2 is a local minimum of the potential (We may find a physical realization of this form of potential in the description of conducting polymers [3, 4], $V(\phi) = \frac{g^2}{2}(\phi - \phi_0)^2 \left(\phi + \phi_0 + \frac{2\mu}{g} \right)^2 + j\phi$).

Integrating over fermions implies calculating the following determinant

$$S_F = -\ln[\det(i\gamma^\mu \partial_\mu - \mu - g\phi)] = -\text{tr}[\ln(i\gamma^\mu \partial_\mu - \mu - g\phi)] \quad (2)$$

In one spatial dimension, it is possible to perform an exact calculation of (2) by making use of inverse scattering methods [2, 5, 6]. For three spatial dimensions, we must resort to approximations.

We may rewrite the effective action as

$$S_{eff}[\phi] = \int d^{\nu}x \left\{ \frac{1}{2}(\partial_\mu \phi)(\partial^\mu \phi) - [V(\phi) - V(\phi_2)] \right\} - \text{tr}[\ln(i\gamma^\mu \partial_\mu - \mu - g\phi)] \quad (3)$$

The field configuration that extremizes (3) must satisfy the Euler-Lagrange equation

$$\square \phi = -\frac{\partial V}{\partial \phi} - Sp \langle x | \frac{1}{i\gamma^\mu \partial_\mu - \mu - g\phi} | x \rangle \quad (4)$$

*Work partially supported by CNPq and FUJB/UFRJ.

We may calculate the Green function by using a functional gradient expansion. To do so, we use the identity [10, 11]

$$\begin{aligned} \mathcal{G}(x, x) &\equiv Sp \langle x | \frac{1}{i\gamma^\mu \partial_\mu + M(x)} | x \rangle = \\ &= Sp \int \frac{d^\nu p}{(2\pi)^\nu} \frac{1}{\gamma^\mu p_\mu + M(x)} \sum_{n=0}^{\infty} (-1)^n \left(\Delta M \left(\frac{1}{i} \frac{\partial}{\partial p}, x \right) \frac{1}{\gamma^\mu p_\mu + M(x)} \right)^n \end{aligned} \tag{5}$$

where

$$\Delta M \left(\frac{1}{i} \frac{\partial}{\partial p}, x \right) = \partial_\mu M(x) \frac{1}{i} \frac{\partial}{\partial p_\mu} + \frac{1}{2} \partial_\mu \partial_\nu M(x) \left(\frac{1}{i} \right)^2 \frac{\partial^2}{\partial p_\mu \partial p_\nu} + \dots \tag{6}$$

Keeping terms up to second order in the derivatives and explicitly performing the integrals, we obtain $\mathcal{G}(x, x) = \alpha_\nu M^{\nu-1} + \beta_\nu M^{\nu-4} \square M$, where α_ν and β_ν are functions of the number of space-time dimensions.

For $\nu = 2$ and $\nu = 4$, these functions are divergent. Nevertheless, we may absorb these divergences in a suitable redefinition of the free parameters of the model. After a redefinition of g , μ and j and remembering that, in our case, $M(x) = -(\mu + g\phi)$, we may explicitly calculate the equation of motion.

For $\nu = 2$, we find (up to order g^2)

$$\square \phi = -\frac{\partial V}{\partial \phi} \left[\frac{(\mu + g\phi)^2}{(\mu + g\phi)^2 + \frac{g^2}{6\pi}} \right] \tag{7}$$

and, for $\nu = 4$,

$$\square \phi = -\frac{\partial V}{\partial \phi} \tag{8}$$

The part of the effective action, S_F , associated with the fermionic determinant has the form $S_F = -g \int d^\nu x \int [D\phi] \mathcal{G}(x, x)$, with the matrix element given by (5).

We note that, in the case of $\nu = 4$, the only effect of the fermions is (to this order of approximation) to renormalize the free parameters of the theory. We will see that this situation is completely changed if we include a gap and bound states in the fermionic spectrum.

Based on the results of our previous work, we shall look for *sphaleron*-like (droplet-like) solutions to the equations of motion obtained above [1, 2, 4, 7].

For the $\nu = 2$ case, we may define $\varphi \equiv \phi + \mu/g$ and, using the thin-wall approximation [1] (i.e., considering a droplet whose radius is much larger than its wall thickness) and imposing the boundary conditions $\varphi_{sph}(x \rightarrow \pm\infty) \rightarrow \varphi_2$ and $\frac{d\varphi_{sph}}{dx}(x \rightarrow \pm\infty) \rightarrow 0$, we obtain

$$\varphi_{sph} = \varphi_2 - \phi_P [\tanh(\xi + \xi_0) - \tanh(\xi - \xi_0)] \tag{9}$$

where $\xi \equiv g\phi_P(x - x_{c.m.})$, $\xi_0 \equiv \frac{1}{2} \cosh^{-1} \left(\sqrt{\frac{\frac{g^2}{2\pi} + \varphi_2^2}{\frac{g^2}{2\pi} - 1}} \right)$ and ϕ_P is a constant.

and where we have assumed $\mu/g \gg 1$ (neglecting corrections of order $O((g/\mu)^2)$), consistent with the conditions of validity of the gradient expansion, in order to obtain a closed form for the function that represents the sphaleron.

For the $\nu = 4$ case, we may assume a solution with radial symmetry so that we have, in the thin-wall approximation,

$$\varphi_{sph}(\tilde{\xi}) = \varphi_2 - \tilde{\phi}_P [\tanh(\tilde{\xi} + \tilde{\xi}_0) - \tanh(\tilde{\xi} - \tilde{\xi}_0)], \quad \tilde{\xi} \geq 0 \tag{10}$$

where we have imposed conditions analogous to the case $\nu = 2$.

Therefore, we have a true vacuum bubble, of radius $\tilde{\xi}_0$, centered at the origin. The situation is the same as we would have encountered in a purely bosonic system [1].

In the previous calculations, we have shown that a bubble-like configuration still satisfies the modified equations of motion (In fact, in the $\nu = 4$ case, we have no changes at all). These bubbles play the role of a background field in the determination of the fermionic spectrum. In fact, in some cases, instead of a simple continuum, we may have the presence of a gap and pairs of bound states [2, 5] (we will consider, for simplicity, just one pair). Therefore, if we have a richer spectrum, the calculation of the fermionic determinant, performed above, should be reviewed to deal explicitly with the bound states. The previous calculation of the determinant is the result of a gradient expansion approximation for the total trace, where we sum over all continuum and bound states. However, as we are interested in an effect that depends crucially on the relative occupation of the bound states [2], we should consider a finite density of fermions, i.e., a partial trace. Thus, instead of summing over all fermionic momenta (the restriction of small momenta is over the bosonic fields only), we shall sum them only up to the (occupied) top bound state.

Therefore, the complete effective action has the following form

$$\begin{aligned} \int S_{eff}[\phi] = & \int d^{\nu}x \left\{ \frac{1}{2}(\partial_{\mu}\phi)(\partial^{\mu}\phi) - [V(\phi) - V(\phi_2)] \right\} - \\ & - \frac{g}{2} \int d^{\nu}x \int [D\phi] \mathcal{G}(x, x) - \\ & - n_+ g \int_0^T dt_1 \int d\vec{x} \int_0^T dt_2 \int d\vec{y} \int [D\phi] \psi_B^*(\vec{x}, t_1, \{\phi_{sph}\}) \times \\ & \times \mathcal{G}(x, y) \psi_B(\vec{y}, t_2, \{\phi_{sph}\}) \end{aligned} \quad (11)$$

where ψ_B is the wavefunction of a bound state and n_+ is its occupation number ("doping").

The only term that remains to be calculated is the last one. Assuming that the occupation of the bound states will not affect in an appreciable way the form of the bubble (in the one-dimensional case, this is an exact result [2, 5]), we may rewrite this term as

$$S_{bound} = n_+ g T \int d\vec{x} \rho(\vec{x}) \phi_{sph}(\vec{x}) \quad (12)$$

where $\rho(\vec{x}) = \psi_B^*(\vec{x})\psi_B(\vec{x})$ is the normalized density of probability distribution of the bound charge. However, it is already known [3, 5] that the charge associated with a bubble tends to concentrate on its surface in a gaussian-like way. For our purposes, we will assume that a delta-like distribution will be a reasonable approximation.

In the $\nu = 2$ case, we may write the density ρ as $\rho = \frac{1}{2}[\delta(\xi - \xi_0) + \delta(\xi + \xi_0)]$.

The energy of the bubble, $E = -S_{eff}/T$, as a function of the radius ξ_0 , has the following form:

$$\begin{aligned} E(\xi_0) \approx & \int_{-\infty}^{+\infty} \frac{d\xi}{g\dot{\phi}_P} \left\{ \frac{1}{2} \left[1 + \frac{1}{12\pi} \left(\frac{g}{\mu} \right)^2 \right] (g\dot{\phi}_P)^2 \left(\frac{d\phi_{sph}}{d\xi} \right)^2 + [V(\phi_{sph}) - V(\phi_2)] \right\} - \\ & - n_+ \tanh(2\xi_0) \end{aligned} \quad (13)$$

where we have incorporated the contribution of the Dirac sea in the first term, by making use of the equation of motion. In fact, the contribution of the continuum is of order $O((g/\mu)^2)$ and may be neglected to this order of approximation. The only relevant contribution of fermions comes from the bound states.

In the $\nu = 4$ case, we may write the density ρ as $\rho = \frac{(g\dot{\phi}_P)^2}{4\pi\xi_0^2} \delta(\tilde{\xi} - \tilde{\xi}_0)$.

The energy of the bubble as a function of the radius $\tilde{\xi}_0$ has the following form:

$$\begin{aligned} E(\tilde{\xi}_0) \approx & \int_0^{\infty} 4\pi \frac{\tilde{\xi}^2}{(g\dot{\phi}_P)^2 (g\tilde{\phi}_P)} \frac{d\tilde{\xi}}{d\tilde{\xi}_0} \left\{ \frac{1}{2} (g\dot{\phi}_P)^2 \left(\frac{d\phi_{sph}}{d\tilde{\xi}} \right)^2 + [V(\phi_{sph}) - V(\phi_2)] \right\} - \\ & - n_+ \tanh(2\tilde{\xi}_0) \end{aligned} \quad (14)$$

To analyze the stability of the bubble-like solutions obtained above, we shall study the behaviour of the the energy of the bubble as a function of the bubble radius ξ_0 , now considered as a dynamical variable, s . The results, for the cases $\nu = 2$ and $\nu = 4$, are plotted in Fig. 1 and Fig. 2, respectively.

Our results for the $\nu = 2$ case should be compared with the exact results, previously obtained by using inverse scattering methods [2] (see Figs.). In this way, we may control our approximations. In fact, the observation of Fig.1 shows that our approximation preserves the "quantum stabilization" brought about by fermions. Nevertheless, we find a quantitative difference between the approximate and the exact results due, mainly, to our naive delta-like approximation for the fermionic density. In order to improve on this approximation, one may use a gaussian-like pattern or even the exact fermionic density in the presence of the sphaleron. However, in doing so, one can no longer use the simple analytic form of our analysis.

From our results, it is clear that the effects of fermions in an arbitrary number of space dimensions are due, almost exclusively, to the relative occupation of bound states. The states of the continuum contribute only to order $O((g/\mu)^2)$, and may be neglected. For $\nu = 2$ and $\nu = 4$, the new charged bubbles have the same functional form as the purely bosonic ones, except for a reparametrization, and have their stability drastically modified by the fermions: besides unstable bubbles, we find metastable bubbles as a result of a "quantum stabilization" brought about by the fermions. For $\nu = 2$, this result was obtained exactly in Ref.[2]. This striking feature may, in principle, be measured in some realistic systems. The two-dimensional case finds a natural application in the physics of linearly conducting polymers [3, 4, 5]. The results for the four-dimensional case may have important consequences for the physics of Baryogenesis and in some problems in Optics [8, 9].

From the results for the energy of the bubbles as a function of their radii, it is possible to calculate decay rates for the metastable states of the scalar field as explicit functions of time. This may be implemented by using the formalism presented in [1] and [2] and allows for a non-equilibrium description of the decay process for both $\nu = 2$ and $\nu = 4$ cases.

References

- [a)] e-mail: barci@symbcomp.uerj.br
- [b)] e-mail: fraga@if.ufrj.br
- [c)] e-mail: aragao@if.ufrj.br
- [1] D. Boyanovsky and C.A.A. de Carvalho, *Phys. Rev.* **D48**, 5850 (1993).
- [2] E.S. Fraga and C.A.A. de Carvalho, *Phys. Rev.* **B52**, 7448 (1995) and references therein.
- [3] Yu-Lu, "Solitons and Polarons in Conducting Polymers" (World Scientific), 1988 (and references therein).
- [4] D. Boyanovsky, C.A.A. de Carvalho and E.S. Fraga, *Phys. Rev.* **B50**, 2389 (1994).
- [5] C.A.A. de Carvalho, *Nucl. Phys.* **B324**, 729 (1989).
- [6] S. Novikov, S.V. Manakov, L.P. Pitaevskii and V.E. Zakharov, "Theory of Solitons" (Consultants Bureau), 1984.
- [7] C.A.A. de Carvalho, C.A. Bonato and G.B. Costamilan, *J. Phys. A: Math. Gen.* L1153-L1157 (1989).
- [8] Luiz Davidovich in *Multiphoton Processes, Proceedings of the 5th International Conference on Multiphoton Processes*, Paris, France, September, 1990. (Edited by G. Mainfray and P. Agostini).
- [9] M.E. Shaposhnikov, in 1991 Summer School in High Energy Physics and Cosmology, Trieste, Italy (World Scientific, Singapore, 1992).
- [10] Zhao-bin Su and B. Sakita, *Phys. Rev.* **B38**, 7421 (1988). Prasanta K. Panigrahi, Rashmi Ray and B. Sakita, *Phys. Rev.* **B42** 4036 (1990).
- [11] C.A.A. de Carvalho, D.G. Barci and L. Moriconi, *Phys. Rev.* **B50**, 4648 (1994).

Figure 1: Energy of the bubble as a function of its radius for $v=2$ (purely bosonic, exact results with fermions, approximate results with fermions)

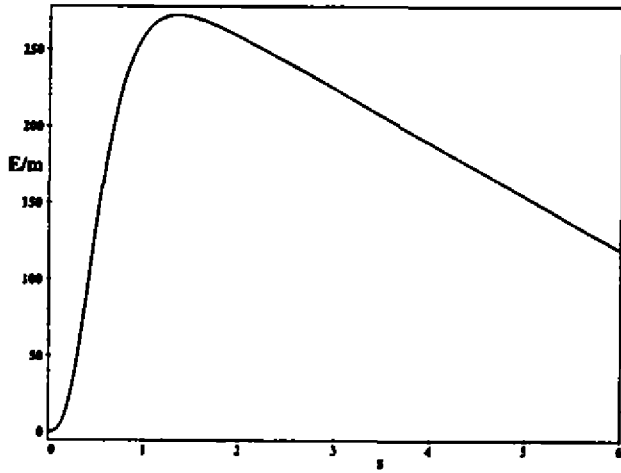
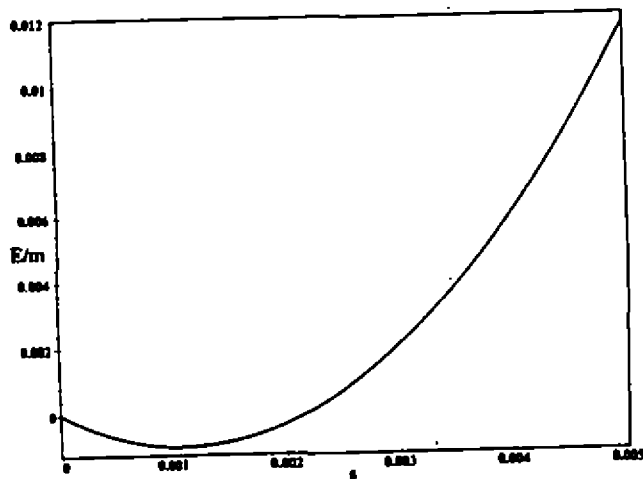
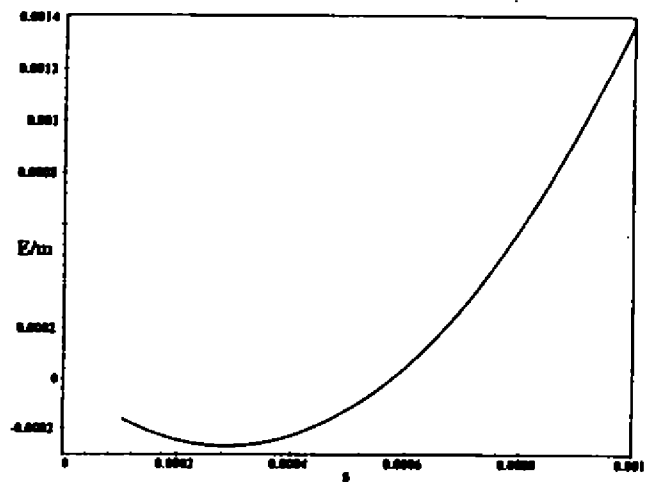
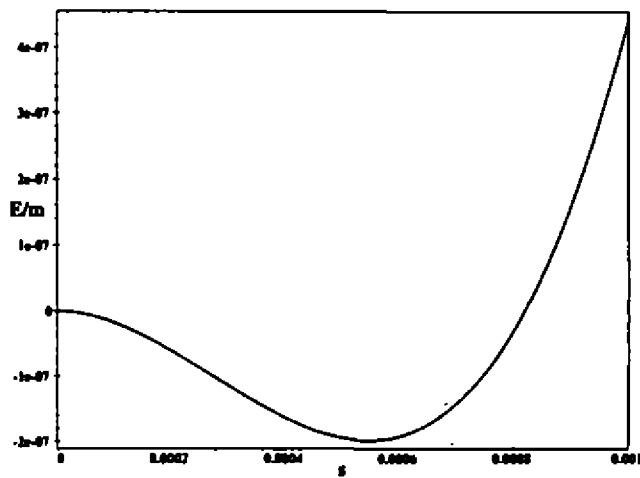
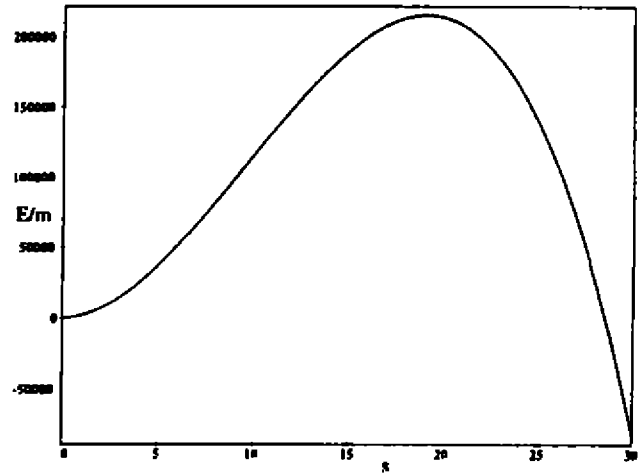


Figure 2: Energy of the bubble as a function of its radius for $v=4$ (purely bosonic, approximate results with fermions)



Cordas Magnéticas Quânticas a Temperatura Finita

D. G. G. Sasaki

Centro Brasileiro de Pesquisas Físicas (CBPF)

E. C. Marino

Universidade Federal do Rio de Janeiro (UFRJ)

We apply the *method of dual quantization* of topological excitations to magnetic strings in the Abelian Higgs Model in (3 + 1)-dimensions. In the approximation of constant absolute value of the Higgs field, we evaluate the correlation function of a closed and circular magnetic string, both at finite and in the zero temperature limit. We show that in zero temperature, only infinite strings exist as genuine excitations. However, the introduction of temperature makes the system unstable and even infinite strings disappear from physical spectrum.

1 Introdução

O objetivo central deste trabalho é determinar a influencia da temperatura no comportamento de cordas quânticas. Com este fim, juntamos a técnica de introdução de temperatura em TQC com o *método de quantização dual* [1], que é uma generalização dos conceitos de dualidade ordem-desordem da Mecânica Estatística. Este modelo foi escolhido porque é o mais simples daqueles que admitem cordas magnéticas como soluções clássicas estáveis.

2 Quantização Dual de cordas

O MHA é definido por:

$$\mathcal{L}_{HA} = -\frac{1}{4} F_{\mu\nu} F^{\mu\nu} + D_\mu \phi D^\mu \phi^* + V(\phi, \phi^*),$$

com

$$V(\phi^*, \phi) = -\frac{\lambda}{4} \left[\phi\phi^* - \frac{2m^2}{\lambda} \right]^2.$$

onde λ e m são parâmetros do modelo.

O potencial é infinitamente degenerado e a sua carga topológica conservada é o fluxo magnético ao longo de um plano transversal à corda.

Inicialmente, definimos uma álgebra dual, que obedece a simetria [2]:

$$\mu(\bar{x}, t) \phi(\bar{y}, t) = e^{i \arg(\bar{y} - \bar{x})} \phi(\bar{y}, t) \mu(\bar{x}, t)$$

e

$$\mu(\bar{x}, t) A_i(\bar{y}, t) = \left[A_i(\bar{y}, t) - \frac{1}{i} \partial_i^{(y)} \arg(\bar{y} - \bar{x}) \right] \mu(\bar{x}, t). \quad (1)$$

O ponto \bar{x} é o ponto em relação ao qual o ângulo $\arg(\bar{y} - \bar{x})$ é definido. Ele determina a posição em que a corda corta um plano transversal à ela.

Em [2] mostra-se que a ação do MHA pode ser escrita como:

$$S_{HA} = \int d^D z \left\{ \frac{1}{4} F_{\mu\nu} \left[1 + \frac{r^2 \rho^2}{(-\square)} \right] F^{\mu\nu} + \frac{1}{2} \partial_\mu \rho \partial^\mu \rho + \frac{1}{2} \rho^2 \partial_\mu \lambda \partial^\mu \lambda + V(\rho) - e \partial_\mu \rho^2 \left[\frac{\partial_\sigma F^{\mu\sigma}}{(-\square)} \right] \lambda - \frac{r^2}{2} \partial_\beta \rho^2 \left[\frac{\partial^\alpha F_{\mu\alpha}}{(-\square)} \frac{F^{\mu\beta}}{(-\square)} \right] \right\}.$$

A função de correlação dos operadores de desordem, no modelo de Maxwell livre são obtidas adicionando-se um campo externo apropriado ao $F^{\mu\nu}$. Então, na aproximação onde o campo de Higgs ρ é constante [2]:

$$\langle \mu(x) \mu^\dagger(y) \rangle = \frac{1}{Z[0]} \int D\rho D\chi DA_\mu \exp \left\{ - \int d^D z \left[\frac{1}{4} (F_{\mu\nu} + \tilde{B}_{\mu\nu}) \times \right. \right. \\ \left. \left. \left[1 + \frac{e^2 \rho^2}{(-\square)} \right] (F^{\mu\nu} + \tilde{B}^{\mu\nu}) + \frac{1}{2} \rho^2 \partial_\mu \chi \partial^\mu \chi + V(\rho) \right] \right\}. \quad (2)$$

tal que

$$\tilde{B}_{\mu\nu}(S) = \frac{2\pi}{c} \int_S d^2 \xi_{\mu\nu} \delta^4(z - \xi),$$

onde S é uma superfície genérica cujos contornos são as cordas L_x e L_y .

A expressão (2) é independente da superfície escolhida. Considere uma outra superfície genérica $S'(L)$, ligando as cordas L_x e L_y . Vamos efetuar a transformação:

$$A_\mu \rightarrow A_\mu + \Omega_\mu.$$

com

$$\Omega_\mu = \frac{2\pi}{c} \int_{V(S,S')} d^3 \xi_\mu \delta^4(z - \xi),$$

onde $V(S, S')$ é o volume limitado pelas superfícies S e S' . Sob esta mudança de variável,

$$F_{\mu\nu} \rightarrow F_{\mu\nu} + \tilde{B}_{\mu\nu}(S') - \tilde{B}_{\mu\nu}(S).$$

Logo, (2), é claramente invariante de superfície.

Sejam duas superfícies S_x e S_y , com orientações opostas e presas, respectivamente, às cordas L_x e L_y , como bandeiras em um mastro. No caso de cordas fechadas, as superfícies assumem a configuração de membranas ligadas a um aro. Escolhendo-as, de modo a se superporem, formando a superfície S , temos:

$$\langle \mu(x) \mu^\dagger(y) \rangle_S = \frac{1}{Z[0]} \int DA_\mu \exp \left\{ - \int d^4 z \left[\mathcal{L}_R + \frac{\pi}{c} \int_{S_x} \delta^4(z - \xi) F^{\mu\nu} d^2 \xi_{\mu\nu} \right. \right. \\ \left. \left. - \frac{\pi}{c} \int_{S_y} \delta^4(z - \xi) F^{\mu\nu} d^2 \xi_{\mu\nu} \right] \right\}.$$

Nesta forma, podemos extrair uma representação explícita do operador de criação de cordas, no espaço de Minkowski:

$$\mu(x) = \exp - \frac{\pi i}{c} \int_{S_x} F^{\mu\nu} d^2 \xi_{\mu\nu}.$$

Calculando-se (2), mostra-se que o operador μ não gera estados topológicos reais [2].

O comutador entre o operador μ e Φ é obtido em [2]:

$$[\Phi, \mu(x)] = \mu(x) \int d^2 z \frac{2\pi}{c} \delta^2(\bar{x} - \bar{y}) = \frac{2\pi}{c} \mu(x),$$

demonstrando que μ gera cordas formadas por $\frac{2\pi}{c}$ unidades de fluxo magnético.

A relação de comutação do μ com A_i [2]:

$$\left[\mu(\bar{x}, t), A_i(\bar{y}, t) \right] = \frac{1}{c} \mu(x) \partial_i^{(y)} \arg(\bar{y} - \bar{x}). \quad (3)$$

Verificamos que (3) e (1), são iguais. Estas relações caracterizam μ como um operador que cria cordas magnéticas quânticas.

2.1 A função de correlação da corda quântica a temperatura finita

Em [2] a expressão foi conseguida:

$$\langle \mu(x) \mu^1(y) \rangle_C = \exp \left\{ -\frac{2\pi^2}{\epsilon^2} \sum_{i,j=1}^2 \lambda_i \lambda_j \oint_{C_{x_i}} d\xi^i \oint_{C_{x_j}} d\eta^j F_M(\xi - \eta) \right\}, \tag{4}$$

onde C_{x_i} é o contorno da superfície $S(C_{x_i})$, $x_1 \equiv x$, $x_2 \equiv y$, $\lambda_1 = 1$ e $\lambda_2 = -1$ e

$$F_M = \mathcal{F}^{-1} \left[\frac{1}{-\square} + \frac{M^2}{(-\square)^2} \right].$$

A introdução de temperatura em TQC é realizada através das regras de Feynman no espaço Euclideo, com as substituições abaixo [3]:

$$\begin{aligned} \int \frac{d^4 k}{(2\pi)^4} &= \frac{1}{\beta} \sum_n \int \frac{d^3 k}{(2\pi)^3}, \\ k_0 &= \omega_n = \frac{2\pi n}{\beta}, \\ (2\pi)^4 \delta^4(k_1 + k_2 + \dots) &= -(2\pi)^3 \beta \delta_{\omega_1 + \omega_2 + \dots} \times \delta^3(\vec{k}_1 + \vec{k}_2 + \dots). \end{aligned}$$

onde β é o inverso da temperatura.

Calculando-se (4) a temperatura finita [4]:

$$\begin{aligned} \langle \mu(\vec{x}, t) \mu^1(\vec{y}, t) \rangle_C &= \exp \left\{ -\frac{2\pi^2}{\epsilon^2} \sum_{i,j=1}^2 \lambda_i \lambda_j \oint_{C_{x_i}} \oint_{C_{x_j}} d\xi^i d\eta^j \left[-\frac{1}{4\pi\beta} \frac{1}{D} \right. \right. \\ &\quad \left. \left. + \frac{1}{2\pi\beta} \frac{1}{D(1 - e^{-\frac{2\pi}{\beta} D})} - \frac{M^2}{8\pi\beta} D - \frac{M^2}{8\pi^2} \ln(1 - e^{-\frac{2\pi}{\beta} D}) \right] \right\}. \end{aligned} \tag{5}$$

Esta expressão para a função de correlação é válida para qualquer configuração de cordas fechadas a temperatura finita, dentro da aproximação considerada. Podemos utilizá-la também para cordas retas e infinitas [2].

A configuração geométrica mais simples é aquela com simetria cilíndrica (Fig. 1).

Para esta configuração a expressão (5) torna-se [4]:

$$\begin{aligned} \langle \mu(\vec{x}, t) \mu^1(\vec{y}, t) \rangle &= \exp \left\{ -\frac{4\pi^3 R^2}{\epsilon^2} \sum_{i,j=1}^2 \lambda_i \lambda_j \left[-\frac{1}{2\pi\beta} \int_0^\pi \frac{d\alpha \cos \alpha}{\sqrt{H_{ij}^2 + 2R^2(1 - \cos \alpha)}} \right. \right. \\ &\quad \left. - \frac{M^2}{4\pi\beta} \int_0^\pi d\alpha \cos \alpha \sqrt{H_{ij}^2 + 2R^2(1 - \cos \alpha)} \right. \\ &\quad \left. + \frac{1}{\pi} \int_0^\pi \frac{d\alpha \cos \alpha}{\sqrt{H_{ij}^2 + 2R^2(1 - \cos \alpha)}} \frac{1}{\beta \left(1 - e^{-\frac{2\pi}{\beta} \sqrt{H_{ij}^2 + 2R^2(1 - \cos \alpha)}} \right)} \right. \\ &\quad \left. - \frac{M^2}{4\pi^2} \int_0^\pi d\alpha \cos \alpha \ln \left(1 - e^{-\frac{2\pi}{\beta} \sqrt{H_{ij}^2 + 2R^2(1 - \cos \alpha)}} \right) \right] \right\}. \end{aligned} \tag{6}$$

onde

$$H_{ij} = \begin{cases} H & \text{para } i \neq j \\ 0 & \text{para } i = j \end{cases}.$$

Se assumirmos de início que $H \rightarrow \infty$, a primeira integral claramente irá se anular e a segunda integral terá um termo dominante H ; no entanto o integrando está multiplicado por $\cos \alpha$ e a integral, neste intervalo, será zero. Finalmente, as duas integrais restantes, só poderão dar uma contribuição não nula quando β , no argumento

da exponencial, for também infinito. Logo, concluímos que a função de correlação a longas distâncias será 1, e portanto trivial, a menos que β seja infinito (temperatura zero).

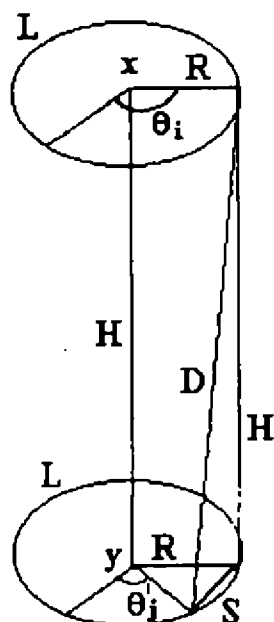


Figura 1.

2.1.1 Limite de temperatura zero

O resultado de (6) no limite de temperatura zero é [4]:

$$\langle \mu(\bar{x}, t) \mu^\dagger(\bar{y}, t) \rangle = \exp \left\{ \sum_{i,j=1}^2 \lambda_i \lambda_j \left[-\frac{\pi^2}{e^2} \frac{H_{ij}^2 + 2R^2}{H_{ij} \sqrt{H_{ij}^2 + 4R^2}} + \frac{M^2 \pi^2 R^2}{2e^2} + \frac{H_{ij} - \sqrt{H_{ij}^2 + 4R^2}}{H_{ij} + \sqrt{H_{ij}^2 + 4R^2}} \right] \right\}.$$

Os termos com $i = j$ são auto-interações das cordas, sendo portanto não físicos. Renormalizamos o operador:

$$\mu_r = \mu \exp \frac{\pi^2 R}{e^2 |\bar{c}|}.$$

para $|\bar{c}| \rightarrow 0$. Substituindo $H_{ij} = H$ e realizando o somatório em λ , então:

$$\langle \mu(\bar{x}, t) \mu^\dagger(\bar{y}, t) \rangle_r = \exp \left\{ \frac{2\pi^2}{e^2} \frac{H^2 + 2R^2}{H \sqrt{H^2 + 4R^2}} - \frac{M^2 \pi^2 R^2}{e^2} + \frac{H - \sqrt{H^2 + 4R^2}}{H + \sqrt{H^2 + 4R^2}} \right\}$$

◊ $H \gg R$

$$\langle \mu(\bar{x}, t) \mu^\dagger(\bar{y}, t) \rangle_r = \exp \left\{ -\frac{8\pi^2}{e^2} \frac{R^4}{|\bar{x} - \bar{y}|^4} + \frac{M^2 \pi^2}{e^2} \frac{R^4}{|\bar{x} - \bar{y}|^2} \right\}.$$

Tomando o limite de longas distâncias ($|\bar{x} - \bar{y}| \rightarrow \infty$), $\langle \mu \mu^\dagger \rangle_r = 1$. Logo, o operador μ cria estados de vácuo.

◦ $R \gg H$

$$\langle \mu(\bar{x}, t) \mu^\dagger(\bar{y}, t) \rangle_r = \exp \left\{ \frac{2\pi^2}{c^2} \frac{R}{|\bar{x} - \bar{y}|} - \frac{M^2 \pi^2}{c^2} R |\bar{x} - \bar{y}| \right\}.$$

O seu comportamento assintótico é $\langle \mu \mu^\dagger \rangle_r = 0$.

Observe que como $R \gg H$, ao fazermos o limite assintótico, automaticamente estamos considerando cordas infinitas. Logo, apenas estas constituem estados legítimos.

A densidade de energia da corda é:

$$\mathcal{M} = \frac{M^2 \pi}{2c^2} H. \quad (7)$$

3 Conclusão

A conclusão pode ser sumarizada do seguinte modo:

◦ Temperatura zero

No caso de cordas com tamanho finito, não existem estados quânticos associados. Somente para cordas infinitas existem tais estados físicos. A densidade de energia da corda circular infinita é idêntica à corda reta infinita.

◦ Temperatura finita

Para cordas finitas, o mesmo comportamento a temperatura zero é mantido. No entanto, para cordas infinitas, os estados quânticos de corda são proporcionais ao vácuo e portanto não se constituem em estados físicos genuínos. A inclusão de temperatura desestabiliza os estados quânticos de cordas fechadas e infinitas, que estavam presentes a temperatura zero. Este é o principal resultado deste trabalho.

References

- [1] E. C. Marino, in *Applications of Statistical and Field Theory Methods in condensed matter. Proceedings of NATO Advanced Study Institute*, D. Baeriswyl, A. Bishop e J. Carmelo Eds., Plenum, New York, 1992.
- [2] E. C. Marino, *Phys. Rev.* **D53** (1996) 1001.
- [3] C. W. Bernard, *Phys. Rev.* **D12** (1974) 3312.
- [4] D. G. G. Sasaki, *Cordas Magnéticas Quânticas a Temperatura Finita*, Tese de Mestrado, CBPF, setembro de 1996.

Blindagem versus Confinamento na QCD em 2 Dimensões

E. Abdalla,* R. Mohayaee

International Centre for Theoretical Physics, Trieste, Itália

A. Zadra

Instituto de Física, USP, São Paulo, Brasil

A propriedade de confinamento dos constituintes fundamentais da matéria ainda não é totalmente compreendida. Trata-se de um dos problemas fundamentais da física teórica. Há dois fenômenos aparentemente relacionados, o confinamento e a blindagem das cargas, que não devem ser confundidos. Para diferenciá-los, foram importantes os estudos da eletrodinâmica quântica em duas dimensões (QED2), conhecida como modelo de Schwinger. Nosso objetivo, neste trabalho, é o de estender estes estudos para o caso não-abeliano: para a cromodinâmica quântica em duas dimensões (QCD2). Discutimos as propriedades de blindagem e confinamento de cargas (de côm), usando uma versão bosonizada da QCD2. Nossos cálculos se baseiam em soluções estáticas das equações semi-clássicas de campo. Levamos em consideração a possibilidade dos campos estarem em diferentes representações. Nossa conclusão é de que prevalece a fase de blindagem, ao invés de confinamento, mesmo quando as partículas (quarks) possuem uma pequena massa. Para confirmar este resultado, esboçamos a construção dos operadores que correspondem aos quarks blindados.

1 Introdução

Nosso objetivo é o de descobrir em que condições (da massa, constante de acoplamento, representação dos férmions) a QCD_2 exhibe confinamento ou está na fase de Higgs (blindagem). Fomos motivados pelos resultados de outros grupos, que dizem obter **confinamento** para férmions massivos na representação adjunta. Adotamos como estratégia a solução semi-clássica do modelo bosonizado da QCD e, ao contrário dos outros grupos, obtemos **blindagem** para férmions massivos.

Lembre-mos da diferença entre confinamento e blindagem. No fenômeno de confinamento, os estados de quark estão *permanentemente ligados*. Por outro lado, a blindagem se caracteriza pela impossibilidade de reconhecermos cargas (*cores*) individuais. Para distinguir estes fenômenos, podemos usar o teste do par quark-antiquark, calculando sua energia potencial de ligação $V_{q\bar{q}}(L)$ em função da distância L entre eles. Na fase de confinamento, a energia varia linearmente com a distância, e o loop de Wilson depende da área A :

$$V_{q\bar{q}} \sim \sigma L \iff \langle W(C) \rangle \sim e^{-\sigma A}$$

Já na fase de Higgs (blindagem), a energia tende assintoticamente a uma constante, e o loop de Wilson obedece à lei do perímetro P :

$$V_{q\bar{q}} \sim 1 - e^{-mL} \iff \langle W(C) \rangle \sim e^{-uP}$$

Este teste pode eventualmente falhar devido à criação de pares. Um critério mais rigoroso consiste em introduzir outros números quânticos (sabores): quando existem estados com sabores observáveis ou distinguíveis, teremos blindagem; se os sabores não forem distinguíveis, teremos confinamento.

*Endereço permanente: Instituto de Física-USP, C.P. 66318, S. Paulo, Brasil.

2 Lições da teoria abeliana

O limite abeliano da QCD bidimensional é o modelo de Schwinger, definido pela lagrangeana

$$\mathcal{L} = \bar{\psi}(i \not{D} - M)\psi - \frac{1}{4} F_{\mu\nu} F^{\mu\nu}$$

onde

$$\not{D} = \gamma^\mu(\partial_\mu + ieA_\mu), \quad F_{\mu\nu} = \partial_\mu A_\nu - \partial_\nu A_\mu = \epsilon_{\mu\nu} F$$

F — campo elétrico

e — constante de acoplamento, dimensão de massa

Na versão bosonizada, este modelo é descrito pela seguinte lagrangeana

$$\mathcal{L} = \frac{1}{2} F^2 + \frac{1}{2} (\partial_\mu E)^2 + \frac{c}{\sqrt{\pi}} FE + 2m^2 [\cos(2\sqrt{\pi}E + \theta) - 1]$$

onde

E — campo mesônico, θ — vácuo-teta

$2m^2 = \Sigma M$, $\Sigma = e \frac{\exp(i\theta)}{2\pi^2} =$ condensado fermiônico

Nesta teoria bosonizada, efeitos quânticos (como geração de massa e vácuo-teta) se apresentam já no nível lagrangeano. Por este motivo, o teste semi-clássico do dipolo fornece respostas corretas. Colocando duas cargas-de-prova externas, segundo a distribuição de cargas

$$\rho(x) = -q \left[\delta\left(x - \frac{L}{2}\right) - \delta\left(x + \frac{L}{2}\right) \right] = \frac{c}{\sqrt{\pi}} \frac{\partial}{\partial x} Q(x)$$

chegamos à seguinte equação de movimento (independente-do-tempo) para o campo $E(x)$:

$$E'' = \frac{e^2}{\pi}(E - Q) + 4\sqrt{\pi}m^2 \sin(2\sqrt{\pi}E + \theta)$$

De sua solução, obtém-se a energia potencial do par de cargas,

$$V(L) = \frac{q^2}{2} L - \frac{qc}{2\sqrt{\pi}} \int_{-L/2}^{L/2} dx E(x)$$

de onde se faz o teste:

SE $V(L) \xrightarrow{L \rightarrow \infty} \text{const.}$ ENTÃO blindagem

SE $V(L) \xrightarrow{L \rightarrow \infty} \infty$ ENTÃO confinamento

Com as hipóteses de campo E "fraco", contínuo e E' contínuo, chega-se aos seguintes resultados:

(i) $m = 0$, $\theta = 0$, q qualquer \implies blindagem:

$$V(L) = \frac{q^2 \sqrt{\pi}}{2e} \left(1 - e^{-L/\sqrt{\pi}} \right)$$

(ii) $m \neq 0$, $\theta = 0$, q qualquer \implies confinamento:

$$V(L) = \frac{e^2 q^2}{2\pi\alpha^3} (1 - e^{-\alpha L}) + \frac{q^2}{2} \left(1 - \frac{e^2}{\pi\alpha^2} \right) L, \quad \alpha = \sqrt{\frac{e^2}{\pi} + 8\pi m^2}$$

(iii) $m \neq 0$, $q = e$: blindagem para $\theta = \pi$ e confinamento para $\theta \neq \pi$

$$V(L) \approx \frac{e^4}{2\pi\alpha^3} (1 - e^{-\alpha L}) + \frac{e^2}{2\pi} \left(1 - \frac{e^2}{\pi\alpha^2} \right) (\theta - \pi)L$$

Estas previsões semiclássicas são confirmadas pela construção dos chamados *estados exóticos*. Com a introdução uma simetria interna $SU(k)$ (sabor), define-se um operador fermiônico que carrega sabor,

$$\mathcal{F}_f = e^{i\sqrt{\pi}\gamma_5 \chi_f + i\sqrt{\pi} \int_{x^1}^{x^2} dx^1 \chi_f(x^0, x^1)}$$

a partir do qual se constroem os mesons (\mathcal{M}) e barions (\mathcal{B}):

$$\mathcal{M} = \mathcal{F}_f \mathcal{F}_j^\dagger \quad \mathcal{B} = \prod_{i=0}^k \mathcal{F}_i$$

Para férmions sem massa ($m = 0$), \mathcal{F}_f comuta com a hamiltoniana, e conclui-se que os quarks **blindados** são observáveis. Se $m \neq 0$ e $\theta = \frac{\pi}{2}$, também se constroem operadores que comutam com a hamiltoniana. Se $m \neq 0$ e $\theta \neq \frac{\pi}{2}$, \mathcal{F}_f não gera auto-estados da hamiltoniana, e assim temos confinamento.

3 Estudando a QCD₂

O modelo fermiônico da QCD com férmions numa representação arbitrária é dado por

$$\mathcal{L} = -\frac{1}{4} \text{tr} F_{\mu\nu} F^{\mu\nu} + \bar{\psi}_i^f (i \not{\partial} \delta^{ij} + e \not{A}^{ij}) \psi_j^f - M \bar{\psi}^f \psi^f$$

onde ψ_j^f : i = índice de cor; $f = 1, \dots, k$ = índice de sabor.

Segundo Gross *et.al.* (hep-th/9511104), cujo critério foi o cálculo do coeficiente-de-área (σ) no loop de Wilson

$$\langle W(C) \rangle = \langle \exp i q \int_C A_\mu dx^\mu \rangle \sim e^{-\sigma A}$$

se $M = 0$, então $\sigma = 0$ (**blindagem**) mesmo quando os férmions estão na representação adjunta (!). Por outro lado, se $M \neq 0$, então eles obtêm $\sigma = 2\Sigma M \neq 0$ (**confinamento**), onde $\Sigma = -\langle \bar{\psi} \psi \rangle$ = condensado fermiônico.

Na tentativa de reproduzir estes resultados, consideramos o modelo de QCD bosonizada, dado pela ação

$$S = S_{YM}[\beta, C] + k\Gamma[\beta] + \sum_f \Gamma[g_f] - (c_v + k)\Gamma[\Sigma] + S_{gh}$$

onde

$\Gamma[\dots]$ = ação de WZW

$$S_{YM} = \int d^2x \text{tr} \left[\frac{1}{2} (\partial_+ C_-)^2 + i\lambda C_- \beta^{-1} \partial_+ \beta \right]$$

$$S_m = m^2 \sum_{f=1}^k (\Sigma g_f^{-1} \beta^{-1} - \beta g_f \Sigma^{-1})$$

g_f = setor sem massa dos fermions bosonizados

(β, C) = setor massivo dos fermions bosonizados

Σ = excitações com métrica negativa

$$c_v = \text{Casimir: } f^{abc} f^{dbc} = \frac{1}{2} c_v \delta^{ad}$$

$$\lambda = \frac{c}{2\pi} (c_v + k)$$

$$m^2 = \mu M, \quad \mu = \text{parametro de renormalizacao}$$

Na construção deste modelo, fizemos a hipótese de que o termo de massa $M \int \bar{\psi} \psi$ possa ser tratado perturbativamente e bosonizado.

Seguindo o teste do potencial quark-antiquark, começamos introduzindo um par de quarks-de-prova de cores q^a e $-q^a$ nos pontos $x = L/2$ e $x = -L/2$, o que se faz pela transformação

$$i(\beta^{-1} \partial_+ \beta)^a \longrightarrow i(\beta^{-1} \partial_+ \beta)^a - \frac{2\pi}{e} q^a \left(\delta(x - \frac{L}{2}) - \delta(x + \frac{L}{2}) \right)$$

na ação acima. Em seguida, resolvemos as equações de movimento, na aproximação linear (i.e. *campos fracos*) e calculamos a energia potencial interquarks pela fórmula

$$V(L) = -(c_v + k) q^a (C_-^a(L/2) - C_-^a(-L/2))$$

Por fim, estudamos o que acontece quando $L \rightarrow \infty$.

Como resultado, temos o seguinte potencial:

$$V(L) = \frac{(c_v + k)^2 q^2}{2k} \times$$

$$\left[\left(\frac{4\pi\lambda^2 - km_-^2}{m_+^2 - m_-^2} \right) \left(\frac{1 - e^{-m_+L}}{m_+} \right) + \left(\frac{km_+^2 - 4\pi\lambda^2}{m_+^2 - m_-^2} \right) \left(\frac{1 - e^{-m_-L}}{m_-} \right) \right]$$

onde

$$c = \frac{c_v}{(c_v + k)}$$

$$m_{\pm}^2 = \frac{2\pi}{t} \left[(\lambda^2 + (1+c)2km^2) \pm \sqrt{(\lambda^2 + (1+c)2km^2)^2 - 8ck\lambda^2 m^2} \right]$$

de onde inferimos que:

- $V(L)$ permanece *finito* quando $L \rightarrow \infty \Rightarrow$ *blindagem*
- há duas escalas de massa, $m_+ > m_-$, para os campos de gauge.
- quando os férmions não têm massa ($m = 0$) então $m_- = 0$ e $m_+ = \sqrt{\pi}/k\lambda$.

$$V(L) = \frac{(c_v + k)\sqrt{\pi} q^2}{2} \frac{1}{t} (1 - e^{-2\sqrt{\pi}\lambda L})$$

- no limite $c_v \rightarrow 0$, reobtemos os resultados do modelo de Schwinger com $\theta = 0$.

4 Conclusão

O estudo semi-clássico da $QC D_2$ bosonizada prevê o fenômeno de blindagem, e não de confinamento, mesmo quando os férmions (numa representação arbitrária) possuem uma pequena massa. Uma verificação rigorosa exige a construção operadores fermiônicos (*estados exóticos*) que carreguem outros números quânticos (sabores). Resta também calcularmos o valor crítico da massa dos férmions para a qual ocorra a transição de fase blindagem — confinamento.

References

- [1] E. Abdalla, R. Mohayaee, A. Zadra, a ser publicado no *Int. J. Mod. Phys. A*, IC/96/51, hep-th/9604063.

The q-Virasoro Algebra Obtained by an Analogue of the Hamiltonian Reduction Procedure

E. Batista*, J.F. Gomes†, I.J. Lautenschleguer‡

Instituto de Física Teórica UNESP

September 1996

In this work we introduce a new kind of q-Deformed Virasoro Algebra. This Algebra is obtained from the Quantum Current Algebra $U_q(\widehat{su}(2))$, by imposing constraints on the currents and performing the Dirac Bracket procedure.

I Introduction

The Hamiltonian Reduction of WZNW models is well established in the literature [2]. WZNW models are 2 dimensional quantum field theories in which the fields take values on a Group Manifold and the action consists of a chiral term and another term of topological origin. The conserved currents of the model satisfy a Kac-Moody Algebra with respect to their Poisson Brackets. The Hamiltonian Reduction process consists in imposing constraints on the currents of the model and reduce, by means of these constraints, the number of fields in the action. Choosing appropriated constraints, the resulting models are the so called Conformal Toda Models. The Dirac Brackets of the remaining currents close an extended Conformal Algebra (W_n). For instance, if the Group Manifold is $SU(2)$, this process gives us the Liouville Model and the Conformal Algebra of the remaining currents is the Virasoro Algebra.

Our approach consists in taking only Current Algebras, discarding the field theoretic substract, given in terms of OPE relations. We then use an specific prescription to define Poisson Brackets associated to OPEs. In order to ensure that our construction is consistent, we apply this method to the classical case, where the results are well known. Finally we take the Quantum Current Algebra $U_q(\widehat{su}(2))$ and construct the Dirac Brackets after imposing the constraints on the currents. Verifying carefully in each step the classical ($q \rightarrow 1$) limit, we obtain a new kind of q-Deformed Virasoro Algebra.

II From OPEs to Poisson Brackets

In the context of Conformal Field Theories it is usual to deal with OPE relations. In 2-dimensional field theories the time ordering is replaced by radial ordering, and contractions among fields usually appear as poles in the complex plane. Let $A(z)$ and $B(w)$ be two fields on a 2-dimensional space, the OPE relation among A and B read

$$A(z)B(w) = \sum_{0 < n \leq h(A,B)} \frac{[AB]_n(w)}{(z-w)^n} + \text{regular terms}, \quad (1)$$

where $h(A, B)$ is the highest order pole appearing in the OPE, which, obviously, depends on A and B . It is possible to define Poisson Brackets associated to OPE relations [3], the Poisson Brackets related to (1) is given by the expression

$$\{A(z), B(w)\}_{PB} = \sum_{n > 0} \frac{(-1)^{n-1}}{(n-1)!} \{AB\}_n(w) \partial_z^{n-1} \delta(z-w), \quad (2)$$

making the correspondence $[AB]_n(w) = \{AB\}_n(w)$.

*Supported by FAPESP

†Supported in part by CNPq

‡supported by CNPq

Some remarks are needed about these Poisson Brackets: First, the time coordinate in this case is the variable \bar{z} . Moreover, the Poisson Brackets ignore double contractions, which appear in OPEs of chains of fields, as stated by Wick Theorem, then we may consider these Poisson Brackets as the "classical" counterpart of the OPE.

III The Classical Case

Let us start with the Current Algebra $\widehat{su}(2)$, with generators $\{I\}$

$$\begin{aligned} H(z) &= \sum_{n=-\infty}^{\infty} H_n z^{-n-1}, \\ E^{\pm}(z) &= \sum_{n=-\infty}^{\infty} E_n^{\pm} z^{-n-1}. \end{aligned} \tag{3}$$

These currents satisfy the following OPE relations ($k = 1$):

$$\begin{aligned} H(z)H(w) &= \frac{1}{(z-w)^2} + \text{regular terms}, \\ H(z)E^{\pm}(w) &= \pm \frac{\sqrt{2}E^{\pm}(w)}{z-w} + \text{regular terms}, \\ E^{\pm}(z)E^{\mp}(w) &= \pm \frac{\sqrt{2}H(w)}{z-w} + \frac{1}{(z-w)^2} + \text{regular terms}. \end{aligned} \tag{4}$$

The associated Poisson Brackets (2) of the OPE relations (4) are

$$\begin{aligned} \{H(z), H(w)\}_{PB} &= -\delta'(z-w), \\ \{H(z), E^{\pm}(w)\}_{PB} &= \pm\sqrt{2}E^{\pm}(w)\delta(z-w), \\ \{E^{\pm}(z), E^{\mp}(w)\}_{PB} &= \pm\sqrt{2}H(w)\delta(z-w) - \delta'(z-w). \end{aligned} \tag{5}$$

If we impose the following constraints in currents (3),

$$\begin{aligned} \chi_1(z) &= H(z), \\ \chi_2(z) &= E^+(z) - 1, \end{aligned} \tag{6}$$

which are of second class, the Dirac Matrix, $\Delta_{ij}(z, w) = \{\chi_i(z), \chi_j(w)\}_{PB}$, read

$$\Delta(z, w) = \begin{pmatrix} -\delta'(z-w) & \sqrt{2}\delta(z-w) \\ -\sqrt{2}\delta(z-w) & 0 \end{pmatrix}, \tag{7}$$

and the inverse is

$$\Delta^{-1}(z, w) = \begin{pmatrix} 0 & -\frac{1}{\sqrt{2}}\delta(z-w) \\ \frac{1}{\sqrt{2}}\delta(z-w) & -\frac{1}{2}\delta'(z-w) \end{pmatrix}. \tag{8}$$

The Dirac Bracket of the remaining current $E^-(z)$, defined by

$$\begin{aligned} \{E^-(z), E^-(w)\}_{DB} &= \{E^-(z), E^-(w)\}_{PB} + \\ &- \int dw' dw'' \{E^-(z), \chi_i(w')\}_{PB} \Delta_{ij}^{-1}(w', w'') \{\chi_j(w''), E^-(w)\}_{PB}. \end{aligned}$$

results in

$$\begin{aligned} \{E^-(z), E^-(w)\}_{DB} &= \partial_w E^-(w)\delta(z-w) - 2E^-(w)\delta'(z-w) + \\ &+ \frac{1}{2}\delta'''(z-w). \end{aligned} \tag{9}$$

This algebra is a Virasoro Algebra with central charge $c = -6$, obtained by the procedure described in previous section from the OPE ($T(z) = E^-(z)$)

$$T(z)T(w) = \frac{\partial_w T(w)}{z-w} + \frac{2T(w)}{(z-w)^2} + \frac{-6}{(z-w)^4} \tag{10}$$

IV The q -Deformed Case

The Quantum Current Algebra $\mathcal{U}_q(\widehat{su}(2))$ is generated by currents [1]

$$\begin{aligned} E^\pm(z) &= \sum_{n=-\infty}^{\infty} E_n^\pm z^{-n-1}, \\ \Psi(z) &= \sum_{n \geq 0} \Psi_n z^{-n} = q^{\sqrt{2}H_0} \exp \left\{ \sqrt{2}(q - q^{-1}) \sum_{n > 0} H_n z^{-n} \right\}, \\ \Phi(z) &= \sum_{n \leq 0} \Phi_n z^{-n} = q^{-\sqrt{2}H_0} \exp \left\{ -\sqrt{2}(q - q^{-1}) \sum_{n < 0} H_n z^{-n} \right\}. \end{aligned} \quad (11)$$

The only OPE relations among these currents having singular terms are ($k = 1$)

$$\begin{aligned} \Psi(z)\Phi(w) &= \frac{(z - wq^3)(z - wq^{-3})}{(z - wq)(z - wq^{-1})} \Phi(w)\Psi(z), \\ \Psi(z)E^\pm(w) &= q^{\pm 2} \frac{(z - wq^{\mp \frac{3}{2}})}{(z - wq^{\pm \frac{3}{2}})} : E^\pm(w)\Psi(z) :, \\ E^\pm(z)\Phi(w) &= q^{\pm 2} \frac{(z - wq^{\mp \frac{3}{2}})}{(z - wq^{\pm \frac{3}{2}})} : \Phi(w)E^\pm(z) :, \\ E^+(z)E^-(w) &= \frac{1}{w(q - q^{-1})} \left[\frac{\Psi(wq^{\frac{1}{2}})}{z - wq} - \frac{\Phi(wq^{-\frac{1}{2}})}{z - wq^{-1}} \right] + \text{r.t.}, \\ E^-(z)E^+(w) &= \frac{1}{w(q - q^{-1})} \left[\frac{\Phi(wq^{\frac{1}{2}})}{z - wq} - \frac{\Psi(wq^{-\frac{1}{2}})}{z - wq^{-1}} \right] + \text{r.t.} \end{aligned} \quad (12)$$

The analogues of classical constraints (6) are given by

$$\begin{aligned} \chi_1^q(z) &= \frac{\Psi(z) - \Phi(z)}{\sqrt{2}z(q - q^{-1})}, \\ \chi_2^q(z) &= E^+(z) - 1. \end{aligned} \quad (13)$$

These constraints have as classical limit ($q \rightarrow 1$) the set of constraints (6). The Dirac Matrix for (13) read

$$\Delta_q(z, w) = \begin{pmatrix} -\frac{[2]}{2} D_{q(z)} \delta(z - w) & \frac{[2]}{\sqrt{2}} q^{-\frac{3}{2}} \delta(zq^{-\frac{3}{2}} - w) \\ -\frac{[2]}{\sqrt{2}} \delta(zq^{-\frac{3}{2}} - w) & 0 \end{pmatrix}, \quad (14)$$

where

$$D_{q(z)} f(z) = \frac{f(zq) - f(zq^{-1})}{z(q - q^{-1})}$$

and

$$[x] = \frac{q^x - q^{-x}}{q - q^{-1}}.$$

The inverse of (14) is

$$\Delta_q^{-1}(z, w) = \begin{pmatrix} 0 & -\frac{\sqrt{2}}{[2]} \delta(zq^{\frac{3}{2}} - w) \\ \frac{\sqrt{2}}{[2]} q^{\frac{3}{2}} \delta(zq^{\frac{3}{2}} - w) & -\frac{q^3}{[2]} D_{q(zq^3)} \delta(zq^3 - w) \end{pmatrix}. \quad (15)$$

In the classical limit the matrices (14) and (15) tend to (7) and (8) respectively.

Finally, let us calculate the Dirac Bracket of the current $E^-(z)$, which gives us a quantum version of the Virasoro Algebra (9). The resulting algebra has the form

$$\begin{aligned} \{E^-(z), E^-(w)\}_{DB} &= q^{-6} (D_{q(wq^{-3})} E^-(wq^{-3})) \delta(z - wq^{-4}) + \\ &- (E^-(w) + q^{-6} E^-(wq^{-2})) D_{q(z)} \delta(z - wq^{-3}) + \\ &+ \frac{q^3}{[2]} D_{q(z)}^3 \delta(z - wq^{-3}). \end{aligned} \quad (16)$$

The classical limit of (16) is the Virasoro Algebra (9).

V Conclusions and Outlook

We have found a new method to obtain a q -Deformed Virasoro Algebra by a quantum analogue of the Hamiltonian Reduction process applied to the Quantum Current Algebra $\mathcal{U}_q(\widehat{su}(2))$. We used an specific prescription to construct Poisson Brackets from OPE relations and then performed the Dirac Bracket procedure after imposing constraints on currents.

Now we are performing the same method in the case of the Quantum Current Algebra $\mathcal{U}_q(\widehat{su}(3))$, in order to construct a new q -Deformed \mathcal{W}_3 Algebra. In both cases, there are no field theoretic substract, that is, there are still no QFT which obey a q -deformed symmetry, described by these algebras. It is necessary to search these new QFT and study their properties.

References

- [1] A.H. Bougourzi and L. Vinet: "A Quantum Analogue of the Boson-Fermion Correspondence", preprint CRM-2181 (1994).
- [2] L. Fehér, L. O'Raifeartaigh, P. Ruelle, I. Tsutsui and A. Wipf: "On Hamiltonian Reduction of the WZNW Theories", Phys. Rep. 222 No 1 (1992) 1-64.
- [3] K. Thielemans: "An Algorithmic Approach to Operator Product Expansions, \mathcal{W} -Algebras and \mathcal{W} -Strings", PhD Thesis (1994).

Remark on Shape Invariant Potential

Elso Drigo Filho¹ and Regina Maria Ricotta²

¹ Instituto de Biociências, Letras e Ciências Exatas, IBILCE-UNESP

² Faculdade de Tecnologia de São Paulo, FATEC/SP-CEETPS-UNESP

For more than a decade, Supersymmetry has provided new information about ordinary quantum mechanical problems, and Supersymmetric Quantum Mechanics (SQM) has become a field of research by itself. It has been shown that the symmetry between two different systems that share the same energy spectra can be interpreted in terms of supersymmetry. From the knowledge of the ground state of a given potential it is possible to find another potential with the same energy spectrum, except for the ground state. In fact, from the use of supersymmetric partner Hamiltonians and their degeneracy spectra it has become possible to determine a ladder of Hamiltonians and their spectra, only through the ground states of the ladder. Concerning the partner Hamiltonians with potentials V_+ and V_- that are similar in shape but differ in the parameters, Gedenstein introduced in 1983 the concept of shape invariance. Here we propose an extension of this concept. It is formulated in terms of the functional form of the whole super-family and not only between any two members of the ladder. We give two examples where all the members of the super-family can be written in a general functional form and conclude that Gedenstein's condition of shape invariance is sufficient but not necessary in order to obtain the super-family.

Gedenstein [1] defined the "shape invariant" potentials by the relationship

$$V_+(x; a_0) - V_-(x; a_1) = W^2(x, a_0) + W'(x, a_0) - W^2(x; a_1) + W'(x; a_1) = R(a_1) \quad (1)$$

where $W(x; a)$ is the superpotential, a_0 and a_1 stand for parameters of the supersymmetric partner potentials V_+ and V_- , $R(a)$ is a constant. The supersymmetric partners are related with the supersymmetric Hamiltonian in an usual way [2], $V_+ = W^2 - W'$ and $V_- = W^2 + W'$.

The relationship between shape invariance and solvable potentials is discussed by several authors (see, for instance, [3] and [4]). Other mathematical aspects of shape invariant potentials are also present in the literature, for example in the supersymmetric WKB approximation, [5], Berry phase, [6], and in the path-integral formulation, [7].

There is a general conclusion about these kind of potentials which is that the concept of shape invariance is a sufficient but not a necessary condition for the potential to become exactly solvable, [4].

In a recent work, [8], the Hulthén potential was studied from the Supersymmetric Quantum Mechanics formalism. This potential has an interesting property, that is when the angular momentum is zero, $l = 0$, it is not shape invariant in the sense expressed in ref.[1]. However, it is still possible to construct a general form of the potentials in the super-family of Hamiltonians:

$$V_n(r) - E_0^{(n)} = W_n^2(r) - \frac{d}{dr}W_n(r) = \frac{n(n-1)\delta^2 e^{-2\delta r}}{2(1-e^{-\delta r})^2} - \frac{[n(1-n)\delta + 2]\delta e^{-\delta r}}{2(1-e^{-\delta r})} + \frac{1}{2}\left(-\frac{n}{2}\delta + \frac{1}{n}\right)^2. \quad (2)$$

where $n = 1, 2, 3, \dots$ labels the n -th member of the super-family whose ground-state is $E_0^{(n)}$, ($n = 1$ and 2 correspond to the two first members V_+ and V_- , respectively, except by additive constants in V_-) and δ is a fixed parameter. For $n = 1$ the potential in (2) leads us to the usual Hulthén potential V_H

$$V_+(r) = V_H(r) - E_0^{(1)} = -\frac{\delta e^{-\delta r}}{1-e^{-\delta r}} + \frac{1}{2}\left(\frac{1-\delta}{2}\right)^2. \quad (3)$$

and from (2) it is easy to note that the condition (1) is not satisfied, i.e., V_H is not shape invariant but the whole super-family has the same functional form given by equation (2).

Taking the previous example, it is possible to suggest an extension of the concept of shape invariance. This invariance would be associated with the functional form of the whole super-family potentials and not only with the first two members (V_+ and V_-), since all the members of super family can be written in a general functional form in terms of one or more parameters (as the natural number n in Hulthén potential case). In other words, it is possible to construct a general expression for all potentials of the super-family.

The simple example of the free particle in a box can be used to make clear the above idea. The Hamiltonian H in this case is

$$H_+ = H - E_0^{(1)} = -\frac{d^2}{dx^2} - 1; \quad -\frac{\pi}{2} < x < +\frac{\pi}{2} \quad (4)$$

where the constant term (-1) sets the eigenvalue of the ground state of H_+ to zero. [9]. In this case the general form for the superpotential is

$$W_n(x) = n \tan(x) \quad (5)$$

where n is a natural number different from zero. ($n = 1, 2, 3, \dots$). The super-family is such that $E_n^{(1)} = n^2$ and the n -th member of the super-family potential is

$$V_n(x) - E_0^{(n)} = \frac{n(n-1)}{\cos^2(x)} - n^2. \quad (6)$$

Thus, it is not shape invariant in the Gedenstein's sense. [1], since $V_+ = -1$ and $V_- = \frac{2}{\cos^2(x)} - 1$, whereas it is shape invariant in the extended sense.

In our definition the potentials are shape invariant when it is possible to construct a super-family whose members have the same functional form. On the other hand, in the usual definition introduced by Gedenstein, once relation (1) is satisfied it is possible to find all the members of the super-family. However, having built a super-family it does not necessarily mean that relation (1) is satisfied, as shown in the two examples above of the Hulthén potential and the particle in a box. In other words, Gedenstein's condition of shape invariance is sufficient but not a necessary condition to obtain the super-family.

The interesting question to be studied now is if the extended shape invariance is a necessary condition to the potential to be exactly solvable. Other questions concerning shape invariance, [5], [6], [7], can also be analysed using this extended concept.

References

- [1] L. Gedenstein, *JETP Lett.* **38** (1983) 356
- [2] F. Cooper and B. Freedman, *Ann. Phys. NY* **146** (1983) 262; R. W. Haymaker and A. R. Rau, *Am. J. Phys.* **54** (1986) 928
- [3] G. Levai, *J. Phys. A: Math. Gen.* **25** (1992) L521; G. Levai *Lect. Notes in Phys.* **427** Ed. H. V. van Gevamb Spring-Verlag (Berlin) (1993) 107; T. Fukuiand and A. Aizawa, *Phys. Lett.* **A180** (1993) 308
- [4] F. Cooper, J. N. Ginocchio and A. Khare, *Phys. Rev.* **D36** (1987) 2458; Cao X. C., *J. Phys. A: Math. Gen.* **24** (1991) L1165
- [5] R. Dutt, A. Khare and U. P. Sukhatme, *Phys. Lett.* **B181** (1986) 295; D. T. Barclay and C. J. Maxwell, *Phys. Lett.* **A157** (1991)
- [6] D. Bhaumik, B. Dutta-Roy, B. K. Bagchi and A. Khare, *Phys. Lett.* **A193** (1994) 11
- [7] R. De, R. Dutt and U. Sukhatme, *Phys. Rev.* **A46** (1992) 6869
- [8] E. Drigo Filho and R. M. Ricotta, *Mod. Phys. Lett.* **A10** (1995) 1613
- [9] E. Drigo Filho, *Rev. Bras. Fis.* **20** (1990) 258

Superspace Formulation for the BRST Quantization of the Chiral Schwinger Model

Everton M. C. Abreu^{1,2} and Nelson R. F. Braga¹

¹ Instituto de Física,

Universidade Federal do Rio de Janeiro,

Caixa Postal 68528, 21945 Rio de Janeiro, RJ, Brazil

² Instituto de Física, Universidade do Estado do Rio de Janeiro,

Rua São Francisco Xavier 524, CEP 20550 Rio de Janeiro, RJ, Brazil

The Lagrangian BRST formalism of Batalin and Vilkovisky (BV) [1, 2, 3] is presently considered the most powerful procedure for the quantisation of gauge theories. The application of this formalism to anomalous gauge theories was first discussed by Troost, van Nieuwenhuizen and Van Proeyen [4], that succeeded in using the Pauli Villars regularization in order to give a regularized meaning to the master equation at one loop order.

The Chiral Schwinger Model (CSM) has been an important device to understand the quantisation of anomalous gauge theories.

The superspace formulation has the nice property of been, by construction, explicitly BRST invariant. The master equation is translated into the existence of a superfield structure associated to the quantum action in such a way that realizing the Wess Zumino mechanism is just equivalent to building up such a superfield without anomaly.

The fermionic nature and the nilpotency of the BRST transformations makes it possible to build up a superspace representation where they are realized as translations in a Grassman variable[7]. One adds to the original space-time variables one Grassmanian degree of freedom θ and associate to each original field $\phi(x)$ a superfield:

$$\Phi(x, \theta) = \phi(x) + \theta \delta \phi(x) \quad (1)$$

in such a way that:

$$\delta_{BRST} \Phi(x, \theta) = \frac{\partial}{\partial \theta} \Phi(x, \theta) \quad (2)$$

When one tries to apply this superspace realization to the case of the field antifield (FA) quantisation one faces a problem. The quantum master equation[1]

$$\frac{1}{2}(W, W) = i\hbar \Delta W \quad (3)$$

involves the operator:

$$\Delta \equiv \frac{\delta_r}{\delta \phi^a} \frac{\delta_l}{\delta \phi_a^*} \quad (4)$$

that represents the possibly non trivial behavior of the path integral measure. One then needs a superspace version for this operator and thus one should introduce functional derivatives with respect to superfields. However, superfields of the form (1) will in general be constrained, as the BRST transform. For an unconstrained superfield:

$$\Omega(x, \theta) = A(x) + \theta B(x) \quad (5)$$

However, as discussed in [5], functional differentiation and integration for constrained superfields is not in general well defined.

The collective field approach to BV consists (in a very summarized way) in starting with a gauge field theory characterized by a classical action $S_0[\phi^i]$, introducing ghosts, antighosts and auxiliary fields associated to the original gauge invariances of S_0 in the usual way, getting an enlarged field set represented as ϕ^A . These fields realize a BRST algebra:

$$\delta_0 \phi^A = R^A[\phi] \tag{6}$$

Then we introduce a new set of fields called collective fields $\tilde{\phi}^A$ and replace everywhere ϕ^A by $\phi^A - \tilde{\phi}^A$. This way we double the field content of the theory and at the same time associate to each field a new trivial shift symmetry. In order to gauge fix these new symmetries we introduce new ghosts, antighosts and auxiliary fields, represented respectively as: π^A , ϕ^{*A} and B^A . We have a large freedom in choosing the BRST transformations for this enlarged set of fields. Following [8] we can define the enlarged BRST algebra as

$$\delta \phi^A = \pi^A ; \delta \tilde{\phi}^A = \pi^A - R^A[\phi - \tilde{\phi}] ; \delta \pi^A = 0 ; \delta \phi^{*A} = B^A ; \delta B^A = 0 \tag{7}$$

and the total action as

$$S = S_0[\phi^i - \tilde{\phi}^i] - \delta(\phi^{*A} \tilde{\phi}^A) + \delta \psi[\phi^A] \tag{8}$$

where $\psi[\phi^A]$ is a fermionic functional representing the gauge fixing of the original symmetries (6). The BV gauge fixed classical action is obtained if one functionally integrates the vacuum functional associated with S over π^A , $\tilde{\phi}^A$ and B^A .

The interesting point is that in this collective field approach all the fields of the sets ϕ^A and ϕ^{*A} have BRST transformations that are independent quantities, unrelated to the associated field, as follows from (7). Therefore, if we introduce superfields of the form (1), at least for this two sets, they will be unconstrained. The component decomposition for the functional derivatives then makes it easy to see that the operator:

$$\underline{\Delta} \equiv \int dx \int d\theta \int d\theta' \frac{\delta_r}{\delta \Phi^A(x, \theta)} \frac{\delta_l}{\delta \Phi^{*A}(x, \theta')} \tag{9}$$

with

$$\begin{aligned} \Phi^A(x, \theta) &= \phi^A(x) + \theta \pi^A(x) \\ \tilde{\Phi}^A(x, \theta) &= \tilde{\phi}^A(x) + \theta(\pi^A(x) - R^A[\phi - \tilde{\phi}]) \\ \Phi^{*A}(x, \theta) &= \phi^{*A}(x) + \theta B^A(x) \end{aligned} \tag{10}$$

represents the operator Δ in superspace.

In the superspace formulation the quantum action, for non anomalous gauge theories, will have the component expansion

$$\underline{W} = W + \theta i \hbar \Delta W \tag{11}$$

and the master equation will read:

$$\frac{\partial}{\partial \theta} \underline{W} = i \hbar \underline{\Delta} W \tag{12}$$

corresponding, order by order in \hbar , (we are considering quantum corrections only up to one loop order):

$$\frac{\partial}{\partial \theta} \underline{S} = 0 : \frac{\partial}{\partial \theta} \underline{M}_1 = i \underline{\Delta} \underline{S} \tag{13}$$

The classical action for the Chiral Schwinger Model (CSM) is:

$$S_0 = \int d^2x \left[-\frac{1}{4} F_{\mu\nu} F^{\mu\nu} + \frac{1}{2} \bar{\psi} \mathcal{D} (1 - \gamma_5) \psi \right] \quad (14)$$

where $D_\mu = \partial_\mu + ieA_\mu$. The BRST transformations of the fields are:

$$\delta A_\mu = \partial_\mu c; \delta \psi = i\psi c; \delta \bar{\psi} = -i\bar{\psi} c; \delta c = 0 \quad (15)$$

where c is the ghost field associated to the gauge invariance of S_0 .

We enlarge, as explained in the previous section, the field content of the theory, introducing the collective fields $\tilde{A}_\mu, \tilde{\psi}, \tilde{\bar{\psi}}, \tilde{c}$ and build up the associated superfields.

The total superfield action will be:

$$\underline{S} = \underline{S}_0 + \underline{S}_1 + \underline{S}_2 \quad (16)$$

with the extended superspace version of the classical action:

$$\begin{aligned} \underline{S}_0 &= \int d^2x \left(-\frac{1}{4} F_{\mu\nu} [\underline{A}_\mu - \underline{\tilde{A}}_\mu] F^{\mu\nu} [\underline{A}_\mu - \underline{\tilde{A}}_\mu] \right. \\ &\quad \left. + \frac{1}{2} (\underline{\bar{\Psi}} - \underline{\tilde{\bar{\Psi}}}) \mathcal{D} [\underline{A}_\mu - \underline{\tilde{A}}_\mu] (1 - \gamma_5) (\underline{\Psi} - \underline{\tilde{\Psi}}) \right) \end{aligned} \quad (17)$$

the gauge fixing of the shift symmetry:

$$\underline{S}_1 = -\frac{\partial}{\partial \theta} \int d^2x \left[\underline{A}_\mu^* \underline{\tilde{A}}^\mu + \underline{\Psi}^* \underline{\tilde{\Psi}} + \underline{\bar{\Psi}}^* \underline{\tilde{\bar{\Psi}}} + \eta^* \eta \right] \quad (18)$$

and the gauge fixing of the original symmetry of S_0 :

$$\underline{S}_2 = \frac{\partial}{\partial \theta} \int d^2x \Lambda [\underline{A}_\mu, \underline{\Psi}, \underline{\bar{\Psi}}, \eta] \quad (19)$$

with the collective field version of the classical action:

We must now build up a superspace Pauli Villars (PV) action, that will regularize the action of the operator $\underline{\Delta}$ on the action. Following the prescriptions of [5] we associate with ψ and $\bar{\psi}$ the PV fields χ and $\bar{\chi}$ and the corresponding collective tilde fields and introduce the action:

$$\begin{aligned} \underline{S}_{PV} &= \frac{1}{2} (\underline{\bar{\chi}} - \underline{\tilde{\bar{\chi}}}) \mathcal{D} [\underline{A}_\mu - \underline{\tilde{A}}_\mu] (\underline{\chi} - \underline{\tilde{\chi}}) \\ &\quad - \frac{1}{2} M (\underline{\bar{\chi}} - \underline{\tilde{\bar{\chi}}}) (\underline{\chi} - \underline{\tilde{\chi}}) - \frac{\partial}{\partial \theta} \left(\underline{\bar{\chi}} \underline{\tilde{\chi}} + \underline{\chi} \underline{\tilde{\chi}} \right) \end{aligned} \quad (20)$$

that represents a copy of the fermionic part of action (17) but with a mass term that, after calculating the regularized δS , allows the removal of the PV fields by taking the limit $M \rightarrow \infty$.

We define the BRST transformations of the PV fields to be similar to the ones from the corresponding fields.

The action of the operator $\underline{\Delta}$ on the regularized total action, if we include the PV fields also in the operator (9), is then:

$$\underline{\Delta}(\underline{S} + \underline{S}_{PV}) = 0 \quad (21)$$

The regularized form of ΔS when we use the PV regularization shows up as a violation of the zero order master equation associated to the presence of the mass term. In the present superspace formulation, this absence of BRST invariance of the total (regularized) classical action $S_T = S + S_{PV}$ is translated into the presence of a θ component in the corresponding superfield:

$$\underline{S}_T = \underline{S} + \underline{S}_{PV} = S_T + \theta \delta S_T \quad (22)$$

The general form of δS_T is

$$\delta S_T = iM(\bar{\chi} - \tilde{\bar{\chi}})(\chi - \tilde{\chi})(c - \tilde{c}) \tag{23}$$

Integration over the fields $\pi^{(\lambda)A}$, $B^{(\lambda)A}$ and $\tilde{\chi}^A$ removes the extended collective field structure, recovering the usual result as in [4], that corresponds in (23) just to the absence of the collective tilde fields. The next step would be to integrate over the PV fields. We will not repeat this procedure here as it is exactly the same as in the component case, that is widely discussed in the literature[3, 4, 9]. The result is:

$$(\Delta S)_{reg.} = \frac{i}{4\pi} \int d^2x (c - \tilde{c}) \left((1-a) \partial_\mu (A^\mu - \tilde{A}^\mu) - \epsilon^{\mu\nu} \partial_\mu (A_\nu - \tilde{A}_\nu) \right) \tag{24}$$

Now going back to the one loop order master equation (13) we have to look for a superfield \bar{M}_1 whose θ component is equal to $i(\Delta S)_{reg.}$.

That realize in superspace the collective field version of the Wess Zumino field transformations. We include a gauge fixing term for the WZ field in the action defining:

$$\underline{S}' = \underline{S} - \frac{\partial}{\partial\theta} \int d^2x \hat{\Omega} \Omega^* \tag{25}$$

From the transformation of Ω one easily realizes that $\Delta S = \Delta S'$. Now we can write a superfield that satisfies $\partial \bar{M}_1 / \partial \theta = i(\Delta S)_{reg.}$.

$$\begin{aligned} \bar{M}_1 &= \frac{1}{4\pi} \int d^2x \left(\frac{(a-1)}{2} \partial_\mu (\Omega - \hat{\Omega}) \partial^\mu (\Omega - \hat{\Omega}) \right. \\ &\quad \left. - \partial_\mu (\Omega - \hat{\Omega}) \left((a-1) (\underline{A}^\mu - \hat{\underline{A}}^\mu) + \epsilon^{\mu\nu} (\underline{A}_\nu - \hat{\underline{A}}_\nu) \right) \right) \end{aligned} \tag{26}$$

in components this superfield reads: $\underline{M}_1 = M_1 + \theta(i\Delta S)_{reg}$ with:

$$\begin{aligned} M_1 &= \frac{1}{4\pi} \int d^2x \left(\frac{(a-1)}{2} \partial_\mu (\omega - \hat{\omega}) \partial^\mu (\omega - \hat{\omega}) \right. \\ &\quad \left. - \partial_\mu (\omega - \hat{\omega}) \left((a-1) (A^\mu - \hat{A}^\mu) + \epsilon^{\mu\nu} (A_\nu - \hat{A}_\nu) \right) \right) \end{aligned} \tag{27}$$

If we remove the collective fields, this corresponds just to the Wess Zumino term found in [6] in the non superspace approach.

Therefore, the superfield $\underline{W} = \underline{S}' + \underline{M}_1$ satisfies the superspace version of the master equation (12), representing the superfield action, that includes, besides the quantum action, also the anomalous contribution from the path integral measure ΔS .

We have shown to represent the quantum action of the Chiral Schwinger model in a BRST superspace. An interesting point of this formulation is that both the action and the ΔS term (that comes from the non trivial behaviour of the path integral measure) show up in the same superfield. The master equation corresponds thus just to a restriction on the structure of this object. We have also shown that the Wess Zumino mechanism can also be realised in this formulation, by adding a superfield that represents the gauge group elements.

This work was partially supported by CNPq, FINEP, FUJB and CAPES (Brazilian Research Agencies).

References

- [1] I. A. Batalin and G. A. Vilkovisky, Phys. Lett. B102 (1981) 27, Phys. Rev. D28 (1983) 2567.
- [2] M.Henneaux and C.Teitelboim, Quantization of Gauge Systems, Princeton University Press 1992, Princeton, New Jersey.
- [3] J. Gomis, J. Paris and S. Samuel, Phys. Rep. 259 (1995) 1.

- [4] W.Troost, P.van Nieuwenhuizen and A. Van Proeyen, Nucl. Phys. B333 (1990) 727.
- [5] E.M.C.Abreu and N.R.F.Braga, "A superspace Formulation for the Master Equation", to appear in Phys. Rev. D.
- [6] N. R. F. Braga and H. Montani, Phys. Lett. B264 (1991) 125.
- [7] S. Ferrara, O. Piguet and M. Schweda, Nucl. Phys. B119 (1977) 493; K. Fujikawa, Progr. Theor. Phys. 59 (1978) 2045.
- [8] J. Alfaro and P. H. Dangaard, Nucl. Phys. B404 (1993) 751.
- [9] F.De Jonghe, The Batalin-Vilkovisky Lagrangian Quantization scheme with applications to the study of anomalies in gauge theories, PH.D. thesis K.U. Leuven, HEP-TH 9403143.

Zeta Function Method for Repulsive Casimir Forces at Finite Temperature

F.C. Santos*, A. Tenório and A.C. Tort†

Instituto de Física, Universidade Federal do Rio de Janeiro

Cidade Universitária - Ilha do Fundão - Caixa Postal 68528

21945-970 Rio de Janeiro, Brasil

We compute the Casimir pressure between an unusual pair of parallel plates, namely, a perfectly conducting plate ($\epsilon \rightarrow \infty$) and an infinitely permeable one ($\mu \rightarrow \infty$) at finite temperature with the generalized ζ -function method.

Since Casimir's paper[3] on the attraction between two parallel (perfectly) conducting plates due to the vacuum fluctuations of the electromagnetic field, a considerable amount of work has been done on this subject, varying from the application of alternative techniques to the investigation of new geometries and theories. Casimir's approach to this problem consists basically in computing the interaction energy between the plates as the (regularized) difference between the zero point energies with and without the boundaries conditions dictated by the physical situation (for instance, perfectly conductor character of the plates). In fact, the great novelty of Casimir's paper of 1948 was not the fact that two neutral objects attracted each other¹, but the simplicity of the method of calculating this attraction in the context of quantum field theory.

However, since Casimir's work, many other techniques were developed which may be more appropriate depending on the physical situation under study. In particular, methods of computing effective actions are in general very powerful for our purposes. We shall be concerned here with one of these methods, namely, the so-called generalized ζ -function method. In this paper we shall apply it to the unusual case of a pair of parallel plates, where one of them is perfectly conducting ($\epsilon \rightarrow \infty$), while the other is infinitely permeable ($\mu \rightarrow \infty$) at finite temperature. This problem, at zero temperature, was solved by T. Boyer[4] two decades ago in the context of random electrodynamics (a kind of classical electrodynamics which includes classical electromagnetic zero-point radiation). In order to apply the generalized ζ -function method, let us introduce the partition function Z for bosons [1]:

$$Z = N \int_{\text{periodic}} [D\phi] \exp \left(\int_0^\beta d\tau \int d^3x \mathcal{L} \right), \quad (1)$$

where N is a constant which has no influence on the final result and the term periodic means that the functional integral is to be performed on fields satisfying the condition:

$$\phi(x, 0) = \phi(x, \beta). \quad (2)$$

The free energy F is related to the partition function $Z(\beta)$ through the relation $F = -\beta^{-1} \ln Z(\beta)$, where $\beta = T^{-1}$. Beside the condition (2) we can consider boundary conditions which are determined by the geometry and nature of the physical fields. Choosing the Cartesian axes such that the axis OZ is perpendicular to both plates with the perfectly conducting plate at $z = 0$ and the infinitely permeable one at $z = d$ (see figure), the boundary conditions are the following: the tangential components of the electric field must vanish at $z=0$, while the tangential components of the magnetic field must vanish at $z=d$. However, since we will be dealing with standing wave modes between the plates, these conditions are equivalent to imposing that tangential components of the electric field vanishes at $z = 0$ (as before) and its z -derivative vanishes at $z = d$. Hence, we can compute the partition function

* e-mail: filadelf@if.ufrj.br

† e-mail: tort@if.ufrj.br

as if the electromagnetic field were a massless scalar field. All we have to do is insert by hand an extra factor of 2 to take into account for the two possible polarizations of the electromagnetic field modes (this can be done only for the plane geometry of this problem). Therefore, the boundary conditions for this scalar field are:

$$\phi(\tau, x, y, z = 0) = 0, \quad \frac{\partial \phi}{\partial x}(\tau, x, y, z = d) = 0. \tag{3}$$

Thus we can write the $\ln Z$ as:

$$\ln Z = \left(-\frac{1}{2}\right) \ln \det(-\square_E | F_d), \tag{4}$$

where the symbol $F|_d$ means a set of functions which satisfy the conditions (2) and (3). The generalized ζ -function method consists basically in the following three steps: (i) first, we compute the eigenvalues of $-\square_E$ and write $\zeta(s; -\square_E) = \text{Tr}(-\square_E)^{-s}$; (ii) second, we make an analytical extension of $\zeta(s; -\square_E)$ to a meromorphic function on the whole complex s -plane; (iii) finally, we compute $\det(-\square_E | F_d) = \exp\{-\frac{\partial \zeta}{\partial s}(s = 0; -\square_E)\}$. Combining the previous equations, we obtain:

$$F = -\frac{\zeta'(s = 0, -\square_E)}{\beta}. \tag{5}$$

The eigenvalues of $-\square_E$ whose eigenfunctions $\phi(\tau, x)$ satisfy (2) and (3) are

$$\left\{ \frac{4\pi^2 n_1^2}{\beta^2} + K_x^2 + K_y^2 + \left(n_1 + \frac{1}{2}\right)^2 \frac{\pi^2}{d^2} \mid K_1, K_2 \in \mathbb{R}, n_1, n_2 = 0, 1, 2, \dots \right\}. \tag{6}$$

The ζ -function then reads

$$\zeta(s, -\square_E) = L^2 \sum_{n_2=-\infty}^{\infty} \sum_{n_1=0}^{\infty} \int \frac{dK_x dK_y}{(2\pi)^2} \left[K_x^2 + K_y^2 + (2n_1 + 1)^2 \frac{\pi^2}{4d^2} + \frac{4\pi^2 n_2^2}{\beta^2} \right]^{-s} \tag{7}$$

where L^2 is the area of the plates. Now, rearranging the terms in summations, we can write this last equation as

$$\begin{aligned} \zeta(s, -\square_E) &= L^2 \frac{1}{2\pi} \sum_{n_1=1,3,5,\dots}^{\infty} \int_0^{\infty} dK_{\perp} K_{\perp} \left[K_{\perp}^2 + n_1^2 \frac{\pi^2}{4d^2} \right]^{-s} + \\ &+ 2 \sum_{n_2=1}^{\infty} \sum_{n_1=0}^{\infty} \frac{1}{2\pi} \int_0^{\infty} K_{\perp} dK_{\perp} \left[K_{\perp}^2 + \frac{n_1^2 \pi^2}{4d^2} + \frac{4\pi^2 n_2^2}{\beta^2} \right]^{-s}, \end{aligned} \tag{8}$$

where $K_{\perp}^2 = K_x^2 + K_y^2$ and the angular integration was already made. Using the following integral representation for the Euler Beta function:

$$\int_0^{\infty} dx x^{\mu-1} (x^2 + 1)^{\nu-1} = \frac{1}{2} B\left(\frac{\mu}{2}, 1 - \nu - \frac{\mu}{2}\right), \tag{9}$$

$$B(x, y) = \frac{\Gamma(x)\Gamma(y)}{\Gamma(x+y)} \tag{10}$$

which is valid for $\Re(\nu + \frac{\mu}{2}) < 1$ and $\Re\mu > 0$, we get

$$\begin{aligned} \zeta(s, -\square_E) &= \frac{T_E L^2}{4\pi} \frac{\Gamma(s-1)}{\Gamma(s)} \left[\left(\frac{\pi}{2d}\right)^{2-2s} \sum_{n_1=1,3,5,\dots} n_1^{2-2s} + \right. \\ &+ \left. 2\pi^{2-2s} \sum_{n_2=1}^{\infty} \sum_{n_1=1,3,5,\dots} \left[\frac{n_1^2}{4d^2} + \frac{4n_2^2}{\beta^2} \right] \right]. \end{aligned} \tag{11}$$

In order to connect the summation on the rhs of the above equation to the ζ_R -function, we use the following trick:

$$\sum_{n_1=1,3,5,\dots} n_1^{2-2s} = (1 - 2^{2-2s})\zeta_R(2s - 2). \tag{12}$$

Furthermore, taking into account the Epstein function which, for any positive N and large enough $\Re z$, is defined by

$$E_N^{M^2}(z; a_1, a_2, \dots, a_N) = \sum_{n_1=1}^{\infty} \sum_{n_2=1}^{\infty} \dots \sum_{n_N=1}^{\infty} \frac{1}{(a_1 n_1^2 + a_2 n_2^2 + \dots + a_N n_N^2 + M^2)^z}, \tag{13}$$

where $a_1, a_2, \dots, a_N > 0$ and using one more trick:

$$\sum_{n_2=1}^{\infty} \sum_{n_1=1,3,5} \left[\frac{n_1^2}{4d^2} + \frac{4n_2^2}{\beta^2} \right]^{1-s} = \sum_{n_2, n_1=1}^{\infty} \left[\frac{n_1^2}{4d^2} + \frac{4n_2^2}{\beta^2} \right]^{1-s} - \sum_{n_2, n_1=1}^{\infty} \left[\frac{(2n_1)^2}{4d^2} + \frac{4n_2^2}{\beta^2} \right]^{1-s} \tag{14}$$

we can write

$$\begin{aligned} \zeta(s, -\square_T) &= \frac{L^2}{4\pi} \frac{\Gamma(s-1)}{\Gamma(s)} \pi^{2-2s} \left[\left(\frac{1}{2d} \right)^{2-2s} (1 - 2^{2-2s}) \zeta_R(2s-2) + \right. \\ &\quad \left. + 2E_2 \left(s-1; \frac{1}{4d^2}; \frac{4}{\beta^2} \right) - 2E_2 \left(s-1; \frac{1}{d^2}; \frac{4}{\beta^2} \right) \right]. \end{aligned} \tag{15}$$

The Epstein function has an analytical continuation to a meromorphic function in the complex plane. For $N = 2$ and $M^2 = 0$ the analytical continuation is given by [2]:

$$\begin{aligned} E_2(z; a_1, a_2) &= -\frac{a_1^{-z}}{2} \zeta_R(2z) + \frac{1}{2} \left(\frac{\pi}{a_2} \right)^{1/2} \frac{\Gamma(z-1/2)}{\Gamma(z)} a_1^{-z+1/2} \zeta_R(2z-1) + \\ &\quad + \frac{2}{\Gamma(z)} a_2^{-1/2(z+1/2)} \pi^z \sum_{n_1, n_2=1}^{\infty} n_2^{z-1/2} (a_1 n_1^2)^{1/2(1/2-z)} \times \\ &\quad \times K_{1/2-z} \left(\frac{2\pi n_2}{\sqrt{a_2}} \sqrt{a_1 n_1^2} \right). \end{aligned} \tag{16}$$

Making the proper substitutions for z, a_1 and a_2 in the Epstein function and after some simple algebra, we obtain

$$\begin{aligned} \zeta_R(s, -\square_T) &= \frac{L^2}{4\pi} \frac{\pi^{2-2s}}{\Gamma(s)} \left\{ \frac{\beta}{2} \pi^{1/2} \Gamma \left(s - \frac{3}{2} \right) \zeta_R(2s-3) \left[\left(\frac{1}{4d^2} \right)^{3/2-s} - \left(\frac{1}{d^2} \right)^{3/2-s} \right] + \right. \\ &\quad + 4 \left(\frac{2}{\beta} \right)^{-s+1/2} \pi^{s-1} \sum_{n_1, n_2=1}^{\infty} \left(\frac{n_2 d}{n_1} \right)^{s-3/2} \times \\ &\quad \times \left[\left(\frac{1}{2} \right)^{-s+3/2} K_{3/2-s} \left(\frac{\beta \pi n_1 n_2}{2d} \right) - K_{3/2-s} \left(\frac{2\beta \pi n_1 n_2}{2d} \right) \right] \left. \right\}. \end{aligned} \tag{17}$$

And finally, using the fact that the derivative of function $G(s)/\Gamma(s)$ at $s = 0$ is simply given by $G(0)$ we obtain

$$\begin{aligned} \zeta'(0, -\square_T) &= \frac{-(\frac{7}{8})\pi\beta L^2}{720d^3} \\ &\quad + \frac{L^2\sqrt{2}}{\sqrt{\beta}} \sum_{n_1, n_2=1}^{\infty} \left(\frac{n_2 d}{n_1} \right)^{-3/2} \left[(2)^{-3/2} K_{3/2} \left(\frac{\beta \pi n_1 n_2}{2d} \right) - K_{3/2} \left(\frac{2\beta \pi n_1 n_2}{2d} \right) \right]. \end{aligned} \tag{18}$$

From equations (5) and (18) we obtain the free energy:

$$\frac{F}{L^2} = \frac{\left(\frac{7}{8}\right)\pi}{720d^3} + \frac{\sqrt{2}}{\beta^{\frac{3}{2}}} \sum_{n_1, n_2=1}^{\infty} \left(\frac{n_2 d}{n_1}\right)^{-\frac{3}{2}} \left[(2)^{-\frac{3}{2}} K_{\frac{3}{2}} \left(\frac{\beta \pi n_1 n_2}{2d} \right) - K_{\frac{3}{2}} \left(\frac{2\beta \pi n_1 n_2}{2d} \right) \right]. \quad (19)$$

The first term in (19) represents the Casimir energy at $T = 0$, the second one the correction due to thermal effects. From this result we can derive easily the Casimir pressure. Notice that for this particular boundary conditions (19) will yield a repulsive Casimir pressure.

Acknowledgements. The authors are indebt to C.Farina for enlightning discussions.

References

- [1] Kapusta, Joseph I., *Finite-Temperature Field Theory*, Cambridge University Press, 1989
- [2] Kirsten, K., *J. Math. Phys.* **35**, 459 (1994).
- [3] Casimir, H. B. G., *Proc. Kon. Nederl. Wetensch.* **51**, 793 (1948)
- [4] Boyer, T. H., *Phys. Rev. A* **9**, 2078 (1974)

Spherical Collapse in Higher Order Gravity.

Fernando Kokubun

Departamento de Física - UFMA

Av. dos Portugueses s/n, CEP 65085-580, São Luis, Ma, Brazil

and

Instituto de Física Teórica - UNESP

Rua Pamplona 145, CEP 01405-900, São Paulo, SP, Brazil

In this work we analyze a spherical model for the nonlinear collapse in the weak field limit of the Higher Order Gravity Theory (HOGT). In this limit, the Newtonian gravitational potential is corrected by an Yukawa-like term. In this approach we obtain some constraints to the initial size of the spherical region. In the case the coupling parameter α is positive, we obtain a critical radius $r_{i,max}$ such that only mass shell with $r_i < r_{i,max}$ would collapse. On the other hand, for negative α only mass shell with $r_i > r_{i,min}$ would collapse.

1 Introduction

Structure formations are one of the most amazing fields of modern cosmology. We know that in the standard Friedmann models, the Universe is highly homogeneous and isotropic as seen by Cosmic Microwave Background [1]. However, we see too, several lumpy of matter in the Universe, all highly non-homogeneous. This apparently contradictory situation is explained assuming that at some instant of Universe evolution, some kind of seed was responsible for triggering structure formations. Unhappily, although great success of existing scenarios - quantum fluctuations in the early Universe, cold and dark matter, cosmic strings [2] - there are not at moment any conclusive results excluding one or other scenarios.

On the other hand, although great success of General Relativity and Friedmann models, several other theories and models was proposed to explain apparently anomalous results due to utilization of standard gravity theory. One of these theories - Higher Order Gravity Theory (HOGT) - is obtained with introduction of $R_{\mu\nu}R^{\mu\nu}$ and R^2 terms in the standard Einstein-Hilbert action [3]. The main interest of HOGT is to obtain a renormalizable quantum gravity theory [4], in such a way that the only appreciable consequences occurs at very small scale. Moreover, one interesting feature of HOGT is that at weak field limit, the resulting gravitational potential is a Newtonian added with a Yukawa-like term [3]. The possible existence of such term in laboratory scale was tested, resulting that its influence if exist is very small [5]. Nevertheless, this not exclude the possibility of its influence in a more large scale. Some observational consequences of this extra term in the gravitational potential at large scale was analyzed by several authors [6].

In this work, we are interested in a possible role of HOGT in the formation of large scale structure. For this purpose, we analyze how an initially spherical regions evolve in the framework of HOGT. The background is assumed to be flat, and expanding like Friedmann model. This can be accomplished assuming that the range of Yukawa term is nearly the same as the size of spherical region. For the sake of simplicity, we assume that spherical region is always $\ll H^{-1}$. In this approach, we avoid any trouble with gauge fixing problem. Thus we can assume that these spherical region evolve under action of a gravitational potential resulting of weak field limit of HOGT. An advantage of this scenario is that we obtain an analytical result of its evolution [7].

2 Non-linear collapse in Spherical Model.

In the weak field limit of HOGT, the gravitational potential is given by [3]

$$\Phi(r) = -\frac{GM_o}{r} [1 + \alpha e^{-\mu r}] \quad (1)$$

where $M_o = 4\pi\rho r^3/3$ is the matter content inside spherical region of radius r . Then the energy of a particle located at distance r is given by

$$\frac{1}{2} \left(\frac{dr}{dt} \right)^2 - \frac{GM_o}{r^2} = E \quad (2)$$

where $M_o \equiv \rho(4\pi r^3/3)(1 + \alpha e^{-\mu r})$.

The initial energy of a given mass shell with radius r_i at instant t_i is

$$E(r_i) = K_i \Omega_i [\Omega_i^{-1} - (1 + \Delta_i)] \quad (3)$$

where $K_i \equiv H_i r_i^2/2$ is its initial kinetic energy, $\Delta_i = 1 + \alpha e^{-\mu r}$ and $\Omega_i \equiv \frac{\rho(r_i)}{\rho_c(t_i)}$, with H_i the standard Hubble constant and $\rho_c(t_i) \approx 3H_i^2/(8\pi G)$ is the critical density.

When $E < 0$ the mass shell would collapse, which in our case result in a constraint

$$\Delta_i = \alpha e^{-\mu r} > \Omega_i^{-1} - 1. \quad (4)$$

Now, if $\alpha < 0$ and $\Omega_i > 1$, we obtain a critical radius

$$r_{i,\min} = \log \left[\frac{|\alpha| \Omega_i}{\Omega_i - 1} \right]^{1/\mu} \quad (5)$$

such that only mass shell with $r_i > r_{i,\min}$ would collapse. In the figure 1 we plot $r_{i,\min} \times \Omega_i$ with three distinct values for α , using $\mu = 1$. In this case, we have first a formations of large structures, which would suffer fragmentation to form small objects. These situations are similar to the scenarios using hot dark matter [8]. However, because the range of Yukawa term is given by μ^{-1} , note that if $\Omega \simeq 1$, there would be no significant differences with Newtonian case.

In the case $\alpha > 0$ and $\Omega_i \geq 1$ the mass shell always collapse. However, if $\alpha > 0$ and $\Omega_i < 1$ we obtain a critical radius

$$r_{i,\max} = \log \left[\frac{\alpha \Omega_i}{1 - \Omega_i} \right]^{1/\mu} \quad (6)$$

such that only mass shell with $r_i < r_{i,\max}$ would collapse. Note that Ω_i and α are constrained by $\Omega_i > 1/(1 + \alpha)$ and assuming $0 < \alpha < 1$ [3], we obtain that $\Omega_i \geq 0.5$. In the figure 2 we plot $r_{i,\max} \times \Omega_i$ for three distinct α values, using $\mu = 1$. When $\Omega_i \rightarrow 1/(1 + \alpha)$, we have $r_{i,\max} \rightarrow 0$.

The equation 6 show that this case ($\alpha > 0$ and $\Omega_i < 1$) is more favorable to formations of small objects. Therefore in this scenario, the hierarchy goes from small to large objects, like models using cold dark matter [9].

Finally, if $\alpha < 0$ and $\Omega_i \leq 1$ there are not collapse at all.

The spherical region with $E < 0$ would reach a maximum radius r_m , and after this instant would begin its contraction phase. At this point the spherical system would be detached from Universe expansion, and its evolution would be determined mainly by local mass concentration. We know that at maximum radius the velocity of spherical shell would vanish, in such a way that all energy would be stored as gravitational potential. Then, it is straightforward to show that at this point the energy is given by

$$E(r_m) = -\frac{GM_o}{r_m} [1 + \Delta_m] = -\frac{GM_o}{r_i} [1 + \Delta_m] \frac{r_i}{r_m} \quad (7)$$

with $\Delta_m = \alpha e^{-\mu r_m}$. Now from energy conservation, we know that $E(r_i) = E(r_m)$, then using equation 3 and 7, we obtain

$$\frac{r_m}{r_i} = \frac{1 + \Delta_m}{1 + \Delta_i - \Omega_i^{-1}} \quad (8)$$

We solved numerically the equation 8 using $\alpha = 2/3$ – which is standard value obtained in HOGT [3] – with $\Omega = 0.90$ and 0.75 , with results displayed in the figure 3. For small r_i we obtain that ratio $r_m/r_i \propto 1 - [\Omega(1 + \alpha)]^{-1}$ with smooth variation near origin of r_i , whereas for $r_i \simeq 1$ this ratio grow exponentially. The data in r_i -axis is constrained to $r_i < r_{i,\max}$. The behaviour of r_m/r_i for different α is show in the figure 4. Note that these are similar to the graphic displayed in the figure 3. When $r_i \simeq r_{i,\max}$, we have $1 + \Delta_i \simeq \Omega_i^{-1}$ (see equation 4), and in this case $r_m/r_i \rightarrow \infty$ as can be seen in the figures 2 and 3. (In the Newtonian case, this happen when perturbation $\delta_i \simeq \Omega_i^{-1} - 1$.)

Nevertheless, with $\alpha < 0$ the behaviour are different. In the figure 5, we plot a graphic of $r_m/r_i \times r_i$ using $\Omega_i = 1.10$ and $\alpha = -1.0, -2/3$ and $-1/3$. In this case we obtain that smaller r_i greater are the ratio r_m/r_i , and with greater r_i , the ratio goes to a constant value for all α . This behaviour is expected (see equation 8), because when r_i is large we obtain $r_m/r_i \rightarrow \Omega_i/(\Omega_i - 1)$.

The spherical region after reaching its maximum size r_m will collapse and virialize forming a bound system independent of Universe expansion. From virial theorem its is straightforward to see that energy after virialization is given by

$$E(r_{\text{vir}}) = -\frac{GM}{2r_{\text{vir}}} [1 + \alpha(1 - \mu r_{\text{vir}})e^{-\mu r_{\text{vir}}}] \quad (9)$$

In non dissipative case $E(r_m) = E(r_{\text{vir}})$ such that

$$r_{\text{vir}} = \frac{r_m}{2} \left\{ \frac{1 + \alpha(1 - \mu r_{\text{vir}})e^{-\mu r_{\text{vir}}}}{1 + \alpha e^{-\mu r_m}} \right\} \quad (10)$$

remembering that in a Newtonian gravity $r_{\text{vir}} = r_m/2$.

In the figures 6 and 7 we show several graphics of $r_{\text{vir}}/r_m \times r_i$ for different α and Ω . Its is interesting to note that HOGT results differs only slightly from standard Newtonian case – a difference of nearly $\pm 10\%$. With negative α , r_{vir}/r_m goes to standard Newtonian value with large r_i , and with positive α this happens with small r_i . These are expected, remembering that when $r \ll \mu^{-1}$ we obtain a standard Newtonian gravity with rescaled gravitational constant $G \rightarrow G(1 + \alpha)$, and with $r \gg \mu^{-1}$ we obtain a standard Newtonian gravity. In the figure 8, we show the behaviour of a overdense region ($\Omega_i = 2.0$) with $\alpha < 0$. Note that when $\alpha = -2/3$ and $\alpha = -1/3$, the curve show a maximum. This happens because in both cases, the minimum radius is very small. Note that when $\alpha < 0$ we have a repulsive term in the gravitational potential. Thus with small mass (corresponding to small radius r_i), the repulsive term is dominant. With expansion, due to its exponential behaviour, its influence decrease and attractive term begins to dominate. This explain the existence of a maximum in those graphics.

An important question is how large is μ^{-1} . This term is related to the range of Yukawa term in the gravitational potential. A natural choice is the size of horizon at decoupling time. If μ^{-1} was smaller than horizon H_{dec} at this time, it would be expected a formations of several bound structures and these lumpy regions would perturb the cosmic microwave background. On the other hand, if μ^{-1} is greater than H_{dec} , we have a gauge fixing problem. To avoid these undesirable features, a natural choice is $\mu^{-1} \simeq H_{\text{dec}}$, which result in a conservative value of $\mu^{-1} \simeq 5$ Mpc.

Now, from our results given in the figures 1 and 3, the case with $\alpha > 0$ is more feasible. In this case, the maximum initial size of perturbations is smaller than horizon scale when $\Omega \leq 0.8 \sim 0.9$. Thus, it is easy to obtain perturbations which evolve to galaxies sizes. On the other hand, with $\alpha < 0$ the situations is more problematic. Only when $\alpha = -1/3$ and $\Omega \geq 1.2$ it is possible to obtain a initial size smaller than horizon. In all other situations (with $\alpha < 0$), to obtain an initial size smaller than horizon, we need a exceedingly high Ω value.

3 Concluding Remarks.

In this work we obtained that the presence of extra term in the Newtonian gravitational potential change the behaviour of a spherical collapse. Depending of α parameter, we can simulate "top down" (hot dark matter) or "bottom up" (cold dark matter) scenarios for large scale structure formations. In particular, $\alpha > 0$ is consistent with standard value $\alpha = 2/3$ obtained in HOGT [3] (It is possible to obtain a negative α , but only with a presence of additional scalar and vectorial fields [11].) To be applicable in the formations of large-scale structures the range

of μ^{-1} need to be as large as galaxies cluster sizes, and in this case this would be undetected in the laboratory experiments, as is the actual case [5]. Nevertheless, it is important to note that our results don't exclude an existence of dark matter. But it show that some expected behaviour can be only a signature of non standard gravity. To obtain a more confident result, it would be important to perform a fully relativistic analysis of perturbations in HOGT including dark matter.

Other aspects which need to be considered are cooling and heating process due to formations of star and supernova bursts during the collapse of spherical region. Although a detailed analysis are complicated, we expect that due to Yukawa term, shells with different radius collapse with distinct time (note that $t_{\text{dyn}} \propto G^{1/2}$ and in our case we can consider G as a function of shell radius, whereas in a Newtonian case it is independent). In this case we expect that shock waves would be formed during collapse. These shocks may be very important in the heating process. A more detailed analysis including cooling process will be performed in a future collaboration.

This work was partially supported by FAPESP, Brazilian financial agency.

References

- [1] G.F. Smoot et al. *Ap.J.* **371**(1991)L1.
- [2] see any good monography about modern cosmology. for example: E.Kolb, and M. Turner *The Early Universe*. (Addison-Wesley, 1990); A. Vilenkin and E.P.S. Shellard *Cosmic Strings and Other Topological Defects*. (Cambridge University Press, 1994); T. Padmanabhan *Structure Formation in the Universe*. (Caqmbriage University Press, 1995).
- [3] Y. Fujii *Nature* **234**(1971)5; R. Acharaya and P.A. Hlogan *Lett.Nuov.Cim.* **6**(1973)668; K.S. Stelle *Gen.Rel.Grav.* **9**(1978)353; R. Utiyama *Prog. Theor. Phys.* **72**(1984)83.
- [4] K.S. Stelle *Phys.Rev D* **16**(1977)953
- [5] G.W. Gibbons and B.F. Whiting *Nature* **291**(1981)626; C. Talmadge, J.-P. Berthias, R.W. Hellings and E.M. Standish *Phys.Rev.Lett.* **61**(1988)1159; C. Jekeli, D.H. Eckhardt and A.J. Romaides *Phys.Rev.Lett.* **64**(1990)1204.
- [6] R.H. Sanders *Astron. Astrophys.* **136**(1984) L21; M. Kenmoku, E. Kitajima, Y. Okamoto and K. Shigemoto, *Int. J. Mod. Phys. D* **2**(1993)123; D.Hadjimichef and F. Kokubun *submitted to publication*(1996).
- [7] J.E. Gunn, J.R. Gott *Ap.J.* **176**(1972)1.
- [8] J. Centrella and A. Mellot *Nature* **305**(1982).196; J.R. Primack, in *Proc. of The International School of Physics "Enrico Fermi"*, ed. N. Cabibbo, (North Holland 1984). 137.
- [9] M. Davis, G. Efstathiou, C. Frenk and S.D.M. White *Ap.J.* **292**(1985).371.
- [10] L. Spitzer *Physical Process in the Interstellar Medium*. Joh Wiley. New York (1978).
- [11] M. Kenmoku, Y. Okamoto and K. Shigemoto *Phys.Rev. D* **48**(1993)578; F. Kokubun *in preparation* (1996).

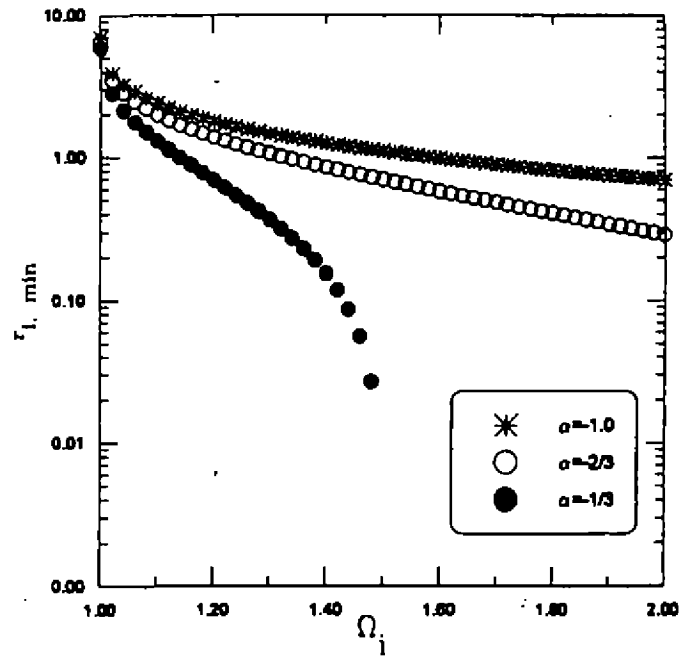
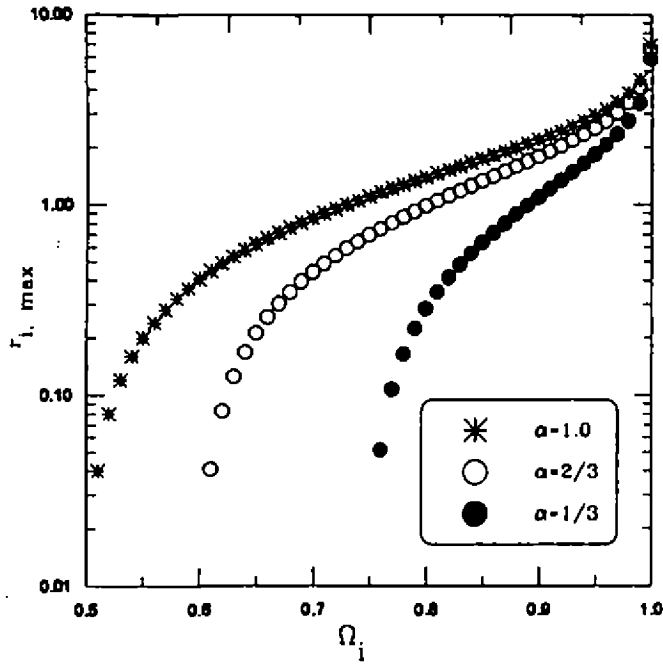


Figure 1. The critical radius $r_{i,max}$ for $\alpha > 0$ and $\Omega_i < 1$. The radius are expressed in units of μ^{-1} .

Figure 2. The critical radius $r_{i,min}$ for $\alpha < 0$ and $\Omega_i > 1$. The radius are expressed in units of μ^{-1} .

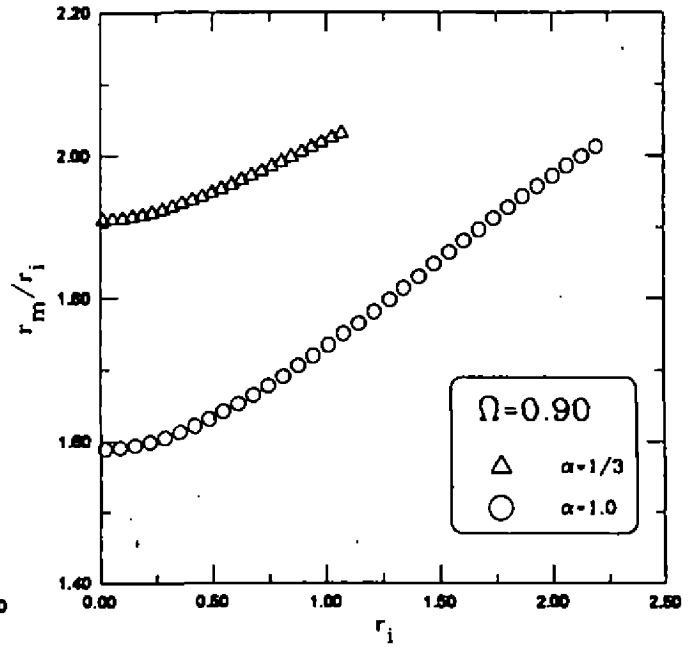
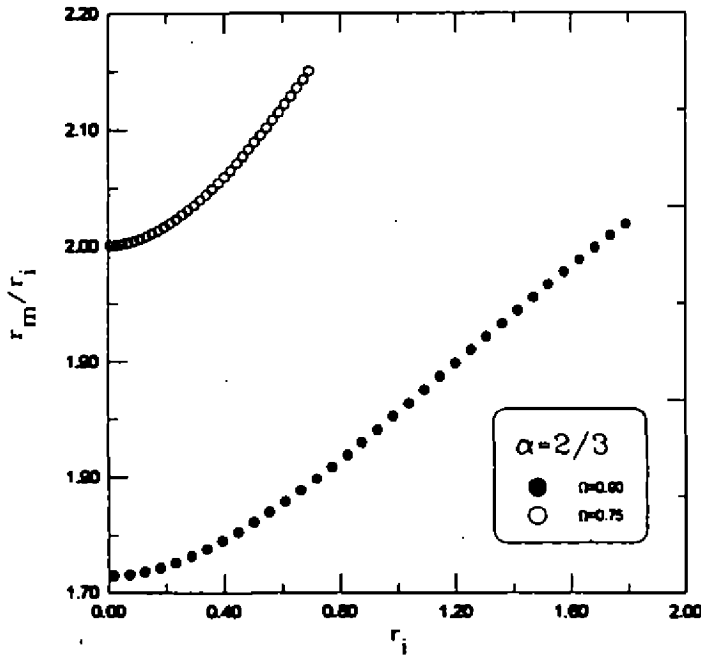


Figure 3. The ratio r_m/r_i with $\alpha = 2/3$ and $\Omega = 0.90$ and 0.75 . The r_i -axis is limited to $r_i < r_{i,max}$, with $r_{i,max} = 1.7918$ and 0.6931 , respectively when $\Omega = 0.90, 0.75$.

Figure 4. The ratio r_m/r_i , with $\Omega = 0.90$ and $\alpha = 1$ and $1/3$. The r_i -axis is limited to $r_i < r_{i,max}$, with $r_{i,max} = 2.1972$ and 1.0986 , respectively when $\alpha = 1, 1/3$.

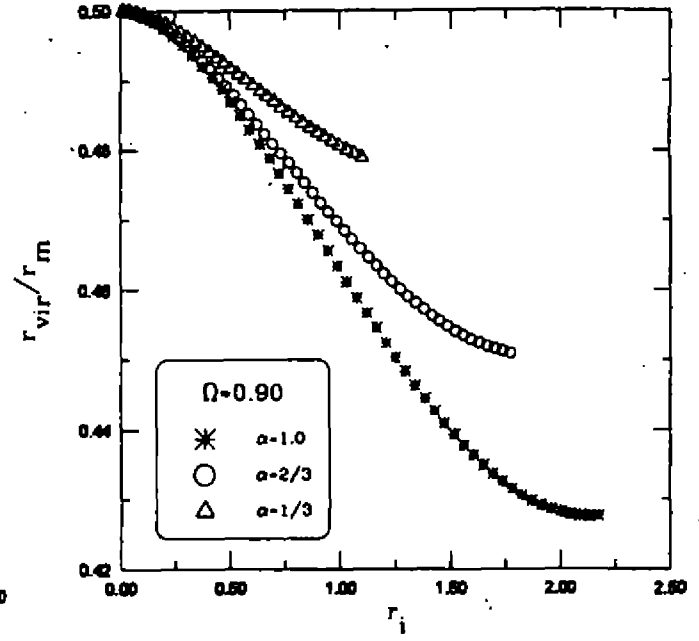
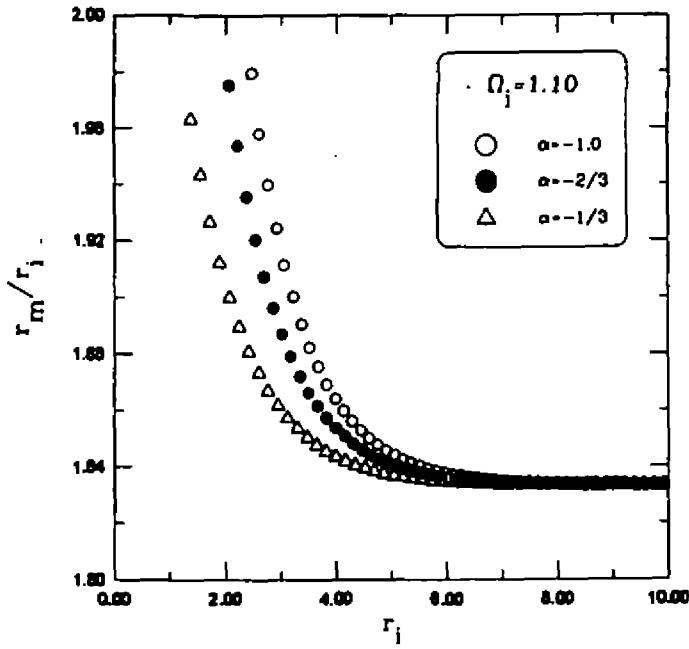


Figure 5. The ratio r_m/r_i with $\alpha < 0$ and $\Omega = 1.10$. The r_i -axis is limited to $r_i > r_{i,\min}$ with $r_{i,\min} = 2.3979, 1.9924$ and 1.2993 , respectively when $\alpha = -1, -2/3, -1/3$.

Figure 6. Graphics of r_{vir}/r_m with $\Omega = 0.90$ and $\alpha > 0$. The r_i -axis is limited to $r_i < r_{i,\max}$, with $r_{i,\max} = 2.1972, 1.7918$ and 1.09 , respectively when $\alpha = 1, 2/3, 1/3$.

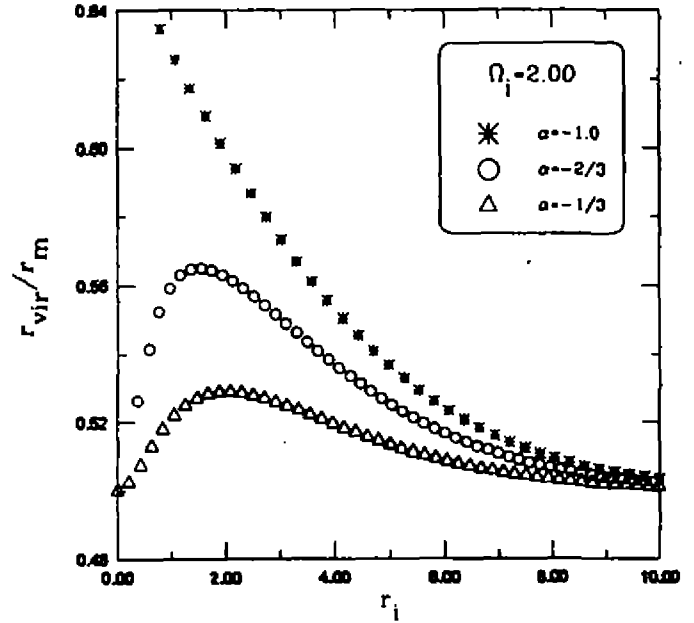
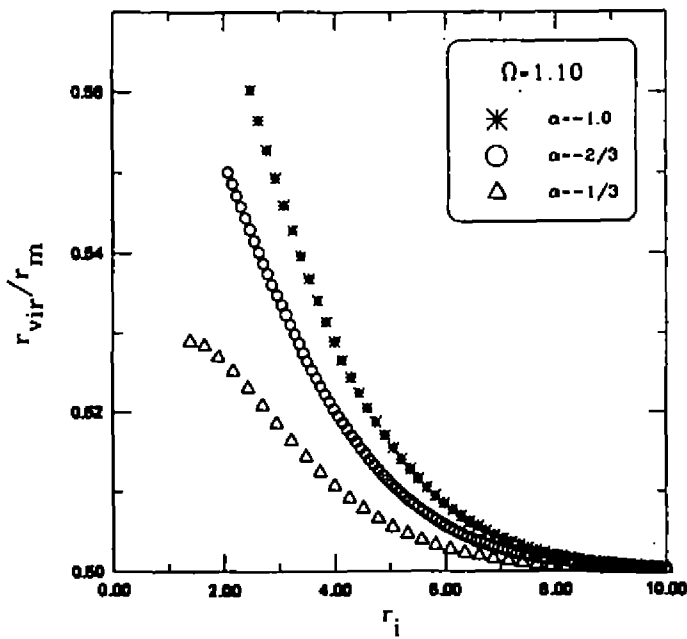


Figure 7. Graphics of r_{vir}/r_m with $\Omega = 1.10$ and $\alpha < 0$. The r_i -axis is limited to $r_i > r_{i,\min}$, with $r_{i,\min} = 2.3979, 1.9924$ and 1.229 , respectively when $\alpha = -1, -2/3, -1/3$.

Figure 8. Graphics of r_{vir}/r_m with $\Omega = 2.00$ and $\alpha < 0$. The r_i -axis is limited to $r_i > r_{i,\min}$, with $r_{i,\min} = 0.6931, 0.2877$ and -0.4055 , respectively when $\alpha = -1, -2/3, -1/3$.

Atomic Levels Shifts Between Plates: the Influence of Vacuum Polarization

G.L. Klimchitskaya*

Departamento de Física

Universidade Federal da Paraíba - João Pessoa

I.L. Tomashevsky

Technical Institute - Arkhangelsk, Russia

It is common knowledge that the vacuum effects of quantum field theory contribute to the atomic energy levels and transition probabilities. The best known example for this type of contribution is the appropriate component of the Lamb shift caused by the ν . In modern quantum optics the atoms inside some cavity are frequently dealt with. In such a situation some boundary conditions are imposed on the photons wave functions resulting in the change of vacuum modes and vacuum contribution to the Lamb shift. Such It is interesting to give a fully relativistic consideration of the part of frequency shift due to the retardation effects (i.e., for large L). For this purpose it is worthwhile to use the photon propagator in the presence of boundary conditions [2] w

$$D_{\mu\nu}(x, y) = D_{\mu\nu}^{(0)}(x - y) + \tilde{D}_{\mu\nu}(x, y), \quad (1)$$

where $D_{\mu\nu}^{(0)}(x - y)$ with $\mu, \nu = 0, 1, 2, 3$ is the usual free-space propagator in covariant gauge.

The second term in Eq. (1) is the boundary dependent part. In the region between the plates it may be presented as

$$\tilde{D}_{\mu\nu}(x, y) = \frac{1}{(2\pi)^3} \int d^3\vec{k} \sum_{s, \sigma} \frac{1 - \sigma e^{i\Gamma L}}{8\Gamma \sin(\Gamma L)} F_{\mu s \sigma}(k, x) F_{\nu s \sigma}(-k, y). \quad (2)$$

Here the indices take the values $\sigma = \pm 1$; $s = 1, 2$ (the coordinate axis x_3 is orthogonal to the boundaries), the three-dimensional vector \vec{k} has the components $\vec{k} = (k_0, k_1, k_2)$, and the notations are used

$$F_{\mu s \sigma}(k, x) = \tilde{e}_\mu^s e^{-ik_0 x^\alpha} (e^{i\Gamma x_3} + \sigma e^{-i\Gamma x_3}), \quad (3)$$

where $\alpha = 0, 1, 2$.

The photon polarization vectors in Eq. (3) are

$$\tilde{e}_\mu^1 = \begin{pmatrix} k_1^2 \\ k_0 k_1 \\ k_0 k_2 \\ 0 \end{pmatrix} \frac{1}{k_1 \Gamma}, \quad \tilde{e}_\mu^2 = \begin{pmatrix} 0 \\ k_2 \\ -k_1 \\ 0 \end{pmatrix} \frac{1}{k_1} \quad (4)$$

with the quantities $k_1 = \sqrt{k_1^2 + k_2^2}$ and $\Gamma = \sqrt{k_0^2 - k_1^2 + i\epsilon}$, where $\epsilon > 0$ which is to say that the propagator is causal. We use units in which $\hbar = c = 1$, $e^2 = 4\pi\alpha$, e is the electron charge, $\alpha = 1/137$ is the fine structure constant.

In the paper [3] using the propagator (2) the expression was obtained for the Rydberg energy level shift of Hydrogen atom. This expression, however, incorporated the summation over all the spectrum of states resulting in impossibility to separate and inve

*On leave from North-West Polytechnical Institute - St. Petersburg, Russia

By the use of the quantum electrodynamical perturbation theory of atomic spectra [4] the general relation for the self-energy corrections to the levels of a Hydrogen atom between the conducting plane parallel plates in the first order of perturbation theory

$$\Delta E_a = \frac{ie^2}{(2\pi)^3} \int d^3\vec{k} \sum_{s,\sigma} \frac{1 - \sigma e^{i\Gamma L}}{8\Gamma \sin(\Gamma L)} \int d^3x \int d^3y \psi_a^*(x) \gamma_0 \gamma_\mu \tilde{e}_\mu^s e^{-ik_\sigma x} \quad (5)$$

$$\times (e^{i\Gamma x_3} + \sigma e^{-i\Gamma x_3}) \sum_{a'} \frac{\psi_{a'}(x) \psi_{a'}^*(y)}{k_0 - \epsilon_{aa'} - i0} e^{ik_\sigma y} (e^{i\Gamma y_3} + \sigma e^{-i\Gamma y_3}) \tilde{e}_\nu^s \gamma^\nu \gamma^0 \psi_a(y).$$

Here the index β takes the values $\beta = 1, 2$, the index a denotes the Dirac electron wave functions (i.e., the set of four quantum numbers n, j, l, m [5]), and $\epsilon_{aa'} = E_a - E_{a'}$.

It is well to notice that the corrections to the energy level due to the change of the wave functions of atomic electron between plates and due to the change of the photon propagator are additive (as it should be in the lower order of perturbation theory).

When taking into account that the energy shift under consideration increases proportionally to n^3 (n being the principal quantum number) [1,3] we may neglect by the fine splitting of the energy levels in calculation of the correction (5). When it

$$|\epsilon_{nn'}(x_3 \pm y_3)| \ll 1, \quad \left| \frac{x_3 \pm y_3}{L} \right| \ll 1, \quad (6)$$

it has been possible to get the following expression after the long but straightforward calculations:

$$\Delta E_n = -\frac{e^2}{\pi L} \sum_{n' < n} \left[\epsilon_{nn'} \langle x_3 \rangle_{nn'}^2 \sum_{m=1}^{\infty} \left(\epsilon_{nn'} + \frac{2i}{Lm} \right) \frac{e^{i\epsilon_{nn'} L m}}{m} \right. \quad (7)$$

$$\left. - \frac{2i}{L} (\langle x_1 \rangle_{nn'}^2 + \langle x_2 \rangle_{nn'}^2) \left(\epsilon_{nn'} + \frac{i}{2L} \right) \sum_{m=1}^{\infty} \frac{e^{i(\epsilon_{nn'} L + \pi)m}}{m} \right] + O\left(\frac{e^2 n^6}{L^4 \alpha^4}\right).$$

The values of matrix elements $\langle x_i \rangle_{nn'} \equiv \langle \psi_n | x_i | \psi_{n'} \rangle$ are given in the monograph [5].

It is not complicated to get the contribution from the general expression (7) to the frequency shift of spectral line (the corresponding correction is determined by $\Delta \tilde{E}_n = \text{Re} \Delta E_n$) and to the change of spectral line width (described by $\text{Im} \Delta E_n$). Let us consider now the first of the mentioned corrections which will look like

$$\Delta \tilde{E}_n = \frac{e^2}{\pi} \sum_{n' < n} \left\{ \frac{\epsilon_{nn'}^2}{L} \langle x_3 \rangle_{nn'}^2 \ln \left| 2 \sin \frac{\epsilon_{nn'} L}{2} \right| \right. \quad (8)$$

$$+ \frac{2\epsilon_{nn'}}{L^2} [\langle x_3 \rangle_{nn'}^2 A_s(\epsilon_{nn'} L) - (\langle x_1 \rangle_{nn'}^2 + \langle x_2 \rangle_{nn'}^2) A_s(\epsilon_{nn'} L + \pi)]$$

$$\left. - \frac{1}{L^3} (\langle x_1 \rangle_{nn'}^2 + \langle x_2 \rangle_{nn'}^2) A_c(\epsilon_{nn'} L + \pi) \right\} + O\left(\frac{e^2 n^6}{L^4 \alpha^4}\right),$$

where

$$A_c(x) = \sum_{m=1}^{\infty} \frac{\cos mx}{m^2} = \arcsin^2 \left(\cos \frac{x}{2} \right) - \frac{\pi^2}{12}, \quad (9)$$

$$A_s(x) = \sum_{m=1}^{\infty} \frac{\sin mx}{m^2}.$$

We emphasize that the summation in the expressions (7), (8) is carried out only over the lower states of the discrete spectrum while the infinite summation occurs only in Eq. (9). Therefore the formula (8) is very convenient for the numerical calculations.

Let us note also that the first item in brackets in Eq. (8) tends to infinity when $\epsilon_{nn'} L = 2\pi l$, ($l = 1, 2, \dots$) and presents the resonant contribution which was obtained in paper [1] in nonrelativistic limit. It can be shown, however, that if the width of the levels is accounted for the magnitude of this item turns out to be of the same

$n' = 1$. Let $\epsilon_{n1}L = 2\pi l$, and Γ_n is the width of the upper level. Then the resonance term has to be written in the form

$$\frac{e^2}{\pi L} \langle x_3 \rangle_{n1}^2 \epsilon_{n1}^2 \frac{1}{\Gamma_n} \int_{-\Gamma_n/2}^{\Gamma_n/2} \ln(\epsilon L) d\epsilon = \frac{e^2}{\pi L} \langle x_3 \rangle_{n1}^2 \epsilon_{n1}^2 [\ln(\Gamma_n L) - 1]. \quad (10)$$

For all the possible values of the width Γ_n the contribution (10) into the level shift does not distinguish considerably by its value from the contribution of the nonresonant items of (8).

We will look now at the imaginary part of the correction (7) which defines the change of the spectral line width. It may be written in the form

$$\begin{aligned} \text{Im } \Delta E_n &= -\frac{e^2}{\pi} \sum_{n' < n} \left\{ \frac{\epsilon_{nn'}^2}{L} \langle x_3 \rangle_{nn'}^2 \arcsin \left(\cos \frac{\epsilon_{nn'} L}{2} \right) \right. \\ &+ \frac{2\epsilon_{nn'}}{L^2} [\langle x_3 \rangle_{nn'}^2 A_c(\epsilon_{nn'} L) - (\langle x_1 \rangle_{nn'}^2 + \langle x_2 \rangle_{nn'}^2) A_c(\epsilon_{nn'} L + \pi)] \\ &\left. - \frac{1}{L^3} (\langle x_1 \rangle_{nn'}^2 + \langle x_2 \rangle_{nn'}^2) A_s(\epsilon_{nn'} L + \pi) \right\}. \end{aligned} \quad (11)$$

The functions $A_c(x)$, $A_s(x)$ were given in Eq. (9).

Note that the item of the order $(e^2 n^6)/(L^4 n^4)$ in Eq. (7) is purely real. By this reason it contributes to the Eq. (8) but does not contribute to the Eq. (11).

The resulting expressions (8) (with regard to the averaging over the width of the levels of the Eq. (10) type) and (11) may be used for the calculations of atomic levels shifts and spectral lines widths which are necessary for the interpretation of partic

This work was partially supported by the International Science Foundation.

References

- [1] Barton G. *Physica Scripta* T21 (1988), 11.
- [2] Bordag M., Robaschik D. and Wieczorek E. *Ann. Phys. (NY)* 165 (1985), 192.
- [3] Bordag M. *Preprint*, NTZ 14-92, Leipzig University, 1992.
- [4] Labzowsky L., Klimchitskaya G. and Dmitriev Yu. *Relativistic Effects in the Spectra of Atomic Systems*. Bristol: IOP Publishing Ltd, 1993.
- [5] Bethe H.A. and Salpeter E.E. *Quantum Mechanics of One- and Two-Electron Atoms*. Berlin: Springer Verlag, 1957.

New Experiment for Obtaining Stronger Constraints on Hypothetical Particles of Modern Field Theory

G.L.Klimchitskaya¹, Ye.P.Krivtsov*, V.M.Mostepanenko², C.Romero, A.Ye.Sinelnikov*

Departamento de Física

Universidade Federal da Paraíba - João Pessoa

**D.I.Mendeleev Institute for Metrology, St.Petersburg, Russia*

¹*On leave from North-West Polytechnical Institute - St.Petersburg, Russia*

²*On leave from St. Petersburg State Technological Institute (Technical University) and A. Friedmann Laboratory for Theoretical Physics, Russia*

The search of additional long-range interactions between macrobodies has been the object of much concentrated attention of a number of authors (see the collection of references on the subject in [1]). Such interactions may be caused by the exchange of light elementary particles, predicted in unified gauge theories, supersymmetry and supergravity [2], between the atoms of distinct macrobodies. Among these particles are axion, scalar axion, dilaton, spin-one antigraviton etc. New interactions may arise also as corrections to the classical gravitational theory at small distances [3]. The potential of a force acting between two atoms separated by the distance r due to the exchange by light particles has the Yukawa form

$$V(r) = \alpha \frac{N_1 N_2}{r} \exp\left(-\frac{r}{\lambda}\right), \quad (1)$$

where $\lambda = m^{-1}$ is the Compton wave-length of a particle with mass m , α is the dimensionless interaction constant. The factors N_1, N_2 , which are the numbers of nucleons in atomic nuclei, were introduced for taking off the dependence of α on the sort of atom, i.e., on the nuclear charges. An action range λ in (1) may vary from one angstrom to hundreds of meters. We use the relativistic units, in which $\hbar = c = 1$. In the following we shall suppose that the long-range interaction field of a macrobody is the additive sum of the Yukawa-type fields of its atoms. Such supposition is justified by the smallness of long-range interactions.

The main objective of a number of investigations is to determine some constraints for the constants α, λ . In the paper [4] the recent constraints were collected resulting from the Eötvös-, Galileo- and Cavendish-type experiments, Casimir and van der Waals force measurements. In the action range $\lambda \geq 1$ m the best constraints on α result from the Eötvös experiment of paper [5]. Then with decreasing of λ the best constraints on α may be deduced (see [4,6]) from the Cavendish-type experiments of papers [7-9]. As a result the permitted region of (α, λ) -plane lies below some curve (see later).

In this paper we suggest to use the precise experimental setup [10] for obtaining stronger constraints on the constants of Yukawa-type interactions. This setup includes the large homogeneous steel sphere with a non-concentric spherical cavity in which the strictly homogeneous, flat gravitational field arises. The sphere may be rotated around some vertical axis coinciding with the technological opening. The rotation of the sphere results in the rotation of the gravitational field relative to the stationary detector mounted in is not homogeneous. The setup of this kind was created originally for the calibration of accelerometers [10]. In a really existing setup the sphere diameter is 600 mm, the cavity diameter is 475 mm. The sphere is made sectional so that the turning of The detector is inserted in the cavity through the opening into the place usually occupied by the accelerometer.

We suggest using the torsional pendulum as a sensitive element of additional interaction. The pendulum string passes into the cavity through the opening and coincides with a vertical rotational axis of the setup. The gravitational

forces acting upon two balls attached to the opposite ends of the pendulum beam of the length $2l$ are the same for any position of rotating sphere. It is a consequence of homogeneity of gravitational field inside the cavity. But the additional forces acting to different balls are not equal to each other to give rise to some torque which have to be registered. The most important characteristic of the detector is its sensitivity to acceleration a_{det} . Below the value $a_{\text{det}} \approx 10^{-12} \text{ cm/s}^2$ will be used, which is realistic one for the high level gravitational experiments (see, e.g., [11]). It surpasses in 10 times the acceleration of the detector test bodies due to thermodynamic fl

In the event of no additional interaction being registered the constraints on the parameters of this interaction will result from the inequality

$$M_{\text{max}} < M_{\text{det}} = 2m_0 l a_{\text{det}}, \quad (2)$$

where M_{max} is the maximal value of the torque produced by the additional interaction, and M_{det} is the sensitivity of the detector to the torque.

Let us start the calculation of the torque with the potential energy of one atom having N_2 nucleons in its nucleus and inserted into the spherical cavity of R_2 radius inside the steel sphere of R_1 radius. This last sphere is characterized by n_1 atoms in a unit volume with N_1 nucleons in their nuclei. The atom under consideration is located at a point M spaced r_1 apart from the center of the sphere and r_2 apart from the center of the cavity. Then its potential energy is

$$U(M) = \int_D d^3r V(r), \quad (3)$$

where $V(r)$ is the potential (1), D is the volume of the sphere with exception of the cavity and r being the distance between the point M and an arbitrary point of D .

Performing the integration in (3) with the use of (1) one gets the result:

$$U(M) = 4\pi N_1 N_2 n_1 \alpha \lambda^2 \left[\frac{R_2 + \lambda}{r_2} \sinh(\tilde{r}_2) \exp(-\tilde{R}_2) - \frac{R_1 + \lambda}{r_1} \sinh(\tilde{r}_1) \exp(-\tilde{R}_1) \right]. \quad (4)$$

Hereafter the tilde means that the corresponding quantity is divided by λ .

Let us consider as a test body the small spherical ball of radius r_0 with its center at a point M . Let the material of a ball have the atomic density n_2 and the number of nucleons in one nucleus N_2 . Integrating Eq.(4) over the volume of this ball we obtain its potential energy:

$$U_b(M) = 3n_2 v_0 f(\tilde{r}_0) U(M), \quad (5)$$

where $v_0 = 4\pi r_0^3/3$ is the volume of the ball,

$$f(x) \equiv \frac{1}{x^2} \left(\cosh x - \frac{\sinh x}{x} \right). \quad (6)$$

Note that the quantity $f(\tilde{r}_0) \approx 1/3$ for all values of r_0, λ to be used later.

Now it is possible to calculate the torque due to additional interaction acting on the torsional pendulum detector.

In Fig. 1 the projection of the torsional pendulum is shown onto the plane orthogonal to the rotational axis of the setup and passing through the centers of the sphere O_1 and the cavity O_2 . The detector itself may be located at some distance h below or above this plane. Using the Eqs.(4),(5) we get the potential energy of the detector:

$$U_d = 12\pi N_1 N_2 n_1 n_2 \alpha \lambda^2 v_0 f(\tilde{r}_0) \left\{ A(\tilde{R}_2) \left[B(\tilde{r}_2^{(+)}) + B(\tilde{r}_2^{(-)}) \right] - A(\tilde{R}_1) \left[B(\tilde{r}_1^{(+)}) + B(\tilde{r}_1^{(-)}) \right] \right\}. \quad (7)$$

where

$$r_i^{(\pm)} = (r_i^2 + h^2 + l^2 \pm 2r_i l \cos \varphi_i)^{1/2}, \quad i = 1, 2. \quad (8)$$

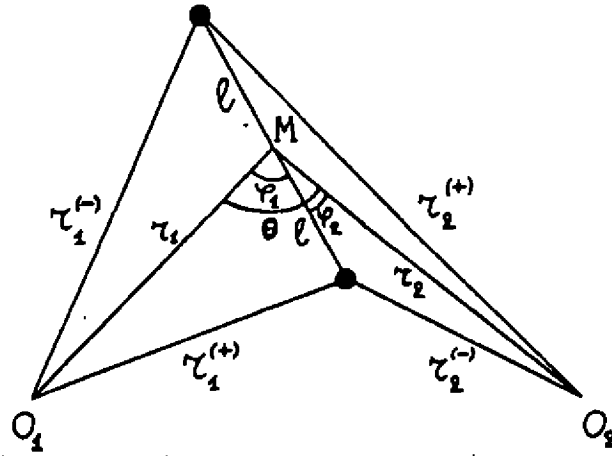


Figure 1.: The position of the detector relatively to the centers of the sphere \$O_1\$ and of the cavity \$O_2\$ (the point \$M\$ is the projection of the setup rotational axis which is orthogonal to the plane of the figure).

In (7) we also used the notations

$$A(x) = e^{-x}(1+x), \quad B(x) = \frac{\sinh x}{x}. \tag{9}$$

From geometrical considerations (see the Fig. 1) it is evidently seen that \$\cos \varphi_2 = \cos(\varphi_1 - \theta)\$. Further we will use the notation \$\varphi \equiv \varphi_1\$.

The torque we are looking for may be expressed as

$$M = -\frac{\partial U_d}{\partial \varphi}, \tag{10}$$

where \$U_d\$ is given by (7).

Differentiating in accordance with (10) we get the result:

$$M = 12\pi N_1 N_2 n_1 n_2 \alpha v_0 f(\bar{r}_0) l \left\{ A(\tilde{R}_2) \left[f(\tilde{r}_2^{(+)}) - f(\tilde{r}_2^{(-)}) \right] r_2 \sin(\varphi - \theta) - A(\tilde{R}_1) \left[f(\tilde{r}_1^{(+)}) - f(\tilde{r}_1^{(-)}) \right] r_1 \sin \varphi \right\}. \tag{11}$$

To obtain the desired constraints for a fixed position of the detector inside a cavity it is necessary to find the maximal value of \$M\$ with respect to \$\varphi\$. In the general case this may be done only as a result of computations which are not very descriptive. But if the detector is located at a plane of the sphere and cavity centers which is orthogonal to the axis of the setup (i.e., \$h = 0\$), the analytical investigation may be performed equally well.

To do this let us expand the energy \$U_d\$ from (7) which is a periodic function of \$\varphi\$ in Fourier series. After long but straightforward calculations[12] we will find

$$U_d = 24\pi^2 N_1 N_2 n_1 n_2 \alpha \lambda^2 v_0 f(\bar{r}_0) \times \left\{ \frac{a_0}{2} + \sum_{k=1}^{\infty} \left[a_k^{(2)} \cos(2k\varphi_2) - a_k^{(1)} \cos(2k\varphi_1) \right] \right\}, \tag{12}$$

where the coefficients are:

$$a_k^{(i)} = \frac{\lambda}{\sqrt{l r_i}} A(\tilde{R}_i) \sum_{m=k}^{\infty} \frac{4m+1}{16^m} \binom{2(m+k)}{m+k} \binom{2(m-k)}{m-k} I_{2m+\frac{1}{2}}(\tilde{r}_i) I_{2m+\frac{1}{2}}(\tilde{r}_i) \tag{13}$$

and \$a_0 \equiv a_0^{(1)} + a_0^{(2)}\$, \$I_\nu(z)\$ are Bessel functions of imaginary argument.

Differentiating the quantity (12) with respect to $\varphi \equiv \varphi_1$ we obtain the net result

$$M = 48\pi^2 N_1 N_2 n_1 n_2 \alpha \lambda^2 v_0 f(\bar{r}_0) \sum_{k=1}^{\infty} k \left[a_k^{(2)} \sin 2k(\varphi - \theta) - a_k^{(1)} \sin 2k\varphi \right]. \quad (14)$$

It is seen from (13) that the coefficients of the series (14) decrease very quickly with the increasing of k so that in the region $\lambda \gtrsim 2$ cm it is quite sufficient to take into account only $a_k^{(i)}$ -terms of (14). Let us represent the maximal value of the torques, which are given in (11) or (14), by the angle φ in the following way

$$M_{\max} = 12\pi N_1 N_2 n_1 n_2 \alpha v_0 f(\bar{r}_0) Q(\lambda, l, r_1, r_2, h). \quad (15)$$

Here the multipliers before Q are extracted as a matter of convenience, Q is the maximal value in φ of all the other multipliers (11) or (14). So in the general case (Eq.(11))

$$Q(\lambda, l, r_1, r_2, h) = l \max_{\varphi} \left\{ A(\bar{R}_2) \left[f(\bar{r}_2^{(+)}) - f(\bar{r}_2^{(-)}) \right] r_2 \sin(\varphi - \theta) - A(\bar{R}_1) \left[f(\bar{r}_1^{(+)}) - f(\bar{r}_1^{(-)}) \right] r_1 \sin \varphi \right\}. \quad (16)$$

In the particular case $h = 0$, where the Fourier expansion (14) is valid,

$$Q(\lambda, l, r_1, r_2, 0) = 4\pi \lambda^2 \max_{\varphi} \sum_{k=1}^{\infty} k \left[a_k^{(2)} \sin 2k(\varphi - \theta) - a_k^{(1)} \sin 2k\varphi \right]. \quad (17)$$

In the case when no additional interaction was registered the constraints on the parameters of this interaction result from the inequality (2). Regarding to Eq.(15) it is seen that the constraints on α, λ do not depend on the parameters of the torsional pendulum balls. In fact, the multiplier before Q in the right-hand side of (15) may be transformed to

$$12\pi N_1 N_2 n_1 n_2 \alpha v_0 f(\bar{r}_0) = 12\pi \frac{\rho \rho_0}{m_p^2} \alpha v_0 f(\bar{r}_0), \quad (18)$$

where ρ, ρ_0 are the densities of the sphere and of the test body, and m_p is the proton mass.

Substituting (15) into (2) taking account of (18) and using the evident equality $\rho_0 v_0 = m_0$ we bring Eq.(2) to the form (with the restored constants \hbar and c)

$$\alpha \leq \frac{m_p^2}{2\pi \rho \hbar c} \frac{a_{\text{det}} l}{Q(\lambda, l, r_1, r_2, h)}, \quad (19)$$

where the approximate equality $f(\bar{r}_0) \approx 1/3$ was used.

The numerous calculations were performed using the result (19) for the different positions of the detector inside a cavity and for the different values of l with $0.1 \text{ cm} \leq l \leq 500 \text{ cm}$. Let us start with the geometrical sizes of the existing setup [10]. In this case the constraints on α, λ practically do not depend on the value of l . Because of this, in the following we shall use the value $l = 4 \text{ cm}$ (the distance between two balls of the torsional pendulum is $2l = 8 \text{ cm}$).

Different positions of the rotational axis have been considered as well as of the detector along the rotational axis. In order to get the strongest constraints it is necessary to make the configuration of the setup maximally non-symmetric. The way to realize it is to place the rotational axis of the setup maximally close to the boundary of the cavity from inside. Our calculations have shown that the best position of the axis is the following. One of the detector's balls is bound to be near the wall of the cavity whereas the axis itself — approximately in the middle between the wall of the cavity and the center of the sphere. For the obtaining of the strongest constraints the detector balls and the centers of the sphere and of the cavity should lie in one plane orthogonal to the rotational axis ($h = 0$) with $\theta = 0$ (see Fig. 1).

Here the constraints may be found by the Eq.(19), using for Q the expression (17) with the Fourier coefficients (13). As the calculations show the region of λ for which the known to date constraints may be strengthened is $0.3 \text{ cm} \leq \lambda \leq 2 \text{ m}$.

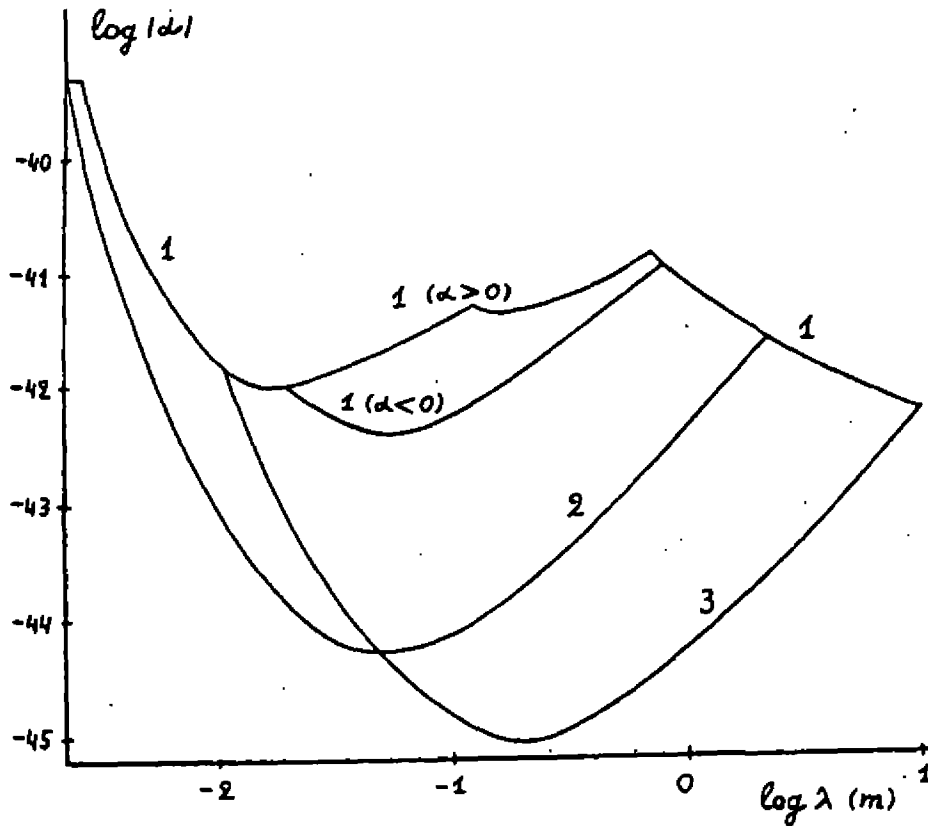


Figure 2.: The constraints on the parameters of Yukawa-type interactions which may be obtained from the proposed experiment (curve 1 — known to date; curve 2 — may be obtained by the use of existing setup; curve 3 — may be obtained by the use of especially designed setup of this kind).

The results of the performed calculations are shown in Fig. 2. The permitted regions of (α, λ) -plane lie below the curves. Curve 2 corresponds to the optimal position of the setup rotational axis giving the strongest constraints on α, λ ($r_1 = 12$ cm, $r_2 = 18$ cm, $\theta = 0$, see Fig. 1). The best strengthening in 400 times holds for $\lambda \approx 6$ cm ($\alpha > 0$).

Let us now consider the constraints which may be obtained by the use of a specially designed setup under discussion. To shift a minimum point of curve 2 in Fig. 2 to the right (where the strength of the known to date constraints is moderately high)

There is evidently a strong interest for carrying out the proposed experiment.

Two of the authors (G.L.K. and V.M.M.) thank the Department of Physics of the Federal University of Paraiba for kind hospitality. C. Romero was partially supported by CNPq.

References

- [1] E. Fischbach et al., *Metrologia* 29 (1992), 215.
- [2] J. Kim, *Phys. Rep.* 150 (1987), 1.
- [3] V.de Sabbata, V.N. Melnikov and P.I.Pronin, *Progr. Theor. Phys.* 88 (1992), 623.
- [4] V.M. Mostepanenko and I.Yu. Sokolov, *Phys.Rev.* D47 (1993), 2882.
- [5] B.R. Heckel et al., *Phys. Rev. Lett.* 63 (1989), 2705.
- [6] V.M. Mostepanenko and I.Yu. Sokolov, *Phys. Lett.* A132 (1988), 313.
- [7] J.K. Hoskins et al., *Phys. Rev.* D32 (1985), 3084.
- [8] Y.T. Chen, A.H. Cook and A.J.F. Metherell, *Proc. Roy. Soc. Lond.* A394 (1984), 47.

- [9] V.P. Mitrofanov and O.I. Ponomareva, *Sov. Phys. JETP* 67 (1988), 1963.
- [10] Yu.V. Tarbeyev, Ye.P. Krivtsov, A.Ye. Sinelnikov and A.A. Yankovsky, *Bulletin Seismol. Soc. Amer.* 84 (1994), 438.
- [11] V.I. Panov and V.N. Frontov, *Sov. Phys. JETP* 50 (1979), 852.
- [12] G.L. Klimchitskaya et al., Preprint: UFPB-DF-002/96, J.Pessoa, 1996.

The $(\lambda\varphi^4 + \sigma\varphi^6)_{D=3}$ Model at Finite Temperature and the Tricritical Phenomena

Gino N.J. Añaños and N.F. Svaiter*

Centro Brasileiro de Pesquisas Físicas-CBPF

Rua Dr. Xavier Sigaud 150, Rio de Janeiro, RJ 22290-180 Brazil

The thermodynamics of the massive $\lambda\varphi^4 + \sigma\varphi^6$ model is analyzed at finite temperature in the two-loop approximation. The behavior of the thermal mass and coupling constant is discussed. We demonstrate in the two-loop approximation the existence of a tricritical point.

1 Introduction

The field theory with a $\lambda\varphi^4$ self-interaction has been extensively studied in the literature. General expressions for Feynman diagrams at zero temperature have been calculated up to the four-loop order [1]. In the same way, some years ago the temperature dependence of the renormalized mass and coupling constant was analyzed [2]. More recently different methods have been used to study finite temperature quantum field theory [3] [4].

The purpose of this paper is to present a two-loop calculation of the $(\lambda\varphi^4 + \sigma\varphi^6)_{D=3}$ model. For simplicity we assume that the dimension of the order parameter is one. We obtain the thermal correction to the square mass $m^2(\beta)$ and coupling constant $\lambda(\beta)$. If the thermal coupling constant $\lambda(\beta)$ becomes negative (for positive square mass $m^2(\beta)$) a first-order phase transition may occur. For negative square mass and positive $\lambda(\beta)$ we have a second order phase transition. The point $m^2(\beta) = \lambda(\beta) = 0$ defines the tricritical point [5]. Some systems such as metamagnets (antiferromagnets in the presence of a strong external field) or the $He^3 - He^4$ mixture exhibit such behavior. A tree-level discussion of the tricritical phenomenon can be found in Refs.[6] [7]. For a treatment using the Callan-Zymanzik equation see for example ref.[8]

We compute $\Gamma^{(2)}(0)$ and $\Gamma^{(4)}(0)$ up to second order in perturbation theory and prove that the two-loop approximation is enough to obtain the tricritical point where a line of second order phase transition merges smoothly at this point with a line of first order phase transition. This paper is organized as follows. In section II we will review some general formalism. In section III the thermal corrections to the mass and coupling constant $\lambda(\beta)$ for the two-loop one particle irreducible diagrams $\Gamma^{(2)}(0)$ and $\Gamma^{(4)}(0)$ are presented. Conclusions are given in section IV. Through this paper we use $\hbar = c = 1$.

2 General formalism

Let us consider the vacuum to vacuum persistence functional in the presence of an external scalar source $J(x)$.

$$Z(J) = \int \mathcal{D}\varphi \exp\left(-\int d^Dx (\mathcal{L}(\varphi) - J(x)\varphi(x))\right) \quad (1)$$

where

$$\mathcal{L}(\varphi) = \frac{1}{2}(\partial\varphi)^2 + \frac{1}{2}m^2\varphi^2 + \frac{1}{4!}\lambda\varphi^4 + \frac{1}{6!}\sigma\varphi^6. \quad (2)$$

The problem we will study is to find a tricritical temperature $\beta^{-1}(m, \lambda, \sigma)$ for a set of values of m , λ and σ where the 1PI diagrams $\Gamma^{(2)}(0)$ and $\Gamma^{(4)}(0)$ vanish. This point defines the tricritical point. Consequently let us examine

*e-mail:nfuxsvai@cal.drpf.cbpf.br

the thermal effects over $\Gamma^{(2)}(0)$ and $\Gamma^{(4)}(0, 0, 0, 0) \equiv \Gamma^{(4)}(0)$. We will calculate explicitly the two-loop contribution to the renormalized thermal mass and coupling constant. The diagrams contributing to the two-point function are:

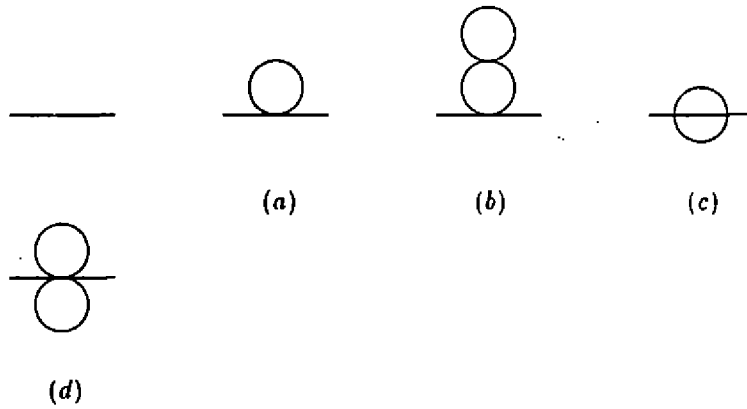


fig.(1) - The diagrams that contributes to the 1PI two-point functions.

The diagrams that contributes to the four-point functions are:

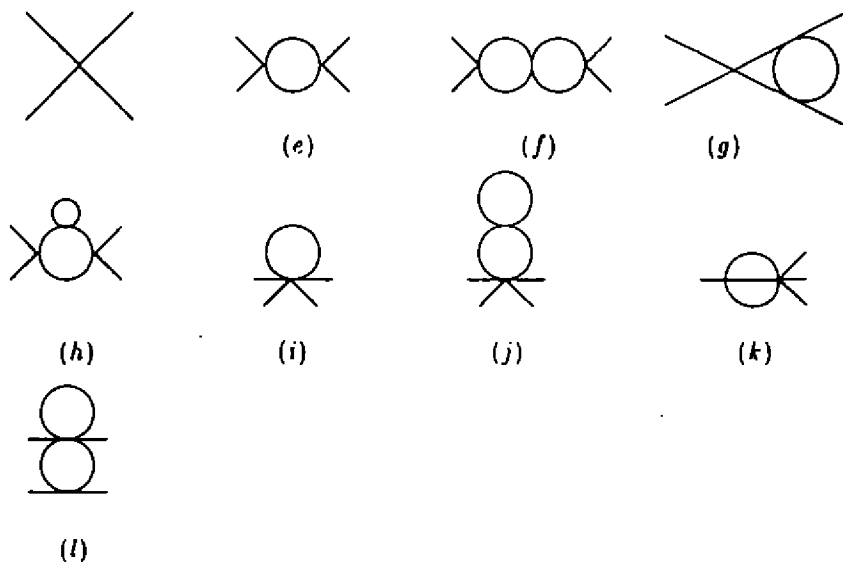


fig.(2) - The diagrams that contributes to the 1PI four-point functions.

It is possible to obtain the expressions for $\Gamma^{(2)}(0)$ and $\Gamma^{(4)}(0)$, given by:

$$\Gamma^{(2)}(0) = m^2 + \frac{1}{2}\lambda(a) - \frac{1}{4}\lambda^2(b) - \frac{1}{6}\lambda^2(c) - \frac{1}{8}\sigma(d) \quad (3)$$

and

$$\begin{aligned} \Gamma^{(4)}(0) = & \lambda - \frac{3}{2}\lambda^2(e) + \frac{3}{4}\lambda^3(f) + 3\lambda^3(g) + \frac{3}{2}\lambda^3(h) \\ & - \frac{1}{2}\sigma(i) + \frac{1}{4}\lambda\sigma(j) + \frac{2}{3}\lambda\sigma(k) + \frac{1}{2}\lambda\sigma(l), \end{aligned} \quad (4)$$

where:

$$(a) = \frac{1}{(2\pi)^D} \int \frac{d^D q}{(q^2 + m^2)} \quad (5)$$

$$(b) = \frac{1}{(2\pi)^{2D}} \int \frac{d^D q_1}{(q_1^2 + m^2)} \int \frac{d^D q_2}{(q_2^2 + m^2)^2} \quad (6)$$

$$(c) = \frac{1}{(2\pi)^{2D}} \int \frac{d^D q_1 d^D q_2}{(q_1^2 + m^2)(q_2^2 + m^2)((q_1 + q_2)^2 + m^2)} \quad (7)$$

$$(d) = \left(\frac{1}{(2\pi)^D} \int \frac{d^D q}{(q^2 + m^2)} \right)^2 \quad (8)$$

$$(e) = \frac{1}{(2\pi)^D} \int \frac{d^D q}{(q^2 + m^2)^2} \quad (9)$$

$$(f) = \left(\frac{1}{(2\pi)^D} \int \frac{d^D q}{(q^2 + m^2)^2} \right)^2 \quad (10)$$

$$(g) = \frac{1}{(2\pi)^{2D}} \int \frac{d^D q_1 d^D q_2}{(q_1^2 + m^2)(q_2^2 + m^2)((q_1 + q_2)^2 + m^2)^2} \quad (11)$$

$$(h) = \frac{1}{(2\pi)^{2D}} \int \frac{d^D q_1}{(q_1^2 + m^2)} \int \frac{d^D q_2}{(q_2^2 + m^2)^3} \quad (12)$$

$$(i) = \frac{1}{(2\pi)^D} \int \frac{d^D q}{(q^2 + m^2)} \quad (13)$$

$$(j) = \frac{1}{(2\pi)^{2D}} \int \frac{d^D q_1}{(q_1^2 + m^2)} \int \frac{d^D q_2}{(q_2^2 + m^2)^2} \quad (14)$$

$$(k) = \frac{1}{(2\pi)^{2D}} \int \frac{d^D q_1 d^D q_2}{(q_1^2 + m^2)(q_2^2 + m^2)((q_1 + q_2)^2 + m^2)} \quad (15)$$

$$(l) = \frac{1}{(2\pi)^{2D}} \int \frac{d^D q_1}{(q_1^2 + m^2)} \int \frac{d^D q_2}{(q_2^2 + m^2)^2} \quad (16)$$

3 The tricritical phenomenon

The aim of this section is to show that there is a temperature where the tricritical phenomenon appears. In order to regularize the model we can choose among a plethora of regularization procedures: Pauli-Villars, dimensional regularization, momentum cutoff, etc. We prefer to use a mixing between dimensional and zeta function analytic regularization. Therefore let us define:

$$I_{\beta}(D, s) = 1/\beta \sum_{n=-\infty}^{\infty} \int \frac{d^{D-1}k}{(2\pi)^{D-1}} \frac{1}{(\omega_n^2 + k^2 + m^2)^s} \quad (17)$$

Writing $\Gamma^{(2)}(0)$ and $\Gamma^{(4)}(0)$ as a function of $I_{\beta}(D, s)$ we have:

$$\begin{aligned} \Gamma^{(2)}(0) &= m^2 + \frac{1}{2}\lambda I_{\beta}(D, 1) - \frac{1}{4}\lambda^2 I_{\beta}(D, 1)I_{\beta}(D, 2) \\ &\quad - \frac{1}{6}\lambda^2(c) - \frac{1}{8}\sigma(I_{\beta}(D, 1))^2, \end{aligned} \quad (18)$$

and

$$\begin{aligned} \Gamma^{(4)}(0) &= \lambda - \frac{3}{2}\lambda^2 I_{\beta}(D, 1) + \frac{3}{4}\lambda^3(I_{\beta}(D, 2))^2 + 3\lambda^3(g) + \frac{3}{2}\lambda^3 I_{\beta}(D, 1)I_{\beta}(D, 3) \\ &\quad - \frac{1}{2}\sigma I_{\beta}(D, 1) + \frac{1}{4}\lambda\sigma I_{\beta}(D, 1)I_{\beta}(D, 2) + \frac{2}{3}\lambda\sigma(k) \\ &\quad + \frac{1}{2}\lambda\sigma I_{\beta}(D, 1)I_{\beta}(D, 2). \end{aligned} \quad (19)$$

Using the analytic extension of the inhomogeneous Epstein zeta function it is possible to obtain $I_{\beta}(D, s)$:

$$I_{\beta}(D, s) = \frac{m^{D-2s}}{(2\pi^{\frac{1}{2}})^D \Gamma(s)} \left(\Gamma(s - \frac{D}{2}) + 4 \sum_{n=1}^{\infty} \left(\frac{2}{mn\beta}\right)^{\frac{D}{2}-s} K_{\frac{D}{2}-s}(mn\beta) \right). \quad (20)$$

where $K_{\nu}(z)$ is the modified Bessel function of third kind [9]

It follows that there is a set of values of the parameters m^2 , σ and λ for each temperature which leads to the vanishing of the thermal physical mass $m^2(\beta)$ and coupling constant $\lambda(\beta)$, i.e., the critical line in the parameter space. Note that the basis of all considerations above assume that the sunset and related diagrams can not modify the tricritical behavior.

A straightforward calculation gives for $I_{\beta}(3, 1)$, $I_{\beta}(3, 2)$ and $I_{\beta}(3, 3)$

$$I_{\beta}(3, 1) = \frac{m}{2\pi} \left(-\frac{1}{2} + \sum_{n=1}^{\infty} \left(\frac{1}{mn\beta}\right) e^{-mn\beta} \right) \quad (21)$$

$$I_{\beta}(3, 2) = \frac{1}{16\pi m} \left(\frac{1}{2} + \frac{1}{e^{m\beta} - 1} \right) \quad (22)$$

and finally

$$I_{\beta}(3, 3) = \frac{1}{16m^3} \left(\frac{1}{2} + \frac{1}{e^{m\beta} - 1} + \sum_{n=1}^{\infty} (mn\beta) e^{-mn\beta} \right). \quad (23)$$

To evaluate the sum in $I_{\beta}(3, 1)$ we use the following trick

$$\sum_{n=1}^{\infty} \left(\frac{1}{mn\beta}\right) e^{-mn\beta} = \frac{1}{m\beta} \sum_{n=1}^{\infty} \frac{(e^{-m\beta})^n}{n} = -\frac{1}{m\beta} \ln(1 - e^{-m\beta}) \quad (24)$$

Eq.(32) can be written as

$$I_{\beta}(3, 3) = \frac{1}{16m^3} \left(\frac{1}{2} + \frac{1}{e^{m\beta} - 1} + m\beta \frac{e^{-m\beta}}{(e^{m\beta} - 1)^2} \right) \quad (25)$$

The idea is to define the quantities $x = m\beta$, $y = \frac{\lambda}{m}$ and $z = \sigma$. In the space (x, y, z) the condition $\Gamma^2(0) = 0$ defines a surface. The same happens for $\Gamma^4(0)$. The intersection of both surfaces defines a tricritical line. (See fig.(3)).

The effective potential as a function of the vacuum expectation value of the field and $m\beta$ can be plotted. The temperature is the parameter that allows us to interpolate between the two configurations: a metastable state at $\langle \varphi \rangle = 0$ in the low temperature regime with first-order phase transition and a second order phase transition in the high temperature regime. (See fig.(4)). At some intermediate temperature the tricritical point appears.

In the high temperature regime it is possible to write

$$I_{\beta}(3, 1) = \frac{m}{2\pi} \left(-\frac{1}{2} + \sum_{k=1}^{\infty} \frac{(m\beta)^{k-1}}{k!} \right). \quad (26)$$

and

$$I_{\beta}(3, 2) = \frac{1}{16m\pi} \sum_{k=0}^{\infty} \frac{B_{2k}}{(2k)!} (m\beta)^{2k-1}, \quad (27)$$

where B_n are the Bernoulli coefficients.

A possible method to deal with the system in the high temperature regime is dimensional reduction (DM). This approach has been used by many authors [10]. The basic idea is that in the imaginary time formalism the free propagator has a form $(\omega_n + p^2 + m^2)^{-1}$. The Matsubara frequency act like a mass so that in the high temperature regime the non-static modes ($n \neq 0$) decouple and we have a three dimensional theory after the integration of the non-zero modes. Of course this effective model will describe the original model only for distances $R \gg \beta$.

4 Conclusion

By studying the $(\lambda\varphi^4 + \sigma\varphi^6)_{D=3}$ model at finite temperature we have obtained a well known result. We proved that for each set of values of m , λ and σ there is a temperature $\beta^{-1}(m, \lambda, \sigma)$ where the physical thermal mass $m^2(\beta)$ and coupling constant $\lambda(\beta)$ vanish. One remarks should be made. The existence of the tricritical point can not be modified with the inclusion of the sunset and related graphs. The inclusion of these graphs will only change the temperature of the tricritical point.

A natural extension of this paper is to calculating the decay rate of the metastable state $\langle \varphi \rangle = 0$ with nucleation of bubbles in the low temperature regime [11]. For $m\beta > m\beta_c$, the solution $\langle \varphi \rangle = 0$ is a unstable minimum of the potential (the false vacuum), and it is possible to evaluate the probability per unit time and volume for the false vacuum to decay into the true vacuum of the model. To calculate the decay rate it is necessary to evaluate the instanton solution and a gaussian integral around the instanton. This subject is under investigation in this model.

Acknowledgment

We would like to thank Prof.A.P.C.Malbouisson for several helpful discussions. This work was supported by Conselho Nacional de Desenvolvimento Científico e Tecnológico-CNPq.

References

- [1] A.A.Vladimirov, *Theor. Math. Phys.* **36**, 732, (1978), F.M.Dittes, Y.A.Kubyshev and O.V.Tarasov, *Theor.Math.Phys.* **37**, 879 (1978).
- [2] K.Babu Joseph, V.C.Kuriakose and M.Sabir, *Phys.Lett* **115B**, 120 (1982), O.J.Eboli and G.C.Marques, *Phys.Lett* **162B**, 189 (1985), H.A.Weldon, *Phys.Lett* **174B**, 427, (1986), K.Takahashi, *Z.Phys.* **C20**, 601 (1985), T.Aither, *Phys.Lett* **B238**, 360 (1990).
- [3] N.Banerjee and S.Mallik, *Phys.Rev.D* **43**, 3368 (1991), M.E.Carrington, *Phys.Rev.D* **45**, 2933 (1992), P.Arnold, *Phys.Rev.D* **46**, 2628 (1992), R.P.Parwani, *Phys.Rev.D* **45**, 4695 (1992), R.P. Parwani and H.Singh, *Phys.Rev.D* **51**, 4518 (1995).

- [4] J.Frenkel, A.V.Saa and J.C.Taylor, Phys.Rev.D **46**, 3670 (1992), F.T.Brandt, J.Frenkel and J.C.Taylor. Phys.Rev D **44**, 1801 (1991).
- [5] M.Blume, V.J.Emery and R.B.Griffiths, Phys.Rev.A **4**, 1071 (1971), E.Eberhand, K.Riedel and F.J.Wegner, Phys.Rev.Lett. **29**, 349 (1972), J.C.Le Guillou and J.Zinn Justin. Phys.Rev. Lett **39**, 95 (1977), D.Boyanovsky and L. Masperi, Phys.Rev.D **21**, 1550 (1980), H.Hamber, Phys.Rev.B **21**, 3999 (1980) and R.Pisarski, Phys.Rev.Lett. **48**, 574 (1982).
- [6] C.Itzykson and J.M.Drouffe,"Statistical Field Theory", Cambridge University Press (1989). Cambridge, England.
- [7] K.Huang,"Statistical Mechanics", John Willey e Sons, Inc (1987) New York.
- [8] C.A.Aragão de Carvalho, Nucl.Phys. **119**, 401 (1977).
- [9] N.N.Lebedev, "Special functions and their applications" Dover Publication. Inc. N.Y.(1972).
- [10] T.Appelquist and R.D.Pisarski, Phys.Rev.D **23**, 2305 (1981), S.Nakarni. Phys.Rev.D **27**, 917 (1983). *ibid* Phys.Rev.D **38**, 3287 (1988), A.N.Jourjine, Ann.Phys. **155**, 305. (1984), R.F.Alvarez Estrada Phys.Rev.D **36**, 2411 (1987), K.Farakos, K.Kajantie, K.Dummukaienen and M.Shaposhnikov, Nucl.Phys. **B245**, 67 (1994) and E.Braaten and A.Nieto, Phys.Rev.D **51**, 6990 (1995).
- [11] A.D.Linde, Nucl.Phys. **B216**, 421 (1983), E.Weinberg and A.Wu. Phys.Rev.D **36**, 2477 (1987), M.Gleiser, G.C.RMarques and R.O.Ramos, Phys. Rev.D **48**, 1571 (1993).

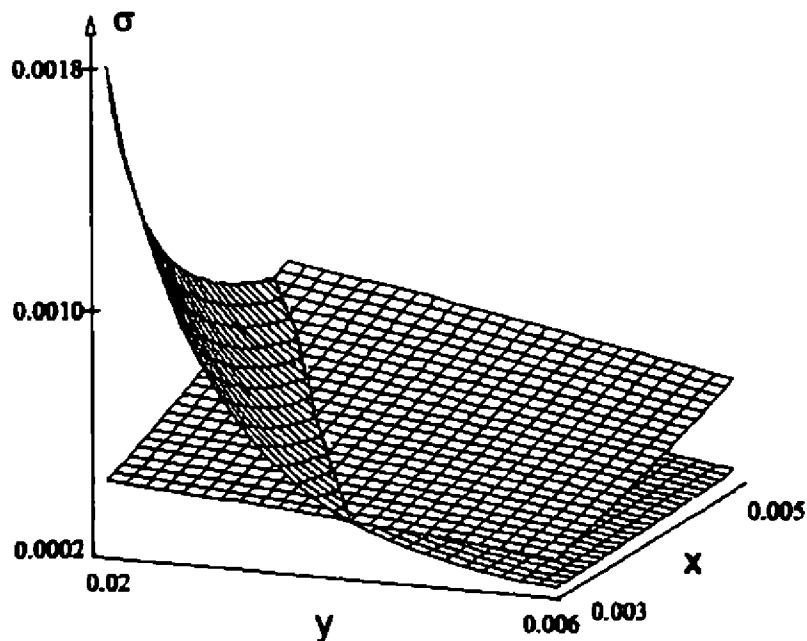


Figure 3. The two surfaces $\Gamma^{(2)}(0) = 0$ and $\Gamma^{(4)}(0) = 0$ in the space $x = m\beta$, $y = \frac{\lambda}{m}$ and $z = \sigma$.

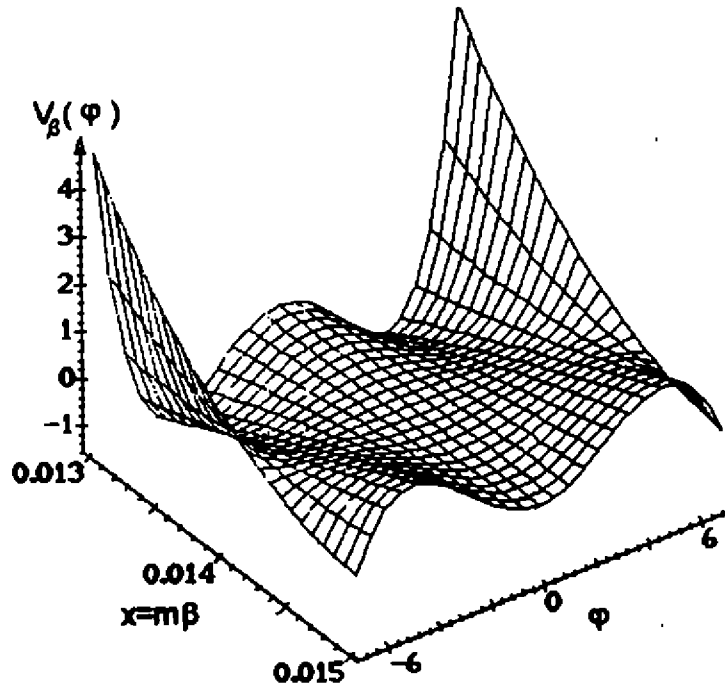


Figure 4. The effective potential as a function of the vacuum expectation value of the field and $m\beta$. In the low temperature regime, there is a metastable minimum at $\langle \varphi \rangle = 0$ (there is a true degenerate minimum outside the origin that does not appear in the figure). Increasing the temperature appears the tricritical temperature β_c^{-1} . In the high temperature regime there is only a second order phase transition.

Vacuum, Chiral Symmetry and Condensates in two-dimensional QCD

H. R. Christiansen*

Centro Brasileiro de Pesquisas Físicas, CBPF - DCP
Rua Xavier Sigaud 150, 22290-180 Rio de Janeiro, Brazil

We analyse the chiral symmetries of flavored Quantum Chromodynamics in two dimensions and show the existence of chiral condensates within the path-integral approach. Our results put forward the question of topological issues when matter is in the fundamental representation of the gauge group.

1 Introduction

In order to understand the complex structure of the QCD vacuum [1] one should analyse possible mechanisms for chiral symmetry breaking and the formation of fermion condensates. Vacuum expectation values (v.e.v.) of quarks composites can be understood as a result of the condensation of pairs of particles and holes. These quantities are particularly useful in the understanding of both spontaneous and dynamical symmetry breaking as well as in some fundamental aspects of Quantum Chromodynamics such as its topological structure.

Two-dimensional models like QCD_2 are preferred frameworks to discuss these phenomena since they present the basic aspects of the four dimensional theory such as the existence of non-trivial topological sectors and chirality properties and, moreover, exact results can be generally obtained.

In the present work we analyse the chiral symmetries of the QCD_2 vacuum by means of fermionic local correlators. Extending the analysis of the Abelian case presented in ref.[2] here we calculate vacuum expectation values of products of local bilinears $\bar{\psi}(x)\psi(x)$, in two-dimensional Quantum Chromodynamics with flavor. Using a path-integral approach which is very appropriate to handle non-Abelian gauge theories, we show that multipoint chiral condensates do not collapse. However, the elementary mass term has a zero v.e.v., a result which is compatible with a vanishing isosinglet chiral anomaly and is consistent with Coleman's theorem. The topological structure of the theory is especially considered and we show the crucial role played by topological flux sectors in obtaining non-zero correlators.

2 Topology

In two space-time dimensions it is generally assumed that the vanishing of the homotopy group $\Pi_1(SU(N))$, implies that QCD_2 exhibits only a trivial topology when fermions are in the fundamental representation of the gauge group. Hence, no vacuum degeneracy is expected to occur. In contrast, when adjoint matter is considered, the relevant symmetry group becomes $SU(N)/Z_N$ rather than $SU(N)$. This is responsible for the appearance of N topologically different sectors and instanton effects become apparent.

Nevertheless, by handling fundamental fermions it can be easily verified that gauge field configurations lying in the Cartan subalgebra of $SU(N)$ generate non-trivial topological fluxes. Thus, one should include these topologically charged configurations in the path-integral domain *also* for fermions in the fundamental representation.

Concerning this last aspect, let us stress that in two dimensions the role of instantons is played by vortices. In the Abelian case, these vortices are identified with the Nielsen-Olesen vortex solutions of a spontaneously broken Abelian

*Electronic address: hugo@cbpfsu1.cat.cbpf.br

Higgs model [3]. This should be contrasted with QCD_4 where four-dimensional instantons are regular solutions of the gauge field equations of motion when fermions are absent; in the two-dimensional case, either Abelian or non-Abelian, no regular solutions with topological charge exist unless complete symmetry breaking is achieved via Higgs fields. When these scalars are included, the resulting static, axially symmetric gauge field configurations give a realization in a two-dimensional Euclidean theory, of regular gauge fields carrying a topological charge. These classical configurations are then identified with two-dimensional instantons, to be used in non-perturbative analysis of a Maxwell theory coupled to massless fermions [4]. The same route can be undertaken in the non-Abelian case since the analogous to Nielsen-Olesen vortex solutions have been shown to exist, again for spontaneously broken gauge theories [5]. It means that, in the spirit of the path-integral approach to QFT one has to take into account these configurations in the measure of the theory without Higgs fields. Once regular gauge field configurations carrying topological charge are identified, the associated fermion zero modes can be found [6]-[7] and then, used to study the formation of fermion condensates.

Our approach starts by decomposing a given gauge field belonging to the n^{th} topological sector in the form [8]

$$A_\mu^a(x) = A_\mu^{a(n)} + a_\mu^a \tag{1}$$

where $A_\mu^{(n)}$ is a classical fixed configuration of n^{th} flux class and a_μ is the path-integral variable which takes into account quantum fluctuations. a_μ belongs to the trivial topological sector and can be then decoupled by a chiral rotation which implies a Fujikawa jacobian.

Topological gauge field configurations and the corresponding zero-modes of the Dirac equation play a central role in calculations involving fermion composites. As in the Abelian case, two-dimensional gauge field configurations $A_\mu^{(n)}$ carrying a topological charge $n \in Z_N$ can be found for the $SU(N)$ case. The relevant homotopy group in this case is Z_N and not Z as in the $U(1)$ case [9]. Taking g_n in the Cartan subgroup of the gauge group we can write a gauge field configuration belonging to the n^{th} topological sector in the form

$$A_\mu^{(n)} = iA(|z|) g_n^{-1} \partial_\mu g_n \tag{2}$$

where $z = x_0 + ix_1$ and $\bar{z} = x_0 - ix_1$.

Zero-modes of the Dirac operator in the background of such non-Abelian vortices, have been analysed in [7]. The outcome is that for topological charge $n > 0$ ($n < 0$) there are Nn ($N|n|$) square-integrable zero modes η_L (η_R) analogous to those arising in the Abelian case. Indeed, one has

$$\eta_R^{(m,i)j} = \begin{pmatrix} z^m h_{ij}(z, \bar{z}) \\ 0 \end{pmatrix}, \quad \eta_L^{(m,i)j} = \begin{pmatrix} 0 \\ \bar{z}^{-m} h_{ij}^{-1}(z, \bar{z}) \end{pmatrix} \tag{3}$$

with

$$h(z, \bar{z}) = \exp(\phi^{(n)}(|z|)M), \quad M = \frac{1}{N} \text{diag}(1, 1, \dots, 1 - N) \tag{4}$$

and ϕ is given by

$$e_{\mu\nu} \frac{x_\nu}{|z|} \frac{d}{d|z|} \phi^{(n)}(|z|) = A_\mu^{(n)}. \tag{5}$$

Here $i, j = 1, 2, \dots, N$ and $m = 0, 1, \dots, |n| - 1$. The pair (m, i) labels the $N|n|$ different zero-modes while j corresponds to a color index.

3 QCD_2 with Flavor

Let us consider two dimensional $SU(N_c)$ Yang-Mills gauge fields coupled to massless Dirac fermions in the fundamental representation of the group in Euclidean space-time

$$L = \bar{\psi}^q (i\partial_\mu \gamma_\mu \delta^{qq'} + A_{\mu,a} t_a^{qq'} \gamma_\mu) \psi^{q'} + \frac{1}{4g^2} F_{\mu\nu}^a F_{\mu\nu}^a. \tag{6}$$

Here the labels $a = 1 \dots N_c^2 - 1$, and $q = 1 \dots N_c$ are summed over, and the partition function is

$$Z = \int \mathcal{D}\bar{\psi} \mathcal{D}\psi \mathcal{D}A_\mu \exp[- \int d^2x \exp L]. \tag{7}$$

In order to compute fermionic correlators containing products of local bilinears $\bar{\psi}\psi(x)$ it will be convenient to decouple fermions from the a_μ field through an chiral rotation within the topologically trivial sector. The choice of an appropriate background like

$$A_+^{(n)} = 0 \quad (8)$$

is crucial in order to control the zero-mode problem. Let us start by introducing group-valued fields to represent $A^{(n)}$ and a_μ

$$a_+ = iu^{-1}\partial_+ u \quad (9)$$

$$a_- = id(v\partial_- v^{-1})d^{-1} \quad (10)$$

$$A_-^{(n)} = id\partial_- d^{-1}. \quad (11)$$

In terms of these fields the fermion determinat can be suitably factorized in an arbitrary gauge by repeated use of the Polyakov-Wiegmann identity [12], resulting in

$$\det \mathcal{D}[A^{(n)} + a] = \mathcal{N} \det \mathcal{D}[A^{(n)}] \times \exp(S_{eff}[u, v; A^{(n)}]) \quad (12)$$

where

$$\begin{aligned} S_{eff}[u, v; A^{(n)}] = & W[u, A^{(n)}] + W[v] + \frac{1}{4\pi} \text{tr}_c \int d^2x (u^{-1}\partial_+ u) d(v\partial_- v^{-1})d^{-1} \\ & + \frac{1}{4\pi} \text{tr}_c \int d^2x (d^{-1}\partial_+ d)(v\partial_- v^{-1}). \end{aligned} \quad (13)$$

Here $W[u, A^{(n)}]$ is the gauged Wess-Zumino-Witten action which in this case takes the form

$$W[u, A^{(n)}] = W[u] + \frac{1}{4\pi} \text{tr}_c \int d^2x (u^{-1}\partial_+ u)(d\partial_- d^{-1}) \quad (14)$$

and $W[u]$ is the usual WZW action.

Once the determinant has been written in the form (12), one can work with any gauge choice. The partition function shows the following structure

$$\begin{aligned} Z = & \sum_n \det(\mathcal{D}[A^{(n)}]) \int \mathcal{D}a_\mu \Delta_{FP} \delta(F[a]) \\ & \exp\left(-S_{eff}[A^{(n)}, a_\mu] - \frac{1}{4g^2} \int d^2x F_{\mu\nu}^2[A^{(n)}, a_\mu]\right) \end{aligned} \quad (15)$$

where $\Delta_{FP}\delta(F[a])$ comes from the gauge fixing.

Correlators in the non-Abelian Flavored Case

As it happens in the Abelian case, the partition function of two dimensional Quantum Chromodynamics only picks a contribution from the trivial sector because $\det(\mathcal{D}[A^{(n)}]) = 0$ for $n \neq 0$ (see eq.(15)). In contrast, various correlation functions become non-trivial precisely for $n \neq 0$ thanks to the zero-mode contributions when Grassman integration is performed.

In order to find a wide expression for general correlators let us just work with the gauge choice (8). Now, the Dirac equation takes the form

$$\mathcal{D}[A^{(n)} + a] \begin{pmatrix} \psi_+ \\ \psi_- \end{pmatrix} = \begin{pmatrix} 0 & u^{-1}i\partial_+ \\ dvd^{-1}D_-[A^{(n)}] & 0 \end{pmatrix} \begin{pmatrix} \zeta_+ \\ \zeta_- \end{pmatrix} \quad (16)$$

where ζ is defined by

$$\psi_+ = dvd^{-1}\zeta_+, \quad \psi_- = u^{-1}\zeta_- \quad (17)$$

Thus, the interaction Lagrangian in the n^{th} flux sector can be written as

$$L = \bar{\psi} \mathcal{D}[a + A^{(n)}]\psi = \zeta_-^* i\partial_+\zeta_- + \zeta_+^* \mathcal{D}_-[A^{(n)}]\zeta_+ \quad (18)$$

which we will write $\bar{\zeta} \tilde{D}[A^{(n)}] \zeta$. In terms of these new fields, the elementary bilinears $\bar{\psi} \psi$ take the form

$$\bar{\psi} \psi = \zeta_-^* u d v d^{-1} \zeta_+ + \zeta_+^* d v^{-1} d^{-1} u^{-1} \zeta_- \tag{19}$$

Concerning the jacobian associated to (17) it is nothing but the effective action defined in the previous section by eq.(13). Hence, an explicit expression for arbitrary non-Abelian correlators reads

$$\begin{aligned} \langle \bar{\psi} \psi(x^1) \dots \bar{\psi} \psi(x^l) \rangle &= \sum_n \int \mathcal{D}u \mathcal{D}v \Delta_{FP} \delta(F[a_\mu]) \exp[-S_{eff}(A^{(n)}, u, v)] \\ &\int \mathcal{D}\bar{\zeta} \mathcal{D}\zeta \exp\left(\bar{\zeta} \begin{pmatrix} 0 & i\partial_+ \\ D_-[A^{(n)}] & 0 \end{pmatrix} \zeta\right) \\ &B^{q_1 p_1}(x^1) \dots B^{q_l p_l}(x^l) \zeta_-^{*q_1} \zeta_+^{p_1}(x^1) \dots \zeta_-^{*q_l} \zeta_+^{p_l}(x^l) + B^{q_1 p_1}(x^1) \dots \\ &B^{-1 q_1 p_1}(x^1) \zeta_-^{*q_1} \zeta_+^{p_1}(x^1) \dots \zeta_+^{*q_1} \zeta_-^{p_1}(x^1) + B^{q_1 p_1}(x^1) \dots \\ &B^{-1 q_1 - 1 p_1 - 1}(x^{l-1}) B^{-1 q_l p_l}(x^l) \zeta_-^{*q_1} \zeta_+^{p_1}(x^1) \dots \zeta_+^{*q_l - 1} \zeta_-^{p_l - 1}(x^{l-1}) \zeta_+^{*q_l} \zeta_-^{p_l}(x^l) \\ &+ \dots \end{aligned} \tag{20}$$

where the group-valued field B is given by $B = u d v d^{-1}$. Notice that we have obtained a general and completely decoupled result, from which one sees that due to color degrees of freedom, the simple product that one finds in the Abelian case becomes here an involved sum.

The introduction of a flavor index implies additional degrees of freedom which result in N_f independent fermionic field variables. Consequently, the growing number of Grassman (numeric) differentials calls for additional Fourier coefficients in the integrand. Dealing with N_f fermions coupled to the gauge field, we can use the fermionic jacobian computed for one flavor to the power N_f , while the bosonic measure remains untouched. As we have previously explained, the Dirac operator has $|n|N_c$ zero modes in the n^{th} topological sector, implying that more fermion bilinears are needed in order to obtain a non-zero fermionic path-integral. Moreover, since the flavor index comes with a factor N_f on the number of Grassman coefficients, the minimal non-zero product of fermion bilinears in the n^{th} sector requires of $|n|N_c N_f$ insertions.

Since the properties of the topological configurations are given by those in the torus of $SU(N_c)$, one can easily extend the results already obtained in the Abelian case. In particular, the chirality of the zero modes is dictated by the same index theorem found in the Abelian theory, this implying that in sector $n > 0$ ($n < 0$) every zero mode has positive (negative) chirality. In this way, the right (left) chiral projections of the minimal non-zero fermionic correlators can be easily computed.

Let us consider $N_c = 2$ and $N_f = 2$ in order to present the simplest illustration of expression (20). The minimal fermionic correlator then looks

$$\begin{aligned} \sum_n \langle \bar{\psi}_+^{1,1} \psi_+^{1,1}(x^1) \bar{\psi}_+^{1,2} \psi_+^{1,2}(x^2) \bar{\psi}_+^{2,1} \psi_+^{2,1}(y^1) \bar{\psi}_+^{2,2} \psi_+^{2,2}(y^2) \rangle_n &= \\ \frac{1}{Z^{(0)}} \sum_{p,q,r,s} \prod_{k=1}^2 \int_{GF} \mathcal{D}u \mathcal{D}v J_B e^{-S_{B_{eff}}^{(1)}(u,v,d)} B_k^{1,pq}(x^k) B_k^{2,rs}(y^k) \times \\ \int \mathcal{D}\bar{\zeta}_k \mathcal{D}\zeta_k e^{\int \bar{\zeta}_k \tilde{D}[A^{(1)}] \zeta_k} \bar{\zeta}_+^{p,k} \zeta_+^{q,k}(x^k) \bar{\zeta}_+^{r,k} \zeta_+^{s,k}(y^k). \end{aligned} \tag{21}$$

where

$$B_k^{q_1 p_1 l_1}(x) = u^{p_1 q_1}(x) (d v d^{-1})^{q_1 l_1}(x), \tag{22}$$

$\bar{\zeta}_+ = \zeta_-^*$ and $\tilde{D}[A^{(n)}]$ stands for the Dirac operator as defined in eq.(18). We have used the notation $Z^{(0)}$ for the partition function since it is completely determined within the $n = 0$ sector, see eq.(15). We have showed every color and flavor indices explicitly indicating sum and product operations. The GF subindex stands for the gauge fixing. The action $S_{B_{eff}}^{(n)}(u, v, d) = N_f S_{WZW}(u, v, d) + S_{Maxwell}(u, v, d)$ is given by the full gluon field $A^{(n)}(d) + a(u, v)$, and yields a high order Skyrme-type lagrangian [10].

The fermionic path-integral can be easily done, amounting to the product of eigenfunctions discussed in the sections above, as follows

$$\int \mathcal{D}\bar{\zeta}_k \mathcal{D}\zeta_k e^{\int \bar{\zeta}_k \tilde{D}[A^{(1)}] \zeta_k} \bar{\zeta}_+^{p,k} \zeta_+^{q,k}(x^k) \bar{\zeta}_+^{r,k} \zeta_+^{s,k}(y^k) = \det \nu(\tilde{D}[A^{(1)}]) \times$$

$$\left(-\bar{\eta}_+^{(0,1)p,k} \eta_+^{(0,1)q,k}(x^k) \bar{\eta}_+^{(0,2)r,k} \eta_+^{(0,2)s,k}(y^k) + \bar{\eta}_+^{(0,1)p,k} \eta_+^{(0,2)q,k}(x^k) \right.$$

$$\left. \bar{\eta}_+^{(0,2)r,k} \eta_+^{(0,1)s,k}(y^k) - \bar{\eta}_+^{(0,2)p,k} \eta_+^{(0,1)q,k}(x^k) \bar{\eta}_+^{(0,1)r,k} \eta_+^{(0,2)s,k}(y^k) \right.$$

$$\left. + \bar{\eta}_+^{(0,2)p,k} \eta_+^{(0,2)q,k}(x^k) \bar{\eta}_+^{(0,1)r,k} \eta_+^{(0,1)s,k}(y^k) \right). \quad (23)$$

Here $\det \nu(\tilde{D}[A^{(1)}])$ is the determinat of the Dirac operator, defined in eq.(18) omitting zero-modes and (e.g.) $\eta^{(0,1)q,k}(x^k)$ is a non-Abelian zero-mode as defined in section 2, with an additional flavor index k . Concerning the bosonic sector, the presence of the $F_{\mu\nu}^2$ (Maxwell) term crucially changes the effective dynamics with respect to that of a pure Wess-Zumino model. One then has to perform approximate calculations to compute the bosonic factor, for example, by linearizing the U transformation, see [10].

4 Conclusions

We have presented correlated v.e.v.s of an arbitrary number of fermionic bilinears in multiflavour non-Abelian gauge theories in two space-time dimensions.

Using a path-integral approach we have shown how topological effects give rise to non-trivial correlators. These results make apparent that the topological structure found in QCD_2 for matter in the fundamental representation is indeed very important. The gauge fields lying in the Cartan subalgebra of $SU(N)$ have to be taken into account to find significant outcomes for fermion condensates.

As a byproduct, our approach gives $\langle \bar{\psi}\psi \rangle = 0$ in any flux sector. This is consistent with Coleman's theorem which prohibits the spontaneous breakdown of the chiral symmetry in two dimensions. In contrast to the Abelian case, in QCD_2 there is no (isosinglet) axial anomaly to give rise to a non-zero mass like condensate $\langle \bar{\psi}\psi \rangle$. Our result is in agreement with numerical outcomes and independent analytical calculations based on dispersion relations and duality. However, in contrast to ours, these last have been only performed in the trivial topological sector with the (additional) assumption of cluster decomposition. Notice that only for an infinite number of colors (large N limit), the Berezinskii-Kosterlitz-Thoules behaviour [13] of such a fermion correlator is compatible with a non-zero outcome (in the bosonized theory, a la Mandelstam). Nevertheless, for any finite value of N , the axial anomaly dynamically breaks the (global) $SU(N)_A$ symmetry allowing the existence of non vanishing correlators for a larger number of points, see e.g. eq.(21).

In contrast to the alternative approaches mentioned above, our treatment enhance the crucial role that topology plays in the QCD vacuum and for this reason it is a suitable scheme to analyse these issues. In particular we do not need of a cluster decomposition ansatz, nor of the large N limit approximation.

Acknowledgements

The author is grateful to Centro Brasileiro de Pesquisas Físicas (CBPF) and CLAF-CNPq, Brazil, for warm hospitality and financial support. F.A. Schaposnik and J. Stephany are acknowledged for enlightening discussions.

References

- [1] see e.g. E. Shuryak, *Rev. Mod. Phys.* **65** (1993) 1.
- [2] H.R. Christiansen and F.A. Schaposnik, *Phys. Rev.* **D53** (1996) 3260. V. Steele, A. Subramanian and I. Zahed, *Nucl. Phys.* **B452** (1995) 545.
- [3] H.B. Nielsen and P. Olesen, *Nucl. Phys.* **B61** (1973) 45.
- [4] S. Coleman, *The Uses of Instantons*, and references therein.

- [5] H. de Vega and F.A. Schaposnik, *Phys. Rev.* **D14** (1976) 1100. G. Lozano, M.V. Manías and F.A. Schaposnik, *Phys. Rev.* **D38** (1988) 601.
- [6] R. Jackiw and P. Rossi, *Nucl. Phys.* **B190** [FS3] (1981) 681.
- [7] H. de Vega, *Phys. Rev.* **D18** (1978) 2932. L. Cugliandolo and G. Lozano, *Phys. Rev.* **D39** (1989) 3093.
- [8] K. Bardacki, L. Crescimano, *Nucl. Phys.* **B313** (1989) 269.
- [9] H. de Vega and F.A. Schaposnik, *Phys. Rev. Lett.* **56** (1986) 2564; *Phys. Rev.* **D34** (1986) 3206.
- [10] E. Fradkin, C.M. Naon and F.A. Schaposnik, *Phys. Rev.* **D36** (1987) 3809.
- [11] D. Cabra, M.V. Manías, F.A. Schaposnik and M. Trobo, *Phys. Rev.* **D43** (1991) 3508.
- [12] A.M. Polyakov and P.B. Wiegmann, *Phys. Lett.* **131B** (1983) 121; *Phys Lett.* **141B** (1984) 223.
- [13] V.L. Berezinskii, *Sov.Phys.JETP* **32** (1970) 493, **34** (1971) 610. J.M. Kosterlitz and D.J. Thoules, *J. Phys.* **C6** (1973) 1181.

Negative Dimensional Integration Method and Massive Feynman Diagrams

Ian G. Halliday¹ Regina Maria Ricotta² and Alfredo Takashi Suzuki³

¹Departamento de Física, Universidade de Swansea, Reino Unido

²Faculdade de Tecnologia de São Paulo, FATEC/SP-CEETPS-UNESP

³Instituto de Física Teórica, IFT-UNESP

A constructive method is proposed to solve a class of massive Feynman integrals within the Negative Dimensional Integration Method. The results are compared with the ones given by known positive D methods and expressed in terms of dimensionally and analytically regularized integrals.

The Negative Dimensional Integration Method (NDIM) was first devised and considered by Halliday and Ricotta, [1], to evaluate Feynman diagrams. It is based in the following integral

$$\int d^D q (q^2)^n = (-1)^n \pi^{D/2} \Gamma(n+1) \delta_{n+D/2,0}. \quad (1)$$

Since by assumption $n \geq 0$, necessarily $D \leq 0$. One possible way of checking this result is to consider the familiar D -dimensional Gaussian integral,

$$\int d^D q e^{-\lambda q^2} = \left(\frac{\pi}{\lambda}\right)^{D/2} \quad (2)$$

which is notably an analytic function of the dimension D . Considering an analytic continuation to negative D , we can expand the LHS of (2), projecting out the powers of the exponential function in the integrand. We have

$$\sum_{n=0}^{\infty} \frac{(-\lambda)^n}{n!} \int d^D q (q^2)^n = \left(\frac{\pi}{\lambda}\right)^{D/2} \quad (3)$$

which can be satisfied if and only if the power of λ is $n = -D/2$, which results in the integral (1).

Thus, by applying the method to compute Feynman amplitudes with propagators raised to some powers, we end up projecting out powers of Gaussian integrals and summing finite series, truncated by the negative powers of the propagators.

Let us now consider the Gaussian-like integral

$$\begin{aligned} I_m &= \int d^D q e^{-\alpha q^2 - \beta[(q-p)^2 - m^2]} = \sum_{i,j} (-1)^{i+j} \frac{\alpha^i \beta^j}{i!j!} \int d^D q (q^2)^i [(q-p)^2 - m^2]^j \\ &= \sum_{i,j} (-1)^{i+j} \frac{\alpha^i \beta^j}{i!j!} J(i, j; p, m). \end{aligned} \quad (4)$$

Notice that the integral $J(i, j; p, m)$ is a D -dimensional massive Feynman integral when D is positive and i and j are negative. By solving directly the D -dimensional momentum integral we get

$$I_m = \frac{\pi^{D/2}}{(\alpha + \beta)^{D/2}} e^{-\frac{\alpha\beta}{(\alpha+\beta)} p^2 + \beta m^2} = \pi^{D/2} \sum_{x,y} (-1)^x \frac{\alpha^x \beta^{x+y}}{(\alpha + \beta)^{x+D/2}} \frac{(p^2)^x}{x!} \frac{(m^2)^y}{y!}. \quad (5)$$

Now, the binomial term is given by

$$(\alpha + \beta)^{-x-D/2} = \sum_{\substack{a,b \\ a+b=-x-D/2}} \frac{(-x-D/2)!}{a!b!} \alpha^a \beta^b \tag{6}$$

so that, inserting it into the previous equation, we have

$$I_m = \pi^{D/2} \sum_{\substack{x,y,a,b \\ a+b=-x-D/2}} (-1)^x \frac{(-x-D/2)!}{a!b!} \alpha^{x+a} \beta^{x+y+b} \frac{(p^2)^x (m^2)^y}{x! y!} \tag{7}$$

Thus, in order to evaluate $J(i, j; p, m)$ we compare powers of α and β of equations (4) and (7). The comparison gives us constraint equations on the sum indices

$$i = x + a ; \quad j = x + y + b ; \quad a + b = -x - D/2.$$

which can be rewritten in a more convenient way as

$$i = x + a ; \quad j = x + y + b ; \quad \sigma \equiv x + y = i + j + D/2.$$

We have, therefore, altogether four summation indices $x, y, a,$ and b with three constraints, such that the solution for the $J(i, j; p; m)$ will be given as a single sum. This remnant sum, of course, can be constructed in four different ways, namely,

$$C_1^4 = \frac{4!}{1!3!} = 4$$

In principle, all this four sums are possible, namely, sums either in $x, y, a,$ or b . For each of these sums, there will be a specific possible external momentum and mass relation. If we leave the summation index x we obtain

$$y = \sigma - x ; \quad a = i - x ; \quad b = j - \sigma$$

and the momentum ratio is given by

$$(p^2)^x (m^2)^y = (p^2)^x (m^2)^{\sigma-x} = (m^2)^\sigma \left(\frac{p^2}{m^2} \right)^x \tag{8}$$

The solution for $J(i, j; p, m)$ is then

$$\begin{aligned} J_1 &= (-\pi)^{D/2} (-m^2)^\sigma \frac{(1+\sigma)_{-\sigma-D/2}}{(1+j)_{-\sigma}} \sum_x \frac{(-1)^x (1-D/2)_{-x}}{(1+i)_{-x} (1+\sigma)_{-x}} \frac{(p^2/m^2)^x}{x!} \\ &= (-\pi)^{D/2} (-m^2)^\sigma \frac{(1+\sigma)_{-\sigma-D/2}}{(1+j)_{-\sigma}} \sum_x \frac{(-i)_x (-\sigma)_x}{(D/2)_x} \frac{(p^2/m^2)^x}{x!} \\ &= (-\pi)^{D/2} (-m^2)^\sigma \frac{(1+\sigma)_{-\sigma-D/2}}{(1+j)_{-\sigma}} {}_2F_1(-i, -\sigma; D/2; p^2/m^2). \end{aligned} \tag{9}$$

On the other hand, if we leave the summation index y we obtain

$$x = \sigma - y ; \quad a = i - \sigma + y ; \quad b = j - \sigma$$

and the momentum ratio is given by

$$(p^2)^x (m^2)^y = (p^2)^{\sigma-y} (m^2)^y = (p^2)^\sigma \left(\frac{m^2}{p^2} \right)^y \tag{10}$$

The solution for $J(i, j; p, m)$ is then

$$J_2 = (-1)^{i+j} i! j! \pi^{D/2} (p^2)^\sigma \sum_y (-1)^{\sigma-y} \frac{(-\sigma-D/2+y)!}{(i-\sigma+y)!(j-\sigma)!} \frac{(m^2/p^2)^y}{(\sigma-y)! y!} \tag{11}$$

Also, if we leave the summation index a we get

$$x = i - a ; \quad y = \sigma - i + a ; \quad b = j - \sigma$$

and the momentum ratio is given by

$$(p^2)^x (m^2)^y = (p^2)^{i-a} (m^2)^{\sigma-i+a} = (m^2)^\sigma \left(\frac{p^2}{m^2}\right)^i \left(\frac{m^2}{p^2}\right)^a \quad (12)$$

In this case the solution is

$$J_3 = (-1)^{i+j} i! j! \pi^{D/2} (m^2)^\sigma \left(\frac{p^2}{m^2}\right)^i \sum_a (-1)^{i-a} \frac{(-i - D/2 + a)!}{a!(j - \sigma)!} \frac{(m^2/p^2)^a}{(i - a)!(\sigma - i + a)!} \quad (13)$$

We note that the system cannot be solved in b , so that the solution given in terms of sum in b , is the empty set:

$$x = \emptyset ; \quad y = \emptyset ; \quad a = \emptyset.$$

Thus, we have three non-vanishing ways of writing the solution for $J(i, j; p, m)$. Two of them, given by (11) and (13), have the same mass-momentum dependence in the sum.

Here we propose the following constructive method: the solution for $J(i, j; p, m)$ will be given by the linear combination of the sums with equal external mass and momentum dependence. In other words, the solution for $J(i, j; p, m)$ will be either $J(i, j; p, m) = J_1$ or $J(i, j; p, m) = J_2 + J_3$, i.e.,

$$J = J_1(i, j; p, m) = (-1)^{i+j} i! j! \pi^{D/2} (m^2)^\sigma \sum_x (-1)^x \frac{(-x - D/2)!}{(i - x)!(j - \sigma)!} \frac{(p^2/m^2)^x}{x!(\sigma - x)!} \quad (14)$$

or the linear combination of the two left solutions that have the same momentum dependence, i.e.,

$$\begin{aligned} J &= J_2(i, j; p, m) + J_3(i, j; p, m) \\ &= (-1)^{i+j} i! j! \pi^{D/2} (p^2)^\sigma \sum_y (-1)^{\sigma-y} \frac{(-\sigma - D/2 + y)!}{(i - \sigma + y)!(j - \sigma)!} \frac{(m^2/p^2)^y}{(\sigma - y)! y!} \\ &\quad + (-1)^{i+j} i! j! \pi^{D/2} (m^2)^\sigma \left(\frac{p^2}{m^2}\right)^i \sum_a (-1)^{i-a} \frac{(-i - D/2 + a)!}{a!(j - \sigma)!} \frac{(m^2/p^2)^a}{(i - a)!(\sigma - i + a)!} \end{aligned} \quad (15)$$

Now we have to express all the factorials in terms of Pochhammers symbols, in order to do the analytic continuation to positive dimension D . We get

$$\begin{aligned} J = J_1 &= (-\pi)^{D/2} (-m^2)^\sigma \frac{(1 + \sigma)_{-\sigma - D/2}}{(1 + j)_{-\sigma}} \sum_x \frac{(-1)^x (1 - D/2)_{-x}}{(1 + i)_{-x} (1 + \sigma)_{-x}} \frac{(p^2/m^2)^x}{x!} \\ &= (-\pi)^{D/2} (-m^2)^\sigma \frac{(1 + \sigma)_{-\sigma - D/2}}{(1 + j)_{-\sigma}} \sum_x \frac{(-i)_x (-\sigma)_x}{(D/2)_x} \frac{(p^2/m^2)^x}{x!} \\ &= (-\pi)^{D/2} (-m^2)^\sigma \frac{(1 + \sigma)_{-\sigma - D/2}}{(1 + j)_{-\sigma}} {}_2F_1(-i, -\sigma; D/2; p^2/m^2) \end{aligned} \quad (16)$$

and

$$\begin{aligned} J = J_2 + J_3 &= (-\pi)^{D/2} (p^2)^\sigma \frac{(1 + \sigma)_{-2\sigma - D/2}}{(1 + i)_{-\sigma} (1 + j)_{-\sigma}} {}_2F_1(1 - \sigma - D/2, -\sigma; 1 + i - \sigma; m^2/p^2) \\ &\quad + (-\pi)^{D/2} (-m^2)^\sigma \left(\frac{-p^2}{m^2}\right)^i \frac{(1 - i - \sigma)_{-j - D/2}}{(1 + j)_{-\sigma}} {}_2F_1(-i, 1 - i - D/2; 1 - i + \sigma; m^2/p^2) \end{aligned} \quad (17)$$

The analytic continuation for $D > 0$ and $i, j < 0$ is then straightforward,

$$J^{AC} = \pi^{D/2} (-m^2)^\sigma \frac{(-j)_\sigma}{(-\sigma)_{\sigma + D/2}} {}_2F_1(-i, -\sigma; D/2; p^2/m^2) \quad (18)$$

and

$$\begin{aligned}
 J^{AC} = & \pi^{D/2} (p^2)^\sigma \frac{(-i)_\sigma (-j)_\sigma}{(-\sigma)_{2\sigma+D/2}} {}_2F_1(1-\sigma-D/2, -\sigma; 1+i-\sigma; m^2/p^2) \\
 & + \pi^{D/2} (-m^2)^\sigma \left(\frac{-p^2}{m^2}\right)^i \frac{(-j)_\sigma}{(i+\sigma)_{\sigma+D/2}} {}_2F_1(-i, 1-i-D/2; 1-i+\sigma; m^2/p^2)
 \end{aligned} \tag{19}$$

These are exactly the results given by any positive D method, see for instance [3]. Notice that equation (19) is the analytic continuation of (18).

What remains to be done is a generalization of the above proposed constructive method to other massive cases. The main idea is to systematically project out powers of the Gaussian-like integrals for any massive Feynman D-dimensional integral. Such projection leaves us with constraint equations on the summation indices that have to be solved for all the possibilities. We are then left with different mass-momentum dependence solutions, like in (9)-(13), such that the final answer will be the linear combinations of the solutions having the same mass-momentum dependence.

We have evaluated all the possible massive two and three point functions, including the cases where the masses in each propagator are different or some of them are zero. Our results are in perfect agreement with the ones given in reference [3].

References

- [1] I. G. Halliday, and R. M. Ricotta, *Phys. Lett. B* **193** (1987) 241
- [2] R. M. Ricotta, *J.J. Giambiagi Festschrift*, ed. by H. Falomir et al., World Scientific, Singapore, 1990
- [3] E. E. Boos and A. I. Davydychev, *Theor. and Math. Phys.*, **89** (1992) 1052

A Note on Moments of Gaussian Grassmann Multivariable Integrals

I. C. Charret*, S. M. de Souza† and M. T. Thomaz‡

Instituto de Física

Universidade Federal Fluminense

R. Gal. Milton Tavares de Souza s/nº

Campus da Praia Vermelha

Niterói, R.J., 24210-310 Brazil

The path integral methods has played a central role in many branches in Physics. Among the physical quantities that can be written as a path integral, we have the grand canonical partition function for self-interaction fermionic system, whose path integral expression is:

$$Z(\beta, \mu) = \int D\psi(\vec{x}, \tau) D\bar{\psi}(\vec{x}, \tau) e^{-\int d\vec{x} \int_0^\beta \bar{\psi}(\vec{x}, \tau) \partial_\tau \psi(\vec{x}, \tau)} e^{-\int_0^\beta d\tau \mathbf{K}}, \quad (1)$$

where $\psi(\vec{x}, \tau)$ and $\bar{\psi}(\vec{x}, \tau)$ are anticommuting variables with continuous label \vec{x} and τ , satisfying anti-periodic boundary conditions in the temperature parameter τ . β is the inverse of temperature ($\beta = 1/kT$), and $\mathbf{K} = \mathbf{H} - \mu\mathbf{N}$, where \mathbf{H} is the hamiltonian of fermionic system, μ the chemical potential and \mathbf{N} the total number of particles operator. The variables of functional integral, $\psi(\vec{x}, \tau)$ and $\bar{\psi}(\vec{x}, \tau)$ are generators of a Grassmann algebra. The interaction part of \mathbf{H} , introduce in the exponential of expression (1), at last, one power term of variables of degree bigger than two. Due to our inability to calculate integrals beyond the gaussian approximation, the contribution from the interaction terms of hamiltonian to the r.h.s. of equation above correspond to the moments of the gaussian Grassmann integral. Formally, these integrals are calculated by introducing an external Grassmann current and taking functional derivatives with respect to it.

Using the anticommuting nature of generators of the Grassmann algebra, we show that the moments of gaussian Grassmann multivariable integral are related to the cofactors of the matrix of the gaussian exponential.

1 Moments of Gaussian Grassmann Multivariable Integrals

It is a known result [1] for a Grassmann algebra of dimension 2^{2N} , composed of the generators $\{\eta_1, \dots, \eta_N; \bar{\eta}_1, \dots, \bar{\eta}_N\}$, that

$$\int \prod_{i=1}^N d\eta_i d\bar{\eta}_i e^{\sum_{i,j=1}^N \eta_i A_{ij} \bar{\eta}_j} = \det(\mathbf{A}), \quad (2)$$

where A_{ij} are the entries of matrix \mathbf{A} and are commuting quantities.

We will show in this article that the moments of integral (1) are co-factors of \mathbf{A} .

We first consider the case where we have one product $\bar{\eta}_i \eta_k$ in the integrand of the gaussian integral (1), that is,

*E-mail: IRAZIET@IF.UFF.BR

†E-mail: SMARTINS@IF.UFF.BR

‡E-mail: MTT@IF.UFF.BR

$$M(l, k) \equiv \int \prod_{i=1}^N d\eta_i d\bar{\eta}_i \bar{\eta}_l \eta_k e^{\sum_{i,j=1}^N \eta_i A_{ij} \eta_j} \tag{3}$$

where l, k are fixed and $1 \leq l, k \leq N$.

Due to the fact that for all Grassmann generators we have: $\bar{\eta}_i^2 = \eta_i^2 = 0, i = 1, \dots, N$, the only non-null terms in eq.(2) are the ones where the integrand has N products of the form: $\bar{\eta}_i \eta_j$. Eq. (2) becomes:

$$M(l, k) = \int \prod_{i=1}^N d\eta_i d\bar{\eta}_i \bar{\eta}_l \eta_k \frac{1}{(N-1)!} \sum_{\substack{i_1, \dots, i_{N-1}=1 \\ j_1, \dots, j_{N-1}=1}}^N A_{i_1 j_1} \dots A_{i_{N-1} j_{N-1}} \times \\ \times \bar{\eta}_{i_1} \eta_{j_1} \bar{\eta}_{i_2} \eta_{j_2} \dots \bar{\eta}_{i_{N-1}} \eta_{j_{N-1}} \tag{4}$$

and the indices are such that $i_n \neq l, n = 1, \dots, N-1$, and $j_n \neq k, n = 1, \dots, N-1$. Once the product $\bar{\eta}_{i_n} \eta_{j_n}$ is a commutative quantity, each term in the sum of (3) appears $(N-1)!$ times.

The $(N-1)!$ distinct terms in (3) can be generated by fixing one configuration for $\{i_1, i_2, \dots, i_{N-1}\}$, for example, we choose: $\{i_1 = 1, \dots, i_{l-1} = l-1, i_l = l+1, \dots, i_{N-1} = N\}$, and, taking all the terms coming from the sum over the indices $j_n, n = 1, \dots, N-1$. Therefore, $M(l, k)$ becomes

$$M(l, k) = \int \prod_{i=1}^N d\eta_i d\bar{\eta}_i \bar{\eta}_l \eta_k \sum_{\substack{j_1, \dots, j_{N-1}=1 \\ j_n \neq k}}^N A_{1j_1} \dots A_{l-1, j_{l-1}} A_{l+1, j_l} \dots A_{Nj_{N-1}} \times \\ \times \bar{\eta}_1 \eta_{j_1} \bar{\eta}_2 \eta_{j_2} \dots \bar{\eta}_{l-1} \eta_{j_{l-1}} \bar{\eta}_{l+1} \eta_{j_l} \dots \bar{\eta}_N \eta_{j_{N-1}} \tag{5}$$

Renaming the variables: $j_l \rightarrow j_{l+1}, j_{l+1} \rightarrow j_{l+2}, \dots, j_{N-1} \rightarrow j_N$, we have that:

$$M(l, k) = \int \prod_{i=1}^N d\eta_i d\bar{\eta}_i \bar{\eta}_l \eta_k \sum_{\substack{j_1, \dots, j_{N-1}=1 \\ j_1, \dots, j_N=1}}^N A_{1j_1} \dots A_{l-1, j_{l-1}} A_{l+1, j_{l+1}} \dots A_{Nj_N} \times \\ \times \bar{\eta}_1 \eta_{j_1} \bar{\eta}_2 \eta_{j_2} \dots \bar{\eta}_{l-1} \eta_{j_{l-1}} \bar{\eta}_{l+1} \eta_{j_{l+1}} \dots \bar{\eta}_N \eta_{j_N} \tag{6}$$

Defining the matrix $\mathbf{B}(l, k)$ as:

$$B_{ij}(l, k) = \begin{cases} A_{ij}, & \text{if } i \neq l \text{ and } j \neq k \\ \delta_{il} \delta_{jk}, & \text{if } i = l \text{ or } j = k \end{cases} \tag{6}$$

and $i, j = 1, 2, \dots, N$.

Using the definition of matrix $\mathbf{B}(l, k)$, the expression of $M(l, k)$ is re-written as:

$$M(l, k) = \int \prod_{i=1}^N d\eta_i d\bar{\eta}_i \sum_{j_1, \dots, j_N=1}^N B_{1j_1} \dots B_{l-1, j_{l-1}} B_{l, j_l} \dots B_{Nj_N} \times \\ \times \bar{\eta}_1 \eta_{j_1} \dots \bar{\eta}_l \eta_{j_l} \dots \bar{\eta}_N \eta_{j_N} \tag{7}$$

Integrating over $\bar{\eta}_i$, and using the definition of determinant [2, 3], we finally have that

$$M(l, k) = \det \mathbf{B} = (-1)^{l+k} A(l, k), \tag{8}$$

where $A(l, k)$ is the minor determinant of matrix \mathbf{A} , when the line l and the column k are deleted. $M(l, k)$ is the cofactor of matrix \mathbf{A} .

Using an analogous procedure, we now consider the case of moments of the gaussian Grassmann multivariable integral when we have m products:

$$\bar{\eta}_{l_1} \eta_{k_1} \bar{\eta}_{l_2} \eta_{k_2} \cdots \bar{\eta}_{l_m} \eta_{k_m}$$

in the integrand of (2), where $m \leq N$.

Consider the fixed sets: $L = \{l_1, l_2, \dots, l_m\}$ and $K = \{k_1, k_2, \dots, k_m\}$. We define $M(L, K)$ as

$$M(L, K) \equiv \int \prod_{i=1}^N d\eta_i d\bar{\eta}_i \bar{\eta}_{l_1} \eta_{k_1} \cdots \bar{\eta}_{l_m} \eta_{k_m} e^{\sum_{i,j=1}^N \eta_i A_{ij} \eta_j} \tag{9}$$

and the products are ordered such that: $l_1 < l_2 < \dots < l_m$ and $k_1 < k_2 < \dots < k_m$.

Using an analogous reasoning, we obtain

$$M(L, K) = \int \prod_{i=1}^N d\eta_i d\bar{\eta}_i \sum_{j_1, \dots, j_N=1}^N B_{1j_1} \cdots B_{l-1, j_{l-1}} B_{l, j_l} \cdots B_{N, j_N} \times \\ \times \bar{\eta}_{l_1} \eta_{j_1} \cdots \bar{\eta}_{l_m} \eta_{j_m} = \det \mathbf{B}(L, K) = (-1)^{(l_1+l_2+\dots+l_m)+(k_1+k_2+\dots+k_m)} A(L, K), \tag{10}$$

where the matrix $\mathbf{B}(L, K)$ is defined as:

$$B_{ij}(L, K) = \begin{cases} A_{ij}, & \text{if } i \neq l_1, \dots, l_m \text{ and } j \neq k_1, \dots, k_m \\ \delta_{il_1} \delta_{jk_1}, & \text{if } i = l_1 \text{ or } j = k_1 \\ \vdots \\ \delta_{il_m} \delta_{jk_m}, & \text{if } i = l_m \text{ or } j = k_m, \end{cases} \tag{11}$$

and $i, j = 1, 2, \dots, N$. $A(K, L)$ is the determinant of the matrix obtained from matrix \mathbf{A} by deleting the lines: $\{l_1, l_2, \dots, l_m\}$, and, the columns: $\{k_1, k_2, \dots, k_m\}$.

In summary, we can say that the effect of the presence of a product $\bar{\eta}_l \eta_k$ within the integrand of the gaussian integral (2), is to replace the line l of matrix \mathbf{A} , A_{ij} , by δ_{jk} , and its column k , A_{ik} , by δ_{il} . In their turn, the determinants of matrices $\mathbf{B}(L, K)$, eq.(10), are easily written in terms of determinants of matrices of smaller dimension. Hence products of Grassmann generators cut down the dimension of the matrices the determinant of which we are to calculate.

Acknowledgements

I.C.C and S.M. de S. thank CNPq for financial support. M.T.T. thanks CNPQ and FINEP for partial financial support.

References

[1] C. Itzykson and J.B. Zuber, *Quantum Field Theory*, McGraw-Hill (1980); U. Wolf, Nucl. Phys. **B225** [FS9] (1983) 391;
 [2] S.M. de Souza and M.T. Thomaz, J. Math. Phys. **31** (1990) 1297;
 [3] D. Kreider et al, *An Introduction to Linear Analysis*, Addison-Wesley, Ontario (1966).

Expansão a Altas Temperaturas para Sistemas Fermiônicos Autointeragentes até ordem β^3

I.C.Charret, S.M. de Souza e M.T.Thomaz,
Instituto de Física - Universidade Federal Fluminense
R. Gal. Milton Tavares de Souza s/nº.
Niterói, R.J., 24210-340. Brasil

E.V.Corrêa Silva
Centro Braileiro de Pesquisas Físicas
R. Dr. Xavier Sigaud nº 150,
Rio de Janeiro, R.J., 22290-180. Brasil

Exploramos a natureza grassmanniana das variáveis envolvidas na expressão da integral de caminho da função de partição grã-canônica para modelos fermiônicos autointeragentes para mostrar, em uma dimensão espacial, uma relação geral envolvendo os termos dessa expansão no limite de altas temperaturas e uma combinação de co-fatores de uma matriz adequada formada por quantidades comutantes. Aplicamos esse tratamento para calcular os coeficientes exatos, até ordem β^3 , da função de partição grã-canônica para o modelo de Hubbard em $d = (1 + 1)$ no limite de altas temperaturas. Os resultados encontrados são válidos para qualquer conjunto de parâmetros que caracterizem o modelo.

1 Motivação:

Devido a natureza anticomutativa dos campos fermiônicos é comum a utilização de diferentes técnicas de bosonização para tratá-los. Esses resultados dependem da decomposição utilizada para os campos auxiliares e, portanto, apresentam ambiguidades, quando utilizamos teoria de perturbação.

O Modelo de Hubbard [1], que descreve elétrons interagentes, apesar de ser muito utilizado para o estudo de magnetismo itinerante em uma grande variedade de dimensões espaciais, apresenta resultados exatos apenas para o caso de uma dimensão espacial e temperatura zero.

Exploramos em um trabalho anterior [2] a natureza grassmanniana dos campos fermiônicos para estudar o comportamento a altas temperaturas da função de partição grã-canônica para o oscilador anarmônico fermiônico. Este modelo tem dimensão espacial zero e uma extensão natural é o estudo do modelo de Hubbard unidimensional.

Em um artigo recente [3] calculamos o coeficiente exato até primeira ordem em $\beta(\beta = \frac{1}{T})$ da expansão da função de partição grã-canônica para o modelo de Hubbard unidimensional no limite de altas temperaturas. Utilizando o método proposto nesse primeiro artigo, os cálculos são realizados para uma rede espacial contendo um pequeno número de sítios espaciais e têm que ser extrapolados para uma rede contendo um número de sítios quaisquer. Isso gera algumas dificuldades numéricas, que são eliminadas através de uma simplificação dos cálculos, levando a um resultado válido para uma rede formada por N pontos espaciais, onde N é qualquer.

2 Integrais Múltiplas e Momentos:

É um resultado conhecido que para uma álgebra de dimensão 2^{2N} temos que:

$$\det \mathbf{A} = \int \prod_{i=1}^N d\bar{\eta}_i d\eta_i \exp\left\{ \sum_{i,j=1}^N [\bar{\eta}_i \mathbf{A}_{ij} \eta_j] \right\}, \quad (1)$$

onde \mathbf{A}_{ij} são os elementos da matriz \mathbf{A} e são quantidades comutantes.

Mostramos em um trabalho recente [4] que:

$$\int \prod_{i=1}^N d\bar{\eta}_i d\eta_i \bar{\eta}_l \eta_k \exp\left\{ \sum_{i,j=1}^N [\bar{\eta}_i \mathbf{A}_{ij} \eta_j] \right\} = (-1)^{l+k} \mathbf{A}(l, k) \quad (2)$$

onde $\mathbf{A}(l, k)$ é o co-fator da matriz \mathbf{A} , após o corte da linha l e da coluna k .

A dimensão da matriz \mathbf{A} está associada a dimensão da álgebra. Portanto, para uma matriz \mathbf{A} não diagonal, a dimensão da rede espacial que pode ser calculada com esse método ficará limitada.

3 Novo Método:

Estamos interessados em estudar o caso em que a matriz \mathbf{A} tem a seguinte forma:

$$\mathbf{A} = \begin{pmatrix} \mathbf{I} & -\mathbf{I} & \mathbf{0} & \dots & \mathbf{0} \\ \mathbf{0} & \mathbf{I} & -\mathbf{I} & \dots & \mathbf{0} \\ \mathbf{0} & \mathbf{0} & \mathbf{I} & \dots & \mathbf{0} \\ \vdots & \vdots & \vdots & \ddots & \vdots \\ \mathbf{I} & \mathbf{0} & \mathbf{0} & \dots & \mathbf{I} \end{pmatrix} \quad (3)$$

$\dim[\mathbf{A}] = M = nN$ onde n representa o número de sítios de temperatura; N representa o número de sítios espaciais e \mathbf{I} a matriz identidade de dimensão $N \times N$.

Exploramos a estrutura de blocos da matriz \mathbf{A} , diagonalizando-a através de uma transformação de similaridade dada por:

$$\mathbf{P}^{-1} \mathbf{A} \mathbf{P} = \mathbf{D} \quad (4)$$

onde:

$$\mathbf{D} = \begin{pmatrix} \lambda_1 \mathbf{I} & \mathbf{0} & \mathbf{0} & \dots & \mathbf{0} \\ \mathbf{0} & \lambda_2 \mathbf{I} & \mathbf{0} & \dots & \mathbf{0} \\ \mathbf{0} & \mathbf{0} & \lambda_3 \mathbf{I} & \dots & \mathbf{0} \\ \vdots & \vdots & \vdots & \ddots & \vdots \\ \mathbf{0} & \mathbf{0} & \mathbf{0} & \dots & \lambda_n \mathbf{I} \end{pmatrix} \quad (5)$$

com λ_i , onde $i = 1, 2, \dots, n$, sendo os autovalores da matriz \mathbf{A} . Cada autovalor tem degenerescência N . Como a matriz \mathbf{A} não é hermitiana, alguns deles são complexos. Após essa transformação, os índices associados ao sítio espacial não são misturados pois a estrutura de blocos da matriz \mathbf{A} é conservada também pela matriz de transformação \mathbf{P} . Utilizando essa transformação de similaridade, as integrais múltiplas são reescritas como:

$$I = \int \prod_{i=1}^{nN} d\bar{\eta}_i d\eta_i [\bar{\eta} \mathbf{Q}]_i [\mathbf{P} \eta]_k \exp\left\{ \sum_{i,j=1}^{nN} [\bar{\eta}_i \mathbf{D}_{ij} \eta_j] \right\}. \quad (6)$$

O cálculo de I se reduz, de acordo com a eq.(2), ao cálculo de cofatores da matriz \mathbf{D} , que é diagonal.

4 Aplicação ao Modelo de Hubbard unidimensional

A expansão a altas temperaturas para a função de partição grã-canônica é dada por:

$$\mathcal{Z} = \text{Tr}[e^{-\beta K}] = \text{Tr}[1 - \beta K + \frac{\beta^2}{2} \text{Tr}[K^2] - \frac{\beta^3}{3} \text{Tr}[K^3] + \dots] \quad (7)$$

onde $K = H - \mu N$, H é a hamiltoniana do sistema, μ é o potencial químico e N é o operador número total de partículas.

Utilizando a álgebra de Grassmann, o traço para qualquer operador fermiônico pode ser escrito como:

$$\begin{aligned} \text{Tr}[K^n] &= \int \prod_{i=1}^{2nN} d\bar{\eta}_i d\eta_i e^{\sum_{i,j=1}^{2nN} \eta_i A_{ij} \eta_j} K^{\mathbb{Q}}(\bar{\eta}, \eta; i=0) \times \\ &\times K^{\mathbb{Q}}(\bar{\eta}, \eta; i=1) \dots \times K^{\mathbb{Q}}(\bar{\eta}, \eta; i=n-1) \end{aligned} \quad (8)$$

para o modelo de Hubbard unidimensional temos que [3]:

$$\begin{aligned} K^{\mathbb{Q}}(\bar{\eta}_\sigma(x_l, \tau_\nu), \eta_\sigma(x_l, \tau_\nu)) &= \\ &= \sum_{i=1}^N \sum_{\sigma \pm 1} (E_0 + \sigma \lambda_B - \mu) \bar{\eta}_\sigma(x_l, \tau_\nu) \eta_\sigma(x_l, \tau_\nu) + \\ &+ \sum_{l=1}^N \sum_{\sigma \pm 1} t [\bar{\eta}_\sigma(x_l, \tau_\nu) \eta_\sigma(x_{l+1}, \tau_\nu) + \bar{\eta}_\sigma(x_l, \tau_\nu) \eta_\sigma(x_{l-1}, \tau_\nu)] + \\ &+ \sum_{l=1}^N U \bar{\eta}_l(x_l, \tau_\nu) \eta_l(x_l, \tau_\nu) \bar{\eta}_l(x_l, \tau_\nu) \eta_l(x_l, \tau_\nu). \end{aligned} \quad (9)$$

Observa-se que esta é a expressão exata do coeficiente β^n da expansão a altas temperaturas da função de partição de sistemas fermiônicos.

Utilizando a transformação dada pela matriz P , os geradores podem ser reescritos da seguinte forma:

$$\bar{\eta}_{\nu N+l} = \sum_{\nu'=0}^{n-1} q_{\nu\nu'} \bar{\eta}'_{\nu' N+l} \quad (10)$$

$$\eta_{\nu N+l} = \sum_{\nu'=0}^{n-1} p_{\nu\nu'} \eta'_{\nu' N+l} \quad (11)$$

Com a utilização desse novo formalismo, mostramos [5] que o número de integrais a serem calculadas é bem reduzido. Além disso, as integrais são muito mais simples, pois estamos trabalhando com uma matriz diagonal. Grande parte das integrais são nulas devido as propriedades da matriz diagonal.

a) Exemplo de Integrais Nulas:

Para $n = 2$, uma das integrais possíveis tem a seguinte forma:

$$I_1 = \int \prod_{i=1}^{2N} d\bar{\eta}_i d\eta_i \bar{\eta}_i \eta_{i+1} \exp\left\{ \sum_{i,j=1}^{2N} [\bar{\eta}_i A_{ij} \eta_j] \right\} \quad (12)$$

Usando a transformação de similaridade para $n = 2$, podemos escrever:

$$\bar{\eta}_i \eta_{i+1} = \bar{\eta}'_i \eta'_{i+1} + \bar{\eta}'_i \eta'_{N+l+1} + \bar{\eta}'_{N+l+1} \eta'_{i+1} + \bar{\eta}'_{N+l+1} \eta'_{N+l+1} \quad (13)$$

Esse resultado corresponde, para qualquer valor de l , ao cálculo de determinantes de matrizes que possuem linhas e colunas identicamente nulas.

b) Exemplo de Integrais Não-nulas:

Para $n = 2$, uma outra integral possível tem a seguinte forma:

$$I_2 = \int \prod_{i=1}^{2N} d\bar{\eta}_i d\eta_i \bar{\eta}_i \eta_i \exp\left\{ \sum_{i,j=1}^{2N} [\bar{\eta}_i \mathbf{A}_{ij} \eta_j] \right\} \quad (14)$$

Usando novamente a transformação de similaridade para $n = 2$, podemos escrever:

$$\bar{\eta}_i \eta_i = \bar{\eta}'_i \eta'_i + \bar{\eta}'_i \eta'_{N+i} + \bar{\eta}'_{N+i} \eta'_i + \bar{\eta}'_{N+i} \eta'_{N+i} \quad (15)$$

Para qualquer valor de l esses resultados são diferentes de zero. Mostramos também que esses resultados independem de l .

Utilizando esse novo formalismo obtivemos os coeficientes exatos para β^2 e para β^3 da expansão a altas temperaturas da função de partição grã-canônica para o modelo de Hubbard unidimensional. Para β^2 obtivemos:

$$\begin{aligned} Tr[\mathbf{K}^2] &= 2^{2N} \left[N^2 \left[(E_0 - \mu)^2 + \frac{1}{2} (E_0 - \mu) U + \frac{U^2}{16} \right] + \right. \\ &+ \frac{N}{2} \left[(E_0 - \mu)^2 + (E_0 - \mu) U + (\lambda_B)^2 + 2t^2 + \right. \\ &\left. \left. + \frac{3}{8} U^2 \right] \right] \quad (16) \end{aligned}$$

e para β^3 :

$$\begin{aligned} Tr[\mathbf{K}^3] &= 2^{2N} \left[N^3 \left[(E_0 - \mu)^3 + \frac{3}{4} (E_0 - \mu)^2 U + \frac{3U^2}{16} (E_0 - \mu) + \frac{U^3}{64} \right] + \right. \\ &+ N^2 \left[\frac{3}{2} (E_0 - \mu)^3 + \frac{15}{8} (E_0 - \mu)^2 U + \frac{3\lambda_B^2}{2} (E_0 - \mu) + \right. \\ &+ 3t^2 (E_0 - \mu) + \frac{15}{16} (E_0 - \mu) U^2 + \frac{3t^2 U}{4} + \frac{3U\lambda_B^2}{8} + \frac{9U^3}{64} \left. \right] + \\ &+ N \left[\frac{3}{8} (E_0 - \mu)^2 U + \frac{3}{8} (E_0 - \mu) U^2 + \frac{3t^2}{2} (E_0 - \mu) - \frac{3U\lambda_B^2}{8} + \right. \\ &\left. + \frac{3t^2 U}{4} + \frac{3U^3}{32} \right] \quad (17) \end{aligned}$$

A partir dessas expressões (exatas), podemos calcular a energia livre de Helmholtz, e obter então, expressões para quantidades físicas, tais como: energia média por sítio, magnetização quadrática média por sítio, etc.

5 Conclusões e Perspectivas:

Obtivemos resultados exatos para cada termo da expansão a altas temperaturas da função de partição grã-canônica para um sistema fermiônico descrito pelo modelo de Hubbard unidimensional e periódico, espacialmente. Esses resultados são válidos para qualquer número de sítios espaciais e qualquer número de partições na temperatura. Não há nenhuma restrição quanto ao modelo fermiônico a ser analisado.

Os cálculos de termos de ordens superiores estão sendo realizados, além do estudo da possibilidade de analisarmos o modelo de Hubbard com dimensão espacial maior do que 1.

6 Agradecimentos:

I.C.C., S.M.S. e E.V.C.S. agradecem o apoio financeiro ao CNPq e M.T.T. agradece o apoio financeiro parcial do CNPq e FINEP.

References

- [1] J.Hubbard, Proc. Roy. Soc. **A277** (1963) 237; **A281** (1964) 401.
- [2] S.M. de Souza e M.T. Thomaz, J. Math. Phys. **32** (1991) 3455.
- [3] I.C.Charret, E.V.Corrêa Silva, S.M. de Souza e M.T.Thomaz. J.Math.Phys. **36** (1995) 4100.
- [4] I.C.Charret, S.M. de Souza e M.T.Thomaz. Braz.Journal.Phys., submetido a publicação
- [5] I.C.Charret, E.V.Corrêa Silva, S.M. de Souza e M.T.Thomaz. J.Math.Phys., submetido a publicação

Violação de Desigualdades Quânticas com Campos Clássicos

J. Acacio de Barros*

Departamento de Física - UFJF

Patrick Suppes, Gary Oas†

Ventura Hall, Stanford University

and

Adonai S. Sant'Anna‡

Departamento de Matemática - UFPR

December 3, 1996

I Esquema Experimental

O esquema experimental usa duas fontes clássicas $\alpha_1(\theta_1)$, com fase θ_1 , e $\alpha_2(\theta_2)$, com fase θ_2 , e uma terceira fonte a ser estudada, $u(\theta)$, com fase desconhecida. A configuração experimental tem duas detecções homodinas, (D_1, D_2) sendo uma e (D_3, D_4) a outra. A geometria do esquema é mostrada na Figura.

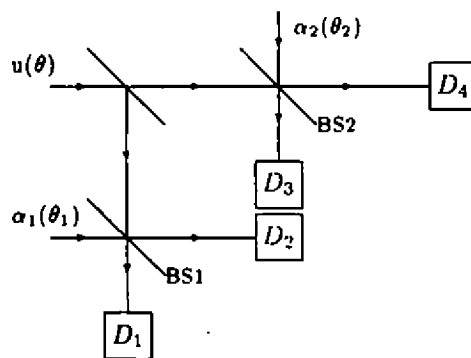


Figure 1.: Configuração Experimental Proposta.

II Funções de Correlação

Nesta seção iremos computar as funções de correlação que violam as desigualdades. A intensidade no detector I_1 pode facilmente ser calculada como

*E-mail: acacio@fisica.ufjf.br

†E-mail: oas@ockham.stanford.edu

‡E-mail: adonai@gauss.mat.ufpr.br

$$I_1(\theta) = \lim_{T \rightarrow \infty} \frac{1}{T} \int_0^T \left[\frac{1}{2} \alpha \cos(\omega t + \theta_1 + \pi/2) + \frac{1}{4} \beta \cos(\omega t + \theta) \right]^2 dt. \quad (1)$$

que é

$$I_1(\theta) = \frac{1}{32} \beta^2 + \frac{1}{8} \alpha \beta \sin(\theta - \theta_1) + \frac{1}{8} \alpha^2. \quad (2)$$

De maneira similar, calculamos as intensidades clássicas para os outros três detectores. Estas intensidades são condicionais na variável θ . Para obter as intensidades incondicionais, assumimos uma distribuição uniforme para θ e integramos as expressões para todos os valores possíveis de θ .

As intensidade incondicionais I_1 , I_2 , I_3 , e I_4 para os detectores D_1 , D_2 , D_3 , e D_4 são

$$I_1 = I_2 = I_3 = I_4 = \frac{1}{32} \beta^2 + \frac{1}{8} \alpha^2. \quad (3)$$

Agora começamos a computar a covariância entre intensidades nos detectores homodinos. A covariância que nos interessa é entre $(I_1 - I_2)$ e $(I_3 - I_4)$.

$$\begin{aligned} \text{Cov}(I_1 - I_2, I_3 - I_4) &= \frac{1}{2\pi} \int_0^{2\pi} [(I_1(\theta) - I_2(\theta)) \times (I_3(\theta) - I_4(\theta))] d\theta \\ &\quad - \frac{1}{2\pi} \int_0^{2\pi} (I_1(\theta) - I_2(\theta)) d\theta \times \\ &\quad \times \frac{1}{2\pi} \int_0^{2\pi} (I_3(\theta) - I_4(\theta)) d\theta. \end{aligned} \quad (4)$$

É simples mostra que de (2) e (4) temos

$$\text{Cov}(I_1 - I_2, I_3 - I_4) = \frac{1}{32} \beta^2 \alpha^2 \cos(\theta_1 - \theta_2). \quad (5)$$

Para computar a correlação, temos que saber a variância das variáveis aleatórias $(I_1 - I_2)$ e $(I_3 - I_4)$, que são definidas como

$$\begin{aligned} \text{Var}(I_1 - I_2) &= \frac{1}{2\pi} \int_0^{2\pi} (I_1(\theta) - I_2(\theta))^2 d\theta - \left[\frac{1}{2\pi} \int_0^{2\pi} (I_1(\theta) - I_2(\theta)) d\theta \right]^2 \\ &= \frac{1}{32} \beta^2 \alpha^2 \end{aligned} \quad (6)$$

e

$$\text{Var}(I_3 - I_4) = \frac{1}{32} \beta^2 \alpha^2. \quad (7)$$

Finalmente, podemos calcular a correlação entre as duas variáveis aleatórias $(I_1 - I_2)$ e $(I_3 - I_4)$. Isto é feito da maneira padrão, simplesmente dividindo a covariância pela raiz quadrada das variâncias:

$$\rho(I_1 - I_2, I_3 - I_4) = \frac{\text{Cov}(I_1 - I_2, I_3 - I_4)}{\sqrt{\text{Var}(I_1 - I_2) \text{Var}(I_3 - I_4)}}. \quad (8)$$

e temos a seguinte expressão para a correlação:

$$\rho(I_1 - I_2, I_3 - I_4) = \rho(\theta_1, \theta_2) = \cos(\theta_1 - \theta_2). \quad (9)$$

III Violação das Desigualdades de Bell

Agora podemos mostrar que as desigualdades são violadas. Podemos escolher fases θ_1 , θ_2 , θ'_1 , e θ'_2 tal que obtemos imediatamente para as quatro correlações $\rho(\theta_1, \theta_2)$, $\rho(\theta_1, \theta'_2)$, $\rho(\theta'_1, \theta_2)$ e $\rho(\theta'_1, \theta'_2)$ uma violação das desigualdades de Bell na forma dada por Clauser, Horne e Shimony [7], escolhendo quatro ângulos tal que

$$\theta_1 - \theta_2 = \theta'_1 - \theta'_2 = 60^\circ, \quad (10)$$

$$\theta_1 - \theta'_2 = 30^\circ, \quad (11)$$

$$\theta'_1 - \theta_2 = 90^\circ. \quad (12)$$

Em particular,

$$\begin{aligned} \rho(\theta_1, \theta_2) - \rho(\theta_1, \theta'_2) + \rho(\theta'_1, \theta_2) + \rho(\theta'_1, \theta'_2) = \\ -\frac{\sqrt{3}}{2} + \frac{1}{2} - 1 - \frac{\sqrt{3}}{2} < -2. \end{aligned} \quad (13)$$

III.1 Localidade

Iremos mostrar nesta seção que o esquema apresentado neste artigo é local, num sentido preciso. Seguimos [12]. Localidade requer o seguinte:

$$E(X|\theta_1, \theta_2, \theta) = E(X|\theta_1, \theta). \quad (14)$$

É óbvio que (14) é obtida imediatamente subtraindo-se as intensidades de cada detector homodino, e observando que o resultado não depende dos ângulos fixados no outro detector. A equação (14) diz simplesmente que qualquer que seja o resultado de uma medida num detector homodino, este resultado tem que depender somente de θ , a variável oculta, e da fase associada a este detector em particular, e não pode ser influenciada pela fase do outro detector.

IV Comentários Finais

Existem vários comentários que temos que fazer para clarear alguns pontos.

- Quando usamos campos clássicos, o número de fótons é extremamente grande. Por outro lado, as desigualdades de Bell, não são suficientes para mostrar que não temos uma distribuição conjunta para campos clássicos.
- Podemos argumentar que se campos clássicos violam as desigualdades de Bell, então, como eles são clássicos, o Teorema de Bell tem que estar errado, e devemos mostrar porque isto é o caso. Contudo, tudo que mostramos neste artigo é que campos clássicos não tem uma variável oculta tipo Bell.

Agradecimentos J. A. B. agradece apoio parcial do Lafex/CBPF, e em particular ao Dr. Nelson Pinto Neto. J.A.B. também agradece à FAPEMIG por apoio financeiro. A. S. S. agradece ao CNPq por apoio financeiro.

References

- [1] A. Aspect, J. Dalibard, G. Roger, Phys. Rev. Lett. **49**, (1982) 1804.
- [2] A. Aspect, P. Grangier, G. Roger, Phys. Rev. Lett. **49**, (1982) 91.
- [3] J. S. Bell, Physics **1**, (1964) 195.
- [4] J. S. Bell, Rev. Mod. Phys. **38**, (1966) 447.
- [5] N. Bohr, Phys. Rev. **48**, (1935) 696.
- [6] N. Bohr and L. Rosenfeld, Det. Kgl. Danske Videnskabernes Selskab., Mat.-fys. Med. **XII**, (1933) 8.

- [7] J. F. Clauser and A. Shimony, *Rep. Prog. Phys.* **41**, (1978) 1881.
- [8] A. Fine, *Phys. Rev. Lett.* **48**, (1982) 291.
- [9] P. W. Holland and T. R. Rosenbaum, *Ann. Statist.* **14**, (1986) 1523.
- [10] M. Loève, *Probability Theory II*, 4rd edition, (Springer Verlag, New York, 1978).
- [11] A. Peres, *Quantum Theory: Concepts and Methods*, (Kluwer, Dordrecht, Holland, 1995).
- [12] P. Suppes and M. Zanotti, in *Logic and Probability in Quantum Mechanics*, ed. P. Suppes (Reidel, Dordrecht, 1976), p. 445.
- [13] P. Suppes and M. Zanotti, *Synthese* **48**, (1981) 191.
- [14] S. M. Tan, M. J. Holland and D. F. Walls, *Opt. Commun.* **77**, (1990) 285.
- [15] S. M. Tan, D. F. Walls, and M. J. Collett, *Phys. Rev. Lett.* **66**, (1991) 252.
- [16] D. F. Walls and G. J. Milburn, *Quantum Optics*, (Springer-Verlag, New York, 1994).

Hamiltonian Structures for the Generalized Dispersionless KdV Hierarchy*

J. C. Brunelli†

Universidade Federal de Santa Catarina

Departamento de Física - CFM

Campus Universitário - Trindade

C.P. 476, CEP 88040-900

Florianópolis, SC - BRAZIL

We study from a Hamiltonian point of view the generalized dispersionless KdV hierarchy of equations. From the so called dispersionless Lax representation of these equations we obtain three compatible Hamiltonian structures. The second and third Hamiltonian structures are calculated directly from the r-matrix approach. Since the third structure is not related recursively with the first two ones the generalized dispersionless KdV hierarchy can be characterized as a truly tri-Hamiltonian system.

An interesting class of nonlinear equations are the so called dispersionless Lax equations which are the quasi-classical limit of ordinary Lax equations. This quasi-classical limit corresponds to the solutions which slowly depend on the variables x, t . Taking the KdV equation $4u_t = u_{xxx} + 6uu_x$ and dropping out the dispersive term (through the substitution $\frac{\partial}{\partial t} \rightarrow \epsilon \frac{\partial}{\partial t}, \frac{\partial}{\partial x} \rightarrow \epsilon \frac{\partial}{\partial x}$ and $\epsilon \rightarrow 0$) we end up with the Riemann equation

$$u_t = \frac{3}{2}uu_x \quad (1)$$

Solutions of (1) can be written through the implicit form $[1] u = f(x - ut)$ and this dependence gives rise to the breaking of the wave shape leading to a transition from conservative to dissipative behaviour [2]. As it is well known the balancing between the dispersive and nonlinear terms is responsible for the soliton solutions and the integrability of the KdV equation. What is interesting is that the Riemann equation, at least before the breaking of its wave solutions, is a integrable Hamiltonian system much like the KdV. As point out by Olver and Nutku [3] equation (1) has an infinite sequence of zero order conserved charges

$$H_1 = \int dx u, \quad H_3 = \frac{1}{4} \int dx u^2, \quad H_5 = \frac{1}{8} \int dx u^3, \dots \quad (2)$$

and has three first-order Hamiltonian structures given by

$$\mathcal{D}_1 = 2\partial, \quad \mathcal{D}_2 = u\partial + \partial u, \quad \mathcal{D}_3 = u^2\partial + \partial u^2 \quad (3)$$

These three Hamiltonian operators are compatible in the Magri's sense [4,5] making (1) a tri-Hamiltonian system, i.e., it can be written in three Hamiltonian forms

$$u_t = \mathcal{D}_1 \frac{\delta H_5}{\delta u} = \mathcal{D}_2 \frac{\delta H_3}{\delta u} = \frac{3}{4} \mathcal{D}_3 \frac{\delta H_1}{\delta u} \quad (4)$$

However, it is important to point out that since $\mathcal{D}_3 \neq \mathcal{D}_2 \mathcal{D}_1^{-1} \mathcal{D}_2$ the Hamiltonian operators are not trivially related. Therefore, the Hamiltonian structures (3) make the Riemann equation a truly tri-Hamiltonian system. From Magri's theorem [4,5] the Hamiltonians (2) are in involution with respect to any of the three Poisson brackets

$$\{H_n, H_m\}_i = \int dx \frac{\delta H_n}{\delta u} \mathcal{D}_i \frac{\delta H_m}{\delta u} = 0, \quad i = 1, 2, 3, \dots \quad (5)$$

*to appear in the Reviews in Mathematical Physics.

†Work supported by CNPq. E-mail address: brunelli@fsc.ufsc.br

Whence, (1) is an integrable Hamiltonian system.

Although we have Lax representations for the Riemann equation we do not know how to use them for an inverse scattering problem or use the pseudo-differential operator algebra to obtain its Hamiltonian structures through the Gelfand-Dickey approach [6]. However, Lebedev [7] has noticed that for the case of Benney's equation an alternative Lax representation is possible. This Lax representation is called dispersionless Lax equation and was also considered by Krichever [8] in his studies about topological minimal models.

The dispersionless KdV equation (1) can be obtained directly, bypassing the dispersionless limit of the KdV equation. Let E_n be the polynomial of degree n in p [8]

$$E_n = p^n + u_{-1}p^{n-1} + u_0p^{n-2} + \dots + u_{n-2} = \sum_{i=0}^n u_{n-i-2}p^i \tag{6}$$

where $u_{-2} = 1$ and the polynomial coefficients u_i are functions of the variable x and various time variables t_k ($k = 1, 2, 3, \dots$). We denote A_+ and A_- the parts of the Laurent polynomial A containing nonnegative and negative powers of p respectively. The generalized dispersionless KdV hierarchy is given by the Lax equation

$$\frac{\partial E_n}{\partial t_k} = \{(E_n^{k/n})_+, E_n\} = \{E_n, (E_n^{k/n})_-\} \tag{7}$$

where the bracket is defined [7,9] to be

$$\{A, B\} = \partial_p A \partial_x B - \partial_p B \partial_x A \tag{8}$$

and $E_n^{k/n}$ is the k th power of the Laurent polynomial $E_n^{1/n}$ satisfying $(E_n^{1/n})^n = E_n$.

Now, for general Laurent polynomials of the form $A = \sum_{i=-\infty}^{+\infty} a_i(x)p^i$ we define its residue as the coefficient of the p^{-1} term ($\text{Res}A = a_{-1}$) and the Adler trace [10] as $\text{Tr} A = \int dx \text{Res}A$.

Let us note from (7) that we can write

$$\frac{\partial E_n^{m/n}}{\partial t_k} = \{(E_n^{k/n})_+, E_n^{m/n}\} \tag{9}$$

for an arbitrary integer m . Taking the trace of (9) and after using $\text{Tr}\{A, B\} = 0$ we obtain $\frac{\partial}{\partial t_k} \text{Tr}(E_n^{m/n}) = 0$. Thus, we define the conserved charges as

$$H_m = \frac{n}{m} \text{Tr}(E_n^{m/n}), \quad m = 1, 2, 3, \dots \tag{10}$$

It is easy to show that $\frac{\partial^2 E_n}{\partial t_1 \partial t_1} = \frac{\partial^2 E_n}{\partial t_3 \partial t_3}$, i.e., the flows given by (7) commute. Therefore, the hierarchy of equations (7) has an infinite number of conserved laws (10) and an infinite number of commuting flows and can be formally be considered integrable.

Let us illustrate these results for (6) with $n = 2$ and $u_{-1} = 0$. We obtain for $E_2 \equiv E = p^2 + u$ and $u_0 \equiv u$

$$\begin{aligned} E^{1/2} &= p + \frac{1}{2}up^{-1} - \frac{1}{8}u^2p^{-3} + \frac{1}{16}u^3p^{-5} - \frac{5}{128}u^4p^{-7} + \dots \\ E^{3/2} &= p^3 + \frac{3}{2}up + \frac{3}{8}u^2p^{-1} + \dots \\ E^{5/2} &= p^5 + \frac{5}{2}up^3 + \frac{15}{8}u^2p + \frac{5}{16}u^3p^{-1} + \dots \\ E^{7/2} &= p^7 + \frac{7}{2}up^5 + \frac{35}{8}u^2p^3 + \frac{35}{16}u^3p + \frac{35}{128}u^4p^{-1} + \dots \end{aligned} \tag{11}$$

From (9) we get the hierarchy of equations

$$\frac{\partial u}{\partial t_1} = u_x, \quad \frac{\partial u}{\partial t_3} = \frac{3}{2}uu_x, \quad \frac{\partial u}{\partial t_5} = \frac{15}{8}u^2u_x, \quad \frac{\partial u}{\partial t_7} = \frac{35}{16}u^3u_x, \dots \tag{12}$$

The conserved charges from (10) are

$$H_1 = \int dx u, \quad H_3 = \frac{1}{4} \int dx u^2, \quad H_5 = \frac{1}{8} \int dx u^3, \quad H_7 = \frac{5}{64} \int dx u^4, \dots \quad (13)$$

Thus, from (12) we get the Riemann equation as the first nonlinear equation in the hierarchy. Also, the charges (13) are exactly the Hamiltonians (2). We call (12) and (7) the dispersionless KdV (Riemann) hierarchy and the generalized dispersionless KdV (Riemann) hierarchy, respectively.

We can derive in a systematic way the first Hamiltonian structure associated with the generalized dispersionless KdV hierarchy of equations (7) following the Drinfeld and Sokolov approach [11] as in [12] for the usual KdV hierarchy. Starting from (7) we get

$$\frac{\partial}{\partial t_k} \text{Tr } E_n Q = \sum_{i=1}^{n-1} \int dy \text{Tr } E_n \{V_i(x, y), Q(x)\} \frac{\delta H_{n+k}}{\delta u_{n-i-1}(y)} \quad (14)$$

where $V_i(x, y) \equiv \delta(x-y)p^{-i}$ and $Q = \sum_{i=1}^n q_{n-i-1} p^{-i}$ is the dual to E_n . Here the q 's are assumed to be independent of the u 's. This yields a linear functional

$$\text{Tr } E_n Q = \int dx \sum_{i=0}^{n-1} u_{n-i-2} q_{n-i-2} \quad (15)$$

If we want to write (14) in Hamiltonian form as

$$\frac{\partial}{\partial t_k} \text{Tr } E_n Q = \{\text{Tr } E_n Q, H_{n+k}\}_1 = \sum_{i=1}^{n-1} \int dy \{\text{Tr } E_n Q, \text{Tr } E_n V_i\}_1 \frac{\delta H_{n+k}}{\delta u_{n-i-1}(y)} \quad (16)$$

(where we have used that $\text{Tr } E_n V_i(x, y) = u_{n-i-1}(y)$) we get after comparing it with (14)

$$\{\text{Tr } E_n Q, \text{Tr } E_n V_i\}_1 = \text{Tr } E_n \{V_i, Q\} \quad (17)$$

In this way, the dispersionless Lax equation (7) can be written in Hamiltonian form with respect to the first Poisson bracket

$$\{\text{Tr } E_n Q, \text{Tr } E_n V\}_1 = \text{Tr } E_n \{V, Q\} \quad (18)$$

for any dual Q and V relative to E_n .

As an example let be $E_2 \equiv E = p^2 + u_{-1}p + u_0$ with the duals

$$V = v_{-1}p^{-2} + v_0p^{-1}, \quad Q = q_{-1}p^{-2} + q_0p^{-1} \quad (19)$$

We get that

$$\begin{aligned} \text{Tr } E \{V, Q\} &= 2 \int dx q_0 v'_0 \\ \text{Tr } EQ &= \int dx (u_{-1}q_{-1} + u_0q_0) \\ \text{Tr } EV &= \int dx (u_{-1}v_{-1} + u_0v_0) \end{aligned} \quad (20)$$

Now, (18) yields (constraining E_2 to $E = p^2 + u$, where $u \equiv u_0$ and $u_{-1} = 0$)

$$\{u(x), u(y)\}_1 = 2\partial\delta(x-y) = \mathcal{D}_1\delta(x-y) \quad (21)$$

which is the first Hamiltonian structure for the Riemann equation (1).

We can try to write the dispersionless Lax equation in other Hamiltonian forms. However, we can use the algebraic structure behind the dispersionless hierarchy and apply the r-matrix formalism to obtain the other Hamiltonian structures. It is well known by now that the so called first Hamiltonian structure of integrable models is

the symplectic structure of Kostant-Kirillov [13] on the orbits of the coadjoint representation of Lie groups [10,14]. For dispersionless equations given by the Lax representation (7) the corresponding Lie algebra is given by the associative algebra of Laurent polynomials endowed with the bracket (8). The Hamiltonian structure (18) can also be obtained from this result. Semenov-Tian-Shansky [15] has shown that the multi-Hamiltonian nature of integrable equations could be explained in terms of the so called r-matrix. Let g be an abstract associative algebra with a non-degenerate trace form $\text{Tr}: g \rightarrow \mathbb{R}$. In this way we can identify g with its dual g^* by $\langle A|B \rangle = \text{Tr} AB$. Also, we can use the natural Lie algebra structure obtained by $[A, B] = AB - BA$ on g . The linear mapping $R: g \rightarrow g$ is a classical r-matrix on g whenever the modified bracket $[A, B]_R = [RA, B] + [A, RB]$ satisfies the Jacobi identity [15]. This gives us a second Lie algebra structure on g . The modified bracket satisfies the Jacobi identity if the modified Yang-Baxter equation holds. The important result for us is that the new Lie product endows $g = g^*$ with new Poisson structures. The first one is

$$\{\text{Tr} EQ, \text{Tr} EV\}_2 = \frac{1}{2} \text{Tr} E \left([Q, R(EV)] + [R(QE), V] \right) \tag{22}$$

where Q and V are duals to E . This expression was given by Semenov-Tian-Shansky [15] and it is the analog of the second structure of Gelfand-Dickey [6]. In references [16] a third Poisson structure was introduced

$$\{\text{Tr} EQ, \text{Tr} EV\}_3 = \frac{1}{2} \text{Tr} E \left([Q, R(EVE)] + [R(EQE), V] \right) \tag{23}$$

and it was shown that the Kostant-Kirillov structure (which gives (18) in our problem), (22) and (23) form a compatible tri-Hamiltonian system, i.e., the three structures are compatible in Magri's sense [4,5].

For Lie algebras that can be written in the form $g = g_+ \oplus g_-$ the r-matrix on g is given by $R = P_+ - P_-$ where $P_\pm g = g_\pm$ are the projections onto the subalgebras. For our particular case of dispersionless equations it is clear that $g_+ = \{A_+ = \sum_{i=0}^\infty a_i(x)p^i\}$ and $g_- = \{A_- = \sum_{i=1}^\infty a_{-i}(x)p^{-i}\}$ with trace already defined for the Laurent polynomials and bracket given by (8). So, the Poisson brackets (22) and (23) assume the form

$$\begin{aligned} \{\text{Tr} E_n Q, \text{Tr} E_n V\}_2 &= \\ &= \frac{1}{2} \text{Tr} E_n \left(\{Q, (E_n V)_+\} - \{Q, (E_n V)_-\} + \{(E_n Q)_+, V\} - \{(E_n Q)_-, V\} \right) \end{aligned} \tag{24a}$$

$$\begin{aligned} \{\text{Tr} E_n Q, \text{Tr} E_n V\}_3 &= \\ &= \frac{1}{2} \text{Tr} E_n \left(\{Q, (E_n^2 V)_+\} - \{Q, (E_n^2 V)_-\} + \{(E_n^2 Q)_+, V\} - \{(E_n^2 Q)_-, V\} \right) \end{aligned} \tag{24b}$$

Let us again use the Riemann equation as an example. Using E_2 and (19) we get, after an straightforward algebra, the following Poisson brackets from (24)

$$\begin{aligned} \{u_{-1}(x), u_{-1}(y)\}_2 &= -2\partial\delta(x-y) \\ \{u_{-1}(x), u_0(y)\}_2 &= -\partial u_{-1}\delta(x-y) \\ \{u_0(x), u_0(y)\}_2 &= (u_0\partial + \partial u_0 - u_{-1}\partial u_{-1})\delta(x-y) \end{aligned} \tag{25a}$$

$$\begin{aligned} \{u_{-1}(x), u_{-1}(y)\}_3 &= -2(u_0\partial + \partial u_0)\delta(x-y) \\ \{u_{-1}(x), u_0(y)\}_3 &= -(2\partial u_0 u_{-1} + u_{-1}^2\partial u_{-1})\delta(x-y) \\ \{u_0(x), u_0(y)\}_3 &= (u_0^2\partial + \partial u_0^2 - u_{-1}\partial u_0 u_{-1} - u_0 u_{-1}\partial u_{-1})\delta(x-y) \end{aligned} \tag{25b}$$

In the second and third brackets (25) u_{-1} is coupled to itself and to u_0 . From $\{u_{-1}(x), u_{-1}(y)\}$ in (25) it follows that $u_{-1} = 0$ corresponds to a second class constraint and we have to use the Dirac reduction. We then obtain

$$\{u(x), u(y)\}_2 = (u\partial + \partial u)\delta(x-y) = \mathcal{D}_2\delta(x-y) \tag{26a}$$

$$\{u(x), u(y)\}_3 = (u^2\partial + \partial u^2)\delta(x-y) = \mathcal{D}_3\delta(x-y) \quad (26b)$$

where we have set $u \equiv u_0$. These are exactly the Hamiltonian structures in (3).

Finally, the k th flow in the generalized dispersionless KdV hierarchy (7) can be written in Hamiltonian form as

$$\frac{\partial u}{\partial t_k} = \mathcal{D}_1 \frac{\delta H_{k+n}}{\delta u} = \mathcal{D}_2 \frac{\delta H_k}{\delta u} = \frac{k(k-2)}{(k-1)^2} \mathcal{D}_3 \frac{\delta H_{k-n}}{\delta u} \quad (27)$$

where $k > 1$ and $\mathbf{u} = (u_{-1}, u_0, \dots, u_{n-2})$. The Hamiltonians H_n are given by (10) and the Hamiltonian structures \mathcal{D}_1 , \mathcal{D}_2 and \mathcal{D}_3 can be obtained from the Poisson brackets (18), (24a) and (24b) respectively. For $n = 2$ we obtain from (27) the dispersionless KdV hierarchy of equations (12).

With our results we can study the higher Hamiltonian structures of other interesting dispersionless systems. For instance, the classical dispersionless long wave equation $u_t + uu_x + h_x = 0$, $h_t + (uh)_x = 0$ can be derived from the Benney's system [17] of equations. It is not difficult to check that it has a simple dispersionless nonstandard Lax representation $\frac{\delta E}{\delta t} = \{E, (E^2)_{\geq 1}\}$ where $E = p + \frac{1}{2}u + \frac{1}{4}hp^{-1}$ and the bracket is given by (8). Here $(E^2)_{\geq 1}$ stands for the purely nonnegative (without p^0 terms) part of the Laurent polynomial obtained from E^2 . For dispersive systems the nonstandard Lax representation was introduced by Kupershmidt in [18] and the generalization of the Gelfand-Dikii brackets was performed in [19]. The derivation of the Poisson brackets for equations with nonstandard dispersionless Lax representation is an interesting and relevant problem and is under investigation. These algebraic techniques can also be applied in the study of the classical limit of W-algebras [20], which are related with the second Poisson structure (22). Also, in the study of the dispersionless KP and dispersionless Toda lattice hierarchies [21] the usual quasi-classical limit from the ordinary KP and Toda hierarchies can be bypassed using the algebraic setup described in this work.

References

- [1] G. B. Whitham, "Linear and Nonlinear Waves" (Wiley, New York, 1974).
- [2] P. Lax, *Am. Math. Mo.* **79**, 227 (1972); J. Cavalcante and H. P. McKean, *Physica* **4D**, 253 (1982).
- [3] P. J. Olver and Y. Nutku, *J. Math. Phys.* **29**, 1610 (1988).
- [4] F. Magri, *J. Math. Phys.* **19**, 1156 (1978).
- [5] P. J. Olver, "Applications of Lie Groups to Differential Equations", *Graduate Texts in Mathematics*, Vol. 107 (Springer, New York, 1986).
- [6] L. A. Dickey, "Soliton Equations and Hamiltonian Systems" (World Scientific, Singapore, 1991).
- [7] D. R. Lebedev, *Lett. Math. Phys.* **3**, 481 (1979).
- [8] I. Krichever, *Commun. Math. Phys.* **143**, 415 (1992).
- [9] D. R. Lebedev and Yu. I. Manin, *Phys. Lett.* **74A**, 154 (1979).
- [10] M. Adler, *Invent. Math.* **50**, 219 (1979).
- [11] V. G. Drinfeld and V. V. Sokolov, *J. Sov. Math.* **30**, 1975 (1985).
- [12] A. Das and W.-J. Huang, *J. Math. Phys.* **33**, 2487 (1992).
- [13] A. A. Kirillov, "Elements of the Theory of Representations" (Springer, Berlin, 1976); B. Kostant, *Lect. Notes in Math.* **170**, 87 (1970).
- [14] B. Kostant, *London Math. Soc. Lect. Notes, Ser.* **34**, 287 (1979); A. G. Reyman, M. A. Semenov-Tian-Shansky and I. B. Frenkel, *Sov. Math. Dokl.* **20**, 811 (1979); W. W. Symes, *Invent. Math.* **59**, 13 (1980); D. R. Lebedev and Yu. I. Manin, *Funct. Anal. Appl.* **13**, 268 (1980).
- [15] M. A. Semenov-Tian-Shansky, *Funct. Anal. Appl.* **17**, 259 (1983).
- [16] L.-C. Li and S. Parmentier, *Comm. Math. Phys.* **125**, 545 (1989); W. Oevel and O. Ragnisco, *Physica* **161A**, 181 (1990).
- [17] D. J. Benney, *Studies Appl. Math.* **52**, 45 (1973).
- [18] B.A. Kupershmidt, *Comm. Math. Phys.* **99**, 51 (1985).
- [19] J. C. Brunelli, A. Das and W.-J. Huang, *Mod. Phys. Lett.* **A9**, 2147 (1994).
- [20] J. M. Figueroa-O'Farril and E. Ramos, *Phys. Lett.* **B282**, 357 (1992).
- [21] K. Takasaki and T. Takebe, *Rev. Math. Phys.* **7**, 743 (1995).

The Connes-Lott program on the Sphere and the Static Magnetic Monopole

Juan A. Mignaco, Cassio Sigaud, Franciscus J. Vanhecke

Depto. de Física Teórica, Inst. de Física

Antonio R. da Silva

Depto. de Matemática Pura, Inst. de Matemática

U.F.R.J. - C.P. 68528 - CEP 21945-970 Rio de Janeiro - RJ

We examine the problem of the Dirac monopole in the light of Serre-Swann's theorem identifying the space of sections of (complex) vector bundles over the sphere and the projective modules over the algebra of complex-valued functions. These modules are defined by projection operators classified by $\pi_2(S^2) \cong \mathbf{Z}$. On these modules we construct hermitian connections with values on the universal differential envelope. The Connes-Lott program is applied using the Hilbert space of complexified inhomogeneous differential forms on the sphere with its Atiyah-Kähler algebra structure. This Hilbert space splits in two minimal left ideals of the Clifford algebra, providing irreducible representations for it. The Dirac (Kähler) differential operator $\mathbf{D} = i(\mathbf{d} - \delta)$ preserves the splitting. Both ingredients induce a representation of the universal differential envelope. In order to recover its differential structure, a quotient with the "junk" is taken and yields the complexified de Rham exterior differential algebra over the sphere. The subsequent steps of the Connes-Lott program allows to define the fermionic action, and the field action is obtained using the Dixmier trace once the connection and curvature are reduced to de Rham forms.

A similar treatment to describe the instantons using the algebra of functions on S^4 with quaternionic values is in progress.

1 Introduction

Non commutative geometry is an attempt to introduce new geometrical contents by taking as primary entities associative algebras instead of the customary spaces. The relation with the usual treatment is provided by a theorem of Gel'fand and Naimark that associates the space of irreducible representations of C^* -algebras with a topological space [1]. For the algebra of functions on a manifold, the resulting space is homomorphic to the original manifold.

In recent years, Connes [2] applied these ideas looking for a geometrical setting for models in elementary particle physics. One of the most interesting results is that the Higgs field may appear as a component of the connection in a generalized algebraic structure. In his work with Lott [[2]] where this result was first made explicit, they wrote a recipe for the construction. In full generality, the procedure is quite elaborated and many corners of it are not clear enough. In this work, we propose a rather simple application with well known physical and mathematical features, in which we display the main operations necessary with a rather modest mathematical apparatus.

This brief report condenses a longer version which will be submitted for publication elsewhere [3]. In the next section we sketch the procedure which leads to the construction of a universal differential envelope for the algebra of C^∞ -functions on the sphere, when this surface is stereographically projected on euclidian charts.

The next section is devoted to the formulation of the projection on algebraic modules, and we show how they are classified by the homotopy group $\pi_2(S^2) \cong \mathbf{Z}$. The connection and curvature are calculated, and the rôle of the topological properties is made explicit.

The last section is a short description of the construction of a "spectral triple" à la Connes. We introduce, at variance with the usual procedure, a Hilbert space formed by the inhomogeneous differential forms, endowed with a Clifford product. The analogue of the usual Dirac differential operator is its version proposed by Kähler [4], which reads $D = i(d - \delta)$, where δ is the codifferential operator adjoint to d within the natural inner product in the space of differential forms.

The results are analogous to the ones provided by the study of the Schwinger model on the sphere [5], and they are applicable to the study of Dirac's magnetic monopole, since the configuration space for it retracts onto the sphere.

2 Differential Geometry on the Sphere S^2

The sphere of radius r is defined as $S^2 \equiv \{p \equiv (x, y, z) \in \mathbf{R}^3 \mid x^2 + y^2 + z^2 = r^2\}$; its stereographic projection on the equatorial plane is given in the austral chart $H_A \equiv \{p \in S^2 \mid z < r\}$ by:

$$\phi_A : H_A \rightarrow \mathbf{R}^2 : (x, y, z) \rightarrow (\xi, \eta), \text{ where } \xi = \frac{x}{r-z}, \eta = \frac{y}{r-z}, \quad (1)$$

whose inverse is easy to find and the analogous projection on the other chart, ϕ_B , too.

A complex coordinate for the plane, $\zeta_A = \xi + i\eta$, is related to the usual polar and azimuthal angles through

$$\zeta_A = \cot(\theta/2) \exp(i\varphi). \quad (2)$$

and corresponding expressions are obtained in the boreal chart for the complex coordinate ζ_B . On the overlapping region, $H_A \cap H_B$ one has $\zeta_A \zeta_B = 1$.

Differential forms ($d\xi, d\eta$) and the zweibein ($\underline{\theta}^\xi, \underline{\theta}^\eta$) are related through

$$\underline{\theta}^\xi = \frac{2}{f_A} d\xi, \quad \underline{\theta}^\eta = \frac{2}{f_A} d\eta \quad (3)$$

with $f_A = 1 + |\zeta_A|^2$. The metric on the austral chart is inherited from the euclidian metric in \mathbf{R}^3 and is

$$g|_A = \underline{\theta}^\xi \otimes \underline{\theta}^\xi + \underline{\theta}^\eta \otimes \underline{\theta}^\eta \quad (4)$$

$$= \frac{1}{2} (\underline{\theta}_A^c \otimes \underline{\theta}_A + \underline{\theta}_A \otimes \underline{\theta}_A^c), \quad (5)$$

with $\underline{\theta}_A = \underline{\theta}^\xi + i\underline{\theta}^\eta$ and $\underline{\theta}_A^c$ its complex conjugate.

A local basis for the space of differential forms on the sphere, $\mathcal{F}^*(S^2)$ is given in H_A by $\{1, \underline{\theta}^\xi, \underline{\theta}^\eta, \omega\}$, with

$$\omega|_A = \underline{\theta}^\xi \wedge \underline{\theta}^\eta. \quad (6)$$

the oriented area element.

The Levi-Civita connection reads

$$\nabla \underline{\theta}^\xi = -(\xi \underline{\theta}^\eta - \eta \underline{\theta}^\xi) \otimes \underline{\theta}^\eta, \quad (7)$$

and an analogous expression for $\underline{\theta}^\eta$.

Through the Hodge duality operator, $*$,

$$* : \mathcal{F}^{(p)}(S^2) \rightarrow \mathcal{F}^{(2-p)}(S^2) \quad (8)$$

one defines an inner product in the space of p -forms, $\mathcal{F}^{(p)}$:

$$\langle \alpha, \beta \rangle = \int_{S^2} \alpha \wedge * \beta. \quad (9)$$

Besides,

$$\alpha \wedge * \beta = g^{-1}(\langle \alpha, \beta \rangle) \omega \quad (10)$$

where g^{-1} is the inner product with values on S^2 .

On the Grassmann algebra of differential forms a Clifford product is introduced for one-forms:

$$\alpha \vee \beta = \alpha \wedge \beta + g^{-1}(\alpha, \beta). \tag{11}$$

The Clifford algebra must be complexified in order to have non-trivial solutions for idempotents:

$$P_{\pm} = \frac{1}{2}(1 + i\omega) \tag{12}$$

that projects on its two minimal left ideals. The Dirac-Kähler differential operator, defined as

$$D = i(d - \delta), \tag{13}$$

where δ is the adjoint of the exterior differential d with the inner product defined as above in $\mathcal{F}^{(p)}$, preserves the minimal left ideals \mathcal{I}_{\pm}^E , and the Hilbert space completion of $\mathcal{F}^*(S^2)$ may be written as the direct sum of the Hilbert spaces generated by each minimal left ideal (with a suitable inner product).

3 The Projective Modules over $C^\infty(S^2) \otimes \mathbb{C}$

The universal differential envelope of an algebra \mathcal{A} is defined as a graded differential algebra

$$\Omega_u^*(\mathcal{A}) \equiv \left\{ \bigoplus_{k=0}^{\infty} \Omega_u^{(k)}(\mathcal{A}), d_u \right\}, \tag{14}$$

with $\Omega_u^{(0)} = \mathcal{A}$ and d_u is a formal differential [1, 6].

A right (left) module of an algebra \mathcal{A} is a set of elements of the algebra that transform among themselves by right (left) multiplication by all the elements of the algebra. The universal differential envelope defined above, $\Omega_u^*(\mathcal{A})$ is a bi-module, and its tensor product over \mathcal{A} with a \mathcal{A} -module \mathcal{M} is well defined. Given a connection in \mathcal{M} :

$$\nabla : \mathcal{M} \rightarrow \Omega_u^{(1)}(\mathcal{M}) = \mathcal{M} \otimes \Omega_u^{(1)}(\mathcal{A}), \tag{15}$$

it can be extended to the whole of $\Omega_u^*(\mathcal{M})$. On a basis $E_i, i = 1, \dots, N$ for a free module, the connection is given by an $N \times N$ matrix with entries in $\Omega_u^{(1)}(\mathcal{A})$:

$$\nabla E_i = E_j \otimes \omega^j_i. \tag{16}$$

The curvature ∇^2 of the connection is a module homomorphism.

A hermitian projective module of finite rank, \mathcal{M}_P , over \mathcal{A} , is obtained from a free module (the algebra itself or a finite tensor product of it) as the image of a projection operator $P, P^2 = P, P^\dagger = P$. In our case, the algebra $\mathcal{A} = C^\infty(S^2) \otimes \mathbb{C}$, and it is enough for our purposes to consider the unidimensional projection from $\mathcal{A} \otimes \mathcal{A}$ which can be written as

$$P(\vec{n}) = \frac{1}{2}(1 + n^\alpha \sigma_\alpha), \tag{17}$$

where the components n^α are real functions on the sphere and are normalized to unity, and σ_α indicates the three Pauli spin matrices. The projection so constructed is then given by a mapping $S^2 \rightarrow S^2$. The mapping is characterized by the second homotopy group, $\pi_2(S^2) \cong \mathbb{Z}$.

Choosing as a representative for a class $[\vec{n}]$ the mapping which preserves the southern pole, $(1, 0, 0)$, is given, on the austral euclidian chart H_A :

$$\left. \begin{aligned} \nu_A &= \zeta_A^k, \text{ if } [\vec{n}] = k \\ \nu_A &= (\zeta_A^c)^{|k|}, \text{ if } [\vec{n}] = -k \end{aligned} \right\} \tag{18}$$

where $k \in \mathbb{Z}^+$ and ν_A is the complex coordinate of $\vec{n} \in S^2$.

A connection ∇_P on a projective module $\mathcal{M}_P = P\mathcal{M}$ is obtained from the one in \mathcal{M} , ∇ , by

$$\nabla_P = P \circ \nabla : \mathcal{M}_P \rightarrow \mathcal{M}_P \otimes_{\mathcal{A}} \Omega_u^{(1)}(\mathcal{A}), \tag{19}$$

and, correspondingly, a curvature is obtained which keeps track of the non-trivial topology content of the projection. It is the contribution inherited from the projection which prevents to write the curvature as a differential of a globally defined connection one-form on the sphere.

4 The Spectral Triple $\{\mathcal{A}, \mathcal{H}, \mathcal{D}\}$

In the sense employed by Connes [2] the spectral triple in our case has the following components:

- $\mathcal{A} = C^\infty(S^2) \otimes \mathbb{C}$
- \mathcal{H} is the Hilbert space obtained by the completion of a minimal left ideal \mathcal{I}_+^E , using a convenient (spinor-like) inner product
- \mathcal{D} is the Dirac-Kähler differential operator restricted to \mathcal{H} ; it is self-adjoint and has a compact resolvent.

On \mathcal{H} there is a faithful \ast -representation π_0 of \mathcal{A} on the bounded operators, $\mathcal{L}(\mathcal{H})$:

$$\pi_0 : \mathcal{A} \rightarrow \mathcal{L}(\mathcal{H}) : f \rightarrow \hat{f} = \pi_0(f), \tag{20}$$

$$(\hat{f}\psi)(\mathbf{x}) = f(\mathbf{x})\psi(\mathbf{x}). \tag{21}$$

The universal differential algebra is mapped in $\mathcal{L}(\mathcal{H})$ as an extension of π_0 with the help of the Dirac-Kähler operator:

$$\pi : \Omega_u^*(\mathcal{A}) \rightarrow \mathcal{L}(\mathcal{H}) : \psi_u \rightarrow \pi(\psi_u) \tag{22}$$

where

$$\pi(f_0 d_u f_1 \cdots d_u f_p) = \hat{f}_0 \left[\frac{1}{i} \mathcal{D}, \hat{f}_1 \right] \cdots \left[\frac{1}{i} \mathcal{D}, \hat{f}_p \right]. \tag{23}$$

The resulting set, however, is not a graded differential algebra, which is obtained by taking the quotient with the ideal formed by $\text{Ker}(\pi) + d(\text{Ker}(\pi))$. At the end, we recover the de Rham algebra of differential forms on the sphere. This allows to obtain the lagrangian for an abelian Yang-Mills field via the Dixmier trace [1, 2].

To proceed with the Connes-Lott program one needs to construct the matter field lagrangian. In our case, this matter field is represented as a vector of a new Hilbert space obtained via the tensor product over \mathcal{A} of \mathcal{H} and the projective module \mathcal{M}_P .

$$\mathcal{H}_F = \mathcal{M}_P \otimes_{\mathcal{A}} \mathcal{H} \tag{24}$$

This allows to introduce a covariant differential operator, \mathcal{D}_∇ , which contains the interaction with the Yang-Mills abelian field.

Minimization of the lagrangian results in a curvature for the Yang-Mills field

$$\rho = d\kappa + \rho_m \tag{25}$$

where κ is a globally defined one-form and ρ_m is a monopole field which in the cartesian chart H_A is

$$\rho_m = \frac{1}{(1 + |\nu_A|^2)^2} d\nu_A \wedge d\nu_A^c \tag{26}$$

and an analogous expression in the other chart. These results are in agreement with those of Jayewardena [5].

For the matter field, minimization leads to the covariant Dirac equation of Benn and Tucker [7].

References

- [1] J. C. Varilly and J. M. Gracia-Bondia, *J. Geom. and Phys.* **12**(1993)223
- [2] A. Connes and J. Lott, *Nucl. Phys.(Proc. Suppl.)* **18B** (1990)29
A. Connes, "Noncommutative Geometry". Acad. Press, London (1994)
- [3] J. A. Mignaco, C. Sigaud, A. R. da Silva and F. J. Vanhecke, "The Connes-Lott Program on the Sphere", in preparation.
- [4] E. Kähler, *Abh. Dt. Akad. Wiss. Berlin, Kl. für Math., Phys. u. Tech., Jahrg. 1960*, **4** (1960); *Rendiconti di Matematica (Roma)*, Ser. V, **21**(1962)425
- [5] C. Jayewardena, *Helv. Phys. Acta* **61** (1988) 636
- [6] R. Coquereaux, *J. of Geom and Phys.* **6** (1989) 425
- [7] I. M. Benn and R. W. Tucker, *Comm. Math. Phys.* **89** (1983)341

The Virasoro algebra of a 1+1 black hole model

J. F. Gomes, F. E. Mendonça da Silveira and A. H. Zimerman

Instituto de Física Teórica - UNESP

In this work, we study a model of the conformally invariant non Abelian Toda type which presents a black hole structure, according to a Hamiltonian reduction procedure. Based on the work of Bilal (A. Bilal, Nuc. Phys. B 422 (1994) 258-288), we follow a WZNW formalism to construct a single black hole action which interacts with the Toda type fields, through a particular choice of a grading operator that acts on a $so(5)$ Lie algebra, for the example of a spin $3/2$ model. We study also the symmetries, generated by the remaining currents of the above Hamiltonian reduction, which satisfy an algebraic structure of the Virasoro type. Finally, we are able to express the currents algebra in terms of free fields.

The $so(5)$ Lie algebra has two simple roots. Let's call them, as in the Weyl-Cartan basis, α_1 and α_2 , and write them as

$$\alpha_1 = e_1 - e_2 \quad (1)$$

and

$$\alpha_2 = e_2, \quad (2)$$

where e_1 and e_2 are typical elements of the Chevalley basis.

These elements satisfy the usual scalar product relations

$$e_i \cdot e_j = \delta_{ij}, \quad (3)$$

with

$$i, j = 1, 2. \quad (4)$$

If we define a grading operator as

$$Q = \frac{2(\alpha_1 + \alpha_2) \cdot H}{(\alpha_1 + \alpha_2)^2}, \quad (5)$$

where the operator H is related to the Cartan generators h_i through

$$h_i = \frac{2\alpha_i \cdot H}{\alpha_i^2}, \quad (6)$$

then we can write an arbitrary element $g \in SO(5)$ as the Gauss decomposition

$$g = NBM, \quad (7)$$

where we define

$$N = \exp(\psi_1 E_{\alpha_1} + \psi_2 E_{\alpha_1 + \alpha_2} + \psi_3 E_{\alpha_1 + 2\alpha_2}), \quad (8)$$

$$B = \exp(\psi E_{\alpha_2} + \phi(\alpha_1 + \alpha_2) + \rho Q + \chi E_{-\alpha_2}) \quad (9)$$

and

$$M = \exp(\chi_1 E_{-\alpha_1} + \chi_2 E_{-\alpha_1 - \alpha_2} + \chi_3 E_{-\alpha_1 - 2\alpha_2}). \quad (10)$$

If we impose the constraints

$$J_{-\alpha_1} = 1, \quad (11)$$

$$J_{-\alpha_1 - \alpha_2} = 0 \quad (12)$$

and

$$J_{-\alpha_1 - 2\alpha_2} = 0, \quad (13)$$

on the J current components in the direction of the elements with negative gradation and the gauge fixing

$$J_{h_1} = 0, \quad (14)$$

$$J_{\alpha_2} = 0 \quad (15)$$

and

$$J_{\alpha_1 + 2\alpha_2} = 0, \quad (16)$$

on the J current components in the direction of the elements with null gradation, we will obtain the expressions for the non-physical fields

$$\chi_1 = \partial_- \phi - \partial_- \rho, \quad (17)$$

$$\chi_2 = \partial_- \chi - \chi(\partial_- \rho + \partial_- \phi) - \chi^2 \partial_- \psi e^{-\phi - \rho} \quad (18)$$

and

$$\partial_- \chi_3 = \chi_3^2. \quad (19)$$

The gauge fixing

$$J_{h_2} = 0 \quad (20)$$

leads to the black hole condition for the model

$$\partial_- \rho + \chi \partial_- \psi e^{-\phi - \rho} = 0. \quad (21)$$

The remaining currents read as

$$J_{-\alpha_2} = \partial_- \psi e^{-\phi - \rho}, \quad (22)$$

$$J_{\alpha_1} = \partial_- \chi_1 + \chi_1^2 + 2\chi_2 \partial_- \psi e^{-\phi - \rho} \quad (23)$$

and

$$J_{\alpha_1 + \alpha_2} = \partial_- \chi_2 + \chi_1 \chi_2 - \chi_3 \partial_- \psi e^{-\phi - \rho}. \quad (24)$$

The Polyakov-Wiegmann term can be written as $Tr(BE_{\alpha_1} B^{-1} E_{-\alpha_1})$, which furnishes the Lagrangian density

$$L = \partial_- \phi \partial_+ \phi + \partial_- \rho \partial_+ \rho - e^{-2\phi} + 2\partial_- \psi \partial_+ \chi e^{-\phi - \rho}. \quad (25)$$

The proposal of the coordinate transformations

$$\psi = \psi' e^{\rho/2} \quad (26)$$

and

$$\chi = \chi' e^{\rho/2} \quad (27)$$

leads to the expressions for the black hole conditions and for the constrained Lagrangian density

$$\partial_- \rho = \frac{-\chi' \partial_- \psi' e^{-\phi}}{1 + \frac{1}{2} \psi' \chi' e^{-\phi}} \quad (28)$$

$$\partial_+ \rho = \frac{-\psi' \partial_+ \chi' e^{-\phi}}{1 + \frac{1}{2} \psi' \chi' e^{-\phi}} \quad (29)$$

and

$$L = -e^{-2\phi} + \partial_- \phi \partial_+ \phi + 2 \frac{\partial_- \psi' \partial_+ \chi' e^{-\phi}}{1 + \frac{1}{2} \psi' \chi' e^{-\phi}} \quad (30)$$

which furnishes the canonically conjugate momenta

$$\pi_\phi = 2\phi, \quad (31)$$

$$\pi_{\psi'} = \frac{2\partial_+ \chi' e^{-\phi}}{1 + \frac{1}{2} \psi' \chi' e^{-\phi}} \quad (32)$$

and

$$\pi_{\chi'} = \frac{2\partial_- \psi' e^{-\phi}}{1 + \frac{1}{2} \psi' \chi' e^{-\phi}} \quad (33)$$

The usual Poisson brackets for the physical fields ϕ , ψ' and χ' , together with the Dirac brackets for the non-local field ρ leads to a Virasoro algebra for the remaining currents. In fact,

$$\{J_{-\alpha_2}(\sigma), J_{-\alpha_2}(\sigma')\} = \frac{1}{2} J_{-\alpha_2}(\sigma) J_{-\alpha_2}(\sigma') \partial_-^{-1} \delta(\sigma - \sigma'), \quad (34)$$

$$\{J_{\alpha_1}(\sigma), J_{\alpha_1}(\sigma')\} = -\frac{1}{2} \delta'''(\sigma - \sigma') + 2J_{\alpha_1}(\sigma') \delta'(\sigma - \sigma') - J'_{\alpha_1}(\sigma') \delta(\sigma - \sigma') \quad (35)$$

and

$$\{J_{\alpha_1+\alpha_2}(\sigma), J_{\alpha_1+\alpha_2}(\sigma')\} = \frac{1}{2} J_{\alpha_1+\alpha_2}(\sigma) J_{\alpha_1+\alpha_2}(\sigma') \partial_-^{-1} \delta(\sigma - \sigma'). \quad (36)$$

Finally, if we consider the coordinate transformations

$$\rho = \rho' - \phi' \quad (37)$$

and

$$\phi = \rho' + \phi' \quad (38)$$

and define the free fields as

$$\psi = f_+, \quad (39)$$

$$\chi = f_- e^{2\rho'}, \quad (40)$$

$$\phi' = f_1 \quad (41)$$

and

$$\rho' = f_2, \quad (42)$$

together with the ansatz for the comutation relations for these free fields

$$\{f_1(\sigma), f_{\pm}(\sigma')\} = 0, \quad (43)$$

$$\{f_1(\sigma), f_1(\sigma')\} = -\frac{1}{8}\partial_-^{-1}\delta(\sigma - \sigma'), \quad (44)$$

$$\{f_2(\sigma), f_2(\sigma')\} = -\frac{1}{8}\partial_-^{-1}\delta(\sigma - \sigma'), \quad (45)$$

$$\{f_1(\sigma), f_2(\sigma')\} = -\frac{1}{8}\partial_-^{-1}\delta(\sigma - \sigma'), \quad (46)$$

$$\{f_2(\sigma), f_-(\sigma')\} = \frac{1}{2}f_-(\sigma')\partial_-^{-1}\delta(\sigma - \sigma'), \quad (47)$$

$$\{f_2(\sigma), f'_+(\sigma')\} = -\frac{1}{2}f'_+(\sigma')\partial_-^{-1}\delta(\sigma - \sigma'), \quad (48)$$

$$\{f_-(\sigma), f_-(\sigma')\} = -f_-(\sigma)f_-(\sigma')\partial_-^{-1}\delta(\sigma - \sigma'), \quad (49)$$

$$\{f'_+(\sigma), f'_+(\sigma')\} = -f'_+(\sigma)f'_+(\sigma')\partial_-^{-1}\delta(\sigma - \sigma') \quad (50)$$

and

$$\{f_-(\sigma), f'_+(\sigma')\} = f_-(\sigma)f'_+(\sigma')\partial_-^{-1}\delta(\sigma - \sigma') + \frac{1}{2}\delta(\sigma - \sigma'), \quad (51)$$

we will be able to reproduce the above Spin 3/2 Virasoro algebra, for the corresponding remaining currents.

References

1. A. Bilal, Nucl. Phys. B 422 (1994) 258
2. A. Bilal and J. -L. Gervais, Nucl. Phys. B 318 (1989) 579
3. J. -L. Gervais and M. V. Saveliev, Phys. Lett. B 286 (1992) 271
4. A. N. Leznov and M. V. Saveliev, Commun. Math. Phys. 89 (1983) 59
5. E. Witten, Phys. Rev. D 44 (1991) 314

Asymptotic Dynamics in QED₃

J. L. Boldo^{*}, B. M. Pimentel[†] and J. L. Tomazelli[‡]

Instituto de Física Teórica

Universidade Estadual Paulista

Rua Pamplona, 145, 01405-900 - São Paulo, SP - Brazil

In QED the method to deal with non-stationary processes as electron scattering by an external potential with the emission of a finite number of low-energy photons, using the S matrix expansion in powers of e^2 , leads to divergences in the probability amplitudes for such processes. These divergences in the low-frequency region are known as *infrared divergences*.

The pioneering program of taking into account the collective effect of low-energy photons was accomplished by Bloch and Nordsieck^[1] in the late 30's. They showed that the probability of emission of a finite number of low-energy photons is zero instead of infinite, as predicted by perturbation theory. On the other hand, when the transition probability is extended to all possible final states one gets a finite result.

One can attribute to the infrared divergences an incorrect choice of the asymptotic states which can be compared with the experimental data, besides the ill definition of the scattering operator, where the asymptotic dynamics is not taken into account. Murota^[2] was the first to incorporate the exact contribution of low-energy photons in the definition of the S operator. Later Kulish and Faddeev^[3] proposed in addition to the redefinition of this operator a modified space of asymptotic states. The Kulish-Faddeev model is based on early arguments, mainly those of Kibble^[4], where the Fock space representation of the Hilbert space, containing a finite number of low-energy photons, is replaced by a coherent-state representation for an infinite number of these photons, in such a way that matrix elements of the Dyson S operator between these states are finite and nonzero.

The investigation of the infrared problem in four-dimensional gauge theories can be extended to the tridimensional case, where a more careful analysis is required^[5]. This study can still be justified if we bear in mind that some physical phenomena, such as the quantum Hall effect and the high T_c superconductivity, can be better understood in the context of quantum electrodynamics in (2+1) dimensions.

Consider a quantum system described by a Hamiltonian H constituted by two terms

$$H = H_0 + V(t), \quad (1)$$

where H_0 is the free Hamiltonian and $V(t)$ is a short-range interaction potential

$$\lim_{t \rightarrow \pm\infty} V(t) = 0. \quad (2)$$

This implies that asymptotically the scattered particles are supposed to be free. Thus, since in scattering processes the particles are observed only in asymptotic regions ($t \rightarrow \pm\infty$), the asymptotic states are eigenstates of H_0 .

Using these ideas, one defines the S operator in perturbation theory assuming that the asymptotic dynamics is given by H_0 :

$$S = W_{out}^\dagger W_{in}. \quad (3)$$

^{*}Supported by CAPES

[†]Partially supported by CNPq

[‡]Supported by FAPESP

where W_{in} are the wave operators

$$W_{in} = \lim_{t \rightarrow +\infty} U(t, 0)^\dagger e^{-iH_0 t} \quad (4)$$

and

$$U(t, s) = e^{-iH(t-s)} \quad (5)$$

Using (5), one rewrites the S matrix as

$$S = \lim_{\substack{t \rightarrow +\infty \\ s \rightarrow -\infty}} e^{iH_0 t} U(t, s) e^{-iH_0 s} \quad (6)$$

From this definition the physical meaning of the S matrix is the following: an asymptotic initial state φ , taken at $t = 0$, is evolved to $s \rightarrow -\infty$ through free dynamics and then evolves from $-\infty$ to $t \rightarrow +\infty$ via $U(t, s)$ and, finally, from $t \rightarrow +\infty$ to $t = 0$ through free dynamics. The transition probability from this state to another final asymptotic state ψ is given by

$$|\langle \psi | S | \varphi \rangle|^2 \quad (7)$$

where the asymptotic states belong to the Fock space.

Solving the equation of motion for the time evolution operator, the S matrix can be rewritten as a time-ordered product

$$S = T \exp \left\{ -i \int_{-\infty}^{+\infty} V^I(t) dt \right\} \quad (8)$$

where $V^I(t)$ is the potential in the interaction picture. If the interaction potential vanishes in remote regions, such that

$$\int_{-\infty}^{+\infty} ds \|V(s)\| < \infty \quad (9)$$

then the Dyson series for the S operator (8) is absolutely convergent. Thus, the S operator is unitary in the Fock space, provided the particles have free dynamics in asymptotic regions.

The above method is not suitable to describing scattering processes when we consider long-range potentials such as the Coulomb potential. In this case, even at far regions this potential cannot be neglected.

In order to illustrate the method employed in the construction of the asymptotic operator $U_{as}(t)$ let us consider the scattering of a charged particle by a Coulomb potential in two dimensions. The Hamiltonian of the system has the following form:

$$H = \frac{\bar{p}^2}{2m} + g \ln r = H_0 + V \quad (10)$$

where m is the mass of the scattered particle and g is the product of the charges of the particle and the scattering center.

First of all one constructs the potential shape in the asymptotic region in the interaction picture and then one obtains the wave packet which will represent the scattered particle in this region. For this purpose one considers the observables \bar{x} and \bar{p} as the position and momentum operators in the interaction picture. In this representation these operators satisfy the following equations of motion:

$$\frac{dO_I}{dt} = \frac{1}{i} [O_I, H_0] \quad (11)$$

Using the Hamiltonian (10) and the above equation, we see that the momentum of the scattered particle is a constant of motion:

$$\frac{d\bar{p}}{dt} = \frac{1}{i} [\bar{p}, H_0] = 0 \quad (12)$$

Similarly, the equation of motion for the coordinates

$$\frac{d\bar{x}}{dt} = \frac{1}{i} [\bar{x}, H_0] = \frac{\bar{p}}{m} \quad (13)$$

whose solution

$$\bar{x}(t) = \bar{x} + \frac{\bar{p}}{m}t, \quad (14)$$

describes the time evolution of the coordinate operator of the scattered particle is identical to the classical trajectory of a particle in uniform rectilinear motion. From these results one can obtain the shape of the interaction potential at large distances, assuming that in this region the particles behave as classical particles with well defined trajectories. Thus, for $|t| \rightarrow \infty$

$$V(t) = g \ln \left(\frac{|\bar{p}|}{m}t \right). \quad (15)$$

This potential, which describes the interaction in the asymptotic region $|t| \rightarrow \infty$, is not absolutely convergent and its contribution to the asymptotic dynamics cannot be underestimated. In other words, the asymptotic dynamics is not governed by H_0 but by the operator

$$H_{as}(t) = H_0 + V_{as}(t) = H_0 + g \ln \left(\frac{|\bar{p}|}{m}t \right). \quad (16)$$

With this Hamiltonian describing the asymptotic dynamics and taking into account that $V_{as}(t)$ in the interaction picture is the same as in the Schrödinger picture, since

$$[V_{as}(t), H_0] = 0. \quad (17)$$

the wave function which describes the behavior of the particle in this region is obtained by solving the Schrödinger equation for H_{as}

$$i \frac{d}{dt} |\alpha, t\rangle = H_{as}(t) |\alpha, t\rangle. \quad (18)$$

where $|\alpha, t\rangle$ is the physical state of the scattered particle. In the momentum representation the above equation becomes

$$i \frac{d}{dt} \Psi(\bar{p}, t) = \left[\frac{\bar{p}^2}{2m} + g \ln \left(\frac{|\bar{p}|}{m}t \right) \right] \Psi(\bar{p}, t). \quad (19)$$

whose solution is

$$\begin{aligned} \Psi(\bar{x}, t) &= \frac{1}{2\pi} \int d\bar{p} \Psi(\bar{p}, t) e^{i\bar{p} \cdot \bar{x}} \\ &= \frac{1}{2\pi} \int d\bar{p} e^{i\bar{p} \cdot \bar{x}} c(\bar{p}) \\ &\quad \times \exp \left\{ -i \frac{\bar{p}^2}{2m} t - ig \left[t \ln \left(\frac{|\bar{p}|}{m}t - 1 \right) - t_0 \ln \left(\frac{|\bar{p}|}{m}t_0 - 1 \right) \right] \right\}. \end{aligned} \quad (20)$$

The choice of this solution is due to certain initial conditions for equation (19). These are determined by considering that the time variation of the coordinate and momentum distributions for the particle represented by the wave packet (20) for $|t| \rightarrow \infty$ must be governed by the classical dynamics.

The wave packet (20) can be written as

$$\begin{aligned} \Psi(t) &= U_{as}(t) \Psi \\ &= e^{-iH_0 t} \exp \left\{ -igt \left[t \ln \left(\frac{|\bar{p}|}{m}t - 1 \right) - t_0 \ln \left(\frac{|\bar{p}|}{m}t_0 - 1 \right) \right] \right\} \Psi. \end{aligned} \quad (21)$$

The previous example shows that the choice of the Hamiltonian which describes the asymptotic dynamics depends on the physical origin of the problem, in contrast with the usual definitions in the formal theory of scattering, where H_0 is taken as the asymptotic operator in the wave operators.

We then redefine the wave operators in the following way:

$$W_{out}^{in} = \lim_{t \rightarrow \mp \infty} e^{-iHt} U_{as}(t) \quad (22)$$

In (2+1) dimensions, the potential which describes the interaction between electrons and positrons with the electromagnetic field in the asymptotic region is given by

$$\begin{aligned} V_{as}(t) &= \frac{1}{(2\pi)} \int d\bar{k} \int d\bar{p} \frac{1}{\sqrt{2\omega}} \frac{p^\mu}{p^0} \rho(\bar{p}) \left[a_\mu(\bar{k}) e^{-i\frac{\bar{k}\cdot\bar{p}}{p^0}t} + a_\mu^\dagger(\bar{k}) e^{i\frac{\bar{k}\cdot\bar{p}}{p^0}t} \right] \\ &= \frac{1}{(2\pi)} \int \frac{d\bar{k}}{\sqrt{2\omega_k}} j_{as}^\mu(\bar{k}, t) \left[a_\mu(\bar{k}) e^{-i\omega t} + a_\mu^\dagger(-\bar{k}) e^{i\omega t} \right], \end{aligned} \quad (23)$$

where

$$j_{as}^\mu(\bar{k}, t) = \int p^\mu e^{i\frac{\bar{k}\cdot\bar{p}}{p^0}t} \rho(\bar{p}) \frac{d\bar{p}}{p^0} \quad (24)$$

is an operator that has the shape of a current distribution of a particle with charge density $\rho(\bar{p})$ and uniform velocity $\frac{\bar{p}}{p^0}$. In fact, the eigenvalues of the operator (24), acting in a space of charged particles, are classical current densities due to the motion of these particles, showing that, asymptotically, the scattered particles behave as classical particles.

As in the non-relativistic case, the Hamiltonian that describes the asymptotic dynamics is given by

$$H_{as} = H_0 + V_{as}(t), \quad (25)$$

where H_0 is the free Hamiltonian. We can obtain $U_{as}(t)$, by solving the Schrödinger equation for the time evolution operator

$$i \frac{d}{dt} U(t) = H(t) U(t), \quad (26)$$

where H is the Hamiltonian of the system. In our problem $H = H_{as}$ and, therefore, the above differential equation must be satisfied by the operator $U_{as}(t)$. In analogy to the non-relativistic result, we look for solutions of the above equation of the following type:

$$U_{as}(t) = e^{-iH_0 t} Z(t), \quad (27)$$

Substituting this operator in equation (26), we obtain the following equation of motion for $Z(t)$

$$i \frac{d}{dt} Z(t) = V_{as}^I(t) Z(t), \quad (28)$$

where $V_{as}^I(t)$ is the asymptotic potential operator in the interaction picture, namely

$$V_{as}^I(t) = e^{iH_0 t} V_{as}(t) e^{-iH_0 t}. \quad (29)$$

The solution of the above equation is the time-ordered product

$$Z(t) = T \exp \left\{ -i \int^t V_{as}^I(\tau) d\tau \right\}, \quad (30)$$

whose solution can be simplified if we note that the commutator of potentials at different times is a c-number:

$$[V_{as}^I(t_1), V_{as}^I(t_2)] = \text{c-number} \quad (31)$$

and, consequently,

$$[V_{as}^I(t), [V_{as}^I(t_1), V_{as}^I(t_2)]] = 0, \quad \forall t, t_1, t_2. \quad (32)$$

Then, the solution for $Z(t)$, with time ordering, can be rewritten as an ordinary product

$$\begin{aligned} Z(t) &= \exp \left\{ -i \int^t V_{as}^I(\tau) d\tau \right\} \exp \left\{ -\frac{1}{2} \int_{t_0}^t d\tau \int_{t_0}^\tau ds [V_{as}^I(\tau), V_{as}^I(s)] \right\} \\ &= \exp \{R(t)\} \exp \{i\phi(t)\}. \end{aligned} \quad (33)$$

where

$$R(t) = -i \int_{t_0}^t V_{as}^I(\tau) d\tau \quad (34)$$

and

$$\phi(t) = -\frac{1}{2i} \int_{t_0}^t d\tau \int_{t_0}^{\tau} ds [V_{as}^I(\tau) \cdot V_{as}^I(s)] \quad (35)$$

From this result we see that the asymptotic operator consists of two factors that commute. The first involves photon operators. The second is a phase factor which can be written as

$$\phi(t) = \frac{1}{4\pi} \int d\bar{q} \int d\bar{p} \frac{p \cdot q}{p^0 q^0} \rho(\bar{p}) \rho(\bar{q}) t \left[1 - \ln \left(2 \left| \frac{\bar{p}}{p_0} - \frac{\bar{q}}{q_0} \right| t \right) \right] \quad (36)$$

showing that this is a relativistic generalization of the above mentioned Coulomb phase. The eigenvalue of this operator acting in a space of charged particles gives the Coulomb interaction among all the particles of the system.

With $Z(t)$ defined in (33), the asymptotic operator is rewritten as

$$U_{as}(t) = e^{-iH_0 t} e^{R(t)} e^{i\phi(t)} \quad (37)$$

and, following the non-relativistic generalization, the operator S is expressed as

$$S = \lim_{\substack{t \rightarrow +\infty \\ t' \rightarrow -\infty}} U_{as}^\dagger(t) e^{-iH(t-s)} U_{as}(s) \quad (38)$$

This definition differs from the Dyson S matrix, given in (4), by the substitution

$$e^{-iH_0 t} = U_{as}(t) \quad (39)$$

showing that the infinite range of the Coulomb potential destroys the behavior of free dynamics in asymptotic regions, in contrast with the Dyson S matrix definition.

The new definition of the S matrix, taking into account the asymptotic dynamics, leads also to the conclusion that the space of asymptotic states consists of coherent states instead of those belonging to the Fock space.

References

- [1] F. Bloch and A. Nordsieck, Phys. Rev. 52, 54, (1937);
- [2] T. Murota, Prog. Theor. Phys. 24, 1109, (1960);
- [3] P. Kulish and L. Faddeev, Teor. Mat. Fiz. 4, 153 (1970) [Theor. Math. Phys. 4, 745 (1970)];
- [4] T. W. B. Kibble, Phys. Rev. 173, 1527; 174, 1882; 175, 1624 (1968);
- [5] B. M. Pimentel and J. L. Tomazelli, J. Phys G. 20, 845 (1994).

Explicit Demonstration of How the Zeta Function Method Removes the Divergences

José Alexandre Nogueira

*Departamento de Física, Centro de Ciências Exatas,
Universidade Federal do Espírito Santo,
29.060-900 - Vitória-ES - Brasil.
E-mail: nogueira@cce.ufes.br*

Adolfo Maia Jr.

*Instituto de Matemática, Universidade Estadual de Campinas,
13.081-970 - Campinas-SP, Brasil
E-mail: maia@ime.unicamp.br
Department of Physics, Brown University,
02912 Providence-RI, USA*

1 Introduction

High-energy physics was the first to perceive the necessity for a Relativistic Quantum Field Theory, and later other speciality physics found a powerful tool in it. Undoubtedly the Quantum Field Theory has obtained its best success in the Quantum Electrodynamics (QED). All Quantum Field Theory is fundamentally of perturbative aspect. So, the quantities with the greatest physics interest, the Green Functions, are constructed by means of perturbative series. However, in all its perturbative aspects it has heavy divergence problems. The treatment of these infinities continues to be one of the most challenging problems in Quantum Field Theory. The mathematical nature of the problem is clear. Divergences occur in perturbative computations because two distributions can not be multiplied at the same point. Several methods have been proposed in order to eliminate this problem. However, only in Quantum Electrodynamics has it been possible to eliminate these infinities consistently and in a physically meaningful manner by absorbing them into the bare parameters of the theory.

A quantity of considerable physical importance is the vacuum energy density which is associated with interesting physics effects, such as, Lamb Shift and Casimir Effect, which occur because of vacuum fluctuation. Nevertheless, there are several variations on the concept of vacuum energy in common circulation, among them the minimum of the effective potential obtained from the approach of functional methods from Quantum Field Theory is largely used. Effective potential principal application is associated with Spontaneous Symmetry Breaking. It is obtained from a nonperturbative method as a series in loop (\hbar). Since in the classical limit, which is the tree approximation, the effective potential becomes the same as the classical potential, therefore it is the classical potential plus the quantum corrections. It also suffers from the same divergences problems.

The usual procedure in order to deal with those divergences has been to employ a regularization method (Dimensional, Cut-off, etc) so as to isolate the divergences and to become the finite theory making use of a regulator and afterwards using a renormalization prescription, subtraction of the poles or addition of counter-terms, to eliminate the isolated divergences and to restore the theory with the elimination of the regulator. Since the subtraction of the poles or addition of infinite counter-terms, although well-founded in flat spaces, become dubious in curved spaces. The Zeta Function Method for the minimum of the effective potential gives only finite amounts, as recommended. However, it is obvious that implicitly in the Zeta Function Method there must take place cancelling of the divergences.

The paper is organized as follows. In Section 2 we explicitly show the cancellation of the divergences in the Zeta Function Method. In Sections 3 and 4 we point out that terms from divergent part of the sum over zero-point energy and scaling parameter or normalization constant, μ , respectively, although they are present in the renormalized minimum of the effective potential, they are not present in the observed energy. Indeed, they are not observed. This takes place because the energy is a relative quantity and it is not an absolute one and therefore differences of energy can only be observed.

2 Cancellation of the divergences

In the approach of the functional methods from Quantum Field Theory, the vacuum energy density can be found by computing the minimum of the effective potential [1-7]. The energy density found of that manner is a loop expansion (or equivalently in powers of \hbar), that is, its classical amount plus quantum correction.

Let $\phi(x)$ be a single real scalar field in a Minkowski space-time, subject to the potential $V(\phi)$. The minimum effective potential to the first order in the loop expansion (or equivalently in powers of \hbar) is given by

$$V_{eff}(\bar{\phi}) = V_{cl}(\bar{\phi}) + \frac{1}{2} \frac{\hbar}{\Omega} \ln \det \left[\frac{\delta^2 S[\bar{\phi}]}{\delta\phi(x)\delta\phi(y)} \right] = V_{cl}(\bar{\phi}) + V_{eff}^{(1)}(\bar{\phi}), \tag{1}$$

where $\bar{\phi} = \langle \phi \rangle$ is the classical field, $S[\phi]$ is the classical action, $\Omega = VT$ is the volume of the background space-time manifold and in the classical potential $V_{cl}(\phi)$ is included mass and self-interactions terms.

Making usual analytic continuation to the Euclidian space-time [2,4], the classical action can be written as

$$S[\phi] = \int d^4x \left[\frac{1}{2} \partial_\mu \phi \partial_\mu \phi + V_{cl}(\phi) \right], \tag{2}$$

where an euclidian summation convention is understood for repeated indexes. From eq.(2) we get the matrix $m(x, y)$ of the quadratic variation of the action $S[\phi]$

$$m(x, y) \equiv \frac{\delta^2 S[\phi]}{\delta\phi(x)\delta\phi(y)} = \delta^4(x - y) [-\delta^{\mu\nu} \partial_\mu \partial_\nu + V''_{cl}(\bar{\phi})]. \tag{3}$$

Now, m is a real, elliptical and self-adjoint operator (because of the Euclidean analytic continuation) and for these kind of operators we can define the so-called generalized zeta function. Let $\{\lambda_i\}$ the eigenvalues of the operator $m(x, y)$. The generalized zeta function associated to $M(x, y)$ ($m = M = \frac{m}{2\pi\mu^2}$) is defined by

$$\zeta_M(s) = \sum_i \left(\frac{\lambda_i}{2\pi\mu^2} \right)^{-s}, \tag{4}$$

where we have introduced a unknown scale parameter μ , with the dimensions of $(\text{length})^{-1}$ or mass in order to keep the zeta function dimensionless for all s . The introduction of the scale parameter or also normalization constant μ , can be best understood when we observe that a hidden division of the divergent integral there is in the proceeding of zeta function regularization, that is, a separation of the divergent and finite parts of the $V_{eff}(\phi)$ (in [4], pag. 208 and in [5], pag 88). It is well-known the relation

$$\ln \det M = - \frac{d\zeta_M(0)}{ds}, \tag{5}$$

Now, effective potential to the first order in the loop expansion can be written

$$V_{eff}^{(1)}(\phi) = - \frac{1}{2} \frac{\hbar}{\Omega} \frac{d\zeta_M(0)}{ds}. \tag{6}$$

We know that the evaluation of the effective potential given by eq.(6) is finite quantity, that is, without divergents terms. This is because the generalized zeta function as defined in the eq.(4) is regular at $s = 0$ [2, 8].

Or alternatively we could have used the relation

$$\ln \det[m(x, y)] = \text{tr} \ln[m(x, y)], \tag{7}$$

and got [4]

$$V_{eff}^{(1)} = \frac{\hbar}{2} \int \frac{d^4 k}{(2\pi)^4} \ln \left[k_E^4 + V''(\bar{\phi}) \right]. \quad (8)$$

where k_E is the quadri-moment and the lower suffixes E denotes euclidian space-time. As can be seen the integral of the eq.(8) is clearly divergent and so we need a regularization procedure in order to isolate the divergences. Of this we conclude that the evaluation of the effective potential using the zeta function, eq.(6), must hide the cancellation of the divergences in some manner.

In order to explicitly point out how the cancellation of the divergences occurs, we write the eigenvalues of the operator $m(x, y)$ as

$$\lambda_{i,\omega} = \omega^2 + h_i^2, \quad (9)$$

where h_i are eigenvalues of the hamiltonian operator H and ω is a continuous parameter labeling the temporal part of the eigenvalues of the operator $m(x, y)$.

Generalized zeta function associated to the operator $M(x, y)$, defined by eq.(4), can be written, using the eq.(9), as

$$\zeta_M(s) = \int_{-\infty}^{\infty} \frac{d\omega}{2\pi} \sum_i \left[\frac{\omega^2}{2\pi\mu^2} + \frac{h_i^2}{2\pi\mu^2} \right]^{-s} T. \quad (10)$$

Using the relation [9]

$$\int_{-\infty}^{\infty} \left(k^2 + A^2 \right)^{-s} d^m k = \frac{\pi^{\frac{m}{2}} \Gamma(s - m/2)}{\Gamma(s)} \left(A^2 \right)^{\frac{m}{2} - s}. \quad (11)$$

we can perform the above integral in $d\omega$ and get

$$\zeta_M(s) = \frac{1}{2\sqrt{\pi}} \frac{\Gamma[s - 1/2]}{\Gamma[s]} \zeta_H(s - 1/2) T, \quad (12)$$

where $\zeta_H(s - 1/2)$ is the generalized zeta function associated to the hamiltonian operator H and it defined by

$$\zeta_H(s - 1/2) = \sqrt{2\pi\mu^2} \sum_i \left(\frac{h_i^2}{2\pi\mu^2} \right)^{1/2 - s}. \quad (13)$$

It is well-known that $\zeta_M(s)$ is analytic at $s = 0$ [8,10-11]. So, $\zeta_M(0)$ is finite. Therefore either $\zeta_H(s - 1/2)$ is analytic at $s = 0$ and $\zeta_M(0)$ vanish or $\zeta_H(s - 1/2)$ is not analytic at $s = 0$ and in this case $\zeta_H(s - 1/2)$ must have the same structure of the simple poles as the gamma function $\Gamma(s)$, so that $\zeta_M(s)$ is analytic at $s = 0$. Then, after some regularization procedure, the generalized zeta function associated to the operator H can be written as

$$\zeta_H(s - 1/2) = F(s) + D(s)\Gamma(s), \quad (14)$$

where $F(s)$ and $D(s)$ are analytic function at $s = 0$. Note that s is the regulator used in specific regularization procedure.

The eq.(14) is evident when we employ the Laurent series expansion

$$\zeta_H(s - 1/2) = \frac{a_{-1}}{s} + a_0 + a_1 s + a_2 s^2 + \dots$$

$$\zeta_H(s - 1/2) = \frac{a_{-1} 2\sqrt{\pi}}{\Gamma(s - 1/2)} \Gamma(s) + a_0 + a_1 s + a_2 s^2 + \dots$$

where $D(s)$ and $F(s)$ are self-evident. Since $\zeta_H(s - 1/2)$ only has a simple pole the expansion is univocally determined.

Now one differentiates the eq.(12) and using eq.(14) we obtain

$$\zeta'_M(s) = \frac{\Gamma(s - 1/2)\Gamma}{2\sqrt{\pi}\Gamma(s)} \left[\psi(s - 1/2)F(s) + \psi(s - 1/2)D(s)\Gamma(s) - \psi(s)F(s) + \right.$$

$$-\psi(s)\Gamma(s)\mathbf{D}(s) + F'(s) + D'(s)\Gamma(s) + \mathbf{D}(s)\psi(s)\Gamma(s)\Big]. \tag{15}$$

Observe that the terms in boldface are divergents, yet they cancel them-selves. Finally we find

$$\zeta'_M(0) = -[F(0) + \psi(-1/2)D(0) + D'(0)]T. \tag{16}$$

The result above explicitly show how the divergences are cancelled in the evaluation of the effective potential using the eq.(6). So, it is clear that hidden in $\zeta'_M(0)$ there is a renomalized prescription, the analytic continuation. The method of evaluation of the effective potential using ζ'_M is completely equivalent to the renormalized prescription employed by Salam and Strathdee [12], as one can see using the relation

$$\frac{2\sqrt{\pi}\Gamma[s]}{\Gamma[s-1/2]} = -\frac{1}{s}, \tag{17}$$

in the eq.(12) and extracting the finite part one multiply by s and after compute the derivative with respect to s at $s = 0$ in order to get

$$\zeta_H^R = -\zeta'_M(0). \tag{18}$$

3 Terms from divergent part

Still we can observe that the last two terms of the right hand side of the eq.(16) depende on the divergent part from $\zeta_H(s-1/2)$, as one can see from eq.(14). Therefore they must not be observed. In order to prove this affirmation we recall that differences of energies are only observed. Another concept of vacuum energy in common circulation and most intuitive than the minimum of the effective potential is the sum over zero-point energy, defined as

$$\epsilon = \frac{\hbar T}{2\Omega} \sum_i h_i. \tag{19}$$

where h_i are the eigenvalues of the Hamiltoniana operator.

Using the generalized zeta function defined in the eq.(13) we write

$$\epsilon = \frac{\hbar T}{2\Omega} \lim_{s \rightarrow 0} [\zeta_H(s-1/2)]. \tag{20}$$

Now, let ϵ^0 be the vacuum energy density in the free space furnished by

$$\epsilon^0 = \frac{\hbar T}{2\Omega} \lim_{s \rightarrow 0} [\zeta_H^0(s-1/2)], \tag{21}$$

with

$$\zeta_H^0(s-1/2) = F^0(s) + D^0(s)\Gamma(s), \tag{22}$$

of form analogous to eq.(14).

The observed energy will be given by the difference between ϵ and ϵ^0 .

$$\delta\epsilon = \epsilon - \epsilon^0. \tag{23}$$

From eq.(s) (20), (21), (14), (22) and (23) we obtain

$$\delta\epsilon = \frac{\hbar T}{2\Omega} \left[F(0) - F^0(0) \right] + \frac{\hbar T}{2\Omega} \lim_{s \rightarrow 0} \left[\left(D(s) - D^0(s) \right) \Gamma(s) \right]. \tag{24}$$

It is well-known that the subtraction procedure (23) cancels the poles becoming finite $\delta\epsilon$. So, it is clear that

$$D(s) - D^0(s) = 0, \tag{25}$$

since $D(s)$ and D^0 are analytic at $s = 0$ by definition and so their subtraction to have a pole structure like $\Gamma(s)$ [11]. From eq.(25) we get

$$D(s) = D^0(s) \quad (26)$$

and

$$D'(s) = D^{0'}(s). \quad (27)$$

What finally yields us

$$\delta\epsilon = \frac{\hbar T}{2\Omega} \left[F(0) - F^0(0) \right]. \quad (28)$$

Now, in the same manner, using the eq.(22) in the eq.(16) we write

$$\zeta_M^{0'}(0) = -\{F^0(0) - \psi(-1/2)D^0(0) + D^{0'}(0)\}T. \quad (29)$$

with

$$V_{ef}^0 = -\frac{1}{2} \frac{\hbar}{\Omega} \frac{d\zeta_M^0(0)}{ds}, \quad (30)$$

being the effective potential in the free space.

Now, the observed energy is given by

$$\delta V_{ef} = V_{ef} - V_{ef}^0, \quad (31)$$

which results, using the eq.(s) (5), (16), (29) and (30),

$$\delta V_{ef} = \frac{1}{2} \frac{\hbar}{\Omega} \left[F(0) - F^0(0) + \psi(-1/2)D(0) - \psi(-1/2)D^0(0) + D'(0) - D^{0'}(0) \right]. \quad (32)$$

Taking into consideration the results (26) and (27) in (32)

$$\delta V_{ef} = \frac{1}{2} \frac{\hbar}{\Omega} [F(0) - F^0(0)]. \quad (33)$$

As we hoped it is exactly alike the result of the eq.(28). The eq.(32) explicitly points out the cancellation of the terms which come from $\zeta_M(s - 1/2)$ divergent part in the observed energy.

4 Scaling parameter μ

As we have already pointed out the evaluation of the effective potential using the derivative of the generalized zeta function associated to the operator of the quadratic variation of the action, eq.(6), involves regularization and renormalization procedures, eq.(18), of a implicit manner. We know the regularization procedure (isolation of the divergences) introduces a scale parameter or normalization constant, μ , with dimensions of mass. It has been introduced for us in order to keep the generalised zeta function dimensionless for all s , eq.(4). It is also well-known physics quantities must not depend on μ (in [1], pag. 329 and in [5], pag. 96, as for exemple). Now we shall show explicitly how the scaling parameter μ is cancelled in the observed energy.

In the definition (4) of the zeta function we have performed a scaling transformation of the operator m ,

$$M = \frac{m}{2\pi\mu^2}. \quad (34)$$

in order to keep the zeta function dimensionless. The eq.(5) can be written as [2, 8]

$$\ln \det[M(x, y)] = -\zeta_M'(0) = -\zeta_m'(0) - \zeta_m(0) \ln(2\pi\mu^2). \quad (35)$$

with $\zeta_m(s)$ defined as

$$\zeta_m(s) = \sum_i \lambda_i^{-s} \tag{36}$$

In agreement with the eq.(10) we write

$$\zeta_m(s) = \frac{1}{2\sqrt{\pi}} \frac{\Gamma[s-1/2]}{\Gamma[s]} \zeta_h(s-1/2)T, \tag{37}$$

with $\zeta_h(s-1/2)$ defined

$$\zeta_h(s-1/2) = \sum_i \left(h_i^2 \right)^{1/2-s} \tag{38}$$

Observing the eq.(12) and (37) we can see they are formally identical, therefore allowing the same anterior consideration about the poles structure of the function $\zeta_h(s-1/2)$ and in a agreement with the eq.(14) we write

$$\zeta_h(s-1/2) = f(s) + d(s)\Gamma(s). \tag{39}$$

Observe that $f(s)$ and $d(s)$ are independent of μ whereas $F(s)$ and $D(s)$ are dependent on μ . Using the eq.(39) in the eq.(37) we get

$$\zeta_m(0) = -d(0)T. \tag{40}$$

Now, substituing eq.(40) in (35) and after in (6) we obtain

$$V_{ef}^{(1)} = -\frac{1}{2} \frac{\hbar T}{\Omega} \zeta_m'(0) - \frac{1}{2} \frac{\hbar T}{\Omega} d(0) \ln(2\pi\mu^2). \tag{41}$$

Since $\zeta_m'(0)$ is independent of μ , it only stands by in the coefficient of the term $d(0)$ which comes from divergent part of $\zeta_h(s-1/2)$ and it must not be observed as we have already asserted.

From eq.(21) and (22) we can write

$$\epsilon = \frac{1}{2} \frac{\hbar T}{\Omega} \lim_{s \rightarrow 0} [\zeta_h(s-1/2)]. \tag{42}$$

and

$$\epsilon^0 = \frac{1}{2} \frac{\hbar T}{\Omega} \lim_{s \rightarrow 0} [\zeta_h^0(s-1/2)]. \tag{43}$$

with

$$\zeta_h^0(s-1/2) = f^0(s) + d^0(s)\Gamma(s). \tag{44}$$

From same foregoing consideration we find

$$d(s) = d^0(s). \tag{45}$$

The observed energy is given by eq.(31)

$$\delta V_{ef}^{(1)} = -\frac{1}{2} \frac{\hbar T}{\Omega} \left[\zeta_m'(0) - \zeta_m^0(0) \right] - \frac{1}{2} \frac{\hbar T}{\Omega} \left[d(0) - d^0(0) \right] \ln(2\pi\mu^2). \tag{46}$$

where

$$V_{ef}^{(1)} = -\frac{1}{2} \frac{\hbar T}{\Omega} \zeta_m^0(0) + \frac{1}{2} \frac{\hbar T}{\Omega} d^0(0) \ln(2\pi\mu^2). \tag{47}$$

From eq.(45) we can see that the last term in the eq.(49) vanish, so one cancelling the μ dependence.

The μ dependence in the renormalization energy becomes clear when we substitute the eq.(44) in the eq.(43) and we employ the renormalization prescription used by Salam and Strathdee, obtaining

$$\epsilon^0 = \frac{1}{2} \frac{\hbar}{V} \left[f^0(0) + d^0(0) + d^0(0) \ln(2\pi\mu^2) \right], \tag{48}$$

which is the Coleman-Weinberg potential when

$$V(\phi) = \frac{1}{2} M^2 \phi^2 + \frac{1}{4!} \lambda \phi^4. \tag{49}$$

5 Conclusion

The regularization procedure of the minimum of the effective potential using zeta function method provides us finite result without the necessity of subtraction of any pole or addition of infinite counter-terms.

This is owing to zeta function is regular at $s = 0$. In this manner dubious proceedings used in order to obtain of a finite result for the minimum of the effective potential are avoided, since as we explicitly showed the divergences are implicitly cancelled by zeta function method.

It is important to point out finite terms come from divergent part of the sum over zero-point energy must not be observed even if they be present in the renormalized potential. Finally we showed that the scaling parameter or renormalized constant μ must not be observed, too. In other words, observed energy must not depend on μ . This occurs because the energy is a relative quantity and it is not absolute one. In order to best understand this we note that μ realizes a similar role as the referencial point (r_0) for which one determine an arbitrary value for classical potential, as it is well elucidated in [13]. One become clear that the observed result must not depend on μ as the referencial point does not depend on μ .

It is also important point out in spite of μ to be present in the renormalized effective potential, the effective potential does not depend on μ in sense that it is invariant under a scale transformation ($\mu \rightarrow \mu' = \lambda\mu$) because one is absorbed by others parameter of theory.

References

- [1] L. H. Ryder, Quantum Field Theory, Cambridge University Press, Cambridge (1985).
- [2] P. Ramond, FIELD THEORY A Modern Primer. The Benjamin/Cummings Publishing Company, Inc., Massachusetts (1981).
- [3] R. J. Rivers, Path Integral Methods in Quantum Field Theory. Cambridge University Press, Cambridge (1987).
- [4] K. Huang, Quarks Leptons & Gauge Fields. World Scientific Publishing Company, Singapore (1982).
- [5] J. V. Narlikar and T. Padmanabhan, Gravity, Gauge Theories and Quantum Cosmology. D. Reidel Publishing Company, Dordrecht (1986).
- [6] J. Iliopoulos, C. Itzykson and A. Martin, Rev. Mod. Phys., **47** (1975) 165.
- [7] R. Jackiw, Phys. Rev., **D 9**(6), (1974) 1686.
- [8] S. Hawking, Commun. Math. Phys., **55** (1977) 133.
- [9] J. A. Nogueira and A. Maia Jr., Phys. Lett., **B358** (1995) 56.
- [10] N. D. Birrell and P. C. W. Davies, Quantum Fields in Curved Space. Cambridge University Press, Cambridge. (1982).
- [11] S. K. Blau, M. Visser and A. Wipf, Nucl. Phys., **B310**, (1988) 163.
- [12] A. Salam and J. Strathdee, Nucl. Phys. **B90**, (1975) 203.
- [13] M. Hans, Am. J. Phys., **51**(8), (1983) 694.

Estudo das Ressonâncias em um Cilindro com Incidência Oblíqua

J. P. R. F. de Mendonça - UFJF e L. G. Guimarães - UFRJ

1 Introdução

O estudo do espalhamento de campos eletromagnéticos por certos obstáculos permite estudar as propriedades de campos evanescentes e assintóticos. Neste trabalho estudamos o espalhamento de ondas planas por microcilindros. O nosso interesse é estudar o papel do ângulo de incidência na localização e larguras das ressonâncias. Estudamos também a propagação do campo elétrico ao longo do microcilindro. Wait [1] foi o primeiro a resolver o problema do espalhamento de ondas planas por cilindros dielétricos. Com o intuito de ganharmos uma visão física sobre as ressonâncias, utilizamos a conhecida analogia óptica-mecânica entre o índice de refração e potencial. Assim obtemos uma equação idêntica a equação de Schrödinger independente do tempo onde o potencial efetivo tem a forma de um poço cercado por uma barreira de potencial que suporta a existência de "estados quase ligados do campo". Dividiremos este assunto em 4 seções. Na seção 1 nós obtemos os potenciais de Debye para o caso de um cilindro dielétrico. Em seguida encontramos uma equação transcendental, a qual contém toda a informações sobre as posições e larguras das ressonâncias. Na seção 2 desenvolvemos uma teoria semi-clássica para os modos ressonantes. Esta teoria permite dar uma interpretação física dos modos ressonantes e características do espalhamento ressonante. Na seção 3 discutimos a dependência da posição e largura de ressonâncias com o ângulo de incidência. Finalmente na seção 4 fazemos um resumo dos principais resultados do nosso trabalho.

2 Os Potenciais de Debye e a Equação Transcendental.

Considere um cilindro cujo o eixo de simetria está na direção z e o vetor de onda \mathbf{k} incidente faz um ângulo ϕ com o eixo do cilindro. A polarização da onda espalhada é relacionada com a polarização da onda incidente. Quando o campo elétrico incidente está contido no plano de incidência (plano que contém \mathbf{k}_{inc} , e o eixo- z) teremos o chamado caso I e na outra situação (campo magnético incidente está contido no plano de incidência) o caso II. Trabalhando em coordenadas cilíndricas (ρ, θ, z) tendo o cilindro raio a , índice de refração é N e admitindo cilindros não magnéticos ($\mu = 1$ em todo o espaço) e para um vetor de onda incidente $\mathbf{k}_{inc} = k(\cos \phi \mathbf{x} + \sin \phi \mathbf{z})$ temos que, os potenciais de Debye (soluções escalares da equação de onda) são dados por:

$$\begin{Bmatrix} \Pi \\ \Upsilon \end{Bmatrix} = \exp[i(\omega t + n\theta - hz)] \begin{Bmatrix} f(\rho) \\ g(\rho) \end{Bmatrix} = F_n \begin{Bmatrix} f(\rho) \\ g(\rho) \end{Bmatrix} \quad (1)$$

com $h = k_0 \sin \phi$, e as funções $f(\rho)$ e $g(\rho)$ satisfazem a equação diferencial de Bessel radial.

$$\frac{d^2 f}{d\rho^2} + \left(\frac{1}{\rho} \frac{df}{d\rho} \right) + \left(k^2 - \frac{n^2}{\rho^2} \right) f = 0 \quad (2)$$

Utilizando os potenciais de Debye que descrevem o comportamento assintótico e no interior do cilindro corretos temos respectivamente que:

i) Para o meio exterior (meio I com índice de refração $N = N_1 = 1$)

$$\begin{Bmatrix} \Pi_n \\ \Upsilon_n \end{Bmatrix} = F_n J_n(\bar{k}_1 \rho) + F_n H_n(\bar{k}_1 \rho) \begin{Bmatrix} a_n \\ b_n \end{Bmatrix}$$

ii) Para o meio interior (meio 2 com índice de refração $N_2 = N$)

$$\begin{Bmatrix} \Pi_n \\ \Upsilon_n \end{Bmatrix} = F_n J_n(\bar{k}_2 \rho) \begin{Bmatrix} d_n \\ c_n \end{Bmatrix} \quad (3)$$

onde $\bar{k}_j^2 = k_j^2 - h^2$, $k_j = N_j k_0$, $H_n(x)$, $J_n(x)$ são respectivamente as funções de Hankel e Bessel cilíndricas e a_n , b_n , c_n e d_n são os coeficientes a serem determinados usando-se as condições de contorno na interface, isto é, conservação das componentes tangenciais dos campos **E** e **H** na interface ($\rho = a$). Fazendo isto obtém-se um sistema de quatro equações lineares que nos permitem obter os coeficientes da expansão acima [1]. Ressonâncias estão relacionadas com os polos desses coeficientes que são os zeros da equação a seguir:

$$\Delta \equiv X_\lambda(\beta)Z_\lambda(\beta) - \left[\lambda \sin \phi \left(\frac{1}{\nu^2} - \frac{1}{u^2} \right) \right]^2 \quad (4)$$

onde definimos os parâmetros de tamanho $\beta = ku$, $\nu = \beta \cos \phi$ enquanto que as funções $X_\lambda(\beta)$ e $Z_\lambda(\beta)$ são dadas por,

$$X_\lambda(\beta) = \frac{\ln' H_\lambda^{(1)}(\nu)}{\nu} - \frac{\ln' J_\lambda(u)}{u} \quad (5)$$

$$Z_\lambda(\beta) = \frac{\ln' H_\lambda^{(1)}(\nu)}{\nu} - N^2 \frac{\ln' J_\lambda(u)}{u} \quad (6)$$

aqui \ln' representa a derivada logarítmica com respeito ao argumento de J_λ e H_λ . Para um dado momento angular $\lambda^2 = (n - 1/2)(n + 1/2)$ e ângulo de incidência ϕ os zeros da equação transcendental acima são complexos e podem ser escritos como $\tilde{\beta} = \beta - iw$ onde β é a posição da ressonância e w a sua largura.

3 Teoria Semi-Clássica para as Ressonâncias

A equação 2 pode ser re-escrita como

$$-\frac{d^2 G}{d\rho^2} + U_{ef} G = k_0^2 G \quad (7)$$

onde $U_{ef}(\rho, \phi) = \frac{\lambda^2}{\rho^2} - k_0^2(\tilde{N}^2 - 1)$, $\tilde{N}^2 = N^2 - \sin^2 \phi$ e $\lambda = (n - 1/2)(n + 1/2)$. Note que 7 é equivalente a equação de Schrödinger independente do tempo sujeita a um potencial efetivo U_{ef} e "energia" k_0^2 .

Assumindo que não há absorção ($\text{Im}(N)=0$) e $\text{Re}\{N\} > 1$ o potencial tem a forma de um poço cercado por uma barreira de potencial, o que suporta a existência de estados quase ligados do campo. Com esta escolha para o índice de refração os campos convergem para o interior da superfície cilíndrica, podendo gerar causticas [2]. Note que para uma dada energia $k_0^2 > 0$ os estados ressonantes envolvem um problema de espalhamento com 3 pontos de retorno clássicos, um interno ρ_1 e os outros dois sendo um o próprio raio do cilindro a enquanto o outro mais externo é denotado por ρ_2 de tal forma que $\rho_1 < a < \rho_2$.

As ressonâncias óticas estão relacionadas com alto valor de momento angular λ e neste caso a solução da equação 4 e não trivial, levando um trabalho computacional tremendamente instável. Assim, para resolvermos numericamente a equação transcendental (eq. 4) precisamos de um bom input inicial. O cálculo deste input pode ser dado através da aproximação WKB, onde vamos admitir que $\beta \gg w$. Analisando a equação 4 vemos que o termo dominante é $X_\lambda(\beta)Z_\lambda(\beta)$, ou seja,

$$\ln' H_\lambda^{(1)}(\nu) = \frac{\nu}{u} C_j \ln' J_\lambda(u) \quad (8)$$

onde

$$C_j = \begin{cases} 1 & j = 0 \quad \text{Casol} \\ N^2 & j = 1 \quad \text{CasolI} \end{cases}$$

Dentro da aproximação de mais baixa ordem WKB a equação acima pode ser escrita com:

$$\frac{\sqrt{\lambda^2 - \nu^2}}{\nu} (1 - ic^{2\Psi}) = \frac{\sqrt{u^2 - \lambda^2}}{u} \tan(\varphi - \pi/4) \left(\frac{\nu}{u}\right) C_j$$

Onde $\varphi = \sqrt{u^2 - \lambda^2} - \lambda \cos^{-1} \left(\frac{\lambda}{u}\right)$ é a fase de Bohr-Sommerfeld enquanto que $\exp\{2\Psi\}$ é a transmissividade da barreira. As soluções da equação acima são complexas, a parte real dessas soluções nos fornece a posição β de uma dada ressonância enquanto que a parte imaginária nos fornece a sua largura w . Usando os resultados WKB como input iniciais podemos numericamente os zeros da equação transcendental $\Delta = 0$ e obter os resultados exatos (numéricos) para a posição e largura de ressonâncias. Com estes valores podemos estudar o comportamento ressonante dos campos espalhado e interno.

4 O Papel do Ângulo de Incidência

Nossos resultados mostram uma extrema sensibilidade a variações do ângulo de incidência tanto para a posição como para a largura da ressonância. O valor da posição da ressonância cresce quando ϕ cresce revelando que a largura efetiva do poço de potencial diminui quando ϕ cresce. Por outro lado, a largura diminui quando ϕ cresce, mostrando que a espessura da barreira a ser tunelada cresce quando ϕ cresce. Observamos também que a eficiência em gerar modos ressonantes é limitada por um ângulo crítico $\phi_c = \sin^{-1} \sqrt{(N^4 - N^2 + 1)^{1/2} - (N^2 - 1)}$ a partir do qual basicamente a energia se propaga através de ondas de superfície.

5 Resumo

Alguns pontos chaves devem ser destacados neste trabalho a saber, é possível controlar o tempo de meia vida do photon dentro de uma fibra variando-se o ângulo de incidência ϕ uma vez que a largura da ressonância é uma função decrescente deste ângulo, além disso existe um ângulo crítico ϕ_c que delimita a propagação entre modos guiados e ondas de superfície.

References

- [1] James R. Wait, *Canadian J. of Physics* **33** 189 (1955)
- [2] L.G. Guimarães, *Opt. Comm.* **103** 339 (1994)

Acoplamento Interplanos e Propriedades Magnéticas em Supercondutor a Alta T_c

L. C. Malacarne, R. S. Mendes and P. R. Veroneze

Dep. de Física - Fundação Univ. Estadual de Maringá

Av. Colombo 5790, 87020-900 - Pr - Brasil

Desde a descoberta dos supercondutores a alta temperatura, tem havido um grande interesse no entendimento do mecanismo que explique os altos valores de T_c . Vários modelos foram propostos para descrever este mecanismo, entre eles gostaríamos de ressaltar aqueles que levam em consideração planos supercondutores interagentes.

De especial interesse são aquelas interações que privilegiam o tunelamento interplanos de pares, pois isto favorece o aumento de T_c [1, 2, 3], quando comparado com o modelo BCS [4].

Por exemplo, nas referências [1, 2] os autores enfocam, essencialmente, interações independentes do momento transferido, já em [3] o comportamento anisotrópico é explorado.

Neste trabalho vamos verificar se, além do aumento de T_c , uma interação, que privilegia o tunelamento de pares, reproduz algumas propriedades características dos supercondutores na presença de um campo magnético. Para tal, vamos usar uma Hamiltoniana, suficientemente simples, que mantenha os aspectos qualitativos principais da interação entre planos via pares.

Além disso, empregaremos o método de integração funcional [5] para obter as equações de Landau-Ginsburg [6] (LG) na presença de campo magnético. A partir dessas equações, verificamos que o modelo empregado apresenta propriedades esperadas para um supercondutor. Por exemplo, quantização do fluxo magnético, efeito Meissner e possibilidade da existência de vórtice e rede de vórtices.

O modelo que estudaremos neste trabalho, para o caso de dois campos, tem sua dinâmica regida pela Hamiltoniana

$$\mathcal{H} = \mathcal{H}_1 + \mathcal{H}_2 + \mathcal{H}_I, \quad (1)$$

onde

$$\mathcal{H}_j = \int dV \left\{ \sum_{s=11} \psi_{sj}^\dagger \left[\frac{-1}{2m} (\vec{\nabla} - ie\vec{A})^2 - \mu_j \right] \psi_{sj} - g_j \psi_{1j}^\dagger \psi_{1j}^\dagger \psi_{1j} \psi_{1j} \right\}, \quad j = 1, 2$$

e

$$\mathcal{H}_I = - \int dV [g_3 \psi_{11}^\dagger \psi_{11}^\dagger \psi_{12} \psi_{12} + g_3^* \psi_{12}^\dagger \psi_{12}^\dagger \psi_{11} \psi_{11}]. \quad (2)$$

As partes \mathcal{H}_1 e \mathcal{H}_2 representam as Hamiltonianas para dois modelos BCS e o termo \mathcal{H}_I dita a interação entre eles. Os campos ψ_{sj} dizem respeito aos elétrons; \vec{A} dita a interação com o campo externo; μ_j são os potenciais químicos; g_1 , g_2 e g_3 são as constantes de acoplamento que regem as interações.

No caso da teoria BCS usual, um campo auxiliar é introduzido [5] representando os pares de Cooper do modelo. Neste trabalho, generalizamos este procedimento introduzindo mais de um campo auxiliar. A função de partição usando estes novos pares de Cooper generalizados é

$$\mathcal{Z}_1 = \int \prod_{s,j} \mathcal{D}\bar{\psi}_{s,j} \mathcal{D}\psi_{s,j} \mathcal{D}\sigma_j^\dagger \mathcal{D}\sigma_j \exp \left\{ - \int_0^\beta d\tau \int dV (\mathcal{L}_0 + \mathcal{L}_a + \mathcal{L}_b) \right\}, \quad (3)$$

onde

$$\mathcal{L}_0 = \sum_{s,j} \bar{\psi}_{s,j} \left[\frac{\partial}{\partial \tau} - \frac{1}{2m} (\vec{\nabla} - ie\vec{A})^2 - \mu_j \right] \psi_{s,j}, \quad \mathcal{L}_a = - \sum_{i,j} \bar{\psi}_{1i} \bar{\psi}_{1i} g_{ij} \psi_{1j} \psi_{1j}$$

$$e \quad \mathcal{L}_b = \sum_i (\sigma_i^* - \sum_j c_{ij}^* \bar{\psi}_{1j} \bar{\psi}_{1i}) (\sigma_i - \sum_l c_{il} \psi_{1l} \psi_{1i}). \quad (4)$$

Na expressão acima, as constantes de acoplamento g_{ij} são os elementos da matriz envolvendo as constantes de acoplamento ($g_{11} = g_1, g_{22} = g_2, g_{12} = g_3$ e $g_{21} = g_3^*$).

Os coeficientes c_{ij} são escolhidos de modo a eliminar os termos quárticos. Além disso, é conveniente definirmos novos campos auxiliares, $\chi_i = \sum_j c_{ij}^* \sigma_j$, que representam os novos pares de Cooper generalizado. Isto nos possibilita expressar a função de partição numa forma mais simplificada.

$$\mathcal{Z} = \int \prod_{i,j} \mathcal{D}\bar{\psi}_{i,j} \mathcal{D}\psi_{i,j} \mathcal{D}\chi_i^* \mathcal{D}\chi_i \exp \left\{ - \int_0^\beta d\tau \int dV (\mathcal{L}_0 + \mathcal{L}_I) \right\}. \quad (5)$$

com

$$\mathcal{L}_I = - \sum_i (\chi_i^* \psi_{1i} \psi_{1i} + \chi_i \bar{\psi}_{1i} \bar{\psi}_{1i}) + \sum_{i,j} \chi_i^* (U^+ g_D^{-1} U)_{ij} \chi_j. \quad (6)$$

U é a matriz unitária que diagonaliza g , e g_D é composta pelos autovalores de g , isto é, $g_D = U^+ g U$. Observe que a generalização destas expressões para o caso de N camadas é imediata, o que passaremos a considerar doravante. Na expressão (5) podemos efetuar as integrações nos campos $\bar{\psi}$ e ψ , resultando em

$$\mathcal{Z} = \int \prod_i \mathcal{D}\chi_i^* \mathcal{D}\chi_i \exp \left[- \sum_i \text{tr} \ln M_i + \sum_{i,j} \chi_i^* (U^+ g_D^{-1} U)_{ij} \chi_j \right]. \quad (7)$$

a menos de termos independentes de \bar{A} , χ_j^* e χ_j .

Onde a matriz M_j é dada por

$$M_j = \delta(\tau - \tau') \delta(\vec{x} - \vec{y}) \begin{pmatrix} [\frac{\partial}{\partial \tau} - \frac{1}{2m} (\vec{\nabla} - ie\bar{A})^2 - \mu_j] & -\chi_j \\ -\chi_j^* & -[-\frac{\partial}{\partial \tau} - \frac{1}{2m} (\vec{\nabla} + ie\bar{A})^2 - \mu_j] \end{pmatrix}$$

Para o $\text{tr} \ln M_i$ empregaremos a relação $\text{tr} \ln M_i = \ln M_0 - \sum_{n=1}^\infty \frac{1}{n} \text{tr} [M_0^{-1} (M_i - M_0)]^n$, onde M_0 é a matriz M_i com $\bar{A} = 0$ e $\chi_j^* = \chi_j = 0$.

Para obtermos as equações de Landau-Ginsburg, que descreve o comportamento da teoria perto da temperatura crítica, T_c , consideraremos somente os quatro primeiros termos da série em (7).

Primeiramente examinaremos o caso com $\bar{A} = 0$. Os termos com n ímpar são identicamente nulos, devido a estrutura matricial de $M_0^{-1} (M_i - M_0)$.

A contribuição para o termo com $n = 2$, usando a representação dos momentos, é igual a

$$- \sum_{i,w',k'} \chi_i^*(w', k') \Pi_i(w', k') \chi_i(w', k'), \quad (8)$$

onde após alguns cálculos podemos escrever

$$\Pi_i(0, k) \simeq -\rho_i(0) \ln \left(\frac{2\gamma\beta w_{D,i}}{\pi} \right) + \frac{\beta^2 \mu_i \rho_i(0)}{24\pi^2 m} \zeta(3, 1/2) k^2. \quad (9)$$

Com $\ln \gamma$, $w_{D,i}$, $\rho_i(0)$ e $\zeta(3, 1/2)$ representam a constante de Euler, energia de Debye, densidade de estados na superfície de Fermi e função zeta de Riemann, respectivamente.

O termo com $n = 4$ vem a ser

$$- \sum_{w',k'} \chi_i^*(w'_1, k'_1) \chi_i(w'_2, k'_2) \chi_i^*(w'_3, k'_3) \chi_i(w'_3 - w'_2 + w'_1, k'_3 - k'_2 + k'_1) \times \mathcal{T}_i(w'_1, k'_1, w'_2, k'_2, w'_3, k'_3), \quad (10)$$

onde

$$T_i \simeq \frac{\rho_i(0)\beta}{16\pi^2 V} \zeta(3, 1/2). \quad (11)$$

Finalmente, usando (7),(8),(9),(10) e (11) podemos escrever as equações de Landau-Ginsburg efetivas para o modelo

$$a_i \nabla^2 \chi_i + b_i' \chi_i + c_i (\chi_i^* \chi_i) \chi_i + \sum_j (U^+ g_D^{-1} U)_{ij} \chi_j = 0. \quad (12)$$

com as constantes a_i, b_i e c_i são dadas por

$$a_i = \frac{\beta^2 \mu_i \rho_i(0)}{24\pi^2 m} \zeta(3, 1/2), \quad b_i' = -\rho_i(0) \ln\left(\frac{2\gamma\beta w_{D_i}}{\pi}\right), \quad c_i = \frac{\rho_i(0)\beta^2}{8\pi^2} \zeta(3, 1/2).$$

Vamos analisar as equações de Landau-Ginsburg homogêneas com dois campos. Observemos primeiramente que, $g_{12} = g_{21} = 0$ reduz o modelo a duas teorias BCS desacopladas. Neste caso, o modelo tem uma simetria global $U(1) \times U(1)$ e daí duas temperaturas críticas de transição de fase de segunda ordem. Se $g_{12} = g_{21} \neq 0$, vemos de (12) que $\chi_1^* \chi_2 = \chi_1 \chi_2^*$, isto é, as fases de χ_1 e χ_2 são iguais a menos de um sinal. Este fato faz com que a simetria contínua do modelo seja reduzida de $U(1) \times U(1)$ para $U(1)$. Conseqüentemente, a quebra desta última simetria leva a existência de uma única temperatura crítica para a transição de fase de segunda ordem. De fato, se um dos parâmetros de ordem, χ_1 ou χ_2 , for nulo, as equações (12) implicam que o outro também será.

Quando os parâmetros correspondentes aos dois campos forem iguais, $b_1 = b_2 = b$ e $c_1 = c_2 = c$, as soluções das equações (12) que minimizam S são $\chi_1 = \chi_2 = \chi_0$ para $d < 0$ e $\chi_1 = -\chi_2 = \chi_0$ para $d > 0$, onde $\chi_0^2 = (-b + |d|)/c$. Estas soluções nos conduzem a temperatura crítica

$$T_c = \frac{2\gamma w_D}{\pi} \exp\left[-\frac{1}{\rho(0)} \left(\frac{g_1}{\det(g)} - \left|\frac{g_3}{\det(g)}\right|\right)\right]. \quad (13)$$

Passemos a considerar a variação espacial dos parâmetros de ordem χ_1 e χ_2 no caso de um supercondutor semi-infinito (contido na região $x > 0$). Para o caso parâmetros iguais ($b_1 = b_2 = b$ e $c_1 = c_2 = c$), as equações (12), com $\chi_1(x) = \chi_0 f_1(x)$ e $\chi_2(x) = \chi_0 f_2(x)$ ($-\chi_0 f_2(x)$) para $d < 0$ ($d > 0$) vem a ser

$$-a f_i'' + b f_i + (-b + |d|) f_i^3 - |d| f_i = 0, \quad i = 1, 2 \quad (14)$$

Considerando que longe de $x = 0$ χ_i deve tender para soluções homogêneas e para $x = 0$ χ_i é nulo, obtemos as condições de contorno $f_1(0) = f_2(0) = 0$ e $f_1(\infty) = f_2(\infty) = 1$ para as equações (14). A solução para este problema de contorno é $f_1(x) = f_2(x) = \tanh(x/\sqrt{2}\xi)$, onde $\xi = \sqrt{a/(-b + |d|)}$ é o comprimento de coerência.

Vemos que as soluções são as mesmas de uma teoria BCS, porém o comprimento de correlação é modificado pela presença da interação entre planos.

A energia livre de LG com $\vec{A} \neq 0$ é obtida introduzindo uma contribuição de energia magnética, $\frac{1}{8\pi} B^2$, e fazendo a substituição $\nabla \rightarrow \nabla - 2ie\vec{A}$, que pode ser verificada através de um cálculo direto.

Portanto, as correspondentes equações de LG são

$$\nabla \times \vec{B} = 4\pi \vec{j}, \quad (15)$$

$$-a_n (\nabla - 2ie\vec{A})^2 \chi_n + b_n \chi_n + c_n |\chi_n|^2 \chi_n + \sum_l (M^\dagger g_D^{-1} M)_{nl} \chi_l = 0, \quad (16)$$

onde

$$\vec{j} = -2ie \sum_n a_n (\chi_n^* \nabla \chi_n - \chi_n \nabla \chi_n^*) - 8e^2 \left(\sum_n a_n \chi_n^* \chi_n\right) \vec{A}. \quad (17)$$

O efeito Meissner é obtido diretamente de (15) e (17) ao empregarmos as soluções homogêneas para χ_n , $\nabla^2 B = \lambda^{-2} B$. No caso de dois campos fermiônicos com parâmetros iguais temos $\lambda^{-2} = 64\pi e^2 a(-b + |d|)/c$ para o comprimento de penetração.

A quantização do fluxo magnético, Φ , pode ser obtida a partir da equação (17), empregando uma condição de contorno conveniente e a unicidade de χ_n . Escolhendo um contorno onde $j = 0$, $B = 0$ e $|\chi_n|$ constante, obtemos

$$\Phi = \sum_j \Phi_{0j} n_j, \quad \Phi_{0j} = \frac{\pi}{c^2} \frac{a_j |\chi_j|^2}{\sum_n a_n |\chi_n|^2}, \quad (18)$$

onde $n_j = 0, 1, 2, 3, \dots$. Quando especializamos esta expressão para o caso de dois campos, a parâmetros iguais, recaímos na quantização usual do fluxo magnético, $\Phi = \Phi_0 n$.

Consideremos, agora, uma solução tipo vórtice para o caso de dois campos com parâmetros iguais. Usando o *ansatz*: $A_r = 0$, $A_\theta = A(r)$, $|\chi_1| = |\chi_2| = f(r)$, e para as correspondentes fases de χ_1 e χ_2 , $\varphi_1 = \varphi_2 = n\theta$ quando $d < 0$ e $\varphi_1 = -\pi + \varphi_2 = n\theta$ quando $d > 0$, obtemos de (15) e (16) equações que são matematicamente iguais aquelas que temos para a supercondutividade usual. Concluímos, então, que no presente caso temos soluções tipo vórtice, porém com os comprimentos característicos diferentes. De maneira análoga, podemos verificar, também, que possível obter uma rede de vórtices.

A partir deste modelo simples verificamos que, além de gerar um aumento de T_c , a introdução de interação entre planos via pares preserva propriedades fundamentais de um supercondutor, como a quantização do fluxo magnético, o efeito Meissner e rede de vórtices. Estes resultados mostram que a análise de interações mais gerais, por exemplo, modelos com constante de acoplamento anisotrópica, poderia fornecer informações mais ricas sobre o comportamento de supercondutores com alto T_c .

References

- [1] Z. Tesanovic, Phys. Rev. B, 36 (1987) 2364; Z. Tesanovic, Phys. Rev. B 38 (1988) 2489;
- [2] T. Scheneider, Z. Gedik and S. Ciraci, Europhys. Lett., 14 (1991) 261;
- [3] S. Chakravarty, A. Sudbo, P. W. Anderson, S. Strong, Science, 261 (1993) 337; A. Sudbo, S. Chakravarty, S. Strong, P. W. Anderson, Phys. Rev. B, 49 (1994) 12245; S. Chakravarty, P. W. Anderson, Phys. Rev. Lett., 72 (1994) 3859; A. Sudbo, Journal of Low Temp. Phys., 97 (1994) 403;
- [4] Bardeen, J. Cooper, L. N., Schrieffer, J.R., Phys. Rev. 108 (1957) 1175;
- [5] Popov, V. N. *Functional Integrals and Collective Excitations*, Cambridge University Press, New York (1990);
- [6] Ginsburg, V. L. and Landau, L. D., JEPT 20 (1950) 1064.

Álgebra Super $\left(W_{\frac{\infty}{2}} \oplus W_{\frac{1+\infty}{2}}\right)$ no Modelo de Super-Autovalores

L. O. Buffon¹, D. Dalmazi² and A. Zadra¹

¹Instituto de Física, USP; ²UNESP, Guaratinguetá

1 Introdução

Os modelos de matrizes aleatórias são importantes na física porque são modelos exatamente solúveis. O modelo discreto de uma matriz hermitiana descreve, no limite contínuo, a família $(p, q) = (2, 2k - 1)$ de modelos conformes mínimos acoplados à gravidade 2-D [1]. A função de partição deste modelo satisfaz a um conjunto de vínculos que podem ser obtidos a partir das equações de Schwinger-Dyson (S-D) associadas aos geradores da álgebra de Virasoro [2]. Estes vínculos são denominados de vínculos de Virasoro e são suficientes para resolvermos o modelo. Os geradores de Virasoro podem ser escritos em termos dos autovalores como os operadores diferenciais $l_n = -\sum_{i=1}^N x_i^{n+1} \partial_i$, $n \geq -1$, onde x_i são os autovalores da matriz $N \times N$. Eles satisfazem à álgebra de Virasoro $[l_n, l_m] = (n - m)l_{n+m}$. Em analogia aos modos de Virasoro que surgem em teorias de campo conforme, vamos associar o spin $s = 2$ ao gerador e ao vínculo de Virasoro.

Contudo, podemos estender essa álgebra introduzindo operadores diferenciais de ordens superiores

$$W_n^{(s)} = (-i\hbar)^{s-1} x^{n+1} \partial^{s-1}, \quad s \geq 1 \quad (1)$$

A ordem da derivada $(s - 1)$ corresponde ao spin (s) do operador. Para $s=2$ reobtemos o gerador de Virasoro: $W_n^{(2)} = -i\hbar x^{n+1} \partial$. Por conveniência, abandonamos os índices i dos autovalores e introduzimos a constante de Planck \hbar , que será útil para estudarmos o limite clássico destas álgebras. Os operadores em (1) satisfazem uma álgebra $W_{1+\infty}$:

$$[W_m^{(r)}, W_n^{(s)}] = -i\hbar \sum_{k \geq 0} (-i\hbar)^k C_{mn}^{rs}(k) W_{m+n-k}^{(r+s-2-k)} \quad (2)$$

onde $C_{mn}^{rs}(k)$ são constantes de estrutura. Estas álgebras de comutadores serão posteriormente denominadas de álgebras quânticas. Atuando com os geradores (1) na função de partição do modelo obtemos vínculos de spins superiores ($s \geq 2$), mas que são redutíveis aos vínculos de Virasoro [3].

No modelo de duas matrizes estes vínculos de ordem superior não são redundantes e as álgebras W_{∞} associadas são necessárias para resolver o modelo.

A extensão supersimétrica $N=1$ do modelo de uma matriz hermitiana é o chamado modelo de super-autovalores [4]. Ele descreve no limite contínuo, as teorias superconformes mínimas $((p, q) = (2, 4m))$ acopladas à supergravidade 2-D. Sua função de partição obedece a um conjunto de vínculos associados aos geradores da álgebra de super-Virasoro $N=1$. Em termos dos autovalores x_i e de seus companheiros supersimétricos θ_i , esses geradores são dados por

$$g_{n+1/2} = \sum_{i=1}^N x_i^{n+1} (\theta_i \partial_i - \Pi_i), \quad \Pi_i = \frac{\partial}{\partial \theta_i} \quad (3)$$

$$l_n^S = -\sum_{i=1}^N \left(x_i^{n+1} \partial_i + \frac{(n+1)}{2} x_i^n \theta_i \Pi_i \right), \quad n \geq -1 \quad (4)$$

que satisfazem à álgebra superconforme $N=1$:

$$[g_{n+1/2}, g_{m+1/2}]_+ = 2l_{n+m}^S, \quad [l_n^S, l_m^S] = (n - m)l_{n+m}^S$$

$$[t_n^s, g_{m+1/2}] = \frac{(n-1-2m)}{2} g_{n+m+1/2} \tag{5}$$

Podemos associar a estes geradores os spins conformes $s=3/2$ e $s=2$, respectivamente. Para os geradores fermiônicos o spin é a ordem da maior derivada mais $1/2$. Os vínculos associados aos geradores (3) e (4) são denominados de vínculos de super-Virasoro e são suficientes para resolver o modelo de super-autovalores.

No trabalho [5], calculamos os vínculos de spins superiores neste modelo e mostramos que eles são redutíveis aos vínculos de super-Virasoro. E também que eles estão associados com os geradores bosônicos da álgebra super $(W_{\frac{3}{2}} \oplus W_{\frac{1+\infty}{2}})$.

Nas seções seguintes vamos mostrar como obter extensões supersimétricas das álgebras w_∞ bosônicas. Primeiro faremos isso no caso clássico com parênteses de Poisson no super-espaço de fase, e depois no caso quântico através de comutadores. O super-espaço de fase é definido pelo par de coordenadas (x, θ) comutante e anticomutante e seus momentos canonicamente conjugados (p, Π) , respectivamente. A álgebra quântica é obtida pelas regras usuais de correspondência entre os momentos e os operadores diferenciais: $p \rightarrow -i\hbar\partial/\partial x$, $\Pi \rightarrow -i\hbar\partial/\partial\theta$ e o limite clássico é dado por: $\hbar \rightarrow 0$ e $\frac{1}{i\hbar}[\cdot, \cdot] \rightarrow \{\cdot, \cdot\}$. Para maiores detalhes do cálculo das álgebras que vamos apresentar ver a referência [6].

Uma possível aplicação dessas álgebras super W_∞ é na solução da extensão supersimétrica do modelo de duas matrizes.

2 Álgebras super- w_∞ clássicas N=1

No caso bosônico a álgebra w_∞ clássica é equivalente à álgebra de Poisson dos difeomorfismos que preservam áreas de superfícies suaves no espaço de fase (x, p) . Estes difeomorfismos são transformações canônicas $f \rightarrow f + \epsilon\{f, \rho(x, p)\}$ geradas via parênteses de Poisson $\{f(x, p), g(x, p)\} = \frac{\partial f}{\partial x} \frac{\partial g}{\partial p} - \frac{\partial f}{\partial p} \frac{\partial g}{\partial x}$, que preservam a área ($\omega = dx \wedge dp$). A função geratriz pode ser expandida como $\rho = \sum_{s,n} \rho_{s,n} w_n^{(s)}$ de forma que os elementos da base $w_n^{(s)} = x^{n+1} p^{s-1}$ satisfazem a álgebra w_∞ clássica

$$\{w_m^{(r)}, w_n^{(s)}\} = [(s-1)(m+1) - (r-1)(n+1)] w_{m+n}^{(r+s-2)} \tag{6}$$

A extensão supersimétrica N=1 dessa álgebra clássica é obtida a partir da álgebra superconforme clássica N=1:

$$\begin{aligned} \{g_m^{(3/2)}, g_n^{(3/2)}\}_+ &= 2w_{m+n+1}^{(2)} \\ \{g_m^{(3/2)}, w_n^{(2)}\} &= \left[(m+1) - \frac{1}{2}(n+1) \right] g_{m+n}^{(3/2)} \\ \{w_m^{(2)}, w_n^{(2)}\} &= (m-n)w_{m+n}^{(2)} \end{aligned} \tag{7}$$

onde assumimos os parênteses de Poisson graduados: $\{x, p\} = 1$, $\{\theta, \Pi\}_+ = -1$.

A realização mais geral destes geradores é

$$g_n^{(3/2)}(\lambda) = x^{n+1}(\theta p - \Pi) + 2\lambda(n+1)x^n\theta \tag{8}$$

$$w_n^{(2)}(\lambda) = x^{n+1}p + (n+1)x^n \left(\lambda + \frac{\theta \Pi}{2} \right) \tag{9}$$

onde λ é constante. Para obtermos a extensão da álgebra para spins superiores, tomamos as seguintes hipóteses:

- i) O spin mais baixo é $s = 3/2$.
- ii) Existe o gerador fermiônico com spin $s = 5/2$.
- iii) A álgebra de Poisson dos geradores fermiônicos obedece a seguinte regra

$$\{g^{(r)}, g^{(s)}\}_+ \propto w^{(r+s-1)} + \text{spins menores}$$

- iv) No gerador $g_n^{(s)}$, s é o spin e n representa a dimensão conforme.

Com isso tomamos a Ansatz mais geral para o gerador $g_m^{(5/2)}$

$$g_{m-1}^{(5/2)} = x^m \theta p^2 + c_m x^m p \Pi + d_m x^{m-1} \Pi + e_m x^{m-2} \theta \tag{10}$$

Impondo o fechamento da álgebra podemos calcular os possíveis valores de λ , c_m , d_m e e_m . Fazendo isso, obtivemos duas álgebras w_∞ supersimétricas:

Tipo 1: Com os geradores:

$$g_n^{(k+3/2)} = x^{n+1} p^k (\theta p - \Pi) \quad (11)$$

$$w_n^{(s)} = x^{n+1} p^{s-1} + \frac{1}{2}(n+1)x^n p^{s-2} \theta \Pi \quad (12)$$

formamos a álgebra- w_∞ :

$$\begin{aligned} \{g_m^{(r)}, g_n^{(r')}\}_+ &= 2w_{m+n+1}^{(r+r'-1)} \\ \{g_m^{(r)}, w_n^{(s)}\} &= [(s-1)(m+1) - (r-1)(n+1)] g_{m+n}^{(r+s-2)} \\ \{w_m^{(s)}, w_n^{(s')}\} &= [(s'-1)(m+1) - (s-1)(n+1)] w_{m+n}^{(s+s'-2)} \end{aligned} \quad (13)$$

onde $r, r' = 3/2, 5/2, \dots$ e $s, s' = 2, 3, 4, \dots$

Tipo 2: Temos quatro famílias de geradores somente com spins pares no setor bosônico:

$$g_n^{(2a+3/2)} = x^{n+1} p^{2a} (\theta p - \Pi) \quad (14)$$

$$\bar{g}_n^{((2a+1)+3/2)} = x^{n+1} p^{2a+1} (\theta p + \Pi) \quad (15)$$

$$w_n^{(2a+2)} = x^{n+1} p^{2a+1} + \frac{1}{2}(n+1)x^n p^{2a} \theta \Pi \quad (16)$$

$$k_n^{(2a+2)} = x^{n+1} p^{2a+1} \theta \Pi \quad (17)$$

formando a álgebra super w_∞ par:

$$\begin{aligned} \{g_m^{(r)}, g_n^{(r')}\}_+ &= 2w_{m+n+1}^{(r+r'-1)} \\ \{g_m^{(r)}, w_n^{(s)}\} &= [(s-1)(m+1) - (r-1)(n+1)] g_{m+n}^{(r+s-2)} \\ \{w_m^{(s)}, w_n^{(s')}\} &= [(s'-1)(m+1) - (s-1)(n+1)] w_{m+n}^{(s+s'-2)} \\ \{\bar{g}_m^{(r)}, \bar{g}_n^{(r')}\}_+ &= -2w_{m+n+1}^{(r+r'-1)} \\ \{\bar{g}_m^{(r)}, w_n^{(s)}\} &= [(s-1)(m+1) - (r-1)(n+1)] \bar{g}_{m+n}^{(r+s-2)} \\ \{g_m^{(r)}, \bar{g}_n^{(r')}\}_+ &= 2[(r'-1)(m+1) - (r-1)(n+1)] k_{m+n}^{(r+r'-2)} \\ \{g_m^{(r)}, k_n^{(s)}\} &= \bar{g}_{m+n+1}^{(r+s-1)} \\ \{\bar{g}_m^{(r)}, k_n^{(s)}\} &= g_{m+n+1}^{(r+s-1)} \\ \{k_m^{(s)}, k_n^{(s')}\} &= 0 \\ \{k_m^{(s)}, w_n^{(s')}\} &= [(s'-1)(m+1) - (s-1)(n+1)] k_{m+n}^{(s+s'-2)} \end{aligned} \quad (18)$$

Esta segunda álgebra é totalmente nova e será chamada de álgebra super w_∞ par. Podemos notar que as duas álgebras tem uma sub-álgebra comum formada pelos geradores $g_n^{(2a+3/2)}$ e $w_n^{(2a)}$, que será chamada de álgebra super w_∞ , pois seu setor bosônico corresponde a um truncamento para spins pares da álgebra w_∞ . Ambas as álgebras estão relacionadas com transformações que preservam a área no super-espaço de fase ($w = dx \wedge dp - d\Pi \wedge d\theta$). Entretanto, a função geratriz dessas transformações não é mais arbitrária como no caso bosônico. Para a álgebra super w_∞ (13) ela é da forma:

$$\rho_A = \phi(x + \frac{\theta \Pi}{2p}, p) + (\theta p - \Pi) \psi(x, p) \quad (19)$$

e para a álgebra super w_∞ par (18) temos:

$$\rho_B = p\phi(x + \frac{\theta \Pi}{2p}, p^2) + \theta \Pi p \varphi(x, p^2) + (\theta p - \Pi) \psi(x, p^2) + (\theta p + \Pi) p \eta(x, p^2) \quad (20)$$

onde ϕ , φ , ψ e η são funções suaves. As funções geratrizes ρ_A e ρ_B formam dois subgrupos invariantes do difeomorfismo. Se a função geratriz for arbitrária $\rho(x, p, \theta, \Pi)$, a álgebra super w_∞ que surge é N=2 [7].

3 Álgebras super- W_∞ quânticas $N=1$

O gerador bosônico de Virasoro pode ser escrito na forma mais geral

$$W_n^{(2)}(\lambda) = -i\hbar (x^{n+1}\partial + \lambda(n+1)x^n) \quad (21)$$

Vamos impor a seguinte condição sobre os geradores da álgebra W_∞

$$[W_m^{(r)}, W_n^{(s)}] = -i\hbar (c_0 W_{m+n}^{(r+s-2)} + c_1 W_{m+n-2}^{(r+s-4)} + \dots) \quad (22)$$

que permitirá obtermos truncamentos para spins pares. Tomando um Ansatz para $W_m^{(3)}$, obtemos as soluções: $\lambda = 1/2$ para a álgebra $W_{1+\infty}$ ($s \geq 1$) e $\lambda = 0$ para a álgebra W_∞ ($s \geq 2$).

Para obtermos a extensão supersimétrica $N=1$ da álgebra quântica W_∞ , tomamos uma série de hipóteses análogas às que usamos no caso clássico e seguimos o mesmo procedimento. Entretanto, neste caso encontramos somente uma álgebra supersimétrica consistente, formada pelos operadores:

$$\begin{aligned} G_n^{(3/2)} &= (-i\hbar)x^{n+1}(\theta\partial - \partial_\theta) \quad , \\ G_n^{(5/2)} &= (-i\hbar)^2 (x^{n+1}\partial(\theta\partial + \partial_\theta) + (n+1)x^n\partial_\theta) \quad , \\ G_n^{(7/2)} &= (-i\hbar)^3 (x^{n+1}\partial^2(\theta\partial - \partial_\theta) - 2(n+1)x^n\partial\partial_\theta - n(n+1)x^{n-1}\partial_\theta) \quad , \\ G_n^{(9/2)} &= (-i\hbar)^4 (x^{n+1}\partial^3(\theta\partial + \partial_\theta) + 3(n+1)x^n\theta\partial^3 + 3n(n+1)x^{n-1}\theta\partial^2 \\ &\quad + (n-1)n(n+1)x^{n-2}\partial_\theta) \quad , \\ W_n^{(2)} &= (-i\hbar) \left(x^{n+1}\partial + \frac{1}{2}(n+1)x^n\theta\partial_\theta \right) \quad , \\ K_n^{(2)} &= (-i\hbar)^2 x^{n+1}\partial\partial_\theta\theta \quad , \\ W_n^{(4)} &= (-i\hbar)^3 \left(x^{n+1}\partial^3 + \frac{3}{2}(n+1)x^n\partial^2 + \frac{1}{2}n(n+1)x^{n-1}\partial \right. \\ &\quad \left. - \frac{1}{2}(n+1)x^n\partial^2\partial_\theta\theta \right) \quad , \\ K_n^{(4)} &= (-i\hbar)^4 (x^{n+1}\partial^3 + (n+1)x^n\partial^2) \partial_\theta\theta \quad , \\ W_n^{(6)} &= (-i\hbar)^5 \left(x^{n+1}\partial^5 + \frac{5}{2}(n+1)x^n\partial^4 + 2n(n+1)x^{n-1}\partial^3 \right. \\ &\quad \left. + \frac{1}{2}(n-1)n(n+1)x^{n-2}\partial^2(1 + \partial_\theta\theta) - \frac{1}{2}(n+1)x^n\partial^4\partial_\theta\theta \right) \quad (23) \\ K_n^{(6)} &= (-i\hbar)^6 (x^{n+1}\partial^5 + 2(n+1)x^n\partial^4 + n(n+1)x^{n-1}\partial^3) \partial_\theta\theta \end{aligned}$$

que formam a álgebra quântica:

$$\begin{aligned} [G_m^{(3/2)}, G_n^{(3/2)}]_+ &= 2i\hbar W_{m+n+1}^{(2)} \quad , \\ [G_m^{(3/2)}, W_n^{(2)}] &= i\hbar(m+1) - \frac{1}{2}(n+1)G_{m+n}^{(3/2)} \quad , \\ [W_m^{(2)}, W_n^{(2)}] &= i\hbar(m-n)W_{m+n}^{(2)} \quad , \\ [G_m^{(5/2)}, G_n^{(3/2)}]_+ &= i\hbar(m-3n-2)K_{m+n}^{(2)} + 2(-i\hbar)^2(m-n)W_{m+n}^{(2)} \quad , \\ [G_m^{(3/2)}, K_n^{(2)}] &= -i\hbar G_{m+n+1}^{(5/2)} + (-i\hbar)^2(n+1)G_{m+n}^{(3/2)} \quad , \\ [K_m^{(2)}, K_n^{(2)}] &= (-i\hbar)^2(n-m)K_{m+n}^{(2)} \quad , \\ [W_m^{(2)}, K_n^{(2)}] &= i\hbar(m-n)K_{m+n}^{(2)} \quad , \\ [G_m^{(5/2)}, W_n^{(2)}] &= i\hbar(m - \frac{3}{2}n - \frac{1}{2})G_{m+n}^{(5/2)} + (-i\hbar)^2 n(n+1)G_{m+n-1}^{(3/2)} \quad , \\ [G_m^{(5/2)}, K_n^{(2)}] &= -i\hbar G_{m+n+1}^{(7/2)} + 2(-i\hbar)^2(n+1)G_{m+n}^{(5/2)} + (-i\hbar)^3 n(n+1)G_{m+n-1}^{(3/2)} \quad , \end{aligned}$$

$$\begin{aligned}
[G_m^{(5/2)}, G_n^{(5/2)}]_+ &= -2i\hbar W_{m+n+1}^{(4)} - 3(-i\hbar)^2(n(n+1) + m(m+1))K_{m+n-1}^{(2)} \\
&\quad + 2(-i\hbar)^3((n+m+1)(n+m+2) - 3(n+1)(m+1))W_{m+n-1}^{(2)} \\
[G_m^{(3/2)}, W_n^{(4)}] &= -i\hbar \frac{1}{2}(n-6m-5)G_{m+n}^{(7/2)} \\
&\quad + (-i\hbar)^2(n(n+1) - 3(m+1)(m+n+1))G_{m+n-1}^{(5/2)} \\
&\quad + (-i\hbar)^3 \frac{1}{2}(m(m+1)(3n+2m+1) + n(n+1)(n-m-2))G_{m+n-2}^{(3/2)}.
\end{aligned}$$

O setor bosônico formado por $W_n^{(2s)}$ e $K_m^{(2r)}$ se desacopla em duas sub-álgebras, uma isomorfa à álgebra $W_{\frac{1+\infty}{2}}$ e outra isomorfa à álgebra $W_{\frac{\infty}{2}}$. Assim, concluímos que o setor bosônico da álgebra toda será chamado de álgebra $(W_{\frac{\infty}{2}} \oplus W_{\frac{1+\infty}{2}})$.

4 Conclusões

Construímos as extensões supersimétricas $N=1$ das álgebras W_{∞} . A nível clássico, encontramos duas álgebras de Poisson que são as super w_{∞} e super w_{∞} par. No caso quântico, encontramos somente uma, a super $(W_{\frac{\infty}{2}} \oplus W_{\frac{1+\infty}{2}})$. O limite clássico ($\hbar \rightarrow 0$) desta álgebra é a super w_{∞} par. Uma questão em aberto é se existe alguma álgebra quântica cujo limite clássico seja a super w_{∞} (13).

Analisando os operadores quânticos (23) disponíveis, encontramos formas compactas para os operadores bosônicos e fermiônicos, respectivamente dadas por $K_n^{(2r)} = p^{r-1} x^{n+1} p^r \Pi \theta$ e $\tilde{G}_n^{(s+1/2)} = p^{s-1} x^{n+1} \theta p + (-)^s x^{n+1} p^{s-1} \Pi$. A questão aqui é se existe algum ordenamento especial que determine estes operadores quânticos a partir dos geradores clássicos.

References

- [1] V. Kazakov, Mod. Phys. Lett. **A4** (1989) 2125.
- [2] E. Abdalla, M.C.B. Abdalla, D. Dalmazi and A. Zadra, "2D gravity in non-critical strings", Lectures Notes in Physics **m20**.
- [3] H. Itoyama and Y. Matsuo, Phys. Lett. **B262** (1991) 233.
- [4] L. Alvarez-Gaumé, H. Itoyama, J.L. Mañes and A. Zadra, Int. J. Mod. Phys. **A7** (1992) 5337.
- [5] L.O. Buffon, D. Dalmazi and A. Zadra, hep-th/9604184.
- [6] L.O. Buffon, D. Dalmazi and A. Zadra, hep-th/9607122.
- [7] E. Bergshoeff, B. de Wit and M. Vasiliev, Nucl. Phys. **B366** (1991) 315.

Sobre o Modelo de Chern-Simons na Frente de Onda da Luz *

Leon Ricardo Ururahy Manssur
Centro Brasileiro de Pesquisas Físicas-CNPq

São revistas algumas propriedades de sistemas físicos a duas dimensões espaciais, com ênfase na possibilidade de existência de spin e estatística fracionários (*anyons*), e na relação disto com o modelo de Chern-Simons abeliano.

Na ref.[1], cuja leitura é recomendada, Dirac afirma que os 10 geradores do grupo de Poincaré (em 3+1 dimensões) usualmente são: as hamiltonianas, relacionadas à evolução dinâmica do sistema no espaço-tempo; e os geradores que sobram (simples, ou *cinemáticos*) se relacionam com um sub-grupo do grupo de Poincaré: eles mantêm invariante a hipersuperfície escolhida para a quantização. Naquele artigo, é discutida a formulação canônica da teoria quântica nas formas instantânea (tendo como suporte a superfície $x^0 = \text{constante}$), sobre o hiperbolóide (dado por $x^\mu x_\mu = \text{constante}$), e sobre a frente de onda da luz (dada por $x^+ \equiv \tau \equiv (x^0 + x^3)/\sqrt{2} = \text{constante}$). Foi notado que na frente de onda temos um gerador cinemático a mais. Além disto, não há raízes quadradas na Hamiltoniana da eq. de Dirac, o que evita o problema de energias negativas.

Nas coordenadas convencionais, dois pontos do hiperplano $x^0 = \text{const.}$ têm em geral separação tipo espaço, que se torna tipo luz se e somente se estes pontos coincidem. Na frente de onda, dois pontos do hiperplano $x^+ = \text{const.}$ também têm em geral um intervalo tipo espaço, mas este intervalo pode se tornar tipo luz, se os dois pontos pertencerem à reta onde o hiperplano tangencia o cone de luz. Logo, podemos, neste hiperplano, ter intervalo tipo luz para dois pontos não-coincidentes, ao contrário do caso anterior. No momento em que quantizamos a teoria, o princípio de causalidade microscópico faz aparecer a não-localidade: requer-se que o comutador

$$[A(x^+, x^-, x^\perp), B(0)]_{x^+=0}$$

onde $x^\pm = (x^0 \pm x^3)\sqrt{2}$, $x^\perp = (x^1, x^2)$, se anule quando o intervalo $(x^2)^2|_{x^+=0} = (2x^+x^- - x^\perp \cdot x^\perp)|_{x^+=0} = -x^\perp \cdot x^\perp$ for tipo espaço. Logo, o comutador é proporcional a $\delta^2(x^\perp)$ (e suas derivadas), e não há nenhuma imposição de localidade em x^- : usando a representação espectral de Lehman para o campo escalar, mostra-se [3] que, na frente de onda,

$$\langle 0 | [\phi(x^+, x^-, x^\perp), \phi(0)]_{x^+=0} | 0 \rangle = -\frac{i}{4} \delta^2(x^\perp) \epsilon(x^-). \quad (1)$$

Na quantização, resulta que o vácuo é mais simples na frente de onda. Ocorre que, para uma partícula massiva em sua camada de massa, os momenta k^\pm são positivo-definidos e portanto a conservação do momento longitudinal total não permite que haja excitações de tais quanta no vácuo da frente de onda. Isto oferece vantagens para o cálculo de efeitos não-perturbativos, e pode esclarecer aspectos do vácuo da QCD: no formalismo convencional este inclui termos de condensados fermiônicos e gluônicos, que não podem comparecer no vácuo da frente de onda.

Em 2 dimensões espaciais, o grupo de rotações tem uma estrutura peculiar: as rotações comutam (o grupo SO(2) é abeliano), e não há *a priori* nenhuma razão para que o momento angular seja quantizado. Espera-se então que a função de onda para um sistema de n partículas satisfaça

$$\Psi(\dots, q_i, \dots, q_j, \dots) = e^{2\pi i \sigma} \Psi(\dots, q_j, \dots, q_i, \dots), \quad (2)$$

q_i denotando o conjunto de números quânticos da i -ésima partícula, e σ o parâmetro de estatística, um número real qualquer (a menos de um inteiro). Os casos particulares de bósons e férmions são dados por $\sigma = 0$ e $\sigma = 1/2$.

*Tese de Mestrado defendida no CBPF em abril de 1996

respectivamente. O caso geral é chamado de *anyon*. Como esperado, neste caso o espectro do operador de momento angular tem valores diferentes de inteiro ou semi-inteiro.

Para obter este efeito a partir de primeiros princípios [11], por exemplo, em Mecânica Quântica não-relativística, basta notar que no espaço de configurações de um sistema de partículas temos que assumir que os vetores de cada uma delas são sempre diferentes uns dos outros, isto é, elas não podem ocupar o mesmo lugar. Do contrário teríamos necessariamente estatística bosônica. Ao excluirmos estes pontos, apenas no caso de 2 dimensões espaciais, o espaço de configurações deixa de ser simplesmente conexo. Então, ao calcularmos, por exemplo, amplitudes de transição, as trajetórias na integral de caminho são inequivalentes, e têm um peso segundo a classe de equivalência a que pertencem. Resulta [16] que surge um campo magnético proporcional à densidade de partículas. Portanto, a título de ilustração, podemos interpretar a interação neste sistema como tubos de fluxo magnético de raio infinitesimal acompanhando cada partícula. Pode-se mostrar que a introdução do termo de Chern-Simons também leva a este resultado. Na passagem a uma teoria de campos relativística, encontramos dificuldades e pouco é conhecido no momento sobre estatística e spin não usuais.

Este modelo tem sido usado para tratar problemas de física da matéria condensada onde o movimento é confinado a um plano, como por exemplo, a supercondutividade a baixas temperaturas e o efeito Hall quantizado (vide [12, 13, 15, 14]).

1 Campo escalar carregado

A teoria considerada aqui é definida pela seguinte densidade de lagrangeana:

$$\mathcal{L} = (\mathcal{D}^\mu \phi)(\tilde{\mathcal{D}}_\mu \phi^*) + \frac{\kappa}{4\pi} \epsilon^{\mu\nu\rho} A_\mu \partial_\nu A_\rho \quad (3)$$

onde κ é uma constante. ϕ é um campo escalar complexo. A_μ é um campo de gauge abeliano e

$$\mathcal{D}_\mu = (\partial_\mu + ieA_\mu) \quad (4)$$

$$\tilde{\mathcal{D}}_\mu = (\partial_\mu - ieA_\mu). \quad (5)$$

Os campos de calibre têm que satisfazer condições de contorno anti-periódicas no infinito ao longo de x^- , pois se não, isto tornaria nula a carga conservada do campo ϕ .

A hamiltoniana na frente de onda, obtida usando o método de Dirac para sistemas vinculados, é então

$$H^{I, J} = \int d^2x (\mathcal{D}_1 \phi)(\tilde{\mathcal{D}}_1 \phi^*), \quad (6)$$

com A_1 dado em termos de ϕ e ϕ^* . Notamos que ela é mais simples que a hamiltoniana a tempos iguais, por exemplo, a da ref. [8]. Entretanto, agora temos não-localidade.

Concluimos que sobram apenas os campos ϕ e ϕ^* como variáveis independentes, em termos dos quais a dinâmica de todos os outros é descrita. Calcula-se facilmente os parênteses

$$\{\phi, \phi\}_D = \{\phi^*, \phi^*\}_D = 0 \quad (7)$$

$$\{\phi, \phi^*\}_D = \{\phi^*, \phi\}_D = K(x-y) \equiv -\frac{1}{4} \epsilon(x^-) \delta(x^1), \quad (8)$$

que reconhecemos como sendo os parênteses de Dirac na frente de onda obtidos por um argumento geral na eq. 1.

A_1 é um gauge puro:

$$A_1 = \partial_1 \Lambda \quad (9)$$

$$\Lambda(x) = \frac{1}{8a} \int d^2y \epsilon(x^- - y^-) \epsilon(x^1 - y^1) j^+(y) \quad (10)$$

Para eliminá-lo, aparece uma fase no campo de matéria $\hat{\phi} = e^{i\Lambda} \phi$, o que resulta em

$$H = \int d^2x (\partial_1 \hat{\phi})(\partial_1 \hat{\phi}^*). \quad (11)$$

Na teoria a tempos iguais [4, 8, 5], podemos analogamente definir um $\hat{\phi}^{e,t}$, com

$$\Lambda^{e,t}(\mathbf{x}) = \frac{1}{4\pi a} \int d^2y \Theta(\mathbf{x} - \mathbf{y}) j^0(y), \quad (12)$$

onde $\Theta(\mathbf{x} - \mathbf{y})$ é o ângulo entre o vetor $\mathbf{x} - \mathbf{y}$ e o eixo dos x^1 , no plano (x^1, x^2) . Notemos que Θ é multivalente, e por este motivo na integração temos que escolher um ramo, fazendo um corte. Este corte se traduz como uma descontinuidade em Θ , e para comutar derivadas em relação a x e integrais em y no intuito de obter uma hamiltoniana livre, obtemos um termo não desejado. Resulta que

$$\hat{\phi}(x)\hat{\phi}(y) - e^{\frac{i}{2\pi a}\Delta} \hat{\phi}(y)\hat{\phi}(x) = 0 \quad (13)$$

$$\hat{\phi}(x)\hat{\pi}(y) - e^{\frac{i}{2\pi a}\Delta} \hat{\pi}(y)\hat{\phi}(x) = i\delta^2(\mathbf{x} - \mathbf{y}) \quad (14)$$

onde $\Delta = \Theta(\mathbf{y} - \mathbf{x}) - \Theta(\mathbf{x} - \mathbf{y}) = \pi \text{ mod } 2n\pi$ (n inteiro), que são as conhecidas relações de comutação graduadas, com o fator de fase multivalente Δ [8]. É argumentado que a tempos iguais há uma **descrição dual da teoria**.

Poder-se-ia pensar que na eq. 10 temos uma outra maneira de representar o ângulo Θ da forma instantânea (eq. 12), apenas mudando os nomes das coordenadas, já que as derivadas das duas expressões dão essencialmente a delta. Mas é demonstrado no apêndice de [9] que elas coincidem apenas para uma classe restrita de funções teste. Elas diferem nas condições de contorno no infinito que impomos aos campos de calibre: a tempos iguais, nulas; na frente de onda, anti-periódicas em x^- .

Entretanto, ocorre que $[\hat{\phi}, \hat{\phi}^*] \neq 0$ e $[A, A] \neq 0$, o que torna as relações de comutação graduadas mais complicadas quando tentamos escrevê-las na frente de onda. Obtemos que

$$\begin{aligned} \hat{\phi}(x)\hat{\phi}(y) - e^{[\alpha(x,y) - \alpha(y,x)]} \hat{\phi}(y)\hat{\phi}(x) &= e^{i\alpha(x,y)} [e^{i\Lambda(x)}, e^{i\Lambda(y)}] \phi(x)\phi(y) + \\ &+ \frac{1}{2} [e^{i\Lambda(x)} e^{i\Lambda(y)} \hat{\phi}(y^-, x^1)\hat{\phi}(y)(1 - e^{\alpha(x,y)}) - (x - y)] \end{aligned} \quad (15)$$

onde

$$\alpha(x, y) = -\frac{i}{8a} \epsilon(x^- - y^-) \epsilon(x^1 - y^1). \quad (16)$$

e o último termo é igual ao anterior com x e y permutados. Notemos que o lado esquerdo é análogo à relação de comutação graduada a tempos iguais, eq. 13, mas as funções que aparecem nos expoentes têm simetrias bastante distintas. Além disto, Θ é multivalente, o que não acontece com α . A conclusão é que, na frente de onda, não se pode obter A multivalente tal que a hamiltoniana seja livre e $\hat{\phi}$ obedeça uma relação de comutação graduada como a eq. 13, devido às condições de contorno.

2 Campo espinorial

Tentaremos repetir a análise da seção anterior para o caso de campos fermiônicos. Em $(2 + 1)$ dimensões, as matrizes gama de Dirac podem ser representadas por matrizes de dimensão 2:

$$\gamma^0 = \sigma_1, \quad \gamma^1 = i\sigma_3, \quad \gamma^2 = i\sigma_2 \quad (17)$$

Definimos então γ^+ e γ^- da maneira usual. Notemos que estas 3 matrizes juntamente com a identidade formam uma base para as matrizes 2×2 e não faz sentido definir γ^5 .

O campo ψ é um espinor de 2 componentes, e define-se $\bar{\psi} \equiv \psi^\dagger \gamma^0$. Nossa densidade de lagrangeana será agora dada por

$$\mathcal{L} = \frac{i}{2} \left[\psi_\alpha^* (\gamma^0 \gamma^\mu)_{\alpha\beta} \mathcal{D}_\mu \psi_\beta - \mathcal{D}_\mu \psi_\alpha^* (\gamma^0 \gamma^\mu)_{\alpha\beta} \psi_\beta \right] + \alpha \epsilon^{\mu\nu\rho} A_\mu \partial_\nu A_\rho \quad (18)$$

Os únicos campos independentes que sobram são ψ_2 e ψ_2^* e, novamente, a distribuição $K(x - y)$ aparece devido às condições de contorno, e as observações anteriores se aplicam.

A hamiltoniana na frente de onda então é escrita

$$H^{l.f.} = \frac{1}{2} \int d^2x \left[\psi_2^* (\mathcal{D}_1 \psi_1) + (\mathcal{D}_1 \psi_1^*) \psi_2 \right], \quad (19)$$

De novo, a hamiltoniana tem um aparência mais simples que a de tempos iguais, mas é não-local e tem um potencial de sexta potência.

Os parênteses de Dirac entre os campos resultam:

$$\{\psi_2, \psi_2\}_D = \{\psi_2^*, \psi_2^*\}_D = 0 \quad (20)$$

$$\{\psi_2, \psi_2^*\}_D = -\frac{i}{\sqrt{2}}\delta^2(x-y) \quad (21)$$

$$\{j^+, j^+\}_D = 0. \quad (22)$$

Notemos que a densidade de carga comuta com ela mesma, e que a eq. 21 fornece um comutador local, contrastando com que vimos anteriormente para bósons. O campo $\hat{\psi}_2$ é definido da mesma maneira que $\hat{\phi}$ na seção anterior. Obtemos que

$$[\hat{\psi}_2, \hat{\psi}_2]_+ = 0. \quad (23)$$

o que se fosse obtido a tempos iguais seria inequivocamente o anticomutador de um campo fermiônico. Aqui, este resultado não é conclusivo, pois não sabemos o que significa um anti-comutador igual a zero *na frente de onda*.

3 Conclusões

Foram estudados campos em 3 dimensões minimamente acoplados a termo de Chern-Simons nas coordenadas da frente de onda, onde 4 (e não 3) dos 6 geradores do grupo de Poincaré são cinemáticos. Resulta que na frente de onda sempre temos um sistema vinculado. Obtidos os parênteses de Dirac, os campos de calibre são completamente eliminados. No caso do campo espinorial, sobra apenas uma de duas componentes e sua conjugada. A Hamiltoniana é não local e o potencial é de sexta potência.

Tentamos obter indícios de estatística não usual (anyônica), a qual é naturalmente proposta em 2 dimensões espaciais. A construção a tempos iguais [8] não leva a uma Hamiltoniana sem interação para o campo transformado $\hat{\phi}$, ao contrário do que é afirmado na literatura, porque há no integrando uma função multivalente [10, 11]. Já na frente de onda, devido às condições de contorno, a Hamiltoniana é livre, mas não encontramos o fator de fase multivalente que alegadamente daria origem à estatística fracionária.

Ainda, nas referências encontramos afirmações de que a estatística fracionária não aparece de forma natural numa teoria de campos relativística porque a exclusão de pontos do espaço de configurações é artificial [10] e que existe anomalia rotacional independente de anyons [6]. Entretanto, não podemos concluir ainda sobre a existência ou não de anyons, pois a teoria é não-linear e não-local.

Agradecimentos

Agradeço Prof. Prem P. Srivastava pela orientação e ao CNPq pelo auxílio financeiro.

References

- [1] P. A. M. Dirac, Rev. Mod. Phys. 21, 392 (1949)
- [2] P. P. Srivastava, Light-Front Quantization of Dynamical Systems With Chern-Simons Term, ICTP-Trieste preprint, IC-305/94, hep-th@xxx.lanl.gov/9412239; ver também Europhys. Letts. (1995)
- [3] S.J. Brodsky e H.C. Pauli, Schlading Lectures, SLAC-PUB- 5558/91; K.G. Wilson, Nucl. Phys. B (proc. suppl.) 17 (1990); P.P. Srivastava, Lectures, Proceedings XIV Encontro Nacional de Partículas e Campos, Caxambu, MG, pgs. 154-192 (1993), Soc. Bras. Fis.; hep-th@ xxx.lanl.gov/9312064 e 9412204, 9412205; P. Srivastava, Quantum Field Theory on the Light-Front: an introduction (Monografia CBPF-MO-003/93)
- [4] S. Deser, R. Jackiw e S. Templeton, Phys. Rev. Lett. 48, 975 (1982); Ann. Phys. 140, 372 (1982)
- [5] C. R. Hagen, Ann. Phys. 157, 342 (1984)
- [6] C. R. Hagen, Phys. Rev. D 31, 2135 (1985)

- [7] R. Mackenzie e F. Wilczek, *Int. J. Mod. Phys. A* **3**, 2827 (1988)
- [8] G. W. Semenoff, *Phys. Rev. Lett.* **61**, 517 (1988); G. W. Semenoff e P. Sodano, *Nucl. Phys.* **B328**, 753 (1989)
- [9] M. S. Swanson, *Phys. Rev.* **D42**, 552 (1990)
- [10] P. S. Gerbert, *Int. J. Mod. Phys. A* **6**, 173 (1991)
- [11] S. Forte, *Rev. Mod. Phys.* **64**, 193 (1992)
- [12] F. D. M. Haldane, *Phys. Rev. Lett.* **51**, 605 (1983)
- [13] R. B. Laughlin, *Phys. Rev. Lett.* **50**, 1395 (1983)
- [14] B. Blok e X. G. Wen, *Phys. Rev B* **43** 8337 (1991)
- [15] M. Stone, *Int. J. Mod. Phys. B* **5**, 509 (1991)
- [16] S. Ouvry, *Ideal Anyons, Mesoscopic Quantum Physics - Les Houches, Session LXI, 1994* - editores E. Akkermans, G. Montambaux e J.-L. Pichard, North-Holland, Amsterdam, PACS numbers: 03.65.-w, 05.30.-d, 11.10.-z, 05.70.Ce, IPNO/TH 94-76
- [17] P. A. M. Dirac, *Lectures in Quantum Mechanics*, Benjamin, New York, 1964
- [18] M. Henneaux e C. Teitelboim, *Quantization of Gauge Systems*, Princeton University Press, NJ, 1992; Hanson, Regge, Teitelboim, *Constrained Hamiltonian System*, *Accad. Naz. dei Licei*, Roma, 1976 ; K. Sundermeyer, *Constrained Dynamics*, *Lecture Notes in Physics* 169, Springer-Verlag, Berlin, 1982

Sewing string tree vertices with ghosts

Leonidas Sandoval Junior*

sandoval@snfma2.if.usp.br

Depto. de Física Matemática

Instituto de Física - Universidade de São Paulo

December 3, 1996

During the early days of String Theory, the way to obtain the vertices for the scattering of a large number N of strings was to take a vertex for the scattering of a small number of strings (usually 3) and "sew" it to other similar vertices. Here we shall be concerned with the sewing of two vertices in order to form a third one. This has been done many times before, but we will use here the method developed by Neveu and West (Comm.Math.Phys. 119, 1988). We will also be concerned with sewing the strings when we include ghosts in the theory.

We shall start with a review of how to do the sewing of two vertices at tree level without any ghosts. What we must do is sew two legs of two vertices, one leg from each vertex. What we have in the beginning are two vertices V_1 and V_2 with N_1 and N_2 legs, respectively (figure 1).

We now sew leg E from V_1 with the adjoint of leg F from V_2 . What we have now is the substitution of the two sewn legs by a propagator (figure 2). When this propagator is written in parametric form, it is an integration over one of the variables (in order to cancel one spurious degree of freedom) and a conformal factor \mathcal{P} which contains terms of L_n 's acting on leg E only.

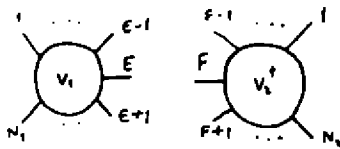


Fig.1: two vertices to be sewn together.

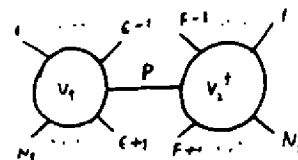


Fig.2: two vertices sewn together.

So the resulting vertex V_c (called the *composite vertex*) has the generic form

$$V_c = V_1 P V_2^\dagger \tag{1}$$

where the hermitian conjugate of V_2 is for the sewn leg F only and

$$P = \int dx \mathcal{P}$$

where x is a suitable variable. In what follows, we shall often write \mathcal{P} instead of P , calling attention to the integration when necessary.

In the work of Neveu and West, vertices without ghosts were sewn together using some overlap identities satisfied by the vertices V_1 and V_2^\dagger . The result they obtained was that two vertices can be sewn together as long as the conformal factor P has the form

$$\mathcal{P} = V_E^{-1} V_F \Gamma \tag{2}$$

where V_E^{-1} and V_F are conformal transformations and $\Gamma z = z^{-1}$.

When we introduce ghosts, the vertices are now surrounded by a "cloud" of ghosts and, in addition to satisfying the previous overlap identities, they must also obey some overlap identities with the conformal operators b^i and c^i , given by

$$b^i(\xi_i) = \sum_{n=-\infty}^{\infty} b_{-n}^i \xi_i^{n-2} \quad , \quad c^i(\xi_i) = \sum_{n=-\infty}^{\infty} c_{-n}^i \xi_i^{n+1}$$

*Work developed under a CAPES grant, in King's College London, and supported by CNPq.

where c_n^i and b_n^i are ghost anticommuting oscillators with anticommutation relations

$$\{c_n^i, b_m^j\} = \delta_{n,-m}.$$

These operators have, respectively, conformal weights 2 and -1 .

The overlap identities for a vertex V with these operators are given by

$$V \left[b^i(\xi_i) - \left(\frac{d\xi_j}{d\xi_i} \right)^2 b^j(\xi_j) \right] = 0, \quad V \left[c^i(\xi_i) - \left(\frac{d\xi_j}{d\xi_i} \right)^{-1} c^j(\xi_j) \right] = 0.$$

We shall be working here with overlap identities for the physical vertex U , which has the correct ghost number, instead of the overlap identities for vertex V . The physical vertex is given by

$$U = V \prod_{\substack{i=1 \\ i \neq a,b,c}}^N \sum_{j=1}^N \sum_{n=-1}^{\infty} e_n^{ij} b_n^j \tag{3}$$

where a, b, c are any three legs of the vertex and the matrix e_n^{ij} is given by

$$\sum_{n=-1}^{\infty} e_n^{ij} \mathcal{L}_n^j = V_j^{-1} \partial_i V_j$$

where the cycling transformations are now defined on the complete generators \mathcal{L}_n^i of the conformal algebra of the bosonic oscillators and of the ghost oscillators. These vectors e_n^{ij} have the following property:

$$\frac{\partial V}{\partial z_i} = V \sum_{j=1}^N \sum_{n=-1}^{\infty} e_n^{ij} \mathcal{L}_n^j. \tag{4}$$

In order to derive the overlap identity for the physical vertex U , we must multiply the overlap identity for V by the same factor as in eq. (??), and pass it through the overlap identities, obtaining

$$U \left[b^i(\xi_i) - \left(\frac{d\xi_j}{d\xi_i} \right)^2 b^j(\xi_j) \right] = 0. \tag{5}$$

$$U \left[c^i(\xi_i) - \left(\frac{d\xi_j}{d\xi_i} \right)^{-1} c^j(\xi_j) \right] + V \sum_{\substack{p=1 \\ p \neq a,b,c}}^N (-1)^p \prod_{\substack{k=1 \\ k \neq a,b,c \\ k \neq p}}^N \sum_{l=1}^N \sum_{q=-1}^{\infty} e_q^{kl} b_q^l \\ \times \sum_{n=-1}^{\infty} \left[e_n^{pi} \xi_i^{n+1} - \left(\frac{d\xi_j}{d\xi_i} \right)^{-1} e_n^{pj} \xi_j^{n+1} \right] = 0. \tag{6}$$

From (??) we can see that there will be an anomalous term in the c^i overlap of the physical vertex U unless both legs i and j are precisely those legs (a, b or c) that do not have any ghosts attached to them. These ghosts which are attached to all the other legs are responsible for the anomalous terms.

By careful analysis of the ghost number and of BRST invariance of the composite physical vertex U_c , resulting of the sewing of the two physical vertices, we can conclude that we need to add some extra ghosts during the sewing procedure, in the same way we added the conformal term \mathcal{P} . These extra ghosts are given by

$$G = (-1)^{N_1+a} \sum_{j=1}^{N_1} \sum_{n=-1}^{\infty} e_n^{aj} b_n^j$$

where a ($a \neq E$) is one of the legs of vertex U_1 that does not have ghosts attached to it.

The composite vertex U_c is then given by

$$U_c = U_1 G P U_2$$

Making the necessary insertions is a long and difficult task. The resulting composite vertex is given by

$$\begin{aligned}
 U_c^{gh} = & \left(\prod_{\substack{i=1 \\ i \neq E, F}}^{N_1+N_2} i(0) \right) \exp \left[\sum_{\substack{i,j=1 \\ i \neq j \\ i,j \neq E, F}}^{N_1+N_2} \sum_{n=2}^{\infty} \sum_{m=-1}^{\infty} c_n^i E_{nm} (\Gamma V_i^{-1} V_j) b_m^j \right] \\
 & \times \prod_{r=-1}^1 \sum_{\substack{j=1 \\ j \neq E, F}}^{N_1+N_2} \sum_{s=-1}^1 E_{rs}(V_j) b_s^j \\
 & \times \prod_{\substack{i=1 \\ i \neq b, c}}^{N_1} \sum_{n,m=-1}^{\infty} \left[\sum_{\substack{j=1 \\ j \neq E}}^{N_1} e_n^{ij} E_{nm}(V_{0j}^{-1} V_j) b_m^j + \sum_{\substack{j=1 \\ j \neq F}}^{N_2} e_m^{iE} E_{mn}(V_{0E}^{-1} V_j) b_n^j \right] \\
 & \times \prod_{\substack{i=1 \\ i \neq d, g, h}}^{N_2} \sum_{n,m=-1}^{\infty} \left[\sum_{\substack{j=1 \\ j \neq E}}^{N_1} e_n^{iF} E_{nm}(V_{0F}^{-1} V_j) b_n^j + \sum_{\substack{j=1 \\ j \neq F}}^{N_2} e_n^{ij} E_{nm}(V_{0j}^{-1} V_j) b_m^j \right].
 \end{aligned}$$

This result has been verified by explicitly sewing the physical vertices U_1 and $U_2^!$.

The one loop measure in String Theory: the case of two finite fixed points

Leonidas Sandoval Junior*

sandoval@snfma2.if.usp.br

Depto. de Física Matemática

Instituto de Física - Universidade de São Paulo

December 3, 1996

In String Theory, we can represent the scattering of an arbitrary number N of bosonic strings in first order of perturbation by a Riemann sphere with N strings worldsheets attached to it (figure 1). Using the conformal invariance of the theory, these worldsheets can be reduced to points on the surface, parametrized by the variables $z_i, i = 1, \dots, N$ (figure 2).

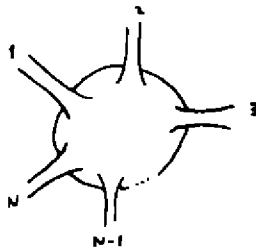


Fig.1: scattering of N closed bosonic strings.

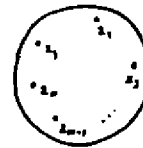


Fig.2: scattering after conformal transformations.

In the case of higher orders of perturbation theory, the Riemann sphere is substituted by Riemann surfaces of higher orders. The total scattering amplitude will be the sum of all the diagrams, represented by all genera of Riemann surfaces (figure 3).

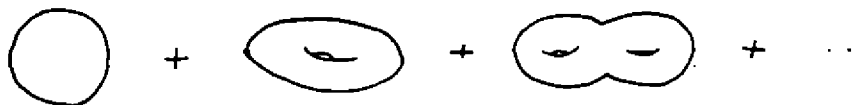


Fig.3: all orders of perturbation theory.

Each of these Riemann surfaces can be continuously deformed into Riemann spheres (for closed strings) with "handles" attached to them (figure 4). Each handle is parametrized by a group of three complex numbers, $v_r, r = 1, 2, 3$.

*Work developed under a CAPES grant, in King's College London, and supported by CNPq.



Fig.4: parametrization of a handle.

So, the scattering of N bosonic strings in some particular order of perturbation is represented by a Riemann surface of genus g , parametrized by N complex variables z_i and $3g$ complex variables v_r (figure 5).



Fig.5: $(g + 1)$ -th order of perturbation.

In the Group Theoretic approach to String Theory, developed by Neveu and West (Phys.Lett. 193B, 1987), the scattering amplitude of an arbitrary number N of bosonic strings can be calculated in a systematic way. It consists of two parts: the *vertex* and the *integration measure* (*measure*, for short), integrated over all the variables z_i and v_r , except three of them, that must be fixed in order to gauge fix the conformal invariance of the theory.

In order to calculate the measure, one needs to use functions that change some of the variables v_r by an infinitesimal amount δv_r . In the one loop case, we can parametrize the three v_r variables by α , β , and w , where α and β are called *fixed points* and w is called the *multiplier*. We may fix the two fixed points and one of the variables z_i so that we only have now the multiplier w and the remaining variables z_i as variables. The functions that change the variable w on a certain covering ξ_j of the Riemann surface by an infinitesimal amount δw are given by

$$f_{w_j}^{(i)}(\xi_j) = \frac{\delta w}{\epsilon w} (\xi_j - \alpha) \left[\zeta(v_i) - \frac{\zeta(\pi i)}{\pi i} \right] \quad , \quad j = 1, \dots, N, \tag{1}$$

where $v_i = \ln(\xi_i - \alpha) - \ln(-\alpha)$ and $\zeta(v_i)$ is the Weierstraß ζ -function, given by

$$\zeta(v_i) = \frac{1}{v_i} + \sum_{w_i, w_i \neq 0} \left(\frac{1}{v_i - w_i} + \frac{1}{w_i} + \frac{v_i}{w_i^2} \right)$$

with periods $w_{i1} = \ln w$ and $w_{i2} = 2\pi i$. The fact that there are N of these functions is that each one has to act on a different covering of the Riemann surface. These coverings are needed in order to avoid singularities at the N points z_j .

Using this function, we obtain the following result for the measure:

$$\bar{f} = w^{-2} \left[\prod_{n=1}^{\infty} (1 - w^n) \right]^{-24} \tag{2}$$

This measure is independent of the number of strings that are being scattered.

In higher order of perturbation theory, it is impossible to fix all the fixed points of the theory, so it would be useful to see how the inclusion of fixed points will change the value of the measure in the case of just one handle.

So, we now fix three of the variables z_i and leave the three variables α , β and w free. We now have to analyze the effects of functions that change the two fixed points by infinitesimal amounts. The functions that change the multiplier w are still the same as before, and the functions that change the fixed points are given by

$$f_{\alpha_j}^{(i)}(\xi_j) = -\frac{\delta\alpha}{\epsilon} \frac{(\xi_j - \beta)^2}{(\alpha - \beta)^2} \quad (3)$$

and

$$f_{\beta_j}^{(i)}(\xi_j) = -\frac{\delta\beta}{\epsilon} \frac{(\xi_j - \alpha)^2}{(\alpha - \beta)^2} \quad (4)$$

respectively.

The measure that results of the inclusion of these new functions is given by

$$\bar{f} = (\alpha\beta)^{N-1} (\alpha - \beta)^{-(N+1)} w^{-2} \left[\prod_{n=1}^{\infty} (1 - w^n) \right]^{-24} \quad (5)$$

The measure depends now on the number of strings that are being scattered.

Actually, the most general functions that change the fixed points α and β are written like

$$f_{\alpha_j}^{(i)}(\xi_j) = \frac{\delta\alpha}{\epsilon} \frac{1}{(\alpha - \beta)^2} [c_\alpha (\xi_j - \alpha)(\xi_j - \beta) - (\xi_j - \beta)^2] \quad ,$$

$$f_{\beta_j}^{(i)}(\xi_j) = \frac{\delta\beta}{\epsilon} \frac{1}{(\alpha - \beta)^2} [c_\beta (\xi_j - \alpha)(\xi_j - \beta) - (\xi_j - \alpha)^2]$$

where c_α and c_β are constants such that $c_\alpha \neq \beta/\alpha$ and $c_\beta \neq \alpha/\beta$. For $c_\alpha \neq 0$, $c_\beta \neq 0$, these solutions imply the measure

$$\bar{f} = (\alpha\beta)^{N-1} (\alpha - \beta)^{-(N+1)} (c_\alpha\alpha - \beta)(c_\beta\beta - \alpha) w^{-2} \left[\prod_{n=1}^{\infty} (1 - w^n) \right]^{-24}$$

This dependence of the measure on arbitrary constants is not yet understood, and may be fixed by some yet unknown feature of the theory.

On Pseudospherically Symmetric Repulsive Gravitational Field

Luis A. Anchordoqui, José D. Edelstein*, Carlos Núñez

Departamento de Física, Universidad Nacional de La Plata

C.C. 67, (1900) La Plata, Argentina

and

Graciela S. Birman*

Departamento de Matemática, Fac. Cs. Exactas, UNCPBA

Pinto 399, (7000) Tandil, Argentina

Received March, 1996

Solutions of Einstein vacuum equations, for a static pseudospherically symmetric system, are presented. They describe a naked singularity and a singular solution with many resemblances to the Schwarzschild solution but with two major differences: its static region, lying inside the null horizon, sees the singularity, and its effective gravitational field is repulsive. We shortly discuss on the phenomenological plausibility of this last solution as a self-consistent system living on a space-time domain, and discuss some features of particle geodesics in its gravitational field.

As a fundamental physical theory, General Relativity is well known for not imposing any constraints on spacetime geometry just but a Lorentzian-manifold structure and Einstein field equations. In specific problems, it may be appropriate to impose additional model-dependent constraints, such as a specific symmetry or asymptotic conditions on the geometry. Thus, the study of Einstein equations and their solutions have attracted so much attention from the point of view of numerical analysis [1] as well as exact solutions coupled to matter [2, 3], solutions in diverse dimensions [4], solitonic solutions [5], etc.

In this contribution, we shall assume the existence of a region in the Universe having spatial pseudospherical symmetry. This region could be thought of as a kind of space-time domain possibly originated in an anisotropy occurred at the Universe expansion. In any case, we shall solve under this hypothesis the Einstein vacuum equations inside the domain, reaching fairly interesting results. We obtain two possible singular solutions depending upon the sign of an integration constant ϖ :

(i) $\varpi < 0$ leads to a naked singularity, while

(ii) $\varpi > 0$ gives rise to a singular space-time with a null-horizon and a repulsive gravitational field. The static region lies inside the horizon and, thus, sees the singularity.

We shall analyse these singular solutions, study particle geodesics in the background metric of solution (ii), and argue on the self-consistency of the resulting effective repulsive gravitational field.

Let us start by considering the Einstein vacuum equations in a space-time domain with spatial pseudospherical symmetry. The solution we shall develop, choosing a pseudospherical gauge, is based on the following metric tensor,

$$g_{\mu\nu} = \text{diag}(e^\nu, -e^\lambda, -r^2, -r^2 e^{2\theta}). \quad (1)$$

In spite of the fact that ν and λ are arbitrary functions of r and t , as in Schwarzschild's case [6], there is a coordinate system where the metric tensor is static, in other words, the universe is stationary for a privileged observer that detects no change in the intrinsic geometry of the space. Concerning θ , it is a pseudospherical parameter valued in the interval $(-\infty, 0]$ [7]. In such a coordinate system, the solution of Einstein vacuum equations reads

$$ds^2 = - \left(1 - \frac{\varpi}{r}\right) dt^2 + \left(\frac{1}{1 - \frac{\varpi}{r}}\right) dr^2 - r^2(d\theta^2 + e^{2\theta} d\phi^2). \quad (2)$$

A naked singularity rises up whenever the integration constant ϖ is negative. We shall consider, in the following, ϖ as a positive constant to be determined from continuity conditions on the boundary of the domain¹. In this

*CONICET

¹Note that as our solution is valid on a bounded region of spacetime, there is no "Newtonian" restriction on the sign of ϖ .

case, it is easily seen from equation (2) that there are pathologies at $r = \infty$ and $r = 0$. In order to clarify about the physical significance of these divergences, let us compute the non-vanishing components of the Riemann tensor. They are simply

$$R_{tr}{}^{tr} = R_{\theta\phi}{}^{\theta\phi} = \frac{\infty}{r^3} \quad \text{and} \quad R_{t\theta}{}^{t\theta} = R_{t\phi}{}^{t\phi} = R_{r\theta}{}^{r\theta} = R_{r\phi}{}^{r\phi} = -\frac{\infty}{2r^3}, \tag{3}$$

showing that an imaginary test observer approaching from infinite must encounter infinite tidal forces at the origin, independently of the route he uses to reach there. This is obvious from the curvature invariant I

$$I \equiv R_{\lambda\eta}{}^{\mu\nu} R_{\mu\nu}{}^{\lambda\eta} = 12 \frac{\infty^2}{r^6}. \tag{4}$$

On the other hand, the Riemann tensor is completely regular at $r = \infty$. Moreover, the proper distance from $r = \infty$ to an arbitrary point r , is well defined in the interval $0 < r < \infty$ as is shown in the following equations

$$\int_{\infty}^r |g_{rr}|^{1/2} dr = [r(r - \infty)]^{1/2} + \infty \ln \left| \left(\frac{r}{\infty} - 1 \right)^{1/2} + \left(\frac{r}{\infty} \right)^{1/2} \right| \tag{5}$$

when $r < \infty$ whereas

$$\int_{\infty}^r |g_{rr}|^{1/2} dr = -\infty \operatorname{arccot} \left[\frac{r^{1/2}}{(\infty - r)^{1/2}} \right] - [r(\infty - r)]^{1/2} \tag{6}$$

when $r > \infty$. It is worthwhile to point out that at $r = \infty$ we have a reversal in the roles of t and r as timelike and spacelike coordinates. The spacetime breaks into two parts, resembling the standard, positive mass, Schwartzschild solution: a time-like static region with the Killing vector in the time direction and a dynamic region with three space-like symmetries; the boundary between these regions, at $r = \infty$, being a null-horizon. One major difference with the Schwartzschild solution is that the static region of the pseudospherical singularity is in the neighbourhood of the origin and, therefore, sees the singularity.

In order to get a deeper insight into the pseudospherical solution, it will be interesting to study the orbits followed by particles immersed in its gravitational field (2). The particle geodesics in this background metric will reveal several interesting features of the pseudospherical singularity. We shall choose the coordinate system in such a way that the radial projection of the orbits coincide with $\theta = 0$. In this oriented coordinate system, the particle will have zero momentum in the θ -direction. The invariances $t \rightarrow t + \Delta t$ and $\phi \rightarrow \phi + \Delta\phi$ define two Killing vectors which we shall identify with the conjugate momenta $p_0 \equiv E$ (particle's energy) and $p_\phi \equiv L$ (an angular momentum-like vector). We will use these conserved quantities, as usual, to obtain a first integral of the equations of motion. Consistency with the equivalence principle, demands test particles to follow the same world line regardless of its mass. Hence the quantities relevant for the motion of particles are: the energy per unit rest mass $E = E/m$ and the ratio $\tilde{L} \equiv L/m$. Taking this into account, the on-shell condition of the particle can be written as

$$-\frac{\tilde{E}^2}{1 - \frac{\infty}{r}} + \frac{1}{1 - \frac{\infty}{r}} \left(\frac{dr}{d\tau} \right)^2 - \frac{\tilde{L}^2}{r^2} - 1 = 0, \tag{7}$$

or, equivalently,

$$\left(\frac{dr}{d\tau} \right)^2 = \tilde{E}^2 - \tilde{V}_{\text{eff}}^2, \tag{8}$$

with the effective potential given by

$$\tilde{V}_{\text{eff}}^2 = \left(\frac{\infty}{r} - 1 \right) \left(\frac{\tilde{L}^2}{r^2} + 1 \right). \tag{9}$$

Interestingly enough, we see that the effective potential is repulsive for $\tilde{L} = 0$ while, contrary to the usual cases, the "centrifugal" term of \tilde{V}_{eff}^2 gives rise to an attractive contribution to the effective potential. We will come back to this striking point later.

The turning point R can be obtained by setting $dr/d\tau = 0$. For a given energy \tilde{E}_0 , restricting ourselves to radial motion ($\tilde{L} \equiv 0$) this results in

$$R = \frac{\infty}{\tilde{E}_0^2 + 1}. \tag{10}$$

Then, the proper time can be simply expressed, from eq.(8), as

$$\tau = \int \frac{dr}{\infty^{1/2}} \left(\frac{1}{R} - \frac{1}{r} \right)^{-1/2}. \tag{11}$$

This integral can be evaluated using the suitable change of variables

$$r = \frac{R}{2}(1 + \cosh \eta), \quad (12)$$

in such a way that the 'proper time' it takes a particle to travel from $r = R$ to $r = 4\varpi^2$ is a finite quantity given by

$$\tau = \frac{R}{2} \sqrt{\frac{R}{\varpi}} \left\{ \operatorname{arccosh} \left(\frac{8\varpi}{R} - 1 \right) + 4 \sqrt{\frac{\varpi}{R}} \left(\frac{4\varpi}{R} - 1 \right) \right\}. \quad (13)$$

In fact, this quantity should be referred to as a proper distance, being calculated inside the dynamical region. In order to compute the 'coordinate time' taken by the particle to reach the null-horizon, it will be useful to introduce appropriate "tortoise coordinates" [8]

$$r^* = -\{r + \varpi \ln(\varpi - r)\} \quad \text{such that} \quad \frac{dr}{dr^*} \equiv \tilde{E} \frac{dr^*}{dt}. \quad (14)$$

It is easy to see from (9) that $\tilde{E}^2 - \tilde{V}_{\text{eff}}^2 \cong \tilde{E}^2$ near $r = \varpi$. Then, after (8) and (14), $dr^*/dt \cong 1$. Thus,

$$r^* = -\{r + \varpi \ln(\varpi - r)\} \cong \varpi \ln(\varpi - r). \quad (15)$$

or, equivalently,

$$r = \varpi - Ce^{-r^*/\varpi}, \quad (16)$$

with $C \equiv \text{constant}$. It can be seen from equations (9) and (14) that the approach of \tilde{V}_{eff}^2 to zero as $r \rightarrow \varpi$ is seen to be exponential in r^* . In the same vein, equation (16) shows that it takes infinite 'coordinate time' to arrive at $r = \varpi$.

Let us briefly discuss, at this point, about the repulsive nature of the pseudospherical solution. It has certainly appeared from the lack of a 'Newtonian' restriction on the bounded region of space-time given by the spatial pseudospherically symmetric domain. This domain can be thought of as a kind of structure that might have appeared in the early universe generating a disconnected region, still unobserved, with pseudospherical geometry. It is important to stress that this symmetry could be generated by a mass distribution external to the domain. This fact is not forbidden, in principle, by Birkhoff's theorem which does not apply whenever symmetries are not spherical. The boundary of the domain could be inside the horizon, this leading to the appearance of a naked singularity.

The main challenge posed by this singular pseudospherically symmetric solution should be to find a matter system that would be able to generate this odd gravitational field, and to carefully study how it smoothly glues with regular solutions outside the domain. This is, of course, a hard problem that should be fulfilled in order to give complete consistency to our pseudospherical solution into a 'Newtonian'-like universe. The study of this issue, as well as a complete analysis of particle geodesics in the background metric of the pseudospherical singularity, is being completed [9]. We hope to be able to give an answer to the matching-conditions problem in the boundary of the domain in a forthcoming work.

We would like to thank Héctor Vucetich for a critical reading of the manuscript.

References

- [1] See, for example, Ph. Papadopoulos and P. Laguna, "Numerical Solutions of Mixed value problems: Investigations in Spherical Symmetry", talk delivered at 14th International Conference on General Relativity and Gravitation, Florence, Italy, 1995.
- [2] See, for example, A. R. Roy and P. K. Maiti, *Astrophys. Space Sci.* **205** (1993) 277.
- [3] A. Rendal, "Solutions of Einstein equation with matter", to appear in the GR14 Conference Proceedings, gr-qc 9505017.
- [4] L. Anchordoqui, G. Birman, S. Perez Bergliaffa and H. Vucetich, *Gen. Rel. Grav.*, in press.
- [5] R. Bartnik and J. McKinnon, *Phys. Rev. Lett.* **61** (1988) 141.
- [6] See, for example, *Théorie des Champs*, L. Landau et E. Lifchitz, (Éditions Mir 1970); §97.
- [7] See, for example, *Differential Geometry*, L. P. Eisenhart, (Princeton Mathematical Series, Princeton University Press, 1940); §49.
- [8] See, for example, *Gravitation*, C. W. Misner, K. S. Thorne, and J. A. Wheeler, (Freeman, San Francisco, 1973); §25.5.
- [9] L. A. Anchordoqui, J.D. Edelstein, C. Núñez and G. S. Birman, in preparation.

²We consider $r = 4\varpi$ a radius where the particle is far away from the influence of the potential.

Scalar-Time Parametrization of Klein-Gordon Equation: The Harmonic Oscillator Solution

Luis A. Anchordoqui^a, Ana G. Grunfeld^a and Mario C. Rocca^{a,b}

^a*Departamento de Física, Universidad Nacional de La Plata
C.C. 67. (1900) La Plata, Argentina*

^b*Departamento de Matemática, Fac. Cs. Exactas, U.N.C.P.B.A.
Pinto 399, (7000) Tandil, Argentina*

The implications of a manifestly covariant formulation of relativistic quantum mechanics depending on a scalar evolution parameter, canonically conjugated to the variable mass, is still an unsettled issue. In this work we find the harmonic oscillator solution in the above mentioned formulation, and we briefly comment on some models where this solution could be applied.

In a fine set of papers, Dirac introduced the idea of elevating the time coordinate x^0 to the rank of operator [1]. The proper time formalism introduces an absolute evolution parameter (related to the proper time in the classical limit), which parametrizes the dynamics of the quantum system [2]. The basic idea of these works, which have probably fallen into oblivion because Dirac himself did not insist on it in his celebrated paper of 1928 [3], shortly returned to view with Feynman and Stückelberg antiparticles interpretation as particles moving backward in time [4, 5]. Since then, various works have appeared in the literature [6, 7, 8, 9, 10, 11], but the precise interpretation of the additional parameter, poses a puzzle to physics which is still unresolved. We shall adopt here, the Collins and Fanchi (CF) formalism [8]. In this scenario, we work out the harmonic oscillator solution of the Klein-Gordon (KG) equation.

We hope that this generalized quantum relativistic mechanics for spinless particles could be applied to current problems in contemporary physics, such as the production of charmed mesons in the frame of Color Transparency [12] and a bound systems of two dyons [13]. Quantum mechanical features of Color Transparency have been studied considering the non-relativistic evolution of a $c\bar{c}$ pair produced, as a small wave packet, inside the nucleus. The interaction between the pair of quarks has been modeled by using a harmonic oscillator hamiltonian [12]. Since relativistic effects are important in this phenomenon, we think it is interesting to apply the scalar time parametrization of the Klein-Gordon oscillator to the non-relativistic model. A similar treatment could be applied to the case of bound system of two dyons which has been studied in [13] with a non-relativistic quantum isotropic oscillator.

Let us briefly sum up the characteristic of the formalism. The square of the amplitude of the wave function Ψ must be interpreted as the probability of an event corresponding to the position of a particle at a particular time. It is worthwhile to point out that the latter interpretation differs from the usual one due to that there is a probability distribution associated with time. Therefore, for each t there is a probability that a particle may or may not be found somewhere in space. This seems to be reasonable, since particles such as mesons have finite lifetimes. Then, the mean value of the position operator \hat{x} , can be written as

$$\langle x^\mu \rangle = \int_{ST} x^\mu \rho d^4x \quad (1)$$

where ρ is a distribution on the spacetime manifold satisfying the two following conditions:

$$\rho > 0 \quad \text{and} \quad \int_{ST} \rho d^4x = 1$$

with integration understood in the Lebesgue sense, over the entire spacetime manifold.

Taking this into account, the on-shell condition must be understood as the expectation value of the $p^\mu p_\mu$ operator. As shown by CF, the aforementioned operator is proportional to $\partial/\partial\tau$, and the light-cone constraint identifies τ with the classical proper time [8]. Thereby, the free particle equation, in natural units, is given by

$$i 2 \bar{m} \frac{\partial \Psi}{\partial \tau} = H \Psi \tag{2}$$

here $H = p^\mu p_\mu$ and \bar{m} is defined as the classical limit of the $p^\mu p_\mu$ expectation value.

Our purpose is to work out the relativistic spinless harmonic oscillator in the frame of the formalism we have commented. The hamiltonian for the relativistic harmonic oscillator was studied by Moshinsky and Szczepaniak [14]. They proposed a new type of interaction in the Dirac equation, linear in coordinates and momentum. The corresponding equation has been named "Dirac Oscillator" because in the non-relativistic limit the harmonic oscillator has been obtained. This kind of interaction was introduced in the Klein-Gordon equation [15, 16]. To get a closed form for the extended relativistic harmonic oscillator hamiltonian, we present first the Klein-Gordon oscillator developed in the Bruce [15] formalism together with the Sakata-Taketani approach [17]. The latter selection determines the following KG equation

$$(\square + m^2 \omega^2 r^2 - 3 m \omega + m^2) \Psi = 0 \tag{3}$$

Now, we want to work out this equation in the frame of the scalar time parametrization taking into account the above definition of the $p^\mu p_\mu$ operator and considering a probability distribution associated with time. To solve this equation we shall consider the wave function $\Psi(x_\mu, \tau)$ as an element of the space of exponentially increasing distributions Λ_∞ [18]. The Fourier transform space in the variable τ , is defined as a tempered ultradistribution U [18, 19, 20]. We can define $(i 2 \bar{m} \frac{\partial}{\partial \tau})^{1/2}$ operating over a Λ_∞ distribution as follows [21]:

$$\left(i 2 \bar{m} \frac{\partial}{\partial \tau}\right)^{1/2} f(\tau) = \mathcal{F}^{-1} \{ \alpha^{1/2} \hat{f}(\alpha) \} \tag{4}$$

where

$$\hat{f}(\alpha) = \mathcal{F} \{ f(\tau) \} \tag{5}$$

With all these requirements eq. (3), takes the form:

$$\left[\square + 2 \bar{m} i \omega^2 r^2 \frac{\partial}{\partial \tau} - 3 \omega \left(2 \bar{m} i \frac{\partial}{\partial \tau} \right)^{1/2} + 2 i \bar{m} \frac{\partial}{\partial \tau} \right] \Psi = 0 \tag{6}$$

Thus, taking into account the Fourier transform, equation (6) could be written as follows :

$$\int_\Gamma \left(\square + \omega^2 r^2 \alpha - 3 \omega \alpha^{1/2} + \alpha \right) \hat{\Psi}_c(x_\mu, \alpha) e^{-\frac{i \omega}{\bar{m}} \tau} d\alpha = 0 \tag{7}$$

where Γ is the usual path which surrounds all the singularities of $\hat{\Psi}_c$ placed on a $2K$ wide band that encircles the real axis. The path Γ runs from $-\infty$ to ∞ along $\text{Im}(z) > K$ and from ∞ to $-\infty$ along $\text{Im}(z) < -K$. Defining the operator

$$\square + \omega^2 r^2 \alpha - 3 \omega \alpha^{1/2} + \alpha = L \tag{8}$$

equation (7) reads,

$$L \hat{\Psi}_c(x_\mu, \alpha) = a(x_\mu, \alpha) \tag{9}$$

where $a(x_\mu, \alpha)$ is an entire analytical function in the variable α . Thus,

$$\hat{\Psi}_c(x_\mu, \alpha) = \hat{f}_c(x_\mu, \alpha) + L^{-1}a(x_\mu, \alpha) \tag{10}$$

with \hat{f}_c a general solution of the homogeneous system,

$$L.\hat{f}_c(x_\mu, \alpha) = 0 \tag{11}$$

The boundary condition we shall impose is to set the entire analytical function ($a(x_\mu, \alpha)$) equal to zero; with this condition we ensure that for a fixed $\alpha > 0$ we obtain the same energy spectrum as in the usual KG formalism. Therefore we obtain,

$$\int_{\Gamma} \left(\square + \omega^2 r^2 \alpha - 3\omega \alpha^{1/2} + \alpha \right) \hat{f}_c(x_\mu, \alpha) e^{-\frac{3\omega}{2\alpha} \tau} d\alpha = 0 \tag{12}$$

On the real axis this expression takes the form,

$$\int_{-\infty}^{+\infty} \left[\left(\square + \omega^2 r^2 \alpha - 3\omega(\alpha + i0)^{1/2} + \alpha \right) \hat{f}_c(x_\mu, \alpha + i0) - \left(\square + \omega^2 r^2 \alpha - 3\omega(\alpha - i0)^{1/2} + \alpha \right) \hat{f}_c(x_\mu, \alpha - i0) \right] e^{-\frac{3\omega}{2\alpha} \tau} d\alpha = 0 \tag{13}$$

If we impose to \hat{f}_c to satisfy the equality

$$\int_{-\infty}^0 \left[(\alpha + i0)^{1/2} \hat{f}_c(x_\mu, \alpha + i0) - (\alpha - i0)^{1/2} \hat{f}_c(x_\mu, \alpha - i0) \right] e^{-\frac{3\omega}{2\alpha} \tau} d\alpha = 0 \tag{14}$$

equation (13) reads,

$$\int_0^{+\infty} \left(\square + \omega^2 r^2 \alpha - 3\omega \alpha^{1/2} + \alpha \right) \left[\hat{f}_c(x_\mu, \alpha + i0) - \hat{f}_c(x_\mu, \alpha - i0) \right] e^{-\frac{3\omega}{2\alpha} \tau} d\alpha + \int_{-\infty}^0 \left(\square + \omega^2 r^2 \alpha + \alpha \right) \left[\hat{f}_c(x_\mu, \alpha + i0) - \hat{f}_c(x_\mu, \alpha - i0) \right] e^{-\frac{3\omega}{2\alpha} \tau} d\alpha = 0 \tag{15}$$

Next, we define as in ref. [19, 18]

$$\hat{f}(x_\mu, \alpha) = \hat{f}_c(x_\mu, \alpha + i0) - \hat{f}_c(x_\mu, \alpha - i0) \tag{16}$$

Bearing this in mind, our system can be reduced to

$$\left(\square + \omega^2 r^2 \alpha - 3\omega \alpha^{1/2} + \alpha \right) \hat{f}(x_\mu, \alpha) = 0 \quad \alpha > 0 \tag{17}$$

$$\left(\square + \omega^2 r^2 \alpha + \alpha \right) \hat{f}(x_\mu, \alpha) = 0 \quad \alpha < 0 \tag{18}$$

which is solved using the standard procedure of quantum mechanics. Thus, introducing $\hat{f} = e^{-iEt} \varphi$, eq. (17) becomes

$$\left(-\Delta + \alpha \omega^2 r^2 - 3\alpha^{1/2} \omega + \alpha \right) \varphi = E^2 \varphi \tag{19}$$

The eigenfunctions that satisfy the last equation are:

$$\begin{aligned} \varphi_{\alpha, N_1, N_2, N_3} &= A_{\alpha, N_1, N_2, N_3} e^{-\alpha^{1/2}(x^2 + y^2 + z^2) \omega^2 / 2} \\ &\times H_{N_1}(\sqrt{\alpha^{1/2} \omega} x) H_{N_2}(\sqrt{\alpha^{1/2} \omega} y) H_{N_3}(\sqrt{\alpha^{1/2} \omega} z) \end{aligned} \tag{20}$$

where H_{N_i} , $i = 1, 2, 3$ are Hermite polynomials and E satisfies,

$$E^2 - 2(N_1 + N_2 + N_3) \alpha^{1/2} \omega + \alpha = 0 \tag{21}$$

with $N_i \in \mathcal{N}$ (natural numbers) ($i = 1, 2, 3$).

Finally we obtain for $\hat{\Psi}$

$$\hat{\Psi}_{\alpha N_1 N_2 N_3} = A_{\alpha N_1 N_2 N_3} e^{-i\alpha\tau/2\bar{m}} e^{-iE(\alpha, N_1, N_2, N_3)t} e^{-(x^2 + y^2 + z^2)\alpha^{1/2}\omega^2/2} \times H_{N_1}(\sqrt{\alpha^{1/2}\omega}x) H_{N_2}(\sqrt{\alpha^{1/2}\omega}y) H_{N_3}(\sqrt{\alpha^{1/2}\omega}z) \tag{22}$$

with $A_{\alpha N_1 N_2 N_3}$ the normalization constant given by

$$A_{\alpha N_1 N_2 N_3} = \frac{\alpha^{1/2}\omega}{\pi} \frac{1}{\sqrt{2\pi\bar{m}} 2^{(N_1 + N_2 + N_3)/2} (N_1! N_2! N_3!)^{1/2}} \tag{23}$$

We now turn to the calculation of Ψ in the case $\alpha < 0$. The equation (18) is now

$$(-\Delta + \alpha\omega^2 r^2 + \alpha)\varphi = E^2\varphi \tag{24}$$

This equation has the following eight independent solutions:

$$\Phi_{\alpha E_1 E_2 E_3}(x, y, z) = \begin{cases} x y z & \Phi_{E_1}(x) \Phi_{E_2}(y) \Phi_{E_3}(z) \\ x y & \dot{\Phi}_{E_1}(x) \Phi_{E_2}(y) \Phi'_{E_3}(z) \\ x z & \Phi_{E_1}(x) \Phi'_{E_2}(y) \Phi_{E_3}(z) \\ x & \Phi_{E_1}(x) \Phi'_{E_2}(y) \Phi'_{E_3}(z) \\ y z & \dot{\Phi}'_{E_1}(x) \dot{\Phi}_{E_2}(y) \Phi_{E_3}(z) \\ y & \dot{\Phi}'_{E_1}(x) \Phi_{E_2}(y) \Phi'_{E_3}(z) \\ z & \dot{\Phi}'_{E_1}(x) \dot{\Phi}'_{E_2}(y) \Phi_{E_3}(z) \\ & \Phi'_{E_1}(x) \Phi'_{E_2}(y) \Phi'_{E_3}(z) \end{cases} \tag{25}$$

with

$$\dot{\Phi}_{E_1\alpha}(x) = \Phi\left(\frac{3}{4} + \frac{i(E_1^2 - \frac{\alpha}{3})}{4(-\alpha)^{1/2}\omega}, \frac{3}{2}, i\sqrt{-\alpha}\omega x^2\right) \tag{26}$$

$$\dot{\Phi}_{E_2\alpha}(y) = \Phi\left(\frac{3}{4} + \frac{i(E_2^2 - \frac{\alpha}{3})}{4(-\alpha)^{1/2}\omega}, \frac{3}{2}, i\sqrt{-\alpha}\omega y^2\right) \tag{27}$$

$$\dot{\Phi}_{E_3\alpha}(z) = \Phi\left(\frac{3}{4} + \frac{i(E_3^2 - \frac{\alpha}{3})}{4(-\alpha)^{1/2}\omega}, \frac{3}{2}, i\sqrt{-\alpha}\omega z^2\right) \tag{28}$$

$$\dot{\Phi}'_{E_1\alpha}(x) = \Phi\left(\frac{1}{4} + \frac{i(E_1^2 - \frac{\alpha}{3})}{4(-\alpha)^{1/2}\omega}, \frac{1}{2}, i\sqrt{-\alpha}\omega x^2\right) \tag{29}$$

$$\dot{\Phi}'_{E_2\alpha}(y) = \Phi\left(\frac{1}{4} + \frac{i(E_2^2 - \frac{\alpha}{3})}{4(-\alpha)^{1/2}\omega}, \frac{1}{2}, i\sqrt{-\alpha}\omega y^2\right) \tag{30}$$

$$\dot{\Phi}'_{E_3\alpha}(z) = \Phi\left(\frac{1}{4} + \frac{i(E_3^2 - \frac{\alpha}{3})}{4(-\alpha)^{1/2}\omega}, \frac{1}{2}, i\sqrt{-\alpha}\omega z^2\right) \tag{31}$$

where $\Phi(\alpha, \beta, s)$ are the degenerate hypergeometric functions [22] and $E_1^2 + E_2^2 + E_3^2 = E^2$ are real numbers. Thus we obtain for $\hat{\Psi}$ the expression:

$$\Psi_{N_1 N_2 N_3 \alpha} = A_{N_1 N_2 N_3 \alpha} e^{-i\alpha\tau/2\bar{m}} e^{-iEt} e^{-i(x^2 + y^2 + z^2)\sqrt{-\alpha}\omega/2} \dot{\Phi}_{\alpha E_1 E_2 E_3}(x, y, z) \tag{32}$$

with

$$A_{\alpha E_1 E_2 E_3} = (|E_1||E_2||E_3|) \frac{\left|\Gamma\left(\frac{1}{4} + \frac{i(E_1^2 - \alpha/3)}{4(-\alpha)^{1/2}\omega}\right)\right| \left|\Gamma\left(\frac{1}{4} + \frac{i(E_2^2 - \alpha/3)}{4(-\alpha)^{1/2}\omega}\right)\right| \left|\Gamma\left(\frac{1}{4} + \frac{i(E_3^2 - \alpha/3)}{4(-\alpha)^{1/2}\omega}\right)\right|}{2^{5\pi/2}\omega^{3/2}(-\alpha)^{3/4}\bar{m}^{1/2}} \tag{33}$$

This functions can be normalized to

$$\delta(\alpha - \alpha')\delta(E_1 - E'_1)\delta(E_2 - E'_2)\delta(E_3 - E'_3) \quad (34)$$

Finally the general solution is given by

$$\begin{aligned} \Psi(\mathbf{x}_\mu, \tau) = & \int_0^\infty d\alpha \sum_{N_1 N_2 N_3} C_{\alpha N_1 N_2 N_3} e^{-i E(\alpha N_1 N_2 N_3) t} e^{-i \alpha \tau / 2 \bar{m}} e^{-i(x^2 + y^2 + z^2) \sqrt{-\alpha} \omega / 2} \\ & \times H_{N_1}(\sqrt{\alpha^{1/2} \omega} x) H_{N_2}(\sqrt{\alpha^{1/2} \omega} y) H_{N_3}(\sqrt{\alpha^{1/2} \omega} z) + \\ & \int_{-\infty}^0 d\alpha \int_{-\infty}^{+\infty} dE_1 dE_2 dE_3 C_{\alpha N_1 N_2 N_3} e^{-i \sqrt{E_1^2 + E_2^2 + E_3^2} t} \\ & \times e^{-i \alpha \tau / 2 \bar{m}} e^{-i(x^2 + y^2 + z^2) \sqrt{-\alpha} \omega / 2} \phi_{\alpha E_1 E_2 E_3}(x, y, z) \end{aligned} \quad (35)$$

Summing up, with the help of tempered ultradistributions and their inverse Fourier transform space (exponentially increasing distributions), we have presented the complete set of eigenfunctions for the harmonic oscillator KG equation in the proper time formalism. It is possible to select $a(x_\mu, \alpha) = 0$ to obtain for fixed $\alpha > 0$, as a particular case, the energy spectrum which coincides with the usual KG harmonic oscillator solution, identifying $m = \alpha^{1/2}$ (being m the mass of the oscillator). This can be deduced from the dispersion relation (see eq. (21)). The eigenfunctions given by eq. (20) are the same of those for the usual KG harmonic oscillator. Contrary to the usual KG formalism, in the proper time model, solutions for negative values of α do exist. These solutions represent tachyonic particles. On the contrary to the usual quantum field theory, solutions with $\alpha < 0$ are well-behaved in the sense that they are oscillating (as for a normal bradyonic particle), instead of exponentially increasing.

We are grateful to L. Epele, H. Fanchiotti and C. García Canal for fruitful discussions. We also knowlege C. Naón, S. Perez Bergliaffa and D. Torres for insightful comments and critical reading of the manuscript.

References

- [1] P. A. M. Dirac, *Proc. R. Soc. London, Ser. A* **110**, 405 (1926); **110**, 661 (1926).
- [2] For an update see: L. P. Horwitz, *Time and the Evolution of States in Relativistic Classical and Quantum Mechanics*, talk to be delivered at the conference on Physical Interpretation of Relativity Theory, Imperial College, 6-9 September, 1996 ([hep-ph/9606330](#)), and references therein.
- [3] P. A. M. Dirac, *Proc. R. Soc. London, Ser. A* **117**, 610 (1928).
- [4] R. P. Feynman, *Phys. Rev.* **84**, 108 (1951).
- [5] E. C. G. Stückelberg, *Helv. Phys. Acta* **14**, 558 (1941); **15**, 23 (1942). See also Fock.
- [6] J. P. Aparicio, F. H. Gaioli and E. T. Garcia Alvarez, *Phys. Rev. A* **51**, 96 (1995).
- [7] J. P. Aparicio, F. H. Gaioli and E. T. Garcia Alvarez, *Phys. Lett. A* **200**, 233 (1995).
- [8] R. E. Collins, J. R. Franchi, *Nuovo Cimento A* **48**, 314 (1978).
- [9] P. N. Kaloyerou and J. P. Vigiér, *J. Phys. A* **22**, 663 (1989).
- [10] P. M. Pearle, *Phys. Rev.* **168**, 1429 (1968).
- [11] A. Kyprianidis, *Phys. Rep.* **155**, 2 (1987);
- [12] J. P. Blaizot, R. Venugopalan, M. Prakash, *Phys. Rev. D* **45**, 814 (1992).
- [13] V. M. Ter-Antonyan, A. Nersessian, [hep-th/9508137](#).
- [14] M. Moshinsky and A. Szczepaniak, *J. Phys. A* **22**, L817 (1989);
- [15] S. Bruce, P. Minning *Nuovo Cim. A* **106**, 711 (1993).
- [16] V. Dvoeglazov, Preprint EPUAZ 94-02
- [17] S. Sakata and M. Taketani, *Proc. Phys. Mat. Soc (Japan)* **22**, 757 (1940).

- [18] M. Hasumi, *Tohoku Math. J* **13**, 94 (1961).
- [19] J. Sebastião e Silva, *Math. Ann.* **36**, 38 (1958).
- [20] M. Marimoto, *Proc. Japan Acad* **51**, 87 (1975); **51**, 213 (1975).
- [21] D. G. Barci, C. G. Bollini, L. E. Oxman and M. C. Rocca, hep-th/9606183.
- [22] I.S. Gradshteyn and I.M. Ryzhik, *Table of integrals, series and products*, (corrected and enlarged edition. Academic Press, Inc. 1980).

More on Renormalization Ambiguities: Effective Action and Mode Summation

Luiz C. de Albuquerque*

*Instituto de Física, Universidade de São Paulo
P.O. Box 66318, 05389-970 São Paulo, SP, Brazil*

The one-loop effective action is formally equivalent to the summation of the energies associated with the vacuum fluctuations of the quantum field. However, renormalization effects may introduce an anomalous scale dependence in the one-loop effective action, and also in the summation of zero-point energies. Recently, it has been argued that these two methods lead to distinct results for the Casimir energy. We show that the one-loop effective action is completely equivalent to the zero-point energy summation, working in a regularized way since beginning. Hence, we clarify some statements made earlier in the literature.

In 1948 Casimir [1] showed that two neutral perfectly conducting parallel plates placed in the vacuum attract each other, due to zero-point oscillations of the electromagnetic field (field strength fluctuations). His starting point resembles an old idea of Euler and Heisenberg [2]. They used the zero-point oscillations of the Dirac field (charge fluctuations) in an external field to define an effective action to the electromagnetic field. The common feature is the summation of the energies associated with the vacuum fluctuations of the constrained quantum field to define the vacuum energy and the effective action. Later, the notion of effective action was elaborated, first as the generating functional of 1PI Green's functions, and nowadays as any effective theory which reproduces the full theory over some energy (distance) scale [3]. Indeed, the effective action at one-loop order is formally equivalent to the older definition of Euler and Heisenberg [4], and so the vacuum energy calculated from it is also formally the same as that embodied in the Casimir argument.

However, due to renormalization effects the complete equivalence of these two definitions is not straightforward. Recently [5], it has been argued that the effective potential method is more reliable than the mode summation (MS) approach in the computation of the vacuum energy. Myers pointed out that in some cases the MS approach neglects a scale dependent contribution. Almost at the same time, another group [6] stated the opposite: that the vacuum energy calculated from the MS approach is more general than the effective potential calculation. In this paper, we use the scalar vacuum energy example to show the complete equivalence between the two definitions of "effective action" (one-loop 1PI and MS), working in a regularized way since the beginning. However, the proof is general and can be extended to other situations, as for example external field calculations in QED.

1. Let $\phi(x)$ be a real massive scalar field, with a $\lambda\phi^4/4!$ self-coupling¹. The one-loop effective potential is given by a bosonic determinant²

$$V^{(1)}(\bar{\phi}) = -\frac{i}{2} \ln \det_k \left(\frac{\mathcal{O}}{\mu^2} \right), \quad (1)$$

where $\mathcal{O}(\bar{\phi}) = k^2 - M^2$, $M^2 \equiv m^2 + \frac{\lambda}{2}\bar{\phi}^2$, $\bar{\phi}$ is a constant background field, and μ is a mass scale used to normalize the determinant. The determinant in (1) is meaningless, unless some regularization is adopted. We will use the generalized zeta function technique [7].

*e-mail: claudio@snfma2.if.usp.br

¹ $D = d + 1$, flat space-time with signature $(+, -, \dots, -)$.

²Note that $\ln \det \mathcal{A}_{x,y} = \text{Tr} \ln \mathcal{A}_{x,y} = \Omega_D \text{Tr}_k \ln \mathcal{A}_k$, where Ω_D is a D -dimensional normalization volume, and k denotes "momentum space".

$$\det_k \left(\frac{\mathcal{O}}{\mu^2} \right) = \exp \left[-\frac{\partial}{\partial s} \zeta_{\frac{\mathcal{O}}{\mu^2}}(s) \Big|_{s=0} \right] \tag{2}$$

$$= (\mu^2)^{-\zeta_{\mathcal{O}}(0)} \exp \left[-\frac{\partial}{\partial s} \zeta_{\mathcal{O}}(s) \Big|_{s=0} \right]. \tag{3}$$

where

$$\zeta_{\frac{\mathcal{O}}{\mu^2}}(s) = \text{Tr}_k \left(\frac{\mathcal{O}}{\mu^2} \right)^{-s} \equiv \int \left(\lambda_n \mu^{-2} \right)^{-s} \tag{4}$$

is the generalized zeta function associated with the D -dimensional operator \mathcal{O} , whose eigenvalues we denote by λ_n . For instance, taking Dirichlet boundary conditions (DBC) in x_1 , $\phi(\bar{x}, x_1 = 0) = 0 = \phi(\bar{x}, x_1 = L)$, we have the discrete set $k_1 = \frac{\pi n}{L}$, plus plane waves in the other $d = D - 1$ dimensions.

The minimum of the effective potential gives the vacuum energy density. Since $m^2 > 0$, this is given by ³

$$\mathcal{E}_0(L) = V^{(1)}(\dot{\phi} = 0) = \frac{i}{2} \frac{\partial}{\partial s} \zeta_D(s; \mu) \Big|_{s=0} = \frac{i}{2} \left[\zeta_D'(0) + \zeta_D(0) \ln \mu^2 \right]. \tag{5}$$

In the specific case of DBC, the generalized zeta function reads

$$\zeta_D(s; \mu) = \frac{1}{(2\pi)^D L} \sum_{n=1}^{\infty} \int_{-\infty}^{\infty} d^d \bar{k} \left[\frac{\bar{k}^2 - \left(\frac{\pi n}{L} \right)^2 - m^2}{\mu^2} \right]^{-s} \tag{6}$$

where $d^d \bar{k} = dk_0 dk_2 \dots dk_d$, and $\bar{k}^2 \equiv k_0^2 - k_1^2$.

The representation given by (6) is valid only for a definite range of the complex parameter s . However, an analytical continuation to the whole complex plane is possible, and indeed must be done before one takes the limit $s \rightarrow 0$. One major virtue of the so-called zeta function method [7] is that $\zeta_D(s)$ is analytic at $s = 0$ for most interesting operators in field theoretical problems. In particular, for an elliptic, positive second-order operator, $\zeta_D(s)$ is a meromorphic function with only simple poles. Thus, $\mathcal{E}_0(L)$ defined in (5) is a finite quantity.

Let us integrate over k_0 . This gives

$$\zeta_D(s; \mu) = (-1)^{1/2-s} \frac{\sqrt{\pi} \mu}{(2\pi)^d L} \frac{\Gamma(s-1/2)}{\Gamma(s)} \sum_{n=1}^{\infty} \int_{-\infty}^{\infty} d\bar{k}_\perp \left[\frac{\bar{k}_\perp^2 + \left(\frac{\pi n}{L} \right)^2 + m^2}{\mu^2} \right]^{1/2-s} \tag{7}$$

Using now (5), we obtain for $\mathcal{E}_0(L)$:

$$\mathcal{E}_0(L) = \frac{1}{2} \mu \frac{\partial}{\partial s} \left\{ \frac{1}{\Gamma(s)} f(s) \int \left(\lambda_n \mu^{-2} \right)^{1/2-s} \right\}_{s=0} = \frac{1}{2} \mu \frac{\partial}{\partial s} \left\{ \frac{1}{\Gamma(s)} f(s) \zeta_d(s-1/2; \mu) \right\}_{s=0} \tag{8}$$

$$f(s) \equiv -\frac{\Gamma(s-1/2)}{2\sqrt{\pi}}, \quad \int = \frac{1}{L} \sum_{n=1}^{\infty} \int_{-\infty}^{\infty} \frac{d\bar{k}_\perp}{(2\pi)^{d-1}}.$$

where $\lambda_n \equiv \bar{k}_\perp^2 + \left(\frac{\pi n}{L} \right)^2 + m^2$ are the eigenfrequencies associated with the d -dimensional (reduced) operator $\hat{\mathcal{O}}$.

For a function $F(s)$ analytic at $s = 0$, we use the approximation $1/\Gamma(s) \approx s + \gamma s^2 + O(s^3)$ to deduce that $\frac{\partial}{\partial s} \frac{F(s)}{\Gamma(s)} \Big|_{s=0} = F(0)$. Hence, suppose that $\zeta_d(s-1/2; \mu)$ is analytic at $s = 0$: Then, we will obtain $f(0) = 1$, and $\omega_n = \lambda_n^{1/2}$

$$\mathcal{E}_0(L) = \frac{1}{2} \mu \zeta_d(-1/2; \mu) = \frac{1}{2} \int \omega_n. \tag{9}$$

³The simplified notation is: $\frac{\partial}{\partial s} \zeta_{\frac{\mathcal{O}}{\mu^2}}(s) \Big|_{s=0} \equiv \zeta_D'(0; \mu)$.

This is exactly the non-regulated MS expression for the vacuum energy, written as a sum of zero-point energies. Of course, (8) is only another way to write (5). However, formula (8) is also a regularized expression for the vacuum energy in a MS like form. The UV divergences, associated with the high-frequency modes in (9), manifests as poles in $\zeta_d(s - 1/2; \mu)$ when we put $s = 0$. Thus, in general, $\zeta_d(s - 1/2; \mu)$ is not regular at $s = 0$ ⁴.

To see this, we make a Mellin transform to relate the generalized zeta function to the trace of the heat kernel, $Y(t) \equiv \text{tr} e^{-t\hat{c}\mu^{-2}}$. As is known [9], the heat kernel possesses an asymptotic expansion for small t . Using this expansion, we get the pole structure of $\zeta_d(s; \mu)$ [6]

$$\zeta_d(s; \mu) = \frac{1}{(4\pi)^{d/2}\Gamma(s)} \left\{ \sum_0^\infty \frac{C_j}{s - (d/2 - j)} + f(s) \right\}. \tag{10}$$

$f(s)$ is an entire analytic function of s . Hence, we see that $\zeta_d(s; \mu)$ is a meromorphic function of s , having only simple poles with residua given by the coefficients C_j .

In particular, coming back to eq. (8), we obtain

$$\begin{aligned} \mathcal{E}_0(L) &= \frac{\mu}{2(4\pi)^{D/2}} \frac{\partial}{\partial s} \frac{1}{\Gamma(s)} \left\{ \sum_{j \neq D/2}^\infty \frac{C_j}{s - (D/2 - j)} + f(s - 1/2) + \frac{C_{D/2}}{s} \right\} \\ &= \bar{\mathcal{E}}_0(L) - \frac{\mu}{2(4\pi)^{D/2}} \psi(1) C_{D/2}(\mu). \end{aligned} \tag{11}$$

One conventional choice is to define the Casimir energy (density) as [8]

$$\mathcal{E}_c = \mathcal{E}_0(L) - \mathcal{E}_0(L_0), \tag{12}$$

where L_0 is some "normalization" set (sometimes, $L_0 = \infty$).

The Casimir energy defined by (11) and (12) will, in general, depend on the scale μ , when $C_{D/2} \neq 0$. For conformally invariant theories in flat space-time and flat parallel plates, $C_{D/2} = 0$ and μ disappears identically. Even in the massive case, however, the definition (12) can remove this dependence. But in general we expect a dependence on μ in the Casimir energy. For example, in an ultrastatic space-time with $ds^2 = (dx_0)^2 - g_{ij}(\vec{x})dx^i dx^j$, we decompose the differential operator $\square \equiv g^{\mu\nu} \nabla_\mu \nabla_\nu = (\partial_0)^2 - \Delta_d$, so that the equation (8) also gives the vacuum energy, provided that $\lambda_n = \lambda_n(\Delta_d)$.

The principal effect of this scale dependence is that the usual scale behavior of the total energy may be violated. The scale μ can be interpreted as a free parameter which takes into account the physics associated with boundaries, curvatures, masses, and couplings [6].

Let us see what is the effect of a change of scale, $\mu \rightarrow \mu'$. From the definition (4), we get

$$\zeta_D(s; \mu') = \left(\frac{\mu'}{\mu} \right)^{2s} \zeta_D(s; \mu). \tag{13}$$

Using (5), (8) and (13), we obtain

$$\mathcal{E}_0(\mu') = \mathcal{E}_0(\mu) - \frac{\mu}{(4\pi)^{D/2}} C_{D/2}(\mu) \ln \left(\frac{\mu'}{\mu} \right). \tag{14}$$

The scale dependence is logarithmic, and proportional to the coefficient $C_{D/2}$ [6].

2. We have just proved, in a rigorous way, the complete equivalence between the MS definition for the vacuum energy and the effective potential at one-loop. Using the zeta function definition of the determinant, we arrived at expression (8), which is a kind of regulated MS expression (perhaps a strange one). However, unlike others regularizations, the zeta function regularization embodied in (8) already contains an infinite renormalization of the

⁴However, the entire expression on the RHS of (8) is analytic at $s = 0$.

theory. Note that the expression (11) for the vacuum energy is finite: $\zeta_d(s)$ possesses only simple poles, which combines with $\Gamma(s)$ in (8) to give a finite result. This is expected, since $\zeta_D(s)$ is analytic at $s = 0$ (see (5)). The arbitrariness of the renormalization process is manifest through the scale μ . In general, the dependence on the scale is logarithmic.

3. However, others regularization prescriptions for the MS definition are possible, and indeed are fairly used [8]. In particular, starting from the unregulated MS formula (8), one could use the following regularization [6]

$$\mathcal{E}_0(s) = \frac{1}{2} \mu \not\int (\lambda_n \mu^{-2})^{1/2-s} = \frac{1}{2} \mu \zeta_d(s - 1/2; \mu). \tag{15}$$

In this case, the pole in $s = 0$ do not cancel against $\Gamma(s)$. Thus, the coefficient $C_{D/2}$ turns into an obstacle to give a finite Casimir energy. As properly emphasized in [6], the total energy is finite, because of its effects over the gravitational field, and so the bare action must contain a term proportional to $C_{D/2}$. The renormalization prescription which removes the pole, on the other hand, is not unique. This entails an ambiguity in the Casimir energy. In particular, in the minimal subtraction scheme employed in [6], the pole is simply removed, and the Casimir energy is defined by (PP=principal part)

$$\mathcal{E}_c \equiv \lim_{s \rightarrow 0} \frac{1}{2} \left\{ \mathcal{E}_0(+s) + \mathcal{E}_0(-s) \right\} \equiv \frac{\mu}{2} \text{PP} \zeta_d(s - 1/2; \mu). \tag{16}$$

Using this definition, Blau et al. [6] derived the formula (14) for the scale dependence of the Casimir energy.

4. Instead of the generalized zeta function, we can use the Schwinger's formula (SF) for the one-loop effective action [10] as a definition of the functional determinant in (1) (see [11] for elementary applications). We proved in [12] the equivalence between the SF and the MS expressions for the vacuum energy, first in a formal way, and then using a regularization prescription. We will repeat only a few steps of the argument of [12], but now introducing a scale.

The regularized SF reads [13]

$$\omega^{(1)} = -\frac{i}{2} \int_0^\infty dt t^{s-1} \text{Tr} e^{-it\mathcal{H}} \mu^{-s}, \tag{17}$$

where s is large enough to make the integral well defined. In this approach, we first compute the integral, then make an analytical continuation to the whole complex plane of s , and finally the limit $s \rightarrow 0$ is carefully taken (sometimes appropriate subtractions have to be made). $\mathcal{H} = \vec{p}^2 - p_0^2 + m^2$ is the proper-time Hamiltonian. After evaluating the trace, we take a derivative with respect to m^2 on both sides of (17), to obtain

$$\frac{\partial \omega^{(1)}}{\partial m^2} = -\frac{\omega T}{2} \mu^{-s} \sum_{n=1}^\infty \int \frac{d^d \vec{k}}{(2\pi)^d} \int_0^\infty dt t^s e^{-it(-\vec{k}^2 + \frac{\pi^2 n^2}{L^2} + m^2)} \mu^{-s}. \tag{18}$$

Using the definition of the Euler Gamma function, the integration over t is readily done. Then, we integrate over k_0 to obtain

$$\frac{\partial \omega^{(1)}}{\partial m^2} = \frac{-1}{2} i^{-\nu} \omega T \Gamma\left(\frac{1}{2}\right) \Gamma\left(\nu + \frac{1}{2}\right) \mu^{-\nu} \sum_{n=-\infty}^\infty \int_{-\infty}^\infty d\vec{k}_\perp \left[\frac{\vec{k}_\perp^2 + \left(\frac{\pi n}{L}\right)^2 + m^2}{\mu^2} \right]^{-(1/2+s)} \tag{19}$$

Integrating on m^2 and identifying $\mathcal{E}_0 = -\frac{\omega^{(1)}}{\Omega D}$, we finally obtain (apart from an irrelevant additive constant)

$$\mathcal{E}_0(s) = \frac{1}{2} \mu G(s) \sum_{n=1}^\infty \int \frac{d\vec{k}_\perp}{(2\pi)^{d-1}} \left[\frac{\vec{k}_\perp^2 + \left(\frac{\pi n}{L}\right)^2 + m^2}{\mu^2} \right]^{1/2-s} \tag{20}$$

where we defined $G(s) = \frac{i^{-\nu}}{1-2\nu} \frac{\Gamma(\nu+1/2)}{\sqrt{\pi}}$ ($G(0) = 1$). Thus, for a general ultrastatic manifold, we write

$$\mathcal{E}_0(s) = \frac{1}{2} \mu \not\int (\lambda_n \mu^{-2})^{1/2-s} = \frac{1}{2} \mu \zeta_d(s - 1/2; \mu). \tag{21}$$

which is just eq.(15). This is yet another and more transparent way to derive the rigorous equivalence between the IPI effective action at one-loop and the MS definition.

Conclusions

We showed by two ways (using the generalized zeta function and the Schwinger's formula) the complete equivalence of two particular definitions of the vacuum energy, e.g. the IPI effective action at one-loop for constant background fields, and the summation of energies associated with zero-point oscillations of the fields (MS approach)⁵. Of course, different renormalization schemes leads to different expressions for the Casimir energy, when $C_{D/2} \neq 0$. However, the scale behavior (14) is a general feature in any definition of the Casimir energy. But in no way is one approach (MS or effective potential) more restrictive than the other, as stated in [6, 5]. In particular, the last author called the discrepancy between the naive MS formula (without the scale factor) and the ζ -function regularized expression (with the scale dependent factor proportional to $\zeta_D(0) = C_{D/2}$, see (5)) of "zero-point anomaly". In fact, the anomalous behavior of the path integral measure under scale transformations is responsible for the conformal anomaly factor (which is proportional to $A_{D/2}$) in the energy-momentum tensor (Hawking, ref. [7], and [14]), but there is nothing new in this remark. In others words, the concept of zero-point anomaly is a misnomer. Anyway, there is no real difference between the two approaches, with regard to the scale behavior of the Casimir energy: in the general case, the Casimir energy develops an anomalous logarithmic dependence in the normalization scale, proportional to $C_{D/2}$.

LCA would like to thank Adilson J. da Silva, Carlos Farina, Marcelo Gomes and Marcelo Hott for reading the manuscript, and also to the Mathematical Physics Department for their kind hospitality. This work was partially supported by CNPq (Brazilian research agency).

References

- [1] H. G. B. Casimir, Proc. K. Ned. Akad. Wet. **51**, (1948) 793.
- [2] W. Heisenberg and H. Euler, Z. Physik, **98** (1936) 714.
- [3] A. V. Manohar, Lectures at the Schlafliing Winter School, UCSD/PTR 96-04.
- [4] S. Weinberg, Phys. Rev. **D9** (1974) 3357.
- [5] E. Myers, Phys. Rev. Lett. **59** (1987) 165.
- [6] S. K. Blau, M. Visser, and A. Wipf, Nucl. Phys. **B310** (1988) 163.
- [7] A. Salam and J. Strathdee, Nucl. Phys. **B90** (1975) 203; J. S. Dowker and R. Critchley, Phys. Rev. **D13** (1976) 3224; S. W. Hawking, Commun. Math. Phys. **55** (1977) 133.
- [8] G. Plunien, B. Müller e W. Greiner, Phys. Rep. **134** (1986) 87.
- [9] B. S. DeWitt, *Dynamical Theory of Groups and Fields* (Gordon and Breach, 1964).
- [10] J. Schwinger, Phys. Rev. **82** (1951) 664.
- [11] L. C. de Albuquerque, C. Farina, and S. J. Rabello, IF/UFRJ/94/07, hep-th/9403002, unpublished.
- [12] L. C. de Albuquerque, C. Farina, S. J. Rabello, and A. N. Vaidya, Lett. Math. Phys. **34** (1995) 373.
- [13] M. V. Cougo-Pinto, C. Farina and A. J. Seguí-Santonja, Lett. Math. Phys. **30** (1994) 169; M. V. Cougo-Pinto, C. Farina and A. J. Seguí-Santonja, ib. **31** (1994) 309.
- [14] K. Fujikawa, Phys. Rev. Lett. **44** (1980) 1733.

⁵There are other definitions of the vacuum energy, either in local form via the VEV of the energy-momentum tensor [8], or through the full effective action in place of the one-loop effective action.

Casimir Mass and Coupling Constant at Finite Temperature

Luiz C. de Albuquerque*

Instituto de Física, Universidade de São Paulo

Caixa Postal 66.318, 05389-970 - São Paulo, SP, Brazil

C. Farina[†] and A. Tort

Instituto de Física, Universidade Federal do Rio de Janeiro

Caixa Postal 68528, 21945-970 - Rio de Janeiro, RJ, Brazil

We compute the mass correction and the coupling constant at finite temperature and with Dirichlet boundary condition in an interacting scalar field theory in D dimensions, at one-loop. Some peculiar results of odd D are noted. Namely, the self-energy is scale-dependent, and the mass counterterm develop a dependence on L (the distance between the plates).

Field theories defined on manifolds not homeomorphic to R^D displays a lot of appealing features, such as dynamical mass generation, vacuum instabilities and symmetry breaking or restoration [1]. This is the case also in finite temperature field theory (FTQFT). The Casimir effect [2] also illustrates the effect of *global constraints* on the dynamical properties of the theory. In fact, external *boundary conditions* (BC) (Dirichlet, periodic, Neumann or any other) affect not only Feynman diagrams associated with energy calculations, but all diagrams: diagrams with and without boundary conditions can have finite numerical differences. So, other physical quantities (such as masses, coupling constants, anomalous magnetic moments, etc.) could, in principle, be affected by these external BC.

Usually, calculations are done with periodic BC. In this letter, we will investigate the case of Dirichlet BC on a spatial sector, plus periodic BC in the imaginary-time. We explicit compute the mass correction and the coupling constant at one-loop in a $\lambda\phi^4$ theory. This generalization reveals unusual (but not quite surprising) properties of the Dirichlet BC.

The Lagrangian is (Euclidean space)

$$\mathcal{L}(\phi) = -\frac{1}{2}\phi\Box\phi - \frac{1}{2}m^2\phi^2 - \frac{\lambda}{4!}\phi^4 - \frac{1}{2}\delta Z\phi\Box\phi - \frac{1}{2}\delta m^2\phi^2 - \frac{1}{4!}\delta\lambda\phi^4 + \dots \quad (1)$$

where the dots indicates counterterms of the form $C_n\phi^n$ ($n \geq 6$) necessary for the renormalization of the model in $D \geq 5$. We adopt the imaginary-time version of FTQFT - the field is periodic in the Euclidean time x_0 , with period $\beta := \frac{1}{T}$ ($\hbar = k_B = c = 1$). Hence, $k_0 = 2\pi Tl$, $l = 0, \pm 1, \pm 2, \dots$. Also, imposing Dirichlet BC in x_1^1 , we have that $k_1 = \frac{\pi n}{L}$, $n = 1, 2, \dots$

The lowest order contribution to the Casimir mass comes from the 1 loop self-energy function

$$\Sigma^{(1)} = \frac{1}{2}(-\lambda)\mu^{D-\omega} \frac{1}{\beta L} \sum_{n=1}^{\infty} \sum_{l=-\infty}^{\infty} \int \frac{d^{\omega-2}\bar{k}}{(2\pi)^{\omega-2}} \left[\bar{k}^2 + \left(\frac{\pi n}{L}\right)^2 + \left(\frac{2\pi l}{\beta}\right)^2 + m^2 \right]^{-1} \quad (2)$$

where $\bar{k} = (k_2, \dots, k_{D-1})$, m is the renormalized mass, and μ is a mass scale introduced to keep $\Sigma^{(1)}$ with the right dimension. We will use a mix between dimensional and analytic regularization, based in the analytical continuation

*e-mail: claudio@snfma2.if.usp.br

[†]e-mail: farina@if.ufrj.br

¹In this Casimir type situation, the plates are located at $x_1 = 0$ and $x_1 = L$, where the field vanishes.

of certain Epstein functions. In eq. (2), ω replaces D ; after elimination of the ultraviolet divergent part, we take the limit $\omega \rightarrow D$. The mass and coupling constant counterterms are defined by imposing the limits

$$\begin{aligned} \lim_{\omega \rightarrow D} [p^2 + m^2 + \delta m^2 - \Sigma^{(1)}] \\ \lim_{\omega \rightarrow D} [-\lambda - \delta\lambda + \Gamma^{(2)}] \end{aligned} \tag{3}$$

be finite [3], in a minimal subtraction (MS) scheme.

Integration of (2) leads to

$$\Sigma^{(1)} = -\frac{2\lambda\pi\mu^{D-\omega}}{(4\pi)^{\omega/2}L\beta} \Gamma(2 - \frac{\omega}{2}) \left[E_1^{m^2} \left(2 - \frac{\omega}{2}; \frac{\pi^2}{L^2} \right) + 2E_2^{m^2} \left(2 - \frac{\omega}{2}; \frac{\pi^2}{L^2}; \frac{4\pi^2}{\beta^2} \right) \right], \tag{4}$$

where we introduced the modified inhomogeneous Epstein function [4, 5]

$$E_N^{c^2}(s; a_1, a_2, \dots, a_N) := \sum_{n_1=1}^{\infty} \sum_{n_2=1}^{\infty} \dots \sum_{n_N=1}^{\infty} \frac{1}{[a_1 n_1^2 + \dots + a_N n_N^2 + c^2]^s}, \tag{5}$$

where $a_1, \dots, a_N, c^2 > 0$ and N is an integer. The above series converges for $\Re s > \frac{N}{2}$.

Using the analytical continuation to the whole complex s -plane of the modified inhomogeneous Epstein function with $N = 1$, namely

$$E_1^{c^2}(s, a^2) = -\frac{1}{2}c^{-2s} + \frac{1}{2} \frac{\sqrt{\pi}}{a} \frac{\Gamma(s - \frac{1}{2})}{\Gamma(s)} c^{1-2s} + 2 \frac{\sqrt{\pi}}{a} \left(\frac{ca}{\pi}\right)^{1/2-s} \frac{1}{\Gamma(s)} \sum_{n=1}^{\infty} n^{s-1/2} K_{1/2-s} \left(\frac{2\pi c}{a} n\right), \tag{6}$$

as well as a recurrence relation between Epstein functions, we obtain for $\Sigma^{(1)}$

$$\begin{aligned} \Sigma^{(1)} = -\frac{\lambda}{(4\pi)^{\omega/2}} \mu^{D-\omega} \left\{ -\frac{\sqrt{\pi}}{2} \frac{m^{\omega-3}}{L} \Gamma\left(\frac{3-\omega}{2}\right) + \frac{m^{\omega-2}}{2} \Gamma\left(1 - \frac{\omega}{2}\right) + 2\left(\frac{m}{L}\right)^{\omega/2-1} \right. \\ \left. \times \sum_{n=1}^{\infty} n^{1-\frac{\omega}{2}} K_{\frac{\omega}{2}-1}(2mLn) + \frac{4\sqrt{\pi}}{L} \sum_{n,l=1}^{\infty} \left[\frac{l^2/(2T)^2}{(\pi n)^2/L^2 + m^2} \right]^{\frac{3-\omega}{4}} K_{\frac{\omega-3}{4}} \left(\frac{l}{T} \sqrt{(\pi n)^2/L^2 + m^2} \right) \right\}. \end{aligned} \tag{7}$$

The divergent contributions to $\Sigma^{(1)}$ is given by $\Gamma(1 - \frac{\omega}{2})$ (poles for $\omega = D$ even), and $\Gamma(\frac{3-\omega}{2})$ (poles for $\omega = D$ odd). Expanding these terms around the simple pole in $\omega = D$, and using (3), we obtain the mass counterterm to the order λ .

$$\begin{aligned} \delta m_+^2 = -\frac{(-1)^{D/2-1}}{(D/2-1)!} \frac{\lambda}{(4\pi)^{D/2}} m^{D-2} (D-\omega)^{-1}, \\ \delta m_-^2 = \frac{(-1)^{(D-3)/2}}{((D-3)/2)!} \frac{\lambda\sqrt{\pi}}{(4\pi)^{D/2}} \frac{m^{D-3}}{L} (D-\omega)^{-1}. \end{aligned} \tag{8}$$

Note the relevant fact that the counterterm depend on L for odd D .

The renormalized mass to the order λ is (see (4)):

$$M^2(T, L) = m^2 - \Sigma_R^{(1)}(T, L) |_{\omega \rightarrow D}. \tag{9}$$

The contributions independent of T and L may be dropped: these arise even when $T = 0$ and $L \rightarrow \infty$, and could be discarded by a finite renormalization². Then, we have

²However, we will keep the logs. Besides, we made a change of scale $\mu^2 \rightarrow \mu^2/4\pi$.

$$M^2(T, L) = m^2 + \frac{\lambda}{(4\pi)^{D/2}} \left\{ f_{\pm}^{\mu}(m, L) + 2 \left(\frac{m}{L}\right)^{D/2-1} \sum_{n=1}^{\infty} n^{1-\frac{D}{2}} K_{\frac{D}{2}-1}(2mLn) \right. \\ \left. + \frac{4\sqrt{\pi}}{L} \sum_{n,l=1}^{\infty} \left[\frac{l^2/(2l)^2}{(\pi n)^2/L^2 + m^2} \right]^{\frac{3-D}{4}} K_{\frac{D-3}{2}} \left(\frac{l}{T} \sqrt{(\pi n)^2/L^2 + m^2} \right) \right\}. \quad (10)$$

$$f_{+}^{\mu}(m, L) = -\frac{\sqrt{\pi} m^{D-3}}{2L} \Gamma\left(\frac{3-D}{2}\right) + \frac{(-1)^{D/2-1}}{(D/2-1)!} m^{D-2} \ln\left(\frac{\mu}{m}\right), \\ f_{-}^{\mu}(m, L) = -\frac{(-1)^{(D-3)/2} \sqrt{\pi} m^{D-3}}{((D-3)/2)!} \frac{1}{L} \left[\ln\left(\frac{\mu}{m}\right) + \frac{1}{2} \psi\left(\frac{D-1}{2}\right) \right]. \quad (11)$$

Note that $f_{\pm}^{\mu}(L \rightarrow \infty) = 0$. For finite L , however, the renormalized mass develops a scale dependence for D odd. This is a bit unusual since, as is well known, in dimensional regularization (for flat unconstrained space-time) the renormalized quantities do not develop such a scale dependence for D odd.

To compare our result with the known one, we take the limit $L \rightarrow \infty$. Hence, using $\frac{1}{L} \sum_{n=1}^{\infty} f\left(\left(\frac{\pi n}{L}\right)^2\right) \Rightarrow \int \frac{dk}{2\pi} f(k^2)$, and the integral [6]

$$\int_0^{\infty} dz (z^2 + 1)^{-a/2} K_a(a\sqrt{z^2 + 1}) = \sqrt{\frac{\pi}{2a}} K_{a-1/2}(a). \quad (12)$$

we obtain the pure thermal correction

$$M^2(T) = m^2 + \frac{\lambda}{(4\pi)^{D/2}} \left[f_{\pm}^{\mu}(m, L \rightarrow \infty) + 2(2mT)^{D/2-1} \sum_{n=1}^{\infty} n^{1-\frac{D}{2}} K_{\frac{D}{2}-1}\left(\frac{m}{T}n\right) \right]. \quad (13)$$

This result was also given in [7].

In the same fashion, taking the limit $T = 0$ we isolate the pure Casimir correction,

$$M^2(L) = m^2 + \frac{\lambda}{(4\pi)^{D/2}} \left[f_{\pm}^{\mu}(m, L) + 2 \left(\frac{m}{L}\right)^{D/2-1} \sum_{n=1}^{\infty} n^{1-\frac{D}{2}} K_{\frac{D}{2}-1}(2mLn) \right]. \quad (14)$$

Of course, the result (14) agrees with the known one ($D = 4$, cf. Toms in [1]).

The first perturbative correction to the coupling constant is given by the four-point function at one-loop,

$$\Gamma^{(2)} = \frac{3}{2} \lambda^2 \mu^{D-\omega} \sum_{n=1}^{\infty} \sum_{l=-\infty}^{\infty} \frac{1}{\beta L} \int \frac{d^{\omega-2} \vec{k}}{(2\pi)^{\omega-2}} \left[\vec{k}^2 + \left(\frac{\pi n}{L}\right)^2 + \left(\frac{2\pi l}{\beta}\right)^2 + m^2 \right]^{-2}. \quad (15)$$

As is clear, we will do this calculation for zero external momenta, for simplicity³.

$\Gamma^{(2)}$ is computed in the same way as $\Sigma^{(1)}$. We will only state the results. The coupling constant counterterm is

$$\delta\lambda_{+} = 3 \frac{(-1)^{D/2-2}}{(D/2-2)!} \frac{\lambda^2}{(4\pi)^{D/2}} m^{D-4} (D-\omega)^{-1}, \\ \delta\lambda_{-} = -3\sqrt{\pi} \frac{(-1)^{(D-5)/2}}{((D-5)/2)!} \frac{\lambda^2}{(4\pi)^{D/2} L} m^{D-5} (D-\omega)^{-1}. \quad (16)$$

There is no coupling constant renormalization for $D = 2, 3$.

After a finite renormalization, the renormalized coupling constant, defined by (see (4))

³As we are mainly interested in the thermal and "compactification length" dependence of the parameters, and not in scattering process, this is a reasonable approximation. Indeed, this choice arises naturally when computing the effective potential for constant background fields, and is equivalent to the definition of the renormalized parameters in the special point $p = 0$. However, we have to keep $m \neq 0$.

$$\Lambda(T, L) = \lambda - \Gamma_R^{(2)}(T, L) |_{\omega \rightarrow 0}, \tag{17}$$

is given by

$$\Lambda(T, L) = \lambda - \frac{3\lambda^2}{(4\pi)^{D/2}} \left\{ g_{\pm}^{\mu}(m, L) + 2 \left(\frac{m}{L}\right)^{D/2-2} F\left(\frac{D}{2} - 2; 2mL\right) + \frac{4\sqrt{\pi}}{L} H^{m^2} \left(\frac{D-5}{2}; \frac{\pi^2}{L^2}, 4\pi^2 T^2\right) \right\}. \tag{18}$$

$$g_+^{\mu}(m, L) = -\frac{\sqrt{\pi} m^{D-5}}{2L} \Gamma(5/2 - D/2) + \frac{(-1)^{D/2-2}}{(D/2 - 2)!} m^{D-4} \ln\left(\frac{\mu}{m}\right),$$

$$g_-^{\mu}(m, L) = -\sqrt{\pi} \frac{(-1)^{(D-5)/2}}{((D-5)/2)!} \frac{m^{D-5}}{L} \left[\ln\left(\frac{\mu}{m}\right) + \frac{1}{2} \psi\left(\frac{D-3}{2}\right) \right]. \tag{19}$$

In the special cases of $D = 2, 3$ only the first term in the RHS of g_{\pm}^{μ} contribute. We see that Λ also develops a scale dependence for odd D .

Again, taking the limit $L \rightarrow \infty$ we can isolate the pure thermal correction

$$\Lambda(T) = \lambda - \frac{3\lambda^2}{(4\pi)^{D/2}} \left[g_{\pm}^{\mu}(m, L \rightarrow \infty) + 2(2mT)^{D/2-2} F\left(\frac{D}{2} - 2, \frac{m}{T}\right) \right]. \tag{20}$$

Exactly as done before, we obtain the pure Casimir correction to the coupling constant taking the limit $T = 0$,

$$\Lambda(L) = \lambda - \frac{3\lambda^2}{(4\pi)^{D/2}} \left[g_{\pm}^{\mu}(m, L) + 2 \left(\frac{m}{L}\right)^{D/2-2} F\left(\frac{D}{2} - 2, 2mL\right) \right] \tag{21}$$

To conclude, let us discuss our results.

Dependence on the renormalization scale is expected in calculations involving one-loop physics. In fact, the renormalization scale reflects the ambiguity inherent in any renormalization process, and in this case summarizes the effects associated with the boundaries and with mass and coupling constant renormalizations. Thus, μ can only be fixed by an additional condition. Guided by Casimir energy calculations, we can dispose any contribution independent of T and/or L . Using this condition, we obtain a definite expression for $M(T, L)$ and $\Lambda(T, L)$ in the case of D even. However, in the odd D case this condition cannot fix the scale.

A closely related issue of odd D is that the counterterms depend on L . It is known that if a theory is renormalizable for a given space-time manifold, then it is also renormalizable in the manifold obtained by the identification of certain coordinates [8], with the same counterterms. However, $\lambda\phi^4$ is not renormalizable for $D > 4$, and so in this case there is no reason why the counterterms could not depend of T and/or L . Indeed, in the thermo field dynamics approach to FTQFT, the analogy between FTQFT in imaginary-time and field theory on a multiply connected space-time is lost. However, Matsumoto et al. [9] proved that if a theory is renormalizable at $T = 0$, it is also renormalizable at $T \neq 0$. As stressed by these authors, this statement do not exclude a possible thermal dependence of the counterterms. Nevertheless, explicit calculations shown that the counterterms are temperature independent. Taking the case of finite T (or periodic BC in a spatial coordinate), it is easy to show that at one-loop in flat space-time the amplitudes can be expressed as the sum of the zero temperature contribution plus thermal(-quantum) contributions [10]. The zero T part is renormalized in the usual way, while the finite T part is automatically regulated by the appropriate statistical distribution function. Using this method in the case of Dirichlet BC, we found that besides the usual (vacuum) divergence (i.e. the second term in square brackets in (7)), there is another divergent piece, which is exactly the first term in square brackets in (7). This contribution originates from the difference in the eigenvalues of k_{\parallel} for Dirichlet BC and periodic BC.

LCA would like to thank Jossif Frenkel and Nami Svaiter for helpful discussions, and to Adilson J. da Silva, Marcelo Gomes and Victor Rivelles for reading the manuscript. This work was partially supported by CNPq, FINEP and FUJB (Brazilian research agencies).

References

- [1] L. H. Ford, Proc. R. Soc. Lond. **A368** (1979) 305; D. J. Toms, Phys. Rev. **D21** (1980) 2805; G. Denardo e E. Spallucci, Nucl. Phys. **B169** (1980) 514.
- [2] G. Plunien, B. Muller e W. Greiner, Phys. Rep. **134** (1986) 87.
- [3] J. C. Collins, Phys. Rev. **D10** (1974) 3320.
- [4] J. Ambjorn and S. Wolfram, Ann. Phys. **147** (1983) 1.
- [5] K. Kirsten, J. Phys **A24** (1991) 3281; J. Math. Phys. **35** (1994) 459.
- [6] I. S. Gradshteyn and I. M. Ryzhik, *Tables of Integrals, Series and Products* (Academic Press, 1965).
- [7] L. H. Ford and N. F. Svaiter, Phys. Rev. **D51** (1995) 6981.
- [8] R. Banach, J. Phys. **A13** (1980) L365.
- [9] H. Matsumoto, Y. Nakano, and H. Umezawa, Phys. Rev. **D20** (1984) 1116; H. Matsumoto, I. Ojima, and H. Umezawa, Ann. Phys. **152** (1984) 348.
- [10] J. I. Kapusta, *Finite Temperature Field Theory* (Cambridge University Press, 1992).

$O(\mathbf{p}^2/m^2)$ Corrections to the Aharonov-Bohm Scattering*

M. Gomes, J. M. C. Malbouisson[†] and A. J. da Silva
 Instituto de Física, Universidade de São Paulo, Caixa Postal 66318,
 05315-970, São Paulo, SP, Brazil.

November 21, 1996

In this work we shall determine relativistic corrections to the Aharonov-Bohm (AB) scattering [1]. Due to its connection to the physics of anyons [2-4], this process can be described by a nonrelativistic (NR) Lagrangian [5],

$$\mathcal{L}_{NR} = \psi^* \left(iD_t + \frac{\mathbf{D}^2}{2m} \right) \psi - \frac{v_0}{4} (\psi^* \psi)^2 + \frac{\Theta}{2} \partial_t \mathbf{A} \times \mathbf{A} - \Theta A_0 \nabla \times \mathbf{A}. \quad (1)$$

Up to one loop, the 2-particle scattering amplitude, calculated in the center of mass (CM) frame, is

$$\mathcal{A}_{NR}^{(1)} = -v_0 - i \frac{2e^2}{m\Theta} \cot \theta + \frac{m}{8\pi} \left(v_0^2 - \frac{4e^4}{m^2 \Theta^2} \right) \left[\ln \left(\frac{\Lambda_{NR}^2}{\mathbf{p}^2} \right) + i\pi \right], \quad (2)$$

where Λ_{NR} is a nonrelativistic ultraviolet cutoff. The renormalization is implemented by redefining the self-coupling constant, $v_0 = v + \delta v$, so that the total renormalized nonrelativistic amplitude is given, up to order e^4 , by

$$\mathcal{A}_{NR} = -v - i \frac{2e^2}{m\Theta} \cot \theta + \frac{m}{8\pi} \left(v^2 - \frac{4e^4}{m^2 \Theta^2} \right) \left[\ln \left(\frac{\mu^2}{\mathbf{p}^2} \right) + i\pi \right], \quad (3)$$

where μ is an arbitrary mass scale, introduced by the renormalization, that breaks the scale invariance of the amplitude [6].

We observe that at the critical values $v_{\pm}^{\pm} = \pm 2e^2/m|\Theta|$, scale invariance is restored and by choosing the v_{\pm}^{\pm} value, corresponding to a repulsive contact interaction, the amplitude reduces to the Aharonov-Bohm amplitude for identical particles which is given by [1, 6]

$$\mathcal{F}_{AB}(|\mathbf{p}|, \theta) = -i \sqrt{\frac{\pi}{|\mathbf{p}|}} \alpha [\cot \theta - i \operatorname{sgn}(\alpha)] + O(\alpha^3), \quad (4)$$

where $\alpha = e^2/2\pi\Theta$.

This work is concerned with the question to what extent the relativistic corrections preserve such criticality. Using an intermediate cutoff procedure [7], which allows the determination of the $|\mathbf{p}|/m$ expansion of the quantum amplitudes, we calculate the 1-loop particle-particle CM scattering amplitude, for low external momenta, up to order \mathbf{p}^2/m^2 . The leading term of the $|\mathbf{p}|/m$ expansion coincides with the above result, as verified in Ref. [8], whereas the subdominant parts do not vanish at the critical self-interaction values and so represent relativistic corrections to the Aharonov-Bohm scattering.

To obtain the relativistic corrections, we consider a charged self-interacting scalar field in 2 + 1 dimensions minimally coupled to a Chern-Simons gauge field [9] described by the Lagrangian density

$$\mathcal{L} = (D_{\mu} \phi)^* (D^{\mu} \phi) - m^2 \phi^* \phi - \frac{\lambda}{4} (\phi^* \phi)^2 + \frac{\Theta}{2} \epsilon_{\sigma\mu\nu} A^{\sigma} \partial^{\mu} A^{\nu} - \frac{\xi}{2} (\partial_t A^i)^2, \quad (5)$$

where $D_{\mu} = \partial_{\mu} - ieA_{\mu}$ is the covariant derivative, $\epsilon_{\sigma\mu\nu}$ is the fully antisymmetric tensor normalized to $\epsilon_{012} = +1$, the Minkowski metric signature is (1, -1, -1), the units are such that $\hbar = c = 1$ and repeated greek indices sum from 0 to 2 while repeated latin indices sum from 1 to 2. The choice of the Coulomb gauge fixing, the same used in Ref.

*Supported by Conselho Nacional de Desenvolvimento Científico e Tecnológico (CNPq) e Fundação de Amparo à Pesquisa do Estado de São Paulo (FAPESP).

[†]On leave from Instituto de Física, Universidade Federal da Bahia, Salvador, 40210-340, Brazil.

virtual gauge field propagator which is independent of k^0 and totally antisymmetric in the Minkowski indices with the only nonvanishing components given by

$$D_{0i}(k) = -D_{i0}(k) = \frac{1}{\Theta} \frac{\epsilon_{ij} k^j}{k^2}, \quad (6)$$

where $\epsilon_{ij} = \epsilon_{0ij}$. The free propagator of the bosonic matter field is the usual Feynman propagator $\Delta(p) = i[p^2 - m^2 + i\epsilon]^{-1}$ and the vertex factors are $-i\lambda$ for the self-interaction vertex and $-ie(p + p')^\mu$ and $2ie^2 g^{\mu\nu}$ for the trilinear and the seagull vertices that always arise from minimal coupling with a scalar field.

In the CM frame, with external particles on the mass shell, one has $p_1 = -p_2 = \mathbf{p}$, $p'_1 = -p'_2 = \mathbf{p}'$ and $p_1^0 = p_2^0 = p_1'^0 = p_2'^0 = \omega_p = \sqrt{m^2 + p^2}$. The tree level particle-particle amplitude is given by

$$A^{(0)} = -\lambda - i \frac{8e^2}{\Theta} \sqrt{m^2 + p^2} \cot \theta \simeq -\lambda - i \frac{8e^2}{\Theta} m \left(1 + \frac{p^2}{2m^2}\right) \cot \theta, \quad (7)$$

where θ is the scattering angle and m is the renormalized mass of the bosonic particle. One sees that, by definiteness, we take the amplitude as being $(-i)$ times the 1PI four point function. This choice is only to facilitate the comparison with the nonrelativistic case discussed in ref.[6].

We shall calculate the 1-loop order scattering amplitude, for low external momenta and up to order p^2/m^2 . The contributions arising from the insertion of the vacuum polarization and vertex corrections into the tree level gives,

$$A^{(1)} \simeq -\frac{2e^4}{\pi\Theta^2} m \left\{ \frac{13}{6} + \frac{19}{10} \frac{p^2}{m^2} \right\}. \quad (8)$$

Diagrams that admixes particle self-interaction and gauge field exchange, do not contribute, due to charge conjugation and the antisymmetric form of the gauge field propagator. The most important, one loop particle-particle scattering comes from the diagrams shown in Fig. 1 where it is also presented the routing of external momenta used in the calculations.

The group (a) is the finite self-interaction scattering, which can be exactly calculated [7-8] and to order p^2/m^2 is given by

$$A^{(a)} \simeq \frac{\lambda^2}{32\pi m} \left\{ \left(1 - \frac{p^2}{2m^2}\right) \left[\ln \left(\frac{4m^2}{p^2} \right) + i\pi \right] + 4 - \frac{p^2}{6m^2} \right\}. \quad (9)$$

The $|p|/m$ expansion of the more involving CS scattering, the (b) and (c) groups of diagrams of Fig. 1, will be calculated employing the following cutoff procedure [7]. First of all, we integrate over k^0 (the frequency part of the loop momentum k) without making any restriction in order to guarantee locality in time. The remaining integration over the Euclidean k plane is then separated into two parcels through the introduction of an intermediate cutoff Λ_I in the $|k|$ integration satisfying

$$i) |p| \ll \Lambda_I \ll m \quad \text{and} \quad (ii) \left(\frac{|p|}{\Lambda_I} \right)^2 \approx \left(\frac{\Lambda_I}{m} \right)^2 \approx \frac{|p|}{m} \approx \eta, \quad (10)$$

which defines η as the small expansion parameter. The auxiliary cutoff Λ_I splits the space of the intermediate states into two parts, the low (L) energy sector ($|k| < \Lambda_I$) and the high (H) energy one with $|k| > \Lambda_I$. In the L sector all the spatial momenta involved are small ($|p|/m$, $|k|/m \ll 1$) and so one can perform a $1/m$ expansion of the integrand while, in the H- region, $|k| \gg |p|$ and the integrand can be expanded in a Taylor series around $|p| = 0$ and then, in both cases, integrated term by term (a regularization scheme has to be used if the graph is ultraviolet divergent). This procedure permits analytical calculations in every order in η , produces Λ_I -dependent results and further expansions in Λ_I/m may be necessary to get the $|p|/m$ expansion of the L and H contributions to the amplitude, up to the desired order. Certainly, for sake of consistence, the Λ_I -dependent parcels of the L and the H contributions of each diagram cancel identically. This process has been explicitly verified to produce the correct $|p|/m$ expansion for the self-interaction scattering (a) [7].

Consider the "right" box diagram corresponding to the direct exchange of two virtual gauge particles, the first parcel of Fig. 1(b). Following the Feynman rules, one has

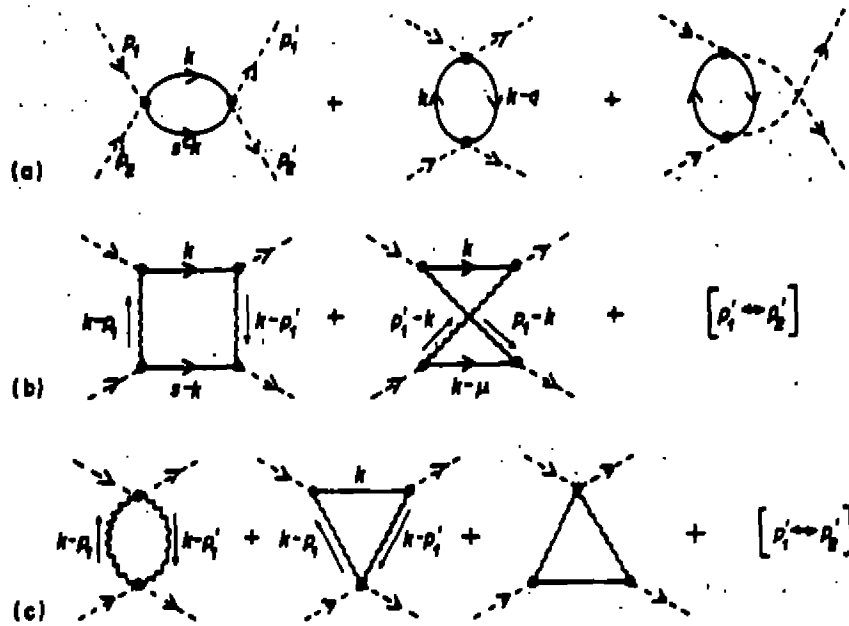


Figure 1: One loop order particle-particle scattering. In the momenta assignment shown, $s = p_1 + p_2$, $q = p_1 - p'_1$ and $u = p'_1 - p_2$.

$$\begin{aligned}
 A^{(b)dir} &= -ie^4 \int \frac{d^3k}{(2\pi)^3} \{ (p_1 + k)^\mu D_{\mu\sigma}(k - p_1) (2p_2 + p_1 - k)^\sigma \Delta(k) \\
 &\quad \Delta(p_1 + p_2 - k) (-k + p_1 + p_2 + p'_2)^\rho D_{\rho\nu}(k - p'_1) (k + p'_1)^\nu \} + [p'_1 \leftrightarrow p'_2] \\
 &= -\frac{4e^4}{\pi^2 \Theta^2} \int d^2k \left(\frac{w_p^2}{w_k} \right) \frac{1}{p^2 - k^2 + i\epsilon} \left[\frac{(\mathbf{k} \times \mathbf{p})(\mathbf{k} \times \mathbf{p}')}{(\mathbf{k} - \mathbf{p})^2 (\mathbf{k} - \mathbf{p}')^2} \right] + [p' \leftrightarrow -p'] , \quad (11)
 \end{aligned}$$

where the k^0 integration was done as a contour integral. The angular integration in the last line above can be cast in the form $\frac{1}{2} [\cos \theta I_0 - I_2]$ where

$$I_n = \int_0^{2\pi} d\varphi \frac{\cos(n\varphi)}{[2 \cos(\varphi - \theta/2) - \beta][2 \cos(\varphi + \theta/2) - \beta]} \quad (12)$$

and $\beta = (\mathbf{k}^2 + \mathbf{p}^2)/(|\mathbf{k}||\mathbf{p}|)$. This integral can be done using the residue theorem and one finds

$$\begin{aligned}
 A^{(b)dir} &= -\frac{e^4}{\pi \Theta^2} \int d(k^2) \left(\frac{w_p^2}{w_k} \right) \frac{1}{p^2 - k^2 + i\epsilon} \\
 &\quad \left[\frac{|\mathbf{k}^2 - \mathbf{p}^2| (k^2 - p^2)}{(\mathbf{k}^2)^2 + (\mathbf{p}^2)^2 - 2\mathbf{k}^2 \mathbf{p}^2 \cos \theta} - 1 \right] + (\theta \leftrightarrow \pi - \theta) . \quad (13)
 \end{aligned}$$

The remaining \mathbf{k}^2 integration is then divided into two pieces, from 0 to Λ_L^2 (L region) and from Λ_L^2 to $\Lambda_H^2 \rightarrow \infty$ (H sector). In the L part, using

$$\frac{w_p^2}{w_k} = m \left(1 + \frac{\mathbf{p}^2}{m^2} \right) \left[1 - \frac{\mathbf{k}^2}{2m^2} + \frac{3(\mathbf{k}^2)^2}{8m^4} + \dots \right] \quad (14)$$

and keeping terms up to order η^2 , one obtains

$$A_L^{(b)dir} \simeq -\frac{2e^4}{\pi \Theta^2} m \left\{ \left(1 + \frac{\mathbf{p}^2}{2m^2} \right) [\ln(2|\sin \theta|) + i\pi] - \frac{\mathbf{p}^2}{m^2} \right\}$$

$$-\frac{1}{2} \cos \theta \ln \left(\frac{1 - \cos \theta}{1 + \cos \theta} \right) \frac{p^2}{m^2} - (1 - 2 \cos^2 \theta) \frac{p^4}{\Lambda_f^4} \left. \right\}. \quad (15)$$

In the H region, the integrand is replaced by its Taylor expansion around $p^2 = 0$ which is given by

$$\left[-\frac{2m^2 \cos \theta}{(k^2)^2 \sqrt{k^2 + m^2}} \right] p^2 + \left[\frac{2m^2(1 - 2 \cos^2 \theta)}{(k^2)^3 \sqrt{k^2 + m^2}} - \frac{2 \cos \theta \sqrt{k^2 + m^2}}{(k^2)^3} \right] p^4 + \mathcal{O}(p^6).$$

Performing the k^2 integrations one obtains, up to order η^2 ,

$$A_H^{(b)dir} \simeq -\frac{2e^4}{\pi\Theta^2} m \left\{ (1 - 2 \cos^2 \theta) \frac{p^4}{\Lambda_f^4} \right\}. \quad (16)$$

Adding (15) and (16), we get

$$A^{(b)dir} \simeq -\frac{2e^4}{\pi\Theta^2} m \left\{ \left(1 + \frac{p^2}{2m^2} \right) [\ln(2|\sin \theta|) + i\pi] - \frac{p^2}{m^2} - \frac{1}{2} \cos \theta \ln \left(\frac{1 - \cos \theta}{1 + \cos \theta} \right) \frac{p^2}{m^2} \right\}. \quad (17)$$

The k^0 integration of the twisted box diagram, the second in Fig. 1(b), gives

$$A^{(b)twist} = -\frac{e^4}{2\pi^2\Theta^2} \int d^2k \left(\frac{w_k w_{k-s} - w_p^2}{w_k w_{k-s} (w_k + w_{k-s})} \right) \left[\frac{(\mathbf{k} \times \mathbf{s})^2 - (\mathbf{p} \times \mathbf{p}')^2}{(\mathbf{k} - \mathbf{p})^2 (\mathbf{k} - \mathbf{p}')^2} \right] + [\mathbf{p}' \leftrightarrow -\mathbf{p}'] \quad (18)$$

where $\mathbf{s} = \mathbf{p} + \mathbf{p}'$ and we recall that $w_{k-s} = \sqrt{(\mathbf{k} - \mathbf{s})^2 + m^2}$. This integration has a rather non trivial angular part but the use of the approximation procedure before performing it allows analytical calculations and one ends up, after adding its final particles exchanged partner, with

$$A_L^{(b)twist} \simeq 0 \text{ and } A^{(b)twist} \simeq A_H^{(b)twist} \simeq -\frac{2e^4}{\pi\Theta^2} m \left\{ \frac{p^2}{2m^2} \right\}. \quad (19)$$

Thus, the total box amplitude, $A^{(b)} = A^{(b)dir} + A^{(b)twist}$, is finite and, up to order p^2/m^2 , is given by

$$A^{(b)} \simeq -\frac{2e^4}{\pi\Theta^2} m \left\{ \left(1 + \frac{p^2}{2m^2} \right) [\ln(2|\sin \theta|) + i\pi] - \frac{p^2}{2m^2} - \frac{1}{2} \cos \theta \ln \left(\frac{1 - \cos \theta}{1 + \cos \theta} \right) \frac{p^2}{m^2} \right\}. \quad (20)$$

The third group, the seagull scattering, has to be treated more carefully since it carries the divergence of the four point function. One can immediately see that each of the k^0 integrations of the gauge bubble and the two triangle diagrams would diverge if made separately. However, taking all the diagrams of group (c) together, the divergences of the k^0 integrations cancel out identically and the angular integrations, which again are linear combinations of I_n , lead to

$$A^{(c)} = -\frac{e^4}{2\pi\Theta^2} \left\{ \int d(k^2) \left(\frac{w_p^2 + w_k^2}{w_k} \right) \frac{\text{sgn}(k^2 - p^2) (k^2 - \cos \theta p^2)}{(k^2)^2 + (p^2)^2 - 2k^2 p^2 \cos \theta} - \int d(k^2) \frac{1}{w_k} \left[\frac{|k^2 - p^2| (k^2 - p^2)}{(k^2)^2 + (p^2)^2 - 2k^2 p^2 \cos \theta} - 1 \right] \right\} + (\theta \leftrightarrow \pi - \theta). \quad (21)$$

Repeating the procedure exemplified with the box diagram one finds

$$A_L^{(c)} \simeq -\frac{2e^4}{\pi\Theta^2} m \left\{ \left(1 + \frac{p^2}{2m^2} \right) \left[\ln \left(\frac{\Lambda_f^2}{p^2} \right) - \ln(2|\sin \theta|) \right] + \frac{p^2}{m^2} + \frac{1}{2} \cos \theta \ln \left(\frac{1 - \cos \theta}{1 + \cos \theta} \right) \frac{p^2}{m^2} + \frac{1}{2} (1 - 2 \cos^2 \theta) \frac{p^4}{\Lambda_f^4} + \frac{\Lambda_f^4}{16m^4} \right\}, \quad (22)$$

$$A_H^{(c)} \simeq -\frac{2e^4}{\pi\Theta^2}m \left\{ -\left(1 + \frac{p^2}{2m^2}\right) \ln\left(\frac{\Lambda_f^2}{4m^2}\right) - 1 - \frac{1}{2}(1 - 2\cos^2\theta) \frac{p^4}{\Lambda_f^4} - \frac{\Lambda_f^4}{16m^4} + \left[\frac{\Lambda_0}{m}\right] \right\} \quad (23)$$

and, thus, the total seagull contribution to the amplitude is

$$A^{(c)} \simeq -\frac{2e^4}{\pi\Theta^2}m \left\{ \left(1 + \frac{p^2}{2m^2}\right) \left[\ln\left(\frac{4m^2}{p^2}\right) - \ln(2|\sin\theta|) \right] - 1 + \frac{1}{2}\cos\theta \ln\left(\frac{1-\cos\theta}{1+\cos\theta}\right) \frac{p^2}{m^2} + \frac{p^2}{m^2} \right\} + \frac{2e^4}{\pi\Theta^2}\Lambda_0. \quad (24)$$

The constant divergent term above can be suppressed by a counterterm of the form $-\frac{2e^4}{\pi\Theta^2}\Lambda_0(\phi^\circ\phi)^2$ introduced in the Lagrangian density. We can also imagine that the bare self-coupling λ carries a divergent part that just cancel the divergence of the four point function. In any case, we take the finite part of (24) as the 1-loop renormalized (c) contribution. This would be the result if we had used dimensional renormalization.

The pure CS exchange scattering, the sum $A^{(b)} + A^{(c)}$, is given by

$$A^{(CS)} \simeq -\frac{2e^4}{\pi\Theta^2}m \left\{ \left(1 + \frac{p^2}{2m^2}\right) \left[\ln\left(\frac{4m^2}{p^2}\right) + i\pi \right] - 1 + \frac{p^2}{2m^2} \right\}, \quad (25)$$

and it is noticeable that the cancellation of the θ dependent terms of the box and the seagull amplitudes happens in both dominant and subleading orders.

The total renormalized 1-loop particle-particle scattering amplitude, $A^{(a)} + A^{(CS)} + A^{(p)} + A^{(v)}$, is independent of the scattering angle θ and, up to order p^2/m^2 , is given by

$$A^{(1)} \simeq m \left(\frac{\lambda^2}{32\pi m^2} - \frac{2e^4}{\pi\Theta^2} \right) \left[\ln\left(\frac{4m^2}{p^2}\right) + i\pi \right] - m \left(\frac{\lambda^2}{32\pi m^2} + \frac{2e^4}{\pi\Theta^2} \right) \frac{p^2}{2m^2} \left[\ln\left(\frac{4m^2}{p^2}\right) + i\pi \right] + m \left(\frac{\lambda^2}{8\pi m^2} - \frac{7e^4}{3\pi\Theta^2} \right) - m \left(\frac{\lambda^2}{192\pi m^2} + \frac{24e^4}{5\pi\Theta^2} \right) \frac{p^2}{m^2}. \quad (26)$$

The leading term of the above expansion, which coincides with the result of Ref. [8], vanishes if the self-interaction parameter is fixed at one of the critical values $\lambda_c^\pm = \pm 8me^2/|\Theta|$ but the subdominant terms do not. The implications of this fact will be discussed next.

Prior to any comparison with the nonrelativistic case, the normalization of states has to be properly adjusted. In the relativistic case one takes $\langle p'|p \rangle = 2w_p\delta(p' - p)$ while the usual normalization in a NR theory does not have the $2w_p$ factor and thus the CM amplitudes, calculated in the last section, must be multiplied by

$$\left(\frac{1}{\sqrt{2w_p}} \right)^4 = \frac{1}{4m^2} \left[1 - \frac{p^2}{m^2} + \dots \right]. \quad (27)$$

The tree level and the 1-loop amplitudes, equations (7) and (26), are then rewritten, up to order p^2/m^2 , as

$$A^{(0)} = -\frac{\lambda}{4m^2} - i\frac{2e^2}{m\Theta} \cot\theta + \left[\frac{\lambda}{4m^2} + i\frac{e^2}{m\Theta} \cot\theta \right] \frac{p^2}{m^2} \quad (28)$$

and

$$A^{(1)} \simeq \frac{m}{8\pi} \left(\frac{\lambda^2}{16m^4} - \frac{4e^4}{m^2\Theta^2} \right) \left[\ln\left(\frac{4m^2}{p^2}\right) + i\pi \right] - \frac{m}{8\pi} \left(\frac{3\lambda^2}{32m^4} - \frac{2e^4}{m^2\Theta^2} \right) \frac{p^2}{2m^2} \left[\ln\left(\frac{4m^2}{p^2}\right) + i\pi \right] + \frac{m}{8\pi} \left(\frac{\lambda^2}{4m^4} - \frac{14e^4}{3m^2\Theta^2} \right) - \frac{m}{8\pi} \left(\frac{25\lambda^2}{96m^4} + \frac{74e^4}{15m^2\Theta^2} \right) \frac{p^2}{m^2}, \quad (29)$$

where calligraphic \mathcal{A} means that the amplitude is written in the nonrelativistic normalization.

Confronting the tree levels, of the relativistic and the NR scattering amplitudes, one sees that the self-interaction parameters are related by $v = \lambda/4m^2$ and the critical values for which the 1-loop NR and leading relativistic scattering amplitudes vanish are also related by

$$v_c^\pm = \frac{\lambda_c^\pm}{4m^2} = \pm \frac{2e^2}{m|\Theta|} = \pm \frac{4\pi}{m} \alpha \operatorname{sgn}(\alpha), \quad (30)$$

where the AB parameter is $\alpha = e^2/2\pi\Theta$. By choosing the value v_c^+ , corresponding to a repulsive contact interaction, the tree amplitude reduces, after multiplying by the appropriated kinematical factor, to the Aharonov-Bohm amplitude for identical particles (4). The leading order vanishes at v_c^+ whereas the subdominant terms that survive, namely

$$\begin{aligned} \mathcal{A}^{\text{sub}} = & \frac{4\pi}{m} \alpha \left[\operatorname{sgn}(\alpha) + \frac{i}{2} \cot \theta \right] \frac{p^2}{m^2} + \frac{17}{3} \frac{\pi}{m} \alpha^2 \\ & - \frac{\pi}{m} \alpha^2 \frac{p^2}{m^2} \left[\ln \left(\frac{4m^2}{p^2} \right) + i\pi \right] - \frac{54}{5} \frac{\pi}{m} \alpha^2 \frac{p^2}{m^2}, \end{aligned} \quad (31)$$

represent relativistic corrections to the Aharonov-Bohm scattering.

Part of the correction of the tree level ($\sim \alpha$) is due to the normalization of states and so has a pure kinematical origin, but not all of it since the scattering amplitude corresponding to the exchange of one virtual gauge particle depends on the CM energy as a consequence of the minimal coupling. The other corrections come from the 1-loop (e^4) contribution to the perturbative expansion and are indeed relativistic. These kind of terms, proportional to α^2 , do not exist in nonrelativistic AB scattering (which exact result is function of $\sin \alpha$) and then may be detected in experiments with fast particles.

References

- [1] Y. Aharonov and D. Bohm, *Phys. Rev.* **115** (1959) 485; for a review see S. Ruijsenaars, *Ann. Phys. (N.Y.)* **146** (1983) 1.
- [2] J. M. Leinaas and J. Myrheim, *Nuovo Cimento* **37B** (1977) 1.
- [3] F. Wilczek, *Phys. Rev. Lett.* **48** (1982) 1144; *Phys. Rev. Lett.* **49** (1982) 957.
- [4] D. P. Arovas, R. Schrieffer, F. Wilczek and A. Zee, *Nucl. Phys.* **B251** (1985) 117.
- [5] C. R. Hagen, *Phys. Rev.* **D31** (1985) 848.
- [6] O. Bergman and G. Losano, *Ann. Phys. (N.Y.)* **229** (1994) 416.
- [7] M. Gomes, J. M. C. Malbouisson and A. J. da Silva, "On the Nonrelativistic Limit of the $\lambda\phi^4$ Theory in 2+1 Dimensions", hep-th/9610247, to be published in *Mod. Phys. Lett. A*.
- [8] M. Boz, V. Fainberg and N. K. Pak, *Phys. Lett.* **A207** (1995) 1; *Ann. Phys. (N.Y.)* **246** (1996) 347.
- [9] R. Jackiw and S. Y. Pi, *Phys. Rev.* **D42** (1990) 3500.

Soluções Tipo Vórtice em Eletrodinâmica Escalar em $D = 2 + 1$ Acoplada à Gravitação

M. S. Cunha, A. Penna Firme, O.S. Ventura

Depto. Campos e Partículas,

Centro Brasileiro de Pesquisas Físicas

Estuda-se o comportamento da matéria escalar carregada acoplada a um campo de Maxwell, em presença de gravitação, em um espaço tempo 3-dimensional. Apesar de não apresentar caráter dinâmico em 3 dimensões, os graus de liberdade gravitacionais são introduzidos como um simples background; as equações de Einstein são analisadas em presença da matéria e do setor de gauge, e a solução proposta para a métrica é parametrizada levando-se em conta as restrições impostas pela dinâmica da matéria e pelas equações de Maxwell em 3D. A partir de dois Ansätze que caracterizam configurações de vórtice em 2 dimensões espaciais, são analisadas as equações não-lineares acopladas que fornecem as configurações de campo e a solução para a métrica. Possíveis soluções, dependendo das condições de contorno, são apresentadas e seu comportamento assintótico é discutido. Procura-se, também, relacionar o ângulo de deficit, característico da geometria associada à gravitação em 3D, com os parâmetros presentes na densidade de Lagrangeana do modelo.

1 Descrição do Modelo

Partiremos de um Lagrangeano que é construído acoplando o Lagrangeano de Einstein ao Lagrangeano de um campo escalar complexo com simetria de gauge $U(1)$:

$$\mathcal{L}_\Phi = \sqrt{-g} \left\{ g^{\mu\nu} (D_\mu \Phi)^\dagger (D_\nu \Phi) - \frac{1}{4} g^{\mu\alpha} g^{\nu\beta} F_{\mu\nu} F_{\alpha\beta} - V(\Phi) \right\} \quad (1)$$

onde $D_\mu \Phi = \nabla_\mu \Phi + e A_\mu \Phi$ e $V(\Phi) = \frac{e^2}{2} R^2 (R - \eta)^2$.

Comporemos as duas partes real e imaginária do campo Φ via $\Phi = R e^{i\psi}$ onde R e ψ são reais.

Nossa análise será efetuada em um espaço tempo de dimensão $D = (2 + 1)$. Neste caso, a métrica mais geral possível que apresenta simetria polar é dada por:

$$ds^2 = e^{2\nu(t,r)} dt^2 - e^{2\eta(t,r)} dr^2 - e^{2\lambda(t,r)} d\phi^2, \quad (2)$$

onde r é a coordenada radial e ϕ é a coordenada polar. Devido à simetria do problema, as funções definidas na métrica somente dependem de r e t . Reescrevendo o Lagrangeano, obtemos:

$$\mathcal{L} = \frac{1}{2} g^{\mu\nu} \partial_\mu R \partial_\nu R + \frac{1}{2} R^2 g^{\mu\nu} (\partial_\mu \psi + e A_\mu) (\partial_\nu \psi + e A_\nu) - V(R) - \frac{1}{4} g^{\mu\alpha} g^{\nu\beta} F_{\mu\nu} F_{\alpha\beta} \quad (3)$$

Assumimos aqui, que o ansatz para o campo A_μ tenha a forma:

$$A_\mu = \delta_\mu^\phi \left(\frac{P(r,t) - 1}{e} \right) \quad (4)$$

Com este Ansatz o tensor momento-energia tem suas componentes expressas por:

$$T_{tt} = \frac{1}{2} \left\{ \dot{R}^2 + R\dot{\psi}^2 + e^{-2\lambda} + e^{2\nu} \left[e^{-2\eta} R'^2 + R^2 \left(e^{-2\eta} \psi'^2 + e^{-2\lambda} \left[\partial_\phi \psi + eP \right]^2 \right) \right. \right. \\ \left. \left. + V(R) + e^{-2(\eta+\lambda)} P'^2 \right] \right\} \quad (5)$$

$$T_{rr} = \frac{1}{2} \left\{ R'^2 + R^2 \psi'^2 + e^{-2\lambda} P'^2 + e^{2\eta} \left[-e^{-2\nu} \dot{R}^2 + R^2 \left(e^{-2\nu} \dot{\psi}^2 + \right. \right. \right. \\ \left. \left. - e^{-2\lambda} \left[\partial_\phi \psi + eP \right]^2 \right) - 2V(R) + e^{-2(\nu+\lambda)} \dot{P}^2 \right] \right\} \quad (6)$$

$$T_{tr} = \dot{R}R' + R^2 \dot{\psi} \psi' + e^{-2\lambda} \dot{P} P' \quad (7)$$

$$T_{\phi\phi} = \frac{1}{2} \left\{ R^2 (\partial_\phi \psi + eP)^2 - e^{-2\nu} \dot{P}^2 + e^{-2\eta} P'^2 + e^{2\lambda} \left[e^{-2\nu} \dot{R}^2 - e^{-2\eta} R'^2 + \right. \right. \\ \left. \left. + R^2 (e^{-2\nu} \dot{\psi}^2 - e^{-2\eta} \psi'^2) - 2V(R) \right] \right\} \quad (8)$$

$$T_{t\phi} = R^2 \dot{\psi} (\partial_\phi \psi + eP) \quad (9)$$

$$T_{r\phi} = R^2 \psi' (\partial_\phi \psi + eP) \quad (10)$$

Como $T_{\mu\nu} \equiv T_{\mu\nu}(r, t)$, somos obrigados a impor que $\partial_\phi \psi = [\partial_\phi \psi](r, t)$, o que vincula o campo ψ à dependência $\psi = \phi h(r, t)$.

O penúltimo termo de (8) é proporcional a $\phi^2 \{ e^{-2\nu} \dot{h}^2 - e^{-2\eta} h'^2 \}$ e, devido à dependência de $T_{\mu\nu}$ em t e r , escrevemos:

$$e^{-2\nu} \dot{h}^2 - e^{-2\eta} h'^2 = 0 \quad (11)$$

Pela mesma razão o segundo termo de T_{tr} implica que:

$$\dot{h} h' = 0 \quad (12)$$

Concluimos, então, que o campo ψ caracteriza a solução tipo vórtice, com $\psi = \phi$.

Ao impormos que o sistema seja estático, obtemos os resultados apresentados por Shaver(Shaver, E., *General Relativity and Gravitation*, 24, 187, 1992), o que implica dizer que há equivalência das soluções em $D = (3+1)$ e $D = (2+1)$ polar, ao eliminarmos a coordenada z . Tomemos aqui a expansão no Ansatz anteriormente apresentado, dada por:

$$A_\mu = \delta_\mu^t \frac{\lambda}{c} + \delta_\mu^\phi \left(\frac{P(r, t) - 1}{c} \right) \quad (13)$$

Mantendo a independência temporal em todas as funções, obtemos as componentes não nulas para o Tensor de Einstein:

$$G_{tt} = -e^{2\nu} \left[\lambda'' + \lambda'^2 \right] \quad (14)$$

$$G_{rr} = \lambda' \nu' \quad (15)$$

$$G_{\phi\phi} = -e^{2\lambda} \left\{ -\nu'^2 - \nu'' \right\} \quad (16)$$

O fator $e^{2\eta}$ foi absorvido na métrica através de uma mudança na coordenada r . Se impusermos $G_{rr} = 0$, a compatibilização da métrica plana para o limite $r \rightarrow \infty$ nos leva a $\nu = const$ em $\nu = 0$, sem perda de generalidade.

Assim, as equações de Euler-Lagrange para os campos A_μ e R bem como as componentes da equação de Einstein, são apresentadas a seguir:

$$P'' - \frac{\omega'}{\omega} P' - e^2 R^2 B = 0 \quad (17)$$

$$\chi'' + \frac{\omega'}{\omega} \chi' - e^2 R^2 \chi = 0 \quad (18)$$

$$R'' + \frac{\omega'}{\omega} R' + R\chi^2 - \frac{P^2}{\omega^2} R - \frac{dV}{dR} = 0 \quad (19)$$

$$R^2 \chi^2 + \left(\frac{P'}{\omega e} \right)^2 = 2V(R) \quad (20)$$

$$R'^2 = \left(\frac{RP}{\omega} \right)^2 + \left(\frac{\chi'}{e} \right)^2 \quad (21)$$

$$\frac{\omega''}{\omega} = -8\pi \left\{ R'^2 + 2V(R) \right\} \quad (22)$$

Estamos tomando $e^\lambda = \omega$.

Na situação em que $P = 0$, as equações (20) e (22) fixam a forma do potencial em:

$$V(R) = \frac{e^2}{2} R^2 (R - \eta)^2 \quad (23)$$

Este potencial acresce um termo cúbico ao tradicionalmente usado, $\lambda\phi^4$. Podemos facilmente verificar que as expressões (19) e (20) são agora equivalentes.

Após a mudança de escala $r \rightarrow \frac{r}{\eta}$, $R \rightarrow \eta R$ e $\chi \rightarrow e\eta\chi$, o sistema torna a forma:

$$\frac{\omega''}{\omega} = -8\pi\eta^2 \left\{ R'^2 + R^2 (R - 1)^2 \right\} \quad (24)$$

$$R'' + \frac{\omega'}{\omega} R' - R^2 (R - 1) = 0 \quad (25)$$

Devemos supor que a métrica tenda à métrica de Minkowsky com um deficit angular quando $r \rightarrow \infty$. Assim consequentemente $\lim_{r \rightarrow \infty} \omega = \alpha r$. O deficit angular é obtido diretamente da equação (25) e é dado por:

$$\alpha = 1 - 8\pi\eta^2 \int_0^\infty \omega(r) \left\{ R'^2 + R^2 (R - 1)^2 \right\} dr \quad (26)$$

2 Conclusão

O problema que nos resta é resolver as equações de campo e fixar as funções R , χ e ω , de tal modo que as configurações do campo escalar, do potencial de gauge e do campo gravitacional fiquem determinadas.

Com as condições de contorno adotadas, a função R , que determina o campo escalar, apresenta solução trivial e a função ω indica ser o espaço-tempo plano.

Portanto, a conclusão a que se chega, de acordo com a resolução explícita das equações dinâmicas, é que a solução de vórtice procurada não deve existir, a não ser que seja introduzido um termo tipo Chern-Simons para o campo A_μ . A presença de tal termo interfere diretamente sobre a função χ e espera-se que forneça soluções não triviais para P e ω . Tal possibilidade, encontra-se em fase de análise.

3 Referências

- (1) E. Shaver, *Gen. Rel. Grav. N° 2*, Vol. 24, (1992)
- (2) E. Shaver, K. Lake, *Phys. Rev. D* **40**, 3287 (1989)
- (3) D. Garfinkle, *Phys. Rev. D* **32**, 1323 (1985)
- (4) T. Kibble, *J. Phys. A* **14**, 1387 (1976)
- (5) A. Vilenkin, *Phys. Rev. D* **23**, 852 (1981)
- (6) A. Vilenkin, *Phys. Rep.* 121 N° 5 263 - 315 (1984)

Método de Gibbons para Função Zeta em Teoria de Campos

M.V. Cougo-Pinto, C. Farina, A. Tenório*

Instituto de Física, Universidade Federal do Rio de Janeiro

O estudo de ações efetivas a 1-laço nos conduz ao cálculo de determinantes de operadores cujos espectros exigem que métodos de regularização sejam empregados. Uma das técnicas de regularização usadas é a da função zeta generalizada, definida como:

$$\zeta(s; \mathbf{H}) = \text{Tr } \mathbf{H}^{-s}, \quad (1)$$

onde \mathbf{H} é um operador e s um número complexo. Por meio da função zeta generalizada é possível prescrever, para o determinante de uma ampla classe de operadores, uma expressão finita, a saber:

$$\det \mathbf{H} = \exp \left[- \frac{d}{ds} \zeta(s; \mathbf{H}) \Big|_{s=0} \right], \quad (2)$$

onde estão subtendidas extensões analíticas apropriadas da função zeta no plano complexo s . Essa expressão regulariza $\det \mathbf{H}$, porque a derivada da extensão analítica da zeta é quase sempre analítica em $s = 0$; condição sempre satisfeita para o caso de operadores elípticos quando aplicados sobre variedades compactas e sem fronteiras.

Um ponto de partida amplamente empregado no cálculo de ações efetivas a 1-laço, $\mathcal{W}^{(1)}$, é a relação¹

$$\frac{\partial}{\partial m^2} \mathcal{W}^{(1)} = \frac{i}{2} \text{Tr } \mathbf{G}, \quad (3)$$

onde \mathbf{G} é o operador de Green; ou seja, seu elemento de matriz $\langle x | \mathbf{G} | y \rangle = G(x, y)$ é a função de Green. Essa expressão, em (3+1) dimensões, entretanto, padece de divergências ultravioletas. A função de Green diverge em pontos coincidentes, fazendo-se necessário fornecer um esquema de regularização.

O método de regularização comumente utilizado na literatura é a separação de pontos. Essa técnica consiste em separar os pontos da função de Green, realizar os cálculos e, ao final, remover os termos que divergem no limite quando os pontos são tomados coincidentes novamente.

A proposta inserida neste trabalho é apresentar um método de cálculo e regularização alternativo a separação de pontos, baseado na função zeta generalizada. Nessa abordagem, a regularização do traço da função de Green é implementada modificando-se a expressão original (3) para

$$\begin{aligned} \frac{\partial}{\partial m^2} \mathcal{W}_s^{(1)} &= \frac{i}{2} \text{Tr } \mathbf{G}^s \\ &= \frac{i}{2} \zeta(s; \mathbf{H}). \end{aligned} \quad (4)$$

Para recuperar a equação original basta calcular $\zeta(1; \mathbf{H})$, que contudo diverge. O imperativo, portanto, antes de tomar o limite $s \rightarrow 1$, eliminar os termos fisicamente espúrios. Este método foi introduzido por Gibbons, em 1975, a fim de computar a função partição do oscilador harmônico quântico; mas nunca foi utilizado no contexto da Teoria Quântica de Campos.

Com a intenção de ilustrar esse método, vamos aplicá-lo em dois exemplos na tentativa de reproduzir resultados conhecidos. O primeiro é o cálculo da pressão de Casimir para um campo escalar real massivo entre duas placas

*e-mail: tenorio@if.ufrj.br

¹O fator a frente do traço pode ser $(i/2)$ ou $(-i/2)$, dependendo da natureza bosônica ou fermiônica, respectivamente, do campo.

infinitas. No segundo exemplo aplicamos o método a Eletrodinâmica Quântica, calculando a Lagrangiana efetiva a 1-laço com um campo magnético externo constante e uniforme.

Efeito Casimir

O efeito Casimir é consequência direta da peculiar estrutura do vácuo quântico. As flutuações quânticas de ponto-zero dos campos têm por resultado gerar um estresse mecânico sobre superfícies materiais que limitem um dada região do espaço. Por exemplo, a interação com o vácuo eletromagnético provoca uma pequena, mas mensurável, força de atração entre duas placas metálicas neutras e infinitas separadas por uma distância a . Originalmente esse efeito foi previsto por Casimir em 1948; e oito anos mais tarde a pressão de Casimir foi medida experimentalmente pela primeira vez por Sparnay, em acordo com as previsões teóricas.

A fim de aplicar o método de Gibbons ao efeito Casimir, devemos relacionar a energia do vácuo \mathcal{E} com a ação efetiva a 1-laço $\mathcal{W}^{(1)}$. Pode-se mostrar a seguinte relação entre essas duas grandezas:

$$\mathcal{E} = -\frac{\mathcal{W}^{(1)}}{T}, \quad (5)$$

onde T é um intervalo de tempo tendendo ao infinito.

Escolhemos computar a energia de Casimir entre duas placas sobre as quais um campo escalar real massivo é nulo, ou seja, obedece condições de contorno do tipo Dirichlet.

Pela expressão regularizada para a ação efetiva (4), observamos que é preciso determinar a função zeta $\zeta(s; \mathbf{H})$ do Hamiltoniano \mathbf{H} desse sistema.

$$\mathbf{H} = -\square + m^2, \quad (6)$$

cujas autofunções φ satisfazem condições de contorno homogêneas sobre as placas, ou seja, $\varphi(x, y, z = 0) = \varphi(x, y, z = a) = 0$. A função zeta generalizada pode então ser escrita como:

$$\zeta(s; \mathbf{H}) = iTL^2 \sum_{n=1}^{\infty} \int \frac{dk_1 dk_2 dk_4}{(2\pi)^3} \left[m^2 + k_1^2 + k_2^2 + k_4^2 + \frac{n^2 \pi^2}{a^2} \right]^{-s}, \quad (7)$$

onde T é o tempo, L^2 é a área das placas, $n = 1, 2, \dots$ e a é a distância entre as placas. Note que na integral executou-se uma rotação que levou $k_0 \rightarrow ik_4$. Daí,

$$\int dk_1 dk_2 dk_4 \rightarrow \oint d\Omega \int_0^{\infty} k^2 dk; \quad k^2 = k_1^2 + k_2^2 + k_4^2$$

$$\zeta(s; \mathbf{H}) = i \frac{2TL^2}{(2\pi)^2} \sum_{n=1}^{\infty} \int_0^{\infty} k^2 dk \left[m^2 + k^2 + \frac{n^2 \pi^2}{a^2} \right]^{-s} \quad (8)$$

A integral em k é conhecida (Gradshteyn & Ryzhik, 8380-3):

$$\int_0^{\infty} dx (x^2)^{\frac{\alpha-1}{2}} (A^2 + x^2)^{\beta-1} = \frac{1}{2} (A^2)^{\frac{\alpha}{2} + \beta - 1} B\left(\frac{\alpha}{2}, 1 - \beta - \frac{\alpha}{2}\right),$$

onde $\text{Re}(\alpha) > 0$; $\text{Re}(\beta + \frac{\alpha}{2}) < 1$; e $B(x, y) = \frac{\Gamma(x)\Gamma(y)}{\Gamma(x+y)}$ é a função beta de Euler. Identificando os coeficientes, obtemos:

$$\zeta(s; \mathbf{H}) = i \frac{2TL^2}{(2\pi)^2} \sum_{n=1}^{\infty} \frac{1}{2} \left[m^2 + \frac{n^2 \pi^2}{a^2} \right]^{\frac{3}{2}-s} B\left(\frac{3}{2}, s - \frac{3}{2}\right). \quad (9)$$

Portanto,

$$\zeta(s; \mathbf{H}) = i \frac{TL^2}{8\pi\sqrt{\pi}} \left(\frac{\pi^2}{a^2}\right)^{\frac{3}{2}-s} \frac{\Gamma(s - \frac{3}{2})}{\Gamma(s)} \sum_{n=1}^{\infty} \frac{1}{(n^2 + \sigma^2)^{s - \frac{3}{2}}}, \quad (10)$$

onde $\sigma = \frac{a}{L}m$. O somatório na equação acima é simplesmente a definição de função Epstein-1:

$$E_1^{\sigma^2}(s, 1) \equiv \sum_{n=1}^{\infty} \frac{1}{(n^2 + \sigma^2)^s};$$

cuja extensão analítica para todo o plano complexo pode ser expressada pela fórmula:

$$E_1^{\sigma^2}(z, 1) = -\frac{1}{2\sigma^{2z}} + \frac{\sqrt{\pi}}{2\sigma^{2z-1}} + \frac{2\sqrt{\pi}}{\sigma^{2z-1}} \frac{1}{\Gamma(z)} \sum_{n=1}^{\infty} (\pi\sigma n)^{z-\frac{1}{2}} K_{z-\frac{1}{2}}(2\pi\sigma n).$$

onde $K_{z-\frac{1}{2}}$ é uma função de Bessel modificada. Substituindo-a, então, na equação (9), obtemos a expressão final para a função zeta.

$$\begin{aligned} \zeta(s; \mathbf{H}) = & i \frac{TL^2}{8\pi^2} \left[-\frac{\sqrt{\pi}}{2} m^{3-2s} \frac{\Gamma(s-\frac{3}{2})}{\Gamma(s)} + \frac{a}{2} m^{4-2s} \frac{\Gamma(s-2)}{\Gamma(s)} \right. \\ & \left. + \frac{2}{\Gamma(s)} a^{s-1} m^{2-s} \sum_{n=1}^{\infty} n^{s-2} K_{s-2}(2amn) \right] \end{aligned} \quad (11)$$

A fim de analisar as divergências que acometem sobre a ação efetiva $\mathcal{W}^{(1)}$, tomamos o limite do regularizador $s \rightarrow 1$. É importante identificar os termos singulares antes de integrar em m^2 , caso contrário o método pode gerar termos divergentes que não podem ser excluídos na etapa subsequente, como veremos no nosso segundo exemplo.

Na expressão (11) o segundo termo é singular; mas, felizmente pode ser descartado por meio do seguinte argumento físico: ao observar sua dependência linear em a , concluímos que esse termo está relacionado a uma densidade de energia uniforme, contida no volume aL^2 , independente da separação das placas. Esse termo obviamente é irrelevante para a interação entre elas.

O primeiro termo da expressão (11), apesar de finito, também deve ser excluído, porque independe da distância a , não contribuindo para a força. Esse termo pode ser encarado como a auto-energia das placas.

Concluimos, portanto, que só o terceiro termo tem relevância física. A expressão para ação efetiva fica reduzida a

$$\frac{\partial}{\partial m^2} \mathcal{W}_{s=1}^{(1)} = \frac{i}{2} \zeta(s=1; \mathbf{H}) = -\frac{TL^2}{8\pi^2} m \sum_{n=1}^{\infty} \frac{1}{n} K_{-1}(2amn). \quad (12)$$

Para efetuar a integração em m^2 , usamos a seguinte propriedade:

$$\frac{\partial}{\partial m^2} \left[\frac{m^2}{a^2} \frac{1}{n^2} K_{-2}(2amn) \right] = -\frac{m}{a} \frac{1}{n} K_{-1}(2amn).$$

Substituindo em (12),

$$\frac{\partial}{\partial m^2} \mathcal{W}^{(1)} = \frac{\partial}{\partial m^2} \left[\frac{TL^2}{8\pi^2} \frac{m^2}{a} \sum_{n=1}^{\infty} \frac{1}{n^2} K_{-2}(2amn) \right]; \quad (13)$$

e finalmente integrando, chegamos a expressão para a densidade de energia de Casimir para um campo escalar real massivo, a saber,

$$\frac{\mathcal{E}(a)}{L^2} = -\frac{m^2}{8\pi^2 a} \sum_{n=1}^{\infty} \frac{1}{n^2} K_{-2}(2amn) + ctc, \quad (14)$$

onde ctc é uma constante de normalização. Essa constante pode ser determinada se lembrarmos que a energia de interação deve ser nula no limite em que a massa associada ao campo escalar tende a infinito ($m \rightarrow \infty$). Nesse limite, o tempo de vida das partículas virtuais tende a zero, não existindo flutuação quântica - no limite clássico não há efeito Casimir. Como a função de Bessel modificada $K_{-2}(z)$ decresce exponencialmente com z , resulta que a constante vale zero ($ctc = 0$).

No limite em que a massa tende a zero ($m \rightarrow 0$), a energia de Casimir vale

$$\frac{\mathcal{E}(a)}{L^2} \approx -\frac{\pi^2}{1440a^3} + \frac{m^2}{96a} + O[m^4]. \quad (15)$$

No limite de massa grande ($am \gg 1$), o resultado é

$$\frac{\mathcal{E}(a)}{L^2} \approx -\frac{1}{32} \left(\frac{m}{\pi a}\right)^{\frac{3}{2}} e^{-2am}. \tag{16}$$

Lagrangiana Efetiva na EDQ

No segundo exemplo da aplicação do método de Gibbons a TQC, calculamos a Lagrangiana efetiva a 1-laço da Eletrodinâmica Quântica para um campo magnético externo constante e uniforme. Para tanto, partimos da seguinte expressão para a ação efetiva:

$$\mathcal{W}^{(1)} = -\frac{i}{2} \text{Tr} \log (\not{f}^2 + m^2) : \quad \not{f}^2 = \pi^2 + \frac{e}{2} \sigma_{\mu\nu} F^{\mu\nu}, \tag{17}$$

onde Tr denota o traço funcional e matricial. Na situação em questão o campo elétrico $\vec{E} = 0$ e o campo magnético $\vec{B} = B\vec{e}_3$. Logo, no tensor de Maxwell $F^{\mu\nu}$ só as componentes $F^{12} = -F^{21} = B$ são diferentes de zero. Daí, calculando o traço matricial,

$$\mathcal{W}^{(1)} = -i \sum_{j=1}^2 \text{tr} \log \left[(-\not{y}^j eB + m^2 + \pi^2) \right]. \tag{18}$$

onde tr denota o traço funcional apenas. Derivando essa expressão em relação a m^2 , obtemos que

$$\frac{\partial}{\partial m^2} \mathcal{W}^{(1)} = -i \sum_{j=1}^2 \text{tr} \mathbf{H}_j^{-1} : \quad \mathbf{H}_j = (-\not{y}^j eB + m^2 + \pi^2) \tag{19}$$

Em (3+1) dimensões, ambos os traços que aparecem na equação (19) divergem, fazendo-se necessário regularizá-la. Empregando o método de Gibbons, obtemos:

$$\frac{\partial}{\partial m^2} \mathcal{W}_s^{(1)} = -i \sum_{j=1}^2 \zeta(s; \mathbf{H}_j) \tag{20}$$

Para computar as funções zeta que aparecem na equação acima, precisamos conhecer o espectro do operador $m^2 + \pi^2$. Os autovalores desse operador são

$$(n + 1/2)2eB + m^2 - k_0^2 + k_4^2.$$

onde o número quântico de energia $n = 0, 1, 2, \dots$ determina um nível de Landau. A degenerescência de cada nível n é $(eB/2\pi)$ por unidade de área.

$$\zeta(s; \mathbf{H}_j) = i\Omega \left(\frac{eB}{2\pi}\right) \sum_{n=0}^{\infty} \int \frac{dk_3 dk_4}{(2\pi)^2} \left[(-\not{y}^j eB + (2n + 1)eB + m^2 + k_3^2 + k_4^2) \right]^{-s}. \tag{21}$$

onde $\Omega = TL^3$ é um volume no espaço-tempo. Integrando (21) de forma inteiramente similiar a integração realizada na equação (7) em nosso primeiro exemplo, após algumas manipulações, obtemos que

$$\zeta(s; \mathbf{H}_j) = i \frac{\Omega}{16\pi^2} (2eB)^{2-s} \frac{\Gamma(s-1)}{\Gamma(s)} \sum_{n=0}^{\infty} \left[n + \alpha + 2 + (-1)^j \right]^{1-s}. \tag{22}$$

onde $\alpha = m^2/2eB$. Mas o somatório na expressão acima corresponde a própria definição da função zeta de Hurwitz $\zeta_H(z; a)$:

$$\zeta_H(z; a) = \sum_{n=0}^{\infty} \frac{1}{(n+a)^z}.$$

o que nos permite escrever:

$$\sum_{j=1}^2 \zeta(s; \mathbf{H}_j) = i \frac{\Omega}{16\pi^2} (2eB)^{2-s} \frac{\Gamma(s-1)}{\Gamma(s)} \left\{ \zeta_H(s-1; 1+\alpha) + \zeta_H(s-1; \alpha) \right\}. \tag{23}$$

Usando a propriedade de função zeta de Hurwitz traduzida por

$$\zeta_H(z; 1+a) = \zeta_H(z; a) - a^{-z}.$$

podemos reescrever a equação (23), de forma que

$$\frac{\partial}{\partial m^2} \mathcal{W}_s^{(1)} = -i \sum_{j=1}^2 \zeta(s; \mathbf{H}_j) = \frac{\Omega}{16\pi^2} (2eB)^{2-s} \frac{\Gamma(s-1)}{\Gamma(s)} \left\{ 2\zeta_H(s-1; \alpha) - \alpha^{1-s} \right\}. \tag{24}$$

Na expressão acima a extensão analítica de função zeta de Hurwitz está subtendida. Obviamente, quando $s \rightarrow 1$, essa expressão ainda diverge, uma vez que não fizemos nada para sanar suas singularidades. A fim de analisar como a derivada da ação efetiva diverge quando $s \rightarrow 1$, usamos a seguinte representação para a extensão analítica da zeta de Hurwitz:

$$\zeta_H(z; \alpha) = \frac{\alpha^{-z}}{2} - \frac{\alpha^{1-z}}{1-z} + \frac{1}{\Gamma(z)} \int_0^\infty \left[\frac{1}{e^t-1} - \frac{1}{t} + \frac{1}{2} \right] e^{-\alpha t} t^{z-1} dt,$$

válida para $\text{Re}(z) > -1$ e $\text{Re}(\alpha) > 0$. Daí,

$$\begin{aligned} \frac{\partial}{\partial \alpha} \mathcal{W}_s^{(1)} &= \frac{\Omega}{8\pi^2} (2eB)^{3-s} \frac{\Gamma(s-1)}{\Gamma(s)} \left\{ \zeta_H(s-1; \alpha) - \frac{\alpha^{1-s}}{2} \right\} \\ &= \frac{\Omega}{8\pi^2} (2eB)^{3-s} \left\{ -\frac{\alpha^{2-s}}{(1-s)(2-s)} + \right. \\ &\quad \left. + \frac{1}{\Gamma(z)} \int_0^\infty \left[\frac{1}{e^t-1} - \frac{1}{t} + \frac{1}{2} \right] e^{-\alpha t} t^{s-1} dt \right\}. \end{aligned} \tag{25}$$

Pode-se mostrar que a integral na expressão acima converge quando $s = 1$; portanto, somente o primeiro termo é singular. Esse termo integrado em α vale:

$$\frac{\Omega}{8\pi^2} \frac{m^{2(3-s)}}{(1-s)(2-s)(3-s)}.$$

Como podemos observar, ele não depende do campo magnético B , podendo ser excluído, apesar de divergir no limite $s \rightarrow 1$. Logo, a expressão para a derivada da ação efetiva em relação a α , em $s = 1$, fica reduzida a equação:

$$\frac{\partial}{\partial \alpha} \mathcal{W}^{(1)} = \frac{\Omega}{2\pi^2} (eB)^2 \int_0^\infty \left[\frac{1}{e^t-1} - \frac{1}{t} + \frac{1}{2} \right] \frac{e^{-\alpha t}}{t} dt. \tag{26}$$

Usando a primeira identidade de Binet para $\log \Gamma(z+1)$ (Whittaker & Watson, 12.31),

$$\log \Gamma(z+1) = \left(z - \frac{1}{2} \right) \log z - z + \frac{1}{2} \log(2\pi) + \int_0^\infty \left[\frac{1}{e^t-1} - \frac{1}{t} + \frac{1}{2} \right] \frac{e^{-\alpha t}}{t} dt,$$

obtemos finalmente uma expressão para a derivada da ação efetiva em relação a α que pode ser facilmente integrada:

$$\frac{\partial}{\partial \alpha} \mathcal{W}^{(1)} = \frac{\Omega}{2\pi^2} (eB)^2 \left\{ \log \left[\frac{\Gamma(\alpha+1)}{\sqrt{2\pi}} \right] - \alpha \log \alpha + \frac{1}{2} \log \alpha + \alpha \right\}. \tag{27}$$

A fim de integrar a equação (27), usamos a seguinte relação:

$$\zeta'_H(-1; 1+x) = \zeta'_H(-1) + \frac{1}{2}(x^2+x) + \int_0^x \log \left[\frac{\Gamma(1+y)}{\sqrt{2\pi}} \right] dy.$$

onde $\zeta'_H(-1; a)$ e $\zeta'_R(-1)$ representam, respectivamente, as derivadas das funções zeta de Hurwitz e zeta de Riemann no ponto $z = -1$ do plano complexo. Daí, integrando de zero até $\alpha = m^2/2eB$, obtemos que

$$\begin{aligned} \mathcal{W}^{(1)}(B) &= \frac{\Omega}{2\pi^2}(eB)^2 \left\{ \log \int_0^\alpha \left[\frac{\Gamma(\gamma+1)}{\sqrt{2\pi}} \right] d\gamma - \int_0^\alpha \left[\gamma \log \gamma + \frac{1}{2} \log \gamma + \gamma \right] d\gamma \right\} + cte \\ &= \frac{\Omega}{2\pi^2}(eB)^2 \left\{ \zeta'_H(-1; 1+\alpha) - \zeta'_R(-1) - \frac{1}{2} \left(\log \alpha - \frac{1}{2} \right) \left(\alpha^2 - \alpha \right) \right\} + cte, \end{aligned} \quad (28)$$

onde cte é uma constante de normalização que pode ser determinada se obrigarmos que a ação efetiva a 1-laço seja nula quando não existe campo magnético externo, $\mathcal{W}^{(1)}(B=0) = 0$. Quando $B \rightarrow 0$, $\alpha \rightarrow \infty$, permitindo usar a seguinte expansão assintótica da $\zeta'_H(-1; a)$ para $|a| \gg 1$ (Elizalde & Soto, Ann. Phys. 162 (1985) 192):

$$\zeta'_H(-1; a) = \left(\frac{a^2}{2} - \frac{a}{2} + \frac{1}{12} \right) \log a - \frac{a^2}{4} + \frac{1}{12} + O(a^{-2}).$$

Substituindo essa expressão na equação (28), observamos que todos os termos resultantes entre as chaves são nulos quando $B = 0$. Isso implica que a constante de normalização também é nula ($cte = 0$). Portanto, a expressão final para a Lagrangiana efetiva a 1-laço na EDQ com campo magnético constante e uniforme é:

$$\begin{aligned} \mathcal{L}^{(1)}(B) &= \frac{(eB)^2}{2\pi^2} \left\{ \zeta'_H \left(-1; 1 + \frac{m^2}{2eB} \right) - \zeta'_R(-1) - \right. \\ &\quad \left. - \frac{1}{2} \left[\log \left(\frac{m^2}{2eB} \right) - \frac{1}{2} \right] \left[\left(\frac{m^2}{2eB} \right)^2 - \left(\frac{m^2}{2eB} \right) \right] \right\}. \end{aligned} \quad (29)$$

Factored coset approach to bosonization in the context of topological backgrounds and massive fermions

M.V.Manías^{a,b}, C.M.Naón^{a,b}, and M.L.Trobo^{a,b}

^a Depto. de Física, Universidad Nacional de La Plata.

CC 67, 1900 La Plata, Argentina.

^b Consejo Nacional de Investigaciones Científicas y Técnicas, Argentina.

We consider a recently proposed approach to bosonization in which the original fermionic partition function is expressed as a product of a G/G -coset model and a bosonic piece that contains the dynamics. In particular we show how the method works when topological backgrounds are taken into account. We also discuss the application of this technique to the case of massive fermions.

In a recent paper [1], Theron et al presented an alternative approach to bosonization in two dimensions using the path integral formalism. They obtained a complete derivation of the bosonization dictionary for both the Abelian and non-Abelian cases. In the Abelian case they started with the generating functional for current-current correlation functions of free Dirac fermions in two dimensional Euclidean space:

$$Z = \int D\bar{\Psi} D\Psi DA \exp\left\{-\int d^2x (\bar{\Psi} i\not{\partial}\Psi - j_\mu A_\mu)\right\} \quad (1)$$

where $j_\mu = \bar{\Psi}\gamma_\mu\Psi$.

In a general gauge, that is without fixing the gauge, the method consists in making a gauge transformation in the fermionic variables which gives rise to a delta of conservation of the fermionic current $j_\mu = \bar{\Psi}\gamma_\mu\Psi$. Appropriately representing $\delta(\partial_\mu j_\mu)$ and making a chiral change of variables Z can be factorized in terms of a G/G -coset fermionic partition function, and a bosonic part which contains the dynamics:

$$Z = \int D\bar{\Psi} D\Psi DB_\mu e^{-S_{cf}} \int D\phi DA_\mu e^{-S_{bos}[\phi, A_\mu]} \quad (2)$$

where S_{cf} is the action of the fermionic coset $U(1)/U(1)$ model.

This is one of the main achievements of the new approach. Indeed, in the standard decoupling technique of the path integral bosonization [2], $Z[A_\mu]$ is expressed as a bosonic partition function multiplied by the vacuum to vacuum amplitude of free fermions. In the framework of Ref.[1] the fermionic factor corresponds to constrained fermions, which are dynamically trivial (in the sense that both fermionic currents are set equal to zero). Thus, the bosonizing character of the procedure becomes more apparent.

Taking this into account it is interesting to analyze the applicability of this new method to the study of other physical situations in which the bosonization procedure is known to be more involved than in the case of free massless fermions. In this work we focus our attention on two of such situations. Firstly we consider a model of fermions coupled to a vector field A_μ , allowing this field to carry a non-trivial topological charge: $\oint A_\mu dx^\mu = -2\pi N$ [3]. One of the more interesting features of this model is the existence of the so called minimal correlation functions which, being zero for trivial topology, develop non-zero values when $N \neq 0$.

Finally we go back to trivial topology and briefly show how to extend the method of [1] to the case in which fermions are massive. This is an important point since much of the pioneering work on bosonization was done in the context of massive models [4].

On the other hand, our discussion concerning this matter could also be helpful in order to use the ideas of [1] in the study of 2D statistical-mechanics models away from criticality. In this context $\bar{\Psi}\Psi$ is the energy density of the system and $m \propto (T - T_c)$.

Let us start with the generating functional introduced in Ref [3]:

$$Z = \sum_N \int D\bar{\Psi} D\Psi DA_\mu \exp\{- \int d^2x \bar{\Psi}[i\partial + A]\Psi\} \tag{3}$$

with $A_\mu = A_\mu^{c(N)} + a_\mu$, where $A_\mu^{c(N)}$ is a fixed (classical) configuration with topological charge N :

$$\oint A_\mu^{c(N)} dx^\mu = -2\pi N \tag{4}$$

while a_μ stays in the topologically trivial ($N = 0$) sector.

Following the procedure developed in [1] to obtain a coset model in a general gauge, we perform a gauge transformation

$$\Psi \rightarrow e^{i\eta(x)}\Psi \qquad \bar{\Psi} \rightarrow \bar{\Psi}e^{-i\eta(x)} \tag{5}$$

in the generating functional (3). We then have

$$Z = \sum_N \int D\bar{\Psi} D\Psi DA_\mu \exp\{- \int d^2x [\bar{\Psi}i\partial\Psi + j_\mu A_\mu + (\partial_\mu j_\mu)\eta]\} \tag{6}$$

This partition function is in fact η -independent so we can integrate over η : we introduce the identity as

$$Z = \sum_N \int D\bar{\Psi} D\Psi DA_\mu \delta(\partial_\mu j_\mu) \exp\{- \int d^2x [\bar{\Psi}i\partial\Psi + j_\mu A_\mu]\} \tag{7}$$

Now we represent $\delta(\partial_\mu j_\mu)$ in the form

$$\delta(\partial_\mu j_\mu) = \int DB_\mu D\theta \exp\{- \int d^2x [B_\mu j_\mu + \frac{1}{\pi} B_\mu \epsilon_{\mu\nu} \partial_\nu \theta]\} \tag{8}$$

Introducing this expression in the generating functional and making the shift $B'_\mu = B_\mu + a_\mu$, we obtain

$$\begin{aligned} Z &= \sum_N \int D\bar{\Psi} D\Psi DA_\mu DB'_\mu D\theta \exp\{- \int d^2x \{\bar{\Psi}i\partial\Psi + j_\mu(A_\mu^{c(N)} + B'_\mu) + \\ &+ \frac{1}{\pi} B'_\mu \epsilon_{\mu\nu} \partial_\nu \theta\} - \frac{1}{\pi} a_\mu \epsilon_{\mu\nu} \partial_\nu \theta\} \end{aligned} \tag{9}$$

In order to factorize out a constrained fermionic model we have to eliminate the linear term in B'_μ . To this end we make a chiral transformation with parameter σ in the fermionic variables. This change yields a Fujikawa Jacobian given by [5]:

$$J_F = \exp\{\frac{1}{\pi} \epsilon_{\mu\nu} \partial_\nu \sigma (B'_\mu + A_\mu^{c(N)}) - \frac{1}{2\pi} \sigma \square \sigma\} \tag{10}$$

The generating functional becomes:

$$Z = \sum_N \int D\bar{\Psi} D\Psi DA_\mu DB'_\mu D\theta e^{-S} \tag{11}$$

where

$$S = \int d^2x \{ \bar{\Psi} i\rlap{\not{\partial}}\Psi + (B'_\mu + A_\mu^{c(N)} + \epsilon_{\mu\nu}\partial_\nu\sigma)j_\mu + \frac{1}{\pi}\epsilon_{\mu\nu}\partial_\nu\theta B'_\mu - \frac{1}{\pi}\epsilon_{\mu\nu}\partial_\nu\theta a_\mu - \frac{1}{\pi}\epsilon_{\mu\nu}\partial_\nu\sigma A_\mu^{c(N)} - \frac{1}{\pi}\epsilon_{\mu\nu}\partial_\nu\sigma B'_\mu + \frac{1}{2\pi}\sigma\Box\sigma \} \tag{12}$$

Now choosing $\sigma = \theta$, we cancel the linear term in B'_μ and obtain

$$Z = \sum_N \int D\bar{\Psi} D\Psi DA_\mu DB'_\mu D\sigma e^{-S'} \tag{13}$$

with

$$S = \int d^2x \{ \bar{\Psi} i\rlap{\not{\partial}}\Psi + (B'_\mu + A_\mu^{c(N)} + \epsilon_{\mu\nu}\partial_\nu\sigma)j_\mu - \frac{1}{\pi}\epsilon_{\mu\nu}\partial_\nu\sigma A_\mu + \frac{1}{2\pi}\sigma\Box\sigma \} \tag{14}$$

In order to write this generating functional as the product of a $\frac{U(1)}{U(1)}$ fermionic coset model and a bosonic part, like in Ref.[1], we make the shift $B'_\mu \rightarrow B'_\mu - \epsilon_{\mu\nu}\partial_\nu\sigma$. Thus we have

$$Z = \sum_N \int D\bar{\Psi} D\Psi DB'_\mu e^{-S'_{cf}(N)} \int D\sigma DA_\mu e^{-S_{bos}(\sigma, A_\mu^{c(N)})} \tag{15}$$

where

$$S'_{cf}(N) = \int d^2x \bar{\Psi} [i\rlap{\not{\partial}} + B'_\mu + A_\mu^{c(N)}]\Psi \tag{16}$$

and

$$S_{bos}(\sigma, A_\mu) = \int d^2x \frac{1}{\pi} [\sigma \frac{\Box}{2} \sigma - \epsilon_{\mu\nu}\partial_\nu\sigma A_\mu] \tag{17}$$

Let us stress that in our case both the $\frac{U(1)}{U(1)}$ fermionic coset factor and the bosonic one have a non-trivial topological structure.

If we want to identify this result with the one obtained in Ref.[3] we have to make a second chiral transformation in the fermionic variables, in order to decouple the B_μ field from the fermions [2]. In this way we recover a factorized generating functional $Z = Z_{Fer} \times Z_{Bos}$, with Z_{Fer} having the same zero modes problem which was studied in Ref.[3].

Calling the parameter of the transformation ϕ , we obtain:

$$\begin{aligned} Z &= \sum_N \int D\bar{\chi} D\chi \exp\{-\int d^2x [\bar{\chi}(i\rlap{\not{\partial}} + A_c^N)\chi]\} \times \\ &\int DA_\mu D\sigma D\phi \exp\{\frac{1}{\pi}\int d^2x [\epsilon_{\mu\nu}\partial_\nu\sigma A_\mu - \frac{1}{2}\sigma\Box\sigma + \epsilon_{\mu\nu}\partial_\nu\phi A_\mu^c + \frac{1}{2}\phi\Box\phi]\} \\ &= Z_{Fer} \times Z_{Bos} \end{aligned} \tag{18}$$

From this expression, one can conclude that only the $N = 0$ sector contributes to the Z , a well established result for massless fermions [3].

Now, in order to compute fermionic correlation functions we have to add source terms in the form:

$$Z_{\rho_R, \rho_L} = \int D\bar{\Psi} D\Psi DA_\mu \exp\{- \int d^2x [\bar{\Psi} i\rlap{/}{\partial}\Psi - j_\mu A_\mu + \rho_R \bar{\Psi}_R \Psi_R + \rho_L \bar{\Psi}_L \Psi_L]\} \tag{19}$$

so that, differentiating n_R times (n_L) with respect to ρ_R (ρ_L) we obtain the minimal correlation function in the n_R (n_L) sector, and making the cross derivatives n_R times with respect to ρ_R and n_L times with respect to ρ_L we arrive to the non-minimal correlator in the $|n_R - n_L|$ topological sector.

Let us consider the minimal functions in the $n_R > 0$ sector (equivalent results are obtained in the $n_L < 0$ sector) as follows:

$$\langle \prod_{i=0}^{n_R-1} \bar{\Psi}_R \Psi_R(x_i) \rangle = Z^{-1} \frac{\delta^{n_R} Z}{\delta \rho_R(x_0) \dots \delta \rho_R(x_{n_R-1})} \tag{20}$$

This expression can be factorized as the product of a fermionic mean value and two bosonic parts in the form

$$\begin{aligned} \langle \prod_{i=0}^{n_R-1} \bar{\Psi}_R \Psi_R(x_i) \rangle &= \langle \prod_{i=0}^{n_R-1} \bar{\chi}_R \chi_R(x_i) \rangle_{fer} \langle e^{\sum_{i=0}^{n_R-1} \beta_i \phi(x_i)} \rangle_{bos} \\ &< e^{\sum_{i=0}^{n_R-1} \beta_i \sigma(x_i)} \rangle_{bos} \end{aligned} \tag{21}$$

where $\beta_i = 2$ for all values of i , and

$$L_F = \bar{\Psi} [i\rlap{/}{\partial} + A^{(N)}] \Psi \tag{22}$$

$$L_\sigma = \frac{1}{\pi} [\sigma \frac{\square}{2} \sigma - \epsilon_{\mu\nu} \partial_\nu \sigma A_\mu] \tag{23}$$

and

$$L_\phi = -\frac{1}{\pi} [\phi \frac{\square}{2} \phi + \epsilon_{\mu\nu} \partial_\nu \phi A_\mu] \tag{24}$$

For simplicity we shall consider a distribution of the topological charge given by

$$\epsilon_{\mu\nu} \partial_\mu A_\nu^G = \sum_{i=0}^{n_R-1} \alpha_i(x) \delta^2(x - x_i) \tag{25}$$

with

$$\sum_{i=0}^{n_R-1} \alpha_i(x_i) = -2\pi N \tag{26}$$

This distribution corresponds to a Nielsen-Olesen configuration [6], in which the vortex width tends to zero (see Ref.[7] for details).

For the fermionic part we obtain

$$F(x_0, \dots, x_{n_R-1}) = \det_0(i\rlap{/}{\partial} + A_c^N) e^{\sum_{i=0}^{n_R-1} \alpha_i \beta_j \square_{x_i, x_j}^{-1}} \prod_{i < j} |x_i - x_j|^2 \tag{27}$$

while the bosonic piece (i.e. the product of the last two factors in (16)) is given by

$$B(x_0, \dots, x_{n_R-1}) = c^{-\sum_{i,j} (\frac{\alpha_i \alpha_j}{2r^2} + \alpha_i \beta_j + \frac{1}{2} \beta_i \beta_j)} \Omega_{x_i, x_j}^{-1} \quad (28)$$

So, the minimal correlation function for the $n_R > 0$ topological sector reads:

$$\langle \prod_{i=0}^{N-1} \bar{\Psi}_R \Psi_R(x_i) \rangle = \det_0(i\cancel{\partial} + A_c^N) \prod_{i,j=0; i \neq j}^{n_R-1} (|x_i - x_j|)^{\frac{-\alpha_i \alpha_j}{(2r)^2}} \quad (29)$$

This result is in full agreement with the one previously obtained in [3].

The computation of non-minimal functions is, though tedious, straightforward. The interested reader will find guiding lines in [7].

To conclude this letter, as promised in the introductory paragraph, we now go back to trivial topology and consider massive fermions. To be more specific let us examine the following generating functional:

$$Z = \int D\bar{\Psi} D\Psi \exp\{-\int d^2x [\bar{\Psi}(i\cancel{\partial} + m + A)\Psi]\} \quad (30)$$

Following the steps of the previous case we make a gauge transformation in the fermionic variables and represent $\delta(\partial_\mu j_\mu)$ as in (8). Calling $B'_\mu = B_\mu + A_\mu$ we arrive at

$$Z = \int D\bar{\Psi} D\Psi DB'_\mu D\theta \exp\{-\int d^2x [\bar{\Psi}i\cancel{\partial}\Psi + j_\mu B'_\mu + m\bar{\Psi}\Psi + \frac{1}{\pi} B'_\mu \epsilon_{\mu\nu} \partial_\nu \theta - \frac{1}{\pi} A_\mu \epsilon_{\mu\nu} \partial_\nu \theta]\} \quad (31)$$

We make now a chiral change with parameter σ in the fermionic variables:

$$Z = \int D\bar{\chi} D\chi DB'_\mu D\theta \exp\{-\int d^2x [\bar{\chi}i\cancel{\partial}\chi + j_\mu B'_\mu + me^{2\gamma_5\sigma} \bar{\chi}\chi + \frac{1}{\pi} B'_\mu \epsilon_{\mu\nu} \partial_\nu \theta - \frac{1}{\pi} A_\mu \epsilon_{\mu\nu} \partial_\nu \theta - \frac{1}{\pi} B'_\mu \epsilon_{\mu\nu} \partial_\nu \sigma + \frac{1}{2\pi} \sigma \square \sigma]\} \quad (32)$$

Again in order to eliminate the linear term in B'_μ we identify $\sigma = \theta$. We then find

$$Z[A_\mu] = \int D\bar{\chi} D\chi DB'_\mu D\sigma \exp\{-\int d^2x [\bar{\chi}(i\cancel{\partial} + me^{2\gamma_5\sigma} + B')\chi + \frac{1}{\pi} (\epsilon_{\mu\nu} \partial_\nu \sigma A_\mu + \frac{1}{2} \sigma \square \sigma)]\} \quad (33)$$

At this point we shall make a perturbative expansion in the fermionic mass m . Obviously, the building block of this expansion is the following object:

$$\bar{\chi}(x) e^{2\gamma_5\sigma(x)} \chi(x) = \chi_2^\dagger e^{2\sigma(x)} \chi_1 + \chi_1^\dagger e^{-2\sigma(x)} \chi_2 \quad (34)$$

Using this explicit expression, $Z_m[A_\mu]$ can be readily written in terms of fermionic and bosonic v.e.v's in the form:

$$\begin{aligned}
Z_m[A_\mu] &= Z_{m=0}^{Fer}[\text{coset}]Z[A_\mu]^{Bos} \\
&\sum_{j=0}^{\infty} \frac{m^{2j}}{(j!)^2} \int \prod_{k=1}^j d^2x_k d^2y_k \langle X_2^{\dagger} X_1(x_k) X_1^{\dagger} X_2(y_k) \rangle_{Fer, \text{Coset}} \\
&< \prod_{k=1}^j e^{2[\sigma(x_k) - \sigma(y_k)]} \rangle_{Bos, \sigma, A_\mu}
\end{aligned} \tag{35}$$

Then, exactly as it happens in the massless case (Eq.(2)) the fermionic coset partition function can be extracted as an overall factor, but no complete factorization takes place, since every term in the mass expansion contains a fermionic v.e.v.. However, if one sets $A_\mu = 0$ the r.h.s. of Eq.(30) becomes the partition function of a bosonic Sine-Gordon model, as expected (Ref.[4],[8]). This fact can be easily verified just by evaluating the fermionic factor in the series, which can be done in a simple way using, for instance, the standard decoupling technique (See Ref.[2]).

In summary we have extended the factored coset approach to bosonization proposed in (Ref.[1]), in two directions. Firstly we discussed the case of massless fermions coupled to an Abelian gauge field with non-zero topological charge. We were able to show that the coset factorization takes place exactly as in the $N = 0$ case, but with both Z_{Fer} and Z_{Bos} containing the topological structure, i.e. the corresponding actions are dependent on N . Finally we considered the case $N = 0$ but with massive fermions. As it is well-known, the massive determinant cannot be exactly solved due to the chiral non-invariance of the mass term. This fact led us to make a perturbative expansion in the mass. Concerning this case our main conclusion is that no complete factorization is obtained because the constrained fermionic action enters the game through the v.e.v.'s which are present in the perturbative series of eq.(35).

References

- [1] A.N.Theron, F.A.Schaposnik, F.G.Scholtz and H.B.Geyer, Nucl.Phys. **437** 187, (1995).
- [2] R.Gamboa-Saraví, F.Schaposnik and J.Solomin, Nucl. Phys. B **185**, 239 (1981).
- [3] K.Bardacki and M.Crescimanno Nucl.Phys.B **313** 269 (1989)
- [4] S.Coleman, Phys. Rev. D **11**, 2088 (1975).
S.Coleman, R.Jackiw and L.Susskind Ann.Phys.**93**, 267 (1975)
- [5] K.Fujikawa, Phys. Rev. Lett. **42**, 1195 (1979) ; Phys. Rev. D **21**, 2848 (1980).
- [6] H.B.Nielsen and P.Olesen Nucl.Phys.B **61** 45 (1973).
- [7] M.N.Manias, C.M.Naón and M.L.Trobo Phys.Rev.D **47**, 3592 (1993).
- [8] C.M.Naón Phys.Rev.D **31**, 2035 (1985).

The Weakly Disordered 2D Electron Gas in a Magnetic Field

N. Bralić

*Facultad de Física, Pontificia Universidad Católica de Chile
Casilla 306, Santiago 22, Chile*

R. M. Cavalcanti

*Departamento de Física, Pontificia Universidade Católica do Rio de Janeiro
CP 38071, CEP 22452-970, Rio de Janeiro, RJ, Brasil*

C. A. A. de Carvalho and P. Donatis

*Instituto de Física, Universidade Federal do Rio de Janeiro
CP 68528, CEP 21945-970, Rio de Janeiro, RJ, Brasil*

We study a relativistic electronic gas in two space dimensions in the presence of a uniform magnetic field and a random static gauge field, which is treated perturbatively. Electron-electron interactions are neglected. We compute, to first order in perturbation theory, the expectation values of the current, $\langle j_\mu \rangle$, and of the conductivity tensor, $\langle \sigma_{ij} \rangle$, averaged over configurations of the random field with a gaussian weight. The implications of our results for the theory of the integer quantum Hall effect (IQHE) are briefly discussed.

1 The system

Let us consider a system of non-interacting relativistic electrons moving in two dimensions, in the presence of a uniform magnetic field perpendicular to the plane and of a random gauge field. The Euclidean electron propagator $S(x, y)$ is the Green's function of the Euclidean Dirac operator,

$$[\not{\partial}_x - i\not{A}(x) - m] S(x, y) = \delta^3(x - y), \quad (1)$$

satisfying the zero-temperature boundary condition $\lim_{|x-y| \rightarrow \infty} S(x, y) = 0$. The gauge field $\mathcal{A} = A + \tilde{A}$ comprises both the external field $A = (i\mu, A_1, A_2)$, where μ denotes the chemical potential and $\epsilon_{ij} \partial_i A_j = B$; and the random field $\tilde{A} = (i\tilde{A}_0, \tilde{A}_1, \tilde{A}_2)$. (In what follows we shall assume that there is no disorder in the magnetic field, i.e. $\tilde{A}_1 = \tilde{A}_2 = 0$.) The electric charge has been set to one. The Dirac matrices γ_μ ($\mu = 0, 1, 2$) satisfy the Euclidean algebra $\{\gamma_\mu, \gamma_\nu\} = 2\delta_{\mu\nu}$.

Once $S(x, y)$ is obtained, one can compute many quantities of physical interest, among them the current density, $j_\mu(\vec{x})$:

$$j_\mu(\vec{x}) = -\text{Tr}[\gamma_\mu S(x, x)]; \quad (2)$$

and the local conductivity tensor, $\sigma_{ij}(\vec{x})$:

$$\sigma_{ij}(\vec{x}) = i \int d^3y \Pi_{i0}(x, y) y_j, \quad (3)$$

$$\Pi_{\mu\nu}(x, y) = \text{Tr}[\gamma_\mu S(x, y) \gamma_\nu S(y, x)]. \quad (4)$$

All physical quantities must be averaged over disorder. Here this will be done using the probability distribution

$$P[\tilde{A}_0] = \exp \left\{ -\frac{1}{2g} \int d^2x \tilde{A}_0^2(\vec{x}) \right\}. \quad (5)$$

which, being gaussian, is completely determined by the one and two-point correlation functions:

$$\langle \tilde{A}_0(\vec{x}) \rangle = 0; \quad \langle \tilde{A}_0(\vec{x}) \tilde{A}_0(\vec{y}) \rangle = g \delta^2(\vec{x} - \vec{y}). \tag{6}$$

Note that we are taking averages over *static* realizations of the random field, otherwise it would be necessary to introduce a dynamics for \tilde{A} .

Since $S(x, y)$ is a highly non-local functional of \tilde{A} , we shall perform the averaging process perturbatively. In terms of the ‘unperturbed’ propagator $S_0(x, y)$, which satisfies

$$[\partial_x - i\tilde{A}(x) - m] S_0(x, y) = \delta^3(x - y), \tag{7}$$

and the same boundary condition as does $S(x, y)$, Eq.(1) can be formally solved for S as (in matrix notation):

$$S = S_0 + S_0 i\tilde{A} S_0 + S_0 i\tilde{A} S_0 i\tilde{A} S_0 + \dots \tag{8}$$

Now, the averaging can be done using (6) and applying Wick’s theorem to evaluate the n -point correlation functions.

The unperturbed propagator, $S_0(x, y)$, can be obtained using Schwinger’s proper time method[1] (for this and other methods, see also[2, 3]). The result is

$$S_0(x, y) = M(\vec{x}, \vec{y}) \int \frac{d^3p}{(2\pi)^3} e^{ip \cdot (x-y)} S_0(p), \tag{9}$$

where ($\omega \equiv p_0 - i\mu$)

$$S_0(p) = -i \lim_{\epsilon \rightarrow 0^+} \int_{\epsilon}^{\infty} \frac{dt}{\cosh Bt} \exp \left\{ -(\omega^2 + m^2)t - \vec{p}^2 \frac{\tanh Bt}{B} \right\} \\ \times \left\{ (\omega \cosh Bt - im \sinh Bt) \gamma_0 + \frac{p_1 \gamma_1 + p_2 \gamma_2}{\cosh Bt} + (\omega \sinh Bt - im \cosh Bt) \right\}, \tag{10}$$

and $M(\vec{x}, \vec{y})$ is a gauge dependent, translation-invariance violating term:

$$M(\vec{x}, \vec{y}) = \exp \left\{ i \int_{\vec{y}}^{\vec{x}} \tilde{A}(\vec{\xi}) \cdot d\vec{\xi} \right\}; \tag{11}$$

the integral is performed along a straight line connecting \vec{y} to \vec{x} .

2 Results

Computing the averaged current density according to the scheme outlined in the previous section, we find, up to second order in g , the following results:

$$\langle j_0(\vec{x}) \rangle = \frac{B}{2\pi} \left(1 - \frac{g \ln 2}{4\pi} \right) \left\{ \frac{1}{2} - \theta(\mu - \epsilon_0) - \sum_{n=1}^{\infty} [\theta(\mu - \epsilon_n) - \theta(-\mu - \epsilon_n)] \right\}; \tag{12}$$

$$\langle j_1(\vec{x}) \rangle = \langle j_2(\vec{x}) \rangle = 0. \tag{13}$$

In (12), $\epsilon_n = \sqrt{m^2 + 2nB}$ (B is assumed to be positive) is the n -th relativistic Landau level. The result for the spatial components is expected to be exact, by rotation symmetry. For the averaged conductivity tensor, the result is the following:

$$\langle \sigma_{11} \rangle = \langle \sigma_{22} \rangle = 0; \tag{14}$$

$$\langle \sigma_{21} \rangle = -\langle \sigma_{12} \rangle = \frac{1}{2\pi} \left(1 - \frac{g \ln 2}{4\pi} \right) \left\{ \frac{1}{2} - \theta(\mu - \epsilon_0) - \sum_{n=1}^{\infty} [\theta(\mu - \epsilon_n) - \theta(-\mu - \epsilon_n)] \right\}. \tag{15}$$

As a matter of fact, (15) can be derived in a much simpler way, using the identity[2, 5]

$$\langle \sigma_{21} \rangle = \frac{\partial}{\partial B} \langle j_0 \rangle. \tag{16}$$

Besides bringing about an enormous simplification, this identity raises an interesting problem: since the Landau energies, ϵ_n , depend on the magnetic field, the differentiation of $\langle j_0 \rangle$ with respect to B will not only reproduce the result for $\langle \sigma_{21} \rangle$, it will also generate some extra terms:

$$\frac{\partial}{\partial B} \langle j_0 \rangle - \langle \sigma_{21} \rangle = \frac{1}{2\pi} \left(1 - \frac{g \ln 2}{4\pi} \right) \sum_{n=1}^{\infty} \frac{\partial \epsilon_n}{\partial B} \{ \delta(\mu - \epsilon_n) - \delta(-\mu - \epsilon_n) \}. \quad (17)$$

This “anomaly” seems to be related to the fact that [6]

$$\lim_{T \rightarrow 0} \sigma_{21}(T) \neq \sigma_{21}(T = 0). \quad (18)$$

In fact, an explicit computation of the finite temperature Hall conductivity of the “clean” (i.e. in the absence of the random field) system shows that the difference between the left and the right side of (18) coincides with the right side of (17) (with $g = 0$). Apparently, identity (16) is correct!

According to (15), the Hall conductivity, $\langle \sigma_{21} \rangle$, shows a staircase structure as a function of the chemical potential μ and of the magnetic field B . The height of the steps depends on the strength of the disorder, g . However, one of the features of the IQHE is the remarkable quantization of the Hall conductivity in units of e^2/h ($= 1/2\pi$ in our units), even in the presence of impurities and defects [7]. For our result to be consistent with the observed accuracy of this quantization (at least one part in 10^5), g would have to be extremely small and, so, one should expect the results of perturbation theory to be reliable.

(We note, however, that the existence of a dependence of the plateau values of $\langle \sigma_{21} \rangle$ on g may be a feature of the probability distribution (5). We have computed the Hall conductivity, in the range $-\epsilon_2 < \mu < \epsilon_2$, using a probability distribution of the form

$$P\{\tilde{A}_0\} = \exp \left\{ -\frac{1}{2g} \int d^2x [(\vec{\nabla} \tilde{A}_0)^2 + M^2 \tilde{A}_0^2] \right\} \quad (19)$$

and, in this case, there is no $\mathcal{O}(g)$ correction to the clean system value of σ_{21} .)

On the other hand, according to the established viewpoint, our results are not enough to explain the IQHE. In QHE experiments in heterostructures, it is believed [7] that j_0 is kept constant while B is varied (however, see [8] for a different viewpoint). Comparing (12) and (15), we find $\langle \sigma_{21} \rangle = \langle j_0 \rangle / B$ and, therefore, no plateaux. We are forced, thus, to conclude that if disorder plays a role in the IQHE it will necessarily be nonperturbative.

Acknowledgments

This work had financial support from Proyecto FONDECYT, under Grant No. 1950794, Fundación Andes, CNPq, and FAPERJ.

References

- [1] J. Schwinger, Phys. Rev. **82** (1951), 664.
- [2] J. D. Lykken, J. Sonnenschein and N. Weiss, Int. J. Mod. Phys. **A6** (1991), 1335; Int. J. Mod. Phys. **A6** (1991), 5155.
- [3] J. O. Andersen and T. Haugset, “Magnetization in 2+1 dimensional QED at Finite Temperature and Density”, preprint, cond-mat/9410084.
- [4] V. Zeitlin, Phys. Lett. **B352** (1995), 422.
- [5] P. Strieda, J. Phys. **C15** (1982), L717.
- [6] S. S. Mandal and V. Ravishankar, “Activated resistivities in the integer quantum Hall effect”, preprint, cond-mat/9607173.
- [7] See, for example, “The Quantum Hall Effect”, eds. R.E. Prange and S.M. Girvin (Springer-Verlag, New York, 1987), and references therein.
- [8] G. A. Baraff and D. C. Tsui, Phys. Rev. B **24**, 2274 (1981).

Chiral Decomposition For Non-Abelian Bosons

Nelson R.F. Braga and Clovis Wotzasek

Instituto de Física, Universidade Federal do Rio de Janeiro

21945, Rio de Janeiro, Brazil

We study the non-abelian extension for the splitting of a scalar field into chiral components. Using this procedure we find a non ambiguous way of coupling a non abelian chiral scalar field to gravity. We start with a (non-chiral) WZW model covariantly coupled to a background metric and, after the splitting, arrive at two chiral Wess-Zumino-Witten (WZW) models coupled to gravity.

1 There are indications that a deeper understanding of such issues as string dynamics and fractional quantum Hall effect phenomenology can be achieved by treating the chiral sectors in a more independent way. However, coupling chiral fields to external gauge and gravitational fields is problematic. In a recent paper[1], we have discussed how the coupling of chiral (abelian) fields to external gravitational backgrounds can be achieved by diagonalization of the first-order form of a covariant scalar action. The theory reduces then to a sum of a left and a right Floreanini-Jackiw actions[2], circumventing the problems caused by the lack of manifest Lorentz invariance. Proceeding along these lines, one can gauge the scalar action before chiral splitting, which is trivial, and thus obtain the correctly gauged chiral scalar action. This procedure was motivated by a previous article by Bastianelli and van Nieuwenhuizen[3] where the coupling of one abelian chiral boson to gravity is achieved by starting with scalar field coupled covariantly to gravity and then imposing a chiral constraint in the first order Lagrangean. An earlier description of the coupling of chiral fields to gravity was given by Henneaux and Teitelboim[4].

In this Letter we extend the chiral decomposition scheme to nonabelian scalar fields and use this result to study the coupling with a gravitational background field.

2 Let us extend the separability condition discussed, for the abelian case, in [1] to non-abelian bosons. The most obvious choice would be to consider an action given by a bilinear gradient of a matrix-valued field g taking values on some compact Lie group G , which would be the natural extension of the free scalar abelian field. This is the action for the principal chiral model that reads

$$S_{PCM}(g) = \frac{1}{2} \int d^2x \text{tr} (\partial_\mu g \partial^\mu g^{-1}) \quad (1)$$

Here $g : R^{1,1} \rightarrow G$ is a map from the 2 dimensional Minkowski space-time to G . This action, however, puts some difficulties. First of all, by examining its field equation we learn that unlike the abelian case, it does not represent a free field. More important for us is the fact that there is no simple way to represent this action in terms of TW dual variables, as in the abelian case. Surprisingly though, we learn that it is still possible to introduce chiral variables in a simple fashion, after the reduction to a first-order action. The reason being that chiral variables only appear as derivatives, unlike the case of dual variables. The Jacobian of the field redefinition does not involve a time-derivative and can be reabsorbed in the normalization of the partition function. Let us write the PCM in its first-order form as

$$\begin{aligned} S_{PCM}(g, P) &= \frac{1}{2} \int d^2x \text{tr} (PgPg) + \int d^2x \text{tr} (\partial_\tau g P) \\ &+ \frac{1}{2} \int d^2x \text{tr} (g^{-1} \partial_\sigma g g^{-1} \partial_\sigma g) \end{aligned} \quad (2)$$

and redefine the fields g and P in a way that mimics the abelian case

$$\begin{aligned} g &= AB \\ P &= \varepsilon (B^{-1} \partial_\sigma A^{-1} - \partial_\sigma B^{-1} A^{-1}) \end{aligned} \tag{3}$$

The action for the PCM now reads

$$\begin{aligned} S_{PCM}(A, B) &= S_\varepsilon(A) + S_{-\varepsilon}(B) \\ &+ \varepsilon \int d^2x \operatorname{tr} [A^{-1} (\partial_\tau A \partial_\sigma B - \partial_\sigma A \partial_\tau B) B^{-1}] \end{aligned} \tag{4}$$

where

$$S_\varepsilon(A) = \int d^2x \operatorname{tr} (\varepsilon \partial_\sigma A^{-1} \partial_\tau A - \partial_\sigma A^{-1} \partial_\sigma A) \tag{5}$$

We see that due to the non-abelian nature of the fields, the cross-term cannot be eliminated, so that complete separation cannot be achieved. However this picture changes drastically with the inclusion of the Wess-Zumino topological term, i.e., when we consider the WZW model. The topological term

$$\Gamma_{WZ}(g) = \frac{1}{3} \int d^3x \epsilon^{ijk} \operatorname{tr} \{g^{-1} \partial_i g g^{-1} \partial_j g g^{-1} \partial_k g\} \tag{6}$$

under the field redefinition (3), splits as

$$\begin{aligned} \Gamma_{WZ}(AB) &= \Gamma_{WZ}(A) + \Gamma_{WZ}(B) + \\ &+ \int d^2x \operatorname{tr} [A^{-1} (\partial_\tau A \partial_\sigma B - \partial_\sigma A \partial_\tau B) B^{-1}] \end{aligned} \tag{7}$$

Next, we can bring results (4) and (7) into the Wess-Zumino-Witten (WZW) action[9], which is described by

$$S_{WZW}(g, P) = \frac{1}{\lambda^2} S_{PCM}(g, P) + \frac{n}{4\pi} \Gamma_{WZ}(g) \tag{8}$$

We mention the appearance of an extra parameter, both in the action and in the canonical formalism, playing the role of coupling constant. In terms of the chiral variables, the WZW model reads

$$\begin{aligned} S_{WZW}(A, B) &= \left[\frac{1}{\lambda^2} S_\varepsilon(A) + \frac{n}{4\pi} \Gamma_{WZ}(A) \right] + \left[\frac{1}{\lambda^2} S_{-\varepsilon}(B) + \frac{n}{4\pi} \Gamma_{WZ}(B) \right] + \\ &+ \left(\frac{\varepsilon}{\lambda^2} + \frac{n}{4\pi} \right) \int d^2x \operatorname{tr} [A^{-1} (\partial_\tau A \partial_\sigma B - \partial_\sigma A \partial_\tau B) B^{-1}] \end{aligned} \tag{9}$$

We can appreciate that the separability condition is only achieved at the critical points, as expected, but also that our choice of ε is now dependent on which of the critical points we choose: $4\pi\varepsilon = -\lambda^2 n$. The result is the non abelian version of the chiral decomposition, and corresponds to the sum of two Lagrangians describing non abelian chiral bosons of opposite chiralities, each one having the form proposed by Sommerschein[6]. We will see that a change of the critical point automatically switches the chirality of A and B by changing the sign of ε . Indeed, in order to obtain separability, we must have either

$$(i) \quad \frac{\lambda^2 n}{4\pi} = -\varepsilon = 1 \tag{10}$$

or

$$(ii) \quad \frac{\lambda^2 n}{4\pi} = -\varepsilon = -1 \tag{11}$$

In the first case we find the set of chiral equations as

$$\begin{aligned}\partial_x (A^{-1} \partial_+ A) &= 0 \\ \partial_- (B^{-1} \partial_x B) &= 0\end{aligned}\quad (12)$$

Now we are in position to consider the coupling of non-abelian chiral scalars to gravity. The coupling of a scalar non abelian field to a background metric $\eta^{\mu\nu}$ can be described by the action

$$S_{WZW}(g, \eta) = \frac{1}{\lambda^2} S_{PCM}(g, \eta) + \frac{n}{4\pi} \Gamma_{WZ}(g) \quad (13)$$

where

$$S_{PCM}(g, \eta) = \frac{1}{2} \int d^2x \sqrt{-\eta} \text{tr} (\eta^{\mu\nu} \partial_\mu g \partial_\nu g^{-1}) \quad (14)$$

The topological term $\Gamma_{WZ}(g)$ is not affected by the metric since the volume element times the antisymmetric tensor makes a covariant scalar. We can write the action for the Principal Chiral Model in a first order form as we did before. Introducing also the chiral variables defined in (3) we get:

$$\begin{aligned}S_{WZW}(A, B, \eta) &= \left[\frac{1}{\lambda^2} S_\epsilon(A, G_\epsilon) + \frac{n}{4\pi} \Gamma_{WZ}(A) \right] \\ &+ \left[\frac{1}{\lambda^2} S_{-\epsilon}(B, G_{-\epsilon}) + \frac{n}{4\pi} \Gamma_{WZ}(B) \right] \\ &+ \left(\frac{\epsilon}{\lambda^2} + \frac{n}{4\pi} \right) \int d^2x \text{tr} [A^{-1} (\partial_\tau A \partial_\sigma B - \partial_\sigma A \partial_\tau B) B^{-1}]\end{aligned}\quad (15)$$

In particular, we note that the separability conditions, Eqs.(10) and (11), are not affected by the presence of the metric. Thus, at the separability points, we get two chiral non-abelian scalars coupled to gravity in the same way as in the abelian case.

5 Concluding, we have proposed a way of splitting the action for the non-abelian boson into two chiral sectors, including the interacting case. This chiral decomposition is related to the holomorphic factorization of the WZW model discussed in [10, 11]. If we go to Euclidean space our light cone coordinates x^+ and x^- will correspond to the conformal coordinates z and \bar{z} and the chiral solutions $B_+(x^+)$ and $A_-(x^-)$ will correspond to holomorphic and antiholomorphic functions respectively.

Acknowledgments. We would like to thank E. C. Marino for kindly reading the manuscript. One of us (NRFB) would like to thank M. Asorey and P. van Nieuwenhuizen for important discussions. CW thanks the hospitality of the Department of Physics and Astronomy of University of Rochester, where part of this work was done. The authors are partially supported by CNPq, FINEP and FUJB, Brasil.

References

- [1] N.R.F.Braga and C. Wotzasek, Mod. Phys. Lett. A10(95)173.
- [2] R. Floreanini and R. Jackiw, Phys. Rev. Lett. 59, 1873 (1987).
- [3] F. Bastianelli and P. van Nieuwenhuizen, Phys.Lett. B217 (1989) 98.
- [4] M. Henneaux and C. Teitelboim, Phys. Lett. B206 (1988) 650.
- [5] A. Tseytlin and P. West, Phys. Rev. Lett. 65, 541 (1990).
- [6] J. Sonnenschein, Nucl. Phys. B309(88)752.
- [7] S.Mandelstam, Phys.Rev.D11 (1975)3026.
- [8] A. M. Polyakov and P. B. Wiegmann, Phys. Lett B131 (1983) 121.

- [9] E.Witten, *Comm. Math. Phys.* 92 (1984) 455 .
- [10] V.G.Knizhnik and A.B.Zamolodcikov, *Nucl.Phys.B*247 (1988)83.
- [11] E. Witten, *Comm.Math.Phys.* 144 (1992) 189.
- [12] B. De Wit, M.T.Grisaru, and P. van Nieuwenhuizen, *Nucl.Phys.B*408 (1993) 299.

Função Partição Generalizada para Campos Quase-Periódicos com Potencial Químico

P. F. Borges*, H. Boschi-Filho† e C. Farina‡

Instituto de Física, Universidade Federal do Rio de Janeiro

CP 68528, Rio de Janeiro, RJ 21945-970, Brazil

Usando o fato de que campos bosônicos a temperatura finita $T = \beta^{-1}$ são periódicos no intervalo $(0, \beta)$ enquanto campos fermiônicos são antiperiódicos, nós discutimos a construção de funções de partição para campos quase-periódicos, isto é, para campos que obedecem a condição $\psi(\vec{x}; 0) = e^{i\theta} \psi(\vec{x}; \beta)$. Nós empregamos o método da função zeta generalizada para calcular o determinante associado com a função partição para campos quase-periódicos. Uma vez que nós queremos discutir a função partição para um gás com densidade finita, nós incluímos o potencial químico μ , relacionado a carga conservada pelos campos.

Nosso ponto de partida está apoiado na observação de que em temperatura finita $T = \beta^{-1}$ campos bosônicos são periódicos no intervalo $(0, \beta)$ enquanto campos fermiônicos são antiperiódicos no mesmo intervalo. Então, uma extensão natural é considerar campos quase-periódicos

$$\psi(x; 0) = e^{i\theta} \psi(x; \beta) \quad (1)$$

A função partição para um sistema descrito por uma Hamiltoniana H com potencial químico μ pode ser escrita como

$$\exp\{-\beta\Omega\} = \text{tr} e^{-\beta(H - \mathcal{N}\mu)} \quad (2)$$

onde Ω é a energia livre e \mathcal{N} é a carga conservada do sistema. Como é bem sabido para campos bosônicos carregados massivos, nós podemos expressar esta função partição como um determinante [1][2], ou seja,

$$\exp\{-\beta\Omega\} = [\det(-D^2 + M^2)_P]^{-1}(\text{bosons}) \quad (3)$$

onde D^2 é o quadrado da derivada covariante D_ν , incluindo o potencial químico, $D_\nu = (-\partial_0 + i\mu), \partial_i$ e M é a massa do campo. O índice P significa que os autovalores do operador $-D^2 + M^2$ estão sujeitos a condições de contorno periódicas e assim são dados por

$$\lambda_{n\vec{k}} = (\omega_n + i\mu)^2 + k^2 + M^2 \quad (4)$$

onde $\omega_n = 2n\pi/\beta$, com $n \in \mathcal{Z}$, são as frequências de Matsubara[3] para campos bosônicos e $\vec{k} \in \mathcal{R}^N$.

Da mesma forma que para bósons, nós também podemos escrever a função partição para férmions como um determinante (por conveniência nós usaremos o operador de Dirac de segunda ordem iterado)

$$\exp\{-\beta\Omega\} = [\det(-D^2 + M^2)_A]^{d/2}(\text{fermions}) \quad (5)$$

onde d é a dimensão da representação do campo de Dirac e o subscrito A significa que os autovalores são calculados com condições de contorno anti-periódicas e portanto dadas por (4) com $\omega_n = (2n + 1)\pi/\beta$.

*e-mail: pborges@if.ufrj.br

†e-mail: boschi@if.ufrj.br

‡e-mail: farina@if.ufrj.br

Nossa generalização consiste em calcular o determinante deste operador, mas agora submetido as condições de contorno quase-periódicas(1), ou seja:

$$\mathcal{Z} = [\det(-D^2 + M^2)_\theta]^\sigma \tag{6}$$

onde o subscripto θ significa que a condição quase-periódica é suposta e nós introduzimos um novo parâmetro σ capaz de reproduzir corretamente os casos particulares bosônico e fermiônico. Observe que quando $\theta = 0$ e $\sigma = -1$ nós reobtemos a função de partição bosônica, enquanto que para $\theta = \pi$ e $\sigma = d/2$ temos o caso fermiônico. Por generalidade, vamos calcular o determinante acima em $N + 1$ dimensões espaço-temporais. Os autovalores neste caso são:

$$\lambda_{n,\vec{k},\theta} = [2n\pi/\beta + i\mu + \theta/\beta]^2 + \vec{k}^2 + M^2 \tag{7}$$

O determinante (6)é uma generalização da versão em mecânica quântica em $0 + 1$ dimensão (com $\mu = 0$) que foi calculado usando funções de Green[4] e o método da função Zeta[5]. Aqui, nós também vamos calcular este determinante usando o método da função Zeta generalizada através da fórmula básica[6]:

$$\det \mathcal{A} = \exp \left\{ \frac{-\partial}{\partial s} \text{tr} \mathcal{A}^{-s} \right\} \Big|_{s=0} = \exp \left\{ \frac{-\partial}{\partial s} \zeta(s; \mathcal{A}) \right\} \Big|_{s=0} \tag{8}$$

onde a função Zeta generalizada é definida por $\zeta(s; \mathcal{A}) = \text{tr} \mathcal{A}^{-s}$ e uma extensão analítica de $\zeta(s; \mathcal{A})$ para todo o plano complexo é tacitamente suposta.

Para o caso em mãos a função zeta generalizada fica:

$$\zeta(s; \mathcal{A}) = \frac{V}{(2\pi)^N} \Omega_N \sum_{n=-\infty}^{+\infty} \int_0^\infty dk k^{N-1} (\lambda_{n,\vec{k},\theta})^{-s} \tag{9}$$

onde V é o volume e Ω_N é a área da hipersfera unitária em N dimensões espaciais, e nós usamos a relação (7). Usando a fórmula [7]

$$\int_0^\infty dx x^{\rho-1} (x^2 + y^2)^{-\tau} = \left(\frac{1}{2}\right) y^{2\tau+\rho} B\left(\frac{\rho}{2}, -\tau - \frac{\rho}{2}\right) \tag{10}$$

nós obtemos

$$\begin{aligned} \zeta(s; \mathcal{A}) &= \frac{C_N}{2} \frac{\Gamma(\frac{N}{2})\Gamma(s - \frac{N}{2})}{\Gamma(s)} \\ &\times \left(\frac{2\pi}{\beta}\right)^{-2s+N} \sum_{n=-\infty}^{+\infty} [\nu^2 + (n + \chi)^2]^{-(s - \frac{N}{2})} \end{aligned} \tag{11}$$

onde nós definimos $C_N = V\Omega_N/(2\pi)^N$, $\nu = \beta M/2\pi$ e $\chi = (i\beta\mu + \theta)/2\pi$. A soma que aparece na fórmula acima é uma generalização da função de Epstein usual[8], para a qual pode-se escrever uma extensão analítica em todo o plano complexo[9]:

$$\begin{aligned} D(s, \nu, \chi) &\equiv \sum_{n=-\infty}^{+\infty} [\nu^2 + (n + \chi)^2]^{-(s - \frac{N}{2})} \\ &= \frac{\sqrt{\pi}}{\Gamma(s - \frac{N}{2})} \times \frac{\Gamma(s - \frac{N}{2} - \frac{1}{2})}{\nu^{2s - N - 1}} \\ &+ \frac{4\sqrt{\pi}}{\Gamma(s - \frac{N}{2})} \sum_{n=1}^{+\infty} \cos(2\pi n\chi) \left(\frac{n\pi}{\nu}\right)^{s - \frac{N}{2} - \frac{1}{2}} K_{s - \frac{N}{2} - \frac{1}{2}}(2\pi n\nu) \end{aligned} \tag{12}$$

onde $K_\alpha(z)$ é a função de Bessel modificada de ordem α . Tomando a derivada de $\zeta(s; \mathcal{A})$ em relação a s , no limite $s = 0$ nós obtemos (a menos de um termo irrelevante que é linear em β e independente de μ):

$$\begin{aligned} \left. \frac{\partial}{\partial s} \zeta(s, A) \right|_{s=0} &= 2\sqrt{\pi} C_N \Gamma\left(\frac{N}{2}\right) \left(\frac{2\pi}{\beta}\right)^N \\ &\times \sum_{n=1}^{+\infty} \cos(2\pi n \chi) \left(\frac{n\pi}{\nu}\right)^{-\frac{1}{2}(N+1)} K_{-\frac{1}{2}(N+1)}(2\pi n \nu) \end{aligned} \quad (13)$$

Usando este resultado nós podemos encontrar o determinante generalizado (6) que interpola continuamente as funções de partição, ou de forma equivalente, a energia livre para um gás relativístico de bósons ou férmions com potencial químico μ :

$$\begin{aligned} \Omega(\beta, \mu) &= \frac{\sigma C_N}{\sqrt{\pi}} (2M)^{\frac{1}{2}(N+1)} \Gamma\left(\frac{N}{2}\right) \beta^{-\frac{1}{2}(N+1)} \\ &\times \sum_{n=1}^{+\infty} \cos(n\theta) \cosh(n\beta\mu) \left(\frac{1}{n}\right)^{\frac{1}{2}(N+1)} K_{\frac{1}{2}(N+1)}(n\beta M) \end{aligned} \quad (14)$$

Se nós particularizarmos os parâmetros θ e σ aos casos bosônico e fermiônico, encontraremos precisamente os resultados conhecidos na literatura [10][11] (ver também [14]).

É interessante calcular as expansões para altas e baixas temperaturas da energia livre para clarificar o papel dos parâmetros θ e σ no cálculo acima. Tomando o limite de altas temperaturas $\beta M \ll 1$ na eq. (14), nós encontramos:

$$\Omega(\beta, \mu) = 2V\sigma \left(\frac{T}{\sqrt{\pi}}\right)^{N+1} \Gamma\left(\frac{N+1}{2}\right) \sum_{n=1}^{+\infty} \cos(n\theta) \cosh(n\beta\mu) \left(\frac{1}{n}\right)^{N+1} \quad (15)$$

No limite de baixas temperaturas, $\beta M \gg 1$, nós temos:

$$\Omega(\beta, \mu) = 2V\sigma \left(\frac{M}{2\pi}\right)^{\frac{N}{2}} T^{1+\frac{N}{2}} \sum_{n=1}^{+\infty} \cos(n\theta) \cosh(n\beta\mu) \left(\frac{1}{n}\right)^{1+\frac{N}{2}} e^{-(n\beta M)} \quad (16)$$

Agora, nós mostraremos que da energia livre (14), ou de forma equivalente, de suas expansões de altas e baixas temperaturas, nós podemos extrair as temperaturas críticas da condensação de Bose-Einstein para um gás de bósons. Tomando $\theta = 0$ e $\sigma = -1$ e o limite de altas temperaturas, nós encontramos para a densidade de carga:

$$\rho \equiv -\frac{1}{V} \left\{ \frac{\partial}{\partial \mu} \Omega \right\} \Big|_{V, T} = \frac{2\mu}{\pi^{\frac{N+1}{2}}} \Gamma\left(\frac{N+1}{2}\right) \zeta(N-1) T^{N-1} \quad (17)$$

onde $\zeta(N-1)$ é a função Zeta de Riemann comum. Em particular, se $N = 3$ nós temos a bem conhecida temperatura crítica para a condensação de Bose-Einstein ($\mu = M$) [10]:

$$T_c = \left(\frac{3\rho}{M}\right)^{\frac{1}{2}} \quad (18)$$

Analogamente, no limite de baixas temperaturas, nós temos: ($\mu = M$)

$$\rho = \zeta\left(\frac{N}{2}\right) \left(\frac{TM}{2\pi}\right)^{\frac{N}{2}} \quad (19)$$

a qual implica que a temperatura crítica para $N = 3$ é [12]

$$T_c = \frac{2\pi}{M} \left(\frac{\rho}{\zeta\left(\frac{3}{2}\right)}\right)^{\frac{2}{3}} \quad (20)$$

Das equações (17) e (19) nós podemos ver que o condensado não é definido em duas dimensões espaciais ($N = 2$), uma vez que a função Zeta de Riemann $\zeta(s)$ tem um polo em $s = 1$. De fato, como a função Zeta é convergente para

$s > 1$ nós encontramos que a condensação de Bose-Einstein para campos massivos (nos limites ultra-relativístico e não-relativístico) ocorre para dimensões espaciais $N > 2$, o que concorda com a literatura[10][13].

Para ver que férmions se excluem e discutir o comportamento geral da interpolação de θ e σ , vamos reescrever a energia livre (14) como

$$\begin{aligned} \Omega(\beta, \mu) &= -\frac{TV\sigma}{(2\pi)^N} \int d^N k \operatorname{Re} \left\{ \ln \left[1 - e^{i\theta} e^{\beta(\omega-\mu)} \right] + (\mu - -\mu) \right\} \\ &= -\frac{TV\sigma}{(2\pi)^N} \int \frac{d^N k}{2} \left\{ \ln \left[1 + e^{2\beta(\omega-\mu)} - 2 \cos \theta e^{\beta(\omega-\mu)} \right] \right\} \\ &\quad - \frac{TV\sigma}{(2\pi)^N} \int \frac{d^N k}{2} (\mu - -\mu) \end{aligned} \tag{21}$$

onde $\omega = \sqrt{k^2 + M^2}$. Como a condensação está relacionada ao estado de momento zero ($\vec{k} = \vec{0}$), neste caso nós temos $\omega = M$. Então, nós podemos ver que a equação acima é bem definida para todo valor de μ , exceto quando $\theta = 0$ (ou $2n\pi$, n inteiro) para o qual $\mu = M$ dá a bem conhecida condição de condensação. Então, nós podemos inferir que nenhuma condensação ocorre para qualquer $\theta \neq 2n\pi$ (n inteiro).

A função de distribuição de uma partícula correspondente a energia livre acima:

$$f_\theta(\beta) = \left\| \frac{1}{1 - e^{i\theta} e^{\beta\omega}} \right\| = \left[\frac{1}{1 + e^{2\beta\omega} - 2 \cos \theta e^{\beta\omega}} \right]^{\frac{1}{2}} \tag{22}$$

Desta função de distribuição generalizada nós podemos encontrar o resultado usual que férmions se excluem, tomando $\theta = \pm\pi$, de modo que obtemos a distribuição usual de Fermi-Dirac. É claro que o mesmo ocorre para a distribuição de Bose-Einstein quando nós tomamos $\theta = 2n\pi$ com n inteiro.

Uns poucos comentários são necessários aqui: Primeiramente, vale a pena dizer que o parâmetro interpolante θ discutido aqui cumpre o papel de um campo de calibre topológico constante $A_\mu = (A_0, 0, 0, 0)$, desde que a condição de contorno θ para o operador de Klein-Gordon implicou que $\omega_n = \omega_n + \theta/\beta$, que pode ser vista como um deslocamento no operador derivada temporal $\partial_0 = \partial_0 + i\theta/\beta$. A discussão dos determinantes bosônico (3) e fermionico (5) com um campo de calibre topológico constante, mas sem relacioná-lo as condições de contorno ou estatística interpolante, foi apresentada antes[14].

Em segundo lugar, nós decorevimos aqui uma espécie de bosonização (fermionização) pela inclusão de arbitrários θ e σ na função partição. Note que, nós mostramos que nenhuma condensação ocorre para campos com $\theta \neq 2n\pi$, entretanto um campo fermiônico interagindo com um campo topológico θ/β com $\theta = \pi$ também condensará, desde que a fase global adicionada a $\exp \beta(\omega \pm \mu)$ seja um inteiro vezes 2π .

Como uma lembrança final, vamos mencionar que nossa abordagem pode ser estendida a outros espaços-tempo com outras topologias. Naturalmente, estes resultados se reduzem aos nossos para um espaço-tempo do tipo $\mathcal{R}^N \otimes S^1$ quando colocamos $\theta = 0, \pi$ e $\sigma = -1, d/2$ em nossa fórmula.

References

- [1] C. Bernard, Phys. Rev. D **9** (1974) 3312.
- [2] J. I. Kapusta, Phys. Rev. D **24** (1981) 426; for a review see J. I. Kapusta, *Finite temperature field theory*, Cambridge, 1989.
- [3] T. Matsubara, Prog. Theor. Phys. **14** (1955) 351.
- [4] H. Boschi-Filho, C. Farina and A. de Souza Dutra, J. Phys. A **28**(1995)L7.
- [5] H. Boschi-Filho and C. Farina, Phys. Lett. A **205** (1995) 255.
- [6] A. Salam and J. Strahleer, Nucl. Phys. B **90** (1975) 203; J.S. Dowker and R. Critchley, Phys. Rev. D **13** (1976) 3224; S.W. Hawking, Commun. Math. Phys. **55** (1977) 133; G.W.Gibbons, Phys. Lett. A **60** (1977) 385.
- [7] I. S. Gradshteyn and I. M. Ryzhik, "Table of Integrals, Series and Products", Academic Press, 1980.
- [8] P. Epstein, Math. Ann. **56**(1903) 615 ; **65**(1907) 205.
- [9] K. Kirsten, J. Phys. A **25** (1992) 6297; **26** (1993) 2421.

- [10] H. E. Haber and H. A. Weldon, Phys. Rev. Lett. **46** (1981) 1497.
- [11] H.-T. Elze, W. Greiner and J. Rafelski, J. Phys. A **6** (1980) L149.
- [12] see, e. g., K. Huang, *Statistical Mechanics*, Wiley, New York, 1963.
- [13] D. J. Toms, Phys. Rev. Lett. **69**(1992) 1152; Phys. Rev. **D47** (1993)2483; Phys. Rev.**D51**(1995)1886; Phys. Lett. **B343**(1995)259.
- [14] A. Actor, Phys. Rev. D **27** (1983) 2548; Ann. of Phys. (N.Y.) **159** (1985) 445; Phys. Lett. B **157**(1985)53; Nucl. Phys. B **256** (1986) 689.

Action Principle for the Classical Dual Electrodynamics*

PCR Cardoso de Mello⁽¹⁾, S Carneiro⁽²⁾ and MC Nemes⁽¹⁾

⁽¹⁾ Departamento de Física, Universidade Federal de Minas Gerais

CP702, 30000, Belo Horizonte, MG, Brasil.

⁽²⁾ Instituto de Física, Universidade de São Paulo

CP66318, 05389-970, São Paulo, SP, Brasil

The purpose of this paper is to formulate an action principle which allows for the construction of a classical lagrangean including both electric and magnetic currents. The lagrangean is non-local and shown to yield all the expected (local) equations for dual electrodynamics.

One of the oldest open problems in the theory of elementary particles is that of the quantization of the electric charge. Although apparently very simple, this experimental result has not yet found theoretical explanation in the context of the standart model of fundamental interactions.

In 1931, PAM Dirac^[1] found an explanation for such quantization based on the lack of symmetry of Maxwell's equations in what concerns their source terms. The presence of magnetic currents in these equations leads, at the quantal level, to the quantization of the electric and magnetic charges.

Since the pioneer work of Dirac, other solutions to the problem have been proposed in the context of unified theories, as GÜT's^[2,3] and Kaluza-Klein theories^[4,5]. However, all these proposals are shown to be connected to the existence of solitonic magnetic monopoles^[6-9].

A great obstacle to the development of an electrodynamics with charges and poles is the absence of an adequate lagrangean formulation. This is intimately connected to the difficulty of constructing a regular 4-potential in all space-time. There have been several proposals to circumvent this problem: the introduction of Dirac's string^[10], of the double-valued Wu-Yang potential^[11], of the singular Bollini-Giambiagi potential^[12] and finally the use of non-local wave functions, proposed by Cabbibo and Ferrari^[13]. However, a lagrangean formulation which gives rise to the complete set of electromagnetic equations, without necessity of any subsidiary condition, is still lacking.

The main purpose of the present work is to show that a non-local lagrangean can be constructed which gives a correct description of the classical dual electrodynamics provided we postulate the following variational principle: *the dynamics of the system charge-field-monopole is such that the action presents a saddle point which is a minimum with respect to variation of the usual degrees of freedom and a maximum with respect to variation of the dual degrees of freedom.*

Following such prescription we construct the lagrangean density

$$\mathcal{L} = \mathcal{L}_e + \mathcal{L}_m - \frac{1}{4} F_{\mu\nu} F^{\mu\nu} - j_\mu A^\mu + g_\mu \tilde{A}^\mu \quad (1)$$

where j_μ e g_μ are the electric and magnetic 4-currents, respectively. Here we have introduced the Cabibbo-Ferrari generalized field tensor^[13]

$$F^{\mu\nu} \equiv \partial^\mu A^\nu - \partial^\nu A^\mu - \epsilon^{\mu\nu\alpha\beta} \partial_\alpha \tilde{A}_\beta \quad (2)$$

and the non-local potentials^[14]

$$A^\mu = \tilde{A}^\mu + \frac{1}{2} \epsilon^{\mu\gamma\alpha\beta} \int_V \partial_\alpha \tilde{A}_\beta d\xi_\gamma \quad (3)$$

*Work partially supported by CNPq and FAPESP

$$\tilde{A}^\mu = \dot{A}^\mu - \frac{1}{2} \epsilon^{\mu\gamma\alpha\beta} \int_{\tilde{P}} \partial_\alpha A_\beta d\xi_\gamma \quad (4)$$

with P and \tilde{P} defined, respectively, by the world lines of the charge and pole.

The first two terms in (1) correspond, respectively, to the free lagrangeans of the electric and magnetic charges, so that the Lagrange's function corresponding to (1) is given by

$$L = L_e + L_g + L_{Maxwell} \quad (5)$$

where

$$L_e = -m(1-u^2)^{\frac{1}{2}} + e \vec{u} \cdot \vec{A} - e A_0 \quad (6)$$

$$L_g = M(1-v^2)^{\frac{1}{2}} - g \vec{v} \cdot \vec{A} + g \dot{A}_0 \quad (7)$$

$$L_{Maxwell} = -\frac{1}{4} \int d^3x F_{\mu\nu} F^{\mu\nu} \quad (8)$$

Here \vec{u} and \vec{v} stand for the charge and pole velocities, m and M standing for their masses. e and g are their charge strenghts.

In the absence of monopoles we can, using the gauge freedom^[13], set $\dot{A}^\mu = 0$ and our lagrangean reduces to the usual lagrangean of electromagnetism. Also, in the absence of electric charges, by setting $A^\mu = 0$ we get, apart from an overall sign, the dual lagrangean

$$\mathcal{L} = \mathcal{L}_o - \frac{1}{4} \tilde{F}_{\mu\nu} \tilde{F}^{\mu\nu} - g_\mu \dot{A}^\mu \quad (9)$$

where

$$\tilde{F}^{\mu\nu} = \frac{1}{2} \epsilon^{\mu\nu\alpha\beta} F_{\alpha\beta} \quad (10)$$

stands for the dual of the field tensor.

From (2)-(4) and (10) we can show the validity of the relations^[17]

$$F^{\mu\nu} = \partial^\mu A^\nu - \partial^\nu A^\mu \quad (11)$$

$$\tilde{F}^{\mu\nu} = \partial^\mu \dot{A}^\nu - \partial^\nu \dot{A}^\mu \quad (12)$$

Variations of the local potentials - for given fixed particles's world lines - lead to variations of the non-local ones. Using (11), (12) and the identity

$$F_{\mu\nu} F^{\mu\nu} = -\tilde{F}_{\mu\nu} \tilde{F}^{\mu\nu} \quad (13)$$

it is a simple matter to check that the extremum condition for the action under such variations leads to Euler-Lagrange equations which correspond to the expected generalized Maxwell's equations

$$\partial_\beta F^{\alpha\beta} = -j^\alpha \quad (14)$$

$$\partial_\beta \tilde{F}^{\alpha\beta} = -g^\alpha \quad (15)$$

Variations with respect to the coordinates of the charge and pole give

$$m \frac{dU^\alpha}{d\tau} = e (\partial^\alpha A^\beta - \partial^\beta A^\alpha) U_\beta \quad (16)$$

$$M \frac{dV^\alpha}{d\tau} = g (\partial^\alpha \tilde{A}^\beta - \partial^\beta \tilde{A}^\alpha) V_\beta \quad (17)$$

where U^μ and V^μ stand for the 4-velocities of the charge and pole and τ is their proper time. Here, the derivatives of the potentials are taken along the world lines of the particles. Thus, using again (11) and (12), we obtain the correct Lorentz's equations

$$m \frac{dU^\alpha}{d\tau} = e F^{\alpha\beta} U_\beta \quad (18)$$

$$M \frac{dV^\alpha}{d\tau} = g \tilde{F}^{\alpha\beta} V_\beta \quad (19)$$

We can see that the proposed lagrangean, although non-local, leads to all desired local equations of motion. Using the field equations it is possible to show that a change of the paths of integration in (3) and (4) corresponds to a gauge transformation of the non-local potentials. Because this result, it is not necessary to consider variations of these paths to obtain the particles's equations.

It is important to note that (11) and (12) do not imply into the homogeneity of (14) and (15). It is due to the fact that the non-local potentials are not regular, do not obeying the Euler condition. In other words,

$$(\partial^\mu \partial^\nu - \partial^\nu \partial^\mu) \mathcal{A}^\alpha \neq 0 \quad (20)$$

and the same for $\tilde{\mathcal{A}}^\alpha$.

The irregular character of \mathcal{A}^μ , as a function of x and t , is evident once one examines expression (3) in the case of a magnetic monopole at rest in the origin. Any path which goes through the origin turns the integral into a divergent one over a semi-infinite line. Such singularity are essential, since they come from the intersection between the charge's world line and the monopole's one, and are already contained in the equations of motion derived from the lagrangean. In fact, Lorentz's equation (18) allows the charge to come indefinitely close to the monopole, over the line connecting them. But when the superposition occurs, the second member of this equation becomes singular, unless the relative velocity between charge and pole goes to zero. We note however that, whatever the charge's trajectory might be, the singularity of \mathcal{A}^μ will always lie in a 4-hemisphere opposed to that of charge's motion. This discussion is valid also for the dual non-local potential.

Let us consider the dual transformation

$$A^\mu \rightarrow -\tilde{A}^\mu \quad (21)$$

$$\tilde{A}^\mu \rightarrow A^\mu \quad (22)$$

$$j^\mu \rightarrow -g^\mu \quad (23)$$

$$g^\mu \rightarrow j^\mu \quad (24)$$

together with $m \rightarrow M$. The lagrangean and action will change sign. As the equations of motion do not depend on the overall sign of these quantities, we can say that the theory remains invariant under such dual transformation.

The sign difference between the free lagrangeans of the electric and magnetic charges (cf. (6) and (7)) may give the impression that the monopole would appear as a particle with negative energy^[15]. This would be of course unacceptable at the classical level. It is possible to see that this is not the case by calculating the total conserved energy of the system charge-field-monopole, using the equations of motion obtained from the lagrangean.

This result apparently contradicts the hamiltonian formulation of the theory. However, the dual simetry and the very form of the lagrangean, obeying a saddle principle, lead us to a hamiltonian formulation which is internally consistent with the theory. In fact, the dual transformation (21)-(24), under which $L_e \rightarrow -L_g$ and $S_e \rightarrow -S_g$, transforms the momentum and hamiltonian of the charge

$$\vec{p}_e \equiv \frac{\partial S_e}{\partial \vec{r}} = \frac{\partial L_e}{\partial \vec{u}} = \frac{m\vec{u}}{(1-u^2)^{\frac{1}{2}}} + e\vec{\mathcal{A}} \quad (25)$$

$$\mathcal{H}_e \equiv -\frac{\partial S_e}{\partial t} = \frac{\partial L_e}{\partial \vec{u}} \cdot \vec{u} - L_e = [m^2 + (\vec{p}_e - e\vec{\mathcal{A}})^2]^{\frac{1}{2}} + e\mathcal{A}_0 \quad (26)$$

into the momentum and hamiltonian of the pole

$$\vec{p}_g = -\frac{\partial S_g}{\partial \vec{r}} = -\frac{\partial L_g}{\partial \vec{v}} = \frac{M\vec{v}}{(1-v^2)^{\frac{1}{2}}} + g\vec{\mathcal{A}} \quad (27)$$

$$\mathcal{H}_g = \frac{\partial S_g}{\partial t} = -\left(\frac{\partial L_g}{\partial \vec{v}} \cdot \vec{v} - L_g\right) = [M^2 + (\vec{p}_g - g\vec{\mathcal{A}})^2]^{\frac{1}{2}} + g\mathcal{A}_0 \quad (28)$$

The above expressions respect the canonical form of Hamilton's equations, since the latter remain invariant under a simultaneous change of sign of \vec{p} and \mathcal{H} . It is also simple to show that (28) corresponds to the correct time evolution generator for the monopole.

We should like to remark that our formulation does not induce any modification for the particles's equations of motion in the gravitational field.

Usually the action for a mass m particle subject to this field is given by

$$S = -m \int ds \quad (29)$$

with

$$ds^2 = g_{\mu\nu} dx^\mu dx^\nu \quad (30)$$

In the case of a magnetic charge, however, one should consider the action in the form

$$S = M \int ds \quad (31)$$

so that it presents, contrary to (29), a maximum and so that the Lagrange's function reduces to the correct one (cf. (7)) in the absence of the gravitational field.

Since the equations of motion are given by $\delta S = 0$ the sign difference between (29) and (31) will not matter. This is in complete agreement with the Equivalence Principle. Besides, the positive definite character of the energy of the monopole guarantees that it will play the same role as any other particle in what concerns the generation of gravitational field.

In conclusion, we have proposed an action principle which allows for the construction of a non-local classical lagrangean which yields all the equations of electromagnetism with charges and monopoles, without having to resort to additional restrictions or constraints on the dynamics of the particles.

The quantization of the theory remains a challenging open problem. The same can be said of its non-abelian extension. In the same way that magnetic monopoles can be obtained as solitons of non-abelian theories, we can think that electric charges would be given as topological solutions of dual theories to the first^[19-21]. This possibility suggests a unified description of electric and magnetic charges as configurations of bosonic scalar and vector fields. The difficulty lies, however, in the lack of a self-dual lagrangean which contains at the same time the bosonic fields and their respective duals, like in (1). The introduction of non-local potentials (non-abelian) may be a way to the construction of a saddle point lagrangean formulation.

References

- [1] Dirac PAM, 1931. Proc.Roy.Soc. A133. 60.
- [2] Georgi H and Glashow SL, 1974. Phys.Rev.Lett. 32. 438:
- [3] Pati JC and Salam A, 1974. Phys.Rev. D10. 275.

- [4] Kaluza Th., 1921, Sitzungsber.Preuss.Akad.Wiss.Math.Phys., 966;
 [5] Klein O., 1926, Nature 118, 516; Z.Phys. 37, 895.
 [6] Gross DJ and Perry MJ., 1983, Nucl.Phys. B226, 29;
 [7] Sorkin RD., 1983, Phys.Rev.Lett. 51, 87;
 [8] 't Hooft G., 1974, Nucl.Phys. B79, 276;
 [9] Polyakov AM., 1974, JETP Lett. 20, 194.
 [10] Dirac PAM., 1948, Phys.Rev. 74, 817.
 [11] Wu TT and Yang CN., 1975, Phys.Rev. D12, 3845; 1976, Phys.Rev. D14, 437.
 [12] Bollini CG and Giambiagi JJ., 1977, Nucl.Phys. B123, 311.
 [13] Cabibbo N and Ferrari E., 1962, Nuovo Cimento 23, 1147.
 [14] Around three decades ago, Rohrlich^[15] introduced similar non-local potentials, making use of a parametrization suggested by DeWitt^[16] for tracking non-local wave functions like the one used by Cabibbo and Ferrari^[13]. In his work, however, he arrives at different results and conclusions.
 [15] Rohrlich F., 1966, Phys.Rev. 150, 1104.
 [16] DeWitt BS., 1962, Phys.Rev. 125, 2189.
 [17] The covariant derivative of the line integral of a tensor $\Lambda^{\alpha\dots\nu}$ with respect to the observation point x^μ , extremum of the path of integration P , along this path, is defined as^[18]

$$\partial^\mu \int_P \Lambda^{\alpha\dots\nu}(\xi) d\xi_\nu \equiv \lim_{dx_\mu \rightarrow 0} \frac{[\int_{P'} \Lambda^{\alpha\dots\nu}(\xi) d\xi_\nu - \int_P \Lambda^{\alpha\dots\nu}(\xi) d\xi_\nu]}{dx_\mu} \quad (32)$$

where P' is obtained from P by adding to this one an extension dx^μ in the x^μ direction. Thus if the derivation is to be performed in a direction which should be orthogonal to that of the integration, the difference in brackets vanishes and so does the derivative. On the other hand, if we derive in the same direction of the integration, we obtain, according to the Fundamental Theorem of Calculus, $\Lambda^{\alpha\dots\mu}(x)$. Thus we have

$$\partial^\mu \int_P \Lambda^{\alpha\dots\nu}(\xi) d\xi_\nu = \Lambda^{\alpha\dots\nu}(x) \delta_\nu^\mu = \Lambda^{\alpha\dots\mu}(x) \quad (33)$$

- [18] Mandelstam S., 1962, Annals of Physics 19, 1.
 [19] Goddard P, Nuyts J and Olive D., 1977, Nucl.Phys. B125, 1;
 [20] Montonen C and Olive D., 1977, Phys.Lett. B72, 117;
 [21] Seiberg N., 1994, preprint IASSNS-HEP-94/98, RU-94-82, Rutgers University.

Schwinger Model With Current-Current Interaction

R. L. P. G. Amaral^b, L.V. Belvedere^b and C. P. Natividade^a

a: Departamento de Física e Química, Universidade Estadual Paulista

Campus de Guaratinguetá, Caixa Postal 205, 12500-000 Guaratinguetá, São Paulo, Brazil

b: Instituto de Física, Universidade Federal Fluminense

Av. Litoranea, S/N, CEP 24210-340, Niterói, RJ, Brazil

In this work we discuss the effect of quartic fermion self interacting terms on the dynamics of the vector and chiral Schwinger models. We consider the operator treatment to obtain the fermion and vector fields solutions. The θ -vacuum structure of the vector and chiral models is displayed. This work complements the functional approach in [1].

1 Operator solution

Let us first analyze to the vectorial case (the left and right couplings are equal) and let us avoid the anomaly keeping the gauge invariance in the bosonization of the model. The Lagrangian density will be in this case:

$$L = -\frac{1}{4} F^{\mu\nu} F_{\mu\nu} + i \bar{\psi} \not{D} \psi - \frac{g^2}{2} \bar{\psi} \gamma^\mu \psi \bar{\psi} \gamma_\mu \psi \quad (1)$$

The solution of the Schwinger model in the Lorentz gauge is [2] $\psi_j = \sqrt{\mu/2\pi x} : \exp(i\sqrt{\pi}\gamma_{j,i}^5(-\alpha_1 - \alpha_2 + \alpha_3) - i\sqrt{\pi} \int_x^\infty \dot{\alpha}_3 dy^1) :$ and $A^\mu = -\frac{1}{m} \epsilon^{\mu\nu} \partial_\nu(\alpha_1 + \alpha_2)$. Here α_1 is a canonical scalar field with mass $m = \epsilon/\sqrt{\pi}$, α_3 is a canonical massless field and α_2 the same but with negative metric while μ is an infrared regulator. The Maxwell equation in the physical subspace is satisfied with the current: $J^\mu = \frac{1}{\sqrt{\pi}} \epsilon^{\mu\nu} \partial_\nu(\alpha_1 + \alpha_2 - \alpha_3)$. These fields define the operator solution to the above Lagrangian in the interaction picture. To boost them to the Heisenberg picture while keeping the Lorentz invariance it is necessary first to verify the validity of the Schwinger condition, $[\Theta_{00}(x), \Theta_{00}(y)] = i(\Theta_{01}(x) + \Theta_{01}(y)) \partial_x \delta(x-y)$ [3]. The Schwinger model hamiltonian is easily seen to verify this condition. The only nonvanishing term in the interaction energy-momenta tensor is $\Theta_{00}^{int} = \frac{g^2}{2} ((J^0)^2 - b(J^1)^2)$. Requiring the Schwinger condition we fix the value $b = 1/(g^2/\pi + 1)$. Now we take the free hamiltonian expressed in terms of the fields α_i and their conjugate momenta Π_i (note that $\Pi_2 = -\dot{\alpha}_2$), add the interaction term resulting in a Hamiltonian that in spite of quadratic has crossed terms among all fields and all momenta. In the Heisenberg picture the new definition of the momenta can be obtained inverting the canonical equations ($\partial_t \alpha_j = \partial_{\Pi_j} H$). They are $\Pi_1 = (1 + \frac{g^2}{\pi}) \dot{\alpha}_1 + \frac{g^2}{\pi} (\dot{\alpha}_2 - \dot{\alpha}_3)$, $\Pi_2 = -(1 - \frac{g^2}{\pi}) \dot{\alpha}_2 + \frac{g^2}{\pi} (\dot{\alpha}_1 - \dot{\alpha}_3)$, and $\Pi_3 = (1 + \frac{g^2}{\pi}) \dot{\alpha}_3 - \frac{g^2}{\pi} (\dot{\alpha}_2 + \dot{\alpha}_1)$.

The original variables α_i are now not free fields. Let us perform a generic linear transformation to new variables. Requiring canonical commutation relations for these new fields we chose the transformations as: $\alpha_1 = \frac{1}{\sqrt{1+g^2/\pi}} \phi_1$, $\alpha_2 = \sqrt{1+g^2/\pi} \phi_2 + \frac{g^2}{\pi\sqrt{1+g^2/\pi}} \phi_1$, and $\alpha_3 = \frac{1}{\sqrt{1+g^2/\pi}} \phi_3 + \frac{g^2}{\pi\sqrt{1+g^2/\pi}} (\phi_1 + \phi_2)$. Substituting these definitions in the hamiltonian we see that ϕ_1 is a canonical field with mass equal to $m(g) = m/\sqrt{1+g^2/\pi}$, ϕ_2 is a negative metric and ϕ_3 a positive metric canonical massless field. This mass coincides with the one in [1]. The solution of the model is obtained from the free one upon the substitution of the old phase space variables by the new ones. The result therefrom any correlation function may be easily computed is:

$$\psi_j = N : \exp \left(\frac{-i\sqrt{\pi}}{\sqrt{1+g^2/\pi}} \gamma_{j,j}^5 (\phi_1 + \phi_2 - \phi_3) - i\sqrt{\pi+g^2} \int_x^\infty \dot{\phi}_3 d\xi^1 \right) : \quad (2)$$

$$A^\mu = -\frac{1}{m(y)} \epsilon^{\mu\nu} \partial_\nu (\phi_1 + \phi_2) \tag{3}$$

As in the Thirring model case we have to redefine the J_1 component with a $1/\sqrt{1+g^2/\pi}$ factor. Only after that the current becomes vectorial and results in: $J^\mu = \frac{1}{\sqrt{\pi}\sqrt{1+g^2/\pi}} \epsilon^{\mu\nu} \partial_\nu (\phi_1 + \phi_2 - \phi_3)$. This current can be also obtained computing the short distance gauge invariant operator product of the fermion fields and normalizing them to have a vectorial field.

We can verify that the Dirac equation becomes satisfied, $\not{D}\psi = g^2 J\psi$. The vector field satisfies the equation: $\partial_\mu F^{\mu\nu} - eJ^\nu = eL^\nu$. As in the Schwinger model the L^μ current, $L^\mu = \frac{1}{\sqrt{\pi}\sqrt{1+g^2/\pi}} \epsilon^{\mu\nu} \partial_\nu (\phi_3 - \phi_2)$, is a null metric field. The Maxwell equation is obeyed in the physical subspace where the expectation values of this current are zero.

In order to obtain the spurious operators one can consider the operators that would result from a gauge transformation: $\psi'_j = \psi_j \times \exp\left(i\sqrt{\pi+g^2} \int_x^\infty (\phi_2) dy^1\right)$; and $A'^\mu = -\frac{1}{m(y)} \epsilon^{\mu\nu} \partial_\nu \phi_1$. As the field ϕ_1 belongs to the operator algebra of the model [4] we can factorize its contribution out of the fermionic fields. The resulting operators commute with the null metric current L_μ and have constant correlation functions. They define the two spurious operators after the introduction of the interaction:

$$\sigma_j = N \times \exp\left(\frac{i\sqrt{\pi}}{\sqrt{1+g^2/\pi}} \gamma_{j,j}^5 (-\phi_2 + \phi_3) - i\sqrt{\pi}\sqrt{1+g^2/\pi} \int_x^\infty (\phi_3 - \phi_2) dy^1\right) \tag{4}$$

These operator expose the origin of the violation of the cluster property. In order to restore it one should define the theta vacua. As in the Schwinger model this would lead to a twofold set of degenerate vacua. The spurious operators σ_1 and σ_2 differ from the ones in the Schwinger model as they are not chiral however. The effect of the interaction appears in their dependence at the same time of the right and left light cone variables. On the other hand we could deal only with the operators present in the algebra of fields of the model and avoid the introduction of the gauge transformation leading the pair of spurious operators. In this case the unique spurious operator will be $\sigma_1^\dagger \sigma_2$ where the effect of interaction will show up in its dimension being changed.

Let us now construct the generators of gauge transformations of the model. Following [5] we take the generators of gauge transformation of the Schwinger model and boost them to the Heisenberg picture. We obtain the generators of gauge transformations in the interacting model:

$$T(\lambda) = \exp\left(\frac{i}{\sqrt{\pi}\sqrt{1+g^2/\pi}} \int dy^1 \left((\phi_3 + \phi_2) \partial_1 \lambda(y) - (\hat{\phi}_3 + \hat{\phi}_2) \partial_0 \lambda\right)\right) \tag{5}$$

Commuting with the fields we can ascertain that these are the correct generators of the gauge transformations. $T \psi(x) T^{-1} = e^{i\lambda(x)} \psi(x)$ and $[T, A_\mu(x)] = -\frac{1}{\pi} \partial_\mu \lambda(x)$.

Following [8] we define $\lambda_{-1/2}(y^0, y^1) = -\pi\Theta(y^0 - y^1 - x^-)$ and $\lambda_{1/2}(y^0, y^1) = -\pi\Theta(y^0 + y^1 - x^+)$. Taking $\lambda_1 = (1 + g^2/2\pi)\lambda_{1/2} + (g^2/2\pi)\lambda_{-1/2}$ we see that this generator reduces to the spurious operator σ_1 , while $\lambda_2 = (1 + g^2/2\pi)\lambda_{-1/2} + (g^2/2\pi)\lambda_{1/2}$ leads to the σ_2 operator. As in the Schwinger model the screening is due to the disappearance, after the switching to the theta vacua, of the physical states carrying quantum numbers associated to the generators of $U(1)$ and chiral $U(1)$ gauge transformations. The difference is that the basic generators are not chiral any more. In any case looking at the true spurious operators obtained with the fields that define gauge invariant algebra of operators of the model, $\sigma_1^\dagger \sigma_2$ we see that they are as in the Schwinger model functions of the scalar operator $\phi_2 - \phi_1$ and not of their chiral components.

Let us note that although the vectorial field expression could be obtained directly from the Schwinger model vector field through a simple redefinition of the electric coupling constant the fermionic field cannot be obtained so

simply with the same transformation. The gauge invariant interacting two point fermionic functions cannot also be obtained from the ones in the Schwinger model through such a transformation. The effect of the interaction after quantization is to define a new class of models.

The value of the chiral anomaly can now be computed. Taking $J_5^\mu = \epsilon^{\mu\nu} J_\nu$ we have $\partial_\mu J_5^\mu = \frac{-m(g)}{2\sqrt{\pi+g^2}} \epsilon_{\mu\nu} F^{\mu\nu} = \frac{-e}{2(\pi+g^2)} \epsilon_{\mu\nu} F^{\mu\nu}$. The spacial integral of J_5^0 gives not properly the chiral transformation generator, Q_5 . To have $[Q_5, \psi] = i\gamma_5 \psi$ the current should be multiplied by $1 + g^2/\pi$, reflecting directly in the value of the anomaly.

Let us turn now to the chiral case. The fermionic Lagrangian is [6]:

$$L = -\frac{1}{4} F^{\mu\nu} F_{\mu\nu} + i\bar{\psi} \not{D}_{(+)} \psi - \frac{G\pi}{2a} \bar{\psi} \gamma^\mu (1 + \gamma_5) \psi \bar{\psi} \gamma_\mu (1 + \gamma_5) \psi \quad (6)$$

Where $\not{D}_{(+)} = \gamma^\mu \partial_\mu + i\gamma^\mu A_\mu (1 + \gamma_5)$ and it is convenient to define the coupling through $G = g^2 a/\pi$. In this case it is more straightforward to bosonize directly the Lagrangian obtaining the equivalent model [7]:

$$L = -\frac{1}{4} F^{\mu\nu} F_{\mu\nu} + \frac{1}{2} \partial_\mu \phi \partial^\mu \phi + \frac{e}{\sqrt{\pi}} (\partial_\mu + \tilde{\partial}_\mu) \phi A^\mu + \frac{ae^2}{2\pi} A_\mu A^\mu - \frac{g^2}{2} J_\mu J^\mu \quad (7)$$

In the operator approach the bosonized expression of the current depends largely on the regularization used on its computation. We choose the current that would appear in the Maxwell equation in the $g = 0$ model. Namely we take $\bar{\psi} \gamma_\mu (1 + \gamma_5) \psi \approx J_\mu = \frac{-1}{\sqrt{\pi}} ((\partial_\mu + \tilde{\partial}_\mu) \phi + \frac{e}{\sqrt{\pi}} A_\mu)$. This regularization differs from the one used in the computation of the $J_\mu A^\mu$ term as the contribution of the very vector field to it is taken with different weight. We could have worked with this regularization without changing the main course of arguments but the expressions involved would be unnecessarily cumbersome to read. Substituting $A_\mu = \partial_\mu \chi + \tilde{\partial}_\mu \lambda$ in the Lagrangian and changing variables to: $\phi = \phi_3 - \frac{e}{\sqrt{\pi}} (1 - G) \lambda_1 + \frac{e(1-G)a}{\sqrt{\pi}(a-1+G)} \chi$ and $\lambda = \lambda_1 - \frac{1-G}{a-1+G} \chi$, results in:

$$L = \frac{1}{2} \square \chi \square \chi - \frac{m_g^2}{2} \partial_\mu \chi \partial^\mu \chi + \frac{1}{2} \partial_\mu \phi_3 \partial^\mu \phi_3 + \frac{e^2(1-G)(a-1+G)}{2\pi} \partial_\mu \lambda_1 \partial^\mu \lambda_1 \quad (8)$$

Where the mass $m_g = e\sqrt{1-G}a/\sqrt{a-1+G}\sqrt{\pi}$ coincides with the one computed in [1]. The solution of the higher derivative field χ is well known [7] leading to $\chi = (\phi_2 - \phi_1)/m_g$ where the field ϕ_1 has mass m_g and positive metric while the massless field ϕ_2 is quantized with negative metric. The solution of the model is obtained expressing the free fermionic field in terms of ϕ and its momentum and substituting the later by $\partial_\mu L$. It is finally:

$$A_\mu = \frac{1}{m_g} \left(\tilde{\partial}_\mu (\phi_2 - \phi_1) - \frac{(1-G)}{(a-1+G)} \partial_\mu (\phi_2 - \phi_1) \right) + \partial_\mu \lambda_1 \quad (9)$$

$$\psi_2 = \exp \left(-i\sqrt{\pi} \left(\phi_3 + \int_r^\infty dy^1 \phi_3 \right) \right) \quad (10)$$

$$\psi_1 = \exp \left(i\sqrt{\pi} \left(\phi_3 + \frac{2\sqrt{1-G}}{\sqrt{a-1+G}} (\phi_2 - \phi_1) \right. \right. \quad (11)$$

$$\left. \left. - \frac{2e(1-G)}{\pi} \lambda_1 - \int_r^\infty dy^1 \phi_3 \right) \right) \quad (12)$$

The Dirac equation will read $i\partial_+ \psi_2 = 0$ and $(i\partial_- - 2A_- - 2g^2 J_-) \psi_1 = 0$ and the Maxwell equation will be $\partial_\mu F^{\mu\nu} = e(1-G) J^\nu + e(1-G) L^\nu$ where the current is:

$$J_\mu = \frac{-1}{\sqrt{\pi}} \left((\partial_\mu + \tilde{\partial}_\mu) \phi_3 + \frac{a}{\sqrt{a-1+G}\sqrt{1-G}} \tilde{\partial}_\mu (\phi_2 - \phi_1) \right. \\ \left. + \frac{e}{\sqrt{\pi}} \left((a-1+G) \partial_\mu \lambda_1 - (1-G) \tilde{\partial}_\mu \lambda_1 \right) \right) \quad (13)$$

and the null metric current given by

$$L_\mu = \frac{1}{\sqrt{\pi}} \left((\partial_\mu + \tilde{\partial}_\mu) \phi_3 + \frac{a}{\sqrt{a-1+G}\sqrt{1-G}} \tilde{\partial}_\mu \phi_2 + \frac{c}{\sqrt{\pi}} \left((a-1+G) \partial_\mu \lambda_1 - (1-G) \tilde{\partial}_\mu \lambda_1 \right) \right) \quad (14)$$

determines the physical subspace out of the complete Hilbert space. The physical fields turn out to be ϕ_1 and $h = \phi_3 - \frac{c(1-G)}{\sqrt{\pi}} \lambda_1 + \sqrt{\frac{1-G}{a-1+G}} \phi_2$. It is interesting to note that the introduction of the current-current interaction in this case can be accommodated in a redefinition of the parameters of the original ($g = 0$) Lagrangian. Indeed making $e \rightarrow e(1-G)$ and $a \rightarrow a/(1-G)$ in the chiral Schwinger model solution leads us directly to the interacting ($g \neq 0$) model solution. This can be understood as a consequence of the fact that the interaction term $J_\mu J^\mu$ would be naively zero if one used the quiral current expressed only in terms of the fermion fields, as this product would be identically zero. What makes this interaction different from zero is exactly the ambiguity in the definition of the currents present in the chiral Schwinger model. This phenomenon has its correspondence in the functional formalism in the fact that the introduction of an identity, $1 = \exp(\langle J_\mu J^\mu \rangle)$, in the integrand together with the ambiguities in the jacobian leads to the redefinition of the parameters of the model.

It is important to note that in the chiral case we cannot define an spurious operator in terms of the algebra of operators that are observables of the theory. There is no theta vacuum.

References

- [1] A. S. Dutra, C. P. Natividade and H. Boschi-Filho, Sobre o efeito da auto-interação quártica de férmions na massa dos fótons em 1+1D, XVI ENFPC, Caxambú, 1995.
- [2] J. Schwinger, Phys. Rev. **128**(1962)2425, J. H. Lowenstein and J. Swieca, Ann. Phys. **68**, (1971), 112.
- [3] M. B. Halpern, Phys. Rev. D, **12** (1975) 1684 and M. B. Halpern, Phys. Rev. D, **13** (1976) 337.
- [4] L. V. Belvedere C. P. Natividade, C. G. Carvalhaes and H. Boschi Filho, Algebraic Isomorphism in two-dimensional gauge theories, in preparation.
- [5] K. D. Rothe and J. A. Swieca, Phys. Rev. D **15** (1977) 541.
- [6] R. Jackiw and R. Rajaraman, Phys. Rev. Lett. **B54**(1985)1219, R. Rajaraman, Phys Lett **B514**(1985)1305, A. Niemi and G.
- [7] D. Boyannovsky, I. Schmidt and M. F. L. Golterman, Annals of Phys. **185**, (1988), 111.
- [8] K. D. Rothe, E. Abdalla and M. Abdalla, Theoretical Methods in Two dimensional Quantum Field Theory, World Scientific, 1992.

SUSY QM for the Two-Component Wave Functions

R. de Lima Rodrigues^{(a)*} and A. N. Vaidya^(b)

^(a)Departamento de Física, Universidade Federal da Paraíba
58.109-970 - Campina Grande - PB, Brazil

^(b)Instituto de Física, Universidade Federal do Rio de Janeiro
Rio de Janeiro, RJ - 21.945-970 - Brazil

December 3, 1996

I Introduction

We studied the supersymmetry (SUSY) in non-relativistic quantum mechanics (QM) [1] involving two-component wave functions [2]. We show that the superpotential for the SUSY QM with two-component wave functions is a Hermitian matrix. We point out that the respective supersymmetric Hamiltonian can be realized from stability equation for two coupled real scalar fields in 1+1 dimensions [3] and for a bidimensional physical system in coordinate space associated to a Neutron in a static magnetic field [4].

II SUSY QM to two-component eigenfunction

Let H_- be the bosonic sector Hamiltonian for a two-component eigenstate Ψ_- , given by

$$H_- = -\mathbf{I} \frac{d^2}{dx^2} + \mathbf{V}_-(x), \quad \Psi_-(x) = \begin{pmatrix} \psi_{-,1}(x) \\ \psi_{-,2}(x) \end{pmatrix} \quad (1)$$

where \mathbf{I} denotes the 2 by 2 unit matrix and $\mathbf{V}_-(x)$ is a 2 by 2 matrix potential which may be written in terms of a 2 by 2 matrix superpotential $\mathbf{W}(x)$, viz.

$$\mathbf{V}_-(x) = \mathbf{W}^2(x) + \mathbf{W}'(x). \quad (2)$$

In general, from a Hamiltonian (H_1) for a two-component wave function in the following bilinear form

$$H_1 = \mathbf{A}^+ \mathbf{A}^- = -\mathbf{I} \frac{d^2}{dx^2} + \mathbf{V}_1(x) \quad (3)$$

we can find the supersymmetric partner, viz.

$$\begin{aligned} H_2 &= \mathbf{A}^- \mathbf{A}^+ = -\mathbf{I} \frac{d^2}{dx^2} + \mathbf{V}_2(x) \\ \mathbf{A}^- &= -\mathbf{I} \frac{d}{dx} + \mathbf{W}(x), \quad \mathbf{A}^+ = (\mathbf{A}^-)^\dagger. \end{aligned} \quad (4)$$

We see that only when the hermiticity condition of the superpotential is readily satisfied i.e.

$$\mathbf{W}^\dagger = \mathbf{W} \quad (5)$$

we may put H_1 with the potential ($\mathbf{V}_-(x)$) given in (2). In this case H_1 becomes exactly H_- .

*This work was partially supported by CNPq. E-mail:rafael@dfjp.ufpb.br

III Two coupled scalar field

The Lagrangian density for two coupled scalar field nonlinear system in the natural system of units ($c = \hbar = 1$), in (1+1) dimensional space-time is given by

$$\mathcal{L}(\rho, \sigma, \partial_\mu \rho, \partial_\mu \sigma) = \frac{1}{2} (\partial_\mu \rho)^2 + \frac{1}{2} (\partial_\mu \sigma)^2 - V(\rho, \sigma), \tag{6}$$

where $\partial_\mu = \frac{\partial}{\partial x^\mu}$, $x^\mu = (t, x)$ with $\mu = 0, 1$. $x_\nu = \eta_{\nu\mu} x^\mu$. $\rho = \rho(x, t)$ and $\sigma = \sigma(x, t)$ are real scalar fields and $\eta^{\mu\nu}$ is the metric tensor. The potential $V = V(\rho, \sigma)$ is any positive semidefinite function of ρ and σ , which must have at least two different zeros, in order to present solitons as solutions.

Since the potential $V(\rho, \sigma)$ is positive it can be written in the following square form, analogous to the case with only single field [5]:

$$V(\rho, \sigma) = \frac{1}{2} M^2(\rho, \sigma) + \frac{1}{2} N^2(\rho, \sigma). \tag{7}$$

The Bogomol'nyi condition of minimum energy associated with the static configurations [5] becomes:

$$\rho' = -M(\rho, \sigma), \quad \sigma' = -N(\rho, \sigma). \tag{8}$$

From the classical stability of the soliton solutions in this nonlinear system, which is ensured by considering small perturbations around $\rho(x)$ and $\sigma(x)$ we obtain:

$$\mathcal{H} \tilde{\Psi}_n = \omega_n^2 \tilde{\Psi}_n, \quad n = 0, 1, 2, \dots \tag{9}$$

where

$$\mathcal{H} = \begin{pmatrix} -\frac{d^2}{dx^2} + \frac{\partial^2}{\partial \rho^2} V & \frac{\partial^2}{\partial \sigma \partial \rho} V \\ \frac{\partial^2}{\partial \rho \partial \sigma} V & -\frac{d^2}{dx^2} + \frac{\partial^2}{\partial \sigma^2} V \end{pmatrix}_{|\rho=\rho(x), \sigma=\sigma(x)}, \quad \tilde{\Psi}_n = \begin{pmatrix} \eta_n(x) \\ \xi_n(x) \end{pmatrix}. \tag{10}$$

We can realize the 2 by 2 matrix superpotential in the following manner

$$\mathbf{W} = - \begin{pmatrix} \frac{\partial}{\partial \rho} M & \frac{\partial}{\partial \sigma} M \\ \frac{\partial}{\partial \rho} N & \frac{\partial}{\partial \sigma} N \end{pmatrix}_{|\rho=\rho(x), \sigma=\sigma(x)} \tag{11}$$

But

$$(\mathbf{W})^\dagger = \mathbf{W} \Rightarrow \frac{\partial}{\partial \sigma} M = \frac{\partial}{\partial \rho} N. \tag{12}$$

The SUSY algebra can be readily realized as

$$H_{SUSY} = [Q_-, Q_+]_+ = \begin{pmatrix} \mathcal{A}^+ \mathcal{A}^- & 0 \\ 0 & \mathcal{A}^- \mathcal{A}^+ \end{pmatrix}_{4 \times 4} = \begin{pmatrix} \mathcal{H}_- = \mathcal{H} & 0 \\ 0 & \mathcal{H}_+ \end{pmatrix} \tag{13}$$

$$[H_{SUSY}, Q_\pm]_- = 0 = (Q_-)^2 = (Q_+)^2. \tag{14}$$

The supercharges Q_\pm become a four by four matrix differential operators.

Indeed the bosonic sector Hamiltonian of H_{SUSY} is given exactly by \mathcal{H} treated in stability equation.

IV A Neutron in Magnetically Bound States

Consider an electrically neutral spin $\frac{1}{2}$ particle of mass M and a magnetic moment $\mu \vec{\sigma}$ (a Neutron) in interaction with an infinite straight wire carrying a current I and located along the z -axis. The magnetic field generated by the wire is given by (we use units with $c = \hbar = 1$) $\vec{B} = 2I \frac{(-y, x, 0)}{(x^2 + y^2)}$, where x and y are cartesian coordinates in the

plane perpendicular to the wire. The Hamiltonian of the particle is given by $H = \frac{\vec{p}^2}{2m} + \mu \vec{\sigma} \cdot \vec{B}$, where $\vec{\sigma} = (\sigma_1, \sigma_2, \sigma_3)$ are the Pauli matrices.

The motion along the z -axis is free and will be ignored in the following. Thus we get a two-dimensional problem with $H = \frac{\vec{p}^2}{2m} + 2I\mu \frac{(-y\sigma_1 + x\sigma_2)}{(x^2 + y^2)}$ [4].

In the space of bound states we have symmetry under the SO(3) group while for scattering states the symmetry group is SO(2,1).

In cylindrical coordinates and because of the translational symmetry in the z -direction we obtain:

$$\psi(\vec{r}) = \frac{1}{\sqrt{4\pi L}} \left\{ \phi_{k+}(\rho) e^{im\phi} \begin{pmatrix} 1 \\ 0 \end{pmatrix} + \phi_{k-}(\rho) e^{i(m+1)\phi} \begin{pmatrix} 0 \\ 1 \end{pmatrix} \right\} e^{i2\xi k z}, \quad k = 0, \pm 1, \dots \quad (15)$$

Using

$$\frac{d^2}{d\rho^2} + \frac{1}{\rho} \frac{d}{d\rho} = \left(\frac{d}{d\rho} + \frac{1}{2\rho} \right)^2 = \rho^{-\frac{1}{2}} \left(\frac{d^2}{d\rho^2} + \frac{1}{4\rho^2} \right) \rho^{\frac{1}{2}}, \quad \phi_{k\pm} = \rho^{-\frac{1}{2}} \xi_{k\pm} \quad (16)$$

we get

$$H \xi_{k\pm} = E \xi_{k\pm}, \quad \xi_{k\pm} \equiv \begin{pmatrix} \xi_{k-} \\ \xi_{k+} \end{pmatrix} \quad (17)$$

where

$$H \equiv -1 \frac{\hbar^2}{2M} \frac{d^2}{d\rho^2} + V\left(\frac{1}{\rho^2}\right) = A^+ A^-, \quad A^\pm = \pm \frac{\hbar}{\sqrt{2M}} \frac{d}{d\rho} + W(\rho). \quad (18)$$

Note that $\mathbf{W}(\rho)$ is the 2 by 2 matrix superpotential. A detailed analysis of this applications will be published elsewhere.

References

- [1] E. Witten, *Nucl. Phys.* **B185**, E. D. Filho, *Mod. Phys. Lett.* **A9**, 411 (1994); E. D. Filho and R. M. Ricotta, *Mod. Phys. Lett.* **A10**, 1613 (1995); F. Cooper, A. Khare, U. Sukhatme, *Phys. Rep.* **251**, 267 (1995).
- [2] T. Fukui, *Phys. Lett.* **A178**, 1 (1993).
- [3] R. Rajaraman, *Phys. Rev. Lett.*, **42**, 200 (1979); R. Rajaraman, *Solitons and Instantons*, (North-Holland, Amsterdam, 1982); L. J. Boya and J. Casahorran, *Phys. Rev.* **A39**, 4298 (1989); R. de Lima Rodrigues, P. B. da Silva Filho e A. N. Vaidya, Proceedings do XV Encontro Nacional de Física de Partícula e Campos, Caxambu-MG, 1995; XIII Encontro de Físicos do Norte e Nordeste, Salvador-BA, 1995; D. Bazeia, M. J. dos Santos and R. F. Ribeiro, *Phys. Lett.* **A208**, 84 (1995).
- [4] R. de Lima Rodrigues and A. N. Vaidya, **Green's Function for a Neutron in Magnetically Bound States**, preprint DF-CCP-UFPB/02/96 (submitted to *Phys. Rev. A*, July, 1996); I. Voronin, *Phys. Rev. A* **43** 29 (1991).
- [5] E. B. Bogomol'nyi, *Sov. J. Nucl. Phys.* **24**, 489 (1976); R. de Lima Rodrigues, *Mod. Phys. Lett* **A10**, 1309 (1995).

Uma Classe de Potenciais Isoespectrais com o q-Oscilador Relativístico 1D

R. de Lima Rodrigues^(a) e Silvanio Bezerra de Oliveira^(b)

^(a) Departamento de Ciências Exatas e da Natureza

Universidade Federal da Paraíba, Cajazeiras - PB, 58.900-000

^(b) Departamento de Física, Universidade Federal da Paraíba

58.109-970 - João Pessoa - PB, E-mail: rafael@dfjp.ufpb.br

December 5, 1996

I Introdução

Nesses últimos anos tem-se discutido com grande interesse, tanto por físicos como por matemáticos, trabalhos sobre a q-deformação quântica [1], que tem despertado estudos em busca de sistemas físicos reais com q-simetrias. Recentemente vários trabalhos tem sido realizados sobre os sistemas de osciladores quânticos relativísticos unidimensionais (1D) e tridimensionais (3D), os quais podem ser construídos via um acoplamento não mínimo da equação de Dirac para uma partícula livre [2]. A partir da equação de Schrödinger relativística via o operador momento linear "diferença" nos proporciona uma segunda possibilidade [3]. Recentemente, a q-SUSI tem sido implementada via o q-oscilador bosônico e q-oscilador fermiônico e seus estados q-supercoerentes [6]. Neste trabalho abordaremos a estrutura algébrica da supersimetria (SUSI) [4], implementando os companheiros q-SUSI em termos de operadores diferenciais de "diferenças finitas" de primeira ordem. Considerando duas transformações SUSI sucessivas sobre um q-oscilador relativístico 1D encontraremos uma classe de potenciais q-deformados exatamente solúveis. Nesse sistema o parâmetro de q-deformação é constante e os seus estados são não degenerados. Utilizaremos o sistema de unidades em que $m = \hbar = c = 1$. O q-oscilador relativístico unidimensional (1D) é governado pelo seguinte hamiltoniano[3]:

$$\mathbf{h} = 2 \left(\frac{\cosh\left(\frac{i}{2} \frac{d}{dx}\right) \cosh\left(\frac{\omega}{4x}\right) \cosh\left(\frac{i}{2} \frac{d}{dx}\right)}{\cosh\left(\frac{\omega}{4x}\right)^2 - 2 \cosh\frac{\omega}{4}} \right) = \frac{P_x^2}{2} + V(x), \quad (1)$$

onde o operador momento linear de diferença finita é dado por:

$$P_x = -\frac{2}{\cosh\left(\frac{\omega}{4}x\right)} \sinh\left(\frac{i}{2} \frac{d}{dx}\right). \quad (2)$$

O sistema descrito pelo hamiltoniano acima é denominado de oscilador relativístico pelo fato de que, no limite não-relativístico, obtém-se o operador hamiltoniano do oscilador harmônico simples, ou seja, $P_x \rightarrow -i \frac{d}{dx} \Rightarrow \mathbf{h} \rightarrow -\frac{1}{2} \frac{d^2}{dx^2} + \frac{1}{2} \omega^2 x^2$. Na q-deformação quântica o comutador pode ser definido pela seguinte relação de comutação generalizada: $[A^-, A^+]_q = A^- q A^+ - A^+ q^{-1} A^-$. No problema considerado acima, o parâmetro constante de q-deformação quântica torna-se: $q = e^{-\omega \hbar / 4 m c^2} = e^{-\frac{\omega}{4}}$, pois $m = \hbar = c = 1$. Usaremos a seguinte propriedade do operador de diferença finita:

$$\sinh\left(\frac{i}{2} \frac{d}{dx}\right) (\varphi(x)\psi(x)) = \left(\sinh\left(\frac{i}{2} \frac{d}{dx}\right) \varphi(x)\right) \left(\cosh\left(\frac{i}{2} \frac{d}{dx}\right) \psi(x)\right) + \left(\cosh\left(\frac{i}{2} \frac{d}{dx}\right) \varphi(x)\right) \left(\sinh\left(\frac{i}{2} \frac{d}{dx}\right) \psi(x)\right), \quad (3)$$

a qual pode ser verificada fazendo as expansões dos respectivos operadores exponenciais que aparecem no operador diferença seno hiperbólico.

II Companheiros q-Supersimétricos

Definindo os operadores A^\pm na forma:

$$A^\pm = -\frac{i\sqrt{2}}{\cos\frac{1}{2}\omega x} \sinh\frac{i}{2}\left(\mp\frac{d}{dx} + \omega x\right) = -\frac{i\sqrt{2}}{\cos[(a^+ + a^-)/2\sqrt{2}]} \sinh\frac{i}{\sqrt{2}}a^\pm. \quad (4)$$

o hamiltoniano do q-oscilador relativístico torna-se,

$$h = \frac{1}{2}\{A^-, A^+\}_q = \frac{1}{2}\{e^{-\omega/4}A^-A^+ + e^{\omega/4}A^+A^-\} = e^{\omega/4}A^+A^- + E^{(0)}, \quad (5)$$

onde o autovalor e a autofunção de energia do estado fundamental são dados pela seguinte condição de aniquilação:

$$A^- \eta_1^{(0)}(x) = 0 \implies E^{(0)} = 2 \sinh\frac{\omega}{4}, \quad \eta_1^{(0)}(x) \propto e^{-\frac{x^2}{2}}. \quad (6)$$

A equação de Schrödinger relativística independente do tempo é a seguinte:

$$h\eta^{(n)}(x) = E^{(n)}\eta^{(n)}(x). \quad (7)$$

O compnheiro q-SUSI de $H_1 = h$ e sua solução não-normalizável são, respectivamente:

$$H_2 = e^{-\omega/4}A^-A^+ + E^{(0)}, \quad A^+\eta_2^{(0)}(x) = 0 \implies \eta_2^{(0)}(x) \propto e^{\frac{x^2}{2}}. \quad (8)$$

Agora consideraremos uma solução geral não-normalizável de H_2 , a saber:

$$\eta_G(x) = \eta_2^{(0)}(x) \left\{ 1 + \alpha \int_{-\infty}^x [\eta_2^{(0)}(\tilde{x})]^{-2} d\tilde{x} \right\}. \quad (9)$$

Note que quando $\alpha \rightarrow 0 \implies \eta_G(x) \rightarrow \eta_2^{(0)}(x)$. Efetuando uma fatorização em termos desta solução não-normalizável, temos:

$$\tilde{H}_2 = e^{-\omega/4}B^-B^+ + E^{(0)} = e^{-\omega/4}A^-A^+ + E^{(0)}, \quad \tilde{V}_2(x) = V_2(x), \quad (10)$$

onde o operador B^+ é construído sob à condição de aniquilação da solução geral $\eta_G(x)$:

$$B^+\eta_G(x) = 0. \quad (11)$$

O potencial do companheiro q-SUSI $\tilde{H}_1 = e^{\omega/4}B^+B^- + E^{(0)}$ de \tilde{H}_2 é dado por:

$$\tilde{V}_1(x) = V_1(x) + [A^-, A^+]_q + [B^-, B^+]_q. \quad (12)$$

O estado fundamental de \tilde{H}_1 satisfaz a seguinte condição de aniquilação:

$$B^-\tilde{\eta}_1^{(0)}(\tilde{x}) = 0 \implies \tilde{\eta}_1^{(0)} = \frac{1}{\eta_G(x)}. \quad (13)$$

Note que $\tilde{V}_1(x) \rightarrow V_1(x)$, as $\alpha \rightarrow 0$. Os novos potenciais são isoespectrais [5] com o q-oscilador relativístico unidimensional.

Um trabalho com uma análise detalhada sobre a construção dessa classe de potenciais q-deformados exatamente solúveis está sendo preparado para ser submetido à publicação num periódico internacional.

Acknowledgments

Este trabalho foi parcialmente financiado pela Capes.

References

- [1] L. C. Biedenharn, *J. Phys. A: Math. Gen.* **22**, L873 (1989); A. J. Macfarlane, *J. Phys. A: Math. Gen.* **22**, 4581 (1989).
- [2] M. Moshinsky e A. Szczepaniak, *J. Phys. A: Math. Gen.* **22**, L817 (1989); J. Jayaraman e R. de Lima Rodrigues, *Proceedings of the XIV Encontro Nacional de Física de Partículas e Campos*, 441 (1993).
- [3] E. D. Kagramanov, R. M. Mir-Kasinov e Sh. M. Nagiyev, *J. Math. Phys.* **31**, 1733 (1990); R. M. Mir-Kasimov, *J. Phys. A: Math. Gen.* **24**, 4283 (1991).
- [4] E. Witten, *Nucl. Phys.* **B185**, 513 (1981); E. D. Filho, *Mod. Phys. Lett.* **A9**, 411 (1994); E. D. Filho and R. M. Ricotta, *Mod. Phys. Lett.* **A10**, 1613 (1995); F. Cooper, A. Khare, U. Sukhatme, *Phys. Rep.* **251**, 267 (1995).
- [5] M. N. Nieto, *Phys. Lett.* **B145** 208 (1984); C. V. Sukumar, *J. Phys. A: Math. Gen.* **18**, 2917 (1985); W.-Y. Keung, U. P. Sukhatme, Q. Wang and T. D. Imbo, *J. Phys. A: Math. Gen.* **22**, L987 (1989); R. de Lima Rodrigues, *Mod. Phys. Lett* **A10**, 1309 (1995).
- [6] San-Ru Hao, Guang-Hua Li e Juan-Yan, *J. Phys. A: Math. Gen.* **27**, 5995 (1994).

Perturbative Analysis of the Schwinger Model (QED_2) for Gauge Non-Invariant Regularizations

Rodolfo Casana Sifuentes^{*}, Marcelo Barbosa da Silva Neto[†], Sebastião Alves Dias[‡]

Centro Brasileiro de Pesquisas Físicas-CBPF

Departamento de Teoria de Campos y Partículas

Abstract

In this article we consider the Schwinger model for gauge non-invariant regularization ($\alpha \neq 1$), and study the perturbative behaviour of some relevant correlation functions.

Now let us consider the Schwinger model defined by the Lagrangian density [1]

$$\mathcal{L}(\psi, \bar{\psi}, A) = -\frac{1}{4}F_{\mu\nu}F^{\mu\nu} + \bar{\psi}(i\partial + eA)\psi. \quad (1)$$

The vacuum functional can be exactly evaluated [2], considering A_μ as an external field

$$\begin{aligned} e^{iW[A]} &= \int d\psi d\bar{\psi} \exp \left[i \int \bar{\psi} (i\partial + eA) \psi \right], \\ W[A] &= \frac{e^2}{2\pi} \int dx \left[\frac{1}{2}(\alpha + 1)A_\mu A^\mu - A_\mu \frac{\partial^\mu \partial^\nu}{\square} A_\nu \right], \end{aligned} \quad (2)$$

where α is an arbitrary real parameter related to different regularization procedures used for calculating the fermionic determinant.

The generating functional for the Green's functions of the fields appearing in the Lagrangian (1) is

$$Z(\eta, \bar{\eta}, J) = \int dA_\mu d\psi d\bar{\psi} \exp \left[i \int dx (\mathcal{L}(\psi, \bar{\psi}, A) + \bar{\eta}\psi + \bar{\psi}\eta + J_\mu A^\mu) \right], \quad (3)$$

for values of $\alpha \neq 1$ the theory is not gauge invariant at quantum level (with A_μ external). However, in order to arrive to a gauge invariant formalism [4] we proceed with Faddeev-Popov [3] method and introduce

$$\int d\theta \Delta_f[A] \delta(f[A^\theta]) = 1, \quad (4)$$

where $d\theta$ represents the invariant measure on $U(1)$, $g = e^{-i\theta} \in U(1)$, and $f[A] = 0$ is the gauge-fixing condition.

^{*}casana@cbpfsu1.cat.cbpf.br

[†]silvanet@cbpfsu1.cat.cbpf.br

[‡]tiao@cbpfsu1.cat.cbpf.br

The generating functional (3) can be written, after inserting (4), as

$$Z[\eta, \bar{\eta}, J] = \int dA_\mu d\psi d\bar{\psi} d\theta \Delta_f[A] \delta(f[A^\theta]) \times \quad (5)$$

$$\times \exp \left[i \int dx \left(\mathcal{L}[\psi, \bar{\psi}, A] + \bar{\eta}\psi + \bar{\psi}\eta + J^\mu A_\mu \right) \right].$$

Under the change of integration variables $A_\mu \rightarrow A_\mu^{\theta^{-1}}$

$$A_\mu \rightarrow A_\mu^{\theta^{-1}} = A_\mu + \frac{1}{e} \partial_\mu \theta, \quad (6)$$

dA_μ is assumed to be invariant. Then (5) can be written as

$$Z[\eta, \bar{\eta}, J] = \int dA_\mu d\psi d\bar{\psi} d\theta \Delta_f[A] \delta(f[A]) \times \quad (7)$$

$$\times \exp \left[i \int dx \left(\mathcal{L}[\psi, \bar{\psi}, A^{\theta^{-1}}] + \bar{\eta}\psi + \bar{\psi}\eta + J^\mu A_\mu^{\theta^{-1}} \right) \right].$$

If we redefine the fermion fields

$$\psi \rightarrow \psi^\theta = e^{-i\theta} \psi, \quad (8)$$

$$\bar{\psi} \rightarrow \bar{\psi}^\theta = \bar{\psi} e^{i\theta}, \quad (9)$$

the Lagrangian turns to the original form. However the fermionic measure is not invariant under (9) but generates the Wess-Zumino action [5], $\alpha(A, g^{-1})$

$$d\psi d\bar{\psi} = d\psi^\theta d\bar{\psi}^\theta e^{i\alpha(A, g^{-1})} \quad (10)$$

where $\alpha(A, g^{-1}) = W[A^{\theta^{-1}}] - W[A]$, is found to be

$$\alpha(A, g^{-1}) = \frac{(a-1)}{2\pi} \int dx \left(\frac{1}{2} \partial_\mu \theta \partial^\mu \theta - e \theta \partial_\mu A^\mu \right). \quad (11)$$

Now the generating functional (3) reads

$$Z[\eta, \bar{\eta}, J] = \int dA_\mu d\psi d\bar{\psi} d\theta \Delta_f[A] \delta(f[A]) e^{i\alpha(A, g^{-1})} \times \quad (12)$$

$$\times \exp \left[i \int dx \left(\mathcal{L}[\psi, \bar{\psi}, A] + \bar{\eta} e^{i\theta} \psi + \bar{\psi} e^{-i\theta} \eta + J_\mu A^\mu - \frac{1}{e} \theta \partial_\mu J^\mu \right) \right].$$

We use the following gauge-fixing condition

$$f[A] = \frac{1}{\sqrt{\xi}} \partial_\mu A^\mu, \quad (13)$$

which gives the final form for the generating functional (3)

$$Z[\eta, \bar{\eta}, J] = \int dA_\mu d\psi d\bar{\psi} d\theta e^{i\alpha(A, g^{-1})} \exp \left[i \int dx \left(\mathcal{L}[\psi, \bar{\psi}, A] - \frac{1}{2\xi} (\partial \cdot A)^2 + \right. \right. \quad (14)$$

$$\left. \left. + \bar{\eta} e^{i\theta} \psi + \bar{\psi} e^{-i\theta} \eta + J_\mu A^\mu - \frac{1}{e} \theta \partial_\mu J^\mu \right) \right].$$

The calculation of the A^μ propagator from (14) is straightforward and yields

$$\langle 0|T A_\mu(x) A_\nu(y)|0\rangle = \quad (15)$$

$$= -i \int \frac{dk}{(2\pi)^2} \left[\frac{1}{k^2 - m^2} \left(g_{\mu\nu} - \frac{k_\mu k_\nu}{k^2} \right) - \frac{2\pi}{e^2(a-1)} \frac{k_\mu k_\nu}{k^2} \right] e^{-ik \cdot (x-y)},$$

we can also compute the complete fermion propagator

$$\begin{aligned} \langle 0|T\psi(x)\bar{\psi}(y)|0\rangle &= & (16) \\ &= i \exp \left\{ \frac{2\pi i}{a-1} \left(1 + \frac{e^2/\pi}{\square} \right) [\Delta_F(0; m^2) - \Delta_F(x-y; m^2)] \right\} G_F(x-y), \end{aligned}$$

$$m^2 = \frac{e^2}{2\pi}(a+1) \quad , \quad i\partial G_F(x-y) = \delta(x-y), \quad (17)$$

$$(\square + m^2)\Delta_F(x-y; m^2) = \delta(x-y). \quad (18)$$

0.1 Perturbative Analysis

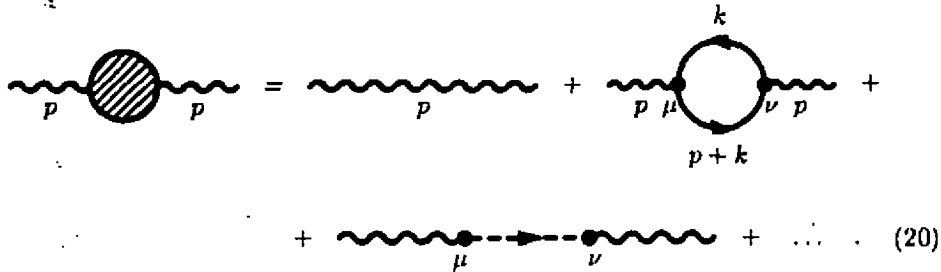
0.1.1 Photon propagator

From eq.(14) we obtain

$$\begin{aligned} \langle 0|T A_\mu(x) A_\nu(y)|0\rangle &= - \frac{\delta^2 Z[\eta, \bar{\eta}, J]}{\delta J^\nu(y) \delta J^\mu(x)} \Big|_{J=0=\eta=\bar{\eta}}, & (19) \\ &= \int dA_\mu d\psi d\bar{\psi} d\theta \left[A_\mu(x) + \frac{1}{e} \partial_\mu \theta(x) \right] \left[A_\nu(y) + \frac{1}{e} \partial_\nu \theta(y) \right] e^{i\alpha(A \cdot g^{-1})} \times \\ &\quad \times \exp \left[i \int dx \left(\mathcal{L}[\psi, \bar{\psi}, A] - \frac{1}{2\xi} (\partial \cdot A)^2 \right) \right]. \end{aligned}$$

Let us compute separately the contributions for this Green's functions

i) Term quadratic in A^μ



$$+ \dots \quad (20)$$

The fermion loop in (20) gives

$$-i\Pi_{\mu\nu}(p) = \frac{ie^2}{2\pi} \left[(a+1)g_{\mu\nu} - \frac{2p_\mu p_\nu}{p^2} \right], \quad (21)$$

so that the second order contribution to the vacuum polarization is

$$\begin{aligned} -i\Sigma_{\mu\nu}(p) &= -i\Pi_{\mu\nu}(p) - \frac{ie^2}{2\pi}(a-1)\frac{p_\mu p_\nu}{p^2}, \\ &= im^2 \left[g_{\mu\nu} - \frac{p_\mu p_\nu}{p^2} \right]. \end{aligned} \quad (22)$$

As usual, eq.(20) is a geometrical series that can be summed to give

$$\text{Diagram: wavy line } p \text{ --- } \text{circle with diagonal lines} \text{ --- wavy line } p = \frac{-i}{p^2 - m^2} \left(g_{\mu\nu} - \frac{p_\mu p_\nu}{p^2} \right) - \frac{i\xi p_\mu p_\nu}{p^4}. \quad (23)$$

ii) Term quadratic in θ

$$\begin{aligned} \text{Diagram: dashed line } p \text{ --- } \text{circle with diagonal lines} \text{ --- dashed line } p &= \text{Diagram: dashed line } p \text{ --- dashed line } p + \text{Diagram: dashed line } p \text{ --- wavy line } p \text{ --- circle with diagonal lines --- wavy line } p \\ \text{Diagram: dashed line } p \text{ --- } \text{circle with diagonal lines} \text{ --- dashed line } p &= \frac{2\pi}{a-1} \frac{i}{p^2} - \frac{i\xi e^2}{p^4}. \end{aligned} \quad (24)$$

iii) Mixed term

$$\text{Diagram: dashed line } p \text{ --- } \text{circle with diagonal lines} \text{ --- wavy line } p \nu = -\frac{\xi e p_\nu}{p^4}, \quad (25)$$

$$\text{Diagram: wavy line } p \text{ --- } \text{circle with diagonal lines} \text{ --- dashed line } p = \frac{\xi e p_\mu}{p^4}. \quad (26)$$

From (19) we obtain the photon (A^μ) propagator referring to the theory defined by (1)-(3)

$$\begin{aligned} \langle 0|T A_\mu(x) A_\nu(y)|0\rangle &= \\ &= -i \int \frac{dp}{(2\pi)^2} \left[\frac{1}{p^2 - m^2} \left(g_{\mu\nu} - \frac{p_\mu p_\nu}{p^2} \right) - \frac{2\pi}{e^2(a-1)} \frac{p_\mu p_\nu}{p^2} \right] e^{ip \cdot (x-y)}, \end{aligned} \quad (27)$$

and we see that it coincides with eq.(15). We observe that the term e^{-2} is not obtained from the perturbative calculation.

0.1.2 Fermion propagator

From eq.(14)

$$\begin{aligned} \langle 0|T \psi(x) \bar{\psi}(y)|0\rangle &= - \frac{\delta^2 Z[\eta, \bar{\eta}, J]}{\delta \eta(y) \delta \bar{\eta}(x)} \Big|_{J=0=\eta=\bar{\eta}} \\ &= \int dA_\mu d\theta d\psi d\bar{\psi} \psi(x) \bar{\psi}(y) e^{i\alpha(A, \theta^{-1})} \times \\ &\quad \times \exp \left\{ i \int dz \left(\mathcal{L}[\psi, \bar{\psi}, A] - \frac{1}{2\xi} (\partial \cdot A)^2 + \theta(z) j(z, x, y) \right) \right\}, \end{aligned} \quad (28)$$

where $j(z, x, y) = \delta(z - x) - \delta(z - y)$, we can calculate the fermion propagator to one-loop order

$$\text{Feynman diagram expansion} \quad (29)$$

The fermion self energy gives

$$\begin{aligned}
 -i\Pi(p) &= -e^2 \int \frac{dk}{(2\pi)^2} \gamma^\mu \frac{1}{\not{p} + \not{k}} \gamma^\nu \left[\frac{1}{k^2} \left(g_{\mu\nu} - \frac{k_\mu k_\nu}{k^2} \right) + \frac{\xi k_\mu k_\nu}{k^4} \right], \\
 &= -\frac{ie^2 \not{p}}{4\pi p^2} (\xi - 1).
 \end{aligned}
 \tag{30}$$

The self energy is finite, which shows that the origin of the divergencies in eq.(16) is not perturbative.

If in eq.(28), we integrate the θ -field we obtain a divergency that can not be cancelled by the normalization factor $Z[0, 0, 0]$. This divergency coincides with the one found previously in eq.(16).

In this subject we disagree with Z.Jian-Ge *et al* [6] when they found a perturbative divergency by considering, in the computation of the fermion self energy, the full photon propagator this can not be made, because the term which gives the divergency (e^{-2})(a Proca-like behaviour for the propagator) is obtained non-perturbatively.

We use the Faddeev-Popov method in order to define the free propagators of the fields involved in the theory. The free photon propagator can not be defined because a theory is non-gauge invariant. The option is to enlarge the number of the quantum degrees of freedom or to consider carefully the contribution of the longitudinal parts.

Acknowledge

We would like to thank CAPES/CNPq that financed the present work.

References

- [1] Our conventions are $g^{00} = -g^{11} = 1$, $\epsilon^{01} = 1$, $\gamma_5 = \gamma_0 \gamma_1$, $\epsilon_{\mu\nu} \gamma^\nu = \gamma_\mu \gamma_5$.
- [2] R.Jackiv, in *Relativity, Groups and Topology II*(Les Houches 1983), eds. B.S.DeWitt e R. Stora (North Holland, Amsterdam, 1984).
- [3] L.D Faddeev and V.N. Popov, *Phys. Lett. B* 25 (1967), 29.
- [4] K. Harada and I. Tsutsui, *Phys. Lett. B* 183 (1987), 311.
- [5] K. Fujikawa, *Nucl. Phys. B* 271(1986), 681.
- [6] Z.Jian-Ge, D.Qing-Hai and L.Yao-Yang, *Phys. Rev. D*43, 613 (1991).

On Bosonization Ambiguities of Two Dimensional Quantum Electrodynamics

S. A. Dias and M. B. Silva Neto*

Centro Brasileiro de Pesquisas Físicas - CBPF

Departamento de Teoria de Campos e Partículas - DCP

We study bosonization ambiguities in two dimensional quantum electrodynamics in the presence and in the absence of topologically charged gauge fields. The computation of fermionic correlation functions gives us a mechanism to fix the ambiguities in nontrivial topologies, provided that we do not allow changes of sector as we evaluate functional integrals. This removes an infinite arbitrariness from the theory.

1 The model

We will study quantum electrodynamics in two dimensional euclidean space described by the action functional

$$S = \int d^2x \mathcal{L}(A_\mu, \bar{\psi}, \psi) = \int d^2x \left[\frac{1}{4} F_{\mu\nu} F^{\mu\nu} + \bar{\psi} D \psi \right], \tag{1}$$

where the Dirac operator D

$$D \equiv \gamma^\mu (i\partial_\mu + e A_\mu) \tag{2}$$

has N zero eigenvalues, the zero modes, which are closely related to the existence of classical configurations in the gauge field sector

$$e A_\mu^{(N)} = -\hat{\partial}_\mu f,$$

where the function $f(x)$ behaves, at infinity, as

$$\lim_{x \rightarrow \infty} f(x) \simeq -N \ln|x|.$$

These configurations carry a topological charge $Q = N$, where Q is given by

$$Q = \frac{1}{4\pi} \int d^2x \epsilon_{\mu\nu} F_{\mu\nu}.$$

and this allows us to write

$$A_\mu = A_\mu^{(N)} + a_\mu,$$

where a_μ has vanishing topological charge. Now we can bosonize the theory in this sector, performing the change of variables

$$\begin{aligned} \psi &\rightarrow \exp(-i\rho + \phi\gamma_5) \psi, \\ \bar{\psi} &\rightarrow \bar{\psi} \exp(i\rho + \phi\gamma_5). \end{aligned}$$

where ρ and ϕ are the scalar fields in terms of which a_μ is written. Taking into account the Fujikawa jacobian, we can write the generating functional in terms of the complete set of eigenfunctions of the Dirac operator $\varphi_{0i}^{(N)}$ as

$$\begin{aligned} Z[J^\mu, \bar{\eta}, \eta] &= \sum_N \int [da_\mu] \delta(a_\mu, A_\mu^{(N)}) \exp\left(\left\langle \frac{1}{4} F_{\mu\nu} F^{\mu\nu} \right\rangle + \langle J^\mu A_\mu \rangle\right) \\ &\times \exp\left(\langle \bar{\eta} \mathbf{S}^{(N)} \eta \rangle\right) \det' D^{(N)} \prod_{i=1}^{|N|} \langle \bar{\eta} \varphi_{0i}^{(N)} \rangle \langle \varphi_{0i}^{(N)\dagger} \eta \rangle. \end{aligned} \tag{3}$$

*e-mail: tiao@cbpfsul.cat.cbpf.br and silvaner@cbpfsul.cat.cbpf.br

where

$$\begin{aligned}\eta' &= \exp(i\rho + \phi\gamma_5)\eta, \\ \bar{\eta}' &= \bar{\eta}\exp(-i\rho + \phi\gamma_5),\end{aligned}\quad (4)$$

and

$$\mathfrak{S}(a_\mu, A_\mu^{(N)}) \equiv \frac{\det' D}{\det' D^{(N)}} N[\phi],$$

with the term $N[\phi]$ being cancelled by subsequent computations.

This ratio will contribute as an effective term to the action. Now we finally have, in terms of the set of orthonormal eigenfunctions of the Dirac operator $\Phi_{0i}^{(N)}$, the expression

$$Z[J^\mu, \bar{\eta}, \eta] = \sum_N \int [da_\mu] \exp\left(-\bar{S} + \langle J^\mu A_\mu \rangle + \langle \bar{\eta}' G^{(N)} \eta' \rangle\right) \prod_{i=1}^{|N|} \langle \bar{\eta}' \Phi_{0i}^{(N)} \rangle \langle \Phi_{0i}^{(N)} \eta' \rangle. \quad (5)$$

where

$$\bar{S} = \left\langle \frac{1}{4} F_{\mu\nu} F^{\mu\nu} \right\rangle + \Gamma[a_\mu] + \bar{\Gamma}[a_\mu, A_\mu^{(N)}] + \Gamma'[A_\mu^{(N)}],$$

and

$$\Gamma[a_\mu] = \frac{e^2}{4\pi} \int d^2x a_\mu \left(a(N) \delta_{\mu\nu} - \frac{\partial_\mu \partial_\nu}{\square} \right) a_\nu, \quad (6)$$

$$\bar{\Gamma}[A_\mu^{(N)}, a_\mu] = \frac{e^2}{2\pi} \int d^2x a_\mu \left(a(N) \delta_{\mu\nu} - \frac{\partial_\mu \partial_\nu}{\square} \right) A_\nu^{(N)},$$

$$\Gamma'[A_\mu^{(N)}] = \frac{e^2 a(N)}{4\pi} \int d^2x f \square f. \quad (7)$$

The parameter $a(N)$ was introduced during a regularization procedure.

There is still the integration over a_μ to be performed. The change

$$\sigma = \rho - \frac{1}{\lambda} \langle \Delta_F(j_\rho + j'_\rho) \rangle \quad (8)$$

$$\varphi = \phi + f \mp e^2 \langle \Delta(m; x-y)(j + j') \rangle \quad (9)$$

where

$$\Delta_F(x-y) \equiv \square^{-1}(x-y) = -\frac{1}{2\pi} \ln|x-y|$$

and

$$\Delta(m; x-y) \equiv [\square(\square - \mu^2)]^{-1}(x-y) = -\frac{1}{2\pi m^2} \{K_0[m|x-y|] + \ln|x-y|\}$$

puts the action into a diagonal form and where we also have defined $\lambda \equiv (1 - a(N))/2\pi$ and $m^2 = (e^2 a(N))/\pi$. Now we have for \bar{S} plus the sources the expression

$$\begin{aligned}-\bar{S}_{sources} &= \frac{1}{2a^2} \left\langle \varphi \square \left(\square - \frac{e^2 a(N)}{\pi} \right) \varphi \right\rangle + \frac{e^2}{2} \langle (j + j') \Delta(m)(j + j') \rangle + \\ &\quad \frac{(1 - a(N))}{2\pi} \langle \sigma \square \sigma \rangle - \frac{1}{2\lambda} \langle (j_\rho + j'_\rho) \Delta_F(j_\rho + j'_\rho) \rangle.\end{aligned}$$

As we have already said, the scalar fields ρ and ϕ are such that a_μ does not carry a topological charge in the limit $|x| \rightarrow \infty$. So it is desirable that the new fields σ and φ behave like the old ones, going to zero at infinity. If this would not be the case, it would be equivalent to perform transformations that change the topological sector, which would lead us to compute jacobians over noncompact spaces, what is very difficult to obtain. So, although keeping in mind the general case, we will restrict ourselves to transformations which do not change the topological sector.

In the case of the σ field we have

$$\begin{aligned} \lim_{|x| \rightarrow \infty} \sigma(x) &= \lim_{|x| \rightarrow \infty} \rho(x) - \frac{1}{\lambda} \lim_{|x| \rightarrow \infty} \langle \Delta_{\mathcal{F}}(x-z)(j_{\rho} + j'_{\rho}) \rangle \\ &= \frac{1}{2\pi\lambda} \lim_{|x| \rightarrow \infty} \left\{ \sum_{i=1}^k (\ln|x-x_i| - \ln|x-y_i|) \right\} \\ &= 0, \end{aligned}$$

once $\lim_{|x| \rightarrow \infty} \rho(x) = 0$, in agreement with the conditions imposed.

For the field φ , we have

$$\begin{aligned} \lim_{|x| \rightarrow \infty} \varphi(x) &= \lim_{|x| \rightarrow \infty} f(x) + \lim_{|x| \rightarrow \infty} \phi(x) \mp \lim_{|x| \rightarrow \infty} e^2 \langle \Delta(m; x-z)(j + j') \rangle \\ &= -N \ln|x| \pm \frac{e^2}{2\pi m^2} \lim_{|x| \rightarrow \infty} ((K_0[m|x-z|] + \ln|x-z|)(j + j')) \\ &= -N \ln|x| \pm \frac{1}{2a(N)^2} |N| \ln|x| \\ &= - \left(N \mp \frac{|N|}{a(N)} \right) \ln|x|, \end{aligned}$$

once K_0 is well behaved in the limit considered and $\lim_{|x| \rightarrow \infty} \phi(x) = 0$. Here, the \mp sign corresponds to sectors with topological charge N and $-N$, respectively. The asymptotic behavior of φ is then

$$\lim_{|x| \rightarrow \infty} \varphi(x) = \begin{cases} - \left(N - \frac{N}{a(N)} \right) \ln|x|, & N > 0, \\ - \left(N + \frac{N}{a(N)} \right) \ln|x|, & N < 0. \end{cases}$$

which is singular unless we have

$$u_{\mathcal{S}}(N) = 1, \quad \forall N \neq 0.$$

2 Conclusion and remarks

In nontrivial topology sectors, as we have seen, there is an infinite amount of ambiguity in the theory, due to arbitrary choices of $a(N)$ for each N . A simple criterium to choose $a(N)$ seems to be the one which does not allow changes in the topological sector. It gives a value for $a(N)$ which coincides with the one obtained through the requirement of gauge invariance. The connection between gauge invariance and preservation of topology is not completely clear and perhaps can only be clarified if one could compute the correlation functions without these criteria. It is our aim to explore also this direction in the near future.

References

- [1] J. Schwinger, *Phys. Rev.* **128** (1962) 2425.
- [2] J. Lowenstein and J. Swieca, *Ann. Phys. (N.Y.)* **68** (1971) 172.
- [3] R. Jackiw and R. Rajaraman, *Phys. Rev. Lett.* **54** (1985) 1219.
- [4] R. Jackiw and K. Johnson, *Phys. Rev.* **182** (1969) 1459.
- [5] S. A. Dias and C. A. Linhares, *Phys. Rev.* **D47** (1993) 1672.
- [6] E. Abdalla, M. C. B. Abdalla and K. D. Rothe, *Non-Perturbative Methods in Two Dimensional Quantum Field Theory*, Singapore (World Scientific, 1991).
- [7] K. Bardakci and M. Crescimano, *Nucl. Phys.* **B313** (1989) 269.
- [8] M. V. Manias, C. M. Naón and M. L. Trobo, *Phys. Rev.* **D41** (1990) 3174.
- [9] S. A. Dias and M. T. Thomaz, *Phys. Rev.* **D44** (1991) 1811.
- [10] S. A. Dias and C. A. Linhares, *Phys. Rev.* **D45** (1992) 2162.
- [11] M. V. Manias, C. M. Naón and M. L. Trobo, *Int. Jour. Mod. Phys.* **A5** (1990) 2853.

Path-integral Computation of Multipoint Spin Correlators in 2d Statistical Mechanics Models

V.I. Fernández^a and C.M. Naón^{a,b}

^aDepto. de Física, Universidad Nacional de La Plata, CC 67, 1900 La Plata, Argentina.

^bConsejo Nacional de Investigaciones Científicas y Técnicas, Argentina

We extend a previously developed technique for computing spin-spin critical correlators in the 2d Ising model, to the case of multiple correlations. This enables us to derive Kadanoff-Ceva's formula in a simple and elegant way. We also exploit a doubling procedure in order to evaluate the critical exponent of the polarization operator in the Baxter model. Thus we provide a rigorous proof of the relation between different exponents, in the path-integral framework.

In a previous work [1] one of us has shown how to compute 2-point correlators of 2D Statistical Mechanics models through a path-integral approach to bosonization [2]. In particular, the critical behavior of the Ising spin-spin correlation function was obtained, by using a slightly modified version of the identity derived by Zuber and Itzykson [3]:

$$F_2^2(x_1, x_2) = \langle \sigma(x_1)\sigma(x_2) \rangle^2 = \langle \exp \int_{x_1}^{x_2} dz J_0(z) \rangle \quad (1)$$

where J_μ is the Dirac fermion current and $\langle \rangle$ means vacuum expectation value in a model of free massless fermion fields.

The purpose of this note is twofold. On the one hand we extend the above mentioned method to compute the 2n-point correlator. On the other hand we adapt the "doubling" technique [4] which led to (1), in order to calculate the correlation function of the polarization operator in the Baxter model [5].

For the sake of clarity we shall begin by briefly summarizing the main points of the spin-spin correlator calculation. In ref.[1] the line integral in (1) was written as

$$\int_{x_1}^{x_2} dz J_0(z) = \int d^2x \dot{\Psi} A \Psi \quad (2)$$

where A_μ is an auxiliary vector field with components:

$$A_0(z_0, z_1) = \delta(z_0)\theta(z_1 - x_1)\theta(x_2 - z_1) \quad (3)$$

$$A_1(z_0, z_1) = 0. \quad (4)$$

This simple manipulation enabled us to express the squared spin-spin correlator in terms of fermionic determinants:

$$F_2^2(x_1, x_2) = \frac{\det(i\cancel{\partial} + A)}{\det i\cancel{\partial}} \quad (5)$$

where the coordinate dependence in the right hand side of (5) is, of course, contained in A .

Finally, one performs a change of path-integral fermionic variables which is chosen so as to decouple fermions from the background field A_μ . It is interesting to note that, in this formulation, the desired 2-point function is just the square root of the Fujikawa Jacobian J_F [6] associated with the transformation of fermionic variables:

$$F_2(x_1, x_2) = J_F(x_1, x_2)^{\frac{1}{2}} \quad (6)$$

As shown in [7], this Jacobian must be computed with a gauge-invariant regularization prescription in order to avoid a linear divergence. This procedure then leads to the well-known power law decay with exponent equal to $\frac{1}{4}$.

Let us now show how to extend the above depicted technique to the computation of the $2n$ -point spin correlation function at criticality. To this end, following ref.[8], we express the squared multipoint correlator as

$$F_{2n}^2(x_1, \dots, x_{2n}) = \langle \prod_{i=1}^{2n} \sigma(x_i) \rangle^2 = \langle \prod_{i \text{ odd}} c x_i \pi \int_{x_i}^{x_{i+1}} dz J_0(z) \rangle \tag{7}$$

where, as before, $\langle \rangle$ in the r.h.s. means vacuum expectation value to be evaluated in a model of massless Dirac fermions. It is now apparent that each line integral in (7) can be cast in the form

$$\int_{x_i}^{x_{i+1}} dz J_0(z) = \int d^2 z J_\mu A_\mu(z; x_i, x_{i+1}) \tag{8}$$

where we have introduced the n classical singular potentials

$$A_0(z; x_i, x_{i+1}) = \delta(z_0) \theta(z_1 - x_i) \theta(x_{i+1} - z_1) \tag{9}$$

$$A_1(z; x_i, x_{i+1}) = 0. \tag{10}$$

Now, in order to rewrite (7) in a more compact way we construct a new vector field B_μ as a simple superposition of A_μ 's:

$$B_0(z) = \sum_{i=1, \text{ odd}}^{2n-1} A_0(z; x_i, x_{i+1}) \tag{11}$$

$$B_1(z) = 0. \tag{12}$$

Thus the $2n$ -point function can be expressed in terms of fermionic determinants

$$F_{2n}^2 = \frac{\det(i\cancel{\partial} + \cancel{B})}{\det i\cancel{\partial}} \tag{13}$$

exactly as it happens in the $n = 1$ case (See (5)), but with A replaced by B . This is our first non-trivial result. The next step is to write B_μ in terms of scalar functions Φ and η as

$$B_\mu = \epsilon_{\mu\nu} \partial_\nu \Phi + \partial_\mu \eta. \tag{14}$$

Performing now a decoupling change of path-integral fermionic variables with chiral and gauge parameters, Φ and η , respectively, one has

$$F_{2n}^2(x_1, \dots, x_{2n}) = J_F(x_1, x_2, \dots, x_{2n}) \tag{15}$$

Solving the system of differential equations for Φ and η obtained by replacing (14) in (11) and (12), and then inserting the result in (15), one gets

$$F_{2n}(x_1, \dots, x_{2n}) = \left(\frac{\prod_{\text{even } i} |x_{ij}|}{\prod_{\text{odd } i} |x_{ij}|} \right)^{\frac{1}{4}} \tag{16}$$

where $i > j$ and even (odd) refers to a constraint on $i + j$. We have also set an ultraviolet cutoff, which divides the coordinate differences, equal to 1. This formula exactly coincides with the famous Kadanoff-Ceva's result [9].

Let us now consider the Baxter model [5], which can be considered as two Ising systems interacting through their spin variables. As shown by Luther and Peschel [10], the scaling limit of this model is described by the Thirring

[11] interaction:

$$\mathcal{L}_{int} = -\lambda J_\mu J_\mu \quad (17)$$

where J_μ is the Dirac fermionic current and the coupling constant λ is proportional to the four-spin coupling of the original lattice model. The Baxter model is known to have two natural order parameters, the magnetization and the polarization $\langle P \rangle = \langle \sigma_i s_i \rangle$, where σ_i and s_i are the spin operators of each Ising system. In the continuous formulation the 2-point correlator for the polarization operator is given by

$$\langle P(x)P(y) \rangle_\lambda = \langle \sigma_x s_x \sigma_y s_y \rangle_\lambda \quad (18)$$

where $\langle \rangle_\lambda$ means v.e.v. with respect to the fermionic model defined by (17). For $\lambda = 0$ the above expression becomes the squared Ising correlator. This suggests the following identification:

$$\langle P(0)P(R) \rangle_\lambda = \langle \exp \pi \int_0^R dz J_0(z) \rangle_\lambda \quad (19)$$

The r.h.s. of the precedent equation can be computed by employing a slightly modified version of the method described above. Indeed, it is easy to show that the introduction of an auxiliary vector field A_μ through a Hubbard-Stratonovich identity, allows to write

$$\langle P(0)P(R) \rangle_\lambda = \frac{Z}{Z_0} \quad (20)$$

with

$$Z = \int \mathcal{D}A_\mu e^{-\int d^2x \frac{A_\mu^2}{2}} \det \left(i\cancel{\partial} + (2\lambda)^{1/2} \beta \right) \quad (21)$$

and

$$Z_0 = \int \mathcal{D}A_\mu e^{-\int d^2x \frac{A_\mu^2}{2}} \det \left(i\cancel{\partial} + (2\lambda)^{1/2} \Lambda \right) \quad (22)$$

where

$$B_\mu = \epsilon_{\mu\nu} \partial_\nu \Phi_B + \partial_\mu \eta_B \quad (23)$$

$$A_\mu = \epsilon_{\mu\nu} \partial_\nu \Phi + \partial_\mu \eta \quad (24)$$

$$\Phi_B = \Phi + \frac{\pi}{\sqrt{2\lambda}} \Phi_c \quad (25)$$

$$\eta_B = \eta + \frac{\pi}{\sqrt{2\lambda}} \eta_c \quad (26)$$

The classical functions Φ_c and η_c are determined exactly as in the Ising case.

Performing now a decoupling change of fermionic variables with parameters Φ_B and η_B one obtains:

$$\langle P(0)P(R) \rangle_\lambda = \langle P(0)P(R) \rangle_0 \langle e^{\int d^2x \Phi \partial_\mu \partial_\mu \Phi_c} \rangle \quad (27)$$

where the first factor in the r.h.s. corresponds, of course, to the doubled Ising correlator, whereas the second one is a v.e.v. to be computed for a model of free scalars Φ . The final result is

$$\langle P(0)P(R) \rangle_\lambda = \left(\frac{a}{R} \right)^{2\Delta_P} \quad (28)$$

where a is an ultraviolet cutoff and Δ_P is the critical exponent associated to the polarization operator, for which we get:

$$\Delta_P = \frac{1}{4} \frac{1}{1 + \frac{2\lambda}{\pi}} \quad (29)$$

Recalling the results for the energy-density ϵ [12] [1] we get:

$$\Delta\rho = \frac{1}{4}\Delta\epsilon, \quad (30)$$

which is the relation predicted by several authors [13] [14] and first derived by Drugowich de Felicio and Koberle [12] in the operator framework.

In summary, we have extended a path-integral approach, previously used to compute 2-point functions in 2D critical systems, to the case in which multipoint correlators are considered. In particular we rederived Kadanoff-Ceva's formula.

We have also obtained the critical exponent of the Baxter polarization operator. This allowed us to give a path-integral confirmation of the relation between exponents first shown in ref[12] within the operator formulation.

Acknowledgement

We thank Fundación Antorchas for financial support.

References

- [1] C.M.Naón, *Journal of Phys.A* **22**, L207, (1989).
- [2] R.Gamboa-Saraví, F.Schaposnik and J.Solomin, *Nucl. Phys.B* **185**, 239, (1981).
- [3] J.B.Zuber and C.Itzykson, *Phys.Rev.D* **15**, 2875, (1977).
- [4] R.A.Ferrell, *J. Stat. Phys.* **8**, 265, (1973).
- [5] R.Baxter, *Phys. Rev. Lett.* **26**, 832, (1971).
- [6] K.Fujikawa, *Phys. Rev. Lett.* **42**, 1195, (1979); *Phys. Rev. D* **21**, 2848, (1980).
- [7] C.M.Naón, *Journal of Phys.A* **23**, L273, (1990).
- [8] B.Schroer and T.T.Truong, *Phys. Lett.B* **72**, 371, (1978).
- [9] L.Kadanoff and H.Ceva, *Phys. Rev. B* **3**, 3918, (1971).
- [10] A.Luther and I.Peschel, *Phys. Rev.B* **12**, 3908, (1978).
- [11] W.Thirring, *Ann. of Phys.* **3**, 91 (1958).
- [12] J.R.Drugowich de Felicio and R.Koberle, *Phys. Rev. B* **25**, 511, (1982).
- [13] I.Enting, *J. of Phys.A* **8**, L35, (1975).
- [14] L.Kadanoff, *Phys. Rev. Lett.* **39**, 903, (1977).

Sobre a Expansão Perturbativa do Modelo de Gross-Neveu $(2+1)D$

V. S. Alves[†], M. Gomes, L. C. Malacarne[§]

S.V.L. Pinheiro[†] e A. J. da Silva

Universidade de São Paulo, Departamento de Física-Matemática, Instituto de Física

[†] *sob licença da Universidade Federal do Pará*

[§] *Universidade Estadual de Maringá*

Este trabalho consiste no cálculo da função beta do modelo de Gross-Neveu em $(2+1)D$ na ordem de dois "loops". Apesar do modelo ser não renormalizável na constante de acoplamento ele será tratado como uma teoria renormalizável no espírito de uma teoria efetiva, válida na região de pequenos momentos (baixas energias).

O modelo de Gross-Neveu massivo é dado pela seguinte densidade de lagrangeana,

$$\mathcal{L} = \bar{\psi}(i\gamma^\mu \partial_\mu - M)\psi - \frac{g}{2M}(\bar{\psi}\psi)^2, \quad (1)$$

onde M é a massa do férmion, ψ é um único campo fermiônico de duas componentes e g a constante de acoplamento.

Em três dimensões¹, o operador $(\bar{\psi}\psi)^2$ possui dimensão canônica igual a quatro, maior que a dimensão do espaço-tempo, caracterizando uma teoria não renormalizável quando tratada perturbativamente na constante de acoplamento, apesar de ser renormalizável no contexto da expansão $1/N$ [1] (com $M = 0$, o modelo apresenta geração dinâmica de massa com quebra de simetria de paridade [2]).

Em teorias renormalizáveis as funções de vértice próprias de N pontos, $\tilde{\Gamma}^{(N)}$, satisfazem a equação do grupo de renormalização.

$$\left(\mu \frac{\partial}{\partial \mu} + \beta \frac{\partial}{\partial g} + \delta M \frac{\partial}{\partial M} - N\gamma \right) \tilde{\Gamma}^{(N)} = 0. \quad (2)$$

Por outro lado, em teorias não renormalizáveis, o lado direito da expressão acima é um polinômio dos momentos externos. Mais precisamente, são os contra-termos que não podem ser absorvidos na redefinição dos parâmetros iniciais da teoria (como a massa, o campo e a constante de acoplamento). No entanto, iremos tratar a teoria descrita por (1) como uma teoria efetiva, válida na região de pequenos momentos ($p \ll M$), de maneira que os efeitos da não renormalizabilidade não seriam importantes. Uma maneira de testar a consistência desta proposta é estudando os pontos fixos da teoria. Em particular, a origem deve ser infravermelho estável, para que a análise perturbativa faça sentido. Tal análise é feita calculando-se a função beta, que determina o comportamento da constante de acoplamento como uma função da escala de massa. Seu cálculo, que é obtido a partir das funções de Green de dois e quatro pontos, será feita na ordem de dois "loops" e o esquema de regularização empregado será o da regularização dimensional.

Primeiramente reescrevemos (1) de maneira usual como,

$$\mathcal{L} = \bar{\psi}(i\gamma^\mu \partial_\mu - M)\psi - \frac{g}{2M}\mu^{3-d}(\bar{\psi}\psi)^2. \quad (3)$$

¹ Neste trabalho usaremos a seguinte representação para as matrizes de Dirac

$$\gamma_0 = \begin{pmatrix} 1 & 0 \\ 0 & -1 \end{pmatrix}, \quad \gamma_1 = \begin{pmatrix} 0 & i \\ i & 0 \end{pmatrix}, \quad \gamma_2 = \begin{pmatrix} 0 & 1 \\ -1 & 0 \end{pmatrix}.$$

e a métrica $g_{\mu\nu} = \text{diag}(1, -1, -1)$.

onde μ é o ponto de subtração . A função de vértice $\Gamma^{(2)}$ é definida como segue

$$\Gamma^{(2)} = - \left[G^{(2)} \right]^{-1} = i(\not{p} - M - \Sigma) . \tag{4}$$

onde $-i\Sigma$ é a auto-energia do férmion, que até dois "loops" possui a seguinte estrutura diagramática,

$$-i\Sigma = \text{diagrama 1} + \text{diagrama 2} \tag{5}$$

(5)

Por outro lado, a função de vértice $\Gamma^{(4)}$, até dois "loops", tem a seguinte estrutura

$$\Gamma^{(4)} = \text{diagrama 1} \cdot \text{diagrama 2} \cdot \text{diagrama 3} \tag{6}$$

(6)

A teoria descrita por (3) possui, para um dado gráfico genérico γ , um grau de divergência superficial igual a $d(\gamma) = 3 - N_F + V$, onde N_F é o número de linhas externas fermiônicas e V o número de vértices. Assim, embora os diagramas de 1- "loop" que contribuem para $\Gamma^{(2)}$ sejam quadraticamente divergentes, eles são finitos se usarmos a regularização dimensional. Enquanto que a contribuição de segunda ordem possui $d(\gamma) = 3$, o que implica que os termos de subtração são proporcionais a M^3 , $M^2\not{p}$, $M\not{p}^2$ e $\not{p}^2\not{p}$, onde p é o momento externo. Observe que os dois primeiros termos contribuem para a renormalização da massa e do campo respectivamente, enquanto que os dois últimos são contra-termos que não podem ser absorvidos numa reparametrização de (3). Desta forma, o resíduo da função de dois pontos, que será representado por $Res^{(2)}$, possui a seguinte decomposição, onde, condensadamente, estamos denotando por p quaisquer dos momentos externos.

$$Res^{(2)} = b_1 M^3 + b_2 M^2 \not{p} + b_3 M \not{p}^2 + b_4 \not{p}^2 \not{p} . \tag{7}$$

e portanto a expressão (4) é escrita como

$$\tilde{\Gamma}^{(2)} = i\not{p} - iM - \frac{ig}{2} M \mu^{3-d} K - \frac{g^2}{4M^2} (2 \ln \mu Res^{(2)} + \text{finito}) , \tag{8}$$

onde K é uma constante e utilizamos um esquema de subtração que remove os pólos gerados pela regularização.

Semelhantemente, os únicos diagramas divergentes que contribuem para a função de quatro pontos são aqueles de dois "loops" (estes possuem $d(\gamma) = 2$), já que os diagramas de 1- "loop", apesar de serem formalmente divergentes, são também finitos quando empregamos a regularização dimensional. Portanto, o resíduo $Res^{(4)}$ possui a seguinte decomposição, onde, condensadamente, estamos denotando por p quaisquer dos momentos externos

$$Res^{(4)} = a_1 M^2 + a_2 M \not{p} + a_3 \not{p}^2 . \tag{9}$$

Note que o primeiro termo da equação acima contribue para a renormalização da constante de acoplamento, enquanto que os demais são contra-termos com estrutura diferente daquelas encontradas em (3). Deste modo podemos escrever, omitindo por simplicidade os índices espinoriais, que

$$\tilde{\Gamma}^{(4)} = -\frac{ig}{2M} \mu^{3-d} - \frac{g^2}{4M^2} \mu^{2(3-d)} f(p, M) + \frac{ig^3}{8M^3} (3 \ln \mu Res^{(4)} + \text{finito}) . \tag{10}$$

com $f(p, M)$ sendo uma função dos momentos externos.

Observe então que no limite de pequenos momentos externos o terceiro e o quarto termo de (7) e o segundo e o terceiro de (9) são desprezíveis, de modo que $\tilde{\Gamma}^{(2)}$ e $\tilde{\Gamma}^{(4)}$ satisfazem a equação do grupo de renormalização (2), fornecendo o seguinte resultado,

$$\beta = g^3 \left[\frac{6}{8} a_1 + \frac{i}{2} (b_1 + 3b_2) \right] , \quad (11)$$

$$\delta = i \frac{g^2}{2} (b_1 + b_2) , \quad (12)$$

e

$$\gamma = i \frac{g^2}{4} b_2 . \quad (13)$$

Para o cálculo de b_1 e b_2 precisamos da função de dois pontos. Dois diagramas contribuem para esta função fornecendo a seguinte expressão

$$I^{(2)} = 4i\mu^{2(3-d)} \left(-i \frac{g}{2M}\right)^2 \int \frac{d^3k}{(2\pi)^3} \frac{d^3q}{(2\pi)^3} \left[\frac{i}{(\not{p} + \not{q} - M)} \text{Tr} \left(\frac{i}{\not{q} - M} \frac{i}{\not{q} - \not{q} - M} \right) - \left(\frac{i}{(\not{p} + \not{q} - M)} \frac{i}{(\not{q} - M)} \frac{i}{(\not{q} - \not{q} - M)} \right) \right] . \quad (14)$$

Um cálculo detalhado da amplitude acima, retendo apenas os termos de pólo, fornece o seguinte resultado.

$$I_{\text{pólo}}^{(2)} = -\frac{i}{26\pi^3} \mu^{2\epsilon} \left(-\frac{ig}{2M}\right)^2 \left[12\pi M^3 + \frac{20\pi}{3} M^2 p - \frac{64\pi}{15} M p^2 - \frac{64\pi}{35} \not{p} p^2 \right] \frac{1}{\epsilon} . \quad (15)$$

de onde se conclui que

$$b_1 = -\frac{3i}{16\pi^2} . \quad (16)$$

e

$$b_2 = -\frac{5i}{48\pi^2} . \quad (17)$$

Para o cálculo de a_1 necessitamos da função de quatro pontos. Trinta e dois diagramas contribuem para esta função. Somando todos estes diagramas de quatro pontos, obtemos

$$a_1 = \frac{8}{\pi^2} . \quad (18)$$

Substituindo os valores de b_1 , b_2 e a_1 em (11) e (12) e (13) encontra-se que

$$\beta = \frac{25}{4\pi^2} g^3 . \quad (19)$$

$$\delta = \frac{g^2}{12\pi^2} . \quad (20)$$

e

$$\gamma = \frac{5}{192\pi^2} g^2 . \quad (21)$$

Note que o sinal da função beta é positivo, portanto ela apresenta um ponto fixo estável no infra-vermelho, validando assim a expansão perturbativa feita em g para pequenos momentos.

O presente trabalho serve também para complementar o uso da interação de Gross-Neveu na aproximação até g^2 como feito na referência [3].

References

- [1] Baruch Rosenstein, Brian J. Warr and Seon H. Park; *Phys. Rev. Lett.* 62, 1433, (1989);
- [2] M. Gomes, V. O. Rivelles and A. J. da Silva; *Phys. Rev. D* 41, 1363, (1990);
- [3] Wei Chen; *Nucl. Phys.* B435, 673, (1995);
- [4] J. C. Collins, *Renormalization*, Cambridge University Press, (1985).

Regularização de um modelo tipo $\lambda\varphi^4$ tensorial, via “point-splitting”.

W.A. Moura Melo e J.A. Helayël-Neto
Centro Brasileiro de Pesquisas Físicas
Departamento de Teoria de Campos e Partículas.

December 3, 1996

1 Introdução:

Num artigo de 1934, Dirac [1] introduziu a idéia de “point-splitting”, para se evitar produtos de campos no mesmo ponto¹ (a causa das divergências ultra-violeta na versão segundo-quantizada da teoria). Esse “splitting” seria feito, por exemplo, redefinindo-se os campos, presentes num mesmo vértice, em pontos diferentes.

Mais recentemente, Osland e Wu, numa série de artigos [2], utilizaram essa idéia de “point-splitting” como método de regularização. Particularmente, obtiveram um Lagrangeano (generalizado) para a QED, cujos termos de interação não apresentavam produtos de campos no mesmo ponto. Por outro lado, este mesmo Lagrangeano apresentava problemas de não-localidade. Mesmo assim, estes autores obtiveram diversos resultados satisfatórios com essa formulação. Com base nessa mesma idéia, chegaram a outros resultados importantes, tais como as massas do Higgs (190 Gev) e do quark top (120 Gev), livre de divergências. No entanto, nenhuma referência é feita a respeito de como seriam as novas transformações de gauge, após a introdução de “point-splitting” (que denominaremos *transformações de gauge generalizadas* e abreviaremos por g.g.t’s).

Em 1994, Gastmans, Newton e Wu [3] provaram a existência das transformações de gauge generalizadas para o caso Abelian². Isto foi feito, introduzindo-se um parâmetro de “point-splitting” (aqui, denotaremos por a) nos argumentos dos campos envolvidos nas transformações de gauge usuais e impondo-se que a *nova forma* dessas transformações, satisfizessem à condição Abeliana. Verificaram, assim, que as g.g.t’s assim obtidas, tomam a forma de uma série de potências infinita (em sua forma infinitesimal) na constante de acoplamento de gauge³ (teorias que acoplam campos de gauge a campos de matéria, como a QED). Nesse mesmo trabalho, são apresentadas as formas explícitas, até 4^a ordem na constante de acoplamento de gauge, para as g.g.t’s, e para um “Lagrangeano Generalizado” da QED, que é invariante sob estas transformações até esta mesma ordem (devido à extensão de tais expressões, não as reproduziremos aqui). Alguns aspectos importantes desse Lagrangeano são: regularidade, não-localidade e a presença de termos imaginários. No entanto, quando fazemos $\lim_{a \rightarrow 0}$ tanto nesse Lagrangeano, quanto nas g.g.t’s, recuperamos suas formas usuais.

2 O Modelo de Avdeev e Chizhov:

Num trabalho recente, Avdeev e Chizhov [5] propuseram um modelo que acopla campos tensoriais de matéria ($T_{\mu\nu}$: real, anti-simétrico e de rank-2; descrevendo-se, assim, partículas de spin-1) a campos de gauge vetoriais (A_μ), inclusive com a presença de férmions (ψ e $\bar{\psi}$). Diversos tipos de interação estão presentes na teoria. No entanto,

¹ Aqui, trabalharemos com espaço-tempo quadridimensional; Métrica de Minkowski: $\text{diag}(\eta_{\mu\nu}) = (+, -, -, -)$; $x = x^\mu$.

² No caso das transformações de gauge usuais, como para a QED, dizemos que a transformação é Abeliana, se o comutador de duas transformações distintas for nulo. No entanto, quando se trata das g.g.t’s, esse caráter Abeliano deve ser estudado ordem a ordem, já que tais transf. são séries infinitas.

³ Devemos salientar que as discussões com respeito à estrutura de tais transformações remontam a Dirac [1] e a Schwinger [4].

Sorella, Lemes e Renan [6] mostraram, via identidades de Ward, que vértices do tipo $\psi\bar{\psi}T$, geram anomalias. Em vista disso, nós estudaremos o modelo na ausência de férmions:

$$\begin{aligned} \mathcal{L}_{A,C}(x) = & \frac{-1}{4}F_{\mu\nu}F^{\mu\nu} + \frac{1}{2}(\partial_\lambda T^{\mu\nu})^2 - 2(\partial_\mu T^{\mu\nu})^2 - 2eA_\mu \left[T^{\mu\nu}\partial^\alpha \tilde{T}_{\alpha\nu} - \tilde{T}^{\mu\nu}\partial^\alpha T_{\alpha\nu} \right] \\ & + e^2 \left[\frac{1}{2}(A_\lambda T^{\mu\nu})^2 - (A_\mu T^{\mu\nu})^2 \right] - \frac{\lambda}{4} \left[\frac{1}{2}(T_{\mu\nu}T^{\mu\nu})^2 - 2T_{\mu\nu}T^{\nu\kappa}T_{\kappa\lambda}T^{\lambda\mu} \right] \end{aligned} \quad (1)$$

Tal Lagrangeano é invariante sob as transformações de gauge usuais:⁴

$$\begin{aligned} \delta A_\mu(x) &= -\partial_\mu \Lambda(x) \\ \delta T_{\mu\nu}(x) &= -e\Lambda(x)\tilde{T}_{\mu\nu}(x) \\ \delta \tilde{T}_{\mu\nu}(x) &= +e\Lambda(x)T_{\mu\nu}(x) \end{aligned} \quad (2)$$

com a definição: $\tilde{T}_{\mu\nu}(x) \stackrel{\text{def}}{=} \frac{1}{2}\epsilon_{\mu\nu\alpha\beta}T^{\alpha\beta}(x)$.

Noutro trabalho, Sorella, Lemes e Renan [7] mostraram que a equação (1) pode ser obtida de:

$$\mathcal{L}_S(x) = -\frac{1}{4}F_{\mu\nu}F^{\mu\nu} + (D_\mu\varphi^{\mu\nu})(D^\alpha\varphi_{\alpha\nu})^\dagger - \frac{\lambda}{8}\varphi_{\mu\nu}^\dagger\varphi^{\nu\kappa}\varphi_{\kappa\lambda}^\dagger\varphi^{\lambda\mu}. \quad (3)$$

se impusermos uma condição de auto-dualidade complexa a $\varphi_{\mu\nu}$:

$$\varphi_{\mu\nu}(x) = +i\tilde{\varphi}_{\mu\nu}(x), \quad \text{com : } \tilde{\varphi}_{\mu\nu}(x) = \frac{1}{2}\epsilon_{\mu\nu\alpha\beta}\varphi_{\mu\nu}(x). \quad (4)$$

que nos conduz a:

$$\left. \begin{aligned} \varphi_{\mu\nu}(x) &= T_{\mu\nu}(x) + i\tilde{T}_{\mu\nu}(x) \\ \varphi_{\mu\nu}^\dagger(x) &= T_{\mu\nu}(x) - i\tilde{T}_{\mu\nu}(x) \end{aligned} \right\} \quad (5)$$

onde $T_{\mu\nu}$ e $\tilde{T}_{\mu\nu}$ são reais e anti-simétricos. As derivadas covariantes são definidas como:

$$\left. \begin{aligned} D_\mu\varphi_{\alpha\beta}(x) &= (\partial_\mu + ieA_\mu)\varphi_{\alpha\beta}(x) \\ (D_\mu\varphi_{\alpha\beta})^\dagger(x) &= (\partial_\mu - ieA_\mu)\varphi_{\alpha\beta}^\dagger(x) \end{aligned} \right\}. \quad (6)$$

Claramente, o Lagrangeano (3) é invariante sob:

$$\begin{aligned} \delta A_\mu(x) &= -\partial_\mu \Lambda(x) \\ \delta\varphi_{\mu\nu}(x) &= +ie\Lambda(x)\varphi_{\mu\nu}(x) \\ \delta\varphi_{\mu\nu}^\dagger(x) &= -ie\Lambda(x)\varphi_{\mu\nu}^\dagger(x) \end{aligned} \quad (7)$$

Observa-se, também, a ausência de termos de massa no modelo (eq. (1) ou (3)). Isso é devido ao fato de que, termos de massa explícitos para $T_{\mu\nu}$ e $\tilde{T}_{\mu\nu}$, quebram a simetria de Lorentz. Assim sendo, para preservarmos essa simetria, tais campos só poderiam adquirir massa através de outro mecanismo, como quebra espontânea de simetria, por exemplo.

Devemos enfatizar que, para os nossos objetivos, o uso da equação (3) em lugar do Lagrangeano original (1) diretamente, facilitará enormemente os cálculos, daí o motivo de toda a discussão precedente.

⁴ Já o setor livre deste Lagrangeano ($\frac{1}{2}(\partial_\lambda T^{\mu\nu})^2 - 2(\partial_\mu T^{\mu\nu})^2$) possui invariância conforme. Além de teorias conformes (supergravidade conforme, por exemplo) tais campos de matéria têm sido utilizados em conexão com a teoria eletro-fracca padrão. Neste caso, a inserção de tais campos como parte de modelos eletro-fracos estendidos [8], pode explicar recentes aspectos fenomenológicos sobre os decaimentos $\pi^- \rightarrow e^- \bar{\nu}_e \gamma$ e $K^+ \rightarrow \pi^0 e^+ \nu$. Um estudo teórico sobre a dinâmica clássica desse setor [9], revelou alguns aspectos interessantes: excitações longitudinais como os graus de liberdade físicos, helicidade zero, dentre outros.

3 “Point-Splitting” para o modelo:

Primeiramente, devemos salientar que os resultados obtidos por Gastmans et al. [3], com relação às g.g.t.’s, têm validade bastante geral, desde que as transformações de gauge para a teoria sejam Abelianas. Deste modo, vamos utilizar estes resultados, adaptando-os quando necessário, às nossas necessidades. A tática de propor as transformações com “point-splitting” diretamente em termos dos tensores $T_{\mu\nu}$ e $\tilde{T}_{\mu\nu}$, ambos reais, revelou-se complicada ao ser aplicada ao modelo. Tal complicação surge devido à relação de dualidade que os envolve. Por outro lado, implementando-se tais transformações nos tensores complexos $\varphi_{\mu\nu}$ e $\varphi_{\mu\nu}^\dagger$, obtém-se uma forma mais simples para estas transformações, dada a independência entre eles. Além do mais, o estudo de invariância do Lagrangeano torna-se muito mais simplificado. Começemos, escrevendo as g.g.t.’s (denotadas por δ_G , com parâmetro de “point-splitting” a) para $\varphi_{\mu\nu}$ e $\varphi_{\mu\nu}^\dagger$, até ordem e^2 (já que a teoria é Abeliana, o “point-splitting” não afetará δA_μ : $\delta A_\mu = \delta_G A_\mu(x) = -\partial_\mu \Lambda(x)$):

$$\begin{aligned} \delta_G \varphi_{\mu\nu}(x) &= +ie\Lambda(1)\varphi_{\mu\nu}(x+2a) \\ &\quad + \frac{1}{2}(ie)^2 [\Lambda(1) + \Lambda(3)] (1,3)\varphi_{\mu\nu}(x+4a) + \mathcal{O}(e^3) \\ \delta_G \varphi_{\mu\nu}^\dagger(x) &= -ie\Lambda(-1)\varphi_{\mu\nu}^\dagger(x-2a) \\ &\quad + \frac{1}{2}(-ie)^2 [\Lambda(-1) + \Lambda(-3)] (-1,-3)\varphi_{\mu\nu}^\dagger(x-4a) + \mathcal{O}(e^3). \end{aligned} \tag{8}$$

com as definições:

$$(m, n) = \lim_{b \rightarrow 0^+} \int_{x+ma+b}^{x+na-b} d\eta^\nu A_\nu(\eta) \tag{9}$$

$$\Lambda(\pm n) = \Lambda(x \pm na) \tag{10}$$

A partir das expressões acima, pode-se mostrar que:

$$[\delta_G(1), \delta_G(2)]_{\Gamma,2} \left\{ \begin{array}{l} \varphi_{\mu\nu} \\ \varphi_{\mu\nu}^\dagger \end{array} \right\} = \mathcal{O}(e^3), \tag{11}$$

(com $[a, b] = ab - ba$), que é a condição Abeliana para as g.g.t.’s, até ordem e^2 (veja “footnote” 2). É fácil ver que no $\lim_{a \rightarrow 0}$, recuperamos as formas usuais (7). Para se obter as g.g.t.’s para $T_{\mu\nu}$ e $\tilde{T}_{\mu\nu}$, basta substituir (5) em (8).

Por outro lado, observemos que os termos de interação presentes na eq. (3) não são invariantes sob (8). Assim sendo, se queremos um Lagrangeano invariante sob g.g.t.’s (até determinada ordem), teremos que construí-lo. Lembremo-nos, no entanto, que nosso objetivo principal é chegarmos a um Lagrangeano regularizado⁵. Para isso, teremos que modificar a teoria original, de forma que os termos de interação não apresentem *produtos de campo no mesmo ponto*. Faremos isto, introduzindo “point-splitting” nos argumentos dos campos, da seguinte forma:

$$(D_\mu \varphi^{\mu\nu}(x))(D^\alpha \varphi_{\alpha\nu}(x))^\dagger \stackrel{P.S.}{=} (D_\mu \varphi^{\mu\nu})_{P.S.}(D^\alpha \varphi_{\alpha\nu})^\dagger_{P.S.} = [\partial_\mu \varphi^{\mu\nu}(x) + ieA_\mu(x+a)\varphi^{\mu\nu}(x+2a)] [\partial^\alpha \varphi_{\alpha\nu}(x) - ieA^\alpha(x-a)\varphi_{\alpha\nu}^\dagger(x-2a)] \tag{12}$$

$$\begin{aligned} \varphi_{\mu\nu}^\dagger(x)\varphi^{\nu\kappa}(x)\varphi_{\kappa\lambda}^\dagger(x)\varphi^{\lambda\mu}(x) &\stackrel{P.S.}{=} (\varphi_{\mu\nu}^\dagger \varphi^{\nu\kappa} \varphi_{\kappa\lambda}^\dagger \varphi^{\lambda\mu})_{P.S.} = \\ &\varphi_{\mu\nu}^\dagger(x-a)\varphi^{\nu\kappa}(x+a)\varphi_{\kappa\lambda}^\dagger(x-a/2)\varphi^{\lambda\mu}(x+a/2) \end{aligned} \tag{13}$$

Agora, reescrevendo-se (3), com o “point-splitting” introduzido:

$$\mathcal{L}_{P.S.}^{(0)} = -\frac{1}{4}F_{\mu\nu}F^{\mu\nu} + (D_\mu \tilde{\varphi}^{\mu\nu})_{P.S.}(D^\alpha \varphi_{\alpha\nu})^\dagger_{P.S.} - \frac{\lambda}{8}(\varphi_{\mu\nu}^\dagger \varphi^{\nu\kappa} \varphi_{\kappa\lambda}^\dagger \varphi^{\lambda\mu})_{P.S.} \tag{14}$$

⁵Os termos quadráticos (cinéticos e de massa, quando houver), não serão afetados pelo “point-splitting”. Termos de massa, por exemplo, como na QED, são invariantes sob estas transformações generalizadas (veja discussão em [3]). Os termos cinéticos, geralmente, não são invariantes. Mas os novos termos que surgem da atuação das g.g.t.’s sobre eles, já são regularizados.

A partir daqui, para construirmos um novo Lagrangeano, que seja invariante sob (8), digo, até ordem e^2 , devemos fazê-lo iterativamente, ordem a ordem. Para isso, aplicamos δ_G a $\mathcal{L}_{P,S}^{(0)}$, e retemos os termos até ordem e . Nota-se, claramente, as novas estruturas que possuem esses termos, em comparação com os originais. A tarefa consiste em encontrar (por *Ansatz*), termos proporcionais a e , tais que, quando acrescentados a $\mathcal{L}_{P,S}^{(0)}$, dando-nos um novo Lagrangeano ($\mathcal{L}_{P,S}^{(1)}$), este seja tal que:

$$\delta_G \left(\int d^4x \mathcal{L}_{P,S}^{(1)} \right) = \mathcal{O}(e^2),$$

ou seja, $\mathcal{L}_{P,S}^{(1)}$ nos dá uma Ação invariante sob δ_G até ordem e . Repetindo-se o procedimento até ordem e^2 , encontramos:

$$\begin{aligned} \mathcal{L}_{P,S}^{(2)}(\varphi, \varphi^\dagger) = & \mathcal{L}_{P,S}^{(0)} + \frac{1}{2}(ie)^2 \left\{ \left[\partial_\mu \left(\frac{1}{2} \left(\frac{\Lambda(-1) + \Lambda(+1)}{\Lambda(-1) - \Lambda(+1)} \right) (-1, +1)^2 \right) + \right. \right. \\ & + [A_\mu(x-a) + A_\mu(x+a)](-1, +1) + ([-1] + [+1])(-1, +1)_\mu \\ & \left. \left[\varphi^{\mu\nu}(x+2a) \partial^\alpha \varphi_{\alpha\nu}^\dagger(x-2a) - \varphi^{\dagger\mu\nu}(x-2a) \partial^\alpha \varphi_{\alpha\nu}(x+2a) \right] \right\} + \\ & - \frac{\lambda}{8}(ie) \left\{ \{-2, +2\}_\mu^\alpha \varphi_{\alpha\beta}^\dagger(x-a/2) \varphi^{\beta\mu}(x+a/2) + \{-3/2, +3/2\}_\mu^\alpha \right. \\ & \left. \varphi_{\alpha\beta}^\dagger(x-a) \varphi^{\beta\mu}(x+a) \right\} + \frac{\lambda}{16}(ie)^2 \left\{ \frac{1}{2} \left[\left(\frac{\Lambda(+2) + \Lambda(+4)}{\Lambda(+2) - \Lambda(+4)} \right) (2, 4)^2 \right] \right. \\ & \left[\varphi_{\mu\nu}^\dagger(x-a) \varphi^{\nu\kappa}(x+5a) \varphi_{\kappa\lambda}^\dagger(x-a/2) \varphi^{\lambda\mu}(x+a/2) + \right. \\ & + \varphi_{\mu\nu}^\dagger(x-a/2) \varphi^{\nu\kappa}(x+3a/2) \varphi_{\kappa\lambda}^\dagger(x) \varphi^{\lambda\mu}(x+5a) + \\ & - \varphi_{\mu\nu}^\dagger(x+a) \varphi^{\nu\kappa}(x+7a) \varphi_{\kappa\lambda}^\dagger(x+11a/2) \varphi^{\lambda\mu}(x+13a/2) + \\ & \left. - \varphi_{\mu\nu}^\dagger(x+9a/2) \varphi^{\nu\kappa}(x+13a/2) \varphi_{\kappa\lambda}^\dagger(x+a) \varphi^{\lambda\mu}(x+6a) \right] + \\ & + \left[\varphi_{\mu\nu}^\dagger(x-3a) \varphi^{\nu\kappa}(x+3a) \varphi_{\kappa\lambda}^\dagger(x-a/2) \varphi^{\lambda\mu}(x+a/2)(-2, +2)^2 \right. \\ & \left. \left(\frac{\Lambda(-2) + \Lambda(+2)}{\Lambda(-2) - \Lambda(+2)} \right) \right] + \left[\varphi_{\mu\nu}^\dagger(x-a) \varphi^{\nu\kappa}(x+a) \varphi_{\kappa\lambda}^\dagger(x-5a/2) \right. \\ & \left. \varphi^{\lambda\mu}(x+5a/2)(-3/2, +3/2)^2 \left(\frac{\Lambda(-3/2) + \Lambda(+3/2)}{\Lambda(-3/2) - \Lambda(+3/2)} \right) \right] + \\ & - \left[\left(\Lambda(-4) \varphi_{\mu\nu}^\dagger(x-5a) \varphi^{\nu\alpha}(x+a) + \Lambda(+4) \varphi_{\mu\nu}^\dagger(x-a) \varphi^{\nu\alpha}(x+5a) \right) \right. \\ & \left. \left(\varphi_{\alpha\beta}^\dagger(x-a/2) \varphi^{\beta\mu}(x+a/2) \right) (-2, +2)^2 \left(\frac{1}{\Lambda(-2) - \Lambda(+2)} \right) \right] + \\ & - \left[(-3/2, +3/2)^2 \left(\frac{1}{\Lambda(-3/2) - \Lambda(+3/2)} \right) \varphi_{\alpha\beta}^\dagger(x-a) \varphi^{\beta\mu}(x+a) \right] \\ & \left[\Lambda(-7/2) \varphi_{\mu\nu}^\dagger(x-9a/2) \varphi^{\nu\alpha}(x+a/2) + \Lambda(+7/2) \varphi_{\mu\nu}^\dagger(x-a/2) \right. \\ & \left. \varphi^{\nu\alpha}(x+9a/2) \right] - 2\{-2, +2\}_\mu^\alpha \{-3/2, +3/2\}_\mu^\nu \}. \end{aligned} \quad (15)$$

com as seguintes definições (além de (9) e (10)):

$$[n] = \frac{1}{2} [(-\infty, n) + (\infty, n)] \quad (16)$$

$$(l, m)^\mu = \lim_{b \rightarrow 0^+} \int_{x+la+b}^{x+ma-b} d\eta^\nu F^{\nu\mu}(\eta) \quad (17)$$

$$\begin{aligned} \{-n, +n\}_\mu^\nu = & \lim_{b \rightarrow 0^+} \int_{x-na+b}^{x+na-b} d\xi^\alpha \partial_\alpha \left[\varphi_{\mu\sigma}^\dagger \left(\frac{\xi}{n} + \frac{n-1}{n}x - na \right) \right. \\ & \left. \varphi^{\beta\nu} \left(\frac{\xi}{n} + \frac{n-1}{n}x + na \right) \int_{-\infty}^\xi d\eta^\lambda A_\lambda(\eta) \right] \end{aligned} \quad (18)$$

É fácil verificar que: $\lim_{\alpha \rightarrow 0} \mathcal{L}_{p,S}^{(2)} = \mathcal{L}_S(x)$. O Lagrangeano acima, está escrita em termos de φ e φ^\dagger . Para obtermos $\mathcal{L}_{p,S}^{(2)}$, em termos de T e \dot{T} , que é o resultado final a que queríamos chegar, basta fazer uso da expressão (5). Devido a sua extensão, não a reproduziremos aqui.

4 Conclusões e Perspectivas:

O Lagrangeano generalizado obtido, eq. (15), possui a propriedade de *regularidade*, ou seja, seus termos de interação *não apresentam* produtos de campos no mesmo ponto. Como consequência, espera-se que eventuais quantidades quânticas calculadas a partir dele, não apresentem problemas de divergências ultra-violeta.

Em contrapartida, este mesmo Lagrangeano é *não-local* (caracterizado pela presença de variáveis de campo integradas no espaço-tempo). Pelo que se sabe, a *não-localidade* pode acarretar problemas sérios à uma versão quantizada da teoria (por exemplo, o fato da não-localidade estar relacionada com a não-causalidade). Além do mais, os caminhos que devem ser seguidos para se quantizar uma teoria *não-local*, não nos parecem bastante claros.

Outro ponto importante, é que a dificuldade técnica em lidar com a regularização de Lagrangeanos, utilizando-se o método estudado, está diretamente relacionada com a *quantidade de campos* (principalmente os de matéria, dada a complexidade de suas g.g.t's) envolvida num mesmo vértice. Noutras palavras, aplicar o procedimento a um vértice de 4-pernas, é tecnicamente mais complicado que a outro de 2-pernas. Até onde verificamos, a natureza dos campos em si (escalar, espinorial, etc.) não nos leva a maiores complicações.

Dentre diversas questões importantes que ainda devem ser elucidadas (pelo que parece, em todo o contexto de regularização via "point-slitting"), gostaríamos de citar:

Como já abordamos, que caminhos devem ser seguidos para quantizarmos $\mathcal{L}_{p,S}^{(2)}$, e daí, calcularmos as quantidades de interesse físico?

Gráficos de Feynman: seriam possíveis? Como ficariam?

Até que ponto a invariância de $\mathcal{L}_{p,S}^{(2)}$ sob $\delta\epsilon$, até ordem e^2 , garante-nos, de fato, a invariância de gauge?

Os novos termos que aparecem em $\mathcal{L}_{p,S}^{(2)}$ (não presentes no modelo original) sugerem novos tipos de "interação". Teriam eles algum interesse físico?

Agradecimentos.

Os autores são gratos ao CNPq pelo auxílio financeiro.

References

- [1] P.A.M. Dirac, Proc. Cambridge Phil. Soc. 30(1934)150;
- [2] P. Osland and T.T. Wu, Zeitschrift f. Physik C 55(1992) 569,585,593; Phys. Lett. B 291(1992)315;
- [3] R. Gastmans, C. Newton and Tai T. Wu, Phys. Lett. B 291(1994) 84;
- [4] J. Schwinger, Phys. Rev. 82(1951)664;
- [5] L.V. Avdeev and M.V. Chizhov, Phys. Lett. B 321(1994)212;
- [6] V. Lemes, R. Renan and S.P. Sorella, Phys. Lett. B 344(1995)158;
- [7] V. Lemes, R. Renan and S.P. Sorella, Phys. Lett B 352(1995)37;
- [8] M.V. Chizhov, Mod. Phys. Lett. A vol. 8 N^o 29(1993)2753;
- [9] L.V. Avdeev and M.V. Chizhov, "A queer reduction of degrees of freedom.", JINR Dubna preprint, hep-th/9407067.

O Tensor Energia-Momentum do Campo de Radiação sob vínculos Macroscópicos e o Efeito Casimir.

Franz P. A. Farias* e Arthur M. Neto†

Abstract

In this work, we determine the physically correct form of energy-momentum tensor from the radiation field by using a suitable redefinition of normal product. Next, we apply it in the calculus of Casimir's pression for a class of boundary conditions. The results obtained are present

1 PRELIMINARES

O tensor energia-momentum (E-M) do campo eletromagnético $T_{\mu\nu}(x)$ envolve expressões quadráticas dos operadores de campo $A_\mu(x)$. Os operadores de campo são, do ponto de vista matemático, distribuições a valor-operador, e como o produto de distribuições em um mesmo ponto, a exemplo de $A_\mu(x)A_\nu(x)$, não é definido [4], [5], surgirão, no cálculo desses produtos, divergências associadas com as singularidades presentes nos mesmos (as distribuições).

Historicamente tem-se tratado as divergências de forma bastante pragmática. Com uma motivação dada pela própria teoria quântica, que mostra que apenas diferenças de energias constituem elemento mensurável, o que se faz é redefinir a grandeza física a partir do valor divergente encontrado, valor este que está relacionado com a situação do sistema livre (i.e., do campo estendido em todo o espaço). Essa subtração constitui a *renormalização* da grandeza física [6].

Seguindo uma idéia originalmente colocada nas referências [4] e [5], propomos uma definição de produto de operadores que aplicada ao tensor E-M conduza a resultados físicos livres de divergências, sem o uso da renormalização. Conseguiremos isto a partir de uma definição apropriada do ordenamento normal no espaço de coordenadas sobre a expressão, na forma de operador, do tensor E-M.

2 O TENSOR ENERGIA-MOMENTUM FÍSICO.

Desde que o tensor energia-momentum do campo eletromagnético [3], [6] envolve produto de operadores de campo aplicamos sobre este a técnica de separação de ponto, em seguida desenvolvemos os termos resultantes os quais fornecem,

$$T_{\mu\nu}(x) = \lim_{x' \rightarrow x} [G_{\mu\nu}^{\rho\lambda\sigma\tau}] \left(\partial_\rho^x \partial_\lambda^{x'} \right) (A_\sigma(x) A_\tau(x')), \quad (1)$$

* Depto. Exatas-Universidade Estadual de Feira de Santana, CEP: 44031-046.

† IFUFBA-Universidade Federal da Bahia, CEP: 40210-340.

$$G_{\mu\nu}^{\rho\lambda\sigma\tau} = \frac{1}{2}g_{\mu\nu} (g^{\rho\lambda}g^{\sigma\tau} - g^{\rho\tau}g^{\sigma\lambda}) - g_{\mu\alpha} (g^{\lambda\rho}g^{\alpha\sigma} - g^{\alpha\rho}g^{\lambda\sigma}) \delta_{\nu}^{\tau} - g_{\mu\alpha} (g^{\alpha\rho}g^{\tau\sigma} - g^{\tau\rho}g^{\alpha\sigma}) \delta_{\nu}^{\lambda}. \quad (2)$$

Como $A_{\sigma}(x)$ e $A_{\tau}(x')$ não comutam, o seu produto (orden) precisa ser bem especificado, admitiremos que este é feito a partir do ordenamento normal. Ademais, considerando as situações nas quais a separação de $A_{\sigma}(x)$ em partes de frequências positiva $A_{\sigma}^{+}(x)$ e negativa $A_{\sigma}^{-}(x)$ pode ser realizada de forma covariante, temos para o produto normal,

$$: A_{\sigma}(x)A_{\tau}(x') : := A_{\sigma}(x)A_{\tau}(x') - [A_{\sigma}^{-}(x), A_{\tau}^{+}(x')], \quad (3)$$

A substituição da eq.(3) na eq.(1) leva a,

$$T_{\mu\nu}^{fis}(x) = \lim_{x' \rightarrow x} [G_{\mu\nu}^{\rho\lambda\sigma\tau} (\partial_{\rho}^x \partial_{\lambda}^{x'}) (A_{\sigma}(x)A_{\tau}(x') - [A_{\sigma}^{-}(x), A_{\tau}^{+}(x')])]. \quad (4)$$

Observamos que o operador $T_{\mu\nu}^{fis}(x)$ está definido independentemente da re-representação particular do espaço de Fock empregada. Admitiremos que a representação associada a situação de campo estendido em todo o espaço seja mais fundamental com relação a qualquer outra e que a forma da eq.(4), assim obtida, constitui a forma correta a ser aplicada nas outras situações. Com $A_{\mu}(x)$ no gauge de Coulomb¹ [9] resulta então para $T_{\mu\nu}^{fis2}$,

$$T_{\mu\nu}^{fis}(x) = \lim_{x' \rightarrow x} [G_{\mu\nu}^{\rho\lambda\sigma\tau} (\partial_{\rho}^x \partial_{\lambda}^{x'}) A_{\sigma}(x)A_{\tau}(x')] - \lim_{x' \rightarrow x} [G_{\mu\nu}^{\rho\lambda\sigma\tau} (\partial_{\rho}^x \partial_{\lambda}^{x'}) \sum_{i=1}^2 h_{\sigma}^i h_{\tau}^i D_0^{+}(x-x')], \quad (5)$$

$$D_0^{+}(x-x') = \int \frac{d^3k}{(2\pi)^3 2k_0} \exp[-ik(x-x')].$$

Notamos que o valor esperado de vácuo livre da eq.(5) é nulo como esperado.

3 O EFEITO CASIMIR.

O efeito Casimir refere-se historicamente ao cálculo realizado por H. B. Casimir (1948) [1] que oxibe a existência de uma força atrativa entre duas placas planas e perfeitamente condutoras quando estas se encontram imersas no campo eletromagnético em seu estado de vácuo. A esta força está associada uma pressão sobre as placas que passou a ser denominada de pressão de Casimir. Mostraremos nesta seção que o método exposto anteriormente permite encontrar a mencionada pressão de forma direta. Realizaremos esses cálculos para os seguintes vínculos,

$$\epsilon_{\mu\nu\rho\sigma} n^{\rho} F^{\sigma\nu} |_{S=0}, \quad \epsilon_{\mu\nu\rho\sigma} n^{\rho} \tilde{F}^{\sigma\nu} |_{S=0} = 0 \quad (6)$$

O primeiro vínculo em (6) transporta-se sobre os potenciais como a condição de contorno de Dirichlet enquanto que o segundo vínculo significa a condição de contorno de Neumann sobre os mesmos. As superfícies de interesse são dadas por um (ou dois) plano(s) localizado(s) em $x_3 = 0$ (enquanto que o outro em $x_3 = d$).

¹Os vetores de polarização h^i são a transcrição dos vetores de polarização e_1 e e_2 , no gauge de Coulomb, para o espaço de coordenadas.

²A métrica utilizada tem assinatura -2.

3.1 O VÍNCULO DE DIRICHLET NO PLANO $X_3 = 0$.

A pressão de Casimir será obtida de acordo com a definição a seguir³ [2],

$$p(x) = \lim_{\delta \rightarrow 0} \langle 0_{conf} | [T_{33}^{fis}(\tilde{x}, x_3 = \delta) - T_{33}^{fis}(\tilde{x}, x_3 = -\delta)] | 0_{conf} \rangle. \quad (7)$$

A justificativa para a eq.(7) reside no fato de que temos campo presente tanto no interior quanto no exterior dos planos e portanto, a eq.(7) fornece a pressão líquida resultante. De (5) segue para o componente T_{33}^{fis} ,

$$T_{33}^{fis}(x) = \lim_{x' \rightarrow x} [G_{33}^{33\sigma\tau}] \left[A_\sigma(x) A_\tau(x') - \sum_{i=1}^2 h_\sigma^i h_\tau^i D_0^+(x - x') \right], \quad (8)$$

Realizando a eq.(8) para a representação de $A_\mu(x)$ deste caso⁴ [9] e calculando o comutador resultante nesta representação obtemos após algumas manipulações,

$$T_{33}^{fis}(x) = \lim_{x' \rightarrow x} [\Gamma_1^{\sigma\tau} + \Gamma_2^{\sigma\tau} + \Gamma_3^{\sigma\tau}] \times \left[:A_\sigma(x) A_\tau(x') : - (h_\sigma^1 h_\tau^1 - h_\sigma^2 h_\tau^2) D_0^+(x - x'') \right]. \quad (9)$$

Na obtenção da eq.(9) temos utilizado as representações livre de D_1^+ e D_2^+ [9]. A notação x'' significa $x'' = (x'_0, x'_1, x'_2, -x'_3)$. Segue da eq.(9),

$$\langle 0_{d1} | T_{33}^{fis}(x) | 0_{d1} \rangle = \lim_{x' \rightarrow x} \left[\sum_{i=1}^3 \Gamma_i^{\sigma\tau} \right] \langle 0_{d1} | :A_\sigma(x) A_\tau(x') : | 0_{d1} \rangle = 0. \quad (10)$$

A estrutura de campo eletromagnético é a mesma de um lado e de outro do plano [9] sendo assim, segue da eq.(7) que a pressão de Casimir é nula nessa situação.

3.2 O VÍNCULO DE NEUMANN NO PLANO $X_3 = 0$.

Seguindo os mesmos passos que no item anterior conseguimos,

$$T_{33}^{fis}(x) = \lim_{x' \rightarrow x} [\Gamma_1^{\sigma\tau} + \Gamma_2^{\sigma\tau} + \Gamma_3^{\sigma\tau}] \times \left[\dagger A_\sigma(x) A_\tau(x') \dagger + (h_\sigma^1 h_\tau^1 - h_\sigma^2 h_\tau^2) D_0^+(x - x'') \right], \quad (11)$$

onde $\dagger \dagger$ denota o novo produto normal de operadores em $A_\mu(x)$. Na eq.(11) temos utilizado as representações livre das funções D_1^+ e D_2^+ [9]. Pelas mesmas razões colocadas em (10) segue da eq.(11),

$$\langle 0_{n1} | T_{33}^{fis}(x) | 0_{n1} \rangle = \lim_{x' \rightarrow x} \left[\sum_{i=1}^3 \Gamma_i^{\sigma\tau} \right] \langle 0_{n1} | \dagger A_\sigma(x) A_\tau(x') \dagger | 0_{n1} \rangle = 0, \quad (12)$$

e de (12) decorre também que a pressão de Casimir é nula neste caso.

³A notação para \tilde{x} na eq.(3.6) significa: $\tilde{x} = (t, x, y, 0)$.

⁴A introdução dos vínculos conduz a espaços de representação 'distintos' para os operadores de campo.

3.3 O VÍNCULO DE DIRICHLET NOS PLANOS $X_3 = 0$ E $X_3 = d$.

Como mostramos nos itens anteriores nas regiões com apenas um vínculo (Dirichlet ou Neumann) a pressão de Casimir é nula. Por esta razão consideraremos, daqui em diante, o cálculo dessa pressão apenas na região $0 \leq x_3 \leq d$. De acordo com (7), a pressão no plano em $x_3 = d$ é dada por,

$$p(x) = \lim_{\delta \rightarrow 0} \langle 0_{conf} | [T_{33}^{fis}(\tilde{x}, x_3 = d + \delta) - T_{33}^{fis}(\tilde{x}, x_3 = d - \delta)] | 0_{conf} \rangle. \tag{13}$$

A realização da eq.(8) para a representação de $A_\mu(x)$ relativa a este caso [9], após as devidas simplificações, fornece o seguinte resultado,

$$\begin{aligned} T_{33}^{fis}(x) &= \lim_{x' \rightarrow x} [\Gamma_1^{\sigma\tau} + \Gamma_2^{\sigma\tau} + \Gamma_3^{\sigma\tau}] (*A_\sigma(x)A_\tau(x')*) \\ &\quad - 2 \cdot \lim_{x' \rightarrow x} [\partial_3^x \partial_3^{x'}] \left[\sum_{\substack{-\infty \\ l \neq 0}}^{\infty} D_0^+(x - x'_d) + \left(\frac{\pi}{d}\right) D_0^+(\tilde{x} - \tilde{x}'; 0) \right] \\ &= -\frac{3}{8\pi^2} \left(\frac{1}{d^4}\right) \sum_{l=1}^{\infty} (l)^{-4} = -\frac{\pi^2}{240d^4}, \quad (\hbar = c = 1) \end{aligned} \tag{14}$$

* * denota o novo ordenamento normal e em (14) utilizamos as representações livre de D_{c1}^+ e D_{c2}^+ [9]. A soma em (14) é a função Zeta de Riemann de valor $(\pi^4/90)$. De acordo com a definição da pressão, os resultados (10) e (14) quando levados para a eq.(7) mostram que a mesma é independente das coordenadas ($x_0, x_1, e x_2$) tendo um valor constante sobre a mesmo. O sinal em (14) indica que a força entre os planos é atrativa.

3.4 O VÍNCULO DE NEUMANN NOS PLANOS $X_3 = 0$ E $X_3 = d$.

Seguindo a mesma idéia do caso anterior resulta,

$$\begin{aligned} \langle 0_{n2} | T_{33}^{fis}(x) | 0_{n2} \rangle &= -2 \cdot \lim_{x' \rightarrow x} [\partial_3^x \partial_3^{x'}] \left[\sum_{\substack{-\infty \\ l \neq 0}}^{\infty} D_0^+(x - x'_d) \right] \\ &= -\frac{\pi^2}{240d^4}, \end{aligned} \tag{15}$$

que concorda com o obtido na eq.(14). Este fato mostra que este resultado continua válido para esta situação, i.e., obtemos o mesmo sinal e magnitude para a pressão de Casimir que encontrada no caso anterior.

3.5 O VÍNCULO DE DIRICHLET NO PLANO $X_3 = 0$ E DE NEUMANN NO PLANO $X_3 = d$.

Os mesmos passos realizados nos itens anteriores conduzem neste caso a,

$$\langle 0_{dn} | T_{33}^{fis}(x) | 0_{dn} \rangle = -2 \cdot \lim_{x' \rightarrow x} [\partial_3^x \partial_3^{x'}] \left[\sum_{\substack{-\infty \\ l \neq 0}}^{\infty} (-1)^l D_0^+(x - x'_d) \right], \tag{16}$$

$$= \frac{3}{8\pi^2 d^4} \sum_{l=1}^{\infty} (-1)^{1+l} (l)^{-4} = \left(\frac{7}{8}\right) \frac{\pi^2}{240d^4}, \quad (17)$$

onde a soma é a função Zeta de Riemann de valor $(7/8) (\pi^4/90)$. Podemos concluir de (17) que a pressão de Casimir para o vínculo misto vale $(-7/8)$ daquela dada em (14), portanto tem intensidade menor e sinal contrário, o que indica que a força presente entre os planos é agora repulsiva.

4 CONSIDERAÇÕES FINAIS.

O vínculo da condição de contorno de Dirichlet pode ser considerada como uma idealização da situação física em que temos uma placa de natureza condutora. O vínculo de Neumann idealiza uma placa de natureza usualmente referida na literatura como permeável. Nas situações com dois vínculos temos a combinação correspondente às das placas. O nosso resultado para o vínculo de Dirichlet sobre os planos $x_3 = 0$ e $x_3 = d$ concorda com aqueles obtidos por Brown e Maclay [7], Bordag, Robaschik e Wieczorek [2] e G. Scharf e W. F. Wreszinski [5]. Os resultados que conseguimos para os sistemas permeável e misto concordam com aqueles obtidos por T. Boyer através do método de soma de modos [8].

References

- [1] H. B. G. Casimir, *Proc. K. Akad. Wet.*, B 51 (1948) 793.
- [2] M. Bordag, D. Robaschik e E. Wieczorek, *Ann. Phys. (N.Y.)* 165 (1985) 192;
- [3] C. Itzykson e J. B. Zuber, *Quantum Field Theory* (McGraw-Hill N.Y., 1980).
- [4] G. Scharf, *Finite Quantum Electrodynamics* (Springer N.Y., 1989).
- [5] G. Scharf e W. F. Wreszinski, *Found. Phys. Lett.* 5 (1992) 479; G. Scharf e W. F. Wreszinski, *IL Nuovo Cim.* 107A (1994) 2879.
- [6] G. Plunien, B. Müller e W. Greiner, *Phys. Rep.* 134 (1986) 87.
- [7] L. S. Brown e G. J. Maclay, *Phys. Rev.* 184 (1969) 1272.
- [8] T. H. Boyer, *Ann. Phys.* 56 (1970) 474.
- [9] F. P. A. Farias, *Dissertação de Mestrado* (UFBa, 1996) (Em fase de julgamento).

Energia de Casimir em geometrias retangulares d -dimensionais sob condições de contorno mistas.

J. C. da Silva

Centro Federal de Educação Tecnológica da Bahia,
Salvador, Bahia

Hebe Q. Plácido, A. E. Santana, Arthur M. Neto
Instituto de Física, Universidade Federal da Bahia,
Salvador, Bahia

Abstract

The Casimir energy and its temperature corrections are presented for the electromagnetic field confined in a d -dimensional hypercavity. The expressions are derived considering Dirichlet boundary conditions for each pair of hyperplanes defining a confined direction (the homogeneous case); or yet, by choosing different boundary conditions (Dirichlet or Neumann) at each hyperplane of the pair (the mixed case).

1 Introdução

Dentre os aspectos abordados em relação ao Efeito Casimir[1] encontrados na literatura, é possível citar a questão do caráter atrativo ou repulsivo do efeito, com respeito ao número de dimensões confinadas versus a dimensionalidade do espaço tempo[2,3] e as correções introduzidas ao considerar-se o sistema à temperatura finita[4-6]. Em acréscimo, aborda-se neste trabalho, a influência das diversas condições de contorno admissíveis para o campo eletromagnético confinado. Estes vínculos levam à modificação dos estados estacionários acessíveis ao campo no espaço-tempo ($d + 1$) dimensional. Tomando-se o tensor totalmente antissimétrico $F_{\mu\nu}$ para descrever o campo eletromagnético, o confinamento por hiperplanos infinitos e perfeitamente condutores é representado por $n^\mu F_{\mu\nu}^* = 0$; sendo $F_{\mu\nu}^*$ o tensor dual e n^μ um vetor do tipo espaço, ortogonal ao hiperplano em questão. Outra condição de contorno possível é obtida exigindo-se que $n^\mu F^{\mu\nu} = 0$, situação adequada para descrever superfícies infinitamente permeáveis[2].

Quando as condições de contorno são homogêneas, vale dizer, somente hipersuperfícies condutoras, toma-se o primeiro dos vínculos para se obter as frequências dos modos normais acessíveis ao campo. Contudo para o problema com fronteiras mistas ou seja, uma hipersuperfície condutora e outra permeável, obtido pela aplicação do primeiro vínculo em um hiperplano e do segundo naquele diametralmente oposto, impõe-se uma modificação nas frequências acima citadas[7].

2 Energia de Casimir em $(d + 1)$ dimensões

Considere o campo eletromagnético definido em um espaço $(d + 1)$ -dimensional, onde $\text{diag}(g_{\mu\nu}) = (-1, \underbrace{1, 1, \dots, 1}_{d-\text{dim}})$ com $\mu, \nu = 0, 1, \dots, d$ e confinado ao interior de um hiperparalelepípedo, com p lados de comprimentos finitos l_1, \dots, l_p e $d - p$ lados de comprimentos $L \rightarrow \infty$. Tem-se então para as frequências associadas aos modos acessíveis ao campo

$$\omega(k_1, k_2, \dots, k_p, k_{\parallel}) = c\sqrt{k_1^2 + k_2^2 + \dots + k_p^2 + k_{\parallel}^2}, \quad k_{\parallel}^2 = k_{p+1}^2 + k_{p+2}^2 + \dots + k_d^2, \quad (1)$$

com

$$k_i^2 = \left[\frac{(n_i + g_i) \pi}{l_i} \right]^2, \quad i = 1, 2, \dots, p, \quad n_i = 0, 1, \dots, \infty, \quad (2)$$

sendo k_{\parallel}^2 uma variável contínua. Os valores assumidos por g_i serão $g_i = 1/2$, para o caso dos pares de hiperplanos confinantes estarem submetidos a condições de contorno mistas; ou $g_i = 0$ quando para eles tenham-se vínculos homogêneos. Assume-se então que o sistema se encontra em equilíbrio termodinâmico à temperatura finita. Sendo assim, a energia livre de Casimir associada a este estado do campo eletromagnético, é obtida através da energia livre de Helmholtz expressa por[6]

$$F_d(T; l_i; p; g_i) = \frac{\hbar c}{2} \left(\frac{L}{2\pi} \right)^{d-p} \int_{-\infty}^{\infty} d^{d-p} k_{\parallel} \sum_{\{n_i\}=0}^{\infty} \sqrt{\left[\sum_{i=1}^p \left(\frac{(n_i + g_i) \pi}{l_i} \right)^2 \right] + k_{\parallel}^2} + \left(\frac{L}{2\pi} \right)^{d-p} \int_{-\infty}^{\infty} d^{d-p} k_{\parallel} \beta^{-1} \times \sum_{\{n_i\}=0}^{\infty} \ln \left[1 - \exp \left(-\beta \hbar c \sqrt{\left[\sum_{i=1}^p \left(\frac{(n_i + g_i) \pi}{l_i} \right)^2 \right] + k_{\parallel}^2} \right) \right], \quad (3)$$

onde $\{n_i\} = n_1, n_2, \dots, n_p$. Após realizar-se as integrações angulares[2] e introduzindo-se a variável $t = k_{\parallel}^2 / K^2$ em (2.3), a expressão para F_d é reescrita como

$$F_d(T; l_i; p; g_i) = \frac{\hbar c}{2} \left(\frac{L}{2\pi} \right)^{d-p} \frac{\pi^{\frac{d-p}{2}}}{\Gamma[(d-p)/2]} \sum_{\{n_i\}=0}^{\infty} K^{d-p+1} \int_0^{\infty} dt (t)^{\frac{d-p-2}{2}} \sqrt{1+t} + \left(\frac{L}{2\pi} \right)^{d-p} \frac{\pi^{\frac{d-p}{2}}}{\Gamma[(d-p)/2]} \beta^{-1} \sum_{\{n_i\}=0}^{\infty} K^{d-p} \int_0^{\infty} dt (t)^{\frac{d-p-2}{2}} \times \ln \left[1 - \exp \left(-\beta \hbar c K \sqrt{1+t} \right) \right] \equiv E_d(l_i; p; g_i) + F'_d(T; l_i; p; g_i) \quad (4)$$

onde

$$K^2 = \left[\frac{(n_1 + g_1) \pi}{l_1} \right]^2 + \left[\frac{(n_2 + g_2) \pi}{l_2} \right]^2 + \dots + \left[\frac{(n_p + g_p) \pi}{l_p} \right]^2, \quad (5)$$

e Γ é a função fatorial. O primeiro termo desta equação E_d , é a energia do vácuo a partir da qual obtém-se a energia de Casimir a $T = 0$. O segundo F'_d , corresponde então à correção introduzida pela temperatura.

2.1 Efeito Casimir em $T = 0$

O primeiro termo da energia livre de Helmholtz E_d , que fornece a energia de Casimir em $T = 0$, é então integrado[2] resultando em

$$E_d(l_i; p; g_i) = \frac{\hbar c}{2} \left(\frac{L}{2}\right)^{d-p} \frac{\Gamma[(-d+p-1)/2]}{\Gamma[(-1/2)]} \pi^{\frac{d-p+2}{2}} \times \sum_{\{n_i\}=0}^{\infty} \left[\left(\frac{n_1+g_1}{l_1}\right)^2 + \dots + \left(\frac{n_p+g_p}{l_p}\right)^2 \right]^{\frac{d-p+1}{2}} \quad (6)$$

Estas somas sobre todos os autovalores da energia de ponto zero dos modos do campo diverge, e um procedimento adequado de regularização é necessário. Para tanto, a técnica de funções Zeta será empregada[8,9]. Este procedimento é implementado definindo-se primeiro

$$E_d(l_i; p; g_i; s) = \frac{\hbar c}{2} \left(\frac{L}{2}\right)^{d-p} \frac{\Gamma[s/2]}{\Gamma[-1/2]} \pi^{\frac{-s+1}{2}} \times \sum_{\{n_i\}=0}^{\infty} \left[\left(\frac{n_1+g_1}{l_1}\right)^2 + \dots + \left(\frac{n_p+g_p}{l_p}\right)^2 \right]^{\frac{-s}{2}}, \quad (Re\ s > 0). \quad (7)$$

A soma na eq.(2.7) é então expressa em termos da função Zeta de Epstein Z_p , expressa por[8,9]

$$Z_p(\mathbf{g}; \mathbf{h}; 1/l_1, \dots, 1/l_p; s) \equiv V_p^{-\frac{s}{p}} \sum_{\{n_i\}=-\infty}^{\infty} \frac{\exp[2\pi i(\mathbf{n} \cdot \mathbf{h})]}{[(\mathbf{n} + \mathbf{g}) \cdot A]^{\frac{s}{2}}}, \quad (Re\ s > 0),$$

onde

$$\mathbf{n} \equiv (n_1, n_2, \dots, n_p), \quad \mathbf{g} \equiv (g_1, g_2, \dots, g_p), \quad \mathbf{h} \equiv (h_1, h_2, \dots, h_p).$$

Os vetores \mathbf{g} e \mathbf{h} acima têm suas componentes reais, A é uma matriz diagonal com $diag(A_{ij}) = (1/l_1, \dots, 1/l_p)$ e $V_p = \prod_{i=1}^p l_i$. A linha no sinal de soma indica que esta deve ser efetuada sobre todos os inteiros n_1, \dots, n_p exceto se todas as componentes de \mathbf{g} forem inteiros, quando então o termo $\mathbf{n} = -\mathbf{g}$ deve ser omitido.

Resulta pois para o caso homogêneo ($g_i = 0$) que

$$E_d(l_i; p; 0; s) = \frac{\hbar c}{2} \left(\frac{L}{2}\right)^{d-p} \frac{\Gamma[s/2]}{\Gamma[(-1/2)]} \pi^{\frac{-s+1}{2}} \frac{1}{2^p} \sum_{\{n_i\}=-\infty}^{\infty} \prod_{i=1}^p [1 + \delta_{n_i}] \times \left[\left(\frac{n_1}{l_1}\right)^2 + \dots + \left(\frac{n_p}{l_p}\right)^2 \right]^{\frac{-s}{2}} \\ = \frac{\hbar c}{2} \left(\frac{L}{2}\right)^{d-p} \frac{\Gamma\left[\frac{s}{2}\right]}{\Gamma\left[(-\frac{1}{2})\right]} \frac{\pi^{\frac{-s+1}{2}}}{2^p} \sum_{j=1}^p 2^{p-j} \times \sum_{\{l_i\}} \left[V_j^{(l_i)} \right]^{\frac{s}{p}} Z_j(0; 0; \{l_i\}; s). \quad (8)$$

Nesta expressão a segunda soma indica que ela deve ser realizada sobre todos os conjuntos de l_i , com $l_i \neq l_j$, dentro de cada ordem j associada à V_j e Z_j . Uma vez que o domínio da função

zeta Z_p é $Re s > 0$, será feita uma extensão analítica para a região onde $Re s < 0$. Isto é implementado fazendo-se uso da fórmula de reflexão[8] que possibilita a escrita de Z_p em termos da função \overline{Z}_p definida por

$$\overline{Z}_p(0; \mathbf{g}; l_1, \dots, l_p; p-s) = V_p^{\frac{p-s}{p}} \sum'_{\{n_i\}=-\infty}^{\infty} \frac{\exp(2\pi i \mathbf{n} \cdot \mathbf{g})}{([\mathbf{n} A^{-1}]^2)^{\frac{p-s}{2}}} \quad Re s < 0 \quad (9)$$

A linha no sinal de soma indica que é excluído o termo em que $\mathbf{n} = 0$. Contabilizando-se as duas polarizações independentes associadas ao campo e com o auxílio da definição anterior escreve-se

$$E_d(l_i; p, 0, s) = \frac{\hbar c}{2^p} \left(\frac{L}{2}\right)^{d-p} \frac{\pi^{\frac{d-p+1}{2}}}{\Gamma[(-1/2)]} \Gamma\left[\frac{p-s}{2}\right] \sum_{j=1}^p 2^{p-j} \sum_{\{l_i\}} [V_j^{(l_i)}]^{\frac{s}{p}} \overline{Z}_j(0; \mathbf{g}; l_1, \dots, l_p; p-s) \quad (10)$$

A energia de Casimir é obtida fazendo-se $s = -(d-p+1)$ resultando em

$$E_d(l_i; p; 0) = -\frac{\hbar c}{2^{d+1}} L^{d-p} \pi^{-\frac{d+1}{2}} \Gamma\left[\frac{d+1}{2}\right] \sum_{j=1}^p 2^{p-j} \times \sum_{\{l_i\}} [V_j^{(l_i)}]^{\frac{-d+p-1}{p}} \overline{Z}_j(0; 0; l_1, \dots, l_p; d+1) \quad (11)$$

Para vínculos mistos ($g_i = 1/2$) a expressão(2.7) é escrita como

$$E_d(l_i; p; 1/2; s) = \frac{\hbar c}{2} \left(\frac{L}{2}\right)^{d-p} \frac{\Gamma[s/2] \pi^{\frac{-d+1}{2}}}{\Gamma[-1/2]} \frac{Z_p(1/2; 0; 1/l_1, \dots, 1/l_p; s) V_p^{s/p}}{2} \quad (12)$$

Realizando os mesmos passos anteriores com vista à regularização de E_d tem-se como resultado

$$E_d(l_i; p; 1/2) = -\frac{\hbar c}{2^{d-p+2}} L^{d-p} \pi^{-\frac{d+1}{2}} \Gamma\left[\frac{d+1}{2}\right] \times V_p^{\frac{-d+p-1}{p}} \overline{Z}_p(1/2; 0; l_1, \dots, l_p; d+1) \quad (13)$$

No caso homogêneo com apenas uma das dimensões espaciais confinada ($p = 1$), a eq.(2.11) torna-se

$$E_d(l_1; 1; 0) = -\frac{\hbar c}{2^d l_1^d} L^{d-1} \pi^{-\frac{d+1}{2}} \Gamma\left[\frac{d+1}{2}\right] \zeta(d+1),$$

onde ζ é a função zeta de Riemann. Este resultado concorda com aquele apresentado por Ambjorn[2]. Tomando-se agora o caso misto sob a mesma restrição anterior, a eq.(2.13) fornece

$$E_d(l_1; 1; 1/2) = \frac{\hbar c}{2^d l_1^d} L^{d-1} \pi^{-\frac{d+1}{2}} \Gamma\left[\frac{d+1}{2}\right] \zeta(d+1) \left[1 - \frac{1}{2^d}\right].$$

No espaço tridimensional ($d = 3$) a expressão acima leva ao resultado obtido por Boyer [7].

Estas últimas equações apontam para valores sempre negativos ou positivos da energia, respectivamente. Isto implica em pressões sempre atrativas ($g_i = 0$) ou repulsivas ($g_i = 1/2$) sobre as fronteiras.

2.2 Correção de temperatura ao Efeito Casimir

A correção de temperatura ao Efeito Casimir é dada pelo segundo termo da energia livre de Helmholtz F'_d na eq.(2.4). Após a substituição da função logaritmo pela sua expansão em série[5] têm-se

$$F'_d(T; l_i; p; g_i) = \left(\frac{L}{2\pi}\right)^{d-p} \frac{\pi^{\frac{d-p}{2}}}{\Gamma[(d-p)/2]} \beta^{-1} \sum_{\{n_i\}=0}^{\infty} \sum_{m=1}^{\infty} \frac{(-1)^{2m+1}}{m} \\ \times K^{d-p} \int_1^{\infty} dx 2x(x^2-1)^{\frac{d-p-2}{2}} \exp(-\beta \hbar c K m x). \quad (14)$$

A expressão anterior é então integrada[5] tornando-se

$$F'_d(T; l_i; p; g_i) = -2^{-\frac{d-p-1}{2}} L^{d-p} \beta^{-\frac{d+p-1}{2}} (\hbar c)^{-\frac{d+p+1}{2}} \pi^{\frac{d-p-1}{2}} \\ \times \sum_{\{n_i\}=0}^{\infty} \sum_{m=1}^{\infty} \left(\frac{K}{m}\right)^{\frac{d-p+1}{2}} K_{\frac{d-p+1}{2}}(\beta \hbar c m K), \quad (15)$$

onde K_ν é a função modificada de Bessel. Para uma análise de F'_d em baixas temperaturas, tomar-se-á a expansão assintótica para $K_\nu(z)$, $z \gg 1$ [5] resultando em

$$F'_d(T; l_i; p; g_i) = -\pi^{\frac{d-p}{2}} L^{d-p} \sum_{k=0}^{\infty} \frac{1}{k!} \frac{\Gamma\left[\frac{(d-p+2)}{2} + k\right]}{\Gamma\left[\frac{(d-p+2)}{2} - k\right]} \\ \times 2^{-\frac{d-p}{2}-k} \beta^{-\frac{d-p+2}{2}-k} (\hbar c)^{-\frac{d+p}{2}-k} \sum_{\{n_i\}=0}^{\infty} K^{\frac{d-p}{2}-k} \\ \times \sum_{m=1}^{\infty} m^{-\frac{d+p-2}{2}-k} \exp(-\beta \hbar c m K). \quad (16)$$

Assumindo $p = 1$ e $d = 3$ seleciona-se os dois primeiro termos da soma em k na equação anterior¹. Sob condições de contorno homogêneas ($g_i = 0$) ou mistas ($g_i = 1/2$) as expressões para F'_d são dadas respectivamente por

$$F'_3(T; l_1; 1; 0) = -L^2 \beta^{-2} (\hbar c)^{-1} l_1^{-1} \sum_{n=0}^{\infty} n \sum_{m=1}^{\infty} m^{-2} \exp(-\beta \pi \hbar c m n / l_1) \\ - L^2 \beta^{-3} \pi (\hbar c)^{-2} \sum_{n=0}^{\infty} \sum_{m=1}^{\infty} m^{-3} \exp(-\beta \pi \hbar c m n / l_1). \quad (17)$$

e

$$F'_3(T; l_1, 1, 1/2) = -L^2 \beta^{-2} \pi^2 (\hbar c)^{-1} l_1^{-1} \sum_{n=0}^{\infty} (n + 1/2) \\ \times \sum_{m=1}^{\infty} m^{-2} \exp\left(-\frac{\beta \pi \hbar c}{l_1} \left(n + \frac{1}{2}\right)\right)$$

¹Observe que sob a condição imposta, o argumento de Γ no denominador da eq.(2.16) indica polos desta função que anulam termos subsequentes aos coletados

$$\begin{aligned}
 & -L^2\beta^{-3}\pi(\hbar c)^{-2}\sum_{n=0}^{\infty}\sum_{m=1}^{\infty}m^{-3} \\
 & \times \exp\left(-\frac{\beta\pi\hbar mc}{l_1}\left(n+\frac{1}{2}\right)\right). \quad (18)
 \end{aligned}$$

O sinal no símbolo da soma na eq.(2.17) indica que o termo $n = 0$ deve ser multiplicado por $1/2$. A partir da expressão (2.18) obtém-se resultados particulares já indicados anteriormente[10].

3 Considerações finais

As expressões gerais para a energia de Casimir obtidas neste trabalho, além de permitir que se recupere uma série de resultados já encontrados na literatura (caso homogêneo), também possibilitam a análise de novas situações (caso misto). Por fim, essas expressões generalizadas apontam para a possibilidade de estudar-se configurações onde coexistam condições de contorno homogêneas e mistas. A abordagem numérica para dimensões espaciais e confinamentos arbitrário ($d > 3$, $p > 1$) está em fase de elaboração.

References

- [1] H. B. G. Casimir; Proc. Kon. Nederl. Akad. Wetenschap 51(1948)793
- [2] J. Ambjorn, S. Wolfram; Ann. Phys. 147(1983)1
- [3] F. Caruso, N. P. Neto, B. Svaiter, N. F. Svaiter; Phys. Rev. 43 D(1991)1300
- [4] J. Mehra; Physica 37(1967)145
- [5] N. F. Svaiter; N. Cimento 105 A(1992)959
- [6] G. Plunien, B. Muller, W. Greiner; Phys. Rep. 134(1991)87
- [7] T. H. Boyer; Phys. Rev. 9 A(1974)2078
- [8] L. A. Ferreira; "Sobre a Energia de Ponto Zero do Campo Eletromagnético na Presença de Meios Materiais", Dissertação de Mestrado, IFT-UNESP, 1980, São Paulo
- [9] H. Bateman; Higher Transcendental Functions, McGraw-Hill, 1955, vol. 3
- [10] J. C. da Silva, Hebe Q. Plácido, Ademir E. Santana, A. Matos Neto; Efeito Casimir Entre Placas de Materiais Distintos à Temperatura Finita", Proceedings of the XV Brazilian National Meeting on Particles and Fields(1994)318

LISTA DE PARTICIPANTES

ADILSON JOSE DA SILVA - IFUSP
ADRIANA BRUNSTEIN LALLA - IFUSP
ÁDRIANO ANTONIO NATALE - IFT
ALEXANDRE TORT - UFRJ
ALFREDO TAKASHI SUZUKI - IFT
ALVARO DE SOUZA DUTRA - UNESP-GUAR
ALVARO FAVINHA MARTINI - UNICAMP
ALVARO LEONARDI AYALA FILHO - UFRGS
ANA GABRIELA GRUNFELD - LA PLATA
ANA LUCIA BARBOSA - IFT
ANA LUCIA FERREIRA DE BARROS - CBPF
ANA PAULA MOURA REIS MICELI - UFRJ
ANDERSON CAMPOS FAUTH - UNICAMP
ANDERSON ILHA DOS SANTOS - ON
ANDRE BESSADAS PENNA FIRME - CBPF
ANDRE GUSSO - IFT
ANDRE TENORIO LEITE - UFRJ
ANIBAL LEONARDO PEREIRA - UERJ
ANNA MARIA FREIRE ENDLER - CBPF
ANTONIO CANDIDO CAMARGO GUIMARAES - IFT
ANTONIO EDSON GONCALVES - UEL
ANTONIO SOARES DE CASTRO - UNESP-GUAR
ANTONIO TAVARES DA COSTA JUNIOR - UFF
ARMANDO BERNUI LEO - CBPF
ARVIND NARAYAN VAIDYA - UFRJ
AYRTON ZADRA MORAES FILHO - IFUSP
BERNARD MARIE MARECHAL -
BRAZ EDSON PALLADINO - IFT
CARLA RIBEIRO DA FONSECA - UFRJ
CARLOS ALBERTO SANTOS DE ALMEIDA - UFCE
CARLOS EDUARDO CAMPOS LIMA - CBPF
CARLOS ENRIQUE NAVIA OJEDA - UFF
CARLOS FARINA DE SOUZA - UFRJ
CARLOS FRAJUCA - IFUSP
CARLOS MARIA NAON - LA PLATA
CAROLA DOBRIGKEIT CHINELLATO - UNICAMP
CLISTENIS PONCE CONSTANTINIDIS - IFT
CLOVIS JOSE WOTZASEK - UFRJ
CRISTIANE GRALA ROLDAO - IFT
CRISTINE NUNES FERREIRA - CBPF
DANIEL GUILHERME GOMES SASAKI - CBPF
DANIEL MULLER - IFT
DANIELLE MAGALHAES MORAES - UFRJ
DENIS DALMAZI - UNESP-GUAR
DEUSDEDIT MONTEIRO MEDEIROS - UFCE
DICKSON CADORE GOULART - UFRGS
DIONISIO BAZEIA FILHO - UFPB
EDISON HIROYUKI SHIBUYA - UNICAMP
EDSON MINORU KUBO - IFUSP
EDUARDO DE MORAES GREGORES - IFT
EDUARDO SOUZA FRAGA - UFRJ
EDUARDO V TONINI - CBPF
ELIEZER BATISTA - IFT
ELSO DRIGO FILHO - IBILCE
ERASMO MADUREIRA FERREIRA - UFRJ
ERICA EMILIA LEITE - IFT
ERICA RIBEIRO POLYCARPO - UFRJ
EVERTON MURILO CARVALHO DE ABREU - UFRJ
FABIO BOSCO MOURA SALEMME - IFUSP
FELICE PISANO - IFT
FERDINANDO GLIOZZI - UNIV. DE TORINO
FERNANDO KOKUBUN - IFT
FERNANDO LUIZ DE CAMPOS CARVALHO - IFT
FERNANDO MIGUEL PACHECO CHAVES - UFSE
FILADELFO CARDOSO SANTOS - UFRJ
FRANCISCO EUGENIO M DA SILVEIRA - IFT
FRANCISCO SALES AVILA CAVALCANTE - UFCE
FRANZ PETER ALVES FARIAS - UEF
GALINA L. KLIMCHITSKAYA - UFPB
GEORGE EMANUEL AVRAAM MATSAS - IFT
GERMAN IGNACIO GOMERO FERRER - CBPF
GIL DE OLIVEIRA NETO - CBPF
GILDEMAR CARNEIRO DOS SANTOS - UFBA
GINO NOVALIS JANAMPA ANANOS - CBPF
GUILHERME DE BERREDO PEIXOTO - CBPF
GUILLERMO SANTIAGO CUBA CASTILLO - CBPF
HATSUMI MUKAI - FUEM
HEBE QUEIROZ PLACIDO - UFBA
HELIO MANOEL PORTELLA - UFF
HUGO R. CHRISTIANSEN - CBPF
HUMBERTO BELICH JUNIOR - CBPF
ILYA SHAPIRO - UFJF
IOAV WAGA - UFRJ
IRAZIET DA CUNHA CHARRET - UFF
IVAN JOSE LAUTENSCHEILGUEER - IFT
J. BEKENSTEIN - U. HEBREW
JOAO BARCELOS NETO - UFRJ
JOAO RAMOS TORRES DE MELLO NETO - UERJ
JORGE ABEL ESPICHAN CARRILLO - UNICAMP
JORGE ANANIAS NETO - UFJF
JORGE CASTINEIVAS RODRIGUEZ - IFT
JORGE EDUARDO CIEZA MONTALVO - UERJ
JORGE HUMBERTO COLONIA BARTRA - UNICAMP
JORGE MARIO CARVALHO MALBOUISSON - IFUSP
JOSE A C NOGALES VERA - UFF
JOSE ACACIO DE BARROS - UFJF
JOSE ALEXANDRE NOGUEIRA - UFES
JOSE AUGUSTO CHINELLATO - UNICAMP
JOSE CARLOS BRUNELLI - UFSC
JOSE FRANCISCO GOMES - IFT
JOSE KENICHI MIZUKOSHI - IFUSP
JOSE LUIS BOLDO - IFT
JOSE LUIZ MATHEUS VALLE - UFJF
JOSE P S LEMOS - ON
JOSE PAULO RODRIGUES F DE MENDONCA - UFJF
JOSE ROBERTO SOARES DO NASCIMENTO - UFPB
JOSE TADEU DE SOUZA PAES - UNICAMP
JUAN ALBERTO MIGNACO - UFRJ
JUAREZ CAETANO DA SILVA - UFBA
JULIO MIRANDA PUREZA - UESC
JUSSARA MARQUES DE MIRANDA - CBPF
KWOK SAU FA - FUEM
LAURA MARIA RUBI FALCO DE FRANCA - IFUSP
LEANDRO SALAZAR DE PAULA - UFRJ
LEON RICARDO URURAHY MANSSUR - CBPF
LEONARDO MACHADO DE MORAES - CBPF
LEONIDAS SANDOVAL JUNIOR - IFUSP
LIN YOUNG -
LUCA ROBERTO AUGUSTO MORICONI - UFRJ
LUCIENE PONTES FREITAS - IFT

LUIS CARLOS BASSALO CRISPINO - IFT
LUIS CARLOS MALACARNE - FUEM
LUIZ AMERICO DE CARVALHO - UNICAMP
LUIZ CARLOS SANTOS OLIVEIRA - CBPF
LUIZ CLAUDIO MARQUES DE ALBUQUERQUE - IFUSP
LUIZ FERNANDO KLIPPEL - UCP
LUIZ MARTINS MUNDIM FILHO - CBPF
LUIZ OTAVIO BUFFON - IFUSP
MANOEL JANUARIO DA SILVA NETO - UNICAMP
MANOELITO MARTINS DE SOUZA - UFES
MARCELLO BARBOSA DA SILVA NETO - CBPF
MARCELO BATISTA HOTT - UNESP-GUAR
MARCELO COSTA DE LIMA - CBPF
MARCELO DE OLIVEIRA SOUZA - UENF
MARCELO EVANGELISTA DE ARAUJO - UNB
MARCELO OTAVIO CAMINHA GOMES - IFUSP
MARCELO SCHIFFER - UNICAMP
MARCIO JOSE MENON - UNICAMP
MARCO AURELIO CATTACINI KNEIPP - CBPF
MARCO AURELIO LISBOA LEITE - IFUSP
MARCO AURELIO SCHMIDT - IFUSP
MARCOS CARDOSO RODRIGUES - IFT
MARCUS VENICIUS COUGO PINTO - UFRJ
MARIA BEATRIZ DE LEONE GAY DUCATTI - UFRGS
MARIA DE FATIMA ALVES DA SILVA - UERJ
MARIA TERESA C DOS SANTOS THOMAZ - UFF
MARIA VIRGINIA MANIAS - LA PLATA
MARIO EVERALDO DE SOUZA - UFSE
MARTA LILLIANA TROBO - LA PLATA
MARTHA CHRISTINA MOTTA DA SILVA - CBPF
MAURICIO BERNARDINO MAGRO - IFUSP
MAXWEL GAMA MONTEIRO - UCP
MIKAEL BERGGREN - UFRJ
MIKHAIL PLYUSHCHAY - UFJF
MIRIAM GANDELMAN - CBPF
NADJA SIMAO MAGALHAES - INPE
NATHAN JACOB BERKOVITS - IFUSP
NAZIRA ABACHE TOMIMURA - UFF
NELSON PINTO NETO - CBPF
NELSON RICARDO DE FREITAS BRAGA - UFRJ
NEUSA AMATO - CBPF
NIKOLAI KUROPATKIN - IFUSP
ODYLIO DENYS DE AGUIAR - INPE
ORLANDO LUIS GOULART PERES - IFUSP
OSCAR JOSE PINTO EBOLI - IFUSP
OSWALDO GOMES -
OZEMAR S VENTURA - CBPF
PATRICIA DUARTE PERES - UCP
PATRICIA MACEDO DA COSTA JORGE - UCP
PATRICIO ANIBAL LETELIER SOTOMAYOR - UNICAMP
PAULO ALEX DA SILVA CARVALHO - UNICAMP
PAULO CESAR BEGGIO - UNICAMP
PAULO DE FARIA BORGES - ETFQ
PAULO SERGIO KUHN - UFRGS
PAULO SERGIO RODRIGUES DA SILVA - IFT
PAULO TEOTONIO SOBRINHO - IFUSP
PEDRO CUNHA DE HOLANDA - UNICAMP
PEDRO GALLI MERCADANTE - IFUSP
R. S. CHIVUKULA - U. BOSTON
RAFAEL DE LIMA RODRIGUES - UFPB
RAIMUNDO MUNIZ TEIXEIRA FILHO - IFUSP
RANDALL GUEDES TEIXEIRA - IFT

RAPHAEL DIAS MARTINS DE PAOLA - PUC/RJ
REGINA CELIA ARCURI - UFRJ
REGINA MARIA RICOTTA - UNESP
RENATA ZUKANOVICH FUNCHAL - IFUSP
RENATO KLIPPERT BARCELLOS - CBPF
RENATO MELCHIADES DORIA - UCP
RENIO DOS SANTOS MENDES - FUEM
REUVEN OPHER - IAG
RICARDO MORITZ CAVALCANTI - PUC/RJ
RODOLFO ALVAN CASANA SIFUENTES - CBPF
ROGERIO ROSENFELD - IFT
RONALD CINTRA SHELLARD - CBPF
RUBENS FREIRE RIBEIRO - UFPB
RUBENS LUIS PINTO GURGEL DO AMARAL - UFF
RUDNEI DE OLIVEIRA RAMOS - UERJ
RUDOLF MURADIAN - UFBA
SAMUEL MAIER KURCBART - U.CALIFORN
SAMUEL ROCHA DE OLIVEIRA - UNB
SANDRO SILVA E COSTA - IFT
SAULO CARNEIRO DE SOUZA SILVA - IFUSP
SEBASTIAO ALVES DIAS - CBPF
SERGIO ANEFALOS PEREIRA - IFUSP
SERGIO EDUARDO DE C EYER JORAS - UFRJ
SERGIO JOFFILY - CBPF
SERGIO LUIZ CARMELO BARROSO - UNICAMP
SERGIO MARTINS DE SOUZA - UFF
SERGIO MORAIS LIETTI - IFT
SERGIO VIZEU LIMA PINHEIRO - IFUSP
SILVESTRE RAGUSA - IFSC
SIMONE ALMEIDA ARAUJO - UCP
STOIAN IVANOV ZLATEV - UFSE
TATIANA DA SILVA - UFRJ
VALDIR BARBOSA BEZZERRA - UFPB
VAN SERGIO ALVES - IFUSP
VERISSIMO MANOEL DE AQUINO - UEL
VICENTE PLEITEZ - IFT
VICTOR DE OLIVEIRA RIVELLES - IFUSP
VICTOR PAULO BARROS GONCALVES - UFRGS
VITORIO ALBERTO DE LORENCI - CBPF
VLADIMIR KOPENKIN - UNICAMP
VLADIMIR M. MOSTEPANENKO - UFPB
WALTER FELIPE WRESZINSKI - IFUSP
WELLINGTON DA CRUZ - UEL
WERNER MARTINS VIEIRA - UNICAMP
WINDER ALEXANDER DE MOURA MELO - CBPF
WLADIMIR SEIXAS - UNESP